Concrete Repair, Rehabilitation and Retrofitting III

Editors:
M.G. Alexander, H.-D. Beushausen, F. Dehn & P. Moyo

CRC Press
Taylor & Francis Group
A BALKEMA BOOK

CONCRETE REPAIR, REHABILITATION AND RETROFITTING III

This page intentionally left blank

PROCEEDINGS OF THE 3RD INTERNATIONAL CONFERENCE ON CONCRETE REPAIR, REHABILITATION AND RETROFITTING (ICCRRR), CAPE TOWN, SOUTH AFRICA, SEPTEMBER 3–5, 2012

Concrete Repair, Rehabilitation and Retrofitting III

Editors

Mark G. Alexander
Department of Civil Engineering, University of Cape Town, South Africa

Hans-Dieter Beushausen
Department of Civil Engineering, University of Cape Town, South Africa

Frank Dehn
Universität Leipzig/MFPA Leipzig, Germany

Pilate Moyo
Department of Civil Engineering, University of Cape Town, South Africa

CRC Press
Taylor & Francis Group
Boca Raton London New York Leiden

CRC Press is an imprint of the
Taylor & Francis Group, an **informa** business
A BALKEMA BOOK

CRC Press
Taylor & Francis Group
6000 Broken Sound Parkway NW, Suite 300
Boca Raton, FL 33487-2742

Version Date: 2012912

International Standard Book Number-13: 978-0-203-12425-3 (eBook - PDF)

Visit the Taylor & Francis Web site at
http://www.taylorandfrancis.com

and the CRC Press Web site at
http://www.crcpress.com

Concrete Repair, Rehabilitation and Retrofitting III – Alexander et al. (eds)
© 2012 Taylor & Francis Group, London, ISBN 978-0-415-89952-9

Table of contents

Service life modelling and prediction of durability

NDE/NDT and measurement techniques

Theme 3: Concrete repair, rehabilitation and retrofitting
Repair methods, materials and techniques

Bonded concrete overlays and patch repairs

Structural repairs and strengthening

Retrofitting techniques and FRP systems

Theme 4: Developments in materials technology, assessment and processing

This page intentionally left blank

Concrete Repair, Rehabilitation and Retrofitting III – Alexander et al. (eds)
© 2012 Taylor & Francis Group, London, ISBN 978-0-415-89952-9

Preface

This conference is the third in a series that ran in 2005, then in 2008, and now in 2012. All have been held in Cape Town, South Africa, and have been a collaborative effort between the Universities of Cape Town and The Witwatersrand in South Africa, and the Multifunctional Construction Materials Group at Leipzig University and the Leipzig Institute for Materials Research and Testing (MFPA Leipzig) in Germany. As in the previous conferences, excellent support has been given by researchers and practitioners from these two countries; nevertheless, this remains a truly international conference, with authors being drawn from 54 countries and numerous research and industrial organisations. This continues to fulfil an aim of these conferences, to strengthen relationships not only between Africa and Europe but also between countries and regions from all over the world.

These Proceedings contain papers presented at the conference, classified into a total of 12 sub-themes which can be grouped under five main themes:

– Concrete durability aspects
– Condition assessment of concrete structures
– Concrete repair, rehabilitation and retrofitting
– Developments in materials technology, assessment and processing
– Concrete technology and structural design

While considerable progress has been made in recent years towards understanding deterioration mechanisms for concrete in its various forms, and repair and rehabilitation technologies have advanced markedly, the fact remains that a vast stock of concrete infrastructure worldwide remains in a serious state of disrepair and needs substantial work to maintain and possibly restore to acceptable levels of service. The challenge still remains of finding new ways to extend the useful life of concrete structures cost-effectively. Confidence in concrete as a viable construction material must be retained and sustained, particularly considering the environmental challenges that the industry and society now face.

A large number of papers discuss performance and assessment of innovative materials for durable concrete construction. Interesting fields, some quite new, are covered such as self-healing techniques, high performance concretes, and strain hardening composites. The number of papers submitted on the topic of service life modelling and prediction of durability confirms the positive international developments towards performance-based methods for durability design and specification. Another fact that is evident from the paper submissions is that large advances have recently been made in the fields of non-destructive testing and condition assessment of concrete structures. The papers in the proceedings cover interesting new techniques for the assessment of reinforcement corrosion and their interpretation. Further, vibration-based evaluation of the structural capacity of reinforced concrete members is discussed, representing a relatively new and promising technique for the assessment of corrosion- or fire-damaged structures.

The majority of papers discuss recent developments in concrete repair, rehabilitation and retrofitting techniques. An important research area lies in the field of specifications for repair materials and systems. Here, an integrated approach is needed, linking assessment techniques and service life modelling to appropriate repair methods. A number of papers deal with these important issues, confirming that the industry is on the right track towards efficient and durable repairs. Based on research reports and case studies, latest developments on repair strategies and materials are presented, ranging from surface protection techniques to full-scale repairs. Bonded concrete overlays and patch repairs remain important fields for most repair projects. Techniques and materials for crack-free overlays with sufficient bond strength are discussed. Numerous papers were submitted on the topic of strengthening and retrofitting, highlighting the need to cope with increasing loads and deteriorating structures and showcasing latest developments in FRP strengthening systems.

ICCRRR 2012 is dedicated to the person and work of Professor Joost Walraven who has made, as a researcher and as an engineer, outstanding and international contributions to the development and application of new construction materials, new structures, and structural models. Already at an early stage in his career, Professor Walraven recognized the aspects of repair and retrofitting of concrete structures to be major economic and technical issues for future activities in the concrete community. He has strongly supported the Editors in creating an independent international platform where researchers and practitioners from different countries and continents can share their knowledge and experience on one of the most future-orientated fields of activity in Civil Engineering. The Editors therefore take the opportunity to cordially thank Professor Walraven for his enduring and amicable support of the ICCRRR conference series and his substantial contribution to concrete research and practice.

This 3rd ICCRRR is also being held in conjunction with the Annual RILEM Week – the first time RILEM has held its annual event in sub-Saharan Africa. The African continent is on the move, and the next decades will provide great opportunities for expansion on this continent of science and technology, industry and culture. For this reason, it is timely that the RILEM Week is being held in Cape Town. We look forward to welcoming RILEM members to the 2012 Annual RILEM Week.

All papers submitted for ICCRRR 2012 were subjected to a full process of peer review, and the Proceedings contain only those papers that were accepted following this process. The review of manuscripts was undertaken by members of the International Scientific Advisory Board and other identified leading experts, acting independently on one or more assigned manuscripts. This invaluable assistance, which has greatly enhanced the quality of the Proceedings, is gratefully acknowledged.

Special acknowledgements are due to the following organisations:

- National Research Foundation of South Africa
- Deutscher Beton- und Bautechnik-Verein
- Cement and Concrete Institute of South Africa
- Deutscher Ausschuss für Stahlbeton
- Concrete Society of Southern Africa
- The South African National Roads Agency
- Deutsche Bauchemie
- RILEM
- fib
- American Concrete Institute
- Sika South Africa
- BASF Construction Chemicals
- Afrisam
- Mapei SA
- Chryso Southern Africa
- a.b.e. Construction Chemicals
- Penetron
- StonCor Africa
- PPC Cement
- S.A. Water Research Commission
- S.A. Department of Water Affairs

Finally, the editors wish to thank the authors for their efforts at producing and delivering papers of high standard. We are sure that the Proceedings will be a valued reference for many working in this important field and that they will form a suitable base for discussion and provide suggestions for future development and research.

M.G. Alexander
H. Beushausen
F. Dehn
P. Moyo
Editors

Concrete Repair, Rehabilitation and Retrofitting III – Alexander et al. (eds)
© 2012 Taylor & Francis Group, London, ISBN 978-0-415-89952-9

ICCRRR Committees

ORGANIZING COMMITTEE

INTERNATIONAL SCIENTIFIC AND TECHNICAL ADVISORY BOARD

Prof. C. K. Leung, *UST, Hong Kong*
Prof. L. Luco, *University of Buenos Aires, Argentina*
Dr. P. Lura, *EMPA, Switzerland*
Dr. J. Mackechnie, *University of Canterbury, New Zealand*
Prof. V. Mechtcherine, *TU Dresden, Germany*
Mr. R. Morin, *Ville de Montréal, Canada*
Prof. A. Nanni, *University of Miami, USA*
Mr. A. Newmark, *BKS Pty Limited, South Africa*
Mr. B. Perrie, *Cement and Concrete Institute, South Africa*
Prof. G. Plizzari, *University of Bergamo, Italy*
Prof. R. Polder, *TNO Built Environment and Geosciences, The Netherlands*
Prof. M. Raupach, *RWTH Aachen, Germany*
Dr. P. Richner, *EMPA, Switzerland*
Prof. M. Santhanam, *IIT Madras, India*
Prof. E. Schlangen, *TU Delft, The Netherlands*
Mr. N. Schroeter, *Deutsche Bauchemie, Germany*
Dr. A. Scott, *University of Canterbury, New Zealand*
Prof. J. Silfwerbrand, *CBI Stockholm, Sweden*
Dr. C. Sodeikat, *Ing. büro Schießl Gehlen Sodeikat, Germany*
Prof. L. Taerwe, *University of Ghent, Belgium*
Dr. A. Taffe, *BAM, Germany*
Dr. R. Torrent, *Holcim Group Support, Switzerland*
Prof. A. Turatsinze, *LMDC Toulouse, France*
Mr. A. Van Grieken, *Aurecon, Australia*
Prof. G. Van Zijl, *University of Stellenbosch, South Africa*
Dr. A. Vaysburd, *Vaycon, USA*
Prof. J. C. Walraven, *TU Delft, The Netherlands*
Dr. H. Wiggenhauser, *BAM, Germany*
Prof. A. Zingoni, *University of Cape Town, South Africa*

Keynote papers

Concrete Repair, Rehabilitation and Retrofitting III – Alexander et al. (eds)
 ISBN 978-0-415-89952-9

Assessing the remaining service life of existing concrete bridges

J.C. Walraven
Delft University of Technology, The Netherlands

ABSTRACT: Service life design has developed to a major aspect of the design of new concrete structures. However, a considerable task of the structural engineer of today is as well to deal with existing structures. Decisions have to be taken with regard to strengthening, retrofitting and protecting. Moreover the structural safety is concerned, since the traffic load is now often substantially larger than assumed in the original design. This paper deals with the strategy to be followed when a large number of bridges, with a substantial significance for the national infrastructure, are subject of reconsideration.

1 INTRODUCTION

The major part of the bridges in function today have been designed in a time that structural safety and serviceability were the governing design criteria. Service life considerations were limited to requirements for minimum cover and maximum crack width. Deterioration of those important structures, and costs and nuisance involved, has led to the consciousness that design for service life should be at least at the same level as design for safety and serviceability. The significance of service life design was already formulated by the Dutch engineer Reinhold De Sitter (1984), who formulated the Rule of Fives:

- If a structure is not maintained, the cost of repair will amount to five times the money that has been saved by not maintaining
- If a structure is not repaired, the cost for building a new structures will amount to five times the money that has been saved by not repairing.

The *fib* Model Code for Concrete Structures (2010) is a recommendation for the design of reinforced and prestressed concrete, which is intended to be a guidance document for future codes. Previous Model Codes have been published in 1978 and 1990. The Model Code 1990 has been a basis for e.g. the actual Eurocodes for Concrete Structures (EN 1992-1-1). The most important difference between Model Code 2010 and the previous Model Codes is the introduction of the factor *time*. This factor is not only involved with regard to time-dependant aspects like creep and shrinkage, but predominantly in the sense of "aging" of structures. Where in earlier considerations *durability* was seen as an important design criterion further to structural safety and serviceability, in Model Code 2010 an integral consideration is introduced: concrete structures should be designed to meet requirements with regard to safety and serviceability *for a specified period of time.* This means that the choice of the structural materials and detailing is made in relation to the service life envisaged. Service life requirements can as well be satisfied by a suitable overall design concept, e.g. offering the option of exchange of structural members, adaption of the structure to a new function, or even total dismantlement at the end of service life (Fig. 1)

For any new structure a maintenance and inspection plan has to be provided. The flow chart given in Fig. 2 shows a scheme for a service life conservation strategy, as given in the Model Code 2010.

For the design of new structures a conservation strategy has to be defined, based on the quality of the structure to be realized and maintained. After construction a condition survey has to be carried out, in order to establish the real quality of the structure (as-built document, or "birth-certificate"). This survey could lead to repair work already in this early stage. Subsequently the definite conservation strategy is defined.

A large part of the work of structural engineers now and in future will be to deal with existing structures, which have not been designed for service life. In order to define a suitable conservation strategy for those structures at first an assessment of the condition of those structures is required. On the basis of this assessment it can be decided whether the structure is still able to carry the loads with sufficient safety and whether serviceability is still sufficient. If this is the case, the remaining service life, without significant intervention, can be determined. If the condition of the structure is such that strengthening or retrofitting is necessary, the structure is treated afterwards principally in the same way as a new structure: a conservation strategy is defined for the specified remaining service life.

Figure 1. Demountable connection in a concrete building designed for a service life of 20 years (Delft, The Netherlands).

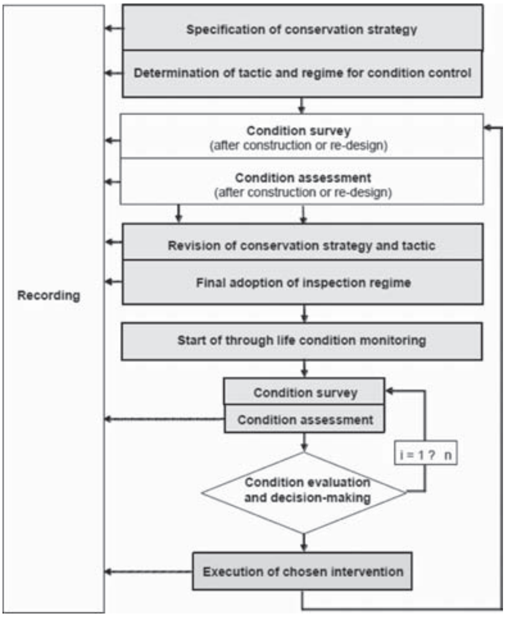

Figure 2. Flow chart for service life conservation and recording of information (fib Model Code 2010).

The diagram shown in Fig. 3 reflects the general problem of the increase of the loads as observed in bridges and the decrease of structural bearing capacity due to material deterioration. Resistance (R) and loads (S) are probabilistic phenomena

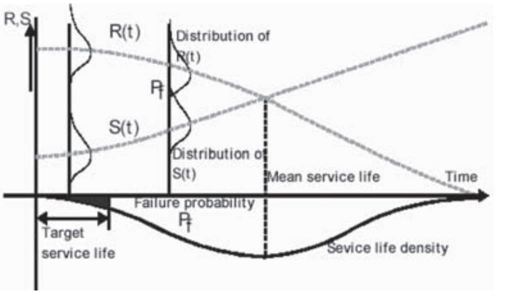

Figure 3. Probabilistic structural safety in relation to service life.

and therefore should be treated with regard to the question whether the structural safety satisfies the demands.

Such a strategy can be followed for individual structures, but as well for large families of structures, which represent the infrastructure of a country or a large part of it. In this way it is possible to foresee consequences of aging of the infrastructure for the national budgets to be reserved for refurbishment and retrofitting.

2 DEGRADATION OF A STOCK OF BRIDGES DUE TO CHLORIDE ATTACK

Chloride ingress in concrete can be described with Fick's second law (*fib* Model Code (2012):

$$C(x,t) = C_s + (C_s - C_i)\, erfc\left(\frac{x}{\sqrt{4D_{app}(t)\cdot t}}\right) \tag{1}$$

where

$C(x,t)$	content of chlorides in the concrete at a depth x and time t as a% of the binder content
C_s	chloride concentration at the concrete surface
C_i	initial chloride content of the concrete
$D_{app}(t)$	apparent coefficient of chloride diffusion through the concrete at time t
t	time of exposure (years)
erf	error function

$$D_{app}(t) = D_{app}(t_0)\left(\frac{t_0}{t}\right)\alpha \tag{2}$$

where

$D_{app}(t_0)$	apparent diffusion coefficient measured at the reference time
α	aging factor giving the decrease over time of the apparent diffusion coefficient.

In order to determine the situation of a stock of thousands of existing concrete bridges and to give a prediction of their remaining service life it is necessary to know more about their history (Fig. 4). A study of this type was carried out in the Netherlands (Gaal, 2004).

The 3500 bridges considered have been constructed in the period 1930 to 2000. The data of the bridges were found in databases of Rijkswaterstaat (the Dutch Ministry of Infrastructure). The first database contained the year of construction and dimensions of the bridge decks. The second database contained the input parameters, related to the concrete quality and design details. These input parameters were determined from site concrete, including data from concrete cores and cover depth measurements. The third database contained the constants that are used in the deterioration models, like corrosion current, critical chloride concentration and aging coefficient. In many cases the chloride profile was determined using drilled cores so that the assumption for the diffusion coefficient could be verified. A special circumstance to be noted is that the type of de-icing salt used in winter changed in time (initially only sand was used). So, the age of the concrete when it was exposed to various concentrations of chloride differed as well. The probability of initiation of corrosion due to chloride ingress and carbonation of all individual bridges was summed up to obtain the total probability of corrosion. The result of this analysis is an arithmetic plot that gives the probability of initiation of corrosion as a function of concrete age

Figure 4. History of construction of existing bridges.

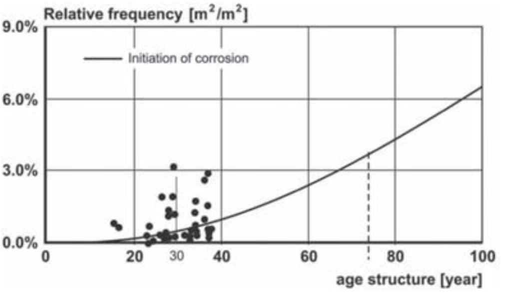

Figure 5. Observed and predicted spalling of 81 Dutch concrete bridges (Gaal, 2004).

(solid line in Fig. 5, Gaal, 2004). A study of spatial variability of the damage was made further to this study (Li, 2004). In Fig. 5 the predictions have been compared with observations on 81 Dutch bridges.

It was noted that older bridges behaved better than newer bridges. This can be explained by the later exposure to serious chloride concentrations.

3 RESIDUAL BEARING CAPACITY OF CONCRETE BRIDGES

3.1 *General considerations*

Figure 3 showed the generally expected tendencies of structural degradation in time against increasing traffic load. For the Dutch government this was a reason to investigate the bearing capacity of a number of representative bridges. The investigations were made on the basis of "unity checks". According to this approach the bearing capacity is calculated without safety factors and compared with the maximum loads on the structure in their most unfavourable position. If the ratio load/resistance is larger than one, this means that the bridge does not fulfill the safety demands. The result of the investigation was alarming at first sight. A large part of the 3500 bridges appeared not to reach the required bridge safety criteria. It should, however, be noted that this analysis was carried out on the basis of design rules, not regarding residual effects, which may require a more advanced calculation. These residual effects might enhance the real bearing capacity and, as such, extend the date that the safety requirements are not met anymore. This is shown by the diagram in Fig. 6, which is an extension of Fig. 3, including the eventual effect of residual bearing mechanisms.

In the sequel at first a survey is given of the results of the unity checks. Subsequently a number of aspects are discussed regarding contributions to resi-dual bearing capacity.

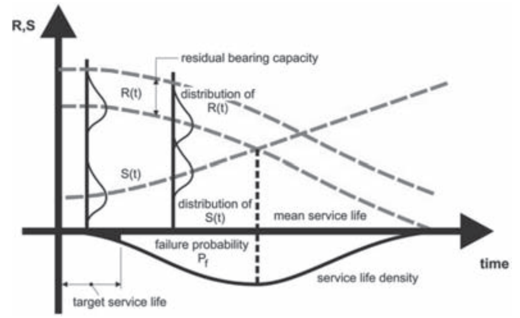

Figure 6. Effect of including residual bearing capacity in service life consideration.

Table 1. Results of unity checks for a selection of bridges.

Year	Type	UC-value
1996	Culvert	1.89
1970	T-beam deck	2.43
1936	Solid slab	4.53
1966	Subway	1.61
1961	Subway	1.18
1959	T-beam deck	3.13
1959	Straight solid slab	2.85
1969	Skew solid slab	3.53

3.2 *Results of preliminary assessment of the bearing capacity of Dutch bridges*

The result of the unity checks, as carried out by a number of design offices, on request of the Ministry of Infrastructure, were remarkable. Table 1 shows a small selection of the verifications for various types of bridges. The assessment of the bearing capacity was carried out under the assumption of actual traffic loads and building codes, whereas for concrete and steel the original design strengths were used. The last column in Table 1 shows the so-called UC values, where UC stands for "Unity Check", giving the ratio between the maximum load at the bridge in use at the most critical position and the bearing capacity, calculated on the basis of existing code rules. If the UC-value is larger than 1,0, this means theoretically that the bearing capacity does not meet the safety standards. The table shows unexpectedly high UC-values. In all cases the shear capacity turned out to be largely insufficient. The highest UC values were found for T-beam bridge decks and solid slab bridge decks.

In spite of the alarming UC-values, however, inspections did not show signs that confirmed the expectation of a serious lack of bearing capacity. Obviously there is a substantial residual bearing capacity, supporting the assumption shown in Fig. 6. It is clear that an accurate determination of the reserve bearing capacity is of large significance and should be regarded before any decision for retrofitting of the bridge is taken.

4 DETERMINATION OF VARIOUS TYPES OF RESIDUAL BEARING CAPACITIES

4.1 *Concrete strength higher than assumed in design*

The first analyses of the bearing capacity of the bridges were carried out using the original design values for concrete and steel. The bridges have originally been built with concrete of strength class C20 (characteristic cylinder strength 20 MPa). However, after the age of 28 days, at which the concrete strength is determined, the hydration process of the cement does not stop. Especially the cement particles in the early days were quite coarse, so that a skin of hydrated cement was formed at the outside, leaving unhydrated cement inside. Since water particles had to diffuse through the hardened skin in order to reach the unhydrated cement, the hydration process continued even until long after the 28-days. Tests on drilled cores, taken from the bridges, showed that the mean concrete compressive strength now is even in the range of 60–90 MPa. The compressive strength is an important design property, but not the most important. Especially with regard to the shear capacity of concrete bridge decks, the tensile strength plays an even more important role. In most design codes, the shear bearing capacity is a direct, or an indirect, function of the concrete tensile strength. With regard to the concrete tensile strength, determined on drilled cores, however a remarkable observation was made, see Fig. 7. Tests on the cylinders, mostly drilled from the bottom side of the slab, showed that the splitting tensile strength was in the range 4–5 MPa, whereas the uniaxial tensile strength was only in the range 1–2 Mpa. According to Eurocode 2 the relation between uniaxial tensile strength and splitting tensile strength should be 0.9, whereas the fib Model Code 2010 proposes even a value 1.0. An important observation in Fig. 7 is that the scatter in the values of the splitting tensile strength and the uniaxial is about the same.

A possible explanation for the difference between the uniaxial tensile strength and the splitting tensile strength is given in Fig. 8. After casting the concrete and vibrating, under the coarse aggregate particles water layers remain due to bleeding. Especially the concrete of those days was sensitive to this phenomenon, since no superplasticizers were used yet, so that excess water was necessary

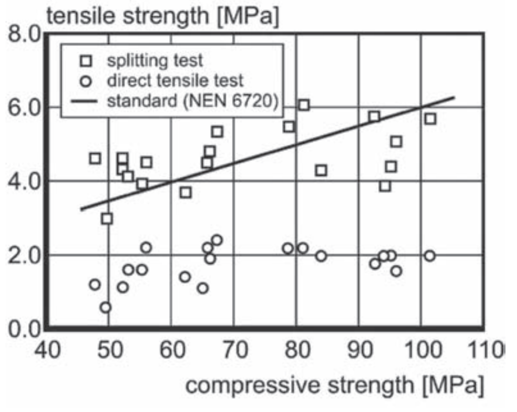

Figure 7. Uniaxial concrete tensile strength and splitting tensile strength as a function of the concrete compressive strength, as determined on cylinders drilled from concrete bridges in the Netherlands.

Figure 8. Cylinder vertically drilled from bridge deck with visual flaw under one of the coarse particles (weakened interface).

for achieving the required workability. The concrete in those days was generally of relatively low strength, which corresponds with the use of excess water. The weakened interfaces between the coarse aggregate particles and the cementmatrix explain the low uniaxial tensile strength of the concrete. As a result of their orientation the weakened interfaces have no influence on the splitting tensile strength. The same holds true for the cylinder compressive strength. In beams and slabs loaded in shear at first vertical bending cracks occur, starting from the bottom of the element. Their direction is perpendicular to the orientation of the weakened interfaces, so that their development is, at least initially, not influenced. Only after the transition from bending cracks into inclined shear cracks there might be some influence, but this applies only to the stage in which the shear crack tends to bend to a low angle with regard to the member axis, in which state the element is already near to shear failure. In order to verify this assumption, large beams were sawn from existing slab bridges, showing the phenomena described, and tested in comparison with similar, newly cast beams made of concrete with the same strength, with the same longitudinal reinforcement, but with a much better workability. The tests showed that the behaviour of the old and the new beams was the same, which confirms that the weak interfaces under the coarse aggregates do not play a significant role with regard to the shear bearing behaviour. Therefore it was concluded that the shear capacity can be calculated with the usual equations, introducing the measured cylinder compressive strength.

4.2 *Sustained loading effect in shear loaded slabs*

In most of the design codes for concrete structures the design concrete compressive strength and the design concrete tensile strength are calculated according to the relations

$$f_{cd} = \alpha_{cc}\frac{f_{ck}}{\gamma_c} \text{ and } f_{ctd} = \alpha_{ct}\frac{f_{ctk}}{\gamma_c} \tag{3}$$

where

f_{ck} = characteristic compressive strength
γ_c = material safety coefficient
f_{ctk} = characteristic tensile strength
α_{cc} = sustained loading factor for compression
α_{ct} = sustained loading factor for tension

For the sustained loading factors α_{cc} and α_{ct} in most codes values are defined of approximately 0.8. Contrary to this, in Eurocode 2 a value 1.0 is recommended. The argumentation behind this is that the sustained loading factors have been determined on specimens with an age of 28 days. The real load on a structure is generally applied at an age substantially over 28 days, so that any sustained loading effect is most probably, at least compensated by the gain in concrete strength by virtue of continued hydration. However, this applies only to *new* structures, where further hydration is a reasonable assumption. However, if for existing concrete bridges, which are mostly more than several decades old, the concrete strength is determined using drilled cylinders, no further hydration will occur. In such a case, where the strength is determined by drilled cylinders, a sustained loading factor should logically be applied, which could significantly reduce the profit of the increased concrete strength.

In order to find out whether there is a sustained loading effect in concrete slabs without shear reinforcement, a substantial number of shear tests was

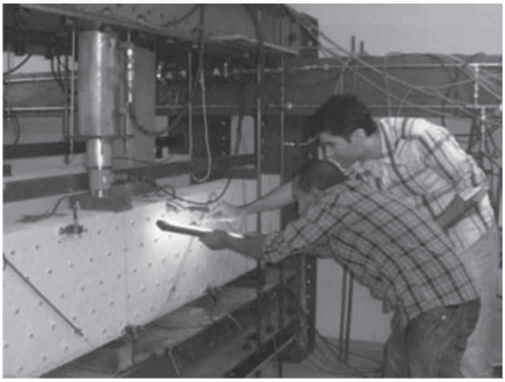

Figure 9. Control of crack propagation in beams without shear reinforcement under sustained shear loading (tests TU Delft, 2012).

carried out. Shear tests on beams without shear reinforcement were conducted under a load application rate of 2–3 minutes until shear failure, as a reference. Subsequently similar beams were subjected to large percentages of the short term shear capacity. It turned out that even for loading levels as high as 90–95% of the short term shear capacity no significant sustained loading effects were observed. The beams, subjected to high load levels of 90–95%, were controlled on crack development for more than 1.5 year (Fig. 9).

It was therefore concluded that no reduction factor for sustained loading in shear needs to be applied.

4.3 *Increased shear capacity in slabs subjected to concentrated wheel load near to line supports*

A critical case in the analysis of the shear capacity of slabs without shear reinforcement is the situation where large wheel loads apply near to line supports. Codes do not give clear specifications on how to apply load spreading and which shear enhancement factor may be applied. A large number of test was carried out on solid slabs with a width of 2.50 m and a thickness of 300 mm, with many different load positions. The tests showed that the load can be spread under 45° from the back side of the loaded area (Fig. 10).

The enhancement factor turned out to be $2.5a_v/d$ which is larger than the factor $2a_v/d$ as given in Eurocode 2 (basically derived for beams).

4.4 *Slab action versus beam action*

All equations for the shear bearing capacity of slabs without shear reinforcement have been derived from tests on beams. With regard to the capacity

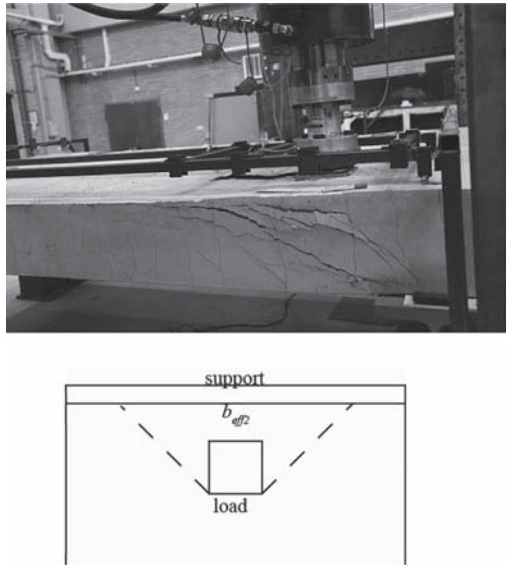

Figure 10. Experiments on load spreading in solid bridge decks subjected to large concentrated loads near to the supports.

to redistribute forces, slabs may be expected to react more favourably than beams. Current practice is that the concrete strength of existing bridges is determined using 6 drilled cylinders. From the strength of those cylinders the characteristic value is determined, which is later used to verify the shear capacity of the slab. However, contrary to beams, slabs will not fail on the basis of the weakest spot. Therefore it was concluded that for slabs the redistribution capacity would be sufficient to allow an increase of the ultimate shear capacity with about 10% compared to beams. The test series was still being carried out at the moment of writing this paper.

4.5 *Compressive membrane action*

The design of concrete bridge decks supported by beams is generally carried out assuming that bending and shear can occur without any confining action. However, in a number of situations confining effects occur, resulting in compressive membrane action (CMA). This mechanism is explained in Fig. 11. As a result of the development of cracks at midfield and at the edges, a mechanism occurs, in which the slab tries to expand in lateral direction. Since this lateral extension is restrained, a compressive arch forms, which is able to generate significant in-plane forces. The increase of the bearing capacity depends on the degree of restraint. The Canadian and New Zealand's

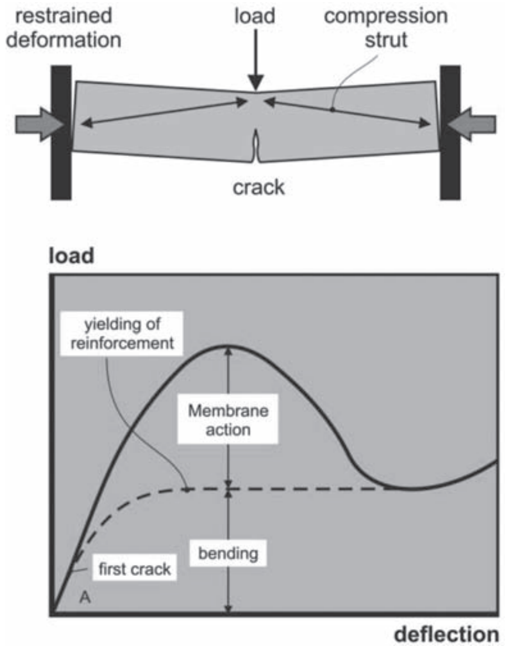

Figure 11. Compressive membrane action in a bridge deck (top) and corresponding increase of bending capacity (below).

Building Recommendations allow the consideration of this effect in design. Although in these recommendations conservative values are given for the effect of compressive membrane action, considerable savings of reinforcement are possible. By considering compressive membrane action a reinforcement ratio of only about 0.5% is due, whereas without consideration of compressive membrane action about 1.7% is required.

The fact that up to now for the design of bridges in most countries compressive membrane action was not regarded, means that there is still a considerable residual capacity with regard to bending and shear. Tests were carried out by Tailor (2007) on a bridge in Northern Ireland. The bridge deck consisted of a solid plate with a cross-sectional depth of 160 mm supported by prestressed beams at a centre to centre distance of 1500 mm. The reinforcement in the deck was applied in the middle of the deck plate. In the experiments loads were reached of 3–5 times the theoretical values, calculated without compressive membrane action. In none of the twelve tests the failure load could be reached: the tests had to be stopped because the limit capacity of the testing equipment was reached.

In The Netherlands 69 bridges are in function with a cross section as shown in Fig. 12. The prestressed deck is more slender than other cases

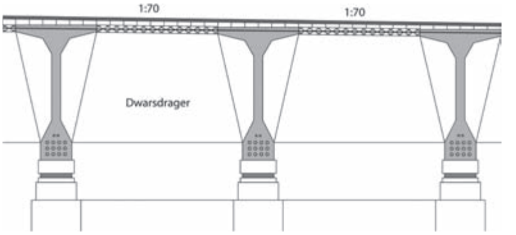

Figure 12. Cross section representative for about 70 bridges in The Netherlands, to be tested for compressive membrane action.

known from literature, in which compressive membrane action was demonstrated, so that it is not sure that the CMA rules can be extrapolated to this case. Therefore tests on compressive membrane action for this type of bridge decks are planned to be carried out in autumn 2012 at TU Delft.

4.6 *Tailor made nonlinear finite element programs*

In order to find out whether a bridge has a sufficient bearing capacity very often nonlinear finite element calculations are used. From experiences with NLFEM calculations it is known that, up to now, this method has been particularly useful for the analysis of test results, known already before.

The reliability of results of predictions, if no calibration has been carried out, depends considerably on the choices made by the analyst. A possibility to enhance the reliability of NLFEM calculations is to carry out calibrations on previous tests on similar types of elements. In the Netherlands calibrations of different NLFEM calculations have been carried out on a collection of prestressed T- and I-shaped bridge beams. By calibration of the test results obtained on the beams from this collection the NLFEM program can be tailored to produce reliable predictions for the behaviour of similar types of bridge beams. Guidelines for such applications have been produced.

4.7 *Proof loading of bridges*

In the previous sections a number of mechanisms have been treated which may contribute to the residual bearing capacity of bridges. In such a way the residual capacity is quantified on the basis of theoretical considerations. Another way of quantifying the residual capacity is to carry out proofloading on the structure. In such a case the challenge is to demonstrate, on the one hand, that the structural safety is (at least) enough to carry the load for a further number of years, but meanwhile to guarantee that no irreversible damage due to proofloading occurs.

The load may only be applied on the structure after an accurate judgment of the conditions of the bridge, during which the dimensions are determined, including the thickness of the topping, the concrete strength is assessed and eventual deficiencies are registrated and evaluated. The effect of the load (deflection, rotation, crack widths, strains in concrete and steel, acoustic emission) are measured. At the beginning of proofloading the permanent load is already present. During the test an additional load F_{aim} is applied on the structure. This load F_{aim} exists of the design value of an eventual additional permanent load, and the design traffic load. An important criterion at proof loading is the limit value of the load F_{lim}. This value is the limit of the load where unwanted damage of the structure is theoretically expected to occur. This value should not be exceeded. Basically there are two possibilities. The first is that F_{aim} is reached before F_{lim}. In this case it has been demonstrated that the structure is suitable to carry the design traffic load. The second is that F_{lim} is reached before the load F_{aim} has been fully applied on the structure. In this case the proofloading procedure should be stopped. Fig. 13 shows a special loading truck, developed for proofloading of short span bridges. This car, named Belfa (German abbreviation for "Belastung Fahrzeug" = loading truck), can lift itself at defined points, so that a critical loading configuration is obtained. The figure shows the application of the proof load on a bridge in Medemblik, The Netherlands.

4.7 *Are reduced safety values for existing bridges acceptable?*

An important practical consideration is to allow a difference in reliability index for new and existing structures. For bridges in national roads in the Netherlands a reliability index of $\beta = 4.3$ is required for new structures to be built (failure probability of $7.9 \cdot 10^{-6}$), whereas for bridges to be repaired a reliability index of $\beta = 3.8$ (failure probability of $7.2 \cdot 10^{-5}$) is allowed. This should go along with a more refined calculation and a realistic estimation of scatter. An important consideration for this decision is that, if for existing bridges as well a β-value of 4.3 would be required, many bridges should be repaired, which would not only result in considerable costs, but as well in traffic congestions and accidents, which might, most probably, result in a larger loss of human lifes than would have been saved by bringing the structure to a theoretically higher level of reliability.

Figure 13. Proof loading of short span bridge with special loading truck Belfa, Medemblik, The Netherlands, 2009.

5 CONCLUSIONS

1. In future building codes service life design will be the leading design principle. It will require specified levels of structural safety and serviceability for a defined period of time.
2. It is worthwhile to apply service life principles to existing structures.
3. Service life principles can be applied not only to single structures, but as well to stocks of structures representing essential parts of the infrastructure. This gives insight in necessary future investments in repair and upgrading.
4. The bearing capacity of structures is often essentially larger than would follow from an analysis on the basis of existing design rules for new structures. Quantifying this may lead to reliable prolongation of service life and considerable cost savings.
5. It makes sense to use a lower level of reliability for existing structures than for new structures.

REFERENCES

Fib Model Code for Concrete Structures 2010, Vol. 1 and 2, *fib-Bulletins 65 and 66, 2012.*

Gaal, G.C.M., "Prediction of deterioration of concrete Bridges", *PhD thesis, TU Delft, June 2004.*

Li, Y., "Effect of spatial variability on maintenance and repair decisions for concrete structures", *PhD-thesis, TU Delft, 2004.*

Sitter, W.R. de, "Costs for Service Life Optimization: the Law of Fives", Durability of Concrete Structures", *Workshop Report, Ed. Steen Rostam, 18–20 May, 1984, Copenhagen, Denmark, pp. 131–134.*

Tailor, S.E., Rankin, B., Cleland & D.J., Kirkpatrick, J., "Serviceability of Bridge Deck Slabs with Arching Action", ACI Struct. Journal, Jan-Feb 2007, pp. 39–48.

Concrete Repair, Rehabilitation and Retrofitting III – Alexander et al. (eds)
© 2012 Taylor & Francis Group, London, ISBN 978-0-415-89952-9

The transformation of the existing building stock: A precondition for a sustainable future

Peter Richner
Department of Civil and Mechanical Engineering, Empa, Dübendorf, Switzerland

ABSTRACT: The role of the built environment for a sustainable development is of paramount importance in all countries. In a highly developed country such as Switzerland, the main challenges are posed by the renewal of the existing infrastructure and the building stock. The latter is a key factor for both energy consumption and greenhouse gas emissions. An integrated approach incorporating new materials, systems engineering and urban physics can lead to new and innovative solutions for the built environment. Thanks to these new developments it will be possible to operate the building stock purely on renewable energies, which will lead to a dramatic reduction in greenhouse gas emissions. Furthermore, the buildings will be more comfortable and more cost efficient.

The built environment plays a key role when it comes to sustainability: It is one of the major economic sectors in every country throughout the world. The ecological importance is given by the consumption of energy related to the construction, operation, maintenance and demolition of buildings and infrastructure and accounts for approximately 50% of the global energy consumption. A similar share of the emissions of greenhouse gases is associated to this number. Furthermore, the quality of life is closely related to the quality of the built environment composed of buildings and infrastructures. Finally, the built environment is an important part of our cultural heritage.

The challenges that have to be met in order to create a truly sustainable built environment are very different in developing countries compared to highly industrialized countries. With the former, it is mostly about creating affordable housing for a growing population at large scales and the buildup of an efficient infrastructure needed for economic growth. The industrialized world is facing a huge building stock and infrastructure that has reached an age where major investments are needed in order to maintain it and to adapt it to the needs of the future.

Thanks to the successful introduction of the building standard "Minergie" which is asking for very low or even zero energy consumption new buildings have an almost insignificant impact on the overall energy consumption of Switzerland. However, heating and cooling of buildings are still responsible for 47% of the end use energy in Switzerland. This is due to the high specific energy demand of buildings built before the introduction of more restrictive energy standards. Most of this energy is based on fossil fuels and therefore contributes heavily to the overall CO_2 emissions of Switzerland. Obviously, Switzerland can only significantly reduce the overall energy consumption and the emission of greenhouse gases if the energy performance of the approximately 1.5 Mio existing buildings is dramatically reduced. This article focuses on how the building stock can be transformed by new developments on different scales: Materials, systems, buildings, neighborhoods and cities.

The high energy consumption of existing buildings is mainly caused by the poor thermal insulation of the building envelope which can be improved by the addition of an additional layer of insulating material such as polymer foams. However, in many cases it is impossible to add this layer of 20 cm or more onto an existing façade, especially not for buildings which are part of the cultural heritage. Since many of these historically valuable buildings have mineral renderings, a rendering system with a very low thermal conductivity of approximately 0.025 W/m*K was developed. This high performance rendering is based on aerogels, a highly porous material (porosity of 80%–99.8%) which is produced by a sol-gel process. Thanks to an optimized combination between the type of aerogel and the binder material it was possible to produce such a rendering system which still can be applied by standard techniques. Presently, the first large scale projects with this material are realized in the field.

A precondition for the wide use of PV systems in buildings is the cost and the integration into the building envelope. Dye-sensitized solar cells (DSCs) are a potentially low-cost alternative to solid state solar cells. On top of that they might exhibit interesting aesthetic features such as transparency and flexibility. Unsymmetrical squaraine dyes proved to be highly efficient in that respect. The squaraines synthesized at Empa are capable of absorbing light in the domain of 500–1000 nm. Theoretically, they are able to absorb up to 53% of the solar radiation. Squaraines allow the production of metal-free cells which will have an inherent cost advantage over ruthenium based systems. From an architectural point of view, it is very interesting to note that DSCs can be at least semi-transparent and that the color can be adjusted to some degree.

Most of the heat demand of reasonably well insulated buildings could be covered by excess heat collected during summer if an efficient and cost-effective method for the storage of low temperature heat could be found. Two different strategies in that area are currently pursued at Empa. The first system is based on aqueous sodium hydroxide that is used in a closed sorption process: The reservoir is charged during summer by evaporating water from the sodium hydroxide solution by solar heat. For heat output, water vapor is absorbed by the caustic solution and the enthalpy of the absorption process is released. The proposed closed sorption storage system has a system-volume-related heat capacity that is 5 times higher compared to conventional water storage if it is used for space heating (output temperature 40°C) and 2.5 times higher if domestic water (65–70°C) has to be delivered. Only recently, Empa started to investigate an alternative system that makes use of the dehydration of ettringite (calcium aluminate trisulfate hydrate) at temperatures between 50–150°C. So-called “metaettringite” with only 10–13 water molecules per formula unit is formed. Subsequent addition of water leads to the rehydration and ettringite is formed again. This process is fully reversible and is associated with an enthalpy change of approximately 600 kJ/kg. The combination of this high energy density and the low operation temperature makes ettringite an interesting candidate for seasonal heat storage.

As mentioned earlier, the biggest challenge is represented by the large existing building stock which is characterized by an extraordinary high energy consumption. A concept for the retrofitting of multistory residential buildings was developed which is based on three pillars: standardization, prefabrication and system integration.

In a first step, a typology for multistory residential buildings erected in Switzerland between 1919 and 1990 was developed which led to a classification with 10 different categories. Different renovation strategies were developed for all categories. The result of this work is a simple tool called *Retrofit Advisor* that can be used by the owner of a building to compare different options including the complete demolition and reconstruction. Modules were developed which include new windows, insulation of the façade, piping for the ventilation of the room and conduits for new electrical outlets. The modules are prefabricated according to the new drawings, based on accurate digital plans of the building which have been acquired by laser scanning earlier. They are transported to the site and quickly mounted without readjustment because any irregularities of the façade would have been taken care of before their arrival.

The importance of the urban scale for a truly sustainable built environment becomes more and more obvious. Many challenges can only be met in a successful manner at this scale, especially in the view of the ongoing global urbanization. The investigation of wind fields in urban areas is on field of research. The pedestrian wind is strongly influenced by high-rise buildings. They can deviate wind in a manner that strong standing vortexes can be generated in front of the building and even higher wind speed can occur around the corners. On the other hand, it is important to guide the wind through street canyons in such a way that pollutants generated by traffic are efficiently swept out. This can also have a cooling effect and mitigate the urban heat island effect to some degree. As the relative fraction of people living in urban areas continues to grow, the same holds true for the overall energy consumption. Therefore, it is important to find ways to optimize the energy consumption on an urban scale by connecting buidlings and neighborhoods in order to exchange, transform and store different forms of energy on a local scale.

A sustainable built environment has to fulfill the requirements of sustainability in all three dimensions: economics, ecology and social values. Huge challenges have to be met before the built environment in Switzerland has reached this state. Based on developments in materials science, systems engineering and multiscale modeling new solutions can be created for the transformation of the existing building stock. The main goals of this development are buildings and neighborhoods which offer a high level of comfort at affordable prices with a minimal environmental impact. The technologies developed in that respect can partially be adapted in other regions of the world according to the local circumstances. It seems to be possible to reach a point where buildings can be operated purely on renewable energy, especially if their energy systems are interconnected without compromising on the level of comfort. However, the transformation is a matter of decades which means that long term planning and a stringent implementation of the strategy are crucial for reaching the ambitious goals.

Concrete Repair, Rehabilitation and Retrofitting III – Alexander et al. (eds)
© 2012 Taylor & Francis Group, London, ISBN 978-0-415-89952-9

The concrete repair industry, actions for improvements

Peter H. Emmons
Baltimore, MD, USA

ABSTRACT: Concrete repair industry has been around for many years to support the world's concrete infrastructure. Until recently, the repair industry has been an informal necessity of concrete structure owners. In the last 30 years, the repair industry has exploded in size and has become a multibillion dollar entity. Material systems, tools and equipment, engineering and contracting have become focused on the repair industry. However, failure rates of repairs remain unacceptably high. Therefore, repair industry has engaged itself to make necessary improvements. In this presentation repair industry action plans will be discussed including the draft of ACI Repair Code first edition content, latest repair (material) system improvements, and the latest research to answer the most difficult questions of repair system performance.

1 INTRODUCTION

The concrete repair, protection, and strengthening industry is driven by deterioration, damage, and defects that commonly occur to concrete structures. Considering that over 500 million yd^3 of concrete are placed every year in the U.S. and that the material is custom made for almost every job using many local materials; that designs are not standard and that construction processes are pressed for time; it is no wonder there are so many repairs.

The annual cost to owners for repair, protection, and strengthening is estimated between $15 and $22 billion in the U.S. alone. The result is a business supported by lawyers, engineers, architects, equipment suppliers, material manufacturers, researchers, educators, testing companies, and contractors. The recent explosive growth of the industry in the past 25 years has resulted in the need for many improvements in materials, design practices, installation procedures, contracting processes, QA/QC procedures, teaching and more. These improvements are necessary to extend service life, reduce costs, and reduce conflicts.

2 VISION 2020

In 2004, a plan was conceived to provide the industry with a roadmap for improvement. Thirteen (13) most important goals were established in the plan with specific strategies and tactics to help the industry evolve faster.

The Vision 2020 goals include:

1. *By the year 2010, the industry will have established mechanisms for industry cooperation to facilitate better faster worldwide creation of concrete repair and protection technology and dissemination of information about the technology.*
2. *Develop and implement means of accelerating the process of document creation and dissemination within industry associations.*
3. *Create a repair/rehabilitation code to establish evaluation, design, materials, field and inspection practices that raise the level of performance of repair and protection systems, establish clear responsibilities and authorities for all participants, and provide the local building officials a means of issuing permits. (By 2012.)*
4. *Develop performance-based guide specifications for specific and generic repair designs to improve specifications. (By 2010 and ongoing.)*
5. *Improve repair material design and performance to eliminate cracking, to carry structural loads, and to have set and cure properties established by the construction process.*
6. *Develop environmentally and worker friendly repair methods, equipment, and materials that will greatly reduce the adverse effects on workers, the public and the earth's ecosystem.*
7. *Develop a means for predicting repair system performance to help ensure the use of proper materials, design details and installation methods based upon predictive models validated by experience.*
8. *Develop and implement strategic research plan for the repair industry.*
9. *Increase the number of material-, engineering-, and construction-related professionals interested in and skilled in repair and protection practice to support the growing need for evaluation, design, new materials, and construction professionals.*
10. *Develop selection processes, contractual agreements, procurement methods and relationship*

arrangements (partnering) that will greatly reduce conflicts, rework, claims, and lawsuits resulting from disagreements among contractors, general contractors, engineers and owners.

11. *Develop facility owner education that will promote awareness of the effects of deterioration and the means to reduce the risks while protecting their investments.*
12. *Develop improved means and methods for accurate and thorough condition assessment.*
13. *Develop specific repair system needs for expanded use, efficiency, and failure reduction.*

Industry leadership teams have used the Vision 2020 documents (Goals and Roadmaps) to guide activities by prioritizing efforts and resources to the established goals and action plans.

Goal 3 To bring repair code into practice, a time table was established that requires the committee work to be completed in 2012, so the new standard could be adopted into the International Building Code and in use by 2015 by local building officials. Committee 562 is on schedule to meet this deadline.

3 PREFACE (DRAFT ONLY)

The purpose of this code is to provide minimum material and design requirements for the evaluation, repair and rehabilitation of structural concrete members to comply with the general existing building code.

Contents

Chapter 1—General Requirements
Chapter 2—Notation and definitions
Chapter 3—Referenced Standards and Reports
Chapter 4—Basis for Compliance
Chapter 5—Loads, load combinations, and strength-reduction factors
Chapter 6—Evaluation and analysis
Chapter 7—Design of structural repairs
Chapter 8—Durability
Chapter 9—Construction
Chapter 10—Quality assurance
Chapter 11—Commentary references

4 SUMMARY

We have entered a new phase on our way to efficient and effective industry development, a place where we know what we want and how to get there.

The Repair Code is a single most important effort defining our point on the industry's path to professionalization. I am optimistic that number of failures and disappointed owners will considerably decrease as our actions unfold.

Concrete Repair, Rehabilitation and Retrofitting III – Alexander et al. (eds)
© 2012 Taylor & Francis Group, London, ISBN 978-0-415-89952-9

Where does rehabilitation fit into the South African dam safety picture?

C. Oosthuizen
Department of Water Affairs, Pretoria, South Africa

ABSTRACT: An overview is given of the developments with regard to risk-based dam safety assessment of dams in the Department of Water Affairs (DWA). Dam safety related terminology is defined to avoid confusion. The ranking and risk-based methodologies used in DWA for dam safety assessments are briefly discussed. With the risk-based methodology the various impacts (i.e. population at risk, social, socio-economic, financial and environmental) as well as the relative risk levels are being quantified, qualified and assessed. These assessments are not only being used for the evaluation of the relative risk at existing dams but also to determine the cost-effectiveness of proposed rehabilitation works. Risk-based dam safety analyses therefore do play a major role in the prioritisation of remedial works.

1 INTRODUCTION

The Department of Water Affairs (DWA) owns 314 dams of which 218 are listed in the ICOLD World Register of Dams. A large number of these dams do not comply with current design criteria. The risk-based dam safety management of DWA dams was formally approved in 1987 by DWA's management.

A brief outline of the present methodology used in DWA (the dam owner) is presented in the full paper. The reults of these analyses are summarised in a series of graphs depicting the various hazards and finally the risk level. An example of these graphs is presented in figure 1 below. Note that the various impacts as well as the risk level are not points on the graphs but areas indicating the confidence levels of the results.

Rehabilitation work is in most cases expensive. One of the tasks for the dam safety engineers is to optimise the rehabilitation budget on a risk-reduction basis. Therefore, rehabilitation merely to comply with present design criteria does not make sense. The hazard and risk reduction of each alternative has to be evaluated.

The question of how unbiased dam safety assessments are was initially the topic of the keynote paper. The author realised that he would step on too many toes and decided to limit the subject to a paragraph or two.

2 CONCLUDING REMARKS

2.1 *Lessons learned*

After more than 25 years of official use, the DWA methodology has proven its value as robust assessment and decision-making tool. Rehabilitation related decisions could be optimised and based on information. Several decisions not to do any rehabilitation have therefore been taken, motivated on risk grounds.

The deterministic approach on the other hand leaves little discretion to the decision maker. The structure is either compliant or not complian, or in short leaving the owner/decision-maker with an instruction either to rehabilitate or not.

2.2 *Limitations*

Neither deterministic nor risk based assessments are exact assessments. Both methods depend on consistent sound engineering judgement. The outcome of both can be biased by the preferences of the engineer(s) performing these analyses and peer review is therefore essential. Limitations of assessments must therefore be disclosed. Compared to determinstic assessments, risk based assessments offer the bigger picture to decision maker.

2.3 *Road ahead*

The methodology focusses on the safety of dams and their immediate surroundings. The need has now arisen to expand it much wider in order to address the whole system. The life cycle, from the decreasing yield of the dam through the conveyances right down to the end user has to be addressed.

Several studies to expand the methodology and to evaluate the validity of the various hazard and risk level graphs are being planned.

> Do not put your faith in what statistics say until you have carefully considered what they do not say
> —William W Watt

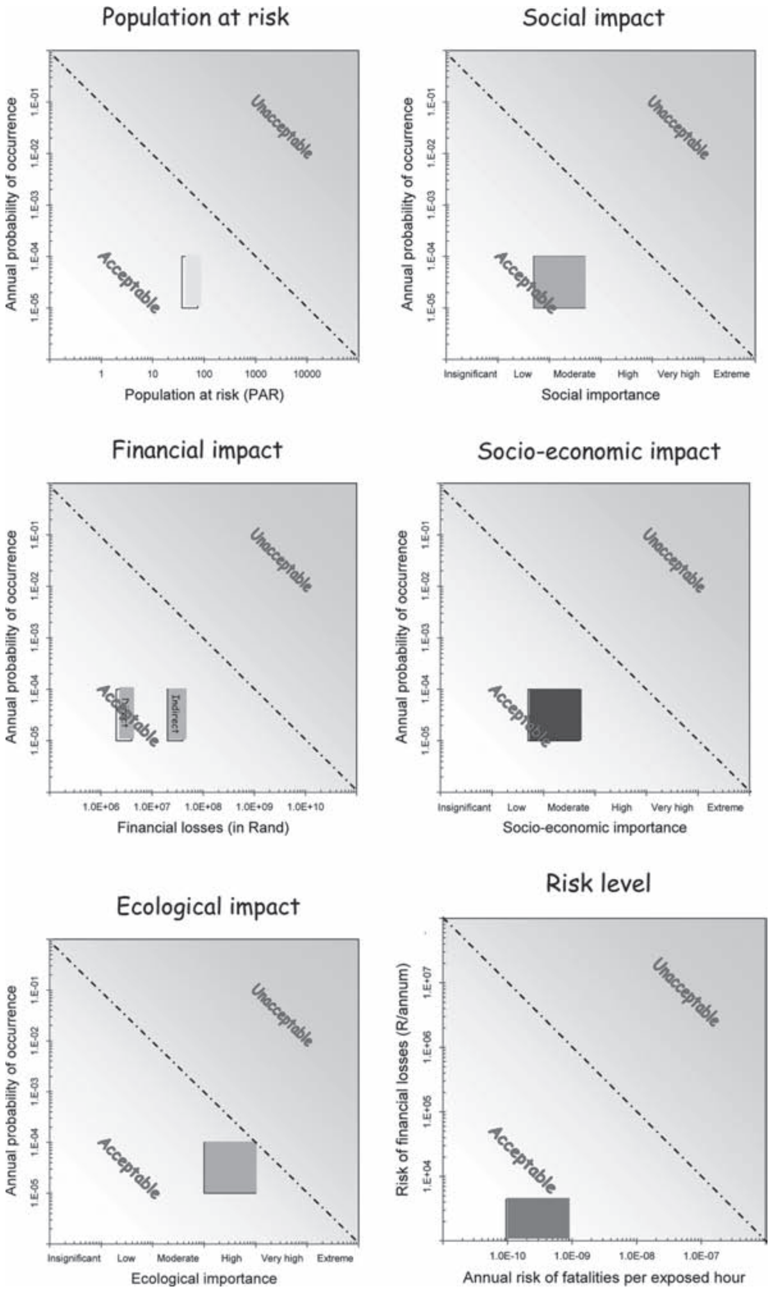

Figure 1. Example of the impact and risk level graphs used to represent results and to provide an indication of the relative acceptability of the values. The size of these blocks gives an indication of the relative level of confidence of the values.

Concrete Repair, Rehabilitation and Retrofitting III – Alexander et al. (eds)
© 2012 Taylor & Francis Group, London, ISBN 978-0-415-89952-9

A life in non-destructive testing!

Michael G. Grantham
Concrete Solutions and Sandberg LLP, UK

ABSTRACT: This paper reviews the career history of Professor Michael Grantham, from humble beginnings as a laboratory technician to his present status as a well known author in the NDT and concrete repair field. It begins with an introduction into the state of the art of NDT in the late 1970's and early 1980's and charts his experiences in construction materials testing, bridge inspections, and later work on other structures . The state of knowledge over that time has changed enormously, with contemporary durability standards simply not being sufficient to provide durable structures against the action of de-icing salt and marine salt especially. Pitting corrosion in bridge substructures had not been identified and it was work under contract to the then Department of Transport that revealed this phenomenon. At the same time, the industry went through a phase of different problems: High Alumina Cement (HAC), Alkali Silica Reaction (ASR), Delayed Ettringite Formation (DEF), all of which required some considerable testing and research. A number of case studies illustrating the wide range of problems encountered are given.

1 INTRODUCTION

This paper deals with the career of Professor Mike Grantham, from humble beginnings as a laboratory technician dealing with plastics and polymers through to his baptism into cementitious materials with Harry Stanger Ltd. in the 1970's and from then to STATS and to the formation of his own company with several partners. In 1992, he became self employed and set up his own consultancy, before his current appointment as a Consultant to Sandberg LLP. During those years there were many changes and challenges in the construction industry, with rapid development of non-destructive testing equipment to the present smaller, faster and better hand held devices for covermeter, half-cell potential, resistivity, ground probing radar and so on.

His career of more than 40 years is illustrated with case studies which show some of the range of work that a forensic engineer has to deal with during both routine and non-routine assessments of structures.

The paper discusses the problems encountered by the industry in understanding chloride induced corrosion in reinforced concrete, which was not fully appreciated in the early 1980's either by most Engineers, or by British Standards, which gave very poor advice on designing for durability in environments such as de-icing salt and marine salt.

Prof Grantham's contributions to publications and to organising the Concrete Solutions series of international conferences on repair—a companion to the ICCRRR series—are also covered.

2 ROUNDTHWAITE BRIDGE IN CUMBRIA

STATS, who I joined in 1980, won a contract to carry out the very first motorway bridge investigation in the UK. This contract was a dual one: its purpose was to both investigate the structure and also a whole range of different testing techniques, to establish which were best for dealing with surveys of bridge structures. This included testing such as half-cell potential, resistivity and gamma ray backscatter in addition to the more obvious choices of covermeter, carbonation testing and so forth. The half cell test proved most useful, despite commercial equipment for half cell potential not being available in the UK in 1980. The structure itself, Roundthwaite Bridge, was in a dire condition, with considerable problems with reinforcement corrosion, and 0.5 m stalactites hanging from the underside. Examination of the carriageway surfacing to investigate depressions in the deck under the asphalt revealed that the concrete was so badly deteriorated in places that you could claw the concrete away with your fingers and expose the top reinforcement!—the effect of leaching of the concrete and freeze-thaw problems.

It was during my three years with STATS that the damage caused by chloride ingress on structures became apparent. Engineers at that time believed that chloride ingress only occurred with bad concrete, yet our surveys were revealing massive chloride ingress in quite good concrete. Guidance given in CP110 (BSI 1972) was very poor

Figure 1. Picturesque Roundthwaite Bridge in Cumbria.

requiring only 40 mm cover for a C30 concrete. This did not improve in BS8110 (BSI 1985), which followed in 1985.

Bamforth published an excellent paper in *Concrete* which examined chloride ingress in detail and confirmed the poor durability to be expected from BS8110 as then published (Table 1).

Table 1. Predicted time to corrosion activation of the reinforcement due to chloride ingress.

Structure	Min. cover (mm)	Effective diffusion coefft. m^2/s	Time to activation (years) $C_t = 0.4\%$	$C_t = 1.0\%$
Old pc concrete	38	4.0×10^{-13}	23.7	53.8
Modern pc concrete BS8110 -General	50	3.0×10^{-12}	5.5	12.4
BS5400 Bridges	65	3.0×10^{-12}	9.2	20.9
BS6349 Maritime	75	3.0×10^{-12}	12.3	27.9

More recently, the advent of EN206 and BS8500 has given much more thought to durability, especially exposure to chlorides. Design lives of 50 or 100 years to depassivation have been calculated, although we won't know whether we will have achieved these in practice for some while yet.

My experience at STATS also included a large survey of the M6 Gravelly Hill Interchange, known as "Spaghetti Junction". This identified pitting corrosion in bridge substructures for the first time—a problem hitherto thought to only be a problem in bridge decks. Half cell potential testing proved effective in locating the corroding anodic areas, which were often associated with stressed areas on the bends in the link reinforcement around the main bars—although occasionally affecting the main bars too.

Figure 2. Aerial view of Spaghetti Junction.

Figure 3. Pitting corrosion caused by chloride attacking the link reinforcement and main bars in a structure.

3 ASR IN CONCRETE AND OTHER PROBLEMS

During the late 1970s and early 1980s, a new phenomenon was beginning to be a concern—Alkali Silica Reaction. Although this had been identified in Europe in 1967, the first case in the UK, on the Val De La Mare Dam in Jersey, was not identified till 1971. Problems began to occur on the mainland as the 1970s progressed, firstly in the South West of England and later in the Midlands and Scotland. It was not for a number of years that the mechanism and significance of the problem was fully understood. The importance of petrography as an analytical tool in assessing structures became apparent and I was fortunate to have a friend at the UK's BRE, Kelvin Pettifer, who was their leading petrographer. That association proved enormously helpful and I learned a great deal about petrography from it.

Early on in my self-employed career I wrote an article for Construction Repair journal on problems the industry was encountering with accuracy of chloride analyses. Together with a contractor, we undertook a covert round-robin trial of laboratories, including both NAMAS (now UKAS) accredited and non-accredited labs, and a range of different fees for the testing. A number of samples of known chloride content, finely ground and carefully sub-sampled to provide a series of accurate control samples, were disguised as dust samples from a fictitious car park and sent to the different labs by the contractor. The results were very illuminating, as only 5 out of 12 labs produced results within plus or minus 10 percent of the correct values. The other seven were variously wrong by larger amounts, with some serious errors. This taught me that if such trials are to be conducted, the laboratory should not know they are being tested. In most such trials, the labs are fully aware of the trial. This inevitably means the results receive extra care and scrutiny and may not reflect the normal practice of the labs!

The UK Concrete Society is currently performing an update of their technical report on the analysis of hardened concrete, which will include an inter-laboratory trial of both cement content and chloride content measurements. In this case, all labs know they taking part in a trial, but it will be interesting to see the findings, which will be available this year.

I remained with MG Associates until recently, when I returned to being self employed and joined Sandberg LLP as a Consultant.

Probably the best way to illustrate my involvement in NDT is via a series of case studies over these years, detailed in the full paper.

4 CASE STUDIES

4.1 *Post tensioned bridges*

The paper deals with a number of investigations in this area as the industry became concerned about the safety of post tensioned structures.

4.2 *Kingsferry lifting bridge, Isle of Sheppey, Kent*

The paper deals with the investigation of a large lifting bridge which carried both road and rail across the River Iwade to the Isle of Sheppey in Kent. This was a fascinating project as the bridge was heavily contaminated with chloride salts but also unintentionally partially protected by a cathodically protected gas pipeline. Details are given in the paper.

4.3 *Failure of lightweight clinker concrete blocks in Northern Ireland*

This relates to very severe problems encountered by a company manufacturing lightweight concrete blocks from ash which contained hard burned quicklime nodules, resulting from the inclusion of limestone in the coal from which the ash was produced. This caused massive expansion of the blocks and several estates of houses and an army barracks had to be rebuilt.

4.4 *Problems with car parks*

This section of the full paper deals with the problems encountered with car parks due to de-icing salt ingress and focuses on one particular case study where chlorides had been cast into the concrete due to a poorly washed marine aggregate.

4.5 *Diesel oil used as a mould release agent!*

This section examines the detective work necessary to find the cause of ugly red staining to a new structure in the course of construction.

4.6 *Wimbledon—centre court*

The investigation of corrosion problems at the famous home of international tennis is described.

4.7 *Delayed ettringite formation in foundation blocks in devon*

This describes a most unusual problem involving massive cracking to foundation blocks exposed to seawater in a very important structure, due to delayed ettringite formation.

5 CONCLUSIONS

This section in the full paper summarises some of the developments in testing methods and the changes in repair techniques over the years.

REFERENCES

See full paper for details.

Concrete Repair, Rehabilitation and Retrofitting III – Alexander et al. (eds)
© 2012 Taylor & Francis Group, London, ISBN 978-0-415-89952-9

Non-destructive testing and continuous monitoring: Modern tools for performance assessment and life time prognosis of structures

C.U. Grosse
Non-destructive Testing, Center for Building Materials,
Technische Universität München, Munich, Germany

ABSTRACT: The sustainability of structures in civil engineering is becoming a more and more important issue. Related to this are problems to assess the structural condition, to measure the performance and to determine the residual lifetime of structures or structural components. Techniques concerning Nondestructive Testing (NDT) and Structural Health Monitoring (SHM) can be valuable to support the engineer during the construction of a new buildings or the maintenance of existing infrastructure and to help making them more sustainable. This requires a comprehensive concept to implement these techniques in existing construction and maintenance plans.

1 INTRODUCTION

Following the recent developments in civil engineering there is a clear trend to involve more and more innovative materials, new construction concepts and optimized maintenance procedures. The question is how non-destructive and monitoring techniques can support these new developments. A combined approach is necessary consisting of monitoring and inspection techniques to improve the sustainability of large structures in civil engineering. The main purpose of monitoring civil structures is to support regular visual examinations or inspections based on non-destructive testing techniques. There are different stages in the lifetime of a structure where NDT and SHM techniques can be helpful.

The paper describe some of these techniques giving examples of application from the background of the author. It is not the intention of this paper to give a comprehensive overview. However, it will demonstrate that NDT and SHM techniques can help at each stage of an individual structure to improve the quality and maintenance. The final section addresses the combination of these techniques in terms of "lifetime NDT supervision".

2 QUALITY CONTROL DURING CONSTRUCTION

The methods currently employed by the construction industry for quality assurance of fresh concrete have already been practiced for many years. They are widely established, although their evidence is quite limited. The main disadvantage of most of the established methods is that they provide only a snapshot of the materials properties and that they cannot be used for investigations of the continuous setting process. Reliable statements, e.g. on the mode of action of the admixtures for concrete can, as a rule, not be obtained with these methods. There are several NDT methods that have the potential to be used for quality control of concrete during setting. Ultrasonic methods are probably the most advanced methods to evaluate fresh cementitious materials.

Using ultrasound techniques the properties of standard concrete and mortar mixtures can be measured—non-destructively, reproducible and largely objective. Of primary interest for quality control of fresh concrete or mortar is that the material parameters critically influencing the quality (e.g. the compressive strength) and workability (e.g. water-cement ratio, air-void contents), consistence, final strength, the effect of admixtures and many more, have a significant effect on the ultrasonic signal parameters, such as wave velocity, amplitude and frequency content. In particular the setting process of fresh concrete and fresh mortar can be investigated in detail. Accordingly, these methods are directly connected with the elastic properties of the materials, rather than with the chemical properties (as with the hydration or maturity measurement methods). Improvements of the technique enable for reliable measurements of elastic moduli on the basis of evaluations of compressional and shear velocities.

Sonic methods for fresh concrete are today so advanced that a recommendation was released by RILEM that could work as a pre-standard.

Although the use of this technology is initially more costly the extra expense is compensated for by the more objective function mode, the improved reproducibility of the measured values and, last but not least, by a noticeable optimization of construction work flow. Areas of application for this method, where these advantages can be exploited are e.g. materials technology (development of new and more efficient concrete admixtures in-situ quality control (sampling no longer necessary), slipform construction (optimization of stability) or precast concrete construction (optimization of work progress).

3 INSPECTION OF STRUCTURES

A major application of non-destructive evaluation methods is the assessment of structures or structural components to reveal defects or deteriorations or to determine the actual condition. NDT methods can support visual or minimal invasive inspections and there is a clear need of accurate, comprehensive and cost-efficient techniques that are robust enough being used in harsh environments. Non-destructive methods are first choice, if the structures prohibit invasive techniques like objects of the cultural heritage. The more traditional methods like the Schmidt hammer are more and more complemented by advanced methods like ultrasound and impact-echo, RADAR and microwave techniques, infrared-thermography, potential field, inductive and capacitive techniques but not to an extend as it would be desired. Technical and commercial boundary conditions that are special for civil engineering structures and the construction industry impeded a broader application of NDT methods in the past.

Devices based on microwave techniques and infrared-thermography usually do not need to be coupled to the surface of a structure under test. This is different from ultrasonic techniques. Using this important method to assess the condition of a large structure had in the past the drawback that the sensors needed to be coupled to the structure by any type of adhesive by hand. There were several developments addressing this issue. Besides investigations to avoid coupling by using air-coupled transducers this is namely the development of dry-contact transducers. This enables for measurements at materials with rough surfaces as they are common in civil engineering. Antenna arrays are available as shear or compressional wave arrays for reflection as well as for through-transmission measurements.

Very close related to efforts overcoming the coupling problem are automatization techniques. Several methods like RADAR, microwaves and thermography do not require a lot of work to conduct measurements on a large scale. Modern microwave devices are rapidly mapping the moisture content of a concrete structure. New developments in RADAR resulted in fully wireless devices.

Infrared-Thermography instead is camera driven and can give images in-situ. Usually the task is to do passively a scanning of the near-surface of structures to detect increased heat flow. Relatively new are active applications, where the heat flow is enforced by an external energy source to produce a thermal contrast between the feature of interest (e. g. defect, moisture) and the background.

Besides of the described techniques also ultrasonic and impact-echo applications need to be automatized investigating large structures. Developments of the Bundesanstalt für Materialforschung und -prüfung in Berlin together with the Fraunhoferinstitut IZFP in Saarbrücken are possibly offering solutions.

Civil Engineering structures are complex in terms of material composition, heterogeneity and geometry. A single NDT method is very often insufficient to detect or even localize deteriorations. To enhance the reliability and the evidence a combination of two or more NDT techniques is required. One solution is the visual comparison of data obtained by different NDT techniques but a more advanced method is the combination of results in terms of data fusion.

To learn more about the influence of boundary conditions it becomes more and more important to simulate the wave propagation effects in particular in heterogeneous media and structures with complex geometry what is common in civil engineering. This can help to determine the limitations of an individual technique no matter if it is based on elastic or electro-magnetic wave propagation. Algorithms are nowadays available for a high-resolution 3D simulation of wave propagation in numerous media; some uses the Elastodynamic Finite Integration Technique. However, tools to model in-situ the propagation of waves and to determine for example best sensor positions are still missing.

The characterization of the sensor's effects is known as sensor calibration. Most of the NDT techniques dealing with elastic waves are mostly based on piezo-electric sensors. The information about the frequency transfer functions of transducers commercially available is very often insufficient. This is in particular true regarding values of the true displacement or true velocity. Several scientists work on a solution for this problem.

4 STRUCTURAL HEALTH MONITORING

Inspection is defined as a singular measurement at a certain occasion related to an assessment of a structural component with the aim to reveal a hidden defect for example. However, some constructions need more attention since their health status is vital for public safety. Besides this, the source for deteriorations or deformations is sometimes difficult to be determined by a singular measurement only. In many cases it is necessary to just detect a deviation of the "usual" behavior of the structure, i.e. an outlier in a time-series. Surveillance techniques can be applied that are usually addressed as *structural health monitoring*. Several NDE techniques are used in this context like vibration analysis, acoustic emission or fiber optical techniques. More traditional SHM techniques like strain gauges and Linear Variable Differential Transformers are generally used as well but more and more in combination with advanced ones based on wireless techniques. A wireless monitoring system could reduce costs significantly. The aerially dense monitoring now made physically and financially possible provides very detailed information about structural state, in so allowing better and more cost effective maintenance schedules. Only after certain changes in the structural behavior have been identified will physical inspection (either by means of non-destructive testing or visual methods) be necessary, and proper repair can be made immediately after the identification of the defect. This reduces the risk of further damage. In fact, such monitoring systems, linked with proper system models, allows for predictive maintenance scheduling so that the actual macroscopic failure never occurs.

The rubric of structural health monitoring can be extended to include the construction process itself. Previously the contractor simply implemented a given design ordered by the owner, but the current trend is for clients to commission certain performance requirements to be met by the finished product—performance-based design. The contracting process becomes the determination of the performance criteria, and delivery becomes a long-term fulfillment of these criteria. This arrangement can only take place if the performance states can be measured and quantified, and the measurement utilized in a decision making process. The processes needed for the evaluation of the structural state at delivery and during operation are increasingly dependent on sensor data and valid models to turn the data into indicators of physical behavior, and decision making tools to determine whether the performance requirements are being met.

Advanced SHM techniques include for example the recording of dynamic vibrational data, the detection of crack propagation or the use of sophisticated measuring techniques using fiber optical sensors. Fiber Bragg Grating can be used as a wavelength-specific reflector and as direct sensing elements for strain and temperature. Optical fibers have numerous advantages because they are nonconductive, electrically passive, immune to electromagnetic interference-induced noise, and able to transmit data over long distances with little or no loss in signal integrity. However, the region being sensitive for strain is relatively small and close by the fiber. Critical issues are in regard to robustness and durability as well as temperature influences.

Acoustic emission (AE) techniques can play a significant role for the monitoring of civil engineering structures since they are able to reveal hidden defects like cracks leading to structural failures long before a collapse occurs. However, most of the existing AE data analysis techniques seem not being appropriate for the requirements of a wireless network including distinct necessities for power consumption. It is costly to implement a large, distributed array of sensors capable of high resolution source location. Power efficient algorithms along with energy harvesting techniques allow now to implement even high-speed data acquisition techniques into wireless sensor networks.

5 COMBINATION OF INSPECTION AND MONITORING TECHNIQUES

It is obvious that the increasing demands for long-living sustainable structures require efficient procedures for quality control, using both, inspection and monitoring. However, procedures addressing all these techniques and planning their efficient use during a lifetime of a structure are rare. The first step could be a problem definition along with identification of appropriate inspection and monitoring techniques—usually along with visual inspections. This should be followed by a schedule or an event definition triggering any type of inspection procedure.

Depending on the type of structure, the extent of deterioration or the accessibility, it have to be decided whether a singular or repetitive inspection is required or monitoring techniques have to be installed. It would be a tremendously help for the stakeholder or the responsible engineer to have valid models simulating the degradation effects and the materials behavior under certain conditions. In addition a competent knowledge is required which NDT methods can be used to access the structural conditions at which level of accuracy. Before SHM techniques can be implemented a non-destructive assessment of certain structural components is in most cases needed. The interaction between inspection and monitoring techniques along with a definition of measuring parameters and profiles (best location, best technique) could be done at an early stage. Ideal would be an in-situ quality control using for example ultrasound, radar, thermography, impact-echo or electro-potential-field methods documented in form of a finger print or birth certificate.

In addition could the success of rehabilitation or retrofitting be a matter of testing.

Concrete Repair, Rehabilitation and Retrofitting III – Alexander et al. (eds)
© 2012 Taylor & Francis Group, London, ISBN 978-0-415-89952-9

Operational Modal Analysis for testing and continuous monitoring of bridges and special structures

A. Cunha, E. Caetano & F. Magalhães
ViBest, Faculty of Engineering, University of Porto, Portugal

ABSTRACT: This paper aims at emphasising the interest and potential of Operational Modal Analysis for testing and continuous monitoring of bridges and special structures, showing in particular different representative case studies previously analysed by the Laboratory of Vibrations and Monitoring (ViBest) of FEUP, such as the Humber suspension bridge, the Infante D. Henrique arch bridge, the FEUP Campus stress-ribbon footbridge or the Braga Stadium suspension roof.

1 INTRODUCTION

Modal Identification of Civil Engineering structures is founded on classical Experimental Modal Analysis techniques based on forced vibration tests.

However, owing to remarkable progress in recent years, Operational Modal Analysis (OMA) became a fundamental tool in Civil Engineering, playing nowadays an outstanding role at different stages along the life cycle of bridges.

Presently, OMA tests are conducted with different purposes, such as: (i) the calibration and validation of finite element models used in the design of new structures; (ii) the confirmation or understanding of structural changes introduced by rehabilitation works; (iii) the evaluation of modal damping ratios, which may be responsible for high levels of vibration induced by wind or traffic loads; and (iv) the design, tuning and evaluation of efficiency of vibration control devices.

At a second level, OMA can also support the development and exploitation of efficient vibration based damage detection continuous monitoring systems, provided that appropriate statistical techniques for removal of the influence of environmental and operational factors on modal properties are duly implemented.

This paper aims at emphasising the interest and potential of OMA for testing and continuous monitoring of bridges and special structures, showing in particular different representative case studies previously analysed by the Laboratory of Vibrations and Monitoring (ViBest) of FEUP (www.fe.up.pt/vibest).

2 DYNAMIC TESTING

Ambient or free vibration tests are simple experimental approaches that enable the very accurate identification of bridge modal properties, and the subsequent experimental validation and updating of finite element models used either at the design and commissioning phases or at modification, rehabilitation or strengthening stages, as evidenced by a large number of case studies.

The potential of OMA techniques can be easily illustrated with the dynamic tests recently performed at the Humber suspension bridge (Figure 1), in UK.

3 CONTINUOUS DYNAMIC MONITORING

3.1 *Infante D. Henrique Bridge*

ViBest/FEUP implemented a permanent dynamic monitoring system in this roadway bridge (Figure 3), which has been in continuous operation since September 2007. The acceleration time series collected every 30 minutes are immediately transferred to FEUP via Internet and processed using appropriate software (DynaMo) specifically developed for this purpose, enabling the detection of structural damage, after removing the influence of temperature and traffic intensity.

Figure 1. Bridge view from the South side.

Figure 2. Measurement sections with indication of the reference sections (R1, R2, RH and RB).

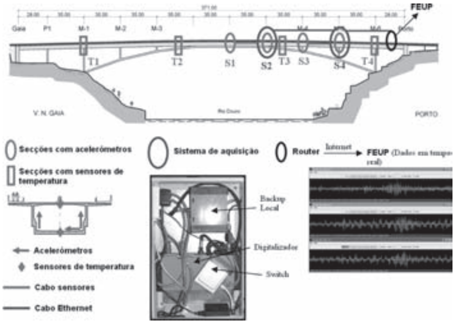

Figure 3. Schematic lateral view of Infante D. Henrique bridge, with characterisation of the continuous dynamic monitoring system installed by ViBest/FEUP.

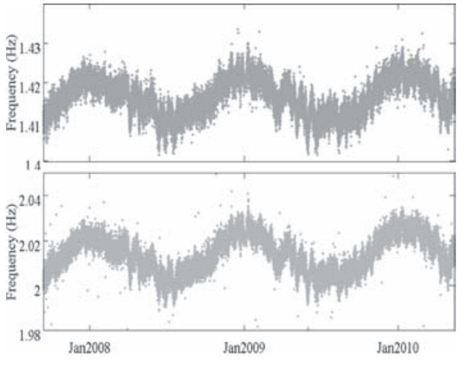

Figure 4. Evolution of the estimates of two vertical bending natural frequencies along three years, using the p-LSCF method.

3.2 *FEUP stress-ribbon footbridge*

ViBest/FEUP implemented a permanent dynamic monitoring system in this footbridge (Fig. 5), which has been in continuous operation since May 2009.

Inspection of collected data shows maximum relative variations of frequency estimates in the range 15–21%, essentially motivated by temperature, but also by the vibration level. Despite the slightly non-linear nature of temperature effects, owing to geometric non-linearity, the correlation between modal frequency estimates is essentially linear, and so PCA technique has been used with success to remove environmental effects and detect damage simulated numerically (Figure 6).

3.3 *Braga stadium suspension roof*

The dynamic properties of the suspension roof (Figure 7) have been continuously monitored since March, 2009, when a dynamic monitoring system was installed by ViBest/FEUP on the west slab.

Ongoing research is currently focused on the interpretation and understanding of the influence of temperature on the variations of the suspended roof modal properties, using also a sophisticated numerical model of the structure previously developed to take into account geometric nonlinearities. In parallel, additional ultrasonic wind sensors have been also implemented in order to better understand the structural behaviour under wind loading using response measurements on the prototype.

Figure 5. Lateral view of FEUP stress-ribbon footbridge.

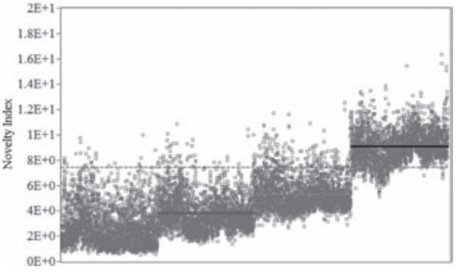

Figure 6. Control chart for damage detection using three different damage scenarios simulated numerically by slightly changing the boundary conditions at the abutments.

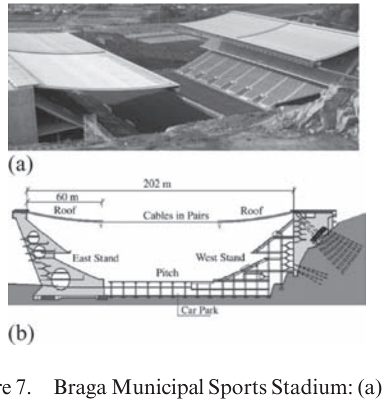

Figure 7. Braga Municipal Sports Stadium: (a) top view of the roof from the west side; and (b) cross section.

Concrete Repair, Rehabilitation and Retrofitting III – Alexander et al. (eds)
© 2012 Taylor & Francis Group, London, ISBN 978-0-415-89952-9

From the instantaneous corrosion rate to a representative value

C. Andrade, N. Rebolledo & F. Pedrosa
Center for Safety and Durability of Structures and Materials (CISDEM-CSIC-UPM), Madrid, Spain

ABSTRACT: Reinforcement corrosion develops due to the penetration of chlorides or of the carbonation front through the concrete pores and corrosion develops if enough moisture is present. However as the corrosion rate changes with temperature and the evolution of the corrosion itself, the representation may not be clear enough to be used for comparative purposes or for prediction of future evolution. The present work proposes a parallel use of accumulated corrosion depth, which is obtained by the integration of each age of the corrosion rate-time curve. This kind of representation enables the determination of corrosion depth at each age and appears the adequate to establish a Representative annual average value for comparative purposes. The procedure is applied to concrete specimens and real size elements exposed to Madrid outdoor conditions.

1 INTRODUCTION

The onset of corrosion consists in the passage of the steel state from a passive or negligible corrosion rate to an active corrosion state identified visually by the appearance of rust (Page et al 1982) with the corresponding loss of bar cross section. The corrosion rate is not commonly measured in spite of its importance to predict the evolution of the loss in structural load bearing capacity. One of the difficulties in the interpretation is linked to the evolution of the values of the corrosion rate with the climate due to its dependence on the degree of concrete water saturation and on the temperature (Vennesland 1997) (Andrade et al. 2002). In present paper are presented examples of variations of the corrosion rate I_{corr} in specimens exposed to natural atmospheres and of the accumulated corrosion penetration, P_{corr}, which has much less variation than the instantaneous corrosion rate.

2 EXPERIMENTAL

For the sake of the illustration, two cases were selected were: 1) small concrete specimens exposed to natural environment in Madrid climate and that have been measured every week (figure 1) and 2) a beam that was measured periodically but no so frequently as the previous specimens (figure 2). Some of the *small specimens* (P-13) were carbonated after the curing period. Specimen P-23 having 3% $CaCl_2$ added in the mix was as corroding from its fabrication.

All the specimens were introduced during their first year to different constant Temperature, T, and RH chambers. After this year some of them were submitted to natural weathering in the Madrid climate. The corrosion parameters were measured by means of a laboratory made potentiostat SVC-2.

The *big samples* used for illustration were: a reinforced concrete T-beam (Andrade et al. 2002) and a square section pile, as illustrated in Figure 2. Both big specimens have been contaminated with 3% chloride by weight of cement added to the mix in the form of $CaCl_2$ to promote corrosion and were exposed outdoors to Madrid climate afterwards. The specimens are 2 meters in length.

Figure 1. Concrete specimens exposed to the action natural atmosphere in Madrid—Spain.

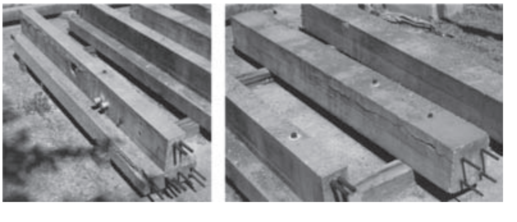

Figure 2. A view of the beam that is also exposed to the action of natural atmosphere.

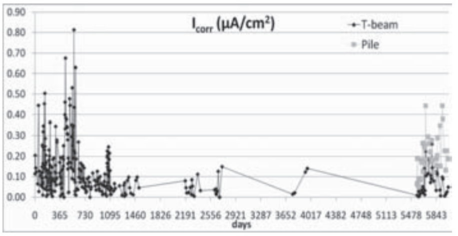

Figure 3. Values of the beam exposed to Madrid atmosphere from 1995 and those of the pillar from 2010.

3 RESULTS

Figure 3 shows as an example the evolution of the instantaneous corrosion rate, I_{corr}, from 1995 of the beam and of the pillar represented in the same figure but recorded only from 2010.

The trends show important changes due to the different seasons which mean different concrete moisture contents and temperatures. As all the samples are non sheltered from rain, they exhibit the higher I_{corr} values in winter and spring presenting very low I_{corr} values in summer due the drying induced by the higher temperatures. Temperature is the main controlling parameter of the concrete moisture which means that, depending on the cover depth, in hot weather the concrete dries and in winter with low temperatures, the concrete remains wet.

4 DISCUSSION

The changes recorded as shown in figure 3 are very difficult of being compared or interpreted. In figures 2 is given the accumulated Corrosion penetration, P_{corr}, values of the beam which result from the progressive integration of the instantaneous values. The trends now appear much clearer from the very beginning because the corrosion penetration is progressive and show near a lineal increase with time. The increase reveals the effect of the wet season and of the hot one because a kind of "steps" appears in the increasing trend. It is also interesting to note the two periods in the Representative or averaged corrosion rate, exhibited by the beam. From the slope of the accumulated or corrosion penetration (P_{corr}) is possible to obtain the representative corrosion rate, $I_{corr,\ REP,}$ which can be used for prediction. They are given for the sake of illustration in figure 4. Regarding the statistical variation, in Table 1 is given the average values obtained from arithmetic calculation of the two periods of the beam and their standard deviation and coefficient of variation. They apparent scatter if high however if the statistical treatment is made on the accumulated corrosion penetration (as I_{acc} or P_{corr} in µm) that scatter from a lineal behaviour (annual constant corrosion rate) is very much reduced as is given by the regression coefficients

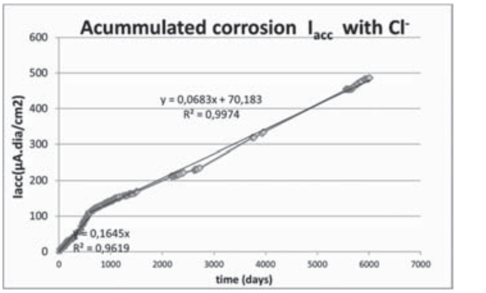

Figure 4. Accumulated corrosion, I_{accr}, or corrosion penetration depth with time of the beam with added chlorides.

Table 1. Descriptive statistics of the beam.

Statistical treatment of the I_{corr} values of the beam				
	Period 1		Period 2	
I_{corr} (µA/cm²)	Arithmetic calculation	From slope figure 9	Arithmetic calculation	From slope figure 9
Average value	0.171	0.164	0.072	0.068
Std. deviation	0.144		0.059	
Coef. Variation	84.1%		82.2%	
Regress. coef.		0.96		0.99

shown on figure 4. Then a Representative Corrosion Rate value can be established with nominal very low scatter, which has to be multiplied by the pitting factor α in the case of localized corrosion.

5 CONCLUSIONS

The corrosion rate values. I_{corr}, fluctuate considerably in outdoor exposition due to the rain periods and the temperature changes. The coefficient of variation found can be around 100%. However this apparently high scatter disappears when the accumulated corrosion penetration P_{corr} is calculated and from its slope an Averaged or annual Representative Corrosion Rate can be deduced with a very high regression coefficient of the fit in spite of the seasonal variations.

REFERENCES

Andrade, C., Alonso, C. & Sarría, J. 2002. *Cement and Concrete Composites* 24: 55–64.

Page, C.L. & Treadaway, K.W.J. 1982. *Nature* 297 (5862): 109–115.

Vennesland, O. 1997. Int. Symposium Norwegian Public Road Administration, Svolvaer-Norway: 253–262.

Concrete Repair, Rehabilitation and Retrofitting III – Alexander et al. (eds)
© 2012 Taylor & Francis Group, London, ISBN 978-0-415-89952-9

Novel cement-based composites for strengthening and repair of concrete structures

V. Mechtcherine
Institute of Construction Materials, Technische Universität Dresden, Dresden, Germany

ABSTRACT: In the last 30 years the construction industry branch having to do with the repair, protection and strengthening of concrete has experienced explosive growth. This has been driven by the need to reverse the deterioration of, damage to, and defects in concrete structures as well as by changes in building use and code requirements. Accordingly, there is great need to improve the materials and techniques used in repair and strengthening. This article focuses on novel High-Performance Fibre-Reinforced Cement Based-Composites (HPFRCCs) for strengthening and repair of buildings and infrastructure made of concrete and, in some cases, masonry. Two new types of such material, Textile-Reinforced Concrete (TRC) and Strain-Hardening Cement-Based Composites (SHCCs), are introduced, highlighting with particular care the benefits and challenges of using HPFRCCs. Specific compositions and production techniques of the composites are presented, followed by a discussion of their mechanical properties in respect of their use on the job. Some reference is made to approaches in considering the load-carrying capacity of the strengthening layers made of HPFRCCs. Furthermore, the transport properties through layers of cracked composites are described as the basis for estimating how well they can protect concrete and its steel reinforcement against ingressing fluids and gases, i.e., against their deterioration. Finally, a number of practical applications of TRC and SHCC are described in order to demonstrate their great potential in the field of rehabilitation of existing concrete structures.

1 INTRODUCTION

Textile-reinforced concrete (TRC) is a composite material consisting of a fine-grained matrix and high-performance, continuous multifilament-yarns made of alkali-resistant (AR) glass, carbon, or polymer. The major advantages of TRC are its high tensile strength and pseudo-ductile behaviour, the latter characterized by large deformations due to its tolerance of multiple cracking (Curbach 2003, Brameshuber 2006, Butler *et al.* 2010).

Biaxial or multi-axial reinforcement fabrics consist of multi-filament yarns comprised of several hundred to several thousand individual filaments approximately 5 to 25 μm in diameter. The fine-grained concrete usually has a water-to-binder ratio of approximately 0.3 with a binder content of 40 to 50% by volume. In strengthening and repair the lamination technique in combination with low-pressure spraying seem to be most suitable.

The mechanical performance of TRC under tensile loading can vary widely depending, first of all, on the quality and quantity of textile reinforcement.

Strain-hardening cement-based composites (SHCC) reinforced by short polymer fibres constitute a relatively new class of building material, which exhibits pseudo-strain hardening behaviour by forming multiple cracks when subjected to tensile loading (Fischer & Li 2006, Toledo Filho *et al.* 2011). The high ductility and strain capacity of SHCC give this material high potential for use in applications in which high, non-elastic deformability is needed. Some of the most promising applications are structural repair and strengthening of existing structures.

The material design of SHCC is based on consideration of the mechanical interactions between fibre and matrix via an interface. The demand of fine fibre distribution makes mandatory the use of only very fine sand as aggregates. Fine Polyvinylalcohol (PVA) and High-density Polyethylene (HDPE) fibre with high aspect ratios were found to be most suitable as reinforcement.

Apart from considerations of strength and toughness, very good workability in the fresh state is essential in order to guarantee the very uniform distribution of fibres throughout the matrix. It was shown that SHCC can be applied by different methods: by pouring into formwork, by spraying, or even by extrusion (e.g., Fischer & Li 2006). For purposes of repair or strengthening, spraying could be the best option in most cases.

2 STRENGTHNING OF EXISTING STRUCTURES

The work of the Collaborative Research Center 528 of the German Research Society at the TU Dresden demonstrated that TRC can be used efficiently in strengthening different structural elements containing steel-reinforcements such as beams, columns, plates, or slabs.

The first practical application of this innovative strengthening method using textile-reinforced concrete was carried out in 2006 in the retrofit of a steel-reinforced concrete roof shell in Schweinfurt, Germany (Weiland *et al.* 2008). The 80 mm-thick steel reinforced concrete hypar-shell has a side length of approximately 27 m and a maximum span of approximately 39 m. Due to its large deformations (drops of up to 200 mm) in the shell's cantilevered areas, the designed tensile stresses in the upper steel reinforcement layer of the shell were exceeded significantly (see Figure 1).

Strengthening with textile-reinforced concrete couples the advantages of a two-dimensional reinforcement layer with a low dead weight. To establish an adequate interaction between the existing concrete and the textile-reinforced strengthening layer sandblasting and subsequent generous wetting of the old concrete surface was carried out. Altogether, three layers of carbon-yarn textile were placed using a lamination technique. The total thickness of the strengthening TRC layer was only 15 mm.

The strengthening of RC structures using SHCC is most advantageous with respect to increasing their resistance to dynamic, energetic loading such as found in earthquakes, soft or hard impact, explosion waves etc. Kim *et al.* (2010) demonstrated the effect of the strengthening of non-ductile frames using precast infill walls made of SHCC. Furthermore, SHCC layers without additional reinforcement might contribute to the shear resistance of thinly walled RC structures.

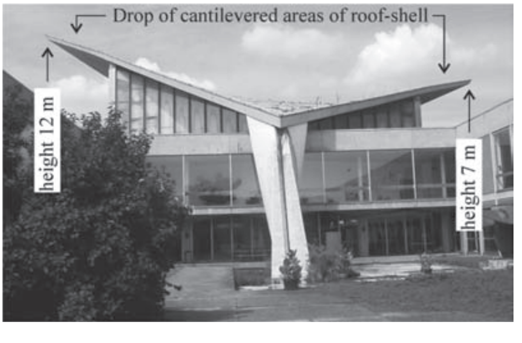

Figure 1. Steel reinforced concrete hypar-shell of FH Schweinfurt, Germany (Weiland *et al.* 2008).

A very promising application is the improvement of overall mechanical performance of existing masonry buildings in general and their earthquake resistance in particular by a thin layer of wet-sprayed, strain-hardening, cement-based composites (SHCC) (Mechtcherine *et al.* 2012). The effectiveness of such strengthening was demonstrated by shear testing on the masonry elements of dimensions 1.25 m × 1.00 m × 0.175 m. The application of SHCC layers on both surfaces with an average thickness of 10 mm provided a tremendous increase in load-bearing capacity under repeated loading.

3 REPAIR AND PROTECTION OF EXISTING STRUCTURES

In the case of using TRC or SHCC for the repair of RC structures, first of all, a protective function is expected of the repair layers. This function can be transferred additionally to the strengthening function or be the main purpose of the repair measure. Since both TRC and SHCC exhibit high deformability due to their fine, well distributed cracking, the repair layers made of such materials are fit to bridge existing and future cracks in the substrate. Furthermore, fine crack patterns can be considered beneficial with respect to the protection of the concrete substrate and its steel reinforcement against the ingress of water, ions and gases.

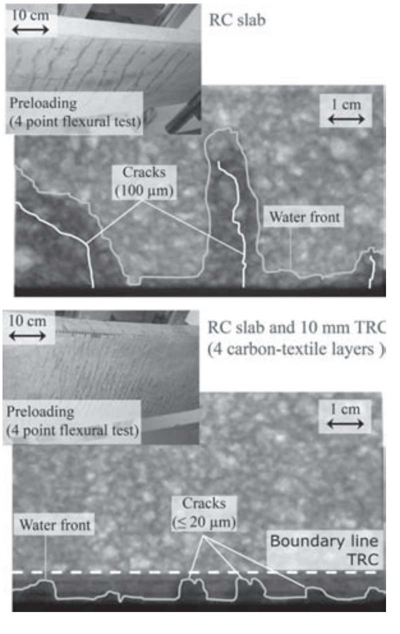

Figure 2. Water uptake by specimens made of ordinary concrete a) without and b) with a protective layer of cracked TRC (with carbon textile) on the bottom side (neutron radiography images after 30 minutes of capillary suction).

Lieboldt *et al.* (2011) investigated the transport mechanisms of water in and through composite concrete specimens made of a cracked ordinary concrete (OC) as a substrate and textile reinforced concrete (TRC) as a cover layer for its strengthening and repair. Neutron radiography served as the testing technique. In ordinary concrete quick and deep ingress of water through relatively wide macro-cracks (100 to 200 μm), followed by transport through the capillary pore system, caused saturation of large areas in a rather short time, see Figure 2a. TRC applied to the OC surface reduced the ingress of water to a large extent, see Figure 2b. Its small crack widths of approximately 20 μm changed suction behaviour fundamentally. In the cracked substrate of ordinary concrete, capillary suction was obviated, and transport through the pore system of the matrix became the prevailing transport mechanism of capillary action. Not only was the mechanism altered, but the transport of water deep into inner regions was significantly retarded as well.

A number of very promising applications of SHCC for repair and protection have been already demonstrated. E.g. SHCC developed at the TU Dresden was used to repair the upper water reservoir of the hydraulic power pumping station Hohenwarte II in Thüringen, Germany. Before repair the reservoir wall showed cracks, defective joints, scaling of the concrete and other defects. The purpose of the pilot project was to restore the water tightness of the wall in just one working step using a single, sprayed layer of SHCC, see Figure 3. Due to its ductility this repair material should durably seal defect joints and cracks, but SHCC should provide as well a smooth, durable cover for the concrete substrate. Since the reservoir walls are exposed to high water saturation and considerable changes in water level, the danger of frost damage is considerable. The use of conventional air-entrainment agents is possible with SHCC, but not when the spaying technique is applied. For this reason superabsorbent polymers (SAP) were introduced as a new additive to improve the frost resistance of the repair layer.

4 SUMMARY

The application of high-performance fibre-reinforced cementitious composites such as TRC or SHCC opens new possibilities in the strengthening and repair of existing concrete structures.

In the case of strengthening with TRC, a significant increase in the ultimate load of existing structures can be achieved. The strengthening of RC structures with SHCC layers without additional reinforcement seems to be most meaningful with respect to increasing their resistance to dynamic, energetic loading as with earthquakes, impact, or exposures. Further possible applications of SHCC are strengthening of masonry and infill walls.

In the case of use of TRC or SHCC for repair of RC structures, a protective function of repair layers is expected in the first place. This function can augment the strengthening function or be the main purpose of the repair measure. Since both TRC and SHCC exhibit high deformability due to fine, well distributed cracking, the repair layers made of such materials are suited to the bridging of existing and future cracks in the substrate. Furthermore, fine crack patterns are beneficial with respect to the protection of the substrate concrete and steel reinforcement against the ingress of water, ions and gases.

Figure 3. Application of SHCC containing SAP as repair material by spraying.

REFERENCES

Brameshuber, W. (ed.). 2006. Textile Reinforced Concrete. State-of-the-Art Report RILEM Technical Commitee 201-TRC. *RILEM Report 36*. RILEM Publications S.A.R.L.

Curbach, M. (ed.). 2003. Textile reinforced structures. *Proc. of the 2nd Colloquium on Textile reinforced Structures (CTRS2), TU Dresden, Germany, 2003.*

Fischer, G. & Li, V.C. (eds). Proc. of Int. RILEM *Workshop on High Performance Fiber Reinforced Cementitious Composites (HPFRCC) in Structural Applications, Honolulu, May 2005: 37–46. PRO 49.* RILEM Publications S.A.R.L.

Kim, S.-W. et al. 2010. Shear performance of precast SHCC infill walls for seismic retrofitting of non-ductile frames. *Magazine of Concrete Research* 62(12): 925–934.

Lieboldt M. et al. 2011. Water transport through textile reinforced concrete. In F.H. Wittmann & O. Mercier (eds), *Basic Research on Concrete and Applications; Proc. of an ASMES International Workshop*: 21–34. Freiburg: Aedificatio Publishers.

Mechtcherine, V. et al. 2012. Strengthening/retrofitting of masonry by using thin layers of sprayed strain-hardening cement-based composites (SHCC). In M. Grantham et al. (eds), *Concrete Solutions; Proc. of 4th Int. Conference on Concrete Repair, Dresden, Germany, 26–28 September 2011*: 741–748. Taylor & Francis Group.

Toledo Filho, R.D. et al. (eds). 2011. Strain Hardening Cementitious Composites (SHCC2-Rio). *RILEM Proceedings PRO 81*. RILEM Publications S.A.R.L.

Weiland, S. et al. 2008. Textile Reinforced Concrete for Flexural Strengthening of RC-Structures—Part 2: Application on a Concrete Shell. In ACI SP-251-3, *Design & Applications of Textile-Reinforced Concrete*: 41–58.

Concrete Repair, Rehabilitation and Retrofitting III – Alexander et al. (eds)
© 2012 Taylor & Francis Group, London, ISBN 978-0-415-89952-9

Rehabilitation and strengthening of concrete structures using Ultra-High Performance Fibre Reinforced Concrete

E. Brühwiler
Ecole Polytechnique Fédérale de Lausanne (EPFL), Lausanne, Switzerland

ABSTRACT: An original concept is presented for the durable rehabilitation and strengthening of concrete structures. The main idea is to use Ultra-High Performance Fibre Reinforced Concrete (UHPFRC) complemented with steel reinforcing bars to "harden" and strengthen those zones of the structure that are exposed to severe environmental influences and high mechanical loading. This concept combines efficiently protection and resistance properties of UHPFRC and significantly improves the structural performance of the rehabilitated concrete structure in terms of durability. The concept has been validated by means of field applications demonstrating that the technology of UHPFRC is mature for cast in-situ and prefabrication using standard equipment for concrete manufacturing. This novel technology is a step forward towards more sustainable structures.

1 INTRODUCTION

Reinforced concrete structures show excellent performance in terms of structural behaviour and durability except for those zones that are exposed to severe environmental influences and high mechanical loading. Rehabilitation of deteriorated concrete structures is a heavy burden from the socio-economic viewpoint since it leads to significant user costs. As a consequence, novel concepts for the rehabilitation of concrete structures must be developed. Sustainable concrete structures of the future will be those requiring just minimum interventions of only preventive maintenance with no or only little service disruptions.

Over the last 10 years, considerable efforts to improve the behaviour of cementitious materials by incorporating fibres have led to the emergence of Ultra-High Performance Fibre Reinforced Concretes (UHPFRC). These novel building materials provide the structural engineer with an unique combination of (1) extremely low permeability which prevents the ingress of detrimental substances such as water and chlorides and (2) very high strength, i.e., compressive strength higher than 150 MPa, tensile strength higher than 10 MPa and with considerable tensile strain hardening and softening behaviour.

Consequently, UHPFRC have improved resistance against severe environmental influences and high mechanical loading thus providing a potential to significantly improve structural resistance and durability to concrete structures.

This keynote paper presents an original concept for the rehabilitation and strengthening of concrete structures and summarizes more than 12 years of intensive research and development of a novel technology to improve concrete structures.

2 CONCEPTUAL IDEA

The basic conceptual idea is to use UHPFRC only in those zones of the structure where the outstanding UHPFRC properties in terms of durability and strength are fully exploited; i.e. UHPFRC is used to "harden" the zones where the structure is exposed to severe environmental conditions (f.ex., deicing salts, marine environment) and high mechanical loading (f.ex. impact, concentrated loads, fatigue). All other parts of the structure remain in conventional structural concrete as these parts are subjected to relatively moderate exposure.

This concept (which is also applicable to new construction) necessarily leads to composite structural elements combining conventional reinforced concrete and UHPFRC.

The combination of the UHPFRC protective and load carrying properties with the mechanical properties of steel reinforcement bars (denominated reinforced UHPFRC or R-UHPFRC) provides a simple and efficient way of increasing the stiffness and load-carrying capacity while keeping compact cross sections (Fig. 1).

Depending on the structural and material properties of the composite system, more or less pronounced built-in tensile stresses are induced in the UHPFRC layer due to restrained deformations at early age. This stress state needs to be analysed and evaluated but is usually resisted by the UHPFRC without crack formation.

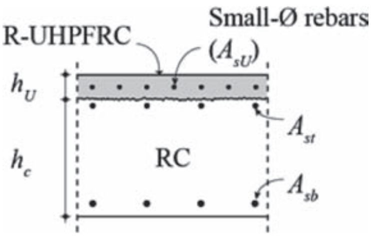

Figure 1. Basic configuration of composite structural elements combining R-UHPFRC and conventional reinforced concrete.

The original conceptual idea (developed in 1999) has been investigated by means of extensive research activities aimed at characterizing UHPFRC materials and their properties as well as the structural behaviour of R-UHPFRC—RC composite structural members, combining material and structural engineering sciences. The concept is well-suited for bridges, buildings, galleries, tunnels and retaining walls.

3 APPLICATIONS

Since 2004, UHPFRC is applied in Switzerland (and in one case in Slovenia following the same concept) on existing reinforced concrete bridge deck slabs as thin watertight overlays (in replacement of currently used waterproofing membranes) as well as reinforcement layer in R-UHPFRC providing both protection and load bearing functions for bridge elements and slabs in buildings without increasing the dead load of the structure.

Specific parts of reinforced concrete structures such as crash barrier walls on highway bridges, bridge piers and retaining walls suffer from severe exposure to concrete aggressive substances such as de-icing salts and impact like action. Such elements usually show insufficient durability when built in conventional reinforced concrete. Again, UHPFRC is suitable to establish the required durability and mechanical performance of such structural elements.

The first field application of UHPFRC in 2004 was for the rehabilitation and widening of a short span road bridge with busy traffic. The entire deck surface of the bridge was rehabilitated in three steps (Fig. 2).

Several more applications (Fig. 3) following the same principle have been conducted under various weather conditions and construction site constraints. Fresh UHPFRC has also been mixed on the construction site and by optimizing additives maximum slopes of up to 10% could be cast with this self-compacting material.

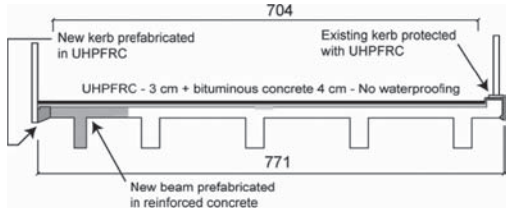

Figure 2. Bridge cross section after rehabilitation (dimensions in cm).

Figure 3. On-site production and casting of UHPFRC.

The relatively high material cost imposes to use UHPFRCs only where maximum benefit of their outstanding mechanical properties can be taken. Obviously, the more requirements (regarding durability, structural/fatigue safety, and functionality) are fulfilled with one UHPFRC layer, the more efficient and economical is the technology.

Analysis of construction costs alone showed that the rehabilitation realized with UHPFRC was in most cases not more expensive and in some cases significantly less expensive than conventional methods (which provides however lower quality in terms of durability and life-cycle costs).

In addition, the UHPFRC technology allows for significant reductions in the duration of construction site reducing thus user costs. Also, it provides significant gains in terms of long term durability and reduction of traffic disruptions (and subsequent user costs) due to multiple interventions (required in the case of conventional approaches).

4 CONCLUSION

An original concept using Ultra-High Performance Fibre Reinforced Concrete (UHPFRC) for the rehabilitation and strengthening of concrete structures has been developed and validated by means of more than 10 site applications under various conditions.

Concrete Repair, Rehabilitation and Retrofitting III – Alexander et al. (eds)
© 2012 Taylor & Francis Group, London, ISBN 978-0-415-89952-9

Textile-based composites versus FRP as strengthening and seismic retrofitting materials for concrete and masonry structures

T.C. Triantafillou
University of Patras, Greece

ABSTRACT: The author reviews experimental studies which have provided fundamental knowledge on the use of a new generation of composite materials, namely Textile-Reinforced Mortars (TRM), as strengthening and seismic retrofitting materials for concrete and masonry structures. TRM are investigated as a means: to provide confinement in plain and Reinforced Concrete (RC), to increase the deformation capacity of old-type RC columns subjected to simulated seismic loading, to increase the shear and flexural resistance of RC members and to increase the out-of-plane or in-plane strength of unreinforced masonry walls. In most cases, the effectiveness of TRM systems is quantified through comparison with equivalent Fiber-Reinforced Polymer (FRP) ones. Based on the results it is concluded that TRM jacketing is an extremely promising new technique, which will enjoy the attention of the research community and will be employed in numerous applications in the next decades.

SUMMARY

The increasing popularity of fiber-reinforced polymers (FRP) as a means of strengthening and seismic retrofitting of existing structures derives from numerous attractive features of these materials, such as: high specific strength (i.e. strength to weight ratio), corrosion resistance, ease and speed of application and minimal change of cross section dimensions. Despite these well-established advantages over other methods, the FRP strengthening technique entails a few drawbacks, which are mainly attributed to the organic resins used to bind and impregnate the fibers. The replacement of organic binders with inorganic ones, e.g. cement-based polymer-modified mortars, would seem as the logical course of action, targeting at the alleviation of all resin-related problems. Nevertheless, the substitution of FRP with fiber-reinforced mortars would be inhibited by the relatively poor bond conditions in the resulting cementitious composite as, due to the granularity of the mortar, penetration and impregnation of fiber sheets is very difficult to achieve. Enhanced fiber-matrix interactions could be achieved when continuous fiber sheets are replaced by textiles, resulting in a new generation of materials, which may be called Textile-Reinforced Mortars (TRM), and may be thought of as an alternative to FRP in the field of strengthening and seismic retrofitting.

Textiles comprise fabric meshes made of long woven, knitted or even unwoven fiber rovings in two (typically orthogonal) or more directions (Fig. 1). The quantity and the spacing of rovings in each direction can be independently controlled, thus affecting the mechanical characteristics of the textile and the degree of penetration of the mortar matrix through the mesh openings. The latter is a measure of the composite action achieved for the mortar-grid structure through mechanical interlock. For the polymer-modified cementitious matrix of externally applied TRM overlays used for strengthening purposes, the following requirements should be met: no shrinkage; high workability; high viscosity; low rate of workability loss; and sufficient shear (hence, tensile) strength, in order to avoid premature debonding. In case E-glass fiber textiles are used, the cement-based matrix should be of low alkalinity.

In this paper, the author reviews experimental studies which have provided fundamental knowledge on the use of TRM as strengthening and seismic retrofitting materials: to provide confinement in plain and reinforced concrete (RC); to increase the deformation capacity of old-type RC columns subjected to simulated seismic loading (Fig. 2, 3);

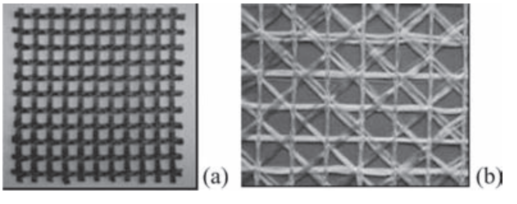

Figure 1. (a) Two-directional textile made of carbon fibers, (b) Three-directional textile made of glass fibers.

Figure 2. TRM confining jacket at column plastic hinge regions.

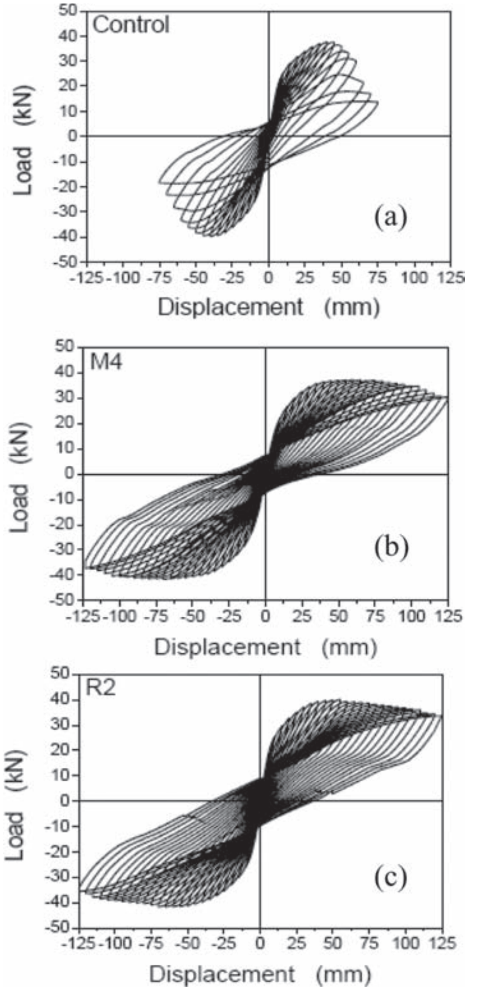

Figure 3. Load-displacement curves for (a) The column specimen without retrofitting, (b) The TRM-confined specimen (M4), and (c) The FRP-confined specimen (R2).

to increase the resistance of RC beams in shear and beams or two-way slabs (Fig. 4, 5) in flexure; and to increase the strength and deformation capacity of masonry walls subjected to out-of-plane or in-plane loading. In most cases, the effectiveness of TRM systems is quantified through comparison with equivalent FRP ones.

From the results presented in this study it is shown that TRM jacketing of RC is nearly as effective as FRP jacketing. The authors believe that TRM jacketing is an extremely promising solution for increasing the confinement as well as the shear and flexural capacity of reinforced concrete members, of crucial importance in strengthening and seismic retrofitting. Extrapolation of the technique to unreinforced masonry walls resulted in substantial increase in strength and deformation capacity, indicating that this new generation of inorganic binder-based composite materials offers a promising solution in the restoration of masonry structures, including monument-type ones.

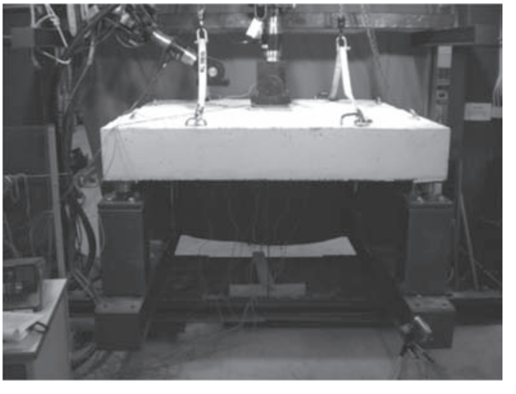

Figure 4. Typical two-way slabs tested.

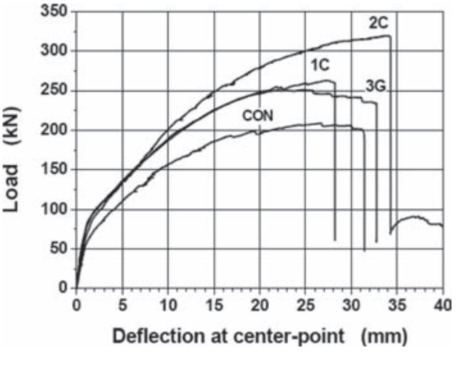

Figure 5. Load – center point deflection curves for slab without strengthening (CON) and slabs with different configurations of externally applied textile reinforcement (C or G denotes carbon or glass fibers, respectively, the number denotes the number of layers).

This page intentionally left blank

Theme 1: Concrete durability aspects

Innovative materials and influences of material composition

This page intentionally left blank

Concrete Repair, Rehabilitation and Retrofitting III – Alexander et al. (eds)
© 2012 Taylor & Francis Group, London, ISBN 978-0-415-89952-9

Curing technologies, strength and durability performance

Rina Wasserman & Arnon Bentur
National Building Research Institute, Civil and Environmental Engineering, Technion, Israel Institute of Technology, Israel

1 INTRODUCTION

The evaluation of curing efficiency is traditionally based on evaluation of strength development since this is the major characteristic used for quality control and specification. However, a major input of curing is its influence on durability. It is now well established that strength is to a large extent a "bulk" property, while durability performance is influenced by processes taking place at the concrete cover zone, "covercrete", and strength may not be sufficiently sensitive to monitor the performance of curing with respect to durability.

In-spite of the wide use of different types of curing technologies, there is very little know-how on their performance with respect to assuring favorable durability performance when considering that their influence on the bulk properties of the concrete may be different than their effect on the cover zone. The object of the present study was the evaluation of such effects, by investigating the influence of various curing technologies on the bulk and surface properties of concretes.

2 EXPERIMENTAL

The curing technologies studied were the standard water ponding (one day in mold, 6 days ponding and thereafter in lab air), two curing compounds (based on silicone and acrylic compositions) and curing fabric which is made up of two portions, a fabric which can absorb water and a polyethylene sheet on top.

The bulk properties were evaluated by compressive tests while the surface properties were characterized by capillary absorption and air permeability tests. For these two tests, 28day old specimens were dried at 60 °C until constant weight and thereafter evaluated for capillary absorption and air permeability. The drying was intended to provide conditions for meaningful comparison to eliminate the effect of differences in moisture conditions on the test results.

3 SUMMARY OF RESULTS

The effect of normal and harsh environments when water ponding for one week is applied suggests that the strength is maintained (Figure 1), while at the same time there is a considerable detrimental influence on penetration characteristics of the concrete surface (increase in capillary absorption and air permeability, Figure 2 for air permeability). This

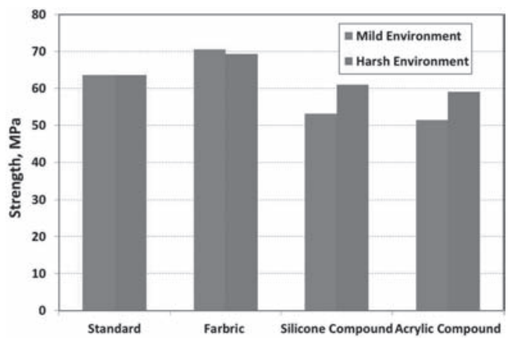

Figure 1. The effect of environment on the strength developed using the various curing technologies.

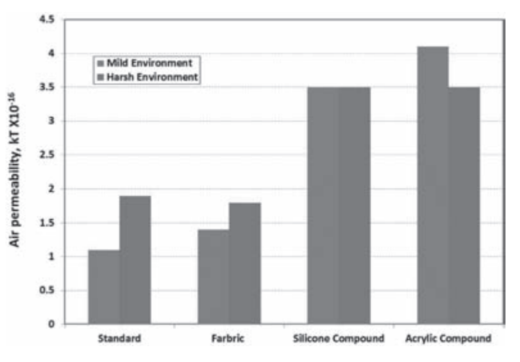

Figure 2. The effect environment on the air permeability of the concretes as a function of the curing technology applied.

is another demonstration of the limitations of using strength as a general performance characteristic for concrete. Comparison of the three curing technologies suggests that the fabric one is clearly superior to the two compound curing treatments. It practically preserves most of the strength and even increases it (Figure 1), while the values of permeability characteristics are being maintained at a level similar to the water ponding standard curing (Figure 2). The two compound curing treatments exhibit reduction in strength and increase in penetration values, especially in the mild environmental conditions.

It is interesting to note the differences in the response of the various curing technologies to the environmental conditions, as summarized in terms of relative values in Figures 1 and 2.

The harsh conditions are detrimental with respect to the fabric curing, leading to mild reduction in strength and marked increase in penetration. Both curing compounds exhibit a different trend, whereby the performance of the curing technology is improved in the harsh environment, with respect to strength as well as penetration resistance. This trend might be explained on the basis of an improved film which coalesces from the curing compounds. Yet, even with this improvement, the overall performance of the curing compounds even in the harsher environmental conditions is inferior to that of the fabric.

Concrete Repair, Rehabilitation and Retrofitting III – Alexander et al. (eds)
© 2012 Taylor & Francis Group, London, ISBN 978-0-415-89952-9

The effect of binder type on chloride threshold values for reinforced concrete

M.C. Alonso & M. Sanchez
Research Centre on Safety and Durability of Structures and Materials (CISDEM), CSIC-UPM, Spain

U. Angst
Institute for Building Materials, ETH Zurich, Switzerland

J.L. Garcia-Calvo
Institute of Construction Science Eduardo Torroja (IETc)c, CSIC, Spain

ABSTRACT: If chloride induced corrosion is the likely failure mechanism, both in the case of condition assessment or service life design, engineers compare the actual or predicted chloride content at the reinforcement steel depth with the chloride content required to initiate corrosion. The latter is usually referred to as chloride threshold value or critical chloride content. Considering the current developments in the cement industry promoting non-traditional and more sustainable binder types, there is a lack of knowledge with regard to their influence on the protection and onset of corrosion of future concrete structures. The present paper gives an overview of the current knowledge on the influence of blended cements on the chloride threshold value and corrosion related durability in general.

1 INTRODUCTION

Penetration of chloride ions from de-icing salts or marine action are common causes of degradation of concrete structures. Efforts are made to develop models for more accurate approaches in the calculation of the service life of concrete structures. Most of the models are based on the phenomenological model of (Tuutti 1982) which considers the service life as two successive stages: an *initiation stage* that describes the process of chloride penetration through the concrete cover and is terminated when corrosion starts (i.e. when the chloride threshold value is reached at the steel), and a *propagation stage* that describes the accumulation of damage owing to propagating rebar corrosion. The *chloride threshold level* is a key input parameter for mathematical service life models. In addition to the chloride threshold level, also the resistance of the concrete cover against chloride ingress governs the duration of the initiation stage.

Despite huge research efforts throughout the last decades, several of the input parameters used in service life models are to a large extent still based on experience with ordinary Portland cement (OPC, CEM I). One reason for this is the fact that these research efforts have not succeeded in providing reliable data for chloride threshold values for various cement types. Nevertheless, the use of OPC has worldwide gradually decreased.

2 EFFECTS OF BINDER TYPE

The binder type affects the corrosion performance of reinforced concrete by affecting the chloride binding capacity, the chloride transport properties and the chloride threshold value.

2.1 *Effect on chloride binding capacity*

Affecting the chloride binding capacity will affect both the chloride threshold value as well as the transport of chloride owing to a "filter effect" associated with high chloride binding capacity.

The effect of mineral additions on the chloride binding capacity was studied by several authors. For the case of silica fume containing cements, the chloride binding capacity was reported to be lower compared to OPC. Fly ash, on the other hand, appears to improve the chloride binding capacity of the binder. Several authors reported also higher chloride binding capacities for ground granulated blast furnace slag containing cements due to improved chemical and physical binding.

2.2 *Effect on chloride transport*

The effect of blended binders on the chloride penetration resistance, such as the pronounced reduction of chloride diffusivity with the use of fly ash or blast furnace slag, is well documented in practical experience. On several other mineral additions (such as limestone or burnt shale), however, not much experience is available.

2.3 *Effect on chloride threshold value*

The impact of different binder types on the chloride threshold level is considered significant as changing the binder can markedly affect two of the most dominant influencing factors of chloride threshold values, viz. the pore solution pH and the steel/concrete interface.

It is well known that the pozzolanic reaction consumes calcium hydroxide liberated during hydration of clinker phases, and thereby reduces the pH and also alkalis are removed from the pore solution and bound in CSH (Garcia-Calvo et al, 2010).

In addition to the pH of the pore solution, the type of binder also affects the microstructure that might be important when considering the steel/concrete interface. Mineral additions can significantly improve the workability of concrete mixes and thus ease compaction; this decreases the risk of macroscopic defects (voids, gaps, etc). It is, however, not yet clear to what extent mineral additions are able to reduce bleed-water zones and other microscopic defects at the steel/concrete interface and specifically if this is sufficient to affect the corrosion initiation mechanism.

In comparison with OPC, lower chloride thresholds have been reported in the literature for silica fume containing cement; for fly ash and ground granulated blast furnace slag, on the other hand, contradictory results have been reported. For binders containing limestone or burnt shale as well as ternary mixes, almost no experience is documented in the literature.

2.4 *Time to corrosion*

To assess the risk of corrosion associated with non-traditional binders, both the chloride transport properties as well as chloride threshold values have to be considered. Binders leading to lower chloride threshold values do not necessarily have to negatively affect the performance of a reinforced concrete structure with respect to chloride induced corrosion. If the chloride diffusion coefficient is significantly lower in the non-traditional binder system compared with OPC, the time until corrosion (initiation stage) might be longer (even with a lower chloride threshold value). Thus, to assess modern binders an approach based on measuring the time required to initiate corrosion might be preferable. The outcome is an "integral result", containing both the chloride penetration resistance and the chloride threshold. However, whatever the experimental approach to assess the risk of corrosion for modern binders, a fundamental challenge are time-effects, viz. the effects associated with time-dependences (maturity) of slow hydration of blended materials and corresponding properties evolution, such as pH decrease or chloride binding and transport etc. that will influence in the performance response of these new binders if accelerated testing is considered.

CONCLUSIONS

It is common to use 0.4% total chloride by cement weight as chloride threshold value, despite the fact that this value is purely based on experience with ordinary Portland cement, the use of which has gradually decreased over the last decades. Only few results are available in the literature with regard to modern binders such as blended cements including fly ash, blast furnace slag, silica fume, limestone, burnt shale, etc. At present, the impact of most of these mineral additions on the corrosion performance of reinforced concrete is unknown. It appears that, on the basis of theoretical reasoning and the few available literature sources, modern binders tend to decrease the chloride threshold value compared with ordinary Portland cement; on the other hand, some mineral additions are clearly able to slow down chloride ingress into concrete. Nevertheless, the overall effect on the service life, i.e. the combined effect of altered chloride transport properties and altered chloride threshold values that together determine the duration of the initiation stage, is not yet clear.

ACKNOWLEDGEMENTS

Alonso, Sanchez and Garcia-Calvo gratefully acknowledge the financial support from Spanish MICINN for the financial support given to this research in BIA2011-22760.

REFERENCES

García Calvo J.L., Hidalgo A., Alonso C. & Fernández Luco L. (2010). Development of low-pH cementitious materials for HLRW repositories Resistance against ground waters aggression, *Cem. & Concrete Res.*, 40: 1290–1297.

Tuutti, K. (1982). CBI Research Report No. 4:82, Swedish Cement & Concrete Research Institute, Stockholm.

Concrete Repair, Rehabilitation and Retrofitting III – Alexander et al. (eds)
© 2012 Taylor & Francis Group, London, ISBN 978-0-415-89952-9

Durability properties of high performance metakaolin concrete in different curing conditions

M. Skazlić, A. Baricevic & M. Peric
Department of Materials, University of Zagreb, Croatia

ABSTRACT: The aim of this investigation was to determine the influence of curing regimes on mechanical properties (compressive strength) and durability properties (chloride diffusion coefficient and coefficient of capillary absorption) of high performance concretes with different addition of metakaolin. Concrete mixtures were prepared using different quantities of metakaolin and different water-cement ratios (0.40. 0.35). Two different curing regimes (laboratory conditions and on site curing) were applied to all concrete mixtures. Results from this experimental study are useful for application of high performance metakaolin concrete in structures exposed to aggressive environment, prepared strictly according to the instructions set below.

1 INTRODUCTION

At present, one of the greatest problems existing in concrete technology is concrete durability in aggressive environmental conditions. In such environments concrete structures deteriorate rapidly due to inadequate material design requirements, construction errors, and lack of structure maintenance. It is for this reason that high-performance concretes are increasingly used today. Having water/binder ratio lower or equal to 0.40 these concrete types achieve reduced permeability and consequently prolonged durability. Named properties are achieved using various mineral admixtures, such as silica fume, fly ash and slag.

Metakaolin is one of more recent types of mineral admixtures. It is obtained under controlled process as primary product, from kaolin clay in rotary kilns at about 800°C. The research carried out up to the present showed a positive influence of metakaolin on mechanical and durability properties of hardened concrete. However, these researches have not covered the influence of curing regimes on the properties of concrete with metakaolin admixture. And it is the curing regime that is of extreme importance for high-performance concrete with mineral admixtures. In this paper, influence of different curing regimes (laboratory and environmental conditions) is illustrated through the results of the durability and mechanical properties investigation.

2 EXPERIMENTAL WORK

The investigation was carried out on a total of six high-performance concrete mixtures (Table 1). The mixture parameters varied were water/cement ratio (0.40 and 0.35) and metakaolin content.

A portion of the specimens were cured in laboratory conditions at 95% relative humidity and 20 ± 2°C for 28 days. Plate-shaped specimens of 50 × 50 × 5 cm were exposed to outdoor environmental conditions immediately after preparation and were cured for 28 days by water splashing. In this way actual concrete curing on site was simulated.

2.1 *Results*

Compressive strength of concrete is tested on cubes of 150 × 150 × 150 mm at the ages of 2 and 28 days. Compressive strength is determined only on laboratory specimens since no influence of ambient exposure to compressive strength is expected. The test results are illustrated in Figure 1.

Chloride diffusion coefficient (D_{Cl-}) and capillary water absorption (S) were tested on cylinders

Table 1. Concrete compositions.

Material	M1	M2	M3	M4	M5	M6
Cement, kg	380	350	330	410	380	350
Water, kg	152	152	152	145	145	145
Aggregate, kg						
0–4 mm	831	831	831	886	886	886
4–8 mm	593	593	593	369	369	369
8–16 mm	554	554	554	591	591	591
Superplasticizer, kg	3.1	3.4	5.7	4.5	5.7	5.7
Metakaolin, kg	0	30	50	0	35	60
Metakaolin, %	0	9	15	0	9	17
Water/binder ratio	0.40	0.40	0.40	0.35	0.35	0.35

having 5 cm in height and 10 cm in diameter. The test results of durability properties at the specimen age of 28 days are presented on Figure 2 and 3.

3 DISCUSSION

3.1 *Influence of water-cement ratio on results*

As the water/cement ratio is reduced the 28-day compressive strength of the concrete without metakaolin is increased by 15% and that of the concrete with metakaolin by 11%. A reduction in water/cement ratio in all the mixtures led to a more rapid gain in strength (Fig.1).

The test results of durability properties show that as the water/cement ratio is reduced the properties of the concrete with and without metakaolin are improved (Figs. 2 & 3).

3.2 *Effect of metakaolin quantity on results*

As the result of the addition of metakaolin, compressive strength is reduced at 2 days and increased at 28 days. Metakaolin, similar to the other mineral admixtures induces slower development of compressive strength although; the increase of the metakaolin quantity assures higher compressive strengths at the age of 28 days. An increase in the metakaolin quantities results in a lower chloride diffusion coefficient and the capillary water absorption.

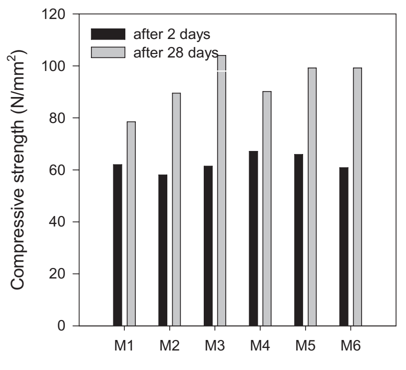

Figure 1. Compressive strength results after 2 and 28 days.

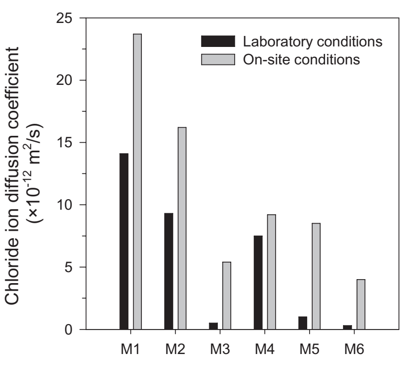

Figure 2. Comparison of chloride ion diffusion coefficient for laboratory and on-site conditions.

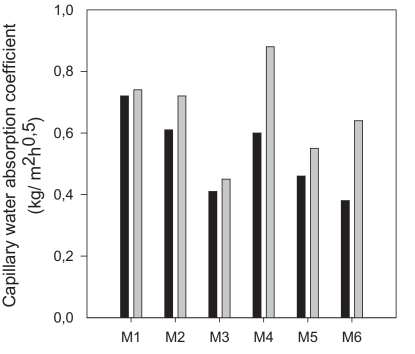

Figure 3. Comparison of capillary water absorption coefficient for laboratory and on-site conditions.

3.3 *Influence of curing regime*

All mixtures exhibited significantly poorer durability properties when cured in ambient conditions than in laboratory conditions.

4 CONCLUSIONS

According to the obtained results following conclusions are made:

– the reduction of water/cement ratio from 0.40 to 0.35 results in a more improved properties of the concrete containing no metakaolin;
– the addition of metakaolin has an influence on the early strength development; 2-day strengths are lower with metakaolin admixture;
– decrease in the amount of CH due to formation of secondary CSH with presence of metakaolin assures increase in 28-day compressive strength, and an improvement in durability properties;
– concretes with or without metakaolin cured in ambient conditions have poorer durability properties than those cured in laboratory conditions;
– 15% of metakaolin exhibits good test results of chloride diffusion coefficient regardless of the curing regime used.

The results discussed in this paper indicate that the use of high performance concrete containing metakaolin is justified in aggressive environmental conditions. For this reason, metakaolin should be grouped into Type II mineral admixtures, and a relevant European standard should be drawn up.

Concrete Repair, Rehabilitation and Retrofitting III – Alexander et al. (eds)
© 2012 Taylor & Francis Group, London, ISBN 978-0-415-89952-9

Quantification of anhydrous GGBFS particles in cement pastes subjected to organic acids: Comparison of selective dissolution and image analysis methods

J. Duchesne & O. Oueslati
Université Laval, Québec, Canada

ABSTRACT: Concrete for agricultural construction is often subject to aggressive environmental conditions. The alteration is translated to a decalcification, an increase of the porosity and a progressive dissolution of phases. Previous studies have shown that the use of Ground Granulated Blast Furnace Slag (GGBFS) largely improve the chemical resistance of the binder. Anhydrous GGBFS particles seem particularly resistant to the acid solution. The purpose of this study is to quantify anhydrous GGBFS particles in blended cement pastes as a function of acid exposition time in order to evaluate their acid resistance. The quantification of the anhydrous particles was measured by selective dissolution and by Back-Scattered Electron (BSE) images analysis. After 28 days of hydration, 60% of OPC and 44% of GGBFS particles were hydrated. The amount of anhydrous particles drops for both materials during acid immersion. After 2 months of acid immersion, the amount of anhydrous particles drops by 49 and 23% for OPC and GGBFS, respectively. This study confirms that GGBFS anhydrous particles present higher acid resistance than OPC.

1 INTRODUCTION

Intensification of farming practice is at the origin of environmental problems directly linked to the excess of effluents such as liquid manure and ensilage effluent. The agricultural effluents are quickly transformed under the effect of bacteria into organic acids. These effluents contain organic acids that constitute a severe chemical threat toward the concrete of agricultural structures. Acetic acid mimics well the aggressiveness of organic acids found in animal manure Bertron et al. (2005) and was used in this study as aggressive agent.

The concrete is a strongly basic environment with a pH greater than 13. In contact with an acidic solution, the chemical equilibrium of the cement hydrates is destabilized and the concrete will undergo an acido-basic reaction. This reaction is responsible for the alteration of the cement matrix that is translated to a decalcification of the material, an increase of the porosity and a progressive dissolution of phases (hydrated or anhydrous). Previous studies have shown that the use of ground granulated blast furnace slag (GGBFS) largely improve the acid chemical resistance of the binder. Anhydrous GGBFS particles seem particularly resistant to the acid solution (Oueslati 2011).

The purpose of this study is to quantify anhydrous GGBFS particles in blended cement pastes as a function of acid exposition time in order to evaluate their acid resistance. The quantification of the anhydrous particles is measured by selective dissolution method and by back-scattered electron (BSE) images analysis on the altered pastes.

2 MATERIAL AND METHOD

2.1 *Materials*

This study was conducted on cement pastes made with ordinary Portland cement (OPC), designated in American Standard as GU (General Use, containing a maximum of 5% limestone filler), blended with 80% of ground granulated blast furnace slag (GGBFS) as partial cement replacement by mass.

The immersion solution was composed of acetic acid (CH_3COOH), a weak organic acid, with a dissociation constant pKa of 4.76 at 25°C. The concentration of the acetic acid was 0.5 M at a pH of 2.8. To avoid hydration of anhydrous particles during the acid immersion, water was replaced by toluene ($C_6H_5CH_3$).

The solution was renewed every week throughout the duration of the experiment in order to maintain the pH of the solution at a value of 2.8.

2.2 *Specimen making and treatment*

Blended pastes containing 80% by mass of GGBFS were made at a water/cementitious material mass ratio (w/cm) of 0.27. Large amount of GGBFS was used because previous studies (Oueslati 2011) have shown that the use of ground granulated blast furnace slag (GGBFS) largely improve the chemical resistance of the binder. Cement replacement level by GGBFS as high as 80% was even better than 60%.

Paste specimens were demolded 24 hours after pouring and stored in wet room at 23°C and 100% RH for 27 days. At the end of the curing period, paste specimens were immersed for 15 days, 1 and 2 months in the acetic acid solutions (0.5M, pH 2.8) at solid-liquid volume ratio of 1/15. After immersion, specimen were slowly dried at room temperature. The external altered zone was easily removed from the specimen due to shrinkage cracking. The quantification of anhydrous particles was measured on these altered zones.

2.3 *Test methods*

The quantification of the anhydrous particles after acid immersion was measured by selective dissolution according to method proposed by Luke & Glasser (1987), Goguel (1995) and Chao (2007) and by back-scattered electron (BSE) images analysis as suggested by Mouret et al. (2001) and Chao (2007).

2.3.1 *Selective dissolution method*

The selective dissolution method is based on preferential dissolution. This technique preferentially dissolves the anhydrous cement particles and the hydration products leaving only the anhydrous GGBFS particles. This technique was run in triplicates on well homogenized sample of 0.25 g of blended pastes ground to <63µm.

2.3.2 *Image analysis method*

Polished sections of blended paste samples were observed under a JEOL JSM-840 A Scanning electron microscope equipped with an energy dispersive x-ray analysis system (EDXA).

Phase discrimination is based on BSE grey level distribution. To simplify the analysis, all images were captured with the same magnification (500 X), contrast and brightness. Image segmentation was the method used to separate the different phases. As the average BSE grey level is directly related to a phase of unique atomic number (Jones 1987, Gu 2003), the segmentation method used the histogram of the grey level distribution of different phases to discriminate each phase. Elemental composition measured by energy dispersive X-ray analysis (EDXA) was used to confirm the identity of each phase. Quantification is based on the number of pixel of each grey tone using an iterative algorithm.

3 RESULTS AND DISCUSSION

Figure 1 presents the evolution of anhydrous GGBFS particles content as a function of the acid immersion time measured by the selective dissolution method while figure 2 presents the same results measured by BSE image analysis.

After 28 days of hydration, 60% of OPC and 44% of GGBFS particles were hydrated. The amount of anhydrous particles drop for both materials during acid immersion. After 2 months of acid immersion, the amount of anhydrous particles drop by 44 and between 18 and 22% for OPC and GGBFS, respectively. This demonstrates the good chemical resistance of GGBFS anhydrous particles against acid attack.

Both methods, selective dissolution and images analysis, gave similar results even if the image analysis method tends to overestimate the quantity of anhydrous particles. GGBFS anhydrous particles present higher acid resistance than OPC. In this research, the goal was to quantifiy the anhydrous OPC and GGBFS particles in cement pastes submitted to an acidic environment. However, these two techniques can be useful to evaluate the hydration rate of OPC and GGBFS in different matrix.

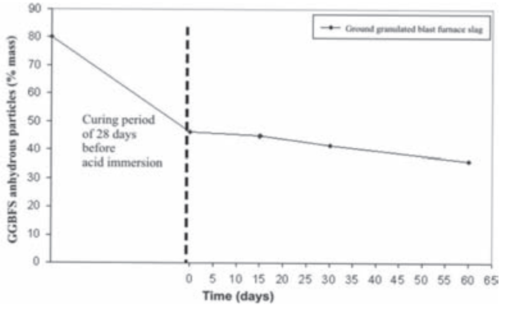

Figure 1. Evolution of the anhydrous GGBFS particles content measured by selective dissolution method.

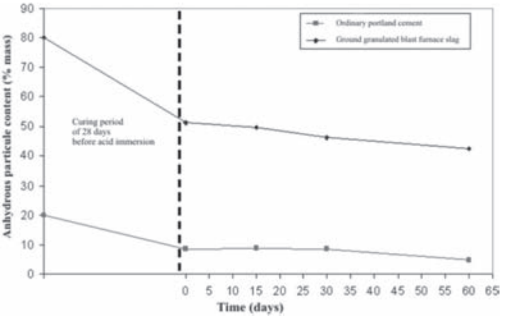

Figure 2. Evolution of the anhydrous particles content as a function of acid immersion time (image segmentation method).

Concrete Repair, Rehabilitation and Retrofitting III – Alexander et al. (eds)
© 2012 Taylor & Francis Group, London, ISBN 978-0-415-89952-9

Performance evaluation of limestone mortars for elevated temperature application in nuclear industry

K. Mohammed Haneefa & Manu Santhanam
Department of Civil Engineering, Indian Institute of Technology Madras, Chennai, India

F.C. Parida
Indira Gandhi Centre for Atomic Research, Kalpakkam, India

ABSTRACT: In fast breeder nuclear reactors, sodium is used as a coolant. Accidental spillage of sodium, which is at an operating temperature of 500–550°C, can cause damage to the structural concrete in several ways. For this reason, a sacrificial layer of limestone aggregate concrete is provided over the conventional siliceous aggregate concrete. This paper presents the performance evaluation of mortars at 550°C, in the absence of sodium, in order to understand the behavior under only thermal exposure. The mortars were made with limestone as fine aggregate and with four types of cement. Apart from studies on mortar with limestone and conventional cements, performance evaluation of geopolymer paste and mortars at elevated temperatures was carried out to study the suitability of this new technology for sodium resistant applications. The different mixes were ranked based on the performance in the compressive strength and mass loss tests and relative performance indices were developed.

1 INTRODUCTION

The alkali metal sodium is used as coolant fast breeder reactors. Accidental spillage of sodium at high temperature from pipes in inert equipment cells or inside reactor cavity can lead to various safety issues in fast breeder reactors due to sodium fire. To prevent the structural concrete from deterioration, a sacrificial layer of limestone aggregate concrete is provided over the conventional siliceous aggregate concrete (Chawla et al. 1985, Pramila et al. 2008, and Das et al. 2009).

Limestone is a sedimentary rock consisting of more than 50% of carbonates of calcium or magnesium. Calcite is the predominant mineralogical component of limestone (Gribble 1988). Impure varieties of limestone may also contain quartz, feldspar, pyrite, clay impurities like alumina and micaceous impurities like biotite. In carbonate aggregates like limestone, $CaCO_3$ decomposes into CaO and CO_2 at 800–900°C and further expands at elevated temperatures resulting in volume changes causing destruction. On the contrary, in siliceous aggregates, the major mineralogical component quartz changes its crystalline phase from α to β at 573°C. This causes siliceous aggregate to be poorer in thermal exposure conditions. In addition, specific heat capacity of calcareous aggregate is 10 times more compared to siliceous aggregates for rise in temperatures up to 600°C (Zing et al. 2011).

Geopolymers are materials that are obtained by alkali activation of pozzolans; the term was suggested by Davidovits in 1970s (Duxson et al. 2007). They are considered eco-friendly as their production does not involve any cement, hence no emission of CO_2. Limited research on performance of geopolymer composites at elevated temperatures showed that their temperature stability is good compared to conventional cement based systems (Kong et al. 2010).

2 MATERIALS AND METHODS

Crushed limestone was used as fine aggregate, which possessed a bulk density, specific gravity and water absorption of 1602 kg/m^3, 2.71 and 0.35% respectively. Mortars were prepared with four types of cement namely ordinary Portland cement (OPC), Portland pozzolana cement (PPC), Portland slag cement (PSC) and high alumina cement (HAC) for a water to cement ratio of 0.55. The effect of different water to cement ratio (w/c) on thermal performance was studied using ordinary Portland cement for a range of 0.40 to 0.60. A specimen size of $25 \times 25 \times 25$ mm^3 was chosen based on safety and handling issues related to experimental setup for sodium interaction studies. Mortars specimens with a mix proportion of 1:2.75 (cement to sand) were cast and cured for 28 days. Compressive strength and mass of specimens were determined before and after thermal exposure. Thermal exposure test was performed in a muffle furnace with an average rise in temperature of 0.60°C/second and the post heated specimens were cooled in air. The specimens were exposed to 550°C for 10, 20 and 30 minutes. X-ray diffraction of powdered samples was carried out to study the mineralogy before and after thermal exposure. Thin section petrography was used to study the petrography of limestone mortar and the porosity of cement paste phase in the mortars qualitatively. Scanning electron microscopy was used to capture backscattered electron images on polished epoxy impregnated samples to study the formation of cracks due to thermal exposure.

To obtain different geopolymer paste, class F fly ash was activated using NaOH solutions by varying the concentration of NaOH solution as 8M, 12M, 16M and 18M. Activating solution to fly ash ratio (A/F) was fixed based on a minimum flow of 150 mm to ensure enough workability to cast the mortar into the moulds. In this respect, A/F was fixed as 0.45 for 8M and 12M, and 0.5 for 16M and 18M solutions. Solid sodium silicate to solid NaOH ratio was fixed at 1.5 for all the mixes. Specimens thus prepared were stored at room temperature for 3 hours and were covered with polythene sheets to avoid evaporation of water, prior to curing at 80°C for 24 hours. Studies on geopolymer pastes were extended to mortar using crushed limestone sand and the fly ash to sand ratio was maintained at 1:2. Thermal exposure studies on conventional cement based mortars were repeated on geopolymer mixes.

3 RESULTS AND DISCUSSION

Mass losses of limestone mortars of ordinary Portland cement were found to be more at higher w/c ratios. A marginal change in mass loss was observed for w/c ratios up to 0.50, but the rate of mass loss increased with higher w/c ratios, which concludes that mass loss has a direct relationship with water to cement ratios. As the w/c ratio increases, compressive strength decreases with increase in exposure time. A marginal reduction in compressive strength was observed for w/c ratios up to 0.50; beyond this point, there was increased reduction in compressive strength with higher w/c ratios.

Based on the performance in the compressive strength and mass loss tests, the eight mixes were ranked separately for the performance with respect to mass loss and compressive strength. The ranking was done on a scale from 1 to 10, 1 being the best and 10 being the worst. This allows a direct comparison of the performances of all eight mortars—M5 with a w/c ratio of 0.60 with OPC is the worst, while the mix M8 with OPC for a w/c ratio 0.40 is the best, which indicates that the effect of water to cement ratio is significant irrespective of type of cement.

Geopolymer paste showed increment in strength with respect to increment in exposure duration and molarities of NaOH solution, except for the mix with 18 M NaOH. Geopolymer mortars showed reduction in strength with increment in exposure duration. Except for the mix with 18 M NaOH, reductions in strength were within 10%. In general, performance of geopolymer composites was comparatively better than conventional cement based systems.

4 CONCLUSIONS

For the mortars with OPC, mixes with lower water to cement ratios ranked high. Among the mortars with different type of cements, Portland pozzolana cement ranked high at similar exposure conditions. Thin section images were effectively used for petrographic interpretation of mortars before and after thermal exposure. Geopolymer pastes exhibited increment in compressive strength with increased duration of exposure, except for the mix made with 18 M NaOH solution. Geopolymer mortars showed reduction in strength with increasing exposure duration.

ACKNOWLEDGEMENT

Partial financial support from Indira Gandhi Centre for Atomic Research, Kalpakkam, Chennai, is gratefully acknowledged.

REFERENCES

Arioz, O. 2007. *Fire Safety Journal, 42:* 516–522.

Chawla, T.C. & Pederesen, D.R. 1985. *Nuclear engineering and design*, 88: 85–91.

Das, S.K., harma, A.K.. Parida, F.C. & Kashinathan, N. 2009. *Construction and building materials,* 23: 3375–3381.

Duxson, P., Fernadez-Jimenez, A. & Provis, J.L. 2007. *The advances in geopolymer Science and Technology,* 42: 2917–2933.

Gribble, C.D. 1988. Rutley's elements of mineralogy, 27th edition, *Unwin Hyman*, London.

Kong, D.L.Y. & Sanjayan, J.G. 2010. *Cement and Concrete Research,* 40: 334–339.

Mehta, P.K. & Moteiro, P.J.M. 2006. Concrete- Microstructure, properties and Materials, Third Edition, *Tata McGraw Hill*, New Delhi.

Pramila, M., Sivasubramanian, K., Amarendra, G. & Sundar, C.S. 2008. *Journal of nuclear materials,* 375: 263–269.

Xing, Z., Beaucou, A.L., Hebert, R., Noumowe, A. & Ledesert, B. 2011. *Cement and Concrete Research* 41: 392–402.

Concrete Repair, Rehabilitation and Retrofitting III – Alexander et al. (eds)
© 2012 Taylor & Francis Group, London, ISBN 978-0-415-89952-9

Optimization of fly ash based geo-polymer concrete

A. Arjun
Indian Institute of Technology Madras, Chennai, India

J. Michel Laye
Lafarge Aggregates and Concrete India Pvt. Ltd., Chennai, India

ABSTRACT: The implementation of the Response Surface Methodology and the Doehlert Experimental Design in order to optimize the constituents for the production of Geo-polymer concrete using sodium activators; fly ash and GGBS (Ground Granulated Blast furnace Slag) being the source materials. From the results of preliminary experimental runs, three variables (i.e., percentage of fly ash, molarity (M) of the hydroxide solution, and relative percentage of silicate solution) have been identified as the potential variables. Thirteen experimental runs as designed by the Doehlert Design fitted very well to the experimental data that it could be used to navigate the design space according to the Analysis of Variance results. The results obtained were exploited using response surface methodology. These responses have been represented and studied in all experimental regions of percentage of fly ash, molarity concentration, and relative percentage of silicate solution. Optimization of geo-polymer concrete designs for economic viability and incorporation into the infrastructure industry has been carried out. The optimal geo-polymer concrete for a given set of domain is obtained with a global desirability of about 98 percent. The Doehlert design model and assessments can help in making optimal decisions on the constituents related to the production of geo-polymer concrete under any given set of domain and environmental conditions.

1 INTRODUCTION

Concrete usage around the world is second only to water. Ordinary Portland cement (OPC) is conventionally used as the primary binder to produce concrete. The amount of carbon-di-oxide released is in the order of one ton for every ton of OPC produced. So, one of the ways to produce environmentally friendly concrete is to replace OPC with by-product material such as fly ash, slag, rice husk etc.

In the case of geo-polymers made from fly ash, the role of calcium in these systems is very important, because its presence can result in flash setting and therefore must be carefully controlled (Lloyd and Rangan 2009).

In this paper, the geo-polymer concrete was framed out of the three variable factor involved in the mix(fly ash 75 to 95%, Molarity of the Hydroxide Solution 5 to 12M and silicate solution 40 to 100%). Sodium based activators were used in the process to dilute the geo-polymer mix.

After screening of the important variables the conventional method used for optimization is the "one factor at a time" method is replaced by Doehlert experimental design of Response Surface Methodology (RSM). . Several researchers have applied these techniques for optimization of different process parameters (Vanot et al., 2002; Dutra et al., 2006; Imandi et al., 2007). Hence, the present study reports the application of Doehlert experimental design to optimize the strength and the cost of the geo-polymer mixes with reference to the above mentioned factors influencing the experiment.

2 EXPERIMENTAL DESIGN

Once the variables having the statistically significant influence on the responses were identified, a Doehlert experimental design [Doehlert, 1970] was used to optimize the levels of these variables. The number of experiments required (N) is given by $N = n^2 + n + n_0$, where n is the number of variables and n_0 is the number of center points. In this study, three factors (i.e., variables) percentage of fly ash (X_1), molarity of the hydroxide solution (X_2) and the percentage of silicate solution (X_3). Therefore, 13 experiments were conducted along with the reference mix in order to keep track on the change in the environmental conditions. The second degree polynomial (Equation. (1)) was fitted to the experimental data by using the statistical package MINITABS 15 to estimate the response of the dependent variable and the regression coefficients.

$$Y = b_0 + b_1X_1 + b_2X_2 + b_3X_3 + b_{11}X_1^2 + b_{22}X_2^2 + b_{33}X_3^2 + b_{12}X_1X_2 + b_{23}X_2X_3 + b_{13}X_1X_3 \quad (1)$$

Where Y is predicted response, X_1, X_2, X_3 are independent variables, b_0 is offset term, b_1, b_2, b_3 are the coefficients for linear effects, b_{11}, b_{22}, b_{33} are the coefficients for squared effects and b_{12}, b_{23}, b_{13} are the coefficients for interaction terms. The significance of the coefficients was evaluated by multiple regression analysis based upon the F-test with unequal variance ($P < 0.05$, $P < 0.01$ and $P < 0.001$).

3 RESULTS AND DISCUSSIONS

The results for 1, 3, 7, 28 and 56 day strengths for all the 13 geo-polymer mixes are as shown in the table 1. The responses dealt are slump retention, 28 and 56 day compressive strengths and cost analysis.

3.1 *Trends in 28 and 56 day compressive strengths and cost*

A detailed statistical modeling of the 28 and 56 day compressive strengths has been carried out in the chosen domain. For both the test days, it was seen that as the fly ash content gets decreased, the strength soar up on the loss of slump retention. Molarity plays a positive role in enhancing the strength as well as the cost, where as silicate has a positive role in enhancing the strength and negative role in the cost analysis of the geo-polymer concrete.

Table 1. Test results for compressive strength.

	Compressive strengths in MPa				
Mix	1 day	3 day	7 day	28 day	56 day
Reference mix 1	7.11	15.78	20.44	29.93	32.15
Geo mix 1	4.00	8.22	12.00	22.67	28.74
Geo mix 2	5.78	16.44	28.89	45.78	43.33
Geo mix 3	2.22	4.89	10.00	18.81	24.67
Geo mix 4	5.33	10.67	18.00	29.56	34.44
Geo mix 5	2.89	6.22	8.22	14.37	18.67
Geo mix 6	6.22	12.00	14.37	36.89	44.44
Geo mix 7	3.56	7.34	13.11	28.15	24.00
Geo mix 8	2.22	6.67	12.00	27.26	32.89
Reference mix 2	7.33	15.33	19.78	28.44	33.78
Geo mix 9	1.78	5.11	11.33	27.11	30.89
Geo mix 10	1.78	3.11	5.56	14.96	18.44
Geo mix 11	7.11	9.56	13.33	21.93	26.44
Geo mix 12	4.22	8.00	10.22	15.11	17.56
Geo mix 13	3.56	6.67	10.00	15.11	16.89
Reference mix 3	7.56	14.67	19.11	28.8	30.22

3.2 *Final optimization*

Finally, the main objective of the paper is to determine the optimal set of conditions for the 28 and 56 day compressive strength and the cost variations with respect to fly ash content, molarity of the solution and silicate sol. The first step was to evaluate the values of the 28 day & 56 day strengths and cost in a range suitable for the economic purpose.

The following domain has been chosen in order to match the viability of the economic purpose and to attain suitable range of 28 and 56 day strengths.

	Goal	**Lower**	**Target**	**Upper**
Cost INR	Minimum	4000	4000	5000
28 day CS	Maximum	30	35	35
56 day CS	Maximum	35	40	40

To optimize all responses under the same conditions is difficult because the interest region of factors is different. To avoid this and to find a compromise, we have resorted to the function of desirability using the software MINITABS. The characteristics of the sample are shown in the table 2 with those calculated from the model. It is important to note the good argument found between the experimental values and those calculated from the model.

4 FUTURE WORK

Further research is to be conducted in order to benchmark the geo-polymer concrete with respect to conventional concrete and develop a rather more sophisticated mathematical solution in order to develop in it any domain possible.

Also, we may consider replacing geo-polymer concrete with the conventional concrete, as it is eco-friendly and develop integrated IS codes for the proportioning of the geo-polymer concrete mixes.

Table 2. Calculated and experimental responses corresponding to the optimal geo-polymer concrete.

	28 day strength	56 day strength	cost
Response	MPa	MPa	INR
Calculated	41.78	40.00	4315
Experimental	40.66	39.11	4485

Concrete Repair, Rehabilitation and Retrofitting III – Alexander et al. (eds)
© 2012 Taylor & Francis Group, London, ISBN 978-0-415-89952-9

Durability studies on glass fiber reinforced High Performance Concrete with fly ash as admixture

H. Sudarsana Rao & Vaishali G. Ghorpade
JNTUA College of Engineering, Anantapur, India

ABSTRACT: Cementatious materials have been used by mankind for construction from time immemorial. The every rising functional requirement of the structures and the capacity to resist aggressive elements has necessitated to develop new concrete composites materials to meet the higher performance and durability criteria. The environmental factors and pressure of utilizing waste materials from industry have also been the major factors in new developments in the field of concrete technology.

High performance concrete has been used in various structures all over the world since last two decades. The development of High Performance Concrete (HPC) has brought about the essential need for additives both chemical and mineral to improve the performance of concrete. Most of the developments across the work have been supported by continuous improvement of these admixtures.

Hence an attempt has been made in the present investigation to study the durability behavior of glass fiber-reinforced High Performance Concrete. To attain the set out objectives of the present investigation, an aggregate binder ratio of 2.0 and w/b 0.30 has been chosen and cement has been replaced partially with fly ash in four different percentages viz. 0, 10, 20 and 30% and glass fibers by with volume percentages of 0, 0.5, 1.0, & 1.5% respectively have been used. Hardened concrete is tested for permeability properties. The results are quite encouraging for use of glass fibers in producing durable High Performance Concrete. The various details of permeability tests on glass fiber reinforced high performance concrete will be presented in this paper.

1 INTRODUCTION

High-performance concrete (HPC) not only have high strength but also have good durability. The main reasons to use HPC to solve the problem of corrosion of steel. (Faguang Leng et al., 2000). The resistance to chloride penetration is one of the simplest measures to ensure the durability of concrete. Since high resistance to chloride penetration can be directly related to low permeability that dominates the deterioration process in concrete structures. This provides a firm basis for the use of high-performance concrete having very low permeability and high durability in the actual structures under severe conditions. (Byung Hwan Oh et al., 2002). The inclusion of fly ash, silica fume, and ground granulated blast furnace slag all significantly reduced the chloride permeability of concrete, as compared with concrete containing Portland cement only. (Ellis, W.E., Jr., Riggs, E.H., & Butler, W.B. 1991)

2 EXPERIMENTAL DETAILS

The cementious materials used in this study were ordinary Portland cement (OPC) 53 grade satisfying IS: 8112-1989. Natural river sand, with a fineness modulus of 3.24 and specific gravity 2.68 was used as fine aggregate. Crushed granite metal with 50% passing 12.5 mm and retained on 10 mm sieve and 50% passing 20 mm and retained on 12.5 mm sieve with specific gravity of 2.73 were used. The Fly ash is obtained from Rayalaseema thermal power station Muddanur, Kadapa district. Specific Gravity of fly ash is 2.20.The specific gravity of the fiber was 2.68. In the present investigation 12 mm fiber length is used. The super plasticiser used in this experiment is SP 337. It is manufactured by FOSROC, Bangalore (India). The control mix was cast using OPC, while the other mixes were prepared by replacing part of cement with fly ash at different percentages i.e. 0%, 10%, 20% and 30% and glass fibers by 0, 0.5, 1.0 and 1.5% respectively with water/binder ratio 0.35 at aggregate binder ratio 2.0. The dosage of super plasticizer is kept constant.

3 DURABILITY TEST

3.1 *Rapid Chloride Permeability Test*

In the present study, RCPT was carried out using disc shaped test specimens of nominal size 100 mm diameters × 50 mm thickness, cut from the 100 mm diameter × 200 mm high cylinders. The test set-up consisted of two acrylic plastic chambers having grooved recesses on one face and closed at the other end. The specimen end faces can snug-fit into the open faces of the chambers. One of the cells is filled with NaCl solution (concentration 2.4 M), while the other is filled with 0.3 M NaOH solution. Copper mesh electrodes are mounted in the cells such that they are in contact with the end faces of the specimen. The whole assembly is held together by long threaded rods with wing nuts at both ends.

The disc shaped specimen, taken out from the curing chamber, is coated with quick setting cooxy on its curved faces and water saturated for 72 hours. It is then mounted with acrylic chambers and assembled. After checking for leak proofness, the chambers are filled with the chloride and hydroxide solutions as stated earlier. A potential difference of 60 V is applied a between the electrodes. The electrochemical cell, constituted by this assembly, results in the rapid migration of chloride ions from the sodium chloride solution to the sodium hydroxide solution, via the pore net work offered by the concrete specimen. The movement of chloride ions is proportional to the intensity of electric current as measured by an ammeter in the power source. The test is carried out for duration of 6 hours and the current is measured at one hour intervals. The total charge carried is computed using Simpson's 1/3rd rule. The test was carried out at the age of 28 days.

4 RESULTS AND DISCUSSIONS

4.1 *Durability test*

4.1.1 *Effect of fly ash content on Chloride Ion Permeability*

The Chloride Ion Permeability in terms of total charge passed in coulombs attained a maximum value of 2128 Coulombs and a minimum value of 249 Coulombs between 0% to 30% of Fly ash content respectively for A/B ratio of 2.0 showing a decreasing rate of permeability with increasing fly ash content. A similar performance was observed for different mixes as shown in the Table 1.

5 EFFECT OF GLASS FIBER CONTENT ON CHLORIDE ION PERMEABILITY

The Chloride Ion Permeability in terms of total charge passed in coulombs attained a maximum value of 2128 Coulombs and a minimum value of 249 Coulombs between 0% to 1.5% Glass Fiber content respectively for A/B ratio of 2.0, showing a decreasing rate of permeability with increasing Glass Fiber content as shown in the Table 1.

Table 1. Fly ash:10% W/C:0.3

Time hrs	G.F- 0%		G.F-0.5%		G. F- 1%		G.F- 1.5%	
0–1	43	45	29	26	24	25	21	22
1–2	41	42	27	24	23	22	19	20
2–3	39	42	25	26	23	22	20	19
3–4	42	39	24	25	21	21	18	18
4–5	38	37	21	24	19	20	18	18
5–6	35	35	21	24	19	20	16	16
R.C.P in columbs	857	864	529	536	464	468	403	407
Average R.C.P in columbs	861		533		466		405	

The Chloride Ion Permeability gives good results when the fly ash content and glass fiber increasing but the compressive strength and split tensile strength results are good for 10% fly ash replacement and 1.0% glass fiber. So the optimum dosage recommended for producing HPC may be 10% fly ash replacement and 1.0% glass fiber.

As per classification system adopted by ASTM C-1202[5], if the charge in coulombs is between 1000–100, then the permeability can be designated as very low and the concrete can be said as HPC. The test result stands at 773 Columbs; It can be treated as low permeable HPC.

6 CONCLUSIONS

1. With the increase in fly ash content from 0 to 30% there is a decrease in chloride permeability of Glass Fiber Reinforced High Performance Concrete.
2. With the increase in Glass fiber content from 0 to 1.5% there is marginal decrease in chloride permeability of Glass Fiber Reinforced High Performance Concrete.
3. Within the tested limits the concrete can be said as low permeable HPC as it is satisfying the strength criteria and also durability aspect as per ASTM standards.

REFERENCES

1. An experimental study on the properties of resistance to diffusion of chloride ions of fly ash and blast furnace slag concrete by Faguang Leng et al., Cement and Concrete Research journal,Vol. 30, Iss-6, June-2000, Pg. 989–992.
2. Development of high-performance concrete having high resistance to chloride penetration by Byung Hwan Oh et al., *Nuclear Engineering and Design, Volume 212, Issues 1–3, March 2002, Pages 221–231.*
3. Comparative results of utilization of fly ash, silica fume and ggbfs in reducing the chloride permeability of concrete. in: durability of concrete. 2nd international conference. by Ellis, W.E., et al., pg. 443–458, 1991, volume-1.

Concrete Repair, Rehabilitation and Retrofitting III – Alexander et al. (eds)

Strength and sulphate resistance of rice husk ash concrete

D.B. Raijiwala
Department of Applied Mechanics, S V National Institute of Technology, Gujarat, India

I.U. Kundan
Department of Applied Mechanics, S V National Institute of Technology, Gujarat, India

ABSTRACT: The huge emission of CO_2 during the production of cement is prompting researchers to adopt a supplementary cementitious material for the production of concrete. Rice husk ash is a highly pozzolanic material which can be used for this purpose. Addition of rice husk ash to Portland cement forms a Calcium Silicate Hydrate (C-S-H) gel around the cement particles which is highly dense and less porous. Apart from the pozzolanic effect, the particle size of rice husk ash provides a filler effect which improves the durability of concrete. In this paper, properly burnt and grinded rice husk ash has been replaced by 10%, 15%, 20% and 30% weight of cement in the production of ordinary concrete. The hardened properties of rice husk ash concrete are evaluated by compressive test, split tensile test, flexural test, and pull out test along with sulphate resistance test which is performed to assess the durability properties of hardened rice husk ash concrete.

Keywords: Rice husk ash; ordinary concrete;

1 RICE HUSK ASH

Rice husk is an agricultural by-product. It constitutes about 20% of the weight of rice. It contains 50% cellulose, 25–30% lignin, and 15–20% of silica. When rice husk is burnt rice husk ash (RHA) is generated. On burning, cellulose and lignin are removed leaving behind silica ash. The controlled temperature and environment of burning yields better quality of rice husk ash as its particle size and specific surface area are dependent on burning condition.

Rice husk ash (RHA) is a very fine pozzolanic material. The utilization of rice husk ash as a pozzolanic material in cement and concrete provides several advantages, such as improved strength and durability properties, reduced material costs due to cement savings, and environmental benefits related to the disposal of waste materials and to reduced carbon dioxide emissions. Reactivity of RHA is attributed to its high content of amorphous silica, and to its very large surface area governed by the porous structure of the particles. Generally, reactivity is also favored by increasing the fineness of the pozzolanic material. However, grinding of RHA to a high degree of fineness should be avoided, since it derives its pozzolanic activity mainly from the internal surface area of the particles.

In the present investigation, rice husk ash was blended with ordinary Portland cement at various percentages by simple replacement method and a realistic assessment of the mechanical properties and sulphate resistance properties has been made and the results were compared with conventional Ordinary Portland cement concrete.

2 EXPERIMENTAL DETAILS

2.1 *Materials used*

Ordinary Portland Cement (OPC):	Conforming to IS 12269-1987 was used for the investigation is given in Table 1.
Graded fine aggregates:	Local clean river sand (fineness modulus of medium sand equal to 2.50) conforming to grading zone II of IS 383-1970 was used.
Graded coarse aggregates:	Locally available well graded aggregates of normal size greater than 4.75 mm and less than 12 mm.

3. TESTS CONDUCTED

(a) Compression test
(b) Split tensile test
(c) Pull out test
(d) Flexure test
(e) Sulphate resistance test (% loss in weight)

Table 1. Composition of OPC & RHA used for investigation.

Constituents	Cement	RHA
Cao	63.90	0.53
SiO_2	22.00	92.95
Al_2O_3	5.60	0.31
Fe_2O_3	4.00	0.26
MgO	1.70	0.55
SO_3	2.30	–
K_2O	–	2.06
Na_2O	–	0.08
LOI	1.10	1.97
Others	0.20	0.12

Table 2. Mix proportion of RHA blended concretes.

Mix designation	RHA (%)	Quantities (kg/m^3) Cement	RHA	Plasticizer (kg/m^3)	Slump (mm)
M25 (control)	0	408	0	2.9	111
R10	10	368	40	3.18	105
R15	15	347	61	3.26	98
R20	20	327	81	3.65	80
R30	30	286	122	6.10	35

Water to binder ratio [C+RHA] 0.54; sand 647 kg/m^3; and aggregate 1095 kg/m^3;

4 RESULTS AND DISCUSSIONS

The results of various tests performed are given below. The following observations have been made:

- As the percentage of rice husk ash concrete increases, the slump decreases because rice husk ash is a hygroscopic material. But this can be compensated by slightly increasing the plasticizer content.
- To maintain workability, the plasticizer requirement of 30 percent replaced rice husk ash concrete is very high and hence, because of slump loss considerations, it is not advisable to replace 30% rice husk ash by weight of cement in the production of ordinary concrete.
- The 7 day strength of rice husk ash concrete is less than ordinary portland cement concrete and it decreases as the rice husk ash percentage increases, possibly because the pozzolanic reaction has not started and the strength is only due to the filler effect of rice husk ash particles and C-S-H gel formation of cement particles.
- The 28 day strength of rice husk ash concrete up to 20% replacement is equivalent to ordinary portland cement concrete.

Table 3. Compression test.

Days	Compression test results (MPa)				
	M25	R10	R15	R20	R30
7	24.8	22.7	21.2	20.8	13.4
28	29.2	30.2	30.4	29.9	23.3
56	31.3	33.2	34.8	33.9	27.1

Table 4. Split-Tensile Test.

Days	Split-Tensile test results (MPa)				
	M25	R10	R15	R20	R30
7	2.36	2.23	2.17	1.93	1.15
28	2.68	2.81	3.12	2.71	2.05
56	3.05	3.12	3.61	3.26	2.78

Table 5. Flexure test.

Days	Flexure test results (MPa)				
	M25	R10	R15	R20	R30
7	3.14	2.70	2.58	2.40	1.57
28	3.87	3.97	4.07	4.05	3.58
56	4.17	4.22	4.37	4.27	3.92

Table 6. Pull-Out test.

Days	Pull-Out test results (MPa)				
	M25	R10	R15	R20	R30
7	6.94	5.55	4.86	4.51	2.52
28	9.19	9.54	9.89	9.71	8.33
56	9.89	10.24	10.76	10.06	8.85

- From the figures of cubes immersed in sulphate solution for 56 days we can see that rice husk ash specimens offered better resistance to sulphate attack as compared to OPC specimens.
- From 56 days results, we can say that with the passage of time, the strength of rice husk ash concrete increases at a faster rate as compared to ordinary ortland cement concrete. Also, from the results, we can observe that up to 15% replacement of rice husk ash, the strength is the highest while beyond that it starts decreasing gradually. Hence, 15 percent replacement levels can be thought of as an optimum replacement level from strength as well as workability considerations.

5 CONCLUSION

From this study we can conclude that 15% is optimum replacement of rice husk ash by weight of cement in the production of ordinary concrete from strength as well as workability considerations.

Concrete Repair, Rehabilitation and Retrofitting III – Alexander et al. (eds)
 ISBN 978-0-415-89952-9

Improvement of repairing mortars in cold environments using coal bottom ash

C. Argiz & E. Menéndez
Instituto de Ciencias de la Construcción Eduardo Torroja (CSIC), Madrid, Spain

M.A. Sanjuán
Instituto Español del Cemento y sus Aplicaciones (IECA), Madrid, Spain

ABSTRACT: Durability in cold environments of mortars made of ordinary Portland cement, bottom ash and pulverized fuel fly ashes obtained from a coal electrical power stations in Spain have been investigated. This paper presents the experimental investigations carried out to study the effect of use of bottom ash (the coarser material, which falls into furnace bottom in modern large thermal power plants and constitute about 10–15% of total ash content of the coal fed in the boilers) as a replacement of fly ash. The performance of both fly and bottom ashes was investigated in terms of the hydration characteristics and microstructure, when exposed to cold environments. The following compositions were considered: Cement + (fly ash + bottom ash) replacement level up to 35%. The (fly ash + bottom ash) consisted of a bottom ash replacement of 50 and 100% of fly ash in the ashes mix. Use of fly ash beyond 35 percent is allowed in Europe, but the use of bottom ash is presently not permitted as pozzolanic addition in cement nor concrete. The use of coal bottom ash in Portland cement is a new dimension in pozzolanic repairing mortars cement and if applied in standarized Portland cement would revolutionize the cement industry, by economizing the production cost and decreasing the ash content. From the results, the use of bottom ash up to 15 percent as pozzolanic addition in cement repairing mortars is strongly recommended.

1 INTRODUCTION

Coal bottom ash (BA) utilisation is an interesting subject of research for economical, environmental and technical reasons. By contrary, the properties of pulverized fly ash have been extensively reported in the literature in comparison with other additions. Traditionally, bottom ash is adequate to substitute natural aggregates (Ramme et al., 1998).

Freezing of water in mortar pores makes the water in the concrete to expand and causes disruption of mortar. In general, the stronger the mortar the more resistant it is. But the performance of low strength mortars can be improved by proper materials selection.

2 EXPERIMENTAL

Coal bottom ash (BA) and fly ash (FA) used in this study were obtained from a Spanish Power Station. It consumes coal from South Africa (90%) and Colombia (10%). A CEM I 42.5 N (EN 197-1:2011) was employed to prepare the cement mixtures. Its specific surface Blaine was of 4050 m^2/kg and compressive strength of 50.98 MPa at 28 days.

Table 1 shows the codes of all the mixes produced and studied. The mortars were prepared accoding to EN 196-1:2005.

Table 1. Cement mixtures of the bottom ash (BA) with fly ash (FA) and cement (CEM I 42.5 N).

	Fly ash + bottom ash mix codification				
Cement mix	% Material	α	β	λ	Ω
CEM I	Fly ash	0%			
	Bottom ash	0%			
	Cement	100%			
CEM II/A-V*	Fly ash		10%	5%	0%
	Bottom ash		0%	5%	10%
	Cement		90%	90%	90%
CEM II/B-V*	Fly ash		25%	12.5%	0%
	Bottom ash		0%	12.5%	25%
	Cement		75%	75%	75%
CEM IV/A-V*	Fly ash		35%	17.5%	0%
	Bottom ash		0%	17.5%	35%
	Cement		65%	65%	65%

* Mix of bottom ash (BA) and fly ash (FA).

3 RESULTS AND DISCUSSION

The chemical compositions of the bottom ash (BA), fly ash (FA) and cement determined by XRF are given in Table 2. The sum of $SiO_2 + Al_2O_3 + Fe_2O_3$ of the bottom ash is 85.6%, which is a similar value to the one for FA (84.4%) which means that this fly ash belongs to ASTM C 618-08a Type F fly ash ($S + A + F \geq 70.0\%$).

3.1 *Pore size distribution*

The pore size distribution determined by mercury pore intrusion (MIP) at 28 days in mixtures with a high amount of BA shows big pores which became smaller when the BA is partially replaced by FA (Figure 1). As expected, after 90-days, hydration products from ashes filled partially the capillary pores above 0.5 μm. Therefore, the width of pore diameter distribution curves became narrower and, finally, their main peak was centered at 0.1 μm.

3.2 *Freeze-thaw resistance*

The Relative dinamic modulus (RDM) evidences a clear trend depending on the amount of ash replacing cement in the mixture. As much ash in the mix, the lower RDM over time (number of cycles) (Figure 2). As expected, the lowest expansion results (Figure 3) were found in the reference cement without any ash (CEM I-α). But also, these data are similar to CEM II/A-V*-β (with FA), this fact disagrees with the RDM results.

Figure 3 shows the increase of volume of the mortars along of 56 cycles of freeze-thaw resistance testing. As expected, the lowest expansion results were found in the reference cement without any ash (CEM I-α). But also, these data are similar to CEM II/A-V*-β (with FA), this fact disagrees with the RDM results, where CEM II/A-V*-β presented lower values than CEM II/A-V*-Ω, with only bottom

Table 2. Chemical composition of the bottom ash (BA), fly ash (FA) and cement (CEM I 42.5 N).

	Chemical composition (%)		
Parameter	Cement	Fly ash (FA)	Bottom ash (BA)
SiO_2	20.9	50.5	52.2
Al_2O_3	4.3	28.9	27.5
Fe_2O_3	3.5	4.7	6.0
CaO	62.7	5.0	5.9
MgO	1.9	1.8	1.7
SO_3	3.4	0.21	0.13
K_2O	0.9	0.80	0.57
Ti_2O_5	0.25	1.56	1.53
P_2O_5	0.10	0.76	0.74
LOI	3.69	3.6	1.8
Soluble residue*	1.04	71.3	75.7
Cl^-	0.023	0.00	0.001

* Na_2CO_3 method.

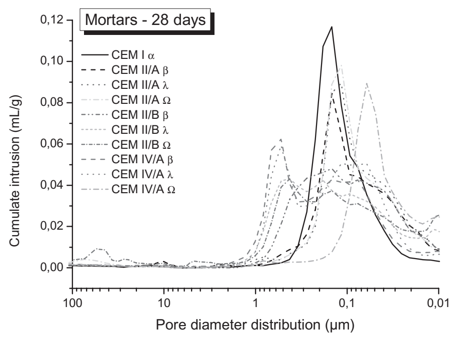

Figure 1. Cumulative mercury intrusion porosimetry (MIP) at 28 days.

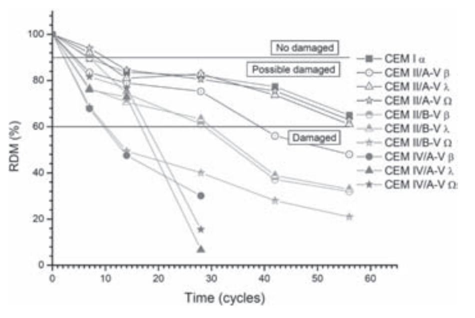

Figure 2. Relative dinamic modulus of mortars made of fly ash and bottom ash exposed to freeze-thaw resistance testing (56 cycles).

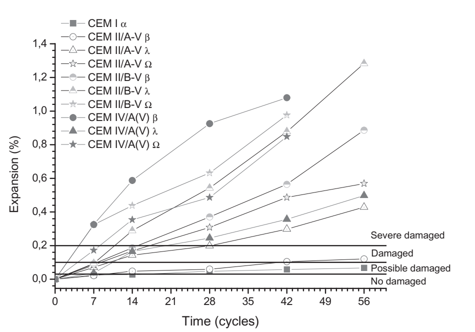

Figure 3. Expansion of mortars without any addition (α) and made of low LOI fly ash (β) and bottom ash (Ω) or a mixture of them (λ) exposed to freeze-thaw resistance testing (56 cycles).

ash replacement, or with the same proportion of BA & FA (λ).

4 CONCLUSION

- Partial or complete replacement of fly ash by bottom ash in Portland-fly ash and pozzolanic cements has a significant effect on the freeze-thaw resistance. However, bottom ash (BA) exhibited a better freeze-thaw resistance as compared to fly ash (FA) especially with higher percentages of substitution.
- Because of the lower loss on ignition (LOI) of bottom ash (BA) than fly ash (FA), repair mortars made of OPC and BA present a better performance in cold environments as result of the higher freeze-thaw resistance.
- Coal bottom ash (BA) chemical composition is quite similar to that of the fly ash (FA) supplied by the same electrical power plant.

Concrete Repair, Rehabilitation and Retrofitting III – Alexander et al. (eds)
© 2012 Taylor & Francis Group, London, ISBN 978-0-415-89952-9

TiO_2 TRC—New features of TRC by titanium dioxide modifications

W. Brameshuber & C. Neunzig
Institute of Building Materials Research of RWTH Aachen University, Aachen, Germany

ABSTRACT: By the addition of titanium dioxide (TiO_2), new fields of application of textile reinforced concrete can be opened up. As a consequence, textile reinforced concrete shall feature pollutant decomposing and self-cleaning properties. In this paper, the effects of the change of different parameters on the pollutant decomposing properties are presented and the use of rhodamine B to assess the self-cleaning properties of fine grained concretes is classified.

1 INTRODUCTION

Textile reinforced concrete consists of fine grained concrete and of inserted technical textiles made e. g. of alkali-resistant (AR) glass or carbon. The advantages of textile reinforced concrete are manifold. In contrast to traditional steel reinforced concrete, the concrete cover can be reduced to a few millimetres because there is no risk of corrosion. Hence, it becomes possible to manufacture filigree, thin-walled components and consequently to build light structures. The surface of the components can be designed arbitrarily and manufactured with a high surface quality.

By the use of nanoparticles made of titanium dioxide (TiO_2), new fields of application and additional functionalities as e. g. self-cleaning and pollutant decomposition are opened up for textile reinforced concrete.

2 MATERIALS

As reference mix, a fine grained concrete mix was used which is based on Brockmann (2005) and further developed within the framework of Collaborative Research Centre SFB 532 (2008) "Textile Reinforced Concrete". The mix design of this grey fine grained concrete is illustrated in Table 1.

At mixes modified with TiO_2, the inert quartz powder was proportionately exchanged by the respective TiO_2. For the examinations presented here, a TiO_2 with a BET-surface of 6 m²/g was used. 5% by mass related to the cement content were added.

The water content was varied and mixtures with $w/c_{(eq)}$-values of 0.4, 0.5, 0.6 and 0.7 were used.

Having been stripped from the formwork, the manufactured test specimens were stored in different ways. Three different storage types were taken into account at the investigations:

- L5: 5 days of water storage at 20°C followed by a storage at 20°C and a relative humidity of 65%,
- 20/65: storage at 20°C and a relative humidity of 65% and
- CO_2-free: CO_2-free storage at 20°C and a relative humidity of 85%.

3 RESULTS

3.1 *Self-cleaning*

For the tests on self-cleaning, rhodamine B was used. Rhodamine B was applied on two reference specimens without TiO_2 and the discolourations were examined with a colorimeter. The first sample was irradiated with a light intensity of 35.5 W/m² in the middle of the sample. The second, how-

Table 1. Mix design of the reference mix according to Brockmann (2005).

Components	Unit	Composition
cement CEM I 52.5 N (c)		490
fly ash (f)		175
silica fume (s), as slurry		35
binder content	kg/m³	700
water		280
quartz powder		500
sand (0.2 mm – 0.6 mm)		714
superplasticiser	% by mass of binder	0.65
w/c	–	0.57
w/c_{eq}*	–	0.47

$*w/c_{eq} = w/(c + 0.4 \cdot f + s)$

ever, was exposed to an irradiation intensity of 15.0 W/m². Due to the different irradiation intensities, different decompositions of rhodamine B were determined. In doing so, the different red intensities were measured. When the irradiation was conducted at 15.0 W/m², about 15% of the rhodamine B was decomposed. At an irradiation of 35.5 W/m², about 40% were decomposed. After the irrigation, a difference in the pollution degree could not be discerned.

In principle, the results show that rhodamine b is decomposed on surfaces without TiO_2 only by artificial sunlight even at an irradiation intensity of 15.0 W/m².

3.2 *Pollutant decomposition*

3.2.1 *General*

The tests on the pollutant decomposition were always performed according to the same scheme. The lamp is turned on for 10 minutes. Afterwards it is turned out for 5 minutes and then turned on again for 10 minutes.

3.2.2 *Influence of the storage*

The investigations regarding the influence of the storage were conducted on series with different storage types. Figure 1 illustrates the pollutant decomposition depending on the storage.

Figure 1 shows that the storage type exerts a significant influence on the pollutant decomposing properties.

3.2.3 *Influence of the water-cement ratio*

To investigate the influence of the w/c_{eq}-value on the pollutant decomposing effect, mixes with w/c_{eq}-values of 0.4, 0.5 and 0.6 were produced. Figure 2 shows that, at titanium dioxide modified fine grained concretes, there is a correlation between the w/c_{eq}-value and the decomposition rate at the pollutant decomposition.

With increasing w/c_{eq}-value, the decomposition rate decreases at the investigations on the pollutant decomposition.

3.2.4 *Influence of the age*

As can be seen from Figure 3, at storage 20/65, there is no significant influence of the age on the decomposition rates at the pollutant decomposition.

4 CONCLUSIONS

The present research results show that, apart from the storage and the w/c_{eq}-value exert a significant influence on the decomposition rates at the investigations of titanium dioxide modified fine grained concretes with regards to the pollutant decomposition. The age does not seem to have a major influence at a storage of 20°C and a relative humidity of 65%.

The investigations on the self-cleaning have so far not yielded any significant results because it turned out during the tests that the applied rhodamine B is not UV-resistant and hence cannot be used any further.

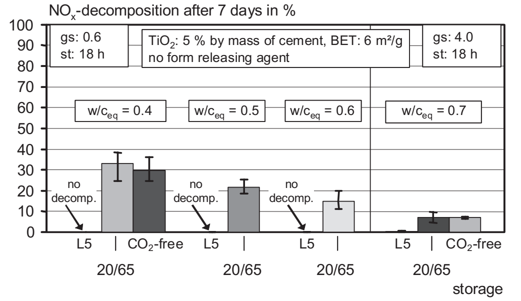

Figure 1. Comparison of the storage conditions at the age of 7 days.

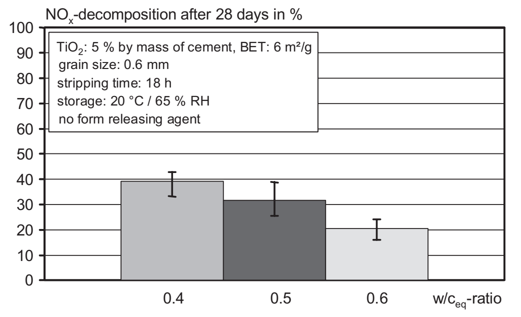

Figure 2. Comparison of the w/c_{eq}-values at the age of 28 days.

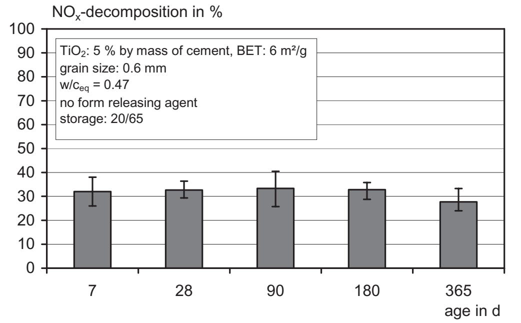

Figure 3. Comparison of the different test ages.

Concrete Repair, Rehabilitation and Retrofitting III – Alexander et al. (eds)
© 2012 Taylor & Francis Group, London, ISBN 978-0-415-89952-9

The use of superabsorbent polymers as a crack sealing and crack healing mechanism in cementitious materials

D. Snoeck, K. Van Tittelboom & N. De Belie
Magnel Laboratory for Concrete Research, Department of Structural Engineering, Ghent University, Belgium

S. Steuperaert & P. Dubruel
Polymer Chemistry and Biomaterials Group, Department of Organic Chemistry, Ghent University, Belgium

ABSTRACT: As concrete cracks due to its low tensile strength and as harmful fluids may migrate into these cracks, the durability of concrete is endangered if no proper treatment or manual repair is applied. To address this need, this research focusses on the use of superabsorbent polymers (1) to seal cracks from intruding potentially harmful substances and (2) to heal the crack due to further hydration and precipitation of calcium carbonate. The first focus relies on hindering the fluid flow by swelling of superabsorbent polymers after they are exposed to a humid environment. The sealing capacity was measured by means of water permeability tests and through visualization of permeability tests by neutron radiography. Superabsorbent polymers are able to seal cracks and thus allow a recovery in water-tightness as a decrease in permeability is noticed. The second focus relies on healing of small cracks in fibre reinforced cementitious materials, restoring the mechanical properties. The regain in mechanical properties was analyzed by four-point-bending tests and the crack closure was microscopically monitored. Cracks close through the combination of further hydration of unhydrated cement particles, precipitation of calcium carbonate and activation of the pozzolanic reaction of fly ash. Desorption of superabsorbent polymers triggers healing in the vicinity of crack faces and cracks up to 130 μm were able to close completely in wet/dry cycles due to the precipitation of calcium carbonate. Mortar samples containing superabsorbent polymers even showed partial healing when stored under a relative humidity of more than 60%. In this way, a smart cementitious material which is reliable and independent from the conditions is acquired.

1 INTRODUCTION

Concrete is often used nowadays because of its high compressive strength. However, concrete is prone to cracking due to its limited tensile strength. The crack formation results in the ingress of water and with that, in the ingress of potentially harmful substances. These substances may deteriorate the concrete from inside out and may endanger the durability of the structure.

How can we solve this?

Concrete has the natural capacity of autogenous crack healing. But three criteria need to be fulfilled: the presence of 'building stones', restriction of the crack width and exposure to a humid environment.

In this paper, self-sealing was investigated by performing water permeability tests. For the second part, the three criteria were combined. The Ca^{2+} ions were already present in the matrix (1), crack widths were limited by mixing in synthetic fibres (2), and, humid conditions were provided by using superabsorbent polymers (SAP) (3). The self-healing efficiency was measured as the crack closure and the regain in mechanical properties.

2 ABSORPTION CHARACTERISTICS

To assess the sealing capacity of SAP, the swelling capacity was calculated from the volume increase between the vacuum dried state and the saturated state after filtration. The measurements were performed with de-ionized water and filtered cement slurry.

The values found for the absorption of SAP in contact with fluid, were compared to water sorption in a 100% relative humidity environment, during dynamic vapour sorption (DVS) measurements (Surface Measurement Systems, London, UK). The solutions, with their pH-value, and the equilibrium values at 100% RH are listed in Table 1. SAP are able to take up moisture from the environment.

3 CRACK SEALING MECHANISM

The first investigated parameter is the self-sealing effect of cracked specimens with embedded SAP. As water enters the crack, the SAP along the crack faces will swell and thus fill the crack. This will

Table 1. (Ab)sorption capacity of SAP A, B and C [g/g SAP].

Used method	pH-value	SAP A	SAP B	SAP C
De-ionized water	6.5	305 ± 4	283 ± 2	11 ± 1
Cement slurry	12.8	61 ± 1	58 ± 2	7 ± 1
DVS		1.68	1.50	1.00

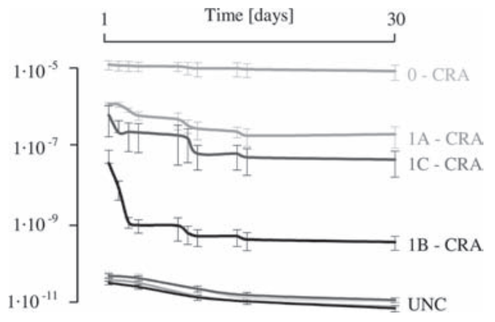

Figure 1. Water permeability k [m/s] in function of time [days]. The error bars show the standard deviation.

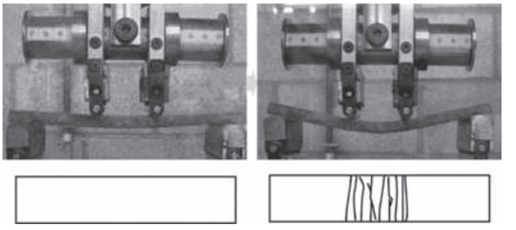

Figure 2. Mixing in PVA-fibres results in great ductility and multiple crack formation. The bottom figures show the crack pattern.

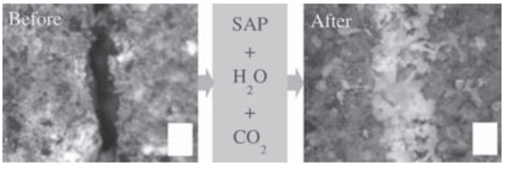

Figure 3. For specimens containing SAP particles, cracks up to 130 μm can close due to autogenous crack healing. The scale bars have a height of 200 μm.

result in a blockage of the crack by swollen SAP and in a decrease in water permeability (Fig. 1).

Cracked specimens without SAP (0 - CRA) have a final k-value of $1\cdot10^{-5}$ m/s (Fig. 1). Cracked specimens containing SAP (1 m% SAP A/B/C), however, show a decrease in permeability. The SAP B particles are able to seal the crack more effectively in comparison to SAP A and SAP C. The difference noticed between SAP A and SAP B is due to the smaller particle size of SAP A. SAP A are not able to effectively seal the total crack. The difference noticed between SAP B and SAP C is due to a lower absorption capacity of SAP C (Table 1). The permeability of a sealed crack with 1 m% SAP B is almost as good as the value noticed for an un-cracked specimen (UNC).

Visualizing the water permeability with neutron radiography shows that SAP are able to seal a crack. The water head in specimens without SAP decreases rapidly in time, and the water head in specimens with SAP decreases only slightly in time.

4 CRACK HEALING MECHANISM

By mixing in microfibres, multiple cracks are formed. Instead of forming one single large un-healable crack, several small healable cracks are formed (Fig. 2). The crack widths were limited to 6–36 μm. Results show that cracks up to 30 μm heal completely and up to 150 μm heal partly when specimens without SAP are subjected to wet/dry cycles. In the presence of air (without any water available), samples cannot heal. But, in specimens with SAP, some healing occurred as crack closure was noticed visually. The sorption equilibrium values at 100% RH are listed in Table 1. SAP are able to take up their weight in moisture from the environment and provided it to the cementitious matrix for autogenous healing.

In wet/dry cycles, cracks up to 130 μm are able to close in specimens containing SAP (Fig. 3). Deposition of crystals is not only due to further hydration, but mainly due to precipitation of $CaCO_3$ crystals. So, not only cracks up to 50 μm are able to heal, but cracks up to 100 μm and further.

Cracks may close with deposited crystals, but what about the strength of the new material?

To answer this question, the regain in first-cracking-strength of the different test series was compared. Without the presence of water, specimens without SAP do not heal. Cracked specimens with SAP do show healing as there is a regain in the first-cracking-strength. When exposed to wet/dry cycles, the specimens with SAP will heal more due to a gradual release of water by the SAP.

5 CONCLUSIONS

Micro-fibre reinforced concrete is durable and provides reliable tensile ductility and multiple cracking. SAP particles swell and block the crack, resulting in a decrease in water permeability. Furthermore, the SAP promote the self-healing ability by providing water upon crack formation, even in a humid environment.

The combination of microfibres and SAP leads to self-sealing and self-healing of cracks.

Concrete Repair, Rehabilitation and Retrofitting III – Alexander et al. (eds)
© 2012 Taylor & Francis Group, London, ISBN 978-0-415-89952-9

Effect of matrix permeability on durability of structural grade geopolymer and conventional concretes

Kwesi Sagoe-Crentsil, Shiqin Yan & Trevor Brown
CSIRO Materials Science and Engineering, Victoria, Australia

ABSTRACT: The factors that control concrete permeability, fluid transport and long-term durability of fly-ash Geopolymer (GP) systems were investigated using equivalent grade Ordinary Portland Cement (OPC) concrete as reference. To assess durability performance, high pressure water and gas permeability tests were conducted on steam-cured Geopolymer and OPC concretes with nominal strengths of 40 MPa and 70 MPa. Measured mean gas (k) and water (K_w) permeability coefficient values for the lower grade concrete were respectively 6.19E-17 m^2 at 300 kPa gas pressure and 1.52E-10 m/s at 525 kPa water pressure. It was observed that water permeability coefficient data for Geopolymer concrete was typically an order of magnitude higher, although gas permeability values were found to be equivalent to reference OPC systems. Analyses of experimental data suggest that transport properties of Geopolymer matrices are largely controlled by the evolution and distribution of its inherent mesoporous capillary pore network structure. The paper further examines implications of increased GP matrix permeability on key durability parameters such as chloride diffusion, carbonation rate, steel reinforcement corrosion and long-term engineering performance.

1 INTRODUCTION

The deterioration of reinforced concrete is generally induced by the penetration of aggressive gaseous or aqueous agents through its interconnected pore network. These agents could be in the form of moisture or ions such as Cl^-, CO_2, SO_4 resulting in cracking, spalling, loss of mass or strength reduction, which further exacerbates the integrity of concrete structures (Basheer et al., 2001, Garboczi, 1990).

Whereas permeability tends to be often controlled by pore connectivity, the elastic properties and strength of concrete are affected by the total volume of pores, in particular, the distribution of macropores which are sized greater than 50 nm (Marsh et al., 1985, Bamforth, 1987). However, for Geopolymer (GP) concrete, the pore connectivity, permeability and the resulting equivalent transport properties responsible for degradation mechanisms are yet to be fully characterized (Criado et al., (2003), Xu & van Deventer, 2000, Steveson, et al., (2005)). This paper therefore examines aspects of the inter-relationships between strength and permeability to address fundamental parameters likely to contribute to long-term GP concrete performance.

2 EXPERIMENTAL

ASTM Type I ordinary Portland cement was used for reference concrete mixtures and Class F fly ash was used for the Geopolymer (GP) mixtures. River sand and local 14/9 mm Hornfels coarse aggregate was used. Both the reference OPC1 and GP1 concrete mixes were designed to achieve target 28 day strength of 40 MPa and 70 MPa respectively for OPC2 and GP2 concrete.

Concrete cylinders for compression testing were tested in accordance with AS 1012.9 (1999). The coefficient of water permeability (K_w) was determined by measuring the amount of water passing through the specimen and calculated using Darcy's law.

3 RESULTS AND DISCUSSION

The mean compressive strength development of steam-cured OPC and GP concretes are shown in Table 1. The results show that GP1 and OPC1 samples varied slightly from the target strengths of 40 MPa at 28 days. In general, the observed post–heat cured compressive strength gain of GP1 concrete was minimal compared to OPC concrete.

Table 2 displays mean water and gas permeability data for all concrete mixes. From Table 2, OPC concretes show reduced permeability values of nearly an order of magnitude.

Fig 1 shows correlations between GP concrete compressive strength and measured gas permeability for GP concretes at 400 kPa pressure. The trends observed show expected inverse correlation between permeability and strength with higher strength samples, which are naturally less porous, delivering lower permeability.

Table 1. Compressive strength development of ambient cured OPC and GP concretes.

Cure duration	GP1 (MPa)	OPC1 (MPa)	GP2 (MPa)	OPC2 (MPa)
1 day	42.3	22.5	63.3	66.0
7 day	42.3	28.0	66.7	72.1
28 day	44.0	38.1	70.3	78.5
91 days	47.8	40.3	71.6	86.4

Table 2. Mean water permeability coefficient values for OPC and GP concretes at 28 days.

Mix ID	Mean permeability (K_w m/s)	Mean gas permeability (m^2) at 300 kPa
GP1	1.52E-10	6.19E-17
OPC1	1.73E-11	6.32E-17
GP2	1.67E-11	1.52E-16
OPC2	7.52E-12	1.93E-16

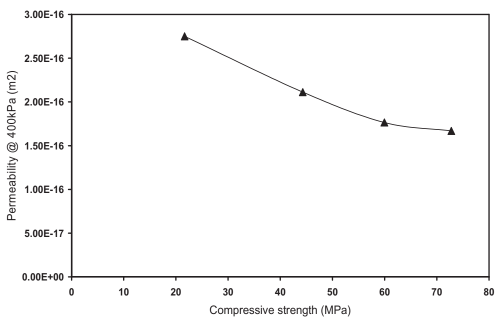

Figure 1. Correlations between GP concrete compressive strength and measured gas permeability for GP concretes at gas 400 kPa pressure.

The transport of fluids through concrete are generally known to occur via networks of continuous capillary and micropores which exist in the concrete's cementitious matrix, as well as the porosity that exist in the interfacial regions with the aggregate (Merchand et al., 1997; Verbeck, 1982). The mechanism of transport through the pore system can be by any combination of diffusion, permeation, capillary action and absorption processes (Garboczi, 1990). There is also some contribution to transport of liquids and gases arising from connected microscopic/gel pores. However, in real structural systems the influence of cracks on transport mechanisms and, eventually, on system durability performance can become very significant depending on the nature and type of crack distribution.

The mechanisms of GP concrete degradation appears to be rather complex. In addition to the transported fluid, the higher inherent alkalinity, the absence of Ca-rich hydration products and the as yet to be fully characterized mesoporous network structure, alongside such system variables as nature and type of reaction products, degree of polymerization, system chemistry, humidity differentials, temperature and other secondary factors all contribute to GP concrete deterioration.

4 CONCLUSION

Measured high pressure water (K_w) and gas (k) permeability coefficient of steam-cured fly ash geopolymer structural grade concrete was respectively found to be 6.19E-17 m^2 at 300 kPa gas pressure and 1.52E-10 m/s at 525 kPa water pressure. The gas permeability values of reference OPC systems were comparable to geopolymer concrete but the corresponding water permeability coefficient data for geopolymer systems were typically tenfold higher.

REFERENCES

Bamforth, P. 1987. The relationship between permeability coefficients for concrete obtained using liquid and gas. *Mag. Concr Res*, 39(138): 3–10.

Basheer, L, Kropp, J. & Cleland, D.J. 2001. Assessment of the durability of concrete from its permeation properties: a review. *Construction and Building Materials* 15: 93–103.

Criado, M., Palomo, A. & Fernandez-Jimenez, A. 2005 Alkali activation of fly ashes. Part 1: Effect of curing conditions on the carbonation of the reaction products. *Fuel*, 84: 2048–2054.

Garboczi, E.J. 1990 Permeability, diffusivity and microstructural parameters. A critical review. *Cement Concr Res*, 20: 591–601.

Marsh, B.K., Day R.L. & Bonner, D.G. 1985. Pore structure characteristics affecting the permeability of cement paste containing fly ash. *Cement Concrete Res* 15(6): 1027–38.

Merchand, J. & Gerard, B. 1997. Microstructure-based models for predicting transport properties. In: Reinhardt HW, editor. *RILEM report no. 16: penetration and permeability of concrete*. E&FN Spon.

Steveson, M. & Sagoe-Crentsil, K. 2005. Relationships between composition, structure and strength of inorganic polymers, Journal of Materials Science 40(8): 2023–2036.

Verbeck, G.J. 1982. Pore structure significance of tests and properties of concrete and concrete making materials. *ASTM Special Tech Publ,* 169 A: 211–219.

Xu, H. & Van Deventer, J.S.J. 2000. The geopolymerisation of aluminosilicate minerals. *Int J Miner Process* 59: 247–66.

Concrete Repair, Rehabilitation and Retrofitting III – Alexander et al. (eds)
© 2012 Taylor & Francis Group, London, ISBN 978-0-415-89952-9

Polymers in concrete repairing according to EN 1504

L. Czarnecki & P. Łukowski
Warsaw University of Technology, Warsaw, Poland

ABSTRACT: Repairs and protection are the important research inspirations of the sustainable development in construction. The role of polymers in this field is particularly interesting. Repairs of the concrete structures are complex and difficult technical task. The series of the European Standards EN 1504 is an attempt of the formal expression of the problem with respect to up-to-date status of the knowledge and technology. The polymers seem to be irreplaceable in concrete repairs and protection. The superior aim shall be obtaining, according to the rules of sustainable development—well defined performance polymer concretes. Implementation of the idea of the sustainable development into the construction, including use of polymers in the concrete repair, will be the source of scientific and engineering inspirations for many years.

1 INTRODUCTION

Sustainable development should satisfies the present needs without limitation of the possibility of satisfying the needs in the future. The construction industry consumes the huge amounts of mass and energy, thus the rules of the sustainable development are particularly important in this area. Durability of the building structures as well as repairs and protection are the important research inspirations of the sustainable development in construction. The role of polymers is here particularly interesting.

Repairing of the concrete elements and structures is the subject of the series of European Standards EN 1504. The set consists of 10 parts under the overall title "Products and systems for the protection and repair of concrete structure. Definitions, requirements, quality control and evaluation of conformity". In ten parts of EN 1504, the term "polymer" can be found 73 times, what is a proof of the big significance of that material in the repairs and protection of concrete; for the comparison, the term "cement" appears 59 times (!) in all parts of the Standard. In this area polymers seem to be irreplaceable.

2 ROLE OF POLYMERS IN REPAIRS AND PROTECTION OF CONCRETE

Polymer concretes are widely and successfully used in the repairs and protection of the concrete structures (Fig. 1). The main advantages are here excellent adhesion to the concrete substrate, tightness and frost resistance, and in the case of the resin concretes also short time to exploitation readiness.

There are areas of the particular usefulness of the given Concrete-Polymer Composites (C-PC) type:

– PCC (Polymer-Cement Concrete) in typical repairs of the concrete structures;
– PC (Polymer Concrete) in the repairs, where quick restoration of usability is required (days or even hours); in the repairs performed under chemical aggression; in the repairs of the concretes of high strength;
– PIC (Polymer Impregnated Concrete) as the way of preserving the monuments and old buildings. The method is used if other ways cannot be employed and requires the conservation agreement.

The polymer concretes are neglected in the European Standard on concrete EN 206-1, and simultaneously they are mentioned a dozen times in the series of the standards on repair and protection of the concrete structures EN 1504. This shows where these materials are particularly needed and what will be the direction of their further development.

3 CONCLUDING REMARKS

Repairs of the concrete structures are complex and difficult technical task. Simultaneously, they are significant from the economical point of view. The series of European Standards EN 1504, dealing with the products and systems for repair and protection of concrete structures, is an attempt of

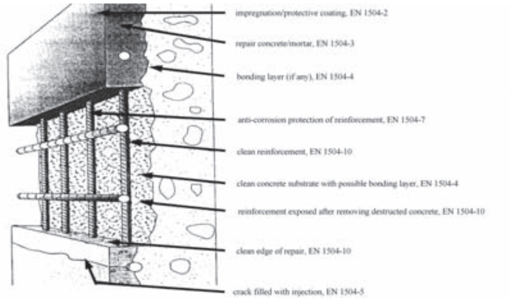

Figure 1. Repair of concrete element according to Czarnecki & Emmons (2002) with attributed suitable parts of European Standard EN 1504.

the formal expression of the problem with respect to up-to-date status of the knowledge and technology. The standards give new inspirations, also in connection with the sustainability in construction.

Polymer is the most expensive component of the polymer concretes, therefore, a development of the methods of material designing can be expected towards decreasing its usage with simultaneous optimisation of the properties involved with usability in the given application. From the other side, polymers seem to be irreplaceable in repairs and protection of the concrete structures. Therefore, the superior aim shall be obtaining—according to the rules of sustainable development—well defined performance polymer concretes. Implementation of the idea of the sustainable development into the construction, including use of polymers in the concrete repair, will be the source of scientific and engineering inspirations for many years.

ACKNOWLEDGEMENT

The paper has been prepared under the framework of the research project financed by National Science Centre, grant No. N 506 257637.

REFERENCES

Czarnecki L., Vaysburd A.M., Mailvaganam N.P., Emmons P.H. & McDonald J.E. 2000. Repair and rehabilitation of structures—some random thoughts. *Indian Concrete Journal* 1: 13–21.

Czarnecki L. & Runkiewicz M. 2005. On the compatibility measure in the repair systems. *2nd International Conference on Concrete Repair, Rehabilitation and Retrofitting, Cape Town, RPA*: 1003–1008.

Czarnecki, L., Kurdowski W. & Mindess S. 2008. Future developments in concrete. *Developments in the Formulation and Reinforcement of Concrete.* Woodhead Publishers Ltd., Abington: Cambridge: 270–284.

Czarnecki, L. 2010. Polymer concretes. *Cement Wapno Beton* 2: 63–85.

Czarnecki, L. & Kaproń M. 2010. Sustainable construction as a research area. *International Journal of the Society of Materials Engineering for Resources*. 17(2): Sept.

Czarnecki L. & Łukowski P. 2010. Polymer-cement concretes. *Cement Wapno Beton* 5: 243–258.

Kibert C.J. 1999. Establishing principles and a model for sustainable construction. *Proceedings of the 1st International Conference CIB TG 16, Florida*: 3–12.

Łukowski P. 2010. Polymer-cement mortars of high bond strength to the concrete substrate. *Restoration of Buildings and Monuments* 4/5: 367–375.

Raupach M. 2006. Concrete repair according to the new European Standard EN 1504. In *Concrete Repair, Rehabilitation and Retrofitting* Alexander M., Beushausen H.D., Dehn F. and Moyo P. (eds.). Taylor & Francis Group, London: 6–8.

Sasse H.R., Stenner R. 1999. Adhesion and the new series of European Standards on protection and repair of concrete structures. *2nd International RILEM Symposium ISAP '99 'Adhesion between Polymers and Concrete',* Drezno: 485–494.

United Nations. 1987. Report of the World Commission on Environment and Development. *G. H. Brundtland Commission, General Assembly Resolution* 42/187.

Concrete Repair, Rehabilitation and Retrofitting III – Alexander et al. (eds)
© 2012 Taylor & Francis Group, London, ISBN 978-0-415-89952-9

Durability properties of inorganic polymer concrete using fly ash and slag

J.R. Mackechnie & A.C.N. Scott
Department of Civil and Natural Resources Engineering, University of Canterbury, New Zealand

ABSTRACT: The potential durability of inorganic polymer concrete made with fly ash and slag was investigated by comparing the durability properties of a range of inorganic polymer and Portland cement-based concrete. Concrete was cured at ambient and elevated temperatures to simulate normal site and precast concrete conditions. Findings from porosity, oxygen permeability and chloride resistance testing show that inorganic polymer concrete has significant differences in microstructure to Portland cement concrete. The higher porosity of inorganic polymer concrete was found to be caused by differences in paste porosity and the presence of compaction voids due to the viscous nature of the material. High strength IPC mixes had moderate permeability but lower strength IPC mix had poor resistance to permeation. Chloride resistance of IPC was not consistent and was generally much poorer than PC-based concrete. Durability properties of inorganic polymer concrete were found to vary considerably depending on mix design and initial curing and did not always follow predictable trends found with PC-based concrete.

1 INTRODUCTION

Inorganic polymer concrete (IPC) is made using waste materials such as fly ash and ground granulated blast-furnace slag. These binders are less reactive than Portland cement and alkali or alkali-silicate activating solutions are used and thermal curing is sometimes required. This produces alkali alumino-silicate gel that is primarily amorphous but may also contain crystalline zeolites. The microstructure of IPC is complex, differs from PC-based concrete and is only starting to be understood by researchers. It is known that the bonding is strong but the material can be porous with significant amounts of unreacted binder. Given the unique microstructure of the material, careful characterisation is required to predict the durability performance.

The objective of this study was to assess the likely durability performance of a range of IPC and PC-based concrete mixes that could be used in structural and precast concrete. Initial curing was either at ambient temperature typical for structural concrete or thermal curing, which is often applied to precast concrete to allow rapid demoulding.

2 EXPERIMENTAL STUDY

Cementitious and pozzolanic binders used were:

PC – Portland cement from Whangarei, NZ
HFA – Fly ash from Huntly power station, NZ
GFA – Fly ash from Gladstone, Australia
LFA – Fly ash from Lethabo power station, SA
PSL – Ground gran. blast-furnace slag from Aus.
SSL – Ground granulated Corex slag from SA

Concrete mix designs used a total binder content of 430 kg/m^3 with a nominal consistence of 180 mm. Fresh concrete assessment included slump and rheology testing. Hardened performance of concrete was assessed at 28 days by measuring density, compressive strength, elastic modulus and drying shrinkage. Durability properties were assessed at 28 and 90 days and included effective porosity, oxygen permeability and chloride resistance.

3 RESULTS

All concrete had relatively high slump (180 ± 30 mm) but workability was found to vary quite significantly when rheology was assessed. PC-based concrete were found to have low yield shear stress and moderate plastic viscosity that was within the expected range considering the high slump and the relatively high binder content used in the material. IPC had higher plastic viscosity values, especially mixes IPAS and IPSA that were very sticky and therefore difficult to compact. Yield shear stress values for IPC were low to moderate with only IPAS being higher at 950 Pa.

Results of hardened concrete properties tested at 28 days are shown in Table 1. Both IPAS and IPSA produced higher compressive strength than

Table 1. Structural properties measured at 28 days.

Property	Temp	PC	FA	SL	IPNZ	IPAS	IPSA
Hard. density	21⁰C	2471	2441	2434	2385	2413	2396
(kg/m^3)	60⁰C	2472	2415	2408	2400	2391	2396
Comp. strength	21⁰C	64.5	69.4	76.6	45.7	75.8	82.2
(MPa)	60⁰C	61.5	58.1	59.6	26.5	75.5	86.5
Elastic modulus	21⁰C	39.5	38.5	40.7	30.3	31.6	32.3
(GPa)	60⁰C	39.0	37.9	38.8	23.5	34.4	34.5
Drying shrink.	21⁰C	584	565	624	539	1352	1499
(mstr)	60⁰C	544	540	582	216	456	552

any PC-based concretes, especially when thermally cured. Thermal curing also enhanced the dimensional stability of high strength IPC mixes.

Porosity of PC-based concrete was significantly lower than concrete made with IPC, which was not consistent with trends found for porosity of equivalent pastes. The relationship between porosity of concrete and paste is shown in Figure 1. The higher level of compaction voids in IPC most likely contributed to this disparity.

Oxygen permeability testing measures the Darcy coefficient of permeability of concrete to oxygen flow. Oxygen permeability index is defined as the negative log of the Darcy coefficient of permeability, with values above 10.0 indicating low permeability concrete while values less than 8.0 indicate high permeability. Figure 2 shows the measured oxygen permeability results for PC-based and IPC concrete at 28 days. IPC was more permeable than PC-based concrete, especially when cured under ambient conditions.

Results of chloride migration testing at 28 days are shown in Table 2 together with apparent diffusion coefficients measured after bulk diffusion testing. The chloride resistance of IPC was inconsistent when compared with other properties and was quite poor.

4 CONCLUSIONS

The lower workability of IPC contributed to the increased porosity of concrete. Durability potential of IPC was found to be compromised by high porosity, which increased permeation of the material. High strength IPC mixes required thermal curing to stabilise the material and provide good structural properties. This material was found however to have poor chloride resistance that could be problematic in some applications, especially if coupled with a loss in alkalinity when exposed to water. The rapid setting of these materials could also limit its application to dedicated precast concrete applications. Durability properties of IPC were found to vary significantly depending on mix design and curing, with performance being less predictable than that of PC-based concretes. Further development of the technology should help improve confidence in the material.

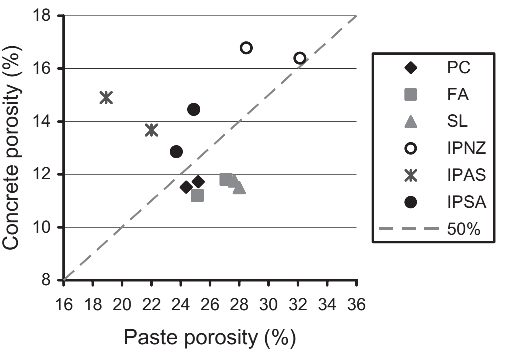

Figure 1. Concrete porosity versus paste porosity.

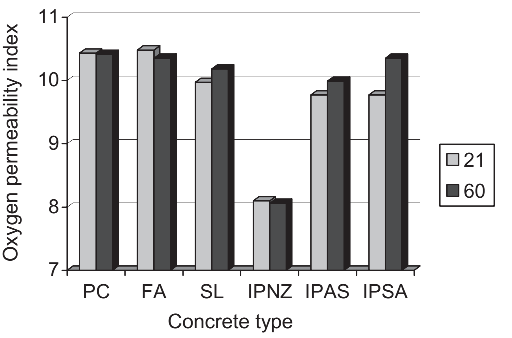

Figure 2. Oxygen permeability results at 28 days.

Table 2. Chloride resistance results after 90 days.

Concrete	Temp	Nordtest D_c	Bulk diff. D_c
PC	21⁰C	6.6×10^{-12}	5.8×10^{-12}
	60⁰C	1.1×10^{-12}	1.8×10^{-11}
FA	21⁰C	1.9×10^{-12}	3.9×10^{-12}
	60⁰C	1.3×10^{-12}	2.7×10^{-12}
SL	21⁰C	1.7×10^{-12}	1.5×10^{-12}
	60⁰C	1.8×10^{-12}	1.9×10^{-12}
IPNZ	21⁰C	4.7×10^{-12}	1.3×10^{-12}
	60⁰C	1.3×10^{-11}	5.3×10^{-12}
IPAS	21⁰C	1.5×10^{-12}	7.9×10^{-11}
	60⁰C	1.7×10^{-12}	2.1×10^{-10}
IPSA	21⁰C	2.5×10^{-11}	Not tested
	60⁰C	2.6×10^{-11}	

Concrete Repair, Rehabilitation and Retrofitting III – Alexander et al. (eds)
 ISBN 978-0-415-89952-9

Aminobenzoate modified hydrotalcites as a novel smart additive of reinforced concrete for anticorrosion applications

Z. Yang
Materials Innovation Institute (M2i), Delft, The Netherlands
Faculty of Civil Engineering and Geosciences, Delft University of Technology, Delft, The Netherlands

H. Fischer
TNO Materials Performance, Eindhoven, The Netherlands

R.B. Polder
Faculty of Civil Engineering and Geosciences, Delft University of Technology, Delft, The Netherlands
TNO Building Materials, Delft, The Netherlands

ABSTRACT: A carbonate form of Mg-Al-hydrotalcite with Mg/Al = 2 and its *p*-aminobenzoate (pAB) modified derivative have been synthesized and characterized by means of XRD, IR and TG/DSC. Mg(2)Al-CO_3 was prepared by a coprecipitation method and was subsequently modified by pAB through the calcination-rehydration technique. The results from the relevant characterizations combined with Total Organic Carbon (TOC) analysis further confirmed that pAB anions were successfully intercalated into the interlayer space of the hydrotalcite. The anticorrosion behavior of Mg(2)Al-pAB was evaluated on the basis of Open Circuit Potential (OCP) monitoring of carbon steel in simulated concrete pore solution at pH 13 contaminated with chloride. The preliminary results from this study demonstrated that ion-exchange indeed occurred between free chloride ions in simulated pore solution and the intercalated pAB anions in Mg(2)Al-pAB structure, thereby reducing the free chloride concentration. The simultaneously released inhibitive p-aminobenzoate anions were found to exhibit the envisaged inhibiting effect and cause a shift of corrosion initiation of the steel to higher chloride concentrations than without the modified hydrotalcite.

1 INTRODUCTION

In this work, magnesium-aluminate-based hydrotalcite, Mg(2)Al-CO_3 (atomic ratio Mg/Al = 2) modified by *p*-aminobenzoate (pAB) was prepared as a model material for a whole family of modified hydrotalcites (MHTs) and experiments were designed to investigate the feasibility of MHTs with the selected intercalating organic species to be able to act as a scavenger for chloride. The primary objective of the paper is therefore to provide preliminary information to explore the promising use of the other various MHTs compositions with selected intercalating inhibitive anions suitable for using as a new type of additive for concrete to reduce chloride-induced corrosion of reinforced concrete.

2 EXPERIMENTAL

2.1 *Synthesis, characterization and anticorrosion evaluation*

The Mg(2)Al-CO_3 was synthesized by a pH-controlled co-precipitation method and the modification of Mg(2)Al-CO_3 with pAB was performed by calcination-rehydration method. Materials characterization was performed by means of XRD, IR and TG/DSC. Total organic carbon (TOC) analysis was employed to analyze the intercalation amount of the corresponding organic anions. The anticorrosion properties of Mg(2)Al-pAB with respect to steel specimens were evaluated by open circuit potential (OCP) in simulated concrete pore solution contaminated with chloride. In these experiments, steel electrodes were immersed in relevant testing solutions and four types of testing solution were prepared as shown in Figure 4.

3 RESULTS AND DISCUSSION

3.1 *Characterisation*

The characteristic peaks in XRD patterns and FT-IR shown in Figure 1–2 indicated that the Mg(2)Al-CO_3 and it's modified derivative Mg(2)Al-pAB were synthesized successfully. Thermal analysis (i.e., TG/DSC) results as shown in Figure 3 combined with TOC revealed that 35.5% pAB anions was intercalated in MHT and the intercalated *pAB* shows a higher thermal stability

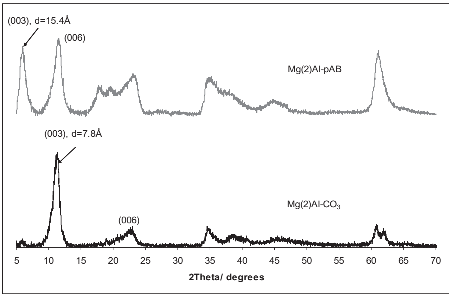

Figure 1. XRD patterns for Mg(2)Al-CO_3 and Mg(2)Al-pA.

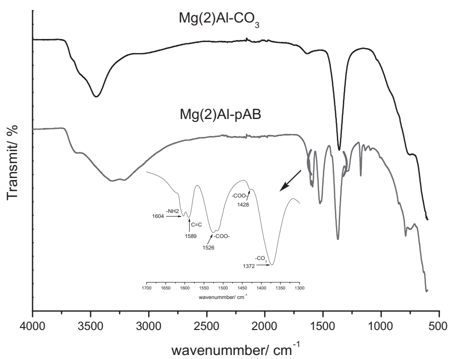

Figure 2. FT-IR Spectra of Mg(2)Al-CO_3 and Mg(2)Al-pAB.

relative to its pure crystalline parent substance, i.e., *p*-amino benzoic acid.

3.2 *Anticorrosion evaluation of Mg(2)Al-pAB on the basis of OCP evolution*

The OCP evolution for the steel electrodes in the testing solutions as shown in Figure 4 clearly revealed that the chlorides have been exchanged with intercalated *p*AB which subsequently show some inhibiting effect and cause corrosion initiation shifting to a higher chloride concentration than without the Mg(2)Al-pAB. As expected from the proposed anion-exchange mechanism, the presence of chlorides leads to release of *p*AB ions. It is worthy to note that MHTs play a double-role against chloride-induced corrosion: simultaneously capturing chlorides and releasing inhibitive anions to protect the steel from corrosion.

4 CONLUSIONS

A carbonate form hydrotalcite (i.e., Mg(2)Al-CO_3) and its *pAB* modified derivative (i.e., Mg(2)Al-pAB)

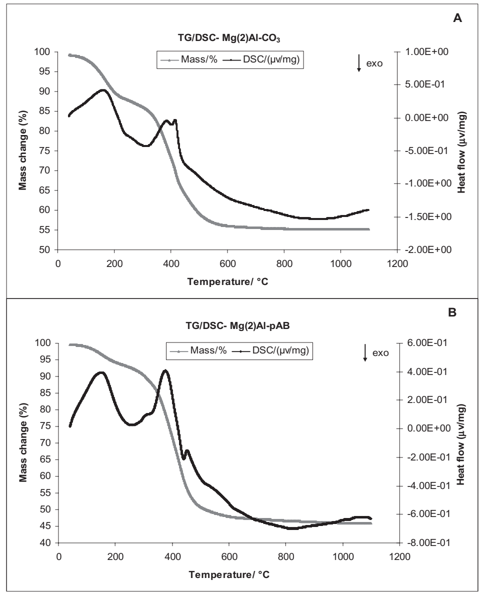

Figure 3. TG/DSC of (A) Mg(2)Al-CO_3 and (B) Mg(2)Al-pAB.

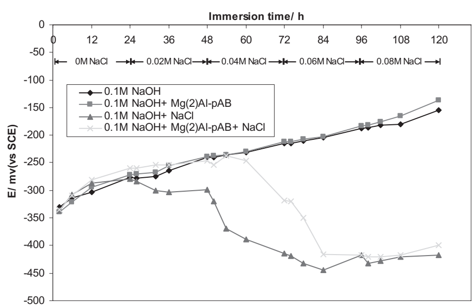

Figure 4. OCP evolution for the steel electrodes in simulated concrete pore solution with and without Mg(2)Al-pAB.

were successfully synthesized and characterized. The anticorrosion behavior Mg(2)Al-pAB was evaluated based on OCP. The preliminary results from this study suggest that ion-exchange indeed occurred between free chloride ions in simulated pore solution and the intercalated *p*-aminobenzoate anions in Mg(2)Al-pAB structure, thereby reducing the free chloride concentration, which is believed to be equivalent to increased binding of chloride present in concrete. The simultaneously released *p*-aminobenzoate anions were found to exhibit some inhibiting effect. The combined effect causes a shift of corrosion initiation on steel to higher chloride concentrations.

Concrete Repair, Rehabilitation and Retrofitting III – Alexander et al. (eds)
© 2012 Taylor & Francis Group, London, ISBN 978-0-415-89952-9

Mix design, mechanical properties and impact resistance of UHPFRCCs

D. Nicolaides & A. Kanellopoulos
Frederick University, Cyprus

M. Petrou
University of Cyprus, Cyprus

M. Soutsos
Queens University Belfast, Belfast, County Antrim, Northern Ireland

ABSTRACT: The research work focused on the determination of guidelines for the production of an UHPFRCC, and the experimental investigation of the quality and the behaviour of this material in a highly demanding application, such as the impact resistance of structures. Specifically, the aim of this study is to present the results of an extended work on the development of an UHPFRCC and the experimental determination of the mechanical properties of the produced material. Furthermore, the paper will present preliminary experimental results on the impact resistance of Reinforced Concrete and UHPFRCC slab specimens.

1 MIX DESIGN AND MECHANICAL PROPERTIES OF UHPFRCCS

All of the principles highlighted in the literature were adopted for the design and development of the first UHPFRCC mixture in Cyprus. Particularly, it was of primary concern the elimination of coarse aggregates from all mixtures, the optimisation of the granular mix, the incorporation of large quantities of small steel fibres and the investigation of post-set heat treatment of the mixes. Moreover, the knowledge acquired and the experiences of other researchers were taken into account in the design and production of the material (Karihaloo et al. 2002, Karihaloo et al. 2005). The optimum derived mix is presented in Table 1.

To determine the mechanical properties of the optimum mix presented in Table 1, compressive (EN 12390–3) and flexural (EN 12390–5) strength tests were conducted, as well as tests towards the evaluation of the Young Modulus (BS 1881–121:1983) of the material. The average results are summarised in Table 2.

2 IMPACT RESISTANCE OF UHPFRCC SLAB SPECIMENS

The impact resistance of UHPFRCC slabs was experimentally verified in real army firing shots, practice which gave the opportunity to the authors to draw conclusions about the impact potential of the material, the experimental setup, appropriate weapons and shooting distances, etc. A wide range of shots, using two different weapons and projectile types were performed.

Table 1. Mix proportions for optimised UHPFRCC mix (per m^3).

Constituents (kg)	Optimised mix
Cement	880
Microsilica	220
Sand 50–250 μm	475
Sand 250–500 μm	358
Water	172
Superplasticiser	67
Fibres: - 6 mm	401
- 13 mm	80
Water/cement	0.20
Water/binder	0.16

Table 2. Mechanical properties of optimised UHPFRCC mix.

Mechanical property	
Compressive strength (MPa)	178.0
Flexural strength (MPa)	30.0
Modulus of Elasticity (GPa)	45.0

For the purposes of this effort, four slab specimens of the same dimensions (100 × 90 × 5 cm) were produced in the laboratory; two UHPFRCC and two Reinforced Concrete (RC). The total amount of short steel fibres in UHPFRCC mixtures was 6% by volume. Reinforced concrete slabs were produced using concrete of characteristic strength equal to 70 MPa (C70). The reinforcement consisted of a steel mesh Y12/8, that aimed at achieving an, approximately, equal amount of steel reinforcement between UHPFRCC and Reinforced Concrete slab specimens. Due to the nature of these tests, and the risk to damage expensive instrumentation, fairly basic measurements were made from the tests. Moreover, it is thought that while the expense and risk to a high-speed video camera is not worth taking, a "broomstick" gauge located behind the target slabs was a very cheap and effective way of measuring both maximum and permanent deflection, to the nearest 1 mm.

Two different types of projectiles were used, namely "Solid Round" projectiles 12.7 mm and "Anti-tank Explosive Shells" 40 mm. Experimental results revealed a substantially improved behaviour of UHPFRCC slab specimens, comparing to Reinforced Concrete slabs, for both types of impact loads (Figures 1a and 1b). Specifically, the damage on UHPFRCC slabs, measured as the size of craters created by "Solid Round" projectiles 12.7 mm, was considerably lower, comparing to the corresponding damage of RC slabs. Furthermore, in several cases, the projectiles did not manage to penetrate the UHPFRCC slab. On the other hand, all of the projectiles managed to penetrate the RC slab. The average diameter of craters in the case of UHPFRCC slabs was 17.3 mm, whereas the corresponding average diameter in the case of RC slabs was 49.8 mm. The magnitude of damage was also visually evaluated, by the density and size of cracks created around each crater. The cracks were significantly more, and of bigger sizes in the case of the RC specimen, while the corresponding cracks were much less in the case of the UHPFRCC slab, due to the existence of high volume of short steel fibres in the specimen. Similar results were obtained in the case of the impact test on specimens using the 40 mm "Anti-tank Explosive Shells". The behaviour of UHPFRCC specimen was substantially improved, comparing to the RC slab. The size of crater created by "Anti-tank Explosive Shells" 40 mm was considerably lower in the case of UHPFRCC, comparing to the corresponding damage of RC slab. The diameter of the crater in the case of UHPFRCC slab was 81 mm, whereas the corresponding diameter in the case of RC slab was 240 mm.

Figure 1a. RC slab after impact loading by "Solid Round" projectiles 12.7 mm.

Figure 1b. UHPFRCC slab after impact loading by "Solid Round" projectiles 12.7 mm.

3 CONCLUSIONS

The experimental verification of the impact resistance of UHPFRCCs in real army firing shots gave the opportunity to draw certain conclusions about the impact potential of the material. UHPFRCCs have exceptionally improved impact performance comparing to Reinforced Concrete. This fact will enable the introduction of this class of materials in new, high value applications which will fully utilize their enhanced properties.

ACKNOWLEDGEMENTS

The authors would like to express their sincere gratitude to the Republic of Cyprus, the Cyprus Research Promotion Foundation (RPF) and the European Regional Development Fund, for funding the research project entitled "Mix Design, Mechanical Properties and Impact Resistance of Ultra High Performance Fibre Reinforced Cementitious Composites" (Contract Number: ΤΕΧΝΟΛΟΓΙΑ/ΥΛΙΚΑ/0609(ΒΙΕ)/01).

Concrete Repair, Rehabilitation and Retrofitting III – Alexander et al. (eds)
 ISBN 978-0-415-89952-9

Durability of lightweight self-consolidating concrete in massive structures

M. Kaszynska
West Pomeranian University of Technology, Szczecin, Poland

1 ABSTRACT

The light-weight self-consolidating concrete combines the advantages of light-weight concrete with properties of self-consolidating concrete. It can save not only by reducing the weight of components, but the lightweight aggregate containing absorbed water is significantly more helpful for concretes made with a low water-cement ratio. The absorbed moisture in the light aggregate is available for internal curing that minimizes the early shrinkage. Thermal stresses evolving from self-heating of concrete masses as a result of exothermic processes during cement hydration can be important in evaluation of concrete structures, such as foundations, bridge abutments and piers. These stresses may cause external cracks in the structural elements resulting in a decrease of stiffness and resistance to various harmful factors occurring during the service life of concrete structures. To determine thermal stresses, it is necessary to establish the relevant processes of setting and hardening of concrete in a structure.

This paper presents test results of workability properties and mechanical properties (compressive strength, tensile strength, modulus of elasticity and shrinkage) of self-consolidating concrete, hardening under adiabatic conditions and isothermal conditions. Various self-consolidating mixtures were considered by replacing a part of fine and coarse natural aggregate with fine and coarse light-weight aggregates.

The tests were performed for concrete mixtures made using Portland cement CEM I 42,5R (European Standard EN 197-1:2000), fly ash, silica fume, Sika Viscocrete 3 superplasticizer, lightweight aggregate Pollytag size of 0-4mm and 4-8 mm, natural sand 0–2mm and natural coarse aggregate size 2–8mm. A constant amount of paste was assumed with a variable proportion of light-weight aggregate to natural aggregate. The aggregate compositions for 9 mixes are shown in Figure 1.

All the considered mixes had initial spread circles within 575–810 mm, as for SF1, SF2 and SF3 slump-flow classes, and classes of viscosity VS2 and VF2.

For evaluation concrete segregation Hardened Visual Stability Index test (HVSI) was used.

The results of compression strength tests are compared in Figure 3.

All concretes after 28 days had the strength in the range of 53,6 MPa through 104,4 MPa.

The relationship between the compressive strength and density of concrete after 28 days of hardening, obtained from tests is shown in Figure 4.

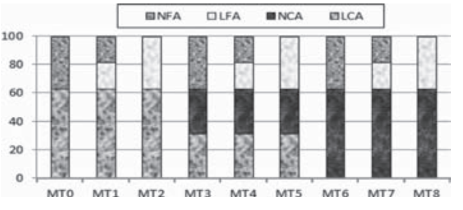

Figure 1. Aggregate compositions by volume in concrete mixes, N-natural aggregate, L-lightweight aggregate, FA-fine aggregate, CA-coarse aggregate.

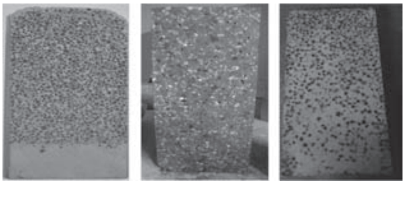

Figure 2. Cross sections of SCC samples with a variable proportion of lightweight aggregate to natural aggregate

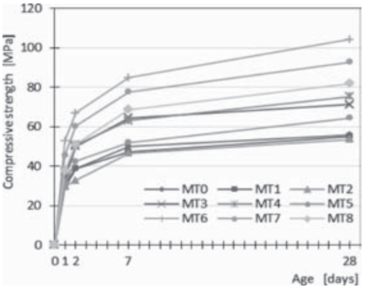

Figure 3. Compressive strength of concrete.

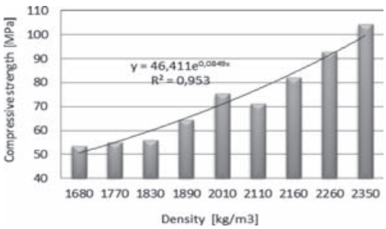

Figure 4. Compressive strength and density of concrete after 28 days of hardening.

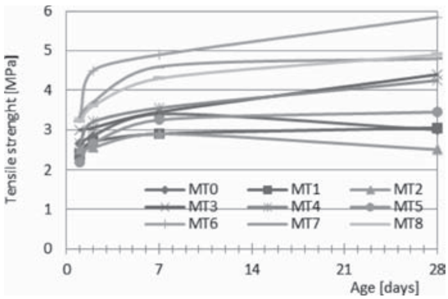

Figure 5. Tensile strength of concrete.

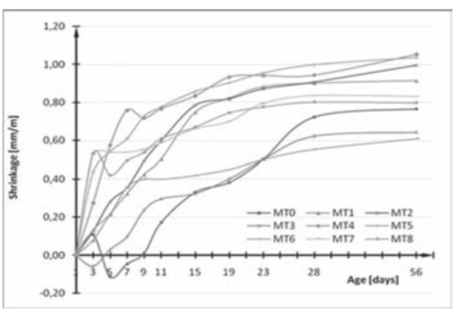

Figure 6. Shrinkage strain versus time.

Splitting tensile test was carried out on cube specimens 100 × 100 × 100 mm. The results of tests are compared in Figure 05.

The shrinkage of concrete was tested on samples of 5 × 5 × 25 cm curing in constant temperature and constant humidity conditions. The results of shrinkage tests are compared in Figure 6.

The assessment and analysis of cement hydration heat in concrete and its mechanical properties were carried out separately in adiabatic conditions. Compressive strength, tensile strength and modulus of elasticity were tested on specimens stored in a calorimeter container at temperature controlled by the temperature of the sample used for testing hydration heat in adiabatic conditions. Investigations have shown that maximum recorded self-heating temperature of concrete was from 44,3°C to 54,4°C.

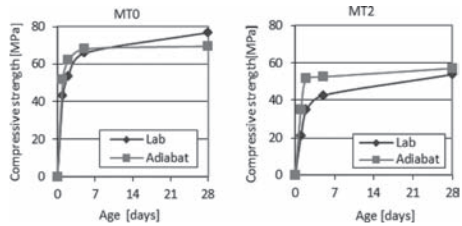

Figure 7. Compressive strength of concrete hardening under isothermal (lab) and adiabatic conditions.

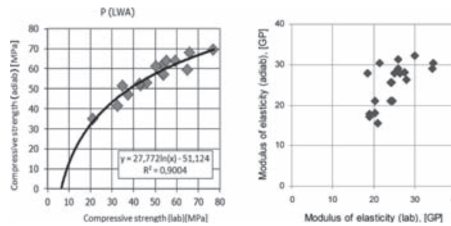

Figure 8. Compressive strength and modulus of elasticity of concretes hardened under isothermal and adiabatic conditions.

Comparison of the test results compressive strength of concrete MT0 and MT2 is presented in Figure 7.

The relationships between the compressive strength and modulus of elasticity of concretes hardened under isothermal conditions (laboratory) and concretes hardening under conditions simulating the curing in massive structures are presented in Fig. 8.

The results of this study confirmed that it is feasible to use light-weight aggregates to obtain a light-weight self-consolidating concrete.

The lightweight self-consolidating concrete requires a careful selection of the aggregates. The weakest link in the mix composition is large diameter aggregate. The highest strength was obtained for concrete with light-weight coarse aggregates and natural fine aggregates.

The higher level of shrinkage was obtained for lightweight SCC with high amount of lightweight sand than normal weight SCC.

The tests showed that the curing temperature has a decisive influence on the growth rate of concrete strength. In practice, after two days of curing in higher temperature, concrete strength approached 78% to 95% of 28 day strength, and after 5 days of curing, from 92% to 97% of the 28 day strength.

Unlike the compressive strength, the tensile strength in higher temperature is not higher than in laboratory conditions.

Modulus of elasticity tests showed a high spread of the resulting values and, therefore, it is difficult to establish any general relationships for lightweight self-consolidating concretes.

Concrete Repair, Rehabilitation and Retrofitting III – Alexander et al. (eds)
© 2012 Taylor & Francis Group, London, ISBN 978-0-415-89952-9

Influence of different recycled aggregate types on strength and abrasion resistance properties of concrete

S.O. Ekolu, L.N. Makama & W.P. Shuluuka
School of Civil & Environmental Engineering, University of the Witwatersrand, Johannesburg, South Africa

ABSTRACT: Different types of recycled aggregates consisting of crushed concrete, recycled rubble stone and crushed clay brick were used as 100% coarse aggregates to prepare concrete mixtures of water/cement ratios of 0.6 and 0.45. Crushed natural dolomite stone was used as control. The various concretes were tested for concrete properties of compressive strength, split tensile strength, the Young's modulus of elasticity and abrasion resistance. It was found that recycled aggregates reduce the workability of concrete mixtures. Use of recycled aggregates of concrete origin also exhibit reduction in compressive strength and split tensile strength by up to 35%. With high strength concrete mixes of at least 50 MPa, the strength losses reduce to negligible levels in some cases. Crushed brick stones gave much higher split tensile strength than all the other recycled stones. The relationship between elastic moduli and compressive strength for concretes made with normal aggregates does not appear to directly apply to concretes made using recycled aggregates. Crushed brick also gave the highest abrasion resistance similar to the performance of the control dolomite stone and better than the other recycled aggregates.

1 INTRODUCTION

Recycling of concrete is an effort towards sustainable development using concrete. The benefits are economic, ecological and environmental. Reduced use of landfill space for waste dumping and conservation of natural rock resources are achieved; and in some cases, concrete recycling for use as aggregates may result in cost savings for construction projects. Concrete recycling is a well exploited practice in some Western countries, with large proportions of concrete waste being re-used. Japan, USA, Germany and Belgium recover 80 to 90% of construction and demolition waste with countries such as Netherlands and Switzerland achieving near 100% recovery. (WBCSD, 2006).

In South Africa, recycling of concrete is still small with some plants for recycling of demolition waste operating in Johannesburg and Cape Town. A large proportion of demolition waste in the country is usually dumped at landfills. With growing infrastructure and population, the promotion of concrete recycling in future will be a beneficial activity to the environment. However, very little research work has been done on recycling of concrete in South Africa.

2 EXPERIMENTAL

2.1 *Recycled aggregate sources*

Crushed dolomite aggregate used as control, and three recycled aggregate types were used in the study. One of the recycled aggregates was a commercially available recycled stone obtained from a plant in Johannesburg that processes rubble for use as fills in civil works. The other recycled aggregates were prepared from concrete chunks and fired clay bricks recovered from a nearby landfill. These were crushed using a laboratory aggregate crusher to produce 19 mm aggregates shown in Figure 1(a)-(d) of full paper.

2.2 *Concrete mixtures and test methods*

Concretes made with recycled stone aggregates were prepared in water/cement ratios (w/c) of 0.6 and 0.45, and corresponding cement contents of 350 kg/m^3 and 430 kg/m^3. No partial replacements for recycled aggregates were made. To isolate the influence of recycled aggregates, the same type of crusher sand was used in all mixes.

3 RESULTS AND DISCUSSION

3.1 *Workability and compressive strength results*

Figure 1 shows that recycled aggregates generally reduce the workability of concrete mixtures. Crushed brick stone exhibited the greatest effect and may be related to its surface characteristics causing mechanical interlocking of particles and resisting rheological flow. To maintain the same slump (without use of plasticizers) would require higher water contents for mixes containing recycled aggregates which in turn would reduce the strengths.

3.2 *Split tensile strength results*

The split tensile strengths determined from 100 mm cubes also showed strength loss as a result of using recycled aggregates but their tensile strength behaviour was different from their effect on compressive strength.

3.3 *Modulus of elasticity*

In Figure 2, it can be seen that there is a strong relationship between the Young's modulus of elasticity (E) and compressive strength (f_{cu}), as expected. The graph also shows a plot of the equation, $E = 4.7\ f_{cu}^{0.5}$, typically used to roughly estimate the elastic modulus from compressive strength of concrete. It is clear that the fitting of the equation to data of recycled aggregates is poor. These results again indicate that while the form of E-f_{cu} relationship for recycled aggregates may be the same as that of normal aggregates, the actual expression relating data for concretes made with recycled aggregates might not apply to that for normal aggregates.

3.4 *Abrasion resistance*

The use of recycled aggregates of concrete origin tends to reduce abrasion resistance regardless of the strength grade of concrete, as shown in Figure 3. The recycled aggregates of brick sources gave good performance in abrasion resistance showing better results than the control mix made of the dolomite aggregate.

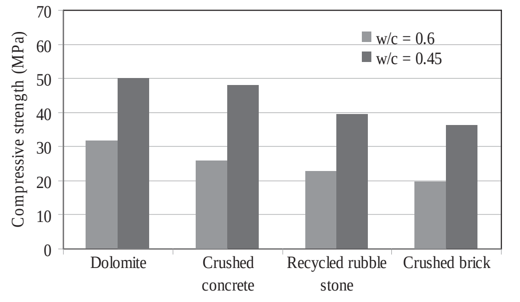

Figure 1. Compressive strength of concretes made using recycled stone aggregates.

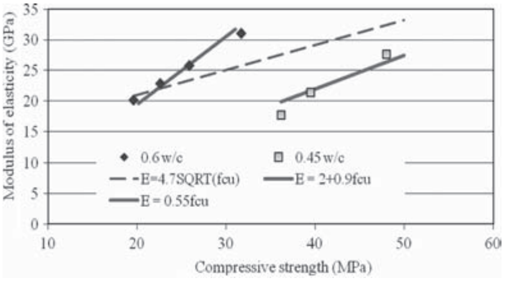

Figure 2. Relationship between compressive strength and elastic modulus of concretes made using recycled stone.

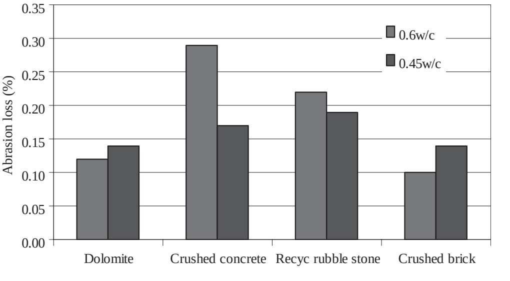

Figure 3. Abrasion resistance of concretes made with recycled stone aggregates.

4 CONCLUSIONS

It was found that all recycled aggregates significantly reduced the workability of concrete.

Results show that use of recycled aggregates of concrete origin reduced strength by up to 35% but the strength loss falls to negligible levels when the aggregates are used in concretes of high strength of at least 50 MPa. Stones of brick origin relatively gave higher strength losses but also produced the best tensile strength and abrasion resistance than all other aggregates.

Concrete Repair, Rehabilitation and Retrofitting III – Alexander et al. (eds)
© 2012 Taylor & Francis Group, London, ISBN 978-0-415-89952-9

Innovative low cost fibre-reinforced concrete—Part I: Mechanical and durability properties

D. Bjegović
Faculty of Civil Engineering, University of Zagreb, Kaciceva 26, Zagreb, Croatia
Faculty of Civil Engineering, Institut IGH, Janka Rakusina 11, Zagreb, Croatia

A. Baricevic & S. Lakusic
University of Zagreb, Kaciceva 26, Zagreb, Croatia

ABSTRACT: Over the past decades, significant attention has been focused on waste tyre management, since the presence of waste tyres in the environment can have negative effects on sustainable development. Just like most EU countries, Croatia also recycles large quantities of accumulated tyres, although not all by-products are equally reused. Researchers from Faculty of Civil Engineering University of Zagreb investigate possibilities for reusing rubber and steel fibres obtained during mechanical recycling in the construction of concrete pavements. Research results show that innovative and sustainable concrete mixtures, meeting criteria set in relevant standards, and offering cost savings on pavement construction and rehabilitation projects, can be prepared using the mentioned by-products. In addition to environmental benefits, recycled fibres are highly likely to be used as choice material in the future because of cost considerations (they are ten times less expensive when compared to industrial fibres).

1 INTRODUCTION

Croatia started building its motorways in late 1970s. Today, Croatia has more than 1.2 thousand kilometres of modern motorways connecting all parts of the country. Traditionally, road pavements in Croatia are mostly built as asphalt pavements, while concrete pavements are mostly used for building short segments on toll stations, as they present better abrasion and freezing resistance properties, and higher ductility, when compared to asphalt pavements.

Investigation on the use of steel fibres recycled from waste tyres for preparation of wet and dry (roller compacted concrete) steel fibre reinforced concrete for pavements implied that recycled steel fibres present viable alternative to the industrially produced steel fibres, if used in higher quantities, or if blended with industrially produced fibres. The analysis of earlier studies reveals that extensive research is needed on possible interactions between industrial and recycled fibres.

2 EXPERIMENTAL RESEARCH

Research on possible interaction of by-products from mechanical recycling of waste tyres, so as to enable production of low cost fibre-reinforced concrete, was performed at the Faculty of Civil Engineering University of Zagreb. Extensive research conducted in collaboration with industrial partners included testing of more than one thousand concrete specimens, so as to determine 16 different properties. Only a part of this research will be presented in this paper. The mixture composition is given in Table 1.

2.1 *Mechanical properties*

Adequate mechanical properties of concrete delay formation of cracks due to traffic load, temperature-induced thermal stresses, freeze-thaw damage, water infiltration, ageing effects, and so forth. With the progress of analysis, it became obvious that incorporation of rubber particles (5 percent of the total volume of aggregate) causes minimum reduction if correlation is done with the mixture containing the air entraining admixture only (Fig. 1).

2.2 *Durability properties*

Durability parameters of a material are of major interest when material is directly exposed to environmental loads, which is obviously true for pavements. It has been established that the presence of de-icing salts during winter is very harmful for the microstructure of concrete. In order to obtain an adequate resistance, the presence of an air entraining admixture in mixture is obligatory. In addition, low modulus of elasticity allows rubber to act as a small spring and absorb pressure of water in capillary pores during freezing.

Table 1. Mixture composition.

Mixture	Cem. (kg)	Water (l)	Aggre. (kg)	Super-pla. (kg)	Air entrai. (kg)	Silica fume (kg)	Industrial fibres (kg)	Polypro. fibres	By—products of mechanical recycling of waste tyres (kg) Steel fibres	Rubber	Textile fibres
100I0R	420	170	1743	2.31	0	21	30	0	0	0	0
100I0RA	420	170	1742	2.31	0.25	21	30	0	0	0	0
100I0RAG	420	170	1656	2.31	0.25	21	30	0	0	18.9	0
100I0RAGP	420	170	1653	2.31	0.25	21	30	2.52	0	18.9	0
70I30RAGT	420	170	1653	2.31	0.25	21	20.87	0	9.13	18.9	2.52
50I50RAGT	420	170	1653	2.31	0.25	21	15	0	15	18.9	2.52
0I100RAGT	420	170	1653	2.31	0.25	21	0	0	30	18.9	2.52

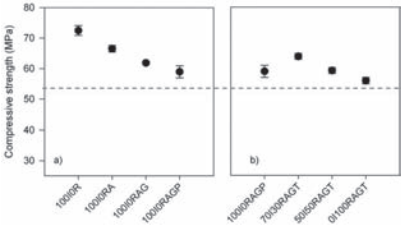

Figure 1. Compressive strength: a) Influence of rubber particles b) Influence of different fibre ratios and by-products.

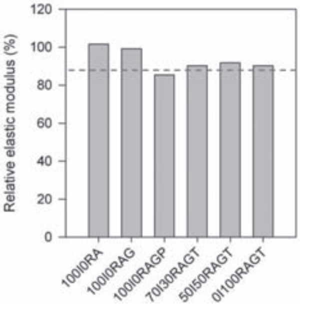

Figure 2. Freezing resistance: a) Influence of rubber particles b) Influence of different fibre ratios and by-products.

After analysis of results, it can be seen that the presence of by-products from mechanical recycling of waste tyres is compliant with all criteria (Fig. 2).

2.3 *Economic eligibility*

Concrete prepared in the course of the study is compliant with all relevant specifications for concrete pavements. In addition, an economic analysis was performed (Table 2).

If calculations are done per m^3, it is clear that savings of up to 33 percent can be made if recycled fibres alone are used. These savings concern only the economic viability of this new low-cost material, although environmental savings are also considerable, which is why this material can rightly be characterized as extremely viable.

Table 2. Price per m^3 of prepared mixtures and possible savings.

Mixture	€/m^3	Savings
100I0RA	€112	0
70I30RAGT	€104	7%
50I50RAGT	€97	14%
0I100RAGT	€80	33%

3 CONCLUSIONS

The present economic situation is certainly favourable for application of innovative low-cost materials. Croatian investments in construction industry amounted to about 7 percent of the GDP in 2009, out of which most sums were invested in the construction and rehabilitation of motorways. Possible reduction in motorway rehabilitation costs, ranging from 7 to 33 percent, makes this research important not only for the scientific community but for the society in general.

The analysis conducted in this paper implies that innovate low-cost fibre reinforced concrete meets all criteria set in standards, thus making introduction of this recycled material reasonable and justified. The main disadvantage of the studied material is its higher external corrosion compared to that exhibited by standard materials (100I0RA). However, this disadvantage is limited to negative visual appearance of the material, and no negative impacts on material properties have been noted.

Additional positive influences of recycled materials, namely of rubber and textile fibres, will be presented in Part II of this paper, in which their influence on concrete ductility, post cracking behaviour, and impact resistance, will be investigated.

Concrete Repair, Rehabilitation and Retrofitting III – Alexander et al. (eds)
© 2012 Taylor & Francis Group, London, ISBN 978-0-415-89952-9

Innovative low cost fibre-reinforced concrete—Part II: Fracture toughness and impact strength

J. Krolo, D. Damjanovic, I. Duvnjak, D. Bjegović, S. Lakusic & A. Baricevic
Faculty of Civil Engineering, University of Zagreb, Zagreb, Croatia

ABSTRACT: Previous investigations acknowledged that reinforcement of concrete with randomly distributed short fibres may improve the energy absorption during static and dynamic loading by comparison to ordinary concrete. This paper presents fibre-reinforced composite concrete, consisting of recycled steel fibres and recycled rubber in combination with industrial steel fibres. As a yield of tire recycling, steel fibres and rubber were obtained and used as by-products in composite concrete. Experimental investigation included six concrete mixtures with ratio of industrial to recycled fibres 100/0%, 50/50% and 0/100%, with or without the addition of recycled rubber. Toughness and impact strength were investigated on the concrete elements consisting of various ratios of the industrial and recycled fibres with addition of recycled rubber particles. Fracture toughness test was performed on Single Edge Notch Bend specimen (SENB or three-point bend). During static loading crack opening and its increase was recorded continuously by means of two LVDT sensors. During impact testing hammer was dropped at the specimens from the specified height. Test configuration included force measurement with sampling frequency of 50 kHz. Test results include toughness, impact resistance and other important properties of fracture mechanics.

1 INTRODUCTION

Purpose of composite material such as fibre-reinforced concrete (FRC) is to increase the bearing capacity after the initiation of the first crack. Optimal ratio of steel industrial fibres to recycled steel fibres, with addition of recycled rubber particles can enhance durability and mechanical properties of such composite or at least retain them.

Impact strength and toughness parameters are investigated in order to evaluate ductility, post cracking behavior and impact resistance of such composite. Investigation of these two parameters is performed for mixtures with different ratios of industrial to recycled steel fibres, with or without addition of recycled rubber particles, polypropylene and textile fibres. Research was conducted for seven different mixtures whose proportions are given in (see table 1).

Impact resistance is usually characterized by the following parameters:

- Number of blows causing the first crack initiation (N_c),
- Work consumed for the first crack initiation (W_c),
- Specific energy consumed for the initiation of the first cracks per unit volume (a_c) (Krolo & Šimić 2011).

$$a_c = \frac{W_c}{V} = \frac{N_c mgh}{V} \quad [J/m^3] \tag{1}$$

Energy of the falling hammer is transferred to the specimen (7 × 7 × 7 cm) placed on the force transducer. Testing was conducted at the Föpple drop weight impact machine.

1.1 *Impact resistance analysis and results*

Specific energy (a_c) is defined as energy per unit volume and it is proportional to work consumed for the first crack initiation (Figure 1.). Improved impact resistance (dynamic energy absorption as well as strength) is one of the important attributes of FRC. Impact strength presents number of blows in a “repeated impact” test to achieve prescribed level of distress. (ACI Committee 544 2009).

2 TOUGHNESS

Toughness evaluation of fibre-reinforced concrete is determined by three point bending test of prismatic specimens (15 × 15 × 55 cm) over 50 cm span.

The sum of energy spent before the first crack formation (fracture toughness corresponding to deflection δ) and different values of absorbed energy corresponding to specified deflection (3δ, $5{,}5\delta$ and $10{,}5\delta$) are defined. Ratio of these two values defines fracture toughness indices (Figure 3).

$$I_5 = \frac{W_{3\delta}}{W_\delta}; \quad I_{10} = \frac{W_{5,5\delta}}{W_\delta}; \quad I_{20} = \frac{W_{10,5\delta}}{W_\delta} \tag{2}$$

Table 1. Mixture composition.

									By – products of mechanical recycling of waste tires (kg)		
Mixture	Cem. (kg)	Water (l)	Aggre. (kg)	Superpla. (kg)	Air entrai. (kg)	Silica fume (kg)	Industrial fibers (kg)	Polypro. fibers	Steel fibers	Rub-ber	Textile fibers
100I0R	420	170	1743	2,31	0,00	21	30		0	0	0
100I0RA	420	170	1742	2,31	0,25	21	30		0	0	0
100I0RAG	420	170	1656	2,31	0,25	21	30		0	18,9	0
100I0RAGP	420	170	1653	2,31	0,25	21	30	2,52	0	18,9	0
70I30RAGT	420	170	1653	2,31	0,25	21	20,87		9,13	18,9	2,52
50I50RAGT	420	170	1653	2,31	0,25	21	15		15	18,9	2,52
0I100RAGT	420	170	1653	2,31	0,25	21	0		30	18,9	2,52

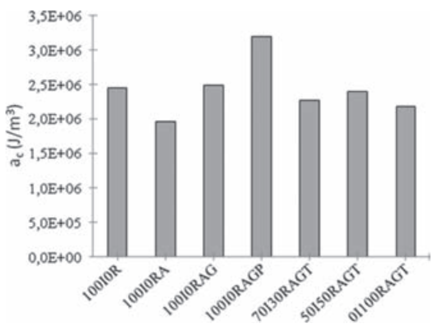

Figure 1. Specific energy consumed for the initiation of the first cracks per unit volume a_c.

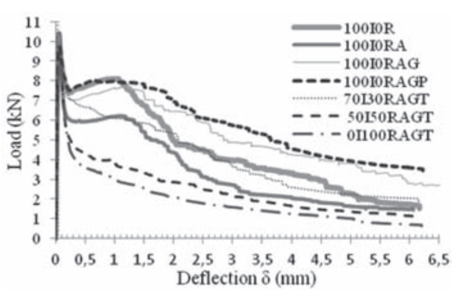

Figure 2. Force—deflection curves.

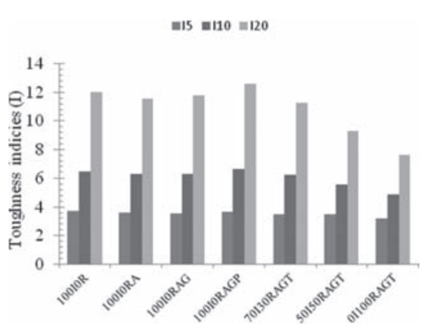

Figure 3. Toughness indices I_5, I_{10} and I_{20}.

Table 2. Total toughness, fracture energy and stress-intensity factor.

Mixture	W_{total} [Nm]	G_F [N/mm]	K_{Ic} [MPa$\sqrt{m}$]
100I0R	27,26	2,02	1,70
100I0RA	23,41	1,73	1,72
100I0RAG	30,14	2,23	1,53
100I0RAGP	37,50	2,78	1,60
70I30RAGT	23,78	1,76	1,81
50I50RAGT	17,39	1,29	1,36
0I100RAGT	12,04	0,89	1,68

When testing a notched specimen, it is possible to ensure stable crack growth. That enables us to determine fracture energy G_F as total energy dissipated over the crack surface (Table 2.).

$$G_F = \frac{W_{total}}{A_{lig}} \tag{3}$$

W_{total} is total work done (Table 2) in order to completely break the specimen and A_{lig} is the area of the resisting unnotched part of the cross section. Toughness of fibre-reinforced concrete can be determined using critical stress intensity factor (K_{Ic}) (Table 2).

3 CONCLUSION

Results of impact strength and toughness parameter investigation for innovative low cost fibre reinforced concrete are satisfactory. Mixtures incorporating recycled steel fibres as a replacement for industrial steel fibres didn't show any improvement. But for some ratios of industrial to recycled steel fibres with addition of recycled rubber particles and polypropylene or textile fibres didn't show significant deterioration of investigated parameters either. When economical and ecological savings are taken into account, possible use and further investigation of this material is reasonable and justified.

Concrete Repair, Rehabilitation and Retrofitting III – Alexander et al. (eds)
© 2012 Taylor & Francis Group, London, ISBN 978-0-415-89952-9

The effect of cement type on the performance of mortars modified by superabsorbent polymers

A.J. Klemm & K. Sikora
School of Engineering and Built Environment, Glasgow Caledonian University, Glasgow, UK

ABSTRACT: Although the use of SAP as internal curing agents in concrete has been widely documented in the literature for over a decade their suitability for general use is still not clearly articulated and cohesive. The research programme, of which a fragment is presented in this paper, endeavours to elaborate on materials characteristics and performance of SAP modified mortars made of CEM I and CEM II type cements. The variations in microstructural features and mechanical/physical properties of composites are the subject of the presented investigations. Application of SAPs in CEM I resulted in reduction of shrinkage. The opposite effect in fly ash cement could be attributed to the altered water management. Differences in strength development in different composites can be attributed to the combined effect of SAP internal curing, fly ash pozzolanic reaction as well collapsing of SAP.

1 INTRODUCTION

Construction industry like any other areas of economic and social life undergoes a continuous modifications and improvements in order to successfully comply with the requirements of sustainable development. To meet the market expectations numerous new composite materials have been developed, including cementitious materials modified by superabsorbent polymers (SAP).

Superabsorbent are cross-linked networks of hydrophilic polymers with a high capacity for water absorption. In contact with liquids SAP hydrate and form a swollen polymer gel. In cementitious matrix of fresh or young material, SAP form a system of evenly distributed pores filled with water which can be gradually released during hydration process. However in a collapsed stage superabsorbent polymers leave behind air filled pores which may result in an inevitable loss of strength.

Over the last couple of years a considerable number of research studies have been undertaken worldwide. They have been predominantly focused on shrinkage behaviour, mechanical characteristics and freeze/thaw performance. Unfortunately, no consensus has been reached on the efficiency of SAP products and their applicability to a wider range of cements in particular to blended cements such as high fly cements.

2 EXPERIMENT

Two sets of samples have been prepared containing different types of cement: CEM I 52.5 and CEM II/B-V 32.5 (LAFARGE). CEM II/B-V 32.5 is the Portland-fly ash cement containing minimum 30% of fly ash. Table 1 presents compositions of mixes.

Table 1. Composition of mixes.

Material	Unit mass [kg/m^3]
Cement (LAFARGE)	700
Silica fume (ELKEM, grade 940)	70
Water, w/c = 0.3	210
Aggregate	1350
Superplasticiser (GLENIUM 51)	12.6

Two types of superabsorbent polymers were used in cementitious composites (BASF). SAP 1 is a crushed type polymer with a lower affinity to water while SAP 2 has spherical shape particles. The w/c ratio in SAP containing mortar had to be adjusted to keep the same flow value, from 0.3 to 0.33 and 0.34.

Samples have been tested after 3, 7 and 28 days of lab curing. Experimental techniques involved: measurement of autogenous shrinkage, compressive and flexural strength and analysis of microstructural features (MIP, SEM).

3 SUMMARY

Preliminary investigations presented in this paper have lead to the following conclusions:

Cement type may have a noticeable effect on autogenous shrinkage in mortars modified by the superabsorbent polymers (Fig.1). Application of SAPs in samples containing CEM I results in reduction of shrinkage while in CEM II has an adverse effect.

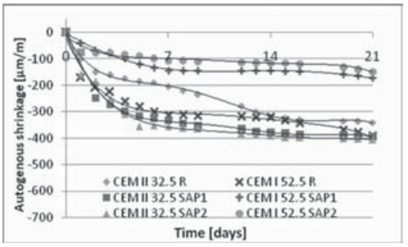

Figure 1. Autogenous shrinkage for composites containing CEM II 32.5 and CEM I 52.5.

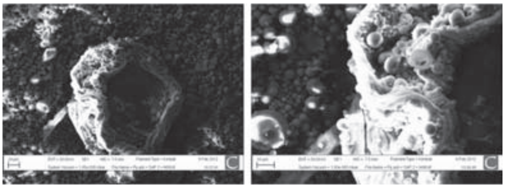

Figure 2. Fly ash particles in SAP gel network (SAP2).

Table 2. Total porosity [%]/Average pore diameter [nm].

		3 days	7 days	28 days
CEM II	R	17.97/27.4	15.19/23.3	12.78/13.3
32.5	SAP1	17.88/24.7	15.77/19.9	12.90/14.8
	SAP2	18.4/21.8	16.51/21.3	13.96/12.2
CEM I	R	13.11/30.3	10.80/22.8	9.02/19.7
52.5	SAP1	14.18/27.7	11.84/22.6	9.71/17.9
	SAP2	13.47/26.0	11.06/21.5	10.40/16.8

Increased value of autogenous shrinkage in CEM II samples modified by SAPs was caused by the altered water management in the system. It is likely that the SAP ability to absorb water is reduced in the presence of fly ash in blended cements or fly ash particles get surrounded by SAP gel leading to increase availability of water in the system. Another possible explanation is associated with superabsorbent gel formation. It is likely that during the initial water absorption at least part of fly ash particles may become surrounded by newly created SAP gel (Fig. 2). This subsequently would lead to increased availability of water and increased flow values.

Fly ash cement results in increased total porosity and decreased average pore diameter. Influence of SAPs is of secondary importance although small increase in porosity is noticeable (Tab 2).

Alterations in pore size distributions were studied for samples of 3, 7 and 28 days of age. Dominant range of pores for both cements was represented by a high peak between 20–70 nm (Fig.3). With the progress of hydration and release of water by SAPs, a tendency to move towards the smaller pores has been observed. Higher peak for very young composites containing SAP 2 was observed for both cements, although slightly smaller in CEM I. The difference between composites containing SAP1 and SAP2 can be attributed to variations in their absorption characteristics, swelling ratios and stabilities.

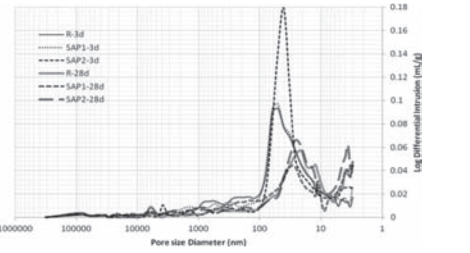

Figure 3. Pore size distribution of specimen with CEM II 32.5.

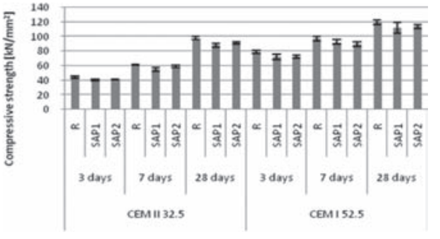

Figure 4. Compressive strength development [kN/mm²].

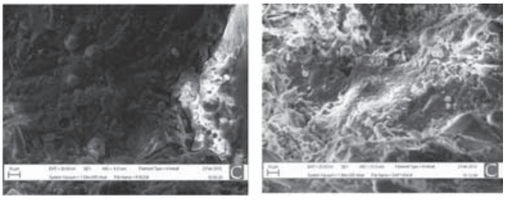

Figure 5. SEM images of composites R and SAP1 samples with CEM II 32.5 after 28 days of lab curing.

Compressive strength of samples containing CEM I is consistently higher than for CEM II (Fig 4). Application of SAPs in both cases has lead to a small reduction of compressive strength. The rate of strength gain in CEM I and CEM II samples is comparable during the first 7 days after which CEM II starts to dominate. Application of SAPs does not affect the general tendency. Enhancement of cement hydration in CEM II is bigger after 7 days.

Although the bond between fly ash and cementitious matrix is low at early ages of curing it improves with time due to densification of microstructure. However some unreacted particles of fly ash can be still identified in mature mortars (Fig 5).

Concrete Repair, Rehabilitation and Retrofitting III – Alexander et al. (eds)
© 2012 Taylor & Francis Group, London, ISBN 978-0-415-89952-9

Effect of super-absorbent polymer on simplification of curing and prevention of micro-cracking of concrete at early age

K. Ichimiya
Department of Civil and Environmental Engineering, Oita National College of Technology, Oita, Japan

H.-W. Reinhardt & A. Assmann
Department of Construction Materials, University of Stuttgart, Stuttgart, Germany

ABSTRACT: Super-Absorbent Polymers (SAP) absorb much water, for example the absorption ratio is from several hundred times to several thousand times of own weight in case of pure water, and maintains the absorbed water for many hours. The effectiveness of SAP on simplified curing technique and prevention of initial cracking of mortar and concrete had been reported in the past research. In order to look at this effect of SAP, mortar specimens which were modified with latest SAP were manufactured, and compressive strength and cracking condition of these specimens were compared.

1 INTRODUCTION

Tuji and others (Tsuji et al. 1999) reported the effectiveness of SAP on simplified curing technique and prevention of initial cracking of mortar and concrete.

In order to look at this effect of SAP, mortar specimens which were modified with latest SAP were manufactured, and compressive strength and cracking condition of these specimens were compared.

2 OUTLINE OF EXPERIMENTS

Two types of SAP were used. SAP-A is a product on the market and SAP-B was developed for concrete admixture. The water absorption ratio of SAP-A:r_A and SAP-B:r_B are 7.5g/g and 22.5g/g respectively. Particle size are as follows: average size of SAP-A is 280 μm, SAP-A-S is less than 63 μm, SAP-A-M is 63 to 125 μm, SAP-A-L is 125 to 250 μm, and average size of SAP-B is 75 μm.

Experimental factors and levels are given in table 1. Tap water, Portland cement (density = 3.15 g/cm^3), standard sand (density = 2.65g/ cm^3) and polycarbo-xylic acid type superplasticizer to adjust the flow value to 230 ± 10 mm were used. Extra water which SAP absorbs was added together with mixing water.

In Exp-1, a cylinder of diameter 5cm and height 10cm was used. The next day after placing, the mould was stripped. After that, specimens were stored in four types of curing condition: 1) water curing (20°C), 2) sealed curing (20°C), 3) water dipping for ten minutes a day and air curing (20°C, 60% RH), 4) air curing (20°C, 60% RH). Compressive strength was measured at seven days.

In Exp-2, a rectangular prism of length 22.5 cm, width 7.5 cm and height 3.0cm and with seven steel bars of D25 arranged as shown figure 1 was used. The order of experiment was storing in oven of 40°C, demolding at the next day after placing, storing in oven of 40°C again and evaluation of cracking at four days.

3 EXPERIMENTAL RESULTS AND CONSIDERRATIONS

3.1 *Experiments for simplified curing technique*

The results of SAP-B modified mixture is shown in figure 2 and figure 3. In case of SAP-B/C = 0.2%, the level and mutual relation of strength are roughly the same as the results of SAP-A/C = 0.4%. On the other hand, the results of SAP-B/C = 0.4% in figure 3 differ from the other mixture. In Japan, water curing is standard for quality control of concrete. On the basis of the strength in water curing, sealed curing and dipping curing are larger than that in water curing and that in air curing is equal to that in water curing. This result means that modifying with SAP-B makes longer water dipping intervals possible. The reason for the compressive strength of air curing is the same level as that of water curing would be explained by internal curing effect of SAP; the amount of occupied moisture from SAP is equal to the amount of released moisture from specimen. On the other hand, the cause of lower compressive strength of water curing than that of sealed curing and water dipping

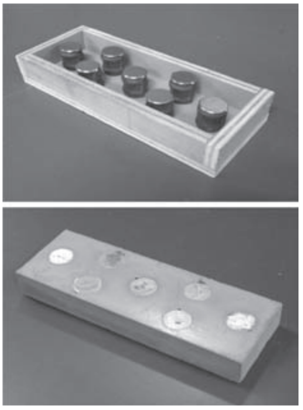

Figure 1. The specimen for experiment of prevention of initial cracking.

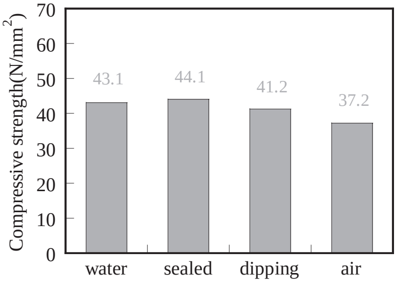

Figure 2. The compressive strength of SAP-B mortar which was cured in different conditions(SAP-B/C = 0.2%).

Table 1. Experimental factors and levels.

	W/C (%)	30,	40,	50
	S/C		1.0	
SAP mass(%) w. resp. to cem.	SAP-A/C	0,	0.4,	1.0
	SAP-B/C	0,	0.2,	0.4

curing are that water saturated pores might have a negative effect on compressive strength.

3.2 *Experiments for prevention of initial cracking*

Cracking conditions of SAP-B modified specimens are shown in figure 4. (a),(b),(c) are W/C = 30%. In both of W/C = 30% and W/C = 50%, SAP-B/C = 0.2% and 0.4% result in few cracks. The mass of water absorption of SAP-B/C = 0.2% is equal to that of SAP-A/C = 0.6%, because water absorption ratio of each SAP is $r_B = 22.5$g/g and $r_A = 7.5$g/g.

The expected SAP-A/C which prevents early age cracking is between 0.4% to 1.0%, and 0.6% is included in this range. If the limits of SAP/C which prevent early age cracking are 0.6% for SAP-A and 0.2% for SAP-B, the effect of cracking prevention might be decided only by the mass of water absorption.

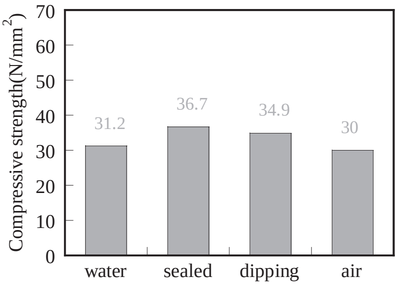

Figure 3. The compressive strength of SAP-B mortar which was cured in different conditions (SAP-B/C = 0.4%).

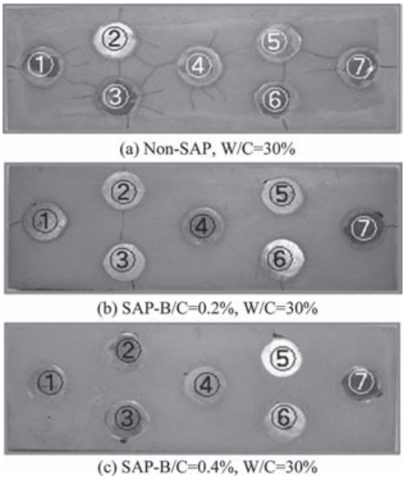

Figure 4. The cracking conditions of non-SAP and SAP-B modified mortar specimens.

4 CONCLUSION

(1) Because the compressive strength is correlated with the void volume of saturated SAP regardless of SAP types, this relation can be explained by void-cement theory.
(2) SAP-A size doesn't influence the compressive strength of mortars which were cured in different conditions.
(3) The compressive strength of SAP modified mortar estimated by SAP-B of 0.4% of cement mass can simplify curing.
(4) Both of SAP-A and SAP-B are able to prevent initial cracking: the minimum mixing ratio in this experiment is 1.0% and 0.2% respectively.

Concrete Repair, Rehabilitation and Retrofitting III – Alexander et al. (eds)
© 2012 Taylor & Francis Group, London, ISBN 978-0-415-89952-9

The influence of the particle size of superabsorbent polymer on internal curing of high performance concrete

Haoliang Huang
Microlab, Delft University of Technology, The Netherlands

Nguyen Van Tuan
Microlab, Delft University of Technology, The Netherlands
Department of Building Materials, Hanoi University of Civil Engineering, Vietnam

Guang Ye
Microlab, Delft University of Technology, The Netherlands
Magnel Lab for Concrete Research, Department of Structural Engineering, Ghent University, Ghent (Zwijnaarde), Belgium

ABSTRACT: In this paper, the influence of the particle size of Superabsorbent Polymers (SAP) for internal curing in High Performance Concrete (HPC) was investigated. Two types of SAP (SAP1 and SAP2) with different sizes were used as curing agents. The autogenous shrinkage of HPC was measured. In addition, the effect of SAP on mechanical properties was also studied. The results reveal that with the same dosage of SAP, the efficiency of internal curing by the SAP with the smaller size (SAP1) is higher than that by the SAP with the larger size (SAP2). By adding SAP into the mixture, the mechanical properties of HPC decrease slightly. By considering the workability, autogenous shrinkage and compressive strength, the SAP with smaller size (SAP1) has better efficiency as an internal curing agent than the other one (SAP2).

1 RESULTS AND DISCUSSION

1.1 *Autogenous shrinkage*

Figure 1 shows the autogenous shrinkage from the time of final setting. From these results, it is noted that autogenous deformation of the HPC mixture without SAP addition is considerable (larger than 700 μm/m in the first 160 hours after the time of final setting). In comparison, when 0.3% SAP (by weight of the cement) was added into the mixture, autogenous shrinkage decreases significantly. The autogenous shrinkage of HPC with SAP2 reduces by 26%. While for the HPC with SAP1, it reduces by more than 65%. Moreover, it should be noted that in the first 10 hours after the final set, the concrete matrix containing SAP1 swells a bit and then shrinks gradually.

From this result, it can be learned that mitigation of autogenous shrinkage of concrete by using SAP1 is more pronounced than that of SAP2, which may be caused by the smaller size of SAP1. With the smaller size, the total surface area of SAP1 is larger than that of SAP2 with a same dosage. Therefore, the total amount of water absorbed by SAP1 will be higher than that by SAP2. Moreover, it is well known that the microstructure of HPC is very dense and thus the moisture transport from SAP particles to its surrounding paste is hindered. Therefore, the effective range of internal curing for each SAP particle is limited. As a result, the better uniform distribution of SAP with a smaller particle size can increase the effectiveness of internal curing in HPC. However, if the particle size of SAP is too small, the amount of water absorbed in each SAP particle is very small. This small amount of water for internal curing can only perform for a very short time. When the water in each SAP particle is consumed completely, autogenous shrinkage of concrete will increases sharply. Therefore, the particle size of SAP should be reasonable in term of internal curing and further investigation is needed to make it clear.

1.2 *Mechanical properties*

Figures 2 and 3 show the compressive strength and flexural strength of HPC samples. From the results, it can be seen that by adding 0.3% of SAP (by the weight of cement), the compressive and flexural strength are reduced by about 8% and 6% respectively, at the age of 150 days. This may be caused by a higher amount of larger pores generated in the paste by SAP (Ye 2012). In this aspect, the SAP

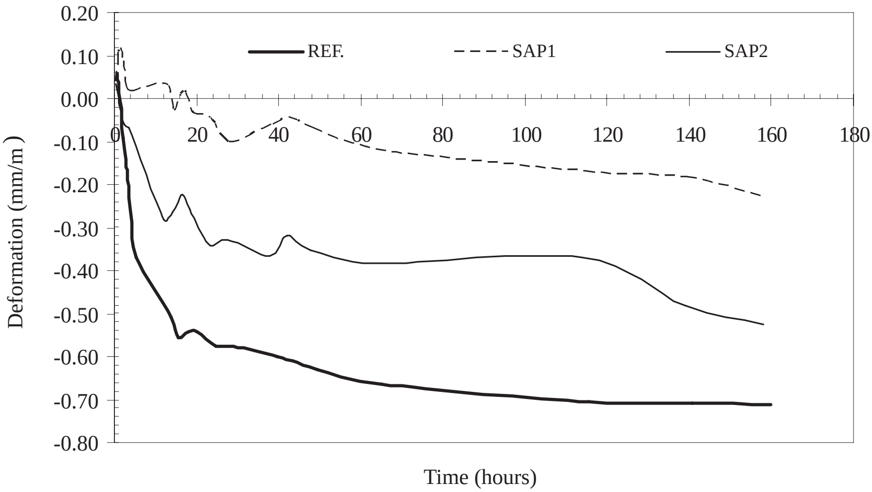

Figure 1. Autogenous shrinkage of HPC containing different SAPs.

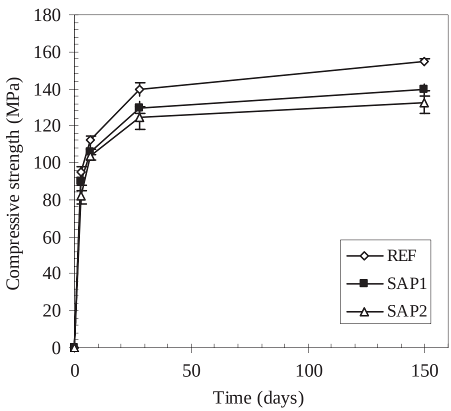

Figure 2. Compressive strength of HPC containing different SAPs.

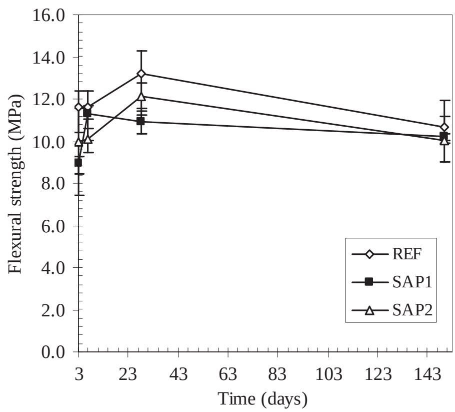

Figure 3. Flexural strength of HPC containing different SAPs.

acts as an air entrainment agent (Bentz & Jensen 2004). These air voids have a negative effect on the mechanical properties of concrete (Craeye 2011). Moreover, it should be noted that the reduction of the compressive strength of the HPC samples containing SAP2 is larger than that of sample containing SAP1. This may be attributed to a higher w/c ratio of the SAP2 mixture. It is also shown that the flexural strength at 150 days is smaller than that at the age of 28 days. It seems that the concrete becomes more brittle during this period. However, further study is needed to make it more evident.

2 CONCLUSIONS

In this study, the effect of the particle size of SAP on autogenous shrinkage and mechanical properties were investigated. Two types of SAP with different particle sizes were used as internal curing agents. From the experimental results, the main conclusions can be drawn as follow:

- The use of SAP1 with a smaller particle size mitigates autogenous shrinkage of HPC more significantly than that of SAP2.
- Both compressive strength and flexural strength of concrete reduce slightly with the addition of SAP.
- By considering the workability, autogenous shrinkage and compressive strength, SAP1 with a smaller size is of better efficiency as an internal curing agent than SAP2.

Concrete Repair, Rehabilitation and Retrofitting III – Alexander et al. (eds)
© 2012 Taylor & Francis Group, London, ISBN 978-0-415-89952-9

Porous network concrete: Novel concept of healable concrete structures

S. Sangadji & E. Schlangen
Microlab, Materials and Environment, Delft University of Technology, Delft, The Netherlands

A. Milenkovic
Grontmij, De Bilt, The Netherlands

ABSTRACT: Self healing concrete has advantages to self repair concrete structures in difficult conditions and to prolong its life time. Researchers used many methods, such as embedded capsules and hollow fibres containing healing materials in the concrete, which indicated some problems of healing agents release. Porous network concrete which is proposed in this paper offer alternative solutions to distribute such healing agent into a crack or cracks in the concrete structures. A porous concrete layer can be placed at the surface or internally in the concrete structure to create a pore network. After concrete hardens, shrinks, swells, deforms, and or cracks, a healing agent e.g. chemical-based, bacteria contained liquid, cement slurry, or mortar can be injected into the porous layer to produce a dense layer and to seal cracks. In this paper a simple system is designed to implement autonomous engineered repair or a self healing mechanism. It was found from the experiments that cracks were filled completely. Comparison of the mechanical properties of concrete beam samples before and after healing/repair shows the effectiveness of the proposed method.

1 INTRODUCTION

1.1 *The problems*

Cracks due to inherent brittleness in concrete structures attract attention since its trigger more serious durability problem. In tackling this problem, researchers proposed self healing systems preferably with automatic or autonomous capability. Several healing mechanisms have been tried in concrete materials such as capsule based and vascular system. Many of them have shown potentials although some impracticality limited their application in real situation.

In this paper we developed a novel approach to make concrete structures healable. We imitate bone morphology by making use of prefabricated cylindrical porous concrete cores, which are placed in the concrete structures interior. The porous network provides alternate means for (1) channeling temporary or permanent materials to form a dense layer and (2) distributing healing agent to cracks into the main body. This morphological analogy can be seen in figure 1. We also proposed a self healing mechanism concept which will be carried out in an autonomous manner. Three basic aspects; sensing, actuating, and adaptive controlling to the environment, will be incorporated into the system.

2 MATERIAL AND METHOD

Three types of the same size of prism specimens were used in this research; plain concrete prism (PLA prism), reinforced concrete prism (RC2 prism), and porous network concrete (PNC prism). RC2 prism reinforced by one Ø2 mm rebar placed at the height of 10 mm from specimens' bottom. To create porous network concrete, a porous concrete core was made and placed in the center interior of a solid concrete prism. The PNC prisms were intended for self healing mechanism testing. Both PLA and RC prisms were meant to be as reference

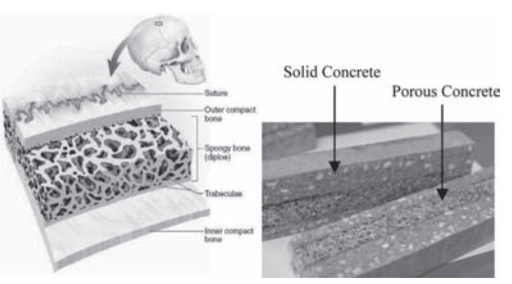

Figure 1. Analogy in terms of morphology between (a) flat bone (after Saladin, 2010) and (b) porous network concrete.

prisms. In this project a two compound epoxy was chosen for healing agents explicitly in order to seal the cracks.

Plain concrete, reinforced concrete prisms, and porous network concrete prisms were loaded by three point bending test. For the reinforced concrete prisms, after first loading cycle, the crack was directly injected with healing agent into the crack plane by means of syringe and needle. Meanwhile for porous network concrete, after the first crack had been created, the injection of healing agent was carried out through the porous core by means of semi-automatic injection action. To achieve complete polymerization of healing agents 24 hours curing time was allowed in the oven at 35°C.

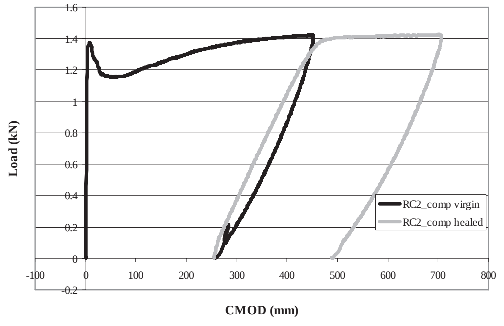

Figure 2. Load versus CMOD of reinforced concrete with second loading after the crack plane was directly injected with healing agents.

3 RESULTS AND DISCUSSION

For the reinforced concrete specimens in which cracks were manually healed by direct injection (pressure grouting using the syringe), the curves obtained during this second loading can also be seen in figure 2. It shows that there was almost no stiffness and strength regain. It was also observed that the crack that was obtained in the first loading cycle just reopened after reloading. It can be concluded that mechanical recovery in terms of strength and stiffness did not work.

In Figure 3 the results for a porous network concrete (with rebar) are presented. For this specimen also a first and second loading regime was applied. In between the porous core was injected with the semi-automatic procedure as explained above. This indicates that regain in strength and in stiffness was obtained due to crack healing action. It was also observed that new cracks were formed upon reloading.

Evidence of the healing efficiency is also provided by a new crack formation which occurred in the prism. The final crack pattern is different from the crack in the first loading. The crack at this new location was not observed to occur in the first cycle, and therefore, this is clear evidence of the effectiveness of the bonding capabilities of the epoxy when used within the concrete specimen.

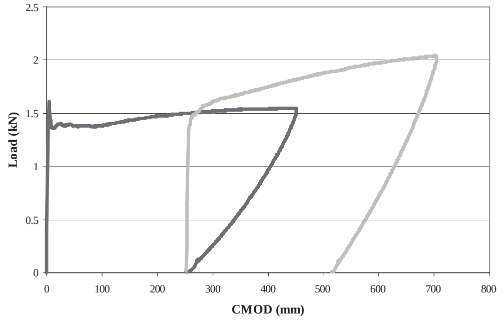

Figure 3. Load versus CMOD of porous network concrete with second loading after the crack was injected with healing agents through porous network in the interior of concrete main body.

4 CONCLUSIONS

Mimicking bone morphology, a prefabricated porous concrete cylinder is placed in the interior of concrete structures. When cracks occur in the main body of concrete structures, this porous network can be used to transfer liquid healing agent into the crack or fracture zone. Provided that the healing agent hardened or polymerized, the crack would be sealed and mechanical recovery might take place. The effectiveness of the proposed concept may be examined by comparing the mechanical response of the two specimens, although it should be noted that the healed specimen will be stronger partly because the porous structure is filled with epoxy, thus, producing a polymer-cementitious composite which enhances the mechanical properties of the healed system.

ACKNOWLEDGEMENT

The Authors would like to thank Mr. Gerrit Nagtegaal for assisting in all mechanical testing. Financial support from the Ministry of National Education, the Government of the Republic of Indonesia in the form of scholarship for the first author is gratefully acknowledged.

Concrete Repair, Rehabilitation and Retrofitting III – Alexander et al. (eds)
© 2012 Taylor & Francis Group, London, ISBN 978-0-415-89952-9

An experimental methodology to assess the self-healing capacity of cementitious composites with "aero-crystallizing" additives

L. Ferrara, V. Krelani, I. Pessina & P. Bamonte
Department of Structural Engineering, Politecnico di Milano, Italy

E. Gastaldo Brac
Penetron Italia, Torino, Italy

ABSTRACT: The self healing capacity of cementitious composites employed for either new or repairing applications opens challenging perspectives for the use of a material intrinsically able to recover its pristine durability levels, thus guaranteeing a longer service life of the designed applications and a performance less sensitive to environmental induced degradation. One possibility of achieving the aforementioned self-healing capacity stands in the use of additives featuring a "delayed crystalline" activity, which, when in contact with water or atmosphere humidity, form chemical compounds which are able to reseal the cracks thus guaranteeing the partial recovery of the pristine mechanical performance. In order to quantify this self healing ability and its effects on the recovery of mechanical properties of the material, a methodology has been developed and will be presented in this paper. It consisted in pre-cracking up to different crack opening levels (a three point bending scheme with COD measurement was employed) prismatic beam specimens, made with both concrete added or not with the aforementioned additives. Specimens were then submitted to accelerated temperature and humidity cycles, representative of autumn climate conditions in northern Italy, for different exposure times. Finally, three point bending tests were performed on either uncracked or pre-cracked specimens and results, in terms of load-crack opening curves, were compared with those obtained from virgin specimens before any "conditioning". This allowed crack "self-closure" to be evaluated and "self healing" indices to be defined and correlated, *e.g.*, to the load-recovery capacity.

1 EXPERIMENTAL PROGRAM

This study focused on the assessment of the self healing capacity of cementitious composites and the reliability of aero-crystallizing additives to trigger and enhance it, quantifying its effects on the mechanical properties of the materials. Two normal strength concretes were mixed (Table 1). 31 beam specimens, 50 mm thick, 500 mm long and 100 wide were cast with each of the mixed concretes. The specimens, were stored in a moist room at 20°C and 95% RH for 35 days.

At the end of the curing period, specimens made with each type of concrete were divided into three groups: specimens of two groups, for each concrete, were pre-cracked in 3-point bending, up to (residual) crack openings equal to about 130 and 270 μm respectively, whereas specimens belonging to the third group were left uncracked. Specimens were then put into a climate chamber and subjected to the temperature and humidity cycle sketched in Figure 1. Specimens were kept into the climate chamber for four weeks. At the end of the first and second week, one third of each group of specimens was taken out of the chamber and subjected to three point bending tests, up to failure. All tests were performed assuming as feedback control variable the Crack Opening Displacement (COD), measured at the mid-span section by means of a clip-gauge.

Table 1. Mix design of investigated concretes.

Constituent	Without additive (kg/m^3)	With additive (kg/m^3)
Cement type II 42.5	300	300
Fine aggregate 0–8 mm	975	975
Coarse aggregate 8–16 mm	975	975
Water	165	165
(w/c)	0.55	0.55
Superplasticizer	3	3
Aero-crystallizing additive	=	3

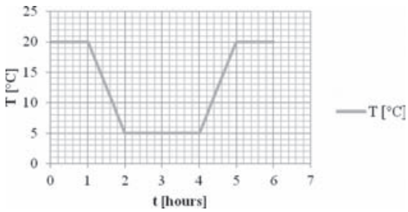

Figure 1. Hygrothermal cycles.

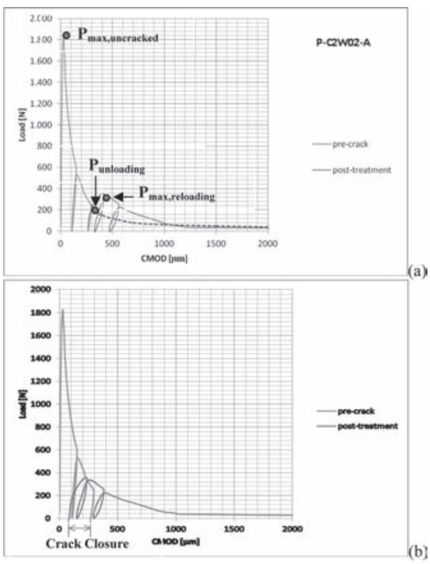

Figure 2. Example of load-COD curve obtained from 3pb tests on the same specimen before and after hygrothermal conditioning showing strength recovery (a) and proposal of a procedure to evaluate crack closure (b).

2 EXPERIMENTAL RESULTS

Figure 2a shows an example of Load vs. COD curve, as recorded from the same specimen tested in 3-point bending before and after the climate chamber exposure. The latter curve has to be interpreted as a reloading of the specimen, following a previous unloading at a prescribed crack opening and the hygrothermal conditioning. The post-conditioning load-COD curve has been rigidly shifted backward along the axis of abscissae (Figure 2b), until its peak load point intersected the softening branch of the virgin load-COD curve. The amount of this shifting was defined as Recovery Index or Index of Crack Self-Healing (ICSH) (Figure 3a–b).

The following statements hold:

– even normal strength concrete, mixed with medium to high water/cement ratios, is likely to exhibit, after conventional aging time (> 28 days), a not negligible capacity to self-heal cracks; this is most likely due to continuing hydration of anhydrous cement particles present on cracked inter faces and exposed to water or even to environment moisture upon cracking. This capacity anyway appears to be randomly scattered and not affected by the duration of the exposure to high relative humidity;
– the addition of aero-crystallizing admixture enhances the aforementioned self-healing capacity, which appears to increase with the time of exposure to high moisture and, most of all, is significant even for higher crack opening.

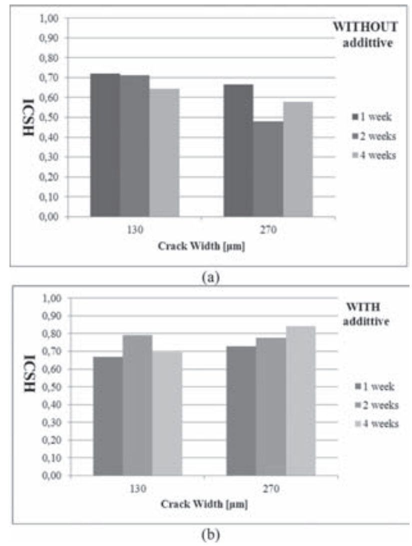

Figure 3. Index of Crack Self Healing (ICSH), evaluated for concretes without (a) or with (b) crystalline admixture, as a function of crack opening and exposure duration.

3 CONCLUSIONS AND FURTHER WORK

Cementitious materials inherently possess, within an acceptable range, some self-healing capacity, most likely due to continuing hydration favored by suitable environment conditions, which is anyway randomly scattered.

The inclusion in the concrete mix of aero-crystallizing admixtures not only enhances the aforementioned self-healing capacity, even up to more than 80% recovery of the crack opening, but also makes it more reliable and consistent.

The proposed methodology needs to be assessed and confirmed on wider variability of natural and artificial exposure conditions (natural exposure, water immersion, wet-and-dry cycles even in marine-like environment etc.).

Concrete Repair, Rehabilitation and Retrofitting III – Alexander et al. (eds)
© 2012 Taylor & Francis Group, London, ISBN 978-0-415-89952-9

Study of the effectiveness of different types of surface protection materials applied in concrete structures

Kalline da Silva Almeida, Manuela Queiroz Oliveira, Victor Pereira & Eliana Barreto Monteiro
Escola Politécnica da Universidade de Pernambuco, Brazil

ABSTRACT: Currently one of the main problems encountered in concrete structures is the corrosion, usually caused by the ingress of aggressive agents from the environment outside. This phenomenon has lead to the development of products that aim to prevent the penetration of aggressive agents, including surface treatments for concrete. Within this context, this paper intends to analyze three types of surface protection systems (hydrophobic agents, coating and pore blocker), usually applied in reinforced concrete structures located in marine environment. Water absorption by immersion and capillarity tests were performed, in addition to accelerated corrosion tests, in order to comparatively evaluate the performance of the studied materials. With the procedure adopted, the advantages of using the hydrophobic agents as a surface product protection in the structures was evident. It was also showed that the hydrophobic agents performance was comparatively better than other studied materials.

1 INTRODUCTION

Commonly are seen numerous cases of reinforced concrete structures that have structural, functional or aesthetic problems. Structures must possess not only the capability to resist loads, but must also be able to resist the action of aggressive agents present in the environment, which can be the main cause of distress.

Evaluation of the effectiveness of the protection system surface, shows to be of great importance because of the need to better understand the operation of this type of product in different types of situations, seeking therefore complement the gaps left by the works already developed.

2 EXPERIMENTAL PROCEDURES

2.1 *Independent variables*

In this work it was decided to consider as independent the variables listed below:

- protection groups—pore liner (hydrophobic agents), coating and pore blocker - [reference (concrete unprotected) + 3 protection systems)];
- State of the concrete substrate to be protected (contaminated and uncontaminated by chloride ions), and;
- Microstructure of concrete—variation of w/c ratio (0.4 and 0.7).

2.2 *Dependent variables*

Variables that are influenced by the variation of the independent variables and, in certain situations, for other dependent variables. The dependent variables of this study are presented following:

- Corrosion potential (Ecorr);
- Water absorption by immersion;
- Capillary water absorption.

2.3 *Materials used in the preparation of specimens*

Surface protection materials

Three different protection systems were used, being all available in the Brazilian market and destined for surface treatment of reinforced concrete structures. The choice of products aimed to compare representatives of the three categories of surface protection systems: pore liner (hydrophobic agents), coating and pore blocker.

Table 1 shows the consumption and the characteristics of the materials studied.

2.4 *Definition of the test series*

The experimental program aimed to evaluate comparatively the influence of three types of surface protection systems for concrete surfaces, varying two parameters:

- water/cement ratio;
- Substrate: with/without chlorides.

Table 1. Description of the systems that are part of the study.

Protection system	Identification	Manufacturer's description	Consumption rate (l/m^2)	Number of coatings	Cure type	Density (g/cm^3)	Setting time (h)
Simple	Hydrophobic agent	Silane—siloxane	0.25	2	Water loss + reaction	0.76	6
Simple	Coating	Acrylic varnish—water-based	0.20	1	Reaction	1.26	2
Simple	Pore blocker	Sodium silicate liquid	0.20	3	Reaction	1.02	½ a 1

Table 2. Name of the series for the water absorption by immersion test.

Series	Product	W/C	Mix proportion
R1	Reference	0.4	1:1.3
R2	Reference	0.7	1:3
H1	Hydrophobic agent	0.4	1:1.3
H2	Hydrophobic agent	0.7	1:3
F1	Coating	0.4	1:1.3
F2	Coating	0.7	1:3
B1	Pore blocker	0.4	1:1.3
B2	Pore blocker	0.7	1:3

Table 3. Name of the series for the capillary water absorption test.

Series	Product	W/C	Mix proportion
R3	Reference	0.4	1:1.3
R4	Reference	0.7	1:3
H3	Hydrophobic agent	0.4	1:1.3
H4	Hydrophobic agent	0.7	1:3
F3	Coating	0.4	1:1.3
F4	Coating	0.7	1:3
B3	Pore blocker	0.4	1:1.3
B4	Pore blocker	0.7	1:3

The specimens were molded with different water/cement ratios with significant variation (a/c = 0.4 and a/c = 0.7). All specimens had the same conditions in the fresh state, that is, they were made within the same range of workability: 260 to 320 mm, determined by the mortar consistency test NBR 7215.

Only the specimens prepared for testing of potential corrosion were cast specimens with and without addition of chloride ions. This procedure aimed to evaluate the behavior of surface protection products with regard to the periods of initiation and propagation of corrosion in new structures (without contamination of chloride ions) and antique structures (contaminated by chloride ions).

Tables 2, 3 and 4 show the series defined for each test performed.

Table 4. Name of the series for the corrosion potential test.

Series	Product	W/C	Mix proportion	Presence of chloride ions
R5	Reference	0.4	1:1.3	–
R6	Reference	0.4	1:1.3	1%
R7	Reference	0.7	1:3	–
R8	Reference	0.7	1:3	1%
H5	Hydrophobic agent	0.4	1:1.3	–
H6	Hydrophobic agent	0.4	1:1.3	1%
H7	Hydrophobic agent	0.7	1:3	–
H8	Hydrophobic agent	0.7	1:3	1%
F5	Coating	0.4	1:1.3	–
F6	Coating	0.4	1:1.3	1%
F7	Coating	0.7	1:3	–
F8	Coating	0.7	1:3	1%
B5	Pore blocker	0.4	1:1.3	–
B6	Pore blocker	0.4	1:1.3	1%
B7	Pore blocker	0.7	1:3	–
B8	Pore blocker	0.7	1:3	1%

3 CONCLUSIONS

Considering the conditions of tests presented here the following conclusion can be obtained:

- With the reduction of water/cement ratio was an improvement in the performance of three types of materials used, with respect to water absorption and therefore reinforcement corrosion due to the action of chloride ions.
- The specimens made with water repellent material showed a better performance than the other specimens made with the other materials of water repellent material showed a comparatively better performance than the other materials with respect to water absorption and therefore the action of corrosion due to chloride ions, especially for the water/cement ratio 0.4.
- With the technique used, it was possible to classify the materials studied in decreasing order of performance, for environments contaminated by chloride ions:
  Hydrophobic agent > Coating > Pore blocker.

Concrete Repair, Rehabilitation and Retrofitting III – Alexander et al. (eds)
© 2012 Taylor & Francis Group, London, ISBN 978-0-415-89952-9

Influence of cement content and environmental humidity on cement-asphalt composites performance

A. Garcia
Empa, Swiss Federal Laboratories for Materials Science and Technology, Switzerland

P. Lura
Empa, Swiss Federal Laboratories for Materials Science and Technology, Switzerland
ETH Zurich, Institute for Building Materials (IfB), Switzerland

M.N. Partl
Empa, Swiss Federal Laboratories for Materials Science and Technology, Switzerland
KTH Stockholm, Department of Civil and Environmental Engineering, Road Engineering/Sealing Components, Sweden

ABSTRACT: Ideally, a material with low-environmental impact and combining the advantages of both asphalt and concrete could be obtained by combining bitumen emulsions and a cementitious material. These bitumen emulsions harden by a process where the water in the mixture is removed both by evaporation and by cement hydration.

In this research, cold asphalt mixtures with different percentages of cement replacement have been prepared and tested with Marshall Stability tests. Furthermore, mixtures with 0% and with 3% of cement replacement were cured under different environmental relative humidity (35, 70 and 90% RH). Additionally, the mass evolution of the specimens cured under different humidity conditions was measured. According to the results of the present study, cement contributes to the hardening of cold asphalt mixtures by creating mortar bridges between the aggregates and by removing water from the mixtures through cement hydration.

1 INTRODUCTION

An ideal pavement material, with the advantages of both asphalt and concrete, could be obtained by combining asphalt emulsions and a cementitious material. The purpose of this combination is to reach higher compressive strengths and lower temperature susceptibility than hot mix asphalt concrete and higher tensile strength and flexibility than cement concrete. Additionally, it would not be necessary to heat up the materials, for mixing them. For this reason, cold mix asphalt would also have the advantage of reducing the energy consumption and the CO_2 emissions. Finally, the composite could be used both for pavement recycling and for new mixtures.

Without cement additions, cold mixes have very poor mechanical performance and very high moisture susceptibility. Moreover, it is well known that the addition of cement improves the Marshall stability of the mixtures, the compressive strength, the stiffness and the microhardness of the binder. For these reasons, between 1 and 3% of ordinary Portland cement by mass of aggregates is usually added to cold asphalt mixtures. Additionally, cement helps the emulsion to break faster, with shorter curing time, as it absorbs water from the emulsion.

The fine particle size of the cement and their partial dissolution upon contact with an aqueous solution induce a faster breaking of the emulsion after placement. The use of very fine particles may however impact the mixture negatively, because water from the emulsion will be used for coating the particles and will be consumed in early-hydration products. As a result, not all aggregates may be covered with emulsion. In the end, cement hydrates form an integral part of the binder, increasing the resistance to permanent deformation and improving moisture and temperature susceptibility of cold mixed asphalt.

Finally, it has been reported that cold mix asphalt concrete could have comparable properties to hot mixtures after curing. To solve this problem, and for obtaining a better understanding of the behaviour of cold mix asphalt, a series of mixtures with different amounts of cement and cured at a constant temperature (20°C) but at different environmental humidity levels (35, 70 and 90% RH) have been investigated. The main objective of this paper is to prepare a solid basis for continuing the exploration of this class of materials in the future.

2 EXPERIMENTAL INVESTIGATION

2.1 *Results*

The evolution of the force resisted by samples with different amounts of cement, and cured during various days, at 90% ambient relative humidity was measured in the research.

It could be observed that just after compaction, the portable capacity of the mixture was close to 0 kN, while the force resisted by the cores increased with the curing time. Additionally, it can be observed that the mixtures hardened faster when the amount of cement was increased.

Additionallly, the evolution of the force and rigidity resisted by cold mix asphalt, without cement, cured at 20 ± 0.5°C and at different relative humidities was measured. As in the cases cited above, the force resisted by the test specimens, as well as their rigidity after compaction, was practically negligible, however it increased progressively with time. Moreover, it can be observed that, during the first days, specimens cured at low relative humidities hardened faster than specimens cured at very high humidities.

Besides, specimens cured under wet conditions did not acquire any measurable mechanical resistance during the curing process. During the experiments, these cores were too loose for being tested and crumbled into pieces during handling.

Additionally, in Figure 1, the relationship between the rigidity and the force, for all the samples studied, is shown. It can be observed that the rigidity of the test samples increased linearly with the force resisted. Also, it can be seen that this curve is the same for all the samples studied, independently of the amount of cement in the mixture and of the environmental relative humidity at which the test specimens were cured.

Finally, when these results are compared with those obtained for hot mix asphalt, it can be observed that even when both materials could resist the same force, the rigidity of cold mix asphalt was always lower than that of the reference hot mix asphalt.

2.1.1 *Water loss*

It was noted that approximately 35% of the water was lost during the first curing day. This happened mainly due to the compaction process of the test specimens, which reduced the total space available for water in the mixture. Additionally, it could be observed that the main mass loss happened during the first 5 days, when the total amount of water in the mixture was reduced to about 25% of the initial value.

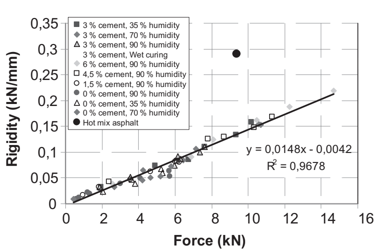

Figure 1. Rigidity (kN/mm)-Force (kN) relationship for test samples with different amounts of cement, cured at 90% humidity.

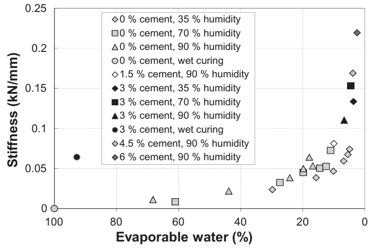

Figure 2. Relationship between the rigidity of the test specimens and the total amount of evaporable water in the mixture.

Cold mix asphalt without cementitious additions was much more sensitive to the environmental humidity than when cement is added. Finally, there was a minimum amount of water that could be eliminated through the evaporation in the air.

In Figure 2 the relationship between the rigidity of test specimens and the total amount of water present in the material is shown. It can be observed that the rigidity of the test specimens appears to be related to the percentage of evaporable water still present in the mixture. Moreover, the mixtures containing cement were more rigid and resisted higher loads, than mixtures without cement.

3 CONCLUSIONS

In this paper, it has been shown that asphalt and cement composites may be suitable for being used as a road material. Cold mix asphalt concrete without cement additions is weak and resists much lower forces than hot mix asphalt concrete, even after 28 days curing at a very low relative humidity. Additionally, cold mix asphalt has also a much lower rigidity than hot mix asphalt. However, when the filler is progressively replaced by Portland cement, the force resisted by the material, as well as its rigidity, increases progressively. Although the rigidity of the cold mix asphalt concrete specimens tested was always below the rigidity of the reference hot mix asphalt, the total force resisted could be higher, depending on the amount of cement added.

Moreover, it was observed that the evaporation rate decreases with the increase in the environmental humidity and that the force and rigidity of the mixtures increase with the water loss in the mixture. Furthermore, it was found that the final percentage of free water in the mixture is reduced and the strength and the rigidity are increased when the amount of cement is increased.

Concrete Repair, Rehabilitation and Retrofitting III – Alexander et al. (eds)
 ISBN 978-0-415-89952-9

Engineered Cementitious Composite as a cover concrete against chloride ingress

Y. Lin, L. Wotherspoon & J.M. Ingham
University of Auckland, Auckland, New Zealand

A. Scott
University of Canterbury, Christchurch, New Zealand

D. Lawley
Reid Construction Systems, Auckland, New Zealand

ABSTRACT: Engineered Cementitious Composite (ECC) is a cement composite reinforced with synthetic fibres. When loaded in tension, ECC exhibits a pseudo strain-hardening characteristic through the process of micro-cracking. The ductile behaviour of ECC makes it an ideal material for remediation of concrete structures, as the differential volume change due to thermal expansion of the original concrete structure and the applied ECC layer can be accommodated. Reinforcement corrosion due to insufficient cover thickness and degradation of concrete is an ongoing issue for concrete structures exposed to marine environments. This study investigates the effectiveness of ECC as a cover concrete for existing concrete structures to delay chloride ingress to the reinforcement and therefore extend the structure's service life.

Six ECC mixes were tested and compared with a 40 MPa concrete mix using three different test methods, namely the ASTM C642 void test, ASTM 1556 bulk diffusion test and AC resistivity. Additionally, the effect of different curing regimes (sealed, water, 3.5% NaCl solution) was investigated on the standard ECC mix. The test results indicated that the best ECC mix could reduce the diffusion coefficient by approximately an order of magnitude compared to a 40 MPa concrete mix subjected to the same environment. It was also determined that the three selected curing options had little effect on the performance of ECC specimens.

1 INTRODUCTION

1.1 *Background*

Reinforced concrete bridge construction in New Zealand (NZ) became common after the 1950s. Due to the nature of design and construction practice during this period, many of the bridges now have insufficient cover concrete compared to the current New Zealand concrete code (NZS 2006) and many bridges now exhibit signs of reinforcement corrosion. To extend the service life of these deteriorated and damaged bridges, immediate remediation is necessary. This study investigated the effectiveness of sprayed Engineered Cementitious Composite as a cover concrete for repair work.

1.2 *Engineered Cementitious Composite*

Engineered Cementitious Composite (ECC) is a ce-ment composite reinforced with synthetic fibres. ECC exhibits a strain-hardening characteristic when subjected to tension through the process of matrix micro-cracking and the transfer of forces through any fibres that bridge the crack. The focus of this study is on sprayed ECC and a typical mix design of sprayed ECC is shown in Table 1, revealing that ECC does not have any aggregates larger than 300 μm in its constituent material.

2 MATERIALS

The test scheme was split into two stages. In stage one, the aim of the test was to determine the effects various additives have on the durability properties

Table 1. Sprayed ECC mix design.

Materials	kg/m^3
300 μm Sand	640
Portland Cement	800
Fly ash	240
Water	374
PVA Fibre	26
Additives (Superplasticizer and stabiliser)	0.3

Table 2. ECC mix designs used.

Mixes	Description
ECC-S	Standard ECC shotcrete mix listed in Table 1
ECC-IFA	Fly ash ratio increased to 0.4 of cement
ECC-CH	Half of fly ash replaced with calcium carbonate
ECC-Si	Silane based water repellent added to ECC-S
ECC-Zn	Zinc stearate water repellent added to ECC-S
ECC-RH	Alternative ECC mix with calcium carbonate replacing fly ash completely and an increased amount of accelerators used
OCM-40	Ordinary concrete mix with a compressive strength of 40 MPa

of ECC. Six different ECC mix designs and a 40 MPa concrete were produced and subjected to three durability tests, with descriptions of each mix design provided in Table 2. In stage two, the aim of the test was to determine the effect of curing on the durability properties of the standard ECC sprayed mix (ECC-S).

3 TEST METHODOLOGIES

The ASTM C642 void test (ASTM 2006), AC resistivity and ASTM C1556 bulk diffusion test (ASTM 2004) were conducted to measure the chloride resistance of cement composites.

4 RESULTS

4.1 *ASTM C642 density, absorption and voids in hardened concrete results*

Void test results are presented in Table 3, showing that in stage one, the majority of ECC mixes had a void percentage between 21 to 25%, which was relatively high compared to the 12% void percentage of the 40 MPa concrete but lower than the 28 to 31% found in the stage two material.

In stage two of the test, it was observed that the cur-ing regime had no significant influence on the quan-tity of voids within the hardened composite.

4.2 *ASTM 1556 bulk diffusion test results*

The average apparent diffusion coefficients of the mixes were determined and are shown in Table 4. All the ECC mixes had a lower apparent chloride diffusion coefficient than that of concrete, indicating that ECC is more resistant to chloride ingress than concrete.

Of the six ECC mixes tested, those with additions of zinc stearate, a silane based water repellant or higher replacement levels of fly ash were all shown to have improved chloride resistance compared to the ECC standard mix.

Table 3. Voids test results.

Mixes	Average void %	CoV
Stage 1 (Sealed)		
ECC-S	24.6	0.01
ECC-IFA	25.0	0.06
ECC-CH	21.4	0.01
ECC-Si	21.0	0.06
ECC-Zn	4.5*	0.02
ECC-RH	22.3	0.01
OCM-40	12.0	0.03
Stage 2 (curing environment stated in brackets)		
ECC-S (Sealed)	28.2	0.02
ECC-S (Water)	31.4	0.11
ECC-S (3.5% NaCl solution)	29.7	0.03

*low measure voids due to impact of additive on testing

Table 4. Bulk diffusion test results.

Mixes	Apparent diffusion coefficient 10^{-12} m^2/s	CoV
Stage 1 (all sealed)		
ECC-S	3.2	0.22
ECC-IFA	2.0	0.47
ECC-CH	4.1	0.16
ECC-Si	2.0	0.13
ECC-Zn	1.7	0.31
ECC-RH	13.4	0.81
OCM-40	19.0	0.30
Stage 2 (curing environment stated in brackets)		
ECC-S (Sealed)	12.5	0.26
ECC-S (Water)	6.9	0.15
ECC-S (3.5% NaCl solution)	–	–

5 CONCLUSIONS

The ECC mixes tested in this study provided a more effective chloride resistant barrier than the 40 MPa concrete control with the standard ECC mix having a chloride diffusion coefficient approximately 6 times lower than the diffusion coefficient of concrete. The inclusion of higher levels of fly ash, a silane water repellant or zinc stearate provided the greatest resistance to the movement of chlorides.

Neither the void test nor the AC resistivity provided an adequate indication of the likely chloride resistance of the different ECC mixes.

The preliminary investigation on the influence of curing showed little difference in void content or AC resistivity though some differences in apparent diffusion coefficient were observed between the sealed and water cured samples.

Concrete Repair, Rehabilitation and Retrofitting III – Alexander et al. (eds)

Fire resistance performance of concretes exposed to high temperatures

Dinakar Pasla
School of Infrastructure, Indian Institute of Technology, Bhubaneswar, India

ABSTRACT: In this paper, the performance of concrete exposed to high temperatures was discussed. The fire resistance properties of concretes were improved by adding polypropylene fibres. An experimental program was designed, in which different types of concrete were investigated including Normal Strength Concrete (NSC), High Strength Concrete (HSC) and Fibre Reinforced Concrete (FRC). The normal concrete was designed without any mineral additions. The high strength concrete was designed with Metakaolin (MK). In both the normal and high strength concretes polypropylene fibers at 0.9 kg/m^3 were also added. The effects of incorporating Metakaolin (MK) and Polypropylene fibre (PP) were also investigated. Spalling was the most critical phenomenon that occurred in concrete specimens that occurred when exposed to high temperatures. The addition of polypropylene fibres slightly enhanced the residual strength of concrete manufactured using Portland cement but not that of MK concrete. PP mitigated the spalling and the explosive behavior of MK concrete. It was also found that by adding PP fibres with the ratio of 0.9 kg/m^3 the fire resistance of the concrete samples improved.

1 INTRODUCTION

The assessment of the residual mechanical properties of concrete exposed to fires or high temperatures is necessary for the evaluation of the serviceability of concrete structures.

2 OBJECTIVES

The main aim of the present study is

- To develop heat resistant concrete which would withstand temperatures upto 700°C.?
- Study the residual strength properties of concretes by using two types of aggregates such as granite and basalt. The residual strength expressed as percentage should be more than 40%.
- Study the effectiveness of polypropylene in reducing the spalling of concretes exposed to high temperatures.

3 MATERIALS AND MIXES

3.1 *Mixtures*

Four mixtures were initially optimised from laboratory tests. The name of every mix consists of two parts indicating the binder type and the fibre reinforcement. For example, NSC is a control mix made with cement as a sole binder and includes no fibre. Similarly, HSCPP is a polypropylene fibre reinforced concrete mix with part of the cement replaced by metakaolin. For mixes containing metakaolin the replacement level was 10% on a weight-to-weight basis. The normal strength concrete mix (NSC) was designed with a nominal target compressive strength of 30 MPa. On the other hand, the metakaolin mix was aimed to be a high strength concrete (HSC) with a target compressive strength of 60MPa.

3.2 *Specimens preparation and curing*

Concrete cubes of 150mm size were cast and the compaction of the fresh concrete of all the mixtures was made on a vibrating table. Then the moulds were covered with a wet cloth for 48 hours. Then the specimens were taken from the moulds and kept in a chamber with 90% relative humidity at temperature 27°C ± 2°C prior to testing. All the specimens were then taken from the chamber not earlier than 1 hour before testing.

4 HEATING REGIME AND TESTING

4.1 *Heating regime*

Drying at 105°C after 7 (seven) days of curing: After curing the concrete cubes for 7 days at 27°C ± 2°C at 90% relative humidity, the cubes were dried at 100°C to 105°C in a drying oven as s. The mark of the concrete before firing was recorded as R100 (in N/mm^2).

Heating upto 700°C after drying at 105°C:
After curing the concrete cubes for 7 days at 27°C ± at 90% relative humidity and drying for 30–32 hours at 105°C to constant weight in a drying oven, the cubes were then fired in a muffle furnace to a temperature of 700°C. The raising of temperature was gradual and it was ensured that the temperature should not exceed 200°C per hour. The heating of the 150mm concrete cubes inside the muffle furnace developed for this investigation was shown in Figure 1. The cubes were measured for dimensions, weight and carefully examined for any surface cracks and then crushed to determine the strength and recorded as R700 (in N/mm^2).

4.2 *Testing of specimens*

The residual compressive strength which is the ratio of R700 to R100, expressed as percentage. All compressive strength tests were carried out in accordance with IS: 516.

5 TEST RESULTS AND DISCUSSIONS

The results of the compressive strengths of concretes developed with granite and basalt aggregates before and after exposing them to temperatures up to 700°C are shown in Tables 2 and 3. The residual strength which is the ratio of R700/R100 are also calculated and tabulated in Tables 1 and 2. All the concretes have satisfied the criteria of achieving the permissible residual strength of more than 40%.

For normal strength concretes (NSC), the residual strength at 700°C for basalt aggregates was about 65%, whereas for granite aggregates it was around 58%. For HSC containing metakaolin, the loss of strength started once the temperature of the specimen started to rise. The loss of the compressive strength was proportional to the increase in the temperature up to 700°C. The rate of strength loss was higher than that of the NSC concrete. The average residual strength of the metakaolin mixes at 700°C was only 47% for basalt aggregates and 43% for granite aggregates. Specimens from the metakolin mix without fibre (HSC) started to spall when the temperature approached 500°C. The spalling increased with the increase of the temperature up to 700°C. This was observed both for the granite and the basalt aggregate concretes.

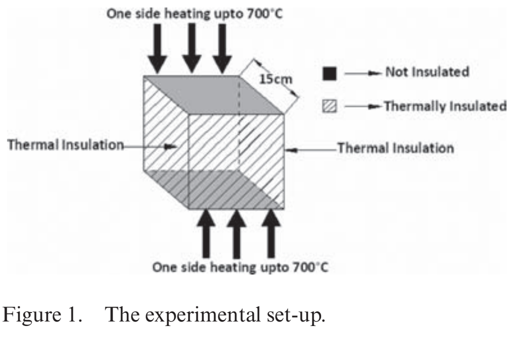

Figure 1. The experimental set-up.

Table 1. Compressive and residual strength results for basalt aggregates.

Compressive strength (MPa)	NSC	NSCPP	HSC	HSCPP
7 day strength	45.42	44.71	66.67	68.85
105°C (R100)	55.81	54.65	76.24	75.76
700°C (R700)	35.20	35.47	35.68	35.56
28 day strength	49.73	51.03	74.85	75.67
R700/R100	63.07%	64.90%	46.80%	46.94%

Table 2. Compressive and residual strength results for granite aggregates.

Compressive strength (MPa)	NSC	NSCPP	HSC	HSCPP
7 day strength	46.05	44.94	67.66	69.42
105°C (R100)	56.17	55.33	78.05	79.91
700°C (R700)	31.52	32.32	34.53	34.34
28 day strength	51.68	49.88	76.89	77.78
R700/R100	56.12%	58.41%	44.24%	42.97%

From the results it can be seen that the residual strengths obtained for concretes manufactured with basalt aggregates are superior to granite aggregates. On the other hand the behaviour of high strength concrete with metakaolin was significantly different from the behavior of concrete manufactured using cement alone, regardless of the presence or absence of PP fibers.

PP fibers mitigated the spalling and explosive behavior of the HSC concrete mixes when exposed to high temperatures. This is in agreement with several investigations HSCPP specimens were sound with no sign of spalling or cracks. HSCPP specimens heated to 700°C developed some minor cracks and spalling but they did not explode, as was observed in the case of HSC concretes without fibers. The inclusion of PP fibers slightly enhanced the performance of the NSC mix as can be seen from comparing mixes NSC and NSCPP. However, the effect of PP fibres was not clear in the presence of metakaolin. Nonetheless, PP fibers had a significant effect on reducing the spalling and the explosive behavior of concrete containing metakaolin.

Concrete Repair, Rehabilitation and Retrofitting III – Alexander et al. (eds)
ISBN 978-0-415-89952-9

Fire-protection coating of reinforced concrete lining in Lefortovsky tunnel

V.R. Falikman
Moscow State University of Civil Engineering, Moscow, Russia

A.A. Shilin
ZAO Triada-Holding, Moscow, Russia

ABSTRACT: In order to protect its high-strength concrete lining and polymer waterproofing gaskets in Lefortovsky tunnel under the Yauza River in Moscow from fire hazards a special fire-protection coating has been developed. It consists of special composite binders and carefully graded fillers. As specified in performance requirements the coating is resistant to aggressive media as well as mechanical wear to withstand high-pressure water cleaning. Applied system places Lefortovsky tunnel to the highest safety level according to the existing international requirements.

Lefortovsky transport tunnel under the Yauza River is the largest underground structure in Moscow. It is situated in the historical part of the city characterized by very complicated geological conditions represented by stratified layers of various strength and hydrostatic pressure up to 0.3 MPa. The total length of the tunnel is 3252 m. The TBM driven section has the length of 2222 m and outer diameter of 14.2 m. The lining is made of prefabricated high-precision reinforced concrete segments 0.7 m thick with two rows of elastomeric gaskets in joints between adjacent rings. Inside the tunnel there is a cast in-situ concrete roadway platform (traffic capacity of 3750 cars per hour). The under-platform space accommodates facilities for evacuation of people, laying of various mains, maintenance purposes.

Unlike fires in buildings above ground, fires in tunnels have certain specific features. These are: quicker increase of an average volume temperature, higher temperature of burning, deterioration of tunnel lining, risk of structural failure, longer burning time, and heavier smoke emission. That's why fire-fighting authorities in several countries adopted new curves to model fire propagation process. However, Russian normative documents provide for the use of a so-called "standard" heating curve.

According to the existing norms one of the critical temperature values was assumed as a limit state: temperature of effective reinforcement inside the concrete slab shall not be more than 300°C; temperature of concrete surface under the fire-protection coating shall not be more than 500°C.

One of the standard protection schemes is to use lightweight plasters: they make the heating curve of the surface concrete gently sloping, thus lowering the temperature gradient as only materials non-susceptible to cracking contact direct flames.

To ensure safety in Lefortovsky tunnel in Moscow it was necessary to choose, on one hand, safe structures and, on the other hand, special facilities and monitoring systems to regulate the traffic and check environmental state. An important part in this complex system belongs to a fire-protection coating of reinforced concrete lining. It was developed specially to meet operational requirements of Lefortovsky tunnel and called the "Barrier" (patented).

The "Barrier" is designated to increase fire-resistance limits of concrete structures up to 2–3 hours and even longer depending on the concrete cover thickness.

This coating is manufactured on the basis of mineral components and contains mechanically activated modified composite cement binder with a low water requirement (so called "Low water demand binder"—LWDB), expanded perlite, exfoliated vermiculite, fine mineral additives. LWDB consist of interground components: Portland cement clinker, modifier that includes dry superplasticizer, gypsum, active and/or inert mineral additions. Grain size as well as components proportion are optimized according to the particular technical requirements and method of application.

The "Barrier" is a ready-to-use dry mix. Approximate consumption of water is 10–12 l per a 20 kg bag. The coating doesn't contain any harmful organic or mineral admixtures that can be emitted during transportation, processing, application, operation (including prolonged high-temperature conditions) or be hazardous to people and environment.

Optimum choice of components as well as dry-mix composition ensure high insulation properties of the system which guarantee long-term protection of reinforced concrete structures from heat emission and open flames as well as resistance to cracking and good adhesion to the substrate. The developed fire protection coating has good performance under dynamic loads within structural operational limits.

Fire testing of reinforced concrete slab samples was carried out to define fire-protection efficiency of the system. Slabs were made of normal-weight concrete (B65) with sand and crushed granite as aggregates according to Russian standard GOST 26633. They were reinforced with a welded mesh of 4 mm plain wires according to GOST 8478. Thickness of the concrete cover (to the lower edge of effective reinforcement) from the heated side was 50 mm. Prior to the application of the coating several chromel-alumel thermocouples were installed on the heated side of the samples. The fire-protection coating was mechanically applied in two steps. First a 20 mm thick layer was sprayed, then a plastering mesh with cells of 40×40 mm was laid over it and finally a finishing layer 30 mm thick was applied. Moisture content of the system prior to testing was 14.0–14.7% whereas moisture of concrete slabs was 2.6–2.7%.

Samples were placed in a testing unit and subject to one-sided heating in a standard mode according to GOST 30247.0. Temperature inside the fire chamber was measured with the help of furnace thermocouples that were installed in three spots distributed uniformly along and across the sample. The time of fire exposure was restricted to 180 minutes.

None of the possible limit states was achieved in the progress of testing. Average temperature of the concrete surface under the fire-protection coating was 87–90°C; average temperature of the reinforcement was 50–51°C. No visible changes of the fire-protection coating were noticed either in the course of testing or during the samples cooling.

Thorough studies allowed to define a precise technological procedure of the fire-protection application. Prior to the coating application the substrate is to be cleaned and dampened by wet shotcreting with the help of appropriate shotcreting units. Dry-mix is delivered to site in 20 kg bags or big-bags of 800 kg. It is stored at positive temperatures and is to be protected from any source of moisture. Storage period in original paper bags shall not exceed 6 months, whereas for damp proof packaging this term is increased up to 2 years.

The substrate shall be free of dust, oil and other contaminants, loose particles. Mechanical cleaning is recommended (wire brush, sandblasting). Chemical cleaning is used if necessary to remove traces of grease from the surface. The cleaned surface is to be wetted. At the time of application ambient temperature shall be 7 ÷ 30°C. Windy and rainy conditions shall be avoided. When applied by the units which both feed and mix the dry product with water feeding rate shall be controlled to obtain the proper mix consistency. The coating is applied in one step if the layer is 1–2 cm thick. If the thickness is to be 3–4 cm, two or more steps are needed. Thick layers require application of a reinforcing mesh to achieve better adhesion to the substrate.

Setting time is 4–6 hours after the application. Compressive strength of the applied coating is minimum 2.5 MPa after 1 day curing at 20°C. After 28 days it grows up to 7.5 MPa. To avoid shrinkage cracking and poor adhesion to the substrate the applied coating is to be protected from wind, direct sunlight and early loss of moisture by using damp proof sheeting or specially wetted materials. Temperature of curing (up to 28 days) shall not be lower than +7°C.

In Lefortovsky tunnel fire-protection coating was applied over a galvanized mesh with the help of shotcreting units equipped with special spraying nozzles. An average rate of two-layer application achieved 350 m^2/day. A decorative finishing coating of 0.5 mm was applied over the fire-protection.

The applied fire-protective coating has a smooth surface of A3 class up to the height of 3.5 m from the roadway level. It is painted in various colors not to look monotonous and thus to avoid the so-called fatigue effect for drivers when they are passing rather a lengthy section in a confined space of the tunnel.

Altogether it took 75 days to complete the fire-protection application. After the system was applied the authorities responsible for its operation and maintenance inspected the tunnel. It was stated that after 28 days the coating had the compressive strength of 16.5 MPa, its vapour permeability was 4 times higher than that of the concrete lining. Adhesion to the lining was 0.84 N/mm^2.

Proper operation and maintenance of the applied system is capable of providing an absolute protection of people and tunnel structures in emergency situations. This system places Lefortovsky tunnel in Moscow to the highest safety level according to the existing international requirements.

Concrete Repair, Rehabilitation and Retrofitting III – Alexander et al. (eds)
© 2012 Taylor & Francis Group, London, ISBN 978-0-415-89952-9

Influence of hydrophobicity and oleophobicity on cleaning graffiti on concrete panels and natural stones

K. Malaga
CBI Swedish Cement and Concrete Research Institute, Borås, Sweden
Federal Institute for Materials Research and Testing (BAM), Berlin, Germany

U. Mueller
Federal Institute for Materials Research and Testing (BAM), Berlin, Germany

ABSTRACT: Anti-Graffiti Systems (AGS) are meant to make the cleaning process more efficient by inserting a layer between the paint and the substrate. This layer can have a low surface energy thus make it difficult for the paint to stick to the substrate or it may be easily removed together with the paint. This paper is presenting results from a study of how hydrophobicity and oleophobicity influence the cleaning efficiency of graffiti paints from concrete and natural stones. The results demonstrated that high hydrophobicity and high oleophobicity are not guaranteeing satisfying cleaning effects. The physical properties of a substrate in combination with the characteristics of the AGS layer decide about the cleaning effect.

1 INTRODUCTION

Many constructions in our built environment are affected by graffiti smearing. Graffiti is not entirely a problem of urban areas but appears also frequently in rural communities and along our traffic infrastructure. Besides the aesthetical impact graffiti causes considerable costs for their removal and subsequent costs for repairing damages caused by improper graffiti cleaning. In particular sensible towards graffiti is concrete with its grey and homogeneous appearance. Therefore, concrete is overrepresented concerning affected areas and the cleaning of these is a very difficult task. Anti-graffiti systems (AGS) are meant to make the cleaning process more efficient by inserting a layer between the paint and the substrate. Studies of the hydrophobicity, oleophobicity and microscopic evaluation of the protecting layer are not included in any of the evaluation methods. High hydrophobicity and oleophobicity are assumed to give the best anti-graffiti protection. The goal of this study was to analyse the link between cleaning efficacy and the hydrophobic and oleophobic effect of a permanent and sacrificial AGS on concrete and natural stone panels.

2 SAMPLE MATERIAL AND METHODS

The selected stone samples were of low, intermediate and high porosity and of different mineralogical composition. All stones had a cut finish. The concrete consisted of a basic panel with a ca. 5 mm thick top layer. Two types of commercially available anti-graffiti products were used: a permanent system, Protectosil-AGS (AGS1), consisting of a fluorinated silane and an associated cleaning chemical, and a sacrificial product, AGS 3502 (AGS2), based on a microcrystalline wax. The panels were conditioned for at least 14 days at 23°C and 50% RH before and after the application of the AGS products. The graffiti paints consisted of different types listed in BASt TP-AGS (2009). The paint was applied with a mask in form of circular patches.

The AGS layers characteristics on the surfaces were analysed by the Scanning Electron Microscopy and by Laser Scanning Confocal Microscopy, and hydrophobicity/oleophobicity was measured by the static contact angle measurements. The cleaning efficacy factor F_{AGS} was calculated as a mean value per type of substrate. The visual evaluation scale ranges from 0 to 5 and the threshold value is set to 2. The scale is as follows:

- 0 - 100% cleaned;
- 1 - only single traces of the paints are left
- 2 - 90–75% cleaned
- 3 - 75–30% cleaned
- 4 - less than 30% cleaned
- 5 - not cleaned

For each of the substrates 10 panels, 30×30 cm^2, were prepared. For the evaluation three panels protected with each AGS and painted with graffiti were cleaned. The fourth AGS coated and graffiti painted panel was not cleaned and served as a reference for the visual evaluation of the cleaning effect of the other three panels. Additionally, uncoated reference panels were painted with the graffiti and cleaned.

3 CONCLUSIONS

The results showed a clear distinction in cleaning efficacy between the two types of AGS. In overall AGS2 gave a very good cleaning efficacy and AGS1 failed for a number of porous substrates. The porosity influence was important for the AGS1 protected samples but not for the AGS2. A possible explanation, why the silane was failing the test on some materials exhibiting a higher porosity and the micro wax was not can be concluded as followed:

- The sacrificial microcristalline wax (AGS2) formed a coating on the surface of the substrates, whether they were low or high in porosity. High porosity materials required a higher amount of agent and the agent penetrated the subsurface pore system as seen in Sandstone (SSt3) and concrete (B). The cleaning efficacy, however, was not affected by this since the agent was still coating over even larger pores. It can be stated that the AGS2 results in homogeneously distributed layer that purely mechanically protects the samples against the graffiti.
- The permanent fluorinated silane (AGS1) formed a coating on the denser substrates but impregnated substrates with a higher porosity. Though in the latter case the surfaces of pores were coated with the silane, larger pores were not coated over as in the case with AGS2. This means that in the case of porous substrates the paint could be mechanically wedged in the pores reaching to the surface, even though the pores walls were hydrophobic and oleophobic. This was also observed on the cleaned substrates of concrete and sandstone SSt3 coated with AGS1 where rests of paint were found in the pore system up to 2 mm below the surface.

For the fluorinated silane (AGS1) the influence of the hydrophobicity and oleophobicity on the cleaning efficacy is important and controls the adhesion characteristics of graffiti paint to the substrate surface (Fig.1). However, these are not the only factors controlling the AGS performance. Total porosity and pore size distribution play a crucial role, in particular with higher porosity substrates or materials with very large pore sizes. Both parameters, total porosity and pore size distribution, influence also the surface roughness of a substrate, which is a third crucial parameter for the final cleaning efficacy.

From the findings presented it can be concluded that anti-graffiti agents, which form a coherent film

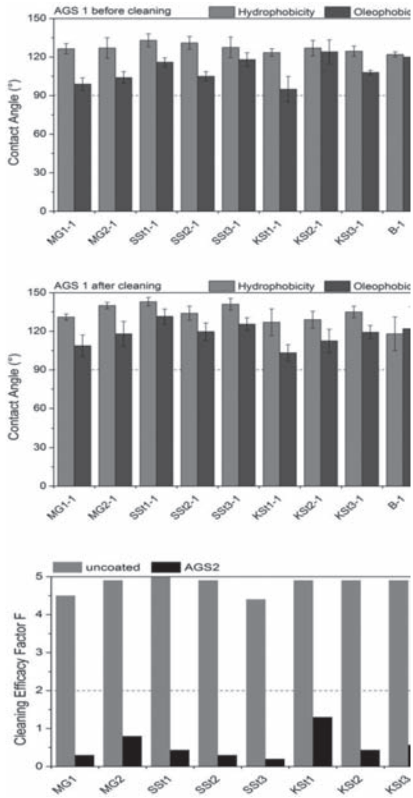

Figure 1. Contact angle for AGS1 treated samples and cleaning efficiency factor for AGS2 treated samples.

may be effective over a wide range of substrates with various porosities and pore size distributions, also for porous materials. However, in order to decide on the applicability of those types of agents other requirements have to be considered as well, such as water vapour transfer. In particular porous substrates usually require coatings with a high water vapour transfer coefficient, otherwise if the coating is applied outdoors; detachment of the coating due to the influence of moisture and/or frost action might be possible. Agents, which do not form a coherent coating but show an impregnating effect, such as silanes/ siloxanes, may fail in performance, when the substrate becomes too porous and/or pore sizes become too large. Paint might be mechanically wedged into the pores, even though hydrophobic and/or oleophobic properties are still fully present.

ACKNOWLEDGEMENTS

VINNOVA, the Swedish Governmental Agency for Innovation Systems is acknowledged for the VINNMER grant and the German Federal Highway Research Institute for the financial support.

This page intentionally left blank

Service life modelling and prediction of durability

This page intentionally left blank

Concrete Repair, Rehabilitation and Retrofitting III – Alexander et al. (eds)
© 2012 Taylor & Francis Group, London, ISBN 978-0-415-89952-9

Developing a modified rapid chloride permeability test for mortar concrete

A.A. Ramezanianpour, A.R. Pilvar, M. Mahdikhani & F. Moodi
Concrete Technology and Durability Research Center, Amirkabir University of Technology, Tehran, Iran

R. Pilvar
Institute for Transport Studies (ITS), University of Leeds, West Yorkshire, England

ABSTRACT: This paper describes the development of a very rapid test method which can measure the permeability of concrete against chloride ions. Once the sample preparation stage has been completed, up to 15 concrete specimens can be tested in one hour using a single conductivity cell. The test involves saturating a concrete specimen with a 30% NaCl solution before measuring the conductivity of the sample. By saturating specimens with a highly conductive solution, they showed virtually the same pore water conductivity. Different concrete samples yield different conductivity levels primarily due to differences in their pore structure. The measured conductivity was observed to be related to the diffusivity ratio as well as the chloride diffusivity of the concrete.

1 INTRODUCTION

Three types of rapid chloride test methods have been developed so far. In all of them, a concrete specimen is placed adjacent to a chloride solution on the one side, and a chloride-free solution on the other. The first type of method is represented by the AASHTO T277 (1983), developed by Whiting et al (1981), in which the total charge passed through a specimen during a six hour period under a 60 V. Then the potential difference is measured and the value used as a chloride permeability index. In the second method which is developed by Dhir et al (1990), the steady state chloride flux is measured under a 10 V potential difference empirically to the chloride diffusion D of the concrete. In the last method which is represented by Tang & Nilsson (1992), the depth of chloride penetration under a 30 V potential after 8 hours is measured and fundamental electrochemical theory is used to calculate D. There is a need for a chloride penetration test that is theoretically sound and also is as more rapid as the AASHTO method. Based on electrochemical theory, a very rapid chloride conduction test has been developed at the University of Cape Town (Feldman et al 1994). The authors present a new test method combining Cape Town method and RCPT method that has no disadvantages of traditional method. This paper deals with the electrochemical principles that led to the development of the new test method for chloride penetration. It is also described the test method as well as the procedure used to determine diffusivity from conductivity measurements.

2 TEST METHOD

The characteristics of the new test are presented in this paper. Since the test involves a single current reading, the apparatus can be used consecutively on a series of samples. The time taken to set up the apparatus for each test determines the rate at which samples can be tested. After passing a short time of the test, few ions relatively migrate and small cells can therefore be used. The conduction test apparatus consists of two 250 ml cells adjacent to a central section containing the concrete sample (Fig. 1). Both cells fix to the central section, thus compressing the silicone rubber collar and clamping the sample. Each cell contains a 23% NaCl solution. The potential difference is applied to stainless steel anode and cathode by 10 V DC power source. A data logger is used to measure the current and potential difference between the solutions accurately.

The apparatus was designed for mortar or concrete samples of 100 mm diameter and the thickness of 25 mm. (Similar apparatus can be designed for other sample diameters). The concrete or mortar is cored with a diamond tipped core barrel fixed to a suitable drill. The core is then sliced using a diamond saw. The average thickness of each disc is measured using a vernier caliper. The concrete discs are placed in an oven at 50ºC for 7 days to remove moisture from the concrete pores. After that the discs are vacuum dried for 3 hours, then vacuum saturated in a 23% NaCl solution for 2 hours and leave to soak in the solution for an additional 18 hours or so.

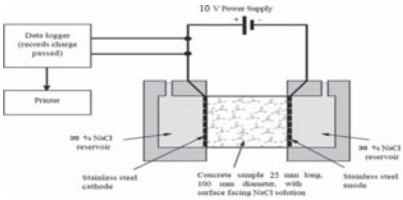

Figure 1. Conduction test arrangement.

The cells containing the NaCl salt solutions are fixed onto the central section containing the sample. The circuit is arranged as shown and the current is measured at the applied voltage (10 V). To determine the conductivity of each sample, the measured current applied voltage and the sample dimensions are substituted in equation 1:

$$\sigma = (i/v) \times (t/A) \tag{1}$$

σ: conductivity of sample [mS/cm]
i: electric current [mA]
v: potential difference [v]
t: thickness of sample [cm]
A: cross-sectional area of sample [cm^2]

3 TEST RESULTS AND ANALYSIS

In order to examine the performance of the instrument built for measuring the permeability of concrete against chloride ions, it is used 19 different mixture proportions in concrete samples, consisting of ordinary concrete, concrete containing silica fume and concrete containing Nano-silica fume. In order for easier interpretation they have also been categorized into groups A, B and C, respectively.

Table 1. Tests results.

No.	Mixtures	Wenner (kΩ.cm)	RCPT (columbs)	MRCPT (mS/cm)
1	A30.45	22	2784	0.464
2	A30.55	16	3461	0.813
3	A30.60	14	3875	0.992
4	A35.45	19	2953	0.548
5	A35.55	14	4354	0.985
6	A35.60	12	4468	1.103
7	B32.50MS0	14	3775	1.355
8	B32.50MS7.5	24	2038	0.900
9	B40.50MS0	10	4856	1.732
10	B40.50MS7.5	25	1886	0.889
11	B32.40MS0	22	2177	0.768
12	B32.40MS7.5	36	1319	0.839
13	B40.40MS0	15	3175	1.006
14	B40.40MS7.5	37	1245	0.675
15	C42.40 NS0	11	6240	1.217
16	C42.40 NS2.5	13	5287	1.016
17	C42.40 NS4.5	15	4725	0.869
18	C42.40 NS6.5	18	3739	0.823
19	C42.40 NS8.5	28	1808	0.659

Table 2. Ranking of concretes in relation to infiltration of chloride ions in different test methods.

Chloride permeability	RCPT (coulombs)	SR (KΩ-cm)	MRCPT (mS/cm)
High	>4000	<14	>0/9
Medium	2000–4000	14–25	0/7–0/9
Low	1000–2000	25–43	0/6–0/7
Very low	100–1000	43–270	0/4–0/6
Negligible	<100	>270	<0/4

Two standard test methods of RCPT (ASTM C1202) and Wenner (FM 5–578) have also been applied to all of the samples in addition to the method developed in this study which is hereafter referred to as MRCPT (Modify Rapid Chloride Penetration Test). Results are showed in Table 1. Using the relationship between these three methods and their associated physical bases, it can be used the categorisation presented in Table 2 in order to rank different concretes in terms of their permeability against chloride ions which have been measured through the MRCPT test. It should be noted that this ranking is also in line with the one specified by ASTM C1202.

4 CONCLUSION

The method presented in this paper, the Modify Rapid Chloride Penetration Test (MRCPT) is based upon robust theoretical bases. It can be claimed that it is one of the fastest methods introduced so far for measuring permeability of chloride ions; as a result it can be repeated many times due to the short duration of the test. Furthermore the concrete samples during the test are not subject to physical or chemical changes, and thus the test can be applied to samples with short curing periods too.

REFERENCES

AASHTO T-277–83, 1983. Standard method of test for rapid determination of the chloride permeability of concrete. Washington D.C. 1229–1234.

Dhir, R.K., Jones, M.R. & Ahmed, H.E.H. 1990. Rapid estimation of chloride diffusion coefficient in concrete Seneviratne. *Mag. Concr. Res.*, 42(152): 177–185.

Streicher, P.E. & Alexander, M.G. 1995. A Chloride Conduction Test For Concrete, *Cement and Concrete Research,* 25(6): 1284–1294.

Tang, L. & Nilsson, L.O. 1992. Rapid determination of chloride diffusivity inconcrete by applying an electrical field. *ACI Mat. Jour*., 89: 49–53.

Whiting, D. 1981. Rapid determination of the chloride ion permeability of concrete, Final Report No. FHWA/RD-81/119. Federal Highway Administration.

Concrete Repair, Rehabilitation and Retrofitting III – Alexander et al. (eds)
ISBN 978-0-415-89952-9

Measuring permeability of cementitious materials

Quoc Tri Phung
Institute for Environment, Health, and Safety, Belgian Nuclear Research Centre (SCK•CEN), Belgium
Magnel Laboratory for Concrete Research, Ghent University, Belgium

Geert De Schutter
Magnel Laboratory for Concrete Research, Ghent University, Belgium

Norbert Maes & Diederik Jacques
Institute for Environment, Health, and Safety, Belgian Nuclear Research Centre (SCK•CEN), Belgium

Guang Ye
Microlab, Delft University of Technology, Delft, The Netherlands

ABSTRACT: At present, it is well-known that permeability is a more fundamental parameter for characterizing concrete durability than the standard compressive strength. Permeability governs the penetration of aggressive substances responsible for degradation and, thereby, has an important effect on the durability of cement-based materials. Despite the importance of permeability, a lot of confusion exists on a wide range of available experimental techniques for quantifying the permeability. This work aims at reviewing existing methods to measure the hydraulic conductivity. In addition, a new method was proposed based on the technique which is used to measure permeability of clay materials at the Belgian Nuclear Research Centre. A constant flow rate was applied to a permeability cell. When steady state was reached, gradient pressure was then determined to calculate permeability. The pressure and water flow was controlled by precise Syringe pumps. Tests were performed on hardened cement pastes with w/c ratio ranging from 0.5 to 0.6 in a temperature control chamber. The tests showed that the proposed method gave reliable results within a reasonable experimental time.

1 INTRODUCTION

Cement-based materials are quite popular for a wide range of civil and infrastructure constructions. In recent years, these materials have also been applied in radioactive waste disposals. Durability and applications mainly depend on permeability. Permeability influences on almost all degradation mechanisms of concrete. Therefore, permeability seems to be a key parameter to characterize long-term performance of concrete. Due to the importance of permeability, many methods to determine permeability have been proposed. However, a lot of confusion still remains.

2 REVIEW OF EXISTING METHODS

2.1 *Direct methods*

Many methods have been used to measure permeability directly relying on Darcy's formula. Basically, direct methods are quite simple and easy to set-up. No additional parameters are needed to interpret the results thanks to using Darcy's formula directly. However, it takes long time to reach a steady state. During this period, permeability could be changed due to hydration. Potential for leaks around the specimen is high. Because of these limitations, the direct methods can only be applied to materials of which the permeability is not very low.

2.2 *Indirect methods*

Indirect methods involve either the application of a transient pressure pulse technique or the application of poromechanical techniques. In general, these methods are much quicker than traditional methods thanks to measurement in non-steady state. Potential of leak is actually decreased. These techniques can determine very low permeability. However, they still require full saturation of the sample. Application of heating or high pressure may also change the microstructure of the cementitious materials. Another disadvantage of these methods is that it is quite complex and difficult for analyses. Moreover, some equations have been proposed to predict the permeability based on other parameters of materials.

3 PROPOSED METHOD TO MEASURE PERMEABILITY IN LABORATORY

3.1 *Principle*

The proposed test method is a direct method. The principle is quite simple. A pressure gradient of around 8 to 10 bar is applied to a permeability cell in which a saturated cement-based core is embedded in a resin. The pressure and water flow are controlled by a precise Syringe pump. A good contact between the cement-based materials and the permeability cell is obtained by optimizing the resin/catalyst ratio.

3.2 *Materials and test set-up*

Tests were performed with cement pastes at w/c ratios at 0.5 and 0.6 in a temperature controlled room. Type I ordinary Portland cement was used. The permeability cell was made of Polycarbonate which has a sufficient strength to bear the applied pressure and can be visualized to check the contact between the resin and the sample. The specimen with a diameter of 94 mm and thickness of 25 mm was embedded into the cell by a resin. The resin hardness can be adjusted by changing epoxy/catalyst ratio. Two Isco Syringe pumps were used to apply either a pressure gradient or constant flow rate on the permeability cell.

3.3 *Experimental procedure*

Cement paste was poured in a cylindrical mould and cured in saturated lime water to prevent Ca-leaching. After 28 days curing, four cores of cement paste with 94 mm diameter were drilled from the raw sample by a diamond driller. The cores were then sliced to small disks at 35 mm thickness. The disks were then embedded into the bodies of the permeability cells. After drying, the specimens were polished to obtain the final sample thickness of 25 mm. The specimens were afterwards saturated in vacuum condition for one day before gluing to 2 permeability cell lids. Prior to permeability testing, all tubes, connections, space were filled up with water.

The applied pressure should not be too high, as micro-cracks can occur in the specimen, but also not too low in order to get a sufficient flow. A constant back pressure of 1 bar was applied to upper side of the cell by one Syringe pump (A). The other side was stepwise loaded by another pump (B) until a sufficient flow was obtained. When the flow was stabilized, the pump (B) was changed from constant pressure mode to constant flow mode. Only pressure readings of the pump (B) needed to be measured to calculate the permeability. Generally, the total time needed for one measurement depends on w/c ratio of sample but it is less than one week for a permeability which is larger than 10^{-13} m/s.

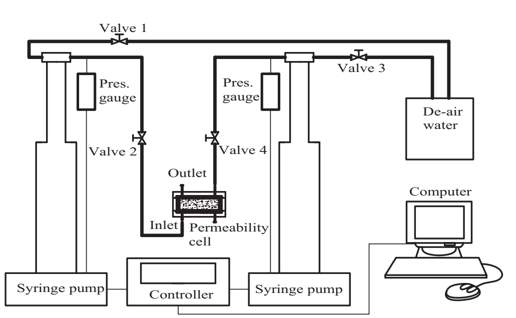

Figure 1. Schematic test set-up.

4 TEST RESULTS AND DISCUSSION

Figure 2 shows the permeability coefficients of cement pastes at three different w/c ratios. It is clear that the permeability is decreasing with the reduction of w/c ratio. In general, the total capillary porosity of cement paste is expected to decrease when its w/c ratio is lower. The decrease in capillary porosity which is composed of lots of large and connected pores leads to a limitation of pathways in cement paste resulting in a reduced permeability. The current test results agree well with previous research data, especially the data of (Powers et al. 1954). It seems that the permeability coefficients obtained from this study are lower than the results

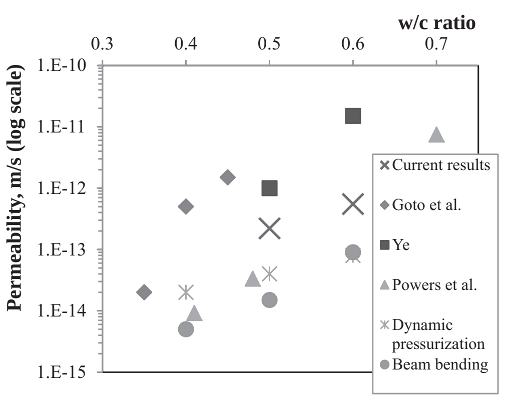

Figure 2. Permeability of cement pastes at different w/c ratios, comparison of the current test results vs. literature data.

of (Ye, Lura, and van Breugel 2006) and (Goto and Roy 1981) while higher than the results obtained from beam bending and dynamic pressurization methods. The differences are attributed to varying curing conditions and the fineness of cement.

5 CONCLUSIONS

A literature survey on existing methods for permeability measurement on cementitious materials is presented pointing out the advantages and disadvantages for the different methods. A novel method to measure hydraulic conductivity of cement-based materials was established. This method seems promising in terms of the required experimental length and the accuracy of measurement. It can determine the permeability coefficient of cement paste in quite a short time compared to other methods (within one week for permeability of 10^{-13} m/s). The permeability of cement paste with different w/c ratios was determined and it was increasing with the increasing w/c ratio. The results compare well with results from studies reported in literature even though there were some variations due to differences in sample preparation.

Concrete Repair, Rehabilitation and Retrofitting III – Alexander et al. (eds)
© 2012 Taylor & Francis Group, London, ISBN 978-0-415-89952-9

The pore structure and water permeability of cement paste blended with fly ash over a long period up to one year

Zhuqing Yu & Guang Ye
Microlab, Civil Engineering & Geosciences, Delft University of Technology, Delft, The Netherlands

ABSTRACT: As a waste residue, Fly Ash (FA) is widely used in construction. Many researches indicated that although the addition of FA reduces concrete strength at early age, blended concrete shows excellent long-term durability. Permeability is one of the most important properties of concrete for estimating durability of concrete. In general, researches focused on the relation between total porosity and water permeability, in most case the curing age was limited to a short-term period. The objective of this paper is to investigate the development of pore structure and its influence on water permeability over a long-term period up to one year, when FA is used as supplement cemetitious materials. In this paper, different contents of FA (30% and 50%) and two different water to binder ratios (w/b ratios) (0.4 and 0.5) were adopted to measure the water permeability and pore structure of blended cement pastes with FA. To explore the relation between pore structure and water permeability, Mercury Intrusion Porosimetry (MIP) method was conducted to obtain the total porosity and pore size distribution of blended cement paste. Direct test method, which is the monitoring of a steady flow through saturated specimens under a hydrostatic pressure gradient, was performed to determine the water permeability of the cement pastes blended with FA. The test results show that the total porosity is not the only factor which can influence the water permeability of pastes. The pore size distribution and critical pore also impact the water permeability of blended cement pastes.

1 INTRODUCTION

The objective of this paper was to investigate the development of pore structure and its impact on the water permeability of cement paste over a long-term period up to one year when FA was used as addition in concrete. In this study, the pore structure determination and water permeability measurement were carried out on cement pastes blended with FA by varying the mixture proportions (i.e., w/b ratio and dosages of FA). The pore structure of cement pastes blended with FA was tested by means of mercury intrusion porosimetry (MIP) at curing age up to 365 days. Meanwhile, The water permeability was measured for the same samples at the same curing age. The correlations between water permeability and pore structure are discussed.

2 MATERIALS AND TEST METHODS

The blended cement pastes were prepared using CEM I 42.5 N (ENCI Company), low calcium FA and distilled water. The dosages of FA were 0% (control sample), 30% and 50% by weight. W/b ratios of 0.4 and 0.5 were employed.

MIP measurements were performed with Micrometrics PoroSizer® 9320. Water permeability test was performed using the direct test method, which is the monitoring of a steady flow through saturated specimens under a hydrostatic pressure gradient.

3 RESULTS AND DISCUSSION

3.1 *Pore structure and permeability*

The relationships between total porosity and permeability coefficient are plotted as shown in Figure 1. It is clear that almost all samples with high porosity are more permeable. The total porosity of control sample and cement pastes blended with 30 and 50% of FA are 31.5%, 30.73% and 35.50%, respectively at 7 days. Although the control sample and cement paste blended with 30% of FA have a similar total porosity, the water permeability of these two samples are different (4.12×10^{-11} and 4.57×10^{-12} m/s).

As shown in Figure 1, the control sample has a much higher permeability. The total porosity measured by MIP cannot explain the diversity of water permeability in different samples which means the porosity is not the only factor which determines the permeability.

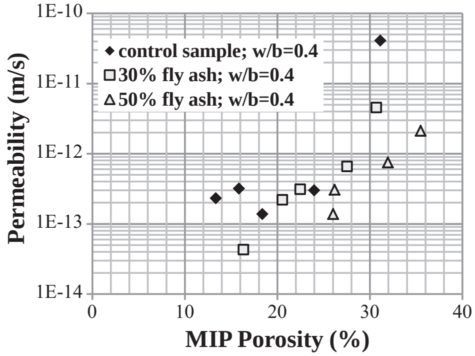

Figure 1. Relationship between permeability and total porosity for cement pastes with same w/b ratio 0.4 up to 365 days.

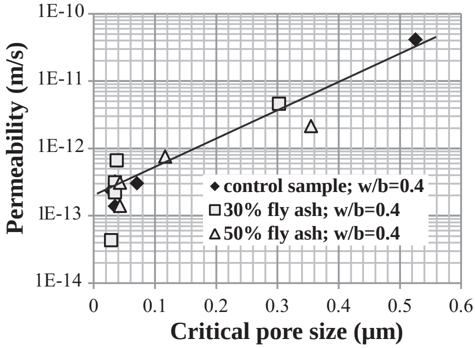

Figure 2. Relationships between water permeability and critical pore size for blended cement pastes with same w/b ratio 0.4 up to 365 days.

The relationships between critical pore size and water permeability for three samples are represented in Figure 2. It is clear that the permeability increases with the increasing of critical pore size. At similar critical pore size (around 0.1 μm), cement pastes blended with FA almost have lower permeability than the control sample. Around 180 days, the Pozzolanic reaction of FA becomes predominant in cement paste blended with FA. Therefore, the critical pore size could reflect the development of water permeability property of blended cement pastes.

Figure 3 shows the pore structure of the control sample and cement pastes blended with different content of FA at curing age of 7 days. The differential curves show that the control sample has higher critical pore diameter, 0.526 μm, which leads to higher permeability (4.12×10^{-11} m/s) compared to that (4.57×10^{-12} m/s) in the cement paste blended with 30% of FA. As discussed previously, pore size distribution and critical pore size are important factors on water permeability of cement pastes.

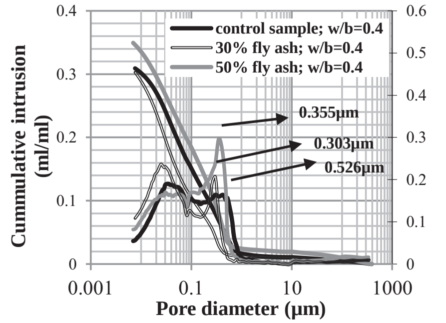

Figure 3. Pore structure of blended cement pastes with different content of FA (w/b ratio = 0.4) at 7 days.

4 CONCLUSIONS

The variation of pore structure must result in the change of permeability in blended cement paste. This study attempts to determine the impact of FA on pore structure and water permeability of blended cement pastes. Then the relationships between pore structure and water permeability for cement pastes blended with FA were explored under long-term curing age up to 1 year. The following major conclusions can be drawn based on the results obtained in this work. In general, cement paste (control sample) almost has lower porosity than cement pastes blended with FA at each curing age, even at long-term curing age. W/b ratio also plays a negative effect on porosity in cement pastes with FA.

1. Besides porosity, pore size distribution and critical pore size are the crucial factors which influence the permeability of blended cement pastes.
2. The water permeability of cement pastes blended with FA is highest at short-term curing age due to higher porosity. But at 7 days, cement pastes blended with FA are less permeable than the control sample because of the effect of higher w/c ratio. After 180 days, the superiority of paste blended with FA is expressed. The cement pastes blended with FA have lower water permeability. Critical pore size plays an important role on the development of permeability at long-term curing age.
3. Higher w/b ratio leads to higher permeability of blended cement paste. At 1 year, cement paste blended with FA with two different w/b ratios have similar permeabilities.

ACKNOWLEDGEMENT

The authors express gratitude to technicians and colleagues in Microlab, TUDelft, The Netherlands.

Concrete Repair, Rehabilitation and Retrofitting III – Alexander et al. (eds)
© 2012 Taylor & Francis Group, London, ISBN 978-0-415-89952-9

Measurement of the air permeability of concrete "in situ": Status quo

R. Torrent
Materials Advanced Services Ltd., Buenos Aires, Argentina

L. Ebensperger
Construtechnik Ltda., Buin, Chile

ABSTRACT: The authors have been involved in the creation, development and preliminary applications of the "Torrent Method" to test, non-destructively, the air-permeability of concrete. The method is suitable for the laboratory but, more important, for site investigation of finished structures. It has been about 20 years since such foundational research and this paper presents a review of the evolution and current situation of the Method, included in the Swiss standards in 2003 (SIA 262/1-E). Application examples conducted in laboratory and civil works (bridges, tunnels and buildings) are presented, including data from different countries worldwide. Correlations between the air permeability coefficient kT and other durability indicators, such as South African Durability Indices, Chloride migration (ASTM C1202), Penetration of water under pressure (EN 12390–8) or Capillary suction are presented. Recent recommendations of the Swiss Federal Highway Administration on the application of the method on site are summarized. Finally, the future prospective uses are discussed, both as quality control tool for new structures and for the condition assessment of existing structures.

1 INTRODUCTION

The so called "Torrent Method" measures the coefficient of permeability to air of the "covercrete", in a completely non-destructive manner. Therefore it aims directly at specifying and controlling the "covercrete" quality of the end product: the finished structure.

2 DESCRIPTION OF THE TEST METHOD

The method serves to measure the coefficient of air-permeability of the cover concrete on site, in a non-destructive manner, and operates as follows (see Fig. 2):

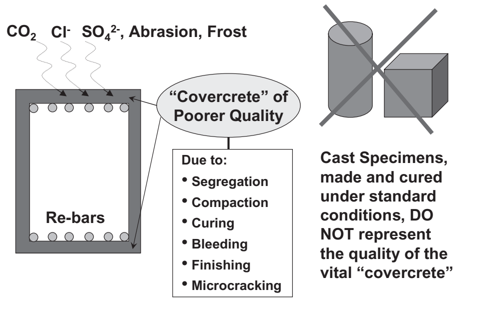

Figure 1. Concept of concrete surface layer ("Covercrete").

Vacuum is created inside the 2-chamber vacuum cell, which is sealed onto the concrete surface by means of a pair of soft rings, creating two separate concentric chambers.

At a time between 35 and 60 sec Valve 2 is closed and the pneumatic system of the inner chamber is isolated from the pump. The air in the pores of the material flows through the cover concrete into the inner chamber, raising its pressure P_i. The rate of

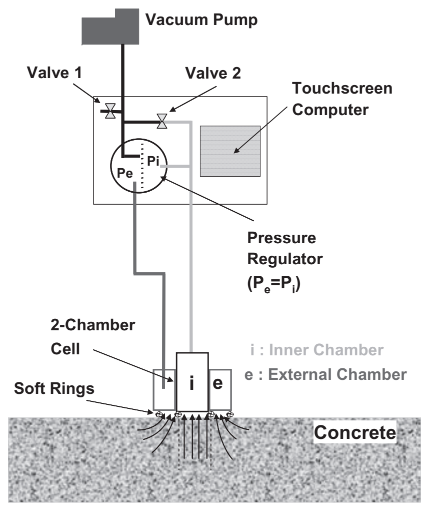

Figure 2. Sketch of test method.

pressure rise ΔP_i (measurement starts at $t_o = 60$ s) is directly linked to the coefficient of air-permeability of the cover concrete.

A pressure regulator maintains the pressure of the external chamber permanently balanced with that of the inner chamber ($P_e = P_i$). Thus, a controlled unidirectional flow into the inner chamber is ensured and the coefficient of permeability to air kT (m^2) can be calculated.

Consequently, depending on the concrete permeability, the test may take from 2 to 6 minutes (12 min for one brand).

The coefficient of permeability kT is calculated as:

$$kT = \left(\frac{V_c}{A}\right)^2 \frac{\mu}{2\varepsilon P_a} \left(\frac{\ln \frac{P_a + \Delta P_i}{P_a - \Delta P_i}}{\sqrt{t_f} - \sqrt{t_0}}\right)^2$$

KT: coefficient of air-permeability (m^2).
V_c: volume of inner cell system (m^3).
A: cross-sectional area of inner cell (m^2).
μ: viscosity of air ($= 2.0 \cdot 10^{-5}$ Ns/m^2).
ε: estimated porosity of the cover concrete (assumed = 0.15).
P_a: atmospheric pressure (N/m^2).
ΔP_i: pressure rise in the inner cell at the end of the test (N/m^2).
t_f: time (s) at the end of the test (2 to 6 or 12 min, depending on the instrument brand).
t_o: time (s) at the beginning of the test (= 60 s).

Table 1. shows the classification of concrete permeability (ages 28–180 days) as function of kT.

3 CORRELATION WITH OTHER TRANSPORT TESTS

Figs. 3 to 6 show comparative data of kT and other well known methods to measure transport.

4 CONCLUSIONS

- The method measures the resistance of the concrete cover against aggressive agents ingress.
- It correlates very well with other methods to measure transport phenomena in concrete.

Table 1. Concrete permeability classes.

Class	kT ($10^{\omega 16}$ m^2)	Permeability
PK1	< 0.01	Very Low
PK2	0.01–0.10	Low
PK3	0.10–1.0	Moderate
PK4	1.0–10	High
PK5	> 10	Very High

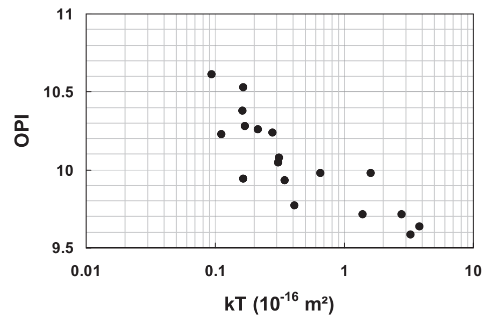

Figure 3. kT vs. South African O_2 permeability index.

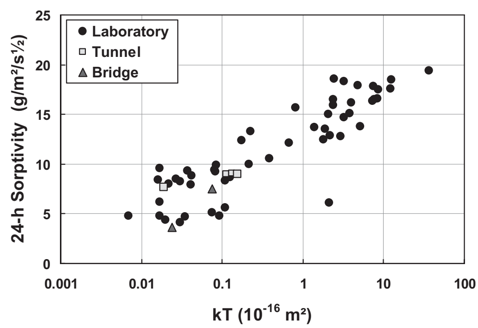

Figure 4. kT vs. capillary suction rate.

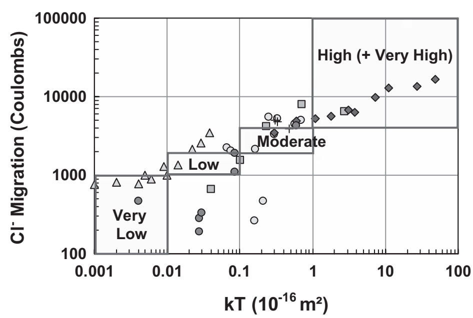

Figure 5. kT vs. chloride migration (ASTM C1202).

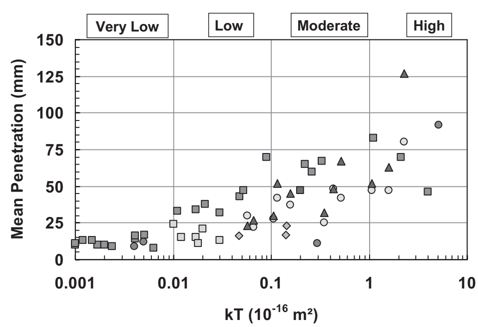

Figure 6. kT vs. water penetration (EN12390–8).

- It encourages the use of specification and control of durability of concrete structures, with the following advantages:
  - By controlling the end product it consolidates a performance oriented mindset in all the parties involved.
  - It tends to eradicate bad practices (uncontrolled water addition to concrete, poor compaction, lack of proper curing, spray of water or cement during floor finishing, etc.).
  - It stimulates the use of innovative solutions that improve the quality of the “covercrete” (permeable formwork membranes, vacuum “dewatering” of slabs and the use of special concretes, such as self-compacting, high performance, self-curing concretes, etc.)
- It constitutes a useful tool for assessing the condition of structures, by identifying the most vulnerable areas where works for repair, rehabilitation or retrofitting may be done.
- The values of kT can be used to design/predict service life of structures on the basis of the real quality and thickness of the "covercrete". Methods already exist for carbonation-induced corrosion whilst methods are being developed to cope with chloride-induced corrosion.

Concrete Repair, Rehabilitation and Retrofitting III – Alexander et al. (eds)
© 2012 Taylor & Francis Group, London, ISBN 978-0-415-89952-9

Evaluation of carbonation progress of existing concrete structure based on air permeability of concrete cover—a case study in Japan

K. Imamoto
Faculty of Engineering, Tokyo University of Science, Tokyo, Japan

A. Tanaka
Hachiyo Consultant, Japan

ABSTRACT: This paper deals with the on-site air-permeability of concrete cover and its relation to carbonation progress of existing RC structures in Japan. The air permeability of concretes and carbonation progresses were measured with 4 buildings and 11 concrete specimens which ages ranged from 12 to 45 years. The carbonation velocity (A) based on the square root theory increases with the increase of air permeability coefficient (kT). Although the relationship between A and kT for all building and concrete specimens has quite large scatter, the relationships between them for individual buildings were comparatively good. This might provide a good perspective for indicate that evaluation of carbonation progress based on the kT should be performed at each building, i.e. environmental condition.

1 INTRODUCTION

In Japan, over 400,000 new reinforced concrete (RC) buildings are constructed every year and approximately 80 billion euros are spent for the maintenance of existing RC structures. Estimating life expectancies of buildings and devising strategies to enhance structural durability are quite important.

This paper deals with the on-site air-permeability of concrete cover and its relation to carbonation depth of existing RC structures in Japan.

2 TORRENT PERMEABILITY TESTER

This method was developed by Torrent (1992). The distinctive characteristic features of this method are a two-chamber vacuum cell and a regulator that balances the pressure in the inner (measuring) chamber and in the outer (guard-ring) chamber. This tester has been adopted to evaluate the carbonation progress of new concrete by Imamoto (2008).

3 OUTLINES OF SURVAYED EXISTING BUIDINGS

4 buildings and 11 old specimens were tested in this study. They are located in north, middle and west region of Japan. Hence, the influence of difference of environmental condition and quality of concrete on the relationship between air permeability and carbonation progress can be discussed. Air permeability of concrete was measured for exposed concrete mainly at indoor in order to eliminate the influence of moisture condition due to rainfall. Appearances and details of buildings and specimens are shown in photos 1 to 5 and table1, respectively. Details of buildings and specimens are introduced in figures 2 and 3 and in table 2 and 3.

4 RELATION BETWEEN AIR PERMEABILITY KT AND CARBONATION PROGRESS OF EXISTING BULDINGS

Figure 4 shows a relationship between carbonation velocity in and the air permeability coefficient (kT) of concrete for all buildings and specimens. It can be seen that the carbonation velocity based on the square root theory, as shown in Eq.(1), A seems to increase with the increase of kT. However its scatter is quite large.

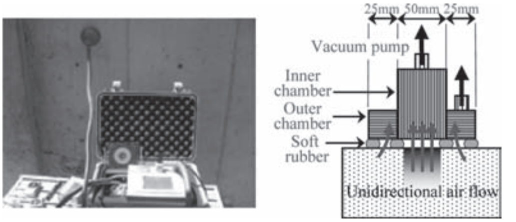

Figure 1. Outline of torrent permeability tester.

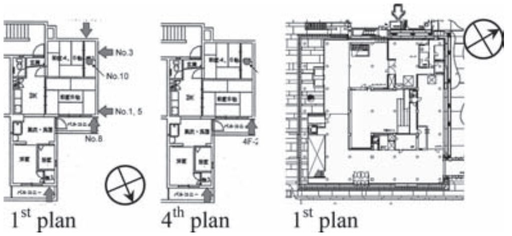

Figure 2. Examples of tested points of Multi-family dwellings in Osaka (HK): Left and National museum of western art in Tokyo (NMWA): Right.

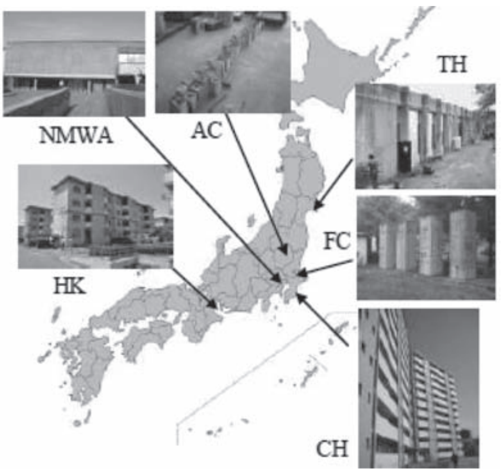

Figure 3. Location of tested buildings and specimens in JAPAN.

Table 1. Details of buildings and exposed specimens.

Name of building	Notation	Location	Year of birth (Age at survey)
Multi-family dwellings	HK	Osaka	Original:1961(49 years) Additive:1992(18 years)
Lab. of Tohoku university	TH	Sendai	1979 (41 years)
National museum of western art	NMWA	Tokyo	1959 (50 years)
Concrete specimen	AC	Tochigi	1977–1997(12–32 years)
Multi-family dwellings	CH	Chiba	1978–9 (41–42 years)
High strength concrete column	FC	Tsukuba	1991 (15 years)

Table 2. Mixture proportion and age of concrete specimens of Ashikaga Institute of Technology in Tochigi (AC).

No. of specimen	Age [Years]	W/C	Unit content[kg/m³] W	C1	C2	S	G
1	30	60	181	301	–	694	1145
2	31	60	178	297	–	736	1038
3	19	60	167	278	–	972	906
4	32	65	205	315	–	852	1216
5	20	55	165	210	90	768	1041
6	30	70	178	254	–	921	1029
7	30	70	179	256	–	769	1112
8	30	50	167	278	–	972	906
9	12	62	173	279	–	861	908
10	28	50	176	347	–	673	1176
11	31	60	179	297	–	717	1054

Table 3. Mixture proportion and age of concrete specimens of high strength concrete columns (Full size specimens) in Tsukuba (FC): Right.

Notation	W/C	s/a	Unit content [kg/m³] W	C	SP	S	G	Ad
Fc100-A	0.2	0.396	160	720	80	531	910	C × 1.7%
Fc100-B	0.2	0.396	160	720	80	531	910	C × 2.0%
Fc60	0.27	0.441	165	611	–	713	910	C × 1.9%

$$C = A\sqrt{t} \tag{1}$$

C: Carbonation depth (mm)
A: Carbonation velocity (mm/years$^{0.5}$)
t : Age of concrete (Years)

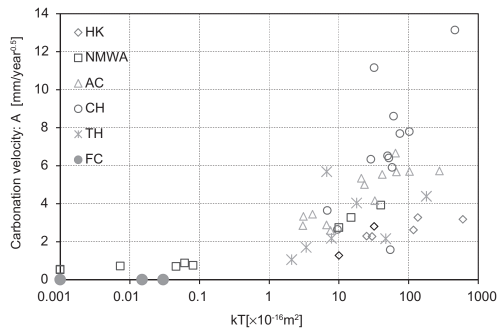

Figure 4. Relationship between kT and A of all buildings and specimens.

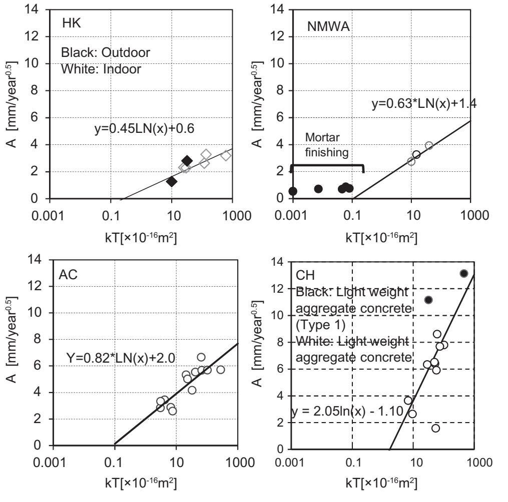

Figures 5 to 8. Relationships between kT and A for each building.

Figures 5 to 8 show relationships of each building. It can be seen that a good agreement can be obtained between them. The tangent of the regression lines differ among each building (for example, the tangents 0.45 for building HK and 0.86 for TH). It is clear that environmental conditions such as temperature and relative humidity R.H. strongly affect the carbonation progress of concrete.

5 CONCLUSIONS AND FUTURE OVERVIEW

The air permeability of existing concrete structures in JAPAN were investigated by nondestructive methods (NDT) and compared to concrete carbonation progress. The relationships between them were comparatively good for individual building. This might indicate that evaluation of carbonation progress based on the kT should be performed at each structure, i.e. environmental condition.

Concrete Repair, Rehabilitation and Retrofitting III – Alexander et al. (eds)
© 2012 Taylor & Francis Group, London, ISBN 978-0-415-89952-9

Lattice Boltzmann simulation of permeability of cement-based materials

M. Zhang & G. Ye
Microlab, Faculty of Civil Engineering and Geosciences, Delft University of Technology, Delft, The Netherlands

ABSTRACT: Due to its importance on the durability assessment and service life prediction of reinforced concrete structures, it is essential to estimate the permeability of cement-based materials. This paper presents a microstructure-based permeability modeling of cement-based materials using the Lattice Boltzmann (LB) method, where a Multiple-Relaxation-Time (MRT) corrosion operator is utilized. The MRT-LB model is applied to simulate the single-phase fluid flow in saturated cement paste. The microstructure of cement paste is generated by HYMOSTRUC3D. Following the onset of steady-state flow, the overall mean velocity is obtained and the water permeability is calculated according to Darcy's law. In the numerical experiments, the effects of water-to-cement (w/c) ratio, degree of hydration and effective porosity on the water permeability of cement paste are evaluated. The simulations are validated with experimental data obtained from the literature. The results indicate that the simulated permeability is close to the measured permeability for the samples at early age. For the samples with effective porosity higher than 20%, the simulation shows a good agreement with the experiment. In addition, for both simulation and experiments, the relationship between the water permeability and the effective porosity is highly correlated. This implies that the effective porosity is a critical parameter which determines the permeability of cement-based materials.

1 MULTIPLE-RELAXATION-TIME LATTICE BOLTZMANN (MRT-LB) SIMULATION

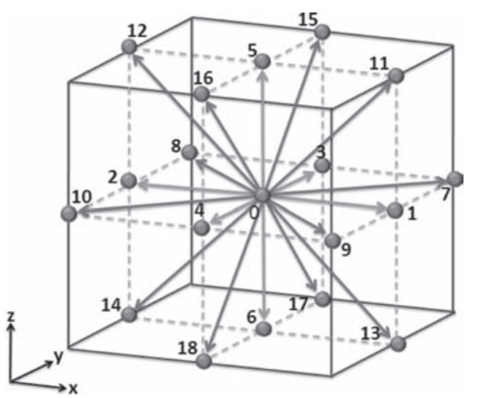

Figure 1. Lattice velocity direction of the D3Q19 model.

2 3D MICROSTRUCTURE OF PORTLAND CEMENT PASTE

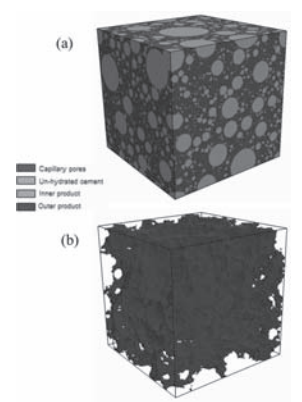

Figure 2. The digitized microstructure and its pore structure of cement paste with w/c = 0.5 at 26 days.

3 RESULTS AND DISCUSSION

3.1 *Fluid flow streamline*

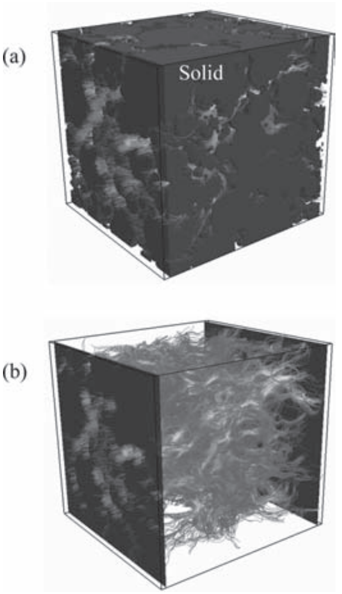

Figure 3. Steady-state flow streamline along the flow direction within the corresponding microstructure and pore structure of cement paste.

3.2 *Permeability*

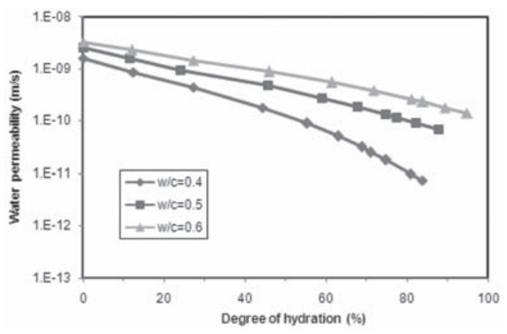

Figure 4. Simulated water permeability as a function of degree of hydration.

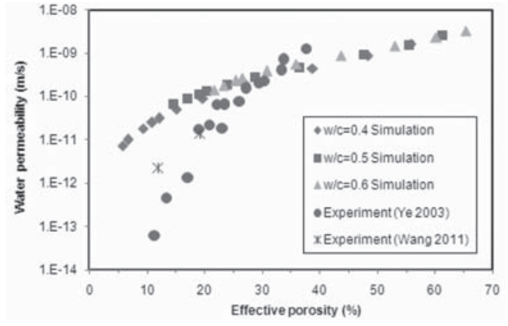

Figure 5. Comparison of simulated and measured permeability as a function of effective porosity.

4 CONCLUSIONS

This work presents a microstructure-based permeability model by using multi-relaxation-time lattice Boltzmann method. From the findings of the present study, the following conclusions can be drawn:

- The LB method provides insight into the internal velocity distribution and allows one to detect preferential flow paths within the specimen, and the LB simulation offers a significant potential for new fundamental insights and understanding of fluid flow processes.
- The simulated water permeability is correlated very well with the microstructure development of cement paste when the degree of cement hydration, w/c ratio and effective porosity are concerned. For the same effective porosity, the permeability values of the samples with different w/c ratios are observed to be very close to each other.
- A good agreement between the simulated and measured permeability can be observed when the effective porosity is higher than 20%. With a decrease in the effective porosity, the difference between the simulated and measured permeability increases. The water permeability significantly depends on the effective porosity which involves the information of porosity and connectivity of pores.

Concrete Repair, Rehabilitation and Retrofitting III – Alexander et al. (eds)
© 2012 Taylor & Francis Group, London, ISBN 978-0-415-89952-9

Morphological nature of diffusion in cement paste

N. Ukrainczyk
TU Delft, MICROLAB, Materials & Environment, The Netherlands
University of Zagreb, Croatia

E.A.B. Koenders
COPPE/UFRJ, Programa de Engenharia Civil, Rio de Janeiro, Brazil
TU Delft, MICROLAB, Materials & Environment, The Netherlands

K. van Breugel
TU Delft, MICROLAB, Materials & Environment, The Netherlands

ABSTRACT: The diffusive transport in cement based materials plays a crucial role in the degradation process of concrete. Rapid development of numerical models has provided novel methods to investigate the influence of microstructure on the evolution of the properties of cement based materials. A virtual 3D porous microstructure created with available hydration models provides a fundamental basis for the analysis of the morphological influence onto the effective diffusion coefficient. Such an approach contributes to a better understanding of the phenomenology and thus improves the predicting reliability of the coupled transport models. This paper investigates the influence of the morphological effect onto the diffusion properties of hydrating cement pastes using the cement hydration and microstructure development model HYMOSTRUC3D. The diffusive properties of the simulated microstructures are analyzed employing a numerical 3D transport model. The modeling results are compared with available literature results.

1 INTRODUCTION

Transport in cementitious materials plays a crucial role in both the degradation process of building materials and the containing of hazardous wastes. A good quality of the concrete cover enhances the durability and reliability of concrete structures. One parameter that is of paramount importance is the effective (macroscopic) transport coefficient. A relevant and reliable method is needed in order to obtain effective diffusion coefficient (D_{ef}) with an acceptable accuracy. Various experimental methods exist but they are either time consuming or have too many drawbacks. Simulating a microstructure evolution during hydration is an advantageous (fundamental) starting point to model the morphological nature of the effective diffusion (transport) coefficient. A virtual 3D microstructure created with an available hydration models provides a basis for the analysis of the morphological influence, including the porosity, tortuosity, constrictivity and the pore water content effect onto the effective diffusion coefficient. Such an approach contributes to a better understanding of the phenomenology and thus improves the predicting reliability of the coupled transport models.

The goal of this paper was to develop a flexible and efficient code within original Hymostruc platform that could be easily used for further developments. A finite difference (FD) program is written in C++ programing language for solving steady state transport problems on virtual 3D digital images generated by Hymostruc (Fig 1.). Hymostruc graphical interface was updated to visualize the transport simulation results.

2 IMPLEMENTATION

FD was chosen rather than finite element method because of the regularity of the digitizing mash and less memory requirement. Furthermore, FD are more physically realistic for transport problems (Garboczi et al. 1998).

The simulation of transport properties is implemented in two ways: 1) through capillary pores only; or 2) through capillary pores and hydration products (more precisely CSH gel). Because the size of the sparse matrix **A** is N times N the matrix is not stored explicitly but only implicitly in the vectors $\mathbf{c}_x$, $\mathbf{c}_y$, and $\mathbf{c}_z$ which store the conductance coefficients of the bonds among voxel faces in the x, y, and z directions, respectively. The system of equations is solved by conjugate gradient algorithm. The bottleneck in this solver routine is the multiplication of matrix A with an arbitrary vector. In order to speed up this

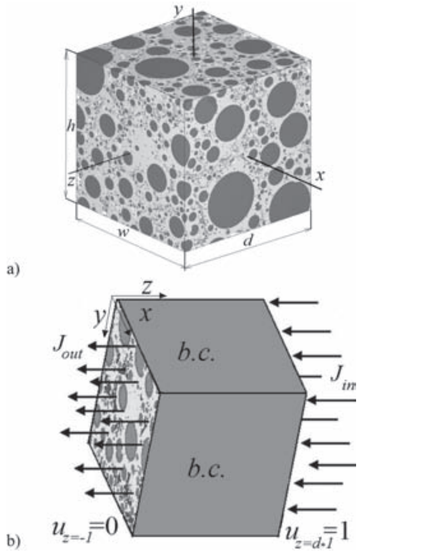

Figure 1. a) 3D simulated microstructure, b) steady state flux (J) across z-axis, with periodic or adiabatic boundary conditions employed on 4 side faces parallel to the imposed flux.

solver one needs to do the multiplication in an optimized way. In the main matrix-vector multiplication according to discretized Laplace equation the result was corrected on boundary nodes in order to account for periodic boundary conditions. The simulated microstructure of hydrated cement paste with visualization of the distribution of water concentrations (relative values 0–1) in cement paste at steady state is shown in Fig 2. The black parts show the high concentrations and the light grey (white) parts the low concentrations of species. Graphical 3D and 2D output interface enables to interactively show 3D and 2D slices with a help of cursors that change the size of cube and z position of microstructure. This enables a full insight into the 3D numerical results.

3 RESULTS

The simulations were run on hydrated cement pastes with two resolutions: voxel length of 1 and 0.5 μm. Only a small difference in results can be observed while increasing resolution. Simulations run on Intel® Xeon® CPU3565 3.2GHz, take 40 s and 9 min for resolution 1 μm/voxel (100^3 voxels) and 0.5 μm/voxel (200^3 voxels), respectively.

The simulated effective diffusion coefficient of tritiated water is higher than the literature value. This discrepancy could be due to a long time needed to obtain steady state conditions in real experiments. During such experimental conditions the continuing cement hydration evolves the microstructure, which is not considered in simulations.

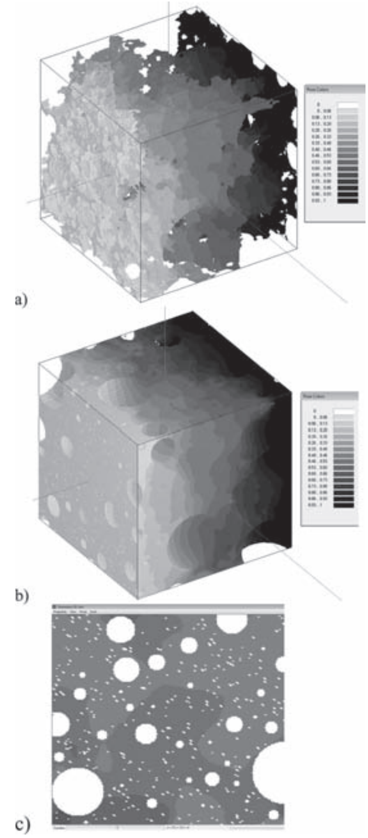

Figure 2. Visualizations of the distribution of water concentrations in cement paste at steady state: a) 3D slices of the capillary pore structure, b) transport through capillary pores and hydration products, and c) 2D slices with cursor that actively changes the z position of microstructure.

4 CONCLUSIONS

This paper presents a full 3D finite difference module that has been implemented within original Hymostruc kernel with which the mass transport through an evolving microstructure can be evaluated.

The numerical model is backed up with a high level of graphical interface to help visually investigate the results of the transport simulations.

The simulation of transport properties as described here can be viewed in a larger general aspect because of the analogy between the following four laws: Fourier's law for heat flow, Ohm's law for electric current, Fick's law for diffusion, and Darcy's law for liquid (and gas) flow in porous materials.

In future work hydration effects (e.g. impacts of portlandite distribution, aluminate-bearing hydration products and fillers) on transport properties will be investigated by linking virtual microstructure simulations and the developed 3D numerical transport model.

Concrete Repair, Rehabilitation and Retrofitting III – Alexander et al. (eds)
© 2012 Taylor & Francis Group, London, ISBN 978-0-415-89952-9

Modeling of moisture distribution in concrete in 3D

J. Skramlik, M. Novotny & K. Suhajda
Brno University of Technology, Czech Republic

ABSTRACT: Into porous material of concrete structures can penetrate moisture in liquid or gaseous form. Humidity affects the physical properties of building material. To express the negative effects of moisture on building materials or building structures more accurately, it is needed to use the most accurate method of detecting moisture diffusion. Capillary conductivity is influenced not only by external fluids and change of heat, but also by the processes inside the porous structure. These influences should be explored in text of European standard EN ISO 15026 where is an informative link that presents the description of the distribution of moisture in porous material based on measurements using NMR (nuclear magnetic resonance), which is essentially a curve of wetting of material in time intervals. The aim of this paper is to present information about detection of distribution of moisture in concrete by means of EMWR (electromagnetic microwave radiation) and to record moisture curve in 3D for calculation of capillary conductivity coefficient and its dependence on moisture by weight.

1 INTRODUCTION

Capillary diffusion of moisture in porous building materials is still quite unexplored area of knowledge in the development of building physics for practical application in the assessment of buildings. The research results in moisture structures have different conclusions of its influence in real conditions. By applying simplified methodology of measurement of capillary conductivity of building materials would by possible to gain a data usable in practical calculations.

2 CAPILLARY CONDUCTIVITY COEFFICIENT

The basic theoretical concept for the description of moisture transport in porous material in this case is based on a combination of continuity equation with Lykov's equation, which expresses capillary conductivity and moisture gradient.

After distribution of moisture in a given time interval (t is constant and x is a function of one variable) can be expressed the capillary conductivity coefficient:

$$\kappa(u(x)) = \frac{1}{2tu'(x)} \cdot \int_x^{\infty} \xi \cdot u'(\xi) d\xi \qquad (1)$$

t = time interval [s], ς = substitution of the distance [–], ω = new variable [–], η = Boltzmann transformation [$m.s^{-1/2}$], x = length of a sample [m], u_1 = max. value of moisture [–], u_2 = moisture by relative humidity [–].

3 DIFFUSION OF MOISTURE ACCORDING TO EUROPEAN STANDARD

The determination of the vapor coefficient according to European standard 15026 is described in EN ISO 12572. Higher water content has an influence on the moisture transport behavior in porous material.

$$K(p_{suc})\frac{\partial p_{suc}}{\partial x} = -D_w(w)\frac{\partial w}{\partial p_{suc}}\frac{\partial p_{suc}}{\partial x} = -D_w(w)\frac{\partial w}{\partial x} \qquad (2)$$

K = liquid conductivity [$s..m^{-1}$], D_w = diffusion of moisture as transfer coefficient [$m^2.s^{-1}$], p_{suc} = suction [Pa], w = moisture by weight [$kg.m^{-3}$].

In annex of this standard are mentioned results of analytical solution in graph and calculated results of humidity in one dimensional form by help of NMR (nuclear magnetic resonance).

4 DETECTION OF MOISTURE DISTRIBUTION BY HELP EMW RADIATION

To detect moisture transport in concrete there was used apparatus developed at the Institute of Building construction, Brno University of Technology (Fig. 1).

5 MONITORING OF MOISTURE IN 3D

At the Fig. 2 is a graphical representation of the changes in moisture by weight obtained by transfer of electromagnetic microwave radiation intensity on the content of moisture in time of a shift of waveguide within the length of sample.

At the Fig. 3 is expression of three-dimensional distribution of moisture material which allows accurate determination of moistening curves.

The values determined with the aid of experimentally assembled apparatus allow calculating the coefficient of capillary conductivity. From distribution of moisture in a given time interval can be expressed the capillary conductivity coefficient (Kutilek):

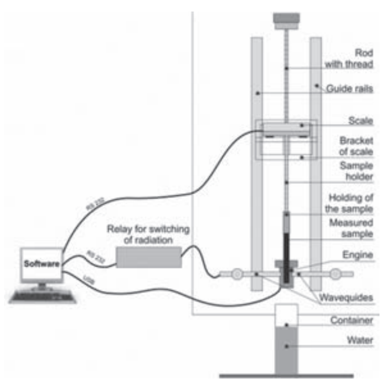

Figure 1. Apparatus for monitoring the moisture transport in 3D view.

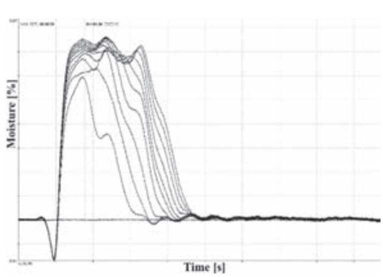

Figure 2. Changes of EMWR intensity depending on the moisture rising in the sample material.

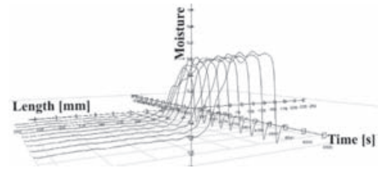

Figure 3. 3D distributions of moisture in the sample material.

$$\kappa(u(x)) = \frac{1}{2tu'(x)} \cdot \int_{x}^{\infty} \xi \cdot u'(\xi) d\xi \qquad (3)$$

where t = time interval [s], ς = substitution of the distance [–], ω = new variable [–], η = Boltzmann transformation [$m.s^{-1/2}$], x = length of a sample [m], u_1 = maximal value of moisture [–], u_2 = moisture by relative humidity [–].

6 CONCLUSIONS

By measurements on the experimental apparatus were attained curves, comparable with the method presented in the ISO standard and there are no differences in the method by use of partial pressures. It has been shown that microwave radiation is sufficient for the detection of moisture. Measurement results can be applied to calculate the coefficient of capillary conductivity. Compared with the gravimetric method are curves for calculation of capillary conductivity coefficient using Mattan method more accurate as well as an integral, which requires more curves on the same material. In addition, more affordable place NMR is EMWR.

ACKNOWLEDGEMENT

This article was supported by GACR P104/10/P388 "Experimental analysis of the effect of microwave radiation for destruction of biological agents" and by GACR P104/10/1390 "The analysis of influence of MW drying while application of chemical grouting into moist brickwork".

REFERENCES

1. Kiessl, K. Kapillarer und dampfförmiger Feuchtetransport in Bauteilen. Essen 1983.
2. European Standard EN ISO 15026 Assessment of moisture transfer by numerical simulation, 2007.
3. Gertis, K. & Kiessl, K. Feuchte Transport in Baustoffen, 1980.
4. Kutilek, M. Dampness porous material, CZ, Prague SNTL, 1992.
5. Krischer, K. Die Wisenschaftliche Grundlagen der Trocknugstechnik, Springer Verlag 1978.
6. Skramlik, J. & Novotný, M. Moisture transfer in building material, PROHITECH 09, Italy, Taylor and Francis Group, UK, ISBN 978-0-415-55803-7, 2009.

Concrete Repair, Rehabilitation and Retrofitting III – Alexander et al. (eds)
 ISBN 978-0-415-89952-9

DC and AC measurements of the chloride diffusion coefficient through concrete

H. Mercado & S. Lorente
Université de Toulouse, UPS, INSA, LMDC (Laboratoire Matériaux et Durabilité des Constructions), Toulouse Cedex 04, France

X. Bourbon
ANDRA, Parc de la Croix Blanche, Chatenay-Malabry, France

ABSTRACT: The chloride diffusion coefficient is an indicator of durability. Among the various methods existing to measure this coefficient, the ones based on natural diffusion are the most time consuming. In order to reduce the duration of experiments, accelerated methods were developed during the past 15 years, among which the electrically enhanced tests. Yet, although the effective diffusion coefficient is a unique parameter depending only on the ionic species of interest and the material (through its pore network), these diffusion coefficients are hardly compared to each others. This paper is an attempt to compare two different methods of chloride diffusion coefficient determination. The first method is based on the application of the Nernst-Einstein equation for which the conductivity of the saturated sample is measured by impedance spectroscopy for two kinds of concrete (based on type I and type V cements). The second method is a migration test in which the flux of chloride measured upstream allows calculating the diffusion coefficient by means of the Nernst-Planck equation. The diffusion coefficients calculated with the two methods are in good agreement provided the metrology of the experiments is carefully controlled.

1 INTRODUCTION

Chloride diffusion is itself a research topic because of the implication of chloride on the corrosion of steel bars used as reinforcement in the concrete structures.

This paper documents a study of ionic transfer through samples of CEM-I and CEM-V concrete. Impedance spectroscopy measurements allowed us to study the relationship between the formation factor and the ionic strength of the pore solution. Next, a comparison is made between the diffusion coefficient calculated from EIS experiments and the diffusion coefficient obtained from a migration test (Khittab et al., 2005).

2 MATERIALS

The concrete samples were based on CEM-I and CEM-V cement with water-to-cement ratio of 0.4 and 0.43 respectively. We also performed pore solution extractions for the two types of concrete from which artificial solutions were prepared.

3 EXPERIMENTS

3.1 *Electrochemical impedance spectroscopy (EIS)*

Impedance measurements were performed with an impedance analyzer (HP 4294 A). The amplitude of the sinusoidal voltage was 200 mV, and the frequency range was 40–110 106 Hz. The values of the impedance were plotted on Nyquist plots.

The diffusion coefficient was obtained from the measurement of the saturated material resistance.

Theoretically, the Nyquist plot corresponding to the equivalent electrical circuit is made of two loops. The system becomes entirely resistive when $\omega \to 0$, $\omega \to \infty$, and for an intermediary value of the angular frequency ω_{mat} for which $Z_{im}(\omega_{mat}) = 0$. In this case, the equivalent circuit impedance is $Z(\omega) = R_{mat}$.

3.2 *Electrokinetic test*

A cylindrical sample of material is placed between two compartments containing any of the artificial solution completed with 20 g/L of NaCl. A constant electrical potential difference is applied between the two faces of the material in a way to create a 400 V/m electrical field.

Since the cathodic compartment contains a renewed volume of solution, it behaves as an infinite reservoir, and the chloride concentration at the surface of the sample on the cathodic side is therefore a constant corresponding to the chloride concentration in the compartment.

4 RESULTS

4.1 *Formation factor and ionic strength*

Concrete cylinders of 30 mm in thickness were vacuum saturated with their corresponding artificial solution. EIS tests were performed and the saturated concretes conductivities were recorded leading to the calculation of the corresponding formation factors. Next, the samples were dried until constant mass before being vacuum saturated again with the same artificial solutions to which 20 g/L of NaCl were added. Again, EIS tests were carried on. Some tests were done immediately after saturation, while another set of samples was kept for one year in saturation with NaCl before EIS tests.

In the case of the CEM-I concrete the formation factor remained relatively constant even when the material was saturated with the solution 1 and NaCl, and kept in this solution for one year. The fact that the formation factor remains constant indicates that, not only F does not vary with the ionic strength, but also does not vary with a change in the pore solution constituents. Such results highlight the character of geometric parameter of the formation factor, a macroscopic geometric parameter which accounts for the pore network tortuosity, and constrictivity.

The case of the CEM-V concrete is rather different. The formation factor increased immediately after the saturation with solution 2 and NaCl. F is even higher when measured after one year of conservation in the saturation solution. This result is in agreement with the works published by Sanchez et al. (2008) who also used a concrete with mineral additions in their study. The pore network is such that the transfer of chloride creates modifications in the concrete microstructure and narrows the pore dimensions leading to an increase of the formation factor. Because the contribution of the smallest pores to the overall porosity in CEM-I concrete is much smaller, the effect of chloride on the pore geometry was not detected.

4.2 *Diffusion coefficients*

The diffusion coefficients measured with the two techniques are in good agreement in the case of CEM-I concrete. In the two different kinds of experiments the metrology was carefully controlled: interface between the electrodes and the samples in EIS experiments, constant boundary conditions in the case of the electrokinetic tests for example.

When the chloride diffusion coefficient is calculated from the Nernst-Planck equation, chloride ions need to be added both to the electrolyte solution that is used in the cathodic and anodic compartments and as saturation solution. This condition ensures null concentration gradients. Because the method is based on the flux of chloride calculations, the amount of chloride transferred through the sample needs to be monitored which requires, obviously, to work with chloride. On another hand, the formation factor measurements through the AC tests proved to be independent of the ionic strength and of the ionic composition of the solution (in the limit of the tested ionic strength range). Therefore the technique may be used to calculate the diffusion coefficient of an ionic species even though the very ion is present neither in the electrolyte compartments, nor in the pore solution.

If the pore network geometry has impact on the electrical charges transport as seen in the previous section, its impact is also obviously present here in the values of the diffusion coefficient measured by Impedance Spectroscopy. We notice that the diffusion coefficient of CEM-I concrete is 3.5 times higher than the one of CEM-V concrete. It is worth highlighting that the technique developed to improve the migration test (specific control of the boundary and initial conditions) leads to a similar ratio between the two diffusion coefficients. This result proves again, but this time in a non direct way, that the geometry of the pore network is the leading factor in the value of the macroscopic parameter which is a diffusion coefficient.

5 CONCLUSION

We presented in this paper a comparison between two different ways to measure the diffusion coefficient of chloride through saturated samples of CEM-I and CEM-V concretes. Artificial solutions were prepared based on the pore solutions compositions of the two concretes. The addition of chloride to the pore solution of the materials does not seem to have a detectable impact on the results of the CEM-I concrete. The CEM-V concrete is relatively sensitive to the chloride transfer with a strong increase of its formation factor in time. The particular structure of the CEM-V concrete pore network combined with the products of the interactions of chloride with the cement matrix lead to narrower pore paths which may explains this result.

Finally the comparison between the diffusion coefficients obtained from EIS tests and electrokinetic experiments indicated a good agreement between the results. Future works will include a search for equivalent electrical models which allow describing the microstructure of the materials.

Concrete Repair, Rehabilitation and Retrofitting III – Alexander et al. (eds)
© 2012 Taylor & Francis Group, London, ISBN 978-0-415-89952-9

Factors affecting $AgNO_3$ colorimetric method for measurement of chloride migration in cement-based materials

C. Shi, X.Wang, X. An & Q. Li
College of Civil Engineering, Hunan University, Changsha, Hunan, China

F. He & C. Chen
Department of Civil Engineering and Architecture, Xiamen University of Technology, Xiamen, Fujian, China

ABSTRACT: In this paper, mechanism of $AgNO_3$ colorimetric measurement, measured and calculated values of chloride concentration at the color change boundary (C_d) were reviewed and discussed. Factors influencing C_d were discussed and error of chloride migration measured by $AgNO_3$ colorimetric method was evaluated. Results indicated that calculated C_d range properly explains why measured C_d reported in many publications varies in a board range. Sprayed volume and concentration of $AgNO_3$ solution are main factors in determining $C_{d.}$ The established $AgNO_3$ spraying procedure and $C_d = 0.2$ mol/L is reasonable for measuring and calculating non-steady-state chloride migration coefficient (D_{nssm}) and apparent chloride diffusion coefficient (D_{app}). Based on established spraying procedure, the error of D_{nssm} can be less than 5% even when $X_d < 5$ mm. However, determination of surface chloride concentration mainly determines error of D_{app}. When average chloride ion chloride concentration in the first 2 mm layer of specimens is similar to that in the contact solution, D_{app} values measured by $AgNO_3$ colorimetric method is very similar to those measured by NT build 443.

Chloride-induced corrosion of steel reinforcement is a dominant factor on durability of concrete structures exposed to marine environments and/or de-icing salts. A local breakdown of the passivating layer occurs when a sufficient amount of chloride ions reaches the steel reinforcement; corrosion is then enabled. In the context of chloride-induced corrosion, it is reasonable to consider the service life of reinforced concrete structures in two stages. Due to the relatively fast development of the second stage and for the sake of safety, the duration of the first stage is sometimes regarded as the design service life of steel-reinforced concrete structures.

The chloride ion penetration front, varying with time and environment, can be used to monitor the movement of chloride ions in concrete and for service life prediction (Stanish 2002). Analysis of chloride ion content in concrete can be conducted by the so-called profile method, which requires a series of special equipment and consumes much time. However, $AgNO_3$-based colorimetric methods can measure chloride ion penetration depth in concrete quickly and simply.

The $AgNO_3$ colorimetric method involves two parameters, X_d and chloride concentration at the color change boundary (C_d). X_d and C_d have been widely used for measuring chloride migration in cement-based materials. For existing concrete structures, periodical spraying of $AgNO_3$ solution can be easily performed to obtain a series of X_d with time, which can provide the kinetic process of chloride penetration. This information can be useful for the assessment of the chloride corrosion risk of existing concrete structures (Baroghel-Bouny et al. 2007a, 2007b, Meck & Sirivivatnanon 1999) or for monitoring the residual life prediction of existing concrete structures (Stanish 2002, Baroghel-Bouny et al. 2006).

Many researchers have studied C_d and noticed that it varied within a broad range. They expressed C_d with three different forms: free chloride concentration (in pore solution), water soluble chloride contents (by the mass of binder), and total chloride concentration (by the mass of binder). The use of a single value instead of actual concentrations may result in significant error in calculated D_{nssm} and D_{app}, the kinetics of chloride penetration process and chloride corrosion risk assessment of existing concrete structures.

Since the 1970s, three $AgNO_3$-based colorimetric methods, i.e. $AgNO_3$ + fluoresceine, $AgNO_3$ + K_2CrO_4 and $AgNO_3$ method, have been proposed to measure the chloride ion penetration depth in concrete in the field and laboratory. $AgNO_3$ method can be conducted more simply and easily than the other two methods. Besides, $AgNO_3$ method can make clear color change boundary in the most cases (Baroghel-Bouny et al. 2007a). Therefore, it is the most practical method for measuring chloride penetration in concrete.

$AgNO_3$ method involves spraying only an $AgNO_3$ solution onto a freshly fractured concrete cross-section, which leads to the formation of white and brown zones with a clear color change boundary. Based on the brightness of color appearing on the concrete surface, Otsuki et al. (1992) recommended the use of 0.1 mol/L silver nitrate solution.

He et al. (2011) investigated chloride concentration at the color change boundary of $AgNO_3$ method. They calculated the C_d according to Ag^+-Cl^-- OH^+-H_2O system.

When $V_{Ag^+}/V_{OH^- + Cl^-} > 2.54C_{OH^-}/C_{Ag^+}$, namely Ag^+ can react with all OH^- and Cl^-, Chloride concentration at color change boundary can be expressed as equation (1).

$$C_{crit\text{-}Cl^-} = 1.6C_{OH^-} \quad (1)$$

When $V_{Ag^+}/V_{OH^- + Cl^-} < 2.54C_{OH^-}/C_{Ag^+}$, ($Ag^+$ can react with only partial OH^- and Cl^-), Chloride concentration at color change boundary can be expressed as Equation (2).

$$C_{crit\text{-}Cl^-} = 0.00695C_{OH^-} + 0.608C_{Ag^+}V_{Ag^+}/V_{OH^- + Cl^-} \quad (2)$$

Where C_{Ag^+}, and C_{OH^-} are the mole concentrations of Ag^+ and OH^-; V_{Ag^+} is the volume of $AgNO_3$ solution added to the NaOH + NaCl solution; $V_{OH^- + Cl^-}$ is volume of NaOH + NaCl solution.

Many factors such as concrete alkalinity, sprayed volume and concentration of $AgNO_3$ solution, pore solution volume of concrete, sampling method and methods used for measuring free chloride in concrete can be responsible for the high variability. Among all factors, sprayed volume and concentration of $AgNO_3$ solution are main ones. 0.1 mol/L $AgNO_3$ solution gives the most clear boundary color, it was suggested to use for the indicator. Therefore, a proper sprayed volume of 0.1 mol/L $AgNO_3$ solution should be determined. However, this important point was not mentioned at all times since the $AgNO_3$ method was applied.

To obtain a small C_d range, sprayed amount of $AgNO_3$ solution should be as less as possible, but the surface of cement-based materials must be completely wetted by $AgNO_3$ solution. For this purpose, a serious of colormetric experiments were conducted and found that when fractured concrete surface was vertically placed, 0.3 ± 0.06 L/m^2 sprayed volume can provide a completely wetted surface without excessive solution owing to drop of small amount of excessive solution from the vertical surface (He 2010).

When taking 0.07 mol/L $AgNO_3$ solution as C_d to use for calculating D_{nssm}, even C_d has a relatively small range, the error still get 20% at about X_d = 5 mm, When C_d = 0.2 mol/L is used for calculating D_{nssm}, the error can be controlled at below 5% even X_d < 5 mm. The established $AgNO_3$ spraying procedure and C_d = 0.2 mol/L can be reasonable for measuring and calculating D_{nssm}.

The established $AgNO_3$ spraying procedure and C_d = 0.2 mol/L can be reasonable for measuring and calculating D_{app}. However, determination of C_S mainly determines error of D_{app}. When average chloride ion chloride concentration in the first 2 mm layer of specimens is very similar to that in the immersion solution used in NT build 443, D_{app} values measured by $AgNO_3$ colorimetric method is very similar with those measured by NT build 443. Therefore, D_{app} in cement-based materials can be rapidly and accurately measured by $AgNO_3$ colorimetric method.

SUMMARY

1. $AgNO_3$-based colorimetric methods are fast and easy to perform. They have been widely applied to measure the chloride penetration depth in field and laboratory.
2. Calculated results of C_d can explain why measured C_d varies within a broad range. Calculated Equation can be very useful to investigate factors influencing C_d and control C_d in a small range for more accurate application of $AgNO_3$ colorimetric method.
3. Many factors such as concrete alkalinity, sprayed volume and concentration of $AgNO_3$ solution, pore solution volume of concrete, sampling method and methods used for measuring free chloride in concrete can be responsible for the high variability. Among all factors, sprayed volume and concentration of $AgNO_3$ solution are main ones. Therefore, a proper sprayed volume of 0.1 mol/L $AgNO_3$ solution should be determined. However, this important point was not mentioned at all times since the $AgNO_3$ method was applied.
4. When C_d = 0.2 mol/L is used for calculating D_{nssm}, the error can be controlled at below 5% even X_d < 5 mm. The established $AgNO_3$ spraying procedure and C_d = 0.2 mol/L can be reasonable for measuring and calculating D_{nssm}.
5. The established $AgNO_3$ spraying procedure and C_d = 0.2 mol/L can be reasonable for measuring and calculating D_{app}. However, determination of C_S mainly determines error of D_{app}. When average chloride ion chloride concentration in the first 2 mm layer of specimens is very similar to that in the immersion solution used in NT build 443, D_{app} values measured by $AgNO_3$ colorimetric method is very similar with those measured by NT build 443. Therefore, D_{app} in cement-based materials can be rapidly and accurately measured by $AgNO_3$ colorimetric method.

Concrete Repair, Rehabilitation and Retrofitting III – Alexander et al. (eds)
© 2012 Taylor & Francis Group, London, ISBN 978-0-415-89952-9

Cement mortars with fly ash and slag—study of their microstructure and resistance to salt ingress in different environmental conditions

M.A. Climent, J.M. Ortega & I. Sánchez
Civil Engineering Department, Universitat d'Alacant, Alacant/Alicante, Spain

ABSTRACT: Several laboratory researches suggest the incorporation of active additions (fly ashes, blast furnace slags, etc.) to concrete, as a useful means of improving the resistance of concrete to salt ingress. Nevertheless, it must be taken into account that concretes with active additions are far more sensible to the quality of curing than OPC concretes. Then, the objective of this research is to contribute to the knowledge of the durability of cement mortars with active additions exposed to two environmental conditions representative of Mediterranean and mild Atlantic climates. The microstructure of the cement mortars was assessed by mercury intrusion porosimetry, and by impedance spectroscopy. Their resistance to salt ingress was quantified in terms of parameters directly related to the relevant ingress and transport mechanisms. As a preliminary conclusion, cements with slag and fly ash, hardened under conditions of Atlantic and Mediterranean climates, can have good service properties in the long term.

1 INTRODUCTION

The use of mineral admixtures in the cement manufacture has many environmental benefits, like the reduction of CO_2 emissions and the use of an industrial waste. The particular cases of ground granulated blast-furnace slag and fly ash, and their effect on the properties of the cementitious materials is a topic of study. Many studies show that in laboratory conditions this kind of materials has good service properties, even better than Portland cement. Real structures are usually hardened in different environmental conditions depending on their geographical location. The different temperature and especially the different relative humidity present in the environment may influence the development of microstructure of concretes and mortars with slag and fly ash. This influence may cause different service properties of these materials, such as the diffusion coefficient of chlorides. In this work, mortars made with three different commercial cement types were tested. The development of their microstructure and their changes in durability-related properties were studied at different hardening ages, as a function of the hardening environment.

2 EXPERIMENTAL SETUP

In this research mortar samples were studied. They were prepared using an ordinary Portland cement (OPC), CEM I 42.5 R (CEM I from now on), a Portland cement with fly ash (content of fly ash from 21 to 35%), CEM II/B-V 42.5 R (CEM II from now on), and a ground granulated blast-furnace slag (GGBS) cement (content of GGBS between 66–80% of total binder), III/B 42.5 L/SR (CEM III from now on), according to the Spanish standard UNE EN 197-1. Mortar samples were exposed to three different conditions: environment A (100% RH and 20ºC, optimum laboratory condition), environment B (85% RH and 15ºC) and environment C (65% RH and 20ºC). Environment B represents the Atlantic climate, present in the north part of Iberian Peninsula (Spain and Portugal), while environment C is representative of Mediterranean climate, present in the east part of Iberian Peninsula. Tests were performed at several ages until 180 days.

The microstructure of the cement mortars was assessed by mercury intrusion porosimetry, and by impedance spectroscopy. The parameters obtained using the abovementioned techniques were the total porosity and the capacitance C_1 respectively. The resistance to salt ingress of cement mortars was characterized using a forced migration test according to Finnish standard NT Build 492. The result of this test was the non-steady-state chloride migration coefficient (D_{NTB}). Finally, their capillary suction coefficient (coefficient K) was determined according to Spanish standard UNE 83.982.

3 RESULTS AND DISCUSSION

For environment A, total porosity, coefficient K and coefficient D_{NTB} decreased and capacitance C_1 increased with time for CEM I, II and III samples. These results could mean that a higher RH accelerates the development of the hydration and pozzolanic reactions, especially the hydration of slag. With these reactions, new solids appear quicker, then total porosity and coefficients K and D_{NTB} decrease at early ages and capacitance C_1 rises. The decrease of total porosity of CEM II samples is delayed in comparison to CEM I and III samples. This could be related with the delaying of the development of pozzolanic reactions of fly ash respect to the hydration of clinker and slag.

For environment B, total porosity hardly changed with time or showed a small decrease for the majority of the samples studied. The capacitance C_1 kept practically constant or increased slowly with age for all types of mortars. On the other hand, the coefficients K and D_{NTB} decreased with time for all mortars studied. However, the decrease of both parameters was slower than observed for environment A. The slower development of microstructure and durability-related properties observed for environment B, could be related with the lower temperature of this condition (15ºC). In an environment with low temperature the hydration reactions of clinker and slag slow down and the formation of solids is also slower. If the clinker hydration is slower, the pozzolanic reactions of fly ash will start later. Then, more time would be needed to observe their effects in microstructure development.

For environment C, total porosity of the majority of CEM I samples kept practically constant until 28 days, decreased since then until 90 days, and increased at 180 days. The capacitance C_1 for CEM I mortars increased until 30 days approximately, since then until 120 days it kept constant, and it decreased at 180 days. Total porosity of CEM II specimens followed practically the same evolution with time as CEM I ones. The capacitance C_1 of these samples kept practically constant until 120 days, and it fell at 180 days. For CEM III samples, total porosity remained constant until 28 days, decreased between 28 and 90 days, and increased at 180 days. On the other hand, the capacitance C_1 showed the highest values of all types of cement studied since 50 days, and at later ages this capacitance decreased. Regarding the durability-related properties, the coefficient K decreased with age for CEM I and CEM III samples (mainly between 28 and 90 days), and kept practically constant for CEM II ones. On the other hand, for CEM I and II samples the coefficient D_{NTB} presented a similar decreasing tendency between 7 and 28 days of age. This tendency continued until 90 days only for CEM II mortars. For both kinds of cements, D_{NTB} increased between 90 and 180 days, but this rise was higher for CEM I mortars. This increase was not observed for CEM III samples hardened under environment C.

The results observed for environment C, may be interpreted as that the lower RH slows down the hydration reactions of clinker and slag, then the microstructure and durability-related properties development happens later (since 28 days hardening). The similar evolution of parameters studied for CEM I and II samples until 90 days of age, could mean that the degree of development of pozzolanic reactions of fly ash is very low at that hardening time. The worsening of properties at later ages observed for most of the samples, especially for CEM I ones, could be due to the formation of shrinkage microcracks as a consequence of lower RH in the environment.

4 CONCLUSIONS

- A low temperature in the environment slows down the development of hydration and pozzolanic reactions. Then, the development of microstructure is slower and more time is needed to reach similar durability properties than for an optimum laboratory condition.
- The improvement of the durability is delayed in environments with relative humidity lower than 100%, but after 180 days hardening these properties have reasonable good values for the majority of the cases studied.
- Relative humidity lower than 100% can produce shrinkage microcracking in mortars at greater hardening ages, as indicated by the increase of total porosity for most of the samples studied.
- In general, CEM III samples show the best properties of durability at 180 days of age.
- Cements with ground granulated blastfurnace slag and fly ash, hardened under environmental conditions of Atlantic and Mediterranean climates, can have good service properties in the long term.

ACKNOWLEDGEMENTS

This work has been financially supported by the Ministerio de Ciencia e Innovación of Spain through projects BIA2010-20548 and BIA2011-25721. J.M. Ortega is indebted to the Ministerio de Educación of Spain for a fellowship of the "Formación Personal Investigador (FPI)" programme (reference BES-2008-002650). Authors would like to thank Cementos Portland Valderribas, S.A., Lafarge España, S.A. & Holcim España, S.A. for providing the cements studied in this work.

Concrete Repair, Rehabilitation and Retrofitting III – Alexander et al. (eds)
 ISBN 978-0-415-89952-9

Capillary suction and chloride migration in fire exposed concrete with PP-fibre

J. Albrektsson & R. Jansson
Department of Fire Resistance, SP Technical Research Institute of Sweden, Borås, Sweden

ABSTRACT: Annually, several concrete structures, such as buildings, bridges, parking garages, tunnels, etc. are exposed to fires. Many fires are small, for example single car fires in tunnels. These fires do not affect the load carrying capability of the concrete structure and thus minor or no reparations are required. In modern concrete for civil engineer applications the use of polypropylene fibres (PP-fibre) to reduce fire spalling is growing. Some studies have been carried out which indicate that the use of PP-fibres will not affect the durability of the concrete. But in case of a fairly moderate fire exposure, a fire exposure that does not lead to structural damage, the PP-fibres can potentially lead to reduced durability. During low intensity fires or at long distances downstream a large fire in a tunnel the PP-fibres melts and form channels in the concrete. After such degradation of the PP-fibres it is plausible that accelerated damage may occur when moisture, de-icing salts and carbon dioxide can more easily penetrate the concrete.

In this experimental study the chloride migration and the capillary suction are studied in moderately heated concrete containing PP-fibres. The chloride migration tests were conducted with heated samples with and without PP-fibres. The capillary suction tests were even conducted with different fibre contents. As a reference the results are compared with results from unheated concrete.

The aim of the project is to define whether or not measures have to be taken to repair concrete structures after small fires and at long distances downstream from large fires in tunnels. If the durability is affected the costs and consequences of not repairing and refurbishing after the fire can potentially be very high especially after a fires in very long tunnel.

1 EXPERIMENTAL STUDY

An experimental study has been conducted in order to investigate the influence of PP-fibres on durability in concrete exposed to a moderate fire. Since most of the deterioration processes are governed by the water or liquid transport in the pore structure of the concrete, a capillary suction test will indicate the ability of the concrete to resist deterioration processes including water. In addition the chloride migration coefficient was determined for such concrete.

1.1 *Concrete mixes*

A typical Swedish tunnel concrete was used in this study. Test samples were prepared with 1.0 and 1.5 kg/m^3 of PP-fibres with the diameter 18 µm, 1.0 kg/m^3 of 32 µm PP-fibres and samples without PP-fibres which was uses as reference.

1.2 *Sampling*

Cores with diameter 100 mm were drilled from the slabs approximately two days after moulding. The cores were then stored in plastic bags for six years. Before the tests the cores were cut in pieces, perpendicular to the axis of the core.

1.3 *Capillary suction test*

The tests were conducted following the procedure prescribed in EN ISO 15148:2003. All the test samples were dried in a heating chamber before the tests. The temperature in the furnace was then increased with 1°C/minute, to avoid high thermal gradients in the samples, up to 250°C and then kept at this temperature for 24 hours.

The capillary suction tests lasted 24 hours. There was significant difference between the heated samples and the unheated samples in weight change rate. Water appears on the upper surface of most of the heated test samples before 2 hours, whereas it took almost 24 hours until all of the unheated samples displayed wetted areas on the top surface. The water absorption coefficients, A_w, are shown in Figure 1.

Chloride migration test Studying the water absorption coefficient of the mixes containing PP-fibres it is can be seen that the water absorption coefficient is increasing with the number of added

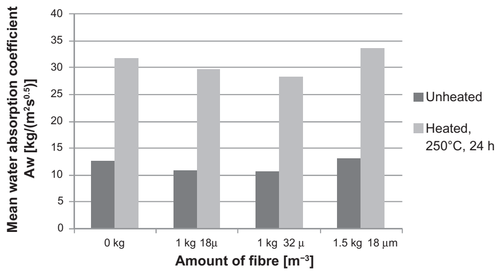

Figure 1. Calculated mean water absorption coefficient, A_w.

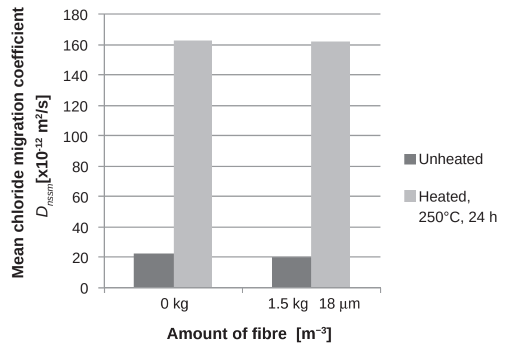

Figure 2. Mean calculated chloride migration coefficient for unheated and heated test samples without and with 1.5 kg/m³ of 18 µm PP-fibres.

PP-fibres, i.e. 1 kg/m³ of 32 µm fibres gives the lowest coefficient and 1.5 kg/m³ of 18 µm fibres gives the highest coefficient for both the unheated and heated samples. However the mix without addition of PP-fibres gives a coefficient in the same level for both the unheated and heated samples.

The tests were conducted following the procedure prescribed in NT BUILD 492:1999. Half of the test samples were heated in a furnace as the samples intended for the water absorption tests. The test durations of the unheated test samples were in accordance with the test method, i.e. 24 hours for such a concrete. Since, the capillary suction tests showed a significant increase of water absorption the test duration for the heated test samples was reduced to about 4 hours. A more distinct chloride front was observed in the unheated samples. The non-steady state migration coefficient was then calculated, the results are shown in Figure 2.

2 CONCLUSIONS

Studies on the microstructure and the transport properties in pre-heated concrete can be found in the literature. It is shown that the porosity increases with temperature and consequently the resistance to gas and liquid transportation decreases with temperature. The porosity increase can mainly be attributed to an increase in fine pores. The evolution of micro cracks after 300°C increases the gas and liquid transportation further. PP-fibres are widely used to reduce the risk of severe fire spalling. Addition of PP-fibres will not influence the cement hydration but the need of a higher amount of superplasticiser, to improve the workability of the mix, gives a higher degree of dispersion of the mix. A high degree of dispersion gives an improved cement hydration but probably also an improved pore structure. A study on the influence of PP-fibres on durability shows that addition of these fibres has no negative effect on durability. At 170°C the fibres melt and leave empty fibre beds but nevertheless the total pore volume is only slightly increased. However, the gas permeability and the water absorption are significantly increased after the fibres have melted. This shows that the connectivity of the pores increases if the fibres melt. This can occur even at small fires or downstream a large fire in a tunnel. The evolution of cracks is also dependent on the load conditions. Experiments show that the crack development is increased parallel to the load direction and decreased perpendicular to this direction. After heating the cement paste may rehydrate in the presence of moisture and the porosity will then consequently decrease.

In this experimental study a significantly increase in water absorption coefficient and non-steady state chloride migration coefficient was obtained for the heated test samples with and without PP-fibres. The influence of the PP-fibres was small compared to the influence of heating. However, the relative change in water absorption coefficient and non-steady state chloride migration coefficient is slightly higher for the samples containing PP-fibres.

3 DISCUSSION

Heating of concretes increases its transports properties and consequently decreases the durability. The addition of PP-fibres influences the transport properties of heated concrete and may decrease the durability further. This limited study indicates that the influence of the PP-fibres is small compared to the influence of heating. However, the influences of these fibres have to be studied further to avoid durability problems. It is also important to study if any recovery from the increased connectivity caused by the fibres at low temperatures will occur and if so, the time needed for recovery.

Concrete Repair, Rehabilitation and Retrofitting III – Alexander et al. (eds)
© 2012 Taylor & Francis Group, London, ISBN 978-0-415-89952-9

Effect of chlorides on moisture content and sorption isotherms

M. Leivo, H. Kuosa, E. Holt & E. Vesikari
VTT—Technical Research Centre of Finland, Espoo, Finland

R.M. Ferreira
C-TAC, University of Minho, Guimarães, Portugal

ABSTRACT: Moisture in concrete is an influential factor in the transport mechanism of aggressive species and therefore directly related to concrete durability. The presence of salts in the pore structure of concrete is known to have a negative influence due to their hygroscopic nature. Despite the well-known thermodynamic behaviour of pure salts, it is not sufficient to explain the effects salts have on certain properties of concrete. In this research the effect salt (NaCl) has on the moisture content and sorption isotherm of concrete was studied.

Six different concrete mixes with varying binder and air content were used for this purpose. To introduce chlorides into the concrete pore structure, specimens ($10 \times 100 \times 100$ mm^3 and $25 \times 100 \times 100$ mm^3) were subject to 16 immersion-drying cycles (5 days immersed/2days drying). Three different mediums were used: water, 3% NaCl solution and 10% NaCl solution. This was followed by determining the sorption isotherms of the concrete specimens by finding the moisture equilibrium at 95%, 65% and 50% relative humidity at 20°C.

Results include, among other tests, the porosity, moisture content, chloride content and the mentioned sorption/desorption isotherms. Moisture uptake and the degree of saturation were also measured.

Experimental results showed that the presence of salt strongly influences the sorption and moisture characteristics of concrete. At each level of relative humidity studied, an increase in the moisture content was observed—in some cases up to 30% higher. As the moisture content of concrete had an influence, this parameter should be considered when evaluating other deterioration attacks such as frost-salt resistance and reinforcement corrosion.

1 INTRODUCTION

The durability of concrete is directly related to the presence of moisture as it is an influential factor in the transport mechanism of aggressive species. The amount of water present in porous materials (moisture content) is a function of several parameters. They can be divided into intrinsic material properties (pore volume, size distribution, geometry and connectivity) and parameters related to external conditions (orientation, capillary rise from ground water, rainfall, wind-driven water, etc.). In addition, the interaction of concrete with air humidity is inevitable.

Salts are often readily water soluble and transported in concrete by water. The presence of salts in the pore structure of concrete is known to have a negative influence due to their hygroscopic nature. Due to fractionation and accumulation in cyclic processes, high salt contents are generated in concrete and may distribute in different positions. Despite the well-known thermodynamic behaviour of pure salts, it is not sufficient to explain the effects salts have on certain properties of concrete.

2 TEST SETUP AND MATERIALS

The aim of this research was to study the influence that varying salt content has on the moisture conditions in concrete. Six different concrete mixes with vary binder and air content were used for this purposed. The water sorption experiments were augmented by other water- and pore-related analyses. The study comprised the determination of the following parameters: moisture contents and isotherms, degree of saturation, final moisture uptake, and chloride contents.

Matured (ca. 80 days curing) concrete specimens of $10 \times 100 \times 100$ mm^3 where subjected to 16 cycles of wetting/drying. Each cycle consisted of 5 days submerged and 2 days drying at 50% relative humidity and 20°C. Three different solutions where used: tap water; 3% NaCl and 10% NaCl (by weight). Additional specimens ($25 \times 100 \times 100$ mm^3) were also used and periodically split to ascertain the depth of the penetration of chlorides. After the cyclic submersion all the 10 mm thick specimens were considered to have been comprehensively penetrated by the chlorides.

To determine the equilibrium desorption isotherm the concrete moisture content was measured manually for all specimens kept at 95%, 65% and 50% relative humidity, and at 20°C until constant weight. All the specimens were then immersed in separate containers (according to the type of solution) for 24 hours. The specimens were weighed after 2, 4, 6 and 24 hours (surface dry specimens). After immersion, the specimens were saturated with an over pressure of 15 MPa to reach full saturation thus assuming all the air pores were also filled with water. Weighing was immediately after the pressure was released. After an additional 2 hours in water at normal atmospheric pressure, all specimens were weighed in water and in air so as to determine the volume of each specimen. This was followed by drying until a constant weight at 105°C to obtain the dry weight. The chloride contents of the concretes and the waters used for the immersion saturation were determined. The amount of chlorides dissolved into the water was measured to assess the effect of the lowering of the chloride content in the concrete in comparison to the concentration prior to water immersion.

The concretes were produced with common Finnish cements, with blast furnace slag and with fly ash additions. Granitic aggregates were used with a maximum aggregate size of 16 mm. A superplasticizer was always used, in addition to an air entraining agent.

The mixes, representing prevailing common industrial mixes in Finland, were produced with an effective water/binder (w/b) ratio of approx. 0.50. This effective w/b ratio excludes the water absorbed by the aggregate, and is calculated by the amount of cement multiplied by 1.0, BFS by 0.8, and FA by 0.4. The main mix design information, i.e. binders and additions, aggregates, w/b ratio and fresh concrete air content (measured value), is presented in the full paper. Standardized cubes ($150 \times 150 \times 150$ mm^3) were cast. The specimens were handled and cured following standardized procedures until the time of testing procedures.

3 RESULTS

The average moisture contents with time, regarding all the concrete mixes, are presented in Figure 1. Time $t = 0$ *days* corresponds to when the specimens were moved to RH 95% after the immersion-drying cycles (112 d). The specimens were moved to RH 65% when $t = 151$ *days* and to RH 50% when $t = 355$ *days*. The specimens reached equilibrium at RH 50% when $t = 559$ *days*.

Chlorides did have an effect on the concrete desorption isotherm (RH-moisture content).

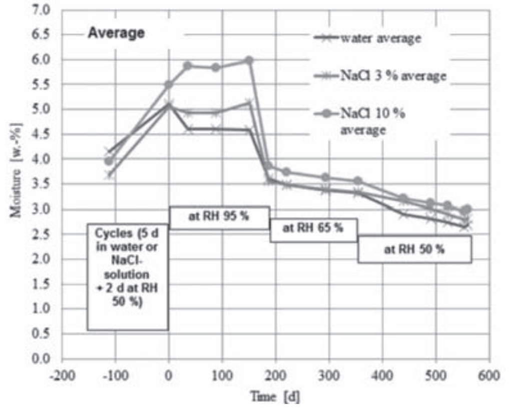

Figure 1. Variation of average moisture contents of all concrete mixes with time.

At RH 95% the average moisture content of the 6 concretes was increased by 12–31% when chlorides were introduced in the concrete before determining the stabilized moisture content.

At RH 65% and at RH 50% the effect of chlorides on the concrete moisture content was not as large as at RH 95%. The average stabilized moisture content at RH 65% was 1–7% higher, and at RH 50% it was 6–12% higher, than without additional chlorides.

4 CONCLUSIONS

The research presented in this paper was based on a limited number of variables and the testing was only performed at three different levels of relative humidity. However, based on the test results obtained, the following conclusions are considered:

- The presence of chlorides in the concrete pore structure strongly influences the sorption and moisture characteristics of concrete. At each level of relative humidity studied, an increase in the moisture content was observed—in some cases up to 30% higher.
- Due to the deliquescence characteristic of salts, the water content in concrete at a given atmospheric relative humidity can be higher than initially expected. As a result, concrete contaminated with salts can perform differently than expected.
- As the moisture content of concrete had an influence, this parameter should be considered when evaluating other deterioration attacks such as frost-salt resistance and reinforcement corrosion.

Concrete Repair, Rehabilitation and Retrofitting III – Alexander et al. (eds)
© 2012 Taylor & Francis Group, London, ISBN 978-0-415-89952-9

Accelerated evaluation of corrosion inhibition by means of the integral corrosion test

C. Andrade & N. Rebolledo
Center for Safety and Durability of Structures and Materials (CISDEM-CSIC-UPM), Madrid, Spain

ABSTRACT: Corrosion inhibitors, either added in the concrete mix or applied in corroding structures, are used to avoid or decrease reinforcement corrosion. Their efficiency is usually noticed by measuring the corrosion rate in several exposure conditions to detect the possible decrease of the corrosion rate or a repassivation. In present paper is presented the use of the named "integral corrosion test" to evaluate the inhibitor efficiency. This test consists in a migration test in which the cubic specimen has a bar embedded in its centre which starts to corrode when the chloride front arrives to it. It is called "integral" because it enables the consecutive detection of the diffusion coefficient, the chloride threshold and the corrosion rate. The diffusion coefficient is measured from the time taken until the steel bar starts to corrode, the chloride threshold by analysing a small sample of the steel/concrete interface just after depassivation and the corrosion rate, by measuring it in a twin specimen after the disconnection of the external voltage. The results indicate that the presence of inhibitors delay the depassivation time and decrease the corrosion rate developed while the chloride threshold appears to be higher. Then the test seems a good accelerated mode of studying inhibitor efficiency and can be also used to classify concrete resistance to chlorides.

1 INTRODUCTION

The use of inhibitors is among the different preventive measures to delay the corrosion initiation (Page et al. 2000). The efficiency of the inhibitors and their long term performance is still a subject of discussion as the data are scarce (Berke et al. 1993) and not always conclusive. One reason of the discrepancies is due to the testing method. In present paper a new method to evaluate in an accelerated manner the inhibition efficiency.

It is based in the principles of migration by accelerating the chloride penetration applying an external electrical field and measuring the time to depassivation. This method has been called "integral" corrosion test because it informs not only on the initiation but also on chloride threshold (Castellote et al. 2001) and on the reduction of the corrosion rate after depassivation, and is covered by the Spanish Standard UNE 83992-2 (Spanish Standard UNE 83992-2) "*Durability of concrete. Tests of accelerated penetration of chlorides. Integral accelerated method*". In present paper is illustrated its use to evaluate the corrosion inhibition by using the concept of "fictitious" diffusion coefficient as the chloride lasts longer to induce depassivation due to the presence of the inhibitor.

2 METHODOLOGY

The cement can be of any class depending of the particular application of the results although in present case an Ordinary Portland Cement was used.

Two types of concrete were fabricated with a characteristic strength of 50 MPa. For the exercise sodium known corrosion inhibitor was added to the mix in proportions, as indicated by the inhibitor manufacturer, of 0, 1.5, 2 y 2.5% of NO_2^- by cement weight.

The specimens are cubes of concrete and of prismatic shape and the recommended size is of 10 mm or 15 mm although also of 7 mm are appropriate. The arrangement is shown in figure 1. The samples have embedded a corrugated bar of 8 or 10 mm in diameter at a distance reproducing the cover depth (around 3 cm in figure 1). A pond was glued to the surface of one of the faces of the specimen as shown in figure 1. A 1.2 M $NaCl+CuCl_2$ solution was used to fill the pond.

A potential drop of 12 to 30 V is applied by means of a potential source through electrodes placed inside the pond (the cathode) and at the opposite face through a sponge (the anode). In order to detect the onset of corrosion, periodically the corrosion potential of the bar by means of a volmeter is measured by first switching off the potential drop during 30 to 180 minutes.

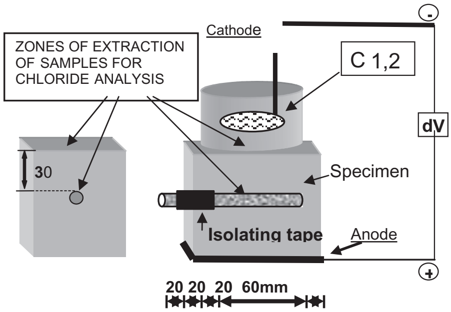

Figure 1. Accelerated chloride migration test setup.

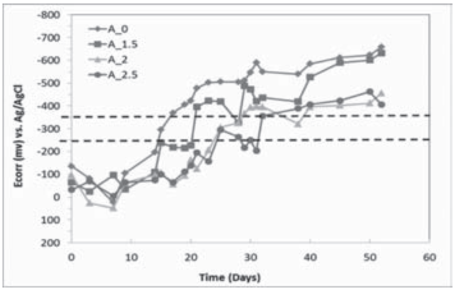

Figure 2. E_{corr} during time for concrete HAC-50.

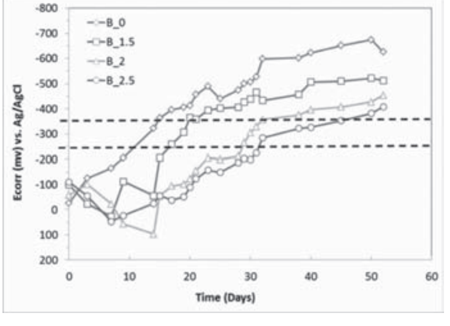

Figure 3. E_{corr} during time for concrete HA-50/F50.

The depassivation can be also detected by measuring the Polarization Resistance through a potentiostat. After depassivation is noticed, the specimen is broken in order to find out the chloride threshold. For it a sample near the bar over the corroded zone is extracted. In order to measure the corrosion rate after depassivation, other specimen is left to corrode naturally by switching off the potential applied during around 15 to 30 days. The non stationary Diffusion Coefficient is calculated by means of the following expressions (Castellote, 2001): $D_{ns} = e^2/ 2 \cdot t_{lag} \cdot \varphi$ [cm²/s]. The accumulated corrosion

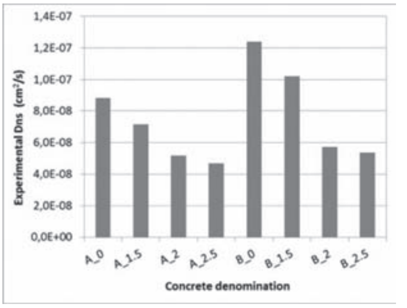

Figure 4. Apparent diffusion coefficients.

P_{corr} is calculated from the Corrosion rate I_{corr} through: P_{corr} (mm) = $0.0116 \times I_{corr}$ (µA/cm²) $\times$ t (years).

3 RESULTS AND DISCUSSION

Figures 2 and 3 show as example the results of Corrosion potential along the experiment. Either the E_{corr} or the I_{corr} indicate fairly well the depassivation onset. Its delay is proportional to the amount of Nitrites added. Figure 4 shows the calculated apparent diffusion coefficients.

The critical chloride content, Cl_{th} measured is also increasing with the amount of nitrites. Regarding the inhibitor efficiency, it can be quantified through the calculation of the percentage of inhibition. The values taken for this calculation are those given in figure 7. The results are shown in figure 9 which enables to deduce that the percentages of 2 and 2.5% give similar efficiencies.

4 CONCLUSIONS

The integral corrosion test standardized in Spain seems suitable not only for the calculation of service life parameters in the case of different concretes, but also it serves for the comparison of the inhibitor efficiency. In the cases tested no deleterious influence of the electrical field applied has been noticed.

REFERENCES

Berke, N.S., Hicks, M.C. & Tourney, P.G. 1993. Evaluation of concrete corrosion inhibitors. In: Proceedings of the 12th international corrosion congress (ICC). Houston, Texas, USA: 74–8.

Castellote, M., Andrade, C. & Alonso, C. 2001. *Cement and Concrete Research*, 31: 1411–1420.

Page, C.L., Ngala, V.T. & Page, M.M. 2000. Corrosion inhibitors in concrete repair systems. *Mag Concr Res*, 52(1): 25–37.

Concrete Repair, Rehabilitation and Retrofitting III – Alexander et al. (eds)
 ISBN 978-0-415-89952-9

Ageing process of cementitious materials: Ion transport and diffusion coefficient

A. Babaahmadi & L. Tang
Chalmers University of Technology, Gothenburg, Sweden

Z. Abbas
University of Gothenburg, Gothenburg, Sweden

ABSTRACT: Risk assessment analysis concerning service life predictions of concrete structures in nuclear waste repositories requires broad knowledge about long-term concrete deterioration processes. It is well known that the degradation process of cementitious materials involves diffusion of internal and external ions, interaction between these ions and re-deposition of the interacted products. However, although diffusion properties play an important role in the deterioration process, there is a lack of reliable data on ion diffusivity in concrete, especially co-existing ions rather than chloride. The aim of this study is to further analyze multi-component ionic diffusion accompanied with surface complexation and selective adsorption. Natural diffusion cell and field immersion tests are used to analyze transport properties of ions present in groundwater surrounding nuclear waste repositories such as chloride, sodium, lithium and calcium ions, through cement paste. Analytical techniques such as Ion chromatography, potentiometric titration, inductively coupled plasma mass spectrometry and X-Ray fluorescence methods are used. Results indicate that the ionic diffusion coefficients differ between different ions and the higher the concentration of the ions, the lower the diffusion coefficient will be.

1 INTRODUCTION

Ionic transport in cementitious materials is one of the key factors governing the deterioration process of concrete structures. However, reliable data regarding ion diffusivity through cementitious materials is scare and information regarding coexisting ions, and differences between their diffusion coefficients and ion-ion interactions, is even rarely available.

In this paper natural diffusion cell tests using sodium chloride, lithium chloride and lithium nitrate solutions are carried out in order to study the effects of ion-ion interactions on individual diffusion coefficients. Furthermore, the dependency of diffusion coefficient on ionic concentration is studied.

2 MATERIAL AND METHOD

Preparing test specimens, Swedish structural Portland cement (CEM I 42.5N BV/SR/LA) was mixed with Milli-Q water at a water-cement ratio of 0.5. Fresh cement paste was cast in acrylic cylinders of an internal diameter of 50 mm.

Conventionally diffusivity of ions in a porous material is measured using a natural diffusion cell test at a certain gradient of concentration (Page 1983). In this study, 18 sets of diffusion cells were used, with three sets per each solution. In order to study transport properties of chloride, sodium, lithium and calcium, 6 different solutions containing these ions were used:

- 5 g, 10 g and 20 g NaCl per liter
- 10 and 20 g LiCl per liter
- 10 g $LiNO_3$ per liter

Monitoring the concentration changes in the downstream cell and using Flick's first law, the steady state diffusion coefficient is calculated (Crank 1975). Using the Q_{Cl}–t curve the "time-lag", which is the duration until a significant linear relationship is observed from the Q_{Cl}–t curve, would be specified. And the non-steady state diffusion coefficient can be calculated (Crank 1975). The natural immersion test involves immersion of the test specimen in a solution containing specific ions of interest and measuring the penetration depth or penetration profile of these ions in the specimen.

The natural immersion test is carried out using a total of 20 cylinders (10 pastes and 10 mortars) of Ø46 × 100 – 250 mm, cured for 6 months and coated with thick (3 – 4 mm) epoxy, sealing all surfaces except one for exposure. The specimens were immersed in ground water 400 meters deep

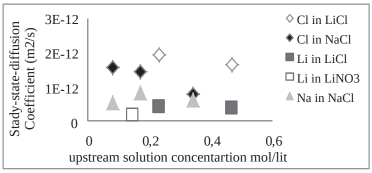

Figure 1. Calculated steady-state diffusion coefficients.

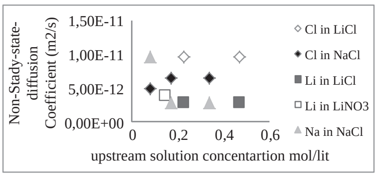

Figure 2. Calculated non-steady-state diffusion coefficients.

under the ground in the Äspö laboratory located in Oskarshamn, Sweden. Assuming that Flick's second law of diffusion is valid the non-steady-state diffusion coefficient is calculated by fitting the experimental profiles to an error-function of Fick's second law of diffusion for a semi-infinite media. (Crank 1975).

3 RESULT AND DISCUSSION

The analysis shows that the higher the concentration of the ions in upstream cell, the higher the concentration gradient (slope of the curve) would be. The Steady-State diffusion coefficients of chloride, lithium and sodium ions are presented in figure 1. The results show that the diffusion coefficient values of cations and anions differ by an order of magnitude. Moreover, the diffusion coefficient values specifically regarding chlorides decreases due to increase in the ionic concentration of upstream cell, which is logical due to the friction effects between ions (Tang 1999). The differences between the cation diffusion coefficients of sodium and lithium can be explained due to their different hydrated ionic size. Lithium ions although smaller than sodium ions in crystalline radius, would carry up a larger water layer around them in solution (Abbas et al. 2009). Consequently larger hydrated ions such as lithium will have a slower movement than sodium ions. Using the definition of time-lag the non-steady state diffusion coefficients are calculated. The results are presented in figure 2.

The samples from the field immersion test were analyzed qualitatively using LA-ICP-MS. The results are presented in figure 3. Considering the constituents of Äspö groundwater, chloride and calcium ions as of having higher concentration in Äspö groundwater, have diffused more than other ions in

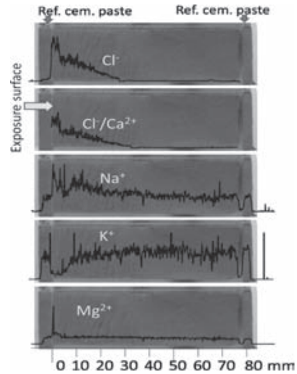

Figure 3. ICP-MS results from the analysis on the samples in field immersion test.

to the specimen. On the other hand, potassium ions have diffused out from the specimen in to the ground water. The amount of chloride and calcium in the sample is quantified using potentiometric titration and non-steady state diffusion coefficient of chloride is calculated by curve fitting to be 8.86E-12, m2/s.

4 CONCLUSIONS

Natural diffusion cell and field immersion tests are performed. The results concerning the ions of interest being Chloride, Sodium and lithium shows:

- Diffusion coefficient of sodium and lithium ions is lower than chloride ions by an order of magnitude.
- The diffusion coefficient value depends on the concentration of ions in the upstream cell.
- The diffusion coefficient value is dependent on the ionic size and the radius of water field around the ion. Because as much as more water field around the ions the harder it gets for them to diffuse and the diffusion coefficient would decrease.

REFERENCE

Abbas, Z., Nordholm, S. & Ahlberg, E. 2009. Monte Carlo simulations of salt solutions: Exploring the validity of primitive models. *J. Phys Chem B*. 113: 5905–5916.

Crank, J. 1975. The mathematics of diffusion. Oxford: Clarendon press.

Page, C.L. & Vennesland, Ø. 1983. Pore solution composition and chloride binding capacity of silica-fume cement pastes. *J. Materials and Structures*, 16, 19–25.

Tang, L. 1999. Concentration dependence of diffusion and migration of chloride ions—Parts 1 & II. *J. Cement and Concrete Research*. 29 (9): 1463–1474.

Concrete Repair, Rehabilitation and Retrofitting III – Alexander et al. (eds)
© 2012 Taylor & Francis Group, London, ISBN 978-0-415-89952-9

The interaction of deterioration caused by chloride ingress and carbonation in mortars exposed to cyclic wetting and drying

J. Backus & D. McPolin
Queen's University Belfast, David Keir Building, Belfast, Northern Ireland

B. Kuen
Vienna University of Technologie, Vienna, Austria

ABSTRACT: Carbonation and chloride ingress are the two main causes of corrosion in reinforced concrete structures. An investigation to monitor the ingress of chlorides and carbonation during a 24-week cyclic wetting and drying exposure regime to simulate conditions in which multiple mode transport mechanisms are active was conducted on a variety of binders.

Penetration was evaluated using water and acid soluble and free chloride profiles, and phenolphthalein indicator. X-ray diffraction was also used to determine the presence of bound chlorides and carbonation.

The effect of carbonation on binding capability was observed and the relative quantity of chlorides also showed a correlation with the amount of chlorides bound in the form of Friedel's salt. As carbonation was mainly observed to be a surface affect in this study it did not alter the overall ability of the materials to resist chloride penetration.

1 INTRODUCTION

Chloride ingress and carbonation together account for over 50% percent of the deterioration of concrete structures. For corrosion to occur, the passivating film that protects steel in concrete needs to be destroyed and both oxygen and sufficient humidity should be present at the steel. Chloride ingress is directly responsible for the destruction of the passivating film.

Similarly, carbonation reduces the pH of the concrete surrounding the steel, making the protective passive film unstable and exposing the steel. When the concrete surrounding the steel is wet, an electrolytic cell is completed and steel starts to corrode.

As modern concretes are free from internal chlorides, the corrosion due to chlorides is caused by those penetrating through the concrete cover from an exposure environment. Sufficient quantities of chloride ions are required to depassivate the reinforcement. This quantity is known as the threshold chloride content. Therefore, the distribution of chloride ions within reinforced concrete is of great importance.

Carbonation also requires carbon dioxide to penetrate from the external environment. Similar to the chloride ingress, there is a threshold pH at which the passive layer breaks down.

The effect of ground granulated blast-furnace slag (GGBS) and pulverised fuel ash (PFA) considered in this study, is to reduce permeability. The reason for this reduction is due mainly to the Pozzolanic reaction of calcium hydroxide (Mehta, 2006). Relevant to all the transport mechanisms, for transport to occur the pores must be continuous and the effectiveness of the transport through continuous pores will also be affected by the size of the pores.

2 EXPERIMENTAL PROCEDURE

2.1 *Specimen preparation*

Three mixes were used in this study, incorporating Portland cement (PC), pulverised fuel ash (PFA) and ground granulated blast-furnace slag (GGBS). A water-binder ratio of 0.42 was chosen for all mixes so as to produce reasonable workability in the range of 300–450 mm. The aggregate binder ratio was 1.67 for all mixes.

The specimens were manufactured according to BS 1881: 125 (1986) using a pan mixer. Specimens were cast within one week and removed from the moulds 24 hours after casting.

2.2 *Curing, preparation, and chloride exposure*

After demoulding, the specimens were stored in a water bath (20 ± 1°C) for three days. They were then removed from the water bath and transferred to a constant temperature room at 20 ± 1°C, 55 ± 1% relative humidity for continued hydration until they were 28 days old. Cores were then cut from the slabs, coated in epoxy emulsion (Sikaguard 680) and a 60 mm pipe placed over them to facilitate ponding.

The cores were ponded with a 0.55M (3.2%) NaCl solution for 1 day and the following day the saline solution was removed and the surface exposed to air for 6 days at 20 ± 1°C, 55 ± 1% RH. This cyclic regime was chosen to simulate real exposure conditions in the splash zone which Bamforth (1997) identified as the most extreme zone with regard to the accumulation of surface chlorides whilst potentially allowing carbonation to occur. This cycle was repeated every week for twenty four weeks.

2.3 *Acid and water soluble and free chlorides*

The acid and water soluble chloride contents of the various mixes was determined by profile grinding at discrete depths of 0–1 mm, 1–2 mm, 2–3 mm, 3–4 mm, 4–5 mm, 5–10 mm, 10–15 mm and 15–20 mm and then digesting in nitric acid and water respectively, according to the method described in BS EN 14629 (2007) and the technique described by Haque, et al. (1995). The pore fluid expressed from twenty one cores, sliced into 3 mm thick discs was used to determine the free chloride concentration.

As would be expected with an external chloride source, all the profiles generally show a high concentration of chlorides near the surface which decreases with depth as the mortars resist the penetration of the chloride ions. The acid soluble profiles for all mortars have a lower chloride concentration in the surface layer and a peak is observed at about 3 mm.

In the water soluble chloride profiles the PFA and GGBS have a less distinct peak. The large difference between acid and water soluble profiles could be explained by chloride binding as both GGBS and PFA would be expected to increase binding while the peaks in the water soluble profiles may be caused by a diffusion gradient from released chloride brought about by the lower pH of the GGBS and PFA mixes.

At the surface layer of the GGBS mix, the water and acid soluble values are the same, suggesting that carbonation occurring during the drying cycles had released all the bound chlorides.

2.4 *Phenolphthalein indicator and pH profile*

A cylinder from each mix was split and sprayed with phenolphthalein indicator and readings taken in accordance BS EN 14630 (2006). While the pH profiles were obtained from the dust samples prepared for water soluble chloride analysis and measured using a Gelplas reference combination pH electrode.

The results from the phenolphthalein indicator would suggest that very little carbonation had occurred in the samples, with only GGBS showing any indication of carbonation occurring.

However, the pH profile identified that the pH for all mixes dropped in the initial layers of the concrete. GGBS has had the most carbonation as indicated by the phenolphthalein, followed by PFA and then PC.

2.5 *X-ray diffraction analysis of dust*

Once again the dust extracted from discrete layers for analysis. The XRD micrographs were analysed to determine the presence of Friedel's salt and calcium carbonate. The presence of calcium carbonate was used to indicate that the cyclic regime resulted in carbonation occurring even although not at sufficient quantity to show up on the phenolphthalein test.

XRD analyses were only carried out in the first 5 mm of the sample, where it can clearly be seen it is present, declining rapidly over the first 3 mm and not present in the last 2 mm. GGBS has the most calcium carbonate present, followed closely by PC mix with PFA having the least as would be expected given the smaller quantity of calcium oxide in its composition.

The quantity of Friedel's salt for each sample, as determined from the peak count in the micrographs revealed that the specimens with the greatest to least quantities of Friedel's salt were PFA, GGBS and PC. These results were not unexpected as from literature it is known that Friedel's salt is formed by chloride ions combining with calcium aluminate hydrate present in the mortar. PFA contains a high quantity of alumina (Al_2O_3) and therefore would be expected to increase the binding. The GGBS mix showed a decrease in binding. This would be expected as Friedel's salts decompose in lower pH environments.

3 SUMMARY AND CONCLUSIONS

The effect of carbonation on binding was significant and it is recommended that it should be measured in conjunction with chloride concentration when using materials with chloride binding capability.

The acid soluble chloride profiles which were obtained had a similar trend to the water soluble and free chloride profiles. Although quantification of the water soluble/free chlorides may be a more accurate way of assessing corrosion risk than acid soluble chlorides, it is a higher risk method as additional bound chlorides are also present in the mortar, which are not accounted for. Should conditions arise which causes liberation of these additional bound chlorides, such as carbonation, there is potential for a massive sudden increase in free chloride concentration within the material.

Through the cyclic exposure in this study both carbonation and chloride ingress occurred and although carbonation did occur, its effect was near surface—resulting in a high surface chloride concentration but it did not significantly alter the overall performance of the materials.

A strong relationship was observed between Friedel's salt and the difference between free/water soluble and acid soluble chloride concentration.

Concrete Repair, Rehabilitation and Retrofitting III – Alexander et al. (eds)
© 2012 Taylor & Francis Group, London, ISBN 978-0-415-89952-9

Influence of carbonation on the chloride concentration in the pore solution of concrete

X. Wan & T. Zhao
Qingdao Technological University, Qingdao, China

F.H. Wittmann
Aedificat Institute Freiburg, Freiburg, Germany

ABSTRACT: Chloride content and pH value of the pore solution in the neighborhood of steel reinforcement are decisive parameters for initiation and rate of corrosion. The pore solution of cement mortar and hardened cement paste has been expressed from the pore space by high pressure. The influence of water-cement ratio, age, and the addition of chloride to the fresh mix on chloride content of the pore solution has been determined by ion chromatography. At the same time the pH value of the pore solution has been determined. It was found that the content of free chloride decreases with increasing water-cement ratio and it increases with the amount of chloride added to the fresh mix. The amount of chemically bound chloride increases with time, but it decreases with decreasing content of dissolved chloride in the pore solution. A significant influence of carbonation on the chloride content of the pore solution has been observed. After complete carbonation of cement mortar and of hardened cement paste with different water-cement ratios (W/C = 0.5 and 0.7) and with different amounts of chloride added to the fresh mix (0%, 0.5% and 1%) the dissolved chloride content increases by a factor between 2 and 12. In parallel the chemically bound chloride decreases significantly due to carbonation. As has been expected the pH value decreases from values around 13.2 to values as low as 8.0. It can be concluded that carbonation not only lowers the pH value but at the same time it liberates chemically bound chloride. This is one obvious reason why combined action of chloride penetration and carbonation accelerates steel corrosion and shortens service life of reinforced concrete structures.

1 INTRODUCTION

Chloride concentration and pH value of the pore solution adjacent to the steel reinforcement are decisive parameters for initiation and rate of corrosion. During cement hydration in presence of chloride Friedel's salt and Kuzel's salt, can be formed in concrete. In addition some chloride can be chemically bound by other hydration products of cement by substitution. Finally part of the chloride will be adsorbed firmly on the huge internal surface area of different hydration products. Theissing et al. (1978) studied the binding of chloride in different hardened cement pastes in presence of NaCl and $CaCl_2$. Their results showed that there is a chemical equilibrium between the chloride concentration in the hydration products and the chloride concentration in the pore solution. In the project described in this paper, the chloride concentration in the pore solution of cement mortar and hardened cement paste has been determined. The pore solution has been expressed under high pressure. The water-cement ratio and the curing age were varied. Some samples were made with chloride added to the fresh mix. Finally the influence of carbonation on the free chloride content was investigated.

2 EXPERIMENTAL

One mortar mix (M) and two hardened cement paste mixes with water cement ratio 0.5 (HCP1) and water cement ratio 0.7 (HCP2) were prepared for these investigations. To some specimens 0.5% or 1% of reagent grade sodium chloride related to the mass of cement has been added. Two types of cylinders with a diameter of ∅ = 50 mm were cast and stored in a humid room until the pore solution was expressed.

One type has a height of 50 mm. The pore solution of these cylinders was expressed after 3 and 7 days. The second type had a height of 10 mm. These thinner discs were exposed to accelerated carbonation before the pore solution was expressed in a device as shown in Fig.1 (Barneyback, R.S. & Diamond, S. (1981)). From each specimen, 4 to 6 ml

Table 1. Total chloride content as determined from the initial chloride content and the chloride added to the fresh mix, amount of dissolved chloride, and amount of chemically bound chloride, mg/V_c.

Mix type	Total chloride content	Amount of dissolved chloride			Amount of chemically bound chloride		
		3d	7d	7d-C	3d	7d	7d-C
M-0	138	6	4	40	132	134	97
M-0.5	372	105	34	216	267	338	156
M-1	607	293	141	375	314	466	232
HCP1–0	216	15	9	31	201	207	185
HCP1–0.5	586	152	45	159	434	541	428
HCP1–1	956	297	175	427	660	781	529
HCP2–0	191	11	8	32	180	182	159
HCP2–0.5	517	117	43	206	400	474	310
HCP2–1	843	313	135	478	530	828	483

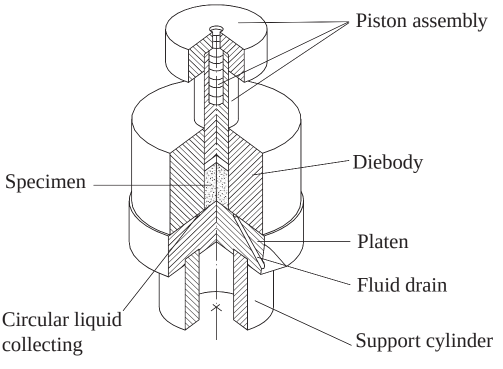

Figure 1. Device for expressing the pore solution.

pore solution could be obtained for chemical analysis. The dissolved chloride ions in the pore solution were determined by ion chromatography (Dionex, ICS-1500). The pH value of the pore solution was measured with a calibrated digital pH meter.

3 RESULTS

The total chloride content and the dissolved chloride content in the pore solution of mortar (M) and hardened cement paste with two different water cement ratios W/C = 0.5 (HCP1) and W/C = 0.7 (HCP2) are shown in Table. 1. The amount of NaCl added to the fresh mix is indicated with 0%, 0.5% and 1% in Table 1 after the corresponding mix designation. From Table 1, we learn that the concentration of the dissolved chloride decreases with ongoing hydration. This can be explained by the fact that more and more chloride is chemically bound as hydration goes on. Part of it will be found in Friedel's salt and in Kuzel's salt while another part will substitute other ions in conventional hydration products and a third part will be adsorbed on the huge internal surface area of hydration products. After carbonation a huge amount of chloride is freed from hydration products and the concentration in the pore solution increases enormously. In this way steel corrosion may be initiated. This is a typical example of synergetic effects of combined actions. Chloride migration and carbonation together aggravate the risk of corrosion in reinforced concrete structures. The amount of chemically bound chloride increases of course with ongoing hydration.

Independent of the age the pH value of the hardened cement paste is slightly higher than 13, as expected. After carbonation values around 8 have been measured.

4 CONCLUSIONS

The analysis of the expressed pore solution gives us new and interesting insight into the chloride distribution in concrete.

The distribution of chloride in concrete depends on the total chloride content. Both the chemically bound chloride content and the concentration of the dissolved chloride increase with increasing total chloride content following a chemical equilibrium.

A considerable amount of chemically bound chloride is freed into the pore solution by carbonation. Under given circumstances this combined action can reduce service life of reinforced concrete structures considerably due to initiation of steel corrosion.

REFERENCES

Barneyback, R.S. & Diamond, S. 1981. Expression and Analysis of Pore Fluids from Hardened Cement Paste and Mortars. *Cem. Concr. Res.* 11: 279–285.

Theissing, E.M., Hest-Wardenier, E.M. & de Wind, G. 1978. The combining of sodium chloride and calcium chloride by a number of different hardened cement pastes. *Cem. Concr. Res.* 8: 683–692.

Concrete Repair, Rehabilitation and Retrofitting III – Alexander et al. (eds)

Modified Wedge Splitting Test (MWST)—a simple tool for durability investigations of reinforcement corrosion in cracked concrete

B. Šavija, E. Schlangen & J. Pacheco
Delft University of Technology, Delft, The Netherlands

R.B. Polder
Delft University of Technology, Delft, The Netherlands
TNO Technical Sciences/Building Materials, Delft, The Netherlands

ABSTRACT: Reliable methods for controlled cracking of reinforced specimens in laboratory conditions are needed in order to experimentally study chloride ingress and reinforcement corrosion in cracks. In the paper, the Modified Wedge Splitting Test (MWST) for specimen cracking is presented. The setup is thoroughly explained, and the implications of proposed modifications are discussed. Load-Crack Opening Displacement (COD) curves are presented, and means of reducing crack closing after unloading are proposed. Cracking patterns are studied visually and destructively and compared to the regular wedge splitting test, commonly used in fracture mechanics testing. Significance of proposed modifications of the setup is discussed in the view of the available literature, especially with respect to their influence on reinforcing steel corrosion. The prospects of the proposed method are critically compared to other procedures for controlled cracking proposed in the literature.

1 INTRODUCTION

Cracks are inevitable in reinforced concrete structures. In order to study corrosion initiation and propagation in cracked concrete, reliable methods for cracking of specimens in the laboratory are needed. This paper proposes one such method.

The wedge-splitting method has long been used in fracture mechanics of concrete. Since the setup is simple and effective, it has been also adopted in some durability studies.

Reinforced concrete has somewhat different cracking behavior than plain concrete. As tension is applied in the reinforcing steel, microcracks form in the steel/concrete interface. Also, debonding of the steel/concrete interface occurs, possibly creating a fast pathway for fluid penetration. The modification of the wedge-splitting test is proposed in order to study the aforementioned phenomena.

2 METHOD

2.1 *Materials and mix design*

Cement used in this research was ordinary Portland cement CEM I 52.5 R. Water to cement ratio of the mix used was 0.45. Mix properties are given in Table 1.

2.2 *Specimen preparation and cracking procedure*

For the specimen preparation, cubic moulds of $150 \times 150 \times 150$ mm^3 are used. Inside the mould, two reinforcing bars of about 120 mm in length are placed. Prior to casting the specimens, a steel profile with a cross section of 40×40 mm^2 is mounted on the mould, in order to create a recess in the sample. This steel profile is removed after around 5 hours. After the curing period, a notch (5 mm thick) is sawn in the specimen using a water cooled saw.

Wedge-splitting specimens were taken out of the climate chamber after 28 days and thereafter stored at room temperature until testing. At the age of 36 days, cracking procedure was performed. In order to control the obtained crack width, LVDTs are placed on both sides of the specimen at the bottom of the notch, where the crack is expected to initiate. Their average is used as a feed-back signal for the machine, and controls the whole loading process. When the

Table 1. Concrete mix composition.

Constituents	Amount
Portland cement	22 kg
Water	10 kg
Fine aggregate (0–4 mm)	50.5 kg
Coarse aggregate (4–16 mm)	61.6 kg
Super plasticizer	308 ml

desired crack width has been achieved, hard plastic wedges are placed inside the notch, in order to reduce the crack closing (recovery) after unloading.

2.3 *Digital image correlation*

Digital image correlation (DIC) is an optical (non-contact) method used for tracing surface displacements of deforming solids. During loading, images of the deforming specimen were taken at an interval of 1s using a digital camera. They were processed and analyzed using DIC.

2.4 *Resistance and cracking*

Electrical resistance of concrete is closely related to durability. The connectivity of the pore network, the size and distribution of pores and environmental conditions like moisture and temperature all have an influence over resistance measurements. In cracked concrete, this continuity of the pore network is broken. Concrete resistance measurements were performed with a LCR meter (120 Hz AC) by attaching a pair of electrodes that allow to measure the resistance over the cracked zone.

3 RESULTS AND DISCUSSION

3.1 *Cracking results*

In total, 7 specimens were prepared and cracked according to the described procedure. In order to study the cracking pattern visually, an additional specimen (not included in the rest of the study) was loaded until the average COD was more than 1 mm, then unloaded and vacuum impregnated using fluorescent epoxy. Then it was cut parallel to the reinforcing steel (Figure 1). During the test, debonding occurs at the steel/concrete interface, which is important for durability investigations.

3.2 *Digital image correlation results*

During this test, 445 images in total were taken. First image was used as a reference, to which others were correlated to. A square grid with a spacing of 20 pixels was applied on the reference image and used for the analysis. Unlike LVDT measurements which only give displacements between designated points, DIC can provide more details on the crack shape, geometry, width, and depth.

3.3 *Cracking and resistance results*

Figure 2 shows the load-displacement curve of a reinforced concrete specimen with embedded electrodes. It is clear that electric resistance is a linear function of COD.

Figure 2 showed that the increase of resistance as a function of COD is linear with a strong correlation factor (R^2). The gradual increase in resistance values can be attributed to the formation of micro-cracks, while sudden increments to crack growth or propagation.

4 CONCLUSIONS

From the obtained results, the following can be concluded:

- Modified wedge-splitting test (MWST) is a simple tool for creating bending-type cracks in reinforced concrete.
- Debonding at the steel-concrete interface occurs, which is important for chloride ingress and corrosion investigations, as stated in the literature.
- Crack recovery can be minimized, though not fully prevented, by using hard plastic wedges.
- Digital Image Correlation (DIC) can be used successfully in fracture investigations of (reinforced) concrete.
- Electrical resistance is a function of COD with a strong correlation.
- Cyclic changes in resistance can be attributed to crack growth.
- Cracked concrete in dry conditions can have high values of resistance which can be misinterpreted as highly durable.

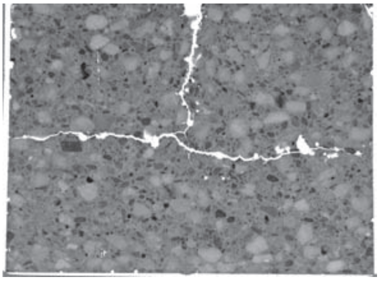

Figure 1. Impregnated crack of the MWST specimen under ultraviolet light.

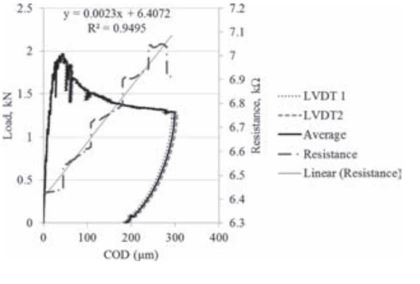

Figure 2. Typical load-COD curve, and the corresponding resistance measurement.

Concrete Repair, Rehabilitation and Retrofitting III – Alexander et al. (eds)
© 2012 Taylor & Francis Group, London, ISBN 978-0-415-89952-9

Effect of concrete and binder composition on cracking sensitivity

Konstantin Kovler, Semion Zhutovsky & Arnon Bentur
National Building Research Institute, Civil and Environmental Engineering, Technion, Israel Institute of Technology, Israel

1 INTRODUCTION

The issue of cracking has been well known in the concrete technology field and a variety of means have been developed to deal with it at the level of the concrete mix design, curing and design of the structure. The cracking problem has been receiving in recent years renewed interest which is due to the advent of modern high-performance concretes which are superb in many of their properties, but some of them exhibit greater sensitivity to cracking. This is due to higher shrinkage values, combined with enhanced phenomena of internal shrinkage, which in combination with thermal stresses can lead to more intensive cracking. The object of the present study was to systematically investigate the nature of high performance concretes with respect to cracking sensitivity, to evaluate the influence of w/c ratio, type of cement and mineral additives, which are the three major parameters used to tailor such concretes.

The sensitivity to cracking was evaluated by means of the ASTM C 1581 ring test, which can take into account autogenous shrinkage effects which occur at a very early stage and also provide more meaningful characterization than the simple approach of evaluating free shrinkage. The latter does not take into account other parameters which control cracking such as the viscoelastic response and the rate of strength development.

The ASTM test provides input parameters to characterize cracking sensitivity, which are either the time to cracking or the strain rate at the time of cracking, and accordingly classifies the cracking sensitivity in terms of four categories: High, Medium-High, Medium-Low and Low. The authors of the current paper have recently modified the categories by characterizing each of them in terms of a new parameter which combines the two ASTM criteria, and is defined as the strain rate divided by the time of cracking.

2 EXPERIMENTAL

The concrete composition variables were the w/c ratio (0.29, 0.33, 0.45 – 567, 506, 450 kg/m^3 cement content, respectively), the cement content in the 0.45 w/c ratio concrete (370, 450 kg/m^3), the type of cement in the 0.33 w/c ratio concretes (CEMI-52.5N, CEMII A-V 42.5N, CEMIII slag cement 42.5 N/B), and the type of mineral additive which was used to replace part of the cement (61 of the 567 kg/m^3 cement) in the 0.29 w/c ratio concrete (metakaolin (MK), fly ash (FA) and microsilica (MS)). Superplasticizer admixtures were added to the mix at a content which was required to achieve 125 mm slump. Rheobuild 700 was used for the 0.45 w/c ratio concretes and Glenium 51 for the 0.33 and 0.29 concretes.

The concretes were tested for compressive strength, free shrinkage and cracking sensitivity in the ASTM 1581 ring test.

3 SUMMARY OF RESULTS

A major driving force for cracking is the shrinkage of concretes during the first few days and weeks. The results in the present study suggest that the differences in shrinkage are relatively small within the wide range of compositional variables evaluated here. However, the differences in cracking sensitivity are very high (Figure 1), suggesting that

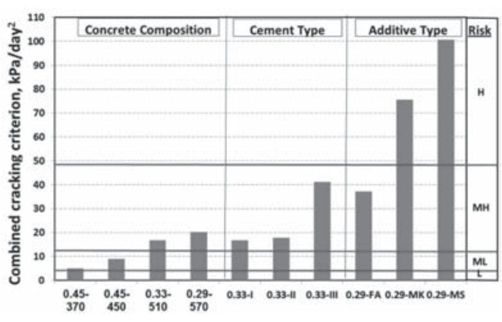

Figure 1. Effect of concrete and binder composition on cracking sensitivity as expressed by the combined criterion of stress rate/time to cracking in the ASTM ring test; Risk levels according to classification by Kovler & Bentur, 2009—H: High, MH: Medium-High, ML: Medium-Low, L: Low.

Concrete composition: First number denotes w/c ratio and the second one the cement content, kg/m3

Cement type: I-CEM I; II-CEMII A-V; CEM III (slag)

Additive type (cement replacement): FA-fly ash; MK-metakaolin; MS-microsilica factors other than shrinkage have a major impact. These could be mechanical and physical properties and their rate of development, such as modulus of elasticity and viscoelastic response. In depth study of each of these basic characteristics is required in order to better understand the internal processes taking place which control cracking sensitivity. The ring test simulates all of these processes and as such the outcome of this test can serve as a good practical indication for cracking sensitivity.

The overall cracking response shown in Figure 1 exhibits the effect of reducing w/c ratio, increasing the cement content, changing the type of cement and the mineral admixtures. The figure shows in particular the large effect of the mineral admixtures, especially the metakaolin and microsilica added to the concrete. Slag (in the CEMIII cement) and fly ash (added to the concrete) increased cracking sensitivity but to an extent which is much smaller than that of the metakaolin and microsilica.

Concrete Repair, Rehabilitation and Retrofitting III – Alexander et al. (eds)
© 2012 Taylor & Francis Group, London, ISBN 978-0-415-89952-9

Towards incorporating the influence of cracks in the durability index testing approach

J. Kanjee, H. Beushausen, M.G. Alexander & M. Otieno
Concrete and Materials Structural Integrity Research Unit, Department of Civil Engineering, University of Cape Town, South Africa

ABSTRACT: In this paper, the need to accurately assess the durability of Reinforced Concrete (RC) structures while taking into account the presence of cracks is reviewed. The development and use of service life models to predict the deterioration of concrete structures are examined. Most of these service life models are based on the philosophy of uncracked concrete, which leads to an over-estimation of the performance of the structure. The South African Durability Index (DI) tests are utilised as indicators to characterise concrete and as input parameters for service life prediction models. The paper reviews literature on the influence of cracks on concrete durability and illustrates current work with regard to accounting for the presence of cracks in the DI approach. The aim of the research discussed in this paper is to improve the service life prediction of (cracked) in-service RC structures.

1 INTRODUCTION

The durability of RC structures depends greatly on the quality of the cover concrete. Therefore, the presence of cracks in the concrete cover can aggravate steel corrosion in RC structures by creating preferential paths for the ingress of various types of potentially deleterious species (such as: H_2O, O_2, CO_2, Cl^-). The result is a shorter time to corrosion initiation, increased corrosion rate and consequently a substantial reduction in service life.

It is becoming increasingly popular to utilize numerical or analytical simulation models to predict the long-term performance of concrete structures. The majority of these service life models have been developed using laboratory test data that consider concrete in an un-cracked state (Ling *et al.*, 2010).

While uncracked concrete exists as an ideal case, frequent cracking occurs in real structures that has a profound impact on their service life performance.

Durability parameters measured using well-cured undamaged specimens may be misleading and may overestimate performance (Weiss, 2003). By using well-cured undamaged specimens as a baseline some models may therefore predict an overly optimistic service life performance that is not representative of the behaviour of the concrete actually used.

2 RESEARCH METHODOLOGY

Literature has shown two main reasons for the presence of cracks being often omitted from various service life models:

i. Insufficient knowledge on the effects of cracks.
ii. Introduction of cracks greatly complicates the analysis.

Furthermore, where cracks have been investigated in previous studies, the influence of aggressive species penetration is normally limited to single isolated cracks. The influence of cracking frequency and the distribution of cracks across a RC structure are not taken into account. Work done by Arya and Ofori-Darko (1996) has shown that the higher the frequency of cracking the higher the corrosion rate, which highlights the need to account for such crack parameters in future research.

However, due to the difficulty of creating desired crack patterns in concrete specimens and the availability of appropriate test methods, a limited amount of studies have been carried out on the permeability of cracked concrete (Picandet *et al.*, 2009).

The complexity of modelling transport in cracked concrete, as well as the pressing need for reliable methods of evaluation and prediction of concrete durability poses a new challenge in the field of concrete research.

Currently, work is being undertaken by the first author to investigate the influence of cracks on the DI-based service life prediction of RC structures. Based on the correlations that will be established using the durability index tests, the influence of cracks can be investigated by considering carbonation and chloride ingress in cracked and uncracked concrete.

Crack widths are the control parameters that are utilised to simulate the cracked specimens. $380 \times 130 \times 120$ mm beam specimens are cast with a notch located in the centre of the beam as shown in Figure 4. The beams are reinforced with one 10 mm diameter mild steel bar, which is positioned to provide a 40 mm cover.

The DI tests will be used to characterize sound (un-cracked) concrete according to the South African service life prediction method, whereas accelerated carbonation and bulk diffusion tests will be used to assess the durability potential of the respective cracked concrete.

Utilising the empirical correlations that exist, the Oxygen Permeability Index can be used to predict carbonation depth development, which can then be compared to the carbonation depth from the accelerated carbonation test of the cracked concrete. Similarly, the Chloride Conductivity Index can be used to obtain the apparent chloride diffusion coefficient, which can be compared to the apparent chloride diffusion coefficient from the bulk diffusion test of the cracked specimen.

This research aims to achieve a number of outcomes with regard to accounting for the influence of cracks on concrete tested for service life predictions. Firstly, the results will illustrate how un-conservative the durability index tests are for a given concrete when compared to a cracked one with respect to carbonation and chloride ingress. Secondly, the possible impact that a given crack width can have on penetration of aggressive species into the concrete, particularly with regard to carbonation and chloride ingress. Lastly on a macro-scale, the significance of crack frequency and species penetration will be considered, and how this can lead to possible macro- and microcell corrosion in RC structures.

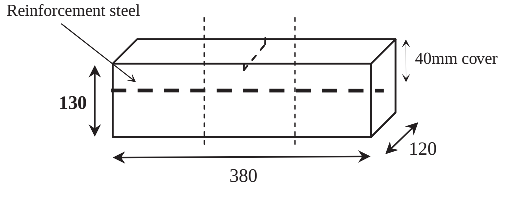

Figure 1. Beam specimens (all dimensions in mm).

Utilising this approach, the influence of cracks on durability testing and its implications on service life predictions can be quantified. This will allow for a more actual prediction of service life with regards to using the durability index tests by taking into account the presence of cracks.

3 CONCLUSION

Based on the studies carried out by various researches, it can be concluded that cracks have a marked influence on the transport properties of concrete, which inherently affects the durability of the structure. Once formed, they present fast routes for transport of aggressive species into concrete. This has a direct impact on the service life performance of the structure.

Durability index testing methods have been developed on the premise of uncracked concrete and currently no compensation has been made to include the influence of cracks. In order to make reliable service life predictions, further research needs to be carried out to consider the influence of cracks on uncracked and cracked concrete using the durability index philosophy.

REFERENCES

Arya, C. & Ofori-Darko, F.K. 1996. Influence of crack frequency on reinforcement corrosion in concrete. Cement and Concrete Research. Vol. 26. No. 3, pp. 345–353.

Ling, G. Lui, Y. Xiang, Z. 2010. Numerical modelling for predicting service life of reinforced concrete structures exposed to chloride environments. Cement and Concrete Composities. No. 32. pp. 571–579.

Picandet, V. Khelidj, A. Bellegou, H. 2009. Crack effects on gas and water permeability of concretes. Cement and Concrete Research 39, pg. 537–547.

Weiss, W.J., 2003. Linking Insitu Monitoring with Damage Modeling for Life-Cycle Performance Simulations in the Concrete Infrastructure, Career Proposal, Sponsor: National Science Foundation.

Concrete Repair, Rehabilitation and Retrofitting III – Alexander et al. (eds)

A model for the prediction of plastic shrinkage cracking in concrete

W.P. Boshoff, R. Combrinck & J. Maritz
Department of Civil Engineering, Stellenbosch University, South Africa

ABSTRACT: Plastic Shrinkage Cracking (PShC) of concrete with large surface areas has been a problem for many years. It is known to increase in severity when the concrete surface is exposed to environmental conditions which result in high evaporation rates. However, the severity of PShC cannot always be directly linked to the evaporation rate. Many other factors have a strong influence, e.g. the initial set time and the bleeding. A new model, PShC Severity, is proposed which is shown in this paper to give a good indication of the PShC to be expected. It is based on the evaporation rate, total bleeding volume and initial set time of the concrete. It iss further shown that the PShC is reduced by adding a low-volume of fibres to the concrete. The reduction is shown to be more significant the higher the volume of fibres.

1 INTRODUCTION

The plastic shrinkage cracking (PShC) of fresh concrete with large surface areas has been a problem ever since concrete has been first used. PShC typically occurs within the first few hours after the concrete has been cast (Domone et al. 2010, Kwak & Ha 2006). These cracks normally do not have a specific pattern and is often referred to as crazed cracking and are known to be more prominent when the evaporation rate is high (Uno 1995).

Many researchers have attempted to model plastic shrinkage of fresh concrete, e.g. Kwak & Ha (2006), Radocea (1994). However, not many, if any, has attempted to model PShC. There are many interlinked time-dependant mechanisms playing a role that it becomes a complex task to incorporate these in a single model.

In this paper, however, a model is proposed to indicate the severity of PShC. This is simple phenomonological approach of which the application is not confined to research laboratories.

2 MODEL FOR PSHC SEVERITY

The proposed model for PShC severity is based on the mechanisms explained in the previous section. It is a basic model which is represented by the total water evaporated from the concrete from the time it is cast until the *initial setting time*. It can be expressed as follows:

$$PShC\ Severity = ER \cdot t_{set} - W_{bl} \tag{1}$$

with ER the evaporation rate [kg/m^2/h], t_{set} the time between laying the concrete and the *initial set time* [h] and W_{bl} the total bleed water [kg/m^2]. Note that the concrete will only start to bleed once it has been placed and the bleeding will cease at the *initial set time*.

The bleeding can be determined with relative ease using the method explained in Section 3.2. The evaporation rate is however more difficult to measure. It is suggested that the model by Uno (1995) be used to determine the evaporation rate for practical applications:

3 EXPERIMENTAL SETUP AND PROGRAM

To demonstrate the model for PShC Severity, a large number of tests were done. These include PShC tests, bleeding tests and setting time tests.

The experiments were conducted in a climate chamber which can create stable environmental conditions ideal for the formation of PShC. The chamber electronically controls temperature and relative humidity to pre-set values with a heating element and a dehumidifier respectively, while a variable airflow is created with two axial fans. The climate chamber can reach a temperature of up to 50°C, relative humidity as low as 10% and uniform wind speed of up to 70 km/h.

Figure 1 shows the test compartment of the climate chamber where the various moulds are placed for testing.

4 TEST RESULTS

All the results are shown in Figure 2 using the PShC Severity model. A relative narrow band is evident correlating the PShC Severity with the

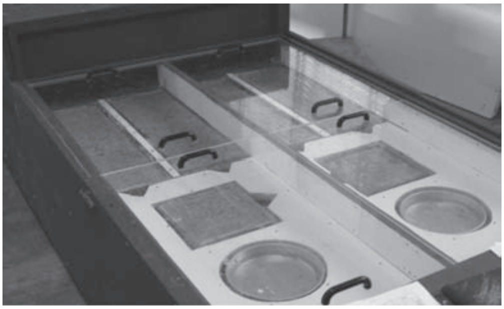

Figure 1. PShC climate chamber.

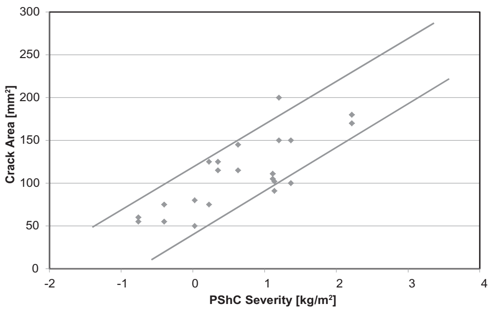

Figure 2. The PShC Severity shown against the Crack Area measured.

crack widths. This indicates that the PShC Severity model is an effective way of modelling the severity of PShC.

5 REDUCING PShC USING FIBRES

Micro synthetic fibres were added to concrete to investigate to which extent it reduces the PShC and how it relates to the PShC Severity model. The fibres used were a combination of polypropylene and polyester.

The results of these tests are shown in Figure 3 together with the band of results for the tests without fibres taken from Figure 2. Effectively, the addition of 0.1% of fibres reduced the PShC Severity with 1.4 kg/m^2.

A further study was done to investigate the effect of different volumes of fibres. The results are shown in Figure 4. It is clear that the higher the volume of fibres, the lower the cracking area. This is useful as it indicates that when an even further reduction of the cracking potential is required, the volume of fibres can be increased in cases where the PShC Severity cannot be decreased.

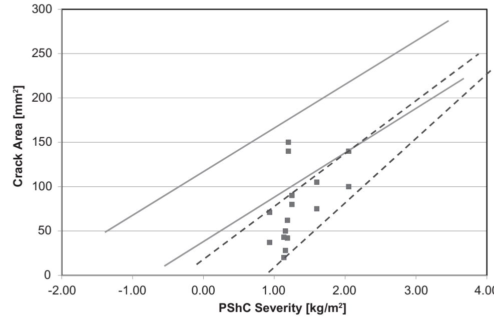

Figure 3. The effect of the addition of 0.1% on the PShC Severity.

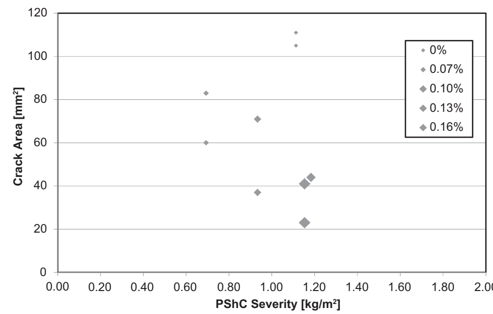

Figure 4. Effect of the volume of fibres on the cracking potential.

6 CONCLUSIONS

This paper proposes a model, defined as Plastic Shrinkage Cracking (PShC) Severity, which is shown to be directly linked to plastic shrinkage cracking potential of fresh concrete. And investigation was also done to show the effectiveness of fibres to reduce PShC. The following conclusions can be made:

- The PShC Severity model is can good indication of the level of PShC that can be expected.
- The PShC Severity can be reduced by altering the:
  - Evaporation rate
  - Bleeding rate and volume
  - Initial setting time of concrete
- The addition of synthetic fibres at low volumes (less than 0.15%) shows a significant reduction of the PShC potential.
- An increasing volume of fibres increases the level of reduction of PShC potential.

The PShC Severity model however needs to be further calibrated to include the effect of different types of admixtures.

Concrete Repair, Rehabilitation and Retrofitting III – Alexander et al. (eds)
ISBN 978-0-415-89952-9

Durability design of reinforced concrete structures submitted to carbonation by using an probabilistic modelling

M. Thiéry & V. Baroghel-Bouny
Université Paris-Est, IFSTTAR, MAT, Paris, France

A. Orcesi
Université Paris-Est, IFSTTAR, SOA, Paris, France

ABSTRACT: A carbonation model has been developed. It is able to take into account the influence of wetting-drying cycles which can slow down the rate of carbonation. Actually it is assumed that carbonation comes to a halt as long as the concrete is too wet. It is considered that wetting is infinitely faster than carbonation or drying. After a wetting step followed by a drying step, carbonation restarts as soon as the concrete is dry enough in the vicinity of the carbonation front. During the wetting step, it has been considered that carbonation stops if the relative humidity RH prevailing in the pores is higher than a threshold value $RH_{\text{lim}} = 90\%$. During the drying step, carbonation classically evolves according to a square root of time law involving the external CO_2 concentration, the average liquid-water saturation degree of the carbonated concrete layer (S), its accessible-to-water porosity (ϕ) and the initial amount of portlandite. The determination of the time evolution of the drying depth X_d at which $RH = 90\%$ is crucial to be able to quantify the carbonation penetration. X_d is assessed by using a simplified moisture transport model which assumes that only the liquid-water movement due to capillary gradients contributes to moisture transport. The main input data required for this moisture transport model are the usual durability indicators ϕ and K_l (liquid-water permeability), two desorption parameters, as well as the surrounding relative humidity RH_{ext}.

This carbonation model has been be developed in a probabilistic framework by calculating a time-dependent probability of failure P_f which expresses the probability that the carbonation front exceeds the concrete cover E by taking into account the variability of the input parameters. In other words, $P_f(t) = P(M_t = E - X_C(t) < 0)$ where M_t refers to the safely margin at time t. The reliability index β has been determined by using the Rackwitz-Fiessler algorithm.

Reliability calculations have been illustrated through three concretes C1, C2 and C3 designed for a service life (SL) of 100 years. C1 and C2 are of class C34/45 whereas C3 is C50/60. Concretes C2 and C3 have been prepared with fly ash. The durability indicators used as input data of this carbonation model have been measured in laboratory, and the probabilistic distributions and coefficients of variation have been inferred from a literature review. It is chosen that the environmental exposure class, in accordance with the European standard EN 206, is XC4, *i.e.*, the most severe sub-class for a corrosion risk induced by carbonation (concrete surface subject to wet and dry periods). According to the Eurocode 2 EC2, and its French Annex in the case of a concrete bridge deck (SL > 100 years), the recommended structural class is S5 for the three studied concretes. As a consequence the concrete cover is fixed at $E = 3.5$ cm.

Whereas the SL prediction according to the performance-based approach (PBA, see Baroghel-Bouny's works) seems in agreement with ours simulations if one considers C1 and C3, PBA leads to an important underestimation of the SL for C2. This con-firms that the analysis of a single parameter, such as the porosity, to assess the performance of a concrete regarding its durability against carbonation, is not relevant. Indeed a defect on the porosity due to a high content of paste or the presence of supplementary ce-mentitious materials like fly ash or slag, which can lead to a more porous microstructure if the measurement of porosity is performed too early, can be counterbalanced by good performances of other DI such as transfer or moisture properties.

A design of the concrete cover E has been carried out by using this probabilistic model. A serviceability target reliability index of 1.5 has been considered according to the EC2. The determination of the optimal value of the concrete cover is illustrated for the three studied concretes in figure 1. For C2, the calculated concrete cover matches with the EC2 spec-ifications whereas a 100-year SL would be insured for C1 only if $E = 4.5$ cm. Figure 1 also highlights that the EC2 specification is 0.5 cm higher than the calculated value for C3 (3 cm *vs.* 3.5 cm). For this last concrete, the structural class has been fixed at S5 according to the EC2 leading to a concrete cover of 3.5 cm. Actually the structural class could have been reduced to S4 by taking into account a high strength class. Nonetheless the presence of fly ash in C3 does not allow such a reduction of the structural class since it is admitted that fly ash weakens the buffering capacity of the cementitious matrix. This model shows that the presence of fly ash, which provides excellent transfer properties if the curing is adequate, does not bring down the durability regarding carbonation, in spite of a reduction of the chemical resistance. In a nutshell the EC2, which is based on the determination of a structural class depending on the strength class and the presence or absence of supplementary cementitious materials like fly ash, shows its limits given that it can lead to an oversizing of the concrete cover.

This paper provides a probabilistic framework for optimizing the times of inspection and maintenance regarding the carbonation-induced corrosion risk. To illustrate this asset, a concrete bridge deck made of C1, C2 or C3 (160 m × 12 m) has been studied. The inspection technique corresponds to the measurement of the carbonation depth by spraying phenolphthalein on concrete cores. At each inspection time t_i, the decision to establish a repair procedure is determined by assessing the event margin $H_{ti} = \gamma \times E - X_C(t_i)$. The γ coefficient represents a detection threshold and implies that the structure is repaired before corrosion initiation has been reached ($\gamma = 0.9$). If the inspection indicates that the repair criterion is reached, the repair consists in rebuilding the carbonated concrete cover by a repair mortar. Three different repair mortars have been selected with three different qualities (M1, M2 and M3). After repair an increase of the variability of the cover E is taken into account to reflect the lower workmanship quality of achieving a fixed cover thickness with a mortar. Such a maintenance policy gives rise to a binary event tree. Figure 2 illustrates the time-dependent evolution of the reliability index β for C1 and C2 concretes in the case of a double inspection at t_1 = 70 years and t_2 = 90 years. It appears that the earlier the inspection is planed, the less the rise of β is obvious. Moreover, the observation is readily drawn that beyond the inspection/repair time the decrease of β is more pronounced because the quality of the repair mortar regarding the carbonation ingress is lower than the quality of the initial concrete cover. This is particularly noticeable in the case of M1 which is of lower quality than M2 and M3. The minimum value of β which is reached during the whole service life heavily depends on the time of initial inspection and the kind of mortar which is used for the repair.

Because targeted inspections are time consuming and expensive, they should be planned and timed for when they produce the most benefit. In the present research, the inspection times are determined by optimizing the total cost of inspection and repair, and by maximizing the reliability index at 100 years. Different inspection intervals have been tested from 10 to 50 years, as well as different moments of first inspection (20, 30, …, 80 or 90 years). The principle of the procedure is to identify the point with the lowest cost able to ensure β_{min} < 1.5. It comes that the optimal solution is provided by a double inspection at years 40 and 90 and a maintenance using M3 as the repair mortar.

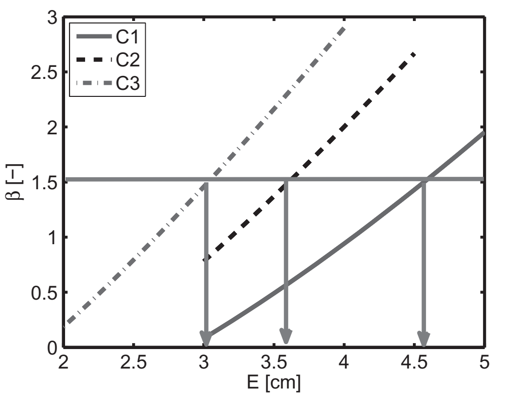

Figure 1. β at 100 years *vs.* the concrete cover thickness E.

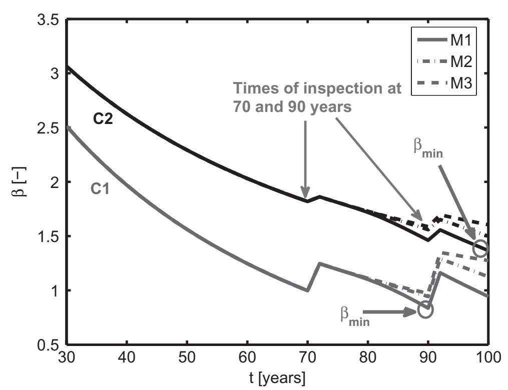

Figure 2. Influence of two inspections at 70 and 90 years on the time-dependent reliability index β for concretes C1 and C2.

Concrete Repair, Rehabilitation and Retrofitting III – Alexander et al. (eds)
© 2012 Taylor & Francis Group, London, ISBN 978-0-415-89952-9

Mix design optimisation—the influence of binder content on mechanical and durability properties of concrete

M. Angelucci, H. Beushausen, & M.G. Alexander
Concrete Materials and Structural Integrity Research Unit, Department of Civil Engineering, University of Cape Town, South Africa

ABSTRACT: Current mix design standards mainly derive from prescriptive type specifications, i.e. recipe-based specifications that prescribe limiting values for certain mix design parameters, such as minimum cement content and maximum water/binder ratio. This has numerous economical, technical and environmental disadvantages and is one of the driving factors behind the development of performance-based specifications to act as alternative means of design of concrete mixes. Such an alternative method in South Africa is the Durability Index (DI) Approach, which has grown increasingly in use. Despite this, a dominant assumption among professionals in the industry is that the durability of a concrete mixture is directly proportional to its binder content. This results in uneconomical, unsustainable and often non-durable concretes due to various implications of high cement contents such as thermal effects and Alkali-Silica reactions. This paper forms part of research that will link mix design parameters such as binder content and water/binder ratio, as well as mechanical properties such as compressive strength, to concrete durability. Issues behind the specification of minimum cement contents are investigated through a review of various pertinent studies conducted previously, followed by a summary of experimental results conducted by the first author. The results gathered in this document suggest that the relationship between durability and binder content is a complex one and hence the specification of minimum cement contents is not an effective means of ensuring durability and should be revisited.

1 INTRODUCTION

Worldwide there is a dominance of prescriptive-type specifications in industry, focusing mainly on minimum cement content, maximum water/binder ratio and compressive strength. According to Wasserman et al. (2009), these specifications resulted from previous practice and experience from times when there was no availability of chemical admixtures or supplementary cementitious materials (SCMs) to contribute to mixture properties. Today, in many cases, such specifications do not prove to be favourable as various problems can arise from their adherence (Wasserman et al. 2009): since cement is the most expensive constituent of concrete mixtures, a higher cement content results in higher costs. From a technical point of view, higher binder content may result in higher strengths, depending on the amount of water used, but it may also result in a higher paste volume, thus making the mixture more susceptible to cracking caused by shrinkage, thermal effects and Alkali-Silica reaction (ASR). As such, there is a worldwide need to reduce the binder content in concrete, a trend which is inhibited by the general opinion among numerous professional engineers that high binder contents are a guarantee for higher durability.

Current specifications for durability in both South African Standards and European Standards follow the prescriptive type, but the increasing argument among researchers is that aspects like mix durability, which is a material performance concept for a structure in a given environment, cannot be determined accurately through the simple prescription of mix parameters. What is needed in order to promote a deeper understanding behind aspects of concrete durability is a study that will investigate the effects that various mix design parameters have on durability properties; this will establish a clear and well-defined relationship between such mix design properties and parameters and durability, which will in turn bring about justifiable and sensible changes to current trends in mix design specifications.

2 METHODOLOGY AND PRELIMINARY RESULTS

The choice of experimental parameters was carried out to encompass mixes suitable for a variety of structural applications common in industry. For this reason, it was chosen to control the binder contents for each w/b ratio through the selection of four water contents that would reflect common modern industry scenarios. Binder combinations were chosen as control 100% CEM I 52.5 N, 70% CEM I/30% FA and 50% CEM I/50% GGBS. Table 1 summarises the mix parameters.

Durability Index Tests (Alexander et al., 2008) were carried out at 28 days for water sorptivity and at 56 days for oxygen permeability and chloride conductivity. Some preliminary results that were obtained are presented and discussed below.

Results from Figures 1 and 2 show that for a fixed water/binder ratio, increasing the water content (and thus binder and paste contents) causes an increase in permeability. However, this increase differs for each binder type. In FA concretes, the difference only seems to be significant at high w/b ratios, while in the CEM I concretes it is noticeable at all w/b ratios. This could be attributed to the higher pore-refinement for FA concretes at low w/b ratios due to the slow-maturing pozzolanic reaction, resulting in improved permeability when w/b ratio is low.

In CEM I concretes it was observed that an increase in w/b ratio does not seem to have any effect on the permeability coefficient, regardless of paste volume. This observation stands in contrast to previous studies carried out by the authors and can at this stage not be explained as further testing and in-depth analysis is needed. One possible reason is that in previous studies, a CEM I 42.5 was used, which is no longer available in South Africa. The finer nature of the cement particles of the CEM I 52.5 used in this study possibly results in an improvement (i.e. densification) of the microstructure to such an extent that an increase in w/b ratio does not bring about any significant changes to permeability of relatively mature concrete. However, to confirm this assumption, further studies are needed.

Additional experimental procedures will involve compressive strength, oxygen permeability, water sorptivity and chloride conductivity testing for all three binder-type mixes. It is anticipated that this will determine whether there exist meaningful and significant relationships between durability and the investigated parameters. Furthermore, results will also aim to show how sensitive mechanical and durability properties are to changes in mix design parameters such as w/b ratio, binder content, binder type and curing regime.

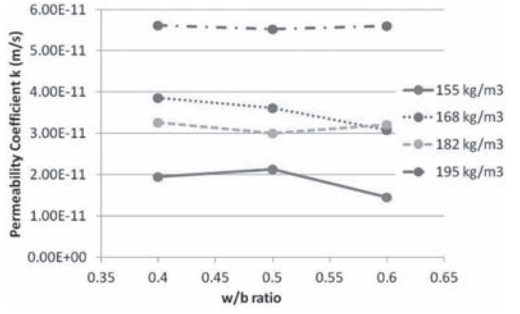

Figure 1. Effect of binder content on concrete permeability for 56 day water-cured samples—100 % CEM I.

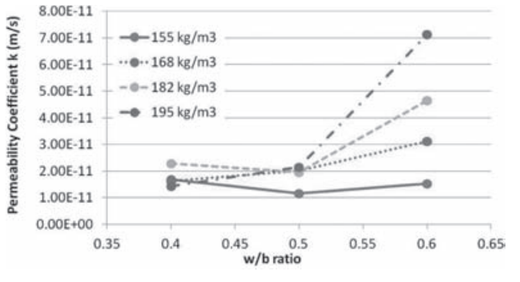

Figure 2. Effect of binder content on concrete permeability for 56 day water-cured samples—70 % CEM I/30 % FA.

Table 1. Mix design parameters.

w/b ratio	Water content (kg/m^3)	Binder content (kg/m^3)
0.40	155	387.5
	168	420.0
	182	455.0
	195	487.5
0.50	155	310.0
	168	336.0
	182	364.0
	195	390.0
0.60	155	258.3
	168	280.0
	182	303.3
	195	325.0

3 CONCLUSIONS

The effect of binder content on physical and mechanical properties of concrete is more complicated than what is suggested by code specifications, where it is simply expressed as a minimum requirement to meet criteria of strength and durability. The findings presented in this paper showed that the beneficial effects associated with an increase in binder content are limited to how much binder is actually used, highlighting the need for a more useful specification parameter that is not minimum binder content *per se*, but a recommended binder content range. The conclusions that were drawn in the studies that were summarized in this paper suggest that current mix design specifications involving the use of minimum binder contents should be revised.

Concrete Repair, Rehabilitation and Retrofitting III – Alexander et al. (eds)
 ISBN 978-0-415-89952-9

Durability and service life of reinforced concrete structures under combined mechanical and environmental actions

T. Zhao, J. Jiang & X. Wan
Qingdao Technological University, Qingdao, China

F.H. Wittmann
Aedificat Institute Freiburg, Germany

ABSTRACT: Initially durability and service life of reinforced concrete structures have been considered under the influence of one single action as for instance chloride penetration, carbonation or frost action. It could be shown in the meantime, however, that the effect of simultaneously or consecutively acting deteriorating processes is more severe than the effect of any single action participating in the deteriorating process. A number of actions, which are known to act frequently in common, has been selected from the huge number of possible load combinations and their deteriorating effect has been studied. Results show that chloride penetration and carbonation after frost action are significantly accelerated. The influence of mechanical tensile and compressive load on rate of carbonation has also been studied. Results can serve as a basis for more realistic prediction of service life of concrete structures exposed to an aggressive environment.

1 INTRODUCTION

Most methods to design service life of reinforced concrete structures are based on one dominant deteriorating mechanism such as carbonation, chloride penetration or frost action. In the meantime it has been shown by a number of publications that the combination of mechanical and environmental actions can be more severe than each load acting separately. In this contribution recent results of test series to investigate durability under combined actions are presented.

In Table 1 some deteriorating actions, which can be observed in concrete, are listed. Some load combinations have been selected on the basis of what is believed to be most important and frequently observed in practice. The influence of prior frost action on carbonation and chloride penetration has been studied. In addition the influence of an applied mechanical load on carbonation and on chloride penetration has been determined.

Table 1. Selection of some major deteriorating processes, which may reduce durability of concrete acting alone or in combination.

Mechanical Load	Migration Processes	Chemical Reactions	Thermal Effects	Hygral Effects
Compression	Ion migration by convection	Carbonation	Heat of hydration	Drying
Tension	Ion migration by diffusion	Chloride in HCP	Thermal gradients	Capillary absorption
Shear	Osmosis	Sulphate in HCP	Thermal decomposition of HCP	Moisture diffusion
Torsion	Electro- osmosis	Ammonium in HCP	Frost action	Shrinkage and swelling
Sustained	Leaching	Hydrolysis	Freeze-thaw cycles	
Cyclic	Electrophoresis	Alkali-aggregate reaction		

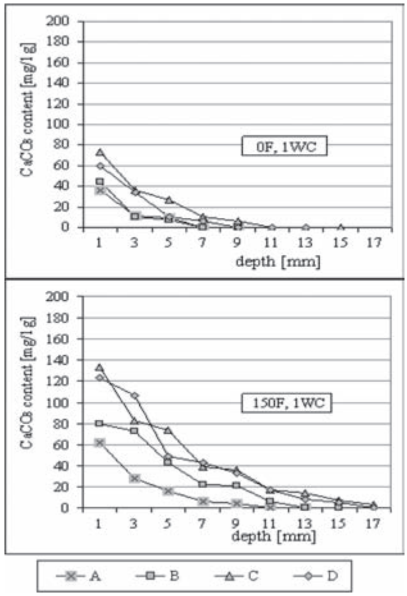

Figure 1. Carbonation profiles as determined on four different types of concrete A, B, C and D without frost damage (upper diagram) and after 150 freeze-thaw cycles (lower diagram) had been applied prior to exposure to accelerated carbonation.

2 INFLUENCE OF FROST ACTION ON CARBONATION AND CHLORIDE PENETRATION

Four different types of rather conventional concrete have been produced and tested to investigate the influence on damage induced by frost action on carbonation and chloride penetration. Concrete A has a water-cement ratio of 0.4, concrete B of 0.5 and concrete C of 0.6. Concrete D has also a water cement ratio of 0.5 but in this case 30% of the Portland cement has been replaced by fly ash. The resulting carbonate profiles as measured in concrete samples after one week of accelerated carbonation are shown in the upper part of Fig.1. In the lower part of Fig. 1 the results as obtained on concrete exposed to 150 freeze-thaw cycles prior to accelerated carbonation.

Similar results have been obtained when chloride penetration before and after frost damage has been observed.

3 INFLUENCE OF MECHANICAL LOAD ON CARBONATION AND CHLORIDE PENETRATION

In order to be able to determine the influence of an applied mechanical load on the rate of carbonation

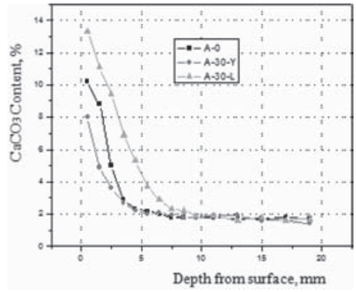

Figure 2. Carbonate profiles as measured in the compression zone (A-30-Y) and in the tension zone (A-30-L) of a concrete beam under four point bending after 30 days of accelerated carbonation. Results obtained on an unloaded companion specimen (A-O) are also plotted in this figure.

concrete beams have been exposed to accelerated carbonation for 30 days under sustained four point bending. Similar but unloaded companion beams have been exposed for the same period to accelerated carbonation. Then the carbonate profiles have been measured in the zone of applied tension as well as in the zone of applied compression. Typical results are shown in Fig. 2 (Wan et al., 2011).

Under tensile stress the rate of carbonation increases steadily. Under moderate compressive stress the rate of carbonation decreases but at a compressive stress higher than 50% of the ultimate stress the rate begins to increase.

The apparent diffusion coefficient of chloride in concrete under sustained tensile and compressive stress shows a similar variation (Jiang et al., 2011).

4 CONCLUSIONS

With the experimental results presented in this contribution it could be shown that durability decreases under the influence of combined actions and service life is shortened significantly.

Under direct tension the rate of carbonation and the rate of penetration of chloride into the pore space of concrete are accelerated significantly. If results of standard test methods without applied load are used for the prediction of service life, results may be misleading and the real service life will be overestimated.

REFERENCES

Jiang, F., Wan, X, Wittmann, F.H. & Zhao, T. 2011. Influence of combined actions on durability of reinforced concrete structures, *Int. Jour. Restoration of Buildings and Monuments* 17: 289–298.

Wan, X., Wittmann, F.H. & Zhao, T. 2011. Influence of mechanical load on service life of reinforced concrete structures under dominant influence of carbonation, *Int. Jour. Restoration of Buildings and Monuments* 17: 103–110.

Concrete Repair, Rehabilitation and Retrofitting III – Alexander et al. (eds)
© 2012 Taylor & Francis Group, London, ISBN 978-0-415-89952-9

Control of concrete cover depth of reinforced concrete structures for durability

G. Nganga, M.G. Alexander & H. Beushausen
Concrete and Materials Structural Integrity Research Unit, Department of Civil Engineering, University of Cape Town, South Africa

ABSTRACT: The durability index-based performance approach in South Africa requires verification of concrete cover properties, its penetrability (using durability indices) and depth. This paper provides a summary of data analysis done on cover depth readings of in-situ structures (bridges) and precast elements (median barriers) from a large scale project in which these specifications were implemented. The assessment of cover depth for a structural element is based on the average of scanned areas. The limit value provided in specifications is 40 mm and it was observed that the average cover depth readings from the bridges and precast median barriers comply with this value. However, no value is provided on permissible proportion below the minimum (30 mm) and above the maximum (55 mm). The variability for in-situ structures was observed to be considerably higher than that of precast elements which indicates that specified cover depths with low variability can be obtained on structures when appropriate quality control is implemented.

1 INTRODUCTION

1.1 *Background*

The extensive deterioration of reinforced concrete (RC) structures due to corrosion is a pervasive concern worldwide. From past studies it has been observed that a major reason for this deterioration is low cover depth that fails to offer adequate protection to reinforcing steel from penetration of environmental agents (CO_2, chlorides, oxygen and moisture) that initiate and propagate corrosion. In addition, it was observed that there is a large variation in cover depth values for site elements.

There are several causes for lack of adequate cover depth which include design faults where cover depth provided is inadequate, poor construction practice and poor structural detailing where reinforcement provisions are not practical on site. Structural designers should avoid increasing design cover depth provisions which may result in cracking and increased penetrability. A recommended approach to address the incidences of inadequate cover depth provision would be to carry out strict controls on quality where cover depths in as-built structures are verified for compliance before and after construction.

1.2 *Provisions for cover depth*

To address the durability concerns in South Africa the Durability Index-based performance approach has been developed where limiting values of durability indices and cover depth are provided based on exposure conditions, required service life and binder type used.

This approach has been implemented by the South African National Roads Agency Limited (SANRAL) in a large scale project, the Gauteng Freeway Improvement Project (GFIP) developed to alleviate the current traffic congestion problems in Gauteng Province. The limit value of cover depth for durability requirements in the project is 40 mm for in-situ and precast elements. This value can be linked to the DI prediction model for carbonation-induced corrosion. The outcome of the model (i.e. carbonation depth development with time for the given input parameters) is illustrated in Figure 1. For a structure to attain the required service life, the carbonation depth should be limited to 40 mm, thus the cover depth provision in the specification. The acceptable ranges of cover depth, allowing for tolerance are minimum cover depth of 30 mm and maximum cover of 55 mm.

2 IN-SITU COVER DEPTH VALUES

Cover depth values were obtained from four bridges in one of the sub-projects in the GFIP. The measurements on bridges were carried out on different structural elements such as abutments, parapets, piers, beams, etc. on a scan area of approximately

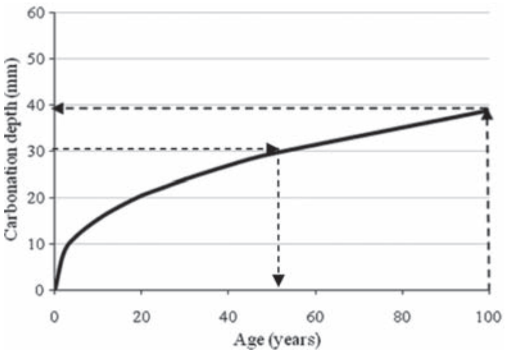

Figure 1. DI prediction model applied to determine limit cover depth value.

1 m^2 that should be randomly located over the entire structure. The total scanned area should represent at least 5% of total surface area of the structure. The average (overall) cover depth for a structural element was determined by obtaining the average of all scanned areas.

From the numerical summary done on cover depth readings, it was observed that the average cover depth complied with the average limit value of 40 mm. However, the variability as measured by coefficient of variation was high ranging from 14.7% to 29.4%. The proportion of values below the minimum value was low with the highest as 1.1% while that of values greater than the maximum was high, as much as 51.4%.

3 PRECAST COVER DEPTH VALUES

The cover depth values for precast elements were obtained from concrete barrier elements used on highways in the GFIP. A total of nine measurements were obtained from a sample of precast elements. The mean cover depth value was 45.1 mm with low variability in readings where the coefficient of variation is 6.3%. The proportion of values below limit value is low at 3.5%. The extent of variability in cover depth readings is low in comparison to that of in-situ structures. This indicates that strict control was exercised in execution of construction practices to ensure that the specified cover depth is attained.

4 DISCUSSION

The payments for cover depth are based on assessment of the overall (average) cover depth of a structural element. For the in-situ and precast elements it is observed that the average values from the cover depth readings considered comply with the limit value of 40 mm. The compliance of the average cover depth with limit value would result in full payment, as provided in project specifications.

This provision may however be inadequate as there is no criterion given for the permissible proportion of values below the acceptable range i.e. the minimum average of 30 mm and maximum average of 55 mm. The practical implication of these high proportions below the minimum would be a reduced service life of the structure (less than 60 years). In addition, a high proportion of values above the maximum value would probably result in increases in crack density and widths, therefore penetrability of the cover with the consequence of reduced service life of the structure.

The variability of precast elements at a CoV of 6.3% was observed to be considerably less than that of in-situ structures (lowest CoV at 14.7%).

5 CONCLUSIONS

The control of cover depth is essential to ensure that a RC structure complies with durability requirements. This paper provides a summary of an analysis of cover depth readings for in-situ and precast structures. It was observed that for the structures considered, precast and in-situ, there was compliance with limit value of 40 mm which would result in full payment. The variability in values of precast elements was considerably lower than that of in-situ structures. Therefore with strict controls in construction, compliance with specified cover depth readings and a low variability in values can be attained.

It is recommended to modify the specifications to determine the permissible proportion of values less than or greater than the minimum and maximum provided. In addition, the payment criteria should be adjusted to consider these proportions to ensure that payments for cover depth are only made on compliance of these values.

Concrete Repair, Rehabilitation and Retrofitting III – Alexander et al. (eds)
© 2012 Taylor & Francis Group, London, ISBN 978-0-415-89952-9

Essential parameters for strength-based service life modeling of reinforced concrete structures—a review

J.O. Ikotun & S.E. Ekolu
School of Civil and Environmental Engineering, University of the Witwatersrand, Wits, South Africa

ABSTRACT: While there are a number of carbonation-induced service life models and extensive data that has been presented in the literature, most do not capture all the necessary parameters to allow their universal application to reinforced concrete structures. Results in the literature generally show an existence of a strong fundamental relationship between carbonation and compressive strength of concrete, but hardly any model has been successful in developing a universal functional relationship for service life prediction. It is often the case that models developed on the basis of a particular data set fail to apply when treated to another data from other authors. These issues indicate the underlying complexity of attempting to determine and emerge the empirical or mathematical functions capable of adequately capturing the key influential parameters affecting observed performance. In a critical review of literature, a variety of parameters in the strength-based models are compiled for a range of potentially plausible models and then examined. Specific interest has been given to models that account or have the potential to account for complex cementitious systems, various types of climates or field exposure conditions. It is found that there is potential to introduce robustness into few selected models that seem, from the literature examination, to closely relate to service life situations and /or needs in Sub-Saharan Africa, among other regions.

1 PAPER SUMMARY

In the recent times, the use of concrete has grown in application to residential, industrial, commercial, innovative structures and constructions. It is pertinent to know that many concrete structures fail to achieve their expected service life due to the limited scientific knowledge on service life design. These issues are some of the major challenges confronting the modern construction industry. Consequently, billions of money is spent annually on repair and maintenance of ageing concrete infrastructure. In 1990, the National Research Council report in the U.S. gave an estimated cost of $2 to $3 trillion required over the next 20 years to repair concrete structures deteriorated by reinforcement corrosion (Hoff 1991) Also, in Sub Sahara Africa and many other parts of the world, a lot of money is spent annually on repairs and rehabilitation of existing concrete structures. The dilemma that has been argued by researchers is the definition of serviceability limit state for evaluation of the service life of the concrete structure. The difficulty is compounded by a myriad of factors such as ageing, global warming, natural disaster, lack of adequate impermeability of concrete, steel corrosion, and internal material reactions (Swamy 2005). Li et al. (2006) suggests that most of the failures in reinforced concrete can be attributed to the emphasis on using factors of safety related to structural strength design with only limited consideration being given to serviceability.

However, the most pronounced form of concrete deterioration in Africa is carbonation-induced corrosion, which normally develops into cracking, delamination and spalling of concrete cover. Several experimental investigations into parameters and design variables that influence reinforcement corrosion have been developed into various models. However, most of these models have been developed basing on short-term accelerated laboratory experiments and their results often show poor agreement with or large variations from the actual real life observations. Also in practice, durability design of concrete is prescriptively done by specifying a minimum concrete cover depending on the exposure conditions, water/cement ratio, compressive strength, corrosion resistance, and diameter of the steel bars. However, there are uncertainties associated with these parameters which are associated to: (i) heterogeneity of concrete, (ii) variability in cover depth, which also hinges on quality control and workmanship during construction, (iii) variability in air CO_2 concentration, relative humidity and temperature of the environment (Zhang & Lounis

2006). These factors eventually lead to considerable uncertainty in service life prediction.

In developing a service life model, it is essential to first examine the accuracy and suitability of corrosion model that will account for essential governing parameters relevant to the local operating environment. In addition, a useful model should be simple but not simplistic, practically easy to execute and should utilize readily available or easily obtainable data. It thus becomes important to consider accelerated test results in conjunction with long—term data from field tests or from existing structures. It is also appropriate to apply stochastic methods of service life evaluation which consider statistically treated variability along with sensitivity analyses of the influential parameters in order to evaluate the impact of their uncertainties on service life (Zhang & Lounis 2006, Otieno et al. 2011, Sarja 2010, Ekolu 2010).

2 CONCLUSION

This paper has been able to review and identify various parameters considered by different authors in modeling of the service life of concrete structures for carbonation-induced reinforcement corrosion. While identifying the essential parameters, limitations and problems in order to make suggestions for an improved robust model that can be suited to application in Sub-Sahara Africa (SSA), among other regions, it is evident that the relationship between the main service life parameters can be universally expressed mathematically to depict the deterioration process in some form of theoretical or empirical model such as the plethora of proposals found in the literature. Most of the service life models are based only on the initiation time to corrosion and give no consideration to corrosion propagation. It has been argued that ignoring the propagation stage may incorporate conservativeness and a safety margin into the model. Another reason favoring the argument is the relatively longer corrosion initiation period compared to the subsequent propagation time which typically lies between 5 to 10 years.

Most of the research studies are laboratory-based experiments where carbonation and corrosion are accelerated in the interest of time. In studies that have included parallel field investigations along with accelerated tests, results typically show strong correlation between the latter and the long-term experimental results. Validation of laboratory results with extensive site specific data on corrosion initiation and propagation is important for wider acceptability and development of empirical models. This aspect presents challenges and at the same time offers opportunities for future research in service life modeling. Existing aged structures can also be used to validate laboratory data for model predictions.

Furthermore, the advent of new binder material systems coupled with new construction technologies rules out suitability of most of the models discussed in the foregone. Extensive coverage of binders and exposure conditions as found in Africa, and incorporation of the effects of new construction materials and technologies are necessary requirements for an effective service life model. Execution of such a model should take into account the randomness of the parameters due to complex interactions of variables. In search of a robust, practically effective service life model, the foregone considerations call for application of the stochastic method along with multivariate analyses.

REFERENCES

Ekolu S.O. 2010. Model validation and characteristics of the service life of Johannesburg concrete structures. *Concrete for a sustainable environment. Concrete Society of Southern Africa. Proc. National Symp., Kempton park, 3–4 September 2010*. Johannesburg: South Africa.

Hoff, G.C. 1991. Durability of offshore and marine concrete structures. Durability of concrete, SP-126. *American Concrete Institute,* Detroit, MI. 33–53

Li, C., Melchers, R.E. & Zheng, J. 2006. Analytical Model for corrosion-induced crack-width in reinforced concrete structure. Technical Paper, *ACI Structural Journal:* 479–487

Otieno, M.B., Beushausen, H.D. & Alexander, M.G. 2011. Modeling corrosion propagation in reinforced concrete structures—A critical review. *Cement and Concrete composites.* (33): 240–245.

Sarja, A. 2010. Reliability principles, methodology and methods for lifetime design. *Materials and Structures.* (43): 261–271.

Swamy, R.N. 2005. Durability design- A holistic philosophy for sustainable construction. *A new concrete code for the 21st Century. Proc. 1st African Concrete Code Symp.* Tripoli, 28–29 November 2005. Libya.

Zhang, J. & Lounis, Z. 2006. Sensitivity analysis of simplified diffusion based corrosion initiation model of concrete structures exposed to chloride. *Cement and Concrete Research. 36*(7): 1312–1323.

Concrete Repair, Rehabilitation and Retrofitting III – Alexander et al. (eds)
© 2012 Taylor & Francis Group, London, ISBN 978-0-415-89952-9

A Virtual Lab for multi-scale modeling of cementitious materials

E.A.B. Koenders
COPPE-UFRJ, Rio de Janeiro, Brazil/Microlab, TU Delft, The Netherlands

E. Dado
Netherlands Defense Academy, Breda, The Netherlands

D.B.F. Carvalho
Pontifícia Universidade Católica, Rio de Janeiro, Brazil

ABSTRACT: Simulating the physical, chemical, material and structural behaviours of cementitious materials has been a challenge to many researchers for many years. Comprehensive analytical and numerical models have been developed for all different scale levels and for all kinds of facets that characterise the materials typical behaviour. In the beginning these models were based on simplified empirical of analytical concepts that were considered to be sufficiently accurate to predict the materials behaviour of a relatively condensed problem mostly at a relatively high scale level (macro scale). Later, after the introduction of the personal computer more computation power became available that could be used to solve more complex models. This enabled the possibility to either simulate the materials behaviour at a more detailed scale level or to simulate more complex multifaceted models at the macro-scale. For cement-based materials, the introduction of the pixel- and particle-based hydration models developed at NIST and Delft could be identified as a milestone and the beginning of a new era in numerical modelling. In-depth schematizations of chemical, physical and morphological processes could be modelled explicitly enabling the simulation of the microstructural evolution of cementitious materials at micro-level scale. In between the micro and macro scale levels, meso-level models (e.g. lattice models) were developed that can be used to simulate fracture processes of two-phase composite systems, i.e. like concrete consisting of paste and aggregates. The latest trend in hydration modelling is to extend the level of modelling detail towards the nano-scale level and to model the development of hydration products explicitly. The development of CSH gel structures can now be schematized explicitly which brings together the formation of hydration products for a given chemical composition and its associated properties. With the introduction of the Virtual Lab called the *"DelftCode"* a multi-scale modelling lab is developed with the aim to line-up the models that are developed for their particular scale-level and to make the results compatible and interchangeable within the modelling framework. The result is a multi-scale simulation tool that covers 10 orders of magnitude, and allows to include various scale effects to be involved in the calculations. The tool can be used for design but also for maintenance and repair assessments of concrete structures.

1 INTRODUCTION

The ongoing tendency towards the miniaturisation of processes is also reflected in research in general and in modelling in particular. The scale level at which material behaviour can be studied is becoming progressively smaller, roughly associating with the developments in optical microscopic techniques as well as with the increase of computer capacity. As a result of this, models have been developed to predict the material behaviours for a specific level of detail, corresponding to a certain range of orders of magnitude such as, macro, meso, micro, and recently also the nano scale level is engaged as a level at which material behaviour can be modelled explicitly. Numerical models are mostly developed for a specific and distinct scale level. Until recently, the three most frequently used modelling levels in materials research were distinguished as, macro-, meso- and the micro scale-level (see Wittmann). At these three levels, the material processes and mechanisms were considered, analysed and implemented into a numerical scheme. In Fig. 1, a schematic overview of these distinct levels is provided.

From the single scale models that operate at the different scale levels as presented, a multi-scale modelling approach that lines-up all the different scale levels would be a next step forward. In this paper a web based initiative for a modelling framework will be addressed that shows a prototype this ambition.

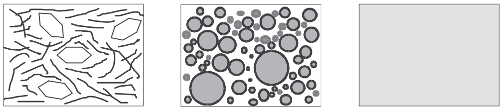

(a) (b) (c)

Figure 1. Schematic overview of (a) Micro-, (b) Meso- and (c) Macro-scale for cement and concrete.

2 THE DELFTCODE

With the ambition to develop a web-based platform that considers the four most decisive scale-levels, i.e. nano to macro, within one single framework, the *DelftCode* has been developed (Fig. 2). The *DelftCode* is an initiative of the Microlab with the aim to line-up numerical models that are developed for their particular scale-level and to make them compatible with the other scale levels within one single modelling framework. The result is a multi-scale simulation tool that covers 10 orders of magnitude and allows for instance to include nano to meso scale level effects into macro scale structures. Each scale level is represented by a "scale-button". After pressing one of these four scale buttons, a model representing that particular scale level will be invoked and numerical experiments (simulations) can be conducted. The calculated data can be shared between the different scale levels optionally.

With the nano scale level being part of the *DelftCode*, the opportunity arises to examine the effect of atomic mutations in chemical structures of the hydration products and how this affects the microstructure. Besides the tailor made design of concrete mixtures, the *DelftCode* structure will also provide the opportunity to examine durability issues and can be used to design the most optimised set op materials properties for repair and rehabilitation of aged concrete elements. The ability to design (new) cementitious materials with improved characteristics towards their expected service-life performance can be evaluated at different scale levels within the *DelftCode* framework. However, the current state of framework is still a preliminary pilot version but modelling tools are being implemented in order to complete the basis of this framework. Different scale level models are currently embedded in the multi-scale framework and will complete the *DelftCode*.

3 MULTI-SCALE MODELLING

In order to be able to transfer data between the different modelling scale levels, multi-scale modelling principles have to be considered as well. Apart from the way how the data is transferred from one scale level to another, most challenging part is how to connect the levels from a modelling point of view.

Figure 2. Home page of the pilot version for the Virtual Modelling Lab, called *The DelftCode*.

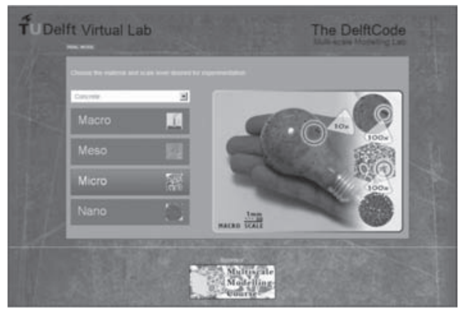

Figure 3. *DelftCode*: Selection of scale level.

Bridging the scale levels can go along with transfer of data only by means of parameters passing or by means of a more complicated integration of models that operate at different scale levels or a possible combination. In either way, bridging the scale levels is an intensive modelling work that requires significant effort both from materials properties as well as from a modelling point of view. With the *DelftCode*, being a virtual modelling lab, the user can choose at which level he/she wants to start the numerical experiments (Fig. 3). It is organized in such a way that data can be calculated in a certain scale level and, when the user decides to proceed with an analysis at another scale level, the data can be taken.

4 CONCLUSIONS

The paper is addressing the pilot version of a Virtual Lab for multi-scale modelling, called the "*DelftCode"*, and is an initiative of the Microlab of TU Delft. The *DelftCode* framework enables the exchange of data among the scale models where the chemical, physical, material or structural data is transferred over the boarders of the nano-micro, micro-meso or meso-macro scale levels. With the *DelftCode* 10 orders of magnitude can be bridged and detailed information be used to optimize design, durability, repair and maintenance concepts of concrete structures.

Concrete Repair, Rehabilitation and Retrofitting III – Alexander et al. (eds)
© 2012 Taylor & Francis Group, London, ISBN 978-0-415-89952-9

Model verification, refinement and testing on independent 10-year carbonation field data

S.O. Ekolu
School of Civil & Environment Engineering, University of the Witwatersrand, Johannesburg, South Africa

ABSTRACT: An extensive range of data generated from a 10-year long-term experimental and field carbonation study was used in this work to test, validate and refine an independent existing model for carbonation prediction in reinforced concrete structures. These data are detailed in the CSIR, 1999 report. In the report, data was generated for twenty one (21) concretes mixtures of nominal strengths 25, 35, 50 MPa made using Ordinary Portland Cement (OPC) or Rapid Hardening Portland Cement (RHC) with or without 15, 30, 50% Fly Ash (FA), each mix being subjected to five (5) different curing regimes prior to exposure of samples to the natural Pretoria weather. Strength and carbonation measurements of the field exposed specimens were determined at the ages of 3.5, 6 and 10 years, along with their compressive strengths. Also determined were compressive strengths at 1, 3, 7, 28, 90, 100 days, 3.5, 6, 10 years for specimens stored under laboratory conditions.

The model has been modified by the author in order to account for the carbonation effect on strength. The good performance by the model on independent data demonstrates its underlying robustness for use in service life prediction.

1 INTRODUCTION

Engineering models typically attempt to capture universal or fundamental concepts and by expressing these in some form of mathematical expressions, the process of determining the future behaviour of a system can be predicted. They are particularly important tools in predicting future performance, which information is usually of value to current knowledge. For example, it is greatly valuable to an owner who invests in physical infrastructure to determine the period of service that can be expected from the structure's physical life.

2 A PLAUSIBLE CARBONATION MODEL

In this paper, a carbonation model which the author of this article considers to be plausible, is subjected to testing and verification (RILEM, 1996).

Previous work (Ekolu, 2010) in which the model was applied to bridges and RC buildings in Johannesburg showed meaningful model predictions and a strong potential for good performance. In this paper, the model is tested and verified against independent, extensive field data of a long-term carbonation study conducted over a period of 10 years and reported in CSIR, 1999.

3 EXPERIMENTAL

The compressive strength and carbonation investigation (CSIR, 1999) conducted from 1988 to 1999 was done using concretes made with OPC, RHC cements. The OPC and RHC cements had 7 day strengths of 41 and 53 MPa respectively, and both cements had 77 MPa at 28 days. The cements are equivalent to CEM I 52.5 and CEM I 52.5R cement classifications of EN 197–1. Fly ash was blended with OPC in proportions of 0 to 50%FA while RHC mixes contained 0 to 25%FA. Three concrete strength grades of 25, 35 and 50 MPa were made according to mix parameters shown in Table 1.

4 STRENGTH DATA

In this analysis, the strength results for laboratory-stored specimen were compared to those for specimen exposed under field conditions at the ages of 3.5, 6 and 10 years as shown in Figures 1 and 2 respectively. There are some interesting observations notable from these strength patterns.

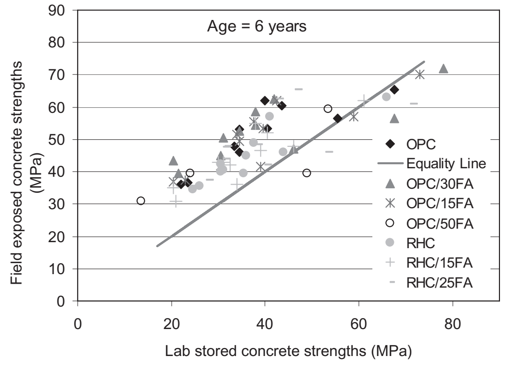

Figure 1. Comparison of 6-year compressive strengths for laboratory-stored and field exposed concretes.

5 CARBONATION DATA AND MODEL PREDICTIONS

Model carbonation rate predictions were conducted basing on different sets of strength results:

1. 28-day strength prior to field exposure (f_{c28})
2. f_{c28} + 8 MPa
3. Strengths of carbonated exposed specimens measured corresponding to the age of field carbonation testing (f_{cbn})
4. Strengths of 50/23 lab-stored specimens measured corresponding to the age of field carbonation testing ($f_{c50/23}$)

No 10-year carbonation data was available, hence model predictions have been limited to 3.5 and 6 year data.

From the foregone model verifications, adjustments to the model are deemed necessary for performance improvement. The model now takes a proposed new form written as:

$$k_c = c_{env} c_{air} a \ (f_c)^{b/s}$$

where, $f_c = f_{ctx}$+ 8 or f_{cbn} such that:

f_{ctx} = mean cube compressive strength at initial time of field exposure

f_{cbn} = mean cube compressive strength of field carbonated concrete at any given age

$1/s$ = strength shift factor for carbonation, given in Table 1

Table 1. Strength shift factor for carbonation.

Cube strength (f_c) used in model	Concrete strength (MPa)		
	<20	20 to 50	>50
$f_{ctx} + 8$	n/a*	1.00	1.00
f_{cbn}	n/a	1.11	1.00

*Note: the model is not applicable to concretes of strengths <20 Mpa.

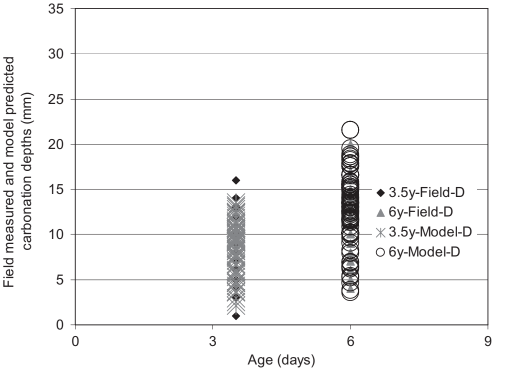

Figure 2. Model tests basing on f_{cbn} after correcting for low strength and high strength concretes.

6 MODEL TESTING

The model tests were conducted for f_{ctx} + 8 MPa and f_{cbn}-based predictions. It can be seen that model prediction results are in agreement with actual measurements.

When the low strength concretes were discarded from the data and a shift factor s = 1.00 was applied to high strength concretes, it can be seen in Figure 2 that the model predicts field carbonation depths much more accurately, with both the measured and predicted carbonation depths lying within the same range of carbonation depth and the extreme points from field measurements being possible outliers.

7 CONCLUSION

A strong correlation was found between predicted and field measured rates and depths of carbonation. The model demonstrates potential robustness for good performance in service life applications.

Concrete Repair, Rehabilitation and Retrofitting III – Alexander et al. (eds)
© 2012 Taylor & Francis Group, London, ISBN 978-0-415-89952-9

Treatment of a stochastic service life prediction model to an evaluation of a distressed two-story RC building

S.O. Ekolu
School of Civil & Envir Engineering, University of the Witwatersrand, Johannesburg, South Africa

Mark Allan
Watch Tower, Johannesburg, South Africa

ABSTRACT: A service life prediction model is applied to a distressed two-storey building structure in Liberia for purposes of examining the model performance. The structure was estimated to be a 30 to 40 year old Reinforced Concrete (RC) structure due to be renovated for use as a residential and office building. Condition survey showed carbonation – induced reinforcement corrosion among structural members. The stochastic parameters used in the model analysis were taken from previous work (Ekolu, 2010). The stochastic model is environmentally sensitive and data from the condition survey was used to assess the model outputs. Basing on the model, the building's service life is estimated to have been in the range of 20 to 30 years. It is found that the model makes generally reasonable prediction of the current condition of the building. But this work also identifies some problems with the model that require research for performance improvement and imbuement of robustness for future use in service life estimation for concrete structures.

1 INTRODUCTION

This paper is an attempt to apply an existing service life prediction model on a reinforced concrete structure so as to evaluate the potential and accuracy attainable. While it is recognised that prediction of service life of a structure is essential for economic aspects associated with repair and maintenance, and risk analysis in certain structures especially the public infrastructure (Ekolu, 2010), accurate prediction of service life of any structure generally continues to be a complex subject of research. There are a number of models (RILEM, 1996; CIB, 2004) in the literature that have been suggested by various authors for different forms of applications, but hardly any of them may bear the acclaim of being universally acceptable or practically suited to various scenarios.

2 BACKGROUND

The two storey RC building in Liberia, estimated to have been constructed in the 1970's, was architecturally designed to be a residential and office building. The owner needed to expand its facilities and intended to renovate the structure for use with its operations. Accordingly, engineering expertise was called upon to examine the condition of the structure and suggest the required repair and/or rehabilitation options. From the outset of the project, it was evident that severe spalling of the concrete cover had occurred leaving exposed steel reinforcement bars. Corroded steel bars were observed in the major structural members especially the slabs and beams. Severe cracking was also found in certain wall sections. With these alarming signs of degradation, it became necessary to conduct a detailed investigation in order to determine the existing capacity of the building. The engineering team then conducted the following assessments (Watch Tower, 2011):

- A condition survey entailing on-site inspection.
- Structural analysis of the existing capacity.

3 CONDITION SURVEY

A condition survey on the building was done as outlined in most of the conventional literature on repair of structures, in order to identify the cause(s) and sources of the distress, determine the extent and severity of the distress, evaluate the appropriate remedial action(s), and prioritize repairs. A photographic record was also made, capturing the distress conditions and features observed in the structural components (see Figures 1 to 3).

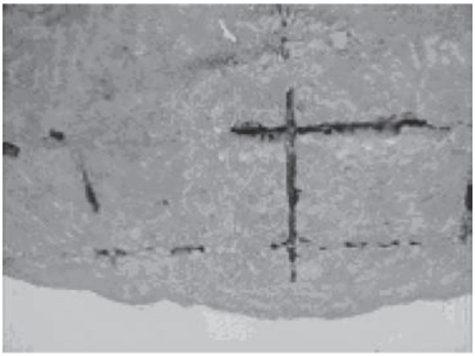

Figure 1. Slab soffits showing a thin concrete cover and corroded rebars.

Figure 2. Field evidence of colour change (to orange) in the outer layer of concrete compared to the original gray colour seen in the interior concrete.

4 LABORATORY TESTS

4.2 *Optical microscopy*

Both tests confirmed that the naturally discoloured region was precisely the carbonation depth. The characteristic features for carbonation can be seen in the micrograph of Figure 3 which was typical of the discoloured concrete region.

6 STOCHASTIC MODEL ESTIMATION OF SERVICE LIFE

Using information determined from field survey and assessment of the R.C structure, the data acquired was treated to stochastic service life estimation. Accordingly, a carbonation (only) prediction model was considered in the analysis.

1. All the seven (7) sites within the structure were classified as ‘sheltered’ from rain.
2. The structural concrete was assumed to be made of ordinary Portland cement (OPC) concrete, although no concrete analysis was conducted to determine the actual type of binder used in the concrete.
3. The mean compressive strengths measured on site were used in the model as opposed to using the characteristic strength value. The strengths from the various structural members generally varied from about 18 to 23 N/mm^2. No adjustments for carbonation effects on strength were considered.
4. The mean concrete cover thickness values determined from field measurements were used in the model.

By considering only the first component of the model, estimation of the time to carbonation of the cover thickness can be made, that is, without considering corrosion propagation. The time to depassivation of steel was taken as the limiting criteria defining the end of service life. Results of

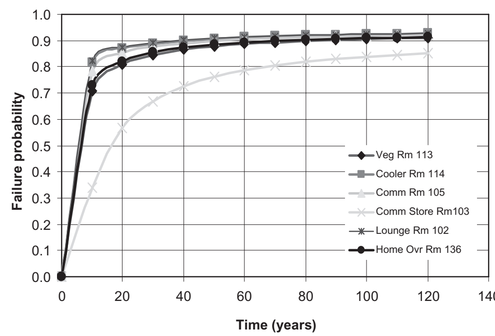

Figure 3. Probability distribution function for carbonation of the structural members.

this analysis are shown in Figure 3 for the seven sites investigated in the RC building. It can be seen that carbonation of the cover thickness progressed quite rapidly in the early ages of the structure. This is consistent with the structurally low strength, low quality concrete. The model also predicts with 80% probability that the full cover thickness of the structural members carbonated within the first 20 years of the structure’s life.

3 CONCLUSIONS

The model predictions appear to place the current service life of the structure in the range of 30 years, while taking note of the broad range of assumptions made for parameters used in the model execution. These predictions also appear to be consistent with the suspected age of the structure. Although the stochastic methodology for service life estimation has been demonstrated, more issues arise concerning the efficacy of the model itself which has been found to be overly sensitive to changes in corrosion rate and bar diameters.

Concrete Repair, Rehabilitation and Retrofitting III – Alexander et al. (eds)
© 2012 Taylor & Francis Group, London, ISBN 978-0-415-89952-9

Methodology for including the age effect of concrete with SCMs in results from accelerated testing

E. Gruyaert & N. De Belie
Magnel Laboratory for Concrete Research, Ghent, Belgium

ABSTRACT: Concrete containing Supplementary Cementitious Materials (SCMs) such as Fly-Ash (FA) or Blast-Furnace Slag (BFS) shows a slower development of its microstructure when compared to mixes with Ordinary Portland Cement (OPC). However, concrete properties are mostly evaluated at the age of 28 days and also accelerated durability tests may start at that age. Therefore, it may be questioned whether the durability of concrete with SCMs is not underestimated when the attack in an accelerated test is concentrated in the initial stage of its lifetime, when its properties have not yet fully developed. On the other hand, when tests are started at later age, e.g. 6 months, one may criticize that in reality the concrete may undergo some degradation already before that age. Therefore, an alternative approach is suggested, in which degradation curves from accelerated tests starting at various ages are first converted to those corresponding with a real environment. Then, the degradation kinetics at different ages are combined into one final degradation curve. This principle is illustrated with data from accelerated carbonation tests in a 10 vol% CO_2 atmosphere, carried out after 1, 3, 6 or 18 months of curing. The results are used to judge whether carbonation-initiated corrosion is a risk for the structure within its life span.

In another approach to compare concrete with SCMs to OPC concrete, some researchers have attempted to determine k-values for fly ash, silica fume and slag with regard to different degradation mechanisms (mainly chloride ingress and carbonation). These k-values may also be time-dependent. An attempt was made to calculate k-values for slag with regard to chloride migration based on experimental test results using a graphical method. The obtained k-values are critically discussed.

1 INTRODUCTION

The durability behaviour of mixes containing blast-furnace slag (BFS) is different from that of ordinary Portland cement (OPC) concrete. In order to evaluate the performance of BFS concrete, accelerated degradation tests are generally executed at the age of 28 days. However, for concrete containing supplementary cementitious materials, it is known that the microstructure develops slower. As a consequence, the results obtained from accelerated degradation tests are sometimes unfavourable and unrealistic for these mixes. On the other hand, concrete structures can sometimes be in contact with aggressive substances at early ages. Therefore, testing at later ages can give too favourable and also unrealistic test results.

In this paper, a methodology for including the age effect in results from accelerated carbonation tests is proposed. Moreover, the applicability of the k-value concept for durability characteristics is evaluated.

2 ACCELERATED DEGRADATION TESTS—MATERIALS AND METHODS

2.1 *Concrete composition*

A reference mixture (S0) containing 350 kg OPC (CEM I 52.5 N), 175 kg water, 791 kg sand 0/4, 425 kg gravel 2/8 and 618 kg gravel 8/16 per m^3 concrete was made. Besides, concrete mixtures with 50% (S50), 70% (S70) or 85% (S85) of the cement replaced by BFS were produced. The specimens were stored in a climate room at 20°C and 95% RH until the time of testing (1, 3, 6, 12 or 18 months).

2.2 *Accelerated carbonation test*

Concrete cubes with a side length of 100 mm were coated (with the exception of one face) and placed in a carbonation chamber (10 vol% CO_2, 20°C and 60% RH). After 2, 4, 8, 16 and 24 weeks, the carbonation depth was measured by spraying phenolphthalein solution on a fresh sawn surface. From the evolution of the carbonation depth (x) (x_0: initial value) in function of square root of time ($\sqrt{t}$), the carbonation coefficient (A) could be calculated (Eq. 1).

$$x = x_0 + A \cdot \sqrt{t} \tag{1}$$

2.3 *Non-steady state migration test (CTH test)*

After a curing time of 1, 3, 6 or 12 months, concrete cores (h 150 mm; ø 100 mm) were drilled out of the concrete cubes and sawn into three identical

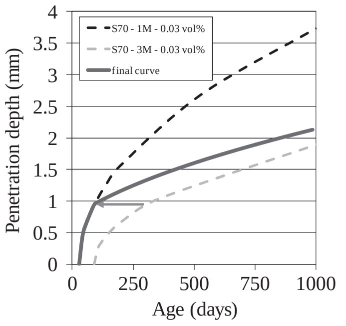

Figure 1. Combination of degradation kinetics at different ages into one final degradation curve.

specimens (h 50 mm; ø 100 mm). The resistance to chloride penetration (D_{nssm}: non-steady-state migration coefficient) was then determined by a non-steady state migration test as described in NT Build 492 (1999).

3 ACCELERATED DEGRADATION TESTS—TEST RESULTS

3.1 *Carbonation*

In comparison to OPC concrete, the performance of BFS concrete is worse with regard to carbonation. Moreover, while a strong decrease of the values of A between 1 (A1) and 3 (A3) months is recorded for BFS concrete, (almost) no change is found afterwards. This means that continuous curing over periods longer than 1 month can still significantly increase the durability properties of BFS concrete, but curing for periods longer than 3 months does not considerably affect the resistance to carbonation anymore.

3.2 *Chloride migration*

The chloride migration coefficients of the reference concrete are significantly higher than those of BFS concrete. No significant differences could be found between the BFS mixes. Moreover, in contrast to the reference concrete, a significant reduction of the migration coefficient is recorded in time for concrete with high cement replacement levels.

4 TIME-DEPENDENT CARBONATION COEFFICIENT

In order to judge whether carbonation-initiated corrosion is a risk for the concrete structure, one may wonder whether the A1 or A3 values must be considered to estimate the carbonation depth within the concrete's life span. While A1 probably give a too unfavourable judgement, A3 maybe gives a too favourable result. Because of all of this, we propose to combine the degradation kinetics at different ages into one final degradation curve, as presented in Figure 1. First of all, the curves from the accelerated tests are converted to those corresponding with a real environment (e.g. 0.03 vol% CO_2). During the first two months (after the concrete is cured for 1 month), it is assumed that the carbonation depth increases with time as indicated by curve 'S70-1M-0.03 vol% CO_2'. However, at the age of 3 months another curve is available which takes into account the ongoing hydration. Since the concrete was already carbonated over ~1 mm (S70-1M-0.03 vol% at 91 days), the curve (S70-3M-0.03vol% CO_2) is shifted to the former (S70-1M-0.03 vol%). Because the carbonation coefficients at 3, 6 and 12 months are roughly the same, the bold curve can be assumed as the final one.

Since curing for 3 months at 20°C and >95% RH is not realistic, we can propose to cure the test specimens for e.g. a few weeks at 20°C and >95% RH, then store them in a climate room at 20°C and 60% RH and determine the values of A at different ages.

5 K-VALUE CONCEPT

An estimation of the k-values was made based on the graphical method. With regard to chloride migration, k-values of 1.3, 1.6 and 1.9 are obtained respectively for BFS in S50, S70 and S85 (3M). This indicates that BFS improves the concrete's chloride resistance considerably. The performance of BFS mixes with regard to chloride ingress corresponded to that of reference mixes with an 'acceptable' w/c ratio. With respect to carbonation, a problem appeared: the worse performance of BFS mixes corresponds to that of reference mixes with a very high w/c ratio. No test results were available for such mixes and uncertain (but also extreme) k-values are obtained.

Remark that the slag-to-cement ratios of the mixes were not limited to the requirements of the k-value concept described in NBN B15-001 (2004).

6 CONCLUSION

In this study, the resistance of BFS and OPC concrete is compared.

- BFS concrete performs better than OPC concrete with regard to chloride attack, while the reverse is the case for carbonation.
- For BFS concrete, the curing time has a significant influence on the resistance. A methodology for including the age effect of concrete with SCMs in results from accelerated carbonation tests is proposed.
- With respect to durability, application of the k-value concept seems to be ambiguous and laborious.

Concrete Repair, Rehabilitation and Retrofitting III – Alexander et al. (eds)
© 2012 Taylor & Francis Group, London, ISBN 978-0-415-89952-9

Lattice model implementation on alkali silica reaction gel expansion in a reacted concrete medium

C. Anaç, E. Schlangen & O. Çopuroğlu
Delft University of Technology, Delft, The Netherlands

ABSTRACT: Modeling of ASR requires consideration of numerous parameters to understand the aspects of gel formation, reaction mechanisms and microstructure of concrete. This study attempts to simulate ASR gel expansion and related crack formation in a concrete matrix. Simulation of local expansion of gel is only possible if the mechanical properties of gel are determined. One of the important input parameters in the model, but also one of the key players in the mechanism of ASR, is the amount of expansion of the gel and as a result the internal forces that are generated by this expansion. A small scale testing set up is used to input to a 2D lattice type model. The expansion of gel formed in a single interface is measured. This study includes internal aggregate deformations due to gel propagation together with ITZ elements in a 2D lattice model.

1 INTRODUCTION

ASR in concrete is often very slow and causes damage after several years. The reaction forms a hygroscopic alkali-silica gel which imbibes water and swells which is the start of the deterioration of the concrete structure. Gel progressively can creep into pores or existing cracks until all space is filled up. Further expansion of the gel will create internal stresses in the concrete matrix, which can lead to cracks propagating radial from the reactive aggregates (Tsuneki 2009).

Modeling efforts are mostly done on material level. Very few attempts have been made on understanding timing and progress of gel in a concrete matrix and link these to accelerated experiment findings.

2 DEGREDATION IN CONCRETE

Modeling ASR requires consideration of numerous parameters with state of art theories. Community is yet far from using a single model to completely simulate the gel formation and generated damage mechanism. In this study authors focus on the damage mechanism of ASR related swelling in hardened concrete medium. Understanding of how cracks propagate in hardened concrete due to disturbance of the internal force system can guide to the development of a rational approach to structural assessment.

Modeling is done in two main groups; (1) modeling of gel formation and its expansion; (2) modeling of ASR related damage. This study attempts to combine both: simulating the correct crack formation and related concrete expansion. The aim is to provide a method for various expansion mechanisms and correlate results with empirical findings.

3 EXPERIMENTAL STUDIES

3.1 *Small scale testing*

As the progress of reaction is slow an accelerated test method needs to be utilized for gel expansion. Based on the work by Andic-Cakir, Copuroglu et al. (2007), a new setup is proposed. Main aim is to create predefined gel continuum surface where expansion and pressure progress can be measured under different boundary conditions.

Designed test setup consisting of a steel box with four-chambers. Each specimen is placed in a chamber and can be tested simultaneously under ultra accelerated conditions (temperature 80°C in 1 M NaOH solution). Two different specimen types are considered for testing. Both have sizes of approximately 20 × 20 × 20 mm. First type is an aggregate-paste "sandwich" where a fixed interface/reaction area is examined. The second type of specimen is a single grain size mortar cube where in addition to the expansion and stress, the crack formations from either boundary condition can be compared. Each pair of samples are subjected to different boundary conditions; free expansion and restrained. The deformation of the specimen is measured using displacement gauge mounted on top. These test results provide information on the

ASR gel formation progress and regarding pressure development.

3.2 *Concrete prism tests—confirmative testing*

Concrete prism test are planned to be partly backward compatible performance tests, based on original mix design from existing structures that have experienced severe expansions due to ASR. The aim is to correlate expansion values and crack patterns to structures with a known reaction history, so the gap between accelerated test results and actual reactions in the field can be linked. For this purpose each test is extended to with 4 additional concrete cubes of sizes 10 × 10 × 10 cm. In the course of the experiments these specimens are taken out used for thin and polished sections analyses on gel progress and damage characteristics. Remaining RILEM tests is based on parameter studies.

4 IMPLEMENTING LATTICE MODEL

4.1 *Image analysis on real samples*

Crack configuration and distribution in the medium influence the post-damage behavior and qualities of concrete (Litorowicz 2006; Mertens and Elsen 2006). Prediction of material properties and damage mechanisms requires quantifying the phases in concrete medium and implementing heterogeneity and irregularity.

In 2009, a highway bridge was demolished for further field and laboratory investigations. Several cores are drilled from the structure at various locations. Digital image analysis has been used to superimpose different phases in concrete section with lattice generated. These polished-section images are converted to a 2D rectangular lattice consisting of 79600 beam elements constituting (Figure 1).

4.2 *Fitting material properties and ITZ*

In the model it is assumed that the gel is formed in ITZ (between aggregate and cement matrix). Local loading has been defined on beam elements located in the ITZ which describes swelling mechanism in this zone. Preliminary simulations assumed all ITZ elements to react simultaneously at the same rate. Then crack formations are compared to real samples. The simulated crack patterns are given in Figure 2.

Crack patterns from impregnated sections and simulations results show close proximity. The simulation has been stopped once the system failed under tension.

For confirmation proposes crack indices are compared. Number of removed elements in the lattice, proportional to over all represented area

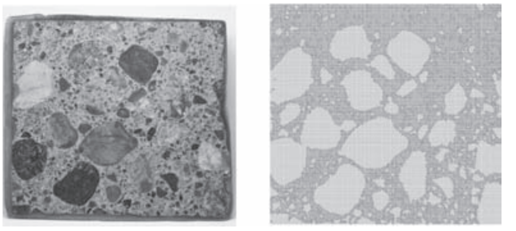

Figure 1. Digitizing 2D section for lattice generation; (1) original impregnated section (2) superimposed lattice elements.

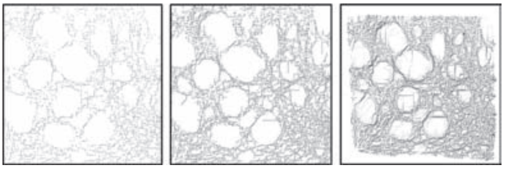

Figure 2. Simulation results—cracked medium after; (1) 3000 steps, (2) 8000 steps, (3) 20000 steps.

can be compared to actual cracks in analyzed section. Binary image analysis and skeleton algorithms will give us approximate crack indices in the image. Also the crack patterns should be quantified and characterized both in the reacted section and the simulation results.

5 DISCUSSIONS AND CONCLUSIONS

Authors emphasis on the fact that implementation of reactive constituents in the model will lead to better representation of damage due to ASR. Forthcoming simulations will involve combinations of aggregate and ITZ elements reacting with varied timing.

In this paper a work-in-progress method is presented to simulate gel swelling with Delft lattice model. Also a procedure and test setup has been explained for identification of local gel properties. Setup enables to create single reaction interface where properties can be tested for various boundary conditions. Lattice model has been developed with the assumption that 2D section is subjected to free expansion. ASR in real life occurs in 3D medium with restraints. However, input for 3D values from real samples is a challenge.

Gel localization may differ for different types and grading of aggregates. These parameters needed to be further tested. Final aim of this study is to provide comprehensive computational tool/method where effects of alkali-silica reaction can be predicted and intensity and distribution of concrete swelling can be quantified throughout the evolution of gel progress.

Concrete Repair, Rehabilitation and Retrofitting III – Alexander et al. (eds)
© 2012 Taylor & Francis Group, London, ISBN 978-0-415-89952-9

A concrete performance assessment tool for structures with alkali silica reaction

C. Anaç, O. Çopuroğlu & E. Schlangen
Delft University of Technology, Delft, The Netherlands

ABSTRACT: This study covers the development of a material Performance Assessment Tool (PAT) on concrete durability by simulating of Alkali Silica Reaction (ASR) deployment. Performance models oblige a multi scale approach from micro to macro level studies. PAT-ASR aims to combine the tasks of guidelines on ASR prevention, performance testing on reactive aggregates, multi-scale material modeling in a comprehensive integrated tool. This project involves experimental studies, among others including the determination of mechanical properties of ASR gel. A computational model, in conjunction with the already developed Lattice Models, will be used for simulating crack patterns in a concrete matrix. Final support tool will provide a guideline for engineers on ASR conscious design.

1 INTRODUCTION

Alkali-silica reactivity generally causes slow (in terms of years) but progressive deterioration due to expansion concrete. Variety of aggregate types, different reactivity and proportions of reactive components in aggregates makes it a challenge to design durable concrete structures with decades of service. Accelerated tests last extremely long and inconclusive to be practical and several variation problems are observed between laboratory test results and real structure measurements. Common practices are to avoid the reactive aggregate, to use low-alkali cement or supplementary cementing materials (SCM). However, understanding the mechanism of the reaction is core for sustainable and durable concrete design.

ASR models mainly base their predictions on curing conditions, temperature, stress and relative humidity effects on free expansion values. Recently, a study is published on three dimensional computational modeling of ASR using finite element model (Comby-Peyrot, Bernard et al. 2009). More recently, Schlangen and Copuroglu (2010) proposed a method on modeling ASR expansion using a new test set up.

2 PERFORMANCE ASSESSMENT

In 2010, Dutch government initiated a research program on advance knowledge management systems for predictive simulation model for service life assessment of concrete structures. In scope of the program, this project aims to develop multi scale material performance assessment tool of ASR development and its effect on durability, namely PAT-ASR. It combines tasks of the available recommendations in a unique integrated tool.

2.1 *Material models and software tool*

Multi-scale models use micro level information for chemical reaction parameters and meso level deformation analysis. Software initially requires chemical and physical properties of materials and concrete mix design parameters to be assigned. This information is used to calculate reactive silicate component of aggregates, parameterization of aggregate properties required for initial threshold values. Users will also be given the option to compare results from literature or existing test results for initial assessment.

Association of expansion values to mechanical properties of ASR gel formation is proved to be challenging task. Schlangen & Copuroglu (2007) proposed a new method for identification of gel properties and proposed a method to use this information in expansion simulation. This method will be further tested with petrographic analysis of reacted specimen. Verification of the model will be done through accelerated test results in the literature, case studies from real structures and experiments in Delft University of Technology (TUD) materials lab. Current efforts are focused on linking experimental results to polished and thin section analysis to rationalize timely progress of reaction products in the matrix.

2.2 *Fracture models*

The modeling part is limited to application of ASR. A numerical model, Delft lattice model (Schlangen 1993) is used for crack formation analysis. Lattice models are capable of simulating fracture mechanism in cement based materials under different loading combinations. Schlangen proved to successfully simulate the softening effect and crack formation on concrete matrix. Specific to ASR, model basically assumes 3 locations for expansion points in the matrix; inside the aggregate, interfacial transition zone (ITZ) or mortar matrix.

Using the quantification and parameterization of aggregate the expansion points in the concrete matrix can be distributed, randomly or specific for the grading. Computational results will be confirmed with the thin section analyses prepared from tests in TUD lab and real structures exposed to ASR (see case studies). The aim is fully simulate an accelerated ASR test. One of the prospect outcomes of this project is to develop standard procedure that allows engineers defining material properties for reliable expansion progress predictions. Then using structural mechanics model, durability performance of structures can be checked for varying or predefined environmental and loading conditions.

3 EMPIRICAL DATA COLLECTION

Two testing approaches are utilized. First is the RILEM recommended accelerated expansion test methods, AAR-3 (at 38°C) and AAR-4 (at 60°C). Both are based on ASTM C1293 and have similar use of concrete prisms. Concrete prism test are planned to be partly backward compatible performance tests, based on original mix design from existing structures. The results provide confirmation and feedback information for proposed damage model. Rest of testing is focused on parameter studies.

Second part is a study of the micromechanical behavior of reactive aggregates. A test set-up is designed and built consisting of a four chamber steel box wherein each chamber a specimen could be tested simultaneously under ultra accelerated conditions, at 80°C. One pair is free to deform and the deformation is measured. Other pair restrained from deformation and the stress generated by the gel is measured. All expansions and stresses measured in a vertical direction (details can be seen on Figure 1). Specimens have same size 203 mm. The first an aggregate-paste "sandwich" where a fixed interface/reaction area is examined, and the second a single grain size mortar cube where in addition to the expansion and stress, the crack formations from either boundary condition can be compared. These test results provide information on the ASR gel formation progress and regarding pressure development.

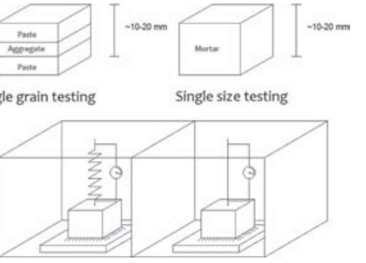

Figure 1. Small scale testing setup by TUD.

By courtesy of our collaborating partners several ASR affected structures are chosen for investigation and analysis. There are ongoing measurements and sampling studies on these structures. Additionally, polished and thin section analysis is done. Norwegian Ministry of Public Works Highways Department has been investigating Nautesund Bridge in Oslo. In 2009, it was demolished for further field and laboratory investigations. Some cores are prepared for thin section and polished section analysis in TUD. They provided extra-ordinary data for our model in defining the micro to meso scale modeling.

In the Netherlands, ASR has been recognized as a major concrete durability issue since 1995. Renewed interest in minimizing distress resulting from ASR emphasizes the need to develop predictable modeling of concrete ASR behavior under field conditions. Data collection for bridges (A59 bridges) started in 2003, involving regular expansion values, relative humidity inside the concrete beams and temperature. Recently there are investigations on several highway bridges. One of these bridges demolished in December 2010, recorded as the first structure demolished due to ASR. Current collaborations with research institutes in the Netherlands will provide more samples from structures linked to ASR damage.

4 DISCUSSIONS

This paper outlines a multi-scale performance assessment tool for ASR affected structures. General principles and methods to be used in this project are listed and discussed as a part of the durable concrete design and service life simulation model. Model covers classification and simulation aspects from micro to macro level issues on ASR in an integrated database. This information can be used in an efficient material management system for durability issues. Model results will be confirmed with case study analysis, real structures and accelerated test results, executed in TU Delft labs. This work will provide a framework of thought which may also be implemented for other degradation processes in cement based materials.

Concrete Repair, Rehabilitation and Retrofitting III – Alexander et al. (eds)
© 2012 Taylor & Francis Group, London, ISBN 978-0-415-89952-9

Relation between mass flow in cement-based composite materials and durability, investigated by means of neutron imaging

F.H. Wittmann
Aedificat Institute Freiburg, Germany

P. Zhang & T. Zhao
Qingdao Technological University, Qingdao, China

ABSTRACT: Mass flow is at the origin of most important deteriorating processes in cement-based composite materials such as mortar and concrete. Water and aqueous solutions can be absorbed by capillary action into the pore space deep and quickly. Pure water leads to leaching and chemical compounds dissolved in water such as sulfates and ammonia can weaken and finally destroy the cement-based matrix by chemical reactions. Chloride dissolved in water can be transported deep into the pore space of concrete by convection and at a later stage even deeper by diffusion. If a critical amount of chloride is accumulated near the steel reinforcement corrosion may be initiated. Neutron imaging is a powerful method to visualize and to determine quantitatively the mass flow in porous materials such as bricks stones and concrete. This advanced method has been applied to study capillary absorption of water and aqueous salt solutions into concrete. The moisture movement into cracks has been studied in particular. It has been shown that water repellent impregnation of the surface of concrete slows down significantly ingress of water and of dissolved aggressive compounds transported with the penetrating water by convection during capillary absorption. Damage caused by frost action accelerates capillary absorption and chloride penetration.

1 INTRODUCTION

The total water content and water movement in porous building materials such as bricks, stones and concrete is most relevant for their durability. By now, there are several destructive and non-destructive test methods to determine water content in cement-based materials. A powerful non-destructive technique is neutron radiography (also called neutron imaging), which is being applied for a wide range of quite different investigations (Zhang et al. (2010a), Zhang et al. (2010b)). In this contribution, we will apply this advanced technique to follow the process of water movement in uncracked and cracked reinforced concrete.

2 EXPERIMENTAL

Mortar specimens having a water-cement ratio of 0.6 have been prepared with the following dimensions: $100 \times 100 \times 300$ mm^3. Part of the mortar prisms have been reinforced with six steel bars having a diameter of 8 mm each. A pre-defined crack width has been introduced by three point bending.

All tests with neutron radiography in this project were performed at the thermal neutron radiographic facility NEUTRA of Paul Scherrer Institute (PSI) in Switzerland (Lehmann et al. (2002)).

3 RESULTS AND DISCUSION

Typical results obtained on a specimen without cracks are shown in Figure 1. The obtained images obtained have been further evaluated by means of existing software IDL. In this way water profiles after certain durations of contact between the surface of the mortar specimens and water have been obtained. Typical results are shown in Figure 2. For the determination of the profiles the rectangular area marked in Fig. 1 has been selected. Moisture profiles move deep into the porous material in a comparatively short time. In practice dissolved ions are transported with the water into the pore space. The penetration depth of ions which is reached by convection during capillary absorption after a few hours would take several years if the transport were based on diffusion.

The process of water penetration into cracked reinforced concrete obtained by neutron radiography is shown in Fig. 3. In this Figure the moisture distribution in the cracked zone is shown after 1 minute, 30 minutes and 60 minutes of contact with

Figure 1. Neutron radiographs taken 30 minutes (left), eight hours (centre) and 72 hours (right) after contact of the surface with water.

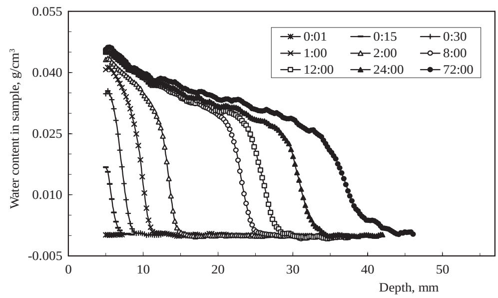

Figure 2. Numerically evaluated moisture profiles in mortar, based on the radiographs shown in Fig. 3, as determined at different durations of capillary absorption.

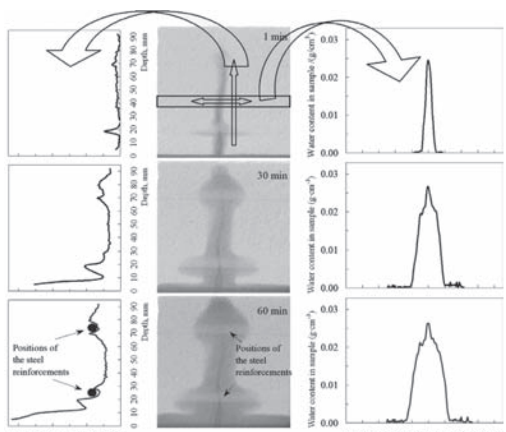

Figure 3. Visualization of water penetrating a crack and migration from the crack into the porous material.

water. The artificial crack (crack width ≈ 0.35 mm) is filled immediately with water. It has also been shown that much finer cracks are also filled with water immediately.

The damaged interfaces between the reinforcement and the cement paste are also immediately water filled. If the surface of a cracked structural element will be in contact with seawater chloride will immediately be in contact with the steel reinforcement.

In order to evaluate the water profiles quantitatively, the water content has been calculated along two axes. The vertical axis has been placed just right of the crack and the horizontal axis slightly below the centre as marked in Fig. 6. The results obtained are shown in the left column and in the right column of Fig. 6 for the vertical moisture movement and the horizontal movement respectively.

It has also been shown that capillary absorption is significantly accelerated it the material is damaged by prior frost action. In this way more chloride can be transported deeper into the pore space of concrete, hence the service life of reinforced concrete structures is considerably shortened by combined frost damage and chloride penetration.

4 CONCLUSIONS

Neutron radiography can be applied to observe water penetration into porous building materials such as concrete and mortar quantitatively with high sensitivity and spatial resolution. Cracks, even fine cracks, are instantaneously filled with water when the surface of concrete is placed in contact with water. In this way dissolved aggressive chemical compounds can be transported deep into structural elements within seconds upon contact with the surface of concrete. Water also penetrates from the crack into the adjacent material following a square root of time law as predicted by theory. Quantitative data obtained from neutron radiography will provide us with the necessary information for development of realistic predictive models to describe uptake of water and aggressive chemical compounds dissolved in water by porous materials such as concrete. Neutron radiography is a very sensitive and non-destructive method. It has also good spatial resolution. Results provide us with a reliable basis of numerical simulation of water ingress and moisture movement both in cracked and uncracked concrete. Capillary absorption is a good indicator for durability of reinforced concrete in marine environment as chloride will be transported first into the pore space by convection.

REFERENCES

Lehmann, E.H., Kuhne, G., Vontobel, P. & Frei, G. 2002. The NEUTRA and NCR Radiography Stations at SINQ as User Facilities for Science and Industry, *Proc. 7th World Conference of Neutron Radiography*, Rome, Italian National Agency for New Technologies, 593–602.

Zhang, P., Wittmann, F.H., Zhao, T. & Lehmann, E.H. 2010a. Neutron Imaging of Water Penetration into Cracked Steel Reinforced Concrete, *Physica B: Condensed Matter*, 405(7): 1866–1871.

Zhang, P., Wittmann, F.H., Zhao, T., Lehmann, E.H., Tian, L. &Vontobel, P. 2010b. Observation and Quantification of Water Penetration into Strain Hardening Cement-based Composites with Multiple Cracks by means of Neutron Radiography, *Nuclear Instruments and Methods in Physics Research Section A*, 620(2/3): 414–420.

Modelling and prevention of reinforcement corrosion

This page intentionally left blank

Concrete Repair, Rehabilitation and Retrofitting III – Alexander et al. (eds)
© 2012 Taylor & Francis Group, London, ISBN 978-0-415-89952-9

Assessment of some parameters of corrosion initiation prediction of reinforced concrete in Persian Gulf region

A.A. Ramezanianpour
Head of Concrete Technology and Durability Research Center, Amirkabir University of technology, Tehran, Iran

E. Jahangiri & F. Moodi
Member of Concrete Technology and Durability Research Center, Amirkabir University of technology, Tehran, Iran

ABSTRACT: Chloride ion ingress is one of the major problems that affect the durability of concrete structures such as bridge decks, concrete pavements, and other structures exposed to harsh saline environments. Therefore, durability based design of concrete structures in severe condition has gained great significance in recent decades and various mathematical models for estimating the service life of reinforced concrete have been proposed. In spite of comprehensive researches on the corrosion of reinforced concrete, there are still various controversial concepts in quantitation of durability parameters such as chloride diffusion coefficient and surface chloride content. Effect of environment conditions on the durability of concrete structures is one of the most important issues. Hence, regional investigations are necessary for durability-based design and vaidation of the models.

Persian Gulf is one of the most aggressive regions of the world because of elevated temperature and humidity as well as high content of chloride ions in sea water. The aim of this study is evaluation of some parameters of durability of RC structures in marine environment from viewpoint of corrosion initiation. For this purpose, some experiments were carried out on the real RC structures and in laboratory. The result showed that various uncertainties in parameters of durability were existed.

1 INTRODUCTION

One of the most corrosive conditions for the reinforced concrete in terms of durability is marine exposure. Damages caused by steel corrosion of structures constructed in marine areas result in extremely high rehabilitation costs annually.

Several factors affect on durability of reinforced concrete structures located in marine environments. However, numerous studies indicate that the predominant reason of reinforced concrete deterioration is chloride-induced corrosion.

In recent decades, several service life prediction models considering material characteristics and exposure conditions have been proposed by various researchers.

In this study, some important parameters of durability that affect on prediction models were evaluated by test on some real RC structures located in Persian gulf region. Additionally, some test was done on samples that similar to concrete composition of structures in laboratory. Structures consist of five jetties that implement at different ages. Finally, corrosion initiation time was estimated by two famous and two local service life prediction models.

2 STRUCTURES AND MARINE CONDITIONS

The under investigation structures are five separate jetties located in the southern part of Imam Khomeini Port Complex having a similar mix design. These structures are constructed at different ages which allow the models to be evaluated in five different ages (A: 2, B: 3, C: 4, D: 5, and E: 6years old). Furthermore, the codes ATM and TID were used to indicate the atmospheric and tidal zones, respectively. Table 1 presents the concrete mix design and Figure 1 shows the structures.

3 EXPERIMENTS

For this study, two series of experiments were performed. First series was performed on concrete

Table 1. Concrete mix design.

w/c	0.35
Cement content [kg/m^3]	450
Silica fume [%]	7%
Fine aggregate [kg/m^3]	864
Coarse aggregate [kg/m^3]	866

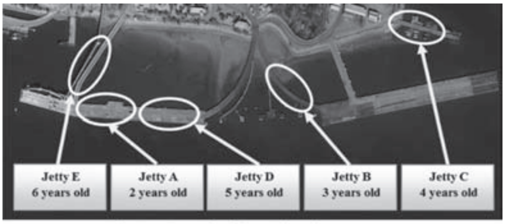

Figure 1. Under investigation structures.

Table 2. In lab test results.

Test	Result
RCMT [mm^2/years] (in^2/years)	169 (0.262)
RCPT [Coulombs]	1365 Low
Resistivity [K.W.cm]	36 Low
Compressive strength [MPa] (Ksi)	75.8 (110)

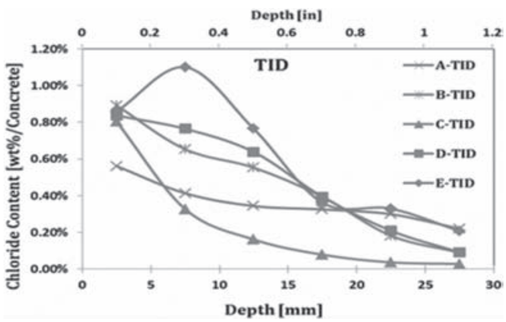

Figure 2. Chloride profiles obtained from the structures.

samples with a concrete mix design similar to structures (Table 2) and the second series of the tests was performed on the structures (Fig. 2).

4 ANALYSIS OF THE RESULTS

4.1 *Laboratory studies*

Results of tests are evidences for considering durable concrete against chloride ion penetration of mentioned structures and all results are confirmed by their related code of practice in terms of durability.

4.2 *In situ studies*

Diffusion coefficient and surface chloride ion content are the most important parameters in estimation of concrete behavior in chloride ion transport into the concrete. Past laboratory studies indicated this fact that apparent diffusion coefficient decreases and surface chloride content increases over time. Obtained results of chloride ion profiles represent this issue in a general case (Fig. 3).

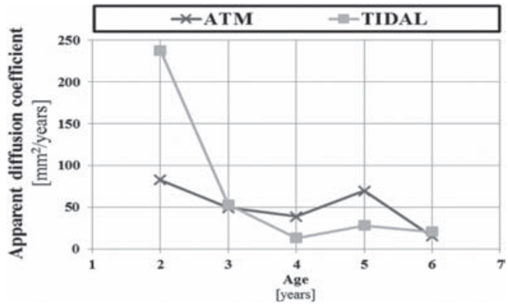

Figure 3. Variation of apparent coefficient of diffusion.

Table 3. Prediction of corrosion initiation time by models.

	Tidal zone	ATM zone
BHRC	15	–
DuarPGulf	66	193
fib	6	22
Life-365	12	23

4.3 *Estimation of the start time of corrosion*

In this section provided models are used to estimate the start time of corrosion for structure's concrete considering the zone weather conditions. These models include: fib, Life-365 and two local models provided by local Research Center (Table 3).

5 SUMMARY AND RESULTS

One of the elements of maintenance plan is analysis of life cycle. In this study, it is attempted to investigate the estimation of service life of reinforced concrete structures from the technical perspective. According to the studied results, it seems that durability parameters that are effective in the estimation of service life have been confronted strong uncertainty. On the other hand, the difference between laboratory results and the actual conditions remind us about this fact that what happens in the reality in the concrete structures will differ from what happens in the experimental results. It indicates that experimental results are valid only if be consistent with test results on the real structures.

Finally, according to performed investigations it seems that making quantitative parameters out of qualitative parameters of durability is one of the most complicated stages of the modeling that generally has confronted strong uncertainties.

REFRENCES

Ashrafi, H.R. & Ramezanianpour, A.A. 2007. Service Life Prediction of Silica Fume Concretes. International Journal of Civil Engineering. 5(3).

Gsosh. P., Hammond, A. & Tikalsky, P.J. 2011. Prediction of Equivalent Steady-State Chloride Diffusion Coefficients. *ACI Materials Journal*.

Nilsson, L.O. 2009. Models for chloride ingress into concrete – from Collepardi to today. *International Journal of Modelling, Identification and Control*, 7(2): 129–134.

Poulsen, E. & Mejlbro, L. 2005. Diffusion of Chloride in Concrete. Taylor & Francis. London & New York.

Ramezanianpour, A.A. & Miyamoto, A. 2000. Durability of concrete structures in the Persian Gulf, *Concrete Journal, Japan Concrete Institute.* 38(3).

Ramezanianpour, A.A. & Pourkhorshidi, A.R. 2004. Iranian code for durable concrete in Persian Gulf and Omman Sea. *Building Engineering and Housing Science Journals*. 2(4).

Concrete Repair, Rehabilitation and Retrofitting III – Alexander et al. (eds)
ISBN 978-0-415-89952-9

Possibilities and restrictions for the use of stainless steel reinforcement

U. Nuernberger
Institute of Materials in the Civil Engineering, University of Stuttgart, Germany

ABSTRACT: The object of this contribution is to provide engineers with an appreciation of the corrosion protection process of stainless steel embedded in concrete. Discussed main focuses are the influence of the steel type, the presence of welds, of the chloride content and of carbonation. The resistance to galvanic corrosion (contact with carbon steel) and cost aspects are also treated. The results consider laboratory tests, field tests and practical experiences. In conclusion, one can say that ferritic stainless steel with at least 12 mass-% of chromium might be the best choice in moderately aggressive environments (carbonated concrete or concrete exposed to low chloride levels). Austenitic stainless steel of type CrNiMo 17-12-2 and ferritic-austenitic (duplex) steel CrNiMoN 22-5-3, even in the welded state, proved to give excellent performance in chloride-containing concrete, even at the highest chloride levels that appear in practice.

1 INTRODUCTION

In reinforced concrete structures the concrete guarantees chemical and physical corrosion protection of the unalloyed reinforcement. Loss of durability caused by poor design and construction only occurs if the passivating oxide layer is rendered unstable due to carbonation of the concrete or to the ingress of chlorides to the steel/concrete interface. In such cases in which it is difficult to achieve the specified design life additional corrosion protection methods are needed. Stainless steel reinforcement which is proposed and used for new reinforced concrete structures and for repair may be an economical and technically attractive approach. Although the initial cost of stainless steel is much higher than that of carbon steel, its use can be justified on the basis that the increase in total project cost is small and is easily overtaken by the benefits of lower maintenance and repair costs.

Stainless steels are corrosion resistant highly alloyed steels which in contrast to unalloyed steel, do not show general corrosion and noticeable rust formation in the atmosphere and in aqueous media. Basic requirement is a minimum concentration of that steel on chromium which is responsible for passivation. Chromium, molybdenum and nitrogen are important elements in relation to pitting corrosion. Nickel especially increases corrosion resistance in acid media. Within the area of concrete reinforcement, three types of stainless steels are generally available in the required product form. These are the chromium alloyed ferritic steels as well as the chromium and nickel alloyed austenitic and ferritic-austenitic (duplex) steels. Interest in the use of these alloys as reinforcing steel for concrete is due to their increased resistance to corrosion, particularly in chloride containing media.

The corrosion resistance required for use in concrete is primarily a resistance against pitting corrosion in chloride containing media. The danger of pitting corrosion decreases with a decline of chloride content and rising pH-value. Therefore, stainless steels are basically more resistant in concrete construction with a pH-value of about 8 to 13 than in atmospheric weather conditions.

Pitting corrosion further depends on the steel composition as well as its surface condition. Weld joints are above all more exposed to the danger of pitting corrosion than are similar non-welded steels, since oxide films (temper colours) reduces passivity.

2 EXPERIENCES WITH APPLICATION

Stainless steel reinforcement has been successfully applied in concrete structures in many countries. Typical applications are structures which are exposed to very aggressive environments. An increasing amount of stainless steel reinforcement is to be found in bridge engineering, multistorey car park decks, tunnels, retaining walls, marine structures like piers at the sea coast, where influence of seawater or deicing salt cannot be excluded.

A case of long-term application of stainless steel reinforcement (1.4301) from the Mexican Gulf is reported. 60 years after construction no significant corrosion was found for the reinforcement, despite the extremely high chloride contents. For other piers at the same place reinforced with ordinary carbon steel, serious chloride corrosion problems occurred.

3 STAINLESS STEEL CORROSION

A number of electrochemical tests, accelerated laboratory tests and long-term site exposure tests have been made with stainless steel rebars (Nuernberger 1996, Nuernberger & Reinhardt 2009). In the following it is reported about own tests (Nuernberger et al. 1993). These are representative for many other investigations. To characterize the corrosion behaviour of stainless steel bars, electrochemical tests to determine the pitting corrosion potential were carried out together with field tests on reinforced elements under typical corrosion conditions. The tests mainly took into consideration the steel type

- 1.4462-X2CrNiMoN 22-5-2 ferritic-austenitic,
- 1.4571-X6CrNiMoTi 17-12-2 austenitic,
- 1.4003-X2CrNi 12 (ferritic)
- one unalloyed steel for comparison.

The materials were tested in the arc-welded and unwelded condition. The concrete was alkaline and carbonated and contained up to 5 mass-% chloride

The following conclusions can be drawn:

- Unwelded ribbed stainless steel reinforcing bars in concrete with chlorides show a higher corrosion resistance, than welded bars.
- The resistance to pitting corrosion decreases gradually in the three steel groups: ferritic-austenitic and austenitic steel-ferritic steel-unal-loyed steel.
- In carbonated concrete the pitting corrosion is more pronounced compared to alkaline concrete with the same amount of chloride.

Figure 1 summarizes the results concerning the corrosion attack by means of corrosion degrees:

- As expected, unalloyed steel bars corrode in carbonated and/or in chloride contaminated concrete. The strongest attack occurred in carbonated plus chloride-contaminated concrete.
- The unwelded low-chromium ferritic steel of type 1.4003 showed a distinctly better behaviour than unalloyed steel. The critical chloride content for pitting corrosion is about 1.5 to 2.5 mass-% depending on state of surface, type of cement (pH-value of pore liquid) and concrete quality. The tendency to concrete cracking is distinctly lower than for corroding unalloyed steel. In chloride contaminated concrete the steel may suffer a stronger attack if the concrete is carbonated.
- For the welded steel within the weld line, chlorides in the order of ≥0.5 mass-% produce locally distinct pitting corrosion. The depth of pitting increases with increasing chloride content and is more pronounced in chloride-containing carbonated concrete. For the ferritic chromium steel the pitting at weld lines is deeper than for unalloyed steel, but the overall general corrosion (loss of weight) is significantly smaller.
- The higher alloyed steels 1.4571 and 1.4462 have a very high corrosion resistance in all the environments tested.

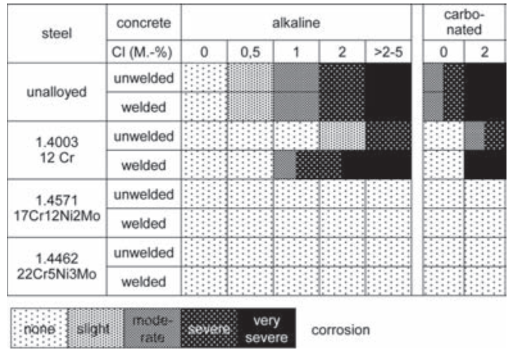

Figure 1. Corrosion attack after 2.5 years field tests (survey).

In conclusion, one can say that ferritic stainless steel 1.4003 might be the best choice in moderately aggressive environments (carbonated concrete or exposed to low chloride levels). Austenitic stainless steel of type 1.4571 and ferritic-austenitic 1.4462, even in the welded state, proved to give excellent performance in highly chloride-containing concrete.

REFERENCES

Nuernberger, U., Beul, W. & Onuseit, G. 1993. Corrosion behaviour of welded stainless reinforced steel in concrete. *Otto-Graf-Journal, FMPA BW Stuttgart*, 4: 225–259.

Nuernberger, U. (1996). Stainless steel in concrete. *European Federation of Corrosion*, book number 657.

Nuernberger, U. & Reinhardt, H.-W. 2009. Corrosion protection of reinforcing steels. *Fib technical report*, bulletin 49.

Concrete Repair, Rehabilitation and Retrofitting III – Alexander et al. (eds)
© 2012 Taylor & Francis Group, London, ISBN 978-0-415-89952-9

Service life extension of concrete structures by increasing chloride threshold using stainless steel reinforcements

H. Mahmoud, M.C. Alonso & M. Sanchez
Research Centre of Safety and Durability of Constructions and Materials (CISDEM) UPM-CSIC, Madrid, Spain

ABSTRACT: Chloride Threshold (CT) of high strength and parent duplex stainless steel (2304 SS type) has been investigated employing accelerated electrochemical tests (potentiodynamic and potentiostatic techniques). The results show that 2304 SS has an excellent long-time corrosion resistance both in direct contact with alkaline environments that simulate the concrete pore solution and in mortar made with OPC. Potentiostatic tests give higher CT than potentiodynamic tests. The CT values measured in alkaline simulated pore solutions indicate that the cold drawn has higher corrosion resistance than the parent stainless steel, moreover the CT increases as the pH of the pore solution also does. The CT measured for 2304 duplex SS embedded in mortar and immersed in 1 M NaCl solutions, using potentiostatic test, also confirm that cold drawn SS shows higher CT (2.8 ± 0.3% total Cl by weight of cement) respect to parent SS (2.3 ± 0.2%).

1 INSTRUCTION

Nowadays, stainless steels are being considered by constructions specialists to increase the service life of concrete structures (Nürnberger 1999, Castro-Borges et al 2007, Alonso et al 2010). The corrosion behaviour of these materials can be evaluated by the determinations of the Chloride Threshold (CT) which is considered as a key parameter in predicting the service life of reinforced concrete structures exposed to chloride environments, (Gulikers 2006). The reported CTs in literature for SS scatter over a large range due to different reasons, as the testing conditions and methods employed (Bertolini et al 2011, Alonso et al 2010). Furthermore, the SS CT implies significant effect of the SS chemical compositions and microstructure (Milan 2010, Hamada 2006), SS surface finishing and welding scale (Nürnberger 2005, Sorensen 1990, Bertolini 2009).

In the present work, CT of high strength and parent 2304 duplex stainless steel was determined. The influence of different significant parameters has been analyzed: the methodology for the CT determination (potentiodynamic and potentiostatic electrochemical techniques), the exposure media (chloride contaminated alkaline solutions, simultaneously added or after passivation and using mortar samples) and the steel microstructure (cold-drawn and parent).

2 EXPERIMENTAL PROCEDURE

Smooth parent and cold drawn duplex 2304 stainless steel wires of 9 and 4 mm in diameter have been tested for chloride threshold determination.

The CT of cold drawn and parent was determined in simulated pore alkaline solutions and in mortar. Fresh alkaline solutions were prepared for each test, all saturated in $Ca(OH)_2$ (pH ≈ 12.5 at 25°C) and some containing also 0.5 M KOH (pH ≈ 13.5 at 25°C). De-ionized water free of CO_2 was used to prepare the test solutions to guarantee the alkalinity of the environment.

- *Potentiodynamic CT test:* The aim of the test is to identify the pitting potential, E_{pit}, indicative of the corrosion onset and also the repassivation capacity E_{rep}, at a critical Cl concentration and pH. In present work, the potentiodynamic curves (CV) were performed using scan rate of 1 mV/s, within the potential region between −1.2 to +0.9 V_{SCE} starting from the cathodic potential.
- *Potentiostatic CT test:* This test was performed by immersion of the tested wires in the alkaline solution and polarization to +250 mV_{SCE} for 24 hours in order to allow the formation of the passive layer. The current of the system is recorded to identify the residual current after passivation. Then the NaCl was added gradually until detecting of the pitting corrosion initiation characterized by sudden increases in the current density.

Potentiostatic CT determinations of cold drawn and parent 2304 stainless steel wires in mortar (cement/sand ratio 1/3 and w/c = 0.5) were performed. Prismatic specimens of 2.4 × 4 × 4 cm size were prepared, without adding chlorides during mixing. Ordinary Portland Cement (OPC) with low alkali and aluminate content was used to reduce the bound chlorides. The mortar specimens were cured in a chamber at 95% RH and 20 ± 2ºC for 15 days previously to initiate the test in order to guarantee the passivation of the SS bars. The potentiostatic tests were performed on mortar samples immersed in 1M NaCl solution. A constant potential of +250 mV_{SCE} was applied during chloride penetration until the onset of corrosion in each SS bar is detected. The total cell current and the current passing through each immersed mortar sample were periodically measured during the potentiostatic test.

3 RESULTS AND DISCUSSION

3.1 *Influence of testing method in CT*

The present CT results obtained form the potentiodynamic and potentiostatic tests indicate that, the cold drawn stainless steel has a relatively higher corrosion resistance than the parent wires. Moreover, the parent wires are more susceptible for pitting corrosion than the cold drawn rebars reflected in higher ΔE. Besides, higher CT values were reported in alkaline solutions with higher pH.

By comparison CT from potentiostatic test of the cold drawn and parent SS, in alkaline solutions it can be observed that, the first shows higher corrosion resistance. The CT determined using CV for cold drawn and parent are lower than from potentiostatic tests in the same solutions (pH 12.5). This observation matches with the results obtained by Bertolini et al 2011, who also stated that potentiodynamic polarization test is a fast technique but lower CT values are obtained than using potentiostatic tests. It can be considered that the differences may be related to the different grown passive films using different electrochemical techniques as suggested by (Sanchez et al 2011).

3.2 *Potentiostatic CT variability of SS in mortar*

The obtained CT values and the depassivation time of the tested stainless steels in mortar specimens are listed in table 1. The CT values are expressed in % of total chloride by cement weight. The test results show that, corrosion initiation was observed on the parent SS in mortar when the chloride content at the steel surface increased above 2.3 ± 0.2% total chloride, while cold drawn SS shows always some higher corrosion resistance, 2.8 ± 0.3% total chloride.

By comparing the CT values in mortar with literature data, it was found that, the data obtained in present work led to reasonable CT values, above 2% and quite similar to those given by Bertolini et all (2011) using also the 2304 SS.

Table 4. CT values in % total Cl by cement weight and depassivation time of cold drawn and parent 2304 SS embedded in mortar.

	2304	
SS	CT (% Cl total)	Depassivation time (days)
R1-Parent	2.14	177
R2-Parent	2.41	240
R1-Cold drawn	2.43	167
R2-Cold drawn	2.45	267
R3-Cold drawn	3.08	237
R4-Cold drawn	2.78	240

4 CONCLUSION

This study focused on the evaluation of the corrosion resistance of 2304 duplex high strength stainless steels through out the determinations of CT in aggressive alkaline solutions and in mortar as well. The results highlight the following:

- The testing method influences in CT, Potentiodynamically CT values are lower than CT by potentiostatic tests.
- The SS microstructure also influences in CT. Cold drawn shows higher Cl corrosion resistance than parent.
- The higher the alkalinity of the environment the higher the CT for pitting corrosion.
- The CT in mortar for duplex SS 2304 varies from 2.8% total Cl for cold drawn to 2.3% for parent.

REFERENCES

Alonso, M.C. et al. 2009. New materials and systems for prestressing structure, European Community, Cost 534 Workshops: 22–36.

Alonso, M.C., Ueli, A., Sanchez, M. & Ann, K.Y. 2010. Onset of chloride induced reinformcent corrosion, Handbook of concrete durability, Middleton publishing Inc., 2-48. Alvarez S.M., Bautista A., Velasco, 2011 Corrosion behaviour of corrugated lean duplex stainless steels in simulated pore solutions. *Corrosion science* 53: 1748–1755.

Bertolini, L. & Gastadli, M. 2009. Corrosion Resistance of Austenitic and low-Nickel duplex stainless steels bars, EUROCOR-Nice 2009.

Bertolini, L. & Gastadli, M. 2011. Corrosion Resistance of low-nickel duplex stainless steels rebars, *Materials and Corrosion*, 62(2): 120–129.

Castro-Borges, P., Cardenas, A., Torrs-Acosta, A., Martinez-Madrid, M., Moreno, E. & Troconis de Rincon, O. 2007. Chloride profiles in a 63-year old concrete pier reinforced with 304 stainless steels in Mexico, *Proceeding of the 5th international conference on concrete under server conditions of environmental and loading*, Toures. France: 143–150.

Gulikers, J. 2006. Considerations on the reliability of service life predictions using a probabilistic approach. *Journal de Physique* IV, 136: 233–241.

Hamada, A.S, Karjalainen, L.P. & Somani, M.C. 2006. Electrochemical corrosion behaviour of a novel submicron-grained austenitic stainless steels in an acidic NaCl solution. *Materials Science and Engineering* A43: 211–217.

Kouril, M., Novak, P. & Bojko, M. 2010. Threshold chloride concentrations for stainless steels activation in concrete pore solutions, *Cement and Concrete Research* 40: 431-436.

Nürnberger U. 1999. Stainless steels reinforcement. Cost action 521-corrosion of steel in reinforced concrete structure, final report: 144-28.

Nürnberger U. 2005. Stainless steels reinforcement—A survey. *Otto-Graf-Journal*, 16: 111–158.

Sánchez, M., Mahmoud, H. & Alonso, M.C. 2011. Electrochemical response of natural and induced passivation of high strength duplex stainless steels in alkaline media. *Journal of Solid State Electrochemistry,* ISSN 1433-0768.

Sorensen, B, Jensen, P.B. & Maahn, E. 1990. The corrosion properties of stainless steels reinforcement—Corrosion of Reinforcement in Concrete, Eds. Page C.L, Treadaway K.W.J, Bamforth P.B. Elsevier Applications Science: 601–610.

Concrete Repair, Rehabilitation and Retrofitting III – Alexander et al. (eds)
 ISBN 978-0-415-89952-9

Working life of cathodic protection systems for concrete structures—analysis of field data

R.B. Polder
Civil Engineering & Geosciences, Delft University of Technology, The Netherlands
TNO Technical Sciences/Building Materials, Delft, The Netherlands

G. Leegwater
TNO Technical Sciences/Building Materials, Delft, The Netherlands

D. Worm & W. Courage
TNO Technical Sciences/Structural Reliability, Delft, The Netherlands

ABSTRACT: Corrosion of reinforcing steel in concrete structures causes concrete cracking, steel diameter reduction and eventually loss of safety. In infrastructure this is mainly due to penetration of chloride ions from de-icing or marine salts. Conventional repair means heavy, labour intensive and costly work, and economic pressures (time and money) work against the required quality level. Consequently, conventional repair is short lived in many cases in practice. Corrosion reappears quickly and the structure needs to be repaired again after a relatively short time, further increasing life-cycle cost. A completely different situation comes about with Cathodic Protection (CP) of steel in concrete as a repair method. Cathodic protection has been applied to concrete structures with corrosion damage for more than 25 years. This paper reports experience and data of costs for maintaining CP systems, based on an inventory of CP systems in the Netherlands installed between 1987 and 2010. For 105 structures with CP, performance and maintenance data were obtained. The large majority provides corrosion protection for a long time. Degradation of components and overall systems seems to occur in limited numbers. Failure of components and total systems as a function of age is quantified. On the average, the time until minor repairs of parts are necessary is about 15 years. Global failure of the anode, which necessitates near complete replacement of the system, is rare. Based on the statistical analysis of field data, the cost of maintaining a CP system was modelled in terms of life cycle cost.

1 INTRODUCTION

Corrosion of reinforcement in concrete infrastructure may occur due to penetration of chloride ions from de-icing salts or sea water. Corrosion causes concrete cracking, steel diameter reduction and eventually loss of safety. A European study of the performance of traditional repairs has shown that they had a short life in practice. Experience with CP suggests it has a much longer life. A survey of CP systems in the Netherlands was carried out.

2 RESULTS

The basic components of a concrete CP system are shown in Figure 1. Between 1987 and 2009, about 150 structures have been provided with CP. The survey produced good documentation of design, performance and maintenance for 105 of them. The large majority of CP systems provides corrosion protection for a long time.

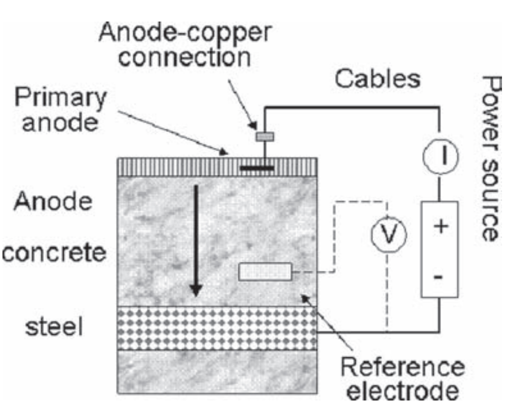

Figure 1. Basic setup of a concrete CP system.

In a limited number of cases, intervention was necessary due to failure of anode-copper connections, primary anodes, reference electrodes and power units. Complete failure of the anode was rare; and no cases have been reported where corrosion had reappeared. Local anode failure occurred in a number of cases, mainly due to local water leakage. Failing parts were replaced or repaired, generally for modest amounts of money, restoring proper CP operation. Thus, maintaining good corrosion protection in previously corroding structures using CP over for example 25 years is a matter of spending some money to maintain the system. Based on survival analysis of the field data a life cycle cost model was built. Results are given for an example case.

3 LIFE CYCLE COST CALCULATION

Based on survival analyses, failure probabilities as a function of time were estimated for the following failure modes: global anode failure; local anode failure; primary anodes; connections; reference electrodes; power units. Combining failure probabilities with unit replacement costs allows predicting the expected cost of maintaining the CP system over a particular period of time. A simple tool is under development for companies and owners to predict the cost of maintaining their structures.

For a building with 500 m^2 of concrete surface, protected using a conductive coating anode, the initial cost of installing CP was € 75,000; annual checkup cost is € 2,000. The rate of interest was 2%. Figure 5 shows the development of total cost, inspection plus replacement cost; and replacement cost alone over 25 years. It can be seen that the actual cost of replacing parts is a relatively small fraction of the annual cost. This fraction, however, increases with time. In any case, the expected present cost of replacing parts over 25 years is 20,000 €. Thus, a CP system working life of 25 years seems possible with a relatively low amount of replacement costs. Of course, annual checkups totalling 40,000 € are also needed. The predictions are based on experience with CP installed on buildings over 20 years.

4 CONCLUSIONS

In order to assess the performance of Cathodic Protection systems in the Netherlands, information on concrete structures with CP was asked from CP and repair companies. Results were analysed using survival analysis. Information on performance was obtained for 105 cases. 50 had been operating for ten years or longer. About two thirds of these required minor interventions, e.g. replacement of components. Survival analysis was used to predict failure rates and the cost to replace failing components. The conclusions apply only when proper maintenance is carried out.

Working lives of CP systems without major intervention of ten to twenty years have occurred; corrosion and related damage to concrete have been absent in all documented cases. Intervention was mainly related to defective details such as local leakage and poor electrical isolation.

Survival analysis of the 105 documented cases suggests that (minor) interventions are increasingly necessary with increasing age. There is a 10% probability that a CP system needs maintenance at an age of about 7 years or less; and a 50% probability that maintenance is needed at an age of 15 years or less.

Complete replacement of the anode was carried out in only two cases, one conductive coating anode (on a bridge) and one titanium anode (of a non-mesh type in a building).

Conductive coatings have shown local deterioration in limited numbers, mainly related to water leakage, which caused the need for local repairs of the coating (ten cases); however, corrosion protection may be provided for another several years even if their condition is (visually) poor.

Anodes based on activated titanium have shown long working lives, up to more than 20 years.

Replacement of primary anodes and anode-copper connections was necessary in a number of cases, in particular with older systems; it appears that such critical details now have improved lives.

Power units and reference electrodes have been replaced in some cases. Simple power units and reference electrodes are relatively inexpensive today, so the cost of these actions is limited.

For an example case it has been shown that life cycle costs of CP systems can be predicted, taking into account failure rates based on survival analysis of field data. The cost of replacement of components is relatively small compared to the usual cost of inspection and electrical checkups. A tool for estimating the cost of maintaining a CP system is under development.

ACKNOWLEDGMENTS

The authors thank CP and repair companies for providing data: Care4-concrete.nl, CORRPRE, ECORemain, RENDON, Van der Heide and Vogel; and the Ministry of Economic Affairs for financial support.

Concrete Repair, Rehabilitation and Retrofitting III – Alexander et al. (eds)
© 2012 Taylor & Francis Group, London, ISBN 978-0-415-89952-9

Assessment of critical chloride content in reinforced concrete by Energy Dispersive Spectrometry (EDS) revisited

J. Pacheco, O. Çopuroğlu, B. Šavija & E. Schlangen
Delft University of Technology, The Netherlands

R.B. Polder
Delft University of Technology, The Netherlands
TNO Building Materials, Delft, The Netherlands

ABSTRACT: Reinforcement corrosion is the most important deterioration mechanism in concrete infrastructure. Chlorides contained in saltwater or de-icing salts penetrate through the concrete cover activating corrosion. When left unattended, corrosion leads to cracking and spalling of concrete cover, reducing the structure's service life. The amount of chlorides required for depassivating the steel is known as critical chloride content or chloride threshold. Because of the importance of the critical chloride content as input for service life prediction models, a precise method for its determination is required. This paper describes a new method for determining critical chloride content in reinforced concrete specimens. Ten reinforced concrete specimens with materials available in the Netherlands were cast, cut, cured, coated, dried and then exposed to chlorides in laboratory conditions. The open circuit potential of the steel reinforcement to an activated titanium electrode was monitored and recorded since the beginning of the exposure period. Specimens were taken from the container seven days after the reinforcement potential dropped more than 150 mV. The chloride content at rebar depth was determined by quantitative Energy Dispersive Spectrometry (EDS).

1 INTRODUCTION

Energy Dispersive X-ray Spectrometry (EDS) is a technique commonly used for material characterization (Scrivener 2004, Zhao 2006, Çopuroğlu 2011), to study the steel-concrete interface (Glass 2001) or chloride profiles (Jensen 1996, Win 2004). A high-energy beam sends electrons to the sample at enormous speed. These electrons interact on the surface and a certain volume of material. Back-Scattered Electrons (BSE) are analyzed for the excitation energy and elements contained in the sample can be quantified.

RILEM committee TC 235-CTC "Corrosion initiating chloride threshold concentrations in concrete" has taken the challenge of developing a new method for determining chloride content in laboratory conditions. In principle, the aim of the recommendation is to describe an experimental procedure that can be replicated in several laboratories. According to a first draft of the recommendation, concrete specimens were cast, prepared, monitored and evaluated by EDS in The Netherlands. This paper describes the preparations for the experiment, the current state and forthcoming experimentation.

2 EXPERIMENTAL

Ten specimens containing a single reinforcing bar and four unreinforced concrete specimens were cast, cut and then cured. A chloride rich solution with a concentration of 3.3% NaCl was prepared and poured into a container. Specimens were exposed to the solution in the container after connecting the rebars to the voltmeter. Open circuit potential (OCP) of specimens was monitored with a high impedance voltmeter, connected to an activated titanium (Ti^*) electrode in the solution. A specimen was considered to have initiated active corrosion when the potential dropped by ate least 150 mV, and remaining so for 7 days. So far, four specimens out of ten have become active.

2.1 *Microscopic and EDS analysis*

Samples of approximately 20 × 20 × 6 mm each were obtained from each cube as shown in From these samples polished sections were prepared to be used under electron microscope in order to increase accuracy of the characterization. More information regarding the procedure can be found in Çopuroğlu (2011).

3 RESULTS

3.1 *Open circuit potentials*

Figure 1 shows the OCP plot of the four active reinforced specimens. Specimens EDS-1 and ED-2 were considered to be actively corroding after 59 days whereas specimens EDS-3 and EDS-4 became active after 120 days.

3.1 *Energy Dispersion Spectrometry (EDS)*

A reference mineral phase was used as reference and constant monitoring of the beam current at Faraday's cup was performed accordingly. Figure 2 shows a Back Scatter Electron image at a 550× magnification. In such figure an aggregate particle, unhydrated cement, calcium hydroxide (CH) and calcium-silicate-hydrate (CSH) phases are visible. In all measurements, the analysis was performed on CSH phases alone. Results of chloride content profiles are shown in Figure 3.

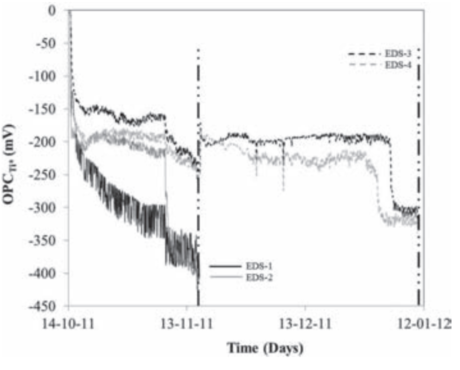

Figure 1. OCP of exposed concrete specimens.

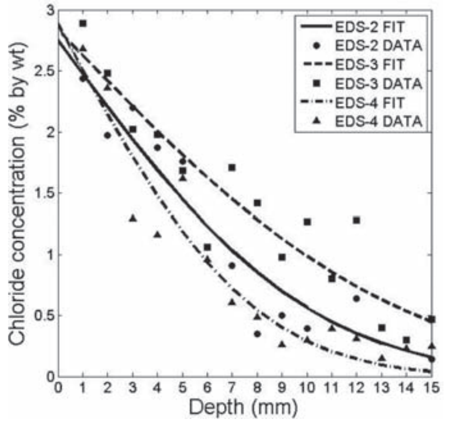

Figure 3. Chloride profiles measured by EDS.

4 DISCUSSION

Results of EDS analysis on polished sections showed that chloride content can be determined by performing measurements on CSH phases at steps of 1 mm from the exposed surface. For EDS-1, results show that the chloride content through the specimen is erratic and with high variations between steps. In fact, it is not possible to find a chloride profile but instead a distributed content. Specimen EDS-1 is disregarded from the following analysis. For EDS-2 results show a more defined profile. The chloride content at the surface ($C_{S\text{-}FIT}$) was estimated by means of curve fitting in Matlab® toolbox. The correlation between the curve fitting and the measured chloride concentrations is above 90%. The estimated diffusion coefficient obtained from the curve fitting (D_{fit}) for EDS-2 is 6.1×10^{-12} m^2/s. For specimens with longer exposure time, EDS-3 and EDS-4, the $C_{S\text{-}Fit}$ in both cases is similar to that found in EDS-2. It seems that the chloride content at the surface had a similar concentration regardless of the exposure time. However, the D_{fit} values of EDS-3 and EDS-4 are lower than that found in EDS-2. This is reasonable since the former specimens had the same mix composition and still required longer exposure to become active.

EDS analysis was performed exclusively on CSH phases on polished concrete samples. Chlorides can be bound to CSH phases at high levels, thus significantly contributing to the total chloride content.

5 CONCLUSIONS

In this paper, the usefulness of EDS is revisited as a technique for chloride content measurements. The main advantage of EDS is that it can percieve differences in chloride content on a microscale level. However, calibration must be performed and a working protocol must be established in order to compare results. The most important findings obtained included:

- Chloride concentration at the exposed surface of concrete specimens was estimated at around 2.8% by curve fitting.
- The chloride content at the level of the reinforcement was between 0.1 and 0.4% by weight of interaction volume.
- Diffusion coefficients obtained from curve fitting were lower than those from Rapid Chloride Migration tests, which could be explained by a higher age of the material.
- Chloride contents obtained from EDS are similar to those reported in literature obtaioned by wet chemical analysis.

Concrete Repair, Rehabilitation and Retrofitting III – Alexander et al. (eds)
© 2012 Taylor & Francis Group, London, ISBN 978-0-415-89952-9

Testing of the chloride threshold values for reinforced concrete structures

H.E. Sørensen, S.L. Poulsen & E.P. Nielsen
Danish Technological Institute, Gregersensvej, Taastrup, Denmark

ABSTRACT: The precision of the existing service life models for chloride exposed concrete structures is highly dependent on the chloride threshold values for the actual exposure conditions and binder compositions. Therefore, a reliable determination of the chloride threshold values for initiation of reinforcement corrosion in concrete structures becomes of paramount importance. A commonly accepted test method for determination of chloride threshold values does currently not exist. However, the RILEM TC 235 CTC group has recently agreed upon the experimental details of an accelerated test method based on open circuit measurements on rebars in concrete specimens exposed to a chloride solution, and an international Round Robin test has been initiated with the purpose of testing the suggested method. This paper presents experiences from our work with determination of chloride threshold values, as well as preliminary results from our participation in the Round Robin test initiated by RILEM TC 235 CTC.

1 INTRODUCTION

A crucial input parameter for modelling of the service lifetime of reinforced concrete structures is the so-called chloride threshold value, which may be defined as the minimum concentration of chloride at the depth of the reinforcement that is able to initiate corrosion of the steel. Without an experimentally determined chloride threshold value, engineers are generally forced to make rather conservative estimates of this value, thus potentially underestimating the service lifetime dramatically. Unfortunately, a commonly accepted method for determination of chloride threshold values is presently lacking. In 2009 a RILEM group (TC 235 CTC) was formed with the purpose of addressing this problem, and after thorough discussions the group agreed on an accelerated test method based on open circuit measurements on rebars in concrete specimens exposed to a chloride solution. Recently, a Round Robin test involving 12 laboratories has been initiated to test the method proposed by the RILEM group.

In 2010 The Danish Expert Centre for Infrastructure Constructions (DECIC) was established. The centre is based on a close cooperation between the Concrete Centre at Danish Technological Institute and the Department of Civil Engineering at the Technical University of Denmark and the activities of the centre are mainly related to durability aspects of reinforced concrete constructions exposed to severe environmental conditions. Part of the research carried out at DECIC is focused on the experimental determination of chloride threshold values for reinforcement corrosion, and the centre is participating in the Round Robin test of the newly suggested method from the RILEM TC 235 CTC group.

2 PRELIMINARY TESTS

A series of preliminary tests have been carried out at DECIC with the aim of developing an accelerated in-lab test method for determination of chloride threshold values for reinforcement corrosion in concrete. The work was done in order to obtain preparatory results and experiences that would serve as useful input for the RILEM TC 235 CTC group.

The basic idea of the preliminary tests is to expose a number of concrete specimens with cast-in rebars to a 6 wt% NaCl solution and subsequently detect the onset of reinforcement corrosion by either open circuit measurement of electrochemical potentials or by observation of a significant increase in the current required to maintain a specific electrochemical potential of the rebar measured against a reference electrode. When corrosion onset is observed the chloride concentration is measured at the depth of the rebars, thus giving the chloride threshold value.

The preliminary tests included eight concrete specimens with a binder composed of 75% Portland cement and 25% fly ash and a water/powder ratio of 0.40. After 28 days of curing each specimen was cut with a diamond saw in order to reduce the concrete cover thickness to either 5 or 15 mm and subsequently the specimens were exposed to a chloride solution.

Generally, no indications of reinforcement corrosion have been observed so far, despite the concrete specimens having been exposed to the chloride solution for more than ten months at the time of writing. Chloride profiles were measured after five and ten months of exposure to examine the status of the chloride ingress in the concrete specimens (Fig. 1), since onset of corrosion was expected to occur within a few months of exposure.

Evaluation of chloride threshold values reported in the literature suggests that corrosion initiation might be expected when the chloride concentration has reached a level approximately between 0.05% and 0.3% (by weight of concrete) at the depth of the reinforcement. Therefore, it also seems reasonable that active corrosion has not been observed during the first ten months of exposure for the concrete specimens having cover thicknesses of either 5 mm or 15 mm, since the chloride profiles in Figure 1 shows that the chloride concentration at depths of 5 and 15 mm is only in the vicinity 0.05% and 0.01% (by weight of concrete), respectively.

The similarity of the two measured profiles suggests that the chloride ingress is affected by an unexpected and unwanted mechanism.

Microscopic investigations indicate that the slow ingress of chloride might partially result from the formation of a dense layer of calcite on the exposed concrete surfaces, which possibly has some blocking effect on the chloride ingress (Fig. 2).

The overall low ingress of chloride observed in the preliminary tests is also related to the high proportion of fly ash in the binder of the concrete, a material which has previously been reported to result in a refinement of the pore structure of the cement paste, as well as enhancement of the chloride binding capacity, thus leading to a higher resistance of the concrete against ingress of chloride ions.

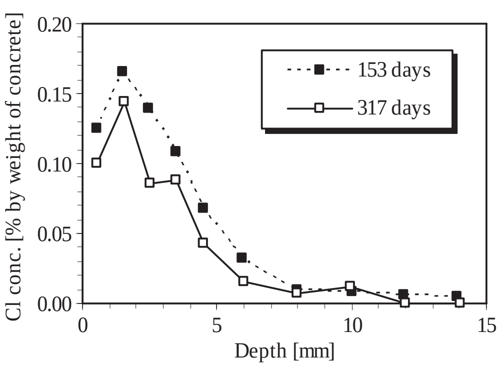

Figure 1. Chloride profiles from two concrete specimens that have been exposed to a 6.0 wt% NaCl solution for 153 days (~five months) and 317 days (~10 months), respectively.

All in all, the preliminary test method is found to be inadequate, at least in connection with the investigated type of concrete, since the method was originally intended to have an overall time frame of only a few months, and consequently, further initiatives that might reduce the time between exposure start and initiation of reinforcement corrosion is needed.

3 RILEM TC 235 CTC: ROUND ROBIN TEST

The basic concept of the method used in the Round Robin test initiated by the RILEM TC 235 CTC group is to expose a series of concrete specimens, each containing a reinforcement bar, to a chloride solution. Subsequently, the electrochemical potential of the reinforcement bars measured against a common standard reference electrode is monitored by a datalogger, and onset of reinforcement corrosion is identified by a significant drop in the measured potential. Prior to exposure, the concrete specimens are partially dried in order to facilitate capillary suction of the exposure solution.

Preliminary results from our participation in the Round Robin test have shown that three weeks of specimen drying (25% relative humidity, 20°C) is sufficient for obtaining the predefined chloride penetration depths due to capillary suction. This was 4 and 7 mm for the two investigated types of concrete, respectively. Reinforcement corrosion has not been detected at the time of writing, but the results are expected to be available for the oral presentation at the conference.

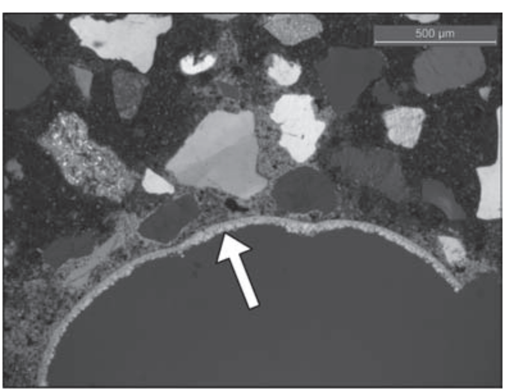

Figure 2. Microphotography of thin section from a concrete specimen that has been exposed to a 6.0 wt% NaCl solution for approx. five months. The semi-circular area in the lower part of the picture is an air void, which was cut during preparation of the exposure surface. A thin and dense layer of calcite (~10 µm thick) is seen along the rim of the air void (see arrow).

Concrete Repair, Rehabilitation and Retrofitting III – Alexander et al. (eds)
 ISBN 978-0-415-89952-9

Protection of steel in concrete using galvanic and hybrid electrochemical treatments

Gareth Glass
Concrete Preservation Technologies, Nottingham, UK

Christian Christodoulou
AECOM, Birmingham, UK

Steven Holmes
Concrete Preservation Technologies, Nottingham, UK

ABSTRACT: In this study, data from galvanic and hybrid electrochemical treatments applied to structures is analysed. It is shown that the protection of steel in concrete using galvanic anodes finds theoretical support from a basis of improving the environment or maintaining a benign environment at the steel. Protection current output responds to the aggressive nature of the environment and, as a result, galvanic anodes have substantially longer lives than originally predicted. Monitoring is preferably focused on monitoring the effect of the protection on the condition of the structure and may be achieved by monitoring either steel corrosion rate and/or steel corrosion potential. Monitoring is preferably combined with a risk management option such as a facility to apply a temporary impressed current treatment to arrest active corrosion if a risk is identified. An allowance for new galvanic protection criteria has been made in the latest European standard on Cathodic Protection of Steel in Concrete.

Corrosion of steel in concrete is an electrochemical process and electrochemical techniques have been used to control corrosion. The simplest of these techniques is galvanic protection. In this case a galvanic anode is connected to the steel and the anode corrodes while delivering a protection current to the steel. Another technique is a hybrid treatment in which a high protection current is briefly impressed off a galvanic anode before galvanic protection is applied (Holmes et al. 2011a). This work looks at data from such systems and considers their performance.

1 GALVANIC ANODES

Galvanic anodes were installed at the edge of patch repairs on a car park deck suffering from de-icing salt induced corrosion. The anodes were installed in drilled holes (25 mm diameter by 40 mm deep) in the parent concrete and were encapsulated in proprietary putty and connected to the steel.

Figures 1shows the potential change relative to an arbitrary reference at some distance from the edge of the patch repairs where the anodes were considered to have no influence on the potentials (Christodoulou et al. 2011). The data shows that in both cases, the anodes had a dominant influence on the potential changes to a distance of about 600 mm

2 HYBRID TREATMENTS

A hybrid treatment briefly impresses a high current off a galvanic anode using a battery or temporary power supply for a period of about a week to arrest active corrosion before connecting the anode to the steel to continue delivering galvanic protection.

Data was collected from hybrid treatments applied to bridge piers and abutments suffering from chloride induced corrosion. Figure 2 shows the effect of the treatment on open circuit steel potentials (Holmes et al. 2011b). The steel potential shifted to much more positive values after 60 days of protection in this example.

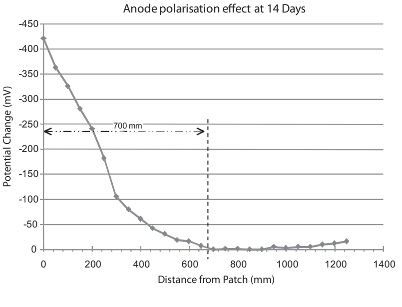

Figure 1. Change in potential induced by anodes in concrete repairs.

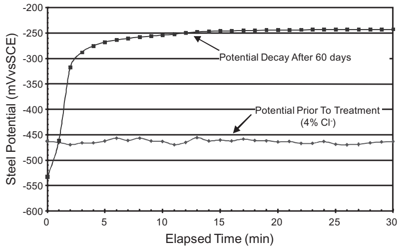

Figure 2. Effect of hybrid galvanic anode treatment on steel potentials.

3 BASIS FOR GALVANIC PROTECTION

The protective effects of electrochemical treatments are broadly described as chloride extraction, re-alkalisation and a negative steel potential shift. However all mechanisms operate in any continuous treatment.

The dominant effect in the cases of continuous electrochemical treatments is most probably an improvement in the environment at the steel (Christodoulou et al. 2010). The evidence for this comes from the long time required to achieve protection and the low protection current densities relative to the localised steel corrosion rate (Glass et al. 2008).

Specific evidence from galvanic systems come from the observation that zinc, thermally applied to concrete surfaces does give adequate protection in aggressive subtropical marine conditions. If it can protect steel in aggressive conditions, then it should also be able to protect steel in less aggressive conditions (Holmes et al. 2011a).

4 RESPONSIVE BEHAVIOUR

Galvanic protection does not have a user controllable protection current output. However the protection current output of a galvanic anode varies with temperature and moisture content in the same way that the corrosion rate of steel varies with these factors. This is termed responsive behaviour.

In cold and dry periods, the current output falls. As a result the life of the anode is increased. The service life of an anode is not determined by a maximum current density, but by a much lower average current density (Holmes et al. 2011a).

5 MONITORING

Monitoring the performance of galvanic anodes is preferably focused on monitoring changes in the condition of the structure that arise as the result of the protection because galvanic protection does not generally sustain high levels of steel polarisation. Examples include corrosion potential as a function of time and/or distance from an anode or edge of the repaired area and/or corrosion rate (Christodoulou et al. 2011).

Corrosion rates up to 2 mA/m^2 are generally considered to be very low or passive. An acceptance criteria might include demonstrating that the corrosion rate at a selected locations representing areas of high corrosion risk is less than 2 mA/m^2.

For corrosion prevention (i.e. stop formation of incipient anodes) an acceptance criterion in this case would be to measure the effect of the anodes on the potential through the concrete along a line extending away from the edge of a repaired area and to show that the influence of the anodes dominates the potential changes to a distance of 300 mm.

6 CONCLUSIONS

The protection of steel in concrete using galvanic anodes finds theoretical support from a basis of protecting the steel by improving the environment or maintaining a benign environment at the steel. Galvanic protection is not generally achieved by sustaining an adequate level of steel polarisation.

Protection current output responds to the aggressive nature of the environment and as a result galvanic anodes have substantially longer lives than originally predicted because the anode is not consumed in cold and dry conditions.

Monitoring the performance of galvanic anodes is preferably focused on monitoring the effect of the protection on the condition of the structure and may be achieved by monitoring either steel corrosion rate and/or steel corrosion potential.

REFERENCES

Christodoulou, C., Glass, G., Webb, J., Austin, S. and Goodier C., "Assessing the long term benefits of Impressed Current Cathodic Protection" Corrosion Science 52 (2010) p. 2671–2679.

Christodoulou C., Glass G., Webb J., Austin S. and Goodier C., 2011, "A new approach for the patch repair of car parks using galvanic anodes", Concrete Solutions 4th International Conference on Concrete Repair, 26–28 September 2011, Dresden.

Glass, G.K., Roberts, A.C., Davison, N., "Hybrid corrosion protection for chloride contaminated concrete" Proceedings of the Institute of Civil Engineers, Construction Materials, 161 (2008) p. 163–172.

Holmes S.P., Wilcox G.D., Robins P.J., Glass G.K. and Roberts A.C., 2011a "Responsive behaviour of galvanic anodes in concrete and the basis for its utilisation" Corrosion Science 53 p. 3450–3454.

Holmes S.P., Wilcox G.D., Robins P.J., Glass G.K. and Roberts A.C., 2011b "Long term assessment of a hybrid electrochemical treatment", Materials and Corrosion 62, p. 1–7.

Concrete Repair, Rehabilitation and Retrofitting III – Alexander et al. (eds)

 ISBN 978-0-415-89952-9

Mechanical behaviour of basalt fibre-reinforced plastics and their durability in an alkaline environment

S. Müller, M. Butler & V. Mechtcherine
Institute of Construction Materials, Technische Universität Dresden, Dresden, Germany

ABSTRACT: Most concrete structures are reinforced with steel bars, and the behaviour of this material combination is advantageous in many respects. However, steel reinforcement close to surfaces is prone to corrosion due to the carbonation and ingress of chlorides, which can lead to severe deterioration in such structures. Alternatively, Fibre-Reinforced Polymers (FRPs) can be used as reinforcement as they are not affected by the corrosion processes typical of steel. In ongoing research the durability of Basalt Fibre-Reinforced Plastics (BFRPs), a new product on the building materials market, is being investigated. The focus of this particular report was on understanding the interactive mechanisms between the rebar and the alkaline environment typical of concrete. The variation parameters were the bar diameter and the surface characteristics of the BFRPs, which were produced by different manufacturers. The mechanical behaviour of the rebars before and after exposure to the alkaline environment was investigated using uniaxial tension tests. The exposure occurred in an alkaline solution at three different temperatures. The deterioration of the rebars was characterised by their mass change and their loss in tensile strength. Furthermore, Environmental Scanning Electron Microscope (ESEM) investigations of the rebar surfaces provided a deeper insight into their specific material behaviour.

1 INTRODUCTION

Fibre-reinforced plastics have become increasingly important over the last few decades and are commonly applied in various high-performance, lightweight elements and structures. In turn, these materials are becoming attractive as a means of reinforcing concrete structures. This project addresses the group of fibre-reinforced plastic rebars made of basalt. The main advantage of basalt-fibre reinforced plastic materials is that they resist corrosion in carbonated concrete. Moreover the material is high strength, light weight, and non-magnetic. Such characteristics make possible the option of a much thinner concrete covering and the elimination of problems related to steel corrosion. However, the alkaline pore solutions in concrete can potentially cause deterioration of both the fibre material and polymer matrix.

2 MATERIAL

The basalt fibre-reinforced plastics (BFRPs) commercially available differ in a wide range of characteristics. This diversity results, for example, from the various chemical compositions to be found in bulk materials, the spinning processes of the fibres, the fibre handling in the pultrusion process, the type of polymer matrix and the surface qualities in order to insure an adequate bond between rebar and concrete.

From customary industrial production the following three different surface types are available:

– sanding of the surface.
– lightly wrapping with basalt fibre yarn.
– tightly wrapping with basalt fibre yarn.

3 TEST METHODS AND PARAMETERS

In the durability experiments specimens were stored in a filtered cement solution, which is similar to the pore solution in concrete. Aging was performed at three different temperatures: 22°C as a reference, 40°C, and 80°C. Higher temperatures were needed to accelerate the chemical reactions and so to achieve a higher degree of material aging. The principles of such accelerated aging are based on the Arrhenius theory.

It is expected that the change in weight and mechanical performance increase with a decrease in the rebars' diameter. Thus, the investigations were concentrated on rebars with diameters of 3 and 5 mm.

Degradation behaviour of wrapped rebar types is similar. For this reason the results presented in this publication are confined to the sanded and the tightly wrapped rebar types.

The duration of the aging tests was 49 days. This storage time at an elevated temperature of 80°C corresponds to a free weathering of around 100 years. But it should be acknowledged here that an exact prognosis of durability behaviour of FRCs on the basis of accelerated tests is very demanding caused by different fracture mechanisms.

4 RESULTS

4.1 *Mechanical behaviour of BFRP rebars*

Table 1 shows results of uniaxial tensile tests on BFRP rebars. The mechanical behaviour of the material strongly depends on its manufacturer. Furthermore, the tensile strength of the smallest rebars is lower then by rebars with increased diameter. This can probably be explained by the less pronounced effect of surface defects.

4.2 *Durability*

4.2.1 *Mass loss investigations*

The durability investigations on rebars in alkaline solution at 20°C and 40°C showed only very little mass changes of treated rebars. Storage in an alkaline solution at a temperature of 80°C caused a decrease in mass for all specimens under investigation.

The weight deficits for wrapped rebars with diameters of 5 and 8 mm are around 3% after 49days of exposure. The 3 mm rebars of this type had a much higher mass loss, around 15%, caused by the unfavourable ratio of surface area to volume.

Sanded rebars with diameters of 5 and 8 mm showed a mass loss far below 1%. The rebars with 3 mm diameter exhibited losses in mass of around 2%. These relatively small mass reductions indicate that the sanded rebars were very resistant to deterioration in an alkaline environment.

4.2.2 *ESEM investigations*

The focus of ESEM investigations was directed at the appearance of the surfaces of the rebars as a whole and also of single fibres after the corrosive removal of polymer. After the strongest accelerated aging (49 days, 80°C), single basalt fibres were found surprisingly not to be prone to corrosion in a highly alkaline environment. This conclusion was deduced from the tightly wrapped rebar type, where the extensive removal of polymer resin from the fibre surface allowed widely unhindered access of the alkaline solution to the basalt fibre. The observed loss of mass on the tightly wrapped specimens can be clearly traced back to the chemical degradation and subsequent removal of the matrix resin of the BFRP. After storage at a temperature of 80°C only some strongly corroded polymer fragments could be seen between single basalt fibres. This pronounced loss of resin seems to be the result of the combined action of the high alkaline level of the solution and the high temperature, which reduces the thermo-mechanical stability of the resin.

This effect requires a critical discussion of the results obtained for the temperature of 80°C. Only a part of the damage measured can be attributed to corrosion processes, which would take place also at lower temperatures under natural conditions. Long-lasting aging testing at lower temperatures is necessary for a more precise estimation of BFRP durability.

In contrast to the wrapped specimens, sanded rebars showed only minor surface alterations after accelerated aging. All fibres of the BFRP were still covered with polymer resin.

4.2.3 *Mechanical behaviour after accelerated aging*

Table 2 shows the tensile strength results obtained on the 5 mm-rebars after 49 days of accelerated aging. In addition, the tensile strength is compared to the values measured on untreated rebars.

Table 1. Results of uniaxial tension tests on BFRP rebars before aging.

Surface structure	Nominal diameter (measured diameter) [mm]	Young's modulus (standard deviation) [MPa]	Tensile strength (standard deviation) [MPa]
Tightly wrapped	3 (2.6)	48270 (2410)	784 (28)
	5 (4.8)		1112 (52)
	8 (8.0)		917 (45)
Lightly wrapped	3 (3.3)	46435 (2950)	1228 (97)
	5 (5.3)		1373 (69)
	8 (7.5)		1155 (62)
Sanded	3 (3.1)	47670 (5050)	1113 (31)
	5 (5.0)		1343 (48)
	8 (8.0)		1439 (94)

Table 2. Tensile strength of 5 mm-rebars after accelerated aging over 49 days.

	Tensile strength (standard deviation)		Reduction of tensile strength compared to untreated rebars	
Temperature [°C]	Sanded rebar [MPa]	Tightly wrapped rebar [MPa]	Sanded rebar [%]	Tightly wrapped rebar [%]
20	1160 (21)	1070 (73)	13.6	3.8
40	1066 (44)	1074 (27)	20.6	3.4
80	749 (28)	686 (55)	44.3	38.3

Aging behaviour with decrease in strength must eventually be considered in defining of corresponding safety factors in structural design. In contrast, the Young's modulus remained constant.

5 SUMMARY

The subset of the results shows that Basalt Fibre-Reinforced Plastics (BFRP) are suited as a concrete reinforcement material. The tensile strength of BFRP is higher than that of steel reinforcement. Young's modulus varies closely around 45000 MPa.

Durability tests demonstrated that the resin can efficiently protect the basalt fibres against alkaline attack and premature failure. The fibre material itself was unaffected by the storing in alkaline environment. But it must be kept in mind that each investigated BFRP had a different specification. Thus, a general statement about BFRP behaviour is not possible at this stage. Therefore, a technical approval seems to be necessary for each rebar type.

Concrete Repair, Rehabilitation and Retrofitting III – Alexander et al. (eds)
© 2012 Taylor & Francis Group, London, ISBN 978-0-415-89952-9

Towards correlating natural and accelerated chloride-induced corrosion in cracked RC preliminary results

M. Otieno, H. Beushausen & M.G. Alexander
Concrete Materials & Structural Integrity Research Unit, Department of Civil Engineering, University of Cape Town, South Africa

ABSTRACT: This paper presents preliminary results of an on-going study on chloride-induced corrosion in reinforced concrete. A total of 210 beam specimens (120 × 130 × 375 mm) were made using two w/b ratios (0.40 and 0.55), three binders (PC, PC/FA and PC/GGBS) and two concrete covers *c* (20 and 40 mm). Other experimental variables included crack width w_{cr} (0, 0.4 and 0.7 mm) and exposure environments (field and laboratory). Accelerated corrosion by cyclic wetting and drying with 5% NaCl solution was used for the laboratory-based specimens while the field-based specimens were exposed to a natural tidal/splash marine zone. Corrosion rate (i_{corr}), half-cell potential and concrete resistivity were measured every two weeks over a period of 30 weeks. Results obtained so far underscore the influence of w_{cr}, *c*, resistivity and concrete quality on i_{corr}, with the general trend showing i_{corr} increasing with increasing w_{cr} and decreasing *c*, resistivity and concrete quality. The results show that for a given set of experimental variables, both natural and accelerated cumulative mass loss follow a linear trend but with the latter having a higher slope. However, long-term results are required to confirm this linear trend with time. The ratios between the natural and accelerated i_{corr} show high variability. This variability should be taken into account when correlating the two.

1 INTRODUCTION

In the development of prediction models for the propagation phase, accelerated corrosion is, in most cases, used to simulate the active corrosion process mainly because it is inexpensive and its effects can be realized quickly compared to natural corrosion. However, there have been critiques of the use of accelerated corrosion to simulate natural corrosion (e.g. Andrade *et al.*, 1993, Alonso *et al.*, 1998) because it is not representative of the natural corrosion process. Despite these critiques, the slow rate of natural corrosion makes it inevitable to use accelerated corrosion to study both the corrosion process and the associated damages on the RC structure.

This study focused on chloride-induced corrosion. Accelerated chloride-induced corrosion can be achieved in different ways including (i) application of a constant direct anodic current or potential, (ii) use of admixed chlorides, (iii) use of cyclic wetting and drying with a chloride-based salt solution, (iv) use of simulated pore solutions, or (vi) a combination thereof. Of these methods, cyclic wetting and drying has been shown to be a better representation of natural corrosion process than the other methods (Yuan *et al.*, 2007), and was therefore used in this study.

The preliminary results presented in this paper are part of on-going research investigating, among other objectives, the potential of using accelerated chloride-induced corrosion (cyclic wetting and drying) to predict marine natural corrosion (tidal/splash zone).

2 EXPERIMENTAL SET-UP

Beam specimens (120 × 130 × 375 mm) were cast using 5 concretes made using two w/b ratios (0.40 and 0.55) and three binders (100% CEM I 42.5 N (PC), 50/50 PC/GGBS and 70/30 PC/FA). However, the 0.55 w/b ratio was not used to make PC specimens based on the fact that it is not used in practice for marine RC structures. Other variables in the experiments included cover depth (20 and 40 mm), crack width (0, 0.4 and 0.7 mm) and exposure environments (laboratory and field). A total of 210 beam specimens were cast. A high yield 10 mm Ø ribbed steel bar was embedded in each beam. A wire was attached to one end of the bar and both ends were epoxy-coated to provide an exposed surface area of approx. 86 cm^2. A 10 mm Ø × 150 mm stainless steel bar was placed in each beam during casting (Figure 1) to act as a counter electrode for i_{corr} measurements.

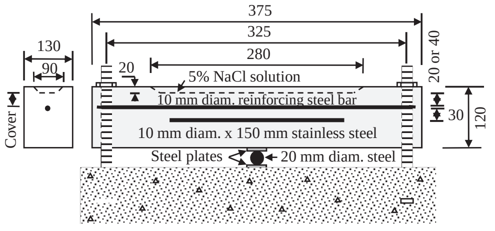

Figure 1. Loading set-up for cracked beams (dimensions in mm).

During casting, 1.0 mm thick and 10 mm deep PVC sheets were placed at the center of each beam (perpendicular to the beam longitudinal axis) to induce cracks at the center of the specimens during pre-cracking. After 28 days of water-curing (at 23 ± 2°C), the beams were pre-cracked under 3-point flexural machine loading. Crack widths were measured using a crack width gauge with a magnification and accuracy of X40 and ±0.02 mm respectively. The cracked specimens remained in specially designed individual loading rigs (Figure 1) for the entire duration of the experimental programme.

Before exposure to the laboratory and field environments, active corrosion was induced in the specimens by applying a very low impressed current (8.6 μA for 10 days) to achieve a corrosion rate of approx. 0.1 μA/cm^2 which is conventionally taken to denote the transition from corrosion initiation to propagation. This process was carried out simultaneously in all beams. The laboratory-based specimens were exposed to controlled temperature and relative humidity of 23 ± 2°C and 50 ± 5% respectively, and subjected to a cycle of 3 days wetting with 5% NaCl solution (contained in a reservoir placed in the cracked face of the beam) followed by 4 days air-drying. Prior to exposure of the field specimens to natural marine tidal/splash zone, all their faces (except the cracked face) were epoxy-coated to ensure a unidirectional chloride penetration. Crack widths of the cracked specimens were monitored. Corrosion rate, half-cell potential and concrete resistivity were measured every 2 weeks in both the laboratory- and field-based specimens. Only the corrosion rate and concrete resistivity results are presented in this paper. The results presented in this paper are those collected up to week 30.

3 RESULTS AND DISCUSSION

3.1 *General corrosion rate trends*

The laboratory and field i_{corr} results showed that, similar to previous studies (Scott, 2004, Otieno *et al.*, 2010), crack width (w_{cr}) affects i_{corr}—with increasing w_{cr} leading to increased i_{corr} but to an extent dependent on concrete cover, quality (or penetrability) and resistivity. Stable corrosion rates were not observed within the 30 weeks period to validate averaging; average i_{corr} are therefore not presented. From the results obtained so far, it is also clear that for a given w_{cr}, i_{corr} varied with both cover depth and concrete quality (or penetrability). The general trend with respect to i_{corr} shows that for a given exposure condition, cover depth and w_{cr}, i_{corr} decreased with increase in concrete quality (binder type and w/b ratio).

The results also clearly show that, in terms of i_{corr}, the blended cement concretes performed better than the PC concretes.

4 CORRELATION BETWEEN LABORATORY AND FIELD CORROSION RATES

The field- and laboratory-based active corrosion rate results suggest that the two can be correlated if sufficient data is available. The empirical correlation will take the form:

$$i_{corr,\,field} = \lambda(i_{corr,\,lab}) \tag{1}$$

where λ is a factor dependent on parameters such as corrosion rate, and not a fixed constant. This will be explored as more results are obtained. Based on the preliminary results, an attempt was made to determine $i_{corr,lab}/i_{corr,field}$ ratios (λ) and a box plot plotted (Figure 2). The many outliers in the box plot indicate high variability between the laboratory and field-based i_{corr}, a phenomenon which

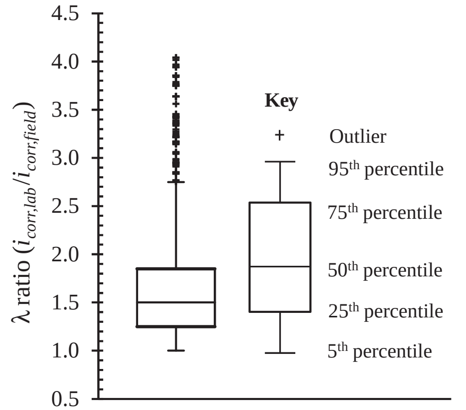

Figure 2. Box plot of *k*-ratios between lab and field active corrosion rates (n = 159, mean = 1.36, std. dev. = 0.25).

should be taken into account when correlating the two. However, more data is required to verify this. Knowledge of this variability is useful in the prediction of i_{corr} in RC structures using laboratory-based test results.

5 CONCLUSIONS

The following conclusions can be made based on the preliminary results presented in this paper:

i. Crack width w_{cr}, cover c, resistivity and concrete quality affect i_{corr}, with the general trend showing i_{corr} increasing with increase in w_{cr} and decrease in c, resistivity and concrete quality.

ii. For field-based specimens, the effect of c on i_{corr} diminishes as w_{cr} increases, in this case from 0.4 mm to 0.7 mm.

iii. For a given set of experimental variables, both natural and accelerated (cyclic wetting and drying) cumulated mass loss follow a linear trend but with the latter having a higher slope. Long-term results are required to ascertain this trend.

iv. Even though it is plausible to find a correlation between natural i_{corr} and accelerated i_{corr} (cyclic wetting and drying), the ratios between the two show high variability. This variability should be taken into account when correlating the two.

Concrete Repair, Rehabilitation and Retrofitting III – Alexander et al. (eds)
© 2012 Taylor & Francis Group, London, ISBN 978-0-415-89952-9

Improving concrete durability through the use of corrosion inhibitors

I.N. Robertson
Department of Civil and Environmental Engineering, University of Hawaii, USA

ABSTRACT: Corrosion of reinforcing steel is a major contributor to early deterioration of concrete structures in a coastal environment. This paper presents the results of a ten year laboratory accelerated corrosion study and an eight year field study involving 25 reinforced concrete panels exposed to a marine tidal zone. Seven different corrosion inhibiting admixtures and two pozzolans were used in the laboratory and field studies to compare their effectiveness at preventing or delaying onset of corrosion. This study was funded by the Hawaii Dept. of Transportation, Harbors Division, in order to evaluate commercially available corrosion inhibiting admixtures when used in concretes made with basalt aggregates common to Hawaii and other Pacific Islands.

The corrosion-inhibiting admixtures included in this project were Darex Corrosion Inhibitor (DCI), Rheocrete CNI, Rheocrete 222+, FerroGard 901, Xypex Admix C-2000, Latex modifier, Kryton KIM, and the pozzolans were fly ash, and silica fume.

Based on an assessment of the performance of field panels and the corresponding laboratory specimens with the same concrete mixtures, it was found that DCI, CNI, fly ash and silica fume all provided improved corrosion protection compared with the control specimens. Kryton KIM performed well in a field panel, but was not included in the laboratory study. As expected, the control mixtures with lower water-cement ratio (0.35) performed better than control mixtures with higher water-cement ratio (0.40).

Concrete mixtures using Rheocrete 222+, FerroGard 901, Xypex Admix C-2000 or Latex-modifier showed mixed results. Some mixtures exhibited improved performance compared with the control mixtures, while others did not. Based on the results of this study, these corrosion inhibiting admixtures cannot be recommended for concrete using Hawaiian aggregates in a marine environment.

1 INTRODUCTION

Reinforced concrete structures exposed to a marine environment often experience corrosion of the reinforcing steel, which may require that the structure be rehabilitated to remain in service. The study reported in this paper was intended to identify effective and reliable corrosion inhibiting measures that will delay the onset of corrosion, prolong the service lives of future structures, and reduce maintenance costs for deteriorating structures.

The experimental program included both laboratory and field studies which are summarized in this paper along with a comparison between the performance of identical concrete mixtures exposed to laboratory and field conditions.

The accelerated laboratory corrosion study was performed based on ASTM G 109–92. Between 4 and 12 specimens were fabricated using each of 100 different mixtures for a total of 656 laboratory specimens. Ponding cycles initiated between 1999 and 2001. When macro-cell current readings indicated that corrosion had initiated, each specimen was removed from cycling and autopsied. After 10 years of cycling, all remaining specimens, whether corroding or not, were removed from cycling and autopsied.

The field study involved panels produced using the more promising inhibiting methods identified in the laboratory study. A total of 25 concrete panels were fabricated and installed at the field site at Pier 38 in Honolulu Harbor one week after concrete placement. Each panel was suspended in the seawater such that the bottom of the panel was always submerged, the middle of the panel was in the tidal zone, while the top of the panel was above the highwater level. Results reported in this paper are based on field observations after 8 years of exposure. A comprehensive final report on the project is currently being prepared.

2 TEST RESULTS

Table 1 provides a comparison between the performance of the 25 field specimens and the corresponding laboratory specimens that utilized the same concrete mixtures. Green, orange and red shading are used to indicate good, moderate and poor performance, respectively. Col. 15 references

Table 1. Details of field and laboratory specimens and comparison of performance.

Mixture Details						Laboratory Specimen Results				Field Half-cell		Field Panel Damage		
Lab Series	Field Panel	w/c Ratio	Aggregate Source	Inhibiting Admixture	Admixture Dosage	Cycles to failure	Average Half-cell	Specimen Damage	Reinft. Corrosion	50% Months	>90% Months	Panel Damage	Months	Field Photos
(1)	(2)	(3)	(4)	(5)	(6)	(7)	(8)	(9)	(10)	(11)	(12)	(13)	(14)	(15)
C2	1	0.4	Kapaa	None	Control	20	-352	None	Mod - Severe	40	40	Crack	84	
C4	7	0.35	Kapaa	None	Control	107*	-313	Minor	Mod - Severe	24	62	None	-	
HC2	2	0.4	Halawa	None	Control	20	-334	Cracks	Mod - Severe	40	40	Cracks and Rust	84	Figure 5
DCI4	3	0.4	Kapaa	DCI	$10\ell/m^3$	34	-221	Minor	Mod - Severe	-	-	None	-	
DCI5	3A	0.4	Kapaa	DCI	$20\ell/m^3$	109*	-195	None	Minor - Mod	-	-	None	-	Figure 6
CNI4	5	0.4	Kapaa	CNI	$10\ell/m^3$	95*	N/A	None	Mod - Severe	24	24	None	-	
CNI4	6	0.4	Kapaa	CNI	$10\ell/m^3$	95*	N/A	None	Mod - Severe	24	46	Rust	80	
CNI4	5A	0.4	Kapaa	CNI	$20\ell/m^3$	95*	N/A	None	Mod - Severe	58	-	None	-	Figure 6
HCNI4	4	0.4	Halawa	CNI	$10\ell/m^3$	95*	-302	Minor	Mod - Severe	40	40	Crack and rust	84	Figure 7
RHE2	15	0.4	Kapaa	Rheocrete	$5\ell/m^3$	93*	-378	Minor	Mod - Severe	62	62	Crack and rust	84	
RHE2	16	0.4	Kapaa	Rheocrete	$5\ell/m^3$	93*	-378	Minor	Mod - Severe	24	24	None	-	
HRHE2	17	0.4	Halawa	Rheocrete	$5\ell/m^3$	87*	-339	Cracks and rust	Mod - Severe	24	40	Rust	84	Figure 8
HRHE2	17A	0.4	Halawa	Rheocrete	$5\ell/m^3$	87*	-339	Cracks and rust	Mod - Severe	58	-	None	-	Figure 8
FER2	20	0.4	Kapaa	FerroGard	$15\ell/m^3$	88	-271	Cracks and rust	Mod - Severe	37	60	Crack and rust	80	Figure 9
-	18	0.4	Halawa	FerroGard	$15\ell/m^3$	N/A	N/A	N/A	N/A	40	62	Crack and rust	84	
-	19	0.4	Halawa	FerroGard	$15\ell/m^3$	N/A	N/A	N/A	N/A	49	62	Rust	84	
XYP2	21	0.4	Kapaa	Xypex	2%	91*	-323	Minor	Mod - Severe	20	37	Crack and rust	84	Figure 10
LATEX5	14	0.4	Kapaa	Latex Mod.	5%	98*	-175	Minor	Minor - Mod	30	38	Crack and rust	74	Figure 11
-	22	0.4	Kapaa	Kryton Kim	2%	N/A	N/A	N/A	N/A	24	-	None	-	
SF2	8	0.36	Kapaa	Silica Fume	5%	106*	-167	None	Minor - Mod	20	-	None	-	Figure 12
SF2	9	0.36	Kapaa	Silica Fume	5%	106*	-167	None	Minor - Mod	13	52	Crack and rust	74	Figure 12
SF2	10	0.36	Kapaa	Silica Fume	5%	106*	-167	None	Minor - Mod	64	-	None	-	
FA4	11	0.36	Kapaa	Fly Ash	15%	100*	N/A	None	Minor - Mod	20	80	None	-	Figure 13
HFA4	12	0.36	Halawa	Fly Ash	15%	69	-122	None	Minor	84	-	None	-	Figure 13
HFA4	13	0.36	Halawa	Fly Ash	15%	69	-122	None	Minor	-	-	None	-	Figure 13
Notes:	N/A - Data not available			* Test series did not fail per ASTM G-109										

figures in the full paper of which Figures 5 and 13 are repeated here as samples of poor performance of a control mixture and good performance of fly ash mixtures.

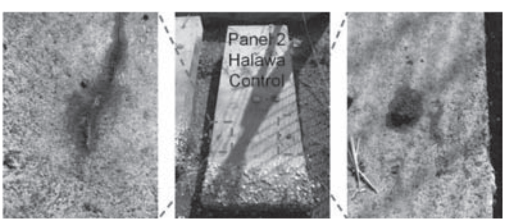

Figure 5. Field panel 2—Halawa aggregate and 0.4 w/c ratio.

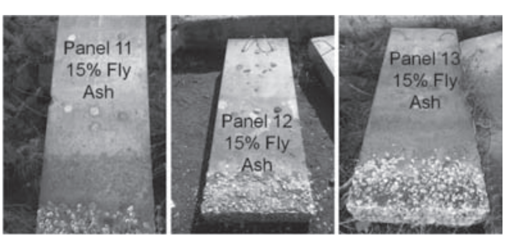

Figure 13. Field panels 11, 12 and 13 with 15% cement replacement with Fly Ash.

3 CONCLUSIONS

Based on observations after 10 years of the accelerated laboratory tests, and 8 years of the field study, the following conclusions were drawn:

1. Mixtures with DCI or Rheocrete CNI at doses of 20 liters per cubic meter showed superior corrosion inhibiting performance compared with the corresponding control specimens.
2. Mixtures with 15% replacement of cement with Fly Ash or 5% replacement of cement with Silica Fume showed superior corrosion inhibiting performance compared with control specimens.
3. A field panel containing Kryton KIM showed superior performance than the control specimen.
4. Mixtures using Rheocrete 222+, FerroGard 901, Xypex Admix C-2000 or latex-modifier showed mixed results and cannot be recommended for concrete using Hawaiian aggregates in a marine environment.
5. The control mixture using Kapaa aggregates with water/cement ratio of 0.35 showed improved corrosion protection compared with the control mixtures with 0.40 water/cement ratio.

REFERENCES

All research reports on this project are available at the UH Civil and Environmental Engrg. Dept. Website: www.cee.hawaii.edu/content/resreport.htm.

Theme 2: Condition assessment of concrete structures

Degradation assessment and service life aspects

This page intentionally left blank

Concrete Repair, Rehabilitation and Retrofitting III – Alexander et al. (eds)
 ISBN 978-0-415-89952-9

Conservation of concrete structures in *fib* Model Code 2010

S.L. Matthews
Principal author of fib Model Code 2010, Chapter 9
Building Research Establishment Ltd., Watford, UK

T. Ueda
Principal author of fib Model Code 2010, Chapter 9
Hokkaido University, Sapporo, Japan

A. Bigaj-van Vliet
Principal author of fib Model Code 2010, Chapter 9
TNO (Netherlands Organisation for Applied Scientific Research), Delft, The Netherlands

ABSTRACT: Chapter 9: *Conservation of concrete structures* forms part of *fib* Model Code 2010, the first draft of which was published for comment as *fib* Bulletins 55 and 56 (*fib* 2010). Numerous comments were received and considered by *fib* Special Activity Group 5 responsible for the preparation of *fib* Model Code 2010. The final version of *fib* Model Code 2010 should be published in early 2012 (*fib* 2012). Chapter 9: *Conservation of concrete structures* is formulated so that it is consistent with the concepts and the overall philosophy adopted in the overall Model Code, which introduces a new integrated life cycle perspective upon the design of concrete structures. In this way, *fib* Model Code 2010 promotes an holistic approach for the design of structures based on defined performance requirements incorporating consideration of safety, serviceability, durability and sustainability.

fib Model Code 2010 has adopted the service life design approach set out in the *Model Code for Service Life Design (fib* MC-SLD), as described in *fib* Bulletin 34 (*fib* 2006), as a rational basis for durability design. In addition to the purely technical design and construction issues, Model Code 2010 takes into account wider philosophical issues such as the through-life management, cost, environmental and societal impacts of concrete structures. To this end *fib* Model Code 2010 seeks to integrate issues relating to the design and construction of new structures with those required for the management of existing concrete structures.

Accordingly Chapter 9: *Conservation of concrete structures* provides a basis for the implementation of through-life conservation and management strategies defined during design, but also processes by which the condition of existing concrete structures can be evaluated and interventions undertaken, as appropriate, to achieve or extend the service life of the concrete structures concerned.

1 BACKGROUND—MODEL CODE 2010

The first draft of the *fib* Model Code 2010 was published for comment as *fib* Bulletins 55 and 56 (*fib* 2010). Numerous comments were received on the draft and these were considered by *fib* Special Activity Group (SAG) 5 during the preparation of the final version of *fib* Model Code 2010, which should be available in early 2012 (*fib* 2012).

fib Model Code 2010 supersedes the earlier CEB/FIP Model Code 1990 (CEB 1991), which itself was a major step forward in the international harmonisation of codes. It served as a basis for Eurocode 2 for the design of concrete structures (CEN 2004–2006), which is now used in most European countries.

fib Model Code 2010 adopts a life cycle perspective, following the sequence of conceptual design, dimensioning, construction, conservation, as well as dismantlement, recycling and reuse.

2 GENERAL—CONSERVATION

In *fib* Model Code 2010 conservation is taken to include all activities aimed at maintaining or returning a concrete structure to a state which satisfies the defined performance requirements.

Commonly two different conservation objectives are distinguished:

- Enabling a structure to meet its intended service life, as envisaged at the time of design;
- Extending the planned service life of a structure or enabling it to meet revised performance requirements (e.g. revised loading or functionality needs).

For a new concrete structure, the condition control activities required for its conservation should be planned when the structure is designed. These plans should be based on the design assumptions and a prognosis of behaviour under the envisaged environmental and loading conditions over its intended service life, considering the defined performance requirements.

For an existing structure, the condition control activities required to extend its intended service life or to accommodate revised performance requirements shall be developed during the re-design process based on knowledge of the current condition of the structure and a prognosis of its future behaviour under the envisaged environmental and loading conditions and recognising the implications of any revised performance requirements.

Special performance requirements may be defined for structures having historical or cultural significance, which may restrict the type of intervention that can be made.

Chapter 9 of *fib* Model Code 2010 comprises the following main sections:

9.1 General
9.2 Conservation strategies and tactics
9.3 Conservation management
9.4 Condition survey
9.5 Condition assessment
9.6 Condition evaluation and decision-making
9.7 Interventions
9.8 Recording

3 DEFINITIONS

In *fib* Model Code 2010 the term '*conservation*' is used to describe the overall process of through-life management which is aimed at maintaining or returning a concrete structure to a state which satisfies the defined performance requirements. Additionally, following the approach used in *fib* MC-SLD, the term '*condition control*' is used to describe the activities and measures performed as a part of the conservation process for the structure.

4 CONSERVATION STRATEGY & TACTICS

The available conservation strategies and the respective tactics are classified as follows:

Strategy A: Proactive condition control activities.
Strategy B: Reactive condition control activities.
Strategy C: Situations where condition control activities are not feasible.

The classification of conservation strategies also recognise whether they involve:

- Adoption of proactive or reactive activities.
- Adoption of planned or unplanned activities.
- Amending the reference performance level of the structure or a component part; whether the activities are to maintain the intended performance level (i.e. a maintenance or repair activity) or are to enhance the current performance level (i.e. strengthening activity).

5 CONSERVATION MANAGEMENT

The through-life conservation process typically involves the following activities:

- Condition survey involves gathering data on the current condition and its development.
- Condition assessment involves review data to assess current performance and make a prognosis of future performance, including identification of deterioration mechanisms.
- Condition evaluation and decision making activities are concerned with establishing the implications for the conservation of an asset, evaluating potential conservation options, selecting an appropriate intervention option(s) and the timing of such works.
- Execution of preventive or remedial works.
- Undertaking through-life condition survey, monitoring and recording of information.

The general flow of the conservation management process is shown in Figure 1 of the full paper. Linked to the above, four condition control levels/inspection regimes are defined:

- CCL3: a proactive approach using a regular inspection, testing and monitoring regime.
- CCL2: a reactive approach which utilises a planned inspection regime (visual only).
- CCL1: a reactive approach using an ad-hoc inspection and testing/investigation regime.
- CCL0: involves no physical inspection, testing or monitoring activities.

ACKNOWLEDGEMENTS

The authors acknowledge the contributions made by other colleagues in *fib* to the development of the concept for Chapter 9 of *fib* Model Code 2010, as well as their helpful comments and suggestions.

REFERENCES

CEN. 2004–2006. EN 1992: *Eurocode 2: Design of concrete structures, Parts 1 to 3*. Comité Européen de Normalisation (CEN), Brussels.

CEB. 1991. *CEB/FIP Model Code 1990 for concrete structures*. Final version CEB Bulletins 203 to 205, Comité Euro-International du Béton (CEB), Lausanne, Switzerland.

fib. 2006. *Model code for service life design of concrete structures. fib* Bulletin 34, Fédération Internationale du Béton (*fib*), Lausanne, Switzerland.

fib. 2010. *Model code 2010 First complete draft – Volumes 1 and 2. fib* Bulletin 55 & 56, Fédération Internationale du Béton (*fib*), Lausanne, Switzerland.

fib. 2012. *Model code 2010 – Final version – Volumes 1 and 2.* To be published in 2012. Fédération Internationale du Béton (*fib*), Lausanne, Switzerland.

Concrete Repair, Rehabilitation and Retrofitting III – Alexander et al. (eds)
© 2012 Taylor & Francis Group, London, ISBN 978-0-415-89952-9

Non-destructive Building diagnosis in the monitoring and inspection of existing building structures

Andrei Walther
Ingenieurbüro BauConsulting Brandenburg, Havel, Germany

Andreas Hasenstab
Bayerischen Ingenieurekammer Bau, Augsburg, Deutschland

Who wants to visit building monuments in Germany, thinks first of centuries—old architectural structures. However, even the modern constructions, often in prestressed concrete, already listed as a monument. Using examples from the construction practice is to show what features of these structures and which have non—destructive methods of verification and inspection of buildings can be expanded. Additionally shown in which frame structures inspected according to current regulations in Germany will have. As part of this inspection, the non—destructive testing methods gain in importance.

Concrete Repair, Rehabilitation and Retrofitting III – Alexander et al. (eds)
© 2012 Taylor & Francis Group, London, ISBN 978-0-415-89952-9

Concrete deterioration in mining structures

A. Masarira & T.L. Bopape
Anglo Operations Limited, Johannesburg, South Africa

ABSTRACT: Concrete structures form a large section of mining infrastructure. They find use both in open-cast as well as mine shafts, containment structures as well as material processing plant structures. Given the huge investments that accompany the design and construction of these structures as well as their criticality in the production line of a mine, it is important that these concrete structures do not experience premature failure or deterioration that would have an impact on production. The reality however is that these structures experience regular failure which requires remedial action. Some of the causes of such failures are due to poor design practices, poor construction and workmanship, failure to fully understand the environmental conditions in which these structures will operate and inaccurate assumptions made during the design process on the loads (especially dynamic loads) which the structures will be expected to carry during their lifetime. Another cause is the operational changes made resulting in these structures being required to carry loads they were not originally designed for. This paper presents some of the common forms of concrete deterioration in mining structures, their possible causes and some of the remedial action taken to restore the integrity of theses concrete structures.

1 INTRODUCTION

Concrete structures form a large component of mining infrastructure. Common concrete application in mining operations is in areas such as shaft lining, material containment structures (silos and bunkers), liquid containment structures (water reservoirs), foundations of material processing equipment such as rock breakers, crushers and mills as well as in building structures such as scrubbing and screening or crushing buildings. The conditions under which these structures operate in mining, in terms of loading and environment, are unique and the structural design needs to consider these. The type and level of concrete deterioration in mining structures is a function of these operating conditions and it is therefore critical that any repair and rehabilitation methods developed take cognizant of these factors.

Concrete mining structures are often exposed to corrosive environments as a result of the wet processes that often take place in these operations. The washing and cleaning of mineral stock which is an integral part of mineral processing is not always done with fresh water, but rather with recycled water. This water permeates through the cracks that usually exist on concrete structures and result in the corrosion induced damage of these structures. Sometimes chemicals are used in mineral processing water, which result in corrosive conditions. There are some mining operations that are located in coastal regions and the chemical composition of sea water makes that environment highly aggressive.

Mining structures are often expected to carry large material loads (rocks and ore) and a number of the processes generate dynamic loads e.g. through crushing, scrubbing, screening or milling processes. The support of heavy equipment and machinery as well as the generation of dynamic loading conditions result in the concrete structures being susceptible to an increased rate of deterioration. In shaft mining, depths to levels such as 2 000 m are easily reached and the concrete structures in such shafts are often under extreme environmental and loading conditions. Mining structures, in general, can be exposed to large temperature fluctuations with differences between the highest and lowest temperatures as high as 40°C. These and other factors result in general concrete deterioration. The various concrete structures in mining are exposed to a wide range of loading and operating conditions. Concrete structures supporting mineral processing equipment are susceptible to dynamic as well as impact loads. Structures in the crushing areas are exposed to impact loads (reversing trucks) or rock-breaker forces.

Concrete deterioration on silos often occurs on the inside wall due to abrasion. Some highly abrasive ore like Platinum ore leads to a high rate of wearing inside the silos. In coal mines, there are relatively frequent cases of spontaneous combustion of coal inside the silos leading to the burning coal causing damage to the concrete. Liquid

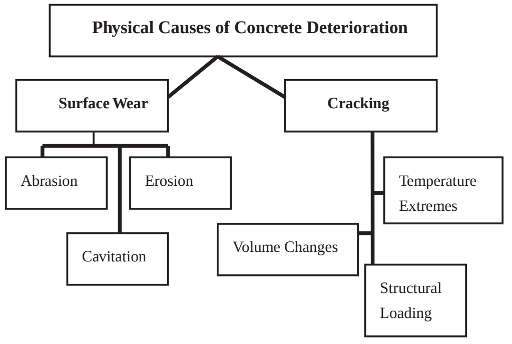

Figure 1. Physical causes of concrete deterioration.

Figure 2. Concrete deterioration.

containment structures such as thickeners or clarifiers could experience leaking of the water through the walls.

The level of deterioration of concrete is indicative of its durability, which is its ability to resist weathering action, chemical attack, abrasion or other processes of deterioration. Concrete structures in mining experience both chemical and physical degradation processes.

There are many stages in the processing of mineral ore which require the use of water. The water mostly used in these processes is recycled and therefore not as clean as fresh drinking water. This water often gets into contact with the concrete structural elements of the processing plants and encourages concrete corrosion. Very often this water is used to clean concrete floors, slabs and other structures and this water often collects on various surfaces of the structures. The deterioration of concrete structures in mining and other industrial operations can lead to structural failures. In order to avoid structural failures and operational downtime, it is imperative that concrete repair and rehabilitation procedures be developed and implemented.

2 REPAIR AND REHABILITATION

The basic stages in the process of concrete repair and rehabilitation are:

- Investigation and analysis of the concrete
- Diagnosis of deterioration of the concrete
- Assessment of maintenance priority
- Develop concrete repair solutions and remedial strategies.

The main objective of the repair procedure and methodology is to stop the progress of any corrosion process that might be taking place in the structure as well as to reduce the probability of corrosion occurring in the future. A clear indication of corrosion damage is the presence of cracks on the concrete. These cracks allow the permeation of moisture into the structure and leading to damage of the steel reinforcement and further concrete damage. It is therefore critical that the presence of cracks be taken seriously and the width of the cracks be considered in determining the repair procedure to use.

2.1 *Surface preparation*

The repair procedure requires a surface preparation i.e. conditioning of the existing concrete to receive repair materials. This can involve the removal of deteriorated, contaminated or damaged concrete in order to provide surfaces that will promote bonding of the repair material.

2.2 *Cleaning of reinforcement*

If corroded reinforcement steel is encountered under the concrete cover, the area around the corroded steel must be uncovered and cleaned.

2.3 *Patch repair*

After the reinforcement steel has either been cleaned (for minimal corrosion) or replaced with new steel, the concrete cover must be reinstated. The most common and efficient method is patch repair i.e. the application of a cementitous repair mortar.

2.4 *Replace structure or member*

In cases where repair is no longer possible the entire structure or structural member would have to be replaced completely.

Concrete Repair, Rehabilitation and Retrofitting III – Alexander et al. (eds)
© 2012 Taylor & Francis Group, London, ISBN 978-0-415-89952-9

Case studies of concrete deterioration in reinforced concrete chimneys

Manu Santhanam
Department of Civil Engineering, IIT Madras, Chennai, India

ABSTRACT: This paper discusses the site investigations and follow-up laboratory tests on three reinforced concrete chimneys—two in central and one in southern India. In the first case, a 2 year old reinforced concrete chimney in central India showed blistering of the outer surface of concrete in many locations, which indicated a possible acid attack that should have progressed outward from the inner surface of the chimney shell. Additionally, the reinforcing bars in these locations showed signs of extensive corrosion, which led to the formation of rust stains on the outer surface. The details of the inspection, analyses, and recommendations are presented in this paper. The second chimney in central India was actually under construction, and poor quality of concrete was noticed at the 90 m level. Site investigation and interviews, followed by laboratory evaluation of cores removed from the structure were able to reveal that the poor quality was a mixture of slow hydrating cement and inadequate construction practices. The analyses and recommendations are presented. In the final case, the failure of the acid resistant brick lining on the top levels of a reinforced concrete chimney in southern India led to an extensive laboratory investigation on the quality of the chimney concrete, using cores removed from the chimney. A combination of chemical and physical tests was used to evaluate the quality, and the details of the methods and results are presented.

1 CASE STUDY 1: ACID ATTACK IN RCC CHIMNEY

The outer surface of the chimney showed signs of damage in a number of locations at regular intervals along the height of the structure. Most of the damage was seen to be in a horizontal direction, while a couple of instances of vertical orientation of the damage were also observed. It is possible that the locations showing the horizontal orientation of damage were joint areas between successive lifts of the slip-form. Rust staining on the surface was visible at most of the locations of damage.

Upon initial assessment, it was clear that the damage was due to leakage of the SO_2 laden flue gases through the concrete shell, its subsequent transformation to sulphuric acid upon condensation, and attack of the concrete. Sulphuric acid severely diminishes the binding nature of cement paste, and the low pH conditions lead to corrosion of the reinforcing steel. At the base of the chimney, there was a pungent smell of gas, indicating the possibility of SO_2. When the access door was opened, extensive dust (ash) collection was seen at the bottom. The air inlets at 1.5 m level were also completely blocked with ash, and some gas leakage could be detected. A yellowish deposit had formed around the inlet, and some liquid discharge was also visible at the surface.

An external scaffolding had been erected at the site, which gave an access to the outer shell of the RCC chimney, and enabled detailed investigation of the concrete at a height of 15 m above ground level. Severe blistering of the concrete had occurred, and rust stains were seen under the damaged area. Some yellow and white deposits were also seen in the blistered area. Samples of this damaged concrete were collected for analysis.

Upon removal of the top layer of concrete, the steel rebar was exposed. In many locations, the hoop steel appeared to have a cover of less than 25 mm (the design cover depth was 50 mm). The steel was found to be undergoing severe corrosion, presumably due to the highly acidic environment caused by the condensation of the flue gases in the interior of the shell.

Some white deposits were also seen on the surface, with signs of wetness. When the external concrete was removed, the inner concrete seemed whitish, which is an indicator of chemical attack of the paste. The inner concrete also appeared warm, and some pungent odour was also detected, indicating a possibility of gas leakage.

The pH results clearly indicate that the concrete at the damaged locations on the external surface is in a severely acidic condition. Specifically, the blistered concrete samples showed pH less than 3.0, indicating highly acidic conditions. The undamaged concrete shows a good alkaline pH of 11.5.

The repair procedure suggested included chipping of damaged concrete, treatment of the reinforcement, patching and finally FRP wrapping.

2 CASE STUDY 2: FAILURE OF ACID BRICK LINING ON TOP LEVELS OF RCC CHIMNEY

Four core samples belonging to concrete from the upper level of a chimney, which was showing possible acidic attack on the inside surface, were received at the laboratory.

Carbonation depth was 4–6 mm for the concrete, which is only a fraction of the cover depth. Though a clear prediction of the probability of carbonation induced corrosion is not possible, it can be stated that the concrete is in good condition at present. The ultrasonic pulse velocity, which was in the range of 3.7–3.8 km/s, indicates that quality of concrete is 'Good' as per IS 13311 (1992). Compressive strength of the concrete core was 27.3 MPa, indicating a satisfactory equivalent cube compressive strength of 36.9 MPa (characteristic strength was supposed to be 30 MPa).

Sulphate contents of the outer deposit as well as the concrete samples from inside were high. The pH of the surface deposit on the inside of the chimney is less than 2, indicating a highly acidic condition. However, the inside samples of the core (with the exception of 2(b)) indicate an alkaline pH. Visual examination of the rebars indicated no signs of corrosion or section loss.

The tests on the core sample revealed that the inside section of the chimney was damaged by possible acid attack. However, the attack was limited to the surface regions, and the interior concrete was found to be in sound condition.

3 CASE STUDY 3: POOR QUALITY OF CONCRETE DURING CONSTRUCTION OF CHIMNEY

The primary issue to be investigated was the quality of concrete between the 86.75 and 89.50 m level of an RCC chimney, of proposed height 250 m, for an ultra-mega power project of 660 MW, which had a poor appearance and was indicating cube compressive strengths much lower than the design characteristic strength of 35 MPa.

A thorough visual inspection of the chimney was conducted during the site visit, and a review of the construction procedures and the concrete quality issues was also undertaken. Following the site visit, a detailed site investigation was carried out. The investigation included non-destructive evaluation using ultrasonic pulse velocity (UPV) and removal of cores from various locations in the chimney. The results from the tests and the extracted cores were sent to the laboratory, where the cores were tested for their strength and integrity.

UPV values in the 2 damage locations of the RC chimney fall under the category of 'Medium' as per the guidelines of IS 13311 (1992). At the laboratory, cores were tested first for ultrasonic pulse velocity. Following this test, the cores were capped using sulphur compound, and tested for compressive strength. With the exception of one core from the 86 m level that showed a UPV of 3.9 km/s, all other cores showed UPV between 4.5 and 5.4 km/s, indicating excellent quality of concrete. Further, all equivalent cube compressive strengths were more than 40 MPa, and the range was 40–75 MPa.

Results of the laboratory investigations of the cores show that the quality of concrete in the chimney between 86.75 and 89.50 m level is good. Thus, the defective concrete in this zone is only at the inner surface region of the chimney shell. Further, the cores from random locations along the chimney elevation also indicate sufficient compressive strength of the concrete. Thus, the recommendations were limited to correcting the surface quality of the concrete in the 86–90 m levels of the chimney. The distressed portion of the chimney was proposed to be chipped until sound concrete was encountered. The methodology of the proposed repair was categorized based on the thickness to which damaged concrete was to be removed to obtain a sound concrete.

REFERENCES

IS 516 1959. Methods of Test for Strength of Concrete—Reaffirmed 2008 Bureau of Indian Standards, New Delhi, India.

IS 2720 1987. Methods of Test for Soils—Part 26: Determination of pH Value. Bureau of Indian Standards, New Delhi, India.

IS 4032 1985. Method of Chemical Analysis of Hydraulic Cement—Reaffirmed 2005. Bureau of Indian Standards, New Delhi, India.

IS 13311 1992. "Non-destructive Testing of Concrete—Methods of Test", Bureau of Indian Standards, New Delhi, India.

Concrete Repair, Rehabilitation and Retrofitting III – Alexander et al. (eds)
© 2012 Taylor & Francis Group, London, ISBN 978-0-415-89952-9

An investigation into failures and problems of industrial floors on the ground—with an emphasis on case studies

R.S. Walls
BSM Baker—Civil & Structural Engineers, Johannesburg, South Africa

S.E. Ekolu
University of the Witwatersrand, School of Civil & Environmental Engineering, Johannesburg, South Africa

ABSTRACT: This paper presents an investigation into the problems encountered in industrial concrete floors on the ground. Shrinkage, acid attack, concrete quality, crazing, curling, durability issues and design considerations are addressed. Case studies from South African companies have been included to illustrate the problems and demonstrate how designs can be done to avoid such issues. Guidelines are proposed for fixing surface beds when problems have occurred. Overall it can be seen that floors are highly susceptible to a variety of problems. However, through good design and construction practices high quality surfaces can be provided for the industrial sector. It has been noted that few engineers and contractors are capable of successfully designing and constructing industrial concrete floors, and this issue must be addressed.

1 INTRODUCTION

We have more problems with surface beds than all other structural issues put together—G. Baker (Pr. Eng. structural engineer with 25 years consulting experience).

1.1 *Issues encountered with concrete surface beds*

Industrial concrete floors on the ground commonly experience problems due to design, construction and usage errors. This paper presents an investigation into the problems associated with industrial concrete floors, having an emphasis on case studies. Industry players have been consulted to obtain much of the information presented. The aim of the paper is to make designers aware of problems that commonly occur such that these might be avoided. Remedial action is suggested for floors in which problems have occurred.

Perrie (2009) lists potential problems in industrial floors as: scaling, crazing, dusting, colour variations, pop-outs, surface irregularities, plastic shrinkage cracks, curling, edge failures, freezing of dowels, faulting, sealant loss, pumping, cracking, corner breaks, shrinkage cracking and vertical slab movement. This long list highlights the difficulties in constructing floors. In this paper, the following problems are specifically addressed due to their high level of occurrence: shrinkage, concrete quality, durability, acid attack, curling, the use of sealants and joints, surface issues, and temperature and lateral restraint effects. The requirements of floors and methods for their construction are briefly addressed because they have a significant influence on the quality of facilities constructed.

2 COMMON PROBLEMS IN CONCRETE INDUSTRIAL FLOORS

Various case studies regarding issues encountered in surface beds, primarily from South Africa, are addressed below.

Figure 1 shows a floor in a bakery which supplies one of South Africa's largest, supermarket chains (Walls, 2009). The bakery was almost closed when the supermarket became aware of the unsanitary condition of the concrete floors. Acid attack from sugars and other chemicals has caused wide spread floor deterioration. It can be seen that in the vicinity of the drain in Figure 1, the concrete quality is the poorest.

An example of delamination is shown in Figure 2, where a delaminated floor in a logistics warehouse is being repaired (Walls, 2009). Readymix concrete was delivered from two separate suppliers. It happened that one delivery supplied was of inferior quality, which led to the delamination. As a result of this flaw, entire sections of the floor had to be replaced.

The delamination of the floor shown in Figure 3 occurred at a factory near Johannesburg. It is believed that the problem was caused by rain falling

Figure 1. Acid attack occurring at a bakery. Note the extensive degradation in the vicinity of the drain (Walls, 2009).

Figure 2. Repair of a delaminated floor at a logistics warehouse (Walls, 2009).

during the casting and floating of the floor, as well as the contractor placing cement onto the floor when floating the concrete to give it a burnished appearance. To remedy the situation a screed from 15–22 mm was pumped onto the surface to create a smooth finish, after the floor had been scarified.

Figure 4 is a case where a series of joint in a warehouse in Johannesburg failed (Baker, 2009). A number of construction errors led to the problems observed. Joints were not sealed for many months, which left slab edges exposed. Joints were incorrectly protected in the interim period, while the floor was allowed to shrink. A soft sealer could potentially have been used in this interim period to reduce the damage. However, excessive concrete shrinkage occurred (which resulted in slab curling) and would have caused a sealer to fail even if it had been used. In this particular case, 3 mm wide sawcuts had been made, but these joints opened to around 6 mm. Most commercially available sealants cannot accommodate strains of 100%.

It is not strictly essential to sawcut and seal a floor. Norton (2009) reports of a toys storage warehouse in America that was built with no joints. Instead the floor was allowed to crack freely. An irregular crack pattern was formed on the floor but its durability and quality was not affected. An epoxy was used to seal the floor and joints. The case suggests a possibility of constructing floors without cutting joints but this construction requires some understanding of the finished product by the client.

Figure 3. Delamination of a floor in a factory.

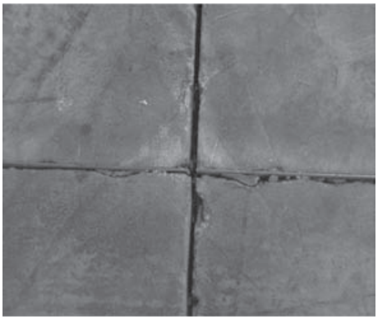

Figure 4. Photo showing a sawcut joint which has been incorrectly sealed and damaged (Baker, 2009).

3 CONCLUSIONS

Industrial concrete floors on the ground are important structural components which are widely used. However, they are also highly susceptible to construction and durability problems. The numerous difficulties cited in this paper have to be addressed when designing and constructing such floors. However, even experienced contractors and engineers will encounter situations where problems arise. At these stages a large variety of repair methods can be used to bring floors back into serviceability.

REFERENCES

Baker, G. 2009. An interview was held with Mr. Geoff Baker (Pr. Eng) on 13 October 2009.

Norton, P. 2009. An interview was held with Mr. Peter Norton, an expert in concrete floors, on 27 October 2009.

Perrie, B. 2009. Common failures in concrete floors and designing and specifying to prevent them. Presentation made at CSSA, Midrand, for the Concrete and Cement Institute on 7 July.

Walls, S. 2009. Numerous interviews were held with Mr. Stuart Walls (Pr. Eng.) in October and November 2009.

Concrete Repair, Rehabilitation and Retrofitting III – Alexander et al. (eds)
© 2012 Taylor & Francis Group, London, ISBN 978-0-415-89952-9

Concrete damage in underground structures

F. Mittermayr, D. Klammer, D. Höllen & M. Dietzel
Institute of Applied Geosciences, Graz University of Technology, Graz, Austria

C. Kurta
Institute of Chemistry—Analytical Chemistry, University of Graz. Graz, Austria

A. Leis
RESOURCES—Institute for Water, Energy and Sustainability, Joanneum Research. Graz, Austria

M.E. Böttcher
Leibniz Institute for Baltic Sea Research, IOW, Rostock, Germany

ABSTRACT: In this paper we present an overview about our findings concerning the damage of underground concrete structures. Case studies were performed in Austrian highway and railroad tunnels and associated structures for drainage and ventilation. In several cases severe damage of the concrete was found owing to sulphate attack, alkali aggregate reactions, leaching and drainage clogging. The focus of this study is to demonstrate by some selected examples how to decipher the causes and reaction mechanisms of damaging reactions. Thus besides conventional mineralogical and hydro-geochemical methods we apply stable isotope and trace element signals within multi proxy approaches. For instance stable isotope results indicate that SO_4^{2-} and CO_3^{2-} from local ground water are mostly responsible for thaumasite formation. More detailed knowledge on individual reactions responsible for concrete damage in underground structures will help to find specific counter measures for already affected buildings and to develop proper concrete recipes, applications and constructive measures for future projects.

1 INTRODUCTION

Remediation and reconstruction of damaged concrete structures in the underground caused by the interaction with the local environment is highly cost intensive and has to be reduced at all means. However, due to the environmental conditions, like geology, temperature and ground water chemistry, underground structures are frequently affected by serious damage (Leemann and Loser, 2011). Glasser et al. (2008) have pointed numerous reactions that may take place in the concrete—water—atmosphere system and may lead to concrete damage. In the present study sulphate attack and subsequent thaumasite formation is highlighted. In spite of enormous research effort there still persist many uncertainties in regard to causes and reaction mechanisms. Thus, the understanding has to be brought to the next level. A powerful tool to approach such matter is the application of stable isotopes (Iden and Hagelia, 2003). With this study we demonstrate that multi proxy approaches including isotopic signatures and trace element contents will lead to a deeper understanding of concrete damage.

2 MATERIALS AND METHODS

We have sampled solids and liquids from Austrian highway and railroad tunnels. Solid samples comprise shotcretes and concretes (unaltered and deteriorated) and secondary formations such as mushy concrete, efflorescences and sinter. Completely disintegrated mushy material was shoveled in plastic bags and consolidated concrete was excavated taking drilling cores. Furthermore natural host rock and soot relicts found in one railroad tunnel were investigated. Samples were analyzed by XRD, SEM and EPMA. Liquid samples comprise drainage solutions, local ground water and interstitial solutions that were expressed from damaged concrete material. In the field temperature and pH of ground and drainage water were measured. The alkalinity was determined by potentiometric titration with HCl in the lab. Concentrations of dissolved ions were analyzed by IC and ICP-MS. Furthermore stable isotope ratios of $^{34}S/^{32}S$, $^{13}C/^{12}C$, $^{18}O/^{16}O$ and $^{2}H/H$ of were measured of solid and liquid samples.

3 RESULTS AND DISCUSSION

XRD pattern of sound concretes and shotcretes display poorly crystalline CSH-phases, portlandite ($Ca(OH)_2$) as well as silicate and carbonate aggregates. Mineralogical investigations (XRD, EPMA, SEM) clearly show that severe concrete deterioration is caused by sulphate attack. Complete disintegrated materials consist mainly of thaumasite, calcite and silicate aggregates. Gypsum was found in small quantities and ettringite could not be identified unambiguously due to the structural similarity and the overwhelming presents of thaumasite. Furthermore significantly reduction and even total lacking of dolomite aggregates were detected by comparing sound and deteriorated material. Surprisingly ground water and drainage water analyses generally showed only low to moderately elevated SO_4^{2-} content with values ranging from about 3 to 500 mg/l. Consequently arising the question: Is dissolved SO_4^{2-} of ground water the only source or are we facing other S sources coming from e.g. internal from concrete/shotcrete, oxidation of pyrite, atmospheric contribution, or organic matter such as soot. The latter source was the most likely candidate for a more than 100 years old railroad tunnel which was not properly cleaned before shotcrete was applied about 50 years ago. In spite of rather low SO_4^{2-} content in the ground water S-isotope measurements clearly indicate that SO_4 in thaumasite is stemming from infiltrating ground water implicating the dissolution of local occurring gypsum and anhydrite rocks. $\delta^{34}S$ values of thaumasite, ground water SO_4^{2-} and host rock are mostly within the range of +14 to +27‰ (Mittermayr et al., 2012a). In a few locations significantly lower $\delta^{34}S$ signals were detected in thaumasite resulting from pyrite oxidation. Interestingly internal sulphate attack or contributions from soot or the Earth's atmosphere can be ruled out by the given $\delta^{34}S$ ranges which opens up a new subject: How does ground water with about 500 mg/l of sulphate or even less may cause intensive sulphate attack? Therefore we analyzed the chemical and isotopic composition of interstitial solutions extracted from heavily damaged concrete samples by using a hydraulic press. Proportions of extracted solutions correspond to about 5 up to 20 wt.% of the solid material and extreme accumulation of Na^+ and SO_4^{2-} is observed compared to the locally occurring ground water. Considering the dramatic increase of univalent cations compared to the local ground water and the rather conservative behavior of e.g. K^+ and Rb^+ suggests evaporation of water to be responsible for extreme SO_4^{2-} concentrations of up to 30000 mg/l (Mittermayr et al., 2011). Proof is gained from analyses of δ^2H and $\delta^{18}O$ values of H_2O molecules which display a strong enrichment of the heavy stable isotopes. The respective kind of isotopic evolution clearly indicates evaporation of H_2O from the local ground water. A further curiosity with a high need to be verified was the incongruent dissolution of dolomite aggregates. Previously we have suggested that dolomite aggregates are preferentially dissolving incongruently governed by high Ca^{2+}/Mg^{2+} ratio in the interacting aqueous solution. Calcite becomes more stable versus dolomite. As long as the pH remains above 10.5 the continuous removal of dissolved Mg^{2+} from the solution is leading to brucite ($Mg(OH)_2$) formation. Surprisingly in all cases where sulphate attack in combination with dolomite aggregates was found, a partial dissolution of the latter and precipitation of secondary calcite and brucite was observed. Thus we assumed carbonate released by dolomite dissolution to have contributed to thaumasite formation. Various studies suggest that the carbonate can be stemming from the absorption of atmospheric CO_2, carbonate aggregates or DIC of ground water. To investigate the carbon source in thaumasite we applied stable carbon isotopes. In contrary to our assumption that carbonate is originating from dolomite aggregates, we found the carbon in thaumasite to be related to the uptake of ground water DIC. $\delta^{13}C$ values from thaumasite and DIC are mostly in the same range from −11 to −5‰ (Mittermayr et al., 2012b). Most carbonates used as aggregates are usually much heavier in isotopic values and are plotting at 0 ± 2‰. In contrary Dietzel (1995) has pointed out that the formation of calcium carbonate related to the absorption of atmospheric CO_2 is leading to a strong depletion of ^{13}C versus ^{12}C. The latter reaction occurs at high pH and is governed by a kinetic isotope fractionation leading to $\delta^{13}C$ values of −25 ± 3‰.

4 CONCLUSION

Applications of multiproxy approaches including stable isotope distributions and trace element contents have shown to be very powerful tools for a deeper and sophisticated understanding of concrete deteriorating processes. Complex reaction paths can be reconstructed and individual causes for the damage can be revealed. Thus repair and remediation measures can be focused and potential threats to the concrete structure should be assessed in the forefront of future projects.

REFERENCES

Dietzel, M., 1995. $^{13}C/^{12}C$ Signatures and $^{18}O/^{16}O$ signatures of calcite precipitations in drainage systems. Acta Hydrochimica Et Hydrobiologica, 23(4): 180–184.

Glauresser, F.P., Marchand, J. & Samson, E., 2008. Durability of concrete—Degradation phenomena involving detrimental chemical reactions. Cement and Concrete Research, 38(2): 226–246.

Iden, I.K. & Hagelia, P., 2003. C, O and S isotopic signatures in concrete which have suffered thaumasite formation and limited thaumasite form of sulfate attack. Cement and Concrete Composites, 25(8): 839–846.

Leemann, A. & Loser, R., 2011. Analysis of concrete in a vertical ventilation shaft exposed to sulfate-containing groundwater for 45 years. Cement & Concrete Composites, 33(1): 74–83.

Mittermayr, F. et al., 2012a. Concrete under Sulphate Attack: An Isotope Study on Sulphur Sources Isotopes in Environmental & Health Studies, 48(1): 105–117.

Mittermayr, F. et al., 2011. Deterioration of concrete—application of stable isotopes. In: M.A.T.M. Broekmans (Editor), 10th International Congress for Applied Mineralogy. Springer, Trondheim: 435–444.

Mittermayr, F., Rinder, T., Klammer, D., Leis, A. & Dietzel, M., 2012b. A Carbon Isotope Study of Thaumasite and Calcite Sinter Formation in Underground Construction, International Congress on Durability of Concrete, Trondheim, pp. in Press.

Concrete Repair, Rehabilitation and Retrofitting III – Alexander et al. (eds)
© 2012 Taylor & Francis Group, London, ISBN 978-0-415-89952-9

Managing risk for concrete repair to multi-storey buildings

P. Storey
Storey ENG (Pty) Ltd, Cape Town, South Africa

J. A. Wium
Department of Civil Engineering, University of Stellenbosch, South Africa

ABSTRACT: The repair of multi-storey concrete frame buildings requires, besides the correct evaluation of the condition of the structure and the selection of the appropriate repair technology, the correct assessment of the risk involved, the apportionment of the risk between the parties involved in the repair process, and the management of the repair process to minimize the risk. This risk includes, amongst others, the absence of design and as built information, the often limited knowledge of the condition of the concrete, the imprecise quantification of the repairs to be carried out, the consistency of the quality of the repairs, and the long term performance of the repair materials. This paper first identifies the risks and explores how information models can reduce some aspects of the risk. It also defines the various parties involved with the repair of a concrete frame building, namely the building owner, consulting engineer, and contractor. It then looks at the manner in which these risks are apportioned and contracted between these various parties. The forms of contract generally found in the construction industry are subsequently discussed with specific reference to how each deals with risk.

1 INTRODUCTION

The concrete frames of many multi-storey buildings are found to be in need of repair. These buildings may be many years old in which the concrete has suffered such damage as carbonation or chloride ion attack. It occurs more and more that even buildings that are only a few years old also suffer degradation due to poor construction techniques or the lack of quality control during construction.

This paper, with specific reference to multi-storey buildings of which the owners have limited funds to expend on repairs, looks at the risks associated with the assessment of the condition of the buildings, the selection of suitable repair techniques, the apportionment of risk between the various parties involved in the repair process, and the carrying out of the repairs. Recommendations are made particularly with the view of ameliorating risk.

2 RISKS ASSOCIATED WITH CONCRETE REPAIR

The repair of damaged concrete carries with it inherent risks. The success of the repair operation is to a large degree dependent on the extent to which the risks are identified and the steps taken to manage and ameliorate the risk. The risks can broadly be categorized as follows:

– The original design and construction of the building.
– The condition assessment.
– The repair designs and specifications.
– The contractual arrangements between the parties involved with the repairs.
– The execution of the repairs.

3 ORIGINAL DESIGN AND CONSTRUCTION

Designs and construction records can provide valuable clues as to the cause of the problems being experienced. Design information includes design loads, concrete strengths, reinforcing content and cover depths, and stress zones (element forces). Construction information includes concrete mix designs, temperature at time of placing of concrete, curing methods, and quality test results.

Historical information is usually not available and construction information is even scarcer.

Recent developments in Building Information Models have shown that these can be used effectively in life cycle management of structures (Hallberg and Tarandi (2011)).

4 CONDITION ASSESSMENT

The successful repair of a concrete structure requires that the condition of the concrete be correctly assessed.

Techniques that have been found to provide reliable results at costs commensurate with the value of the buildings and funding available for repairs include visual inspections, and carbonation and chloride ion testing.

Façade mapping is extremely useful as an estimating tool when preparing repair budgets. The building façade is divided into equal sized zones. For each zone the extent of the damage identified during the assessment is indicated. These areas are measured and multiplied with an estimated depth of repair to arrive at a repair budget. In each zone the actual extent of the repairs carried out are indicated.

5 REPAIR DESIGNS AND SPECIFICATIONS

Before any designs and specifications can be prepared it is essential that the responsible practitioner develops the correct understanding of the cause of the problems. This can be difficult as there is often a lack of available information and assessments of the condition of the building at best reveal only part of the picture. Hence it is vitally important that suitably experienced practitioners prepare the designs and specifications.

Designs must take into account the age of the building, the structural systems employed, the cause of the problems, and how the repairs can be carried out

Repair designs must consider the influence of structural failure on the degradation in the condition of the concrete.

Many repair products are available, and for the most part are quality products produced by reputable manufacturers. Care must in particular be taken to ensure that the repair products do not increase the potential for further problems developing, for example the incorrect use of metal oxide coatings can lead to rapid corrosion of reinforcing steel adjacent to the coated areas.

6 CONTRACTUAL ARRANGEMENTS

The success or failure of any concrete repair is a team effort with each party, building owner / client, consulting engineer / repair practitioner, and contractor, having a specific role to play and share of the risks and rewards.

The paper discusses the specific roles of each of the owner, consultant and contractor, and their responsibilities which will reduce the risk on the project.

Central to ensuring that the various parties understand and take on their roles and responsibilities in a concrete repair project, are the forms of contract entered into between them. Different forms of contract are discussed and the advantages and disadvantages of each are identified.

7 MANAGEMENT OF REPAIR PROCESS

The final and most critical stage in the concrete repair process is the execution of the work. During this stage all of the risk management done in the assessment, design and specification, and bid procurement stages can be undone. The paper identifies the responsibilities of the owner, consultant and contractor and finally shows that all parties must work together as a team, recognizing the responsibilities and skills each brings to bear.

REFERENCES

FIDIC Client/Consultant Model Services Agreement: White Book, FIDIC, 2006.

Guideline Scope of Services and Tariff of Fees for Persons Registered in Terms of the Engineering Profession Act, 2000, (Act No. 46 of 2000). Engineering Council of South Africa.

Hallberg, D. & Tarandi, V. On the use of open BIM and 4D visualisation in a predictive life cycle management system for construction works. Journal of Information Technology in Construction. February 2011.

NEC 3 Engineering and Construction Contract, Institute of Civil Engineers, 2005.

Concrete Repair, Rehabilitation and Retrofitting III – Alexander et al. (eds)
© 2012 Taylor & Francis Group, London, ISBN 978-0-415-89952-9

Condition assessment and repair strategy for seawater intake structure in Saudi Arabia

M.K. Rahman, M. Ibrahim, S.M. Shaahid & M. Barry
Research Institute, King Fahd University of Petroleum & Minerals, Saudi Arabia

M. Alkami
Saudi Aramco, Saudi Arabia

M.R. Taha
Department of Civil Engineering, University of New Mexico, USA

ABSTRACT: A reinforced concrete seawater intake structure is in service over the past three decades in a hypersaline marine environment in Saudi Arabia. Concrete spalling/delamination and corrosion of reinforcing steel were observed in the portion of the structure above the waterline. Condition assessment of the intake structure from outside and inside above and below the water line was conducted. Non-destructive and partially destructive investigations above and underwater, chloride and sulfate ion profiles, chloride ion permeability, water absorption and petrographic study of concrete cores was carried out. The overall structural rating of the structure is "Poor to Fair" with some zones being rated as "Serious". Reinforcement in the splash zone and above, in the walls, girders and beams, and top slab inside the seawater intake chamber are in an active state of corrosion after 32 years in service in harsh marine environment. A repair strategy was developed to enhance the service life of the structure.

1 INTRODUCTION

The seawater treatment plant under study treats seawater that is mainly used for injection in the oil fields for production and secondary oil recovery. The plant with a capacity of 7 million bpd has been serving the oil fields for the last 32 years. The reinforced concrete seawater intake structure has three chambers and seawater enters into these chambers through openings on the front side. The cleaning the seawater takes place at the bar screens and the drum screens. The seawater clear of all debris then passes through the baffle walls into the interconnected chamber. The seawater from this chamber is pumped by vertical lift pumps (1200 mm suction pipe) to the filtration units for treatment.

The coastal structures are in general under high exposure to physical, biological and chemical attack. A wide range of chemicals in seawater can attack concrete under water. Underwater inspection is important for coastal structures to prevent failures that could lead to financial losses and long duration inactivity of critical facilities.

Severe spalling and delamination of concrete and corrosion of reinforcing steel was observed in the portion of the structure above the waterline. A condition assessment of the intake structure was carried out involving inspection of the structure above and below the water line for outer walls, the roof slab, and the inlet chambers housing the bar screen, drum screen and lift pumps. For the purpose of inspection, the seawater intake structure was divided into five zones (Zone-I to Zone-V) based on accessibility for inspection. Areas with common access were grouped in one zone. The inspection and assessment was carried out based on American Society of Civil Engineering (ASCE) guidelines for inspection of structure, and various zones of the structure were rated according to these ASCE guidelines.

2 INSPECTION OF THE INTAKE STRUCTURE

ASCE provides three levels of inspection for routine inspections: (1) **Level I**: Visual inspection of underwater components without removal of marine growth, (2) **Level II**: Partial marine growth removal of statistically representative sample—typically 10% of all components and (3) **Level III**: NDT and PDT of statistically representative sample—typically 5% of all components.

Underwater inspection work in Zone I (outer walls) began with a baseline Level I inspection, recording existing conditions prior to partial cleaning of the exterior of the structure below the water line. A Level II inspection then followed by partial cleaning of the submerged surfaces by hydro jetting.

The Level II inspection included underwater video, documenting observed defects and deterioration. This was followed by a Level III inspection including PDT, with underwater cores extracted from Zone I. The submerged concrete in Zone I appeared sound and free of significant defects or deterioration from marine fouling including algae, barnacles, mollusks and tubeworms.

The reinforcement in the exposed surface of the top slab (Zone II) was found to be in active state of corrosion, being exposed to air and salt-laden seawater spray. In Zone III (representing the lift pump basin chamber) cracking, spalling and corrosion of reinforcement were observed in all areas where top slab openings exist. Leaching of salts was observed at some cracks. A beam near vertical lift-pumps shows severe distress with spalling and reinforcement corrosion. Almost all of the bottom side of the shear stirrups was gone in some portions (Figure 1).

The concrete in the portions of Zones IV (three chambers housing the drum screen) in the intake structure, which are typically submerged, appeared sound and free of significant damage or deterioration. Light to moderate marine growth (typically barnacles) was evident in both areas. Similar observations were made in Zone V (bar screen chamber). Efflorescence, rust staining, cracking and delamination of concrete was observed at several locations in the slab of Zones IV and V.

3 FIELD AND LABORATORY STUDIES

NDT conducted for the intake structure included sounding by hammer, ultrasonic pulse velocity measurements, mapping of cracks, spalling corrosion, mechanical damage, and coring above and below the water line. Ultrasonic pulse velocity measurements were performed on concrete walls and beams using the V-Meter. Half-cell potential test was also carried out on various elements to determine the corrosion activity of the reinforcing steel. Concrete cores and powder samples extracted from the structure were used to obtain water-soluble chloride and sulfate contents by weight of concrete.

Tests were conducted on the concrete cores and the powder samples obtained from various zones of seawater intake structure including, petrographic examination of concrete, compressive strength of concrete, pulse velocity in cores, chemical analysis, water soluble chloride ions, XRF analysis, sulfate content, pH of concrete, absorption tests, rapid chloride permeability test, and Scanning Electron Microscope examination.

Figure 1. Beam showing spalling and corrosion.

The compressive strength tests show that a good quality concrete was used in the construction of the seawater intake structure. The chloride concentrations in different structural members were found to range between 0.085% and 0.26% by weight of concrete at the rebar level (Threshold concentration 0.03–0.05%). The sulfate concentration varied from 0.23% to 0.43% by weight of concrete (Allowable sulfate concentration as per BS 8110 part 124 is 0.6% by weight of concrete).

Petrographic examination of concrete cores showed that concrete used in the structure is non-air-entrained, dense and well-consolidated. The Portland cement content is estimated to be 330 to 350 kg/m^3; and is found to have high ferrite (iron) content. The water-cement ratio varies from 0.38 to 0.42; and air content is estimated to be less than 1 percent. Petrographic examination of underwater concrete shows that there is no evidence of any chemical (chloride or sulfate) attack of seawater or related deteriorations in the concrete.

Based on the studies conducted, the overall structural rating of the structure is "Poor to Fair". Delamination, spalling and cracking is evident in Zone III, IV and V in several concrete structural members. The structural condition inside the intake structure is in advance stages of deterioration. The worst condition was observed in Zones II and III, where the ratings range from "Serious to Poor". Only one zone in the structure, the splash zone in Zone III, is rated as "Serious", indicating its significance on the overall structural safety and its need for urgent repair. The portion of the structure below the water line was found to be in good condition; however, there are indications that the corrosion potential of the reinforcing bars has surpassed the threshold.

4 CONCLUSIONS

Inspection and assessment of the seawater intake structure, show significant deterioration including corrosion of reinforcement, delamination of concrete and cracking of concrete structural elements in the intake structure in various zones. Some of the deterioration identified in the inspection is "**serious**" in ranking and if not addressed, the structural capacity will continue to degrade over time and may result in failure. Repairs are therefore needed for inhibiting or slowing down the rate of corrosion in concrete elements so that they may continue to provide adequate structural capacity for another ten years. A repair strategy is proposed to ensure the long-term serviceability of the structure.

Concrete Repair, Rehabilitation and Retrofitting III – Alexander et al. (eds)
ISBN 978-0-415-89952-9

Corrosion damage of concrete structures in ammonium nitrate-based environments

I. Pepenar
ICECON GROUP-The Research Centre CERTINCON, Bucharest, Romania

ABSTRACT: The paper presents the results of the research on the long-term corrosion behaviour of the reinforced concrete structures, after 30 to 50 years of service in ammonium nitrate-based industrial environments, in respect of the damage generated by the corrosive action of aggressive agents. Investigation of the damage state of reinforced concrete structures, on site and in the laboratory, showed that many of examined elements presented severe damage due to corrosion. This damage was in various stages of development and had a different influence on the resistance, stability and durability of the elements. The conclusions underlie the complexity of the corrosion process on reinforced concrete structures exposed to ammonium nitrate-based environments, also affecting concrete and steel reinforcement. The considerations on the mechanisms of the corrosion processes of concrete and steel reinforcement under the action of ammonium nitrate environments are also described. The possibility of apparition and development of stress corrosion cracking phenomenon of steel reinforcements associated with non-controlled reduction of physico-mechanical characteristics of concrete by corrosion, led in the end to significant diminution or loss of bearing capacity and sudden break (collapse) of reinforced concrete elements/structures.

1 INTRODUCTION

The corrosive action of ammonium nitrate-based aggressive environments, encountered mainly in the industry of chemical fertilizers, has various damage effects upon reinforced concrete structures.

2 SERVICE BEHAVIOUR OF STRUCTURES

2.1 *Types of structures*

There were investigated two representative types of reinforced concrete structures:

- An industrial multistoried building of fabrication;
- Granulation towers of ammonium nitrate, calcium ammonium nitrate and complex fertilizers.

2.2 *Aggressivity of environments*

The reinforced concrete elements were subjected to a long-term action of a strongly aggressive environment, made from various aggressive agents: ammonium and calcium nitrates, compounds with nitrates etc.

2.3 *Damages by corrosion*

Based on specific investigation techniques, the analysis of damage state of reinforced concrete elements after 30 to 50 years of service, pointed out severe damages mainly generated by the strongly corrosive action of the ammonium nitrate. These are concise presented as follows:

- concrete cracking, along the longitudinal steel reinforcements, more accentuated in the marginal area. The corrosion was caused by expansion of the concrete under the action of nitrates. In a further phase, spalling of the concrete cover occurred and afterwards corrosion of the interior concrete;
- fragile fractures, without reduction of the cross-section of steel stirrups (seen in some areas) caused by stress corrosion cracking (columns);
- fragile fractures, without reduction of the cross-section, of longitudinal and transversal reinforcements, caused by stress cracking corrosion induced by the nitrates (beams, slabs, walls). There were also observed local (pitting) and general corrosion phenomena of the steel;
- failures of the beams and slabs due to fracture of reinforcements by stress corrosion cracking.

3 LABORATORY TESTS

The main results of the laboratory tests performed on a large number of concrete and steel reinforcement samples extracted from the corrosion affected elements, showed the following:

- the compressive strength of apparently undamaged concrete varied between 16,3 and 29,5 MPa, while the compressive strength of corroded concrete was diminished to 0;
- the water soluble concentrations of NO_3^- and NH_4^+ ions in the concrete samples damaged by corrosion ranged between 0.70 and 9.02% NO_3^- and 0.15 and 2.15% NH_4^+ (by weight of concrete);
- the pH of aqueous suspension of the concrete samples damaged by corrosion varied between 5.5 and 8.5;
- the steel reinforcements present three main types of corrosion: general and local corrosion, being the types of common corrosion in case of mild carbon steels for reinforced concrete; stress corrosion cracking, the specific type of corrosion found in high strength steel used as tendons in prestressed concrete structures;
- the examination of the reinforcements surfaces revealed (in some samples) the existence of thin cracks, placed perpendicularly to the samples axes, some of them inducing incomplete fracture of the reinforcements;
- the fracture aspect of samples affected by stress corrosion cracking had a fragile character (without reduction of cross-section), due to the presence of typical corrosion induced crack;
- the cracks propagation had an intergranular aspect, some samples showing a visible corrosive attack at the grain boundaries, especially in the superficially decarburized areas.

4 CORROSION MECHANISMS

4.1 *Corrosion mechanism of concrete*

The corrosion action of ammonium nitrate-based aggressive environments on concrete consists in two successive stages:

- decalcification phenomena having as effect the desalkalinization of concrete:
$$2NH_4NO_3 + Ca(OH)_2 + 2H_2O \rightarrow Ca(NO_3)_2 \cdot 4H_2O + NH_3\uparrow \quad (1)$$
- expansion phenomena (similar to sulphate corrosion):
$$Ca(NO_3)_2 \cdot 4H_2O + 3CaO \cdot Al_2O_3 \cdot 6H_2O \rightarrow 3CaO \cdot Al_2O_3 \cdot Ca(NO_3)_2 \cdot 10H_2O \quad (2)$$

These decalcification and expansion phenomena lead to de-alkalinisation, cracking and finally to a rapid concrete destruction by corrosion.

4.2 *Corrosion mechanism of steel reinforcement*

The general corrosion of steel in ammonium nitrate environments is caused by high oxidation capacity on NO_3^- ions and complexing action of Fe^{2+} ions by the NH_4^+ ions. The global corrosion reaction is:

$$9NH_4NO_3 + 14NH_3 + 4Fe \rightarrow 4[Fe(NH_3)_6)] \cdot (NO_3)_2 + 3H_2O \quad (3)$$

The steel corrosion products in these environments comprises of a mix of $[Fe(NH_3)_6)] . (NO_3)_2$ and Fe_3O_4, unadherent and unprotective products towards steel.

The local corrosion of the steel in ammonium nitrate environments is caused by the depassivating action of NO_3^- ions, similar with that caused by Cl^- ions, with formation of corrosion points (pitting). Local destruction of the passivation film, formed at the steel surface in the concrete pores electrolyte, is produced by a mechanism based on anionic penetration reactions.

The stress corrosion cracking is a specific corrosion type of steel in ammonium nitrate environments, characterized by the cracking and fracture of the steel reinforcement, without reduction of cross-section and without visible loss of metal. It is produced by electrochemical selective dissolution of the anodic areas (active path corrosion) and the crack growth is by an anodic mechanism, with an intergranular aspect.

5 CONCLUSIONS

The results of the research on the long-term corrosion behaviour of reinforced concrete structures, after 30 to 50 years of service in ammonium nitrate-based industrial environments, has pointed out the existence of a severe corrosion-induced damage, which affected the resistance, stability and durability of the structures.

The aggressiveness of ammonium nitrate environments against reinforced concrete elements/structures acts in a complex and specific manner, both upon the concrete and its steel reinforcement, by different mechanisms.

The possibility of apparition and development of stress corrosion cracking phenomenon of steel reinforcements associated with non-controlled reduction of physico-mechanical characteristics of concrete by corrosion, can lead in the end to significant diminution or loss of bearing capacity and sudden break (collapse) of reinforced concrete elements/structures.

In order to assure normal service conditions of structures in ammonium nitrate-based industrial environments, intervention measures to remedy existing damages and systematic monitoring of the service behaviour of reinforced concrete elements/structures is required.

Concrete Repair, Rehabilitation and Retrofitting III – Alexander et al. (eds)
© 2012 Taylor & Francis Group, London, ISBN 978-0-415-89952-9

Condition assessment and repair of antenna towers concrete foundations

I. Banjad Pecur, N. Stirmer & B. Milovanovic
Department of Materials, Faculty of Civil Engineering, University of Zagreb, Zagreb, Croatia

ABSTRACT: Deterioration of telecommunication antenna tower foundations is becoming an issue of critical importance in the Croatian electronic communications network since little attention has been directed toward the design against failure and premature deterioration of concrete footings and buried tower components in the design period. In this paper, a case study of comprehensive condition assessment and repair works of defective concrete foundations of 3 self-supported antenna towers exposed to extreme environmental loads is presented. In the first step of investigation, visual examination for the preliminary assessment was done, while in the second step, the detailed examination was provided. The mechanical and durability properties were tested in-situ and in laboratory. Factors affecting the durability of tower anchorages and foundations are discussed together with introduction of repair methods of tower foundations. As presented case studies illustrates, concrete deterioration and distress must be carefully monitored and evaluated to determine the appropriate repair method.

1 INTRODUCTION

Deterioration of telecommunication antenna tower foundations is becoming an issue of critical importance in the Croatian electronic communications network. The overall layout of telecommunication towers is governed by the requirements to the transmission and receiving conditions which leads to tall structures in mountainous areas. Added hereto the access and working conditions for installation and service many solutions often lead to various problems with regard to design, construction and maintenance.

In addition, the predominant loads of antenna towers are natural loads as wind and ice, loads that also effects the deterioration. While the telecommunication equipment and the load bearing steel structure is well maintained, little attention has been directed toward concrete footings and buried tower components.

2 DESCRIPTION OF THE INVESTIGATED TOWERS

Defective concrete foundations of 3 self-supported antenna towers, Licka Pljesivica, Mirkovica and Ucka, were investigated, figure 1. These towers were erected in 1978, beginning of the 1960s and beginning of 1980s, respectively.

Available data about the antenna towers was negligible, while the basic designs of the towers were found, the data about strengthening and upgrade that happened during the exploitation of all three towers was missing.

Self supported towers have one central concrete foundation with as many attachment points as the sides of the tower structure. The attachment points are anchored deep into the central foundation through the concrete pedestals.

3 DEGRADATION OF TOWER FOUNDATIONS

Visual inspection revealed that all three antenna towers were poorly refurbished.

The cracks width spanned from 0.1 to 0.5 mm, while the delaminations of the repair mortar on Mirkovica and Ucka towers appeared at the 70 and 75% of the foundation surface, respectively.

Generally, the concrete can be characterized as unambiguous, full of voids due to missing fine aggregates in the concrete mix and poor concreting technology. The designed values of the concrete built-in were intended to be C20/25. From the results of compressive strength testing it is visible that overall compressive strength of the concrete does not satisfy prescribed values, table 1.

The homogeneity of concrete foundations surface layer was also tested using Schmidt hammer method which also indicate the inhomogeneous concrete.

The water absorption and gas permeability, tables 2 & 3 of the concrete cores were also tested in order to detect durability problems and in addition to provide the information about timely and cost-effective protection of the concrete structure.

Figure 1. Photograph of the self-supported antenna tower Ucka.

Table 1. Results of the compressive strength testing.

Antenna tower	Licka Pljesivica	Mirkovica	Ucka
Number of tested specimens	8	12	15
Minimum value [MPa]	16.90	5.49	3.80
Maximum value [MPa]	49.70	28.93	38.10
Average value [MPa]	35.79	11.71	13.95
Standard deviation [MPa]	11.75	7.05	10.28

Table 2. Results of the capillary absorption testing.

Antenna tower	Licka Pljesivica	Mirkovica	Ucka
Coefficient of capillary absorption, average C [$g/mm^2/h^{-0,5}$]	–	15.86E-4	11.82E-4
Standard deviation [$g/mm^2/h^{-0,5}$]	–	4.13E-4	6.50E-4

Table 3. Results of the gas permeability testing.

Antenna tower	Licka Pljesivica	Mirkovica	Ucka
Coefficient of gas permeability, average [cm^2]	–	8.49E-13	7.79E-13
Standard deviation [cm^2]	–	3.07E-13	4.51E-13

In general, the concrete from tested foundations can be characterized as poor quality concrete.

Pull off test was used to determine the adhesive and tensile strength of concrete foundations, together with the mode of failure they were determined to be important performance properties that would be used as an input parameter in determining the characteristics of repair materials.

The pull off test results gained showed very low adhesion strength while the predominant fracture mode was across the concrete substrate. This indicates the necessity of creating a stronger bond surface between concrete and repair mortar.

4 REPAIR OF ANTENNA TOWER FOUNDATIONS

All of the results presented in this paper are direct evidence of poor construction technology of the antenna tower foundations due to demanding construction conditions and harsh environmental conditions on the antenna tower locations.

In order to provide solutions which would restore the strength and durability of the defective concrete foundations so that adequate safety margins could be achieved, the following steps were carried out to achieve a successful repair of all three antenna tower foundations that were examined:

– Removal of existing repair mortar and unsound concrete, roughening and cleaning of undeteriorated concrete
– Repairing of cracks and internal voids by epoxy injection
– Applying bond coating to concrete surfaces using polymer cement products
– Encasing the foundation with 2 cm thick layer of polymer-modified micro-reinforced mortar
– Removal of rust and flakes from corroded steel of the antenna tower itself and renewal of anti corrosion coating.

In order to achieve the best possible repair of the antenna tower foundations, requirements for the repair materials were prescribed.

5 CONCLUSIONS

A case study involving the concrete foundations of 3 antenna towers, located in extreme conditions has been presented in this paper.

Poor construction of the antenna tower foundations due to demanding construction conditions and extreme environmental conditions on the antenna tower locations during the lifetime resulted with degradation of the foundations.

The evaluation of concrete properties was useful to determine if the tower foundations were safe for use under the design load, and a reduced load that takes into account the damage. The concrete properties were also used to design the concrete encasement necessary for the repair process of tower foundations.

Results of site investigation, test data, and design records were interpreted in order to determine the appropriate repair method.

Concrete Repair, Rehabilitation and Retrofitting III – Alexander et al. (eds)
© 2012 Taylor & Francis Group, London, ISBN 978-0-415-89952-9

Repair and restoration of "Dalle de Verre" concrete windows

M. Ünal & H.-C. Kühne
BAM Federal Institute for Materials Research and Testing, Berlin, Germany

ABSTRACT: On historically important concrete glazing damages occur frequently in form of cracks, chipping and corroded reinforcement. The present article focuses on the analysis of current damages and causes for damage and the development of repair concepts. The observation of compressive strength, carbonation depth, reinforcement layer and diameter as well as moisture and salt content profiles were determined on several reference objects. The carbonation-induced corrosion of the reinforcement was determined as the main cause of the present damage. The frequent occurrence of carbonation-induced corrosion is well-founded by the low concrete cover of the reinforcement. It is caused by the specific manufacturing process in the production of concrete-glass windows. Standards dealing especially with the repair of concrete glazing do not exist. Therefore appropriate repair and maintenance techniques in accordance with DIN EN 1504 and German guidelines for repair and protection of concrete (RL SIB 2001) were developed. The requirements for a repair mortar for these specific applications are described. Furthermore, the basics of cathodic corrosion protection with zinc are presented.

1 INTRODUCTION

1.1 *History and motivation*

After the Second World War new experimental form of art and architecture was developed with concrete and glass. Concrete glazing consists of casted forms, slatted or sliced Dalle de Verre, which is put together with concrete as structural element. These glass pieces are placed corresponding to the artistic design, surrounded by a steel reinforcement mesh and then casted with concrete. All of these techniques is common, however, that comparatively slim concrete elements created with only small element thicknesses and little coverings of reinforcement. The quality of the manufactured glass was significantly worse. The knowledge about performance and durability of the materials used was lower at that time as compared to today.

Hence, as a result the first severe problems appeared on some constructions already after 15 years. We are now confronted with corroded reinforcement, concrete spalling, slivered glass, and deformation of elements, which can even lead to loss of structural safety.

2 STANDARDS AND REGULATIONS

There are a number of national and international standards and guidelines available for the repair of concrete structures, depending on the field of application. The repair of concrete structures in Germany is regulated by the German guidelines and standards for repair and protection of concrete structures RL SIB of the German Committee for Reinforced Concrete (DAfStb). Not all parts of the European standard EN 1504 are applied in Germany. The repair of stained glass is made according to the guidelines for the preservation and restoration of stained glass of the corpus Vitrearum (CVMA). A set of rules tailored to the specific needs of the repair of Dalles de Verre is not available.

3 MAINTENANCE PLANNING

3.1 *General*

For a permanent repair the actual state analysis of the structure is an essential foundation. In that analysis the damages and the causes of damage are investigated. Visual inspection of the building is one of the essential actions of the current state analysis. There are a number of testing methods that can be used to evaluate the degree of damage.

For listed buildings agreements and close cooperation with Monument Protection Authorities are essential.

3.2 *Current state analyses of reference objects*

Within the research project current state analyses were conducted on selected reference objects. The aims were the representative selection of various

Dalle de Verre constructions and the consideration on a wide range of causes and damage patterns. Depending on the causes of damage and accessibility different investigation methods were used. In agreement with the relevant conservation and municipal authorities several inspection and test methods were applied.

4 DAMAGE AND DAMAGE MECHANISM

The investigation results show that carbonation-induced corrosion of reinforcement is the main reason of the current damages. The high pH value of concrete causes the formation of a protective layer of iron oxides on the surface of the steel reinforcement. This passive layer protects steel permanently against corrosion and it is durable and self-repairing as long as high alkalinity is present. However, this characteristic can change if CO_2 from the environmental air or from water penetrates into the hardened concrete and reacts with the $Ca(OH)_2$ to $CaCO_3$ and H_2O. This reaction, known as carbonation, can reduce the pH value below 9. Due to this process the passive layer around the steel is destroyed, which leads to corrosion of the reinforcing steel if oxygen and water are present. The increased volume of the corroded steel results in spalling, delamination and loss of stability. The damages intensified by the corroded and partly exposed steel frame. An additional cause of damage is the steep anchoring of the Dalle de Verre window that does not allow thermal expansion and thus leads to internal stresses in glass and concrete.

The manufacture of the windows was made at different times and often by a variety of unskilled builder's laborer. This led to significant variations in the quality of workmanship and quality of used building materials as well.

The extent of glass damage is highly influenced by the position of the glasses in the windows, the craftsmanship, the weather conditions and the force transmission. The spalling of concrete due to corrosion of reinforcement cause significantly damages to glass. Due to the lack of expansion joints restraint stresses occur, which lead to cracking and spalling of the glass and concrete. Furthermore, the lower concrete glass elements are loaded by the dead weight of the upper elements.

5 MAINTANANCE

Maintenance has the aim of restoring the required target state. For this purpose the resistance of the construction against the penetration of corrosive substances will be increased. In the RL SIB are four maintenance principles for restoration of the corrosion resistance of reinforcement described. Depending on the causes of damage and the construction situation procedures for repair of Dalle de Verre windows can be derived. Primarily concrete repair is aimed to restore the alkaline environment. This can be ensured by local or area reprofiling with a polymer modified mortar.

Depending on the extent of damage a rebuild of Dalle de Verre elements can be inevitable. In such cases stainless steel bars should be preferred.

The lowering of water content in concrete can also reduce the corrosion rate to negligible values. This can be achieved by suitable surface protection systems according to RL-SIB.

Another possibility consists in use of cathodic corrosion protection, at not advanced corrosion of reinforcement. Systems with external power anodes are due to the filigree construction and the high installation effort less suitable. An interesting alternative are systems with sacrificial anodes. The cathodic corrosion protection is realized by an electric connection of the zinc anode (spray coating) with the steel reinforcement.

6 CONCLUSIONS AND OUTLOOK

The standards and guidelines for concrete repair cannot be transferred without additional modifications to the restoration of Dalle de Verre windows. While the concrete standards are based on a technical optimum, the maximum preservation of the original substance and the reversibility of the actions are in the focus of historic preservation. Having regard to those aspects, the loss situation of selected reference buildings are investigated and documented. BAM Federal Institute for Materials Research and Testing has developed maintenance techniques and mortars, tailored to the specific construction conditions. Adapted to the specific characteristics of Dalle de Verre windows, new test specimens and testing scenarios were developed. The practicability of developed formulations and repair techniques were validated on special test samples. Further research is needed on the applicability of cathodic protection systems on Dalle de Verre windows.

ACKNOWLEDGEMENTS

We acknowledge the financial support from the Federal Ministry of Economics and Technology. This research project is funded by the Central Innovation Programme for SMEs (ZIM). In the end, the project partners Glasmalerei Peters, Paderborn and the University of York, UK are thanked for their excellent cooperation.

Concrete Repair, Rehabilitation and Retrofitting III – Alexander et al. (eds)
© 2012 Taylor & Francis Group, London, ISBN 978-0-415-89952-9

Residual structural performance of a 26-year-old corroded reinforced concrete beam

W.J. Zhu & R. François
Université de Toulouse, UPS, INSA, L.M.D.C. (Laboratoire Matériaux et Durabilité des Constructions) Toulouse, France

1 INTRODUCTION

The corrosion of reinforcement which is caused by the chloride ions at the surface of reinforcement in concrete is considered to be the most common reason for the deterioration of the reinforced concrete structures that is being reported in an increasing number by the engineers and researchers all over the world (Page 1999, Du 2007, Andrés 2007). During the period of last few decades, quite a lot of research about corrosion of concrete beams has been conducted (Tuutti 1982, Rodriguez 1997, Dimitri 2007). In the corrosion process, the steel is transformed into rust, which leads to: 1) reduction of the cross-section of reinforcing bars; 2) loss of the bond between bars and concrete; 3) volume expansion which can generate splitting stress strong enough in the concrete nearby the rust, resulting in cracking and spalling of the concrete cover (Coronelli 2004, Auyeung 2000).

However, most of the research is limited in the study of the causes and mechanisms of the reinforcement corrosion (Hanjari 2011), relatively less work is executed the practically important aspect of evaluating the residual structural performance of the corroded concrete structures. Andrés A. et al. (2007) has focused in an experimental investigation about the relationship between the loss of flexure capacity and the loss of steel cross-section of the corroded beams, and obtained the conclusion that the maximum pit depth was the most important factor impacting the load capacity reduction in the corroded beams. Mark G. Stewart (2009) has studied the mechanical behavior of pitting corrosion, including the flexural and shear reinforcement which can significantly affect the mechanical behavior and the ductile yielding, whereas a higher corrosion loss can lead to brittle fracture. But there is still a weak point that most of the corrosion process in the research was accelerated either by the application of an impressed current or an admixture of $CaCl_2$ into the concrete (Xu 2010), the conclusions of different models can vary largely, which still need improving so as to be applied in the real condition.

The aim of this paper is to present the analysis of the residual mechanical performance of a corroded beam B2Cl2 at the age of 26 by loading it in three-point loading system until failure. Indeed effect of load is important (François 1998, Zhang 2009, Vidal 2007). The same mechanical test was carried out in the control beam B2T. The main interest is that corrosion results of a natural process (no impressed current) for a long term of propagation period since corrosion was initiated after 5 years of aging in chloride environment.

2 DIAMETER LOSS OF THE TENSILE BARS

The diameter loss of the two corroded tensile bars was measured by vernier caliper. The loss was shown in Figure 1.

3 TENSION TEST ON THE TENSILE BARS

The tensile bars of the corroded beam B2Cl2 and the control beam B2T were retrieved to perform a tensile test, so that the mechanical behaviors of the bars were investigated (see figure 2).

Considering the influence of the corrosion on the corroded bar, the loss of mass was measured to get the exact cross-section of the corroded bars.

The mechanical behaviors of the tensile bars had been impacted by the corrosion obviously, including the yield strength, the strengthen stage and the ductility. From Figure 2, the yield strength fy of the control bar was considered to be 550 MPa. The impact on ductility is very different from one bar to another and is not correlated to the loss of cross-section but to the shape of corrosion. Pits lead to a more important notch effect and then a huge reduction of ductility since more generalized corrosion lead to weaker notch effect and then weaker loss of ductility.

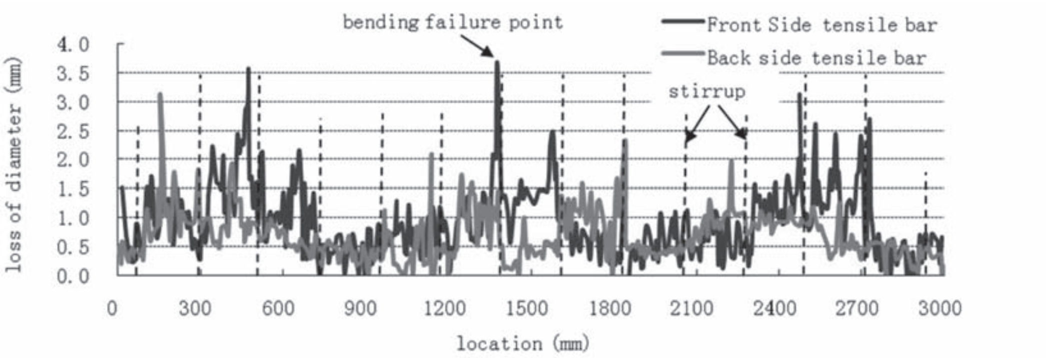

Figure 1. Diameter loss of the two corroded tensile bars.

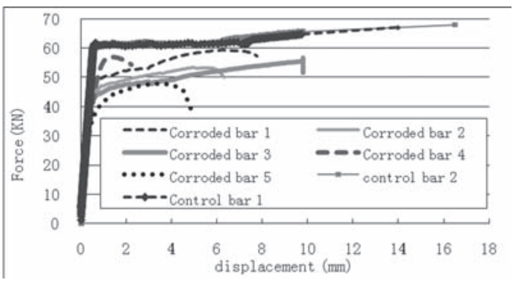

Figure 2. Load-displacement curves for the tensile bars.

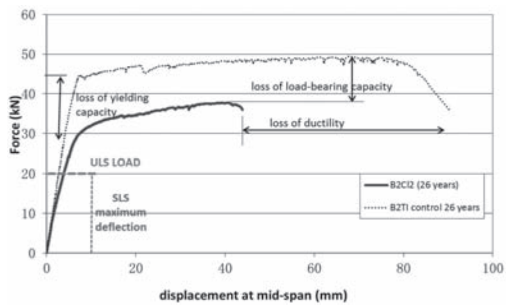

Figure 3. Load-deflection behavior of both 26 years old beams (corroded and control).

4 RESIDUAL MECHANICAL BEHAVIOR

Figure 3 shows the loads-deflection curves. For under-reinforced beams which failed by tensile rebars failure, the corrosion do not change the failure mode but reduced strongly the ductility of the beam. The loss of capacity is linked to the loss of steel-cross section at the failure location. Nevertheless, it seems that corrosion slightly modify the post-yielding hardening properties of steel bars, which lead to a difference in yielding capacity versus the ultimate capacity.

Concrete Repair, Rehabilitation and Retrofitting III – Alexander et al. (eds)
© 2012 Taylor & Francis Group, London, ISBN 978-0-415-89952-9

Experimental and numerical study on the residual strength of deteriorated prestressed concrete bridge beams affected by chloride attack

Y. Tanaka, T. Shimomura & T. Yamaguchi
Nagaoka University of Technology, Nagaoka, Japan

ABSTRACT: In this research, corroded prestressed concrete beams, which had been in service for 35 years in coastal area, were selected as a research object. Four beam specimens were loaded in a flexural or in a shear test to investigate the residual load carrying capacity of corroded prestressed concrete beams. Not only maximum load but also failure mode depended on the distribution of corrosion. Through the measurement of weight loss of PC strands, it was clear that the strands were completely destroyed due to the corrosion in some positions. As a result of these experimental works, it is clear that the average weight loss of prestressing steel is somewhat correlated with the area of cracks per unit concrete area. Analytical studies were conducted to simulate the remaining strength. By taking the development length into consideration, both flexural failure load and shear strength are predicted reasonably.

1 OUTLINE OF TEST PROGRAM

Urokozaki bridge which had been in service for 35 years near Japan sea was chosen to be loaded until failure because this bridge had deteriorated due to chloride attack.

Urokozaki bridge consists of four pre-tensioned I-beams. Two of these beams (beam A and B) were tested in bending and the others (beam C and D) were tested in flexural shear.

2 FLEXURAL TEST

Beam A and B were loaded in flexure. Figure 1 shows the load to center span deflection curve in the flexural test. FE analysis was conducted to estimate the failure load in case of no corrosion. While the sound beam by FE analysis and Beam A failed in shear, Beam B failed in flexure at a smaller load.

Figure 2 shows crack patterns observed after loading test. In case of Beam A, flexural cracks were induced at equal interval in constant moment span. On the other hand, flexural crack was concentrated in Beam B. These differences were caused by the variations in the amount of corrosion.

Figure 3 shows the average weight reduction of PC strands. Weight reduction of beam B is higher than that of beam A. That is the main reason why the maximum load of beam B is less than that of beam A. The location of maximum weight reduction is coincident with the location where flexural failure occurred in beam B.

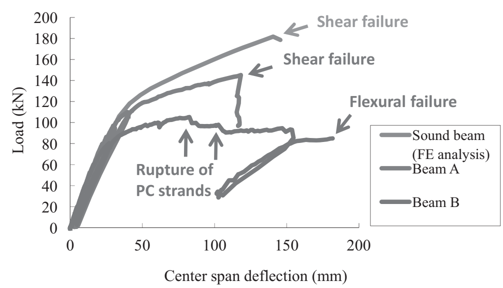

Figure 1. Load to center span deflection curve in flexural test.

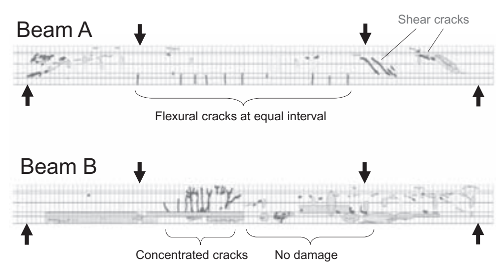

Figure 2. Crack patterns observed after flexural test.

3 FLEXURAL SHEAR TEST

As shown in Figure 4, asymmetric 3 point loading condition was adopted for flexural shear test. Shear span to effective depth ratio (a/d) was selected as the test factor.

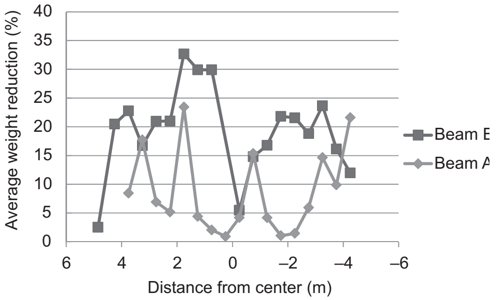

Figure 3. Average weight loss of PC strands in each block.

Figure 4. Loading condition in flexural shear test.

Table 1. Summary of flexural shear test.

No.	a (mm)	a/d	Flexural cracking load (kN)	Diagonal cracking load (kN)	Max. load (kN)	Failure mode
C-I	400	1.08	250	300	350	Yielding
C-II	1200	3.25	102	107	107	Diagonal tension
D-I	600	1.63	85	□	96	Rupture of PC strands
D-II	900	2.44	150	150	180	Shear compression

Table 1 shows summary of flexural shear test. Various failure modes were observed although every specimen was expected to fail in shear.

Flexural strength is calculated with the remaining percentage of PC strands measured after loading test. Figure 4 shows the comparison between experiment and evaluation in flexural failure load. In case of perfect bond, failure load tends to be overestimated. On the other hand, failure load is estimated safely in case development length is considered.

4 FINITE ELEMENT ANALYSIS

Structural performance of beam C and D was simulated by FE analysis. Remaining strands were carefully expressed by line element.

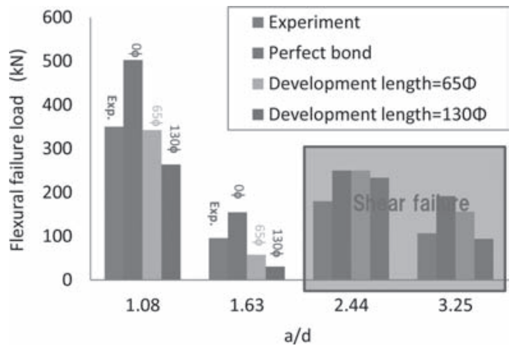

Figure 5. Tested and estimated flexural failure load.

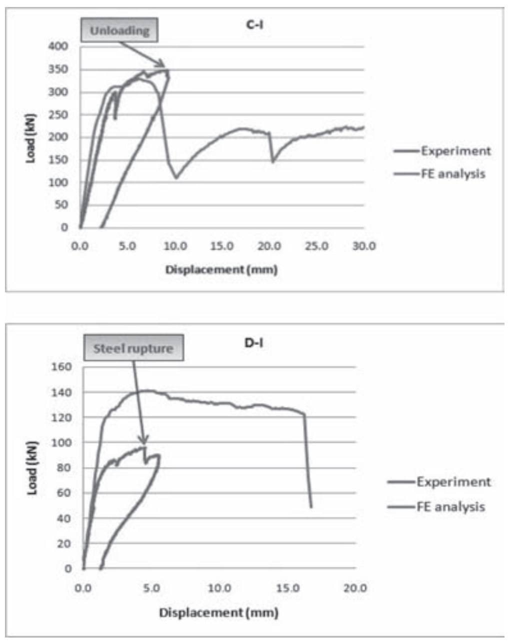

Figure 6. Comparison between FE analysis and experiment on load—displacement relationship (Displacement at loading point).

Figure 5 shows the relationship between load and displacement at point load. FE analysis succeeded in predicting maximum load in all types of specimen except for D-I specimen. Accuracy of numerical results depends on failure mode. Because our program does not consider the rupture of wire, analytical result overestimated the strength of D-I which was failed due to the rupture of strands.

Concrete Repair, Rehabilitation and Retrofitting III – Alexander et al. (eds)
 ISBN 978-0-415-89952-9

Method to evaluate the residual strength in concrete elements exposed to fire using physic-chemical and microstructural parameters

E. Menéndez
Institute "Eduardo Torroja" of Construction Science (IETcc-CSIC), Spain

L. Vega
Ministry of Development, Spain

C. Andrade
Research Centre of Security and Durability of Structures and Materials (CISDEM-CSIC), Spain

ABSTRACT: After the exposition of concrete to fires, it is necessary to evaluate the residual strength of the concrete affected elements. Some methods to evaluate the residual capacity are based on the knowing of the depth of concrete affected by temperatures higher than 500ºC. The layer of concrete that have been exposed to temperatures upper than 500ºC must be not taken into account to do the structural recalculation. In the present work different physic-chemical parameters are used in order to define the alteration zones from the surface exposed to high temperature to the interior. Different layers of concrete exposed to fire are analyzed, from the surface, determining different physic-chemical parameters related with thermal behavior, using DTA-TG, and determining the main crystalline compounds, using XRD. Also, the microstructural analysis by BSE-EDX permits to corroborate the situation of concrete exposed to high temperature.

1 INTRODUCTION

The deterioration of concrete exposed to fire progress from the surface to the interior especially hydrated products of the cement paste. (Fletcher, I.A. et al 2007, Hajpál, M. 2002, Lottman, B.B.G. 2007). The portlandite decomposes approximately 450ºC–550ºC and calcium carbonate approximately 700ºC–900ºC. (Taylor, H.F.W. 1997). Different instrumental techniques are used with the aim of analyzing the behavior of the concrete exposed to a real fire or laboratory tests.

The fire engineering use some simplified methods to evaluate the residual service life of the concrete structural elements after fire. One of the most used simplified methods is denominated method of the isothermal 500ºC. The residual strength of concrete is calculated only with the material no exposed at higher temperature than 500ºC. It is important to determine the depth of the concrete in which the temperature has been higher than 500ºC (Menéndez, E. et al 2012a, Menéndez, E. & Vega, L. 2010).

2 EXPERIMENTAL

Materials: Two types of materials have been analyzed: (i) Cement paste samples manufactured with OPC cured during 51 days in cured water and burned under controlled conditions until 650ºC and 1,000ºC during 48 hours. At 650ºC the portlandite should decompose totally, and at 1,000ºC is produced general decomposition of the cement paste and all of its hydration products. (ii) Concrete cores from the Windsor building, which had an important fire in 2005 in Madrid (Spain).

Instrumental techniques: The main crystalline phases were analyzed by means of X-ray diffraction (XRD). The presence of portlandite and calcium carbonate phases has been determined in concrete samples affected no affected by fire.

A microstructural analysis was carried out by means of backscattered electronic microscopy (BSE) both in laboratory tested cement pastes and samples from concrete cores exposed to fire.

The thermal behavior of the cement samples was analyzed using simultaneous equipment for differential and thermogravimetric analysis (DTA-TG). Was analyzed the dehydroxilation of the portlandite (450–550ºC) and decomposition of the calcium carbonates, between 700ºC and 850ºC.

3 RESULTS AND DISCUSSION

Analysis by X-ray diffraction: In field concrete exposed to fire it is observed that in the surface the portlandite has completely disappeared due to the increase of temperature upper than 650ºC because of the fire action and there is calcium carbonate.

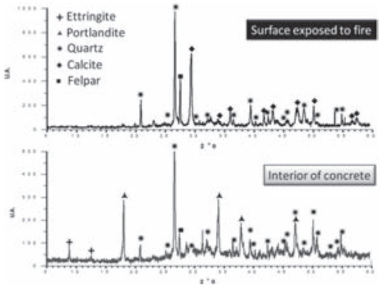

Figure 1. XRD of surface and interior of the concrete in fire.

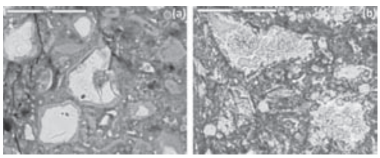

Figure 2. Cement paste exposed to 650ºC (a) and 1,000ºC (b).

While in the interior of the concrete the portlandite remains without presence of calcium carbonate (Fig. 1). Aggregates are siliceous, and there is not interference with paste compounds.

Microstructural analysis: Main damage is produced at cement paste level. Cement paste exposed to 650ºC has microcracks and loss of cohesion in CSH gel; while a layer of dense hydration products remain around the anhydrous particles. Cement paste exposed to 1,000ºC is shown high degradation in CSH gel and around anhydrous particles (Fig. 2a,b).

Field concrete exposed to fire shown degradation especially near to the surface. There is an important degradation close the surface (80 microns) and damage in cement paste some millimeters in depth.

Also, microcracks have been formed close to the exposed surface and progress mainly throughout the cement paste, surrounding aggregates and anhydrous particles. A typical distribution of microcracks is identified in field concrete exposed to fire. The pattern of microcracks is parallel to the surface exposed to high temperature (Fig. 3).

Thermal analysis: Decomposition of portlandite and carbonates are analyzed. Decomposition of portlandite indicates that concrete has been exposed to temperatures higher to 500ºC. Depth of concrete in which the temperature was up to 500ºC is determine to apply the isothermal 500ºC simplified method for residual strength.

Three zones are defined in field concrete exposed to fire according the decomposition of portlandite: Zone I (affected by fire), zone II (partially affected by fire) and zone III (No affected by fire) (Fig. 4). The depth until the concrete has been exposed to temperatures higher than 500ºC

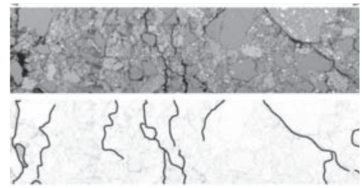

Figure 3. Pattern of microcracks parallel to the surface exposed to fire.

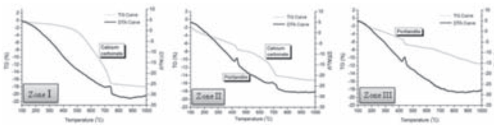

Figure 4. DTA-TG curves in the different zones of exposition.

is between 30–50 mm, depending on the structural element from which the concrete proceed.

Evaluation of the structural damage: The residual resistance is determined at the section level from a reduced section of concrete, excluding the real section from the areas within it which have undergone temperatures of more than 500ºC. The mechanical characteristics of the reduced section are considered, for the purposes of calculations, equal to those corresponding to the concrete at ambient temperature. Reduction of 30–50 mm in concrete with relation to the parametric curves indicates a fire resistance of 90–180 minutes. It is corroborated that the project exigencies were correct in order to ensure the required safety levels related with the evacuation of buildings, using for these calculations.

4 CONCLUSIONS

- Instrumental techniques (XRD, BSE and DTA-TG) give information about the concrete damage due to high temperature.
- Using XRD type of aggregates and potential carbonation of the cement paste are determined. Microstructural characterization by BSE give information about damage level of cement paste and depth until the concrete has had damage. Transversal sections of field concrete expose to fire are showing a typical pattern of microcracks parallel to the exposed surface. By DTA-TG analysis is determined the decomposition of portlandite that is related with the exposition of concrete to temperatures higher than 500ºC.
- The progress of temperature inside the concrete can be used to apply the simplified method of isothermal 500ºC to estimate the residual strength of the concrete element. And, to corroborate the hypothesis of calculus to define the fire resistance of structural concrete elements.

Concrete Repair, Rehabilitation and Retrofitting III – Alexander et al. (eds)
 ISBN 978-0-415-89952-9

Rehabilitation of a large arch dam: Importance of dam safety surveillance

L. Hattingh
Hattingh Anderson Associates, Pretoria, South Africa

C. Oosthuizen
Department of Water Affairs, Pretoria, South Africa

ABSTRACT: Kouga dam is a 69 m above riverbed high double curvature concrete arch dam located on the Kougha River in the Eastern Cape Province of South Africa and completed in 1969. The major concern at the dam is the swelling of the concrete due to Chemical Reaction (SCR) (SCR is also generally known as Alkali-Aggregate Reaction (AAR)). This has the potential of compromising the long-term integrity of the dam especially the arch action during earthquake loads. The importance of proper dam safety surveillance before making any decision on the rehabilitation of dam is highlighted by a discussion of the dam safety surveillance results.

Kouga Dam has been extensively monitored during and after its completion in 1969. Initially the dam reacted as expected but since 1972, it became clear that some form of SCR (swelling due to a chemical reaction) in the concrete was occurring. (SCR is also generally known as alkali-aggregate reaction (AAR)) In addition to this, some inelastic movement of the right flank foundation followed a few years later that complicated the behaviour model of the structure even further.

The results of the 3D-crack gauges confirm slight asymmetric primary arch action in the deepest section directly related to the water level, cantilever action of the blocks on the flanks as well as additional "stiffness" in the left flank arch section created by the parking area and chute spillway.

Seasonal cyclical tangential displacements are evident on the flanks and are decreasing in magnitude towards the centre of the wall. The magnitude of the tangential displacement on the left flank is of a larger magnitude than what is observed on the right flank;

The results of the 3D-crack gauges have been confirmed by the results of the ambient vibration measurements that were done in 2010 highlighting the importance of the 3D-crack gauge network in the interpretation of the behaviour of Kouga Dam.

From the results of the geodetic monitoring system it is clear that although the vertical swelling appears to virtually have stopped in 2000, the horizontal swelling has continued unabated ever since.

The maximum permanent vertical displacements due to swelling is observed in the centre of the arch while the maximum permanent horizontal displacements are evident at the quarter points of the arch (with right flank showing more permanent horizontal displacement than the left flank).

Clearly evident from the vertical displacement is the inelastic deformation of the upper part of the wall during low water levels. Inelastic downstream displacements of the upper part of the wall after periods of extended lower water levels similar to what has been observed at other concrete arch dams in South Africa, is also evident.

Upon closer examination some inelastic downstream displacement after periods of extended lower water levels is also evident. It must be mentioned that similar inelastic deformations are also observed after prolonged periods of low water levels in several other concrete arch dams in South Africa (Hattingh & Oosthuizen 2011). It is hypothesized that these inelastic deformations could be attributed to the shrinkage of the concrete during long periods of low water levels (drying).

It is important to note that recent research highlighted the very long term expansion due to SCR as a result of alkali supply from various sources, alkali recycling as gel transformation and alkali release from the aggregates (Charlwood & Scrivener 2011).

The vertical displacement at the centre of the dam, 4 m below full supply level, is represented as Figure 1. Horizontal displacement at a quarter point of the dam on the right flank, 4 m below full supply level looking downstream is represented as figure 2.

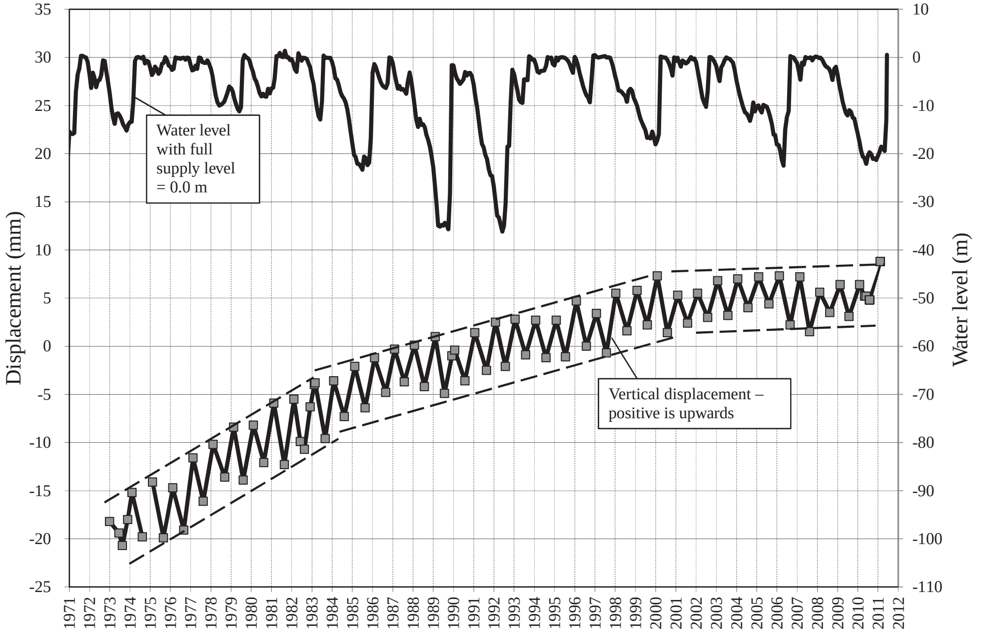

Figure 1. Vertical displacement at the centre of the dam 4 m below full supply level.

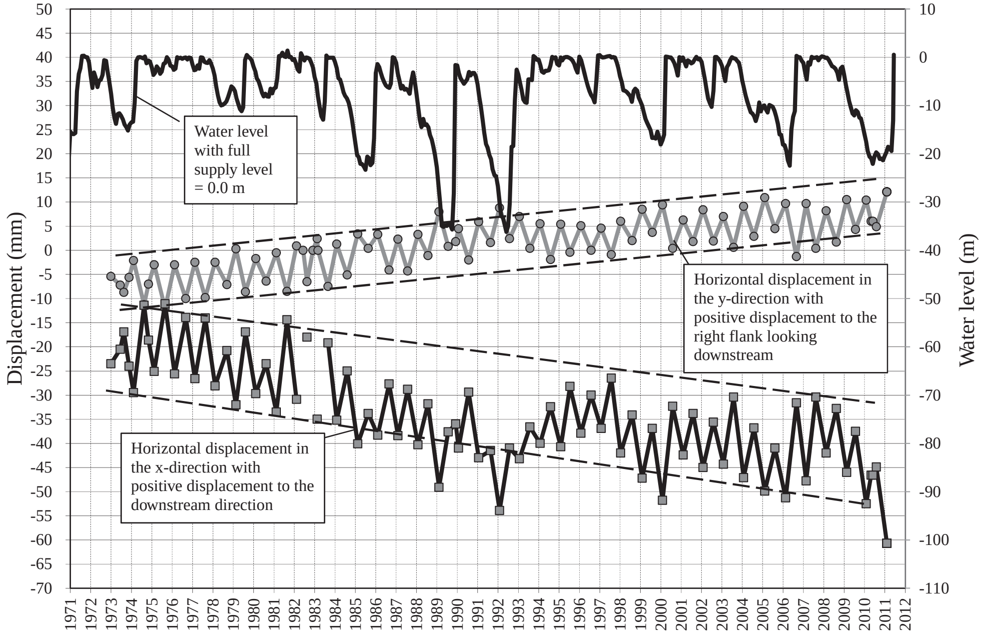

Figure 2. Horizontal displacement at a quarter point of the dam on the right flank 4 m below full supply level looking downstream.

Concrete Repair, Rehabilitation and Retrofitting III – Alexander et al. (eds)
© 2012 Taylor & Francis Group, London, ISBN 978-0-415-89952-9

Multiple arch dam: Challenges with the rehabilitation of one of the thin, unreinforced, double curvature arches of the Stompdrift Dam

J.L. Schoeman & C. Oosthuizen
Department of Water Affairs, Pretoria, South Africa

ABSTRACT: Stompdrift Dam is a multiple (three) double-curvature arch dam supported by two buttresses in the centre and a curved gravity section on the right flank. The dam has to be rehabilitated because of its insufficient spillway capacity and unfavourable cracks that have developed at its third arch. Four alternatives were investigated for strengthening the third arch. The existing thin arch could be converted into a double-curvature thick arch, a multiple buttressed arch, a gravity arch or a cylindrical thick arch. Various challenges encountered with the selected alternative are discussed, i.e. the seasonal movement of the existing structure, bonding of the joint between existing and new concrete, the effect of heat of hydration of the cementitious materials and to retain the unique view of the dam.

1 INTRODUCTION

The dam is comprised of four distinct sections. Three dome-shaped arches make up the left hand side of the dam wall, while the right hand side consists of a curved gravity section. An upstream view of the dam is shown in figure 1.

It was decided to rehabilitate the dam to dam safety concerns. One of these concerns was unfavourable cracks that have developed at the third arch. This paper's focus is on the strengthening of the third arch.

The third arch (the right-most arch looking downstream) has effectively cracked around its perimeter as there is a horizontal crack that runs along the base of the third arch and the vertical contraction joints on its left and right abutments. Horizontal cracks not corresponding to construction joints were also observed in the centre of the arch approximately 6 and 12 lifts respectively from the non-overspill crest (NOC).

Figure 1. An upstream view of Stompdrift Dam viewed from the right flank.

Some of the abovementioned cracks are caused by swelling of the concrete on the upstream face due to alkali aggregate reaction (AAR). Slight movements were also measured in the foundation of the buttress.

2 ALTERNATIVES INVESTIGATED FOR THE STRENGTHENING OF THE THIRD ARCH

During the preliminary design phase three alternatives were initially considered for the refurbishment of the third arch. A fourth alternative was added for consideration as a result of the foundation investigation results.

2.1 *Alternative 1: Double curvature medium thick arch*

The ratio of the existing arch's bottom width to height (b/h) is 0.1, classifying it as a thin arch. The new medium thick arch will have a b/h ratio of 0.2. The arch will be thickened by adding concrete to its downstream face. It turned out to be very expensive due to the construction restraints. A secondary aspect was the additional stresses added to the existing foundations.

2.2 *Alternative 2: Multiple buttressed arch*

This alternative involves constructing a series of buttresses that support the downstream face of the arch. The "buttressed" alternative supports the individual blocks of the third arch and does not add significant forces to the existing foundations. This alternative was, however, quite expensive due to the complexity of the formwork.

2.3 *Alternative 3: Gravity arch*

An ogee shaped crest terminating in a 2.5:1 sloped downstream face was investigated. The b/w ratio of the concrete added next to the downstream face of the existing dam is 1.1.

This alternative allowed for unfavourable foundation conditions and would be easy to construct. Bonding of the new concrete to the existing concrete was not required. It proved to be very expensive, because a relatively large amount of concrete (or RCC) would be required, approximately 45 000 m^3.

The low risk gravity arch alternative was initially selected for refinement. However, during initial foundation explorations it was discovered that the competency of the foundations at the third arch was of a better quality than previously expressed. The better quality foundations made is possible to change the design to a fourth alternative: a cylindrical thick arch discussed below.

2.4 *Alternative 4: Cylindrical thick arch*

A cross section of cylindrical thick arch is shown in figure 2.

In this alternative the downstream face of the arch was vertical, which makes it relatively easy to construct. The combination of new and existing concrete has a b/w of 0.5, which classifies it as a thick arch.

This alternative requires approximately 20 000 m^3 of concrete—less than half the amount that is required by the gravity arch alternative.

A plain strain section of this alternative does, however, not provide adequate resistance to overturning or sliding. It is therefore necessary for the new and old concrete to act monolithically. This alternative was eventually chosen as the preferred choice as it satisfies the design philosophy.

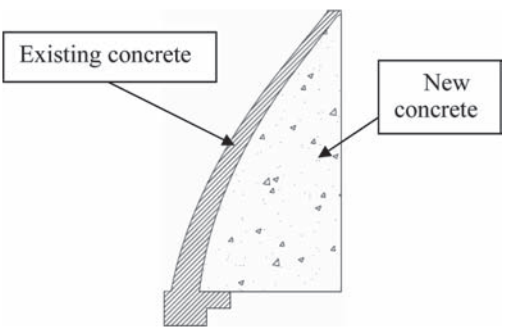

Figure 2. A cross section of the third arch for the cylindrical thick arch alternative. Note the vertical downstream face of the new concrete.

3 CHALLENGES OF THE CHOSEN ALTERNATIVE

3.1 *Seasonal movement of the third arch*

Relatively large seasonal movements have been observed near the centre of the crest of the third arch. This movement is caused by thermal expansion and contraction of the dam wall. Placement of the concrete against the existing dam wall will therefore be timed to coincide with the downstream seasonal movement of the dam to cause a compressive stress at the bond between the new and existing concrete.

3.2 *Bonded vs. unbonded joint*

A bonded joint between the existing concrete and the new concrete of the rehabilitation work would have the following critical advantage over an unbonded joint: The new and existing structures could act monolithically. This is especially important for dynamic load cases. The factors taken into account to ensure a proper bond between the existing and new concrete are:

- Seasonal movement of the existing dam.
- Thermal contraction of the new concrete.
- Grouting system.

3.3 *Programme control of pour sequence*

In order to minimize differential thermal contraction due to uneven loss of heat of hydration, the casting sequence and casting rate have to be carefully controlled. Adequate time for the dissipation of hydration heat has to be provided for each of the blocks before fresh concrete is poured against or on top of it. This will be done by pouring during cooler periods of the day (if necessary, at night) and monitoring the temperature in each lift.

ACKNOWLEDGEMENTS

The authors wish to thank DWA for permission to publish this paper. The opinions expressed are however those of the authors and do not necessarily reflect the views of the Department of Water Affairs. The authors wish to express their gratitude to the following persons:

- Comfort Mahlabela for his valuable contributions during the initial phase of the project; and
- Louis Hattingh for the final editing.

Concrete Repair, Rehabilitation and Retrofitting III – Alexander et al. (eds)
 ISBN 978-0-415-89952-9

Lombardi slenderness coefficient as one of the criteria for the preliminary evaluation of proposed rehabilitation works at Kouga dam

C. Oosthuizen & C. Mahlabela
Department of Water Affairs, Pretoria, South Africa

ABSTRACT: Kouga dam is a 72 m high double curvature arch dam constructed during the 1960's. The dam has been earmarked for rehabilitation in several phases mainly to address deep-seated foundation movements on the right flank and swelling of the lower part of the arch due chemical reaction. The proposed rehabilitation phase addressing the change in distribution of forces from the dam wall onto its foundation as well as problems experienced with the maintenance and operation of the chute spillway is described. The integrity of the central arch with the possibility to raise the dam progressively in subsequent phases is discussed briefly. The use of Lombardi's slenderness coefficient graphs to evaluate the feasibility of five scenarios of the chosen options during the preliminary design of the rehabilitation works is demonstrated.

1 BACKGROUND

Kouga dam is a 72 m high double curvature arch dam situated in the Kouga River 27 km west of the town Patensie in the Eastern Cape. The dam was originally designed to be raised from the existing FSL by 13.72 m at a later stage.

After completion the dam initially behaved as expected. In 1972 however, it became clear that the dam was not behaving as expected. For the next three decades, only the swelling action due to chemical reaction of the concrete (AAR) was observed. However, during 2006 deep-seated foundation movement in the right flank was measured by the Trivec instruments. In addition, unusual natural frequency modes were detected during ambient vibration measurements in 2010 that gave rise to the suspicion that some of the right flank blocks are not in direct contact with each other during low water levels (Moyo & Oosthuizen 2010). A detail analysis of the results of the 3D crack gauges during a 5-yearly dam safety evaluation confirmed the independent movement of the upper parts of the arch (Hattingh & Oosthuizen 2012).

Figure 1. Downstream view of Kouga dam with the gated spillway chutes on the left flank and a stress pad clearly visible on the right flank.

It then became necessary to restore the structural integrity of the upper parts of the arch, secondly, to improve the force distribution on the flanks of the dam, thirdly, to address the operation and maintenance problems experienced with the chute spillways and fourthly, allowing the possibility for the dam to be raised to its full height. Finally, the rehabilitation has to be done in such a way that it does not jeopardise the aesthetics of the dam.

2 PROPOSED REHABILITATION WORKS INCORPORATING A FUTURE RAISING

Several options for phases 3 and 4 were investigated. The spectrum of options ranged from a solution comprised of a series of buttresses to a Roller Compacted Concrete (RCC) gravity arch solution at the other end of the spectrum. The most feasible option was a thick arch solution.

Changing the dam from a medium to thick arch by adding additional concrete on the downstream face of the arch proved to be the most cost-effective solution. The additional benefit is that the present downstream view of the dam would not be changed drastically.

3 EVALUATION OF THE CRACKING POTENTIAL

3.1 *Lombardi slenderness coefficient*

Giovanni Lombardi (Lombardi 1988 & Lombardi 1991) developed a coefficient that can be used to assess the susceptibility of arch dams to cracking, with particular emphasis on shear effects. The coefficient termed the Lombardi "slenderness coefficient" is expressed as follows:

$$C = \frac{F^2}{VH} \tag{1}$$

Where F is the surface area of the dam across the valley; V is the volume of concrete and H is the height of the dam. The interaction between C and H is illustrated in figure 2 below.

From the graph, it can be deduced that in order to minimize the crack potential of a dam, the value C of the well-dimensioned dam should be kept below the dotted line, i.e. crack potential line.

3.2 *Applying Lombardi slenderness coefficient to Kouga dam*

The Lombardi slenderness ratio for the proposed rehabilitation works at Kouga dam was evaluated for five different scenarios as shown in figure 2. A brief description of each of the scenarios is given in table 1 below.

Scenario A1: The C versus H combination for this scenario meets the required slenderness criteria (the combination falls below the cracking potential line). Therefore, the cracking as observed in the dam should only be due to AAR and not due to slenderness.

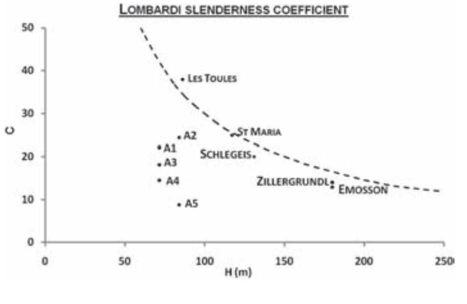

Figure 2. Lombardi slenderness coefficient graph with the positions of a few well-known dams as well as the five scenarios considered for an uncracked Kouga dam shown as A1 to A5.

Table 1. Description of the various scenarios.

Scenario	Description
A1:	Existing dam
A2:	Original raising
A3:	Thickened flanks, existing full supply level (FSL)
A4:	Thickened complete dam, existing FSL
A5:	Thickened complete dam, raised FSL

Scenario A2: In this scenario the non-overspill section is raised by 12 meters. Evaluating this scenario using the cracking potential revealed that this option would result in C versus H combination close to the cracking potential line. This option is risky considering that Kouga dam is already experiencing cracking due to AAR.

Scenario A3: This scenario was used to evaluate the cracking potential for phase 3, i.e. thickening of the non-overspill flanks only but keeping the FSL to existing level. The C versus H combination is below the cracking potential line. This option seems to provide a reasonable margin of safety from cracking due to shear stresses (excluding the long term effect of AAR).

Scenario A4: This scenario evaluates the cracking potential when the dam is thickened to the existing FSL. The C versus H combination meets the required slenderness criteria. This scenario should be ample to cater for both cracking due to AAR and shear stresses.

Scenario A5: This scenario evaluates the cracking potential if the dam's FSL is raised and the entire arch is thickened. The C versus H combination for this scenario meets the required slenderness criteria. This scenario seems to provide a huge safety margin against cracking due to shear stresses.

4 CONCLUDING REMARK

The main advantage of using the Lombardi slenderness coefficient is that only geometric properties of the dam, such as cross sectional area across the valley, the volume of concrete used and the height of the dam are required to calculate the values. No strength parameters are required. Those aspects have to be evaluated subjectively.

The Lombardi slenderness coefficient therefore proved to be quite useful to provide indications of the relative levels of safety for the various scenarios investigated during the screening process. The chosen option can now be refined much more cost-effectively by means of accurately modeled finite element analyses.

Concrete Repair, Rehabilitation and Retrofitting III – Alexander et al. (eds)
© 2012 Taylor & Francis Group, London, ISBN 978-0-415-89952-9

Observations from the calibration of an arch dam model using ambient modal properties

R. Makha & P. Moyo
Concrete Materials and Structural Integrity Research Unit, University of Cape Town, South Africa

ABSTRACT: The Westergaard method was used to represent the ambient dynamic action of the water body and the dam wall on an arch dam finite element model. This study follows the measurement of the modal properties of the actual dam using the ambient vibration testing technique. After the effects of diverging dam reservoir walls, finite reservoir, upstream curvature and flexibility of the dam wall were considered, good correlation was achieved between analytical results and the experimental ones. These factors were ignored in the derivation of the original Westergaard method. Despite that the method was derived for use in the seismic safety analysis of gravity dams where large deformations are expected, the small deformations assumption was made which justified the ignoring of water compressibility. Conversely, in the ambient dynamic behaviour of dams, deformations are generally small hence water compressibility can be neglected. It is in such cases where it is proposed that the Westergaard method can effectively represent the dam-water interaction provided factors such diverging reservoir walls effects are included.

1 INTRODUCTION

Ambient vibration testing (AVT) was carried out on Roode Elsberg arch dam with a view of calibrating a finite element (FE) model of the dam using the natural frequencies and mode shapes extracted from the testing. Among other factors, natural frequencies and mode shapes of a dam are affected by the interaction of the water body entrained in the reservoir with the dam wall (Okuma et al., 2008; Darbre & Proulx, 2002).

Thus, it is important that this factor is included in the properly calibrated finite element models of dams which are used to predict dams' dynamic behaviors. Field data is used to calibrate models. Once a model is calibrated and through the use of automated AVT on dams, strange behavior can be spotted in dams and catastrophic events can then be avoided.

In order to represent the dynamic effect of the water on the dam wall, the added mass concept which originated from a study carried out by Westergaard (1933) has been used extensively in previous studies. When the added mass formulation is used in FE models, there is no need to include fluid finite elements in the model as only the mass of the fluid is considered important in this case.

It is this feature of not modeling the water body using fluid finite elements that makes the added mass formulation the most attractive approach for the purposes of monitoring the dam's daily ambient behaviors. The fluid elements approach can prove to be very cumbersome. Despite its attractiveness through its ease of applicability, the added mass formulation was derived to be used for seismic analysis of dams and not for ambient dynamic behavior. The method was proved to be highly inaccurate for certain cases of seismic analysis (Chopra, 1967).

Hence, the work of this research specifically involved assessing whether the Westergaard added mass formulation can be satisfactorily used to determine the ambient dynamic behavior of arch dams.

2 FE MODEL AND ITS PROPERTIES

The geometry of the dam was captured into the commercial program, Abaqus, with the help of the design drawings to produce a model as shown in Figure 1. The reduced integration, 3-dimensional and 20-noded brick elements which use quadratic shape function to interpolate between nodes were used in the modeling.

Roode Elsberg is a double curved arch dam. The original Westergaard formulation was however developed for a rigid dam with a vertical upstream face. The formulation was extended by Kuo (1982) to further make it applicable to flexible dams with a curved upstream surface. This formulation by Kuo is known as the generalized Westergaard method in literature.

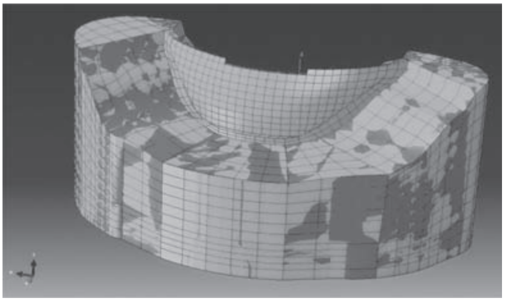

Figure 1. The finite element model of Roode Elsberg dam.

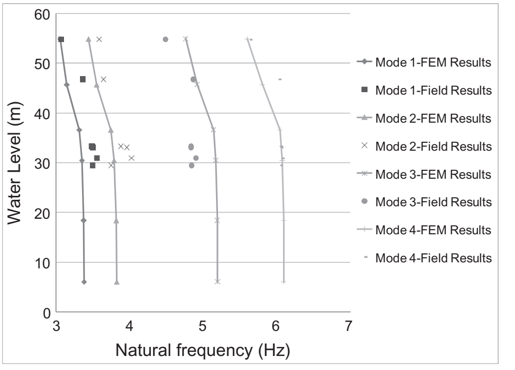

Figure 2. The best calibration achieved between field results of December 2008 and FE model results where 25% of the original calculated Westergaard masses were used.

3 RESULTS AND DISCUSSIONS

3.1 *FE model results versus experimental results*

Following the application of the original Westergaard added mass method, the variations of both the measured and the experimental data with water level were compared. For higher water levels in the dam, there seemed to be considerable discrepancies between the field data and the analytical data.

The mismatch of the field results with the analytical results called for the careful scrutinizing of the applicability of the original Westergaard method and all the pertaining assumptions which were made in its derivation, to the case study. It was realised that the Westergaard added mass concept was derived for a prismatic dam reservoir while Roode Elsberg dam has diverging reservoir walls. On the study conducted by Kuo (1982), it was shown that dams of diverging reservoir walls experience less dynamic pressures along the height of the crown cantilever than the same sized prismatic dams under same conditions. The generated pressures are directly proportional to the added mass.

It is estimated that the effect of the diverging reservoir walls in Roode Elsberg dam, where the reservoir angles are at an angle of about 25° to the reference plane, can be an overestimation of the added mass by about 25%.

3.2 *The generalized Westergaard method*

The generalized method improves the original Westergaard method to extend the method's application to flexible dams with curved upstream face.

The observed experimental mode shapes suggest that the dam vibrates largely in the upstream-downstream direction. This, together with that the generalized Westergaard method mass at a point depends on the direction cosines of the unit normal vector at that point; suggest that the original Westergaard masses are likely to be greater than the generalized Westergaard masses at any point. Hence, the original Westergaard masses were reduced until a good correlation was achieved between the analytical field results and field results of same ambient conditions.

The results are summarised in Figure 2.

There are discrepancies observed for lower water levels' frequencies and some higher modes at higher water levels as well. This can be attributed to the effects of temperature which were not considered in the analysis. Temperature can clearly have an effect on the natural frequencies of a system since it affects the stiffness of the system.

4 CONCLUDING REMARKS

The success of any analysis procedure is ultimately judged on its ability to reproduce or predict the observed behaviour. The use of the Westergaard added mass method to represent the dynamic interaction of the water body and the dam wall in Roode Elsberg dam eventually provided analytical results which were comparable to the field results. This was after the assumptions that were made in the derivation of the Westergaard method were reviewed which led to modifications being made where necessary. The effects of the diverging reservoir walls and the finite reservoir proved to be very important in the application of the added mass method in the Roode Elsberg dam dynamic model.

Concrete Repair, Rehabilitation and Retrofitting III – Alexander et al. (eds)
© 2012 Taylor & Francis Group, London, ISBN 978-0-415-89952-9

Modal parameter estimation from ambient vibration measurements of a dam using stochastic subspace identification methods

P. Bukenya, & P. Moyo
Department of Civil Engineering, University of Cape Town, Western Cape, South Africa

C. Oosthuizen
Department of Water Affairs, Pretoria, South Africa

ABSTRACT: Dynamic testing of concrete dams under ambient vibration excitations such as wind and water waves has advantages such as no artificial excitations is required which makes it a cheaper option. It also tests the structure in its operation conditions so there are no interruptions. In ambient vibration testing, only output responses from the structure are used in modal parameter identification. Stochastic subspace identification algorithm is the state of art technique in modal parameter estimation for civil engineering structures. This paper evaluates the performance of three SSI algorithms namely; unweighted principal component, principal component and canonical variate analysis in the identification of modal parameters (natural frequencies and damping ratios) of a Roode Elsberg dam in South Africa. It is demonstrated that all the three algorithms are close to each other in estimating natural frequencies but not damping ratios. Natural frequencies estimated by the SSI algorithms are compared with the FEM results and it is shown that they did not pick some modes.

Keywords: modal parameter identification, stochastic subspace identification, ambient vibration testing

1 INTRODUCTION

The dynamic behavior of a concrete dam under wind, water waters and other live loads depends on the structural properties such as mass, stiffness and damping. These properties can be determined using finite element modeling. However, these may differ from the real properties of the structures due to the assumptions made in the geometry of the structure and analysis. Therefore the real behavior of dams remains to be verified from full scale vibration tests. These vibration tests help in the estimation of modal parameters (natural frequencies, modal damping and mode shapes). The modal parameters can be used for updating and validating mathematical models and structural health monitoring of dams.

Vibration testing of dams are divided into force vibration tests (FVT) and ambient vibration tests (AVT) also known as operational modal analysis (OMA). In FVT, a structure is excited by mechanical exciters such as servo hydraulic shakers and both the input and output are measured. In OMA, a structure is excited by natural or environmental forces such as wind, water waves and traffic and only output responses from the structure are measured. The use of mechanical exciters in FVT makes this method an expensive one since it involves buying and transportation of the equipment to the dam. In addition to this the excitations may sometimes cause damage to the structure. In such cases, OMA becomes the cheaper option of doing full scale vibration tests of dams. OMA has advantages of (i) being cheap and fast since no exciters are needed, and (ii) the testing does not interfere with the operation of the structure.

OMA algorithms are divided into three categories namely: (i) time domain based methods, (ii) frequency domain based methods and (iii) time-frequency domain based methods (Zhang et al. 2005). In this paper, the performance of a time domain based method known as stochastic subspace identification (SSI) in estimation of modal parameters (natural frequencies and damping ratios) from ambient vibration measurements of Roode Elsberg dam. The three SSI algorithms evaluated here are unweighted principal component (UPC), principal component (PC) and canonical variate analysis (CVA). The measured natural frequencies are compared with those from the Finite element model.

2 AMBIENT VIBRATION TESTING OF ROODE ELSEBERG DAM

Ambient vibration tests were performed on Roode Elseberg dam located in Western Cape Province, South Africa. Q-Flex QA-700 accelerometers with sensitivity of 6 V/g and resolution <1 μg were used to measure signals. Data acquisition was done via the National Instruments 8 channel dynamic signal analyzer with a 24 bit resolution. The ambient vibration data was acquired using a sampling frequency of 1000 Hz during more than 10 minutes in each test.

Modal parameters from ambient vibration measurements were estimated using commercial OMA software called ARTeMIS Extractor Pro 2010. This software implements frequency domain decomposition (FDD) method which is frequency domain based and SSI methods which are time domain based methods. In this study, ambient vibration measurements were analyzed using the three classical versions of the SSI time domain techniques.

3 RESULTS

The results presented in the section are based on the three SSI techniques (UPC, PC and CVA) and all based on stabilization diagram criterion. Modes below 10 Hz were obtained after low-pass filtering, decimation to 16.67 Hz. Table 1 summarizes the results for the five modes from ambient vibration tests carried out in this study in terms of natural frequencies and numerical values. The first natural frequency is around 3.3 Hz and the fifth mode is around 8 Hz. There was no big difference in the picked modes from all the algorithms. The three algorithms did not pick up the fourth mode because it was not well excited so could not be stable in the stabilization diagram. The divergence between the measured natural frequencies for the PC algorithm and the numerical values is analyzed in Figure 2 with a correlation value of 0.98. This figure shows that there is a need for model updating of the finite element model of the dam model.

Table 1. Experimental natural frequencies, damping ratios and FEM natural frequencies.

Mode	FEM f(Hz)	SSI-UPC f(Hz)	SSI-UPC ξ(%)	SSI-PC f(Hz)	SSI-PC ξ(%)	SSI-CVA f(Hz)	SSI-CVA ξ(%)
1	3.36	3.53	1.47	3.53	1.97	3.50	1.44
2	3.52	3.92	1.42	3.99	2.09	3.91	2.57
3	5.03	4.83	1.46	4.86	1.42	4.69	2.92
4	6.39	0	0	0	0	0	0
5	7.63	7.99	0.21	8.05	3.31	7.99	1.96

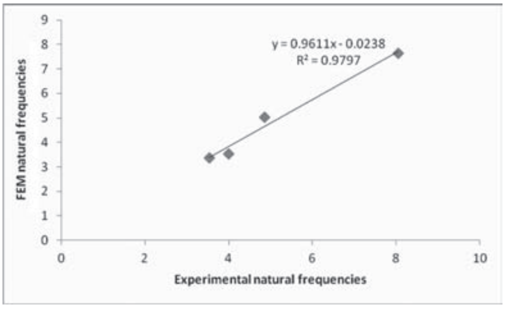

Figure 1. FEM results vs. experimental results.

4 CONCLUSIONS

This paper has presented ambient vibration testing of Roode Elsberg dam. Stochastic subspace identification was applied to ambient vibration measurements from the dam. Evaluation of the performance of the three SSI methods (UPC, PC and CVA) has been made. Experimental natural frequencies and those obtained from the finite element modeling have been compared. The following conclusions can be made from the study:

- Five natural frequencies were identified which range between 3 and 8.5 Hz.
- All the SSI algorithms did not pick up the fourth mode because it was a weak mode and did not meet the stabilization criterion used in the analysis.
- The different SSI algorithms give almost identical results in terms of natural frequencies. The general trend is that the required state space dimensions is of the order PC < UPC < CVA as shown in the stabilization chart.
- Use of projection channels, filtering and decimation gives better stabilization and it also reduces the calculation time.
- There was no correlation in damping ratios as it is always been a challenge to experimentally determine this factor.
- The use of stabilization diagram requires user expertise and also time consuming as there are so many parameters.

Concrete Repair, Rehabilitation and Retrofitting III – Alexander et al. (eds)
© 2012 Taylor & Francis Group, London, ISBN 978-0-415-89952-9

Macroscopic ice lens growth: Observations on Swedish concrete dams

M. Rosenqvist
Vattenfall Research & Development AB, Älvkarleby, Sweden

K. Fridh
Division of Building Materials, Lund University, Lund, Sweden

M. Hassanzadeh
Vattenfall Research & Development AB, Stockholm, Sweden

ABSTRACT: The arch dam at Selsforsen and the buttress dam at Storfinnforsen are two concrete dams of which both have suffered from severe surface spalling on the upstream face, far below the full water supply level. A hypothesis is that macroscopic ice lens growth, similar to frost heave in soil, could have occurred within the dam walls. After initial deterioration of the concrete dams by frost damage or cracking, the formation of macroscopic ice lenses could have been made possible. In an attempt to test the hypothesis, specimens of low strength concrete were exposed in the laboratory to climatic boundary conditions similar to those of the dams. After one week of freezing, the upper part of the concrete specimens was separated from the lower part due to cracking. The gradual propagation of the crack, which appeared about 25 mm below the top surface, was caused by macroscopic ice lens growth.

1 INTRODUCTION

1.1 *Background*

Severe surface spalling, similar to frost heave in soil, has been observed far below the full water supply level on the upstream face of two Swedish concrete dams—the arch dam at Selsforsen (1944) and the buttress dam at Storfinnforsen (1954). The damage was sometimes found to be deeper than the thickness of the concrete cover. This left reinforcement bars open in the water. The concrete used during the construction time had only little or no frost resistance.

Mature concrete is considered to be deteriorated by only two types of frost damage; scaling and internal frost damage. The former will deteriorate the surface, while the latter will lower the strength. Macroscopic ice lens growth, similar to frost heave in soil, could possibly cause a complete segregation of the concrete. The macroscopic ice lens growth theory has however never been considered to cause damage in mature concrete of normal strength.

1.2 *Working hypothesis*

The aim of this study is to investigate if an already deteriorated concrete also could facilitate the formation of macroscopic ice lenses. If this is the case, it may explain the severe extent of the damage to the upstream faces of the two dams. The study has been performed in a laboratory by exposing concrete specimens of low strength to climatic boundary conditions similar to those of the dams.

2 THEORETICAL CONSIDERATIONS

2.1 *Frost heave in soil and young concrete*

The formation of macroscopic ice lenses in soil has been found to be perpendicular to the heat flow direction. The ice lens growth continued as long as the loss of heat from the ice lenses towards the soil surface was balanced by the quantity of heat brought up by the water uptake and later set free during phase change. A continuous water uptake and a low pressure on the ice lenses were two other conditions governing the macroscopic ice lens growth in soil.

A young concrete has properties reminding of the properties in a frost susceptible soil—the permeability is high and the access to water is favourable. However, it has been shown theoretically that a tensile strength of the concrete of about 0.1 MPa is sufficient to prevent macroscopic ice lens growth in young concrete. In addition to the increasing tensile strength, the permeability and the access to water will decrease during the curing time.

2.2 *Macroscopic ice lens growth in mature concrete*

So far, studies have focused on the conditions for macroscopic ice lens growth in young concrete. Only a few observations have been made of macroscopic ice lens growth in mature concrete, but no clear evidence yet exists. The conditions for macroscopic ice lens growth in deteriorated concrete are therefore not fully known. This study will hopefully contribute to an increased knowledge about these conditions.

3 MATERIALS & METHODS

3.1 *Test setup*

The winter mean air temperature around the Storfinnforsen dam is about −15°C and the reservoir water temperature is +4°C. The test setup was designed to correspond to the conditions present at the two dams; one side of the concrete specimens subjected to constant freezing temperature and one side in contact with water. To ensure one dimensional heat flow, the specimens were insulated on the remaining surfaces. The specimens were placed in a box filled with water, letting the lower surface to stay in contact with water (Fig. 1). The air temperature was set to −20°C and the water temperature to +4°C.

3.2 *Concrete specimens*

Two concrete types of w/c-ratio 1.0 and 0.85 were used in the study. The w/c-ratios were chosen to represent a permeable and low strength concrete. Some of the specimens were provided with sheets of paper; with the purpose of creating deteriorated concrete inside the specimens. The deterioration, in the form of cracks, would perhaps facilitate formation of macroscopic ice lenses. The distance between two paper layers was 20 mm. This resulted in three paper layers in each specimen. The fulfillment of the conditions for macroscopic ice lens growth would then hopefully coincide with one of the paper layers.

4 RESULTS

After three to four days of freezing, a crack appeared about 25 mm from the top surface of the specimen of w/c-ratio 1.0. The crack had propagated around the specimen at the level of the top paper layer. After another three to four days of freezing, the crack had widened to about 1–2 mm. An ice lens was visible in the crack. The specimen of w/c-ratio 0.85 with paper layers showed no signs of cracking; neither did the specimens without paper layers. The same results were obtained when the test was repeated. In the future, the experimental work will continue with extended freezing time, different temperatures, etc.

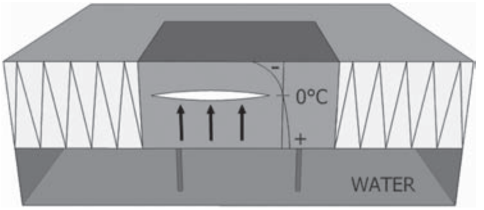

Figure 1. The test setup used for exposing specimens to an air temperature of −20°C and a water temperature of +4°C.

5 DISCUSSION

The potential use of non-frost resistant concrete or the use of low strength concrete in the damaged parts of the dams during the construction time might explain the observed surface spalling. However, these two explanations could not by themselves explain the severe extent of the damage. Macroscopic ice lens growth could on the other hand be a plausible explanation to the severe surface spalling.

The cracking of the specimen of w/c-ratio 1.0, provided with paper layers, could be described in the following manner—the cooling slowly extended downwards in the specimens and the water in the pores began to freeze. When balance in the heat flow was reached at some level, the loss of heat from the growing ice lenses towards the surfaces was balanced by the quantity of heat brought up by the water uptake and later set free during phase change. Since the specimens were weakened by the paper layers, the concrete could not resist the internal pressure from the growing ice lenses. Consequently, all three conditions for macroscopic ice lens growth were fulfilled. The absence of cracks in the other specimens could be explained by a too short time of freezing or by a lower permeability of the second concrete type.

The conditions for macroscopic ice lens growth in concrete dams might be fulfilled if the concrete has previously been deteriorated by frost damage or cracking. In these cases, water uptake is favourable due to high permeability of the concrete and likewise the tensile strength is decreased by the deterioration mechanisms. This line of argument is similar for the specimens, provided with paper layers, where macroscopic ice lens growth was facilitated.

6 CONCLUSION

In this study, indications have been obtained that the conditions for macroscopic ice lens growth could be fulfilled in specimens of low strength concrete. The specimens provided with paper layers, with the purpose of creating deteriorated concrete, cracked at the level of the top paper layer. The cracking was caused by macroscopic ice lens growth. The severe damage to the upstream faces of the arch dam at Selsforsen and the buttress dam at Storfinnforsen might have been caused in the same manner.

ACKNOWLEDGEMENTS

This study was carried out in collaboration between Vattenfall Research & Development AB and Lund University. The funding was provided by Elforsk AB, SBUF and SVC. The authors wish to thank V. Carlsson and H. Eriksson for providing information about the Selsforsen and Storfinnforsen dams.

NDE/NDT and measurement techniques

This page intentionally left blank

Concrete Repair, Rehabilitation and Retrofitting III – Alexander et al. (eds)
© 2012 Taylor & Francis Group, London, ISBN 978-0-415-89952-9

Strength monitoring of concrete structures by using non destructive testing

C. Sashidhar, N.V. Ramana & D. Pavan Kumar
JNTUA College of Engineering, Anantapur, India

ABSTRACT: Structures are assemblies of load carrying members capable of safely transferring the superimposed loads to the foundations. But after it is completed, it is inevitable that the process of deterioting starts on account of natural forces like rain, sun etc. Structural deficiency is also due to defect in construction, use of inferior material, poor workmanship and negligence in quality control and supervision, leakages from roofs, walls and other parts of the structure and corrosion in the reinforcement are the evidences. A correct diagnosis of the defects in structure and proper selection of materials for repairs is very essential. The diagnosis should establish the cause, nature and extents of damage and weakness or deterioration caused in the structure and assess the serviceability of the structure. Now days there are many methods and techniques available and Non Destructive Evaluation (NDE) techniques are one of the methods to evaluate any damage in structure. Non destructive techniques can be used effectively for investigation and evaluating the actual conditions of the structures. These techniques are relatively quick, easy to use and cheap and give a general indication on the property of hardened concrete. The choice of particular NDT depends upon the property of concrete to be observed such as strength, corrosion, crack monitoring etc. In this paper, the NDT tests conducted on different case studies are discussed. The NDT tests conducted on Storage tank or silo (cylindrical shape) of a Cement Factory of height 81 meters and multistoried residential apartment. In these cases, the problems are different for each structure. NDT tests has been conducted to check the performance after rehabilitation done to these structures. From NDT experimentation it was found that the results are satisfactory.

1 INTRODUCTION

To keep a high level of structural safety, durability and performance of the infrastructure an efficient system for early and regular structural assessment is required. The quality assurance during and after the construction of new structures, the characterization of material properties and damage as a function of time and environmental influences is becoming a serious concern. Non-destructive testing (NDT) methods have a large potential to be part of such a system.

NDT Methods in general are widely used in several industry branches such as aircrafts, nuclear facilities, chemical plants, electronic devices and other safety critical installations are tested regularly with fast and reliable testing technologies. A variety of advanced NDT methods are available for metallic or composite materials. In recent years, innovative NDT methods, which can be used for the assessments of existing structures have become available for concrete structures but are still not established for regular inspections. The purpose of establishing standard procedures for nondestructive testing (NDT) of concrete structures is to qualify and quantify the material properties of in-situ concrete without intrusively examining the material properties.

The quality of new concrete structures is dependent on many factors such as type of cement, type of aggregates, water cement ratio, curing, environmental conditions etc. Besides this, the control exercised during construction also contributes a lot to achieve the desired quality. The present system of checking slump and testing cubes, to assess the strength of concrete in structure under construction are not sufficient as the actual strength of the structure depend on many other factors such as proper compaction and effective curing. Considering the above requirements, need of testing of hardened concrete in new structures as well as old structures to assess the actual condition of structures. Non-Destructive Testing (NDT) techniques can be used effectively for investigation and evaluating the actual condition of the structures. These techniques are relatively quick, easy to use, cheap and give a general indication of the required property of the concrete. This approach will enable us to find suspected zones thereby reducing the time and cost of examining a large mass of concrete.

The choice of a particular NDT method depends upon the property of concrete to be observed such as strength, corrosion, crack monitoring etc.

The NDT being fast, easy to use at site and relatively less expensive can be used for

i. Testing any number of points and locations.
ii. Assessing the structure for various distressed conditions.
iii. Assessing damage due to fire, chemical attack, impact, age etc.
iv. Detecting cracks, voids, fractures, honeycombs and weak locations.
v. Assessing the actual condition of reinforcement.

2 LITERATURE REVIEW

Non destructive methods gives correct analysis in finding out the strength of Concrete, however in the absence of information on the conditions of curing and hardening of the concrete under investigation, the results of nondestructive tests can be very misleading[1]. The use of nondestructive testing in the laboratory is well-documented and standard specifications are available. However, when these nondestructive testing methods are used on site, additional factors have to be taken into consideration to enable meaningful interpretation of measurements obtained. The methods of calibration in the laboratory are reviewed and the ways to check on equipment and its calibration during site work are proposed. The information to be recorded and the interpretation of data are discussed by C. T. Tam 1991[2].

The ultrasonic pulse velocity (UPV) method has been used for decades to characterize concrete structures. In this method, ultrasonic transducers are attached to the concrete surface using a coupling agent. The coupling process is both time and labor intensive and, in some cases, may limit the ability to collect data. This paper describes the development of a fully contact-less (air-coupled) UPV method. By adding a matching layer between the transducer crystal and air and using signal processing methods, air-coupled through-thickness compression wave measurements in concrete are made possible. A scanning test setup was proposed and applied to a concrete test specimen that had different thicknesses and contained internal defects. The thicknesses of the test specimen represent realistic values for concrete elements. (Gonzalo P. Cetrangolo and John S. Popovics[7] showed that defects and thickness variations within the concrete were visualized when the UPV data were presented in a two-dimensional (2D) scan image. A data interpretation algorithm was used to accurately locate the embedded defects within the test specimen.

In the view of literature review a good reliability was shown towards the usage of NDT. Based on this, NDT with rebound hammer experimentation was conducted on two structures and detailed discussion presented below.

1. **Storage tank or silo (cylindrical shape) of a Cement Factory (height 81 m):**
The silo was constructed for storage of cement in cement factory. During construction stage it was observed that there is spalling of concrete on outer face at 42 m location in the silo at a cement factory as shown in fig. 1. The reason for spalling of concrete may be due to improper care during pouring and compaction of fresh concrete. The slip form technology was adopted for construction of silo. After the cracks appeared rehabilitation work was recommended. Before commencement of rehabilitation the silo was tested with rebound hammer in and around the affected area and the obtained results were presented Table 2.
The area around the affected portion was removed and treatment was given with good quality cement mortar. After the treatment (Fig. 2), it is cured for 28 days and it was once again tested with rebound hammer. Form the results it is observed that the average strength is above 30 N/mm^2 at the affected portion which is on par with the mix design strength of concrete i.e $30 N/mm^2$.
2. **Residential apartment:**
The residential five stories building was located near a public bus stand. The age of building was 12 years old. The building authorities were noticed delaminated and spilled concrete for their building. For quality assurance and rehabilitation technology regarding the safety and renovation against the cracks developing NDT was conducted with rebound hammer. After through visual view it came to know that certain area are water patched. These areas are much serious for first floor. This may be due to, porous texture of concrete. At few locations corrosion of reinforcement was also observed in first floor. This floor is much prone to water leakages from bath rooms. Due to poor quality of concrete, the deposited reinforcement in

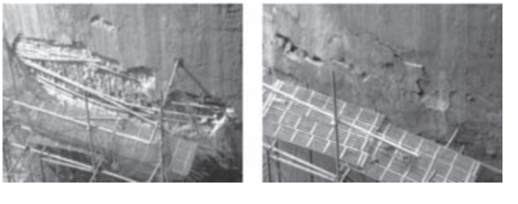

Figure 1. Affected area of silo (before treatment).

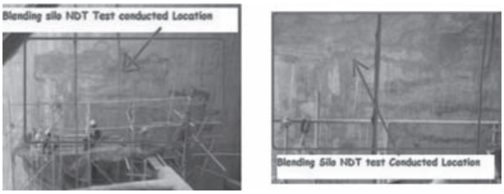

Figure 2. Rehabilitated area of silo (after treatment).

the beams was corroded. In addition to this the building was constructed very near to public bus stand. The emissions are releasing from the bus station may be one of the cause to expedite the corrosion action. Due to diffusion of corrosion activity, the volume of expansion was taken place to existing reinforcement which leads cracking the concrete along the deposition of steel bars in the structural elements. Due to this volume expansion of reinforcement, in some locations the concrete was delaminated and in some other locations the concrete is to be tending to peel off.

For rehabilitation purpose the damaged places was cleaned with brush and small cracks were widened with cutter equipment. Later the gaps were sealed with the help of rapid setting cement, cementatious elastomeric water proof and plasticized expanding grout admixture. The mixing proportion was adopted as per specification. The concrete surrounding this damaged reinforcement was cleaned with wire brush and nittozinc primer base (epoxy zinc rich primer) was applied as anti corrosion treatment. After this treatment the cement mortar was applied over this reinforcement. The treated area was allowed for 28 days curing. (The rehabilitation process was shown in Fig.3.) The slab area was grouted with cement mortar to make more impermeable up to possible extent. Later the concrete was tested with Rebound Hammer to assess the quality. From Non Destructive Test

Figure 3. Rehabilitation process for affected residential building.

results it is observed that the quality of concrete is ahead of mix design concrete (15 N/mm^2). It is concluded that the treated process is effective and this may enhances the durability of the structure.

3 CONCLUSIONS

Based on the inspection and strength monitoring of concrete structures the following conclusion were drawn.

1. The rehabilitation process could be enhancing the durability of the structure.
2. The strength monitoring of structure is needed periodically, thereby it is easy to assess the strength and durability of the structure.
3. Non destructive tests (NDT) more useful to assess the structure quality rather than the distractive tests.
4. Non destructive tests are reliable to assess the quality of concrete.

Concrete Repair, Rehabilitation and Retrofitting III – Alexander et al. (eds)
 ISBN 978-0-415-89952-9

Main challenges of non destructive evaluation of on-site concrete strength

D. Breysse
University Bordeaux, I2M, UMR 5295, Talence, France
CNRS, I2M, UMR 5295, Talence, France
Arts et Metiers ParisTech, I2M, UMR 5295, Talence, France

1 THE CHALLENGE OF NON-DESTRUCTIVE STRENGTH ASSESSMENT

Strength assessment of existing buildings is a key challenge for structural engineers who need to feed structural computations with material data. The quality of assessment is limited due to sources of uncertainties arising at various levels and caused: by the testing method, by systematic interferences with the environment, by random interferences (due to material intrinsic variability), by human factor influence and by data interpretation, including errors in the model between what is measured and what is looked for. Rebound measurement and ultrasonic pulse velocity (UPV) are among the most widely used NDT methods regarding concrete strength assessment. A main point is that of “calibration”, i.e. that of building and using a reliable relationship between NDT values and strength.

Many factors can influence the value of the NDT measurement. One example is that of the aggregate type: the conversion model ($f_c(V)$ or $f_c(R)$) changes with the aggregate type since heavier or harder aggregates tend to increase the UPV and rebound value more than concrete strength. Each influencing parameter would require a correction/calibration stage, notwithstanding with possible interactions between parameters. This process quickly comes to be unpracticable.

The calibration approach is another way to answer this issue. Figure 1 synthesizes how EN-13791 standards recommend to identify strength from on-site NDT measurements. Information obtained on cores can be used: (a) either for establishing a specific model (correlation curve)—Approach A, (b) or for correcting, by shifting, the first estimates given by a prior model—Approach B.

2 SONREB METHOD AND ITS CALIBRATION

Combining several NDT techniques is an old idea. We will restrain here to the case (“Sonreb”) of combining UPV and rebound measurements. The underlying concept is that if the two methods are influenced in different ways by the same factor, e.g. moisture of the concrete, their combined use can cancel the effect of this factor and improve the accuracy of the estimated strength. Like with a single NDT, a conversion curve can be used: $f_c(V, R)$.

Literature survey has shown that the double-power law ($f_c = a\ V^b\ R^c$) is the most common. However a, b and c coefficients show a large variation. This confirms that there is no universal model and that calibration remains necessary. The methodology described for calibration in Figure 1 has been adapted and two approaches can be used. Approach A consists in looking for a multivariate regression function between the (R, V) values measured on the concrete specimens and f_c values measured on cores or cubes. Approach B consists in using a known prior model, e.g. a ($f_{c\ est} = a\ V^b\ R^c$) model, where b and c are given, and to calibrate the coefficient a value. Calibration can be done by calculating the mean value of estimated strength $f_{c\ est,\ mean}$ and the mean value of experimental strength $f_{c\ exp,\ mean}$:

$$k = f_{c\ est,\ mean} / f_{c\ exp,\ mean}$$

Thus the calibrated model writes:

$$f_{c\ est\_cal} = (a/k)\ V^b\ R^c$$

In the following, the prior model will be

$$f_{c\ est} = a\ V^{2.60}\ R^{1.30}$$

with $a = 1.15\ 10^{-10}$. The choice of the a, b and c value, somehow arbitrary, has been done in agreement with literature survey. In any case, the a value will be modified after calibration.

3 STRENGTH ESTIMATE IN PRACTICE

The efficiency of these two approaches has been compared on a variety of data taken from the literature, both from laboratory studies and from real structures, in order to cover a wide field of

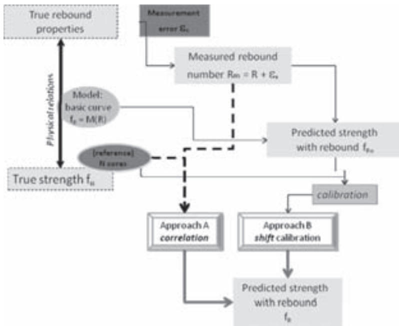

Figure 1. Schematic view of approaches for calibration, from EN 13791.

situations. The strength estimates are identified by comparing four options: (1) Prior model = Gasparik model, (2) Prior model = author's model: $f_{c\ est} = 1.15\ 10^{-10}\ V^{2.60}\ R^{1.30}$, (3) Approach A, (4) Approach B, author's model after calibration with k.

All estimations are compared regarding three criteria: the r^2 coefficient of determination, the root mean square error (RMSE) and the average value of the absolute relative error ε.

3.1 *Calibration results on laboratory data*

The strength assessment process has been applied to 15 datasets published by various authors in the literature, which amounts a total number of 645 series of measurements. These data cover a variety of concretes (average strength from 23 to 130 MPa) which are at maximum 1-year old. For each dataset (i.e. each author-study, the same process has been used and all individual strength estimates have been compared to real values).

Figure 2 plots the 645 UPV-strength pairs of data. The comparison between experimental and estimated strength is given for Model 4 at figure 3. It corresponds to a $r^2 = 0.93$ and a RMSE = 6.4 MPa, which corresponds to the average estimation error on strength. It was found that:

- uncalibrated models have obviously larger errors with RMSE of about 10% against 4 to 6% for calibrated models. Similar conclusions can be made for r^2.
- calibration with Approach B is slightly less efficient than calibration with Approach A, but it must be reminded that it is based on a single "universal" curve and a simple multiplication.

3.2 *Calibration results on on-site data*

The same work was carried out on data obtained on structures. These data are more difficult to get and only four datasets were considered, amounting a total of 64 series of measurements.

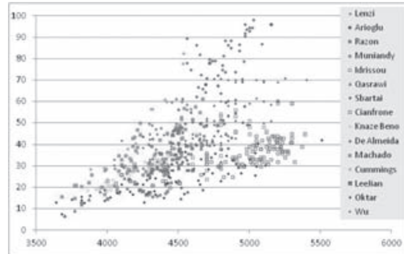

Figure 2. Strength and UPV individual values for the whole population.

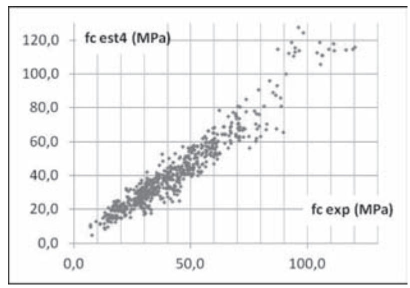

Figure 3. Comparison between measured and estimated values, with calibration, model 4.

The interest of combining the techniques is confirmed in some cases where it reduces the RMSE but not in others. The reasons are known: combination is useless if the quality of one technique is much lower than that of the other technique, which was the case in two out of four datasets. The Approach A is the most efficient since it is based on a specific calibration (possible as soon as one has enough specimens), even if the model remains case-specific. The same reason explains that Approach B may lead to deceptive results, since the b and c exponents of Equation 4 are adapted to plain concrete. Other influencing factors (carbonation, cracking, coring induces damage…) may exist on site, which deserve a careful attention.

3.3 *How many cores for calibration?*

Synthetic simulations have been carried out to analyze how the number of cores influences the quality of assessment. An interesting result is that, in practice, the quality of assessment remains correct even if the number of cores is reduced well below what is suggested by standards. Calibration Approach A is the most efficient when one has more than 6 cores while Approach B has better (and acceptable) results if one has only 3 or 4 cores.

Concrete Repair, Rehabilitation and Retrofitting III – Alexander et al. (eds)
© 2012 Taylor & Francis Group, London, ISBN 978-0-415-89952-9

Test method to determine durability of concrete under combined environmental actions and mechanical load

L. Wang, Y. Yao, Z. Wang, P. Huang & X. Guan
China Building Materials Academy, State Key Laboratory of Green Building Materials, Beijing, China

1 INTRODUCTION

Concrete in working condition is usually subject to the influence of both mechanical load and environmental factors. It is necessary to develop a widely acceptable test method to determine the durability of concrete subject to multiple damage factors. During the last ten years, research fellows in the Chinese Building Materials Academy have been devoted to standardizing the evaluation procedures of concrete performance under multiple damage factors. An innovative device has been developed to facilitate the preloading of samples, maintenance of stable loads and monitor the change in indicative parameters.

2 DEVELOPMENT OF THE TEST DEVICE

Three major damage factors have been emphasized in our research. They are 1) bending load, 2) freeze-thaw cycles, and 3) saline solution attack. The combination of the three factors can effectively simulate actual working conditions of reinforced concrete beams and those of cement concrete pavement.

A number of difficulties are related to the success of designing a test device. First, it is hard to maintain and monitor the stress applied to concrete specimens in severe experimental conditions such as freeze-thaw cycles and saline solution attack. Second, it is important to arrange as many as possible large size specimens in a container so that parallel comparative tests can be conducted simultaneously. Another difficulty is the selection of indicative parameters to measure and the design of acquisition and processing system for dynamic data flow.

The early designed testing device is made up of 5 parts. They are: 1) a preloading unit that provides four-point bending stress, 2) an automatic test unit that performs repeated freeze-thaw cycles, 3) a monitor unit that measures dynamic elastic modulus of samples, 4) an intelligent resistance strain surveying unit, and 5) a CT-2B potentiostat unit.

Concrete samples of larger size (10 cm × 10 cm × 40 cm) are chosen so that 5–20 mm diameter stone and rebar can be used in concrete samples. A pie-shaped load sensor is used to control the compressive load at desired value (Fig. 1).

During 2008 to 2010 the prototype device underwent substantial improvement by Zhendi Wang and Ling Wang in the research on the deterioration of concrete exposed to multiple damage factors.

The device consists of 3 parts: 1) a preloading unit, 2) a freeze-thaw test unit, and 3) a data collecting unit for strain, load, temperature and resistivity (Fig. 2).

The adoption of a signal isolator and a hydraulic pump provides the preloading unit with more accurate control of external flexural loading and also greatly improve the stability of long time load maintenance. Another innovation is the arrangement of test concrete samples in the freeze-thaw tank. They are placed vertically to save room for more samples (Fig. 3). In this way totally nine concrete samples can be placed in the tank at one time. The increase in the capacity of freeze-thaw tank is very helpful particularly for comparative studies where more duplicate samples can be tested under the same treatment.

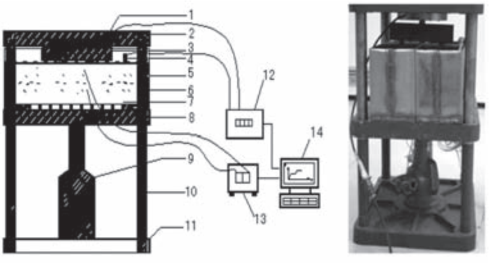

1. pie-shaped load sensor; 2. steel plate; 3. load balancing weight; 4. temperature transducer; 5. stainless steel sink; 6. corrosion solution; 7. concrete sample; 8. steel plate; 9. screw jack; 10. steel upright post; 11. steel plate; 12. intelligent digital receiver; 13. intelligent resistance strain surveying instrument; 14. computer.

Figure 1. Schematic diagram and photo of the preloading device.

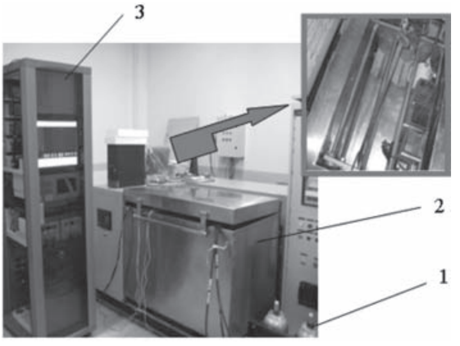

1. improved stress preloading unit; 2. automatic accelerated freeze-thaw test unit; 3. data sampling unit.

Figure 2. The improved edition of test device.

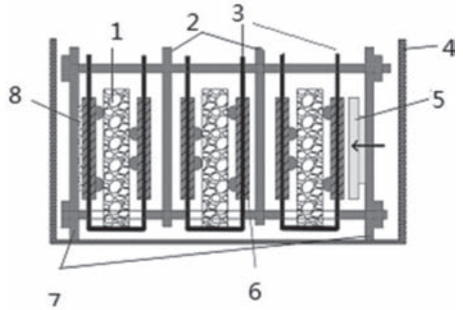

1. concrete specimens; 2. slide board; 3. samples box; 4. tank; 5. force supplier; 6. steel board; 7. stationary board; 8. stress sensor

Figure 3. Schematic diagram showing the test samples in the vertical position.

With these improvements, testing and data collecting are quicker and more accurate. The device can collect the data signals of strain, load, temperature and resistivity during the whole process of the deterioration, making it easier to monitor the change of strain and resistivity over time.

The device can be used to test the effects of all combinations of three major damage factors that concrete may confront in working condition, namely freeze-thaw cycles, chloride salt attack and external flexural load. The treatments that the device can perform and test are grouped into three categories—single damage factor (SDF), double damage factors (DDF) and multiple damage factors (MDF) (Table 1).

Table 1. The treatments that can be studied with the improved test device.

Treatment type	Combination of damage factors
SDF	Repeated freeze-thaw cycles
	Flexural loading
	Chloride salt attack
DDF	Repeated freeze-thaw cycles + chloride salt attack
	Repeated freeze-thaw cycles + external four point flexural load
	Chloride salt attack + external four point flexural load
MDF	Repeated freeze-thaw cycles + flexural loading + chloride salt attack

3 CONCLUSIONS

Concrete structure is usually subject to the influence of both mechanical load and environmental agents. The new device has been developed to help the researches on concrete durability subject to the influence of multiple damage factors.

The device can accurately apply an external flexural load to specimen samples, while steadily maintaining the load for extended period of time. The device can simulate all combinations of three common damage factors that influence concrete structure, namely frost damage, de-icing salt attack and bending load. The device can collect data signals of strain, load, temperature as well as resistivity of the concrete specimen during its deterioration process. Having been tested successfully in laboratory studies, the device can be used to monitor the degradation of concrete structure under the attack of multiple damage factors.

A number of indicative parameters, such as dynamic elastic modulus, strain, relative corrosion current density, resistance and electrical resistivity have shown that the performance of concrete degrades more rapidly when exposed to the attack of multiple damage factors. The higher the flexural load applied, the more rapid the deterioration of concrete progresses. The application of heavy mechanical load would accelerate the structural failure of reinforcement concrete. The results can be used in the optimization of the composition of concrete infrastructures.

Concrete Repair, Rehabilitation and Retrofitting III – Alexander et al. (eds)
© 2012 Taylor & Francis Group, London, ISBN 978-0-415-89952-9

Structure testing with ultrasonic-echo and impulse radar technique

C. Sodeikat
Engineering firm Schießl Gehlen Sodeikat GmbH, München, Deutschland

ABSTRACT: Ultrasonic-Echo and Impulse Radar Technique are powerful non-destructive testing methods and have been successfully used for years in the building industry. In the last years both methods gained big progress concerning test equipment, accuracy of test results and practical use for engineering firms, that means beside of research institutes. Typical tasks for Ultrasonic—Echo and Impulse Radar Technique use are: construction testing for planning repair and rehabilitation measures, determining the condition of existing infrastructure buildings like tunnels and bridges in the course of routine inspections, determining existing structures due to a lack of planning documents, which are needed in the course of renovations and conversions and the quality confirmation of new built constructions in the course of the technical acceptance.

1 INTRODUCTION

Non-destructive testing methods (NDT methods) have been successfully used for decades in the building industry. These methods enable the survey of a structure's condition, without causing further destruction. However destructive testing methods are impossible to avoid altogether. But based on the results of previously conducted non-destructive testing methods, the destructive testing methods can be implemented at specific targets and therefore limit the damage to only the necessary amount, which is better for both the property owner as well as the structure. The low-frequency ultrasonic echo method and the impulse radar make it possible today to answer questions in the assessment of concrete structures and reinforced concrete structures, which with previous NDT methods were not solvable or only solvable with restrictions.

Typical issues concerning existing structures are finding flaws and hollow sections, determining the amount of the reinforcement and the concrete cover of deep laying reinforcement, finding the location of tendons, determining the thickness of structural components (decks, floor slabs, screeds), identifying the dimensions of inaccessible components (foundations, earth banked walls) and generally identifying the layout of the structure when plans are not available.

But ultrasonic and impulse radar are can also be used for controls in the context of structure monitoring and quality control for example in the acceptance of newly built structures.

2 BASIS OF ULTRASONIC ECHO AND IMPULSE RADAR TECHNIQUE

Ultrasonic waves and short electromagnetic pulses are reflected at the interface of discontinuities in an otherwise homogeneous material—changing of the acoustic impedance for ultrasonic waves, changing of the dielectric characteristics for electromagnetic pulses (radar waves). From the elapsed time of the reflected pulse, the distance of the inhomogeneity from the probe can be determined and through scanning generally their extent can also be concluded (Fig. 1).

3 PRACTICAL USE OF ULTRASONIC ECHO TECHNIQUE

3.1 *Measuring device and typical inspection task*

Since the late 1990s, ultrasonic probes have been available which can be connected to concrete surfaces without any coupling agent. A suitable device used in our firm with a small, robust, dust and moisture resistant design consists of a transmitter-receiver unit with 24 point-contact probes, which are assembled in a transmitting section and a receiving section each with 12 probes (Fig. 2). The battery operated control unit generates the transmission pulse and receives and stores the reflected pulses and displays them as images with their depth in millimetres on a small monochrome LCD screen. The data can be further evaluated on the PC in different scan ways.

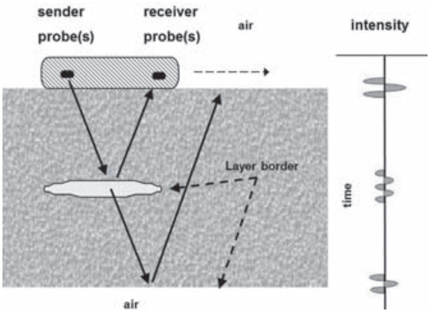

Figure 1. Principle of wave reflection for ultrasonic echo and impulse radar technique.

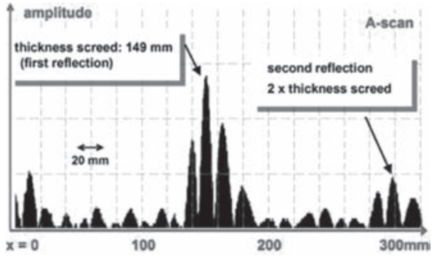

Figure 2. Ultra-Sonic-Echo single-measurement for determining the thickness of an industrial screed; A-scan Multi Array.

Among others typical inspection tasks, which can be solved with this device are:

- Thickness measurements of e.g. Industrial floors, screeds, ceiling systems
- Verifying the integrity of tunnel linings (lining test, see the follow practical example)
- Detecting rock pockets, voids e.g. in the base of triple walls
- Locating installation components and reinforcement elements such as central expansion joints, shear studs, conduits, hollow bodies
- Determining the location and coverage of tendons
- Under certain conditions: Investigating the grouting condition of ducts
- Given a known component thickness: Using the wave velocity to determine the E-Modulus and the compressive strength of the concrete.

3.2 *Determining the thickness of a screed*

Measuring Task and Procedure. As a result of a local screed opening in a new construction the construction manager contested that the thickness of the built in industry screed corresponds to the desired thickness. As part of a court opinion, therefore, the thickness of the screed had to be determined everywhere.

Results. Based on the ultrasonic measurements, areas of the base plate could be detected where the thickness of the screed had fallen significantly under the target thickness of 150 mm. The measurement error of the process, determined through subsequent drilling, was less than 5%. The following Figure 2 shows the representation of corresponding A-scans (as an envelope of the signal) with a recognizable second reflection of the signal (caused by the fact that some of the transmitted signal was also reflected at the top of the screed).

4 SUBWAY TUNNEL TESTING WITH RADAR

In the course of repair measures of a 40 years old German Subway tunnel hints for differences between the drawings and the execution were found.

Measuring Task: The owner ordered us to create an inspection measure to detect potential irregularities in the tunnel shell. The results should be the basis of probably necessary recalculations and repair measures.

Results: Most irregularities in tunnel shells occur in the area of the tunnel roof due to the local difficult pouring process. We executed one measuring line along the tunnel roof and intensified the tests in areas with detected irregularities. The results showed that the thickness of the tunnel shell was locally reduced by 40% (Fig. 3). Furthermore in many areas the reinforcement was located in an incorrect position (Fig. 4). The bottom layer of the reinforcement was obviously pushed upwards during concrete pumping due to a too stiff concrete consistency.

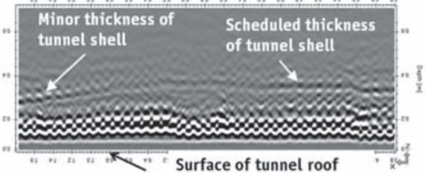

Figure 3. Some areas of the tunnel shell at the roof showed a reduced thickness by 40%.

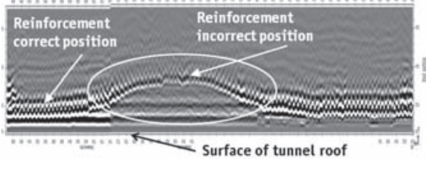

Figure 4. Due to the concrete pumping process with an already too stiff concrete the reinforcement was pushed upwards.

Concrete Repair, Rehabilitation and Retrofitting III – Alexander et al. (eds)
© 2012 Taylor & Francis Group, London, ISBN 978-0-415-89952-9

Influences on layer thickness measurements of concrete coatings by mobile NMR on steel-reinforced concrete constructions

J. Orlowsky & M. Raupach
Institute of Building Materials Research (IBAC), RWTH Aachen University, Aachen, NRW, Germany

ABSTRACT: A large number of infrastructural concrete buildings are protected against aggressive environments by coating systems. The functionality of these coating systems is mainly affected by the composition and thickness of the individual polymeric layers. For the first time ever, a mobile Nuclear Magnetic Resonance (NMR) sensor allows a non-destructive determination of this important parameter directly on the building site. However, before this technique can be used on steel-reinforced concrete elements, the potential effect of the reinforcement on the measurement, i. e. the NMR signal, needs to be studied. This has been done in the frame of a wide test program at the IBAC, RWTH Aachen University. Content of the present paper are the description, results and the analysis of these investigations. The results show a shift of the NMR profile as well as an increase of the signals amplitude in the case of the reinforced samples, while calculating the thickness of concrete coating lead to identical results.

1 INTRODUCTION

The use of coating systems on infrastructural concrete buildings as protection against aggressive environments has increased in the last ten years. The concrete coatings usually consist of individual layers of polymers or cement-based materials. Concrete coatings are also called "surface protection systems" in Germany.

To ensure the target functions of a surface protection system, the following aspects are important: Thickness of the individual coating layers, application method of the coating materials, consideration of environmental parameters such as temperature, humidity, and wind as well as preparation of the substrate.

Up to now, there are no non-destructive test-methods to determine:

- The total thickness of the surface protection system as well as the thickness of the individual layers,
- the water transport through the surface protection system,
- the drying process of the concrete after application of a surface protection system,
- changes of the material due to weathering,
- quality and conformity of the applied material.

The NMR MOUSE® (Mobile Universal Surface Explorer, registered trademark of RWTH Aachen University) was recently found to exhibit a great potential for investigating these issues in a non-destructive way. However, before the mobile NMR can be applied at construction sites, the potential influence of steel reinforcements on the NMR signal has to be investigated. A parameter study on this influence will be the main focus of this paper.

2 NMR MOUSE—THE INVESTIGATION METHOD USED

In contrast to conventional NMR spectroscopy, which uses highly homogeneous magnetic fields, the method used here relies on inhomogeneous magnetic fields applied from a single side. The advantage of single-sided NMR is the virtually unlimited sample size as well as the potential to construct mobile devices that can eventually be used on construction sites. A compact unilateral sensor developed for non-destructive testing of materials containing hydrogen atoms, the so-called NMR MOUSE (PM 5) was used for the described work. The PM 5 has a measuring field of 20 by 20 mm in the cross-section and the thickness can be chosen between 10 and 100 μm (sensitive volume). The NMR signal is collected in the described sensitive volume which can be moved up to 5 mm deep into the specimen by using a stepper-motor driven, high-precision automatic lift which changes the distance between the sensor and the sample.

The most important parameters determined by the NMR MOUSE are the signal amplitude which is indicative for the number of protons in the sensitive volume and the transverse relaxation time T_2 which relates to the molecular mobility. These information are obtained by using the Carr-Purcell-Meiboom-Gill (CPMG) pulse sequence and analysing the resulting spin echos. In order to assess the number of protons, the first 5 to 10 spin echos were integrated. The depth profiles shown in the results section were constructed by plotting these values versus the measuring depth.

3 PARAMETER STUDY ON THE INFLUENCE OF STEEL REINFORCEMENTS

In order to realize an investigation with a wide variation of parameters, a simplified test method had to be developed without using coated, steel-reinforced concrete plates. For that, sandwich elements with a total thickness of approx. 3 mm consisting of a 2.6 wt-% copper sulphate solution embedded between two glass plates were produced (g-c-g elements). Secondly, a rectangular polyethylene framework was built having 48 bore holes to host the steel bars. Sandwich element and box were mounted on the table of the NMR lift.

4 RESULTS AND OUTLOOK

Figure 1 shows two depth profiles which were recorded using the test setup described before. In the first example, no steel reinforcement was present above the g-c-g element, while in the second one, two reinforcement bars with a diameter of 8 mm and a spacing of 10 cm were arranged 2 cm above the sandwich element with an orientation of 90° to the magnetic field lines. Since there are only very few hydrogen atoms in the glass plates, a signal can only be recorded within the aqueous copper sulphate solution. To extract the layer thickness of the copper sulphate solution, the measuring depths corresponding to the "half height", i.e. half of the mean maximum amplitude on the ascending and descending branches were determined. The layer thickness is then given by the distance between these two points.

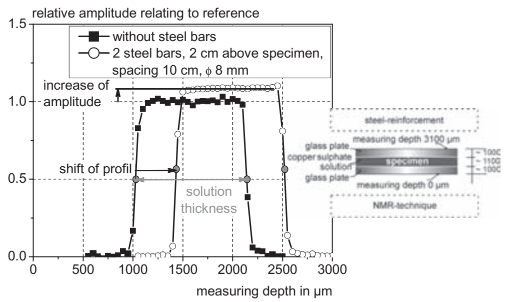

Figure 1. Depth profiles for the g-c-g element as determined by the NMR MOUSE. The measuring depth of 0 µm is located at the borderline between NMR sensor and lower glass plate as illustrated on the right.

The points used to calculate the thickness of the copper sulphate solution also allow calculating the displacement of the sensitive volume (profile shift) originating in the presence of the steel bars. The attraction of the steel causes a shift in the magnetic field of the NMR MOUSE towards the steel. Thus, the position of the sensitive volume is shifted to larger measuring depths by about 400 µm. Moreover, the magnetic field experiences a homogenization by the steel. The resulting decrease of the gradient causes an increase of the volume activated in the specimen which results in an increase of the amplitude.

The results illustrated in the paper show that the existence of steel in the range of the measurements conducted with the NMR MOUSE has the following effects on the determination of depth profiles:

- Shift of the profile towards the steel,
- increase in the measured amplitude,
- but unchanged layer thicknesses!

For measuring the layer thicknesses of coatings on steel-reinforced concrete buildings, this means that the measured layer thickness is independent of the steel reinforcement. Only the position and the amplitude of the coating layers are influenced by the reinforcement in the concrete. To what extent the position and the amplitude of the coating layers are changed depends on the following parameters:

- Concrete cover (the larger, the smaller the influence; at 7 cm only minimal influence)
- Steel diameter (the larger, the larger the influence; decisive at concrete covers ≤4 cm)
- Horizontal distance between the steel bars and from the measuring field (the larger, the smaller the influence; decisive at concrete covers ≤4 cm)
- Amount of steel (the more, the higher the influence)
- Orientation of the steel to the magnetic field (90° has a larger effect than 0°; decisive at concrete covers <4 cm)

To measure and to correct the profile shift due to reinforcement different methods are discussed in the paper. The simplest way is the application and measurement of a marker at the building surface. The profile shift resulting from reinforcement can be taken into account at any measurement by means of the marker. As the layer thickness as such is not influenced by the reinforcement, a correction is not necessary in this place. A correction is also not required for the amplitude because this relative value always experiences the same shift independent of the coating material and because the absolute magnitude of the amplitude is not decisive when measuring the profile. Those cases, in which the absolute magnitude of the amplitude at varying steel reinforcement is relevant (e. g. water penetration front into a material) can, however, not be answered without the model.

Concrete Repair, Rehabilitation and Retrofitting III – Alexander et al. (eds)
© 2012 Taylor & Francis Group, London, ISBN 978-0-415-89952-9

Shape factors of four point resistivity method in presence of rebars

A.J. Garzon, C. Andrade, N. Rebolledo & J. Fullea
Centro de Investigación en Seguridad y Durabilidad Estructural y de Materiales (CISDEM-CSIC-UPM), Madrid, Spain

J. Sanchez & E. Menéndez
Instituto de Ciencias de la Construcción Eduardo Torroja (IETcc-CSIC), Madrid, Spain

ABSTRACT: Concrete resistivity is increasingly being used for diverse applications like the detection of fibers, the evaluation of the degree of water saturation and then of the risk of rebar corrosion, the prediction of the service life or as indicator of the porosity of the concrete. There are several methods to measure the electrical resistivity of the concrete which basically are based in a direct measurement using regular geometries of the specimen and of the electrodes or the measurement by the "disc" or the four point (Wenner) method. It is said that the measurement has in any case to be made in absence of a rebar in the specimen or below the measurement place due to the presence of a metallic piece modifies the measurement. In present work is described the study made to calculate the resistivity by the Four-Point method in specimens containing a centered bar. The theoretical calculations were carried out by a finite element method and the results were verified in several specimens having the same resistivity than the numerical examples. Shape factors and a mathematical expression are given for different variables tested.

The electrical resistivity of concrete is an indication of the volume of pores and of the degree of water saturation and therefore it has a strong relation to the concrete durability and in particular to the corrosion of reinforcements. Andrade et al. (Andrade and d'Andrea 2008) proposed a service life model based in the measurement of the resistivity in saturated concrete.

There are several methods to measure the resistivity, ρ, in concrete structures but the most common used method is the Wenner or Four-point method. The method has been applied from long time ago but always preventing on the need to avoid to be near the metallic bars as if they are in the zone of influence of the current applied, the resistivity will be different and then not representing the concrete bulk. In present paper the disturbance is quantified experimentally and modelled by numerical analysis in order to study whether there are some functions or relations that could be established on the proportion of disturbance and then define a "bar presence" factor, f_b, in addition to the shape factor, f_s, and the geometrical factor ($2\pi a$):

$$\rho = f_b f_s \, 2\pi a \, R \tag{1}$$

Where R is the ratio of the voltage and the current, and a is equal to the electrode spacing

The specimens fabricated were of cylindrical and prismatic shape. The same mortar mix was made for all of them: water-cement (CEM I 42.5 R/SR) ratio of 0.5 and sand-cement ratio of 3. In some of the specimens were embedded a carbon steel B 500 SD bar of 8 mm in diameter. The specimens were cured at 20 ± 2ºC and 100% relative humidity in a chamber during 28 days.

The resistivity was measured by the standard arrangement of the classical Wenner Four Points method, in which the current is applied in the external electrodes and the difference in potential is measured by means of the two internal reference electrodes. The external electrodes were small pieces of reinforcing steel and the two internal ones were Ag/AgCl reference electrodes. Currents of 1.0 mA were applied for the set of experiments and the voltage difference between the reference electrodes was measured every 1 ms after the galvanic pulse. Previously, the potential was measured during 0.1 s in order to find the initial condition potential. The equipment used for all the measurements was the AUTOLAB PGSTAT 30. The specimens were measured during its 28 first days.

Specimens with and without rebar were modelled with COMSOL Multiphysics Finite Element program. Figure 2 shows the theoretical results obtained for a prismatic geometry without and with rebar, a = 35 mm and $\rho_{concrete} = 10^3\ \Omega$m. The

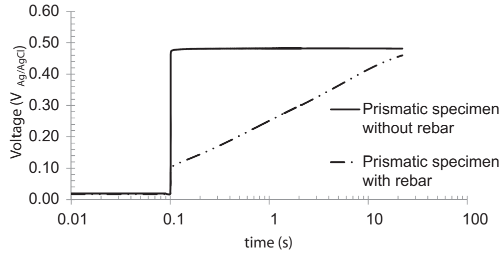

Figure 1. Experimental galvanic pulse on prismatic specimen without and with rebar at the same concrete age (1 day).

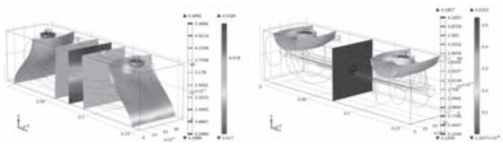

Figure 2. Prismatic geometry 4 × 4x16 cm without rebar (left) and with rebar (right). Isopotential surfaces, central slice of current density and current streamline distribution. FEM calculation.

current lines spread along all geometry, but the current lines are focus between the electrodes in the rebar absence case (Figure 2 left) and they are concentrated in the rebar in the other case (Figure 2 right).

From the results obtained in the theoretical calculations and taking into account the equation 1, it is possible to obtain the bar presence factor, f_b, and the shape factor, f_s.

The shape factor is obtained for the prismatic and cylindrical specimen without rebar where the bar factor f_b = 1. Following equations give the shape factor in function of the electrode spacing, a [=] m, for the prismatic and cylindrical geometry without rebar respectively:

$$f_s = -25.006 \cdot a + 1.0472 \tag{2}$$

$$f_s = -8.5074 \cdot a + 1.0282 \tag{3}$$

The bar factor is present in the prismatic and cylindrical specimens with rebar at the same time that the shape factor. Following equation shows the values of both factors in function of the electrode spacing, a [=] m, for the prismatic and cylindrical specimen with rebar.

$$f_b f_s = -36.117 \cdot a + 0.5945 \tag{4}$$

$$f_b f_s = -3.3636 \cdot a + 0.9618 \tag{5}$$

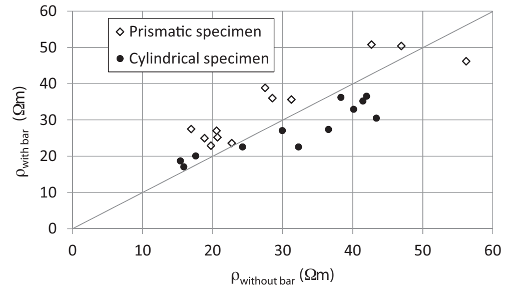

Figure 3. Experimental resistivity values for specimens with and without rebar applying the corresponding factors.

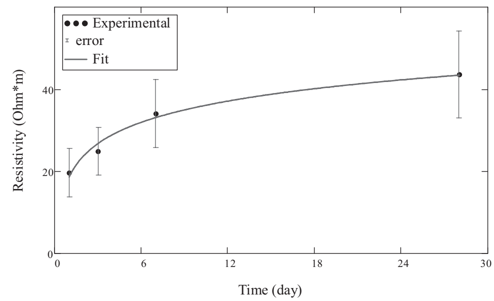

Figure 4. Resistivity evolution during the concrete aged for specimens with and without rebar.

Applying the corresponding theoretical equation obtained by FEM calculations to the experimental values for each geometry, it is possible to obtain the resistivity. Figure 3 shows the resistivity values for specimens with the same dimensions with and without steel bar. The scatter data takes by the steel bar presence is reduced taking into account the proper factors. Figure 4 shows the resistivity evolution of all specimens and its variability. All the specimens belong to the same mix, so they get the same resistivity. This variability is inherent of the concrete material and it does not depend for the geometry.

Concrete Repair, Rehabilitation and Retrofitting III – Alexander et al. (eds)

Statistical analysis of electrical resistivity as a tool for estimating cement type of 12-year-old concrete specimens

J. Pacheco
Faculty of Civil Engineering and Geosciences, Delft University of Technology, The Netherlands

O. Morales-Nápoles
TNO Structural Reliability, Delft, The Netherlands
Faculty of Electrical Engineering, Mathematics and Computer Sciences, Delft University of Technology, The Netherlands

R.B. Polder
Faculty of Civil Engineering and Geosciences, Delft University of Technology, The Netherlands
TNO Technical Sciences/Building Materials, Delft, The Netherlands

ABSTRACT: Statistical tests on values of concrete resistivity can be used as a fast tool for estimating the cement type of old concrete. Electrical resistivity of concrete is a material property that describes the electrical resistance of concrete in a unit cell. Influences of binder type, water-to-binder ratio, moisture and temperature can be detected by changes in resistivity. Data on resistivity at relatively young concrete are available for a wide range of compositions. Measurements are performed in a non-destructive manner with either the Wenner-probe or the Two Electrode Method. The relationship between resistivity and concrete durability is still under research. This paper shows that statistical analysis of electrical resistivity might be a useful tool for estimating the concrete binder. In 1998, concrete specimens with several cement types and water-to-binder ratio were cast and then exposed to salt/dry cycles for 26 weeks. Afterwards, they were left unsheltered in The Netherlands for most part of the subsequent 12 years. In 2010, the identification labels became unreadable. Nested Factorial Design (NFD) mad Kolmogorov-Smirnov Two Sample Test (KS) were applied on values of concrete resistivity obtained from measurements on concrete specimens after 2.5 and 12 years, respectively. Results showed that cement type had the strongest influence on values of resistivity. Also, the probability found in 1995 remained recognizable even after 12 years. This procedure may have significant value for concrete scientists investigating old concrete structures that lack proper documentation on the concrete composition.

Keywords: resistivity, statistical analysis, assessment

1 INTRODUCTION

Concrete resistivity is a material dependant property that describes the electrical resistance over a unit cell. Measured values are usually between 10^1 to 10^5 Ωm and are dependent on type of concrete composition, age and environmental conditions (Polder 2001). In concrete, electric current is carried by ions contained in the pore solution. The chemical composition of this pore solution depends on the cement type and composition and the presence of other binders like GBFS or fly ash.

2 EXPERIMENTAL DESIGN

In 1998, concrete specimens made from four types of cement and three water/binder ratios (in total 12 compositions) were cast and then exposed to salt/dry cycles for 26 weeks, accelerated carbonation and mixed-in chlorides. In this paper, the results of the specimens exposed to salt/dry cycles are described.

Statistical analysis of concrete properties has been performed extensively over the past decades. In this paper, two statistical tools: Nested Factorial Design (NFD) and Kolmogorov-Smirnov Two Sample Test (KST); were applied on values of concrete resistivity after 2.5 and 12 years in order to estimate the most probable cement type in concrete specimens.

Nested Factorial Design is a statistical tool that allows identifying the influence of different parameters on a specific variable. In this case, the influence of cement type, water-to-binder ratio and cover depth over resistivity. The Kolmogorov-Smirnov Two Sample test (KST) compares the probability distributions of two samples. One of

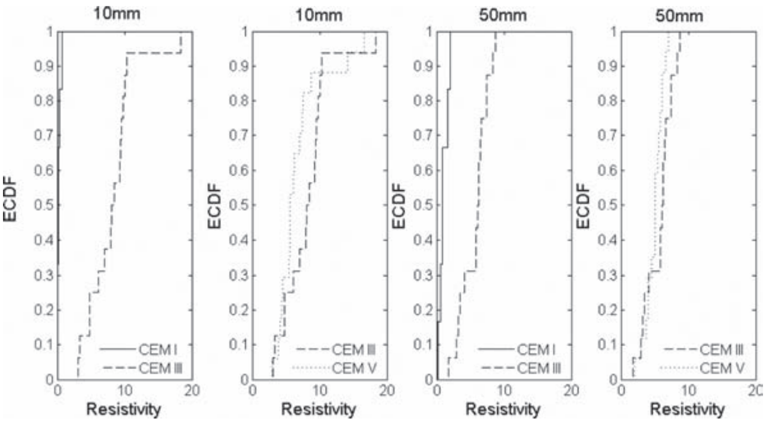

Figure 1. KS test on concrete specimens at 10 and 50 mm of cover depth after 12 years.

the main advantages of the KST is that each sample (group of specimens) may have a different number of replicates, i.e. concrete specimens. By measuring the distance between the empirical cumulative distribution functions (ECDF) of concrete resistivity, the KST can accept or reject the null hypothesis. The null hypothesis assumes that the ECDF of two samples are the same, in this case, they have the same mix design. Rejecting the Ho (Ho = 1) shows that samples have different concrete compositions.

3 RESULTS AND DISCUSSION

3.1 *Preliminary analysis*

Nested Factorial Design (NFD) was performed reported values of concrete resistivity on identified specimens during 2001 (Polder 2001a). This analysis was focused on three parameters: cement type, water-to-binder ratio and cover depth. By rejecting the Ho, the NFD identifies which of the three parameters had the strongest influence on concrete resistivity. The KST analysis on values of concrete resistivity after 2.5 years (identified) was carried out over the same specimens studied with the NFD.

3.1 *Identification of cement type after 12 years.*

Figure 1 shows the results of KST in samples containing CEM I, CEM III and CEM V after 12 years.

3.2 *Discussion*

It was observed that cement type has the strongest influence on concrete resistivity. CEM I and CEM II had lower values of concrete resistivity, while CEM III and CEM V show the highest and similar values. After 2.5 years since the fabrication of the specimens, the addition of GBFS in CEM III and both GBFS and fly ash in CEM V developed a concrete matrix with similar properties.

CEM I is significantly different to those from the rest of cement types. The KST analysis showed of these analyses is several orders of magnitude lower than those found when comparing CEM III and CEM V.

In summary, Portland cement specimens had the lowest values of resistivity regardless of age or cover depth. CEM II had low values at 2.5 years, but close to those of CEM III and CEM V after 12 years. Also, CEM II has a more pronounced dependency on the cover depth compared to CEM I. Concrete specimens made from CEM III and CEM V had similar results. However, as age increased so did the values of resistivity until reaching 5 times higher after 12 years.

4 CONCLUSION

The identification of cement type by statistical analysis on concrete specimens led to:

- NFD analysis showed that after 2.5 years cement type had the strongest influence on concrete resistivity.
- KST identified cement type in 17 of 20 cases with 95% of confidence.
- KST showed that even when the specimens were identified some concrete compositions, containing CEM III and CEM V, could not be distinguished with the same accuracy.
- After 12 years, KST showed that concrete containing supplementary cementitious materials like Fly Ash or GBFS developed a denser pore structure.

Concrete Repair, Rehabilitation and Retrofitting III – Alexander et al. (eds)
 ISBN 978-0-415-89952-9

Measurement and visualisation of the actual concrete resistivity in consideration of conductive layers and reinforcement bars

K. Reichling & M. Raupach
Institute of Building Materials Research, RWTH Aachen University, Aachen, Germany

ABSTRACT: The resistivity of concrete is a major factor regarding the durability of reinforced concrete structures. In combination with a suitable calibration the values may be correlated e.g. to the permeability, the water content of the concrete and the corrosion rate of the reinforcement. However, typical measurement techniques based on four electrodes allow a determination of an apparent resistivity which usually differs from the actual resistivity of the concrete. The major influencing effects are given by surface near layers with a different resistivity compared to the bulk concrete (e.g. due to carbonation or wetting) as well as steel reinforcement. For the evaluation of the actual concrete resistivity the applicability of the Electrical Resistivity Tomography (ERT) has been discussed. By means of this method the resistivity distribution of the concrete section could be determined and illustrated graphically which allows an identification of layers and components with different resistivities.

1 INTRODUCTION

The electrical resistivity is a valuable parameter to assess the durability of concrete structures. However, the commonly used measurement techniques are sensitive to material heterogeneities, e.g. reinforcement bars or resistivity gradients (layers). The four-electrode setup, as it is typically used on reinforced concrete structures, delivers one apparent resistivity value without any evaluation of an influence from heterogeneities in the structure. As a result misinterpretations are not unusual and difficult to detect.

In the present paper two typical cases are discussed; concrete with a water saturated surface layer and the presence of a reinforcement bar in homogeneous concrete. For these cases a method based on the Electrical Resistivity Tomography is presented for the determination of the concrete resistivity.

2 ELECTRICAL RESISTIVITY TOMOGRAPHY

The Electrical Resistivity Tomography (ERT) is typically used in geophysics. By means of electrical measurements from the surface of a structure, the composition of the subsurface can be examined. The main difference to the methods typically used in civil engineering is, that for ERT several measurements are carried out with different electrode positions and distances.

The electrode setup may vary depending on the field of application. Basically one reading is based on a four electrodes setup. Apart from the setup the electrode distances control the depth of measurement. By increasing the electrode spacings the readings are influenced by deeper areas. Surface near areas show typically the highest sensitivities.

The applicability of two-dimensional ERT for reinforced concrete structures has theoretically been studied by considering an array of 20 equally spaced electrodes. An apparent resistivity pseudosection can be determined by combining all data points into a contour plot.

3 CALCULATION OF THE RESISTIVITY DISTRIBUTION

The interpretation of a pseudosection is linked with considerable uncertainties. The evaluation of the resistivity distribution is more reliable after the application of an inversion routine. In the following section the apparent resistivity pseudosections mentioned above are handled as measurement readings. A distinction must be made between the apparent resistivity (measured) pseudosection and a calculated pseudosection. The latter is determined based on a first assumption of the resistivity distribution and is compared with the measured pseudosection by application of the method of non-linear least-squares. This procedure is iteratively repeated until the relative change between two iteration steps is lower than a threshold value, which was set in the present cases to 5%.

The calculated resistivity distribution for the case of a conductive layer on top of concrete with a higher resistivity is shown in figure 1. In figure 2

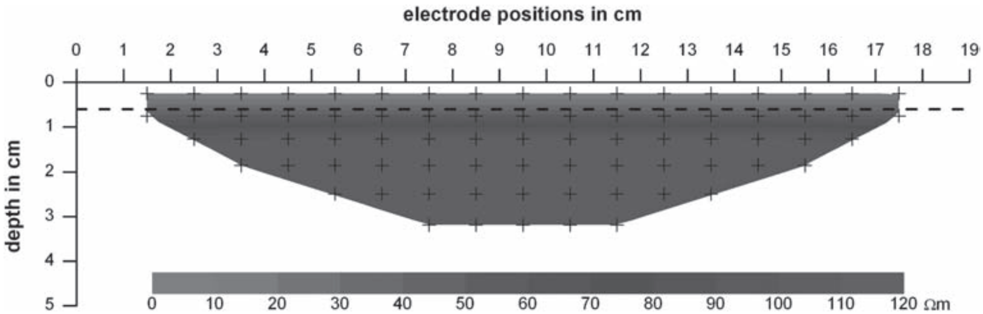

Figure 1. Measured and calculated pseudosection and resistivity plot for concrete with a surface layer (case 1, figure 8).

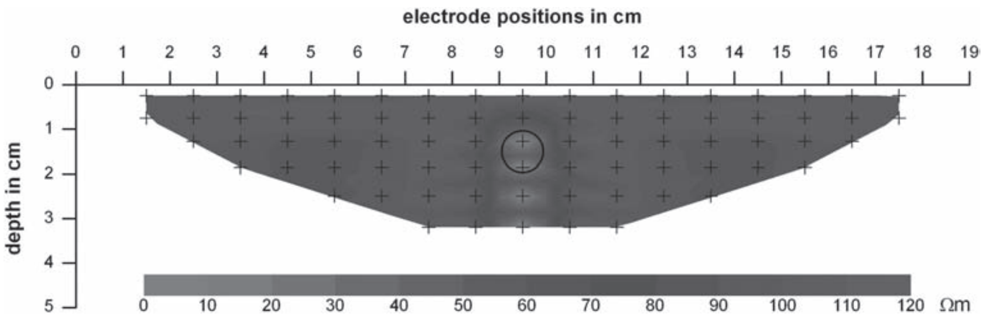

Figure 2. Measured and calculated pseudosection and resistivity plot for concrete with reinforcement bar (case 2, figure 8).

the resistivity distribution for the case of a reinforcement bar is shown. The surface layer and the reinforcement could clearly be detected. The concrete cover correlates well with the underlying geometry. Underneath the rebar further areas with low resistivities were determined. This is the effect of a poor sensitivity of the data points in this area.

It can be shown that ERT is a promising tool for resistivity evaluations in civil engineering. To counteract the inaccuracies the method will be the objective of further studies for adaptation to the needs of civil engineers.

4 CONCLUSIONS AND OUTLOOK

From the results described in the paper the following conclusions can be drawn:

- layers with different resistivities and steel reinforcement bars can deform the shape of the electrical field and thus the potential distribution at the concrete surface.
- in the case of homogeneous and large scaled specimens the current spreads out semi spherically.
- in thin conductive layers a cylindrical approach for the potential distribution is appropriate. The commonly used cell constant provided by Wenner is not suitable to determine the layer resistivity accurately.
- surface near layers and components with different resistivities could be identified by using the ERT (Electrical Resistivity Tomography).
- by means of the ERT a resistivity section can be determined and illustrated graphically which allows innovative approaches for the assessment of reinforced concrete structures.
- the inaccuracies shall be minimised in further studies.
- spectral induced polarisation measurements will be the objective of further studies to determine the concrete resistivity.

Concrete Repair, Rehabilitation and Retrofitting III – Alexander et al. (eds)

Practical operation of data-logging covermeters and the interpretation of results

J.F. Fletcher & C.I. Woolhouse
Elcometer Limited, Manchester, UK

ABSTRACT: Covermeters are widely used for the non-destructive testing of concrete structures to determine if reinforcement bars are adequately covered with concrete and to determine the location of safe spots for drilling, for strengthening, for repair work and for refurbishing the structure.

The use of Covermeters and the requirements of their accuracy for use are described in BS 1881 Part 204. Reinforcement bars can be detected using a pulsed electromagnetic field generated by a coil. Secondary search coils detect the resulting eddy currents induced in the bars and the location, orientation, depth (concrete cover) and diameter of the bars can be determined from this return signal.

Developments in Covermeter design has resulted in the addition of data-logging features as a key aspect of portable Covermeters with software that provides support for the analysis and presentation of data sets generated as a result of surveys carried out on site.

Covermeters now make use of intelligent sensor technology to allow a range of interchangeable sensors to be used with a single Covermeter, including borehole sensors for finding pre-stressing or post-tensioning tendons deep within the reinforcement structure, sensors for the detection and measurement of stainless steel reinforcement and Half-Cell for the assessment of corrosion conditions.

Consisting of either a copper electrode in a copper sulphate solution (Cu/CuSO4) or a silver electrode in a silver chloride solution (Ag/AgCl), each Half-Cell is a sealed unit making site surveys easy to perform.

This paper describes the use and capabilities of such a combined Covermeter and Half-Cell unit. Field data from a survey carried out in the UK will be presented to show the analytical capability of the system. The interpretation and presentation of the data will be discussed.

Keywords: concrete, corrosion, covermeter, data-logging, reinforcement, rebar, drilling.

1 INTRODUCTION

A Covermeter is a basic tool for the non-destructive testing of both old and new concrete structures. The location, orientation and sizing of reinforcement bars and the determination of the depth of concrete cover provide essential information about the structure for acceptance, for maintenance and for planning modifications to structures.

The use of Covermeters and the requirements of their accuracy for use are described in BS 1881 Part 204. Reinforcement bars can be detected using a pulsed electromagnetic field generated by a coil. Secondary search coils detect the resulting eddy currents induced in the bars and the location, orientation, depth (cover) and diameter of the bars can be determined from this return signal.

Recent developments in the design of Covermeters have added new features including the ability to log data in memory and to then analyse this information by means of a software package. In addition Half-Cell measurements to determine the potential for corrosion in the reinforcement bar can be undertaken using the same software package. This allows both the cover and the Half-Cell potential to be assessed simultaneously.

This paper describes the use and capabilities of a Covermeter with Half-Cell capability and discusses the analysis, interpretation and presentation of the data using field data collected on a site in the UK.

2 THE COVERMETER INSTRUMENT

The detection and measurement methodology of the Covermeter described by John Alldred is the basis of the current Covermeter design. This design has features for linear and grid data logging and is compatible with data management software. This Covermeter is also capable of operating with a Half-Cell sensor to assess the potential for active corrosion at the points where the concrete cover has been determined.

3 COVERMETER OPERATION

3.1 *Locating and orientating reinforcement bars*

Covermeters can locate either a single layer of reinforcement bar or two layers at right angles to each other. When the search head approaches a single bar the gauge emits a sound, which increases in pitch as the search head gets nearer to the bar.

4 HALF-CELL POTENTIAL MEASUREMENTS

The Half-Cell potential can be determined using an electrode to form one half of the cell and the reinforcing steel to form the other half.

The measurement is accomplished using a high input-impedance voltmeter and one of two reference electrodes, copper/copper sulphate or silver/silver chloride.

The measurement characterizes the electrochemical behaviour of the structure.

5 DATA LOGGING

5.1 *Statistics*

The Covermeter displays the results of a number of statistical calculations such as the mean, the standard deviation, the coefficient of variation, the lowest and the highest reading and also records the number of readings in the group.

5.2 *Batching*

There are two batching modes in the Covermeter. The Linear batch is used when the readings are taken in a single row or column and the Grid batch is used when an array of rows and columns is recorded.

6 DATA ANALYSIS

6.1 *Transferring data to a computer*

Data stored in batches can be transferred to a computer using the utility within the CoverMaster® software. The software can analyse and chart the results and prepare reports in electronic format or as printed documents.

6.2 *Charts*

The software provides methods for viewing the data including topographic views. These are ideal for determining the potential for corrosion in an area from both cover values and Half-Cell potentials.

7 CASE STUDY

The Covermeter and Half-Cell unit was used for a survey carried out by Mott MacDonald's on a concrete road bridge in the North West of the UK.

8 LIMITATION OF USE

The interpretation of the signal strength display and the sound emitted by the Covermeter in the location and orientation mode does require some operator skill.

When using the search head over welded mesh or joined bars, the centre bar of a double or figure of eight loop will create a very strong return signal and these locations must not be used for cover measurement.

When using the Half-Cell survey it is important to note that the values of potential between the steel bars and the cell probe are only indicative of the likelihood of corrosion occurring.

9 CONCLUSIONS

The use of a Covermeter can provide a lot of useful information for both new & older structures. Confirmation that the reinforcement bars have been correctly positioned and are covered by the appropriate depth of concrete provides confidence on the service life of a new structure.

For older structures, the issue could be the safety of the structure, maintenance strategies or even preparation for a change of use.

The combination of the Covermeter function with the Half-Cell operation allows surveys of older buildings and structures to be carried out so that areas with corrosion problems can be located and monitored.

Concrete Repair, Rehabilitation and Retrofitting III – Alexander et al. (eds)
© 2012 Taylor & Francis Group, London, ISBN 978-0-415-89952-9

Modern damage detection by using static assessment methods for efficient rehabilitation

F. Scherbaum, J. Mahowald, D. Waldmann & S. Maas
Faculté des Sciences, de la Technologie et de la Communication, Université du Luxembourg, Luxembourg

A. Zürbes
Fachbereich Technik, Informatik und Wirtschaft, Fachhochschule Bingen, Bingen, Germany

ABSTRACT: The existing bridges become increasingly older, which leads to the fact that bridge inspections will be even more important, in the future. The assessment of the remaining useful life of bridges and the damage detection, apart from the continuous supervision of a structure investigation and the assessment methods, as well, become more relevant. Normally, the above mentioned methods are costly and time consuming.

Therefore, the University of Luxembourg carries out a project to investigate an efficient application of different assessment methods, taking into account praxis relevant test conditions. Within the context of non-destructive testing methods are static assessment methods analyzed and explained by the example of a two span box girder bridge. The presented bridge is a 102 m long prestressed concrete bridge, which was demolished after the performed tests due to a changed urban planning. Thereby the practicability of damage detections, by using static load tests, can be investigated. Within these test series the structure was damaged step by step, by artificial damage: with each damage scenario a part of the prestressed tendons were cut, which finally lead to a local cracking. By the analysis of the load-deformation-behavior, damages can be detected and located. A statement about the level of the damage can also be made.

1 INTRODUCTION

The existing bridges become increasingly older, which leads to the fact that bridge inspections will be more and more important in the future. But normally these inspections are time consuming and cost intensive. That is the reason why the University of Luxembourg investigates non-destructive testing methods. As a part of this project the damage detection, by using an in-situ load test, was investigated at a real bridge in Luxembourg (Scherbaum & Mahowald 2011b). By measuring the vertical deflection the possibility of a clear demage detection is investigated.

2 BRIDGE DESCRIPTION

The investigated bridge is a two span prestressed concrete bridge with different span lengths (Figure 1 and Figure 2). The superstructure of the bridge is a prestressed box girder with 32 parabolic, 24 upper straight lined and 20 lower straight lined subsequently injected tendons. In 1987, 56 external prestressed steel cables were added into the box girder of the large field.

3 EXECUTED TEST PROGRAMME

To simulate an increasing damage of the bridge the superstructure was damaged stepwise by four damage scenarios. Table 1 describes these damage scenarios. In each scenario the bridge was loaded and unloaded by using 38 steel beams, which illustrate an experimental load of 245 t (Figure 3 & Figure 4). Throughout the tests, the vertical deflection was measured by displacement transducers in section B and in section C (Figure 5) at the surface of the bottom plate from the box girder. Additionally to this, the vertical deflection was measured in 6 sections (section A to F) along the bridge on the top of the superstructure (Figure 5) by a digital leveling.

Figure 1. Side view of the bridge.

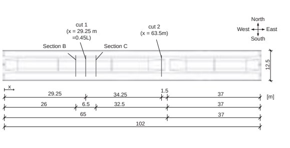

Figure 2. Longitudinal section of the bridge.

Table 1. Description of the damage scenarios according to the cutting sections.

Damage scenario	Damage
# 0	Undamaged State
# 1	Cutting straight lined tendons in the lower part of the bridge at 0.45 L (20 tendons)
# 2	Cutting 8 straight lined tendons in the upper part of the bridge over the pylon
# 3	Cutting external tendons (56 wires)
# 4	Cutting 16 straight lined tendons in the upper part of the bridge and also 8 parabolic tendons

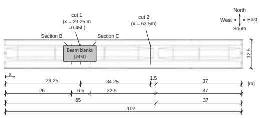

Figure 3. Position of the experimental load.

Figure 4. Experimental load.

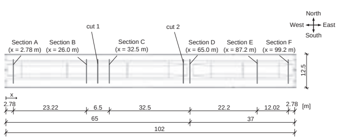

Figure 5. Position of the measurement sections.

3.1 *Vertical deflection of the superstructure*

Figure 6 presents the vertical deflection measured by displacement transducers in section B and section C. The two lines in the upper part of the figure represent the vertical deflection. In the lower part of the figure temperature variations are illustrated.

It can be seen, that each loading and unloading step, in each damage scenario can be recognized by measuring the vertical deflection. Moreover, it can be observed that the vertical deflection increases with a strong damage (damages scenario #1 and #3). In these two scenarios also a crack formation in the bottom plate and in the sidewalls was observed. However, a small damage, like damage scenario #2 does not really lead to an increase of the vertical deflection under load. In this damage scenario 8 tendons were cut, which did not lead to a new crack formation.

In Figure 6 it can also be identified, that the changing of the temperature leads to the deformation of the superstructure. In relation to the damage detection, it can be seen, that temperature changes can leads to a larger vertical deflection than damage scenario #2.

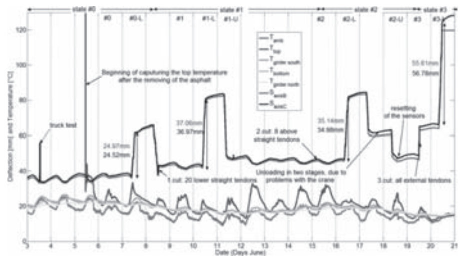

Figure 6. Vertical deflection in section B and C and temperature changes during the test period.

3.2 *Comparison of displacement transducer and digital leveling*

The comparison of the digital leveling and the displacement transducer reveals that both systems illustrate nearly the same global behavior. In the loaded damage scenario #3, a maximum deviation of 1.8 mm was measured between the digital leveling and the displacement transducer.

4 CONCLUSION

The static load test shows, that a damage which leads to a crack could be detected by measuring the vertical deflection. In damage scenario #1 and #3 the vertical deflection increases in relation to the undamaged state respectively to the previous damage scenario #2. But it is important to know, that the influence of the temperature changing could even be higher than from a small damage. So this influence has to be considered in the analysis of the static load test. To be aware of the influences due to temperature, the deflection behavior of an undamaged structure should be analyzed for varying temperatures.

It is also important to take into account the measuring accuracy of the different measuring systems.

REFERENCES

Bungard, V., Walterin, M., Waldmann, D., Maas, S. & Zuerbes, A. (2009). Comparison of static behaviour and nonlinear vibration characteristics of gradually damaged prestressed concrete slabs and reinforced concrete beams. Proceeding of the EVACES 09 conference. Wroclaw. Poland.

Bungard, V. (2010). Condition assessment of concrete structures and bridges using vibration monitoring in comparison to changes in their static properties. PhD-Thesis at the University of Luxembourg.

Gutermann, M. (2002). Ein Beitrag zur experimentell gestützten Tragsicherheitsbewertung von Massivbrücken. Dissertation. Technische Universität Dresden. Deutschland.

Mahowald, J. (2010). Report VII, University of Luxembourg.

Scherbaum, F. & Mahowald, J. (2011b). Report Bridge Champangshiehl 2, University of Luxembourg.

Concrete Repair, Rehabilitation and Retrofitting III – Alexander et al. (eds)
© 2012 Taylor & Francis Group, London, ISBN 978-0-415-89952-9

Strengthening of reinforced concrete slabs built around the year 1910

S. Gmainer & J. Kollegger
Institute for Structural Engineering, Vienna University of Technology, Austria

ABSTRACT: In the city center of Vienna there are still a large number of reinforced concrete structures in use which were built with ribbed reinforced concrete slabs during the first decades of the twentieth century. While the load carrying capacity of these slabs in bending is in accordance with contemporary structural standards, the shear carrying capacity does not always reach the level required today. The paper reports on experimental load carrying tests on 100 year old reinforced concrete slabs. Moreover, the practicability and performance of reinforcing measures were checked. It can be shown that the shear carrying capacity of these slab systems is smaller than the load carrying capacity in bending. A method for the strengthening of these slabs is presented. Destructive load tests on strengthened slabs have demonstrated the practicability of the proposed strengthening method.

1 INTRODUCTION

1.1 *Historical slab system Rella*

The Rella slab system is a slab with concrete ribs that was formed by hollow bodies shaped by the patented and quickly stiffening Bruyn-substance. This mass consisted in essence of lime, gypsum and burnt-out coal slag. Preferably, the hollow bodies had dimensions of 50 times 50 cm and 26 cm height, could be produced on site and put on the scaffolding. Thus it was possible to build various dimensions (Pauser 1994).

In this slab system the reinforcement is placed side by side. At the support part of the reinforcement was bend-up and anchored at the upper side of the slab. No further stirrup reinforcement was placed. The advantage of this system was the profitable lost formwork.

2 LOAD CARRYING TESTS ON EXISTING SLABS

As the building was rebuilt into a hotel and dwelling house, the existence had to be analysed concerning the load capacity based upon presently valid standards. It can be stated that the slab system Rella which was used in this building was produced without any shear reinforcement and so it didn't correspond with any actual standards. Therefore the 100 year old rib slabs were tested on their load capacity, especially on their shear force capacity as there are no stirrups. After removing the concrete ribs the bending reinforcement with the anchoring at the support can be seen. For the bending reinforcement two smooth bars with a diameter of 22 mm were placed. At the support the bending up of one bar is shown (see Figure 1).

Therefore it has to be investigated if the ribbed reinforced concrete slabs are failing due to yielding of the longitudinal bars, or if the support area has failed shortly before that. In contrast to a failure due to bending, an unannounced fracture of the slab would occur in case of a failure of the anchorage. This should be avoides.

The slab system Rella is spanned over 6.25 m. The thickness of the plate is 6 cm and the ribs are approximately 6.5 cm wide and 25 cm high. The supporting of the slab took place on massive outside and intermediate walls made of clay brick masonry. The average concrete strength of the concrete ribs was determined by cylindrical cores and amounts to 45 N/mm^2.

2.1 *Tests with the unreinforced slab system Rella*

Two ribbed concrete slab strips of the second floor of the building were chosen for the testing. The unreinforced test specimens A and B were supposed to show the amount of bearing load of the existing slab. For the preparation of the experiments the assembly and the bottom side of the slabs were removed.

The loading was managed by two hydraulic jacks, thus the tests were carried out displacement-controlled. The hydraulic jacks were placed in the outer quarter points of the slab strip with the aim of simulating a distributed load. The hydraulic jacks were anchored with threaded bars on both lower placed slabs to transfer the load of the Rella slab. Supports were installed in such a way that the

Figure 1. Bend-up reinforcing bars in the supporting area.

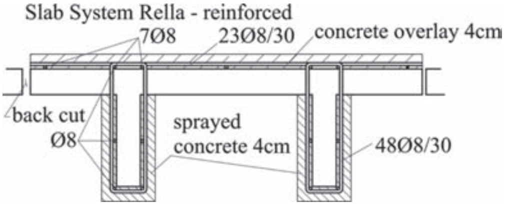

Figure 2. Cross section of the slab system with reinforced ribs.

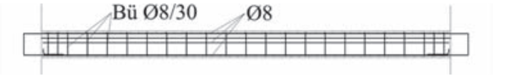

Figure 3. Longitudinal section of the slab system with reinforced ribs.

weight of the upper slab has an effect on the force of the hydraulic jack. As a consequence, the weight of both slabs could operate as an abutment. Swimming pools were established to increase the weight of the slabs.

The test was carried out in load steps of a maximum of 10 kN per jack. The failure load occurred at F = 68.6 kN (specimen A) and 76.5 kN (specimen B). The failure could be observed without any strengthening due to extracting the bending tensile bars at the support.

2.2 *Tests with the reinforced slab system Rella*

Beside the old slabs reinforced rib slabs were tested as well. In these tests the efficiency of the load capacity due to a strengthening was to be checked.

For the reinforced test specimens C and D a strengthening with additional reinforcement (stirrups with a diameter of 8 mm) and a concrete overlay was suggested, in order to create a good compound structure between compression and tension area. The static lever arm between compression and tension area is also increased by the concrete overlay. Moreover, the concrete overlay is useful for the derivation of horizontal forces.

The stirrups were put in drilled holes and fixed to the upper reinforcement as shown in Figure 2 and 3. To guarantee fire protection a 4 cm thick sprayed concrete layer was placed on the ribs.

The placement of the reinforced concrete slabs with ribs should be done in an equal manner as for the unreinforced slabs.

The failure load occurred at F = 127.2 kN (specimen C) and 129.7 kN (specimen D). The failure took place due to yielding of the longitudinal reinforcement in the middle of the slab.

3 CONCLUSION

In case of the discussed and investigated strengthening methods, the load capacity of the ribbed concrete slabs can be increased to the required level by additional reinforcement and stirrups. The sprayed concrete layer and the concrete overlay with a thickness of 4 cm ensure a sufficient concrete covering which is necessary for the durability of the fire restistance, the effect of the compound structure and the protection of corrosion.

The work for the strengthening of the slabs could be carried out without any troubles. The test specimens failed in a very ductile manner.

Comparative calculations have shown that the strengthening of the slabs is more economical than a replacement of the slabs. Furthermore, a shorter construction time could be achieved.

It can be said that tests on old slab systems are very important to research and above all, the preservation of such architecturally and historically prized buildings is worthwile.

Concrete Repair, Rehabilitation and Retrofitting III – Alexander et al. (eds)
 ISBN 978-0-415-89952-9

Analysis of the strain transfer mechanism between a truly distributed optical fiber sensor and the surrounding medium

J.M. Henault, J. Salin & G. Moreau
EDF R&D, Chatou, France

M. Quiertant, F. Taillade & K. Benzarti
Université Paris-Est, IFSTTAR, Paris, France

S. Delepine-Lesoille
ANDRA, Chatenay-Malabry, France

ABSTRACT: Distributed Optical Fiber Sensors (DOFS) are a key tool for monitoring the health of large infrastructures. An optoelectronic device, paired with an optical fiber in a cable, provides strain profiles over several kilometers with few micro-strains accuracy. However, due to shear deformation of the cable's protective coating, strain measurements provided by DOFS may differ from actual strains in the embedding medium. A methodology was developed to determine the relationship between measured/actual strains, called Mechanical Transfer Function (MTF) of the cable. In a first step, tension and pull-out tests were carried out to assess the mechanical properties of the cable components (optical fiber, coating layers) and the interface laws. These parameters were then introduced into a finite element model to determine the cable's MTF and its domain of validity. Finally, an inverse analysis based on this MTF made it possible to evaluate the strain profile within the host structure from the DOFS measurements, and to quantify the crack openings as well.

Structural health monitoring (SHM) is a key procedure in infrastructure lifecycle management, since it enables a real-time diagnosis of the state of wear/damage of a structure. As a complement to conventional sensors, fiber optic sensing systems are an attractive tool for SHM. Distributed Optical Fiber Sensors (DOFS) measuring chain consists of an optoelectronic unit paired with one or more optical fibers wrapped in a sensing cable. It enables to record temperature or strain profiles along kilometres of fibers embedded into a host structure.

Different interrogation units are available, whose operating principles are based on the analysis of the backscattered light in silica. The collected signal corresponds to the continuous record of scattering phenomena along the fiber. Rayleigh and Brillouin scatterings are both strain and temperature sensitive. Brillouin interrogators offer typically a spatial resolution of 1 m with a distance range of several tens of kilometers and a strain sensitivity of 20 μm/m. Rayleigh interrogators offer a high spatial resolution of 1 cm, with a distance range in the order of 100 m and a strain sensitivity of 1 μm/m.

Optical fiber sensors usually consist of one or several fibers wrapped by a protective coating, and forming cables with outer diameters of few mm. The aim of the coating is to protect the optical fiber against mechanical/chemical aggressions. For a sensing purpose, the coating must also be designed to ensure an optimal transfer of temperature and strain from the host material (concrete matrix, soil, composite laminates…) to the optical fiber. However, due to shear deformation of the cable's coating, strain measured in the optical fiber may differ from that in the host structure. It is thus necessary to model the stress transfer mechanism through the protective coating so that the strain field in the host material can be derived from experimental data provided by the core optical fiber.

For this reason, a generic methodology was developed to determine the relationship between strain fields in the optical fiber and in the host material, *i.e.* the mechanical transfer function (MTF) of the cable in the host structure. Such a methodology is independent of the types of cable and host material, and involves both mechanical testing and modelling. On the other hand, obtained results (MTF and its domain of validity) are dependent on both the type of cable, the installation technique (cable embedded or surface mounted) and the nature of the host material.

This paper illustrates the methodology for one particular couple of cable and host material. The sensing cable, shown in Figure 1, is a commercial multi-fiber cable with a diameter of 2 mm.

In a first part of the proposed methodology, tension and pull-out tests were carried out to characterize mechanical properties of the different components of the sensing cable (optical fibers, coating layers and interface laws), and subsequently, to determine domains of linear elasticity and perfect-bonding. n a second part, such experimental results were used to fit the parameters of a Finite Element (FE) modelling based on a cable embedded in the host material.

Then, simulations made it possible to assess the strain level in the optical fiber while imposing a mechanical loading to the host material, thus leading to the determination of the cable's MTF (Figure 2).

The strain profile in the optical fiber is measured with an optoelectronic interrogator which has a given spatial resolution. Equation 1 expresses the relationship between the strain profile measured by the interrogator ($\varepsilon_{measured}$) and the strain profile in the host material (ε_{HM}), considering the cable's MTF and the spatial resolution of the device ($\Pi_{interrogator}$), which can be represented by a rectangular function. The width value of the rectangular function corresponds to the spatial resolution of the interrogator.

$$\varepsilon_{measured}(s) = \varepsilon_{HM}(s) \otimes MTF_{cable}(s) \otimes \Pi_{interrogator}(s) \quad (1)$$

Figure 1. Picture of the multi-fiber cable.

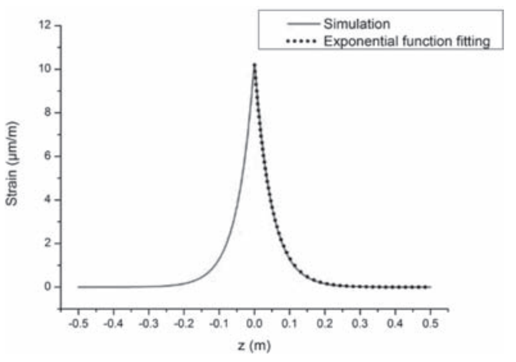

Figure 2. Modelled strain profile within the optical fiber = cable's MTF.

If the MTF has a FWMH of about 10 cm and the interrogator has a spatial resolution of 1 cm, the MTF will have a major influence on the determination of the strain profile in the host material.

In the final part of the paper, the sensing cable was inserted longitudinally into a 3.4 m-long reinforced-concrete beam submitted to a four-point bending test. Further details of this experimentation are available elsewhere. Strain profiles were measured using a Rayleigh interrogator with a centimeter spatial resolution. As an illustration, the strain profile recorded along the sensing cable located in the tensile side of the beam is depicted in Figure 3.

In these conditions, it can be assumed that the strain profile in the host medium is a summation of the elastic strain of concrete (trapezoid shape predicted by the Strength of Material Modelling theory) and Dirac distributions related to cracks. A proper use of Equation 1 and the knowledge of the cable's MTF made it possible to derive the strain profile in the host concrete from the experimental data provided by the sensing cable (Figure 4).

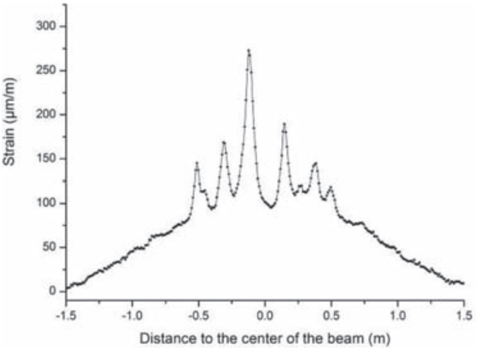

Figure 3. Strain profile as measured by the sensing system in the tension zone of the beam subjected to 4-point bending (70 kN applied load).

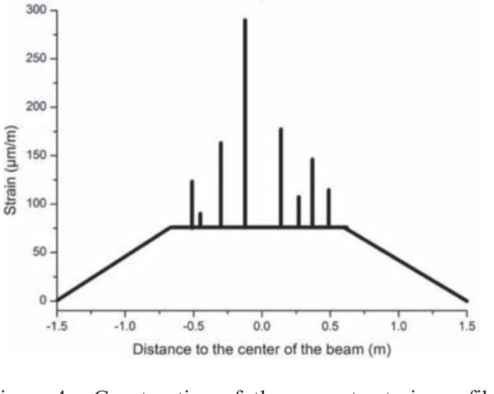

Figure 4. Construction of the concrete strain profile based on a deconvolution of measured strain profile by the cable's MTF.

Concrete Repair, Rehabilitation and Retrofitting III – Alexander et al. (eds)
 ISBN 978-0-415-89952-9

Investigation of the crack opening and damage monitoring of textile reinforced cementitious composites using Digital Image Correlation

E. Tsangouri & D. Van Hemelrijck
Vrije Universiteit Brussel, Department of Mechanics of Materials and Constructions, Brussels, Belgium

ABSTRACT: The stress-strain behaviour of glass textile reinforced cementitious composites in tension is highly non- linear. Focusing at the multiple cracking stage, cracks are initiate and propagate across the cementitious matrix. The opening of these cracks is influenced by the volume fraction of reinforcement, the strength of the matrix, the geometry of the specimen, the debonding phenomena at the matrix- fibre interface and several other parameters. Investigation of the strain profile and the crack width, on this phase of tensile loading, is done in two different composites: E- glass textile reinforced inorganic phosphate cements and AR- glass textile reinforced fine- grained cements. In both cases, Digital Image Correlation (DIC) is used to visualize the crack pattern and the strain distribution. This initial research for a system with low crack width (lower than 100 μm) under tension would be used for the future application of self- healing mechanism on cementitious composites.

1 INTRODUCTION

1.1 *Investigating limited crack width*

Studies have shown that self healing (SH) in concrete is managed only in regions of damage with tight crack width, likely less than 100–150 μm, which is very difficult to achieve in a consistent manner for concrete in the field. In our work, the feasibility of yet another solution to the problem is investigated namely the use of glass fibre reinforced cementitious composite skins as self healing systems which are able to limit the crack width to less than 50 μm (ideal for the healing efficiency). This paper is focusing at the estimation and visualization of the crack pattern at the most critical stage under tensile loading of fibre textile reinforced cementitious composites (TRC), results from two different TRC systems will be compared and the most appropriate would be chosen for further application of SH mechanisms.

2 TENSILE THEORY, MATERIAL AND TEST SET-UP

2.1 *Cracking phenomena during tensile testing*

First cracking phenomena under tensile loading appear when the tensile strength is reached (linear relationship between stress and strain till that point). As tensile load is increasing, additional cracks occur (multiple cracking phase). The number of initial cracks and the cracking distance at this stage depend on the fiber volume fraction and the bond characteristics between reinforcement and matrix and affect the nonlinearity of the stress-strain curve. In the state of stabilized crack pattern further crack occurs. The post initial cracking stage is characterized by opening of distributed cracks.

Characterization of the crack pattern created during multiple cracking of the matrix is the information required to apply SH mechanisms on cementitious composites efficiently.

2.2 *Advanced optical technique as a tool to visualize crack patterns on two different TRC series*

The ability to “see” and become aware of the crack opening and propagation of the two skin reinforcing systems is critical in our effort to choose the optimized self-healed TRC. On this direction, the crack propagation is investigated by the use of Digital Image Correlation (DIC), an advanced and well established optical Non Destructive Technique (NDT). Literature review of the geometry, the test set-up, the loading case and the material shows that Inorganic Phosphate Cement (IPC) and fine grained concrete (FGC) elements reinforced by fiber textile and tested under tension give a first and representative view of the cracking phenomenon appeared on TRC composites. Both cementitious matrices, combined with glass fibre reinforcement, produce strong, durable and thin

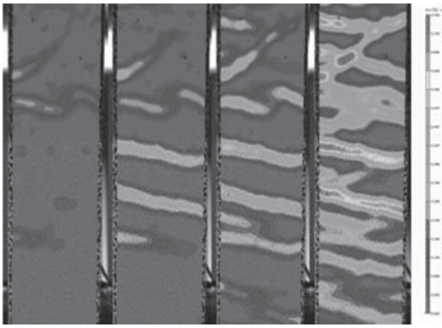

Figure 1. Crack formation at several stages of loading from the beginning till the end of multi-cracking stage.

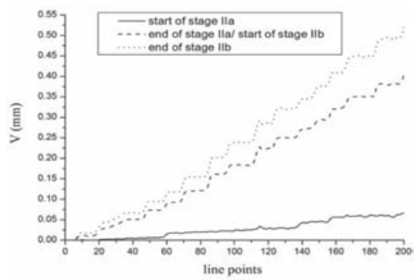

Figure 2. Crack opening displacement as measured during ACK stage II of FGC specimen under tension.

composite laminates with relatively small tensile crack width (50–100 μm).

3 RESULTS

As it is shown in the DIC strain profiles of Fig.1, several cracks appear at different load levels, propagate, open and create a strain concentration area around them.

The crack opening at the beginning and at the end of multiple cracking stage is the most important information derived from DIC analysis. Utilizing the deformation at the direction of loading measured by DIC at several points across the specimen, the graphs (Fig. 2, 3) of cumulative crack opening is used to compare the crack width of IPC and FGC series.

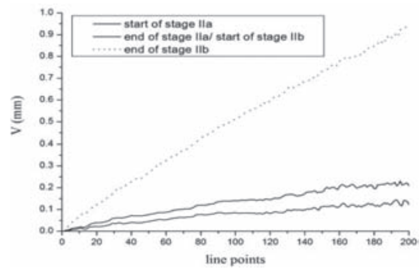

Figure 3. Crack opening displacement as measured during ACK stage II of IPC specimen under tension.

4 CONCLUSION

Summarizing the results from DIC analysis combined with the experimental stress-strain curves and literature review, final conclusions are obtained:

1. Both series of specimens develop crack openings small enough to make them ideal for self healing applications.
2. Apart from the main parameters and set-up that has to be fixed carefully, attention should be paid at the gripping conditions. Flatness at the area of the hydraulic grips is required to avoid stress concentrations and localized grip pressure caused by uneven thickness of the specimen.
3. Crack width and opening during tensile testing is successfully calculated by applying DIC method. FGC crack pattern seems ideal in the case of designing a SH system with limited crack width. Results from this primary analysis should be used as a basis for future investigation of cracking phenomena.

ACKNOWLEDGEMENTS

The authors wish to acknowledge the IWT for financial support under the SIM- Engineered Self-Healing Materials project.

Concrete Repair, Rehabilitation and Retrofitting III – Alexander et al. (eds)
© 2012 Taylor & Francis Group, London, ISBN 978-0-415-89952-9

A non-destructive test method for the performance of hydrophobic treatments

U. Antons, J. Orlowsky & M. Raupach
Institute of Building Materials Research (IBAC), RWTH Aachen University, Germany

ABSTRACT: The efficiency and durability of hydrophobic treatments on concrete surfaces depend amongst others mainly on their penetration behaviour. Up to now the penetration depth of hydrophobic treatments applied on buildings can only be determined on drilled cores. The portable NMR-MOUSE® based on unilateral nuclear magnetic resonance spectroscopy now has been evaluated as tool for non-destructive performance tests. In this paper it's shown that the time depending penetration and distribution of hydrophobic agents in concrete as well as the tracking of the degradation processes can be visualized with this measuring method. Consequently the results confirm different penetration depths of silanes with different length of the alkyls. In addition the temperature stability of the hydrophobic layer after 200°C exposure and the final destruction after 350°C exposure is presented.

1 INTRODUCTION

Hydrophobic treatments are not visible, which is a considerable advantage concerning the preservation of the ordinary building appearance. However disadvantages of hydrophobic treatments are uncertainties concerning the durability of the treated surfaces. These uncertainties are based on the lack of investigation methods to control the efficiency of hydrophobic treatments applied on buildings and insufficient knowledge about the degradation mechanisms of silane treated concrete surfaces. Up to now the penetration depth of hydrophobic agents as well as the residual efficiency can only be measured by using destructive testing methods, i.e. taking drill cores. Within the research project "Durability of hydrophobic treatments on concrete" founded by the German Research Foundation tests with the so called "NMR MOUSE®" (Nuclear Magnetic Resonance Mobile Universal Surface Explorer, registered trademark of RWTH Aachen University) PM 25 based on the unilateral nuclear magnetic resonance spectroscopy have been taken out at ibac RWTH Aachen University. One result of this extensive research is the possibility of a quasi online monitoring of the penetration and distribution of hydrophobic agents in concrete immediately after the material application. These results will be discussed in this paper. Furthermore it will be shown how the degradation of the hydrophobic treatment on concrete surfaces can be monitored with the NMR MOUSE.

2 HYDROPHOBIC AGENTS AND SPECIMENS

In this research project 8 different hydrophobic treatments were used. Their active agents are displayed in table 1. In order to achieve a good comparability between the test results the amount of the active agent per square meter was kept constant. Due to the different degrees of purity the applied mass vary between 130 to 320 g/m^2.

Except for hydrophobic treatments 1 and 2, which are based on 3, none of the investigated products were thinned. For 1 and 2 an aliphatic thinner was used to lower the ratio of the active agent to 40 and 80%. Unlike the dispersions 1 to 6 the hydrophobic treatment 7 was applied on the specimens as crème.

Specimens out of two different types of cements were produced for the investigations. Both concretes had the same water cement ratio (0.6) and the same amount of aggregates.

Besides the possibility of testing on construction sites non-destructive testing also has advantages in laboratory investigations. In this case non-destructive testing with NMR MOUSE allows the examination on the same specimen position at different times. Every specimen had been measured four times already before an accelerated ageing began. This allows determining the explicit changings of each specimen. As a result the influences of inhomogeneities of the concrete can be minimized.

The first measurement took place at the end of the 28 days storage under water. It gave a valuable

Table 1. Active agents.

Hydrophobic agent No.	Active agent
1, 2, 3	Iso-Butyltrimethoxysilane
4	Octyl trimethoxysilane
5	N-Isobutyltriethoxysilane
6	Iso-Octyltriethoxysilane
7	Alkoxysilane
8	Octyl triethoxysilane

clue about the porosity within the specimen. In addition the specimens were measured directly before application. Only on one side of the Specimens a hydrophobic treatment was applied. 5 minutes after the hydrophobic treatment was applied the next measurement took place. For a time period of 7 days the specimens were stored at laboratory conditions. Followed by 2 to 3 days under water, the saturated specimens were measured once again.

3 RESULTS

To visualize the penetration process of the impregnations the fresh hydrophobated specimens had to be measured in short time steps. The deepest ingress of hydrophobic agent 3 was measured 2 hours after application. In contrast to the Iso-Butyltrimethoxysilane (3) the Iso-Octyltriethoxysilane (6) reacts much slower. The deepest ingress of 6 was measured 24 hours after application. However the observed maximal penetration depth and the hydrophobic layer thickness of all investigated hydrophobic agents were equal.

Figure 1 show the effect of a 200 and 350°C temperature exposure on with 7 (tab. 1) hydrophobated concrete. After application of the hydrophobic agent the indirect measurements on water saturated specimens show the hydrophobic layer. After 4 h at 200°C the indirect measurement was carried out again. Water which had been trapped in the hydrophobized areas and a part of the chemically bound water of the concrete was able to vaporize during the 200°C temperature exposure. The 200°C exposure had no influence to the thickness or performance of the hydrophobic layer of any investigated hydrophobic agent. After the 4 h storage at 200°C and the NMR measurement the same specimens were stored for further 4 h at 350°C in the oven. Under this condition all investigated hydrophobic agents had lost there effectiveness. Consequently 4 h at 350°C destroys the hydrophobic layer. By knowing this behavior of the used hydropho-bic agents changes could be related to causes like i.e. UV radiation as long as the temperature during the exposure doesn't exceed 200°C.

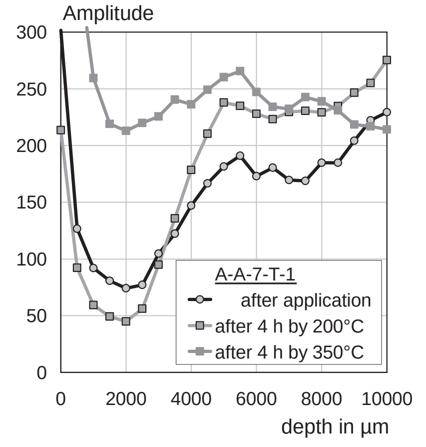

Figure 1. Temperature caused changes of a specimen treated with Alkoxysilane.

4 SUMMARY AND OUTLOOK

This paper introduces a new, non-destructive test method to investigate hydrophobic treatments of concrete surfaces in the laboratory. This test method can be transferred to the construction site. With the new method following aspects can be investigated:

- The time depending penetration depth and distribution of recently on concrete applied hydrophobic agents.
- Changes of the hydrophobic layer inside the concrete due to weathering, abrasion and other influences like high temperatures from fire events.

It's shown that the penetration depth of recently applied hydrophobic agents on concrete can be com-pared with the thickness of the hydrophobic layer. The hydrophobic layer can be determined at any age after the hydrophobic treatment has been applied on the concrete surface. However this measurement requires a concrete with significantly more humidity beside the hydrophobic layer as within. The large impact of the inhomogeneities inside the concrete shows the importance of a measuring method for the construction site, which allows a reliable quality control. Finally it is shown that temperatures of 350°C destroy the hydrophobic layer inside the concrete while temperatures below 200°C have no effect. Focus of further investigations with this non-destructive test method is the durability of hydrophobic treatments on concrete. Therefore the specimens are currently treated with different weathering cycles like UV and freeze thawing.

The authors gratefully acknowledge the financial support of the German Research Foundation within this research project.

Concrete Repair, Rehabilitation and Retrofitting III – Alexander et al. (eds)
© 2012 Taylor & Francis Group, London, ISBN 978-0-415-89952-9

Examination of the hydration of cementitious binders with fly ash and blast furnace slag using in-situ XRD

A. Vollpracht & W. Brameshuber
Institute of Building Materials Research (IBAC), RWTH Aachen University, Germany

ABSTRACT: XRD is used to identify crystalline phases based on their characteristic diffraction pattern that result from the specific crystal structures of the minerals. Quantification is possible using the Rietveld method. Portland cement consists almost completely of crystalline phases whereas fly ash and blast furnace slag contain large amounts of amorphous phases. These phases can be quantified using an internal standard, e. g. quartz powder. In this research work the hydration of ordinary Portland cement, Portland cement plus fly ash and Portland cement plus ground granulated blast furnace were examined using a polyimid foil to prevent evaporation of water and carbonation. During the first 24 h diffraction patterns were recorded automatically. For later ages single measurements were performed on the same sample. The formation of the crystalline phases ettringite and portlandite and the reaction rate of the clinker phases during the fist 28 days of hydration are compared. Thermogravimetric analysis and pore water analysis are used to check the results.

1 INTRODUCTION

In-situ X-Ray diffraction is a promising tool to examine the hydration process of hardening cement pasts. Different experimental set-ups are described in literature. Scrivener et al (2004) used a climate chamber with a relative humidity of 95 ± 2% to minimize the evaporation of water during the first hours of hydration. Hesse et al (2009) used a foil made of polyimid to protect the fresh cement paste and recorded the hydration during the first 22 hours.

These experiments were performed on pure Portland cement pastes. In this study fly ash and ground granulated blast furnace slag were added and some simplifications and enhancements of the existing strategies for the analysis of the diffraction patterns are proposed.

2 MATERIALS

A commercial Portland cement (CEM I 42.5 R) was used in combination with a ground granulated blast furnace slag (GGBS) and a fly ash (FA) respectively. The GGBS was mixed with the cement at a ratio of ggbs/c = 1 and the FA with f/c = 0.33. The chemical compositions of the materials were determined using X-Ray fluorescence analysis. The mineralogical composition was determined with X-Ray powder diffraction and Riedveld analysis. The blast furnace slag is almost completely amorphous. Small amounts of alite, belite and portlandite were found. The glass content was determined to 94.6 ma.-% via optical microscope. The main crystalline phases of the fly ashes were mullite, quartz, hematite, magnetite, anhydrite, srebrodolskite ($Fe_2Ca_2O_5$) and traces of lime, portlandite and silimanite ($SiAl_2O_5$). Via optical microscope a glass content of 86.5 ma.-% was measured, which is in rather good agreement with the XRD analysis (84.1%).

3 METHODS

The hydration process was examined using in-situ-XRD, thermogravimetric analysis and porewater analysis. The experiments are described below.

3.1 *In-situ-XRD*

For the in-situ measurements quartz powder was used as internal standard. At first the dry powders were thoroughly mixed. Then water was added and the pastes were mingled for 2 min. The weighted samples of the components are given in Table 1. The pastes were filled in special sample holders, flattened and covered with polyimid foil (Kapton). The sample holders were placed in the diffractometer X'Pert Powder from PANalytical. The measurements were performed using CuKα - radiation. The generator operated with 40 mA and 40 kV.

Diffraction patterns were recorded automatically during the first 24 h. Afterwards single measurements were performed at the age of 2, 4, 7, 14, 21 and 28 days.

Table 1. Weighted samples of the components for the in-situ-XRD.

Component/ parameter	Paste c g	Paste c + GGBS g	Paste c + FA g
Cement	2.000	1.330	2.000
GGBS	–	1.330	–
FA	–	–	0.660
Quartz powder	2.000	1.330	1.330
water	1.009	1.334	1.151
w/c_{eq}*	0.50	0.50	0.51

*equivalent water/cement ratio for FA: $w/c_{eq} = w/(c + 0.4 \cdot f)$ and for GGBS: $w/c_{eq} = w/(c + ggbs)$

3.2 *Extraction of pore solution and thermogravimetric analysis*

The samples for the thermogravimetric analysis were prepared without quartz powder with an equivalent water/cement ratio of $w/c_{eq} = 0.5$. At defined time intervals the pore solution was squeezed. The compacted cement paste samples were crushed and dried at 105 °C for the TG analysis. The TG measurements were performed with a TGA/DSC1 STARe System from METTLER. The heating rate was 10 K/min and the temperature range was 30 to 900 °C.

4 INTERPRETATION OF THE DIFFRATION PATTERNS

The Kapton foil causes an elevated back ground in the angular range of 15 to 30 °2θ. The influence of the Kapton foil was removed by subtracting the diffraction pattern of the foil from the measured diffraction patterns of the covered samples. Afterwards the Rietveld analysis was performed with the program HighScore Plus from PANalytical.

The ettringite content tends to be overestimated; it was corrected using the sulphate content of all identified crystalline phases and the sulphate content of the binder.

To compare the results of the different binders the content of all crystalline phases was related to the cement content of the pastes.

5 RESULTS

The content of alite decreased strongly during the 28 days of hydration, but no significant reaction of belite can be observed. The highest reaction rate of alite is observed for the GGBS-sample. The FA-sample shows a higher reaction than the pure cement paste as well, probably be due to the higher water content of the paste.

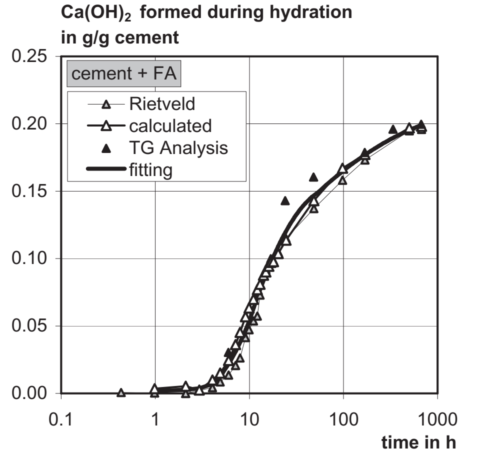

Figure 1. Portlandite formed in the course of hydration of the cement paste with FA determined with TG Analysis, Rietveld analysis and calculated from the consumption of alite.

The portlandite content as it was determined by Rietveld analysis was compared with the portlandite content calculated from the alite consumption (see Fig. 1 as an example). The portlandite contents determined with TG analysis are also pictured.

The agreement between TG analysis and Rietveld analysis is satisfactory for all three binders. For the pure cement paste and the paste with FA there is a good agreement with the calculated portlandite content as well. For the paste with GGBS higher portlandite contents are calculated at later hydration times. Obviously the GGBS has consumed portlandite, were as the FA has not reacted. The reason for this might be the rather coarse grain size distribution of the fly ash.

Both additives lead to an increase in ettringite formation, especially the FA.

The analysis of the pore solution confirmed that the FA did not influence the hydration process during the examined time period. In contrast to that the GGBS leads to a decrease of the alkalinity and the sulphate concentration of the pore solution.

REFERENCES

Hesse, C., Goertz-Neunhoeffer, F., Neubauer, J., Braeu, M & Gaeberlein, P. 2009. Quantitative In-Situ X-Ray Diffraction Analysis of Early Hydration of Portland Cement at Defined Temperatures. *Powder Diffraction* 24: 112–115

Scrivener, K.L., Füllmann, T., Gallucci, E., Walenta, G. & Bermejo, E. 2004. Quantitative Study of Portland Cement Hydration by X-Ray Diffraction/Rietveld Analysis and Independent Methods. *Cement and Concrete Research* 34: 1541–1547

Concrete Repair, Rehabilitation and Retrofitting III – Alexander et al. (eds)
© 2012 Taylor & Francis Group, London, ISBN 978-0-415-89952-9

Passive infrared thermography as a diagnostic tool in civil engineering structural material health monitoring

M. Scott, H. Luttig, M. Strydom, M. Gonelli & D. Kruger
University of Johannesburg, Johannesburg, Gauteng, South Africa

R.G.D. Rankine
Rod Rankine Engineering Solutions, Gauteng, South Africa

T. Broodryk
Yellotec, Gauteng, South Africa

ABSTRACT: Infrared thermography is now a highly evolved non-destructive testing technology with a myriad of proven applications in aeronautical, electrical and mechanical engineering applications. Although it has been successfully used in diagnosing distress in civil structures for two or three decades, civil applications have been limited mainly to qualitative use of this technology due to difficulties in scanning such large objects in a transient state (which can only be passively warmed using unpredictable sunshine) and a lack of appropriate data/experience. The cost of infrared cameras has reduced considerably in recent years but, at the same time, these instruments have become increasingly sophisticated and far better suited to the civil practitioner's needs. Most of South Africa has an ideal climate for passive thermography since we have been blessed with abundant sunshine and large diurnal temperature swings. Recent collaborative research at the University of Johannesburg has explored the ability of a range of thermal cameras to observe delamination-type defects of different sizes embedded in concrete at different depths from various viewing distances and angles under differing weather conditions and seasons. The fruits of this work will culminate in a guideline document for South African practitioners. A parallel study has developed an emissivity cabinet to accurately measure the range of emissivities of common building materials with different surface finishes and degrees of weathering to provide data necessary for more accurate quantitative estimation of surface temperatures of structural elements. This research has shown that common materials such as concrete and steel may exhibit a wide range of emissivities depending on the method of manufacture and weathering encountered.

1 INTRODUCTION

The use of infrared thermography as a means of structural health monitoring has significantly increased in recent years, due in large part to the advancement of infrared cameras and the considerable reduction in their cost. Infrared thermography offers a non-contact, non-destructive analytical technique that has demonstrated the potential to visually display subsurface deterioration in concrete structures.

Essentially, there are two different methods in which infrared thermography can be deployed for a thermographic inspection. In general, this is either in an active or passive fashion. In active thermography, energy is imparted into the target through the use of an artificial external heat source. In passive thermography, however, materials and structures are passively warmed using unpredictable sunshine. Fortunately, South Africa is blessed with abundant sunshine and large diurnal temperature swings and thus has an ideal climate for passive thermography. Civil applications of infrared thermography are very much limited to passive thermographic inspections due to the size of the structures being evaluated and the difficulties associated with trying to actively heat such large structures with relatively small external heating sources.

When passive infrared thermography is used to inspect concrete structures, the heat flow through the concrete is a direct consequence of the surrounding ambient environment. Climatic factors such as wind speed and cloud cover have a significant influence on the development of thermal contrasts. However, as the passive heat source, the sun and its apparent motion, produced by earth's daily rotation about its axis and its annual revolution around the sun, provides the primary means for conducting a passive thermographic inspection and thus has the greatest influence on the development of thermal contrast. Ultimately, the sun's position in the sky influences the intensity of radiation received by different facing elevations of a structure on the ground. Typically, during winter in the southern hemisphere, the north facing surface of a structure receives the greatest intensity of radiation while the south facing surface receives the least. This of course influences the limits of defect detection. Therefore, when passive infrared thermography is used for structural health monitoring, a strong understanding of the environmental conditions required to provide adequate thermal gradients is crucial.

The research reported in this paper focused on determining the effect of solar loading on the ability to detect subsurface features in concrete using infrared thermography. Furthermore, this paper reports on the results of a parallel study in which an emissivity cabinet was developed to accurately measure the range of emissivities of common building materials with different surface finishes and degrees of weathering.

2 BACKGROUND

Infrared thermography offers an alternative approach to non-destructive testing. Through the technology of infrared cameras and the application of infrared thermography, the temperature gradients on the surface of concrete elements can easily be determined. Infrared cameras, as radiometers, are not capable of measuring temperature directly. Instead, they measure and transform radiation intensity into a radiometric signal through complex algorithms within the camera, thereby displaying and indicating the surface temperature of objects on a thermal image, commonly referred to as a thermogram.

3 EXPERIMENTAL

To evaluate the limits of defect detection when utilising passive heating from the surrounding environment, two concrete test blocks were constructed.

Test Block "A" was 1.5 m × 1.05 m with a thickness of 0.15 m. The block was free of steel reinforcement. Rectangular and triangular expanded polystyrene sheets 150 mm in height and 10 mm thick were used as embedded targets to provide subsurface features that would influence the propagation of heat through the test block. The targets were placed at depths of 65 mm, 30 mm, 20 mm and 10 mm from the north facing surface of the test block. Test Block "B" was 1.05 m × 0.9 m with a thickness of 0.195 m. A triangular expanded polystyrene sheet 300 mm in height, 400 mm wide and 10 mm thick installed behind a cross shaped frame, constructed from Y16 and R12 reinforcement bars welded at the point of contact, was used as an embedded target to simulate a subsurface defect obstructed by the presence of steel reinforcement between the defect and the viewer. This would assist in determining if steel reinforcement would influence the thermal contrast on the surface of a concrete element created by an internal delamination parallel to the surface. The target was placed at a depth of 50 mm from the north facing surface of the test block.

4 RESULTS

The results of the inspections carried out on Test Block "A" illustrate the influence that the depth and size of the embedded targets had on the ability of the cameras to detect their presence. The results also report the influence of distance and viewing angle at which thermal images were captured. The results of the inspection carried out on Test Block "B" illustrate the influence that the steel reinforcement had on the thermal contrast created by the triangular target embedded in the concrete.

5 CONCLUSION

This paper has reported the results from an investigation into the use of passive infrared thermography in which the sun was utilised as the passive heat source. Although the potential of this technology is appreciated, its limitations are not fully understood. This lack of understanding can in part be attributed to significant deficiencies in existing research, in particular, the performance of passive infrared thermography under field conditions. These deficiencies offer an excellent opportunity to study the performance of this technology and work towards a set of guidelines that the practitioner can utilise in the field.

In this initial pilot study, the limits of defect detection were reported by considering the effect of the depth and size of the embedded targets, the distance and viewing angles at which these targets were visible and the influence of reinforcing steel on the thermal contrasts created by internal defects beneath the concrete's surface. The investigation confirmed that, under ideal conditions in Johannesburg during the winter solstice, passive infrared thermography is capable of detecting small internal defects up to a depth of 65 mm below the surface of vertical north facing surfaces.

While this investigation achieved respectable outcomes, a number of aspects were not addressed that would certainly influence the limits of defect detection. However, research is ongoing and will be investigating the influence that larger defect areas and perimeters have on thermal contrast development, thermal contrasts developed on elevations other than north and on surfaces other than vertical, as well as investigating the optimum timing of thermographic inspections by quantifying the relationship that exists between solar radiation and thermal contrast development for defects embedded at different depths. Seasonal differences will also be investigated by continuing the research over the summer and winter solstice during which all elevations will be observed. The objective of this work will be the development of a suitable guideline document for South African practitioners.

Concrete Repair, Rehabilitation and Retrofitting III – Alexander et al. (eds)
© 2012 Taylor & Francis Group, London, ISBN 978-0-415-89952-9

Active thermography as a quality assurance for structural engineering

F.U. Vogdt, F. Schaudienst & M. Walsdorf-Maul
Technische Universität Berlin, Department of Civil Engineering, Chair of Building Physics and Construction, Berlin, Germany

ABSTRACT: In the area of building physics, the application of passive thermography in structural engineering makes it possible to determine the surface temperatures of structures or whole buildings. With this method thermal bridges in the building envelope can be qualitatively detected based on localised temperature differences. In this respect, thermography has become established as a measuring method for evaluating a building from an energy point of view and is influenced by the relevant European standards. Active thermography is another area of application for non-destructive analysis of building elements. The analysed building elements are heated up by using an external heat source so that the time-dependent cooling process is thermographically investigated. Therefore, the transient heat flux is observed by recording the temperature change at the surface as a function of time. If there are temperature differences on the surface of the building element, inhomogeneities inside the building element can be measured. Two preconditions for reliable results are necessary: the structure of the building element and material are the same. This application offers new possibilities for detecting voids and honeycombing in concrete. Furthermore safety relevant defects like voids in tendon ducts and cracks in concrete are visible.

This paper deals with investigations of consoles from stucco in one of the oldest mosques in Germany and the application of active thermography as practice in structural engineering.

1 INTRODUCTION

1.1 *History*

The Berlin Mosque is the oldest surviving Mosque in Germany. The building was built from 1924 to 1928 by architect Karl Alfred Herrmann and was opened early during its construction in 1925. In the second World War the minarets were destroyed by artillery fire. The dome of the mosque was hit and the adjoining building was badly damaged. The outside facade of the mosque was hardly affected. Already in 1952 the mosque was provisionally repaired for worship. In 1976 the mosque was equipped with floor heating and the outside facade was painted with plastic dispersion paint. Apart from 1996, the adjoining building was renovated and the minarets were rebuilt between 1999 and 2001. Between 2004 and 2005 the dome was renewed.

1.2 *Motivation for investigations*

The aim of the investigation of the consoles was to locate non visible cracks which developed due to frost. Additionally the condition of the anchorage of concrete products to the masonry shall be determined, since the consoles were already dropped (shown in figure 1).

2 EXPERIMENTAL SETUP

The experimental setup consist a heating unit and an infrared camera. The appropriate computer system for real-time recording of the thermograms is not shown. For measuring the cooling process, VarioCAM hr inspect 680/30 mm' (InfraTecGmbH) IR-camera was used and has an uncooled Focal Plane Array. The camera's distance to the console was set at 2,10 m. With a frequency of 60 Hz, the thermal imaging data is transferred to and stored on a computer. Subsequent to the recording of the cooling process, the thermography sequences can be evaluated via appropriate software. For conducting the measurements, consoles were manually

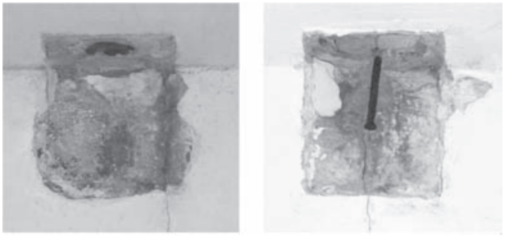

Figure 1. Photos of dropped consoles.

heated for 120 minutes each at a distance of 40 cm to the surface. The observation period after heating was 90 minutes.

3 EVALUATION AND RESULTS

In order to locate delaminations, cracks and voids, thermograms with a maximum contrast in temperature during the cooling process are selected from the recorded thermography sequences. Here, the temperature values are ascertained through environmental parameters of the consoles (temperature and humidity), measuring parameters (i.a. camera distance, measuring range, object lens), and internally recorded parameters of the infrared camera. For all thermograms presented in the following, a homogenous emissivity of the measuring surfaces of 0,90 was presumed. Temperatures are depicted as grey values, which in each image were scaled to a minmum and maximum value. The amplitude image represents the vectorial sum's amplitude of the incidental and reflected thermal wave. The phase image shows the phase shift between stimulation and measured signal at respective frequencies. Amplitude images can be affected by additional reflexions on the surface, the heat source's inhomogeneous energy distribution and an inhomogeneous emissivity distribution. To the large extent, however, these influences are filtered out in phase images. Figure 2 shows two measured consoles. As in the left figure the colour flaking is obviously visible, in the right figure cracks in the painting are visible.

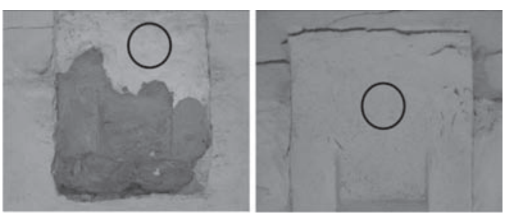

Figure 2. Photo showing consoles with colour flaking (console 1, left) and some visible cracks (console 2, right).

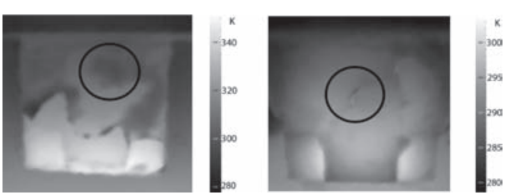

Figure 3. Thermogram after 200s for (console 1, left) and (console 2, right).

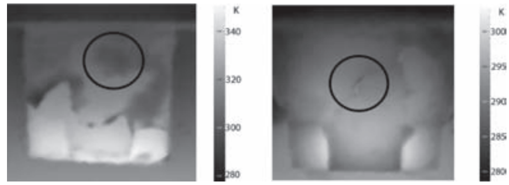

Figure 4. Phase image at 0,01 Hz (console 1, left) and at 0,037 Hz (console 2, right).

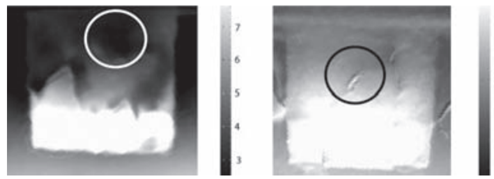

Figure 5. Amplitude image at 0,0334 Hz (console 1, left) and at 0,0334 Hz (console 2, right).

Figure 3 (left) shows thermograms of same consoles. Different temperatures at the surface lead to suspect defects (figure 3, left) and a crack under the painting (figure 3, right). The crack of console 2 is not visible on the photo but is indicated on the thermogram. As expected, the phase images and amplitude images show a better contrast than the thermograms (shown in figure 4 and figure 5).

4 CONCLUSION AND OUTLOOK

In the above mentioned investigations, active thermography was applied to detect defects and delaminations very close to the surface. Data analysis bases Fast Fourier Transformation (FFT) enhances the contrast of defects to be detected. Also the FFT reduces the influence of inhomogeneous heating which occurs if the surface is heated manually and outside affected by the wind and the weather.

Thermography is able to adequately locate delaminations of painting (not visible colour flaking) as well as cracks under painting. The results were, among other things, evaluated within the frequency range. The recorded thermograms as well as the amplitude and phase images facilitate the detection of the simulated adhesion defects. As expected, the amplitude and phase images showed a greater contrast compared to the thermograms. As far as anchorings in concrete are concerned, it is not visible that the consoles are still safely fixed. The investigations demonstrate deep cracks in some consoles.

This could induce that the passivation of the steel anchoring in the concrete is not guaranteed anymore.

Concrete Repair, Rehabilitation and Retrofitting III – Alexander et al. (eds)
© 2012 Taylor & Francis Group, London, ISBN 978-0-415-89952-9

Infrared Thermography applications for the quality control of concrete elements strengthened with FRP

G. Concu, B. De Nicolo & C. Piga
Dipartimento di Ingegneria Civile, Ambientale e Architettura, Università di Cagliari, Italy

N. Trulli
Dipartimento di Architettura, Design e Urbanistica, Università di Sassari, Italy

ABSTRACT: In recent decades there has been widespread use of FRP materials in the rehabilitation of damaged structures and in the upgrading of their seismic behavior.

The technology most widely used is the application of laminates and sheets of carbon fiber through the use of epoxy resins. Despite the undeniable advantages of this intervention, such as excellent strength and stiffness, high strength to weight and stiffness to weight ratios, good durability and high resistance to corrosion, there are nevertheless some limitations related to the quality of the adhesion between the FRP and the concrete substrate. In this light, non-destructive testing techniques seem very promising for the quality control of FRP setting.

The present paper reports the preliminary results of an experimental campaign focused on the use of the Infrared Thermography (IRT) for non destructively evaluating sound and damaged concrete specimens strengthened with different kinds of FRP. The research aims at verifying IRT reliability in detecting and sizing adhesion anomalies and defects. For this purpose, several small concrete beams have been realized, and some artificial defects of various sizes and depth have been deliberately settled in the interface between the reinforcement and the concrete substrate. The beams have been investigated before and after FRP straightening, in order to assess the feasibility of IRT in detecting different kinds of adhesion deficiencies.

1 INTRODUCTION

Externally bonded Fiber Reinforced Polymers (FRP) have great advantages over conventional materials and techniques for strengthening, repairing and retrofitting of existing structures due to their mechanical and physical properties such as their considerable strength-to-weight and stiffness-to-weight ratios, high durability, high corrosion resistance. Structural efficiency of the reinforcement is dependent on how well it has been bonded to the substrate. Indeed a perfect adhesion between FRP and concrete substrates should be obtained in order to assure the durability of the reinforcement. For this reason an important role is played by the quality control of FRP applications by using Non Destructive Testing Techniques (NDT). Some FRP characteristics, including anisotropy, radio transparency and non-magnetic properties, do not allow a large number of classic NDT, such as X-ray and magnetic methods, which have instead provided excellent results in other materials quality control, to be applied with significant results.

In this work the Infrared Thermography (IRT) has been experimented for non destructively evaluating thirty small concrete beams strengthened with FRP systems, with the aim of verifying the uniformity of FRP application and the feasibility of this technique in detecting and sizing adhesion anomalies and defects.

2 INFRARED THERMOGRAPHY

Infrared Thermography is a non destructive technique for remote measurement of surface temperatures through infrared radiation emission. IRT measures the radiated electromagnetic energy in the infrared zone of the electromagnetic spectrum. Each object having a temperature higher than the absolute zero emits in the infrared spectrum and the emitted energy is proportional to the temperature. IRT application in the field of materials NDT is based on the principle that heat transfer in any material is affected by the presence of subsurface flaws or any other change in the thermal properties of the material. The changes in heat flow cause localized energy differences on the surface of the test object, which can be measured using an infrared detector. IRT can be applied through active or passive approaches. In passive Thermography instruments are used to analyze and record data without applying artificial heating or cooling to the object, thus allowing the evaluation of its temperature distribution due to both natural phenomena or heating developing during its ordinary life. Active Thermography involves a deliberate change in temperature: a stimulus is directly applied to the object to cause heating or cooling.

3 EXPERIMENTAL CAMPAIGN

3.1 *Materials*

For the experimental tests 30 small beams $0.15 \times 0.15 \times 0.60$ m have been prepared. The beams have been sorted into two groups, each made of 15 specimens, and have been strengthened using FRP laminates and FRP sheets respectively. For each group, three beams, named respectively A1, A2, A3 for FRP laminates reinforced beams, and B1, B2, B3 for FRP sheets reinforced beams, have been carefully reinforced in order to achieve a perfect adhesion between the reinforcement and the substrate, while in the other specimens some artificial adhesion defects have been settled in the interface between the reinforcement and the concrete substrate, e.g. PTFE, plastic button, collect glue.

3.2 *Method*

IRT has been carried out on each specimen before and after the reinforcement application, in order to evaluate IRT reliability in detecting and classifying defects and adhesion problems. For the experimental tests an active Thermography approach has been applied. The samples have been heated and the exposed surfaces have been monitored with a thermal infrared camera Flir S65. The tests have been run using external heating by means of a 400-W halogen lamp, and special attention has been given to uniformly apply thermal energy onto the test object. During each test two beams have been analyzed simultaneously: one with perfect adhesion between the reinforcement and the concrete substrate and the other one with the adhesion defects. During the tests several thermograms have been acquired and recorded during both the heating and the cooling phases. IRT measurements have been made also before reinforcements application, in order to assess the thermal response of the beams. This allowed the homogeneity of samples thermal behaviour to be verified. After that, reinforcements have been applied, and measurements have been repeated. During the heating phase grate care has been paid to not reach glass transition temperature of the epoxy resin used for FRP application.

In order to give better evidence to the adhesion defects and the areas characterized by thermal anomalies and to reduce errors in thermograms interpretation, further processing has been performed with Matlab® by applying the Singular Value Decomposition (SVD) method.

4 CONCLUSIONS

An experimental program has been started with the aim of verifying the reliability of Infrared Thermography in detecting adhesion anomalies and defects in concrete beams strengthened with different externally bonded Fiber Reinforced Polymers (FRP).

For this purpose thirty beams with different anomalies and different FRP reinforcement types have been prepared. Some artificial adhesion defects have been settled in the interface between reinforcements and concrete substrate. The beams have been tested with active IRT before and after the settlement of the reinforcement.

Throughout the achieved results several conclusions can be drawn as follows:

- Active IRT highlights the presence of both PTFE and plastic button defects and locates them in beams reinforced with FRP laminates and sheets;
- Active IRT allows the presence of debonding between FRP laminates and concrete substrate to be detected;
- Singular Value Decomposition of the thermograms, performed in Matlab®, permits to better detect and locate the adhesion anomalies.

The IRT is a powerful technique that can be carried out on large portions of structures allowing a real-time analysis to be performed in a quick and inexpensive way. Results since now achieved show that IRT is a useful tool for a first location of adhesion defects by means of the identification of areas with abnormal distribution of temperature. However, results are strongly influenced by environmental factors and by optical and thermal properties of the investigated materials.

Further research is ongoing, aimed at deepen the investigation of IRT reliability by analyzing different cases of anomalies and defects, modifying IRT heat source, testing numerical approaches for predicting anomalies size. Moreover, test on full scale reinforced elements will be performed to confirm the effectiveness of the method.

Concrete Repair, Rehabilitation and Retrofitting III – Alexander et al. (eds)
© 2012 Taylor & Francis Group, London, ISBN 978-0-415-89952-9

Structural reliability targets for assessment of ageing infrastructure

M. Kabani, P. Moyo & M.G. Alexander
University of Cape Town, South Africa

ABSTRACT: The constraints faced by civil infrastructure managers have prompted innovative reliability optimisation approaches to minimise life cycle costs. This minimisation has been effective at design stage. The design based optimisation is constrained by societal expectations and notions of safety. The constraints applied in the optimisation at assessment stage are different due to increase of information on loads, resistances, costs and benefits specific to the structure under consideration. A review of these constraints is presented here together with possible areas of modifications when dealing with assessment of structures.

1 INTRODUCTION

Management of civil infrastructure encompasses optimum use and ensuring acceptable levels of safety. Probabilistic methods are now being developed for safety assessment of old structures (Liu et al., 2009; Stewart, 2001; Stewart et al., 2001). In this discussion, the level of safety is related to the probability of failure p_f of a structure under intended use. The acceptable level of safety follows therefore as the maximum probability of failure that is acceptable. The acceptable level of safety can also be given by other measures such as reliability index and risk. Reliability index β is derived probability of failure.

2 NOTIONAL PROBABILITY OF FAILURE

An evaluation of acceptable safety levels of a structure is based on notional probability of failure p_{fN} which is gives the maximum tolerable failures and fatalities levels. The acceptable safety level derived in this way is determined by society. Structural failure usually results in fatalities in terms of death or injuries, economic loss and other environmental impacts. Other factors such as the occurrence of many deaths or injury at a single event can lead to concern from the general public (Burdekin, 2007).

When setting acceptable safety levels, a distinction has to be made between individual risk (*IR*) and societal risk (*SR*) as well as voluntary and involuntary risks (Bhattacharya et al., 2000). *IR* in the UK, given as fatalities is set to an upper tolerable limit of occurrence of 10^{-4} per year while in Netherlands it is set at 10^{-6} per year (Trbojevic, 2009). Although the given measures of IR and SR refer to risk, they are not risk measures and merely give probabilities and the notation is retained for consistence with original literature. The target values have been used to rank design options based on probability of failure even though this falls short of truly risk based design.

3 RELIABILITY TARGETS FOR DESIGN

Reliability is the ability of a system to comply with given requirements under specific conditions during its design life (Holick´y, 2009). Reliability dex β derived from probability of failure is used in design codes to give the safety level. Reliability targets for design have largely been obtained through code calibration if structures deemed to have satisfactory performance (Sarveswaran & Roberts, 1999). It is assumed that the safety level of old structures that have performed well in the past is adequate for present and future needs. Code calibration approach of formulating design codes does not give room for the re-evaluation of safety targets and may place limits for novel applications and technologies.

Target reliability indices β_{target} values can also be derived from minimum acceptable probability of failure. Bhattacharya et al. (2000) pointed that measures of safety margin such as probability of failure and reliability should address uncertainty in loads and resistance, modelling uncertainty consequences of failure, unknown failure mechanisms or loadings, human error and maintenance strategies.

3.1 *Reliability based optimisation*

Reliability based optimisation aims to minimise the life-cycle costs and maximize the benefits a structure through social economic analysis

(Melchers, 1999; Madsen & Egeland, 1989). Optimisation research however, has focused on minimisation of costs in to arrive at acceptable design reliability levels (Frangopol & Maute, 2003):

$$\begin{aligned} &\min C(d_k) \\ &\mathit{Subject\ to}: \beta_i(d_k, X_i) \geq \beta_{tj}\ (i = 1, \ldots, m_p) \\ &d_i^L \leq d_i \leq d_i^U \end{aligned} \tag{1}$$

where $C(d; X)$ is the cost function, d_k is the design variable vector, X is a random variable, β_i is reliability index of the ith mode and β_{ti} is the allowable reliability index for the critical section, d_i^L and d_i^U are lower and upper bounds of the design variable. The minimisation procedure above can be applied to the assessment problem.

4 RELIABILITY TARGETS FOR ASSESSMENT

Reliability targets for assessment are important as triggers for maintenance and upgrade decisions. Assessment Despite the importance of target values in civil infrastructure management decisions, they have been generally assumed in a seemingly arbitrary way. A wide range of nominal values have been used in literature with β ranging from 4.2 to 1.65 depending on limit states involved (Kwon & Frangopol, 2010; Bhattacharya et al., 2005). The assessment problem is generally formulated as below:

$$\begin{aligned} &\min C_{Total} \\ &\text{Subject to } \beta \geq \beta_{Life} \end{aligned} \tag{2}$$

where C_{Total} are the total expected costs, β is reliability at assessment and β_{Lifet} is the target at design life.

The end of life target is the minimum tolerable limit often based on safety considerations and cannot serve as a reference point during service life It may lead to delayed intervention in maintenance. This problem can be circumvented by using the end of life design target and evaluating a corresponding target at the time of assessment.

Furthermore assessment targets should reflect the benefits and consequences of failure as obtained in reliability optimisation schemes. Björgvinsson & Wide, 1996 have stated that society's tolerance to failure is low when the benefits expected in the future are high (Björgvinsson & Wide, 1996). Such an approach to targets will be consistent with social-economic analysis used in reliability theories (Madsen & Egeland, 1989).

Reliability targets for assessment should be obtained from optimisation schemes with design β as upper bound unless an upgrade is undertaken and end of life targets bound profile of a structure largely dictated by safety concerns. This approach is consistent with social economic approach of life cycle cost management.

5 CONCLUDING REMARKS

Acceptable safety level targets are the basis of decisions in design and assessment situations. Structural design codes give a set of procedures which if satisfied ensure that a minimum reliability index is obtained for a given structure. The code approach is simplified and reduces to checking individual components.

Safety targets for assessment have been generally assigned in an arbitrary manner despite their importance as a decision point. A combination of information from structural health monitoring and reliability based optimisations can be used determine appropriate levels of safety consistent with social-economic analysis methods.

REFERENCES

Bhattacharya, B., Li, D., Chajes, M. & Hastings, J., 2005. Reliability- Based Load and Resistance Factor Rating Using In-Service Data. *Journal of Bridge Engineering ASCE* Vol 10 No.5, 530–543.

Björgvinsson, T. & Wilde, G.J., 1996. Risky Health and Safety Habits Related to Perceived Value of the Future. *Safety Science* 22 No1–3, 27–33.

Frangopol, D.M. & Maute, K., 2003. Life-cycle reliability-based optimization of civil and aerospace structures. *Computers and Structures* 81, 397–410.

Holick´y, M., 2009. Reliability analysis for structural design. *Sun Press*, Stellenbosch.

Kwon, K. & Frangopol, D.M., 2010. Bridge fatigue reliability assessment using probability density functions of equivalent stress range based on field monitoring data. *International Journal of Fatigue* 12, 1221–1232.

Liu, M., Frangopol, D.M. & Kim, S., 2009. Bridge System Performance Assessment from Structural Health Monitoring: A Case Study. *Journal of Structural Engineering ASCE* 135 No.6, 733–742.

Madsen, H.O. & Egeland, T., 1989. Structural Reliability-Models and Applications. *International Statistical Review* 57, No 3, 185–203.

Sarveswaran, V. & Roberts, M.B., 1999. Reliability analysis of deteriorating structures-the experience and needs of practicing engineers. *Structural Safety* 21, 357–372.

Stewart, M.G., 2001. Reliability-based assessment of aging bridges using risk ranking and life cycle cost decision analyses. *Reliability Engineering and System Safety* 74, 263–273.

Trbojevic, V., 2009. Another look at risk and structural reliability criteria. *Structural Safety* 31, 245–250.

Concrete Repair, Rehabilitation and Retrofitting III – Alexander et al. (eds)
© 2012 Taylor & Francis Group, London, ISBN 978-0-415-89952-9

Impact of mobile cranes on medium span bridges

V. Gaya & P. Moyo
Department of Civil Engineering, University of Cape Town, South Africa

ABSTRACT: This paper presents an experimental study of the impact factors of mobile cranes on short span bridges. Previous studies have looked at the impact factors for abnormal vehicles in general but there has been no focus on mobile cranes which have different suspension system and axle configurations. Field tests were performed on a medium span concrete to measure the dynamic impact caused by a 36 tons mobile crane. A wooden plank was placed across the instrumented beam to model a deteriorated road surface. Field measurements were used to calibrate a finite element model representing the vehicle-bridge interaction. The study has found that the impact caused by the mobile crane is dependent on its speed, suspension system, weight and condition of road surface.

1 INTRODUCTION

Impact factor is defined as the ratio of the maximum response under a moving load to the maximum response for the same static load.

$$I_m = 1 + \left(\frac{Rd - Rs}{Rs} \right) \tag{1}$$

where Rd = Dynamic response; and Rs = Static response.

The main parameters which contribute to the dynamic impact factors are the bridge span length, number of lanes, radius of curvature, surface roughness, vehicle braking, suspension system, speed, positioning and weight of the vehicle. The fundamental frequency and damping of a bridge also contributes to the impact factors. These parameters can be expressed in terms of dynamic impact factors for longitudinal moment, shear and displacement of the bridge.

Even though mobile cranes are considered as abnormal vehicles, they have different axle's configurations and suspension system when compared to trucks. Mobile cranes operate mostly on a hydro-pneumatic suspension while most heavy vehicles use a leaf spring system.

Hydro-pneumatic suspensions allow mobile cranes to adjust their suspension stiffness by varying the force on the suspension cylinder. This is important since these types of vehicles operate mainly on rough terrains where a level control needs to work frequently and reacts quickly. Hydro-pneumatic suspensions usually function independent of each other and therefore they may have different spring rates and damping.

2 FIELD EXPERIMENT

2.1 *Description of tested bridge*

The Berg River Bridge is located on the R44 road going towards Wellington in Western Cape Province, South Africa. The bridge has been chosen since it is used by both normal and abnormal vehicles. It was constructed in 1974 and is a twelve-span bridge carrying two opposite lanes traffic. The total length of the bridge is 336 m with each span measuring 28 m long and 13.4 m wide. Each span consists of eight simply supported I-beams which are 1.7 apart. Instrumentation.

2.2 *Test procedure*

A 36 tonnes 3-axles Grove GMK 3055 crane (Figure 1) was used for the purpose of this research. Each axle supports 12 tonnes which is the legal axle load in South Africa. The crane can travel at a maximum of 80 km/hr. The length and width of the crane are 10.895 m and 2.550 m respectively.

Displacements and strains were captured with the crane travelling at 5 km/hr, 10 km/hr, 40 km/hr and 75 km/hr. A severely deteriorated road surface was modeled by stacking three planks each having a thickness of 18 mm thickness each on top of each other placed at mid-span.

3 EXPERIMENTAL RESULTS

3.1 *Impact factors*

The impact was measured by taking the peak difference between the static and dynamic curve and

Figure 1. 3-Axles 36 tons mobile crane.

dividing by the peak static value. Measured impact factors without the plank are given in Table 1.

The highest impact factor obtained from the field experiment is 1.16 for a speed of 60 Km/hr. This is lower than recommended design values.

The maximum displacement impact factor measured when the crane was travelling over the plank is 1.29. This is higher than the recommended impact factor of 1.18 for a 28 m span bridge using the South African curve.

4 FINITE ELEMENT MODEL

4.1 *Vehicle-bridge interaction*

The interaction between the mobile crane and the Berg River Bridge system was simulated in Adina finite element software as a mass-spring-damper system crossing a simply supported Bernoulli-Euler beam. The instrumented **I**-beam was modeled having a constant cross section and mass per unit length.

The mobile crane's axle was defined as three triangular loads of 12 tons each moving on the bridge. Each axle was represented as a single degree of freedom system (SDOF). The model assumes that the wheels of the mobile crane remain in contact with the bridge at all times. The different speed scenarios were modeled by varying the load arrival time.

4.2 *Validation*

The displacement impact factors at mid-span are almost similar for both the FE Model and the field experiment for speed between 5 and 60 Km/hr. However the FE Model gives a greater impact at a speed of 75 Km/hr. The finite element software modeled the bridge as one simply supported beam carrying the whole weight of the crane whereas in reality, the weight of the vehicle is distributed to the 1st two beams since the distance between the two beams are 1.7 m and the vehicle width is 2.55 m. The FE Model also does not consider the cross beam at quarter and mid-span which help reduce the impact. Moreover, the field impact factor for the 75 Km/hr scenario would have been bigger if the crane travelled on the construction joint to the bridge.

Table 1. Impact factor at mid-span.

Speed (Km/hr)	Impact Factor	
	Field Experiment	FE Model
10	1.01	1.01
20	1.01	1.01
40	1.03	1.05
60	1.02	1.04
75	1.08	1.22

Table 1 compares the displacement impact factor obtained from the field experiment to the one obtained from the model impact at a speed of 75 Km/hr.

5 CONCLUSIONS

Even though visual inspections and field experiments are still the most effective way of assessing the health of a bridge, they are an expensive and tedious Adina Finite Element software has been used in this research to model the interaction between the mobile crane and the bridge. Field experiment was performed to calibrate and validate the FE model. There is a good correlation between the experimental and FE results.

The study revealed that the safest speed at which the mobile crane can use the bridge together with normal traffic is 20 km/hr. The highest impact factor measured is less than the impact allowed by the South African codes.

The planks have shown that a deteriorated road surface causes the dynamic amplification factor to exceed the allowable impact factor. Therefore a proper maintenance of the bridge is very important to minimize the effects of impact forces.

An increase in vehicle weight causes dynamic strain and displacement to increase but however the impact factor decreases due to an increase in the static response.

This page intentionally left blank

Materials and structural assessments

This page intentionally left blank

Concrete Repair, Rehabilitation and Retrofitting III – Alexander et al. (eds)
 ISBN 978-0-415-89952-9

Lessons from the Big Dig

D.W. Fowler
University of Texas at Austin, Texas, USA

1 INTRODUCTION

The Big Dig was the most expensive construction project ever completed in the U.S at a cost of $14.8 billion, as compared to the original estimate of $2.8 billion, an overrun of $12 billion. On July 10, 2006, a passenger car occupied by a 46-year-old driver and his 38-year-old wife was traveling eastbound in the I-90 connector tunnel. A portion of the suspended concrete ceiling fell onto the vehicle, crushing the right side of the car roof, killing the passenger.

2 CEILING CONSTRUCTION

The ceiling framing supporting the 15 precast concrete panels in the accident module consisted of four steel beams parallel with the roadway. Each beam was supported by eight vertical rods with turnbuckles to permit vertical adjustment. The rods were attached to the support beams at the bottom and hanger plates at the top. The hanger plates were attached to the tunnel roof by stainless steel anchors inserted into holes drilled in the concrete roof and held in place with epoxy.

The ceiling module at the accident site consisted of the framing and 15 reinforced concrete panels. All 10 of the larger panels fell onto the roadway, with only one corner of one panel remaining attached to the ceiling support structure.

3 ANCHORAGE SYSTEM

Originally, the ceiling designer planned to specify the use of undercut anchors to attach the hanger plates to the concrete roof, but the project manager (PM) insisted on adhesive anchors. The adhesive system finally selected by the contractor was a two-part epoxy consisting of a resin and hardener. The epoxy was formulated by an epoxy manufacturer, packaged by a middleman, and sold by a distributor. The anchors were 5/8-in. by 8-in. (16-mm by 20-mm) threaded steel rods. The anchor detail is shown in Figure 1.

The middleman purchased the epoxy from the manufacturer and packaged, marketed and distributed it as a standard set epoxy although they also produced a fast set version. The accident investigation later showed that the epoxy provided by the distributor was nearly always the fast set formulation. The distributor's manual at the time of the design provided different values for the fast set and standard set versions for tensile strength, flexural strength and slant shear strength, but no mention was made of any differences in the bond strength or long-term behavior including creep for anchor applications.

In 1996, the distributor had the standard set epoxy tested in accordance with ICBO and ASTM criteria, both related to adhesive anchors. The standard set passed the 120-day creep test specified by ICBO but the fast set failed the test. The important point is that before the anchor installation the distributor knew that the fast set could not pass the creep test.

The project manager (PM) directed that *all* anchors be tested to 125 percent of their maximum design service load. The contract between the contractor and owner required that the epoxy manufacturer's

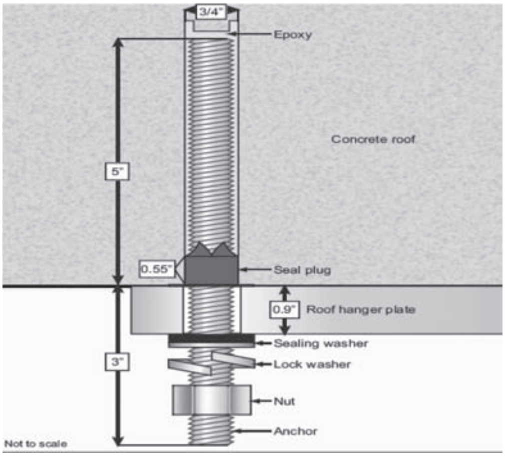

Figure 1. Adhesive anchor detail.

instructions for installation and testing be followed. Drilling of the holes began on June 10, 1999 and proof testing of the anchors soon followed. By the end of September 1999, 548 tests with 38 failures, or a 7 percent failure rate, were documented.

4 PRE-ACCIDENT ANCHOR FAILURES

There were numerous warnings of problems during construction. Some anchors began pulling out even though no signs of problems were noted at the time of installation. In some cases workers noticed that the hangar plates attached by the anchors were beginning to separate from the ceiling. As time went on, other failures were encountered. Additional load tests were performed. Some anchors pulled out. Examination of the anchors indicated several deficiencies: lack of sufficient epoxy to fill the hole; concrete dust on the epoxy around the bolt, indicating that the hole had not been cleaned properly; and brittle epoxy near the tip, indicating incomplete mixing of resin and hardener. Apparently, according to the engineer, in spite of the defects the anchor was able to just pass the original proof load test but after weeks of constant loading by the ceiling module, "the bond was broken, and the bolt began to slip out."

The CM directed the contractor to proof test all replaced anchors to a higher load, and eventually, the two parties agreed on a test load of 6,350 lbs (2,886 kg). The contractor agreed to replace all failed anchors and proof load the new anchors to the higher load. In addition all previously installed anchors in the HOV ramp area would be retested to the higher value.

5 POST COLLAPSE FINDINGS

At the time of the ceiling collapse, all 20 anchors attaching the ceiling support beam pulled out. All but one of the 20 failed anchors were found to have void areas that ranged from 1 to 40 percent (average 10 percent) of their embedment area. Five showed evidence of adhesive failure, all were missing epoxy, and 13 had yellowed epoxy Twelve of the 20 anchors were bent, and all but one showed evidence of overflow epoxy, generally extending 0.75 in. (18 mm) below the embedment area.

Of the 65 anchors outside the failure row, 62 were found to have void areas ranging from 1 to 70 percent (average 15 percent). Twenty-three of the anchors showed evidence of adhesive failure, 44 were missing epoxy, 27 had yellowed epoxy, and 40 of the 65 anchors had displacements ranging from 0.625 to 2.65 in. (16 to 66 mm) before removal.

In examining other anchors from the tunnel, it was noted that the yellowed epoxy was found only on anchors that had significant displacement; no yellowed epoxy was found on anchors that had not displaced. It was theorized that the discoloration was a result of environmental exposure. The yellowed portion was typically about 0.3 in. (7.5 mm) greater than the displacement length.

A hand-held borescope was used to investigate the inside of the anchor holes. All but one of the 20 holes imaged had epoxy voids ranging from 3 to 38 percent of the hold surface area, with 11 holes having void area fractions of 20 percent or more. The void areas were generally in the longitudinal direction. Eleven holes had adhesive failure areas. All of the holes had fractured epoxy covering 42 to 93 percent of the hole surface area.

As part of the investigation of the collapse, 188 anchors were pulled out of the eastbound and westbound D Street portal tunnels to determine the peak load before the anchors pulled out. The peak loads ranged from 1,121 lbs (510 kg) to 24,242 lbs (11,019 kg). All loads were less than the 25,400 lb (11,545 kg) capacity indicated in the Powers literature. Of the 188 anchors, 45 had displacements up to 2.625 in. (66 mm) prior to the pull-out tests. The displaced anchors required about half as much force to remove as those that had not displaced. Only five of the 21 anchors requiring less than 5,000 lbs of force to pull them out had not displaced at all.

Nine anchors that had shown no evidence of displacements were subjected to sustained loads of 1000, 2000 and 3000 lbs (455, 910 and1365 kg) for up to 3 months. One supporting 2,000 lbs for 84 hours pulled out, and one supporting 3000 lbs for 7 hours pulled out. Another anchor supporting 3000 lbs was relieved of its load after 377 hours due to impending failure. Generally failures occurred in the epoxy, and only one failed due to spalling of the concrete. The anchors that sustained the load for the test duration showed displacements of 0.03 to 0.14 in. (0.75 to 3.5 mm).

Laboratory tests showed that the standard set epoxy exhibited no significant movement, while the fast set epoxy exhibited significant displacements at all load levels.

6 SUMMARY OF NTSB FINDINGS

The NTSB report listed 20 findings on the cause of failure. However, the probable cause of failure "was the use of an epoxy anchor adhesive with poor creep resistance, that is, an epoxy that was not capable of sustaining long-term loads."

Concrete Repair, Rehabilitation and Retrofitting III – Alexander et al. (eds)
 ISBN 978-0-415-89952-9

Differing results from inspection and load rating of Sikanni Chief Bridge

P. Phillips
Delcan Corporation, Calgary, Alberta, Canada

R. El-Hacha
University of Calgary, Calgary, Alberta, Canada

ABSTRACT: The Sikanni Chief River Bridge, 256.1 km of the Alaska Highway, British Columbia, Canada, is a five-span structure which was built in 1968. Results from five detailed visual condition evaluations of this bridge, completed over the last decade, are provided within this paper. Findings from the load rating of this structure are also outlined. Deficiencies were detected both from the inspections and the load rating calculations; however, the deficiencies noted based on the load ratings are in fact not observable in the field. The focus of this paper is to show that the findings from the two evaluations differed and to provide the decisions that were made with respect to those differing findings.

1 INTRODUCTION

A live load capacity factor (LLCF) structural evaluation (load rating) and a detailed visual condition inspection of the Sikanni Chief River Bridge (Sikanni), 256.1 km along the Alaska Highway, British Columbia, Canada were performed in September 2009 by Delcan Corporation (Delcan) for Public Works and Government Services Canada (PWGSC), who owns and maintains the structure. Delcan has visually inspected this bridge in 2001, 2005, 2007, and 2011 as well.

Chapter 14, 'Evaluation', of the Canadian Highway Bridge Design Code (CHBDC), CAN/CSA S6-06, was followed when performing the LLCF evaluation. Sikanni was checked for CL1-625 kN truck/lane live loads—normal Canadian traffic. As well, Sikanni has been checked for many heavy-load, permit-controlled (PC), vehicles with gross vehicle weights as high as 1835 kN.

This paper describes the details of the condition evaluations completed for this structure, existing conditions of this structure and how they have changed over the last decade, details and results of the LLCF evaluation, difference in findings between the two evaluation types performed, decisions that were made by Delcan with respect to those differing findings, and recommendations made to PWGSC regarding maintenance and rehabilitation of this structure.

2 LLCF STRUCTURAL EVALUATION

A LLCF evaluation was undertaken to check the existing capacity of Sikanni under its current loading and to establish which of its members were understrength currently, if any. LLCFs are indicators of the amount of capacity that a member currently has available for live loads (LLs). LLCFs greater than one are deemed adequate for the prescribed LLs and LLCFs less than one generally require bridge strengthening, replacement, or posting.

2.1 *Normal traffic*

Table 1 shows the LLCFs that have been calculated for Sikanni's simply-supported precast prestressed inverted concrete U-girders under normal traffic. All ultimate limit state (ULS) checks pass. Sikanni's girders, however, do not pass the serviceability limit state (SLS) checks at the bottom fibres of their bottom flanges at midspan. This would indicate that under unfactored loads the girders should be cracked in their tensile regions. No evidence has been found onsite that the girders are overstressed in positive bending. Therefore, the results from the LLCF evaluation differ from the actual conditions in the field.

In accordance with Clause 14.5.2.3 of the CHBDC: "Where there is no evidence of serviceability-related defects, the evaluation need not consider the SLS if neither the use nor the behaviour of the bridge is changed." Therefore, the LLCF evaluation performed by Delcan did not need to consider the SLS. That being said, the calculations were performed, due to prestressing being present in Sikanni's girders, and they show the following:

– That the girders are susceptible to cracking under the SLS under normal traffic loads.

– That the SLS LLCF evaluation loadings and resistances calculated in accordance with the CHBDC are conservative.

2.2 *Heavy-load vehicles*

Figure 1 shows the LLCFs that have been calculated for Sikanni's girders under 33 different PC vehicles.

The gross vehicle weights of the PC vehicles are much larger than the weight of the CL1-625 kN truck. Since, however, the individual axle weights of the PC vehicles are less than the heaviest axle weight of the CL1-625 kN truck, the PC trucks themselves are all longer than the length of any of Sikanni's individual spans (and therefore the entire weight of a PC truck cannot be completely on one span at any one time), and the PC trucks were instructed to drive down the centreline of Sikanni at reduced speeds and without any other traffic on the bridge at the times of their crossings, the effects of the PC vehicles are actually less than that of normal traffic.

3 RECOMMENDATIONS

Following are the recommendations made to PWGSC regarding the 2011 inspection of Sikanni. The estimated total cost of maintenance and rehabilitation required to this bridge in 2011 Canadian dollars is approximately $300,000. Note however that this work is not all to be performed right away.

Work to be completed within one year:

– Rehabilitate North embankment slope with the addition of riprap ($25,000).
– Repair spalling concrete adjacent to the expansion joint at pier 1 ($10,000).
– Repair pot holes in the bituminous-surface-treatment of the approach roadways ($3600).
– Repair erosion gullies at Northwest and Southwest corners of this bridge with riprap ($2000).
– Realign approach barrier at Southwest corner of this bridge ($200).

Work to be completed within five to ten years:

– Repair deteriorated ends of the pier caps at piers 2 to 4 (total cost of $25,000).
– Repair deck delaminations ($115,500).

Work to be completed annually (costs per year):

– Remove driftwood from around the piers ($2000).
– Clean bearing seats and expansion joints ($9000).

The recommendations made to PWGSC regarding the 2009 LLCF evaluation of Sikanni are that:

– Repeated overloading may cause the girders to crack. Therefore, the girders should be regularly inspected. Heavier axle loads than those of normal traffic should not be allowed on the bridge.
– All members of the bridge are capable of carrying their current loadings. No bridge strengthening or posting is currently required.

Table 1. LLCFs for the girders under normal traffic.

Calculation	Location	$LLCF_{min}$
Stress (SLS)	Midspan (bottom fibre)	0.64
	Midspan (top fibre)	7.34
Flexure (ULS)	Midspan	1.49
	End	1.56
Shear (ULS)	Midspan	4.88
	End	2.46

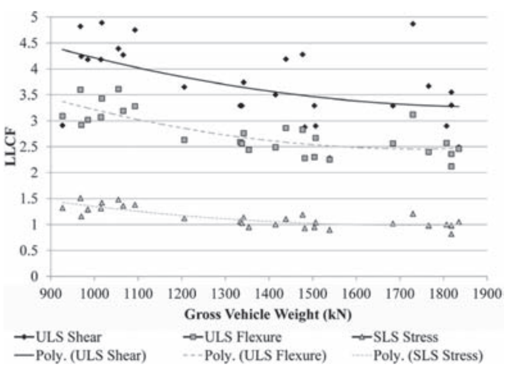

Figure 1. LLCFs for the girders under PC vehicle loadings.

4 CONCLUSION

This paper describes the results of the inspections and LLCF evaluation of Sikanni. There exists a difference in findings between the calculated SLS capacity of this bridge's girders and their actual physical conditions. The calculations indicate that under service loadings the girders should be overstressed and cracked in their positive moment tensile regions, however no cracks exist currently in the field. Delcan's recommendation to PWGSC regarding this difference is to regularly monitor the girders for cracking and to limit axle weights of the trucks on the bridge to those of normal traffic.

DISCLAIMER

Sikanni is well maintained by PWGSC. None of the results contained within this paper should dictate otherwise or are intended to dictate otherwise. In no way does the public need to be concerned with the integrity, safety, stability, or strength of this bridge.

Concrete Repair, Rehabilitation and Retrofitting III – Alexander et al. (eds)
© 2012 Taylor & Francis Group, London, ISBN 978-0-415-89952-9

A new life for ultra low strength concrete, Brisbane City Hall

Albert N. van Grieken
Aurecon, Australia

ABSTRACT: The foundation stone for the Brisbane City Hall was laid by the Prince of Wales in 1920. Since it was officially opened in 1930, the City Hall has become one of the most significant heritage buildings in Queensland and the community and cultural centre of Brisbane. The City of Brisbane now wants the City Hall to be upgraded and the structure to support the loads of a modern public building. This posed significant structural challenges. Preliminary analysis of initial compressive testing of the superstructure concrete, confirmed a characteristic compressive strength of 6 MPa. Examination and analysis of the concrete mix lead to the conclusion that sand bulking, due to volume batching by hand, and increased water content led to this reduced concrete strength. To arrive at a renovation design strength, more than 300 additional core samples were extracted and tested. The results were analysed in detail and using different statistical analysis models and a design compressive strength of only 3.4 MPa was finally adopted. In conjunction with ground penetration radar surveys of the structure, this enabled the identification, selection and design of structural strengthening options, which caused the least disruption to the heritage fabric. The building is currently being refurbished and will resume its place as one of Brisbane's most important and loved public buildings with a stronger structure to meet current and future needs.

1 INTRODUCTION AND HISTORICAL BACKGROUND

The Brisbane City Hall is among Brisbane's and Australia's most prestigious and valuable heritage buildings. The City Council decided to renovate and upgrade the building to improve the standard and utilization for council occupancy and commercial purposes and increase the lifespan of the structure.

This required a detailed understanding of the capacity of the superstructure, including the strength of the concrete, about which little was known, other than that it had a very low compressive strength.

2 CONCRETE QUALITY AND STRENGTH

2.1 *Scope of investigation and tests*

The challenge of establishing the structural capacity of 30 different columns, 81 different primary beams and 65 different secondary beams was compounded by the knowledge that these were constructed with very low strength concrete of variable quality.

Thus a full understanding of materials and establishment of design strengths was essential. This led to the following systemic program of investigations and tests:

- Review of historic data
- Review of information contained in the 2008 reports by a concrete technologist based on 3 cores
- Testing an additional 318, 75 mm diameter cores extracted from selected locations
- Compression strain measurements on four 150 mm diameter cores
- Ground penetrating radar scans to establish reinforcement details and correlate these with existing drawings
- Probability modeling of data obtained
- Structural modeling using the adopted characteristic compressive strength

2.2 *Initial analysis of mix design*

Following concerns raised by the Brisbane City Council, a well respected concrete technologist, David Beal, was commissioned in 2008, to advise on the quality and properties of the concrete. This is due to the lack of historical and technical information about this very old concrete, as it was already clear then, that the quality and strength of this concrete was abnormally low.

Tests on cores taken from three locations in the City Hall produced compressive strengths of 5.2 – 13 MPa.

2.3 *Further core tests and analysis*

In the hope of yielding higher compressive strengths from a much broader sample data basis, an additional 318, 75 mm diameter, core samples were extracted for compressive tests in 2010, as

Figure 1. Failed cylinder.

part of Aurecon's investigation. Results ranged from 2 MPa to 35 MPa. These results were subjected to a vigorous regime of probability analysis using 7 different distribution curves. After selecting log–Pearson 3, Pearson 5, Chi-squared and log normal curves as the most representative, a final strength of 3.4 MPa was adopted. This was not the hoped for result.

2.4 *Stress strain tests*

An additional four, 150 mm diameter cores were extracted and tested by Melbourne Testing Services. 120 Ω strain gauges were bonded to the faces of the cylinders which were subjected to 4 load cycles until a peak compressive stress was achieved. Failure occurred early and in the form of surface crumbling and splitting (Figure 1).

The resulting stress strain curves varied considerably showing that some of the concrete is not quite brittle and exhibited some level of ductility (Figure 2).

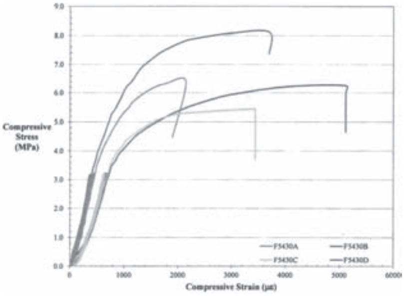

Figure 2. Stress strain curves.

3 STRUCTURAL REFURBISHMENT

After identifying and considering many alternative options, the following strengthening works were adopted.

- To strengthen the beams, the preferred option was to construct a reinforced concrete overlay.
- Where the heritage floor could not be disturbed, steel beams were attached to the soffit.
- The preferred solution to strengthen the columns was to install a high strength 32 MPa concrete 'jacket' around the columns where an increase in size could be tolerated. The non preferred alternative was to remove the outer layer of the columns and replacing the removed concrete with 32 MPa concrete to match the existing size.
- Selected seismic strengthening, involving the construction of new concrete walls against existing masonry walls in the foyers and light wells.

Figure 3. Brisbane City Hall under refurbishment.

4 CONCLUSION

The ultra low strength and variable quality of the concrete to the City Hall structure, necessitated an extensive testing program and analysis of data. These resulted in the adoption of a compressive strength of 3.4 MPa.

Due to the extensive investigations, testing and modelling, the scope of strengthening works and the resulting disruption to the heritage surfaces and features could be kept to a minimum. Work is now well underway (Figure 3).

Concrete Repair, Rehabilitation and Retrofitting III – Alexander et al. (eds)

Testing, maintenance and reinforcement of the Pietrastretta RA05 motorway viaduct

A. Contin, E. Viviani & M. Cavetti
E2B s.r.l., Padua, Italy

M. Viviani
HEIG-VD, Yverdon-les-Bains, Switzerland

ABSTRACT: Located in the Italian RA 05 motorway, the viaduct Pietrastretta is an example of large infrastructures constructed in the 1970s. This post-tensioned concrete viaduct, seriously damaged by several different chemical and physical aggressions, needed to undergo both structural reinforcement and maintenance of the concrete structures recently. This article delivers an insight into inspections and testing conducted, into the problems highlighted and into the solutions adopted to refurbish, repair and reinforce some of the 21 spans of this 850 m motorway viaduct.

1 INTODUCTION

The Pietrastretta viaduct is composed by two separated series of simply supported beams for a total of 21 × 2 spans with average length of about 44 m. Each span is composed by three longitudinal beams equally spaced of about 3.2 m, transversally connected and stiffed by 6 concrete beams, equally spaced of about 8.75 m. Longitudinal beams are of variable cross section with an axis of symmetry in the midspan, which is also the deeper point of the beam. Longitudinal beams are post tensioned by means of six cables with parabolic path. The deck is 9.5 m wide.

The pietrastretta viaduct deck is difficult to access and inspection from the ground is nearly impossible, given the steep mountain side, the friable rock and the intense traffic, which does not allow for an easy closure of the viaduct for inspection (Figure 1).

The features and the traffic volume of the RA05 configure it as an important motorway but, for historical reasons, it has never been classified as a true motorway. For the commercial traffic of an important portion of the Basilicata region, there is no acceptable alternative to this link.

2 STRUCTURAL DETAILS AND DAMAGES

Prestressed precasted beams used in the 60's to 70's were often very similar among them: a deeper section in the middle span, delta shape, a series of round holes created on the top flange, very close to the web, used for rain water evacuation. The great advantage of these beams is the easiness of construction, the good production rate and the better overall quality of the concrete obtained using a partially industrialized production technique. On the down side, the use of this type of precast element requests a careful management of the construction process and details, among them the joints' installation and the evacuation of the water from the deck. In the case of Pietrastretta viaduct the detail of the water evacuation was not well managed The percolation of salted water and the combination with the cold weather concurred to create a combination of freeze-thaw and deicing salt damage especially to the external side of the lateral beams. Although Basilicata region is in the south of Italy, the climate is far from being "Mediterranean". Winters in the region of Pietrastretta are cold and rainy and temperatures are frequently under zero. The metrological station of Potenza, the main city of the Basilicata region, records more than 35 days per year of in which the temperature is consistently under zero °C. It is then not surprising that the penetration of corrosive salts was fast and the action of freeze-thaw intense. freeze-thaw and deicing salts were main causes of concrete degradation however, other ones; even if less extensive, required a particular care. During previous works, some wood boards had been forgotten in place, close to the piles. The rotten wood kept the concrete surface moist for most of the winter, further damaging the concrete by physical and chemical action. Furthermore, in many spots of the piers and under the

Figure 1. A view from the Pietrastretta viaduct.

deck, the condition were favorable to moss-growth on the concrete surface.

3 CONDITION ASSESSMENT AND REPAIR OPTIONS

The extent of damage found during the visual inspections was so important that some lanes had to be closed to the traffic. Some weeks after the closure of these lanes and the end of the inspections a sudden failure of a beam occurred, eventuality not neglected by the engineers that had already taken some measures to avoid the fall of the beam during the field operations by laying a steel beam on the top of the deck along the broken beam and connecting the two by means of Dywidag bars.

The visual inspections and the tests conducted led to the conclusion that some spans of the Pietrastretta viaduct could not be refurbished or strengthened, but needed to be substituted. Further reasons to propose substitution of these spans were highlighted during the visual inspection of the beams: there was no mortar attached to the exposed prestress ducts and the concrete had a grey color lighter than in other spans. These are considered by senior engineers an indicator of high porosity concrete, possibly due to a non-programmed high water/cement ratio (water addiction to correct an inappropriate rheology of fresh concrete or an error). Substitution had a disadvantage: It was clear that it was impossible to demolish the beams in place as well as it was unwise to push them onto the ground. The only possibility was to saw the deck and carry away the beams.

A solution to move the beams out of the field was found: the beams were to be lifted by a pair of full gantry cranes travelling on rails and then be charged on a truck, in order to be evacuated. The same cranes would be used to lay the beams of the new bridge. A series of steel cantilever beams (orthogonal to the bridge axis) were created in order to accommodate one of the crane rails, while the other was laid onto the existing piers caps. A large concrete saw permitted to separate the concrete beams of the viaduct and then to lift them. The greatest challenge in Pietrastretta field was the geometric design of the rail supports. Full gantry cranes available in this field could travel on rails with a prescribed maximum curvature and slope and, in order to minimize the derailment risks, the geometry of the rails should not have any angle. Rails supports do not have to bend excessively in order to avoid imbalance of the crane and excess of load transfer on one of the rails. Furthermore, the span number 18 was so damaged that had not any bearing capacity and certainly would not have sustained the load of the trucks that had to tow the beams of span number 19. Indeed one of the beams of span 18 was collapsed. This fact had not been forgotten by the engineers that had supported the broken beam with a steel beam in order to sustain the truck load and not only to prevent a complete failure of the beam. Finally, the new steel beams were laid and a concrete deck casted. The total intervention time was of about 10 months.

Not all the Pietrastretta's spans had to be demolished: most of them had to be refurbished (concrete was generally in bad condition), some of them had to be strengthened by means of external presteressing cables (since most of the cables had a tension lower than the designed one). After these maintenance and reinforcement operations, a load testing took place.

4 CONCLUSION

Pietrastretta viaduct is a typical 60–70's construction: concrete was believed to be eternal. The increase of the traffic and the extensive use of deicing salts proved that concrete was all but not eternal. The case of Pietrstretta shows that durability often depends on construction details: where the elements of construction were carefully designed and assembled, the bridge had no sign of degradation; where the details were not well conceived, the structure had to be refurbished or reinforced and unfortunately, in some zones substituted, with great nuisance for the user and cost for the collectivity. Today's knowledge will hopefully avoid damages of this magnitude on structures.

ACKNOLEDGEMENTS

The authors would like to thank the owner, ANAS Potenza, the contractor, FIP industrial, for the support, the contractors' engineers for the teamwork: Mauro Scaramuzza, Luigi De Zuccato and Pino Scalese, as well as the E2Bs' engineers Michele Pasqualotto and Cristian Mazzocco.

Concrete Repair, Rehabilitation and Retrofitting III – Alexander et al. (eds)
© 2012 Taylor & Francis Group, London, ISBN 978-0-415-89952-9

Residual structural performance of deteriorated RC bridge girder with reinforcement corrosion

T. Shimomura, Y. Tanaka & T. Yamaguchi
Nagaoka University of Technology, Niigata, Japan

ABSTRACT: The residual structural performance of a real RC bridge that had been in service for 80 years in a coastal area of Japan was tested in the laboratory. The load bearing capacity of the bridge was examined, with the test results showing that the residual load bearing capacity of a heavily corroded RC girder was lower than indicated by the corrosive loss in reinforcement cross-sectional area. A simulation by nonlinear FE analysis implied that the very low ultimate load bearing capacity of the tested girder is attributable to the presence of reinforcement that is unable to bear tensile force due to damage to the lap splice joints. Laboratory tests using RC beam specimens with lap splices were carried out to clarify the reason for the damage to the lap splice joints.

1 INTRODUCTION

It is of importance to estimate the residual structural performance of the existing infrastructure taking into account material deterioration. This paper describes the loading tests on the removed RC girders and the numerical analysis carried out later. The reason of remarkable reduction in load carrying capacity of the deteriorated girder is then clarified based on systematic laboratory tests on RC beam specimens.

2 LOADING TESTS ON ACTUAL RC BRIDGE GIRDERS

Two girders were cut out from an actual RC bridge known as the Nougawa Bridge, which was constructed in 1930 and had been in service in a chloride-prone environment in coastal Japan for 79 years. The concrete cover was repaired by patching with mortar in 1959, 30 years after construction.

Figure 1 indicates the location of the tested girders in the bridge. The average weight loss of reinforcement in the inner girder was 14% while that in the outer girder was 26%. Figure 3 shows the load versus center span deflection relationships. The concrete cover spalled during the test. Accordingly, some lap splices were exposed as shown in Figure 3. The maximum load carrying capacity of the outer girder was only 45% of that of the inner girder. This great difference cannot be explained by only the above-mentioned loss of cross-sectional area of the longitudinal reinforcement due to corrosion.

Nonlinear finite element analysis was carried out using ATENA ver. 4.1.4 to simulate the loading tests. It was confirmed through experiment and analysis that the extremely low loading capacity of the outer girder is attributable to the fact that some of the reinforcement was unable to carry tensile load due to the deterioration of lap splice joints. However, the actual reason for the deterioration of the lap splice joints is not clear at this moment. A number of possibilities can be considered, as follows.

– Presence of lap splices in the tensile zone.
– Corrosion in lap splices.
– Patching work around lap splices after corrosion.
– Corrosion in lap splices after patching work.

In order to clarify the main reason for the deterioration of the lap splice joints as observed in the tested outer girder, a series of laboratory tests was conducted.

3 LABORATORY TEST TO SIMULATE DETERIORAITON OF THE ACTUAL RC BRIDGE GIRDER

Ten RC beam specimens were tested. Figure 4 shows an example of a tested RC beam specimen. The experimental parameters of the ten test specimens

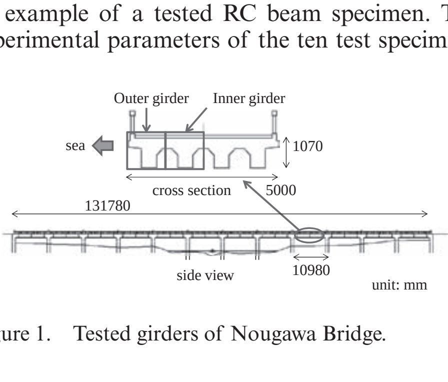

Figure 1. Tested girders of Nougawa Bridge.

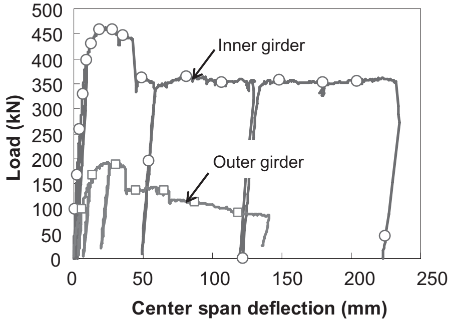

Figure 2. Test results: load-deflection curves.

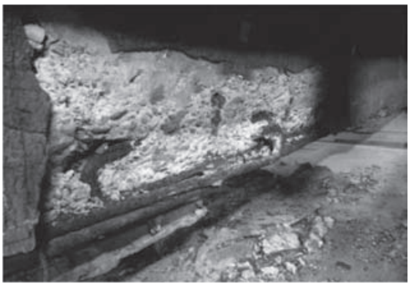

Figure 3. Spalling of concrete cover and exposure of a lap splice joint in the outer girder.

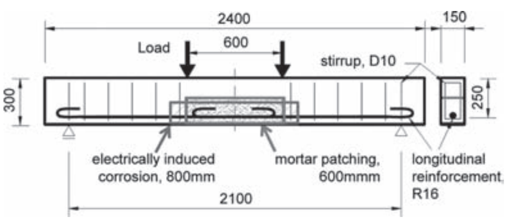

Figure 4. RC beam specimen.

are the existence of a lap splice, corrosion, repair with mortar patching and corrosion again after patching. The test procedure is shown in Figure 5.

In the series of specimens with lap splice joints, shown in Figure 6, specimen H with corrosion of the lap splice joint lost load carrying capacity and deformation capacity. However, specimen I, which had been repaired by mortar patching after corrosion, did not fail at the lap splice joint and exhibited as much load carrying capacity as sound specimen F. On the other hand, specimen J, which had suffered further corrosion after being repaired, failed at the lap splice joint and had very low load carrying capacity and deformation capacity.

Based on the results of these laboratory tests, it is inferred that the main reason for the deterioration of the lap splice joints observed in the tested

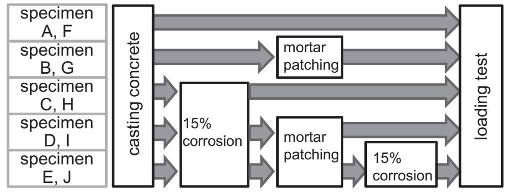

Figure 5. Test procedure.

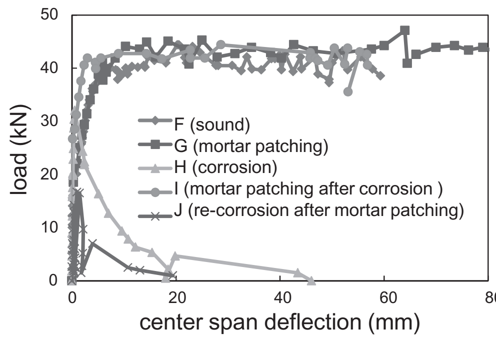

Figure 6. Test results for specimens with lap splice joints.

outer girder was corrosion cracking and spalling of the concrete cover around the lap splices due to corrosion after repair work. Further, it is also inferred that the structural performance of the girder was recovered at one time through the repair work with mortar patching.

4 CONCLUSION

1. If reinforcement anchorages in the concrete have not deteriorated, the structural performance of a reinforced concrete member with corroded reinforcement can be evaluated by considering the reduction in cross-sectional area of the reinforcement due to corrosion.
2. When reinforcement lap splice joints have corroded and the concrete cover has been damaged by corrosive expansion, reinforcement anchorage is lost and the structural performance of the member might be heavily degraded.
3. Even if lap splice joints have corroded and the concrete cover is damaged, anchorage performance can be recovered by repairing the structure with concrete cover patching work.
4. It is difficult to detect deterioration of reinforcement anchorages from surface appearance only. Therefore, in assessing the residual performance of concrete structures that have suffered deterioration, it is important to clarify the position of reinforcement anchorages from design drawings or by some other suitable detection method.

Concrete Repair, Rehabilitation and Retrofitting III – Alexander et al. (eds)
© 2012 Taylor & Francis Group, London, ISBN 978-0-415-89952-9

Residual shear capacity of continuous reinforced concrete beams

Y. Yang, J.A. den Uijl & J.C. Walraven
Delft University of Technology, Delft, The Netherlands

ABSTRACT: In order to better evaluate the residual shear capacity of existing concrete structures, such as multi-span concrete slab bridges, shear tests have been carried out on beams sawn from a bridge constructed in 1961. The test setup is designed to generate moment distributions of both simply supported and continuous structures. The test results are compared with numerical simulations and results derived from earlier tests done on similar specimens. It turns out that other than the initial stiffness, the presence of existing cracks and other faults in concrete have a quite limited influence upon the inclined cracking load. The Eurocode formula is able to predict the inclined cracking load with reasonably accuracy.

1 INTRODUCTION

Residual capacity of existing infrastructures such as bridges has been gaining more and more attention in recent years. In the case of the Netherlands, one of the issues widely discussed is the residual shear capacity of concrete solid slab bridges. Most of those structures have no transverse reinforcement, thus the concrete within the slabs has to carry the shear force. Therefore accurate prediction of the brittle shear failure becomes crucial to structure safety. There are still several aspects making the task more challenging.

The loading history since the structure was build has generated cracks. On the other hand, unlike what is common in experiments, most bridge structures are statically indeterminate, and loaded under complex loading conditions. Besides, existing cracks close to the point of inflection in a continuous beam can influence the shear behaviour significantly.

To study the aforementioned aspects in a more realistic scenario, a series of tests have been executed on beams sawn from the same bridge deck including an intermediate support.

2 SPECIMENS AND TEST SETUP

The tested specimens are sawn from Gestelsestraat Bridge that was constructed in 1961. The bridge is a three span flat slab bridge without shear reinforcement. It was located in the highway surrounding the city Eindhoven in the Netherlands and it has to be demolished for the renovation of the highway system.

Simulations before the tests showed that there was a big chance that the steel bars in the specimens would yield before shear failure could develop in most load cases due to the rather low steel grade available in the 1960s. Therefore, it was decided to increase the flexural strength of the specimen by gluing four Carbon Fibre Reinforced Polymer (CFRP) laminates with 1.4 × 100 mm cross sections on the top surface of the specimens.

Besides, to acquire more information form the same specimens, the undamaged east ends were also tested. In that case the specimens were simply supported and loaded by a single point load. In some of the tests, the specimens are strengthened at the bottom surface by CFRP laminates as well.

The test setup of the continuous beam tests is shown in Figure 1. Two hydraulic actuators are used to applied point loads onto the specimens, namely P_1 and P_2. The ratio between P_1 and P_2 is fixed during the test, to ensure constant moment ratio M^+/M^-.

3 TEST RESULTS

In total nine experiments have been carried out on the four specimens. Because of the complex reinforcement arrangement, the failure mode at the ultimate load varies. Shear failure was not observed in all the tests. Nevertheless, inclined cracks were observed in most of the tests. And the shear forces when this inclined crack originates, V_{cr}, are of more concern in the tests. For beams with relatively large shear slenderness ratio ($a/d > 3.0$), the development of an inclined crack in the shear span usually defines the load capacity in an experiment. In case of smaller a/d, a direct strut will form between the loading plate and the support after origin of the inclined crack, and the shear force can still be increased further. On the other hand, the situation

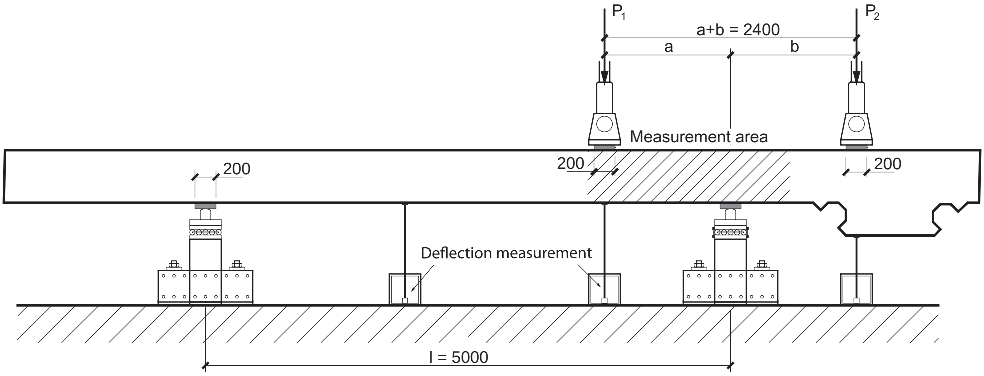

Figure 1. Test setup simulating moment distribution on continuous beams.

in the real world is different, because the location of the traffic load is not fixed. Once an inclined crack has formed, the development of a direct bearing strut is not guaranteed since the load may move. Hence, the shear capacity is defined by the origin of the inclined crack.

In Figure 2, the inclined cracking loads V_{cr} of the presented test program are plotted against M/Vd. As comparison, the results of the previous tests on beams from the same bridge are plotted in the same figure. The predicted τ_{cr} by Eurocode formula is given as a reference. Both continuous and simply supported tests show clear correlation between V_{cr} and M/Vd.

Besides, to check the influence of faults such as existing cracks in the specimens, reference tests simulated by the Non-Linear Finite Element software package ATENA2D is employed. The measured load deflection relationship compares well with the simulations using f_{ct} from splitting tests.

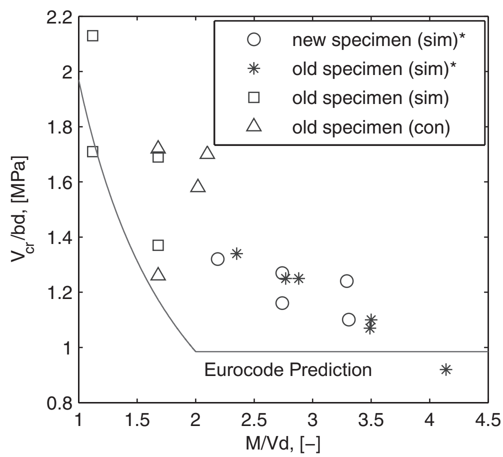

Figure 2. Relation of inclined cracking load V_{cr}/bd and M/Vd. In which sim stands for simply supported tests; con stands for continuous supported tests; *stands for the tests carried out in previous study.

4 CONCLUSIONS

The shear capacity of 50-years old concrete beams has been tested under both simply and continuously supported loading conditions to study the influence of both material and boundary conditions. The test results are compared with numerical simulations and results from earlier tests on specimens sawn from the same bridge deck. The following conclusions can be drawn:

- Existing cracks in the specimens result in a reduced initial stiffness, but their influence upon the inclined cracking load is limited.
- For both old and new concrete specimens, the inclined cracking load V_{cr} is clearly correlated to the maximum M/Vd ratio in the shear span, irrespective the simple or continuous support conditions.
- Using the measured compressive strength, the Eurocode formula on shear capacity of reinforced concrete members without shear reinforcement gives a good prediction of the inclined cracking load of the old and new concrete specimens.

Concrete Repair, Rehabilitation and Retrofitting III – Alexander et al. (eds)
© 2012 Taylor & Francis Group, London, ISBN 978-0-415-89952-9

Shear assessment of solid slab bridges

E.O.L. Lantsoght, C. van der Veen & J.C. Walraven
Delft University of Technology, Delft, The Netherlands

ABSTRACT: The capacity of solid slab bridges in shear is assessed by comparing the design beam shear resistance to the design value of the applied shear force due to the permanent actions and traffic loads. The transverse distribution of loads which occurs in slabs is thus not taken into account. Experiments on slabs under concentrated loads are carried out at Delft University of Technology. The results of these experiments are the basis for recommendations for the assessment of solid slab bridges. A slab factor and a horizontal load spreading method to determine the effective width are proposed. Preliminary results from an additional series of experiments confirm the hypothesis of superposition.

1 INTRODUCTION

As a result of increased traffic loads and intensities, the demands on bridges that were built several decades ago, are higher than calculated with the governing codes at the time of design. In the Netherlands, 600 reinforced concrete solid slab bridges are under discussion. A global assessment of the existing slab bridges ("Quick Scan method") aims at providing a fast and simple tool to evaluate these slab bridges (Walraven 2010).

In current practice, the shear capacity of one-way slabs is calculated based on semi-empirical formulas derived from beam shear experiments. The full width is replaced by the effective slab width, which depends on the chosen horizontal load spreading method. In Dutch practice horizontal load spreading is assumed under a 45° angle from the center of the load towards the support. In French practice (Chauvel et al. 2007), load spreading is assumed under a 45° angle from the far corners of the loading plate towards the support (Fig. 1). Taking the sources of additional capacity, such as the transverse load distribution capacity of slabs, into account leads to a better estimate of the physical bearing capacity, such that retrofitting might become unnecessary.

2 EXPERIMENTS

In the first series of experiments, a total of 30 specimens are tested, on which 133 experiments are carried out. The following parameters are varied in the experiments: the distance between the load and the support, the moment distribution at the support, the amount of transverse flexural reinforcement, plain bars as compared to deformed bars, the size of the loading plate, line supports versus elastomeric bearings, the concrete compressive strength, the location of the load along the width and the total width. This paper shows the properties and results of S15 to S18; the results of the slabs on line supports (S1 – S14) and the slab strips (BS1 – BX3) are reported by Lantsoght et al. (2011a, b).

3 BASIS FOR RECOMMENDATIONS

A database of 207 experiments on wide beams and slabs (Lantsoght 2011a) is compiled. The database is subdivided into different categories: simply supported slabs, continuously supported slabs, bridges tested in the field and cantilevering slabs. The failure mode (wide beam shear failure, punching shear failure or a combination of both) is determined based on pictures or drawings of the crack patterns from the original sources.

A comparison between all experimental results (both from the experiments at Delft University of Technology and the experiments from the slab database) and the values calculated with EN 1992-1-1:2005 is carried out, taking into account two methods of horizontal load spreading. These

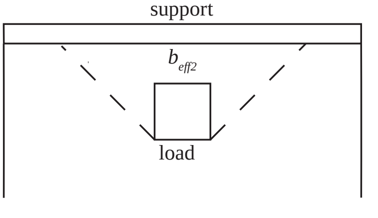

Figure 1. Effective width assuming 45° horizontal load spreading from the far corners of the load: b_{eff2}; top view of slab.

results show that the load spreading method from Figure 1 is to be preferred. Also, experiments on a series of specimens with increasing widths: 0.5 m, 1 m, 1.5 m, 2 m and 2.5 m indicate the existence of the effective width. Comparing the effective width as calculated from these experiments to the effective width as determined based on a horizontal load spreading method, confirms that the load spreading method from Figure 1 gives the best results. The minimum effective width of $4d_l$ becomes governing when the load is placed close to the support ($a/d_l = 1.51$) and near the edge (Lantsoght 2011b).

To take into account the higher shear capacities of slabs as a result of transverse load distribution, the introduction of a slab factor of 1.25 is proposed (Lantsoght 2011b). The slab factor can be used to reduce the contribution of concentrated loads to the total shear force.

4 RESULTS

It is advised to use EN 1992-1-1:2005, taking into account the factor $\beta = a_v/2d_l$ for the reduction of the loads close to the support, which can be combined with the slab factor for concentrated loads of 1.25 into $\beta_{new} = a_v/(2d_l \times 1.25) = a_v/2.5d_l$. The results of $V_{TU}/V_{EC,beff2}$ (V_{TU} = the ultimate shear force as observed in the experiments; $V_{EC,beff2}$ = the shear capacity as calculated form EN 1992-1-1:2005 using b_{eff2} form Fig. 1) when using all the recommendations are given in Table 1, which show that the suggested approach is conservative, even when assuming normal distributions (characteristic value (Char) = average (AVG) – 1.64 standard deviation (STD)).

Based on the load model from EN 1991-2:2002, the most unfavorable position of the wheel loads can be determined. Previously, this position was determined by placing the face of the first axle at a clear distance (a_v) of d_l from the support. The traditional load spreading method resulting in the effective width b_{eff1} was used. This results in the axle load of 300 kN then being spread over a small effective width, leading to a large contribution to the shear force v_{Ed} [kN/m].

By using $\beta_{new} = a_v/2.5d_l$ the most unfavorable position based on the load model from EN 1991-2:2002 becomes the position leading to a clear shear span a_v of $2.5d_l$. Placing the load further away from the support than in current practice leads to a larger effective width over which the first axle load is spread and thus a smaller contribution to the total shear load v_{Ed} [kN/m].

The unity checks for 8 practical cases are carried out at 3 sections per case. The checks are done first according the Dutch Code NEN 6720 combined with its corresponding most unfavorable position for the trucks, and then according to EN 1992-1-1:2005 with the recommendations. While the shear force has significantly decreased by using the recommendations, the maximum shear stress cannot be easily compared.

Table 1. Comparison between experimental results and calculated shear capacity taking the recommendations into account.

Specimens	AVG	STD	COV	Char
all slabs	1.24	0.14	11%	1.01
S1–S10	1.25	0.14	12%	1.01
Plain bars: S11–S14	1.16	0.12	10%	0.96
Elastomeric bearings: S15–S18	1.29	0.10	8.1%	1.11

5 THE HYPOTHESIS OF SUPERPOSITION

The described method assumes that superposition of the reduced contribution of the wheel load (determined from the slab shear tests) over the effective width with the uniformly distributed traffic loads and the dead loads can be applied. To study this hypothesis, a series of slabs is subjected to a combination of a line load, resulting in 50% of the ultimate shear stress found as an average from BS1 and BS3, and a concentrated load. If the principle of superposition holds true, then the shear stress (calculated over b_{eff2}) of the experiment with a concentrated load only, $\tau_{tot,cl}$, should be similar to the sum of the shear stress due to the loads which act over the full width b (line load, dead load and vertical prestressing load), τ_{line}, with the shear stress due to the concentrated load acting over b_{eff2}, τ_{conc}. The first results seem to confirm the hypothesis of the superposition of a reduced concentrated load with a line load.

6 CONCLUSIONS

For the assessment of solid slab bridges, it is recommended to combine EN 1992-1-1:2005 with $\beta_{new} = a_v/2.5d_l$ and calculate the effective width based on the load spreading method as used in French practice, with a minimum of $4d_l$. These recommendations are supported by a large series of experiments from Delft University of Technology, as well as a database of experiments from the literature. As a result, the most unfavorable position of the wheel loads in the load model from EN 1991-2:2002 is found by placing the face of the first axle load at $2.5d_l$ from the face of the support. Preliminary results from a second series on experiments of slabs under a combination of loads show that the hypothesis of superposition holds true when the concentrated load is spread over the effective width resulting from the recommended load spreading method.

Concrete Repair, Rehabilitation and Retrofitting III – Alexander et al. (eds)
© 2012 Taylor & Francis Group, London, ISBN 978-0-415-89952-9

Upgrading of bridges across rivers to resist ship impact

R. Wensauer, M. Keuser & R. Lenner
Institute of Structural Engineering at the University of German Armed Forces, Munich, Germany

W. Keuser
VE Engineering, Koblenz, Germany

ABSTRACT: A change in the ship traffic volume is expected as a result of upgrading of many European waterways. Correlated to improved waterways passage is the increase of ship size and frequency of larger ships. On one hand, the ecological and economic advantages of upgrading process cannot be disputed, but on the other hand, the changed shipping traffic results in additional risks, especially to bridge substructures. Most of current bridges were built more than 30 years ago and were generally not dimensioned for horizontal forces expected from a large ship impact. Due to the increased capacity and the presence of larger ships the bridge substructures are expected to withstand much higher impact loads. These loads can be taken into account in the design of new structures. However, the bulk of existing bridges must be assessed concerning the higher load and if necessary strengthened.

1 INTRODUCTION

Ships are very efficient transportation equipment for mass goods, especially with consideration of the ever increasing ships capacity. On one hand the ecological and economical advantages of larger ships cannot be disputed, but on the other hand, the new situation in shipping traffic also results in some negative effects. Most of bridges, which were built more than 30 years ago, were designed only for relatively small horizontal forces (relevant at the time of design) resulting from a ship impact. Due to the higher capacity of the upgraded waterways and the resulting utilization by heavier ships, the possible impact force on a bridge also significantly increases.

2 REGULATIONS IN EUROCODE AND DIN

Horizontal loads resulting from the effect of a ship impact were much smaller in the older codes and guidelines, when compared to those in the actual Eurocode (DIN EN 1991-1-7 2010). With the increased use and the development of inland waterways in the last few years the regulations in Eurocode and German engineer standards, were also updated and the increased traffic loads were adjusted.

For a bridge, which shall serve as an example in the further text of this contribution, only 500 kN force has been applied as an impact load. Such load is only a fraction of about the 10 MN load, as described by the current codes for the actual ship traffic accounting for much larger ships.

3 THEORETICAL PRINCIPLES

Ship impact load cases are not simple problems, due to many complex variables involved. In one case, a heavy weight, high stiffness object collides with a stiff element—a bridge pier made of concrete or masonry. In other case the object collides with a comparably soft object—protective elements or a sheet pile wall. This issue has been examined in detail by the German Federal Institute for Hydraulic Engineering. In DIN Fachbericht 101 (2003) the concept of a realistic approach to the determination of shock loads based on a probabilistic safety concept is shown. Hence the basic parameters for a both safe and economical consideration of ship impact have been provided.

There are basically two different bridge impact scenarios. The geometry dictates, whether the ship impacts the bridge on the superstructure or the substructure. In many cases the impact on both has to be considered. The main focus of this article is the impact on bridge pier.

Subjected to the maximum value of the dynamic impact force F_{dyn} there are two different types of force-time functions. It needs to be distinguished between the elastic and the plastic impact. The elastic approximation can be only assumed to the upper limit of 5 MN dynamic force. When the maximum dynamic load exceeds the limiting 5 MN value a plastic impact needs to be considered.

In order to calculate the internal forces in the structure resulting from the impact a static equivalent load can be chosen as an alternative for minimization of the complexity. The static equivalent load can be described by Equation 1.

$$F_{stat} = F_{dyn} \cdot DLF \quad (1)$$

Where the dynamic load factor (*DLF*) has a value of 1.3 for all dynamic loads over 10 MN and a value of 1.7 for loads less than 5 MN. Intermediate values of the *DLF* may be interpolated.

4 SHIP IMPACT EXAMPLE

4.1 *Bridge description*

The example bridge is a prestressed concrete box girder with five spans crossing the river Main as a part of the federal road B 26 with a total length of 227m and with a radius of 500 m. The bridge was completed in 1971. The superstructure consists of a single box girder with a 9.3 m roadway width between the railings.

4.2 *Numerical calculations*

In the numerical calculations two different models of the structure were used: a simple cantilever model (A) and the whole structure (B). Results are listed in Table 1 & 2.

The calculated average internal force value reduction in comparison to the results obtained by the static equivalent load applied on the simplified cantilever system can be observed. The results highlight the fact that the resulting internal forces at the Pier 20 decrease almost by 50% when a more detailed and more realistic modeling of the entire structural system is utilized.

Table 1. Calculated bending moment and shear force for Pier 20 (System A).

Load	Static calculation	Dyn. cal. linear	%	Dyn. cal nonlinear	%
M [kNm]	82745	63648	77	61897	75
Q [kN]	12350	9500	77	9024	73

Table 2. Calculated bending moment and shear force for Pier 20 (System B).

Load	Dyn. cal. linear	%	Dyn. cal nonlinear	%
M [kNm]	38827	47	44810	54
Q [kN]	7023	57	7521	61

5 CONCEPTS FOR STRENGTHENING OF THE BRIDGE

5.1 *General aspects*

Three essential components have to be considered regarding bridge upgrading in terms of resisting the loads resulting from a ship impact on the bridge substructure.

5.2 *Foundation*

To ensure the safety against sliding and overturning the existing foundation can be supplemented with additional piling. Special piles with suitable characteristics should be utilized. Normally, the construction space for strengthening is quite limited; hence the emphasis should be given to the possibility of installing the additional piles with small machines and tools and with as little vibrations as possible.

5.3 *Bridge pier*

One of the easiest ways to strengthen a bridge pier is through addition of a reinforcement layer.

As a first step the surface of the existing pier has to be roughened by sand or water jets. After the installation of additional steel reinforcement including stirrups, shotcrete can be used as quite simple way to place the concrete. Concrete layer ensures the protection of the steel against corrosion and at the same time it secures the transfer of forces between the new and the old structure through the achieve bond.

6 CONCLUSION

In summary, it can be stated that it is possible to design/strengthen bridges against impact loads with more economy when a dynamic linear or nonlinear calculation is utilized in calculation of internal forces.

For the construction of new bridges and especially for the strengthening of old bridges, the structural engineer should find individual solutions for each object consistently with the local conditions. The main focus should be aimed towards the bridge foundation, the piers and the bearing systems.

REFERENCES

DIN EN 1991-1-7. 2010. Eurocode 1: *Einwirkungen auf Tragwerke–Teil 1–7: Allgemeine Einwirkungen—Außergewöhnliche Einwirkungen.* Berlin: Beuth Verlag.

DIN Fachbericht 101. 2003. *Einwirkungen auf Brücken*. Berlin: Beuth Verlag.

Concrete Repair, Rehabilitation and Retrofitting III – Alexander et al. (eds)
© 2012 Taylor & Francis Group, London, ISBN 978-0-415-89952-9

Through-life management of LPS dwelling blocks, including their structural assessment for accidental loads and actions

S.L. Matthews
BRE Ltd., Garston, Watford, UK
Joint-Convener fib Special Activity Group 7: Assessment and Interventions upon Existing Structures

B. Reeves
BRE Ltd., Garston, Watford, UK

ABSTRACT: Societal and sustainability are drivers which are generally encouraging the extension of the service life of existing buildings. In the UK there are many high rise Large Panel System (LPS) built dwelling blocks, generally constructed in the 1960's, which are expected to remain in service for an extended period. This poses challenges because LPS dwelling blocks in the UK are treated as a special class of building as a result of the collapse in 1968 of one corner of Ronan Point, a 22 storey LPS dwelling block situated in London, following a piped gas explosion. As these buildings continue to age, and some have now been in service for over 45 years, deterioration processes are expected to affect aspects of their future performance.

Owners of LPS dwelling blocks have an ongoing responsibility for the safety of these blocks, which requires their periodic inspection and structural assessment. Historically the guidance used for structural assessment of LPS dwelling blocks for accidental loads has been the Ministry of Housing and Local Government Circulars 62–68 and 71–68 (MHLG 1968a & 1968b), produced in 1968 shortly after the Ronan Point incident. These MHLG Circulars, along with other related guidance from that era, were never withdrawn and notionally remain in force today. However, this guidance has become outdated by subsequent developments.

The paper outlines an approach to the through-life management of LPS dwelling blocks, together with associated procedures for their structural assessment for accidental loads and actions. This is based upon the outcomes of a programme of work carried out by BRE over an extended period (mid-1990's to 2011) to develop new guidance, which was recently published as BRE Report 511 '*Handbook for the structural assessment of large panel system (LPS) dwelling blocks for accidental loading*' (Matthews & Reeves 2012).

1 INTRODUCTION

The structural hazards to which LPS dwelling blocks are exposed include internal and external gas explosions, fire, as well as the possibility of impacts arising from road vehicles, trains and aircraft. Whilst the probability of the accidental occurrence of these hazards is very small, from a historical perspective overpressure loading and damage arising from an internal gas explosion in an LPS dwelling block has been the type of accidental loading raising the greatest concern.

The BRE programme of load testing of three existing LPS dwelling blocks established that they were able to resist a simulated overpressure in excess of 17kN/m^2, which means they would have been able to resist the accidental loads associated with a severe internal gas explosion which might occur in a building without a piped-gas supply.

Even though the risks of structural damage and collapse arising from these hazards might be *"regarded as insignificant and adequately controlled"* (HSE 2002), there is still a need for LPS dwelling blocks to be assessed and managed in accordance with ALARP principles, which are central to the UK approach to health and safety management. This concept guides the approach and methodology described below.

2 METHODOLOGY FOR THE THROUGH-LIFE MANAGEMENT OF LPS BLOCKS

To establish appropriate procedures and processes for the through-life management of an LPS dwelling block, consideration needs to be given to the following (presented as an indicative sequence of activities/issues to be addressed):

1. Hazards and risk environment associated with internal gas explosions, external gas explosions and vehicular impacts to establish threats and

potential accidental loads and actions to be considered.
2. Environmental conditions within and outside the LPS dwelling block which influence its current condition and its future durability.
3. The performance and assessment requirements for the LPS dwelling block; by reference to the LPS block characteristics considering details such as the number of floors, the presence of a basement, the existence of a piped gas supply, the anticipated future service life required etc.
4. Managing the risks associated with LPS dwelling blocks by adopting risk assessment procedures and by using hazard elimination and risk reduction measures, which are likely to include the provision of diagrammatic warning/prohibition signs in the public areas within an LPS dwelling block explaining the hazards associated with the use or storage of potentially explosive substances within the block.
5. Establishing proportionality criteria for hazard and risk reduction measures.
6. Undertaking a structural assessment of the LPS dwelling block for accidental loads and actions to identify risks that are not *"regarded as insignificant and adequately controlled"*.
7. Establishing whether the LPS dwelling block complies with the structural assessment requirements for accidental loading. This involves meeting one or more of the LPS assessment criteria, LPS Criteria 1 to 3.
8. Alternatively, if the LPS dwelling block does not satisfy the above (LPS Criteria 1 to 3), establish what structural works need to be undertaken to enhance the safety/collapse resistance/reduce the prospect of progressive collapse or disproportionate damage—structural strengthening options are discussed in Section 13 of Matthews & Reeves (2012).
9. Establishing proportionality criteria for structural works undertaken to enhance the safety/collapse resistance/reduce the prospect of progressive collapse or disproportionate damage.
10. Implementing the structural works required to enhance the safety/collapse resistance/reduce the prospect of progressive collapse or disproportionate damage where risks are not *"regarded as insignificant and adequately controlled"*.
11. Establishing whether the LPS dwelling block is adequately durable for the anticipated future service life required. This requires a prognosis of the durability and deterioration effects, together with any associated implications for the structural performance of the LPS dwelling block over the period until the next proposed structural assessment is undertaken—refer Section 10.3 of Matthews & Reeves (2012).
12. If the estimated durability is not adequate, establishing what preventive or remedial interventions are required to meet the future service life required.
13. Implementing the durability related works considered to be required.
14. Updating of the overall through-life management strategy following strengthening or other actions. Establishing a regime for the ongoing durability inspection and monitoring of the LPS dwelling block, with appropriate links to a periodic structural assessment of the block. Preferably using a risk-based philosophy. Further details of the suggested supporting regime involving periodic inspection, monitoring and structural assessment activities are given in Section 12.9 of Matthews & Reeves (2012).
15. If one does not exist, establishing and maintaining a service life/assessment history file containing all technical data relating to an LPS block (i.e. assessment/inspection reports, maintenance records, remedial works details, drawings etc.). Such records, which may also be referred to by other terms such as a technical log/technical file, are expected to be kept by current health and safety legislation.

ACKNOWLEDGEMENTS

The paper draws on previous BRE research projects and the authors acknowledge this material and the valued contributions made by current and former BRE colleagues, the funding bodies, and the assistance given by other organisations.

REFERENCES

HSE. 2002. *Reducing risks, protecting people.* Health and Safety Executive (HSE), London.

Matthews, S.L. & Reeves, B. 2012. *Handbook for the structural assessment of large panel system (LPS) dwelling blocks for accidental loading',* Building Research Establishment (BRE) Report 511, IHS-BRE Press, Bracknell, UK.

MHLG 1968a. *Flats constructed with precast concrete panels. Appraisal and strengthening of existing high blocks: Design of new blocks.* Ministry of Housing and Local Government (MHLG) Circular 62/68, London.

MHLG 1968b. *Flats constructed with precast concrete panels. Appraisal and strengthening of existing high blocks: Design of new blocks.* MHLG Circular 71/68, London.

Concrete Repair, Rehabilitation and Retrofitting III – Alexander et al. (eds)
© 2012 Taylor & Francis Group, London, ISBN 978-0-415-89952-9

Condition assessment and repair of concrete tunnel lining after fire

K. Mavar & E. Marušić
Institute IGH d.d., Zagreb, Croatia

ABSTRACT: Principle influence of fire i.e. high temperatures in concrete are physical changes (loss of compressive strength, tensile strength, modulus of elasticity, increase of porosity, spalling and cracking) and chemical decomposition of certain components in concrete depending on temperature reached (calcium hydroxide at 400°C, limestone at 900–1000°C).

In this paper a case study of Tunnel St Elijah through mountain Biokovo will be presented. Its secondary concrete tunnel lining was exposed to high temperature when formwork caught fire. Concrete was 10–16 hours old. The first performed visual inspection revealed different coloration on area caught in a fire. It depends on distance of centre of fire, position of formwork during fire and direction of wind. By visual inspection, the positions for in-situ testing and cores drilling for laboratory testing were determined. Those included the following: determination of compression strength and density on samples from sound and discolored concrete and comparison of values, determination of adhesive strength by pull off testing on sound areas and discolored areas, difference between Schmidt hammer test results, determination of loss on ignition to establish if decomposition of C-S-H gel occurred. Test results, condition assessment and repair of secondary concrete tunnel lining will be presented.

1 INTRODUCTION

During the performance of secondary concrete lining there was a spontaneous ignition from which the fire spread to the rest of the tunnel. The exact time of a fire is not known, so the age of burned concrete class C25/30 was estimated less than 16 hours.

Scope and area for testing and samples' examination were based on concrete surfaces color changes. When exposed to high temperatures, concrete with limestone aggregate changes color according to the literature. This change is permanent, so it can be used to estimate damage areas.

2 INVESTIGATION WORKS

The object of field investigation was to determine the condition of concrete and steel reinforcement of secondary lining of the tunnel after fire ignites inside the tunnel cladding. Activities performed

Figure 1. The view from bellow at the burned section after tunnel's scaffolding have been moved to the previous section.

Figure 2. The view from below on the top of arch at the junction of concrete and reinforced section—directly above the fire centre.

Classification of damage with a tentative proposal for rehabilitation

Area position	Concrete visual appearance	Damage	Damage category	The necessary undertakings
Segment 1 – area of approx 40 cm, with deep crack	Burned appearance, dark gray—tan color	Concrete with altered properties where there is likely to internal stratification	**V**	Complete removal of 50 cm wide zone, at full depth; concrete repair
Segments 1 & 2 (3 m length), above the height of 4,6 m		Deep cracks to the first reinforcement layer (5–7 cm), decreased strength and density, concrete does not meet the requirement for C25/30. Apparent increased porosity of the surface layer of concrete. Bond strength of concrete surface layer 1–2 cm significantly reduced.	**IV**	Removing concrete layer of approx. 7 cm thick, concrete repair (patching mortars)
Segment 3, above the height of 4,6 m	Concrete gray color, a shade lighter than common concrete	Several thin crack depth of about 3 cm, reducing strength and density. The resulting strength is reduced compared to the sound strength of concrete, but significantly greater than the minimum strength requirements for the C25/30.	**III**	Removing the layer of concrete approx. 3 cm thick, from the 4,6 m height to the top, concrete repair mortars
Segments 4, 5, 6 & 7 above the height of 4,6 m	Largely irregular dark gray spots	Crack mesh (about 1 cm depth). The compressive strength meets the requirements of the designed class C25/30. At the height of 4.6 m to 5.6 my entire 7 segment color changes are significantly smaller	**III**	Surface protection and removal of concrete thickness of approx. 1 cm in area where there are dark spots or mesh of cracks; surface repair of concrete
The sides of the tunnel lining up to 4,6 m	The gray color of concrete	There are no cracks. There is segregation, which is the result of installation. The resulting strength meets the requirements of the designed class C25/30.	**I**	Nothing

on the damaged and sound concrete were visual inspection, then compressive strength and density, surface adhesion strength, Schmidt hammer rebound, and loss on ignition testing.

2.1 *The final classification of damages*

Concrete has sustained expected damage. The greatest reduction in compressive strength, density and adhesion strength of the surface layer of concrete, which indicates a significant reduction in tensile strength of concrete and the cracks, occurred in the zone which was located directly above the centre of the fire. The change of appearance and color of concrete is consistent to the test results conclusions. Concrete of the areas adjacent to the area that has suffered the greatest damage has a number of cracks with depth to 3 cm.

Concrete of the other parts of the observed section, higher than 4,6 m, despite the reduction in compressive strength compared to the sound concrete, is satisfying the conditions of class C25/30.

Concrete below the height of 4,6 m has not suffered damage due to fire.

Apart from pollution, reinforcement bars did not suffered significant damage.

Final classification of damages and necessary undertakings are given at following table.

3 REHABILITATION DESIGN

Rehabilitation works includes replacement of damaged concrete tunnel lining in a 7 cm thick layers (at areas closer to the fire), i.e. the thickness of 1 cm (at areas further to the fire). That includes hydrodynamic removal of concrete layers in both thickness and application of new shotcrete of designed class C25/30 at 6 cm layer and fine restoration mortar class R3 at 1 cm thickness (in order to smooth the concrete surface).

4 DISCUSSION

The paper shows scope of investigation works and condition assessment which have to be accomplished for any damaged reinforced concrete structure prior to repair design.

In the case of tunnel concrete lining exposed to fire, degradation of concrete is detected by concrete de-coloration and cracks occurring, by determination of concrete compressive and adhesion strength reduction and by loss on ignition.

Repair works design has to be performed according to principles and methods given at norm HRN EN 1504-9:2008; which includes removal of concrete layers of different thickness and application of new layers of structural concretes and mortars.

Theme 3: Concrete repair, rehabilitation and retrofitting

Repair methods, materials and techniques

This page intentionally left blank

Concrete Repair, Rehabilitation and Retrofitting III – Alexander et al. (eds)
© 2012 Taylor & Francis Group, London, ISBN 978-0-415-89952-9

Random thoughts on concrete repair specifications' ills and treatment prescriptions

R.M. Snover
Appledore Marine Engineering, Inc., Portsmouth, NH, USA

A.M. Vaysburd
Vaycon Consulting, Baltimore, MD, USA

B. Bissonnette
Laval University, Quebec, Canada

D.F. Burke
US Navy Engineering Service Center, Port Hueneme, CA, USA

1 INTRODUCTION

The present situation with regards to repair specifications demonstrate that many of them are confusing, misleading, and contribute to the problems, instead of contributing to solutions (Fig. 2). This situation can be generally categorized in terms of army slang: "SNAFU"—Situation Normal, All Fouled-Up.

2 A GLIMPSE AT SPECIFICATIONS

The specifications are as important and critical for meeting the performance requirements as the structural design of the project. Too often specification work is delegated to an employee of minor rank compared to that of the designer. Specifications should be as carefully "crafted" as structural analysis and details of a project, and should be carefully tailored to each situation. They should be, therefore entrusted only to engineers with broad experience in concrete technology and understanding of design, construction, materials, durability aspects, inspection, and a progressive philosophy of concrete repair engineering. Creative specifications require experts willing to use progressive ideas, common sense, to think a project through, and in the strength of their knowledge and convictions stand up and defend their provisions, if need be.

It makes no sense to reference "direction by the Engineer", as is presently common practice in many specifications. The study and knowledge of what really is required will usually eliminate need for these meaningless phrases leaving an impression that the specifier is uninformed or lazy. It is also an unfortunate fact that some engineers who are intended by specifications to direct, are not always "literate" enough in concrete technology. Why should a contractor and his staff put their best foot forward if they are to be shot down at every important turn by an engineer who maybe is not qualified "to direct"? Also such an uncertainty in specifications makes sound project bidding impossible. It is a game of "Russian Roulette" to work with such specifications.

3 DURABILITY ISSUES

The true qualification of the term "durability" in concrete repair is its expected useful service life to the next remedial action, or to the replacement of the structure. Several issues concerning the durability factors to be addresses in concrete repair specifications are discussed herein.

3.1 *Permeability*

Of course, the material's micropermeability has to be considered and limited, but only after the issues of macropermeability are successfully addressed by specifying an allowable drying shrinkage value and specifying the ASTM C 1581, "Standard Test Method for Determining Age at Cracking and Induced Tensile Stress Characteristics of Mortar and Concrete under Restrained Shrinkage".

Not a single case of setting the limit for drying shrinkage, when concrete is specified as a repair material, was found during a review of numerous concrete repair specifications. When pre-packaged repair materials are specified, the limits of available shrinkage value may be provided, but without any indication at what age this limit should be met, making such requirements of little value.

3.2 *Repair materials*

There is a widespread common misconception in specifications that the use of high-strength repair materials, not compatible with the concrete substrate, is beneficial. Not a single specification was found to provide limits for maximum allowable compressive strength of hardened repair material. This unjustifiable trend ignores the well-known fact that a stronger and stiffer cementitious material is more likely to crack, because the higher modulus of elasticity increases the tensile stress arising from drying shrinkage and other restrained volume changes.

The strength gain acceleration in cementitious materials has a negative effect on their transport properties. Based on the analysis presented above, it can be concluded that for concrete and other cementitious materials, especially those exposed to severe environments, the rate of strength gain is critical to durability. Materials with slow strength gain, for instance those containing fly ash or slag, might perform more satisfactorily under these conditions.

Specification of high early-strength repair materials should be avoided wherever possible. Rather, if practical, the 100% ultimate compressive strength should be specified at a stage later than the traditional 28 days. The specified compressive strength should not be in excess of what is necessary for load-carrying purposes. Actual 'in-place' 28 days compressive strengths should be kept at levels similar to the 'specified' strength, which should be similar to the existing substrate.

4 PERFORMANCE VS. PRESCRIPTIVE SPECIFICATIONS

Performance specifications are becoming quite popular lately, and, in general, it is not a bad idea in the concrete repair field. However, challenging as they may be, performance requirements often cannot be successfully adapted and used to the exclusion of prescriptive specifications until required performance criteria and reliable evaluative techniques have been developed and widely accepted. This need can be met only through continuing effective research and development. Many specified performance requirements are not more than bold statements simply because there are no practical means to control them. If a particular property, characteristic or other specified item cannot be practically tested, measured, or controlled it should not be specified.

With respect to the performance requirements for repair materials, the situation can be greatly improved by following the guidance of the ACI 546.3R, "Guide for the Selection of Materials for the Repair of Concrete". Nevertheless, many other repair characteristics, such as electrochemical activities, are practically unpredictable.

Caution needs to be exercised in establishing performance requirements for repairing corrosion-affected structures subject to chloride and marine environments. The performance approach may be applicable where the potential future performance is well understood. However, it is unsuitable in cases of corrosion-affected structures being repaired because there is no proven link between available testing methods and actual in-situ performance.

The risk of continuing corrosion and even its acceleration due to the electrochemical incompatibility between "old" and "new" is always present, unless the "global" cathodic protection is addressed.

The synergetic effects of several critical diverse environments present along the electrically continuous reinforcement in addition to differentials in stress states, significantly add to the complexity of the problem. The influence of the repair phase on the existing phase, change in chemical composition, distribution of aggressive agents, oxygen, moisture, and other factors on the electrochemical properties of the repair system all need to be considered, but guidance to do so does not exist. This is why a successful repair of a corrosion-affected structure lasting without problems for 10–15 years is more of a "holy grail", than a reality.

Another concern with the concept of performance specifications is associated with awarding of repair work contracts based solely on the basis of "lowest-bid." Specialized repair contract bidding and award system should in fact be awarded to contractors having relevant experience and that are pre-qualified to complete specialized concrete repair work. It is critically important that both performance and prescriptive specifications contain Contractor, Worker, Field Test Technician, and QC Inspector qualification requirements in the Submittal and Quality Assurance sections. Qualification requirements should include submitting evidence of recent concrete repair experience and that the QC Inspector be a licensed Professional Engineer. Unfortunately, the specified qualification requirements, if any, are still too often disregarded in the bidding process.

At the same time it has to be recognized that even prescriptive specifications cannot realistically contain instructions on every single step needed to achieve the final goal. This would be overwhelming and even confusing in practice.

5 CONCLUDING REMARKS

The concrete repair specifications for "true" durability advocated in this paper is a complex engineering task requiring extensive knowledge of science, engineering and field practices. It also entails considerable standards of responsibility on the part of the professionals developing specifications. Too often, concrete repair is perceived as the problem, rather than the solution. The engineer/specifier has to choose to be either a part of the solution or the part of the problem.

While repair failures cannot be treated as a prerogative of incompetence of the engineer/specifier, it would be irresponsible on the part of the engineer to ignore them as mere mischance and hide them away. Instead, it is necessary to take a close look at the shortcomings, misconceptions and mistakes, analyze them and learn the right lessons to prevent future repair failures.

Concrete Repair, Rehabilitation and Retrofitting III – Alexander et al. (eds)
 ISBN 978-0-415-89952-9

Concrete repair as an engineering task: An approximate solution to an exact problem

A.M. Vaysburd
Vaycon Consulting, Baltimore, Maryland, USA

P.H. Emmons
Structural Group, Hanover, Maryland, USA

B. Bissonnette
Laval University, Quebec City, Canada

ABSTRACT: The condition of the world infrastructure and the present economic difficulties demand high-end repair projects to be designed and executed. Some of these projects are underway, and there seems to be little doubt that more and more will be carried out in the coming years. However, at the same time, a large amount of repair projects are being designed and constructed based on sketchy, inadequate condition evaluation of the existing conditions. Such projects often result in premature failures. Durability planning and setting realistic service life objectives are impossible without comprehensive condition evaluation, which allows the ability to establish the exact problems and their causes. Repair projects are open-end projects with usually several alternative "approximate" solutions to address the problems of the concrete structure in trouble. For the repair project to be successful, the "approximate" solution must address the exact problem. The very best design, materials, and workmanship will fail if the exact problems of the structure and their causes are unknown and only the symptoms are addressed. The problems of repair durability and service life are discussed in this paper in terms of critical importance of comprehensive and reliable condition evaluation (pathology investigation) and durability planning prior to detailed design and specifications.

1 INTRODUCTION

By definition concrete repair is generally an action taken to reinstate, to an acceptable level, the current functionality of a structure or its components that are defective, deteriorated, degraded or damaged in some way, and it should be completed without restriction upon the materials or methods employed.

The absence of such restrictions makes the repair solution an open-end "approximate" solution.

In repair, after all, the purpose should be that of the "Mikado" of Gilbert and Sullivan fame, which was to make the punishment fit the crime. Therefore, to meet such a purpose, the crime must be established.

What, then, defines concrete repair as an engineering task? The authors would like to define it as an open-end "approximate" solution to an exact problem. And in case of repair, in our opinion, an approximate solution to the exact problem is more meaningful in assuring performance than the exact solution to an approximate problem.

Unfortunately, often the repair solutions are approximate solutions to approximate problems.

In addition to condition evaluation problems and solutions, this paper discusses the durability planning measures that should be considered prior to detailed design and specification process in order to eliminate or minimize the need for premature repair of repairs. The role of durability planning in deciding on which remedial and/or protection solutions are more appropriate to meet project objectives durability and economy-wise and perform more satisfactorily is addressed.

2 CONDITION EVALUATION TASK

A durable repair project cannot be successfully designed if the designer does not know precisely the problems, their extent and what caused them to occur.

Establishing the cause(s) carries three main difficulties. The first is that no two repair cases are ever identical. Every case should be analyzed and judged on its own merits. The second is an inadequate understanding of electrochemical behavior of steel exposed to various environments.

The final is that malperformance usually represents the combined effect of several factors. Usually some of these factors lead the way to contributory action of the others, but it can be difficult to perceive which are affected initial damage.

One cannot evaluate the concrete structure and its troubles that one does not thoroughly understand. A better understanding of concrete as a composite material and embedded in it reinforcing steel, and of the context of particular structure made from those and their interference with service environment, etc., will certainly make the condition evaluation engineer aware that he has directed his efforts to real problems instead of factors of secondary importance or no importance at all. For instance, it makes very little sense to have blind reliance in analysis of causes on parameters, such as chloride threshold number, permeability of concrete based on the results of the ASTM C 1202 test, etc.

3 SAMPLING

It is important, prior to sampling and testing, to (a) decide what information is desired from the evaluation and (b) choose the evaluation procedure such that necessary information can be obtained efficiently and economically. Once these decisions are made, the type and amount of data required can be logically deduced, the sampling plan can be selected, and the data obtained.

Moisture is essential to most of the types of deterioration that affects reinforced concrete. However, very seldom moisture condition of concrete in different parts of the structure is being tested.

Electrical resistivity of concrete is often a neglected issue in condition evaluation. The electrical resistivity of concrete is critical for electrochemical processes, corrosion activities, and corrosion mitigation. The resistivity depends on:

– the water content of the concrete,
– the degree of water continuity (cracks, voids, porosity), and
– the moisture conductivity in the porous system (chloride and other chemicals content, temperature).

4 STRUCTURAL ISSUES

The overall condition of a concrete structure, its durability and deterioration status is very much influenced by the structural system itself. For example, structures with many joints are much less durable than more monolithic structures. In the case of bridges and navy piers, for instance, joints are perhaps the single biggest cause of premature deterioration of the bridge components.

It should be noted the mistakes and shortcomings very common in condition evaluation reports where nature and cause of cracking is concerned.

It is clear to an engineer, or at least it must be, that cracks are always due to the fact that the stress exceeds the material strength. Stresses are always the cause of cracking or discontinuities produced in materials. Stresses may be induced by several actions, such as:

– restrained strains due to drying or thermal shrinkage,
– loads,
– local swelling (e.g., steel corrosion products, ettringite formation),
– differential settlements, and/or
– alkali-aggregate reaction products.

In all of the above cases, the basic mechanism of cracking is the exiding of extensibility of cement-based material when it is subjected to tensile stresses.

The sad reality is that very seldom the tensile strength (i.e., direct tensile strength) of existing concrete is being tested and reported in condition evaluation documents.

5 INTERNAL ENVIRONMENT

Without an internal environmental condition in evaluated existing structure and prevailing transport processes input from the adequately performed and documented condition evaluation, the necessary considerations of the possible deterioration and transport processes in a new composite repair system would be impossible. The basic rule of thumb is that reducing transport processes will normally improve durability.

6 DURABILITY PLANNING

Durability planning must become a fundamental part of the repair design process that affects the specifications and detailed design and needs to be carried out before specifications and drawings are prepared.

Three basic questions need to be considered before the appropriateness of remedial actions can be finalized.

1. What is the cause of deterioration?
2. Can steps be taken to slow or stop the processes?
3. What are the structural consequences of the existing and projected damage?

The adequate condition evaluation, the engineering task of finding the exact problems with existing concrete structure, allows us to learn the enemy's plan of attack and develop defensive tactics and alternative solutions, not always by frontal attack, but sometimes by flanking movement or just continuing to further watch the enemy's actions. After all, there are always several choices, based on comprehensive assessment of condition evaluation:

- replacement,
- repair and/or strengthening,
- protection, and/or
- doing nothing and continuing to monitor.

Repair options each have advantages and limitations that are pertinent to a specific structure and specific project objectives, and these should be considered in the durability planning phase of the project. The durability planning has to take into account the constraints of lack of control of ambient conditions, accessibility to the repair location, downtime for completion of the work, the need to keep facility open while repairs are being carried out, etc.

In durability planning, it is very important to realize the importance of materials to be used to replace the deteriorated concrete. The repair material must be compatible with existing substrate and crack-resistant. There are no universally good materials; there are no magic "high-performance" materials. There are horses for courses. The whole myth of "high-performance" cementitious materials, the whole fallacy of it, is built-up by attributing impossible properties to non-existent materials.

7 REPORTING

The writing of the report requires much careful thought, review and drafting. The meaning of each sentence must be critically examined. The report will often be used by non-technical readers and lawyers, and it must therefore be simple and clear, based on factual data, technically accurate, precise and objective in approach.

Any reservations or limitations implicitly in methods and technique employed or interpretations of results should be clearly stated.

Concrete Repair, Rehabilitation and Retrofitting III – Alexander et al. (eds)
© 2012 Taylor & Francis Group, London, ISBN 978-0-415-89952-9

Concrete repair materials, polymers and green chemistry—how far synergistic are they?

Anjan K. Chatterjee
Conmat Technologies Private Limited, Salt Lake, Kolkata, India

ABSTRACT: Repair, restoration and renewal are unavoidable measures in extending the service life of concrete structures. The materials used, to start with, were based on Portland Cement in the form of mortars, concrete, shotcrete, etc. Because of their intrinsic deficiencies in many instances of actual repairs, there has been a preferred shift towards total or partial substitution of Portland Cement with polymeric or monomeric binders. In the process a significant departure is observed from the demands of green chemistry and associated sustainability requirements. This article is an attempt to highlight this issue along with the emerging corrective strategies to synergize the repairs systems with green chemistry.

1 INTRODUCTION

Global investments for maintenance, repair and restoration of concrete structures are continuously on an increasing trend. As all buildings are generally unique with own histories, individual solutions become necessary for their maintenance and repair. This, in turn, has led to the developments of different strategies and solutions including material development. Towards this objective the use of polymers has turned out to be almost imperative.

2 CONCRETE REPAIR MATERIALS

Going by the circumstances prevailing in the past, the first generation repair materials were developed on the basis of hydraulic cement alone. Although these materials, such as the dry pack mortar, preplaced aggregate concrete, shotcrete, replacement concrete, etc., are still being used, they suffer from shortcomings of delayed setting and hardening, low tensile strength, unsuitability for thin section repair, injectability difficulties, poor bond strength, etc. These shortcomings led to the extensive introduction of polymeric materials in partial of full replacement of the hydraulic binders. As a result, materials like epoxy-bonded dry pack mortars, organo-hydraulic grout-injected preplaced aggregate concrete, epoxy resin bonded concrete or prepacked polymer concretes came into wider application. Apart from surface or patch repairs, acrylic and epoxy resins, alkyl-alkoxy silane monomers, polymeric siloxane, etc, are being used for hydrophobic treatment of concrete with varying performance. Epoxy and polyurethane resins are in use for crack repairs in different environmental conditions. The exterior use of these organic materials has solved some problems and created many others.

By way of illustrations the problems pertaining to the use of epoxy resin, methacrylate monomer, vinyl ester resin, polyurethane, etc. have been briefly dealt with in the main paper. The problems obviously relate to sustainability, safety, health and environment in multiple ways. It, therefore, becomes necessary to synergize the use of polymeric substances with green chemistry concepts.

3 CONCEPTS OF GREEN CHEMISTRY

There are twelve principles of green chemistry as detailed in the main paper, which can be grouped in five key statements: use of fewer chemicals, solvents and energy; safe raw materials; process and solvents; efficient process without wastes to the extent possible.; wastes, if at all, should be degradable; sustainability or renewability of raw materials, solvents and energy. These green concepts in the present instance should be realized both in product selection and product application.

4 STRATEGY FOR SYNERGIZING REPAIRS WITH GREEN CHEMISTRY

The first approach is to select polymers made through benign synthesis routes. It is well known that these processes in general involve primarily certain ingredients including solvents. Attempts are being made to develop new reaction processes using green ingredients and solvents. For example, it is possible to eliminate the use of phosgene in the production of urethane; similarly one may look forward to the use of non-petrochemical solvents like ethyl lactate in the coatings industry.

The second step is to promote the use of low VOC emulsions in the paints and varnishes.

The third important avenue is to use more extensively organo-hydraulic composites rather than pure polymer mortars and concretes for repair purposes.

The fourth measure is to encourage the development of novel environment friendly repair systems. The adoption of glass systems in sewage plants with high risk of biogenous sulfuric acid attack or a shift towards nano-technology in coatings or promotion of anti-bacterial protection with nano-silver particles are the future directions of embracing green chemistry.

5 CONCLUSIONS

Concrete repair can have a larger contribution to the environmental impact of a structure than a new construction on a unit volume basis. The premature loss of embodied energy in the concrete is compounded by the removal and disposal of deteriorated concrete. Use of traditional polymeric repair materials with larger environmental impacts further adds to the problems of deviating from green chemistry and sustainability. Selection of polymers made with more benign synthesis, use of non-petrochemical solvents, application of low VOC emulsions, development of newer protective systems with inorganic glass or nano particles, etc. are some of the avenues to explore in synergizing the concrete repair systems with green chemistry and sustainability. Demolition of concrete structures is specially energy intensive. Because of this, the prevention of the need to repair concrete is much more beneficial to the environment and it is more cost-effective when the strategy of service life extension is adopted.

Concrete Repair, Rehabilitation and Retrofitting III – Alexander et al. (eds)
 ISBN 978-0-415-89952-9

Performance and service life of repairs of concrete structures in The Netherlands

J.H.M. Visser & Q.F. van Zon
TNO Build Environment and Geosciences, The Netherlands

ABSTRACT: In 2010, an inventory to the performance of repairs in the Netherlands has been executed, in response to reported low performances of repairs in an European inventory conducted five years earlier. The results indicate that the failure rates of the Dutch repairs are similar to that of the European failure rates: ca. 20% failed within 5 years and 90% failed within 25 years. The failure of the repairs mostly was contributed to an insufficient execution (50%), in contrast to the European investigation. Here, more than 50% of the failure was contributed to incorrect diagnosis or incorrect design of the repair. The service life of most repairs was difficult to establish since either it had not yet ended or because the precise moment of failure (inside or outside the required service life) could not be established.

1 INTRODUCTION

From 2002 to 2006, a European investigation to the performance of repairs of concrete structures has been executed (Tilly & Jacobs, 2007). This research, called ConRepNet, was started in reply to the general impression that the performance of the current concrete repairs is mediocre. Although this impression was expressed throughout Europe, no study was available anywhere that could either confirm or deny it. ConRepNet collected a total of 230 repair cases from practice to establish the performance. Analyses of the results indicated among others that 20% of the repairs had failed within 5 years after application, while 55% failed within 10 year and 90% within 25 years.

The high failure rates in the ConRepNet project raised the question in the Netherlands whether these failure rates were also applicable in this country. With more and more performance based maintenance contracts being defined, designed and under execution, an answer to this question was badly in need. Therefore, a similar inventory as in ConRepNet was conducted specifically for the Netherlands.

2 RESULTS AND DISCUSSION

Compared to the European data base of ConRepNet, the Dutch data base is twice as small (230 in ConRepNet versus102 in the Dutch data base). For both, the data bases are small with respect to their total populations. The interpretations and discussions in this chapter therefore have to be considered with some caution.

2.1 *Failure of the structures*

In the Dutch research, the observed cause of failure on the basis of which the structures have been repaired consisted of more than 50% of a too low cover thickness. In all these cases, this was accompanied with corrosion of the reinforcement. The corrosion was in half of the cases initiated by carbonation. Also other defects such as aggregate clusters, shrinkage cracks and other types of cracks resulted in corrosion. In the European research, cause and effect have been presented as one population. Similar interpretations as for the Dutch case therefore cannot be made. However, in more than half of the cases also corrosion of the reinforcement was observed but in only approximately 10% a too low cover thickness is reported. Tilly & Jacobs (2007) remarked that this low percentage is unlikely. They speculated that it might be a consequence of a lack of recognition of this construction error.

2.2 *Performance of the repairs*

In Figure 1, the failure rates of the Dutch repairs compared to the European repairs are shown. After 5 years, a failure rate of 20% was found in the European research. In the Dutch case, the percentage is somewhat lower (12%). After 10 years, the failure rates are almost similar. Further comparison of the database in not possible because the number of data in these classes are too small. The small differences in failure rates and the smallness of the data bases considered, there is no reason to presume that the failure rates of the repairs in the Netherlands are different from those in Europe.

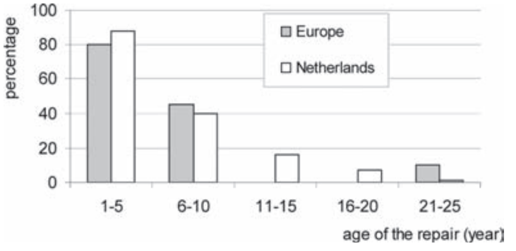

Figure 1. Performance of the repairs with age, expressed as percentage still well performing repairs.

2.3 *Cause of failure of the repairs*

In the Dutch case, approximately half of the failure of the repairs were contributed to a bad or unsuitable execution, whereas use of unsuitable material is mentioned approximately 25%. Errors in diagnoses or design of the repair system are mentioned less than 10%. In Europe the incorrect design of the repair or diagnoses of the cause of damage of the structure was reported as cause of failure (54%). In the Netherlands, this seems to be less of a problem: a wrong diagnosis or design was reported as cause of failure of the repair only in 9%.

The way the repairs fail in the European research mostly was correlated to a wrong diagnosis. This includes ongoing corrosion but also ongoing damage due to ASR and leakage. Collected in four main classes of failure (debonding, corrosion, cracking and 'other'), the distributions of the cause of failure in the two researches are comparable.

2.4 *Service life assessment of the repairs*

For the Dutch data base, an assessment of the service life of the repairs was made. In 26 cases, a service life was demanded. These varied between 1 year (short term repair prior to replacement) to 100 year (too low cover for a just completed structure). Of the 16 failed repairs, only in two cases it could be proven that they failed within their required service life. Of three other cases, it was uncertain if they had failed within their service life because the inspection took place well beyond their required service life and on the hand of the inspection reports no failure time could be narrowed down. Of the remaining failed repairs, no further information on the requested service life was available.

A similar analysis was made for the repairs that showed first signs of degradation and the repairs that were still looking good. Only one repair case showed degradation within its requested service life, the other cases with degradation being either uncertain (meaning outside their requested service life) or unknown. Similarly, only in two repair cases in good shape it could be proven that they performed well longer then requested, i.e. they were already outside their service life. The others were still in their service period or their service life is unknown.

3 CONCLUSIONS AND RECOMMENDATIONS

The analysis of the collected data with respect to the performance of repairs in the Netherlands shows that there is no reason whatsoever to presume that the failure rates of the repairs in the Netherlands are different from those found in.

It proved to be a considerable effort to collect sufficient and sufficiently detailed data concerning repairs. There is a whole set of reasons for this: missing records, lack of knowledge in various companies with respect to repairs and fragmentation of all the required information among various departments and organizations. To form all the different types and pieces of information into one, coherent data entry proved not always to be possible.

This research has demonstrated that it is possible to determine the service life of repairs, even on the basis of a very simple 3-step criterion (good—start of degradation—failed). It would give a tremendous impulse towards a performance based repair methodology if this was further developed. However, the most beneficial step to take is to record the performance of the repairs on a more regular basis. Then, more cases become available for the current databases. Possibly enough data then can be collected to distinguish between the performances of the various materials, for example as a function of the exposure class and so on. With the current data set this was not possible. Only then a choice of the best performing repair material for the required remaining service life can be made, resulting in a truly performance based choice of repair and maintenance.

REFERENCES

Tilly, G.P. & Jacobs, J. 2007. *Concrete Repairs: Performance In Service And Current Practice*, Watford: BRE Press.

Visser, J.H.M. & van Zon, Q.F. 2010. *Performance of Repairs of Concrete Structures. Phase 1. Inventory Repairs.* TNO Report TNO-03402010–04985 Delft: TNO.

Concrete Repair, Rehabilitation and Retrofitting III – Alexander et al. (eds)
© 2012 Taylor & Francis Group, London, ISBN 978-0-415-89952-9

Development of repair mortars for the restoration of natural stone in cultural heritage

P. Ramge & H.-C. Kühne
BAM Federal Institute for Materials Research and Testing, Berlin, Germany

ABSTRACT: Compared with concrete repair, the repair of natural stone is generally a similar task but at the same time very different. For listed buildings and monuments, historical, cultural and aesthetical interests become the ruling parameters. Especially from the demands of total reversibility of repair measures and strict prevention of the slightest original substance loss, which are not known in concrete repair, various restrictions are derived. From an aesthetical point of view, the same appearance as the original stone is desired for the mortar, whereas from a technical point of view, a monolithic behaviour of the repaired stone with homogeneous material properties would be favoured. This creates a need for a multitude of different property combinations and the whish for an independent adjustability of technical and aesthetical properties. A research project dealing with the development and optimisation of modular stone repair mortars is currently carried out at BAM Federal Institute for Materials Research and Testing.

1 INTRODUCTION

In cultural heritage preservation the reparation of natural stone is a major task. Worldwide a lot of unique buildings of historical and cultural value are in need of repair and maintenance. The necessity of intervention may be caused by different reasons. The original substance can be damaged due to changing environmental or building physical boundary conditions, due to changed designated use, due to war damage or simply due to the natural degradation of the used material over time. Technically the partial or total replacement of damaged stone by new stone pieces would often be the most reliable and durable solution, but as soon as cultural heritage is involved this is often not an option any more. For the preservation of cultural heritage the preservation of the original substance in the original context deserves the highest priority. Therefore the remodeling of damaged stone with repair mortars is a good solution. As the variation of natural stone is wide, the requirements on stone repair mortars are wide as well, far wider than those on concrete repair mortars.

2 GENERAL REQUIREMENTS ON NATURAL STONE REPAIR

In contrast to concrete repair neither the structural strengthening nor the protection of reinforcement steel play a key role in natural stone repair. However, the need to match the original substance in terms of aesthetical appearance and to provide compatibility in terms of physical, chemical and mechanical properties becomes more pronounced.

3 FIRST EXPERIMENTS

3.1 *Overview*

The aim of the research project RESDOSYS is the development of a repair mortar system on a modular basis. To archive this, various parameter studies will have to be conducted. The experimental studies, which are presented in this paper, deal first of all with the development of a useful basic-mixture that allows the comparable execution of parameter studies in regard to different fields i.e. influence of the sand, of the binder of inert powders, pigments admixtures etc.

For a proper evaluation of parameter studies ideally not more than one parameter should be changed at a time. This is however technically not possible therefore compromises have to be accepted in laboratory practice.

The intention of the first experiments was to evaluate the possibilities to vary the mechanical properties (compressive strength, flexural strength and stiffness) while consistency and the appearance should not change. Aspects of building physics are not subject of these first experiments; they will be studied in further steps of the research project.

For natural stone repair the visual and haptic appearance of the repaired spot is of major interest. For sandstone this appearance is mainly governed by the aggregates of the mortar, i.e. the sand and its volume fraction. Therefore the following considerations are based on volume fractions (bulk volume without air content) and volumetric replacements.

3.2 *Preliminary tests*

In a series of preliminary tests a basic mixture was found, in which a compromise of various demands was found. A mixture setup with three different powder components was selected: two binder components and one inert component. This allows for example a variation of the cement content while water/powder ratio and paste volume can be kept at a constant value.

3.3 *Variation of the binder composition*

The purpose of this test series was to find out if the theoretical idea is working, that it is possible to create a mixture whose mechanical properties (strength, stiffness etc) can be altered while the appearance and the consistency of the fresh mixture remain constant. The ratios of the powder content that originally consists of a strong binder (cement) a weaker binder (hydraulic lime) and an inert filler (limestone powder) in equal parts were changed systematically. 9 mixture compositions were examined in which the powder composition was varied while sand and water as well as the total powder volume remained unchanged.

3.4 *Use of polymer dispersions*

When stiffness and strength are adjusted solely by the variation of the binder content or the binder water ratio, it is often not possible to influence selected properties independently. Polymer dispersions as used in PCC mortars, however, allow the independent alternation of stiffness compressive strength and tensile strength in certain ranges. Two commercial polymer dispersion powders were tested in the basic mixture in different dosages. The aim of this series was to verify the general functionality of the polymer dispersions in mortars with rather low cement content and to find out in which range the stiffness can be altered compared to the alternation range achieved by the binder content variations.

4 RESULTS

4.1 *Variation of binder composition*

Compressive strength, flexural strength and stiffness are significantly ruled by the cement content. The contribution of the hydrated lime is of secondary importance but yet not neglectable. For higher cement contents the influence of the lime gains on impact on the compressive strength. Even though the tendencies are the same for all three properties there are slight differences in the characteristics. The functions are not linear, which becomes more obvious if relations between the properties are regarded. For the prevention of constraining cracks, the ratio of tensile strength to stiffness is of interest. For a wide range of the experiments this value does not change much. Only for cement contents lower than 1/3 of the powder, the ratio decreases strongly which is unfavorable in terms of constraining crack prevention.

For the shrinkage the influence of cement and hydrated lime seem to be equally strong. For the basic mixture setup only the increase of the inert part of the powder can reduce the shrinkage deformations.

For the powder variations the flow diameter fluctuates in a range between 12 and 17 cm. The hydrated lime had the strongest impact on the consistency.

4.2 *Use of polymer dispersions*

The main focus of these experiments was on the mortar's stiffness and its strength/stiffness ratio. With increasing polymer content the stiffness decreases. Compared with the powder variation test row, similar results i.e. a reduction of stiffness from 9500 MPa down to 6500 MPa would be achievable by reducing the cement content in the powder from 33% to about 16%. In this respect the effect of the polymer dispersion does not seem to be dramatic, but it must be taken into account that far better flexural strength/stiffness ratios are obtained.

In normal strength mortars polymer dispersions are known for a reduction of the compressive strength, however, in the range of low strength mortars they significantly increase both the flexural strength and the compressive strength. This effect may however be overruled by other effects, for example by an increased air entry resulting in a higher porosity of the hardened mortar specimens as seen in the presented case.

5 CONCLUSION AND OUTLOOK

The chosen basic mixture proved to be suitable for various parameter studies. The possibility to systematically exchange powder constituents (reactive or inert) while the total powder volume remains constant is an important precondition for comparable parameter studies.

In the further run of the research project parameter studies for the adaption of the colour (use of pigments, use of sand variations) and the texture (variation of the sand grain size, sand grading curve and sand volume) will be necessary, as well as studies on the physical and chemical properties. This should be all possible on the presented basic mixture. Also various admixtures and their interactions need to be investigated.

Concrete Repair, Rehabilitation and Retrofitting III – Alexander et al. (eds)
© 2012 Taylor & Francis Group, London, ISBN 978-0-415-89952-9

Maintenance of aged concrete structures of the Hong Kong Housing Authority

H.W. Pang, Bosco Au & K.C. Lau
Hong Kong Housing Authority, Hong Kong, China

ABSTRACT: The Hong Kong Housing Authority (HKHA) maintains a stock of about 720,000 flats in more than 1,100 reinforced concrete buildings with the oldest ones aged over 50. Driven by the policy to sustain the buildings as far as possible, HKHA launched in 2005 the Comprehensive Structural Investigation Programme (CSIP) to probe into the structural conditions of the older buildings and establish durable repair to prolong their service life. Through the investigations in the past years, considerable experiences were garnered relating to the diagnosis of concrete defects as well as establishment of repair solutions with the deployment of state-of-the-art techniques to effectively cope with the structural problems in aged buildings. This paper outlines the structural investigation methodology, and depicts the techniques of diagnosing root causes of concrete defects as well as the repair strategy and repair solutions for the aged buildings taking into durability, practicability, cost-effectiveness and environmental considerations. Illustrative examples of tailor-made repair methods are also given and discussed.

1 INTRODUCTION

The Hong Kong Housing Authority (HKHA) is the major government institution responsible for constructing public housing and for maintaining its housing stock. The current policy of the HKHA is that redevelopment would be undertaken only when necessary to replace housing blocks which are no longer safe or economic to maintain; or when there would be a significant increase of building area after redeveloping an aged estate. As an essential part of this strategy, the Comprehensive Structural Investigation Programme (CSIP) was launched in 2005 with the purpose of ascertaining structural conditions of the older buildings and established the required repairs to better sustain them.

2 COMPREHENSIVE STRUCTURAL INVESTIGATION PROGRAMME (CSIP)

A five-step approach for the CSIP is adopted embracing 5 major activities as detailed in the following paragraphs.

2.1 *Information search*

The involves the searching for information including repair history kept in the computerised database, record drawings, past appraisal and monitoring reports, past improvement/strengthening work and records of structurally sensitive structures.

2.2 *Visual inspection*

Inspection will record all surface concrete defects and other information relevant to subsequent assessment of the causes of defects in common areas and tenants' flats.

2.3 *Testing*

Tests are carried out at various locations in the buildings to identify the extent and severity of any defects, and to determine the root causes of defects so that effective repair methods can be established.

2.4 *Structural assessment*

Structural analysis will be carried out to assess the structural adequacy of the structure. Durability assessment will also be conducted to determine the susceptibility of the elements to corrosion.

2.5 *Developing repair solutions*

Appropriate repair solution will be developed according to the findings and structural assessment.

3 DIAGNOSTIC TESTS

Testing regimes are tailored on an estate basis, which would involve the use of state-of-the-art testing equipments and techniques, for the purpose of not only identifying the root causes of defects to develop effective repair solutions, but also to collect information for assessing the long-term performance of the buildings and repair so that appropriate actions can be taken to uphold the structures. The tests commonly used in the CSIP are broadly categorized into non-destructive and destructive tests. Non-destructive tests include moisture survey, hammer tapping, covermeter survey, corrosion rate measurement, water ponding test with fluorescent dye, infrared thermography survey, radar scan, half-cell potential survey and concrete resistivity measurement. Destructive tests include carbonation test, core compressive strength test, chloride content test and petrographic analysis.

4 REPAIR SOLUTIONS DEVELOPED THROUGH CSIP

4.1 *Developing repair solutions*

From previous CSIP, we have found that there is a diversity of causes of concrete deterioration and contamination; and conventional repairs were ineffective to address particular structural defects. So we need to establish tailor-made solutions making using of advanced techniques to cope with the problems. Some examples of our repair solutions are as follows.

4.1.1 *Protection against water ingress*

The multi pulse sequencing system, making use of electro osmotic water repelling force, was adopted to stop water seeping into the basements.

4.1.2 *Electrochemical protection*

To avoid 'patch accelerated corrosion' occurring at chloride-laden concrete, a galvanic electrochemical protection system, sacrificial anodes, was put forward to protect the rebar from further corrosion.

4.1.3 *Increasing maintainability*

Access openings were formed to ease inspection and repair to some confined areas with soil pipes inside.

4.1.4 *Improving micro-environments*

To prevent water ingress to the public areas of some domestic buildings, the existing grille block walls were converted to solid walls with windows.

4.1.5 *Concrete restoration*

To avoid disruption to tenants due to decantation of flats with seriously spalled steel bars, the concrete slabs were restored by replacing the defective concrete with high performance concrete sprayed on to the exposed concrete.

4.1.6 *Omitting vulnerable elements*

The concrete fins at external facades vulnerable to deterioration were removed.

4.1.7 *Replacing vulnerable elements*

To avoid repetitive repair of concrete refuse chutes at domestic blocks, they were replaced by more durable aluminum ones.

5 CONCRETE REPAIR STRATEGY—A PEOPLE-ORIENTATED APPROACH

Concrete repair solutions are established taking into consideration not only the durability of repair, cost effectiveness, construction practicability but more importantly the tenants' acceptability and expectation and how disturbance and nuisance can be kept to a minimum.

To avoid the drawback of conventional mechanical methods for removing concrete, hydro-scarification, having the major advantages of causing no adverse effect to concrete and reinforcing bars and largely reducing structural-borne sound and vibration, has been adopted. Used for the first time in Hong Kong, the machines were tailor-made to resolve different constraints at public rental blocks.

6 CONCLUSIONS AND WAY FORWARD

Through the implementation of the CSIP, the HKHA has identified the root causes of defects of her aged buildings and based on which developed repair solutions to effectively cope with the problems, by deploying state-of-the-art techniques and materials so that the repairs would be durable, cost-effective, practicable, people-orientated and environmentally friendly. The HKHA will review the effectiveness of repair through continuous performance monitoring and make further development to better sustain her housing stock.

Concrete Repair, Rehabilitation and Retrofitting III – Alexander et al. (eds)
© 2012 Taylor & Francis Group, London, ISBN 978-0-415-89952-9

Sustainability-focused maintenance strategy for the public rental housing estates in Hong Kong

S.T. Chan, H.W. Pang & Bosco Au
Hong Kong Housing Authority, Hong Kong, China

ABSTRACT: The Hong Kong Housing Authority (HKHA) manages and maintains over 1,100 high rise reinforced concrete buildings. HKHA builds around 15,000 flats in some 20 buildings annually. In 2005, the HKHA embarked on a new maintenance strategy with a view to better sustaining this growing building stock. It embraces structured programmes covering the regular inspection of the tenant-occupied flats, in-depth condition assessment of the older buildings, and the general improvement of the estate to give the tenants a revitalized environment. This paper outlines the key considerations and philosophy behind the three-throng strategy as well as the achievements so far. It points to the need for test-based understanding of actual performance of buildings of advanced age but inferior durability design, for treating maintenance as both a service and work, and for sustaining the estates as communities as well as built entities.

1 INTRODUCTION

Established in 1973, the Hong Kong Housing Authority (HKHA) takes charge of constructing and maintaining majority of public buildings in Hong Kong. HKHA currently is maintaining more than 1,100 buildings comprising over 720,000 flats to accommodate about 2.1 million people. It builds around 15,000 flats annually. Hong Kong's climate is sub-tropical, warm and humid. Effect of acid rain, coastal environment and use of sea water for flushing in the toilets also increase the risk of chloride contamination of the buildings. The inherent problems of earlier design also made the buildings more vulnerable to ingress of water and contaminants into the concrete.

2 THE SUSTAINABILITY-FOCUSED MAINTENANCE STRATEGY

To sustain the aging estates while coping with the changing needs over time of the community, the HKHA establishes her maintenance strategy that can keep the buildings staying sustainable economically, socially and environmentally, which embraces the Total Maintenance Scheme, the Comprehensive Structural Investigation Programme and the Estate Improvement Programme.

3 TOTAL MAINTENANCE SCHEME (TMS)

Launched in 2005, the TMS is carried out at 5-year cycles to buildings aged over 10. This introduces proactive and customer-oriented services to in-flat maintenance. Rather than reacting to complaints or requests for repair, trained In-flat Inspection Ambassadors pay visits to flats to check if repairs are necessary. Minor repairs are carried out on the spot while works orders are issued immediately for more serious problems. The Ambassadors would also make use of the inspection opportunity to educate tenants how to address minor maintenance problems promptly to prevent deterioration. A computerized system has been developed to support the TMS. Inspection findings are recorded on personal digital assistants (PDAs) by the Ambassadors. When repair is required, a works order can be issued immediately with the PDA with a printout to the tenant for record. The maintenance-service-on-request modeled on the TMS, known as Responsive In-flat Maintenance Service (RIMS), is implemented to meet the in-flat maintenance needs of tenants between TMS cycles and for young estates not covered by the TMS. In 2011, the independent customer satisfaction surveys revealed an encouraging customer satisfaction level of 81.3% on the TMS repair, a marked improvement from 43% before the scheme. The TMS work has received a host of awards.

4 COMPREHENSIVE STRUCTURAL INVESTIGATION PROGRAMME (CSIP)

Launched in 2005, the CSIP is carried out to the estates approaching 40 years of age and at 15-year intervals afterwards. This seeks to ascertain whether the estates are structurally safe and economically sustainable, or otherwise needing consideration of clearance. The structural investigation embraces 5 major activities, namely, information search, visual inspection, testing, structural assessment and developing repair solutions. Testing regimes are tailored on an estate basis, which would involve the use of state-of-the-art testing equipments and techniques, for the purpose of identifying the root causes of defects. To effectively address particular structural defects, tailor-made solutions were established, making use of advanced techniques and materials to cope with the problems. So far, more than 40 repair solutions have been developed under the CSIP to address the structural problems in the aged buildings. The repair work was found effective to resolve the structural problems that had long existed. Not only did the CSIP earn the appreciation from the tenants, it won a series of awards to acknowledge its achievement. The CSIP work has also been positively and widely reported by the media.

5 ESTATE IMPROVEMENT PROGRAMME (EIP)

The HKHA implemented the EIP for each old estate after the CSIP, placing great importance in sustaining the older estates in three fronts: economical, social and environmental. The key concerns of the tenants for a particular estate will be found out through surveys and consultation. Improvements will put people first and cater for the needs of different age groups, in particular the elderly, rather than facility-based. Lifts are added to the blocks lacking lift access, and also at estates where large differences exist between the levels of the various building platforms. The estate common areas and non-domestic premises will be brought up to date to suit the tenants' needs. Recreational facilities will be enhanced to cater for different age groups and re-shaping public space for better social interaction including installation of fitness equipment for the elderly. Weather-protected passage and barrier-free access will be integrated into a master pedestrian network to improve pedestrian circulation especially with the needs of the aged and disabled tenants in mind. The external façade and public areas will be face lifted and upgraded to provide a pleasing living environment for the tenants.

6 APPLICATION OF NEW TECHNOLOGY

The HKHA has established tailor-made solutions making using of advanced techniques to cope with the problems that could not be effectively addressed by conventional methods. For instance, we adopt the multi pulse sequencing system to stop water seeping into the basements, sacrificial anodes to protect the rebar from further corrosion, high performance concrete to repair seriously deteriorated elements, hydro-scarification for removing defective concrete to minimize construction noise and vibration, etc. Besides, Radio Frequency Identification (RFID) and PDA are used in routine maintenance.

7 "ECO" CITY

HKHA acts pro-actively to enhance energy efficiency in public housing estates with a view to reducing greenhouse gas emission and providing a green environment to our tenants. A number of energy saving initiatives have been implemented in the past decades and achieved good results.

8 MAINTENANCE AS A SERVICE

To push for quality service, HKHA established a scheme, known as Quality Maintenance Contactor (QMC) Scheme, in 2000 to enroll maintenance contractors who were dedicated to quality reform and cultural change, and able to demonstrate their sound management, good quality of works and reliable service. These QMCs have been given more tender opportunities. The annual public housing recurrent survey saw good results on the satisfaction index related to maintenance services. This rose from 30% in 2001 to 64% in 2011.

9 CONCLUSION AND WAY FORWARD

The HKHA is committed to provide affordable quality housing to meet the needs of her tenants in a proactive and caring manner. HKHA has developed her maintenance strategy centering on sustainability of the estates, focusing on people. The ageing of sitting tenants, ageing of housing buildings, the changing in tenants' expectation and general improving living standard at large do exert high demand on quality of service in maintaining the buildings. Tapping tenant's need in good time and continual enhancing the maintenance practices to suit rising aspiration is a must for sustaining the buildings. HKHA will continue in this direction and will look for improvement in her maintenance practices as well as latest technology advancement to better her housing stock to meet the need of her customers.

Concrete Repair, Rehabilitation and Retrofitting III – Alexander et al. (eds)
 ISBN 978-0-415-89952-9

The effect of pulse current on energy saving during Electrochemical Chloride Extraction (ECE) in concrete

Tian R. Sun, Mette R. Geiker & Lisbeth M. Ottosen
Department of Civil Engineering, Technical University of Denmark, Denmark

ABSTRACT: Energy consumption is a factor influencing the cost of Electrochemical Chloride Extraction (ECE) in concrete. The aims of this work were to investigate the possibility for energy saving when using a pulsed electric field during ECE and the effect of the pulsed current on removal of chloride. Four experiments with artificially polluted concrete under same charge transfer were conducted. Results showed that the energy consumption was decreased 15% by pulse current in experiments with 0.2 mA/cm^2 current density, which was higher than that of 0.1 mA/cm^2 experiments with a decrease of 9.6%. When comparing the voltage drop at different parts of the experimental cells, it was found that the voltage drop of the area across the concrete was the major contributor to energy consumption, and results indicated that the pulse current could decrease the voltage drop of this part by re-distribution of ions in pore fluid during the relaxation period. However, probably due to the observed re-adsorption of chloride by concrete in pulse current, there was no significant difference between constant and pulse current experiments in relation to removal of chloride. Use of an anion exchange membrane impeded the H^+ ions from the anodic reaction entering the concrete, and the pulse current also demonstrated a positive effect on the energy consumption across the membrane by diminishing the concentration polarization.

1 INTRODUCTION

The electrokinetic remediation technology has been wildly utilized on various porous materials. The possibility of removing chlorides from concrete by using an electric current has been shown in previous investigations.

As result of electrode reactions, the electrolyte close to the anode will turn acidic during the ECE treatment. The concrete is not an acid resistant material, and thereby, the exposed concrete surface will be etched and weakened during the ECE. This issue can be avoided by adding a buffer such as lithium borate or calcium hydroxide to the electrolyte, but at same time, this will reduce the efficiency of extraction due to distributing the charge over more ions than in case of using electrolyte. Ion exchange membrane, as an approach hindering selected ions passing, could be introduced to the ECE process. Membrane enhanced electrokinetic remediation technique has been investigated with soil, fly ash, and harbor sediment.

Due to the introduction of external electric field, the energy consumption becomes a factor influencing the application of ECE. It has been reported that the application of pulsed electric field could improve the removal efficiency of chloride from concrete by releasing the bonding chloride at current off period. But no clear investigation about the effect of pulsed electric field on the energy consumption has been given. Therefore, the other objective of this work is to investigate the possibility of a pulsed electric field for energy saving during ECE and the effect on the removal of chloride. The theoretical considerations in the use pulse current are: (i) diminishing the polarization process and (ii) restoring the equilibrium condition at the cement-electrolyte interfaces.

2 EXPERIMENTAL SETUP AND DESIGN

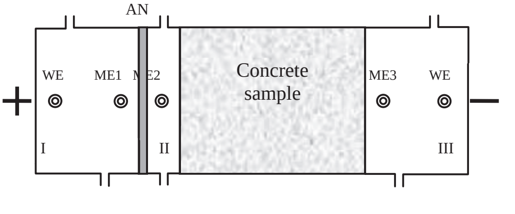

Figure 1. Schematic diagram of the laboratory cell for ECE. (AN = anion exchange membrane, WE = working electrode, ME = monitoring electrode).

Table 1. Experimental design.

Experiments	Current density (mA/cm^2)	Current type	Duration (h)
1C	0.1	Constant	240
1P	0.1	Pulse	360
2C	0.2	Constant	240
2P	0.2	Pulse	360

3 RESULTS AND DISCUSSION

3.1 *Energy consumption*

Figure 2 shows the variation of voltage (between working electrodes) as a function of experimental time.

In general it can be seen that the voltage increased with the increasing of current density since 1C, 1P and 2C, 2P were comparable. For each experiment, after a period of initial increasing, the voltage decreased with time. This is probably due to the transport of OH^- ions from the cathodic reaction into the concrete. OH^- ions have a much higher mobility than other negative ions. A comparison of constant and pulse current experiments showed that the voltage of pulse current experiments were lower than that of constant current experiments although with different extents, which means that the pulse current showed positive effect for energy saving in these experiments.

3.2 *Removal of chloride*

The residual concentration of chloride in the concrete slices after treatment is shown in Figure 3. It can be seen that the chloride concentration in each slice was lower than initial value.

The removal of chloride from the concrete was highly related to the applied current density, the removal efficiency (defined as the decrease in chloride mass divided by the initial chloride mass) in 2C (59%) and 2P (59%) was higher than that in 1C (43%) and 1P (45%). However, there was no significant difference of chloride removal between constant and pulse current experiments for any of the current densities.

The energy consumption was 1.7, 1.5 and 4.7, 4.0 Wh per percent removed chloride in 1C, 1P and 2C, 2P, respectively. In slice 2-4, the chloride concentrations in the pulse current experiments were lower than that those of the constant current experiments. Re-equilibrium between bound and free chlorides gave rise to a high conductivity at the pore fluid during the relaxation period. However, in slice 1, a reverse phenomenon was observed in which the chloride concentration in

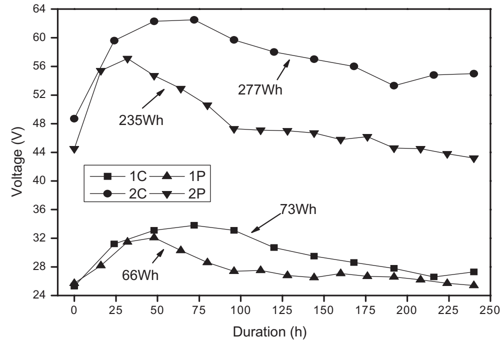

Figure 2. Voltage variation between working electrodes.

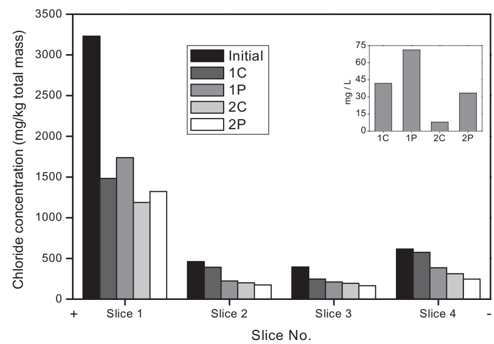

Figure 3. Chloride concentration of each slice in concrete after the treatments. The superimposed graph is the chloride concentration in compartment II of each experiment.

the pulse current experiments was higher. This could be explained by the transport by diffusion and re-adsorption of chloride from compartment II when the current was switched off. The superimposed figure in Figure 3 is the chloride concentration in compartment II, and it shows that the chloride concentration in the pulse current experiments was higher than that of constant current experiments. This is probably due to the interdiffusion between Cl^- ions from the anolyte and OH^- ions from compartment II, since the diffusion of Cl^- ions from the anolyte will be restricted by the diffusion potential.

ACKNOWLEDGEMENT

The reported work was done based on the financial support from the Department of Civil Engineering at the Technical University of Denmark.

Concrete Repair, Rehabilitation and Retrofitting III – Alexander et al. (eds)
 ISBN 978-0-415-89952-9

Modern repair technique for an ancient temple

R. Anupadma, M.S. Mathews & G. Appa Rao
Department of Civil Engineering, Indian Institute of Technology Madras, Chennai, India

T. Satyamurthy
REACH Foundation, Chennai, India

ABSTRACT: The Kailasanatha temple, a 1250 years old temple is located in Utteramerur, Kancheepuram district, Tamil Nadu. The superstructure of the temple is made of brick masonry, which is seated over granite stone basement. The cracks which have appeared in the stone basement were repaired using 'stone stitching method', which is popular under concrete fastening techniques and is implemented on the stone basement. Before the implementation, miniature samples were prepared and tested in the laboratory. They were stitched using steel bars in the normal and inclined to the crack direction. The cracks were bound together and drill holes were made across the cracks. Anchor bars were arranged in the drilled holes after proper cleaning, followed by filling with chemical agent for bonding. After curing, the stitched miniature samples were tested under flexure and shear loading conditions. The test results showed that the stitched miniature samples were found to carry the expected load. Further, as the embedment depth of the anchor bars increased, the load carrying capacity was found to increase.

Keywords: Modern technique, stone stitching, repair, load carrying capacity, embedment length, Utteramerur, Ancient temple.

1 INTRODUCTION

Post-installed bonded anchors, which have been developed recently, are used extensively in practice. An adhesive or bonded anchor is simply a reinforcement bar or a threaded rod inserted into a predrilled hole in hardened concrete, whose diameter is slightly greater than the diameter of the anchor. Typically the drill hole diameter is only 10 to 25 percentage larger than the diameter of the anchor rod. The gap between the drill hole surface and the anchor surface is filled with an adhesive as a bonding agent between the concrete and the steel after setting and hardening. The anchors transfer the loads to concrete through mechanical interlock, friction, chemical bond or combination thereof. The anchorages facilitate for attachment of structural systems. Anchorage system must be designed to ensure durability and robustness, and should also have sufficient load carrying capacity and deformability. Fastening techniques are used for joining old concrete-to-old concrete or old concrete-to-new concrete.

The failure load is best described by uniform bond stress model incorporating the nominal anchor diameter, d with mean bond stress, τ associated with the adhesive (Cook et al. 1998). The above explained fastening technique used for concrete, is tested and implemented for the stitching of stones. Up till now similar damages were conserved or repaired using the existing techniques like by means of supports or by using iron bands or steel stirrups (Lakshmana Murthy, 1997). But very few of these were derived as an output from research. One such innovative repair method is stone stitching, which is test with laboratory experiments on granite and sandstone samples. This method is implemented on the conservation of Kailasanatha temple, Uttaramerur, Kancheepuram, Tamilnadu with granite substructure. As most monuments in north India are made of sandstone, sandstone samples were also tested.

2 SUMMARY

The experiments were carried out in the laboratory based on concepts of repairing RC structures and implemented on stone samples. The samples were tested to find the load carrying capacity of the repaired beams in comparison with reference beams. Reference samples were the beams made of the stone to be used for repairing the temple at site. The testing was carried out in 3 stages based on working stress method for reinforced concrete beams. In the first stage, reference beams were tested to obtain their flexure and shear capacities. From the test results on the reference beams, appropriate steel reinforcing bars and their sizes were calculated.

With both granite and sandstones, the load carrying capacity of the stitched beams was found to be better than that of the reference beams. In the repaired granite beams under shear, diagonal cracks were formed. In shear loading granite beams exhibited failure before reaching their target load due to inadequate embedment length. Hence the beam dimensions were varied to increase the embedment length and the beams were tested. Embedment length was provided equally on either side of the crack.

It clearly shows that the load carrying capacity of the beams with increased embedment length increased. The stitched region of the beam was found to be intact. Shear cracks did not propagate in the repaired area, were formed next to the repaired zone. In the repaired sandstone beam tested in shear, diagonal cracks were formed. The stitched region was found to be intact and the cracks occurred away from the repaired area, showing that the technique was successful. Totally 36 beams made from granite and sandstone were tested in flexure and shear loading. Thus, this system was experimentally proved successful for repairing the stone beams and is proposed for both granite and sandstone monuments. This method is implemented in Kailasanatha temple, Utteramerur.

The Kailasanatha temple, a 1250 years old temple is located in a heritage village, Utteramerur, Kancheepuram district, Tamil Nadu. The temple was built towards the end of 8th century. The temple is made of brick super structure seated over a stone basement. The temple before restoration was in total ruins, with dense vegetation growing over its Vimana. Masonry on the exterior of superstructure was also damaged at places. Several cracks were found in the granite basement. The plinth's granite slab has moved from its original position. The Vimana was conserved and restored, using state-of-the-art techniques. Its broken stucco figurines were re-created.

The challenge of reconstructing stone base was solved using an innovative technique called stone stitching. Using this technique, the cracks in the plinth were stitched with stainless steel rods and water proof epoxy based chemical anchor without disturbing the original structure. The load bearing capacity was tested and proved to be sufficient through laboratory testing of granite sample beams.

With results drawn from laboratory experiments, it was found that the stitching would bear desired load. Thus we confidently implemented the technique at site. Holes were drilled along the cracks at alternate locations in the cross inward direction. The holes were cleaned and chemical anchor was filled in. Corrosion resistant, stainless steel rods were then inserted and finished with parent rock powder to hide the repair work.

3 CONCLUSION

An attempt has been made to evolve a research based repair method for structural damages. Stone stitching method has been developed and evaluated. The reference beams were tested under flexure and shear and the failure loads were recorded and compared with the repaired beams. In flexure, the embedment length and rod sizes were derived as per working stress method and found that the load carrying capacities of repaired beams were increased.

In shear loading, granite beams failed due to insufficient embedment length. Further increase of embedment length, the load carrying capacities were found to be satisfactory. Sandstone samples performed well under shear loading. Hence stone stitching method is suggested to overcome structural damages in granite as well as sandstone monuments. This finding was implemented as a trial application in Kailasanatha temple, Utteramerur.

REFERENCES

Cook, R.A., Kunz, J. & Fuchs, W. 1998. Adhesive anchor under tensile loading, *ACI Journal:* 9–25.

Lakshmana Murthy K. 1997. Structural conservation of monuments in south India (1), *Sundeep Prakashan, New Delhi, 1997*.

Concrete Repair, Rehabilitation and Retrofitting III – Alexander et al. (eds)
© 2012 Taylor & Francis Group, London, ISBN 978-0-415-89952-9

Repair of deteriorated concrete containing recycled aggregates

A. Badr
Advanced Engineering & Sciences, University of Bolton, UK

L. McGivern
Civil Engineering, University of Bolton, UK

ABSTRACT: Research into concrete repair techniques, repair mortars and test practices is extensive. However, there is scant information on the repair of deteriorated concrete made with recycled aggregates. This paper reports the results of an experimental program aiming to assess the suitability of current repair methods for more modern, sustainable concretes such as those containing recycled aggregate. The results proved that concretes made with recycled aggregates could be successfully repaired to form monolithic elements that act compositely and exhibit properties close to the original non-deteriorated specimen.

1 INTRODUCTION

The construction industry is a massive consumer of natural resources and is considered a main producer of waste. Therefore, sustainable construction has become a great concern in major construction activities (Cachim 2009). As part of the construction industry, the concrete industry is looking for ways of making the production of concrete more environmentally friendly. Recycling construction waste into concrete is a promising way towards sustainable construction. Indeed, there is extensive research into the use of recycled aggregate and waste glass into concrete at different replacement levels (Rao et al. 2007, Rahal 2007, Shayan & Xu 2004, Xiao et al. 2012).

If concrete is to be considered a truly sustainable material, repair and strengthening techniques are required, suitable for both traditional and 'modern' concrete containing recycled constituents. The concrete industry realizes the need for effective techniques of repairing deteriorated concrete structures. However, there is little information about the repair of concrete made with recycled aggregate.

The aim of this research was to investigate the feasibility of repairing deteriorated concrete made with recycled aggregate and waste glass.

2 MATERIALS, MIXES AND REPAIR

2.1 *Materials for original mixes*

Natural limestone (LM), recycled aggregate (RA) and waste glass (WG) were used. The nominal aggregate size on all cases was 100 mm. The compositions of the three mixes used are given in Table 1.

2.2 *Materials for repair mortars*

Portland cement mortars (PC), rapid hardening mortar (RH), and a proprietary quick set mortar (QS) were used in the proportions shown in Table 2.

2.3 *Repair of damaged and deteriorated specimens*

Cube and cylinder specimens were loaded to failure and then used as damaged specimens to be repaired.

Cube specimens have been deteriorated by being subjected to freeze-thaw cycles inside an environmental chamber. Details are given in Badr (2010).

The damaged and deteriorated specimens were repaired by 'jacketing' using the repair mortars.

Table 1. Mix proportions (kg/per m^3) of original mixes.

Mix ID	CEM1	Limestone	Recycled	Glass	Sand	w/c	Slump
LM	407	892	–	–	895	0.4	70
RA	407	446	355	–	895	0.4	40
GW	407	446	–	403	895	0.4	50

Table 2. Mix proportions (kg/per m^3) of repair mortars.

ID	CEM1 N	CEM1 RH	QS Mor	Sand	PPF	Water	SP
PC	524	–	–	1223	9	262	52
RH	–	524	–	1223	9	262	52
QS	–	–	1743	–	–	327	–

3 RESULTS AND DISCUSSION

3.1 *Effect of recycled coarse aggregate*

The compressive strength of original and repaired specimens can be seen in Figure 1. The average restored compressive strength due to repair was about 80% of the original strength. The control specimens without recycled aggregate (mix LM) restored 79% of the original strength. The corresponding values for specimens with recycled aggregate (mix RA) and glass (mix GW) were 75% and 86%, respectively. Therefore, it is suggested that repairing specimens containing recycled aggregate or glass was as successful as repairing specimens made with limestone.

Similar results were obtained for restored splitting strength. The control specimens restored 83% whereas, the corresponding values for specimens with recycled aggregate and glass were 85% and 89%.

3.2 *Effect of type of repair mortar*

The effect of the type of the mortar can be detected from Figure 2. The best performance was obtained from specimens repaired using the ready mixed mortar (QS). In fact, the restored strength (41.5 MPa) was more than the original strength (29.3 MPa) representing an increase of more than 40%. However, the laboratory prepared repair mortars (PC & RH) provided satisfactory repair by restoring more than three quarters of the original strength, with slight advantage of the Portland cement mortar PC.

3.3 *Bond with repair mortar*

Figure 3 demonstrates that the failure is caused by cracks initiated and propagated within the repair mortar. There was no sign of delamination between the original concrete and the repair mortar, confirming satisfactory bond.

4 CONCLUSIONS

For the concrete and test conditions used in this investigation, the following conclusions are made:

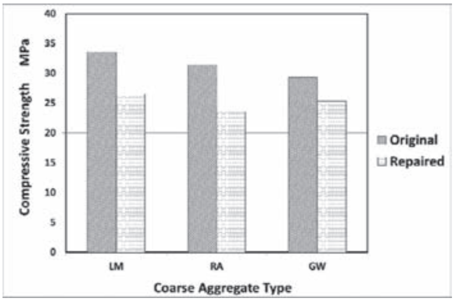

Figure 1. Compressive strength of specimens repaired with RH.

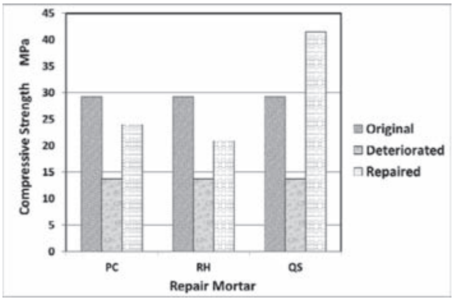

Figure 2. Effect of type of repair mortar on restored strength.

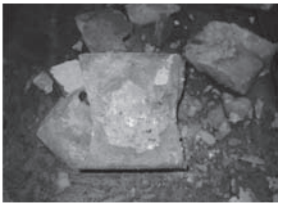

Figure 3. Repaired cube specimen after compression test.

- Concrete specimens containing recycled coarse aggregate or waste glass could be repaired successfully using conventional repair mortars designed for conventional concrete.
- Control specimens without RA restored 79% of the original compressive strength. The corresponding values for specimens with recycled aggregate and glass were 75% and 86%. Similar trend was observed for splitting tensile strength.

REFERENCES

Badr, A. 2010. Freeze-thaw durability of Portland cement and silica fume concretes. In Costa-Borges et al. (eds), *Concrete under Severe Conditions,* CRC Press, (1): 559–666.

Cachim, P.B. 2009. Mechanical properties of brick aggregate concrete. *Construction and Building Materials,* 23(10): 1292–1297.

Park, S.B., Lee, B.C. & Kim, J.H. 2004. Studies on mechanical properties of concrete containing waste glass aggregate. *Cement and Concrete Research,* 34(12): 2181–2189.

Rahal, K. 2007. Mechanical properties of concrete with recycled coarse aggregate. *Building and Environment*, 42(1): 407–415.

Rao, A., Jha, K.N. & Misra, S. 2007. Use of aggregates from recycled construction and demolition waste in concrete. *Resources, Conservation and Recycling*, 50(1): 71–81.

Shayan, A. & Xu, A. 2004. Value-added utilization of waste glass in concrete. *Cement and Concrete Research,* 34(1): 81–89.

Xiao, J., Li, W., Fan, Y. & Huang X. 2012. An overview of study on recycled aggregate concrete in China (1996–2011). *Construction and Building Materials,* 31(6): 364–383.

Concrete Repair, Rehabilitation and Retrofitting III – Alexander et al. (eds)
© 2012 Taylor & Francis Group, London, ISBN 978-0-415-89952-9

Physico-chemical properties and durability of polymer modified repair materials

I.L. Tchetgnia-Ngassam, F. Lespinasse, S. Marceau & T. Chaussadent
Université Paris-Est, IFSTTAR, MAT, Paris, France

ABSTRACT: The proprietary materials used to repair concrete structures are often polymer-modified hydraulic binders. The influence of the presence of polymer on the properties of these composites has been studied, but few works have focused on the evolution of these properties when the material is applied on a structure exposed to an environment that can be aggressive to concrete. In this paper, the properties of polymer-modified mortars made in the laboratory are reported and compared to those obtained on similar commercial products but whose precise composition is unknown. Thus, the influence of the type and quantity of polymer on the consistency, the setting time, the microstructure, the porosity and the mechanical properties of the mortars are analyzed. Special attention is given to the study of the influence of the curing conditions on the final properties of the hardened material.

1 INTRODUCTION

Repair of concrete structures has become essential to extend the service life of infrastructures in agreement with sustainable development policies. Actually, considerable resources are used to rehabilitate damaged concrete structures. The main degradation observed is due to corrosion. It induces large financial costs spent each year for the repair of deteriorated concrete works. Moreover, despite multiple repair solutions, repair failures, as cracking or debonding of the coating, occur frequently within ten years, involving short-term interventions and additional costs of repair and service interruptions (Guettala & Abibsi 2006).

Accordingly, proprietary repair products have been formulated to match the demands of the field. These materials can be classified in two types: classical hydraulic mortars or polymer-modified mortars. The polymers used for the modification of mortars are generally latex or redispersable powders. During the setting of the material, chemical reactions take place between polymers and ions in the pore solution of mortars and/or on the surface of cement particles during hydration leading to the hardened microstructure (Ohama 1998). After hardening, a network structure is obtained, where cement hydrates and polymer interpenetrate to form a co-matrix (Beeldens et al. 2005).

The overall objective of our project is to investigate the durability of repairs carried out using polymer-modified cementitious materials after aging in different exposure conditions. The influence of the presence of polymer and of the curing conditions on the properties of the hardened materials at short and long term is especially studied.

For this aim, seven proprietary polymer-modified mortars used for repair have been studied in order to determine their properties. However, the precise composition of these materials is unknown. Accordingly, polymer-modified mortars, whose composition is controlled, have been prepared in the laboratory. The first results of this study are presented in this article, concerning the effect of type and quantity of polymer in the mortar on the physico-chemical, microstructural and mechanical properties of the materials. The properties of the proprietary and of the laboratory-made products will be compared.

2 EXPERIMENTAL

Seven proprietary repair materials (CM1 to CM7) were selected to represent the generic type of polymer-modified repair mortars that are used for the repair of deteriorated concrete.

In addition to these commercial mortars, polymer-modified mortars were also prepared in the laboratory. They are based on ordinary Portland cement and standard sand CEN 196-1. Two commercially available polymer powders (SA and EVA) were used.

The consistency of the mortars has been fitted by adjusting the water-to-cement (W/C) ratio, in order to obtain the average value measured for the commercial products.

After casting, three different curing conditions have been used in order to assess the influence

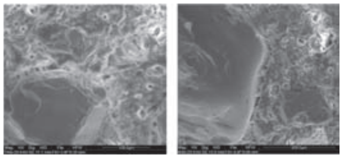

Figure 1. Interface between the cement paste and an aggregate in a 20% EVA-modified mortar.

of the curing conditions on the properties of the hardened mortars:

- water immersion cure: the samples are immersed in 20°C water, corresponding to the recommended cure for pure hydraulic mortars (EN 1504),
- dry cure: 21°C and 60 ± 10% RH, corresponding to the recommended cure for polymer-modified mortars (EN 1504),
- hot cure: 40°C, corresponding to a hot-dry environment on a repair yard.

3 RESULTS AND DISCUSSION

The global properties of the proprietary and of the laboratory-made mortars are in the same order of magnitude.

The addition of polymer in mortars improves its workability and the amount of water to add to achieve a given consistency decreases. This result is mainly explained by the "ball bearing" effect of the polymer particles and the dispersing effect of the surfactants.

For low amount of polymer in the mortar, the setting time increases. This is due to the adsorption of of polymer particles on the surface of anhydrous ce-ment particles during the mixing. This leads to a slower diffusion of water molecules used for the hy-dration of the cement. For P/C ratio higher than 10%, the setting time decreases. The hardening of the material could be governed by the polymer film formation.

The analysis of the microstructure showed that the presence of polymers in mortars increases the resistance to acid attack. The polymer also strengthens the interface between sand aggregates and cement paste. The presence of filaments of polymer bridging cracks and porosities has been revealed (figure 1). The formation of a continuous film of polymer throughout the structure is then confirmed.

In the case of laboratory-made mortars, the porosity is higher for the pure mortar, and decreases as the polymer/cement ratio increases, especially for SA-modified mortars. The porosity is also lower for high temperature curing conditions.

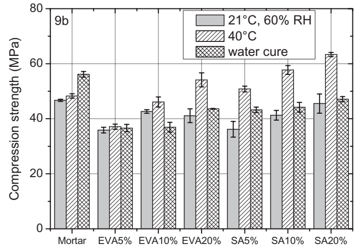

Figure 2. Compressive strength of the laboratory-made mortars.

The characterization of the mechanical strength of composite mortars showed an increase of the strength of the materials with the P/C. The result is related to the decrease of the porosity of the mortars. This increase of the mechanical properties is especially clear for hot-dry curing conditions: the formation of a polymer film with a dense structure is easier in a dry atmosphere or when the temperature is high (Hassan et al. 2000).

It can be concluded that polymer-modified mortars exhibit improved strength under a hot-dry curing environment (Hassan et al. 2000, Marceau et al. in press). This result is relevant because the curing conditions in repair yards are often severe and rarely controlled. Thus, it could be easier to use a polymer-modified repair product whose properties increase when the temperature increases.

This study will be continued by the analysis of the durability of these materials by measuring the diffusion kinetic of species that can damage the concrete (water, CO_2, chlorides ...). Finally, the adhesion of the repair mortars on a concrete support will be characterized before and after accelerated aging tests with different curing conditions and in several environments.

REFERENCES

Beeldens A., Van Gemert D., Schorn H., Ohama Y. & Czamecki L. 2005. From microstructure to macrostructure: an integrated model of structure formation in polymer-modified concrete, *Materials and Structures* 38: 601–607.

Guettala A. & Abibsi A. 2006. Corrosion degradation and repair of a concrete bridge, *Materials and Structures* 39: 471–478.

Hassan K.E., Robery P.C. & Al-Alawi L. 2000. Effect of hot-dry curing environment on the intrinsic properties of repair materials, *Cement and Concrete Composites* 22: 93–101.

Marceau S, Lespinasse F., Bellanger J., Mallet C. & Boinski F. In press. Microstructure and mechanical properties of polymer-modified mortars, *European Journal of Environmental and Civil Engineering*.

Ohama Y. 1998. Polymer based admixtures, *Cement and Concrete Composites* 20: 189–212.

Concrete Repair, Rehabilitation and Retrofitting III – Alexander et al. (eds)
© 2012 Taylor & Francis Group, London, ISBN 978-0-415-89952-9

Polymer-modified Self-Compacting Concrete (PSCC) for concrete repair

K.A. Bode & A. Dimmig-Osburg
Bauhaus-Universität Weimar, Germany

ABSTRACT: In the field of concrete repair, the requirement for a heritage-oriented redevelopment is increasing. A disadvantage of previous solutions is that the often required original textures of listed concrete building surfaces / facades cannot be produced. One solution is the application of the here presented Polymer-modified Self-Compacting Concrete (PSCC). Due to the special mix design of the material, the required properties of a repair material, such as a low Young's modulus, improved bond strength and customized pigmentation can be met specifically. Due to the self-compacting properties, it is possible to imitate formwork textures similar to the original surfaces, also in thin layers.

1 INTRODUCTION

The restoration of buildings is often to be carried out under preservation aspects and the number of listed concrete buildings requiring restoration, such as industrial monuments and modern churches, is increasing. In the field of restoration of listed buildings visual aspects are of high significance. Standard repair methods, such as reprofiling with shotcrete, often reach their limits, as the required true to original surfaces, i.e. formwork texture, cannot be realized. To obtain these, formwork has to be build in front of the surface to be reprofiled and a suitable concrete has to be filled in. One problem here is the usually thin layer thickness, which makes proper casting and compacting of normal concrete difficult.

The aim of this investigations was therefore to develop a self-compacting concrete (SCC), which is suitable for applications in thin layers, mainly for the restoration of vertical concrete surfaces. In addition the material should have improved bonding strength to the substrate. Because of their high flowability and self-levelling properties, SCCs are predestined for the application in complex structures even in the presence of congested reinforcement. The investigations focused on polymer-modified self-compacting concrete, as this material has the ability to let entrapped air escape without applying vibration energy to the concrete or the formwork. Furthermore, the addition of polymers improves the bond strength of mortars and concretes to substrate. The favoured thermoplastic dispersion based on styrene-acrylate copolymer has the added advantage that the segregation stability and rheological properties of SCC can be improved significantly. The PSCC becomes more robust and less sensitive to small variations in the proportions and conditions of the other mix components. Another decisive factor of the mix design was a low Young's modulus in order to lower the risk of cracks and delaminating due to hardening of the concrete. Polymer additions as well as aggregates with low Young's modulus contribute to this characteristic. Another important point in restoration of listed buildings is a true to original coloration of the repair material. In order to achieve a light-colored concrete, light-colored cements (e.g. CEM II and CEM III) and filler materials were used. With the additional use of pigments, a repair concrete with very similar coloration as the original material can be obtained. Studies were conducted to determine the strength properties, the shrinkage and segregation behavior. In a durability test changes of the concrete surface were assessed visually. In order to determine the performance of the polymer-modified self-compacting concrete with regard to mixing and placing under practical working conditions, several field tests on different buildings were carried out. The results of these tests confirm the suitability of the tested mix design as repair material.

2 INVESTIGATIONS

To characterize the concrete as well as for comparative studies, general fresh and hardened concrete properties were determined. The consistency of the fresh concrete was determined with the slump-flow test. For all tested mixes, the slump-flow was set to >700 mm. At the same time, the segregation was evaluated visually. The compressive and flexural tensile strength were determined after a curing time of 28 days; the static Young's modulus and shrinkage behavior were tested after 90 days of curing.

As expected, the parameters of the mixes with CEM I 42.5 R and CEM III/B 42.5 N were higher than of the mixes with CEM III/B 32.5 N. However, in restoration of concrete, high strength characteristics of the repair material are not crucial. As a low Young's modulus is of much higher importance, the mixes with CEM III are favorable. Regarding the shrinkage behavior it was found, that the PSCC with CEM III 42.5 shrinks more than the other concretes. Generally the shrinkage behavior can be regarded as uncritical. The pull-out test was carried out on five samples on concrete pavement slabs ($30 \times 30 \times 5$ cm^3). The measured values for bonding strength after 28 days were always higher than 2 N/mm^2. The failure occurred in most cases in the substrate. Only minor adhesion failures could be detected in edge zones of the slabs. The segregation behavior of the mixes was tested on 2 m long tubes with a diameter of 10 cm. These were filled vertically with polymer-modified SCC. After 28 days the samples were demoulded and the surfaces were examined visually with regard to entrapped air, casting layers and segregation. The samples were then cut longitudinally into half in order to determine the segregation of aggregates. The surfaces of all samples were smooth and without pores of entrapped air. Essential is, that even with a free fall of more than 2 meters, the concrete did not segregate. The designed polymer-modified self-compacting concrete mixes are therefore practical to be applied in narrow formwork with a free fall up to 2 meters. In order to determine the weathering resistance, beam samples of all concrete mixes were subjected to artificial weathering at the age of 7 days. The test routine complied with the at the FIB developed performance test for concrete with regard to alkali-silica reaction (ASR). One test cycle is 21 days long and the routine is as follows: 4 days dry-storage at temperatures between 5 and 65°C; storage for 14 days at 45°C and 100% RH; 3 days cycles of freezing and thawing. Only the samples with CEM III showed slight surface changes (blushing), which could only be detected when examining very closely. The developed mixes can therefore be considered durable against weathering. In order to determine the practicability of producing and handling of the PSCC mixes under practical working conditions, field tests were carried out. To a prefabricated concrete wall a reinforcement mesh was fixed and timber formwork was constructed. The layer thickness was 4 cm. In another test, two sample layers (each 1 m wide × 2 m high) were cast with CEM II 42.5 and CEM I 42.5, respectively. Based on the obtained positive experiences sample layers on a listed concrete building were carried out. The test object is a modern church, the “Weißfrauenkirche” in Frankfurt/Main, Germany. On 5 test areas the workability, especially the mixing procedure and the filling of the formwork, as well as the properties of the hardened concrete, e. g. the adhesive bond, were tested. Also the optical impression on the building in relation to the existing concrete was assessed.

3 SUMMARY

The production of polymer-modified self-compacting concrete—PSCC—and its application for thin and mainly vertical repair layers is possible. However, in each case general requirements have to be identified. The choice of adequate aggregates is important with regard to Young’s modulus, maximum grain size and grain size distribution. On the other hand good adhesion bond to the substrate has to be ensured. This can be obtained by applying polymer dispersion as a concrete additive. The here developed PSCC is suitable for the application under listed building aspects and its practicability on building sites has been shown. The segregation stability and the robustness of the mix designs against variations in production method and proportioning of the components could be proven. It can furthermore be improved by pre-batching and pre-mixing of the dry components in a laboratory. The PSCC is durable, particularly with regard to surface changes due to weathering. With regard to listed building aspects, visible formwork textures and very thin layers can be realized. In spite of the previous positive results, PSCC have the potential for improvement. For example the shrinkage and the Young’s modulus should be decreased further. Another current research topic is the development of new applications of the material, e.g. in the field of mechanical engineering as machine bases.

ACKNOWLEDGEMENTS

The presented study is part of the research project “Methods and building materials for the restoration of buildings under user-oriented”. It is funded by the Federal Ministry of Education and Research, Germany (BMBF) and belongs to the “Entrepreneurial Regions” initiative “Innoprofile”. The verification tests on real buildings were supported by Landesamt für Denkmalpflege Hessen (D), Diakonische Werke Frankfurt/Main (D), architects Sichau & Walter (Architekten BDA Fulda-Dresden/D), Consulting Engineers Trabert and Partners (Geisa/D), and Dynapox GmbH (Weimar/D).

Furthermore thanks to Dipl.-Ing. Franziska Baldy for her support by translating this paper.

Concrete Repair, Rehabilitation and Retrofitting III – Alexander et al. (eds)
© 2012 Taylor & Francis Group, London, ISBN 978-0-415-89952-9

Effect of weathering on polymer modified cement mortars used for the repair and waterproofing of concrete

Ajay Krishnan, Priya S. Nair & Ravindra Gettu
Department of Civil Engineering, Indian Institute of Technology Madras, Chennai, India

ABSTRACT: Polymer modified cement mortar has been used for the repair and waterproofing of concrete structures extensively. In the work reported here, mortars with different types of commercially-available water proofing materials have been subjected to weathering consisting of exposure to UV light and wetting-drying cycles. The effect of the weathering was assessed on changes in water permeability, bond and flexural strength, all of which are critical for long term performance. The results show that there is significant increase in the strength parameters and a marginal decrease in the bond strength and water impermeability for polymer based water proofing materials due to the accelerated weathering. In the case of the cement mortar with a lignosulphonate based integral waterproofing material, the reduction in the properties was much more than for the other polymer based materials (i.e., latexes).

Concrete structures are often exposed to weathering, rain, temperature changes, ambient salinity, pollution, etc. that induce several deterioration and durability problems. In general, the most effective means of limiting such damage is to prevent further ingress of water into the concrete by applying a protective coating. Though there are several types of waterproofing materials, the present study deals with polymer-modified cement-based repair materials, whose advantages include the ease of application, physical and chemical compatibility with concrete, non-toxicity and cost effectiveness. Obviously, the durability of the repair material is of utmost importance but is difficult to evaluate before the application due to the dependence on the environment to which it is exposed to and its chemical nature.

In this paper, the alteration in the performance of cement modified with commercially available polymer based water proofing materials (WPM) due to weathering conditions is assessed. This was compared to the performance of unmodified cement mortars and commonly used lignosulphonate based integral waterproofing agents (IWP). Two series of mortars comprising of unmodified and WPM modified cement mortars were adopted in the test programme: one series of mortars has the same water to cement ratio (w/c) of 0.35 and second series ("constant flow") has mortars with the same flow as measured by the flow table spread; this is closer to the mortars used in practice where the applicator adds water until the required consistency is obtained. The w/c used in the constant flow series and dosages of the WPM are given in Table 1.

The strength parameters and moisture permeability of the mortar, and bond strength between the base concrete and the mortar are the parameters that were considered to evaluate the samples. Specimens from both series are subjected to UV radiation and alternate wetting and drying, and the performance of the materials are assessed by comparing them with those obtained before weathering. The specimens were subjected to cycles of 8 hours exposure to UV light and 4 hours exposure to a relative humidity of 90%, following the ASTM G-154A standard, for 30 days.

The retention of strength in the unmodified and IWP modified cement mortars after weathering was found to be much less than in the polymer based WPM modified cement mortars. This may be attributed to the microcracks and voids formed by the wetting and drying in the unmodified and IWP mortars, and the polymer bridges and plugs formed in the microstructure of the polymer modified mortars. Though the polymers do not contribute much to the initial strength of the mortars, they make the mortar more resistant to deterioration

Table 1. WPM dosage and w/c for different mortars having the same flow.

Mortar	*Dosage as per manufacturers specifications*	*w/c for flow table spread of 20 cm*
OPC		0.50
N-SBR	9 litres for 50 kg of cement	0.37
N-AR	5% by weight of cement	0.37
F-IWP	200 ml for 50 kg of cement	0.48

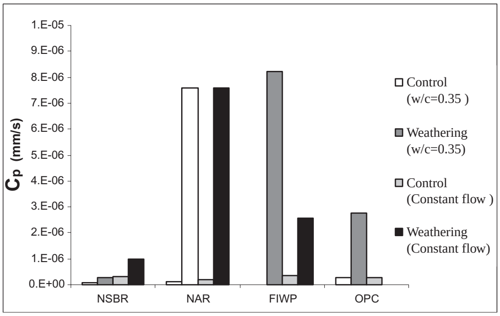

Figure 1. Water permeability of unmodified and WPM cement mortars; Note that F-IWP is impermeable at 1 bar pressure for control (w/c = 0.35).

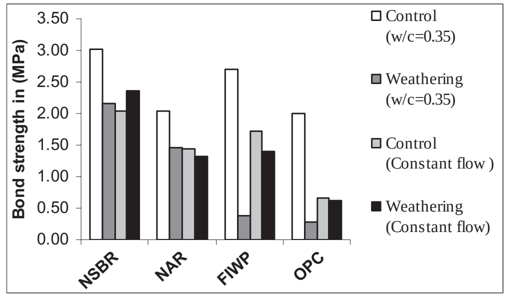

Figure 2. Bond strength of unmodified and WPM cement mortars.

on exposure to weathering conditions. It was also seen that the flexural strength of polymer modified cement mortars increases after weathering and UV exposure possibly due to the polymer bridging that is enhanced due to the wetting-drying cycles.

Figure 1 shows that water permeability (C_p in mm/sec) increases in all cases after exposure to accelerated weathering. It was observed that the unmodified cement mortar with w/c = 0.50 was highly permeable after weathering compared to that of the SBR latex based cement mortars. This is possibly because the SBR is resistant to degradation on exposure to UV radiation and therefore the partial filling of micropores and voids by the polymer continues to prevent the ingress of water.

The bond strengths of unmodified and WPM cement mortars before and after weathering are illustrated in Figure 2. The results confirm that better bonding can be obtained by the incorporation of polymers even after weathering. The decrease of bond strength of all the mortars with w/c = 0.35 on weathering is far less in case of SBR and acrylic based mortar than the unmodified and IWP cement mortars.

From the above results it is clear than the performance of polymer based WPM cement mortars after weathering is superior to that of the unmodified and IWP cement mortars. This can be attributed to the deterioration in the specimens due to the wetting and drying cycles. There is also an increase in porosity due to the leaching of water soluble salts. Such phenomena decrease the strength and durability of the repaired surface. In the case of the IWP based cement mortars, there is some degradation on exposure to UV radiation, and, therefore, it is recommended that lignosulphonate based IWPs may be applied in only in indoor and concealed areas where exposure to UV light will be less.

In the case of polymer based WPM cement mortars, the polymer forms a network in the pore system of the hardened mortar. Though acrylics also undergo degradation, the particles are water insoluble and therefore continue to prevent the permeation of water into the cement matrix. SBR based mortars exhibited, as observed from the above work, superior properties on exposure to UV light and alternate wetting and drying, when compared to unmodified cement mortars and other WPM based mortars. It was also seen that the repaired surface with SBR based mortars gave a glossy appearance after the weathering conditions. The results confirm that the polymer based water proofing agents can be employed in areas that are exposed to UV light and wetting-drying conditions.

From the above study on the influence of weathering on performance of portland cement mortar with and without the addition of water proofing materials, the following conclusions were arrived at. The properties of the mortar with a lignosulphonate based IWP before weathering were superior to the other mortar samples in which the polymer based WPMs were added. However, after weathering, the performance of polymer based WPM cement mortars was far superior in terms of strength and bonding with the base concrete. Between the two types of polymer latexes used in the study, the SBR latex exhibited better performance than the acrylic.

Concrete Repair, Rehabilitation and Retrofitting III – Alexander et al. (eds)
© 2012 Taylor & Francis Group, London, ISBN 978-0-415-89952-9

Case history of polymer-modified cementitious membrane used to protect new and repair concrete

P. Nieuwoudt, P. Zaffaroni & C. Pistolesi
Mapei S.p.A.—Via Cafiero, Milan, Italy

1 INTRODUCTION

Some ancient concrete constructions are still in a perfect state, while certain modern constructions are seriously deteriorating. This is due to the corrosion of the reinforcement, limiting the lifetime of the concrete structure. There are two main types of corrosion, caused either by carbonation, or by chlorides. Corrosion occurs only where water and oxygen are present. The service life of structures can be modelled in two live spans: time of initial corrosion in which the aggressive substances penetrate the concrete cover, and the time for corrosion propagation, when the corrosion attack proceeds. To increase the service life of new and repaired reinforced concrete constructions and delay the onset of corrosion, protective solutions are used to prevent the aggressive species from penetrating into the concrete.

Some protective coatings reduce water absorption, improving the resistivity of the concrete and therefore the propagation time. Cementitious mortars for concrete repair show similar problems to those of reinforced concrete, since metallic reinforcements are often present and can be protected with the same technology.

2 MATERIALS

2.1 *Polymer-modified cementitious coating*

The continuous surface coatings as defined in norm EN 1504-2 does not determine an increase of the critical chloride contents, but create a physics barrier. They slow down the penetration of the aggressive species and delay the onset of corrosion. Corrosion can only be slowed down by treatments or coatings that hinder the passage of water, such as polymer-modified cementitious waterproofing slurry, which features impermeability to water, salt solutions and carbon dioxide; good crack-bridging ability; good adhesion to the substrate; as well as good ageing resistance.

The polymer-modified cementitious elastic coating used in the experiments consists of powder (A), a mix of OPC cement (24%), fine silica sand up to 0.3 mm (60%), calcareous filler (15%), fibres, some admixtures (1%); and liquid (B) made up of modified styrene-acrylic copolymer dispersion (50% solid), blended with some admixtures with Tg (glass transition temperature) of –40°C. Components A and B are mixed together in a 3:1 ratio by weight. The coating has been hand-applied in one layer in a dry thickness range of 1.8 to 2.2 mm. All tests were started after a curing time of 28dd at 20°C and 55% RH. Three substrates were used: concretes with water/cement ratios (0.8 and 0.4) and a standard mortar.

3 TESTS AND RESULTS

3.1 *Impermeability to water*

The waterproofing test has been carried out according to EN 14891, with water pressure of 1.5 bar applied for 7 days, followed by visual inspection. The unprotected concrete measured an average weight gain of 470 g, while the same concrete coated by the test membrane showed weight gain of only 12 g.

3.2 *Impermeability to salt solutions*

Two test methods were used to test the polymer-modified cementitious elastic coating's ability to withstand chloride penetration. Method EN 13396 determined the amount of chloride in the standard mortar after immersion in sodium chloride solution at 3% for 1, 3, 6 and 12 months. The chloride concentration was measured at 8–10 mm depth from the surface of the specimen in contact with solution. The same test was carried out with the same mortar protected with the cementitious coating, showing negligible chloride penetration.

Method ASTM C1202 determined the resistance to chloride ion penetration, based on the determination of the electrical conductance of the concrete to provide a rapid indication of its resistance to the penetration of chloride ions. This electrical current passed through 51 mm thick slices of 102 mm cylinders, measured over a 6-hour period. A potential difference of 60 V dc was maintained across the ends of the specimen. One was immersed in a sodium chloride solution and the other in a sodium hydroxide solution. This test has been carried out with unprotected and protected mortar with elastic coating.

According to ASTM C1202, the standard mortar should be classified as HIGH chloride ion penetrability, while the same protected with the elastic coating is classified as VERY LOW.

3.3 *Impermeability to carbon dioxide*

The carbonation penetration has been evaluated through accelerated CO_2 penetration tests. The samples were put in a chamber for 90 days where a CO_2 enriched environment (30% in volume) was created. At various fixed times, the carbonation penetration depth was measured through a phenolphthalein test. The increased CO_2 penetration for very bad quality concrete with a high w/c ratio (0.8), was reduced significantly for a good quality concrete (w/c = 0,4) and the penetration became negligible when a protective covering was applied.

3.4 *Permeability to water vapour*

The test carried out according to ISO 7783 measured the water vapour transmission through the elastic membrane and the calculation of Sd coefficient, which represents the air equivalent layer. EN 1504-2 specifies requirements for the identification and performance of products and systems to be used for surface protection of concrete. According to this standard, the coating with Sd < 5 m is considered permeable to water vapour. The polymer-modified cementitious elastic coating showed an Sd of 2.4 m.

3.5 *Crack-bridging ability*

This describes the capacity of the membrane to cover micro-cracks that can occur on the concrete and repair mortar surface. The mechanical properties of a coating which is formed by drying a liquid component above the minimum film formation temperature, depend on the temperature. At low temperatures, the polymer film is glassy and brittle. It becomes soft and elastic above certain temperatures. The transition temperature from hard to soft is the glass transition temperature and depends on the polymer's composition. The results of crack-bridging ability measured in the range from –25°C up to 30°C are almost constant in all ranges. This is peculiar, as many polymer dispersions tend to become extremely brittle when the test temperature drops below –5°C, resulting in the coatings becoming very rigid.

3.6 *Pull-off adhesion*

Substrate adhesion is crucial for a positive outcome of the concrete surface intervention. Pull-off tests on concrete according to EN 1542 were done and adhesion tension kept around 1 MPa.

3.7 *Ageing tests*

The resistance to accelerated ageing has been carried out according to ASTM G155, by exposure to weather-ometer equipment simulating years of normal environment conditions. Polymer-modified cementitious coating has been tested before and after 1000 aging cycles measuring the elongation and the pull-off strength. The elasticity has sustained a moderate reduction, while the support adhesion has remained integrally unchanged.

4 CONCRETE PROTECTION CASE

4.1 *Concrete beam bridge reparation and protection*

This project refers to a 50-year old, 600 m highway bridge made of pre-stressed reinforced concrete steel beams and normal reinforced concrete piers. The concrete was degraded by diffused carbonation corrosion. Remedial concrete repairs to the piers started 10 years ago. The construction has been reinforced with polymer-modified cementitious elastic coating. The lower piers have been repaired with special shrinkage compensated thixotropic structural mortar type R4, according to EN 1504-3, spray-applied with variable thickness of 8 to 12 cm and reinforced by adding metallic reinforcements.

The steps followed were selective hydro-demolition of the contaminated concrete and positioning of the new metallic reinforcement; spray application of the mortar type R4 according to EN 1504-3; pressure washing of the final mortar layer; and spray application of the polymer-modified cementitious elastic coating in a single layer. For the highest piers, a micro-concrete Self Compacting Concrete (SCC), based on a special SCC binder, has been used. The application of 8–12 cm material thickness has been done by pumping through formwork, starting from the pillar base. The mortar type R4 and SCC concrete used for the pier reinforcement were designed to have a low w/c ratio for good strength and barrier against the penetration of aggressive substances. Both have been protected with the polymer-modified cementitious elastic coating, to extend the service life of the repaired structure.

Nine years after project completion, cores were taken from the repaired piers to measure the penetration of carbon dioxide. In all samples, there was no carbonation. The amount of chloride has also been measured in the same samples, showing negligible readings. (<0.02%). The compressive strength tests showed results of between 22–34 MPa. This investigation is going to be continued over the next few years to collect further data.

Concrete Repair, Rehabilitation and Retrofitting III – Alexander et al. (eds)
© 2012 Taylor & Francis Group, London, ISBN 978-0-415-89952-9

Use of starch modified concrete as a repair material

A.A. Akindahunsi & H.C. Uzoegbo
School of Civil and Environmental Engineering, University of Witwatersrand, Johannesburg, South Africa

S.E. Iyuke
School of Chemical and Metallurgical Engineering, University of the Witwatersrand, Johannesburg, South Africa

ABSTRACT: Corn is a rich source of carbohydrate, starch extracts and a source staple food for majority of sub-Saharan African population. Starch and its derivatives have been widely described as rheology-modifying admixtures; in an ongoing research the effect of using corn starch modified concrete is reported. Its effects on concrete properties such as compressive strength, sorptivity and permeability were determined on samples with 0, 2.5 and 5% addition of starch by weight of cement. The result showed 9 and 3% increase in strength for 2.5 and 5% starch additions respectively when compared with the control after 56 days of curing, while the sorptivity and permeability tests compared well with the control. At certain proportion, corn starch-modified cement and concrete exhibit low slump and accelerated setting time. These properties make them suitable for certain applications such as concrete repairs and pavement design.

Keywords: cassava starch, concrete, compressive strength, sorptivity, permeability

1 INTRODUCTION

The incorporation of a rheology modifying admixtures (RMA) in fluid concrete can allow the making of a homogenous and yet very fluid concrete. Starch and its derivatives generally have been found to have rheology modifying properties and are now being used as such. These are admixtures used to modify the cohesion and stability of cement-based structures. They can be either mineral additions or polymeric admixtures. The latter are typically polysaccharides such as biogums, cellulose ethers or modified starches (Izumi et. al., 2006; Schmidt et. al., 2009; Akindahunsi et al., 2011; Khayat, 1998). The presence of these admixtures at a given water cement ratio will affect the rates of hydration of cement in concrete and eventual strength development. The use of rheology modifying admixture allows for alteration of flow properties and rheology of mortar and concrete. This property can be used to optimize different types of concrete. An example is shotcrete that requires relatively high yield stress and viscosity to control adhesion and rebound behavior respectively. The benefits of properties provided by starch and its derivatives led to the investigation of the use of corn starch in modifying concrete properties for repair works in this paper.

2 METHODOLOGY

2.1 *Materials*

Modified corn starch (MCS) was used for the study. The cement that was used is ordinary Portland cement 42.5 N, CEM 1. Andesite stones with maximum size 19 mm were used as coarse aggregates while crusher stone dust of specific gravity of 2.88 was used as the fine aggregates.

2.2 *Concrete preparation*

Concrete used for the study was prepared according to ACI Standard 211.1–91. Three types of concrete specimens were prepared. A type was cast as the control, another with 2.5% addition of starch by weight of cement and the last 5% addition of starch by weight of cement.

2.3 *Oxygen permeability and sorpivity tests*

Oxygen permeability and sorptivity tests were carried out according to durability index testing procedure manual of Cement and Concrete Institute (2010) of South Africa.

3 RESULTS AND DISCUSSION

The compressive strength development pattern of the control, 2.5 and 5% starch is presented in Figure 1.

The results of the oxygen permeability tests for the concrete specimens are presented in Figures 2–4. The results of sorptivity tests carried out on concrete disc specimens are presented in Figures 5–7.

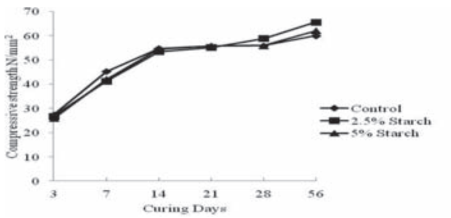

Figure 1. Compressive strength test.

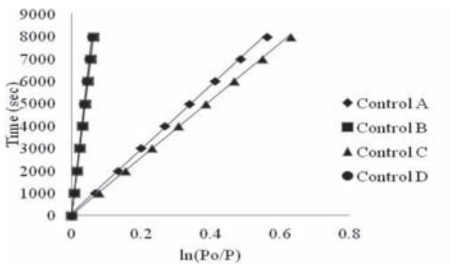

Figure 2. Oxygen permeability test (Control).

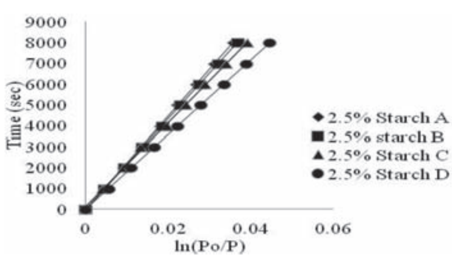

Figure 3. Oxygen permeability test (2.5% Starch).

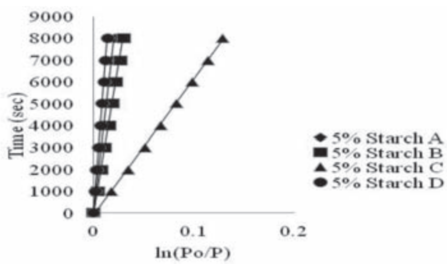

Figure 4. Oxygen permeability test (5% Starch).

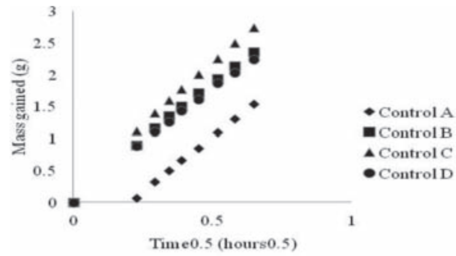

Figure 5. Sorptivity test for control specimens.

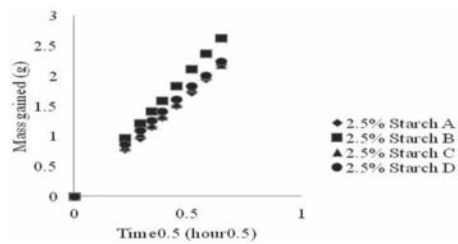

Figure 6. Sorptivity test for 2.5% starch specimens.

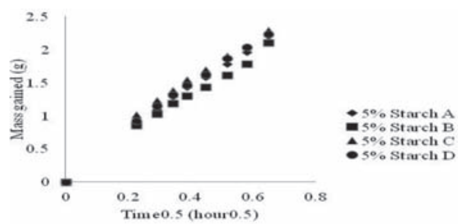

Figure 7. Sorptivity test for 5% starch specimens.

4 CONCLUSION

The effect of use of starch in modifying viscosity of concrete has been demonstrated in this work and from the results obtained the following conclusions can be drawn:

i. Addition of starch in concrete reduce the slump and increase the strength of concrete as seen in concrete specimens with 2.5 and 5% addition of starch
ii. Samples with 2.5 and 5% starch are less porous when compared with the control as shown by the oxygen permeability test. The sorptivity results also compares well with the control.
iii. These characteristics exhibited by starch in concrete makes it a material that can used in concrete repairs

This work is jointly sponsored by SPIN project through the ACP/EU funding and WITS University. The authors wish to acknowledge their support.

Concrete Repair, Rehabilitation and Retrofitting III – Alexander et al. (eds)

Mitigation of ASR affected concrete in Boston, MA, USA: A case study

A.F. Bentivegna
CTL Group, Skokie, Illinois, USA

T. Drimalas
The University of Texas at Austin, Austin, Texas, USA

J.H. Ideker
Oregon State University, Corvallis, Oregon, USA

S. Hayman
University of New Brunswick, Fredericton, New Brunswick, Canada

ABSTRACT: This paper presents the results of investigations into ASR affected traffic barriers in Boston, Massachusetts, USA. Several different treatments were utilized to potentially reduce or arrest ASR. Topical coatings of silane and lithium nitrate were applied to sections of the affected barriers. Additionally, several control sections were left untreated. Lithium nitrate was applied via topical sprays and vacuum impregnation and showed similar or worsened expansion versus untreated control sections, rendering the treatments unsuccessful at mitigating the reaction. The application of silane coatings was successful at lowering the internal relative humidity of the concrete and reducing the expansion of the concrete. The untreated control barriers had an average relative humidity of 86.0% over 4 years. The treatments using two different commercially available silanes, 40% isopropyl-based and 20% isopropyl-based, lowered the relative humidity below the critical threshold of 80.0% RH. This research results indicate that lithium salts applied via topical spray or vacuum impregnation were unable to penetrate and mitigate expansion due to ASR; however the application of topical silanes proved effective and thus minimized the potential for future damage and prolonged the service life of the barriers.

1 RESEARCH OBJECTIVES

The objectives of the research presented in this paper are to assess the effectiveness of both topical application and vacuum impregnation of lithium nitrate and breathable sealers for reducing deleterious ASR. The combination of a wide variety of application methods coupled with instrumentation and monitoring of each application type, were used to determine the best type of application which provided the most effective means of limiting future damage caused by ASR.

2 RESEARCH PROGRAM

This case study investigated concrete traffic barriers on State Route 2 near Boston, Massachusetts, USA. Signs of cracking in the stretch of barriers were first noticed as early as two years after construction. The site location for this specific investigation was considered the worst in terms of cracking for barriers in the state. However, there are other sites where barriers exhibit similar signs of distress.

A total of 24 barriers were topically treated with lithium and/or breathable sealers. Table 1 summarizes the treatments that were applied. A total of 8 treatments were applied and evaluated on these barriers with, three barriers per treatment type.

Eight sections of barriers were treated using the vacuum impregnation method. Four different

Table 1. Topical Treatments and Nomenclature.

Nomenclature	Treatment
T1-A, T1-B & T1-C	Single Application Lithium
T2-A, T2-B & T2-C	Double Application Lithium
T3-A, T3-B & T3-C	Quadruple Application Lithium
T4-A, T4-B & T4-C	Double Application Lithium Followed by 40% silane sealer (Isopropyalcohol Based)
T5-A, T5-B & T5-C	40% Silane Sealer (Isopropyalcohol Based)
T6-A, T6-B & T6-C	20% Silane Sealer (Isopropyalcohol Based)
T7-A, T7-B & T7-C	Water-based silane sealer
T8-A, T8-B & T8-C	Lithium silicate based sealer
C1-A & C1-B	Control Section

Table 2. Vacuum treatments and nomenclature.

Nomenclature	Treatment
VA-1 & VA-2	Short-term Vacuum Treatment of Lithium Nitrate
VB-1 & VB-2	Short-term Vacuum Treatment of Lithium Nitrate Followed by Topical Application 40% silane sealer (Isopropyalcohol Based)
VC-1 & VC-2	Long-term Vacuum Treatment of Lithium Nitrate
VD-1 & VD-2	Short-term Vacuum Treatment of Lithium Nitrate Applied Twice
C2-A & C2-B	Control Section

treatments were evaluated (two sections per treatment). Table 2 summarizes the different vacuum treatments completed.

3 RESULTS

The average vertical expansions for the topically applied treatments are shown in Fig. 1a) topical lithium treatments and Fig. 1b) topical silane treatments. Treatments T1, T2, and T3 had similar or greater expansion than the control section. T4, T5, T6, and T7 showed significant signs of shrinkage and possible reversal of stress caused by ASR. Treatment T8 appeared to increase the reaction and cause more expansion than the control sections.

The average vertical expansion of the barriers treated with vacuum impregnation procedures are shown in Fig. 2. All vacuum impregnation

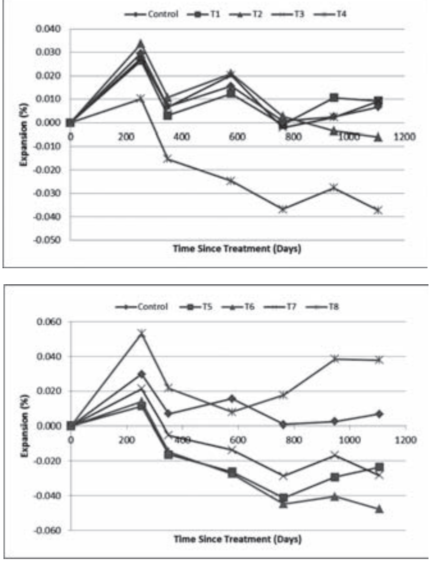

Figure 1a. Average vertical expansion for topically treated lithium nitrate barriers, 1b. Average vertical expansion for topically treated silane nitrate barriers.

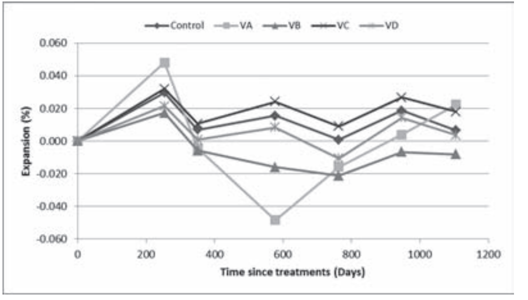

Figure 2. Average vertical expansion for vacuum impregnation treatments.

treatments appear to have negligible effects on expansion of the ASR affected barriers.

In 2007, the research team began monitoring the internal relative humidity of the control specimens and those treated with the breathable sealers. A gradual reduction in relative humidity was observed over the duration of monitoring of treatments T4, T5, T6 and T7. In May 2010, these treatments had an average internal relative humidity of three instrumented holes at a depth of 76.2 mm of 81.4%, 74.0%, 73.5% and 81.7%, respectively, which is near the critical threshold of 80% RH which is required for ASR to presume. However, the control sections had an internal average RH of 86.0%.

4 CONCLUSIONS

The following conclusions can be made from the topical and vacuum impregnation application of lithium nitrate from this field study:

– The topical application of the lithium nitrate had no benefits on reducing expansion rate or cracking propagation compared to control sections.
– Vacuum impregnation showed no signs of mitigating the reaction when used with lithium nitrate.

The following conclusions can be made from the topical and vacuum impregnation application of the breathable sealers from this field study:

– Breathable sealers such as silanes have the greatest potential for mitigating expansion due to ASR in existing structures.
– Isopropyalcohol and water-based silanes appear to be the most promising treatments.
– Treatments T4, T5, T6 and T7 lowered the relative humidity of the section to near or below the critical threshold for ASR.

ACKNOWLEDGEMENTS

The authors would like to acknowledge the support of our research sponsors the United States Federal Highway Administration (FHWA) and the assistance of the Massachusetts Department of Transportation (MassDOT).

Concrete Repair, Rehabilitation and Retrofitting III – Alexander et al. (eds)

Shrinkage cracking of steel fibre-reinforced and rubberized cement-based mortars

T.-H. Nguyen, A. Toumi & A. Turatsinze
Laboratoire Matériaux et Durabilité des Constructions (LMDC)
INSA-UPS, Toulouse cedex, France

ABSTRACT: This paper presents an experimental investigation on the dimensional variations due to restrained shrinkage of Steel Fibre-Reinforced and Rubberised cement based Mortar (SFRRM) and the subsequent cracking. The cementitious materials contain rubber aggregates from grinded used tires and/or steel fibre-reinforcement, while a control material is a plain cementitious mortar. SFRRM was cast using rubber aggregates partly replacing 20 and 30% by volume of mineral aggregates and/or steel fibre contents of 20, 30 and 40 kg.m^{-3}. The shrinkage dimensional changes of SFRRM were measured and compared to the one of the control mortar. Ring type specimens were used for restrained shrinkage cracking tests. It allowed the evaluation of the effect of rubber aggregates and of fibre reinforcement on early age cracking. Their synergetic effect was also analyzed. The study demonstrates the effectiveness of rubber aggregates along with their positive synergetic effect when combined with steel fibre reinforcement to improve resistance to shrinkage cracking.

1 INTRODUCTION

Previous findings showed that the use of overlay materials having a low Young's modulus is a suitable solution to reduce the risk of cracking of cement-based applications. On the other hand, the reinforcement of the mortars by metallic fibres has proven to improve several of its properties, mainly their ductility. In all cases, regardless of the type of reinforcement used, it does not avoid the crack initiation but contribute to restrain the cracking kinetics. In such conditions an enhanced strain capacity of cementitious materials is the property that should be targeted. To achieve this objective, rubber aggregates from the grinded of discarded tires were used, an approach that is likely to address the demand for the conservation of a clean environment by recycling industrial by-product. In this study, the use of rubber aggregates has been tested in combination with the fibres reinforcement.

2 MATERIALS DESIGN AND EXPERIMENTAL STUDIES

For the control mortar, the sand content was 1600 kg.m^{-3}. For SFRRM, two contents of rubber aggregates, partly replacing 20 and 30% by volume of mineral aggregates and commercially available amorphous metal fibres were used. A classification of the different compositions allowing them to be easily referenced was adopted. For example, 20R20F means the mortar incorporating 20% of rubber aggregates and reinforced by 20 kg.m^{-3} of fibres. The contents of cement (500 kg.m^{-3}), of water (325 kg.m^{-3}), of stabiliser (0.9 kg.m^{-3}) and of plasticizer (3.25 kg.m^{-3}) were maintained constant.

In order to quantity resistance to cracking due restrained shrinkage, ring tests were used according to the ASTM C1581-04 standard. Two specimens with a 38 mm thickness, 330 mm inner diameter and 152 mm height were cast around the steel ring. After the pouring, the specimens were immediately cured at 20°C and 50% R.H. The restrained shrinkage of the mortar composite caused compressive strain to develop in the steel ring. This last is measured by two strain gages bonded to the inner surface. The day of the crack initiation was determined thanks to the stress relaxation induced in the steel ring and the resulting sharp drop in the confining strain-time curve. After the cracking of the mortar, the crack width was monitored by a video-microscope with the maximum enlargement of ×175. Figure 1 shows a crack through the entire height of a specimen type 0R0F.

3 RESULTS AND DISCUSSION

Drying shrinkage versus the Young's modulus of the studied composites is presented in figure 2. These results highlight the fact that the decrease of Young's modulus induced by rubber aggregates is the factor that helps explain the high values of

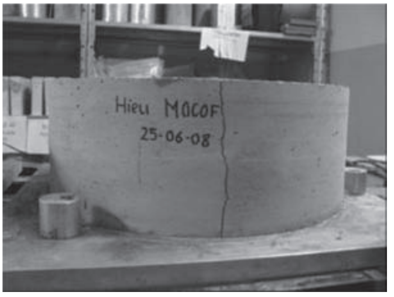

Figure 1. A crack crossing the entire height of 0R0F ring specimen.

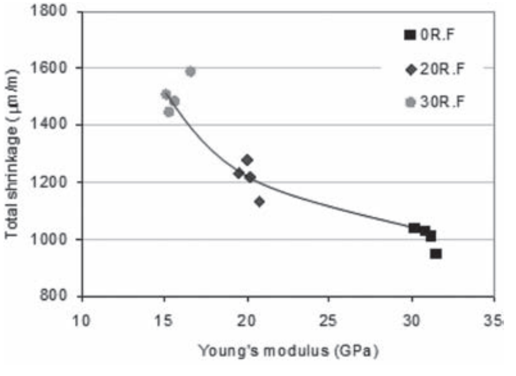

Figure 2. Total shrinkage versus Young's modulus.

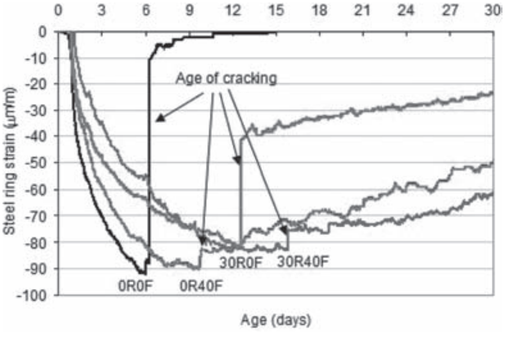

Figure 3. Steel ring strain versus specimen age: Age for crack initiation and post cracking residual steel ring strain.

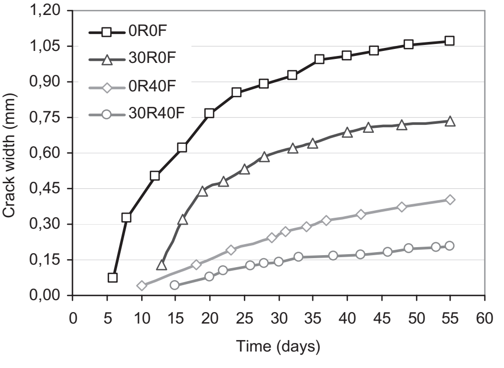

Figure 4. Measured crack widths versus time.

the shrinkage length changes. However, one must ensure that rubber aggregates have no effect on the mass loss that can also explain the observed trends in terms of dimensional changes. Results show that for a given mass loss, the shrinkage length change is more important for the composites incorporating rubber aggregates. Thus, it is indeed due to their low stiffness and not by their influence on mass loss that rubber aggregates amplify the shrinkage length changes.

In order to investigate the balance of the benefit due to the improved strain capacity and the detrimental effect due to higher shrinkage, restrained shrinkage cracking tests were performed by means of ring-tests. The aim was to obtain a good idea of the potential of rubberised cement-based composites to reduce propensity of the composite for shrinkage cracking. Figure 3 shows the variation of steel ring strain versus specimen age of the studied composites. The age (in days) for the crack initiation and the crack width increasing are presented in figure 4.

These results show that rubber aggregate incorporation is a suitable solution to delay initiation of the crack due to restrained shrinkage. It means that, with respect to propensity for cracking, the benefit due to improved strain capacity outweighs the disadvantages of increased shrinkage length change of rubberized mortars. With respect to these properties, results show a positive synergetic effect from combination of rubber aggregates and fibre-reinforcement.

4 CONCLUSION

A combination of rubber aggregates and of fibre-reinforcement appeared to be a suitable solution to limit the propensity for cracking due to restrained shrinkage of cement based applications. It can result in enhanced durability for large surface area which are highly sensitive to cracking due to length change. A second aspect can be highlighted since the use of rubber aggregates obtained from grinding used tires provides an opportunity to recycle used tyres and a contribution to maintain a clean environment. An ongoing work is focusing on a field experience of pavements on soil with the aim to validate the findings of this research study under actual conditions of operation.

Concrete Repair, Rehabilitation and Retrofitting III – Alexander et al. (eds)
© 2012 Taylor & Francis Group, London, ISBN 978-0-415-89952-9

Development of a liquid bio-based repair system for aged concrete structures

V. Wiktor, A. Thijssen & H.M. Jonkers
Delft University of Technology, Civil Engineering & Geosciences, Section of Materials & Environment—Microlab, Delft, The Netherlands

ABSTRACT: The present study focuses on the development of a bio-based repair system. In this paper, the authors investigated (i) the effect of the pH of two transportation solutions on the bacterial activity, the biological part of the repair which mediates mineral formation and (ii) the influence of the nutrient source on the cement paste microstructure, with or without bacterial activity. The results emphasized that the pH of the transportation solution should be alkaline to prevent a rapid leaching of calcium and hydroxide ions from the cement paste. Furthermore, an alkaline pH also promotes bacteria activity resulting in Ca-based mineral formation. The bio-based repair system composed of bacteria, and Na-gluconate in water glass appears to be the most promising as it results in bacterial activity, densification of the microstructure of the cement paste and limited leaching of calcium.

1 INTRODUCTION

The bio-based repair system as presented in this paper is a liquid-based system which transports a bio-based agent into concrete. The bio-based repair agent consists of concrete compatible bacteria and feed which produce calcite-based minerals decreasing concrete matrix porosity. The first step in the development of this bio-based repair system is to determine the best combination between the nutrient source for bacteria and the transportation solution in order to have an optimum bacterial activity but also to insure a good compatibility with the concrete matrix.

In this paper, the authors investigated (i) the effect of the pH of two transportation solutions on the bacterial activity and (ii) the influence of the nutrient source on the cement paste microstructure, with or without bacterial activity.

2 MAIN RESULTS AND DISCUSSION

2.1 *Na-gluconate + NaS + bacteria*

ESEM observations at 7 days show a dense surface area, a very thin gel-like surface layer (<5 μm) and Ca-based layer at the interface of the two. Similarly to the treatment with Na-gluconate+bacteria, bacteria seem to be active. Moreover, the high pH of the present repair solution prevents leaching of calcium and the water glass can react with the cement paste to densify the microstructure (Fig. 1a).

At 28 days a thick multi-phase layer is observed. The gel-like layer noticed at 7 days is most probably Na-gluconate which turned into Ca-gluconate due to lower solubility of the latter at 28 days (Fig. 1bc).

Furthermore, formation of a Ca-based layer on top of the gluconate layer suggests that bacteria are active and convert Na/Ca-gluconate to promote calcium carbonate formation. This is supported by the observation of bacteria imprints on a Ca-based mineral formed at the surface of the mortar specimen (Fig. 1c-d). Moreover, compressive strength results show higher value for this treatment.

2.2 *Na-gluconate*

The thin section observations at 7 days show the absence of a surface layer and the presence of very porous microstructure of the surface area. On the contrary the surface area appears denser at 28 days with the presence of Ca-based surface layer of few microns thickness. Moreover, the shift of the Si-O stretching band to higher wave numbers on the FT-IR spectra between 7 and 28 days suggests a decalcification of the C-S-H.

The low pH of the Na-gluconate solution compared to that of the pore solution results to the leaching of calcium ions. However, the very porous surface area suggests that the leaching in this treatment is more important than the one with H_2O treatment.

Considering that Ca-gluconate is much less soluble than Na-gluconate (35 g/L and 590 g/L respectively), the calcium leached from the cement paste probably immediately precipitate within the repair solution. This creates the driving force for the important Ca^{2+} leaching.

At 28 days, the surface layer observed is most probably a mixture of Ca-gluconate and calcium carbonate. This is due to pH gradient and Ca concentration gradient in the pore solution between the

Table 1. Summary of the different treatment performed with the composition of the repair solutions.

	Repair system solution composition				
Treatment	Bacteria	Carbon source	Transportation solution	pH	Studied effect
Control	∅	∅	∅	∅	Carbonation of the cement paste
H_2O	∅	∅	(*) demi H_2O	~ 6	Leaching of Ca^{2+} from the cement paste
H_2O + bacteria	10^6 spores/mL	∅	demi H_2O	~ 6	Effect of non-active bacteria
Na-gluconate	∅	Na-gluconate (148 g/L)	demi H_2O	~ 7	Influence of the C-source on the cement paste microstructure
Na-gluconate + bacteria	10^6 spores/mL	Na-gluconate	demi H_2O	~ 7	Influence of the pH on the bacterial activity
Na-gluconate + NaS	∅	Na-gluconate	water glass	~ 11	Influence of the pH on the C-source behavior
Na-gluconate + NaS + bacteria	10^6 spores/mL	Na-gluconate	water glass	~ 11	Influence of the pH on the bacterial activity

(*) demi H_2O = demineralized water

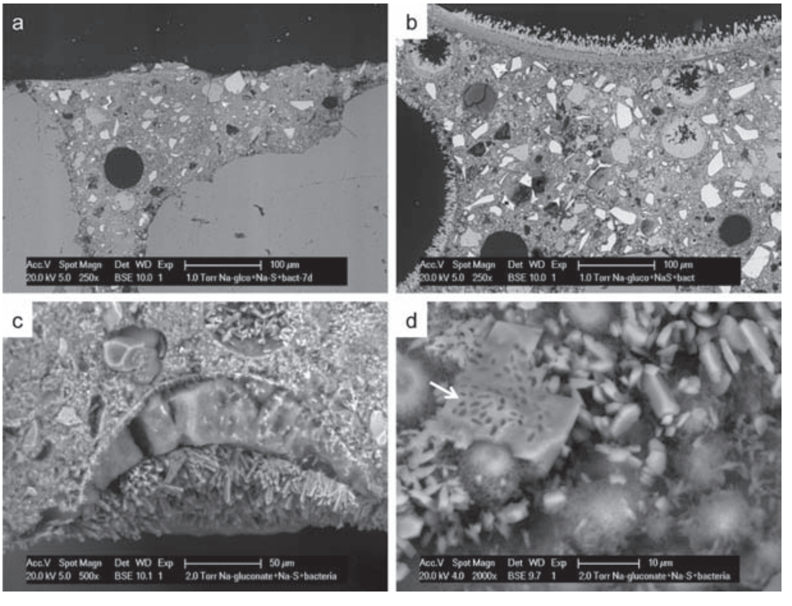

Figure 1. ESEM observations of specimens treated with Na-gluconate + NaS + bacteria—polished section at (a) 7 days and (b) 28 days, (c) details on a pore at the surface of the specimen showing a calcium-based layer on top of a gluconate-based layer, (d) surface observation exhibiting calcium carbonate crystals and bacteria imprints (arrow).

surface area and the non altered area. Between 7 and 28 days, more portlandite and C-S-H are being dissolved to balance these gradients and Ca precipitate in/on the surface area as Ca-gluconate or calcium carbonate as no more leaching is possible.

3 CONCLUSION

First, the results emphasized that the pH of the transportation solution should be alkaline to prevent a rapid leaching of calcium and hydroxide ions from the cement paste. Furthermore, an alkaline pH also promotes bacteria activity resulting in Ca-based mineral formation.

Then, results suggest that the lower solubility of Ca-gluconate compared to that of Na-gluconate acts as a driving force for the dissolution of portlandite and C-S-H.

Finally, the bio-based repair system composed of bacteria, and Na-gluconate in water glass appears to be the most promising as it results in bacterial activity, densification of the microstructure of the cement paste and limited leaching of calcius.

Concrete Repair, Rehabilitation and Retrofitting III – Alexander et al. (eds)
© 2012 Taylor & Francis Group, London, ISBN 978-0-415-89952-9

Development of bio-based mortar system for concrete repair

M.G. Sierra-Beltran & H.M. Jonkers
Microlab, Delft University of Technology, Delft, The Netherlands

ABSTRACT: The overall performance of concrete repair systems depends to a great extent on the durability of and compatibility between the concrete substrate and the repair material. This paper focuses on the development of a concrete-compatible and sustainable bio-based repair system. To promote the compatibility, cement-based mortars have been chosen for this study. The shrinkage and mechanical behaviour of four different High-Performance Fibre-Reinforced Cementitious Composites (HPFRCC) have been studied. According to the test results, the material composed with cement, fly ash and limestone powder developed the lower drying shrinkage while exhibiting a compressive and flexural strength similar to other materials. Then, the limestone powder in this chosen material was partially replaced by a bio-based agent and the mechanical properties of this new composite were studied. The bio-based agent will promote the crack healing and improve the bonding with the concrete substrate.

1 INTRODUCTION

A large number of concrete structures worldwide suffer from deterioration or distress. These structures need constant maintenance or repair. The overall performance of concrete repair systems depends to a great extent on the durability and compatibility between the concrete substrate and the repair material. Bad adhesion is still one of the major sources of damage and poor durability of concrete-repair systems.

Compatibility between the repair material and the concrete substrate is understood as the balance between deformations and physical and chemical properties of both materials. This balance ensures that the repair system will stand the stresses induced by restrained shrinkage as well as chemical changes. To promote this compatibility, a cement-based material, known as Engineered Cementitious Composite (ECC) is studied in this research.

ECC is a class of high performance fibre reinforced cementitious composites (HFRCC), which has been micromechanically designed to have large values of strain capacity with a low percentage of randomly distributed polymer fibres. Due to the presence of the fibres, the material behaves ductile under tension stress and develops multiple micro-cracks before failure. The high ductility and multiple-cracking behaviour can release the stresses induced by differential shrinkage in concrete repair. In conventional ECC the absence of coarse aggregates together with a higher cement and binder content leads to a quite high value of shrinkage. ECC type materials have been studied as repair systems for concrete structures.

This paper proposes a bio-based agent, present in the mortar, to improve the durability of the repair system by promoting crack healing and improving the bonding with the concrete substrate. The bio-based agent consists of bacteria that are compatible with concrete and organic compounds that serve as food for the bacteria. Previous research has shown the capacity of this bio-based agent to produce calcite-based minerals, filling up cracks and reducing the concrete permeability.

2 EXPERIMENTAL PROGRAM

Four different ECC-type mixes were studied. All the mixes were prepared with cement type CEM I 42.5N and 2% per volume poly-vinyl-alcohol (PVA) fibres. Mix 1 was prepared with blast furnace slag (BFS), and limestone powder (LP) as filler. Mix 2 has BFS, fly ash (FA), and sand with a maximum grain size of 500 µm. Mix 3 has FA and sand. Mix 4 has FA and LP.

3 RESULTS AND DISCUSSION

The compressive strength of the mixes varies from 38.4 MPa for Mix 1 to 51.9 MPa for Mix 2. The compressive strength of Mix 1, the mixture with considerably lower cement content, is lower than for the other mixtures.

The flexural behaviour of the mixes was studied at 7, 28 and 60 days. All ECC thin beams have similar behaviour under bending load (Figure 1). Apart from Mix 3, the flexural strength increases with increasing age. For Mix 3, the test results after

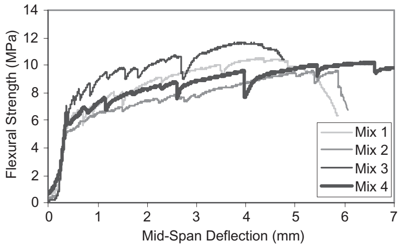

Figure 1. Typical flexural strength-deflection curves at 28 days.

28 days show a decrease of flexural strength. The ultimate deflection capacity of Mixes 1, 2 and 3, decreases with increasing age. This is characteristic of ECC type materials. Mix 4 exhibited a maximum deflection capacity at 28 days.

Mix 1 has the lower compressive strength at 28 days and high bending strength at all ages compared to the other mixes. An improved fibre distribution together with a decreased matrix toughness leads to a higher ultimate flexural strength in this mix.

The drying shrinkage of all mixes was measured up to 120 days. Mix 1 has the highest shrinkage (2900×10^{-6}), and mixes 3 and 4 have the lowest (1870×10^{-6}). The presence of sand particles in mixes 2 and 3 contributes to reduce the drying shrinkage. Unhydrated fly ash particles in Mix 4 contribute to the lower shrinkage of this mix.

3.1 *Effect on mechanical properties of addition of healing agent*

Based on the compressive strength, flexural performance and drying shrinkage test results, Mix 4 was chosen for the bio-based repair mortar system. The limestone powder of this mixture was partially replaced with lightweight particles containing the healing agent. The healing agent considered for this research is alkali-resistant spore-forming bacteria and calcium lactate, which is a nutrient source for the bacteria. A higher amount of water and superplasticizer was necessary to achieve consistent rheology properties.

The mix with the healing agent (Mix 4 H) achieved a higher compressive strength at 28 days than the mix without the agent. This may be due to the presence of calcium lactate in the healing agent.

The flexural strength of Mix 4 H, 9.6 MPa, is slightly lower than that of Mix 4, 10.2 MPa (Figure 3). This reduction is partially because of the higher water-to-binder ratio and higher amount of superplasticizer used in Mix 4 H. In Mix 4 the only filler is limestone powder, which has smaller size particles than the lightweight particles containing the healing agent. The small particle size of limestone powder contributes to a better

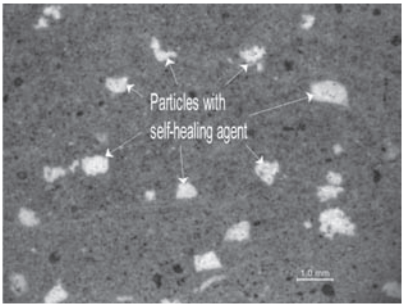

Figure 2. Lightmicroscopic image of particles with healing agent distributed through the ECC material.

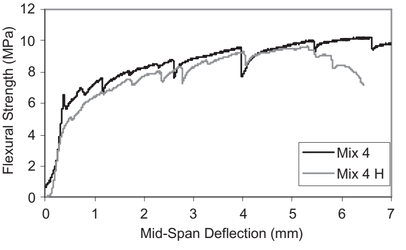

Figure 3. Typical flexural strength-deflection curves of Mix 4 and mix 4 H at 28 days.

packing of the matrix around the fibre, increasing the fibre-matrix properties and therefore the ductility of the mix.

4 CONCLUSIONS

Four different ECC-type materials were studied as possible concrete repair material. The mixture with the lower drying shrinkage was chosen, since drying shrinkage is an important material property for a concrete repair system. The bio-based healing agent was added to the chosen mixture and the effect of the healing agent on the mechanical properties of the material was studied. Test results suggest that the healing agent has a positive effect on the compressive strength while inducing a slight reduction on the flexural properties. Nevertheless, the strength and ductility of the mix with healing agent remain acceptable for an ECC-type material. The ductility is considerably greater than the ductility of conventional concrete and normal fibre reinforced concrete.

Further research includes measurements of the drying shrinkage of Mix 4 H and the restraint shrinkage of the mix when applied as a concrete repair system. The behaviour of this novel bio-based mortar repair system will be assessed and compared with currently commercially available repair systems.

Concrete Repair, Rehabilitation and Retrofitting III – Alexander et al. (eds)
© 2012 Taylor & Francis Group, London, ISBN 978-0-415-89952-9

Full scale application of bacteria-based self-healing concrete for repair purposes

Henk M. Jonkers & Renée Mors
Delft University of Technology, Civil Engineering & Geosciences, Section of Materials & Environment—Microlab, Delft, The Netherlands

ABSTRACT: In the last four years we have developed in our laboratory an experimental mortar mixture with self healing capabilities. This mixture is based on a two component additive, composed of bacteria and organic feed, latter acting as mineral precursor compound for the production of crack-filling material. Experimental results obtained so far show that occurring cracks, which dramatically increase matrix porosity and cause leakage problems, are significantly better healed in bacteria-based than in reference (control) specimens. The goal of the current follow-up research project is to further develop bacteria-based self-healing concrete into a series of products which can be successfully applied outdoors. One specific product comprises a cement-based liner to be applied on concrete constructions to prevent leakage and at the same time repair existing cracks in the underlying concrete in a durable manner. Specific challenges in this project concern technical voluminous and economical production of the two component healing agent needed for full scale application. First results show that powder compression techniques allow economical production of high volumes of healing agent.

1 PROBLEM AND PRIMARY GOAL OF THE PROJECT

Bacteria-based self-healing concrete has been developed in the laboratory during the last 5 years within the framework of DCMat (Delft Centre for Materials) and Agentschap NL—IOP financed projects 'Development of bacteria-based self healing concrete'. The self-healing capacity of concrete specimens based on an experimental concrete mixture was established and quantified in the laboratory. The obtained experimental results showed that cracks, which dramatically increase matrix porosity and cause leakage problems, were significantly better healed in bacteria-based than in reference (control) specimens.

The primary goal of this project is to further develop the laboratory obtained proof-of-principle of bacteria-based self-healing concrete into a series of products which can be successfully applied outdoors. This asks for a development strategy in which a set of target products, covering a wide area of concrete applications, will be specifically developed, characterized, and tested both in the laboratory and under outdoors conditions at intermediate—and full scale. The developmental step from lab table to outdoors application comes with several scientific and technical challenges. Does the observed laboratory-based functionality depend on, and is thus affected by, the concrete mixture composition, quality, and quantity? Therefore, the self-healing capacity of a series of different types of bacteria-based concrete products will be quantified in this project both under laboratory—and intermediate—to full scale outdoors conditions. One specific technical issue that will also be addressed in this project is the necessary issue of process up-scaling.

For full scale applications mass production of healing agent and incorporation in bulk material is needed and therefore technical as well as economical feasibilities needs to be addressed, e.g. is the final product economically competitive with existing market products? As outdoors conditions differ substantially from those in the climate-controlled lab environment, application of self-healing concrete in different environments ask for tailor-made adaptations of the amount and type of healing agent and in general the overall concrete mixture composition. The primary goal is therefore the development of a series of specific concrete products, each of which can be applied in a specific concrete application field. The project consists therefore of five interconnected stages.

Until now, the proof-of-principle of the self-healing capacity of bacteria-based concrete has been established and quantified in the laboratory. This was done using a model (standardized) concrete mixture composition based on a 0 to 8-mm aggregate size composition. Self-healing functionality of test specimens with incorporated bacteria-based healing agent was found to be superior over control specimens. However, for successful outdoors application, specific practical application fields and respective tailor-made concrete products have to be developed and thoroughly tested first, both in the laboratory and under outdoors conditions. For the development of a repair mortar for concrete constructions featuring an in-built self-healing mechanism two types are targeted:

1. A self-healing repair mortar to be applied on existing (thus non-self-healing) and damaged concrete constructions
2. A spray concrete that can be applied as liner on constructions to prevent leakage of, and ingression of chemicals in, the underlying classical (non-self-healing) concrete

Thus for each application field the concrete mixture and healing agent composition needs to be optimized, its resulting concrete characterized, and its functionality tested. Benefits of these novel concrete repair products are that they extend the service life of structures while requiring at the same time less maintenance and repair than currently existing types of repair materials. Practical application of this novel generation of self-healing repair materials will thus result in less resource consumption (cement, aggregate material and energy). Moreover, in combination with the fact that the incorporated autonomous healing agent is of biological origin and fully renewable, this concrete can be considered innovative as it is not only substantially more durable but particularly more sustainable than currently available types of concrete.

2 UP-SCALING PRODUCTION OF HEALING AGENT AND DISCUSSION

The healing agent which is incorporated in the concrete repair material consists primarily of a specific group of spore-forming alkali-resistant bacteria of the genus *Bacillus* and a suitable type of feed for the bacteria. The feed is metabolically converted into limestone what acts as sealer of occurring cracks, thus reducing leakage and ingression of adverse chemicals. The principle mechanism of bacterial crack healing is that the bacteria themselves act largely as a catalyst, and transform a precursor compound to a suitable filler material. Thus for effective self healing, both bacteria and a biocement precursor compound should be integrated in the material matrix. Bacteria that can resist concrete matrix incorporation exist in nature, and these appear related to a specialized group of alkali-resistant spore-forming bacteria. The applied self-healing agent consists thus in fact of two components: one is the bacteria, which thus mainly act as catalyst in a biochemical reaction, and the second is the mineral precursor component, usually calcium lactate, which is converted by the bacteria to calcium carbonate based minerals:

$$Ca(C_3H_5O_2)_2 + 5Ca(OH)_2 + 7O_2 \rightarrow 6CaCO_3 + 10H_2O$$

Both bacterial spores and ‘feed’ can be stored in reservoir capsules such as expanded clay particles prior to addition to the concrete mixture.

Advantage of the expanded clay-based healing agent is that crack-healing in concrete is significantly better than in control concrete (Figures 1 and 2). Disadvantage of this type of healing agent however is that the volume of healing agent-impregnated expanded clay particles needed for obtaining significant self-healing effects reduces strength of the mortar substantially. This is due to the fact that only up to 20% of the expanded clay particle volume can be used as healing agent storage space as most (80%) of the internal pores are not connected. Our novel approach therefore is to produce a tablet type of healing agent using powder compression techniques. This method yields strong particles which are composed of almost 100% effective concrete healing ingredients, i.e. bacteria and feed (see picture). The functionality of this second generation of healing agent in a variety of concrete products is currently under investigation in our laboratory.

ACKNOWLEDGEMENTS

Financial support from the Delft Centre for Materials (DCMat: www.dcmat.tudelft.nl) and Agentschap NL (grant SHM01018) for this work is gratefully acknowledged.

Concrete Repair, Rehabilitation and Retrofitting III – Alexander et al. (eds)
© 2012 Taylor & Francis Group, London, ISBN 978-0-415-89952-9

Evaluation of crack patterns in SHCC with respect to water permeability and capillary suction

C. Wagner, A. Dollase & V. Slowik
Leipzig University of Applied Sciences, Leipzig, Germany

ABSTRACT: Strain-Hardening Cement-Based Composites (SHCC) are characterized by a high strain capacity of up to 5%. This behavior may be attributed to the formation of numerous closely spaced cracks with comparatively small widths. When SHCC is used for crack-bridging repair layers on concrete surfaces, the durability of the respective repair layer will depend on its water permeability and the latter is strongly influenced by the crack pattern in the SHCC. The present study deals with the characterization of crack patterns which are characteristic for SHCC. An evaluation method is proposed which considers both the crack density and the crack width distribution. The latter may be presented as so-called Crack Width Polygon (CWP) the format of which resembles the one of grain size distribution curves. For the comparison of different crack patterns by a single numerical value which is based on the CWP, the so-called Cumulated Crack Width Value (*CCV*) is proposed. The results of the crack pattern evaluation are compared to those of permeability and capillary suction measurements at cracked SHCC specimens. The objective of the presented work is to estimate the durability of cracked SHCC repair layers on the basis of observed crack patterns.

1 INTRODUCTION

The water permeability is an important indicator for the durability of concrete structures. On the one hand, the water may directly affect the material properties of the concrete and, on the other hand, it is the transport medium for other substances which might be damaging. Hence, the water permeability of concrete members should be minimized. This may be accomplished by restricting the number of cracks as well as the crack widths. Restricting crack widths is conventional practice in design codes for ordinary steel reinforced concrete structures. Currently, the number of cracks is not taken into account in technical regulations. A large number of closely spaced cracks might lead to a lower durability, for example in case of Strain-Hardening Cement-Based Composites (SHCC).

The authors' motivation for the characterization of crack patterns in SHCC results from the applicability of this material for repair layers on cracked concrete surfaces (Rokugo et al. 2005, Wagner et al. 2008). Repair layers made of SHCC are capable of bridging comparatively large crack opening displacements in the substrate because of their high deformability. The mechanical behavior under this type of loading has been investigated by Kunieda et al. (2004) and by Wagner & Slowik (2011).

Because of the small crack widths in SHCC, an improved durability is expected. Whether this assumption is correct, is one of the questions addressed in recent studies on the behavior of SHCC.

As stated before, the water permeability of materials or structures may be used as an indicator for the durability. The intention of the presented work was to link the water permeability to the crack pattern. It soon became apparent that the maximum crack width as well as the average crack width should not be used for the evaluation of the water permeability. Furthermore, the strain level is also not directly connected to the water transport properties since the resulting crack pattern will depend on the particular loading conditions. It is proposed to base the estimation of the water permeability on the actually observed crack patterns. The latter should be characterized by considering both the crack width distribution and the number of cracks. An attempt is made to link the characteristics of observed crack patterns to calculated theoretical water flow rates Q_t whereby this calculation is based on the Hagen-Poiseuille equation (see eq. 1). Obviously, the crack width w is the dominant influence on the water permeability of an individual crack.

$$Q_t = \frac{\Delta p \cdot w^3 \cdot l}{d \cdot 12 \cdot \eta} \tag{1}$$

2 EXPERIMENTAL PROGRAM

For the permeability tests, dog-bone shaped specimens with a length of 310 mm were prepared. The inner part with constant cross-section had a length of 100 mm. The specimens were subjected to uniaxial tension until certain strain levels (0.25%, 0.50% 1.00%, 1.50%) were reached. The crack patterns on the front and back side of the unloaded specimens were photographically documented and evaluated. Thereby, the number of cracks, the distance between the cracks, and the crack widths could be measured.

For the permeability tests, a standardized test setup was used. At the age of 28 days, the unloaded specimens were on one side subjected to water pressure. The applied pressure gradient was ranging from 0.5 MPa/m to 5 MPa/m.

The capillary water absorption was investigated at the same samples. The center parts (length 80 mm) of the dog-bone shaped specimens had been cut out before and subjected to drying at 50°C until constant mass was reached. Prior to the tests, the cut surfaces of the samples had been sealed. One of the cracked faces of the respective sample was dunked into water with a depth of 2 ± 1 mm. Capillary suction was quantified by measuring the increasing weight of the sample.

3 CHARACTERIZATION OF THE CRACK PATTERNS

The pressure gradient induced water flow rate depends on the crack density (*CD*), i.e., on the number of cracks per unit length, and on the crack width distribution. The latter is of high relevance because of the predominant effect of the crack width on the water flow rate, see eq. 1. A model is proposed which links the water permeability to the crack pattern. As a prerequisite, it is necessary to present measured crack width distributions as so-called Crack Width Polygons (CWP) and to characterize the crack width distribution by a single numerical value (Cumulated Crack Width Value, *CCV*). This eases the comparison of different crack patterns and the identification of correlations with other experimental results, for instance with the water flow rate. The *CCV* is corrected by using a weight function based on eq. 1 in order to consider the influence of different crack widths on the water permeability ($CCV_{Permeability}$). Then, the theoretical flow rate for a given crack pattern may be calculated.

4 RESULTS

The water flow rate is influenced by the variation of the crack pattern characteristics throughout the specimen thickness. This complicates the correlation of the measured water flow rates with the crack pattern parameters. The water flow coefficient linking the actually occurring flow rate to the theoretical one (see eq. 1) could not be identified with sufficient accuracy because of the large variation, especially in the case of small $CCV_{Permeability}$. Consequently, an exact quantitative determination of real water flow rates based on observed crack patterns appears to be impossible at the moment. This may be attributed to the large number of not quantifiable influences which are for example the roughness of the crack surfaces, crack branching, and bottlenecks on the crack paths. However, an estimation of the water permeability of cracked SHCC should be possible.

Regarding capillary absorption, a clear correlation between the water absorption coefficient w_{24} and the crack density was observed. The slope of the water absorption coefficient versus crack density curve, however, decreases significantly with the time of exposure. This points to a strong influence of the crack density *CD* especially at the beginning of the water absorption. Within the first hour, the specimens with higher *CCV* (wider cracks) exhibit stronger water absorption than the specimens with smaller *CCV* but the same *CD*. The comparatively large scatter of the measured water absorption values may possibly be attributed to different distributions of the crack spacing. This should be subject of further investigations.

5 CONCLUSIONS

A method is proposed which links the water permeability to the characteristics of existing crack patterns. A constant water flow coefficient could not be identified because of the large variation especially in case of small $CCV_{Permeability}$. Consequently, an exact quantitative determination of real water flow rates based on observed crack patterns appeared to be impossible. However, based on the observed crack pattern, the water flow rate may be estimated. For this purpose, a physical relationship between crack parameters and water flow rate has been derived. Using this relationship it is possible to compare different crack patterns with respect to the water permeability.

In water absorption tests, the effects of the crack width distribution and of the crack density were investigated. The latter turned out to be the predominant influence.

For the prediction of the water absorption behavior on the basis of observed crack patterns, a suitable weight function for the crack widths needs to be identified that allows to determine a Cumulated Crack Width Value $CCV_{Absorption}$. Furthermore, the influence of the crack distance distribution on the water absorption should be studied.

Concrete Repair, Rehabilitation and Retrofitting III – Alexander et al. (eds)
© 2012 Taylor & Francis Group, London, ISBN 978-0-415-89952-9

Cathodic protection of concrete structures with thermally sprayed sacrificial zinc anodes—critical parameters for the protective ability of the sprayed-on anode

Bror Sederholm
Swerea KIMAB, Stockholm, Sweden

Anders Selander & Jan Trägårdh
Swedish Cement and Concrete Research Institute, Stockholm, Sweden

ABSTRACT: This paper presents an ongoing project regarding Cathodic protection of concrete structures with thermally sprayed sacrificial zinc anodes. The results from the first stage show that the resistivity of the concrete has a great influence on the protective ability of the sprayed-on anode. Further, the life length of the zinc anode depends on the external environmental conditions at the anode. In conclusion it can be stated that the prospect of using cathodic protection with thermally sprayed zinc sacrificial anodes is promising but in order to optimize the use, threshold values need to be determined regarding for example the humidity, carbonation depth and the chloride content of the concrete.

1 INTRODUCTION

Reinforcement corrosion is a major problem for concrete structures and it often sets the limit for the service life of the structure. If the detoriation process is identified in time it is often possible to stop or slow down the process. However, many structures are in a state where the corrosion is difficult to stop by conventional methods.

Sacrificial anodes are often discussed and in theory they present a simple and cost effective method and a thermally sprayed zinc layer is maybe the most interesting. The zinc layer (200–500 μm) is sprayed on the concrete surface and connected to the steel reinforcement via drilled holes. The difference in electrochemical potential between the metals makes the reinforcement cathode and prevents or decreases further corrosion.

Thermally sprayed zinc is not a common choice in Sweden due to lack of knowledge and experience in combination with the sometimes difficult evaluation. Some of our nuclear plants use the method on their concrete walls in their water intake buildings but beside that only on special test sites such as the Öland bridge.

2 RESULTS FROM STAGE 1

A full report of the results from stage 1 can be found in Sederholm & Selander (2011). The results presented in the paper will focus on the most important results regarding adhesion, electrochemical potential and visual inspection and in this summary mainly on the electrochemical potential.

2.1 *The Öland bridge*

The Öland bridge which connects the island Öland with the mainland over the Kalmar straight is in many ways a unique construction in Sweden. When it comes to reinforcement corrosion it is the blending water which makes it special. The water was taken from the brackish Baltic Sea, which outside Kalmar contains about 0.7 percent salt.

Table 1 shows the results of the electrochemical potential measurements on the Öland bridge. The results are measured on drilled cores from the edge beam on the bridge. There are no special regulations for thermally sprayed sacrificial anodes but for a cathodic protection system with impressed current the SS-EN 12696 require a 100 mV depolarization after disconnecting for 24 h. At the bridge the measurements were done after 30 minutes disconnection. As can be seen in the table the results are already between 54 and 60 mV which indicates that the depolarization should reach above 100 mV within 24 h.This means that the protective ability is satisfactory for the system and even if the depolarization stops at this level a similar investigation on the Öland bridge, with less depolarization (30 to 50 mV after 24 h) gave 79% reduction in corrosion rate. The results in terms of corrosion products were a reduction of 97% after two years exposure.

Table 1. Electrochemical potential measured on drilled concrete cores from the edge beam on the Öland bridge.

Specimen (mV)	Ö1	Ö2	Ö3
Change in steel reinforcement potential after disconnecting 30 min	54	57	60

Table 2. Electrochemical potential measured on drilled concrete cores from the edge beam on the Forsmark III.

Specimen (mV)	F1	F2	F3
Steel reinforcement potential after disconnecting 30 min	85	92	–

2.2 *The Forsmark nuclear plant*

The concrete walls of the water intake building at Forsmark III is partially below sea level and this can be seen on the concrete surface as well as the zinc layer. The self-corrosion of zinc is relatively high under water and after eight years beneath see level the major part of the zinc layer is corroded.

The electrochemical potential presented in Table 2 on the other hand showed a higher depolarization than on the Öland bridge. A more humid environment could be the explanation for this observation.

3 DESCRIPTION OF STAGE 2

Stage 2 contains two major parts. The first which regards laboratory work is focused on finding and quantifying the critical parameters which has a great influence on the protective ability of the sprayed-on anode. The second is identifying typical construction parts with problems related to chloride induced corrosion. High chloride content and high humidity inside the concrete is the important. The measurements on the field sites will include electrochemical potential, corrosion current as well as continues logging of the humidity and chloride profiles.

The laboratory work is focused on defining and identifying threshold values for different factors believed to have a major influence on the function of the zinc anode such as concrete humidity, thickness of the covercrete, w/c-ratio and chloride contetnt. The different humidity levels will be obtained by saturated salt solutions and the chloride ions will be mixed in.

Figure 1 shows a sketch of the experimental setup. The electrochemical potential will be measured, the corrosion current and the amount of corrosion products in a final stage. The function of the anode will be related to the resistivity of the concrete.

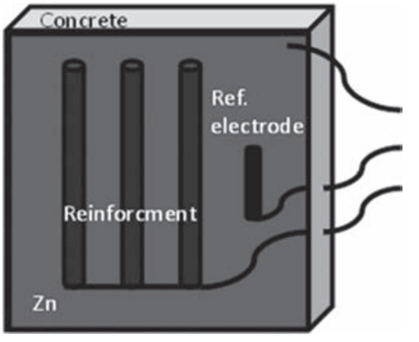

Figure 1. A sketch of the laboratory concrete slab. $150 \times 150 \times 50$ mm.

4 CONCLUSIONS

The following conclusions can be draw based on previous research and the results from the water intake building on Forsmark III (8 year service) and the edge beam on the Öland bridge (11 year service):

- The protective ability of thermally sprayed zinc sacrificial anodes is dependent on the surrounding environment.
- The resistivity of the concrete, which is dependent of the humidity of the concrete, has a great influence on the protective ability of the sprayed-on anode.
- The life length of the zinc anode depends on the external environmental conditions at the anode.
- Thermally sprayed zinc sacrificial anodes have a satisfactory adhesion to the concrete surface.

In conclusion it can be stated that the prospect of using cathodic protection with thermally sprayed zinc sacrificial anodes is promising but in order to optimize the use, threshold values need to be determined regarding for example the humidity and the chloride content of the concrete. The presented laboratory study aims to determine these threshold values.

ACKNOLEDGEMENTS

Elforsk and the Swedish Transport Administration are gratefully acknowledged for their financial support in this project.

REFERENCES

Sederholm, B. & Selander, A. 2011. Katodiskt skydd av betongkonstruktioner…—Etapp I" Elforsk BET 102 (In Swedish).

Concrete Repair, Rehabilitation and Retrofitting III – Alexander et al. (eds)
© 2012 Taylor & Francis Group, London, ISBN 978-0-415-89952-9

Repair of concrete members of seaside apartment buildings deteriorated by steel corrosion

W. Schwarz & F. Müllner
CAS Composite Anode Systems GmbH, Wien, Austria

A. van den Hondel
Cathodic Protection Supplies, Rotterdam, The Netherlands

ABSTRACT: Apartment blocks erected on or near the seaside, especially on the Atlantic coast, are exposed to high sea salt loads. The sea salt is transported inland as a marine aerosol over long distances. Deposition on concrete structures, in combination with high humidity (>80% near sea side), may induce severe damages due to the corrosion of steel in concrete. Conventional repair would require replacement of the with chlorides contaminated concrete, cleaning and subsequent re-encapsulation of the steel rebars and reprofiling. In many cases, e.g. balconies, these conventional repair techniques are not applicable. In the Netherlands, since about 8 years, an innovative technology, based on Cathodic Protection (CP) has been successfully employed using the composite anode system, for the repair and protection of balconies and concrete members of facades of apartment buildings near the marine coast line. The composite anode is easy to apply—like a conventional paint system—and has particular the advantage that only concrete that is mechanically damaged or is disbonded from the reinforcement has to be replaced. Structurally sound concrete may be left in place. The technology was successfully employed for the sustainable repair, protection and maintenance of apartment buildings in Scheveningen, Zandhorst, Bussum, Katwijk und Delft in the Netherlands.

1 INTRODUCTION

Apartment blocks erected on or near the seaside, especially on the Atlantic coast, are exposed to high sea salt loads. Conventional repair would require replacement of the with chlorides contaminated concrete, cleaning and subsequent re-encapsulation of the steel rebars and reprofiling. In many cases, e.g. balconies, these conventional repair techniques are not applicable.

In the Netherlands, since about 8 years ago, an innovative technology, based on cathodic protection (CP) has been successfully employed using the composite anode system, for the repair and protection of balconies and concrete members of facades of apartment buildings near the marine coast line. The advantage of the technology is that the concrete contaminated with chlorides has not to be removed and replaced with repair mortar. In concrete members in whom the steel reinforcement is difficult to access from the surface, like beams supporting balconies, discrete galvanic anodes are installed.

2 COMPOSITE ANODE SYSTEM—TECHNIQUE & APPLICATION

CAST^{x+} is a two component aqueous alkaline (pH 12,7) alumo-silicate/polymer composite paint for the active cathodic corrosion protection of reinforcing steel in concrete. The alumo-silicate component forms the proprietary micro capillary matrix that assures high adhesion to the concrete at current loads up to 30 mA/m^2 and up to 70 mA/m^2 for short periods.

The composite paint is applied like any other concrete paint either by rolling or by air-less spray. Current distributors—termed as primary anodes—are embedded into the composite paint (figure 1). Finally, a decorative cover paint is applied.

Corrosion protection of the steel reinforcement is achieved by applying a voltage in the range of 2–5 Volts between the composite paint and the steel reinforcement, inducing a DC current of 1–5 mA/m^2. Start-up and operation of the composite anode system follows the rules and recommendations of EN-ISO 12696 (2012).

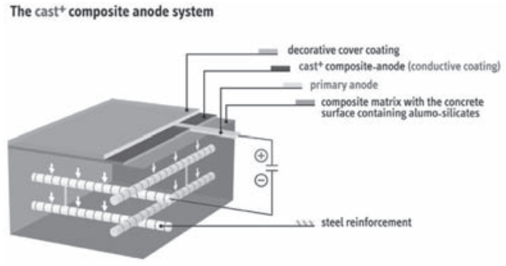

Figure 1. Schematic presentation of the CAST+ composite anode system, based on the CAST+ composite anode paint.

3 CASE STUDIES

From 2004 until 2011, several apartment buildings in Delft, Groningen, Den Haag, Scheveningen, Katwijk, Assen, Bussum and Zandvoort were repaired with the composite anode system technology.

3.1 *Apartment buildings on Scheveningen Strand*

Scheveningen, a district of Den Hague—the capital of the Netherlands—is a modern and a prominent beach resort in the Netherlands. Overlooking the beach, close to the famous pier and the Kurhaus concrete elements of the façade of an apartment complex were repaired and protected with the composite anode system covering a total area of 1600 m^2 (figure 2).

3.2 *Apartment buildings in Zandvoort*

In 2011, the new $CAST^{3+}$ composite anode system was applied on two apartment buildings in Zandvoort. The $CAST^{3+}$ paint is the 3d generation of the composite paint systems exhibiting high durability, high weathering resistance (UV-resistance, frost resistance, frost thaw salt resistance).

The performance and efficiency of CP systems is measured according to EN ISO 12696 by interrupting the applied current for at least 24 hours. Steel rebars are reliably protected against corrosion, if the potentials of the steel rebars shift by at least 100 mV towards the positive direction within not more than 24 hours.

Results show that the steel rebars in the concrete members protected by the $CAST^{3+}$ composite anode system are reliably protected from corrosion. Installation costs are competitive with conventional repair techniques.

Figure 2. Installation of the CAST+ composite anode system on apartment buildings in Scheveningen 2008.

Table 1. Depolarisation values according to EN ISO 12696, measured on 22 November 2011, Apartment building Zandvoort (applied voltage 2,00 Volt).

Zone	On	Inst. Off	60 min Off	1 hour Depol.
North				
Ref 1	0,704 V	0,494 V	0,356 V	*138 mV*
Ref 2	0,619 V	0,533 V	0,282 V	*251 mV*
East				
Ref 3	0,925 V	0,482 V	0,373 V	*109 mV*
Ref 4	0,649 V	0,481 V	0,326 V	*155 mV*
South				
Ref 5	0,695 V	0,592 V	0,453 V	*139 mV*
Ref 6	0,601 V	0,453 V	0,319 V	*134 mV*

4 CONCLUSION

Sea side apartment buildings are exposed to high loads of marine salt that cause severe damages to the concrete structures induced by the corrosion of the steel reinforcement. The $CAST^{3+}$ Composite Anode System offers a cost efficient and reliable technology for the repair and protection of concrete members exposed to marine salt. The technology is highly sustainable as it produces nearly 0-waste, requires minimum concrete preparation—in comparison with water jetting at 2000 bars for conventional repair techniques and involves minimum traffic impairment. In the Netherlands, this technology has now a successful record of over 8 years in the repair, protection and maintenance of sea side apartment buildings. There were no problems in meeting the 100 mV criterion from ISO-EN 12696. Furthermore no signs of ageing visually or electrochemically are observed.

Concrete Repair, Rehabilitation and Retrofitting III – Alexander et al. (eds)
© 2012 Taylor & Francis Group, London, ISBN 978-0-415-89952-9

Galvanic corrosion protection of steel in concrete with a zinc mesh anode embedded into a solid electrolyte (EZA): Operational data and service time expectations

W. Schwarz & F. Müllner
CAS Composite Anode Systems GmbH, Wien, Austria

A. van den Hondel
Cathodic Protection Supplies, Rotterdam, The Netherlands

ABSTRACT: The efficiency of the Galvanic Corrosion Protection (GCP) of the steel reinforcement of a novel Embedded Zinc Anode (EZA) is evaluated on three types of civil structures—a road bridge (cantilevers, part of the underside the bridge deck and an abutment) in the Styrian Alps in Austria, concrete abutments of a steel bridge and support-beams for the bearings of a road bridge in the Netherlands. The EZA is applied to the surface of concrete members whose steel is to be protected from corrosion by embedding a zinc mesh (2–4 kg/m^2) into a proprietary mortar that hardens to a solid electrolyte. The efficiency of the GCP was monitored with embedded reference cells, concrete resistivity—and macro cell sensors. Data collected over a period of up to nearly 5 years show that the EZA protects the steel reinforcement efficiently and reliably. Based on these data, estimation of expected service time is discussed.

1 INTRODUCTION

Galvanic corrosion protection was first employed to protect a bridge deck in Illinois in 1977 within the cooperative highway research program, with mixed results (Kepler et al. 2000). A problem with the initially applied sacrificial anodes was that their protection current decreases with time, and they eventually become passive, so most systems have a relatively short useful life (Virmani & Clemena 1998).

In the 1990's, sacrificial anode systems based on sprayed zinc anodes, zinc foil glued to the concrete surface (zinc hydrogel system), zinc mesh pile jackets around bridge columns filled with sea water were starting to be evaluated and used for the protection of bridge structures.

To a limited extent, zinc anodes embedded into the concrete overlay, are used to protect the steel reinforcement especially accompanying concrete repair.

The driving voltage is set by the properties of the anode, the interface of the anode to the concrete and by the electrolytic conductivity of the concrete overlay. Sprayed zinc anodes require sufficient humidity and high chloride contents to operate satisfactorily (Bäßler et. al.).

A novel galvanic zinc anode system, composed of a zinc mesh embedded into a proprietary mortar that solidifies into a solid electrolyte, was developed by CAS. The solid electrolyte of the embedded zinc anode system (EZA) is based on a tecto-alumosilicate-binder containing additives that prevent passivation of the zinc anode, assure high and durable galvanic activity of the zinc anode and high and durable adhesion towards the concrete overlay.

The efficiency of the galvanic corrosion protection (GCP) of the steel reinforcement with a novel embedded zinc anode (EZA) is evaluated on three types of civil structures—a road bridge (cantilevers, part of the underside the bridge deck and an abutment) in the Styrian Alps in Austria, concrete abutments of a steel bridge and support-beams for the bearings of a road bridge in the Netherlands. The results of the evaluation of the performance and estimation of the service time of the galvanic anodes system are presented.

2 DESCRIPTION OF THE SYSTEM

The galvanic EZA system is composed of a zinc mesh embedded into the proprietary solid electrolyte (figure 1) that ascertains an optimum electrolytic contact between the zinc anode and the concrete overlay. The zinc anode, a zinc mesh, is embedded into the proprietary solid electrolyte that ascertains an optimum electrolytic contact between the zinc anode and the steel reinforcement.

The efficiency of corrosion protection by the EZA may be evaluated according to the procedure described in EN 12696—the 24 h depolarisation criterion.

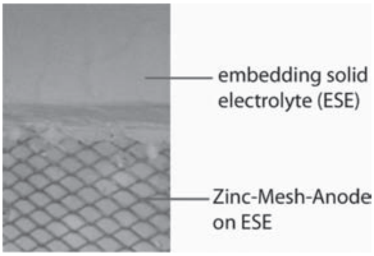

Figure 1. Embedded galvanic zinc anode (EZA): zinc mesh embedded into the TASC mortar from which the embedding solid electrolyte forms.

Figure 2. County road bridge "Alplgrabenbrücke" in the Styrian Alps on the county road B72.

3 FIELD INSTALLATIONS

3.1 *Alpine road bridge*

For the evaluation of the efficiency and durability, the EZA system (2 kg Zinc/m^2) was installed on concrete members of a road bridge in an alpine region of Styria (Austria).

The galvanic currents of the EZA system decrease over a time period of about 1,5 years (Figure 3) towards nearly stable values.

Considering self corrosion and local variations of the current flow, a service time expectancy of minimum 15 years, including "hot spots"—areas of high chloride content and humidity—may be safely assumed for a EZA containing a zinc mesh with 2 kg/m^2. Results indicate that, provided the EZA is covered with a protective coating, galvanic chloride extraction and immobilization in the EZA will be efficient enough to prevent renewed corrosion of the steel after the end of service time.

3.2 *De Meernbrug Steel Bridge & 'Hubertusviaduct' in Den Haag*

The EZA system was installed on the abutments of the De Meernbrug Steel Bridge in Utrecht 2010 (fig. 4) and on the beams supporting the bearings of the Hubertusviaduct' in Den Haag 2008 (fig. 5).

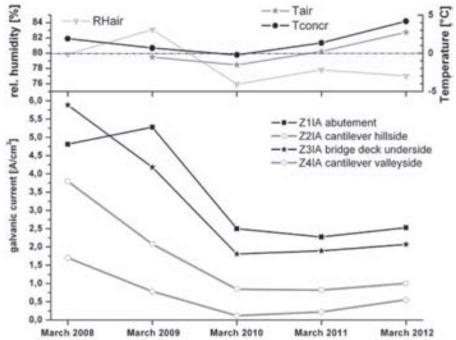

Figure 3. Galvanic currents ZxIA, ambient (Tair) and concrete temperature (Tconcr) and ambient humidity (RHair) averaged over 1–26 March of each year.

Figure 4. One of the abutments of the De Meerenbrugg steel bridge in Utrecht protected with the EZA system.

Figure 5. Support for the bearings on one of the abutments of the Hubertus viaduct in Den Haag.

REFERENCES

Bäßler, R., Burkert, A., Eichler, G. & Mietz, J. 2006., In M.G. Grantham, R. Jaubertie, C. Lanos, (Eds.), Integrated Protection System for Chloride Deteriorated Concrete Structures.*Concrete Solutions,* 220–234. Garston Watford.

Kepler, J.L., Darwin, D. & Locke Jr., C.E. 2000. Evaluation of Corrosion Protection Methods for Reinforced Concrete Highway Structures, Structural Engineering and Engineering Materials SM Report No. 58, University of Kansas Center for Research Inc., Lawrence, Kansas, May 2000

Virmani, Y.P. & Clemena, G.G. 1998. Corrosion Protection—*Concrete Bridges Report No. FHWA-RD-98-088,* Federal Highway Administration, Washington, D.C.

Concrete Repair, Rehabilitation and Retrofitting III – Alexander et al. (eds)
© 2012 Taylor & Francis Group, London, ISBN 978-0-415-89952-9

The use of discrete sacrificial anodes in reducing corrosion rate in chloride contaminated reinforced concrete

P.A. Arito, H. Beushausen, M.G. Alexander & M. Otieno
Concrete Materials and Structural Integrity Research Unit, Department of Civil Engineering, University of Cape Town, South Africa

ABSTRACT: The increasing number of corrosion-affected Reinforced Concrete (RC) structures in South Africa requires an urgent need for economical, technically sound and innovative concrete repair technologies. Currently, in South Africa, the most commonly used repair techniques are patch repairs and corrosion inhibitors. Other potentially successful methods such as sacrificial anodes are rarely exploited. This paper presents the preliminary results from an on-going study aimed at investigating the effectiveness of Sacrificial Anode Cathodic Protection (SACP) systems for service life extension of chloride contaminated RC structures in South Africa. The experimental set-up comprised two RC slab specimens. The SACP system that was used in this study comprised discrete zinc disks placed in a cylinder of a proprietary high alkaline mortar. The provisional results show that corrosion rates in chloride contaminated reinforced concrete can successfully be reduced by the discrete anodes used in this study.

1 INTRODUCTION

Cathodic protection (CP) is an electrochemical technique that has been used to control corrosion of steel in new RC structures and also to retard rebar corrosion in existing structures. It relies on the application of voltage to the reinforcing steel. CP systems can be categorized into two: Impressed current CP (ICCP) systems and sacrificial anode CP (SACP) systems. SACP systems can be configured as surface applied, encapsulated and non-encapsulated systems.

Discrete zinc disks (also known as 'point anodes' or 'hockey puck' anodes) are a type of encapsulated SACP systems. They comprise zinc plugs/disks in a cylinder of a proprietary high alkaline mortar for installation in cored holes in concrete. They are usually installed in a manner that ensures that they are in contact with a purpose designed backfill in cavities within the concrete. These anodes are usually used in patch repairs in buildings and in the mitigation of corrosion in repaired bridge deck spalls and patches in inland and marine substructure components.

This paper presents the preliminary results of an on-going study on sacrificial anodes in reducing the corrosion rate of steel that is embedded in chloride contaminated concrete.

2 EXPERIMENTAL SET UP

The effectiveness of sacrificial anodes in service life extension of chloride contaminated concrete was evaluated with respect to chloride concentration and binder type on two $100 \times 1000 \times 1500$ mm RC slabs. 10 mm diameter rebars—at a spacing of 100 mm centres in each direction—were embedded in the slabs. The slabs were exposed to an outdoor environment in Cape Town, South Africa.

The slabs were cast using: CEM I 42.5 N; Fly ash (Class F); 13 mm greywacke stone; Klipheuwel sand; a commercially available sacrificial anode; 10 mm diameter high yield steel bars and Sodium chloride. A summary of the concrete mix design is shown in Table 1.

Each slab was divided into two halves. One half of each slab was admixed with 0.6% chlorides by mass of binder while the other half was admixed with 1.8% chlorides by mass of binder during casting. The cast RC slabs were water cured for 4 weeks. Water was poured on the concrete three times a day during the entire curing period.

After 8 weeks from the last date of casting, corrosion rates were induced in the slabs over a period of one week using a direct anodic current of 14.14 μA. Sacrificial anodes were installed after a period of 22 weeks from the last date of casting. 6 No. $100 \times 100 \times 60$ mm deep cavities at a square grid of 450×450 mm were excavated in each slab. Thereafter, sacrificial anodes were installed in the slabs according to the manufacturer's instructions. A cementitious repair mortar was used as the backfill during the installation process. The mortar was water cured for 1 week using hessian and a plastic sheet.

The corrosion rate in the slabs was monitored using a Gecor-6 corrosion rate meter. Auxiliary data such as the atmospheric temperature and relative humidity were measured using temperature and relative humidity probes.

Table 1. Summary of concrete mix design.

Material (kg/m^3)	100% OPC	70/30 OPC/FA
CEM I 42.5 N	405	283
Fly ash	–	121
Klipheuwel sand	850	767
Greywacke (13 mm)	990	1039
Water	190	190
w/b ratio	0.47	0.47

Table 2. A summary of corrosion rate measurements in the test slabs.

Parameter		Slab ID	
Slab type and designation		A	B
Binder type		100% OPC	70/30 OPC/FA
Average corrosion rate after withdrawal of current (μA/cm^2)			
Portion of slab	0.6% admixed chlorides	1.64 ± 0.02	0.50 ± 0.12
	1.8% admixed chlorides	2.97 ± 0.63	1.50 ± 0.79
Average corrosion rate after installation of SACP (μA/cm^2)			
Portion of slab	0.6% admixed chlorides	0.12 ± 0.10	0.16 ± 0.01
	1.8% admixed chlorides	0.14 ± 0.06	0.68 ± 0.42

3 RESULTS AND DISCUSSIONS

A summary of the changes in corrosion rate within the slabs is shown in Table 2 and Figure 1.

A two-point moving average trend line of corrosion rate in the test slabs is shown in Figure 1.

A diagrammatic illustration of the changes in corrosion rates is shown in Figure 3.

The average corrosion rate before the SACP system was installed was calculated as the arithmetic mean of the corrosion rate values in each of the two portions of the slabs within the period under consideration. The average corrosion rate after the installation of the SACP system was calculated from the arithmetic mean of the last two corrosion rate values (i.e., corrosion rate values after day 84 in Figure 1).

From Table 2 and Figure 1, it can be observed that the installation of sacrificial anodes in the slabs resulted in a reduction in average corrosion rates in the test slabs. The corrosion rates in Slab A decreased by 1.52 μA/cm^2 (i.e., 93%) and 2.83 μA/cm^2 (i.e., 95%) in the portions that were admixed with 0.6% and 1.8% chlorides respectively. In Slab B, the corrosion rates decreased by 0.35 μA/cm^2 (i.e., 69%) and 0.82 μA/cm^2 (i.e., 54%) within the portions that were cast with 0.6% and 1.8% chlorides respectively. From these results, it can be observed

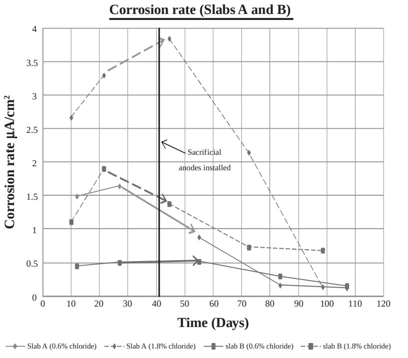

Figure 1. Two-point moving average trendlines of corrosion rates in slabs A and B.

that the slab that was cast using 100% CEM 1 experienced a higher reduction in corrosion rate than the slab that was cast using 70/30 CEM I/FA. This observation could be attributed to the high conductivity (low electrical resistivity) of 100% CEM I concrete which facilitates easy flow of galvanic currents from the discrete anode. The reduction in corrosion rate in the slab cast using 100% CEM I was 3–4 times the reduction in the slab cast using 70/30 CEM I/FA. The reduction in corrosion rates were high in the portions of the slabs that were cast using 1.8% chlorides than those cast using 0.6% chlorides.

4 CONCLUSIONS

This paper is aimed at investigating the use of sacrificial anodes in service life extension of reinforced concrete structures in South Africa. This objective was achieved through an investigation into the effectiveness of sacrificial anodes with respect to concentration of chlorides and binder type. The preliminary results that have been collected and analyzed show that corrosion rate in chloride contaminated reinforced concrete can be reduced using discrete sacrificial anodes. Furthermore, the preliminary results show that the RC slab that was cast using 100% CEM 1 experienced the greatest reduction in corrosion rate.

ACKNOWLEDGEMENTS

The authors acknowledge the general financial support offered by the following organizations for research carried out by the Concrete Materials and Structural Integrity Research Unit at the University of Cape Town: Cement and Concrete Institute, National Research Foundation, Pretoria Portland Cement, Afrisam, Sika South Africa.

Bonded concrete overlays and patch repairs

This page intentionally left blank

Concrete Repair, Rehabilitation and Retrofitting III – Alexander et al. (eds)
© 2012 Taylor & Francis Group, London, ISBN 978-0-415-89952-9

Concrete overlays for pavement rehabilitation summary

Peter C Taylor
National Concrete Pavement Technology Center, Ames, Iowa, USA

Dale Harrington
Snyder and Associates, Ames, Iowa, USA

1 INTRODUCTION

Highway agencies are continually being asked to do more with less when managing their pavement networks. Concrete overlays offer an opportunity to address these needs in that they make use of the equity in the existing infrastructure while delivering long term serviceability at reasonable cost. In addition, they contribute to more sustainable practices by reducing the amount of waste material generated, and use of virgin non-renewable resources.

2 WHAT IS A CONCRETE OVERLAY?

A concrete overlay is a method of pavement rehabilitation that involves placing a layer of concrete over an existing pavement. The following alternative approaches to rehabilitating existing systems can be considered:

- Remove the existing systems and start again
  This approach can provide a high quality, long-term solution but also creates a large amount of waste material that must be disposed of at high cost and environmental impact.
- Apply patches to localized distressed areas
  This approach may extend the life of the pavement for a few years but is, at best, simply a delaying tactic.
- Overlay the existing pavement
  This makes use of existing equity already in place while providing a smooth, long term solution. Disadvantages are that connections with cross streets and services require attention and clearances under bridges may limit the thickness of the new layer.

3 SELECTION OF OVERLAY TYPE

Overlays can be applied to all types of existing pavement including asphalt, concrete and composite systems.

Overlays are considered in two different forms: Bonded and unbonded, regardless of the substrate:

- Bonded overlays are structurally connected to the existing layers and depend on them for load carrying capacity. As such they can be relatively thin but the substrate has to be in reasonable condition. Panel sizes are normally small to reduce the effects of curling and warping.
- Unbonded overlays are separated from the substrate, thus removing problems associated with joints, cracks or horizontal movement in the substrate. The substrate can therefore be in relatively poorer condition but unbonded pavements generally have to be thicker to carry applied loads.

The decision whether to use a bonded or an unbonded overlay is largely based on the condition of the existing pavement.

Typically, bonded systems are about 2 to 5 in. (50 to 125 mm) thick, and deliver a life of 15 to 25 years, depending on traffic loading. Unbonded pavements are normally 4 to 11 in. (100 to 280 mm) thick. Existing concrete can be in poor condition, including material-related distress, but must be stable and uniform.

4 DESIGN

Bonded concrete overlay systems are primarily intended to improve pavements that are structurally sound but need increased structural capacity and/or correction of surface defects. Unbonded concrete overlay systems are usually designed to provide a service life associated with new pavements. They are typically designed to tolerate joint degradation, cracking, and localized failures in the underlying pavement structure by isolating movement between the existing pavement and the overlay.

There are a number of pavement thickness design tools available including the AASHTO 1993 empirical method. ACPA has published a tool called WinPas (2011) that is based on the AASHTO 1993 approach (ACPA 2011a). ACPA also released a web application in 2011 (ACPA 2011b) for thickness design of bonded concrete overlays on asphalt based on work by Roessler (2008).

Another mechanical empirical approach called DARWIN ME (2011) has recently been published by AASHTO. A limitation of this approach is that the model is not set up to assess concrete layers less than 6 inches thick.

4.1 *Bonded overlay*

Conventional concrete mixtures can be used for bonded concrete overlays, although mixtures that are slightly sticky are preferred. Conventional concrete mixtures can be proportioned for rapid strength gain if required. High-modulus structural fibers in the mixture can improve the toughness and post-cracking behavior of the concrete and help control plastic shrinkage cracking. In concrete overlays, aggregate with CTE similar to or lower than that of the existing concrete pavement will help ensure the two layers move together, thus reducing stresses at the interface.

For bonded overlays on concrete the joint type, location, and width must match those of the existing concrete pavement in order to create a monolithic structure. Matched joints prevent reflective cracking. To minimize curling and warping stresses, some additional transverse and longitudinal joints may be sawn in the overlay between the matched joints.

4.2 *Unbonded overlay*

The separation layer design is a primary factor influencing the performance of unbonded overlays on concrete pavements. The separation layer provides a shear plane that helps prevent cracks from reflecting up from the existing pavement into the new overlay. A common separation layer is a conventional 1 in. (25 mm), well-drained asphalt surface mixture, which provides adequate coverage over irregularities in the existing pavement. The separation layer does not provide significant structural enhancement; therefore, the placement of an excessively thick layer should be avoided. Some states are experimenting with geotextile separation layer materials.

Care must be exercised when using an asphalt separation layer under heavy truck loading to prevent stripping when the asphalt is not well drained.

Conventional concrete mixtures are typically used for unbonded overlays of concrete pavements. Early opening can be aided by use of accelerating admixtures and maturity measurements.

Doweled joints are used for unbonded overlays of pavements that will experience significant truck traffic, typically pavements 8 in. (200 mm) and thicker.

During evaluation and design of a bonded concrete overlay project, existing subgrade drainage should be evaluated. If necessary, steps should be taken to ensure adequate drainage in the future.

5 CONSTRUCTION BEST PRACTICES

In bonded overlays on concrete, repairs may be necessary to achieve the desired load-carrying capacity and long-term durability.

The objective of milling is not to obtain a perfect cross section or to completely remove ruts. In general, the depth of milling should be minimized in bonded systems because it results in loss of structural support.

For bonded overlays on concrete, surface preparation of the existing pavement is required to produce a roughened surface that will enhance bonding between the two layers. Construction.

Conventional concrete paving practices and procedures are normally followed for all concrete overlays.

Curing is especially critical on a concrete overlay because its high surface area to volume ratio makes the thin concrete layer sensitive to rapid moisture loss.

Timely joint sawing is necessary to prevent random cracking.

6 CLOSING

There are many millions of square feet of overlays that have been placed in the USA over many years. In general they provide excellent service, but like any construction system, attention has to be paid to details in design and construction to allow for the different characteristics of the layers of the pavement system. Making use of the equity in the existing system helps to make rehabilitation of deteriorated pavements efficient and sustainable.

Concrete Repair, Rehabilitation and Retrofitting III – Alexander et al. (eds)

Optimizing the steel fibre and mesh combinations used in repairing existing pavements with Ultra Thin Continuously Reinforced Concrete Pavements (UTCRCP)

E.P. Kearsley & H.F. Mostert
Department of Civil Engineering, University of Pretoria, South Africa

ABSTRACT: As part of the National Highway renewal programme currently in progress in South Africa, full-scale experimental trial sections of Ultra Thin Continuously Reinforced Concrete Pavements (UTCRCP) have been constructed. The UTCRCP consists of a 50 mm thick layer of 90 MPa concrete containing approximately 100 kg/m^3 of steel fibre as well as a steel mesh of 5.6 mm reinforcing bars at a spacing of 50 mm to 100 mm centre to centre. The UTCRCP can handle high deflections and it is intended for use as an overlay to rehabilitate weakened pavement structures. The design, construction and quality control of the material has proven to be a challenge. Pavement design engineers normally see concrete pavements as rigid pavements that fail in a brittle manner. The un-reinforced concrete pavements with closely spaced movement joints built in the past were rigid brittle structures, but the use of continuously reinforced concrete pavements, has resulted in both a reduction in the volume of concrete required for any given pavement, and a more flexible behaviour of the pavement. Optimization of the concrete mix composition through the use of modern superplasticizers and steel fibres can not only significantly enhance the flexural strength of the concrete, but also result in a more ductile failure. UTCRCP can result in a significant saving in the volume of material required for a pavement designed to take a given traffic load. Since 2006 researchers at the University of Pretoria have been involved with analyzing and testing materials for use in these pavements and in this paper an overview will be given of design, construction and quality control issues encountered. Conventional design procedures cannot be used to determine the required reinforcement diameter and spacing or suitable fibre content. This paper focuses on the optimization of the combination of mesh reinforcing and fibres in the UTCRCP.

1 BACKGROUND

Concrete pavements are increasingly being used to extend the service life of old flexible pavements (Kannemeyer et al., 2007). As part of the National Highway renewal programme currently in progress in South Africa, full-scale experimental trial sections of Ultra Thin Continuously Reinforced Concrete Pavements (UTCRCP) have been constructed. The UTCRCP can handle high deflections and it is intended for use as an overlay to rehabilitate weakened pavement structures. The design, construction and quality control of the material has proven to be a challenge. Pavement design engineers normally see concrete pavements as rigid pavements that fail in a brittle manner. The un-reinforced concrete pavements with closely spaced movement joints built in the past were rigid brittle structures, but the use of continuously reinforced concrete pavements, has resulted in both a reduction in the volume of concrete required for any given pavement, and a more flexible behaviour of the pavement. Optimization of the concrete mix composition through the use of modern superplasticizers and steel fibres can not only significantly enhance the flexural strength of the concrete, but also result in a more ductile failure. If the actual failure mechanism of UTCRCP is taken into account, significant savings can be made in the volume of material required for a pavement designed to take a given traffic load.

Pavement engineers design concrete pavements to carry a given number of axle loads by limiting the actual flexural stress in the concrete to a fraction of the flexural strength. The flexural strength of concrete is normally determined from a beam in four point bending or a Modulus of Rupture (MOR). The MOR is however not a true material property (Denneman et al., 2010) and the actual strength of the UTCRCP differs significantly from that used in the mathematical models. The MOR does not take into account size effects, the post-cracked strength of fibre reinforced concrete, the alignment of fibres or the fact that the actual stresses in the pavement acts in three dimensions, while the MOR is a two dimensional test.

The actual behavior and failure of the UTCRCP can only be accurately modeled by taking the post-cracked behavior of the reinforced concrete into account, yet the standard tests used to determine the properties of concrete are conducted in load control and only the peak load is recorded.

Promising results have been obtained from testing round discs according to ASTM C1550. The disc thickness has been reduced to 55 mm (which is similar to the UTCRCP thickness) and the disc diameter was reduced to 600 mm. The reinforcing that will be placed in the road is placed in the discs and the discs are cured in water and tested in the direction of casting after 28 days. The discs are supported on ball bearings at 3 points, resulting in a span diameter of 550 mm. A load is applied at centre point and the test is conducted in deflection control (1.5 mm/min) using a closed loop material testing system. The midpoint deflection and the load are recorded and the area under the load deflection graph is used to calculate the energy absorption in Joules. This test method has been used on the UTCRCP trial sections constructed for the South African National Roads Agency Limited (SANRAL). The SANRAL specification requires a total energy absorption of 1000 Joules for a deflection of 25 mm. Many of the discs were tested at the University of Pretoria and for the high strength concrete the small contact area at the loading point as well as the three supports seem to cause local failures, significantly altering the test results. A concrete pavement would never be subjected to point loads smaller than a wheel load and therefore it was decided to determine the effect of changing the area of load application as well as the support conditions of the discs.

The effect of support conditions was determined by casting two sets of 6 discs containing hooked ended, 30 mm long hard drawn wire fibres and 5.6 mm high yield reinforcing bars were placed at 50 mm × 100 mm spacing in the discs in the same position (cover) that would be used for the concrete pavement. Half the discs were supported on ball bearings at 3 points while the rest of the discs were supported on a continuous steel ring with a diameter of 550 mm. Both sets of discs were tested using a larger load point than normal and the test results are discussed in this paper.

During field tests with the Heavy Vehicle Simulator (HVS) it was established that a combination of 50 mm × 50 mm × 5.6 mm mesh and 80 kg/m^3 30 mm long hooked-ended steel fibre in a 55 mm thick 80 MPa concrete slab resulted in the longest service life for the UTCRCP (Kannemeyer et al., 2007). The length of the steel fibre, the diameter of the reinforcing bars and the exact spacing of bars has not yet been optimized and current research is aimed at optimizing the reinforcing combination.

2 CONCLUSIONS

UTCRCP can be used to rehabilitate and strengthen existing flexural pavements. There are challenges in both designing and constructing the UTCRCP as the current standard test methods cannot be used to determine the actual material properties of fibre reinforced concrete. Alternative test methods must be developed that can be used to determine material properties that can be used for both non-linear finite element analysis during design and quality control during construction of UTCRCP. Suitable test methods need to take into account factors such as size effects, alignment of fibres, post-cracked strength and three dimensional behavior of UTCRCP.

The round disc test, as detailed in ASTM C1550 can be adapted to provide suitable test results. Punching problems can be eliminated by increasing the area used to apply the load to the high strength discs, while the repeatability of the test can be significantly improved by replacing the 3-point support with a continuous support. The crack pattern at failure of the discs with continuous support resembles the crack pattern observed with full scale testing, indicating that the continuously supported round disc could give a fair indication of the actual behavior of the UTCRCP. More tests would be needed to confirm whether the results obtained from these discs can be used to model the behavior of an actual pavement.

As the UTCRCP is a flexible pavement, it is possible that the riding quality of the pavement can deteriorate to the point where the extent of the vertical movement of the pavement reduces the riding quality of the pavement to an unacceptable level. More research is therefore needed to determine a suitable deflection limit for the round discs. It may be of value to set a minimum energy absorption requirement for a deflection value that would define total failure on the UTCRCP.

The effect of steel fibre length on the load carrying capacity of discs was investigated and it was proven that longer fibres result in higher load bearing capacity. Visual inspection indicated that the mesh did not have a detrimental effect on the ability of the longer fibres to penetrate through the openings in the steel mesh. The long term behavior of UTCRCP could in future be improved by using longer steel fibres.

Although the 50 mm × 50 mm × 5.6 mm mesh with a 60 mm long hook-ended steel fibre content of 80 kg/m^3 outperforms the other combinations, it is possible to meet the current SANRAL requirement of an energy absorption of 1000 Joules for deflections up to 25 mm without using any mesh by increasing the fibre content to 230 kg/m^3. It is difficult to place and compact the UTCRCP containing very high fibre contents and further research should be conducted to establish whether it is practically possible to successfully place UTCRCP with such high fibre contents.

Concrete Repair, Rehabilitation and Retrofitting III – Alexander et al. (eds)
 ISBN 978-0-415-89952-9

Effect of repair materials on durability indexes of concrete

P. Parbhoo, H. Lyimo & S.O. Ekolu
School of Civil & Environmental Engineering, University of the Witwatersrand, Johannesburg, South Africa

ABSTRACT: In this paper, durability index test methods were employed to assess the influence of repair materials on the durability of concrete. Five (5) commercially available repair materials were studied viz:- two special coatings of masonry and carbothane aliphatic paints, and three repair mortars consisting of general purpose, cement-based, and epoxy resin. The oxygen permeability and the water sorptivity test methods were used to determine and compare the performances of the various repair materials. In addition, three types of substrate surface preparation methods were investigated namely chiseling, cutting and brushing of the substrate. The results of the tests show that repair materials do have significant effect on increasing the durability of concrete. It was found that substrate preparation is an important factor in making a durable repair with wire brushed surface preparation giving best performance and chiseling giving least improvement in results. The epoxy resin repair material uniquely showed water-repellant properties in the sorptivity test, not typical of common concrete material behaviour. Accordingly, the applicability of the index test methods on testing of repaired concrete surfaces in the field may require prior knowledge of the characteristics of the repair material used in order to aid interpretation of their durability index test results.

1 INTRODUCTION

Much research has been conducted in the field of concrete durability and a vast amount of repair materials have been developed to improve the durability performance of concrete. These repair materials are highly specialised and are generally highly priced. Although a variety of tests (strength, chemical and electrochemical) are usually conducted on the materials before they are put into production, the long term durability properties of these materials are not well established, in most cases. This investigation work therefore set out to determine the effect that repair materials have on the long term durability of concrete structures.

It should be noted that the repair materials considered in this investigation are not strength enhancers but are designed to protect the reinforcing steel from chemical attack when the surface of concrete has been compromised. Protection of the steel is crucial as reinforcement contributes largely to the load carrying capacity of reinforced concrete and if weakened could cause failure of the concrete structure. Furthermore, different surface conditions were applied onto the concrete by mechanical methods so as to simulate the range of surface preparations that may be carried out before repair materials are applied in practice.

2 LITERATURE REVIEW

In a study conducted by Al-Zahrani, 2003 to evaluate nine polymer- and cement-based repair mortars, the mechanical properties of elastic modulus, compressive, tensile and flexural strength; shrinkage and thermal expansion were tested along with durability properties of chloride permeability, electrical resistivity and carbonation depth. They reported that the mechanical properties of the selected repair mortars did not vary significantly from each other although the elastic modulus of the polymer-based repair mortars was generally less than that of the cement-based repair mortars. There was less drying shrinkage cracking in the polymer-based materials but their electrical resistivity results were higher than those of cement-based repair mortars. Also, enhanced carbonation was noted in some of the polymer-based repair mortars. Both the polymer-based and cement-based repair mortars gave low chloride permeability results.

3 EXPERIMENTAL

3.1 *Sample preparation*

The five generic types of repair materials used in the investigation were the general purpose mortar (cementitious), epoxy resin mortar (resistant to acids and alkalis), cement-based mortar (weather and crack resistant), masonry and carbothane aliphatic paints.

3.2 *Test methods*

The oxygen permeability and sorptivity indexes developed through a joint research program of the University of the Witwatersrand and University of Cape Town in the 1990's (Alexander et al., 1999) were used in this investigation. These methods are being used widely in the industry for quality control and are in the process of being drafted into national standards (SANS 516-1,2,3: 1999).

4 RESULTS AND DISCUSSION

4.1 *Permeability performance of repair materials*

The results clearly show the benefit of applying the repair materials on permeability of concrete. Figure 1 shows that regardless of the type of surface preparation, significant reductions in permeability resulted in all the concretes whose surfaces were repaired with mortar or surface coating.

4.2 *Sorptivity results*

From the graphs, it can be seen that the *epoxy resin mortar* performed the best as it absorbs the least water, followed by the *cement-based mortar* and the *general purpose mortar*. As expected, the control (with no repair material applied on) performs the least.

5 CONCLUSIONS

The general trend in results shows that repair materials significantly improve concrete durability through an increase in OPI values and a decrease in water absorption rate. A brushed surface gives the best result with over 75% decrease in oxygen permeability of concrete relative to the control, followed by the cut surface preparation, while chiselled samples gave the least favourable results presumably due to possible microcracking arising from mechanical action of surface preparation.

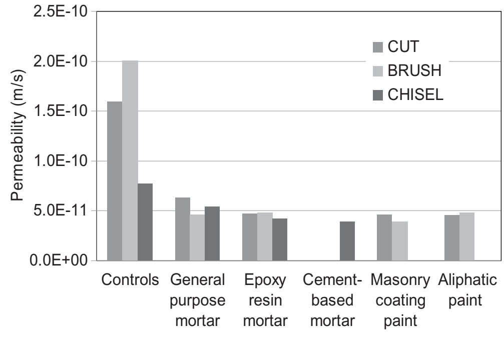

Figure 1. Oxygen permeability results for mix 1 as influenced by the various repair materials and surface preparation methods.

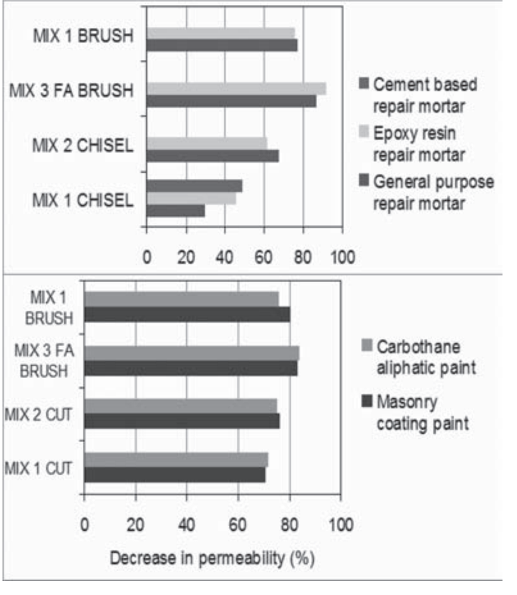

Figure 2. Decrease in oxygen permeability for various mixes and various surface preparation methods.

The epoxy resin repair mortar performed the best in both the OPI and sorptivity tests. It was found that this material has water-repelling qualities.

Concrete Repair, Rehabilitation and Retrofitting III – Alexander et al. (eds)
© 2012 Taylor & Francis Group, London, ISBN 978-0-415-89952-9

Concrete heritage: Tentative guidelines for the 'Patch Restoration Method'

J. Valença
ICIST, Polytechnic Institute of Coimbra, Coimbra, Portugal

C. Almeida
University of Coimbra, Coimbra, Portugal

E.S. Júlio
ICIST, Technical University of Lisbon, Lisbon, Portugal

ABSTRACT: Most outstanding constructions of the XXth Century were built in concrete. Some of these, due to their architectural, historical and/or cultural relevance, are part of the World's heritage. In order to preserve this legacy, interventions must be performed according to very strict restoration requirements. However, when referring to concrete, there is an almost generalized lack of concern relatively to this subject. The study described focuses on a wide spread repairing method of concrete structures, known as 'Patch Repair Method'. This method consists in removing deteriorated concrete from small areas and replacing it by repairing mortars. However, the Patch Repair Method cannot be used straight forward in concrete heritage since, besides durability, material compatibility and structural performance, it is also important to draw special attention to color and texture matching between the original concrete substrate and the repairing mortar. Tentative guidelines are provided relatively to the application of the Patch Repair Method to concrete heritage. A new method is presented, herein called 'Patch Restoration Method', covering the whole process, from assessment to intervention. It includes the following main steps: (i) evaluation of color and texture in the neighborhood of the area to be repaired using image processing; (ii) design and application of a customized repairing mortar, with specific color and texture requirements to match the substrate, also taking into account the effect of ageing; and (iii) monitoring the patch restoration, also using image processing. The method was first applied to mortars, designed and tested in laboratory, aiming to calibrate and validate it. Afterwards, a concrete heritage example was considered as case study—the buildings of the Fundação Calouste Gulbenkian in Lisbon, Portugal—to test the method on site. Finally results are discussed, conclusions drawn, and tentative guidelines are proposed to apply the new 'Patch Restoration Method' in practice.

1 INTRODUCTION

In this paper, a new method is presented, herein called 'Patch Restoration Method'. The method was designed to support restoration operations on concrete heritage, covering the whole process, from assessment to intervention.

The Patch Restoration Method procedure is supported by Digital Image Processing (DIP), which comprises the following steps: (1) Image acquisition. The method can be applied to images in the visible spectrum or in the infrared band; (2) Identification of areas of intervention. In this step, a previously developed method, 'SurfCrete' (Valença *et al.*, 2011), can be applied to detect anomalies in concrete surfaces, e.g, cracking, delamination, detachment or crushing of the concrete, and interventions in terms of inadequate restoration; (3) Characterization of the concrete substrate. This step applies DIP to define the color and texture parameters of the surface. The 2D-LRA method (Santos & Júlio, 2008) is also applied to measure the surface roughness. This information is used to set the restoring mortar; (4) Design and application of a customized repairing mortar, with specific color and texture requirements to match the substrate, and also taking into account the effect of ageing; (5) Evaluation of intervention. Periodic surveys should be performed for monitoring the changes of the restoration mortar with ageing. For this stage, it is essential to acquire all the images under identical exposure and brightness conditions.

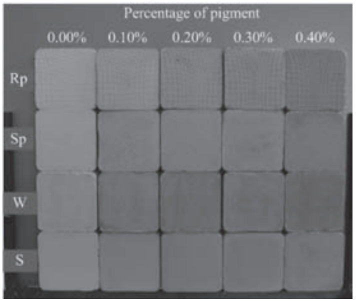

Figure 1. Mosaic of repairing mortars produced.

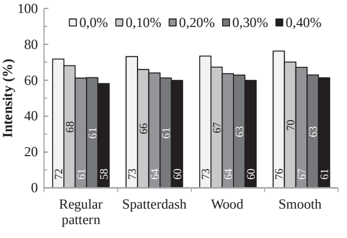

Figure 2. Color changes of the restoration mortar for different textures and percentage of pigments.

2 EXPERIMENTAL STUDY

An experimental study was conducted to validate the method, namely, to study the viability of DIP to assess color of concrete surfaces and to examine, qualitatively, the influence of surfaces textures in the color perception. The laboratorial test was performed on mortar specimens ($100 \times 100 \times 20$ mm^3) produced with different colors and textures. The specimens were produced with a standard white repairing mortar, mixing five different percentages of black pigment: 0.0%, 0.1%, 0.2%, 0.3% and 0.4%, respectively. The specimens were cast aiming to induce four types of textures: (Rp) Regular pattern; (Sp) Spatterdash; (W) Wood texture, and (S) Smooth texture (Figure 1).

To evaluate the color change of the repairing mortar in time, accelerated ageing tests were performed, namely, carbonation attack performed in a carbonation chamber.

Figure 2 shows the measures of intensities of pixels in the four textures produced, before starting the ageing tests. The capacity of the method to identify the color of the specimens' surfaces is clear. Regardless the texture of the surface, the evolution of the color with the percentage of pigments leads to correlations higher than 0.95. The results allow identifying that, for the same mortars, the color intensity slightly increases with the increasing of the roughness of the surface.

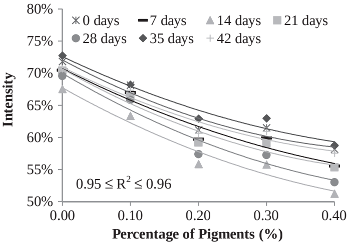

Figure 3. Evolution of the color due to carbonation: Regular pattern texture.

Figure 3 represent the evolution of the color of the specimens during the accelerated ageing test (Regular pattern texture as example). The differences of results, always less than 10%, are not perceptive to the human eye. Moreover, it is possible to observe an almost completely overlap between the first and last week of testing. These results demonstrate that there was no change in color of the repairing mortar during the experimental test.

3 CONCLUSIONS

The 'Patch Restoration Method', based in DIP techniques, allows to define and to assess repairs on concrete heritage. The method can be a powerful tool to assist the entire process of intervention, from assessment and diagnosis to definition of restoration requirements and monitoring the final result. The method allows to characterize the requirements for concrete heritage. The application of DIP in color evaluation showed promising results. It was also proved the applicability in distinguishing the color perception of the repairing mortar when applied to different surface texture.

Interventions on concrete heritage require a holistic survey and should be focus in the following guidelines: (1) A detailed diagnosis has to be conducted to understand the materials' properties, design criteria, construction methods and structural behavior is fundamental; (2) Conservation procedures should be adapted to each reality; (3) Principles of minimum intervention and compatibility should be fulfilled; (4) To perform the patch repairs with restoration requirements, by developing specific and customized repairing mortars to match the original concrete substrate (color and texture). A research study should be conducted to define the repairing mortar, taking into account the environmental attacks, i.e. the effect of ageing (accelerated ageing test are recommended); (5) To assess the evolution of the intervention is fundamental to define and to calibrate the trend of the color evolution of mortars with time, provided by the experimental study.

Concrete Repair, Rehabilitation and Retrofitting III – Alexander et al. (eds)
© 2012 Taylor & Francis Group, London, ISBN 978-0-415-89952-9

Fatigue crack propagation model for bi-material interfaces

Sonalisa Ray & J.M. Chandra Kishen
Department of Civil Engineering, Indian Institute of Science, Bangalore, India

ABSTRACT: In this work, an analytical model has been proposed to predict crack propagation behavior of concrete-concrete bimaterial interface crack by utilizing the concepts of dimensional analysis and self-similarity. The appropriate idealizations in the formulation of a mathematical model are made through various assumption of self-similarity of the phenomenon under consideration based on its physical behavior. The developed model includes the various crack growth influencing fracture parameters together with the elastic mismatch moduli. To use the proposed model for crack growth predictions of cyclically loaded concrete members, calibration and validation studies have been performed utilizing the available experimental data. The proposed model is observed to follow the experimental trend satisfactorily. A sensitivity analysis is carried out to understand the influence of each involved quantities.

1 INTRODUCTION

Existing structures need to undergo repair and rehabilitation during maintenance program in order to extend their service life and to restore their original strength. Since, replacement of an existing structure is not always feasible and cost effective, repair is done which may involve the application of a fresh material over the parent material thereby, creating an interface. Furthermore, in large concrete structures involving mass concreting, constructions are carried out in many stages forming a cold jointed interface between successive lifts of concrete. An interface is considered to be one of the weakest zones in comparison with the parent and newly applied material and is more prone to crack propagation due to the mismatch in modulus of elasticity between two different materials on either side of it. The chances of failure along the interface are higher because of stress concentration and rapid change in stress level along it. Further, most of these structures are subjected to millions of repetitive load cycles during their service life and get deteriorated with age resulting in strength and stiffness reduction. Hence, cracking analysis of interfacial cracks under fatigue loading is of great concern.

Failure mechanisms near cementitious interface are mainly governed by the cracking on the interface or kinking of the crack into either of the two materials. Thus, the understanding of the crack propagation behavior at interfaces under the action of cyclic loads is an important research problem and has been attempted in the present work.

2 FORMULATION OF CRACK ROPAGATION MODEL FOR BIMATERIAL INTERFACES

An analytical model has been proposed to predict the crack growth rate at an interface of different materials using the concept of dimensional analysis and self-similarity. In the development of a mathematical model appropriate idealizations are made through various assumptions of self-similarity of the phenomenon under consideration based on its physical behavior. Using this approach, the developed fatigue crack growth model is

$$\frac{da}{dN} = G_f^{\,1-\gamma_1-\gamma_2}\,\Delta G_I^{\,\gamma_1}\,\sigma_t^{\,\gamma_2-1}\,a^{\gamma_2}\left(1+\alpha\right)^{\gamma_3}\left(1-\mathrm{R}\right)^{\gamma_4}\Phi_4 \quad (1)$$

In Equation 1, E_{eff} is the effective modulus of elasticity of an interface beam derived from an equivalent homogeneous beam giving rise to equal deflection at the load point as that of an interface beam.

Equation 1 represents the functional form for the crack propagation rate with four constants γ_1, γ_2, γ_3, γ_4. These coefficients are determined using the experimental data. The best suited values of the coefficients to the experimental data γ_1, γ_2 and γ_3 are obtained as 1.21, 4.29 and –0.968 respectively. The coefficient γ_3 corresponds to the elastic mismatch parameter which depends on the type of interface. A linear relationship as shown in Figure 1 is proposed between the mismatch parameter of the interface specimen and the corresponding coefficient is expressed as, $\gamma_3 = \mathrm{P}_1\alpha + \mathrm{P}_2$. The values of P_1 and P_2 are 129.19 and 1.27 respectively.

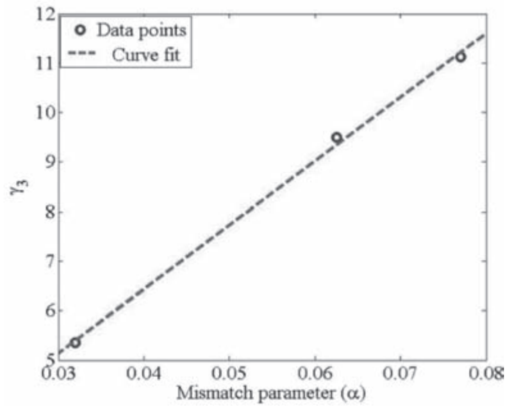

Figure 1. Relationship between α and γ_3.

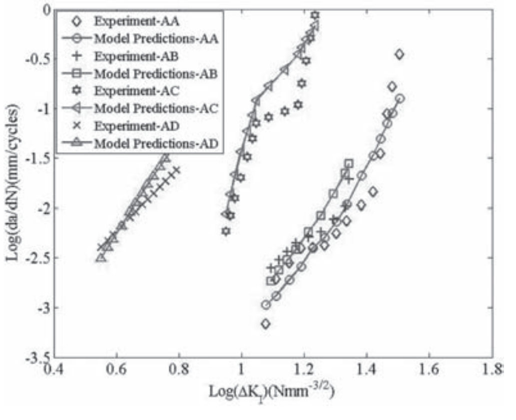

Figure 2. Logarithmic plot of stress intensity factor range and rate of crack propagation (Medium size).

To verify the applicability of the proposed model, different experimental data points other than those used for the calibration study have been used to predict the crack growth rate and compared with the experimental results. Logarithmic plots of cyclic stress intensity factor range and crack propagation rate are shown in Figure 2 for medium size specimen. In this figure, it can be observed that the developed model is able to capture the interfacial crack growth fairly well and the predicted results agree with experimental data points. In Figure 2, crack growth rate has been predicted for medium specimen considering all the four types of interfaces AA, AB, AC and AD. It can be seen that the crack growth rate increases from interface specimen AA to AD.

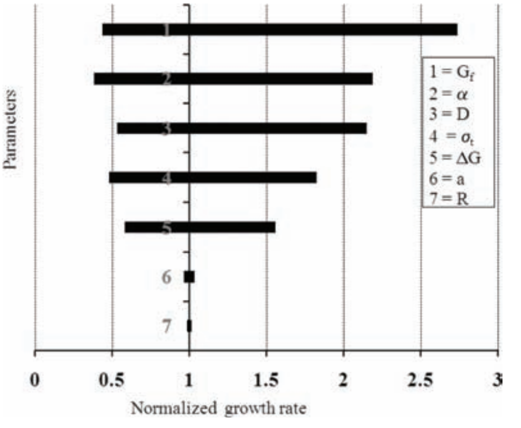

Figure 3. Tornado diagram.

To determine which of the parameters play a dominant role in the crack propagation, a comparative study is performed using a deterministic sensitivity analysis commonly referred as Tornado diagram analysis. The results for the sensitivity study represented as Tornado diagram are shown in Figure 3. It is observed that fracture toughness is most sensitive to the crack growth rate followed by the mismatch parameter and structural size.

3 CONCLUSIONS

The model is developed using the fundamental principles dimensional analysis thereby primarily avoiding the empirical nature. The crack growth model includes various geometrical, material and loading parameters such as crack length, structural size, tensile strength, fracture toughness, loading parameter and stress ratio. Though a sensitivity study on the developed model, fracture toughness is found to be the most sensitive one to the crack growth rate followed by the mismatch parameter and structural size. The fracture toughness for an interface material is related to elastic mismatch parameter and is different than the homogeneous one. With the increase in difference in compressive strength and elastic mismatch parameter the fracture energy decreases. Hence, the crack propagation behavior is strongly dependent on fracture toughness and difference in elastic moduli. The least sensitive parameter is found to be stress ratio.

Concrete Repair, Rehabilitation and Retrofitting III – Alexander et al. (eds)
© 2012 Taylor & Francis Group, London, ISBN 978-0-415-89952-9

Mechanical properties of old concrete—UHPFC interface

Bassam A. Tayeh, B.H. Abu Bakar & M.A. Megat Johari
School of Civil Engineering, Universiti Sains Malaysia, Engineering Campus, Pulau Pinang, Malaysia
Engineering Division, Islamic University of Gaza, Gaza, Palestine

ABSTRACT: The uniqueness of Ultra-High Performance Fiber Concrete (UHPFC) is its extremely low porosity gives its low permeability and high durability, making it potentially suitable for rehabilitation and retrofitting reinforced concrete structures or for use as a new construction material. This experimental study was performed to assess the bond strength between UHPFC as a repair material and Normal Concrete (NC) substrate as an old material; split tensile strength and slant shear tests were performed to quantify the bond strength in indirect tension and shear respectively, also the correlation between split tensile strength and slant shear were studied. The result showed that UHPFC has been cured by steam, gives high bond strength at the early age of the repair process, and interacts well with the surface of NC, as a result the failure occurred mostly in the NC substrate. A good correlation between the slant shear test results and the split tensile test results has been observed.

1 INTRODUCTION

In the field of rehabilitation and strengthening the bond strength between the new and old concrete generally presents a weak link in the repaired structures (Momayez, Ehsani, Ramezanianpour, & Rajaie, 2005). Good bond is one of the main requirements for successful repair (Gorst & Clark, 2003). UHPFC could be used as a repair materials as it has strong mechanical bond is formed between the UHPFC as an overlay material and the substrate material (Sarkar, 2010) and (Harris, Sarkar, & Ahlborn, 2011).

The main purpose of this paper to evaluate the bond strength between UHPFC as the repair material and normal concrete (NC) substrate as old concrete using split test and slant shear test to quantify the bond strength in indirect tension and shear, respectively.

2 EXPERIMENTAL PROGRAMME

2.1 *Normal concrete substrate and UHPFC properties*

The mixing design of NC used in this study ensures average compressive strengths 45 MPa at 28 days. The control specimens used consists of (i) 100 mm diameter by 200 mm high cylinder for the split indirect tensile strength test and (ii) $100\ \text{mm} \times 100\ \text{mm} \times 300\ \text{mm}$ tall prism for uniaxial compression strength test. The NC was tested for 28 days strength and experimental results showed the NC has an average split tensile strength and tall prism compression strength of 2.75 MPa and 38 MPa respectively.

The UHPFC used has achieved an average 28 days cube compressive strength of $f_{cu} = 170\ \text{MPa}$.

2.2 *Specimens preparation*

Each of the tested specimen comprised of two different materials, being the NC as a substrate and UHPFC as a repair material. The fresh NC was sealed and left to set in its moulds for 24 hours after casting. After 24 hours the NC specimens were demoulded and were cleaned and cured for another two days in a water curing tank. At the age of three days, the NC substrate specimens were taken out from the water tank for surface preparation. In this study, the experimental parameter is the surface texture of the substrate. Five different types of surface were prepared, that is (i) as cast without roughening (AC), (ii) sand blasting (SB), (iii) wire brushing (WB), (iv) drill holes (DR) and (v) grooves (GR).

The specimens represent the first half substrate for the slant shear test. Prior to the casting the UHPFC onto this roughened NC surfaces, the NC specimens were further cured in a water tank until the age of 28 days since the casting date. At the age of 28 days, the NC substrate specimens were transported to a curing room (which come with an ambient temperature of 26°C ± 2°C and relative humidity of 75%) for duration of two months.

Before casting the UHPFC, the surfaces of the NC substrate specimens were moistening for 10 minutes and wiped dry with a damped cloth. The NC substrate specimens were then placed into steel-made moulds with the slant side face upward. Mixing of the UHPFC was carrying out using a pan mixer. The moulds were then filled with UHPFC.

Figure 1 shows the complete composite specimens for the split cylinder strength tests and slant shear strength tests. The composite specimens were steam cured for 48 hours at a temperature of 90°C. After the steam curing, and then cured in a water tank. The splitting tensile and slant shear tests were performed on the 3th and 7th day.

2.3 *Split tensile test*

The splitting tensile test, as an indirect tension test, was conducted to determine the bond strength between the NC substrate and UHPFC, according to ASTM C496. In this test procedure, UHPFC was cast and bonded to the NC substrate specimens to form a cylindrical composite cylinder (100 mm diameter and 200 mm height) as shown in Figure 1a.

2.4 *Slant shear test*

The slant shear test was used in this study to determine the bond strength between the NC substrate and the UHPFC, according to ASTM C 882 test procedure. Following this test procedure, UHPFC was cast and bonded to the NC substrate specimens on a slant plane inclined vertically at a 30° angle to form composite prism specimens (100 mm × 100 mm × 300 mm) (Figure 1b.).

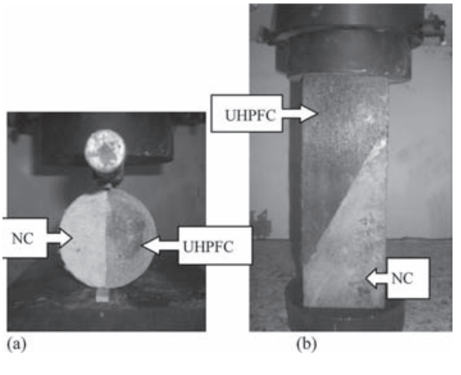

Figure 1. (a) Split cylinder specimen and (b) slant shear test specimens.

3 CONCLUSION

This paper report the experimental results on the bond behaviour between normal concrete (NC) which is the substrate and UHPFC as the repair material using slant shear test and split test to quantify the bond strength in shear and indirect tension, respectively. In the study, the NC and UHPFC used can achieve cube compression strength of 45 MPa and 170 MPa respectively. The experimental parameter was the surface texture of the substrate. Five different types of surface were prepared, that is (i) as cast without roughening, (ii) sand blasting, (iii) wire brushing, drill holes and groove surfaces. The following summarised the conclusion drawn from the experimental programme.

i. The result of the split cylinder tensile strength test shows UHPFC overlays generally have "*excellent bond quality*" with the surface of NC substrates as per the quantitative requirement of (Sprinkel & Ozyildirim, 2000), since most of the failure mode in the split cylinder tensile strength test was through the NC substrate specimen which indicated the bond strength between UHPFC and NC substrate is stronger than the cracking strength of the NC.
ii. The results of slant shear strength test show that the bond strength was very strong and tough since the interface failure occurred after the damage in the NC substrate. In some cases, the failure occurred only in the NC substrate and no separation between the NC substrate and the UHPFC which indicates that superior bond behavior of UHPFC.
iii. The results showed that, a good correlation between the slant shear test results and the split tensile test results has been observed.
iv. Without much statistical supporting evidence on the bond behavior and surface preparation type of the NC substrate and the UHPFC overlay, it is recommended (for the time being) all the NC substrate surface shall be sand blasted prior-to the overlay of the UHPFC as the repair material.

REFERENCES

Gorst, N., & Clark, L. 2003. Effects of thaumasite on bond strength of reinforcement in concrete. *Cement and Concrete Composites, 25*(8): 1089–1094.

Harris, D.K., Sarkar, J., & Ahlborn, T.M. 2011. *Interface Bond Characterization of Ultra-High-Performance Concrete Overlays.* Paper presented at the Transportation Research Board 90th Annual Meeting.

Momayez, A., Ehsani, M., Ramezanianpour, A., & Rajaie, H. 2005. Comparison of methods for evaluating bond strength between concrete substrate and repair materials. *Cement and concrete research, 35*(4): 748–757.

Sarkar, J. 2010. Characterization of the bond strength between ultra high performance concrete bridge deck overlays and concrete substrates: Master of Science in Civil Engineering, Michigan Technological University.

Sprinkel, M.M., & Ozyildirim, C. 2000. *Evaluation of high performance concrete overlays placed on Route 60 over Lynnhaven Inlet in Virginia.*

Concrete Repair, Rehabilitation and Retrofitting III – Alexander et al. (eds)
© 2012 Taylor & Francis Group, London, ISBN 978-0-415-89952-9

Bond characteristics of substrate concrete and repair materials

M.I. Khan, T.H. Almusallam, S.H. Alsayed, Y.A. Al-Salloum & A.A. Almosa
Department of Civil Engineering, College of Engineering, King Saud University, Saudi Arabia

ABSTRACT: Good adhesion of a repair material to concrete is of vital importance in the application and performance of concrete repairs. This paper reviews and compares techniques and results of bond strength test methods that induce shear, including a tensile slant-shear test. The effect of surface preparation and modulus mismatch between repair and substrate are illustrated by experimental and theoretical data. While these tests can provide individually useful information on bond strength and a limited picture of bond characteristics, they can, taken in isolation, result in a misunderstanding of the behaviour of bonded cementitious materials. An experimental study was performed to evaluate the slant shear between two concrete layers, for different techniques for increasing the roughness of the substrate surface. Slant shear tests were conducted to quantify the bond strength in shear.

1 INTRODUCTION

The bond strength between the repair material and concrete substrate plays a vital role in determining the efficiency of a repair material used in concrete structures. The properties and durability of repair systems are governed by properties of the three phases namely, repair, existing substrate, and interface (transition zone) between them. Properly designed, implemented, and functioning man-made systems, with a minimum number of undesirable side effects, require the application of a well-integrated systems approach.

In Saudi Arabia, the majority of the concrete structures constructed more than three decades ago suffer because of lack of quality control and severe weather conditions. Therefore, the structures deteriorate and need urgent repair. In this investigation, bond strength in slant shear test of nine candidate materials are reported.

2 EXPERIMENTAL PROGRAM

2.1 *Material selection*

Nine candidate materials, three from each micro-concrete repair materials, cementitious repair mortars and cementitious polymer modified mortars, were selected. The selection of the repair material was based on the best selling materials manufactured by the top three companies Fosroc, Sika and MBT available in the Kingdom of Saudi Arabia. The designation, properties and application of these micro-concrete repair materials (MCRM), cementitious repair mortars (CRM) and cementitious polymer modified mortars (CPMM).

2.2 *Testing procedure*

Slant shear tests are typically employed to measure the bond strength between the repair material and concrete substrate. The adopted geometry is shown in Figure 1. Bond strength in shear was calculated by dividing the maximum load at failure by the bond area and was obtained from an average of 3 specimens determined at the ages of 7, and 28 days of curing.

3 RESULTS AND DISCUSSIONS

Bond strength development in shear of micro-concrete repair materials is presented as shown in Figure 2. At 7 days, strength development of MCRM-1, MCRM-2 and MCRM-3 is almost similar. At 28 days, the bond strength development of MCRM-1 is insignificant (6%), however, MCRM-2 and MCRM-3 showed increase in the bond strength. The rate of increase in 7-day strength to 28-day strength was highest about 56% for MCRM-2 whilst MCRM-3 showed about 28% increase from 7 to 28 days. It is clearly evident from the results that MCRM-2 attained the best bond strength amongst the three materials under investigation. It is clearly shown that the failure has occurred in the concrete (substrate) whilst repair material and bond remained intact.

From Figure 3, CRM-1 and CRM-2 showed higher bond strength as compared to CRM-3 at all ages investigated. At 7 day, CRM-1 and CRM-2 showed bond strength about 18 MPa and 20 MPa, respectively, whereas CRM-3 showed only 9 MPa. The rate of increase in the bond strength

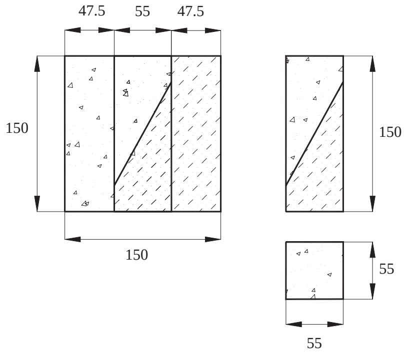

Figure 1. The adopted geometry for slant shear test.

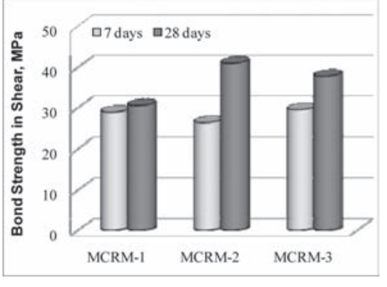

Figure 2. Bond strength development in shear of micro-concrete repair materials.

development from 7 to 28 days is almost similar for CRM-1 and CRM-3 (about 15%) whereas CRM-2 showed slightly higher value (about 22%). At 28 days, the bond strength development in shear of CRM-1, CRM-2 and CRM-3 are 21 MPa and 24 MPa and 10 MPa, respectively. The values of bond strength are lower than that of micro-concrete samples, as expected. Clearly CRM-1 and CRM-2 are better than that of CRM-3.

Bond strength development in shear of CPMM-1, CPMM-2 and CPMM-3 at 7 days is about 2 MPa, 9 MPa and 20 MPa, respectively (Figure 4). At 7 days CPMM-1 did not show any significant strength whereas CPMM-2 managed to reach up to 9 MPa. At 7 days, CPMM-3 showed good strength which is matching with CRM-1 and CRM-2. At 28 days, the bond strength development in shear of CPMM-1, CPMM-2 and CPMM-3 were 14 MPa and 10 MPa and 24 MPa, respectively. The rate of increase in the bond strength development from 7 to 28 days for CPMM-2 and CPMM-3 was 14% and 17%, respectively. However, for CPMM-1 the rate of increase was very high.

Similar to the cementitious repair mortars, most of the samples failed at the bond line between substrate and repair material. It is evident that CPMM-3 is better as compared to that of CPMM-1 and CPMM-2.

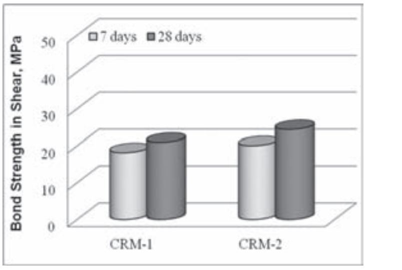

Figure 3. Bond strength development in shear of cementitious repair mortars.

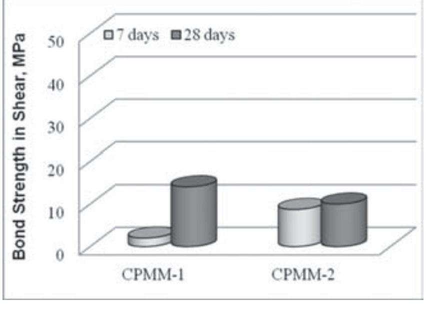

Figure 4. Bond strength development in shear of cementitious polymer modified mortars.

It is worth to mention here that in case of the micro-concrete samples most of the failure took place in substrate concrete whereas in case of cementitious repair mortars failure was mostly in the bond line.

4 CONCLUSIONS

1. Early bond strength development in shear of micro-concrete repair materials (MCRM-1, MCRM-2 and MCRM-3) is almost similar, however, at later age MCRM-2 attained the best bond strength amongst its companions.
2. CRM-1 and CRM-2 showed higher bond strength as compared to CRM-3 at all ages investigated.
3. CPMM-3 showed better bond strength as compared to that of CPMM-1 and CPMM-2.
4. In most micro-concrete samples failure took place in substrate concrete whereas in case of cementitious repair mortars and polymer modified mortars failure was mostly in the bond line.
5. Cementitious repair materials demonstrated better performance as compared to cementitious polymer modified mortars.

Concrete Repair, Rehabilitation and Retrofitting III – Alexander et al. (eds)
© 2012 Taylor & Francis Group, London, ISBN 978-0-415-89952-9

Investigations on the performance of concrete repair mortars in composite specimen tests

P. Ramge & H.-C. Kühne
BAM Federal Institute for Materials Research and Testing, Berlin, Germany

ABSTRACT: In the scope of a recent research project investigations on the performance of repair mortars for concrete structures were carried out at BAM. One of the key points of the project was the systematic investigation on the mode of action of single constituents and their interactions with special emphasis on their influence on the mortars' stiffness and shrinkage behaviour. The mortar's shrinkage can be the reason of many following problems, which can be a direct result, i.e. the damage of the bond interface caused by constraining forces, or an indirect result, such as an increase in carbonation depth or chloride penetration due to shrinkage induced constraining cracks, which will subsequently lead to durability problems. Especially when repairing weak substrate concretes the proper adjustments of the mortar's stiffness and shrinkage behaviour to the properties of the concrete is of essential importance for functionality and durability of the repair task.

1 INTRODUCTION

The performance of a repair mortar is strongly dependant on the sound interaction between mortar properties and substrate concrete. For the success of a concrete repair task not only the durability of the repair mortar itself is of importance, but also the interaction of repair mortar and substrate concrete to function as composite material. Therefore the properties of the repair mortar have to be adjusted to the subsurface in such a way that cracks can be precluded and that a long lasting bond is assured. Stiffness and deformation behaviour of mortar and subsurface must show equal or well adjusted properties, otherwise inner constraining forces, can lead to defects up to a total delamination. Special attention needs to be given to shrinkage induced constraining forces. In this article shrinkage induced hazards to the performance and durability of repair measures are demonstrated on the example of composite specimen tests. The damage can thereby be a direct or indirect result of the shrinkage.

2 INTERACTION BETWEEN SHRINKAGE, STIFFNESS AND TENSILE STRENGTH

Whenever a deformation is hindered, constraining forces develop according to Hooke's law. Due to the bond to the concrete the mortar's shrinkage will always evoke tensile tensions if applied to a pre-existing structure. The case of free unhindered shrinkage, which would be most favorable in terms of constraint prevention, does practically not exist. The crack formation is dependent on the interaction between shrinkage, stiffness and tensile strength. Increasing the tensile strength while decreasing stiffness and shrinkage counteracts the shrinkage induced crack formation. However, for cementitious mortars a material specific relation between stiffness and strength exists. Most technological measures that increase the tensile strength increase also the stiffness and vice versa. Therefore the control of the shrinkage deformations is a very effective tool as the shrinkage can be altered rather independent of strength and stiffness. Even if no cracks in the repair mortar occur, still a threat to the durability of a repair measures exists if shrinkage and stiffness are too high. The occurring constraining forces can cause severe damage to the substrate concrete.

3 EXPERIMENTAL PROGRAM

Several mortar compositions were tested in composite specimen tests. On the composite specimens consisting of substrate concrete specimens sized $30 \times 30 \times 10$ cm^3 coated with a 2 cm repair mortar layer the pull off strength is tested after different storage conditions. Results of the application on low strength concrete and of freeze-thaw cycling tests with de-icing salt exposition are presented in the following, completed by investigations on the mortars' hindered shrinkage behavior in shrinkage gutters.

4 RESULTS—SHRINKAGE INDUCED DAMAGE IN COMPOSITE SPECIMEN TESTS

4.1 *Damage of the substrate concrete by constraining forces*

With several different mortar compositions sprayed applications on special low strength substrate concrete specimen were conducted. These tests on low strength substrate specimens were especially developed to evaluate the suitability of repair mortars for the repair old hydraulic engineering constructions. Although the fracture always took place in the substrate concrete, the limit mean value of 1.2 MPa was only achieved for one of the mortar mixtures. In the other cases a damage of the substrate concrete took place. It is assumed that due to the good bond between repair mortar and substrate concrete a weakening of the substrate concrete's structure was caused by the imposed shrinkage deformations of the mortar. The damage or weakening does, however, not take place in the actual bond interface, but distinctly in the substrate concrete itself. The conditions for the occurrence of this effect are a proper bond between repair mortar and substrate concrete, a high shrinkage of the repair mortar, and a stiffness of the repair mortar, which is significantly higher than that of the substrate concrete.

4.2 *Shrinkage induced crack formation*

The mortars' behaviour at hindered shrinkage was investigated in "shrinkage gutters". Considering the high stiffness of the steel gutters, a total deformation hindrance of the mortar can be assumed. The values of the accumulated crack width are always lower than the values of the free shrinkage. Due to the deformation hindrance the mortar is initially subjected to tensile stress. Due to the bond to the steel surface the elastic strain is maintained in the areas between the cracks. Creep and relaxation can lead to a partial decline of the tension so that the occurrence of new cracks may be suppressed even at ongoing shrinkage. However, there is a good correlation between accumulated crack width in the hindered shrinkage gutter and the free shrinkage. Also for the maximum crack width a general dependence to the free shrinkage does exist. The results show that the reduction of the mortar's shrinkage is an effective tool to control crack intensity and maximum crack width.

4.3 *Damage of the substrate concrete in freeze thaw cycling tests*

Premature failure in the substrate concrete also occurred on normal strength substrate concrete specimen after freeze-thaw cycling with de-icing salt exposition. In this case the weakening of the substrate concrete is not caused by the implementation of constraining forces, but due to cracks allowing the freeze-thaw cycling impact to penetrate to the substrate concrete. Even if the mortar which is directly exposed to the de-icing salt solution during the test shows a good resistance against the freeze-thaw attack and mortar and substrate concrete show good compatibility concerning their temperature related strain, a severe damage to the repair system can happen if cracks in the mortar allow the penetration of the de-icing salt solution to the substrate concrete's surface. In a majority of the bond strength tests after freeze-thaw cycling that were performed during the project, the fracture took place in the substrate concrete well below the target value and well below the average bond strength value achieved on control samples of the used substrate concrete despite a proven general sufficiency of the performance of the respective mortars on this substrate concrete. Even though the cracks may exhibit crack widths well below the limit value of 0.1 mm, they are very effective transport channels for chlorides. The cracks therefore are not only endangering the freeze-thaw and de-icing salt resistance of the concrete or mortar but are a considerable threat concerning the chloride induced steel corrosion of reinforced concrete structures. Already the smallest cracks allow a rapid and deep penetration of chlorides. The mortar's own chloride penetration resistance is of minor interest in this matter, as the chlorides bypass the mortar through the cracks to spread in the substrate concrete.

5 CONCLUSIONS AND OUTLOOK

Constraining cracks and constraining forces can cause severe damage and drastically decrease the durability of a repair task. Traditionally the durability of concrete or cementitious materials is believed to be proportional to its compressive strength. This statement may be generally true for "normal" concrete, however, it is not necessarily valid for more specialized concrete and it is certainly not true for concrete repair mortars if they are regarded as part of a composite system consisting of the substrate concrete on the one hand and the repair layer on the other hand. Optimising a mixture proportioning, always includes a compromise, depending on the priorities of the individual properties for the specific application task. For certain applications of repair mortars it is therefore necessary to accept a reduced compressive strength if this allows better tensile strength to stiffness ratios to prevent the risk of shrinkage induced cracks or shrinkage induced bond disruptions. The control of the mortar's shrinkage deserves special attention in this respect. The sustainability of a repair task is always linked to the positive co-action of repair mortar and original substructure, neither the mortar nor the sub-concrete should be considered isolated.

Concrete Repair, Rehabilitation and Retrofitting III – Alexander et al. (eds)
 ISBN 978-0-415-89952-9

Topography evaluation methods for concrete substrates: Parametric study

L. Courard
University of Liège, Belgium

A. Garbacz
Warsaw University of Technology, Poland

B. Bissonnette
Laval University, Québec, Canada

ABSTRACT: Research projects performed at the University of Liege, Laval University and the Warsaw University of Technology have pointed out the importance of taking care about the surface roughness of concrete substrate with regards to the adhesion of repair materials. This paper wants to make a State-of-Art on this specific problem: surfometry methods, interface analysis, adhesion measurements, …etc are presented, interpreted and compared. Surfology, which is a more wide concept, contributes to understand what will make the contact effective or not, and allow interactions of variable intensities between the materials. Different scales of observation—micro to macro—are needed to exactly represent what happens when materials are put into contact.

In addition to adhesion and cohesion, another parameter often considered affecting the tensile bond between repair material and existing concrete is the substrate roughness. Nevertheless, this subject has been controversial for years. It was concluded that there could be a roughness "threshold value" beyond which further improvement on the roughness would not enhance bond strength (Courard *et al.*, 2010). According to these test results, the "threshold value" ought to be close to the surface roughness of the typical sandblasted surfaces (Courard *et al.*, 2009). However, it remains the opinion of many specialists in the industry that a rougher surface is beneficial to bond strength. Since roughness directly depends on the surface preparation method, the proposed research is intended to shed new light on the subject and ultimately resolve the controversy.

According to American National Standards Institute, the methods for measuring roughness and surface texture can be classified into three types: contacting methods, taper sectioning, and optical (non-contacting) methods.

Among the contacting methods there are stylus type profilometers, tactile tests, measurement of kinetic friction, measurement of static friction, use of rolling ball measurements, and measurement of the compliance of a metal sphere with a rough surface.

Optical (non-contacting) methods include optical reflecting instruments, light microscopy, electron microscopy, speckle metrology, interferometry and laser profilometry (Fukuzawa *et al.*, 2001).

A variety of approaches have been set all over the years to characterize the surface roughness of concrete: evaluation of the proportion of the surface occupied by aggregates, measurement of the maximum roughness amplitude (Courard, 1998), adhesion tests (Pretorius *et al.*, 2001 and Garbacz *et al.*, 2005), calculation of surface parameters based on image analysis or on microscopic observations, etc. However, these methods are unable to provide a sufficiently detailed representation of the actual surface profile for the calculation of morphological and statistical parameters, and are not user-friendly under field conditions. In order to achieve a reliable quantitative analysis of superficial concrete morphology after surface preparation (Bissonnette *et al.*, 2006), different profilometry and surfometry techniques can be used (Perez *et al.*, 2005). The data obtained with such techniques enable a real quantitative assessment of the surface profile by means of statistical parameters calculated from the total superficial profile and from the filtered waviness (low frequency/macro roughness) and roughness (high frequency/microroughness) profiles (Courard *et al.*, 2003 and Courard *et al.*, 2004). Some of these parameters—for instance the profile arithmetic mean and the flatness coefficient—are particularly discriminating both for the shape of valleys and peaks, as well as for their amplitude and frequency.

The selected characterization techniques were compared for effectiveness, accuracy, consistency and field applicability. The following techniques were analyzed on a comparative basis:

- the evaluation of surfaces with sand patch test according to ASTM E965 (very close to EN 13036-1: 2002);
- mechanical profilometry technique, in which a high-precision extensometer is moved all over the surface to obtain a 3-D mapping (x, y, z coordinates), from which morphological parameters are computed;
- laser technique, where the superficial elevation (distance from the laser beam source) of each point is calculated on the basis of the laser beam transit time;
- concrete surface profiles (CSP) plaques 03732.

The aim of this paper is the identification of the different available techniques (laboratory and field use), as well as their comparison for evaluating relevant quantitative roughness characteristics.

Concrete substrates (300 × 300 × 50 mm) of C20/25 class were made from the concrete mix: CEM I 32.5, 2/8 limestone, 0/2 quartz sand. The following types of mechanical treatments were used to prepare the concrete substrates:

- grinding (GR),
- sandblasting (SB),
- shotblasting (SHB35 and SHB45, with treatment time of 35, and 45 s, respectively),
- hand (HMIL) and mechanical (MMIL) milling.

Comparison between Surface Rough Index and parameters measured on the base of profilometry techniques has been performed: an equivalent correlation exists between the mean waviness obtained by means of the two profilometry techniques and SRI, respectively.

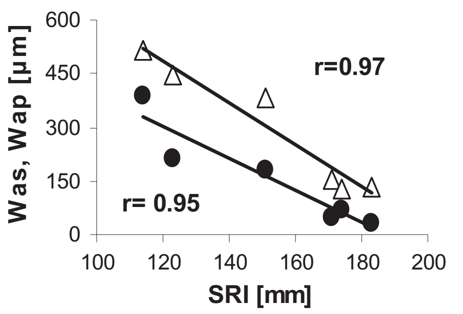

Figure 1. Surface Rough Index vs arithmetic mean of waviness; (p,Δ) and (s,•) for mechanical and laser profilometers (Garbacz *et al.*, 2006).

The mean roughness values are close to each other for the treatment types and the both profilometry methods.

The total height and the mean value of the waviness profile measured with the laser profilometry are 1.3–4.3 times higher than the ones deduced from the mechanical method.

The results of surface geometry characterization with the four methods can be summarized as follow:

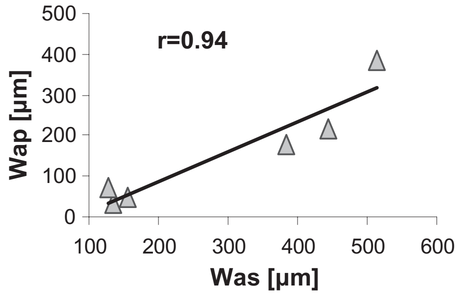

Figure 2. Comparison of mean waviness; "p" and "s" for mechanical and laser profilometers (Garbacz *et al.*, 2006).

- in the case of the profilometry methods, the waviness parameters are about 5% (mechanical profilometry) and 9% (laser profilometry) smaller than the one corresponding to the total profile. This confirms that the global shape of the profile has been preserved through the waviness filtration;
- the mean roughness values are close to each other for the treatment types and the both profilometry methods (Rap = 17 ± 2 and Ras = 19 ± 7, respectively). However, the total height of the roughness profile determined with laser profilometry was 2.8 – 5.5 times exceeding the one obtained with mechanical profilometry with the same filtration method.
- both the total height and the mean value of the waviness profile measured with the laser profilometry are 1.3 – 4.3 times higher than the ones deduced from the mechanical method. In the case of the parameters of Abbott's curve this ratio was even 7 times higher. However, values of these ratios do not correspond to the waviness level.

Even if the accuracy of the evaluation method has to be discussed with regard to the preparation technique—that means the height of the peaks and holes—it seems that all the methods are giving quite correlated results.

Concrete Repair, Rehabilitation and Retrofitting III – Alexander et al. (eds)
© 2012 Taylor & Francis Group, London, ISBN 978-0-415-89952-9

Modeling water absorption of the concrete substrate in concrete repairs

M. Luković, B. Šavija & G. Ye
Delft University of Technology, Delft, The Netherlands

J. Zhou
Sinoma Research Institute, China Sinoma International Engineering Co., Ltd., Beijing, China

ABSTRACT: Moisture exchange between the repair material and the concrete substrate plays an important role in the development of properties of the repair system. Capillary absorption increases the contact area between repair material and concrete substrate, improving the mechanical interlocking of the system. On the other hand, this can result in the change of the water content at the interface, increase the differential shrinkage, and affect further cement hydration and microstructure development of the repair material. Quantification of absorption is especially important for repair materials with low w/c ratio where water loss can significantly affect the quality of the repair. Therefore, this paper proposes a 3D lattice network model based on the unsaturated flow theory to predict the water absorption and water content in the concrete substrate. The corresponding transport properties are assigned to the lattice elements which are idealized as conductive "pipes". As a result, the water content distribution, cumulative water absorption and penetration depth of the water front can be easily quantified in any elapsed time. Comparison of the results of the lattice model and previously developed model is presented. The simulation results are in good agreement with the experimental results.

1 INTRODUCTION

After placing a cementitious repair material on a concrete substrate, the moisture exchange between these two materials takes place. The concrete substrate absorbs water from the repair material. Since the repair material is still "liquid", the water loss causes a reduction in the w/c ratio in the bulk repair material and at the interface. The resultant w/c ratio has two effects on the cement hydration of the repair material. On one hand, the reduced water content initially retards the cement hydration and affects the quality of the bond. On the other hand, a lower w/c ratio results in a lower porosity and a denser pore structure with probably higher strength of the repair material and the repair-substrate interface. Moreover, capillary absorption plays an important role in the mechanical interlocking, since it facilities the penetration of the liquid repair material into the cavities of the concrete substrate and increases the contact area between the two materials (Courard 2000).

Therefore, in order to get optimal performance of concrete repairs, absorption of the unsaturated concrete substrate has to be quantified. With the use of the numerical model described in following and experimental results obtained from gravimetric test, moisture distribution within the sample can be quantified.

2 NON-SATURATED MOISTURE TRANSPORT

The physics of the unsaturated flow is expressed in the extended Darcy's equation which, combined with mass-conservation equation, in one dimensional system, gives (Hall 1994):

$$\frac{d\theta}{dt} = \frac{d}{dx}\left(D(\theta)\frac{d\theta}{dx}\right) \tag{1}$$

where $D(\theta)$ is the hydraulic diffusivity and θ is moisture content. Introduction of the Boltzmann variable, reduces equation (1) to an ordinary differential equation. Since diffusivity is a strongly non-linear function of the moisture content, exponential form for modeling absorption in concrete is used (Leech et al. 2003):

$$D(\theta) = D_0 e^{n\overline{\theta}} \tag{2}$$

where D_0 and n are empirically fitted constants, while $\overline{\theta}$ denotes the reduced moisture content.

After a value of n is chosen and sorptivity, S, is experimentally determined from gravimetric test, the value of D_0 can be calculated from the equation (4) (Lockington et al. 1999):

$$D_0 = \frac{n^2 S^2}{(\theta_s - \theta_i)^2 e^n (2n-1) - n - 1} \quad (3)$$

3 LATTICE MODEL APPROACH

Lattice models have been widely used to simulate fracture, moisture transport and chloride diffusion in cement-based materials (Schlangen 1993; Bolander & Berton 2004; Šavija et al. 2012). In this work, a regular lattice is used to model moisture transport caused by water absorption of the concrete substrate in concrete repairs. The proposed model treats concrete as an assembly of one-dimensional linear elements, through which moisture transport takes place. A generic governing partial differential equation for diffusion-type transport phenomena has the form described in the equation (1). If this equation is discretized using the standard Galerkin method, the following set of linear equations arises:

$$M\dot{\theta} + K\theta = f \quad (4)$$

where M = the element mass matrix; K = the element diffusion matrix and f = forcing vector. Vector θ is the vector of unknown quantities (moisture content) and dot over θ indicates the time derivative.

Using the Crank-Nicholson procedure, the system of linear equations is discretized in time and solved for each discrete time step (Δt).

4 VERIFICATION OF THE MODEL

4.1 *Water sorption in mortar*

The lattice model previously described was applied to simulate the moisture transport in mortar. The experimental results obtained by Hall et al. (1990) are compared to results obtained from the simulation (figure 1).

As can be seen, predicted values match well with measured water profiles, and confirm that lattice model can be used successively for prediction.

4.2 *Water sorption in concrete*

Reliability of lattice model applied to absorption of the concrete substrate was verified on results obtained by repair moisture model (Zhou 2010).

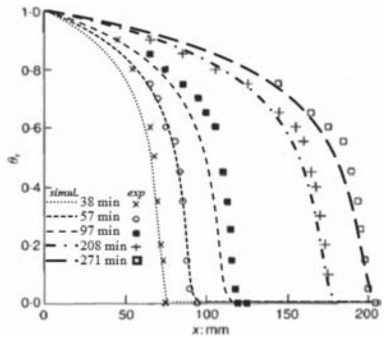

Figure 1. Comparison of reduced water content of mortar between simulation results and experimental results obtained by Hall et al. (1990).

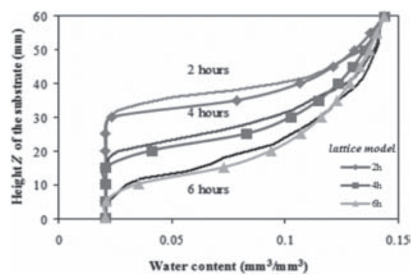

Figure 2. Comparison of water prediction obtained by Zhou (2010) and lattice model.

5 DISCUSSION

The presented model enables easy and fast quantification of moisture content in the concrete substrate if the sorptivity, porosity and initial moisture content of the concrete substrate are known. Various researchers state that different substrates and repair materials correspond to different optimum interface moisture conditions at the time of casting. Therefore, predicting and modeling capillary absorption of the concrete substrate is very important. By controlling moisture transport, optimum moisture condition for a given combination of substrate and repair material can be designed.

6 CONCLUSIONS

Based on the above discussion, the following can be concluded:

- Reliability of the proposed approach was verified with experimental results obtained on mortar and concrete samples. The results show that lattice model can be used as a tool to model capillary absorption of the unsaturated concrete substrate.
- Gravimetric test accompanied with lattice simulation may give very accurate prediction of water distribution and wetting front within the sample.
- Application of this model will enable insight in the moisture transport phenomena and therefore, enable predictability of obtained properties and performance of the repair system.
- Coupled with moisture loss due to hydration of the repair material, this model can be a very valuable tool to design optimal level of water content in the concrete substrate, which could provide the best bond for the different repair systems.

Concrete Repair, Rehabilitation and Retrofitting III – Alexander et al. (eds)

Textile reinforced sprayed mortar for the repair of hydraulic engineering structures

J. Orlowsky & M. Raupach
Institute of Building Materials Research (IBAC), RWTH Aachen University, Aachen, Germany

ABSTRACT: Massive, several decades old hydraulic engineering structures often show lower strength concretes as well as cracked construction joints and cracks with temperature induced changes of the crack width. When using unreinforced repair mortars, changes in the crack width cause a propagation of the cracks into the repair mortar. Water can penetrate these cracks entailing negative effects on the durability of the sprayed mortar and its bond to the existing concrete. The following paper deals with the application of textile reinforcement in customary sprayed mortars. By means of textiles, moving cracks in the substrate are transformed into a finely distributed crack pattern in the repair mortar which is uncritical with regard to durability. Within the framework of a research project funded by the Federal Waterways Engineering and Research Institute (BAW), different textile variations were combined with a sprayed mortar and the properties of the manufactured bond specimens were characterised in the laboratory. Afterwards, the new composite material was used in the context of a test repair on the Neckar weir at Horkheim.

1 INTRODUCTION

Within the framework of a research project initiated and commissioned by the Federal Waterways Engineering and Research Institute (BAW) and carried out by the Institute for Building Materials research (ibac) of RWTH Aachen University, in this context, it should be investigated to which extent a crack existing in the old concrete substrate can be distributed on many fine cracks in the repair mortar when textile reinforced sprayed mortars are used.

To put this aim into practice, a sprayed mortar was chosen and reinforced with four different textiles. At first, laboratory investigations were performed to characterise the new composite material; afterwards it was tested at a hydraulic engineering structure.

2 LABORATORY INVESTIGATIONS

In order to characterise the new composite material, textile reinforced sprayed mortar slabs with a thickness of 30–40 mm (depending on the textile reinforcement) were manufactured applying the dry spraying method. Four strip specimens with a length of 500 mm and a width of 100 mm were sawn from each slab. The ultimate load of these strip specimens was determined in a tensile test with a test rate of 0.5 mm/min. The load was transferred by glued-on steel flaps with a length of 100 mm.

On the basis of a crack existing in the concrete substrate, the crack bridging specimens illustrated in Figure 1 were manufactured to determine the crack distribution in the reinforced repair mortar. In order to increase the free elongation length of the repair layer, a load transmission between the old concrete and the sprayed mortar was prevented in the crack area by means of a 10 cm wide separating strip made of adhesive tape. During the test, the crack opening in the concrete specimen was continuously measured on both sides by inductive displacement transducers.

Cyclic tests with crack openings in the concrete specimen of up to 0.7 mm followed. In this context, the crack widths, number of cracks and crack spacings in the repair mortar were determined depending on the load.

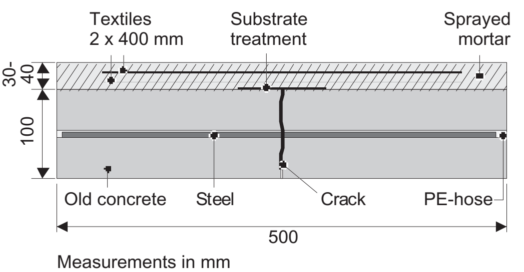

Figure 1. Crack bridging specimen to investigate textile reinforced sprayed mortar.

3 INVESTIGATION RESULTS

From the tensile tests on strip specimens can be discerned that, after the first crack of the sprayed mortar, the reinforcement transfers loads and that further cracks develop. With the carbon textile the highest ultimate loads at the lowest strains were obtained. Especially with the reinforcement impregnated with epoxy resin, a finely distributed crack pattern with crack spacings of about 2 to 3 cm was yielded. All textiles were well embedded into the sprayed mortar, there was no formation of blow holes in the test specimens.

In Figure 2 the crack opening in the old concrete is plotted over the load. Figure 2 shows the load development in the textile reinforced sprayed mortar layer during a crack opening of up to 0.7 mm. The measured load decreases each indicate a crack and a micro-crack formation in the repair system. Generally, with all four reinforcement variations, it was hence achieved to distribute the crack width change of the single crack in the substrate on several cracks in the sprayed mortar layer. In this process, most of the cracks in the sprayed mortar could be generated with the AR-Glass textile impregnated with epoxy resin.

4 TEST ON THE HORKHEIM WEIR

The Horkheim weir was built from 1927 to 1929 by architect Paul Bonatz. It separates the shipway from an old river bed of the Neckar. The construction consists of three weir fields with four massive weir pillars. The weir pillars show numerous cracks and open construction joints. The crack widths are between 0.1 and 3.00 mm.

For a comprehensive test of the new composite material, eight test surfaces were created on the Horkheim weir. Seven surfaces are located on a weir

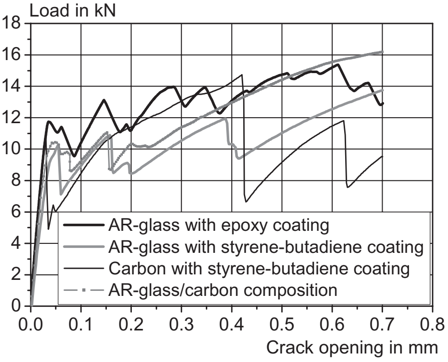

Figure 2. Loads in the textile reinforced sprayed mortar layer during crack opening in the old concrete up to a crack width of 0.7 mm.

pillar in the area of the upstream water, the eighth surface is situated downstream in the zone of changing water levels. The total area amounts to just under 50 m². With regards to their exposure, all surfaces must be classified as exposed to outdoor weathering. Surfaces 7 and 8 are located differently. In contrast to the front side, both surfaces are not exposed to direct insolation. Moreover, at high water, surface 8 is directly exposed to the water. The same mortar as in the laboratory tests we used as sprayed mortar.

In order to measure the crack movements, displacement transducers were installed outside as well as inside the test surfaces. The movements in the repair system at the height of the textiles are measured with strain gauges. The data are recorded continuously and transmitted by modems to ibac.

The textiles are fastened using glass fibre anchors with stainless steel plates. In general, it was sufficient to fasten the textiles with two anchors at the upper edge and, if necessary, another anchor was used where the textiles overlap.

5 SUMMARY

Laboratory tests showed that sprayed mortars can be reinforced with textiles without any problems. A sufficient bond between textile and sprayed mortar could be verified.

Furthermore, it was shown that the movements of a crack in the substrate can be distributed onto several finer cracks in the reinforced repair mortar by means of textile reinforcement. In laboratory tests, the textiles with epoxy resin impregnated AR glass turned out to be best suited. With regards to the application, however, the carbon textile features the advantage that it is directly available at the market and that it can be better handled in the dry spraying process.

The applicability of textile reinforced sprayed mortar layers under on-site conditions at a building was successfully demonstrated at the Horkheim weir. At the visual inspection about 6 months after the application, cracks in the sprayed mortar could not yet be detected. The strain gauges however show the movement of some old concrete cracks. The continuation of the investigations will allow conclusions regarding the functionality of the new repair system at the building.

Moreover, within the framework of a present research project, further investigations in the laboratory as well as on other buildings with lower strength substrates are planned. The testing of new materials, the improvement of the targeted local bond failure in the crack area and, most essential, the additional strengthening of the bond between old concrete and sprayed mortar are in the focus of these scheduled investigations.

Concrete Repair, Rehabilitation and Retrofitting III – Alexander et al. (eds)
© 2012 Taylor & Francis Group, London, ISBN 978-0-415-89952-9

Shrinkage stress damage effect in concrete patch repair

M.A. Shazali
INCO Precast Engineering, Industrial Contractors Co. Ltd., Dammam, Saudi Arabia

M.K. Rahman
Research Institute, King Fahd University of Petroleum & Minerals, Saudi Arabia

M.H. Baluch
Department of Civil Engineering, King Fahd University of Petroleum & Minerals, Saudi Arabia

ABSTRACT: The performance of concrete patch repair is of great concern to concrete repair industry striving to ensure repair overlays that are safely maintained in working and durable condition. The strength and durability performance of concrete repair may be measured in terms of its resistance to cracking and to its primary dependence upon moisture transport. Addressing the performance of concrete patch repair therefore requires a multi-facetted approach to the identification of failure modes related to interaction between moisture flow, shrinkage resistance and associated creep relief. In this paper a coupled approach regarding nonlinear moisture diffusion that includes the effect of shrinkage associated stress damage in concrete patch repair system was considered in modeling the moisture transport criterion. Since distressed repair surfaces cannot be expected to connect surface to environmental moistures in accordance with constant surface factor approach, it follows that shrinkage associated damage adjusted moisture transfer coefficient, in addition to moisture dependent diffusion coefficient, should be considered elemental transport properties with regard to realistic simulation, analysis, and design strategies for structural problems of concrete patch repair under service field conditions. In order to assess the effectiveness of the coupled moisture and shrinkage dependent diffusivity analysis, patch repair problem was investigated with and without considerations of the effects of shrinkage associated stress damage on structural repair response histories. In the light of improved prediction accuracy to an experimental data achieved in the present study, effects of shrinkage associated stress damage must not be neglected in modeling moisture migration in restrained and highly shrinking materials like repair mortar overlays.

Keywords: concrete, durability, repair, moisture, diffusivity, drying, shrinkage, creep, stress, cracking, damage

1 INTRODUCTION

Problems of drying shrinkage in concrete repair have been studied by theoretical analysis as well as by experimental observations (Baluch et al. 2002, 2011). In this paper, moisture diffusion and shrinkage stress analysis models are developed in order to predict drying shrinkage stress in concrete repair. Accordingly, influence of stress damage associated with shrinkage is explicitly accounted by an extended diffusivity definition used to drive the nonlinear moisture prediction model in an improved manner.

2 PROBLEM FORMULATION

There are many types of shrinkage that affect concrete. In a concrete patch repair, however, drying shrinkage related to moisture loss makes up the most significant portion of the total shrinkage strains (Australia 2002). In general, drying shrinkage in concrete is a phenomenon in which the concrete undergoes volume change due to the loss of moisture. The loss of moisture occurs when concrete exposed to a drier environment reaches moisture equilibrium by surface evaporation. The transient moisture flow is described by the following governing partial differential equation:

$$\frac{\partial C}{\partial t} = \nabla[D_a(C)\nabla C] \tag{1}$$

where C is the moisture content, $D_a(C)$ is the diffusivity, and t is time. Equation 1 has to satisfy initial and boundary conditions of the problem. In case of patch repair, a convective boundary is expressed as:

$$q_n = f_m \cdot (C_s - C_e) \tag{2}$$

where q_n is the moisture flux; f_m is the surface factor; C_s is surface moisture, and C_e is the environmental moisture. The moisture-shrinkage relation found in (Baluch et al. 2011) is linear:

$$\varepsilon_{sh} = \alpha_m \cdot M \tag{3}$$

in which ε_{sh} is the free shrinkage; α_m is coefficient of moisture contraction; and M is the moisture loss. Shrinkage strains, together with the elastic strains from structural loads form the total strain (ε_{tt}):

$$\varepsilon_{tt} = \varepsilon_{el} + \varepsilon_{sh} \tag{4}$$

in which ε_{el} is the elastic strain. In combining the drying shrinkage strain, it is seen that moisture contraction affects the computation of shrinkage-stress problem and its structural mechanics application:

$$\nabla\sigma + F = 0; \sigma = C : \varepsilon - \beta M; \varepsilon = \frac{1}{2}[\Delta u + \Delta u^T] \tag{5}$$

which refer to equilibrium, the constitutive law, and the kinematics condition, respectively. The definition of the stress problem is thus completed by a set of boundary conditions compatible with a specific problem application.

The definition of diffusivity is extended to permit moisture-shrinkage effects:

$$D_a(C,S) = D_o \cdot F_{cc}(C) \cdot F_{sc}(S) \tag{6}$$

where D_o is the moisture diffusivity at standard or reference conditions; while F_{cc} and F_{sc} are appropriate diffusivity influence functions for moisture content (C) and shrinkage associated stress damage (S) effects.

3 MODELING, APPLICATION & RESULTS

The heat transfer module offered by Comsol (Comsol 2012) was applied using the appropriate analogs the moisture-shrinkage stress problem. For validation purposes of the Comsol results, the experimental results in Rahman et al. (2000) are reproduced as part of Figure 1. Their calculation considered moisture only dependent diffusivity shrinkage stress analysis using Shrcpan, a research bespoke software. It is seen that when strain reached its ten days value, the mismatch between the two results is quite significant as the numerical curve continue to fall well below the experimental results. The results accomplished by the Comsol analysis with and without shrinkage dependency are also plotted in Figure 1. It is seen that both the Shrcpan and the Comsol results match in response to their consideration of only moisture dependency (Da[C]).

The parity between the Shrcpan and the Comsol results validate the feasibility of the Comsol with much better proximity to the observed data. The analysis for the coupled diffusivity (Da[C,S]) plotted in Figure 1 shows it has achieved clear equivalence with the experimental curve. It should be noted that the solution with shrinkage effects was found to be sensitive to the surface moisture transfer coefficient (f_m) in the flux boundary condition. A simulation strategy in which f_m was adjusted, in this case for the shrinkage distress effects, was applied (Worch 2004).

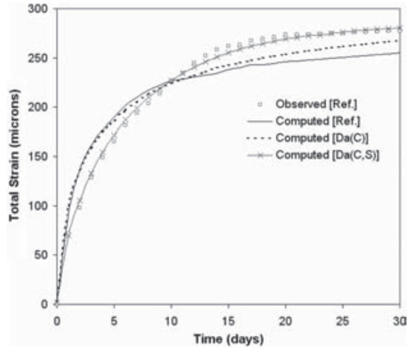

Figure 1. Comsol computed total strains i) with shrinkage effect, case [Da(C,S)]; ii) without shrinkage effect, case [Da(C)].

4 CONCLUSIONS

The model for calculating moisture-shrinkage induced mechanical distress in concrete patch repair using shrinkage adjusted moisture diffusivity introduced in this paper seems to be promising. Clear equivalence was achieved between experimental results and results calculated here in Comsol. The model predicts that drying shrinkage accelerates moisture diffusion, which in turn increases the shrinkage strain. It follows therefore that concrete repair specialists should be aware of using an accurate definition of moisture diffusivity for concrete patch repair.

The results presented in this paper essentially summarize research developments that are at an intermediary stage. Risk factors associated with repair failures are typically studied under the limiting assumption of moisture only dependent diffusivity (Baluch et al. 2002). As such future works on this subject are intended to include consideration of shrinkage associated stress damage in order to permit a better assessment of such factors with improved prediction accuracy.

ACKNOWLEDGEMENTS

The support of Civil Engineering Department and Research Institute at King Fahd Univ. of Petroleum & Minerals (KFUPM) is gratefully acknowledged.

Concrete Repair, Rehabilitation and Retrofitting III – Alexander et al. (eds)

Performance of engineered cementitious composite for concrete repairs subjected to differential shrinkage

J. Zhou
Sinoma Research Institute, Sinoma International Engineering Co., Ltd., Beijing, China

G. Ye
Microlab, Faculty of Civil Engineering and Geosciences, Delft University of Technology, Delft, the Netherlands

T. Sui
Sinoma Research Institute, Sinoma International Engineering Co., Ltd., Beijing, China

1 INSTRUCTION

The differential shrinkage often causes the cracking of the repair material and the debonding of the repair material from the concrete substrate. The cracking of the repair material facilitates the penetration of aggressive agents, and therefore causes reinforcement corrosion and concrete deterioration. Engineered Cementitious Composite (ECC), a fiber-reinforced cementitious material, has been proposed to be one of the most promising repair materials. This group of materials is characterized by high ductility in the range of 3–7% and tight crack width of around 60 μm. When ECC is used as a repair material, ECC can accommodate larger deformation, induced by differential shrinkage or external load, while maintaining a high load capacity. Moreover, the tight crack width of ECC retards the penetration of aggressive agents and thus improves the durability of the repaired structures.

In this paper, the performance of ECC used in concrete repairs is investigated, compared to a fiber-reinforced polymer-modified (FRPM) mortar. The surface cracking in the repair materials and the delamination of the interface caused by the differential shrinkage between the repair material and the concrete substrate were monitored.

2 EXPERIMENTAL PROGRAM

2.1 *Materials*

The concrete substrate used in this study was a three-year-old concrete. Its compressive strength and Young's modulus were 88.9 MPa and 36.3 GPa, respectively. The newly developed ECC, made of limestone powder and blast furnace slag (BFS) was used as repair material. Another repair material, the FRPM mortar, was a commercial premix product. Its water-to-solid ratio was 0.14.

2.2 *Compressive test and uniaxial tensile test*

Compression test and uniaxial tensile test were used to investigate the mechanical properties of the repair materials at the ages of 3, 7, 28 and 90 days.

2.3 *Free shrinkage*

The free shrinkage of the repair materials was measured according to European standard EN 12617-4. After 24-hour curing covered with plastic paper and under a temperature of 20°C, the specimens were exposed to a temperature of 20°C and RH of 50%.

2.4 *Surface cracking and interface delamination*

The surface cracking and interface delamination of the composite beams due to differential shrinkage were investigated, as shown in Figure 1.

The surface of the concrete substrate was grit-blasted. After placing the repair materials, the fresh repair materials were covered with plastic sheet and cured for 24 hours. Then, the composite beams were moved into a room with a temperature of 20°C and RH of 50%. The surface cracking in the repair materials was observed with a portable microscope. The interface delamination was measured with two LVDTs, which were attached on the ends of the composite beams. The measurements on the composite beams lasted for 90 days.

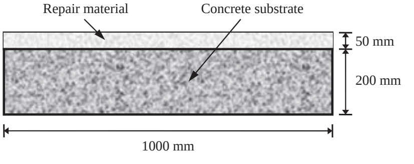

Figure 1. Composite beam with a layer of the repair material and a layer of the concrete substrate.

2.5 *Direct tensile test for measuring bond strength*

The bond strength between the repair material and the concrete substrate was measured by a direct tensile test according to European standard EN 14488-4. The tested specimens were layered cylinders with a diameter of 60 mm. The thicknesses of the repair material and the concrete substrate were both 60 mm.

3 EXPERIMENTAL RESULTS

The ultimate tensile strength, tensile strain capacity and compressive strength of ECC and FRPM mortar are given in Table 1. ECC shows a free shrinkage about 2 times higher than the RFPM mortar in the first 90 days.

The average crack width the repair materials, caused by differential shrinkage, are shown in Figure 5. The first surface crack in the ECC repair system was observed at the ECC age of 3 days, while it was at 5 days in the FRPM system. During the 90-day measurement period, ECC exhibits smaller crack width and a larger number of cracks than the FRPM mortar. At the repair material age of 90 days, 51 cracks with the width ranging from 10 μm to 60 μm were observed on the surface of ECC, while only 9 cracks with the width ranging from 100 μm to 130 μm were observed on the surface of the FRPM mortar. Crack width in ECC is normally smaller than 60 μm. The tight crack width in ECC can greatly reduce the water permeability and retard the penetration of aggressive agents. The durability of the repair system is, therefore, enhanced.

The ECC composite beam shows an earlier and larger interface delamination than the FRPM mortar composite beam. The interface delamination in the ECC composite beam was initiated at 1.5 days, while the interface delamination in the FRPM mortar beam was initiated at 4 days. After 90 days, the ECC composite beam exhibited an average interface delamination of 0.11 mm, while the FRPM mortar composite beam exhibited an average interface delamination of 0.035 mm. In the ECC composite beam, the interface delamination occurs mainly in the first 20 days and reaches the average value of 0.094 mm. Afterwards, the interface delamination in the ECC composite beam did not show a big increase. However, in the FRPM mortar composite beam, the differential shrinkage resulted in a continuous increase in the interface delamination.

As given in Table 2, ECC have a bond strength 47% lower than the FRPM mortar. The ECC specimens all failed in the interface, while the FRPM mortar specimens all failed in the substrate. Since the bond strength between ECC and the concrete substrate is too low, especially at the early stage, the differential shrinkage may cause severe interface delamination rather than cracking, as observed in the first 3 days.

Table 1. Ultimate tensile strength, tensile strain capacity and compressive strength of ECC and the FRPM mortar.

Repair material	Age [d]	Ultimate tensile strength f_t [MPa]	Tensile strain capacity ε_u [%]	Compressive strength f_c [MPa]
ECC	3	3.7 ± 0.2	5.1 ± 0.7	14.3 ± 0.1
	7	4.2 ± 0.4	3.6 ± 0.2	23.9 ± 1.5
	28	4.6 ± 0.5	3.1 ± 0.7	40.1 ± 1.2
	90	4.8 ± 0.3	2.6 ± 0.3	50.3 ± 0.8
FRPM mortar	3	3.9 ± 0.4	< 0.03	58.2 ± 0.4
	7	–	–	69.0 ± 1.0
	28	5.6 ± 0.8	< 0.03	76.8 ± 0.6
	90	–	–	82.3 ± 1.2

Table 2. Repair-substrate bond strength of ECC and the FRPM mortar.

Repair material	ECC	FRPM mortar
Bond strength [MPa]	1.35 ± 0.10	2.57 ± 0.12

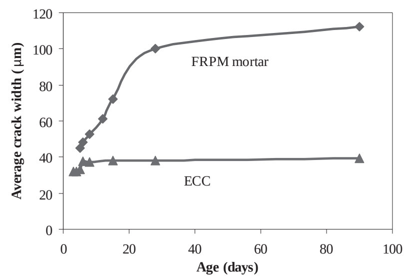

Figure 2. Average crack width at the surface of the repair materials.

The interface is, therefore, the weakest point of the ECC repair system. In order to avoid the interface debonding, the bond strength between ECC and the concrete substrate need to be enhanced.

4 CONCLUSION

The performance of the ECC repair system subjected to differential shrinkage was experimentally investigated compared to a FRPM repair system. Compared with the FRPM, ECC shows smaller crack width and the crack width does not have an obvious increase in the first 90 days. Although ECC cracks, the shrinkage of ECC is much lower than the tensile strain capacity. Consequently, ECC can carry more load and accommodate more deformation. This contributes to the load-carrying capacity of the repair system. It was also found that the bond strength is another crucial factor. To enhance the bond strength becomes more meaningful on achieving durable ECC repairs.

Concrete Repair, Rehabilitation and Retrofitting III – Alexander et al. (eds)
 ISBN 978-0-415-89952-9

Cracking characteristics of cement mortars subjected to restrained shrinkage

M. Chilwesa & H. Beushausen
Concrete Materials and Structural Integrity Research Unit, Department of Civil Engineering, University of Cape Town, South Africa

ABSTRACT: Restrained shrinkage cracking in bonded overlays including patch repairs is a serious problem that compromises overlay and patch performance. In this study, cracking characteristics of cement mortars subjected to retrained shrinkage were investigated. Five mortar types were subjected to a restrained shrinkage test, the ring test, in order to determine their age at cracking and extent of cracking (crack area). Material properties such as free shrinkage, elastic modulus, tensile relaxation and tensile strength were also measured in order to determine their influence on overlay cracking. The experimental results indicate that crack resistance of overlays depends upon the combined influence of the different material properties. In particular, tensile stress relaxation appears to have the largest influence.

1 INTRODUCTION

Cracking in concrete due to restrained shrinkage is a major problem that affects members such as slabs on grade, pavements, toppings, linings and patch repairs. In this paper, these members are considered under the general theme of "bonded overlays". Shrinkage arises as a result of moisture loss by concrete to the environment and also through internal moisture consumption. Loss of moisture can lead to plastic shrinkage in newly cast concrete or drying shrinkage in aging concrete, while a temperature gradient will cause thermal shrinkage. Free shrinkage will cause lateral compressive strains which, if concrete is restrained, results in tensile stresses. In bonded overlays, the differential shrinkage between concrete substrate and repair material generates tensile stresses. These stresses may lead to cracking of concrete if the tensile strength of the overlay concrete is exceeded, thus compromising both the durability and serviceability requirements.

Overlay resistance to crack initiation, development and propagation depends on a number of time-dependent properties of the concrete. In addition to free shrinkage and tensile strength, several other factors can influence the potential for cracking including tensile relaxation and elastic modulus, as well as degree of restraint and environmental conditions such as relative humidity. The advent of cracking will depend upon the interaction of these material properties.

The investigation covered in this study contributes towards efforts aimed at harnessing early age shrinkage cracking in concrete.

2 EXPERIMENTAL PROGRAM AND RESULTS

Five mortars, comprising three Commercial Repair Mortars (CRM1, CRM2 and CRM3) and two laboratory made mortars (M45 and M60), were selected for investigation. A ring test similar to the one described in ASTM C 1581-04 was adopted. Direct uni-axial tensile strength, free shrinkage, and tensile relaxation were measured on dog bone specimens measuring 170 × 40 × 40 mm in the prismatic section.

Results for free shrinkage, tensile strength, tensile relaxation, elastic modulus, age of cracking, and crack area are presented in Figures 1, 2, 3, 4, 5, and 6, respectively.

3 CONCLUSION

Shrinkage and tensile strength are often used as the main material parameters considered in judging the potential cracking performance of overlays and repair patches. The research discussed in this paper shows that shrinkage and strength values in isolation cannot determine the cracking behaviour of cement mortars. Both CRM1 and CRM3 had very high values of free shrinkage strain, yet

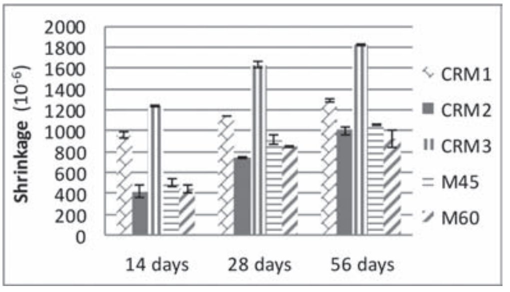

Figure 1. Free shrinkage strain results of mortar specimens.

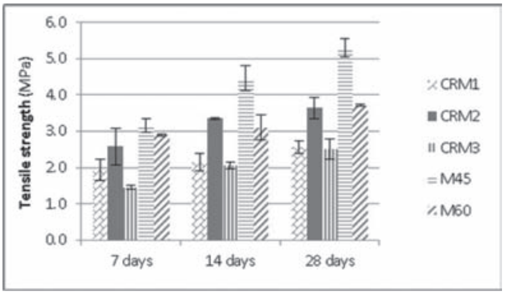

Figure 2. Tensile strength results.

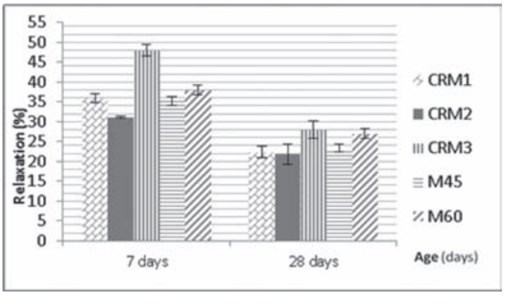

Figure 3. Tensile relaxation results.

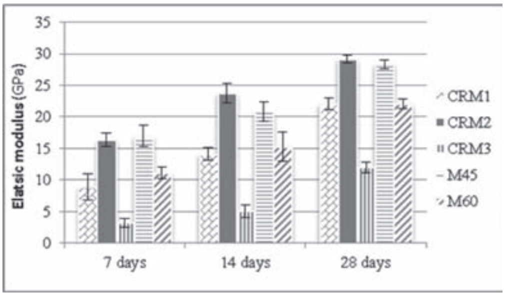

Figure 4. Elastic modulus results.

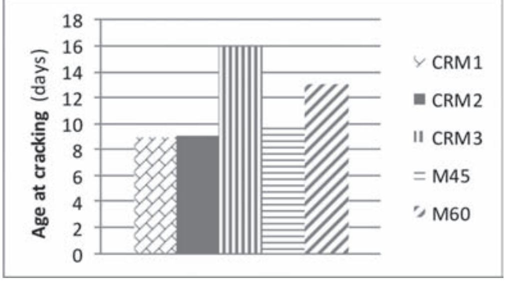

Figure 5. Age at cracking in ring test specimens.

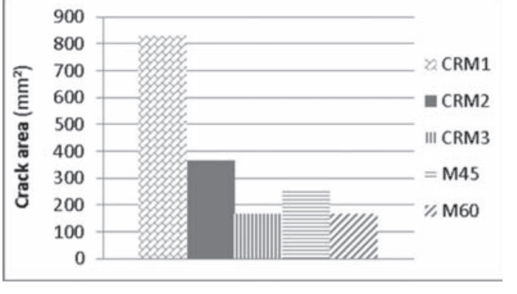

Figure 6. Crack area in ring test specimens.

CRM1 recorded the shortest time to cracking while CRM3 recorded the longest time to cracking. Also CRM1 and CRM2 specimens had the same age at cracking despite them having different material properties. This confirms that crack resistance of repair mortars depends upon the combined influence of a number of factors such as shrinkage, elastic modulus, tensile relaxation and tensile strength.

Tensile relaxation has a very big influence on age at cracking. Tensile relaxation reduced tensile stresses by approximately 20–48% in the mixes tested.

Structural repairs and strengthening

This page intentionally left blank

Concrete Repair, Rehabilitation and Retrofitting III – Alexander et al. (eds)

Retrofitting of Bridge B421 over the Olifants River after flood damage

W. Findlay & F. Kromhout
BKS(Pty) Ltd., Engineering and Management, South Africa

ABSTRACT: Bridge B421 is located on Route R555 between eMalahleni (Witbank) and Middelburg in Mpumalanga, South Africa. On 6 January 2011, after heavy rains, road users reported that a large sinkhole has formed in the road behind the eMalahleni Abutment. The routine road maintenance contractor investigated the cause of the sink hole and found that the abutment and wing wall on the downstream side of the bridge has failed. The South African National Roads Agency SOC Limited (SANRAL) contacted an experienced consulting bridge engineer to investigate the reason for the failure.

Bridge B421 is a simply supported 4-span bridge with span lengths of 16 m each. The deck consists of simply supported reinforced concrete voided slabs. The piers are wall-type on spread footings and the abutments are wall-type closed abutments with splayed wing walls. The three piers and the Middelburg Abutment were founded on weathered mudstone, but contrary to good practice, the eMalahleni Abutment was founded on clayey sand. The shift in the river channel due to scour during 32 years had shifted the position of river scour to the one abutment. When the Witbank Dam sluice gates were opened on 6 and 7 January 2011, the lack of foundation support due to undermining scour and rapid drawdown water pressure behind the abutment wall combined to cause half of the abutment to fail completely. Route R555, which carries more than 14 000 vehicles a day was closed for traffic.

This paper describes the investigations done and the actions taken to support the deck temporarily while constructing a new abutment, supported on piles, underneath the overhanging deck structure, as well as additional works to upgrade the bridge.

1 INTRODUCTION AND BACKGROUND

Bridge B421 is located on the R555 between Witbank (eMalahleni), and Middelburg in the province of Mpumalanga. It is a four span bridge, with each span comprising a simply supported voided slab. The piers are wall-type on spread footings and the abutments are wall-type closed abutments with splayed wing walls on spread footings.

During December 2010 and January 2011 heavy rains fell that led to the opening of the Witbank dam sluice gates twice between the 6th and the 10th of January 2011.

2 FLOOD DAMAGE TO OLIFANTS RIVER BRIDGE

2.1 *Flood damage to Witbank Abutment*

The opening of the sluice gates twice between the 6th and the 10th of January caused the water level in the river to rise above the edges of the wing walls. The sudden increase in flow height and velocity of the water resulted in a whirlpool to start on the downstream side of the Witbank Abutment. The whirlpool caused the backfill material behind the wing wall to be saturated and scour to occur at the back of the wing wall and below the wing wall foundation. This resulted in the wing wall footing to start rotating forward. This led to the abutment and wing wall to collapse and leave a large sinkhole in the road, which resulted in the road being closed.

2.2 *Flood damage to Middelburg Abutment*

The increase in water level at the Middelburg embankment resulted in the fill behind the abutment and wing wall to become saturated. This resulted in the Middelburg Abutment wall to crack at the horizontal construction joint at mid height of the wall.

3 INVESTIGATING POSSIBLE REPAIR SOLUTIONS

3.1 *Geotechnical investigation*

A detailed geotechnical investigation was carried out in order to determine the founding conditions and level to bedrock. The drilling results indicate that the Middelburg Abutment and eastern piers are founded on very soft to soft rock Mudstone, with the Witbank Abutment founded on silty sand

and the bedrock located at a depth of approximately 7.5 m below the top of the existing base. During the geotechnical investigation phase the horizontal crack in the centre of both the abutment walls were monitored and showed that only the Witbank Abutment was bulging forward.

3.2 *Investigating possible repair method of the Witbank Abutment*

The first remedial action considered was to investigate whether the abutment could be repaired with the road open to traffic. To determine this, a detailed analysis of the deck in its current state was required, which showed the repair to the abutment under traffic was not a viable option.

In order to protect and stabilize the upstream abutment footing against settlement and possible future scour damage, the following measures would be required:

- Due to the depth of bedrock the spread footing would have to be founded on piles.
- Jet grouting below the spread footing instead of installing piles.
- The installation of diaphragm walls to support the spread footing.
- Soil anchors would have to be installed.
- The possible installation of sheet piling to safeguard the backfill was also considered.

Considering the above and taking all the potential risks into account, the only solution that would guarantee the long term stability of the Witbank Abutment would be to replace it with a new abutment.

3.3 *Repair method of the Middelburg Abutment*

To ensure the long term stability of the wall, two rows of soil-nails were installed one row on either side of the horizontal construction joint.

4 DESIGN OF THE NEW WITBANK ABUTMENT WALL

4.1 *Temporary support-work of the deck and protection thereof*

The construction and design of the temporary support-work was the contractor's responsibility. The temporary support work was protected, against future flooding by means of a cofferdam around the temporary support-work.

4.2 *Installation of the piles and its effect on the temporary support-work*

The founding level for the new base slab was determined to be approximately 1,5 m below the founding level of the existing abutment. The installation of the 350 mm square precast driven piles was restricted by the following factors, which precluded the use of Auger piles or Continuous Flight Auger piles.

- A maximum rake for the front piles of 1:3.
- A minimum clearance of 1,750 m between centre of piles and deck soffit.
- The piles had to be socketed through the very soft rock and onto the soft rock.

The position and level of the temporary supportwork was calculated to ensure that during the excavation of the new pile cap and demolishing of the existing abutment, would not jeopardise the temporary supportwork. In order to ensure the stability of the temporary support, the settlement and lateral displacement of the support slab had to be monitored during the installation of the piles.

4.3 *Strengthening of the deck over the temporary support*

The position of the jacks on the temporary supportwork altered the mechanism of the deck from simply supported between the bearings, to have a 5 m cantilever over the support for which the deck had to be strengthened over the support.

5 UPGRADING AND REHABILITATION OF BRIDGE B421

The repair to the Witbank Abutment provided an opportunity for the upgrading of the bridge in terms of safety to pedestrians and road users and the rehabilitation of certain elements (bridge joints, pedestrian barriers etc.) of the bridge.

6 CONCLUSION

The R555 was reopenend 10 months after the closure to the public.

ACKNOWLEDGEMENTS

The authors of this paper wishes to acknowledge the active role the South African National Roads Agency Limited played in the successful repair of the Olifants River Bridge as well as kind permission given to publish this paper.

Concrete Repair, Rehabilitation and Retrofitting III – Alexander et al. (eds)

Strengthening of traffic barriers on bridges along the Kaaimans Pass

B.P. Durow & G.A. Visser
SSI Engineers and Environmental Consultants, Pietermaritzburg, South Africa

E.J. Kruger
The South African National Roads Agency SOC Limited, Pretoria, South Africa

ABSTRACT: During the past decade traffic accidents on bridges along the Kaaimans Pass in the Southern Cape have caused minor damage to the barriers on these bridges. Recently the complete dislodgement of barrier panels on one structure occurred. This prompted SANRAL to commission an investigation of the reasons for the failure and to plan for strengthening of these components, if found necessary. Design checks indicated theoretical compliance with the applicable TMH7 code requirements. However, visual inspection of the failed components gave rise to concern about the adequacy of the grouted connection between the precast barrier panels and the bridge decks. It was therefore decided to prepare a design aimed at strengthening the barriers, by fastening stainless steel plates to the barrier front faces, connected to threaded anchor bars which pass through and are secured at the underside of the decks. Analysis by finite element simulation of impact forces confirmed that the original barrier design barely achieved the code ultimate load requirements, whilst the strengthened design was assessed to have an acceptable ultimate load capacity of 135 kN per barrier panel. SANRAL elected to proceed with the implementation of 1000 m of barrier strengthening on four of the Kaaimans Pass bridges, which is currently in progress and due for completion by December 2012.

1 INTRODUCTION

1.1 *Location and topography*

The Kaaimans Pass is located on a portion of the N2 through mountainous terrain, between George and Wilderness in the Southern Cape. Within this length of the Pass the N2 crosses nine bridges which were constructed in the 1980s. Four of these are framed viaduct type structures in areas of very steep crossfall, where half of the four lane highway is supported on these bridges and the other half is constructed in cut. The viaducts numbered B1411, B1412, B1413 and B1414 are the focus of this paper, with particular regard to the adequacy of their barriers.

1.2 *Bridge barriers*

The New Jersey type traffic barriers on the Kaaimans viaducts were originally designed as in situ reinforced concrete components in terms of the TMH7 code requirements (70 kN ultimate impact force at 0,7 m above roadway). Approval of an alternative precast concrete barrier design during construction led to the installation of 2,5 m long barrier panels attached to the decks with 16 mm dia. stud anchors grouted into continuous wedge shaped channels in the deck slabs.

Whereas traffic accidents on these bridges had previously caused minor damage to the barriers, in April 2008 the potential deficiency in these components came to light when two 2,5 m long barrier panels were completely dislodged from bridge B1413 by the impact of a light delivery vehicle.

2 STRUCTURAL ASSESSMENT

2.1 *Initial investigations*

SANRAL appointed consulting engineers to investigate and report on the reasons for the barrier failure and prepare a design for strengthening the barriers, if found necessary.

The alternative design carried out 25 years earlier was based on cone pull-out theory and the use of welded steel stud anchors developed in the USA. A re-check of the original design indicated theoretical compliance with the TMH7 code requirements, but raised questions about the failure mode of the barrier. Unfortunately it was found impractical to confirm the quality of the embedment of the parapets on the grout.

2.2 *Site inspections*

An inspection of the damaged bridge and dislodged barrier panels revealed that the stud anchors together with attached grout cones had torn out of the grout channel, and that the cover concrete had peeled off the looped reinforcing bars at the edge of the deck. However, it was unclear whether the loss of the covercrete from the compression zone beneath the barrier contributed to the failure of the barrier, or was the result of the dislodgement of the barrier.

2.3 *Testing of components and materials*

Tension tests on samples of the stud anchors, cut from the underside of the dislodged barriers, showed that the yield strength of the studs exceeded the calculated tension forces in the anchors by a large margin. Laboratory concrete testing of the precast concrete barriers indicated that the concrete in the lower portions of the barriers was in good condition and unlikely to have contributed to any deficiency in the strength of the barriers.

3 STRENGTHENING PROPOSALS

In view of the uncertainties about the strength of the as-built barriers, SANRAL resolved that a design for strengthening of the barriers on bridge Nos. B1411, B1412, B1413 and B1414 should be prepared, followed by modeling and testing, of both existing and strengthened barriers, using a finite element computer programme capable of simulating the impact loading.

The proposed method of strengthening was based on the use of grade 316L stainless steel components, and included: 10 mm steel plates fastened by dowels to the barrier sloping front faces, and connected to 20 mm diameter threaded anchor bars, which pass through the deck slab; securing the anchors at the deck soffit with lock nuts after pretensioning these to 20 kN.

4 FINITE ELEMENT ANALYSES

4.1 *Finite element model and analysis procedure*

The structure geometry, materials properties, boundary conditions and applied loads were modelled for analysis using the LS-DYNA programme to carry out a non-linear finite element analysis to determine deformation and stress levels in the grout, concrete and anchors. This enabled an assessment and comparison of designs of both the as-built and strengthened barriers.

4.2 *Findings of analyses*

The predicted failure mode of the as-built barriers was indicated as cracking of the grout and deck concrete, causing tearing out of the studs from the grout, with an ultimate load capacity of 75 kN.

In the case of the modified design it was found that, provided the shear dowels at the front of the barrier each have a shear capacity of 35 kN, the strength of the modified design would be controlled by yield of the anchors through the deck, with an ultimate load capacity of at least 135 kN.

5 COURSE OF ACTION

In view of the small ultimate strength margin of the as-built design compared with the code requirements and the risk factors concerning the adequacy of barriers on bridges in the Kaaimans Pass, SANRAL resolved that the barriers should be strengthened. They instructed that the design should be fully developed, ready for implementation as soon as practical. Tenders for the strengthening of the traffic barriers of bridges B1411, B1412, B1413, together with various other rehabilitation measures to these and four other bridges in the Kaaimans Pass were received at the end of 2011. This work is due for completion by December 2012.

6 CONCLUSION

The following important issues arise from the need to strengthen the Kaaimans Pass bridge barriers:

- Caution needs to be exercised when approving a change in barrier design from in situ to precast, especially when the mode of ultimate load failure of the alternative is uncertain.
- Consideration needs to be given to the recalibration of barrier design loads and partial safety factors, in relation to the various risks which influence the adequacy of bridge barriers in South Africa.

ACKNOWLEDGMENT

The meticulous work carried out by Dr A.M. Hay and Prof R.J. du Preez PrEng of Advanced Structural Mechanics (Pty) Ltd in analysing and assessing the Kaaimans Pass bridge barriers is acknowledged with thanks.

Concrete Repair, Rehabilitation and Retrofitting III – Alexander et al. (eds)
 ISBN 978-0-415-89952-9

Assessment and strengthening of R/C hospital building—case study

Osama M.A. Daoud
Building and Road Research Institute, University of Khartoum, Sudan

ABSTRACT: This paper presents an experience in assessment and strengthening of a R/C building carried out in Sudan during the last year. A four stories R/C framed hospital building was constructed five years ago in the middle of Sudan, by the White Nile River. Due to differential upheaval movement of the underneath expansive clay soils (15–25 cm), the building had experienced serious instability problems and sever structural cracks. A comprehensive assessment of the building skeleton including geotechnical investigation, DT and NDT methods revealed the need of five different strengthening and retrofitting techniques, these are, transformation of foundation system from isolated footings to strap foundation to increase the stiffness and rigidity of footings, concrete jacketing of basement floor columns, metal jacketing of the second floor columns, construction of shear walls to enhance the stability of the building and finally CFRP laminates for strengthening of basement floor cover slab. The building had been monitored during and after completion of strengthening and retrofitting works to measure any movements during the last year rainy season. Measurements revealed the efficiency of implemented strengthening and retrofitting techniques.

1 INTRODUCTION

Kosti Military Hospital is a four stories R/C framed building constructed five years ago in Kosti city in the middle of Sudan, by the White Nile River. Because of inadequate geotechnical investigation prior to construction, the building was constructed in an area of highly potential expansive soils, without any special considerations for this type of soil.

The building is a R/C frame type building, the frame is a column-flat slab type, supported on isolated footings. As reported by the local governmental authorities, few years after completion of construction of the hospital, the building starts to suffer from cracks and visible movements of the expansion joints. Lack of routine inspection and maintenance and poor previous rehabilitation works, had led to continuous and fast development of cracks and movements.

2 ASSESSMENT PROGRAM AND RESULTS

A comprehensive structural-geotechnical assessment program including visual inspection, lab oratory testing, destructive and non-destructive testing of concrete was designed and implemented.

2.1 *Visual inspection & excavations*

Visual inspection of the structural members of the building revealed that the building was unstable, expansion joints were undergone excessive rotations and severe structural cracks were seen in some columns. Excavation around footings has been done on some of the foundations with great difficulty because of the saturation of the clay soil, and in some cases, water gushed profusely about the footings. Because of the upheaval movement of the soils, and probably of the weakness of concretes some of the basement columns were buckled and crushed (see Fig. 1). All sanitation system of the building was damaged. Leakage and accumulation of waste water and chemicals (waste of hospital's laboratories) around the columns and in contact with the basement cover slab had caused deterioration and corrosion of reinforcement of columns and slabs.

2.2 *Analysis of geotechnical results*

Geotechnical investigations showed that the soil profile at the hospital region consists of top 5.0 to 7.5 m layer of highly plastic silty clay (CH). This is underlained by alternative layers of very stiff low plastic silty clay (CL) and very stiff low plastic silt (ML) and very stiff highly plastic silty clay (CH) extending down to the end of boreholes at 15 m

Figure 1. One of buckled basement columns.

depth. The index properties of the investigated soils indicated high swelling potential for the clayey layers. The chemical test results showed acidic soils of high contents of harmful chemicals. Isolated footings foundations placed at about 2.9 m depth below the ground surface level. At this depth the bearing capacity of the soil was assessed to be 140 kN/m2.

2.3 *Core test results*

Core specimens were extracted from the foundations and floor slabs. Visual inspection of the core specimens before compression tests revealed that entrapped air voids were noticed in the core specimens which indicate that the concrete was not properly vibrated and compacted. The concrete mix was found to be over sanded and many decayed aggregate particles were noticed in the mix. Also the maximum size of aggregate found was less than 15 mm and the grading observed was not uniform. The average value of the compressive strength test results was 14 N/mm2.

2.4 *NDT tests results*

Ultrasound pulse velocity was performed to assess the quality of concretes of columns and to evaluate the degree of compaction. According to Whitehurst classification method, the quality of concretes of the columns of different floors were found to be varying between poor and doubtful, whereas some points were found to indicate very poor quality.

Rebound hammer values obtained from different columns at different floor levels showed low surface hardness and high variability in the properties of concretes of columns.

2.5 *Structural analysis*

The structural analysis showed that all the basement columns, second floor columns and the basement cover slab were loaded beyond the ultimate limits.

3 SUGGESTED STRENGTHENING METHODS

After a comparative socio-economic feasibility study of the two options of demolishing and strengthening, it was decided by the different consultancy and authorized parts involved to go through strengthening of the building.

3.1 *Modification of foundation system*

To increase the stiffness and tightness of the foundation; hence redistribute the bearing stresses and the non-uniform uplift soil pressures the foundation system was modified from isolated footings to semi-raft type. Also this will eliminate any stress concentrations on underneath soils.

3.2 *Concrete jacketing of short columns*

Strengthening of basement columns via concrete jacketing was apparent since the load carrying capacity of these columns was much less than the applied axial forces and bending moments.

3.3 *Metal jacketing of columns*

In order to increase the load carrying capacity of the second floor columns while maintaining the same cross-section, metal jacketing was the best solution. The gaps between the concrete and the added steel frame were filled with a suitable epoxy mortar.

3.4 *CFRP for basement cover slabs*

The basement cover slab was strengthened using Carbon Fiber Reinforced Polymer laminates fixed at the soffit of the concrete slab using selected epoxy resin (Bank, 2006). This technique was the best solution to cater for the two deficiencies of the slab; structural cracks due to foundation movements and corrosion of reinforcements due to chemical attack (see Fig. 2).

3.5 *Shear walls installation*

To enhance the stability of the building and to rectify the openings at the expansion joints concrete shear walls were installed at both sides of each expansion joint along the total height of the building.

4 CONCLUDING REMARKS

This case study high lights the following facts:

- Clever combination between different strengthening and retrofitting techniques can save a lot of money and time.
- When strengthening and rehabilitation of structures, it is essential to establish the nature of the problems, extent, severity and exact causes. If this is not done the symptoms could be treated not the cause.
- Careful and continuous monitoring during and after installation of strengthening and retrofitting works is vital to evaluate the efficiency of such works.

Figure 2. Strengthening of basement cover slabs with *CFRP*.

Concrete Repair, Rehabilitation and Retrofitting III – Alexander et al. (eds)
© 2012 Taylor & Francis Group, London, ISBN 978-0-415-89952-9

Repair and dynamic-based condition assessment of impact damage to a freeway overpass bridge near Mossel Bay, South Africa

A.A. Newmark
BKS (Pty) Ltd, Cape Town, South Africa

P. Moyo
Civil Engineering Department, University of Cape Town, Cape Town, South Africa

E.J. Kruger
The South African National Roads Agency SOC Limited, South Africa

ABSTRACT: This freeway overpass bridge is located near Mossel Bay, South Arica. It consists of a four span beam and slab type structure. Vehicle impact damage to the bridge occurred as a result of an illegally loaded vehicle passing underneath. The impact caused significant damage to an edge beam during which the functionality of this beam was largely destroyed. (Figure 1) As a result the beam was mainly supported by the transverse diaphragm beams connected to adjacent beams.

It was concluded from a detailed assessment and further design evaluations that repairs would require reconstruction of a section of the beam and the reinstatement of longitudinal tension capacity over the full extent of the beam. The final repair method included positive load application to ensure that the longitudinal and transverse load characteristics of the structure were reinstated. This was done by utilizing post tensioned tendons which were cast into a new in-situ beam web section attached to the inside face of the damaged beam. A new steel plate which would also act as edge armouring provided the optimum solution to reinstate part of the original capacity.

On instruction of the owner, the South African National Roads Agency SOC Limited (SANRAL), the effectiveness of the installation was assessed by means of dynamic based condition assessment before and after completion. These tests were performed by the University of Cape Town, Department of Civil Engineering.

Following the dynamic testing and strain measurements during the retro-fitment of this bridge it was concluded that the damage to the tendons of the outer beam did have a significant impact on global stiffness in the longitudinal direction. Damage to the tendons also had a significant impact in the transverse direction as reflected in change of natural frequencies and redistribution factors. This is in agreement with the analysis carried out by the consulting engineers and the testing confirmed that the rehabilitation intervention was successful in restoring the interaction between the damaged

Figure 1. Extent of damage to web and tendons.

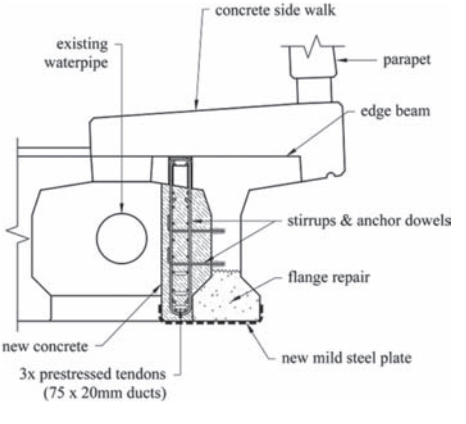

Figure 2. Final design proposal.

beam and the rest of the bridge and improving the load transfer between the damaged beam and the rest of the bridge.

PROJECT TEAM

Owner: The South African National Roads Agency SOC Limited
Consulting engineers: BKS (Pty) Ltd
Dynamic testing: Civil Engineering Department, University of Cape Town
Contractor: Steffanuti Stocks
Prestressing sub-contractor: Amsteel Prestressing

REFERENCES

Maia, N.M.M., Silva, J.M.M., He, J., Lieven, N.A.J., Lin, R.M., Skingle, G.W., To, W.M. & Urgueira, A.P.V. 1997. Theoretical and experimental modal analysis.
Nuno, M.M, Maia, J.M & Silva, M. (eds) *1st Ed*. Research Studies Press Ltd, Baldock, England.

Concrete Repair, Rehabilitation and Retrofitting III – Alexander et al. (eds)
© 2012 Taylor & Francis Group, London, ISBN 978-0-415-89952-9

Upgrading of three historic arch bridges over the Orange River near Keimoes, South Africa

A.A. Newmark & E.J. Smuts
BKS (Pty) Ltd, South Africa

E.J. Kruger & E. Lourens
The South African National Roads Agency SOC Limited, South Africa

ABSTRACT: This project is located on National Route R27 near Keimoes in the Northern Cape Province of South Africa. The overall objective is to improve traffic capacity and safety of the route, with the main focus being the widening of four single traffic lane bridges over the Orange River floodplain. This paper reviews the upgrading of the three main historic arch bridges. The project included a detailed hydrological and hydraulic assessment which resulted in the raising of two of the structures by approximately 2.5 m to prevent overtopping of the structures during larger flood events. The raising and/or widening had to comply with heritage requirements as these structures, completed in the early 1930's, have significant historical importance. This resulted in the original form and appearance to be retained by using a similar arch configuration and detailing. Construction is currently due for completion early 2013.

1 INTRODUCTION

The main focus is on the widening of five bridges over the Orange River floodplain, four of which only allows single lane traffic. This paper reviews the upgrading of the three historic arch bridges built in the 1930's.

Due to the current single lane configuration and limited flood capacity of two of the bridges, the overall objective of the construction project is to increase the capacity and improve the safety of this route. The extent of the widening of the three arch bridges are significant and requires an additional overall bridge width of 8.7 m to obtain the proposed width of 12.4 m. This paper reviews the key planning, design and construction aspects that were considered for this project.

2 RIVER HYDRAULICS AND HYDROLOGY

The Orange River, South Africa's largest river, is used to provide for irrigation as well as domestic and industrial demands along the river and in adjacent catchments through various transfer schemes. The potential flood impact on the R27 bridge crossings of the Orange River at Keimoes is significant. Floods in excess of 8000 m3/s have been recorded in this river reach during the previous 30 years. Some of the larger floods as recorded at Upington were 7400 m^3/s (1934), 5700 m^3/s (1967), 9500 m^3/s (1974), 5200 m^3/s (1976), 8400 m^3/s (1988) and 5470 m^3/s (2011).

The hydrological review required a quantification of the probability of inundation and determining of the flood peaks for the design recurrence intervals.

After due consideration of the above, especially the impact of large floods, the option of raising only B2461 and B2462 by 2,5 m was considered appropriate as this would provide acceptable capacity for a 1: 20 year flood.

3 ENVIRONMENTAL CONSIDERATIONS

A Basic Assessment was required. In consultation with heritage specialists, it was resolved that the necessary safety improvements would be acceptable, provided that this was done in such a way that the character of the bridges were retained. It was agreed that the fundamental approach would be to match the existing details, retain as much of the original fabric of the bridges as possible and that the form of the arches are acknowledged in any new work. In addition it recognised that it was acceptable for the new work to be distinguishable from the old.

4 ASSESSMENT, DESIGN AND CONSTRUCTION STARTEGIES

Typically, each arch bridge was constructed as a series of two-hinged reinforced concrete arches, with expansion joints at each pier and abutment. The piers are of the mass concrete type, whereas the abutments are lightly reinforced. Spread footings are founded

Figure 1. Bridge B2463, a ten span filled arch bridge, over the Orange River.

Figure 2. Bridge B2463 during the 2011 floods.

on shallow rock. The existing balustrades presented no protection for errant vehicles and called for urgent attention. The narrow bridges were originally not constructed with dedicated pedestrian walkways. This has proven to be hazardous, especially for cyclists.

In general the structures were found to be in a fairly good condition.

Considering related background, it was decided to replace Bridge B2461 and B2462 with similar arched structures that comply with the new road width-, geometric-, safety- and hydraulic requirements. This was believed to be a reasonable compromise between heritage concerns and modern requirements. Frequent flood events in the area motivated a precast reinforced concrete, composite, beam and slab solution. The precast beams, however, had to closely resemble the existing arch bridges which resulted in a number of design and construction related complexities.

The final deck cross section comprises twin decks, each consisting of two L-shaped and one inverted T-shaped beams per span. An opening between the decks was introduced to accommodate future services. The top slabs will be linked by means of an infill slab. A 100 mm thick concrete pavement, fully bonded to the deck top slab has been specified for all the arch bridges in view of overtopping and durability considerations.

Guide blocks between the decks, at supports will prevent transverse movement of the deck during future flood events. Buoyancy forces due to total inundation are countered by means of special sand filled chambers in the deck.

In the precast yard the arch beams were post tensioned with longitudinal temporary horizontal tie bars. The tie bars provide structural stability and serviceability limit state compliance to the beams during construction and will be removed once the cast in situ portion of the decks have been completed as well.

It was not required to amend the vertical alignment of bridge B2463, from a hydraulic point of view. The existing deck will therefore be retained, but will require strengthening and substantially widening, as indicated in the figure below.

A precast beam solution was again motivated by flood concerns. The final deck cross section will comprise unsymmetrical twin decks, with an opening between each deck to accommodate future services. The top slabs will be linked by means of an infill slab.

A special beam launching vehicle was specified at tender stage for the transport of the 54t, precast arches from the precast yards to the different bridge sites.

As the widened portion (B2463) of the deck is joined along its length to the existing deck, the new deck had to match the arch behaviour of the existing deck. The completed deck will therefore have 10 arched spans, with expansion joints at each support. Horizontal thrust forces will be transferred to the abutments.

The precast beams were therefore specially designed to receive thrust bearings between adjacent beams to transfer horizontal thrust forces along the length of the structure to the abutments. Articulation of the deck at supports will be provided by elastomeric rubber bearings. Several solutions were considered to strengthen the existing deck. The soffit curvature of the arches makes it difficult to effectively introduce an externally bonded system. Instead, an internal, post tensioning system, in combination with additional vertical stiffening webs, was considered.

5 CONCLUSION

The project provided the structural engineers with not only challenging problems, but also an opportunity to practice their art by upgrading a vital transportation link and so enhancing the lives of the people and towns to whom this road serves as a life line. The scheduled completion for the upgrading of the arch bridges is April 2013.

ACKNOWLEDGEMENTS

The South African Roads Agency SOC Ltd (SANRAL) has kindly granted permission to publish this paper. BKS (Pty) Ltd is the consulting engineer and Botes & Kennedy Manyano is acknowledged as the main contractor.

REFERENCES

BKS (Pty) Ltd. 2010. Contract NRA R027-110-2008/1F—Detailed Assessment and Design Report for the improvement of structures, including widening of 4 bridges on the R27, Sections 10 & 11. SANRAL.

Concrete Repair, Rehabilitation and Retrofitting III – Alexander et al. (eds)
© 2012 Taylor & Francis Group, London, ISBN 978-0-415-89952-9

Analysis and retrofitting design of a single-span R.C. bridge

D. Meloni, B. De Nicolo & A. Cabboi
Department of Structural Engineering, Cagliari, Italy

ABSTRACT: This paper deals with the case history of a damaged one-span prestressed concrete bridge on a crucial artery near the city of Cagliari (Sardinia), along the sea-side. After being involved in a disastrous flood, attention has arisen on the worrying safety state of the deck, submitted to an intense daily traffic load. Evident signs of this severe condition were the deterioration of the beams concrete and the corrosion, the lack of tension and even the rupture of the prestressing cables. After performing a limited in situ test campaign, consisting of sclerometer, pull out and carbonation depth tests, a first evaluation of the safety of the structure was performed. After collecting the data of dynamic and static load tests as well, a comprehensive analysis have been carried out, also by means of a properly calibrated F.E. model. Finally the retrofitting design is presented, consisting of the reparation and thickening of the concrete cover, providing flexural and shear FRP external reinforcements and an external prestressing system, capable of restoring a satisfactory bearing capacity, according to the current national codes. The intervention has been calibrated by the former F.E. model with respect to transversal effects and influence of local and overall deformation of reinforced elements.

1 PRESENT CONDITION OF THE STRUCTURE

The bridge, built between 1963 and 1964, is placed along an important highly trafficked artery, along the seaside in the west of the city of Cagliari. It consists of a unique 17.50 m long span, supported by 14 precast and prestressed concrete beams. The superposed slab is 0.20 m thick and cast in place. Transversal rigidity, apart from the slab, is ensured by three intermediate crossbeams and two head crossbeams, cast in place as well. The structural scheme is that of a simply supported deck on reinforced concrete shoulders (Fig. 1). The prestressing reinforcements scheme of the beams, according to original documents, is made of 82 straight high-strength steel braids (3×24 mm). Apart from the above information and the position of the resultant prestressing tendon, the original documents don't provide further data about the actual internal distribution of reinforcements neither about the concrete strength class. The structure is currently subjected to a daily high vehicle traffic, but recently a tragic flood undermined the foundations and caused serious damages on the shoulders, putting forward the need of an emergency repair and raising attention to the deck structural conditions, characterized by a widespread and severe material deterioration. In the following discussion only the deck of the bridge will be focused.

2 INVESTIGATION AND DIAGNOSIS

A quick in-situ investigation has been performed, consisting of visual inspections, sclerometric and pull-out tests and a carbonation penetration depth check. The investigation highlighted a widespread state of deterioration of the beams concrete and, due both to the scarcity of concrete cover (within $5 \div 15$ mm) and to carbonation, the prestressing braids, at least the outer layers, seems definitely endangered (Fig. 2), to the extent that some of them are slack or even broken. Both sclerometric and pull-out tests confirmed a concrete class higher than C32/40. On conic samples formerly extracted from the RC members by pull-out equipment, the colorimetric carbonation depth test by means of 1% solution of phenolphthalein in ethanol has been carried out, revealing a carbonation penetration far beyond the scarce concrete cover available.

The in-situ investigations, though partial, confirmed first impressions of a superficially degraded concrete, incapable of protecting prestressing braids, due to aggressive environment and thinness of concrete cover. Therefore the authors were persuaded that at least external prestressing tendons are unsafe and unreliable.

3 STRUCTURAL ANALISIS

According to the instructions of the competent authority and taking into account the high

Figure 1. View of the intrados of the deck.

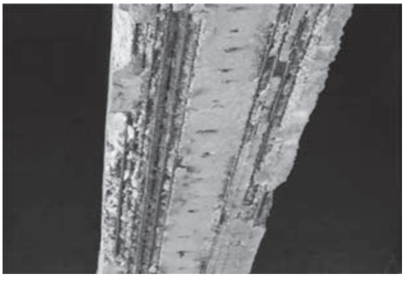

Figure 2. Intrados view of one of the beams.

intensity of daily traffic, the bearing capacity of the deck has been checked with respect to the current Italian codes NTC2008. The structural analysis has been performed both with analytical means, according to Guyon–Massonnet–Barès tables, and with an accurate F.E. model implemented in the F.E. code Straus 7. Being the RC members clearly incapable to ensure the requested safety level and in the absence of an experimental evaluation, the authors estimated the residual bearing capacity by discarding all the peripheral braids, most of whom are clearly damaged or oxidised, and in any case widely embedded in the carbonated layer of concrete, as proved by in-situ investigations. This hypothesis, leading to a loss of 50% of original prestressing, has been the basis of the retrofitting design presented in the following.

4 RETROFITTING DESIGN

The restoration design has been developed accordingly to the following principles, mostly corresponding to client requests and imposed restraints:

- presence of a residual bearing capacity;
- the intervention needs to be properly adjustable afterwards;
- only brief interruptions of vehicle traffic could be sustainable;
- the intervention is supposed to be provisional, since new projects have already been scheduled to modify the current transport circulation in the area.

Therefore the resulting design consists of:

- reconditioning of all the deteriorated RC members and providing a proper concrete cover for the reinforcements (at least 45 mm);
- shear retrofitting at the ends of the beams in terms of carbon fibres fabrics glued on both sides of the beams web, acting like external reinforcements;
- an external un-bonded prestressing system capable of restoring the needed prestressing level, consisting of a certain number of high-strength steel strands in sheaths, placed on both sides of each beams and connected by means of steel anchorages and deviators.

The proper number of strands and the needed tensioning force have been accurately calibrated by the above mentioned F.E. model (Fig. 3), capable of tackling the loss of prestressing force caused by local and overall elastic deformations and the transversal redistribution of prestressing from one element to the other. All verifications have been performed with respect to Ultimate and Serviceability Limit States, for the main load scenarios.

5 CONCLUSIONS

The presented retrofitting intervention satisfies all the design assumptions and provides the following advantages:

- possibility of intervention from the intrados of the deck without, except for short time periods, any interruption of vehicle traffic;
- easiness of execution;
- possibility of adjusting and recalibrating the intervention afterwards in order to take into account any modification of structural conditions.

This can be granted provided a checking system is implemented during execution stages and a periodical checking program is scheduled during the residual lifespan of the structure.

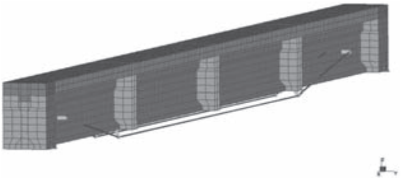

Figure 3. External prestressing applied to the F.E. model.

Concrete Repair, Rehabilitation and Retrofitting III – Alexander et al. (eds)
© 2012 Taylor & Francis Group, London, ISBN 978-0-415-89952-9

Verification of bridge repair assisted by numerical simulation

V. Cervenka & J. Cervenka
Cervenka Consulting Ltd., Prague, Czech Republic

ABSTRACT: Computer simulation is an efficient tool for assessment of strengthening provisions in case of repair and rehabilitation of existing concrete structures. It is based on a non-linear finite element analysis and corresponding safety formats. Special numerical models can capture strengthening elements used to improve the bearing capacity, such as steel or carbon fiber reinforcement and special coating layers. This approach is illustrated on the case of existing railway bridge, which was thoroughly investigated in situ as well as by numerical simulations. Assessment of design resistance in accordance with present safety formats can be based on numerical simulation, while the safety check can be enhanced by exploiting a probabilistic approach.

SUMMARY

Numerical simulation of existing railway bridge, which was strengthened after 50 years of service is demonstrated. The investigation was a part of the European project Sustainable Bridges where a bridge in Örnsköldsvik in northern Sweden was tested to demonstrate the new assessment methods developed during the project (Elfgren et al. 2006, Figure 1). The bridge was planned to be demolished in 2006 and it was possible to utilize it for an investigation of its remaining ultimate load carrying capacity after a service period of 50 years and strengthening.

The project included an investigation of a strengthening by the method based on "Near Surface Mounted Reinforcement".

Numerical simulation was performed with the finite element package ATENA (2006) specialized for simulation of real structural behavior. Several numerical models were developed for the simulation of bridge behavior based on a 2D plane stress simplification as well as on a full 3D representation. It was possible to explore the simulation results obtained before the loading test—a prediction, and after the test—a best fit to known behavior.

The 2D model, is composed of four-node isoparametric quadrilateral elements for concrete and truss bar elements for reinforcement. The load was applied in the middle of the left span in the field experiment.

The results of the simulations are summarized in the form of lod-displacement diagrams in Figure 3, where the mid-span force on the vertical axis and mid-span deflection on the horizontal axis are plotted for various case. (Label meaning: (Original—based on available properties and data

Figure 1. Rayilway bridge at Örnsköldsvik before testing.

Figure 2. 2D model of the bridge.

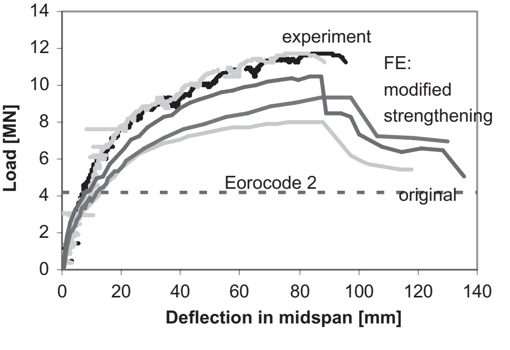

Figure 3. Load-displacement diagrams resulting from 2D simulations.

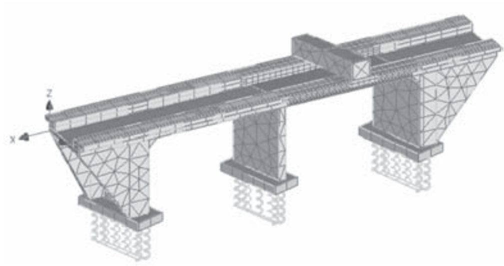

Figure 4. 3D numerical model of the bridge.

prior testing; Strengthening—CFR bars applied; Modified—including the shear reinforcement detected by inspection). The agreement between calculated and observed failure modes (diagonal crack with compression strut) was very good.

Furthermore, a numerical model based on 3D representation was exploited in order to explore how realistic a numerical simulation can be. It reflected real geometry, reinforcement and strengthening by carbon fiber bars with relevant material properties, Figure 4.

In addition to the simulation of real behavior and assessment of remaining bearing capacity a reliability of the bridge was also investigated within the scope of new safety formats introduced in the *fib* Model Code 2010 (MC 2010). The assessment of design resistance for following safety formats was performed (More about safety formats see also in Cervenka 2008):

1. Full probabilistic analysis with the program system SARA.
2. Partial safety factor method (PSF).
3. Global safety format according to Eurocode EN1992-2-Bridges with global safety factor of resistance is defined by $\gamma_R = 1.27$.
4. Safety format based on estimate of coefficient of variation of resistance (ECOV), see Cervenka (2008).

CONCLUSIONS

The presented study has demonstrated the capability of numerical simulation based on nonlinear finite element analysis for assessment of structural capacity of existing structures. Strengthening and assessment of resistance in case of repair can be efficiently modeled by numerical simulation.

Simplified models based on 2D representation and limited knowledge of material properties and boundary conditions leads to conservative but safe estimates of resistance.

Improved assessment of resistance can be achieved by enhanced 3D models, reflecting real geometry, boundary conditions and measured material properties.

Model validation by in-situ testing can be used to calibrate the numerical model and significantly improve the quality of simulation. It is clear that a model validation by testing to failure used in the present case is only exceptionally available. However, a calibration based on similar structures can well serve to this purpose.

It was shown, that numerical simulation can be used as an efficient tool for verification of design of repair provisions in existing structures in accordance with available safety formats.

ACKNOWLEDGEMENT

The presented research originated in part from the project supported by the Czech Grant Agency P105/12/2051, “Model uncertainties in resistance assessment of concrete structures”. The investigation of railway bridge was done in cooperatin with Lulea University of Technology in Sweden supervised by Lennart Elfgren within the Europen project “Sustainable Bridges” headed by SKANSKA. Autors express their sincere thanks to all partners, whose financial and personal contributions made this research possible.

REFERENCES

ATENA 2006. Program Documentation, Cervenka Consulting, www.cervenka.cz

Cervenka V. 1998. Simulation of shear failure modes of R/C structures. In: Computational Modeling of Concrete Structures (Euro-C 98), eds. R. de Borst, N. Bicanic, H. Mang, G. Meschke, A.A.Balkema, Rotterdam, The Netherlands, 1998, 833–838.

Cervenka V. 2002. Computer simulation of failure of concrete structures for practice. 1st fib Congress 2002 Concrete Structures in 21 Century, Osaka, Japan, Keynote lecture in Session 13, 289–304.

Cervenka, J., Cervenka, V. & Janda, Z. 2007. Safety assessment of railway bridges by non-linear analysis, Proc. conf. Sustainable bridges, Wroclow, ISBN 978-83-7125-161-0

Cervenka V. 2008. Global Safety Format for Nonlinear Calculation of Reinforced Concrete. Beton—und Stahlbetonbau 103 (2008), Special Edition, Ernst & Sohn: 37–42.

Elfgren, L 2006. D7.3 Field Test of a Concrete Bridge in Örnsköldsvik, Sweden, Sustainable Bridges Project Report. Lulea University of Technology.

Model Code 2010. First complete draft. Volume 1—fib bulletin 55. Volume 2—fib bulletin 56. ISSN 1562–3610. ISBN 978-2-88394-095-6. International Federation for Structural Concrete (fib), Lausanne, Switzerland. 2010.

Concrete Repair, Rehabilitation and Retrofitting III – Alexander et al. (eds)
© 2012 Taylor & Francis Group, London, ISBN 978-0-415-89952-9

Repairing preloaded square columns by ferrocement jackets made of non-structural WWMs

S.M. Mourad & M.J. Shannag
King Saud University, Riyadh, Kingdom of Saudi Arabia

ABSTRACT: In some situations, Welded Wire Meshes (WWMs) that conform to ACI standards may not be available in the market, consequently, that can result in using other WWMs that are intended for non-structural purposes with less yield strength as compared to that specified by ACI standards. This research investigates the performance of ferrocement laminates made of high strength mortar and non-structural WWMs in strengthening and repairing square reinforced concrete column specimens. The ferrocement laminates were applied on unloaded and preloaded columns with 60%, 80% and 100% of its axial capacity. The overall response of the tested specimens under axial compression was investigated in terms of load carrying capacity, axial stress and strain, lateral displacement, and ductility. Test results indicated that ferrocement jackets made of 2 layers of WWMs have a promising performance. The test results also indicated that repairing similar reinforced concrete columns, after preloading them to failure, with the same ferrocement jacket almost restored their original load capacity and stiffness.

1 INTRODUCTION

Most of the rehabilitation works consist of repairing old deteriorating structures, and structures damaged by earthquakes and natural disasters. Hence the development of cost-effective and long-lasting repair/retrofit methods can greatly reduce maintenance requirements, increase life safety and increase the service life of concrete structures.

Using ferrocement laminates in repairing and strengthening reinforced concrete columns has been proven to be efficient in providing additional strength and ductility. In addition such technique has a major advantage among others, that it is being considered as a low cost repair technique. However, in some situations, WWMs that conform to ACI Committee 549 standards (2000) may not be available in the market, consequently, that can result in using other WWMs that are intended to be used in non-structural purposes. Those types of meshes are made from galvanized steel, used in fencing and other purposes, are commercially available in hardware shops with low prices. Utilizing such ordinary WWM in ferrocement jacket structural applications need more investigation.

The main objectives of this research are to investigate the effectiveness of applying ferrocement jackets containing ordinary locally available welded wire meshes (WWM) encapsulated in high strength mortar when subjected on one-third-scale reinforced concrete square columns; and to study the behavior of damaged and preloaded columns after repairing them with such jackets, in terms of strength gain, ductility and failure modes.

2 EXPERIMENTAL PROGRAM

The experimental program consists of testing one-third scale square (150 × 150 mm) column specimens with a height of 1000 mm in three phases as follows; Phase 1: Control column specimens without any preloading and without ferrocement jackets, Phase 2: Jacketed column specimens without any preloading but with ferrocement jackets, and Phase 3: Strengthened preloaded column specimens include columns strengthened with ferrocement jackets after preloading them with 60%, 80% and 100% of their ultimate axial strength. The number and details of the square reinforced concrete column specimens are given in Table 1.

3 DISCUSSION OF TEST RESULTS

The axial and lateral strains of the column were obtained from the measured axial and lateral displacements that were obtained from the average readings of the LVDTs. Similar behavior was observed in similar specimens, therefore only the results of one specimen are demonstrated in the graphs for clarifying purposes. The axial load-axial and lateral displacements relationships as well as

Table 1. Details of tested column specimens.

	Designation	Preload (%)	Ferrocement jacket
Phase 1	SC-1 SC-2	0	None
Phase 2	SJ-0-1 SJ-0-2	0	2 layers of welded
Phase 3	SJ-60-1 SJ-60-2 SJ-80-1 SJ-80-2 SJ-100-1 SJ-100-2	60 60 80 80 100 100	wire mesh encapsulated in high strength mortar

SC: Control specimens; SJ-XX: Jacketed specimens after preloading by XX% of ultimate load

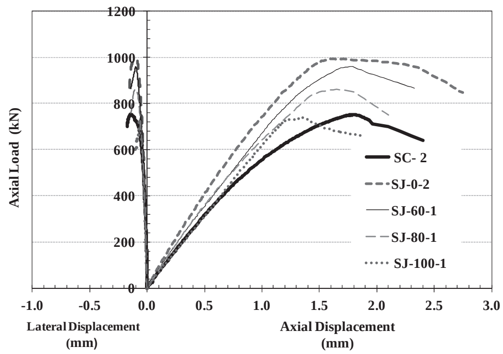

Figure 1. Load–displacement relationships for tested specimens.

Table 2. Test results of control, jacketed and preloaded jacketed columns.

Specimen designation	Ultimate load (kN)	%*	Ultimate axial stress in concrete (MPa)	%*	Initial axial stiffness (MPa)	%*
SC-2	750	–	29	–	26,870	–
SJ-0-2	994	133%	39	135%	33,760	126%
SJ-60-1	960	128%	37	128%	28,816	107%
SJ-80-1	860	115%	35	121%	26,880	100.4%
SJ-100-1	740	98.7%	31	107%	25,840	96.2%

*value relative to that of the control columns

the axial concrete stress-axial and lateral strains relationships were obtained for each tested specimen. Figure 1 shows the axial load-axial and lateral displacements relationships for one specimen of control columns (SC-2), jacketed columns (SJ-0-2) and strengthened preloaded columns (SJ-60-1 and SJ-80-1) as well as the strengthened failed column (SJ-100-1).

Results of tested specimens are summarized in Table 2.

Results indicated that repairing tied reinforced concrete columns that were preloaded up to 60% and 80% of their ultimate load carrying capacity, caused 28% and 15% increase in load carrying capacity. Insignificant increase in axial stiffness was observed for preloaded specimens. The test results have also shown that repairing severely damaged (failed) columns using the same ferrocement jacket restored almost the original load carrying capacity and stiffness of control columns prior to failure, with a significant loss in ductility that can be overcome by using meshes with better mechanical properties matching those present in the ACI committee 549 (2000).

4 CONCLUSIONS

As indicated from test results, using ferrocement jackets made of WWMs having yield strength of about 80% of that specified by ACI committee 549, 2000, has a promising effect in enhancing the load carrying capacity of square columns. Test results indicated that strengthening unloaded reinforced concrete columns of 150 × 150 mm square cross section and a height of 1000 mm, with ferrocement jackets containing 2 layers of non-structural WWM encapsulated in high strength mortar showed about 33% and 26% increase in axial load carrying capacity and stiffness respectively, as compared to control columns. Also, test results indicated that repairing similar reinforced concrete columns of square cross section preloaded up to 60% and 80% of their ultimate load carrying capacity, with the same jackets showed about 28% and 15% increase in axial load carrying capacity as compared to control columns. In addition, test results indicated that repairing similar reinforced concrete columns of square cross section preloaded up to failure with the same jacket restored almost the original load carrying capacity and stiffness of control columns.

Concrete Repair, Rehabilitation and Retrofitting III – Alexander et al. (eds)
© 2012 Taylor & Francis Group, London, ISBN 978-0-415-89952-9

Experimental results of RC columns strengthened with Fibre Reinforced Cementitious Mortars

P. Colajanni, F. De Domenico, N. Maugeri, A. Recupero, & N. Spinella
Department of Civil Engineering, University of Messina; Italy

G. Mantegazza
Ruredil S.P.A., S. Donato Milanese (Milano), Italy

ABSTRACT: The structural behaviour of reinforced concrete columns strengthened with a system made by fibre nets embedded into an inorganic stabilized cementitious matrix was investigated. Specimens with circular and square cross section were cast and subjected to monotonic uniaxial compression to investigate the efficiency of Polypara-phenylene-benzo-bisthiazole (PBO) Fibre Reinforced Cementitious Mortars (FRCM) system in increasing both carrying capacity and ductility. The experimental results show that the confinement by PBO fibre produced a noticeable increment in strength and ductility, even if low mechanical ratios of fibre herein considered were not always able to ensure an hardening behaviour up to rupture.

1 INTRODUCTION

Wrapping with advanced materials is an appealing strategy to increase strength and deformation capacity of concrete members.

New fibre-reinforced composite material has been developed in which epoxy resin is replaced by stabilized inorganic material (cement mortar) binding carbon fibres with the concrete or masonry substrate.

Recently the use of a synthetic polymeric fibre, namely Polyparaphenylene BenzobisOxazole (PBO), has been suggested, capable of establishing chemical bonds with hydrated compounds in a special inorganic binder by means of a hydraulic reaction. The formation of these chemical (interphase) bonds helps to obtain high mechanical properties of the composite. An experimental research has been started at the Department of Civil Engineering of Messina University aiming at investigating the effectiveness of the use of PBO-FRCM for wrapping low strength concrete elements.

2 EXPERIMENTAL PROGRAM

The experimental program was carried out in two phases. In the first one, namely series A, 8 cylindrical specimens with diameter D = 154 mm and height h = 335 mm were cast; in the second one, namely series B, seven cylindrical specimens with diameter D = 200 mm and seven specimens with square cross-section having side a = 200 mm, all of them with height h = 425 mm. Corners of square specimens were rounded with a curvature radius of 20 mm. All specimens were axially unreinforced because the jacketing reinforcement interaction was outside the scope of the present study.

2.1 *Concrete*

Concrete designed to have a cylindrical compressive strength of 25 MPa were prepared by using Portland cement (ASTM International Type I The cement:sand:gravel proportions in the concrete mixture were roughly 1:2.61:2.15 by weight, and the maximum size of the coarse aggregate was 16 mm. The water cement ratio (w/c) was set to 0.57., resulting in a fluid consistency (S4) and a good workability.

2.2 *Fibre*

A synthetic polymeric textile, made up of Polyparaphenylene BenzobisOxazole (PBO) fibre has been used (Fig.1), capable of establishing chemical bonds with hydrated compounds in a special inorganic binder by means of a hydraulic reaction. The formation of these chemical (interphase) bonds between fibre (dispersed phase) and matrix (continuous phase) helps determine the mechanical properties of the FRCM.

3 EXPERIMENTAL RESULTS

3.1 *Circular specimens*

The axial stress-strain curve for the cylindrical specimens of series A, unconfined and confined with two

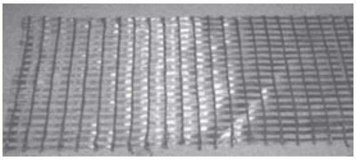

Figure 1. PBO fibre textile.

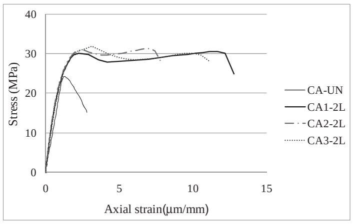

Figure 2. Axial stress-strain curve (CA series - 2 layer).

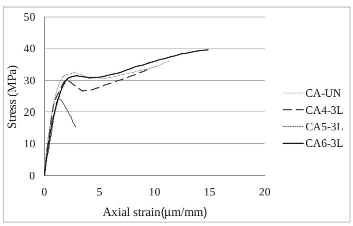

Figure 3. Axial stress—strain curve (CA series – 3 layers.

and three layers of textile are shown in Fig. 2 and 3 respectively. The curves show that in both cases noticeable increments in specimen strength and ductility are achieved by the FRCM. However, when the confinement volumetric ratio ρ is limited to $\rho = 0.236\%$, (2 layers) the stress-strain curve exhibit a flatten post-peak branch at a strength value that is roughly 23% greater than that for the unreinforced specimens; by contrast three layer of textile ($\rho = 0.354\%$) ensure a strain hardening behaviour up to the failure, with a mean value of the maximum strength that is 51% greater than the unreinforced concrete strength. The increments in ultimate strain are noticeable for both the analysed amounts of confinement volumetric ratio, with average ratios of the ultimate strain for confined and unconfined specimens ranging from 3.57 to 3.90.

In the second series (B) cylindrical specimens, had a greater diameter (D = 200 mm, h = 420 mm); thus ρ was decreased to 75% of the values considered for series A. The textile overlapping length has been increased to 250 mm. The figures show that the amount of fibre was not able to ensure a post-peak hardening behaviour, and the increment in the specimen strengths were 19% and 33% for 2 and 3 textile layers respectively. Despite the reduction of confinement volumetric ratio with respect series A; in both cases of use of 2 and 3 textile layers, the increment in the ultimate strain was larger, and a fibre efficiency factor $k_e = 0.81$ was reached

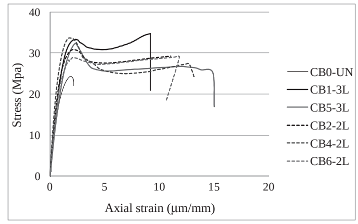

Figure 4. Axial stress—strain curve (CB series).

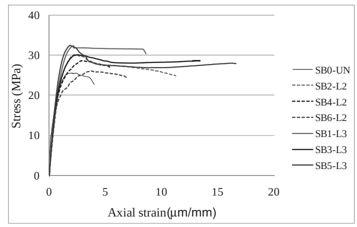

Figure 5. Axial stress—strain (SB series).

3.2 *Square specimens: series B*

The square specimens were characterized by the lowest confinement volumetric ratio ρ, namely $\rho = 0.175$ and $\rho = 0.263$ for specimens with two and three layers of textile respectively. Therefore an hardening behaviour in the post-peak branch was not expected. The axial stress-strain curve depicted in Fig. 12 shows that the textile was able to ensure a ductile behaviour for all the specimens. that the strength increments were roughly 20% smaller than the corresponding ones for cylindrical specimen; worthy of note was the ultimate deformation increment with two layers of textile was 60% of the value obtained for cylindrical specimens, but almost the same when specimens with three layers of textile were considered; in these cases a mean value of the ultimate strain $\varepsilon_{ccu} = 12.66‰$ was obtained.

All specimens showed the same collapse mode due to telescopic jacket textile failure (Banholzer *et al., 2006)* after the formation of wide vertical cracks in the textile overlapping region.

ACKNOWLEDGEMENTS

This study was sponsored by RUREDIL SpA, Italy.

Concrete Repair, Rehabilitation and Retrofitting III – Alexander et al. (eds)
© 2012 Taylor & Francis Group, London, ISBN 978-0-415-89952-9

The enhancement of performance on road tunnel lining by epoxy injection and carbon fiber reinforcement

JinHo, Choo, HongKyun, Kim, TeaJong, Lee, SungWoo, Park, TeaGook & Yoon
Department of Inspection Division, KISTEC, South Korea

ABSTRACT: Two road tunnels have been inspected to provide a precise diagnosis for condition and safety by KISTEC. The typical defects of the road tunnel were cracking, leakage, spalling, corrosion, carbonation, and collapse. Among the investigated defects, cracks were mainly analyzed for shape, location and direction: longitudinal cracks, transverse cracks, inclined cracks, and round shaped cracks. Two types of cracks in tunnels with duct slabs were analyzed with numerical analysis and countermeasures were determined by field investigation and NDT. One type of crack was longitudinal cracks caused by structural reasons, the other was a network of fine cracks beneath the duct slab which was suspected to have been caused by shrinkage, difference of temperature for curing, and connection of rebar between lining and duct slab. The longitudinal cracks were repaired by epoxy injection and carbon fiber reinforcement. The quality of injection within the cracks was proved by coring with Φ43 mm core samples and the strength of attached reinforcement was verified with pull-off tests. The analyzed tension zone was rehabilitated and its stability evaluated. Also, guidelines for maintenance were suggested for the repaired and rehabilitated area.

1 TUNNEL DESCRIPTION

HGM (L = 1,892 m, 3 lane) tunnel and JR (L = 1,650 m, 3 lane) tunnels had been constructed from December 1991 to April 1999 by two different companies with NATM used to pilot tunnelling in advance by TBM (D = 6.5 m). The duct slab of these tunnels was installed for ventilation as a semi-transverse system. To deal with toxic gas and vehicle emission, a 0.6 × 0.6 m port was designed within the duct slab. The estimated traffic at the design stage was 3,500/hour for each tunnel. In this paper, the method of repair and rehabilitation is mainly described for cracks in road tunnels in current service.

1.1 *Cracks*

The most common defect found was a round-shape crack at the crown and a triangular-shape crack at the bottom adjacent to construction joints in the NATM. Regardless of the duct slab, the longitudinal crack at the crown was the most typical. Transverse and inclined cracks at the lining were also investigated. The longitudinal cracks in the lining within 1.2 m above the duct slab and a network of fine cracks beneath the duct slab were focused on in this paper. Firstly, the longitudinal crack was verified with more than 30 numerical analyses conducted by 3 different companies' experts. Each case modeling classified the boundary condition, the location of elastic link, and the state of rebar connection. It was analyzed that the presumably expected reason for the tension crack was the state of rebar connection. The investigated tension zone was mostly identical in both HJM and JR tunnels. Secondly, The networks of fine cracks beneath duct slab could be caused by the self-weight and thermal shrinkage at the curing stage. Also, It was verified that the hydration and shrinkage of the concrete were greater than the free-end boundary condition by the numerical analysis.

1.2 *Additional inspections*

An automatic measuring system was adopted to monitor the progress of the structural cracks at the duct slab for 6 months. 10 points were chosen by the width and length of cracks. Two sections of convergence measurement were also monitored. GPR was conducted on the lining to find any anomalies below the lining and the interval of embedded rebar of lining. With more 3 lines survey of whole tunnel length, the thickness of lining, type of lining construction, and the embedded steel support have been analyzed. As the fundamental items for diagnosis of the tunnel condition, the strength of the lining, the possibility of corrosion, and the material of the lining by laboratory tests were conducted. To assess the repair state of the previous crack injections check coring was conducted for each tunnel.

2 REPAIR AND REHABILITATION

2.1 *Longitudinal crack on lining above duct slab*

It was found that tension cracks were rarely detected because of the reinforcement with rebar especially under a shallow ground surface and residential area. With that reinforcement (2 array D22@100), it could resist the tension caused by the fixed installation of the duct slab. Except for those areas, the longitudinal cracks were checked with the previous repair state and the newly required countermeasures were estimated. The state of repair with injection was checked by hand coring for 38 cracks at the HJM tunnel and 22 cracks at the JR tunnel. To estimate crack condition, the ultrasonic technique forer crack depth and check-coring(Φ43 mm bit mounted Hilti TE76) were implemented. It was found that the depth of cracks was approximately more than 200 mm, so epoxy injection with lower pressure was used which was normally sustained 2 days to infiltrate epoxy into the void.

The quality of injection by stricter repair codes was maintained such as narrow spacing of inlet, check-coring per every 20 ~ 30 cracks, and ensuring the putty surface leveling. After completion of the epoxy injection, the plastered putty was removed by grinding as well as in the tension zone on the lining.

Among the several rehabilitation methods, carbon fiber reinforced plastics were chosen since the tension zone had a round shape surface, utilities cables nearby, and inconvenient access to work. The reinforced fiber was impregnated 4 times on lining with hardening agent. The pull-off adhesion test with DYNA Z16 according to ASTM D4541 (ISO 4624) was conducted. There were 8 tests with random selection, so it was concluded that the adhesive strength of the reinforced plaster ranged from 3.9 to 11.2 MPa which was good enough for the criterion of 1.5 MPa. Special care was needed for the rehabilitated zone which was susceptible to delamination because of losing the adhesion and mal-installation in future.

2.2 *Networks of fine crack beneath duct slab*

From the analysis, we decided that the cracking beneath the duct slab had occurred due to non-structural reasons such as fixed boundary conditions and shrinkage, and temperature during curing at the construction stage. With regard to traffic combustion, defects caused by carbonation such as corrosion, spalling, and deterioration can be rapidly developed. In particular, the carbonation within crack zones can even more drastically damage the reinforced concrete. The goal of repair for the fine cracks focused on sustaining the durability. Cracks larger than 0.3 mm in width were injected by epoxy pressured with rubber band, and then the hair crack zone (approximately 6 m wide beneath the duct slab) was rendered three times with cement paste by painter roller. In addition, approximately 28 cracks were checked for the warranty of injection by hand coring. More care was needed for the repair of the portal area due to deterioration by atmosphere and concentration of combustion products (exhaust fumes etc).

3 CONCLUSION

Two operational road tunnels have been inspected for safety and diagnosis by KISTEC. The cracking and leakage were mainly analyzed to provide information for a suitable repair and rehabilitation regime. The longitudinal cracks in the lining above the duct slab and fine cracks beneath the duct slab have been mainly described in this paper. The method of repair and rehabilitation was chosen considering the depth of cracks and carbonation as well as field circumstances.

The longitudinal cracks caused by structural reasons were repaired with epoxy injection and rehabilitated with carbon fiber reinforcement. The fine cracks in the soffit of the duct slab which may cause possible damage to the reinforced concrete were repaired with injection and render.

To ensure the quality, check coring and pull-off adhesion tests were conducted as well as the process of repair and rehabilitation in quality control. Furthermore, the guideline of maintenance was suggested for annual and periodical inspection by the owner or specialized management company.

Concrete Repair, Rehabilitation and Retrofitting III – Alexander et al. (eds)
© 2012 Taylor & Francis Group, London, ISBN 978-0-415-89952-9

Strengthening of R/C Beams using Ultra High Performance Concrete

E. Fehling & M. Alkhoury
Institute of Structural Engineering, Faculty of Civil and Environmental Engineering, University Kassel, Germany

ABSTRACT: For strengthening and repair of existing structures different techniques, such as addition of steel sections, gluing of CFRP sheets or strips are customary. Also the use of additional reinforcement in conjunction with sprayed concrete is possible. As an alternative to these conventional methods, the use of thin layers of Ultra High Performance Fiber Reinforced Concrete (UHPFRC) has been studied experimentally. Results of an experimental study comprising bond tests as well as beam tests on ordinary R/C beams strengthened by thin layers of UHPFRC will be presented.

1 INTRODUCTION

1.1 *Standard methods for strengthening of reinforced concrete structures*

For strengthening and repair of Reinforced Concrete Structures different methods are common, such as

- additional steel profiles,
- casting or spraying of additional layers of concrete with bar reinforcement,
- gluing of GFRP or CFRP sheets or strips.

While the use of additional steel profiles in many cases requires additional cover both for architectural reasons as well as for fire protection, additional layers of conventional concrete often make a substantial increase of cross sectional dimensions necessary. The use of GFRP or CFRP strips requires special attention to the aspect of end anchorage. Moreover, skew cracks can cause problems with regard to the brittle behavior of high strength glass or carbon fiber laminates. In order to overcome such difficulties, UHPFRC can be an interesting alternative.

2 EXPERIMENTAL PROGRAMME

2.1 *Test program*

The experimental investigations comprise preliminary tests for flowability of UHPFRC in narrow formwork ducts, the bond behavior of UHFRPC at the interface to normal strength concrete interfaces as well as two series of T-beam tests with failure in bending or shear. Figure 1 shows typical cross sections of the bending beam specimens with and without strengthening UHPFRC layer. The thickness of this layer was typically 40 mm. While the concrete strength of the conventional concrete amounted to approximately $f_c = 20$ MPa while the UHPFRC layer showed a cylinder strength of about 177 MPa.

In order to study strengthening in shear, a second series of beam tests has been conducted. Here the strengthening layer reached over the full beam depth. In order to be able to anchor the shear reinforcement, bore holes (diameter 40 mm) have been drilled into the upper flange. Beam 5 served as a reference beam without strengthening but also failing in shear.

The cross sections and the reinforcement of the test specimens for strengthening in shear can be seen from Fig. 2 and 3.

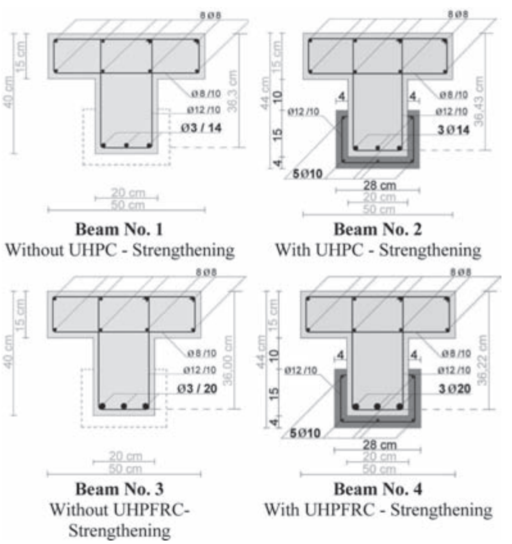

Figure 1. Typical cross sections for beam tests in bending.

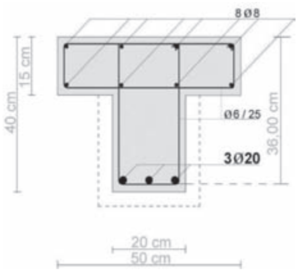

Figure 2. Cross sections for Beam no. 5.

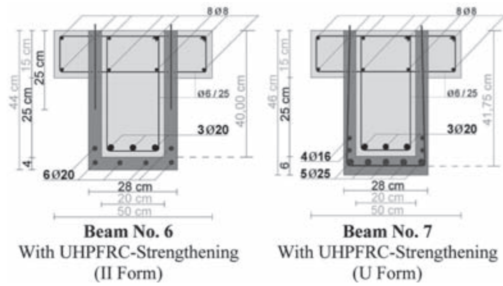

Figure 3. Cross sections for Beams 6 and 7.

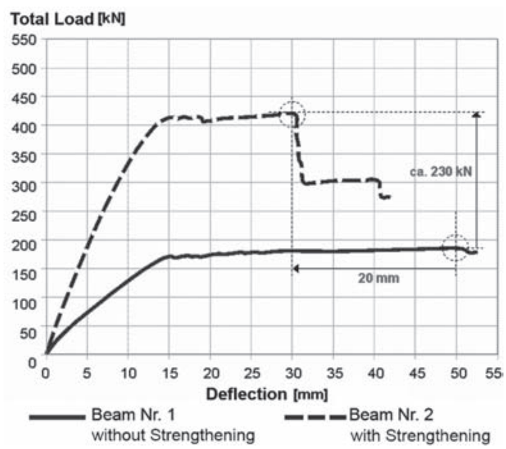

Figure 4. Force-deflection graphs for Beams 1 and 2.

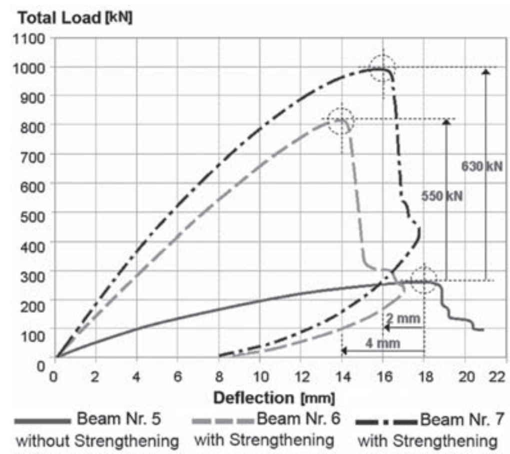

Figure 5. Force-deflection graphs for Beams 5 to 7.

2.2 *Test results*

A typical force deflection diagram of the tests with bending failure is presented in Fig. 4. It becomes evident, that a significant increase of bending resistance was possible, not only by the supplied additional rebars but also by the capacity of the UHPFRC due to the fibers.

The results of the beams tested to investigate strengthening in shear show that a very effective increase of shear capacity can be attained. In order to explain the observed increase, not only the additional web reinforcement in the UHPFRC shell has to be taken into account but also the load carrying capacity of UHPFRC in tension.

The full length paper discusses the results in more detail with regard to load carrying and deformation capacity and gives more insight into the governing mechanisms. A full documentation is contained in the dissertation by Alkhoury 2012. Further information with regard to the topic can be found in the references below.

In order to fully understand the behavior of the beams strengthened in shear, a nonlinear finite element analysis is in preparation.

3 CONCLUSIONS

The experimental study has demonstrated the general applicability of thin UHPC layers for strengthening of R/C beams both in bending and shear. It will be supplemented by further numerical studies.

REFERENCES

Alkhoury, M. 2012. Untersuchung der Verstaerkung bestehender Stahlbetonkonstruktionen unter Nutzung Ultrahochfesten Betons (UHPC) im Vergleich mit herkoemmlichen Verstaerkungsmassnahmen. *Dissertation.* University of Kassel, submitted to the faculty.

Fehling, E. & Stuerwald, S. 2011. Flexural Behavior of UHPC with Fibers and Rebars. *Concrete engineering for excellence and efficiency, fib Symposium PRAGUE 2011*, *June 2011*, 1: 535–538.

Fehling, E. & Thiemicke, J. 2011. Shear Bearing Behavior of Ultra High Performance Concrete (UHPC). *Concrete engineering for excellence and efficiency, fib Symposium PRAGUE 2011*, *June 2011,* 2: 975–978.

Concrete Repair, Rehabilitation and Retrofitting III – Alexander et al. (eds)
© 2012 Taylor & Francis Group, London, ISBN 978-0-415-89952-9

Experimental investigation on the effectiveness of patch repair on the flexural behavior of corroded post-tensioned beams

M. Shekarchi, F. Ghasmzadeh, S. Sajedi & S.A. Razavizadeh
Construction Materials Institute (CMI), School of Civil Engineering, University of Tahran, Tehran, Iran

M.J. Mohebbi
R&D of Persian Gulf Mining and Metal Industries Special Zones (P.G.S.E.Z), Iran

ABSTRACT: Corrosion of steel rebar is the most common source of degradation in reinforced concrete structures of marine environments. The effect of plain reinforcement corrosion on the flexural response of Post-Tensioned (PT) concrete structures is, however, not fully assessed yet. This paper presents the results of an experimental study involving the flexural behavior of sound, deteriorated and repaired PT beams under monotonic loading. The effect of concrete removal from the beam due to the corrosion of reinforcing bars and the efficiency of high performance patch repair for restoring the load-bearing capacity of deteriorated beam have been investigated. It was found that repairing with high performance concrete can enhance the structural performance of deteriorated PT beams with non-corroded tendons.

1 INTRODUCTION

The advantages of prestressed design strategy have allowed the construction of economically competitive bridges with significantly longer spans and greater load-carrying capacity. The increase in bearing capacity, however, has not been accompanied by a corresponding increase in durability especially in harsh environmental conditions.

Deterioration of PT structures in the south of Iran, in the severe environment of the Persian Gulf region, has also been noticeably observed in recent years which results in reduced service life of such structures and higher life cycle costs (Shekarchi et al. 2009, Parhizkar et al. 2006). Fortunately, the most prevalent form of deterioration in PT structures of this region is the spalling of concrete cover due to the corrosion of deformed bars.

2 EXPERIMENTAL PROGRAM

Flexural behavior of deteriorated and repaired PT beams are investigated and compared with the control beam. Table 1 shows a list of tested specimens.

2.1 *Specimens preparation and materials*

Geometry of the PT beams and reinforcement layout are shown in Figure 1.

The cementitious materials used in this study for repair concrete and substrate were Portland cement (PC) equivalent to ASTM Type I, slag blended cement and silica fume (SF).

2.2 *Testing procedures*

2.2.1 *Mechanical tests*

Samples for mechanical testing were prepared in accordance with ASTM C192 and then were evaluated through a set of well-known experimental procedures.

2.2.2 *Accelerated corrosion process*

An electrolyte corrosion technique was used to accelerate the deformed steel corrosion. The specified portion of beams F2 and F3 were submerged

Table 1. List of PT specimens.

Beam ID	Category
F1	Un-corroded
F2	Corroded, deteriorated and cleaned
F3	Corroded, deteriorated and cleaned, repaired

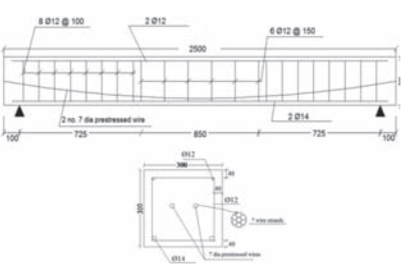

Figure 1. Geometry of the PT beams and reinforcement layout (mm).

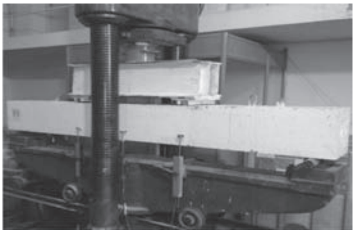

Figure 2. Flexural PT beam test setup.

in the 5% NaCl solution as the electrolyte in a plastic tank. Power supplies with adjustable voltage and direct current of 600 mA were chosen for the electrolyte corrosion process. The corrosion was limited to the central zone with length, width and height of 85 cm, 30 cm and 7.5 cm, respectively.

2.2.3 *Patching repair process*

Damaged concrete was removed to a depth of approximately 8–10 cm from 85–90 cm mid section of the F2 and F3 beams. The reinforcement was then cleaned using a water jet in order to remove surface micro-cracks and dust. Finally one of the beams (F3) was repaired with patch repair method.

2.3 *Loading test setup*

Load was applied in increments by a hydraulic jack and measured with a load cell as shown in Figure 2.

3 RESULTS AND DISCUSSIONS

3.1 *Mechanical properties*

Table 2 shows the mechanical properties of repair concrete and substrate.

3.2 *Degree of corrosion*

Table 3 shows the exact degree of corrosion in the deformed rebars of F2 and F3 beams.

3.3 *Flexural behavior of investigated beams*

Figure 3 shows the comparison of the load-deflection responses of PT beams.

Table 2. Mechanical properties of repair concrete and substrate.

	Substrate	Repair
Compressive strength (MPa)	60	64
Flexural strength (MPa)	2.95	3.70
Tensile strength (MPa)	4.40	5.30
Modulus of elasticity (GPa)	37	35
Tensile bond strength (MPa)	5.2	
Shear bond strength (MPa)	2.97	

Table 3. Degree of corrosion in PT beams.

Type of rebar	Beam F2	Beam F3
Longitudinal	14%	16.1%
Shear	14.9%	15.5%

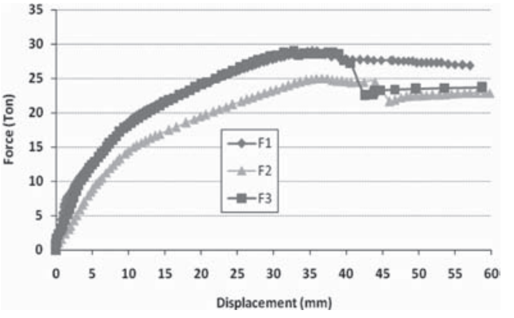

Figure 3. Corroded reinforcement.

As seen in Figure 3, steel corrosion and removal of concrete from beam F2 have lead to reduction of flexural stiffness and the yielding load of deformed bars and prestressed tendons. After applying patch repair material to the deteriorated areas, it was found that the load-carrying capacity and flexural rigidity of deteriorated beam can be restored.

4 CONCLUSIONS

1. After conducting the accelerated corrosion test on the PT beams F2 and F3 for the period of 75 days, 15.4% and 15.75% average degree of corrosion were obtained for longitudinal and transverse reinforcement of such beams, respectively.
2. The load-carrying capacity and stiffness of the PT beam was decreased significantly for the specimen with corroded exposed reinforcement. It was found that by applying patch repair in the deteriorated areas without replacing the corroded rebars, the load carrying capacity and flexural behavior of the beam can be restored.
3. The main cause of reduction in the flexural rigidity and load-bearing capacity of beam F2 was the removal of concrete from corroded PT beam.

REFERENCES

Parhizkar, T., Ramezanianpour, A.A., Hillemeier, B., Rais Ghasemi A.M. & Mozafari N. (2006). Compatibility of Repair Concrete in the Aggressive Environmemt of the South of Iran. *Arab J for Sci and Eng*, 31(1C).

Shekarchi, M., Moradi-Marani F. & Pargar F. (2009). Corrosion Damage of a Reinforced Concrete Jetty Structure in the Persian Gulf: A Case Study. *Struct Infrastruct Eng*, 7(9): 701–713.

Concrete Repair, Rehabilitation and Retrofitting III – Alexander et al. (eds)
 ISBN 978-0-415-89952-9

Numerical investigation on the effectiveness of patch repair on the flexural behavior of corroded post-tensioned beams

M. Shekarchi, S. Sajedi, F. Ghasemzadeh, S.A. Razavizadeh & A. Manafpour
Construction Materials Institute (CMI), School of Civil Engineering, University of Tahran, Tehran, Iran

ABSTRACT: This paper presents an assessment of the flexural behaviour of sound, deteriorated and repaired Post-Tensioned (PT) beams of companion paper (Shekarchi et al. 2012) by three-dimensional non-linear Finite Element (FE) analysis. The effects of stress relaxation of strands, exposing of the corroded reinforcement, and interface characteristics between repair concrete and substrate have been considered in the FE models. By comparing the model predictions and the experimental results, it was found that the model is capable of sufficiently good prediction of the structural response of investigated PT beams with bonded tendons.

1 INTRODUCTION

Allow for a quick low-cost construction, slender components, high load-carrying capacity, minimal deflection, and improved crack control are some advantages of the use of PT structures in comparison with other forms of structures. Corrosion of reinforcing and prestressing steels, however, have been fairly common especially in PT structures exposed to severe marine environments which have ample supply of saltwater and oxygen.

In this paper, numerical modeling of sound, deteriorated and repaired PT beams under monotonic loading has been investigated by ANSYS software.

2 NUMERICAL SIMULATION

2.1 *Finite element model*

ANSYS software package was used to simulate the 3-D FEM modeling of sound, deteriorated and repaired PT beams. Figure 1 shows the model of quarter part of deteriorated and repaired PT beams in ANSYS software.

2.2 *Concrete modeling*

Solid65 element was used to model the reinforced concrete. The compressive uniaxial stress-strain relationship for the concrete model was obtained using the following equations to compute the multi-linear elastic stress-strain curve (MacGregor 1992):

$$f = \frac{E_c \varepsilon}{1 + (\frac{\varepsilon}{\varepsilon_0})^2} \quad (1)$$

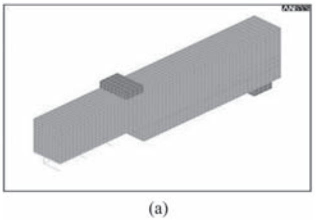
(a)

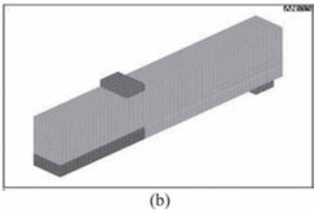
(b)

Figure 1. Modeling of quarter part of (a) deteriorated and (b) repaired PT beams.

$$\varepsilon_0 = \frac{2 f'_c}{E_c} \quad (2)$$

For calculating the linear part, the first point is assumed as $0.3 f'_c$.

2.3 *Post-tensioned strand and reinforcing bars*

Link 8 (truss) element with the capability of plastic deformation is used to model the strand and bars. Perfect bonding between the concrete and reinforcement was considered.

2.4 *Steel plate model*

An eight-node solid element, Solid 45, was used for modeling the steel plates in place of the support of the beam and loading. This element is modeled as a linear isotropic element.

2.5 *Contact behavior*

When the shear and tensile stresses at the interface exceeds the maximum allowable shear and tensile strengths, shear and tensile failures occur, respectively. In order to model these two types of failure, contact pairs (TARGE170 and CONTA174) with debonding capability (CZM) were implemented.

3 RESULTS AND DISCUSSIONS

Figure 2 presents the comparison between experimental data and the finite element analysis for the beam F1 in terms of mid-span load versus deflection. As seen in Figure 2, there is a good agreement between the results of the FE analysis and experimental study.

Comparison of the results obtained from numerical simulation and the experimental results for beam F2 is shown in Figure 3. It is clear from this figure that the load-deflection curve is in a close agreement with the experimental findings until the PT cable reaches its yield stress at the load of 23.05 ton.

Figure 4 shows the comparison between experimental data and numerical results for beam F3. As

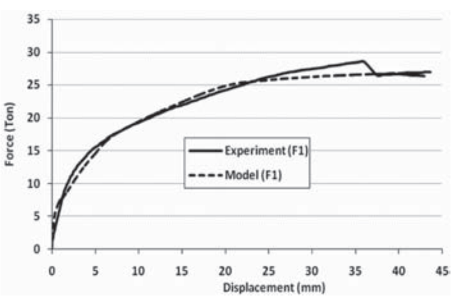

Figure 2. The load-deflection curves for the mid-span of beam F1.

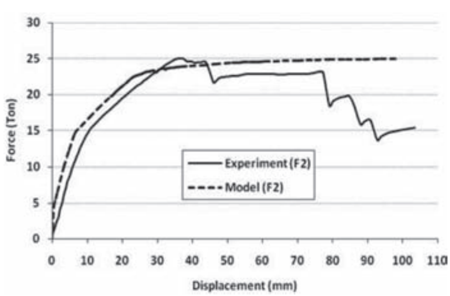

Figure 3. The load-deflection curves for the mid-span of beam F2.

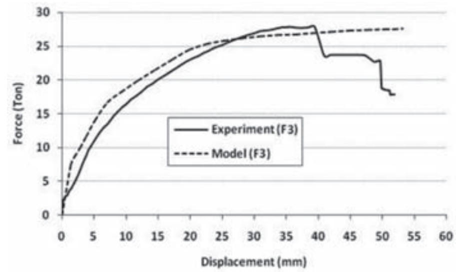

Figure 4. The load-deflection curves for the mid span of beam F3.

can be seen from Figure 4, the current FE model can be used to predict the load-deflection response of repaired PT beams with acceptable accuracy. In repaired PT beams, more attention should be given to the behavior of interface between the repair concrete and substrate.

From the examination of Figures 3 and 4, it can be concluded that the load carrying capacity of the deteriorated beam can been restored to some extent by application of patch repair in the deteriorated parts.

4 CONCLUSIONS

1. Sufficiently accurate prediction of load-deflection curve for sound, deteriorated, and repaired PT beams can be estimated by the applied finite element method. However, this method is unable to simulate the flexural behavior of PT beams after peak load.
2. It was found that the concrete removal from a PT beam can reduce the flexural rigidity and bearing capacity of the beam. By conducting the high performance patch repair in the deteriorated parts it is possible to restore the bear capacity and improve the structural performance of deteriorated PT beams.
3. Further investigation should be done to fully explain the contact behavior at the interface of repaired concrete members especially in harsh environmental conditions.

REFERENCES

MacGregor, J.G. (1992). Reinforced concrete mechanics and design. *Prentice-Hall, Inc., Englewood Cliffs,* N.J.

Shekarchi, M., Mohebbi, M.J., Ghasemzadeh, F., Sajedi S. & Razavizadeh S.A. (2012). Experimental investigation on the effectiveness of patch repair on the flexural behavior of corroded post-tensioned beams. *3rd International Conference on Concrete Repair, Rehabilitation and Retrofitting, September 3–5, 2012*, Cape Town, South Africa.

Concrete Repair, Rehabilitation and Retrofitting III – Alexander et al. (eds)
© 2012 Taylor & Francis Group, London, ISBN 978-0-415-89952-9

Flexure retrofitting of ribbed one-way reinforced concrete slabs through external reinforcing bars

F. Minelli & G.A. Plizzari
University of Brescia, Italy

ABSTRACT: The paper reports results of physical tests on three different ribbed slab typologies, extensively utilized in Italy in the 60's. As many of those structures nowadays do not satisfy the requirements of the new building codes, both at ultimate (ULS) and service (SLE) conditions, the behavior of a slab before or after strengthening was compared toward the evaluation of the efficiency of the strengthening technique, in terms of increase in the post-cracking stiffness, ductility and bearing capacity. The proposed technique results a valuable and promising methodology for an effective strengthening of ribbed slabs.

1 INTRODUCTION

The use of lightweight ribbed one-way reinforced concrete slabs is quite common in Italy and southern Europe, especially in residential buildings, as they allow for a reduced self weight in comparison with a whole concrete section having similar bearing capacity, resulting in a lower seismic action.

This modern technology, characterized by a high degree of prefabrication, is a results of many decades of utilization of similar techniques, but lower-in-technology, as in Figure 1, which shows a rather popular semi-prefabricated slab, referred to as "SAP" (which stands for "self-supporting structure without scaffolding") in Italy.

To decrease the construction time, the idea of prefabricating, in situ, reinforced masonry beams was developed with every single masonry block pre-assembled along small diameter rebars through suitable holes produced in the masonry blocks. Each block contained 3 bottom and two top holes for including up to five smooth rebars having a diameter of 6 or 8 mm, depending on the external load and length of the beam. This allowed a first degree of prefabrication in the field and, moreover, allowed for a rather significant reduction of the construction scaffolding.

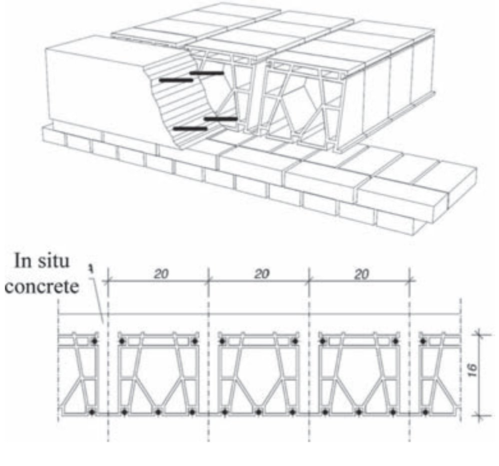

Figure 1. SAP one-way ribbed slab (measures in cm).

In many cases, lack of a proper design can be nowadays reported in existing similar one way ribbed slabs, in relation to the following key-points:

- High span over effective depth ratios;
- Disregard or bad evaluation of superimposed-live load;
- Change in use, which can results in more onerous loading;
- Lack of top 40–50 mm concrete layer;
- Lack of any top reinforcement;
- Small concrete covers;
- Disregard of long-term deformations;
- Lack of skill labor during execution;
- Steel corrosion, concrete and masonry degradation.

2 EXPERIMENTAL PROGRAM

Experimental results refer to two tests on a reproduction of a SAP slab (Fig. 2). In the first case, the slab (sample SAP) was tested up to failure for the complete characterization of the behavior of an existing structure. In the second case (sample R-SAP), an identical slab was loaded up to a target service load (in the cracked stage), then the specimen was reinforced by means of external threaded bears and then loaded up to failure.

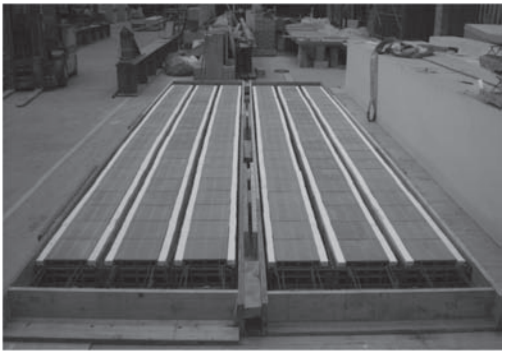

Figure 2. Geometry of the samples reproducing the SAP slab before pouring the concrete.

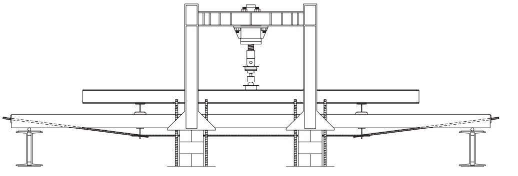

Figure 3. Details of the external reinforcement (double harping point) and reaction frame.

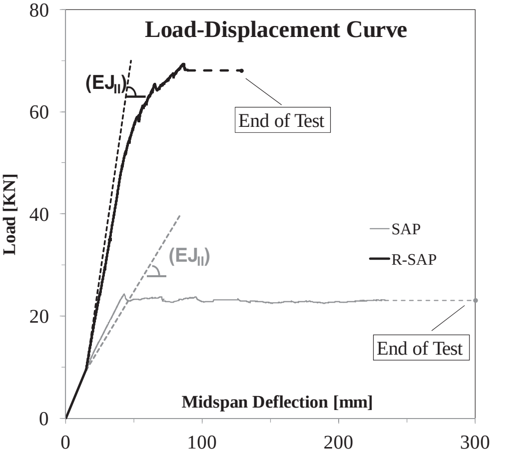

Figure 4. Load-deflection curves of the unreinforced (SAP) and reinforced (R-SAP) specimen.

As reported in Figure 2, the two identical elements consist in three masonry block lines, which identify two central and two half external concrete ribs, simulating three concrete ribs and three corresponding masonry elements.

The samples had a length of 6 m, a span of 5.6 m and a width of 1.08 m.

For R-SAP specimen, the main point was the design of the external reinforcement. 2ϕ20 bars were designed as sufficient external retrofitting for the members. Only the two central concrete ribs were retrofitted, each one with 1ϕ20 bar. The two threaded bars were inclined from the support to the load point (l/4, see Fig. 3) then, by means of a deviator, they laid horizontally in the area under constant moment. In the central zone, the 20 mm bar was substituted by 2ϕ14 mm bars (with negligible variation in area) for ease in construction.

Figure 4 reports the load-deflection curves for both unreinforced and reinforced specimen, with a clear indication of the rather significant influence of the external reinforcement on the overall member response. Note, in both cases, the dotted lines in the last portions of the two responses: for safety reasons, all instruments were removed at the end of the solid line and measurements were made by hand at certain steps.

The flexural collapse of the SAP sample took place for a load of about 25 kN; as expected for lightly longitudinally reinforced members, a concrete crushing, associated with yielding of rebars, was observed. In addition, for a load of 10 kN, many cracks and a significant deflection were already seen.

A significant increase in both the stiffness and the bearing capacity can be attributed to the external reinforcement. The ultimate load was 2.8 times higher than the one of the unreinforced member and the stiffness of the sample R-SAP was about 4.5 as much as that of the unreinforced slab. Both the two aspects are quite significant as they determine an increase in the safety coefficient with regard to the collapse at ULS and, moreover, an enhanced behavior at SLS, especially associated with a lower deflection. A more brittle, even though expected (the retrofitting was just in tension), concrete crushing occurred at a load of about 69 kN, without yielding of the external reinforcement.

3 CONCLUSIONS

A novel strengthening technique for reinforced concrete ribbed slabs that employs external reinforcing bars anchored at the supports was presented in this paper. A 20 mm bar, utilized as external unbounded reinforcement for each reinforced concrete rib and positioned at 100 mm from the bottom fiber provided an increase in bearing capacity of about 3 times and an increase in the stiffness of 4.5 times, compared with the unreinforced specimen, allowing for a complete compliance with both SLS and ULS.

Concrete Repair, Rehabilitation and Retrofitting III – Alexander et al. (eds)
© 2012 Taylor & Francis Group, London, ISBN 978-0-415-89952-9

Analysis of structural rehabilitation of historical masonry with reinforced concrete

N.G. Maldonado, P.E. Martín & I.A. Maldonado
National Technological University. Regional Mendoza Faculty. CeReDeTeC, Mendoza, Argentina

ABSTRACT: This building is declared in the heritage of Mendoza, Argentina. The masonry structure is fired bricks 50 cm thick, without columns or braces. The original design is for educational building, it only has one level, with a principal claustral courtyard, surrounded by galleries next to the classrooms. There is a second courtyard with a block of classrooms and a third one for health services. During its lifetime, more than 90 years, the school has suffered considerable damages due to local earthquakes, changes in architectural materials and lack of maintenance of hydraulic protection. The study methodology used has included the following stages: a detailed study, emergency decisions, analysis of the conditions of the building and diagnosis and rehabilitation proposals. In high seismic risk zone for earthquakes from nearby sources, it is difficult to strictly follow the principles of the different letters of restoration and the task is a challenge for structural engineering. Using data from field and laboratory, the building has been modeled by finite elements, which include interaction with the ground, in this case with a very low bearing capacity and the behavior of different materials for rehabilitation like concrete or steel are analyzed. The costs and availability of local technology for implementation are also analyzed. The advantage of using concrete in their rehabilitation is to achieve the lowest cost and structural performance in accordance to current rehabilitation standards, but from the standpoint of heritage we prefer the combination of steel structures that do not interfere with original structure and with the rehabilitation of reinforced concrete foundation.

1 INTRODUCTION

The renovation of existing structures will be an increasing condition to the sustainability of local communities. This problem is exacerbated in a seismic zone and in the case of restoration of historical buildings with heritage value. The structural challenge is more important when it comes to public use (as in schools, churches and museums).

School infrastructure in the province of Mendoza, Argentina, from the early twentieth century masonry has used unassembled fired ceramic (Grementieri & Shmith 2010). The geological conditions of the region imply that the structures are at greatest risk of earthquakes in the country, near-source earthquakes (INPRES 1989). Therefore the study of the vulnerability of these buildings is justified by the social function of the schools.

In the last decade, the work methodology has included a comprehensive technical and historical survey of the construction, emergency decisions regarding the use restrictions, the analysis of the storage conditions, diagnosis and rehabilitation of viable proposals (Maldonado et al. 2000).

2 STUDIED BUILDING

2.1 *Historical antecedents and survey*

It is a characteristic monumental masonry building, 7 m in height, designed for school use of handmade bricks fired ceramic, seated with lime mortar and cementitious plaster and walls 0.50 m thick. The roof is made of cane and mud and has a covering of corrugated iron, with the support structure of boards and timber.

2.2 *Repair techniques used*

The effect of earthquakes has been very important due to the damages caused in the unreinforced masonry. The first intervention after the Lavalle´s earthquake of 1927, led to the placement of tensors at threshold level in one direction; but this solution was not sufficient enough to achieve adequate structural behavior. The 1985 Mendoza´s earthquake caused the cracking of front masonry at 45 degrees and the evacuation of the building. A major earthquake of August 2006 led to the separation of the front with bracing to prevent crashes (see Figure 1).

Figure 1. State of front (2011).

2.3 *Analysis of conditions of conservation*

The original building has had various interventions, and some of them have generated even more problems than pathologies.

An intervention that brought some problems was the replacement of wooden floating floor to tile floor, with cancellation of the air chambers, which avoided the presence of moisture in the walls in the 1960's. In addition to this, a technical criteria of maintenance such as oil paint in classrooms was inappropriately used as it displaced in height the appearance of moisture in the masonry walls, with a corresponding deterioration.

From the standpoint of soil behavior, lack of maintenance on stormwater drainage systems and sewage water generated significant losses that affected the behavior of existing soil and building foundations, producing significant settlements and the consequent state of cracking existing load-bearing masonry (especially arcs).

To evaluate the structural behavior environmental vibration measurement at different locations in the building has been conducted.

The soil study has also included traditional tests, the measurement of shear wave velocity and the exploration of the foundations. Shallow foundations and silty-clay soils of great power, are very deformable and masonry easily accuses these presence. Some laboratory tests have taken place to characterize the materials used and that have been applied in modeling the behavior.

2.4 *Diagnostic*

To assess the compromise that presents the current building was modeled using finite element method, introducing a predefined deformation of the same order damage presented by the displacement of the front (0.02 m) to evaluate the stress state and verify that the structure is cracked because it has exceeded over 2 times its service status (47 kN/m^2 vs. 115 kN/m^2) for failure of bearing capacity for the foundation used (Plaxis BV 2006). From the point of view of safety has a high degree of structural uncertainty, thus requiring rehabilitation and reinforcement

2.5 *Viable rehabilitation*

To complete the structural requirements we propose:

- To optimize the existing foundation, strengthening the foundation of rubble by the inclusion of a high beam foundation similar to the height of the existing foundation and the construction of Roman piles to reach bearing soil stratum (–4,5 m). The beam foundation, will partially invade the existing foundation, and will be lashed by sectors to transmit loads to the foundation piles.
- To form a chained outside with a metal grid on top of the building, so bracing in both directions masonry walls by steel beams anchored to the walls and metal profiles, triangulating the space to cover. The metal grid is positioned so that the suspended ceiling will not leave in evidence and can in turn be used to locate plumbing facilities (electricity and air conditioning).
- To generate external reinforcements or vertical support efforts to convey the structure to the foundations by metal columns anchored in the masonry structure and the structure foundation.
- Exterior and vertical reinforcements form a lattice that stiffens the structure and that is able to withstand seismic loads for the actual destination of construction.
- To replace existing water drainage systems by better technology and materials.

3 CONCLUSIONS

- A traditional rehabilitation would result from structural changes in the use of various non-traditional materials, hence the intervention suggests a semi-reversible, since it could be strengthened again in the future, with an irreversible intervention in foundations, the stability of the building is ensured.
- In this rehabilitation is modified to 45% of original weight of the building but security is guaranteed performance of the foundation in front of the seismic action, leaving the capital requirements without objection.
- The integrity achieved by the rehabilitation is monitored through the measurement of ambient vibrations.

Concrete Repair, Rehabilitation and Retrofitting III – Alexander et al. (eds)
© 2012 Taylor & Francis Group, London, ISBN 978-0-415-89952-9

Dual function carbon fibre strengthening and cathodic protection anode for reinforced concrete structures

C.V. Nguyen, P.S. Mangat, P. Lambert & F.J. O'Flaherty
Centre for Infrastructure Management, Materials & Engineering Research Institute, Sheffield Hallam University, UK

G. Jones
C-Probe Systems Ltd, UK

ABSTRACT: A novel technique has been proposed and researched in which Carbon Fibre Reinforced Polymers (CFRP) are employed to provide both structural strengthening and electrochemical corrosion protection to Reinforced Concrete (RC) elements suffering from corrosion related damage. CFRPs fabric or rod was used for both flexural strengthening of pre-corroded reinforced concrete beams and operated in a dual functional capacity as an Impressed Current Cathodic Protection (ICCP) anode. After a period of ICCP operation at high current density (>64 mA/m^2 of steel surface area for rod and >128 mA/m^2 of steel surface area for fabric), the beams were subjected to flexural testing to determine the load-deflection relationship. The potential decays of the steel met recognised ICCP standards and the CFRP remained effective in strengthening the corroded reinforced concrete beams. The ultimate strength of the dual function CFRPs reduced slightly when compared with control reinforced specimens used for strengthening only. This is attributed to the application of the ICCP at high current densities influencing the bond at the concrete/CFRP interface. A number of methods for maintaining and enhancing bond are presently being investigated, together with the optimisation of current densities for operating the CFRP anodes.

1 INTRODUCTION

Corrosion of embedded steel in concrete can result in the deterioration and reduction of durability of reinforced concrete structures. Steel in concrete is generally in a passive state due to the high alkalinity of the surrounding cement paste, but exposure to carbonation and chloride ions can result in the steel corroding and producing rust which occupies volumes several times that of the original steel. This can cause internal stress that results in cracking, delamination and spalling of the concrete cover. In addition, corrosion of the reinforcement leads to a loss in its section area and an associated reduction in the service life of the structure (Ahmad 2003, Mangat & Molloy 1992, Al-Sulaimani et al. 1990).

This paper presents some initial results on a novel technique in which CFRPs not only provides additional structural strength to the element being repaired but also works as a cathodic protection anode capable of passing current to electrochemically protect the embedded steel.

2 EXPERIMENTAL PROGRAMME

The test programme included 12 beams in two series. Series 1 includes 6 beams to assess the effect of dual function CFRP fabric (ICCP anode and strengthening). Series 2 had 6 beams to evaluate the effect of dual function CFRP rod (ICCP anode and strengthening).

The specimens were under-reinforced concrete beams, each 900 mm long, rectangular cross-section of 150 mm depth by 100 mm width. Each beam was reinforced by two plain steel bars of 10 mm diameter. There was no shear reinforcement.

The longitudinal tensile steel reinforcement was subjected to forced corrosion by means of an anodic impressed current supplied by a DC power. The current density of 1 mA/cm^2 was used to simulate general corrosion. This current density had previously been succesfully adopted on earlier experiments (O'Flaherty 2008), and was found to provide an appropriate level of corrosion within a reasonable timescale.

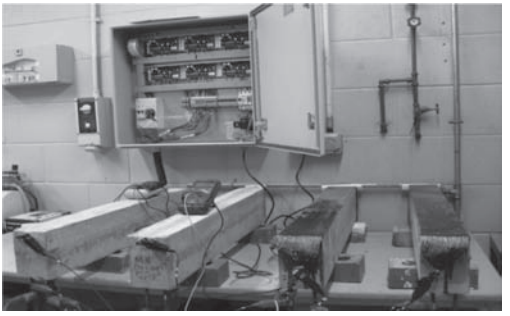

Figure 1. Application of ICCP to corroded reinforced concrete beams.

CFRP fabrics were applied to the surface of corroded beams using Sikadur300. CFRP rods were bonded to pre-formed grooves on the tensile face of beams using a geopolymer developed by Sheffield Hallam University filled with chopped carbon fibres to enhance conductivity. CFRP fabric and CFRP rods were used both for strengthening the corroded reinforced concrete beams and to act as ICCP anodes (Figure 1).

ICCP was applied to the corroded reinforced concrete beams by connecting the reinforcing steel to the negative terminal and the CFRPs anode to the positive terminal of a CPI power supply designed for cathodic protection use. The system was cathodically protected in a controlled laboratory environment (temperature 20°C, RH = 60 ± 5%) where the resistivity of concrete may be expected to be relatively high. The electrical potential of steel and potential decay were monitored and analysed. These beams were finally tested in flexure to determine the load-deflection characteristics.

3 RESULTS AND DISCUSSIONS

The test results showed that CFRPs can be used as an ICCP anode for reinforced concrete structures. CFRP anode can be operated at high current densities of >64 mA/m^2 of steel surface area for CFRP rods and >128 mA/m^2 of steel surface area for CFRP fabric. Based on the data collected, the potential decays are greater than 150 mV after 4 hours. According to the Concrete Society Technical Report No.73 (2011), this demonstrates that CP has been achieved (Figure 2).

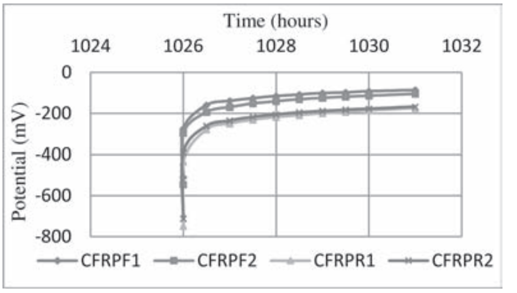

Figure 2. Potential decays of reinforcing steels.

Although there was some slight de-bonding at the concrete/CFRP interface, the CFRP remained effective for strengthening the corroded reinforced concrete beams. The ultimate strength of the dual function CFRPs reduced by approximately 13.5% compared with the CFRP used for strengthening only. This is attributed to the application of ICCP causing the reduction of bonding at CFRP fabric/concrete interface, CFRP rod/geopolymer interface and geopolymer/concrete interface.

4 CONCLUSIONS AND FURTHER WORK

CFRP elements (fabric or rods) applied to reinforced concrete members provide sufficient electrical conductivity to establish an electrochemical circuit with the reinforcement steel through the concrete cover. Additionally, they can be used to strengthen the corroded RC beams, maintaining the structural integrity and increase the ultimate strength of damaged beam. CFRPs increase the stiffness of beams and reduce their ultimate deflection.

In comparison with traditional CP for reinforced concrete, the CFRP anode appears to be capable of operating at much higher current densities. By combining the function of strengthening and CP within a single component, the system is significantly simpler and should also deliver cost savings in addition to easier maintenance.

The enhancement of bonding between CFRPs and concrete needs to be further researched. Some methods for avoiding de-bonding problems such as U-wrapping and near surface mounting are currently being examined. The optimisation of current densities for operating the ICCP anode is also being investigated.

Concrete Repair, Rehabilitation and Retrofitting III – Alexander et al. (eds)

 ISBN 978-0-415-89952-9

Repairing and retrofitting prestressed concrete water tanks in seismic areas

K.C. Kuebitz
Middle East Branch, DYK Incorporated, CA, USA

T. Bloomer
DYK Incorporated, CA, USA

ABSTRACT: During the late 1990s and early 2000s, thirty-two prestressed concrete water tanks in the San Francisco Bay Area were repaired and seismically retrofitted to meet current standards. The prestressed concrete water tanks retrofitted were constructed between 1935 and 1965 using techniques common at that time. Prestressed concrete tanks using this same system were also constructed in other parts of the world, including South Africa and Zambia. In the San Francisco Bay Area, the local water agency considered the costs of replacement against the cost of repair and retrofitting their old prestressed concrete water tanks. Repair and retrofitting was selected. The methods of analysis and the favorable results are a model to other water agencies with similar prestressed concrete water tanks.

Beginning in 1935, the East Bay Municipal Utilities District (EBMUD) in California, USA began constructing water storage tanks which combined the emerging technologies of prestressed concrete and thin shells. This combination of technologies allowed water-containing structures to have the advantages of concrete, without problems associated with cracking and leaking. Since that time, hundreds of similar structures have been built in the San Francisco Bay Area, the majority of which have been in continuous service for decades. In the aftermath of the 1989 Loma Prieta Earthquake, a study of existing water tanks was made in order to assure uninterrupted supply in the event of another large earthquake or other emergency. Older prestressed concrete water tanks, designed and constructed before modern seismic design, were designed for the hydrostatic load only. Many of these older tanks were determined to be in a condition which would not be able to provide water immediately after an emergency. EBMUD decided to rehabilitate and retrofit thirty-two existing water storage tanks to modern seismic design standards and to repair defects. To the great benefit of EBMUD, the water storage tanks were successfully retrofitted and rehabilitated in much less time and for much less cost when compared to demolition and new construction. Learning from the process which EBMUD has now completed can be used as a model for other water agencies with similar structures.

The theory behind prestressed concrete water tanks can be understood by considering a cylindrical shell with free connections at the base and top. Liquid pressure acting on the inside of the cylinder develops hoop stress in the shell. Due to the symmetry of a cylinder with simple boundary conditions, the hoop stress at any elevation is a function of the liquid density, the cylinder radius, and the depth. The post-tension design of such a cylinder required the placement of wires or strands at elevations to counteract the effects of the hoop tension. Additional post-tensioned reinforcement is also added to consider the effects of stress losses and to counteract the effects from differential temperatures and dryness.

In theory, this method works very well. In practice, it was later determined that the stress in each wire might vary due to the cooling of the wire after the friction induced by the die, the speed at which the wire was pulled through the die, and by using worn dies. Die drawing is still used today as a method of prestressing, however, the temperature and force in the wire should be constantly monitored to ensure quality control. Besides die drawing, there are also mechanical methods of prestressing cylinders. Mechanical methods generally employ a means of differential gearing to elongate wire or strand in order to achieve the desired force. The force in these systems can be monitored by special load cells and a feedback loop can send the differential gears continuous instructions in

Figure 1. A Prestressed Concrete Water Tank in Africa Exhibiting Signs of Corrosion.

Figure 2. Crockett Reservoir, California, USA. Constructed in 1935, retrofitted in 2004.

order to adjust the force and maintain a force tolerance of +/– 1.5%. This level of precision is only achievable with mechanical prestressing methods. Without knowing or measuring what level of prestressing is actually being applied, it is possible that the hoop tensile stress could exceed the compression in the concrete. This would place the concrete in a state of direct tension, which usually leads to leaking and corrosion. The ability to measure the force in the prestressed reinforcement is essential to ensure that the proper compression is achieved at every elevation along the height of the prestressed cylinder.

After wrapping the cast-in-situ concrete cylinder with sufficient prestressing wires, a layer of gunite or shotcrete is placed over the wires to protect them against corrosion. Gunite or shotcrete is pneumatically applied fine-aggregate concrete. It is sprayed over the wires to prevent corrosion much in the same way concrete prevents reinforcing bars from corroding. The alkaline chemical environment causes a passivating film to form on the surface of the steel making it resistant to corrosion. Shotcrete is used today in modern prestressed concrete water tanks to cover the prestressing strands or wires. The shotcrete cover coat is essential to the longevity of the water tank. Should the shotcrete fail for any reason, the primary reinforcement will be vulnerable to corrosion.

In total EBMUD upgraded, repaired, and retrofitted 32 prestressed concrete reservoirs. The execution of this was timely, effective, and successful. In the words of EBMUD General Manager, Dennis M. Diemer, "EBMUD's outstanding accomplishments … made it possible to deliver a water system that will protect lives, improve fire service, and distribute the highest quality of water to the millions of customers in its service area, even in the wake of a major earthquake." [2004–2005 Progress Report, Seismic Improvement Program, EBMUD, 2005] The great success of this project can be attributed to the wise choice of originally selecting prestressed concrete water tanks in the first place, then choosing a qualified expert to repair and retrofit them.

When faced with the challenge of having a deteriorating prestressed concrete water reservoir, many water agencies and governments may consider replacement. Most of the consultants that they might hire to evaluate the structure would recommend replacement because they are unfamiliar with the system and the technique. Replacing a prestressed concrete water tank, in most cases, would be a missed opportunity. In addition to the obvious reasons of feasibility, duration, budget, and constructability, repairing and retrofitting a prestressed concrete water tank is an ethical choice when considering environmental impact. It uses much less materials and equipment than constructing a new reservoir would take. It also builds on the tradition of optimizing the brilliant concept of prestressing a concrete cylinder for liquid containment.

Concrete Repair, Rehabilitation and Retrofitting III – Alexander et al. (eds)
© 2012 Taylor & Francis Group, London, ISBN 978-0-415-89952-9

Post-installed bars under low installation temperatures

C. Mahrenholtz, R. Eligehausen, W. Fuchs & J. Hofmann
Institute for Construction Materials, Universität Stuttgart, Stuttgart, Germany

ABSTRACT: The post-installation of reinforcing bars at low ambient temperatures may increase the creep rate and decrease the strength. The relationship between a low curing temperature and the short-term and long-term capacity has not been investigated in detail yet. In a first step tests employing an epoxy based mortar were carried out to investigate the creep behavior under various temperatures at the time of curing, sustained loading and pullout to achieve a better understanding of the effects caused by reduced hardening and incipient post-curing. The tested product was sensitive to decreased installation temperatures: While the pullout strength was influenced only when tested at higher temperatures, the creep displacement became excessive already when conducted at moderate temperatures.

1 INTRODUCTION

1.1 *Background*

Post-installed reinforcing bar systems allow the designer and contractor to find versatile solutions for seismic retrofit measures and design modifications or to realize more economic and efficient construction methods.

Epoxy resins based mortars are often used for the post-installation of reinforcing bars. Like many other mortar systems based on synthetic resins, epoxy mortars are prone to creep.

Epoxy is a thermoset which is irreversibly formed by the chemical reaction of resin and hardener. The two components are provided in a ratio that in theory the thermoset can perfectly cure, i.e. that the conversion α reaches ideally 100 percent which means that all potential cross-links are formed. The degree of cross-linking is a function of time and temperature.

At lower temperatures and curing times to be anticipated for epoxy mortars used at construction sites, the conversion remains comparatively low. As a consequence, the epoxy mortar behaves generally softer and passes the glass transition point at a lower temperature.

Provided that the connection does not encounter a premature failure by excessive creep deformation, the situation is remedied over time to some degree by the counteracting post-curing. Over time, the polymers diffuse and allow additional cross-links to form which increases the conversion.

Figure 1(a) illustrates the influence of the conversion on the mechanical short-term property in terms of the load-displacement behavior. Not only the stiffness but also the strength of the epoxy mortar depends on the degree of cross-linking—the lower the conversion the lower the bond strength of the relevant epoxy. The influence of the conversion on the creep behavior as a mechanical long-term property is shown in Figure 1(b).

2 EXPERIMENTS

2.1 *Test setup*

The complex load transfer mechanism was simulated for the tests carried out within the scope of this paper by a specially designed test setup.

An epoxy mortar system which is qualified for the post-installation of adhesive anchors and reinforcing bars was used. The product is approved for low installation temperatures. The manufacturer's product installation instruction (MPII) was obeyed. After curing, the test stand with the prestressed disk springs was mounted. Next, the load was transferred to the bar via a pulling rod and a fixation.

After the completion of the long-term creep test, the test stand was removed from the climate cabinet. Immediately after releasing the load, a short-term pullout test was carried out under confined conditions to determine the residual capacity.

2.2 *Test program*

Two test types were carried out: Short-term tests, consisting of 2 phases: Curing and pullout testing. Long-term tests, consisting of 3 phases: Curing, creep testing under sustained load, pullout testing. A discrete temperature is assigned to each phase. The short-term tests and the long-term tests were

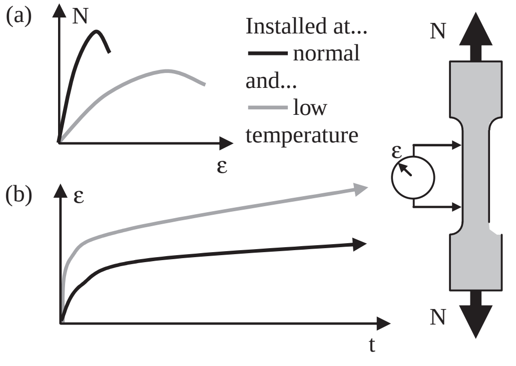

Figure 1. Influence of the conversion on the mechanical properties (schematic): (a) Short-term; (b) Long-term.

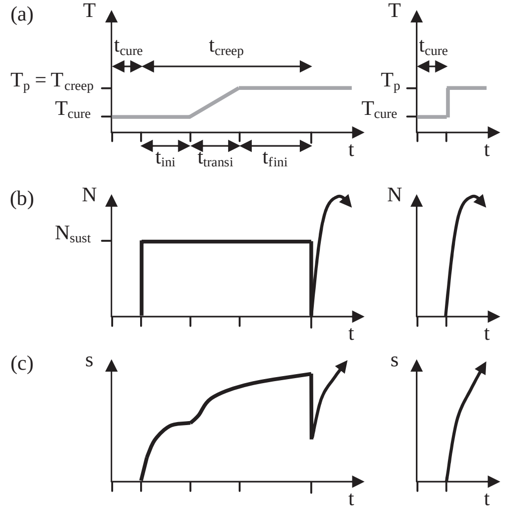

Figure 2. Schematic histories of long-term tests (left) and short-term tests (right): (a) Temperature T; (b) Load N; (c) Resulting displacement s.

carried out to determine the influence of low temperatures of T_{mini} during installation and curing.

Figure 2 visualizes the histories of temperature T, load N and resulting displacement s. The temperature time-history deviated from the standard in order to follow a more realistic approach. The curing temperature was kept constant at T_{cure} after installation over curing time. The first time step of the creep test was carried out at the same temperature, followed by a gradually increase of the temperature stretched over a period of t_{transi}. Finally, the target creep temperature T_{creep} was kept constant for a period of t_{fini}. Assessment Procedure and Criteria.

2.3 *Exemplary evaluation, general performance*

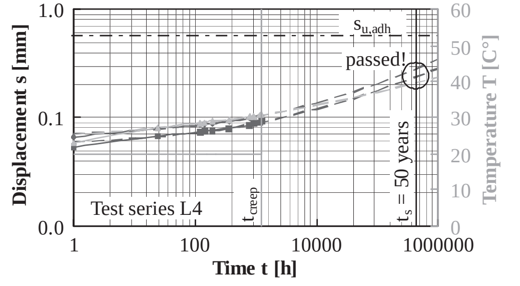

Figure 3. Combined displacement and temperature-time-history diagram of one test series (comprising three tests) as an example.

Figure 3 shows the combined displacement and temperature time-history diagram of one test series (installation and test at 20°C) as an example. Apparently, the extrapolated displacements (dashed curves) of all three tests remain below the displacement $s_{u,adh}$ (dash-dotted line) till the service life t_s (solid line). Therefore, the product passed the test in respect of Criterion 2.

In the following, critical findings are summarized:

– The bond strength of specimens cured at $T_{cure} = 5°C$ and tested at $T_p = 43°C$ is lower than installed and cured at $T_{cure} = 20°C$ and tested at $T_p = 43°C$.
– The creep deformation reaches excessive values if cured at $T_{cure} = 5°C$ and subjected to higher temperatures thereafter. This effect can be observed already for creep tests conducted at moderate temperatures of $T_{creep} = 20°C$.
– The residual capacity was always higher than the capacity of the corresponding short time pullout test for all long-term temperatures tested. The tested strengths exceed the strength achieved after minimum curing time at normal temperatures, demonstrating the beneficial effect of post-curing.

3 CONCLUSIONS

The tests carried out showed that curing at low temperatures and loading at raised temperatures has to be considered as the worst case which might occur in actual practice. Therefore, it is recommended to amend the qualification testing guidelines by tests specifying low installation temperatures and high testing temperatures for both, post-installed reinforcing bar and bonded anchor testing guidelines. Further research is required to develop more realistic temperature histories and to check if extrapolation approaches could yield reliable results.

Concrete Repair, Rehabilitation and Retrofitting III – Alexander et al. (eds)
© 2012 Taylor & Francis Group, London, ISBN 978-0-415-89952-9

Application of post-installed anchors for seismic retrofit of RC beam-column joints: Design and validation

G. Genesio
Engineering Office IEA, Stuttgart, Germany

R. Eligehausen
University of Stuttgart, Stuttgart, Germany

A. Sharma
Bhabha Atomic Research Centre (BARC), Mumbai, India

S. Pampanin
University of Canterbury (UC), Christchurch, New Zealand

ABSTRACT: Many Reinforced Concrete (RC) structures, built in seismic-prone countries before the introduction of the modern seismic oriented codes and usually designed for gravity loads only, necessitate an upgrade in terms of strength and ductility against lateral loading. In this paper the possibility of using post-installed anchors for seismic retrofit solutions is investigated. Post-installed anchors are usually fast and easy to install and they represent a valuable low-invasive solution to transfer high loads with quite low costs. The retrofit of RC beam-column connections with a diagonal haunch element fastened to the existing structural element using post-installed anchors is proposed. The design method based on experimental and analytical investigations is presented. At last, the numerical validation of the retrofit design is discussed.

1 INTRODUCTION

In seismic-prone countries worldwide there is a large amount of buildings that were built before the introduction of modern seismic oriented design codes. Earthquakes during the last decades have shown that these structures designed with substandard detailing need urgently retrofitting and strengthening measures, either to withstand future seismic events with moderate damage, or at least without any collapse.

Large earthquakes that occurred in the recent past showed that deficiencies in the detailing of exterior beam-column joints (i.e. lack of transverse reinforcement, poor anchorage of the beam longitudinal bars in the core and use of plain round bars) are usually responsible for the non-ductile brittle failure mode of the beam-column connections that can induce a collapse of the entire moment resisting frame (Figure 1).

Many retrofit solutions have been proposed and investigated in the recent past to improve the seismic response of beam-column connections and more specifically to avoid brittle failure modes such as column or joint shear failure in favor of more ductile plastic mechanisms such as beam flexural hinging. Various retrofitting techniques are available such as concrete jacketing, steel jacketing, wrapping with fibre reinforced polymer (FRP) sheets, external prestressing, etc. These techniques have proved over the years to be quite effective with each of the above having its own advantages, disadvantages and limitations. However, retrofitting of beam-column joints is still a major topic of concern. One of the major challenges is to practically implement a retrofitting scheme, because there is only a restricted access, if any, to the real joint core to perform any retrofitting technique.

In this study an economical and low invasive technique, the Haunch Retrofit Solution (HRS), is considered. As explained in Section 2 the simplification of this retrofit solution by using post-installed anchors is proposed.

Post-installed anchor systems find extensive application in many different retrofit solutions by attaching new elements to an existing structure. For the design of the anchorages it is necessary to take into account cyclic and impulsive actions and the conditions of the anchorage material, e.g. cracked and low strength concrete. In most of the

Figure 1. Typical failures of beam-column joints observed in recent earthquakes: Italy (2009)—Photo: A Brignola.

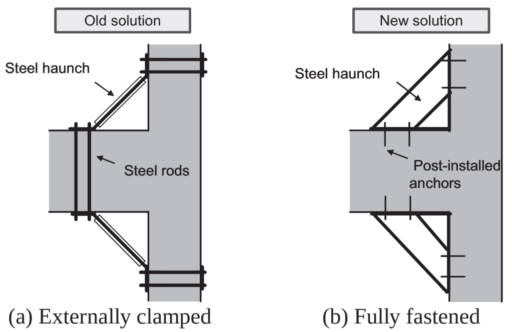

Figure 2. Haunch Retrofit Solution for exterior beam column joints.

applications the anchorages are expected to be over-designed in such way that stiff connections between old and new structural elements may be ensured. However, a proper design of such anchorages is often neglected and the real demand on the anchorage in terms of strength and ductility is underestimated. In the frame of a research cooperation between the University of Stuttgart, the University of Canterbury (UC) and the Bhabha Atomic Research Centre (BARC) the application of post-installed anchors in different seismic retrofit solutions is investigated.

2 RETROFIT STRATEGY

The "Haunch Retrofit Solution" (HRS) (Figure 2a) was developed at the UC in order to modify the internal hierarchy of strength of the beam-column connection and to induce the formation of a ductile flexural hinge in the beam rather than a brittle shear failure in the joint panel. Compared to a wrapping of the joint e.g. using fibre reinforced polymers, this solution represents a cheaper and less invasive way to retrofit a beam-column connection. Although both solutions have the same goal, the functioning principles are very different. With wrapping the shear strength of the joint panel is increased, while with the application of the diagonal steel haunches the joint is protected reducing the shear demand.

The installation of a metallic haunch would be easier and less invasive if the external threaded rods used to fasten the steel diagonals on the beam and on the column could be substituted by post-installed anchors (Figure 2b). In this way no drilling through the floors and the infill walls of the building would be necessary. The results of a numerical analysis, performed with the finite element code MASA developed at the University of Stuttgart, showed that the efficiency of this solution depends mainly on the stiffness of the haunch connection and its slippage on beam/column surface.

As already mentioned, if properly designed, the retrofit solution is able to modify the internal hierarchy of strength of the beam-column connection. In the schematic example shown in Figure 3a, for an assumed column axial load, Nc*, the as-built joint is expected to fail due to joint shear cracking. The retrofit solution should prevent joint and column to fail. The beam flexural strength should be the smallest resistance achieving in this way a ductile plastic mechanism of the beam-column connection. The design parameters to be chosen to achieve the desired hierarchy of strength are the inclination, α, length, L_h and stiffness, K_d of the haunch. If the HRS has to be realized as in Figure 2b another additional parameter is the choice of the anchorage in terms of type and number post-installed anchors.

3 CONCLUSIONS

In this paper an application of post-installed anchors for the refinement and simplification of a retrofit solution for RC beam-column joints, based on the use of two metallic diagonal haunches, was presented. The main required modifications of the design for a safe and economical use of post-installed anchors in HRS were explained. The feasibility of the new solutions was experimentally validated. The analytical design approach was numerically verified.

Retrofitting techniques and FRP systems

Concrete Repair, Rehabilitation and Retrofitting III – Alexander et al. (eds)
© 2012 Taylor & Francis Group, London, ISBN 978-0-415-89952-9

Anchoring FRP laminates for the seismic strengthening of RC columns

R. Sadone & M. Quiertant
Université Paris-Est, IFSTTAR, Paris, France

E. Ferrier
LGCIE site Bohr, Université de Lyon, Université Lyon 1, INSA-LYON, Villeurbanne, France

S. Chataigner
LUNAM Université, IFSTTAR, Nantes, France

J. Mercier
Freyssinet International, Vélizy, France

ABSTRACT: This paper aims to examine the effectiveness of seismic strengthening of Reinforced Concrete (RC) columns by externally bonded Fibre Reinforced Polymer (FRP). Particularly, a novel strengthening system, designed for the flexural strengthening of columns is studied. This flexural strengthening is achieved by FRP plates bonded longitudinally and anchored at the column-stub junction. The proposed system is validated through an experimental campaign carried out on full-scale RC columns. Different strengthening configurations have been applied on columns, which were tested under combined constant axial and reversed cyclic lateral load. The experimental results demonstrate that bonded FRP enhance the bending moment capacity and flexural deformation capacity of strengthened columns. Those tests helped us to analyze the behaviour of columns depending on the FRP confinement (FRP jacket) and the coupling of the confinement with the anchored flexural strengthening. It was then found that the proposed anchoring system is a promising constructive disposition for the seismic strengthening of columns, but this system needs to be improved.

1 INTRODUCTION

This study aims to evaluate the strength and ductility enhancement resulting from longitudinally bonded Fibre Reinforced Polymer (FRP) laminates anchored at the column-stub junction. The anchoring system was previously successfully tested on small concrete blocks (Sadone *et al.* (2010)) but they needed to be tested on representative-scale structures. The originality of the proposed anchoring system is that it is not an additional device but the extension of the Carbon FRP (CFRP) laminate bonded to achieve the flexural strengthening. To study the effectiveness of the proposed anchoring system, real scale reinforced concrete (RC) columns were tested under a quasi-static loading path intended to be representative of a seismic solicitation.

1.1 *Test specimens*

A total of 6 representative scale RC column specimens were constructed (see Figure 1).

The confining jacket was made using the wet-lay up process. Saturated carbon fibre sheets were wrapped around the column while flexural reinforcement was achieved by bonding pultruded CFRP plates.

1.2 *Anchoring system*

The anchored strengthening system was fabricated with a pultruded carbon plate from which the end has been modified. The anchorage system and the CFRP strengthening system (the plate) were then a single continuous element (Sadone et al. (2010)). Principle of the installation of the system to strengthened a column is schematized on Figure 2.

1.3 *Strengthening configurations*

As established in Sadone *et al.* (2012), there is no noticeable difference between the behaviour of a confined column, and a column combining confinement

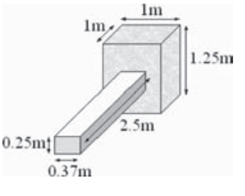

Figure 1. Column dimensions.

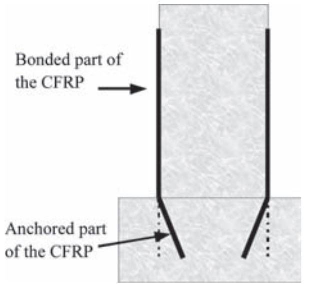

Figure 2. Scheme of the anchoring principle of the flexural strengthening.

and un-anchored laminates for flexural reinforcement. The 3 studied strengthening configurations are then:

- no strengthening (reference specimens PRef1 and PRef2),
- a combination of confinement and laminates (the confinement being the only efficient strengthening system) for specimens PCL1 and PCL2
- and a combination of confinement and anchored laminates (PCLA1 and PCLA2).

1.4 *Loading procedure*

Testing was carried out in the Structures Laboratory of IFSTTAR, located in Paris. Seismic load was simulated by applying cyclic lateral displacements gradually increasing (representative of a seismic loading), while the column was simultaneously subjected to a constant axial load (simulating gravity load). The constant axial load of 700 kN was corresponding approximately to 20% of the axial load carrying capacity of the column. After the application of the axial load, the specimen was subjected to progressively increasing lateral displacement cycles. Two fully reversed cycles were applied for each displacement step. Those displacement steps, referred here as "drift ratio", were defined as a ratio of the column height: 0.25%; 0.5%; 1%; 2%; 4%; etc. until failure.

2 EXPERIMENTAL RESULTS AND CONCLUSIONS

As ever underligned, previous experimental investigations conducted on full-scale RC columns (Sadone *et al.* (2012)) showed that the FRP un-anchored longitudinal reinforcement coupled with confinement does not noticeably change the behaviour of the strengthened columns when compared to simply confined columns (columns without longitudinal FRP). Then, in the following analysis, columns PCL1 and PCL2 are considered as simply confined columns (un-anchored longitudinal reinforcement is not considered).

Considering that a good reproducibility of tests was obtained for each strengthening configuration, results of only one specimen by series are plotted

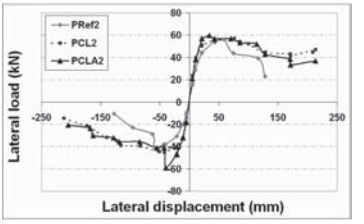

Figure 3. Load-lateral displacements envelope curves.

on Figure 3, which shows the applied lateral force versus displacement drift ratio envelope curves.

On Figure 3 it can be observed that the ultimate lateral displacement of PCL2 and PCLA2 is about twice the ultimate displacement of Pref2, hence demonstrating that the two strengthening configurations are efficient to enhance structural ductility. However, considering that PCL2 and PCLA2 exhibit similar post-peak behaviour, it can be then concluded that the confinement seems to be the main strengthening system to enhance the ductility of specimens.

PCLA2 showed the same failure process as PCL2, but this specimen also experimented a premature failure of anchorages. Indeed, when the anchored plates were loaded in compression during the first cycles, a crushing of end-anchored parts happened. However, before crushing of anchorage, PCLA2 exhibits a maximum lateral load about 40% higher than the maximum load obtained for PCL2 or PRef2.

Finally, within the conditions and the limits of this study, the following conclusions were drawn:

- considering flexural deformation capacity, better performances are observed for strengthened columns, the confinement being the major strengthening system,
- the anchored plates can provide an important increase of the lateral load carrying capacity of strengthened columns. But this benefits is limited due the premature failure of the anchorages by crushing.

REFERENCES

Quiertant M. & Clement J.-L. 2010. Behavior of RC columns strengthened with different CFRP systems under eccentric loading, *Construction and Building Materials*, 25(2): 452–460.

Sadone R., Quiertant M., Chataigner S. & Mercier J. 2010. Behavior of an innovative end-anchored externally bonded CFRP strengthening system under low cycle fatigue. Proceedings of the 5th International Conference on FRP Composites in Civil Engineering CICE 2010 pp. 537–540. Beijing, 27–29 Sept. 2010.

Sadone R., Quiertant M., Mercier J. & Ferrier E. 2012. Experimental study on RC columns retrofitted by FRP and subjected to seismic loading. 6th International Conference on FRP Composites in Civil Engineering CICE 2012, Rome, 13–15 June, 2012. 1.

Concrete Repair, Rehabilitation and Retrofitting III – Alexander et al. (eds)
© 2012 Taylor & Francis Group, London, ISBN 978-0-415-89952-9

Confinement of short concrete columns with CFRP wraps subjected to concentric and eccentric loading

Asad-ur-Rehman Khan & Shamsoon Fareed
NED University of Engineering & Technology, Karachi, Pakistan

ABSTRACT: This paper presents the results of an experimental study on the behaviour of CFRP-confined short concrete columns with low unconfined concrete strengths subjected to eccentric loading. A total of twenty four (24) concrete columns were tested. Three unconfined and three reinforced concrete columns were used as control specimens. Confinement was provided by using CFRP wraps of different heights and spacing. Different confinement schemes were used to determine the effect of schemes on the load carrying capacities of eccentrically loaded columns. All the columns were tested in uniaxial compression, with the load applied at an eccentricity from centre of the column. Results indicate that load carrying capacities of CFRP-confined concrete columns was enhanced in all confinement schemes used during the study and use of CFRP wraps to improve performance of eccentrically loaded concrete columns was found to be an effective method.

1 INTRODUCTION

Deterioration of reinforced concrete columns has been a major issue and to repair and retrofit it involves special techniques. Use of FRP has recently increased to strengthen/retrofit the deteriorated reinforced concrete infrastructure. Results have shown it to be a promising technique. This study presents the behaviour of short concrete columns with unconfined concrete strength in the range of 21 MPa when confined with externally bonded Carbon Fibre Reinforced Polymer (CFRP) wraps. This range of compressive strength was selected as this is representative of average compressive strength of the concrete used in local construction. In this study, concrete columns having cross section of 107 mm × 107 mm and 600 mm in height were tested. Confinement was provided by using CFRP wraps of different heights and spacing. Results indicate that load carrying capacities of CFRP-confined concrete columns were enhanced in almost all confinement schemes used during the study and use of CFRP wraps to confine concrete is an efficient method to improve performance of concrete.

2 EXPERIMENTAL PROGRAM

In order to evaluate the behaviour of short concrete square columns subjected to concentric and eccentric loading confined with CFRP wraps, 24 concrete columns having cross section of 107 mm × 107 mm and 600 mm in height were tested under concentric and eccentric loading. Confinement was provided by using unidirectional CFRP wraps of different heights and spacing. CFRP wraps used in the study have ultimate tensile strength of 4100 MPa, tensile modulus of elasticity of 231000 MPa and fibre density of 1.78 gms./cm^3. In all confined specimens overlap of 102 mm was provided and corners of rectangular columns were also rounded to avoid sharp edges. The pattern of fabric was perpendicular to the applied load. Three plain concrete (PC) and reinforced concrete (RC) columns served as control specimens. Three columns were cast for each confinement scheme; one was tested with concentric load whereas two were tested with eccentric load. All the columns were tested in uniaxial compression with load applied at either at zero eccentricity or an eccentricity of 19 mm to determine the load carrying capacities of confined and unconfined columns.

3 RESULTS AND DISCUSSIONS

3.1 *Columns subjected to concentric loading*

Load carrying capacities, strength enhancement and failure modes of columns tested under concentric loading are discussed in this section. An addition of -C with specimen names is to distinguish specimen tested under concentric loading from those tested under eccentric loading. Specimens tested under eccentric loading will have an addition of -E in addition to the specimen name.

Enhancement in load carrying capacities of confined columns when compared to PC-C and

RC-C were in following order: WF-C, TT-C, WH-C, TA-C and OT-C, showing an increase of 36% and 16%, 32% and 12%, 21% and 3%, 5% and 0% enhancement and 0% enhancement and 0% enhancement respectively. It is important to note that irrespective of CFRP wrapping pattern used for confinement of columns, load carrying capacities are either higher than the reinforced concrete control specimen RC-C or in the same range, except for specimens TA-C and OT-C which were wrapped with 50 mm wide continuous strip wrapped at 100 mm c/c spacing and at one-third of its length respectively, thereby providing better or equivalent confinement as compared to the confinement provided by internal steel stirrups. Almost similar strength enhancements were achieved when columns were wrapped with CFRP wraps along full length (WF-C) and at two third of its length (TT-C), leading to the conclusion that in order to attain maximum strength wraps must be provided at least along two-third length of the column.

3.2 *Columns subjected to eccentric loading*

Load carrying capacities of control specimens PC-E and RC-E were found to be 133 kN and 188 kN respectively. The load carrying capacity of plain concrete column with 50 mm wide continuous strip wrapped angularly at 100 mm c/c spacing (TA-E) was found to be maximum i.e. 291 kN, showing an strength enhancement of 119% and 55% in comparison to control specimens PC-E and RC-E. Enhancement in load carrying capacities of confined columns when compared to PC-E and RC-E were in following order: WH-E, WF-E, TT-E, TS-E and OT-E, showing an increase of 114% and 52%, 110% and 48%, 106% and 46%, 90% and 35% and 80% and 27% respectively. It is important to note that irrespective of CFRP wrapping pattern used for confinement of columns, load carrying capacities are higher than the reinforced concrete control specimen RC-E.

Almost similar strength enhancements were achieved when columns were wrapped with CFRP wraps along full length (WF-E), two third of its length (TT-E) and at half of its length (WH-E), leading to the conclusion that in order to attain maximum strength wraps must be provided at least along half of the length of the column.

4 CONCLUSIONS

On the basis of the results of compressive strengths of PC columns confined with externally bonded CFRP wraps main conclusions drawn from the study are summarized as follows:

1. CFRP wraps provided either better or equivalent confinement as compared to internal steel stirrups, irrespective of CFRP wrapping pattern used to confine columns tested under concentric loading. Load carrying capacities are higher than the reinforced concrete control specimen, except for OT-C which has wraps only at one-third of its length and TA-C which was wrapped angularly with 50 mm wide strip at 100 mm c/c spacing. Maximum gain in strength was observed in columns that were wrapped with 50 mm wide strip at 100 mm c/c spacing (TS-C).
2. In case of specimen tested under eccentric loading, CFRP wraps provided either better or equivalent confinement as compared to internal steel stirrups. Increase in load carrying capacities is observed in all the wrapping patterns as compared to control specimen RC-E. Maximum gain in strength was observed in columns that were wrapped angularly with 50 mm wide strip at 100 mm c/c spacing.
3. Irrespective of wrapping patterns used in the specimen tested under concentric loading, CFRP wraps proved to be beneficial as not only an increase in strength was observed but mode of failure was also changed i.e. from crushing of concrete to CFRP rupture except for OT-C and TA-C specimen in which mode of failure was by crushing of concrete. In case of specimen tested under eccentric loading mode of failure in all the cases was rupture of CFRP wraps.
4. For specimen tested under concentric loading the beneficial effects of CFRP wraps on strength were observed by providing wraps at or more than two third of its length. Whereas, for specimens tested under eccentric load, all the wrapping schemes proved to be beneficial in increasing the load carrying capacity of specimen. In order to attain maximum strength wraps must be provided at least along half of the length of the column.

Concrete Repair, Rehabilitation and Retrofitting III – Alexander et al. (eds)
 ISBN 978-0-415-89952-9

Corner beam-column joints retrofitting with HPFRC jacketing

C. Beschi & P. Riva
Department of Design and Technologies, University of Bergamo, Italy

A. Meda
Civil Engineering Department, University of Tor Vergata, Rome, Italy

ABSTRACT: The effectiveness of a new retrofitting technique, based on the application of High Performance Fiber Reinforced Concrete jacketing for seismic upgrade of RC corner beam-column joints is investigated herein. Three full-scale experimental tests on beam-column corner joint specimens subjected to seismic loads have been performed. The specimens have been designed according to the Italian construction practice of the 60's–70's with typical structural deficiencies, such as use of smooth bars with hooked-end anchorage and lack of stirrups in the joint panel. The tests, performed on the unretrofitted specimens, underline the high vulnerability of the joint panel zone and the critical role of smooth reinforcement bond-slip effect. Moreover, the test showed that the retrofitting proposed solution allows increasing the bearing capacity of columns and the strength of beam-column joints, whit very little visible damage, reaching also an adequate level of ductility.

1 INTRODUCTION

1.1 *The need for RC beam-column joints retrofit*

The Abruzzo earthquake (6th April 2009) dramatically demonstrated that a large amount of the Italian existing RC structures was not able to sustain earthquake actions, maily due to structural deficiencies such as: inadequate material properties, absence of capacity design principles, lack of confinement in the potential plastic regions (typically no transverse reinforcement in the joint regions), poor reinforcement detailing, such as improper anchorage detailing, use of smooth bars for both longitudinal and transverse reinforcement.

From the observation of the effects of past earthquakes, it is widely recognized that beam-column joints represent a critical region in frame buildings subjected to seismic loads. Thus, the strengthening of existing RC beam-column joints has become an important and urgent issue in Italy.

During the last decades, several techniques have been proposed for the seismic retrofitting of RC elements (Fib Bulletin 24 2003, Fib Report 1991): RC jacketing, externally bonded steel plates and FRP wrapping. Recently, a new technique based on the use of High Performance Fiber Reinforced Concrete (HPFRC) jackets has been developed (Martinola et al. 2007, Maisto et al. 2007). The proposed technique consists in encasing structural elements in a thin layer of HPFRC (30–40 mm). The HPFRC material exhibits a hardening behavior in tension coupled with a high compression strength, larger strain capacity and toughness when compared to traditional FRCs.

The results of experimental tests on two unretrofitted joints (CJ1 and CJ2) and a retrofitted one (RCJ1) are given in the following. The test procedure started first with the application of the serviceability loads combination, then of cyclic horizontal displacements of increasing amplitude (Figure 1).

2 EXPERIMENTAL TEST

2.1 *Specimens geometry and materials details*

The specimens are representative of an exterior joint of the first level of a RC four-storey frame designed for gravity loads only according to the

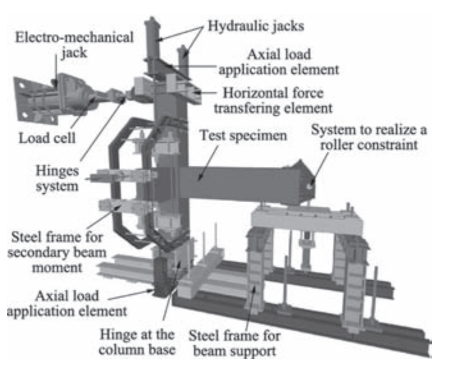

Figure 1. Test set-up.

Italian design provisions in force before the 70's provided by the national standards (R.D. 16/11/1939) and suggested by the technical literature of that time (Santarella 1945).

The beams and the column are characterized by a 30×50 cm and 30×30 cm cross section, respectively, with smooth reinforcing bars and hook-ended anchorages. No transverse reinforcement have been placed inside the joint.

2.2 *Test results*

The experimental results on the unretrofitted specimens confirmed the high vulnerability of corner beam-column joints, with significant damage in the joint core.

In addition, the pronounced cyclic stiffness degradation, with pinching effect in the hysteresis loops, showed the fundamental role played by bar-slip phenomena.

The test on the retrofitted specimen showed that the application of a HPFRC jacket allows to increase the shear strength of the joint. For positive displacements the application of a HPFRC jacket increases the shear strength of about 43% if compared to the unretrofitted specimen maximum strength, while for negative displacements the joint shear strength increases of about 36%.

With respect to the residual strength, it can be noticed that, both for positive and negative directions, the behavior of the retrofitted joint tends to that of the unretrofitted one, since for high drift the tensile contribution of the HPFRC jacket is totally lost, with differences in the order of 10% the most cases.

Figure 2 shows the specimens at the end of the tests. For the unretrofitted specimen CJ2 (the same considerations can be extended to specimen CJ1) three failure mechanisms could be clearly identified: beam failure with a vertical crack at beam-joint interface, joint shear failure with diagonal cracks in the panel zone with the formation of a concrete wedge and cover spalling due to the thrust of the hooked-end anchorages of the longitudinal beam reinforcement at the bottom of the joint.

For the retrofitted specimen, even if some thin cracks could be observed on the outer face of the joint in correspondence with the main beam, the failure was clearly a beam failure as confirmed by the beam-joint interface crack passing through the entire beam section.

It is worth pointing out that no cracks were observed in the outer face of the joint in correspondence with the secondary beam, so that it is possible to state that encasing the joint in a HPFRC jacket avoid the damage due to the thrust of the hooked-end beam bars at the bottom of the joint.

Figure 2. Specimens CJ2 and RCJ1 at the end of the test.

3 CONCLUSIONS

The results of experimental tests on corner beam-column joints subjected to horizontal cyclic loads, confirmed the possibility to improve the seismic performances of corner beam-column joints retrofitted with a HPFRC jacketing, avoiding the damage in the joint panel.

With respect to the unretrofitted specimens, the retrofitted one showed a more limited pinching effect in the hysteresis loops, due to limited joint damage and bond-slip effects.

The application of a HPFRC jacket allows at improving also the ductility of the joint: the retrofitted specimen reached a drift equal to 6% against the 3% reached by the unretrofitted specimens.

Moreover it is worth paying attention to the fact that the retrofitted joint behavior was approximately symmetric in the positive and negative direction, which can be favorable if the joint is subjected to load reversal, as in the case of a seismic event.

REFERENCES

Fib Bulletin No. 24. Seismic assessment and retrofit of reinforced concrete buildings. State-of-art report, International Federation for Structural Concrete, August 2003, 312 pp.

Fib Report 1991. Repair and strengthening of concrete strengthening of concrete structures. Guide to good practice. Thomas Telford Ltd. 1991, 37 pp.

Maisto, L., Meda, A., Plizzari, G.A., & Rinaldi, Z. 2007. R/C beams strengthening and repair with high performance fiber reinforced concrete jacket. In *Proceedings of 4th International Conference on the Conceptual Approach to Structural Design, Venezia (Italy), 27–29 June 2007.*

Martinola, G., Meda, A., Plizzari, G.A., & Rinaldi, Z. 2007. An application of high performance fiber reinforced cementitious composites for R/C beams strengthening. In *Proceedings of FRAMCOS 6, Catania, 18–21 June 2007.*

Regio Decreto R.D. 16/11/1939 n. 2229. Norme per la esecuzione delle opere in conglomerato cementizio semplice e armato. G.U. n. 92, 18/04/1940.

Santarella, L. 1945. Il cement armato—Le applicazioni alle costruzioni civili e industriali, Edizioni Hoepli, Milano, 1945, 559 pp.

Concrete Repair, Rehabilitation and Retrofitting III – Alexander et al. (eds)

Cracking behaviour of RC members strengthened with CFRP strips

W. Ibrahim & J. Hegger
RWTH Aachen University, Aachen, Germany

A. Sherif
Helwan University, Cairo, Egypt

ABSTRACT: This paper discusses the influence of the reinforcing ratio [A_{CFRP}/A_{Steel}] on the cracking behaviour of RC members reinforced with steel bars [A_{Steel}] and strengthened with near-surface mounted (NSM) carbon strips [A_{CFRP}]. The experimental program involves ten tests to study the crack width, crack spacing and cracking behavior of reinforced concrete members strengthened with NSM carbon strips subjected to cyclic tensile load. The strengthening with NSM carbon strips significantly increases the tensile strength and ductility of RC members. In addition, it significantly reduces the crack width in RC members. The paper proposes a formula for predicting the crack width in reinforced concrete members strengthened with near-surface mounted carbon strips.

1 INTRODUCTION

Strengthening of reinforced concrete members using near-surface mounted CFRP technique is today a well-accepted technique that is becoming popular among designers and contractors [1]. In this technique, slots are cut into the surface of structural member and CFRP strips are bonded into the grooves with an adhesive (epoxy resin). This technique is often able to mobilize a greater proportion of the strength of the FRP because of superior bond characteristics that help to prevent debonding failures. The influence of the reinforcing ratio [A_{CFRP}/A_{Steel}] on the cracking behavior of reinforced concrete members strengthened with near-surface mounted has not been sufficiently investigated [2][3]. Ten uniaxial tensile tests are carried out. Three specimens without CFRP strips are used as reference specimens, and seven specimens are strengthened with CFRP strips. The influence of the reinforcement ratio [A_{CFRP}/A_{Steel}] and the type of load [static and cyclic] on the crack width, crack spacing of RC members strengthened with near-surface mounted CFRP strips is studied.

2 CONCLUSIONS

The following are several conclusions of this study:

1. The specimens with higher reinforcing ratios [ρ_e] have smaller crack widths due to the increased stiffness of the specimens compared to the specimens with lower reinforcing ratios.
2. The influence of the cyclic loading [Until 400.000 cycles] on crack width was insignificant and less than 5% compared to static loading. More research is needed to study the effect of cyclic loading in case the cycle's numbers more than 400.000 load cycles.
3. The analytical procedure described herein provides reasonable estimate of the width and spacing of cracks in the RC members strengthened with CFRP strips.

Concrete Repair, Rehabilitation and Retrofitting III – Alexander et al. (eds)
© 2012 Taylor & Francis Group, London, ISBN 978-0-415-89952-9

Shear strengthening of RC hollow box bridge columns using FRP and RC jacketing

M. Fischinger & T. Isaković
University of Ljubljana, Faculty of Civil and Geodetic Engineering, Ljubljana, Slovenia

Bridges, which were built before the modern principles of the earthquake engineering were established, often comprise construction details that are nowadays considered inappropriate for the seismic regions. The deficiencies are mostly related to the transverse reinforcement in columns, which typically cannot ensure adequate shear strength and confinement of concrete core and cannot prevent the buckling of the longitudinal reinforcement bars.

While a number of different strengthening solutions for circular, rectangular or diamond shape bridge columns are broadly available, the investigations of the seismic response and seismic strengthening of hollow box columns are rather limited.

Moreover, the hollow box columns in several bridges in Central Europe comprise specific substandard construction details that were not addressed in the literature at all. An example of bridge supported by such columns is presented in Figure 1. This bridge was constructed on one of the main highways in Slovenia. There have been several concerns regarding its seismic safety. In the paper only those issues, which are related to the non standard reinforcement details in the columns are addressed:

1. The lap splices are constructed near the column foundation, in the region of potential plastic hinges.
2. The transverse reinforcement is placed on the inside of the longitudinal bars.
3. The amount of the transverse reinforcement gradually reduces from the base to the top of the column.
4. Plain bars are used for the longitudinal as well as for the transverse reinforcement.

The response of these columns was investigated experimentally and analytically. These investigations demonstrated their insufficient shear strength. Therefore the shear strengthening was performed considering two strengthening techniques: RC jacketing and CFRP wrapping. The design of strengthening was not trivial, since it was possible to provide it only on the outer side of the column. The outer jacket should to provide the sufficient shear strength, but it could not be too strong, because it could worsen the response of the inner parts of the column.

The typical column, with an aspect ratio of 1.86, was chosen to be examined experimentally. The main properties of the 1:4 scale model are presented in Figure 1.

The model was subjected to a horizontal cyclic load. The column was loaded up to failure. Although the as-built column included several substandard construction details that could induce the buckling of the longitudinal bars prior to their yielding, the column failed due to the insufficient

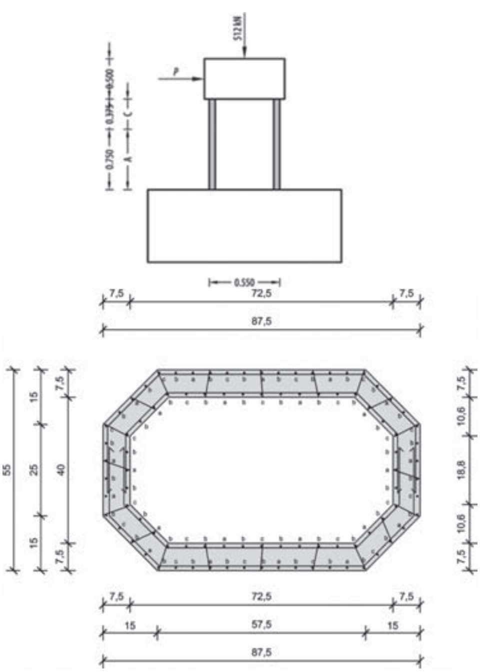

Figure 1. The 1:4 scale model of the as-built column.

shear strength after yielding of the longitudinal bars (see Fig. 2). Considering poor construction details a relatively large displacement ductility capacity of 4 was obtained (see Fig. 2). It was provided by the favorable hollow box cross-section with large compression zone, by the low axial force, and by the relatively high strength of the concrete.

The shear strength of the as-built columns was estimated using the procedures defined in the Eurocode 2 standard (CEN 2004), Eurocode 8/3 standard (CEN 2005) and the procedure proposed at UCSD (Priestley et al. 1996). The UCSD method was the most accurate in the investigated case.

The main purpose of strengthening was to increase the shear strength of the investigated column. The strengthened column was investigated analytically and experimentally on 1:4 scale model. A minimum amount of jacketing was provided. The strengthened column was tested cyclically in a similar way as the as-built column.

The cyclic response of the strengthened column is presented in Figure 3. The concrete jacket efficiently prevented the shear failure of the column. The type of the strengthened column failure was completely different than that of the as-built column. As long as the shear failure was prevented the other unfavorable failure mechanisms induced by other column deficiencies were activated. The spalling of the concrete cover at the outer and inner edges was first ob-served. It was followed by buckling and the rupture of the longitudinal bars. The pull-out of some of the longitudinal bars was also observed. A pronounced horizontal crack was observed at the bottom of the column near the footing. The rupture of the longitudinal bars was followed by substantial rocking of the column.

The alternative way of strengthening using carbon fiber reinforced polymer (CFRP) strips was also analyzed experimentally. The scale of the investigated specimen (1:4) as well as the cross-section dimensions and reinforcement details was kept the same as in the previous cases. Minimum possible amount of CFRP strips was used to strengthen the column.

The cyclic response of column wrapped by CFRP strips was, in general, similar to that of the column strengthened by RC jacketing. The shear failure was efficiently prevented. However, the response was somewhat less favorable (see Fig. 4). There was no additional layer of concrete, which would prolong the spalling of the concrete around longitudinal bars and their buckling, as in the case of the concrete jacketing. The deterioration of the column strength was more pronounced and the energy dissipation capacity was evidently lower. However it should be noted, that the less favorable response of the column wrapped by CFRP strips is partly caused by the pre-corrosion of some of the longitudinal bars.

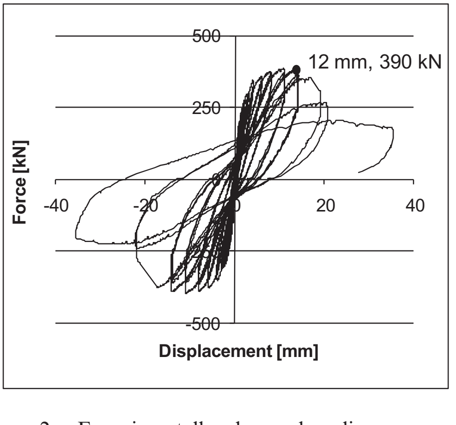

Figure 2. Experimentally observed cyclic response of the as-built column.

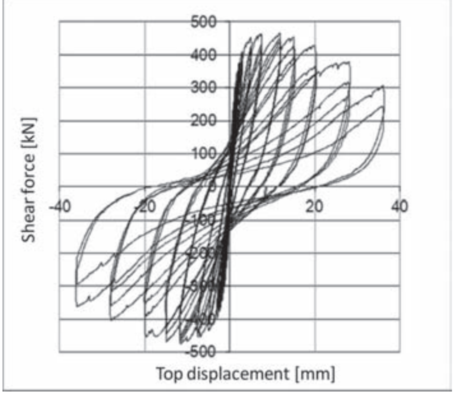

Figure 3. Cyclic response of column strengthened using concrete jacket.

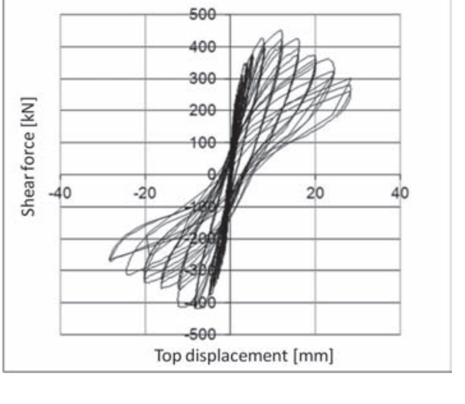

Figure 4. Cyclic response of column strengthened using CFRP strips.

Concrete Repair, Rehabilitation and Retrofitting III – Alexander et al. (eds)
© 2012 Taylor & Francis Group, London, ISBN 978-0-415-89952-9

Flexural performance of repaired reinforced concrete beam containing DFRCC materials

S.F.U. Ahmed
Department of Civil Engineering, Curtin University, Perth, Australia

ABSTRACT: Corrosion induced damage of Reinforced Concrete (RC) structures is the major concern worldwide as it requires costly repair and retrofitting. Different materials are used for such repair and retrofitting, they are conventional repair mortar, combined use of epoxy grout and cement mortar, Fibre Reinforced Polymer (FRP), etc. However, they exhibit limitations in terms of post-repair ductility of the repaired structure due to their inherent brittle material properties. This paper presents the behaviour of corrosion damaged RC beams repaired by Ductile Fibre Reinforced Cementitious Composites (DFRCC). DFRCC is short fibre reinforced cement based composites that exhibits deflection hardening and multiple cracking behaviour in bending. Its ductility and fracture toughness is much higher than that of conventional mortar. In this study six series of specimens are considered. The first series is kept as control (uncorroded), while the other five series are repaired using different repair materials namely the Fibre Reinforced Polymer (FRP) and the DFRCC. The repaired specimens are then structurally tested to evaluate and compare the performance of DFRCC repaired RC specimens with its counterpart FRP repaired specimens. It is observed that DFRCC provides comparable performance in terms of ultimate load and deflection capacity to that of FRP repaired beams and warrant excellent potential for repair and retrofitting of RC structures using this material.

1 INTRODUCTION

Reinforced concrete (RC) infrastructures are deteriorating rapidly worldwide. One of the major causes of such deterioration is due to corrosion of reinforcing steel in RC. The volume expansion of corrosion products exert internal pressure in RC and cause extensive cracking along the reinforcements in the concrete cover followed by spalling and delamination of concrete cover in the vicinity of reinforcements. The ultimate results are the reduction of load carrying capacity and overall reduction of ductility of RC structure. In order to restore the damaged structure to its original state (restoring the structural integrity) extensive repair and retrofitting works are required using different materials and techniques. The commonly used repair materials are repair mortar (Shannag & Al-ateek, 2006), polymer modified repair mortar (Ali & Ambalavanan, 1999; Pellegrino et al., 2009; Rio et al., 2005; Park & Yang, 2005) and use of fibre reinforced polymer (FRP) sheets or laminates (Kutarba et al., 2007). However, they exhibit limitations in terms of extremely low tensile strain, cracking due to shrinkage and debonding of FRP. The above mentioned repair materials particularly mortar and polymer modified mortar are susceptible to cracking during service life due their extremely low tensile strain capacity. Hence, it is often difficult to limit the cracks which form due to mechanical and environmental loads. If these cracks exceed the critical crack width limit, the aggressive substances penetrate through the cracks and restart the corrosion of steel, which require early repair during the maintenance phase. Recently, ductile fibre reinforced cementitious composites (DFRCC) are developed that exhibits deflection hardening and multiple cracking in bending with higher tensile strain capacity than that of ordinary repair mortar or polymer modified repair mortar. DFRCC is short fibre (either metallic or polymeric or both) reinforced cement based composites where fibres are randomly distributed and exhibit excellent ductility under flexure. The DFRCC exhibits multiple cracking with extremely small crack widths which is otherwise not possible using ordinary mortar and polymer modified mortar.

This paper presents the preliminary experimental results of the flexural behaviour of reinforced concrete beams repaired and retrofitted using DFRCC materials containing steel and polyvinyl alcohol (PVA) fibres. Data on such behaviour have not previously been available, and hence the results of this study are expected to contribute to

Table 1. Experimental program.

Series no.	Repair materials used	No. of specimens	Note
1	None	2	Control series
2	Carbon fibre reinforced polymer (CFRP) sheet	2	One layer of CFRP sheet is bonded to the soffit of the beam using epoxy resin
3	DFRCC—steel-2%	2	Approx. 40 mm thick DFRCC is used to repair the bottom cover of the beam
4	DFRCC—PVA (1)-2%	2	Same as above
5	DFRCC—steel-1% + PVA(1)-1%	2	Same as above
6	DFRCC—steel-1% + PVA(2)-1%	2	Same as above

introducing successful repair and retrofitting system and to illustrate the structural behaviour of RC elements repaired using these materials.

2 RESULTS

2.1 *Flexural behaviour of DFRCC repair materials*

All DFRCC exhibited deflection hardening behaviour with different deflection capacities at peak load depending upon the fibre types and combinations. In all DFRCC a total fibre content of 2% by volume is considered. The DFRCC containing 2% steel fibres exhibited the highest ultimate flexural load but low deflection capacity at peak load. On the other hand, the DFRCC containing 2% PVA-1 fibres exhibited the lowest ultimate load but highest deflection capacity at peak load. The DFRCC containing hybrid fibres exhibited simultaneous improvement of both load and deflection capacities.

2.2 *Flexural behaviour of repaired beams*

The CFRP repaired beam exhibits similar ultimate load carrying capacity to that of control beam. The deflection capacity at peak load and the stiffness of both beams are comparable to each other. However, the flexural toughness of CFRP repaired beam is higher than that of control beam.

In the case of DFRCC repaired beams mixed results are obtained with DFRCC containing 2% steel fibre exhibits higher ultimate load carrying capacity while the other fibre combinations don't reach the capacity of that of control. The repaired beam containing steel fibre reinforced DFRCC materials exhibited better performance than that of CFRP repaired beam, with about 8% increase in ultimate load and 15% increase in deflection capacities at peak load. The better ductility of the former one is due to the deflection hardening and multiple cracking behaviour of repair material in flexure. However, the stiffness of the DFRCC repaired beam containing 2% steel fibre is lower than that of CFRP repaired beam. This could be due to low modulus of DFRCC material compared to that of CFRP in tension. Another reason could be that the DFRCC repair layer did not behave in composite manner which is evident from the sign of delamination of DFRCC layer in the flexural test. Similar to that of flexural stiffness, the flexural toughness value is also smaller in the DFRCC repaired beam containing 2% steel fibre than that of CFRP repaired beam; however, it is higher than that of control beam.

3 CONCLUSIONS

The following conclusions can be drawn from this simplified experimental study:

1. The DFRCC exhibit good prospect of repair and strengthening of corrosion damaged RC beams.
2. The DFRCC repaired beam containing 2% steel fibres achieved the load carrying and deflection capacities of that of control and CFRP repaired beams.
3. The stiffness of DFRCC repaired beams is about 30% less than that of control and CFRP repaired beams. This is due to observed delamination of DFRCC layer in the repaired beams.
4. The flexural toughness of most of the DFRCC strengthened beams is comparable to that of control beam.

Concrete Repair, Rehabilitation and Retrofitting III – Alexander et al. (eds)
© 2012 Taylor & Francis Group, London, ISBN 978-0-415-89952-9

Retrofitting bridges to accommodate single point interchanges on the Gauteng Freeways Improvement Project

R. Nel, S.S. Kramer & R.G. Miller
ARQ Pty Ltd., South Africa

ABSTRACT: This paper describes the unique retrofitting methodology adopted on three major bridge interchanges as part of the Gauteng Freeways Improvement Project (GFIP). William Nicol Drive, Rigel Avenue and Garstfontein Road Bridges were all widened over high traffic volume freeways to accommodate new single point interchanges.

1 INTRODUCTION

This paper describes the retrofitting of three bridges to suite new road geometric designs for improved traffic management. The bridges, all situated on the N1, formed part of the Gauteng Freeway Improvement Project (GFIP), which was initiated and financed by the South African National Road Agency Ltd. (SANRAL). What distinguishes these bridges from the rest is their special geometry resulting from the nature of the single point interchanges located over the bridges.

The existing diamond type interchanges at the William Nicol Drive Bridge and the Rigel Avenue Bridge were modified to form single point interchanges. Whilst Garstfontein Road Bridge, originally only an overpass bridge, was changed to a one sided single point interchange. Traffic studies had shown that this interchange system provided significant improvements to the flow of traffic through these interchanges.

2 GEOMETRY

The existing road reserve of SANRAL imposed limits on the horizontal alignment of the interchange distribution roads. However, the layout of the single point interchange aligned towards the center of the bridge instead of outwards beyond the road reserve provided the advantage that expropriation could be kept to a minimum.

A disadvantage of the single point interchange is the need for curved flares on the plan area of the bridge itself (see figure 1 below). This geometry is difficult to both design and construct especially over a busy freeway.

3 WILLIAM NICOL DRIVE BRIDGE

3.1 *Description of structure*

William Nicol Bridge originally consisted of a four span reinforced concrete deck with circular void formers. The deck was 30 m wide and had a total length of 73 m. For the new design the deck was widened on both sides to create the approaching flares for the single point intersection (see figure 1)

3.2 *Design philosophy and methodology*

The widening works consisted of in-situ outer spans and precast middle spans.

The precast elements where designed as open box sections shaped specifically for their location in the bridge. Their shape and size made it impossible to be transported by road and they therefore needed to be manufactured on site as close as possible to their final position.

The cast in-situ outer decks, which were constructed first, provided an ideal platform for the manufacture of these elements. From this location

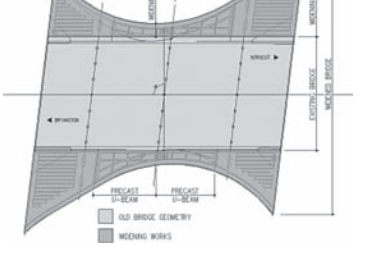

Figure 1. Wiliam Nicol Drive—bridge extensions.

Figure 2. Wiliam Nicol Drive—lowering thwe 110t concrete box girder into place.

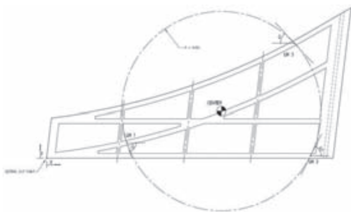

Figure 3. Typical plan of precast flange beam.

they could easily be lifted into position with a mobile crane (see figure 2).

The center of gravity of the precast sections needed to be calculated exactly to ensure force equilibrium during the lifting process. Figure 3 shows the center of gravity of the section as well as the proposed lifting points.

4 RIGEL AVENUE AND GARSTFONTEIN BRIDGE

4.1 *Description of structures*

The existing superstructures of the Rigel Avenue and Garstfontein Road bridges comprised two 27 m span post-tensioned concrete decks.

Triangular shaped flares were added to the corners of the bridge decks to allow for the approach roads of the new single point interchange (figure 4).

4.2 *Methodology*

The widening of these two bridges was twofold. The deck was widened by means of precast U-beams and the triangular flares were achieved with extended cantilevers.

4.2.1 *Main girders*

SANRAL wanted the deck soffit and pier layout of the bridge widening to architecturally match the old bridge as closely as possible. In order to have minimum impact on traffic, it was decided to use “designed for purpose” precast pre-tensioned U-beams on these bridges.

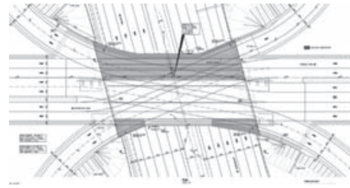

Figure 4. Rigel Avenue Bridge—single point interchange.

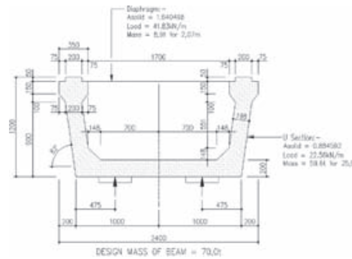

Figure 5. Cross section of precast concrete U-beam.

The beams (see figure 5) had a span length of 26.5 m and a mass of 70t. Each beam was lifted and placed whilst the road was closed for a few minutes during a period of low traffic flow, normally on a Sunday morning.

4.2.2 *Structural parapet*

The introduction of structural parapets on the extended cantilevers or “flares” of the bridges provided a solution to the maintenance of integrity for both the serviceability limit state and the ultimate limit state.

The parapet strengthened the cantilever such that the high design point loads were distributed over a wide area.

5 CONCLUSION

Widening and retrofitting these bridges to suite the new single point interchanges was challenging especially since they cross one of the busiest freeways in South Africa. The design and construction methods developed for these structures have introduced new possibilities for the design of bridges over existing freeways.

The precast concrete members that were developed to help minimize traffic flow interruptions can be reused with success on future projects.

The incorporation of structural parapets was unique in the sense that it utilized material that was normally dead weight which worked against the structure. Now as structural elements they contribute towards the overall strength of the bridge.

Concrete Repair, Rehabilitation and Retrofitting III – Alexander et al. (eds)
© 2012 Taylor & Francis Group, London, ISBN 978-0-415-89952-9

Investigation of shear bonding behavior between base concrete and polymer-modified mortar with CFRP grid

Junlei Zhang, Kentaro Ohno, Kimitaka Uji & Atsushi Ueno
Department of Civil and Environmental Engineering, Tokyo Metropolitan University, Tokyo, Japan

Yuko Ogawa
Department of Civil and Environmental Engineering, Hiroshima University, Hiroshima, Japan

ABSTRACT: Carbon Fiber Reinforced Plastic (CFRP) materials have been widely used as reinforcements for concrete elements, due to their non-corrosion characteristics and high strength-weight ratio. Experimental investigation was carried out to study the effect of CFRP grid and polymer-modified mortar on the shear bonding behavior of existing elements repaired by the materials. In the experiment, Acoustic Emission (AE) technique was applied to investigate the failure process of the specimens. Failure process of the test was estimated by SiGMA (simplified Green's functions for moment tensor analysis) procedure.

1 INTRODUCTION

Recently, retrofitting technique by using sprayed polymer mortar and Carbon Fiber Reinforced Plastic (CFRP) grids has been adopted because CFRP have such good characteristics as high tensile strength and high corrosion resistance. However the shear bonding behavior between existing concrete and sprayed mortar with CFRP at the side of concrete member has not been fully clarified.

In this study, in order to investigate the shear bonding behavior between base concrete and polymer-modified mortar with CFRP grid, pull-out test was carried out. In the experiment, acoustic emission (AE) technique was applied to monitor failure process in specimens. The shear bonding behavior was investigated based on strain distribution of CFRP grid in the specimen and the results of the AE monitoring.

2 EXPERIMENTAL PROCEDURE

Specimens consist of three materials of a base concrete, CFRP grid and polymer-modified mortar as shown in Figure 1. Six specimens have several parameters of sectional area of CFRP grid, grid interval, surface treatment of the base concrete and the use of primer on surface of the base concrete as summarized in Table 1.

In the experiment, applied load was given by pulling out an appearing longitudinal CFRP reinforcement. During the pull-out test, strains of CFRP grid were measured near the crossing points on the grid (grid points) which have a laminated structure. Eight AE sensors were attached to the surface of the specimen as shown in Figure 1.

3 RESULTS AND DISCUSSION

3.1 *Failure mode and crack pattern*

Table 2 shows the failure mode and ultimate load for all specimens. Three failure patterns were observed in the experiment.

In the case of the same CFRP grid (No.1 and No.2 specimens or No.3 and No.4 specimens), loading capacity for the shear bonding became high by using short grid interval. In the case of the same grid interval (No.1 and No.3 specimens or

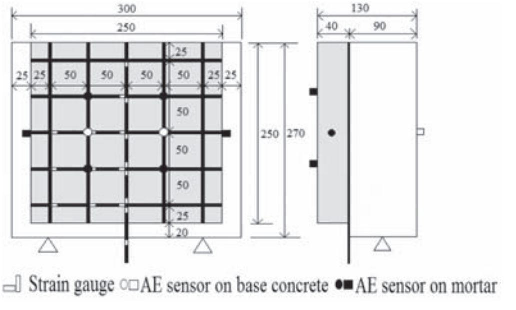

Figure 1. Constitution of specimen (grid interval: 50 mm).

Table 1. Parameters of specimens.

No.	CFRP grid	Grid interval (mm)	Primer	Surface treatment
1	CR6	50	Used	Sand blast
2	CR6	100	Used	Sand blast
3	CR8	50	Used	Sand blast
4	CR8	100	Used	Sand blast
5	CR8	100	Used	Sand paper
6	CR8	100	Not used	Sand blast

Table 2. Results of pull out test.

No.	CFRP grid	Failure mode	Ultimate load
1	CR6	Failure of CFRP	14.92 kN
2	CR6	Failure of CFRP	8.11 kN
3	CR8	Removing of mortar	17.42 kN
4	CR8	Splitting failure	12.23 kN
5	CR8	Splitting failure	14.21 kN
6	CR8	Removing of mortar	8.78 kN

No.2 and No.4 specimens), higher loading capacity for the shear bonding was obtained by applying large cross section area of CFRP grid. As for the treatment of surface of the base concrete, loading capacity for the bonding strength in No.5 specimen which was treated by sand paper became higher than that of No.4 specimen which was treated by sand blast. It is found that the use of the primer brings higher loading capacity for shear bonding by comparing No.4 and No.6 specimens. From results of the experiment, the highest loading capacity for shear bonding could be obtained by using high cross section area of CFRP grid, short grid interval and applying primer to the base concrete.

3.2 *Detail of the failure in No.1 specimen*

This 2-page summary only include results of the No.1 specimen, all specimens are described in the full paper. Strain distributions of a tensioned CFRP reinforcement in No.1 specimen are shown in Figure 2. Focusing on grid points (50 mm, 100 mm, 150 mm, 200 mm and 250 mm from bottom of the specimen), maximum value of strain in the CFRP reinforcement was obtained at 150 mm from bottom of the specimen. At 250 mm from bottom of the specimen, maximum strain was obtained at 14.48 kN before the applied load reached ultimate load as shown in Figure 2. It is found that No.1 specimen failed when grid points in the tensioned CFRP reinforcement broke. This is because the strength or adhesion of laminated grid points in CFRP grid might be low in this specimen. Focusing on upper part of strain distribution, it is clearly found that upper part of CFRP grid hardly bears for the applied load.

Figure 3 shows results of the AE monitoring in No.1 specimen. A lot of AE sources are localized at around the tensioned CFRP reinforcement. It is realized that these AE events mainly generated by friction between the tensioned CFRP reinforcement and polymer-modified mortar or base concrete. AE events generate at lower part of the specimen at first. Then, a lot of AE events generate at upper part of the specimen. From results of the AE monitoring, it is realized that locations of cluster of AE sources shift to upper part of the specimen during the test.

Based on crack patterns, strain distributions and the results of the AE monitoring, the shear bonding bearing area varies with type of CFRP grid and grid interval. Figure 4 shows the assumption of the shear bonding bearing area in No.1 specimen. At the early stage, the areas of bottom of mortar and center of the grid mainly bear for the applied load as shown in Figure 4(a). As increasing the applied load, the shear bonding bearing area shifts to upper part of the specimen as shown in Figure 4(b).

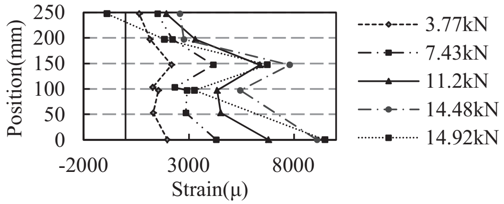

Figure 2. Strain distributions of tensioned CFRP reinforced CFRP in No.1 specimen.

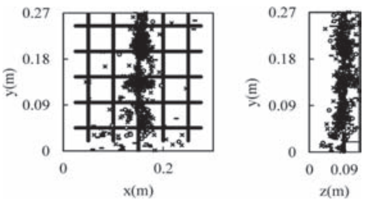

Figure 3. Results of the AE monitoring in No.1 specimen.

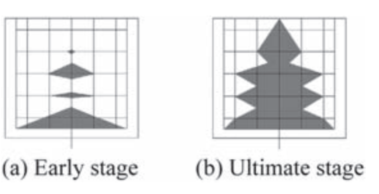

Figure 4. Bearing area of shear bonding in No.1 specimen.

4 CONCLUSIONS

The failure modes of the pull-out test are classified into three patterns. In the case that the strength or adhesion of the grid points which have laminated structure is low, the grid points failure occur. In the case of higher rigidity of CFRP grid, the mortar removes from the base concrete or the mortar split off at near the edge of specimens on loading side. The use of primer to the base concrete surface is effective to obtain the sufficient loading capacity for shear bonding.

Failure process in each specimen is clearly found by results of the AE monitoring. AE sources are concentrated at around a tensioned CFRP reinforcement for all specimens. Locations of cluster of AE sources move from bottom to upper part of the specimens as increasing the applied load in all specimens.

The shear bonding bearing area is estimated based on results of the AE monitoring, strain distributions and crack patterns. As a result, the area of bottom of the mortar and center of the CFRP grid mainly resist for applied load at early stage. Then the shear bonding bearing area shifts to upper part of the specimens.

Concrete Repair, Rehabilitation and Retrofitting III – Alexander et al. (eds)
 ISBN 978-0-415-89952-9

The influence of externally bonded longitudinal TRC reinforcement on the crack pattern of a concrete beam

S. Verbruggen, J. Wastiels, T. Tysmans, O. Remy & S. Michez
Department of Mechanics of Materials and Constructions, Vrije Universiteit Brussel, Brussel, Belgium

ABSTRACT: Often it is more economical to strengthen or repair structures than to demolish and afterwards rebuild them. Several strengthening and repair systems are commercially available at the moment; one of the most common systems is the externally bonded Carbon Fibre Reinforced Polymer (CFRP) strip. This interesting system shows however some drawbacks like its bad resistance to high temperatures and the high cost of the used carbon fibres. The use of strips made of glass fibre reinforced Inorganic Phosphate Cement (IPC) can possibly offer an answer to these drawbacks. High fibre contents (20% in volume and more), which can be obtained with fibre mats, allow for thin and light strips, which are easy to install.

This paper experimentally investigates the influence of external longitudinal reinforcement, made of glass fibre reinforced IPC, on the crack pattern and cracking moment of a plain concrete beam. During a four point bending test, Digital Image Correlation (DIC) monitors the displacements, and thus strains, at the side and the bottom surfaces of the beams in the constant moment zone. In this way, the crack pattern evolution can be visualized. An important observation during these tests is that the first cracks appear at the calculated cracking moment, but that the beams retain their high initial bending stiffness up to an applied moment that is approximately 50% higher than the calculated one. This phenomenon can be ascribed to the restraining effect of the IPC strip on crack opening and propagation.

1 INTRODUCTION

Recent developments in Textile Reinforced Cements (TRC) enable the use of these materials in structural applications, like strengthening and repair of concrete structures. At the Vrije Universiteit Brussel (VUB) Inorganic Phosphate Cement (IPC) is developed, a cementitious material which can be combined with standard E-glass fibres.

The use of TRC, and especially of glass fibre reinforced IPC, for the strengthening of concrete structures has some advantages in comparison with the existing techniques, namely the material's resistance against fire and high temperatures, and the possibility to lower the cost for certain applications by using cheap E-glass fibres instead of carbon fibres. Therefore this paper investigates the effect of externally bonded glass fibre reinforced IPC reinforcement on the crack pattern of an unreinforced concrete beam.

2 TEST SET-UP

A four point bending test with third point load is performed on plane concrete beams with a length of 650 mm, a distance between the supports of 600 mm, a height of approximately 95 mm and a width of approximately 70 mm. The beams are reinforced by placing a 4 mm thick glass fibre reinforced IPC strip over the entire bottom surface of the beam, using different application methods and pretreatments (Table 1).

3 EXPERIMENTAL RESULTS

3.1 *Load-deflection curves*

Figure 1 (glued application) and 2 (glued and bolted application) compare the load-deflection curves for various pretreatments. The dashed horizontal lines represent the analytically calculated cracking moment (4.22 kN) and failure load (8.16 kN or 16.20 kN) respectively.

The ultimate load for the unbolted beams is based on failure due to peeling-off of the external reinforcement. For the bolted beams, the failure mode is calculated to be concrete crushing and IPC TRC in tension. The experiments confirm these failure modes. The different failure mode explains the higher failure load (50%) of the bolted beams (Fig. 2) in comparison with the unbolted beams (Fig. 1). The failure load of the bolted beams is

Table 1. Overview of the different beam types.

Beam type #	Application method	Pretreatment
1	Reinforcement glued on concrete	None
2	Reinforcement glued on concrete	Diamond saw
3	Reinforcement glued on concrete	Chemical treatment
4	Reinforcement glued on concrete	Extra roughening
5	Reinforcement glued and bolted to concrete	Diamond saw
6	Reinforcement glued and bolted to concrete	Chemical treatment
7	Reinforcement glued and bolted to concrete	Extra roughening

quite well predicted by the analytical calculation (Fig. 2). The experimental failure load of the non-bolted beams is significantly higher (28%) than the calculated one (Fig. 1). The latter is the consequence of different boundary conditions in theory and experiment, e.g. the fact that the reinforcement continues over the end supports.

The initial stiffness of the beams remains constant until a load of about 6 kN, which is significantly higher than the calculated cracking moment of 4.22 kN.

Both test series indicate no significant difference in the behaviour of beams with a different pretreatment.

3.2 *Crack pattern evolution*

To study the fracture evolution with increasing load at the beam surface, the technique of Digital Image Correlation (DIC) is used.

With this technique the multiple cracking of the concrete is clearly visible. Cracks initiate at a load of 4.29 kN, which corresponds well to the calculated cracking moment (4.22 kN). However the cracks do not grow significantly until a total load of more than 6 kN is applied. As a result of which the beam retains its high initial stiffness up to a 50% larger moment than the calculated cracking moment.

This technique also shows that the strains are spread over the whole length of the IPC TRC reinforcement. The IPC TRC thus possesses a crack bridging capacity, which may explain the preservation of the beam's initial stiffness and the apparent retardation of the cracking moment of the beam.

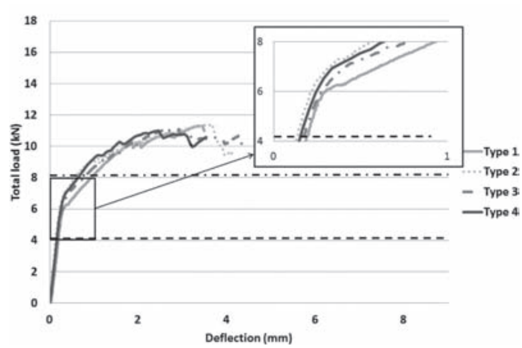

Figure 1. Load-defection curves beam types 1 to 4.

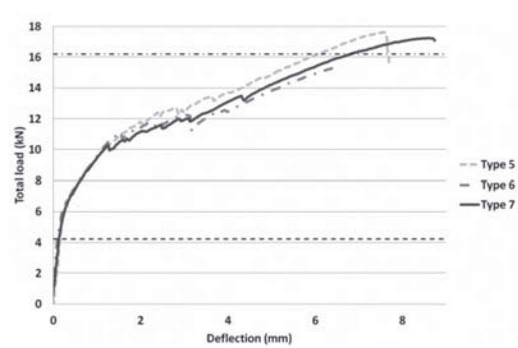

Figure 2. Load-defection curves beam types 5 to 7.

4 CONCLUSIONS

Four point bending tests on plain concrete beams, externally reinforced with IPC TRC, indicate that the beam's stiffness of the first uncracked zone of the load-displacement curve does not reduce until a significantly larger moment (50%) than the calculated and measured cracking moment is applied. A possible explanation for this phenomenon can be found in the crack bridging capacity of the IPC TRC.

A different pretreatment, resulting in a different roughness of the beam surface, does not influence the load-deflection behaviour nor the crack pattern evolution of IPC TRC externally reinforced concrete beams.

While a beam, externally reinforced by glued TRC IPC, fails by peeling-off, the use of both glue and bolts as reinforcement connection results in beam failure due to a combination of concrete crushing and failure of the tensile reinforcement. As a consequence, the addition of bolted connections increases the failure load with 50%.

Concrete Repair, Rehabilitation and Retrofitting III – Alexander et al. (eds)
© 2012 Taylor & Francis Group, London, ISBN 978-0-415-89952-9

Retrofitting of structural concrete after damage caused by impact or explosion

M. Keuser & R. Lenner
Institute of Structural Engineering at the University of German Armed Forces, Munich, Germany

M. Fuchs
Haumann + Fuchs Ingenieure AG, Traunstein, Germany

ABSTRACT: Accidental loads—for example blast and shock waves caused by detonations or more commonly an earthquake or a vehicle impact—lead to a localized damage in Reinforced Concrete (RC) structures. Both the damage assessment as well as the repair techniques of concrete is an important topic with respect to the durable use of infrastructure. Following the damage assessment it is usually necessary to repair the damaged areas. Therefore fundamental investigations concerning the use of different repair techniques have been carried out with respect to damage resulting from an accidental action. This contribution studies different repair and grouting techniques that focus on some example repairs of cracks, concrete microstructure and weakened bond strength between the reinforcing bars and concrete in the surrounding damage zone. Furthermore, this contribution includes application oriented experimental investigations concerning the possible repair of severely blast damaged reinforced concrete elements by grouting and injection.

1 INTRODUCTION

In structural engineering not only static loads are decisive, but also dynamic loads need to be considered. Most of the time, the excessive dynamic loads can be characterized by an accidental loading situation. When highly dynamic loads are considered, then impact and blast loads serve as an example. There are many sources of accidental loading including blast and impact, such as explosions in the industrial facilities.

Damage resulting from accidental loading can possess different characteristics when compared to damage resulting from ultimate/service situations. Accidental load damage typically consists of perforations and craters caused by spalling and scabbing that characterized by a visually recognizable central "target area" as discussed in Gebbeken & Keuser (2012). Another result of accidental loading is the presence of apparently invisible damage in the material surrounding the central area. This is caused by the shock wave travelling through the concrete as well as displacement and vibration of the reinforcement. Consequently the damage supplemental to the main target area is characterized by cracks in the reinforced concrete element. These apparently invisible cracks are often concentrated along the axes of the reinforcing bars and lead to a weakened bond between concrete and reinforcement. As a result stiffness and load bearing capacity are reduced. A possibility how to repair the structure and increase its stiffness is to close the cracks by injecting them with a powder cement suspension or epoxy resin. As a consequence, the concrete matrix and bond behavior of concrete and reinforcement are affected. This leads to a different structural behavior of the whole RC structure. This paper deals with experimental investigation conducted in order to determine, whether it is possible to conduct repairs of RC elements damaged by an accidental loading and, at the same time, to gain information concerning the bond behavior between reinforcement steel and concrete after the repair.

2 RETROFITTING GOALS

For this study the main goals have been set in accordance with the national requirements. Deutscher Ausschus für Stahlbeton (2001) state that by a closure of cracks through grouting or injection and by filling up the spalled concrete volumes the following four objectives should be completed:

1. Closure: prevents corrosive material from entering.
2. Sealing: prevents water from entering; waterproofing.

3. Flexible Joint: provides flexible connection of the crack edges for recurring loading (i.e. temperature loads).
4. Friction-locked Joint: provides friction-locking of crack edges for accidental loading situations.

The above Points 1–3 are achievable by applying various surface protection techniques for the superficial cracking. However, in order to obtain a friction locked joint grouting/injection is necessary.

3 FUNDAMENTAL INVESTIGATION

Theure fundamental investigations aimed at the assessment of grouting/ injection effects of the damaged RC elements repaired according to the Section 2 Goals. In order to investigate the bond behavior and the effect of grouting repair, two tests, pull-out and uniaxial tension, were carried out by Fuchs (2006).

3.1 *Bond behavior*

3.1.1 *Uniaxial tensile test*

The tests show that the bond behavior of reinforced concrete repaired by grouting/injection largely depends on the successful injection and is in turn dependent on the existing crack width. Generally, it can be stated the greater the crack width greater the injection success. The highest increase of bond stiffness can be observed at a crack width of about 0.5 mm. If the crack width is very large (over 0.5 mm) then the increase of bond stiffness is only marginal even at very successful injection repair. This could be possibly contributed to a fact, that at large crack widths there may be missing interlocking effect between the reinforcing bar ribs and the concrete (especially for cracking widths above 2 h_f, that is twice the rib height).

3.1.2 *Pull-out test*

The cracked specimens were repaired by gravity fed epoxy resin with very low viscosity. After the repair and allowed time for the resin hardening the classical pull-out test was carried out in order to obtain relevant information regarding the bond behavior. It was apparent that the increase of bond stiffness of repaired elements when compared to the damaged ones is considerable.

4 COMPRESSION TEST

4.1 *Cube compression*

The compression tests were carried out on concrete cube specimen. Each cube had a crack induced via splitting in order to simulate the accidental load damage. The variable angle between the load and crack direction was used as the main parameter of the investigation.

Three principal directions were used during the testing:

1. Perpendicular to load direction.
2. Skewed to load direction.
3. Parallel to load direction.

The results of uniaxial compression tests showed very similar values for all repaired cubes and reference specimen regardless the principal direction of the crack. This can be explained by the epoxy´s high strength and high stiffness. It is in fact much higher than concrete strength.

5 CONCLUSIONS

The aim of this contribution was to study the suitability of the selected repair techniques while looking at the behavior and effects of the repairs. The fundamental experimental investigations of repaired crack RC structures by utilizing powder cement suspension grouting or epoxy based resin with load pressure injection show reasonable results in improvement of material stiffness and strength as well as bond behavior between reinforcing bars and concrete while accomplishing the goals set by the national standards.

Accidental loads are characterized by large degree of damage with many spalled areas and loose material. The selected low pressure technique was successfully applied. It was proven as a safe repair technique, which prevented further possible damage to the structure. The tests on full scale RC slabs loaded with contact detonation show the applicability of the grouting methods used. However, the judgment of successful full scale repair has been quantified only by applicability and is not sufficient with respect to development of full engineering models.

REFERENCES

Deutscher Ausschus für Stahlbeton. 2001: *Richtlinie des DAfStb: Schutz und Instandsetzung von Betonbauteilen.* Berlin: Beuth Verlag.

Fuchs, M., Keuser, M. & Sendzek, S. 2006. Injektion von Feinstzementsuspension—Verbundverhalten instand gesetzter Stahlbetonbauteile. *Beton*, 10: 468.

Gebbeken, N., Keuser, M., Linse, T. & Wensauer, R. 2012. Betonstrukturen unter Explosion und Impakt. *BetonKalender* 2012: 201–278. Berlin: Ernst & Sohn.

Concrete Repair, Rehabilitation and Retrofitting III – Alexander et al. (eds)
© 2012 Taylor & Francis Group, London, ISBN 978-0-415-89952-9

Debonding of external CFRP plates from RC structures caused by cyclic loading effects

A.J. Badenhorst & G.P.A.G. van Zijl
Civil Engineering Department, Stellenbosch University, South Africa

ABSTRACT: The delamination of Carbon Fibre Reinforced Polymer (CFRP) from Reinforced Concrete (RC) subjected to cyclic loading under various loading amplitudes is reported here. A RC model in the shape of an inverse T-section was designed for this purpose. It was pre-cracked and subsequently reinforced with a 50mm wide CFRP strip. Upon curing, the T-section was tested by bolting its lower end to the loading plate of a materials testing machine, and gripping the CFRP strip at the upper end. The eccentricity of the CFRP caused a combined tensile axial force and a bending moment in the RC specimen, simulating debonding of the CFRP strip from a RC member under bending and tension. The debonding of the CFRP strip in the vicinity of the crack was observed. Monotonic pull-off tests were done to determine the failure envelope. Cyclic experiments followed at 85% and 65% of the peak pull-off load. The experimental results were compared to two dimensional plane stress Finite Element Analyses (FEA) of the same section, with careful simulation of boundary conditions, geometry and at the bonded interface with a suitable constitutive model, calibrated by triplet shear test data. The FEA results proved to represent the experimental results reasonably, justifying the use of the model to analyse responses to cyclic loading at 75%, 55% and 45% of the peak pull-off load. From the data conclusions can be drawn on initiation of delamination, delamination rate, and final unstable, near-instantaneous pull-off, both as function of the load level and number of cycles.

1 INTRODUCTION

Sound methods of strengthening infrastructural elements are in demand to ensure or extend their service life, or to increase their load bearing capacity beyond that originally designed for in cases of upgraded functionality. External strengthening of existing bridge beams by means of CFRP strips bonded onto the tensile face of the reinforced concrete (RC) beams was the focus of this work. Of particular interest was the delamination of the CFRP strip from the beam face in the vicinity of a crack in the concrete.

Debonding is a well known failure mechanism of CFRP-strengthened RC elements. In previous studies on fatigue, improvement of fatigue behaviour by CFRP strengthening was reported and ascribed to lowered stresses in steel reinforcement by crack width limitation of CFRP-reinforcement. Failure of CFRP-strengthened RC beams under fatigue loading has been found to be due to rupture of steel reinforcement. However, to the knowledge of the authors, in depth investigation of debonding under cyclic loading has not yet been reported. This paper reports results of such an investigation.

2 EXPERIMENTAL PROGRAMME

A combined physical and computational experimental program was designed and performed. The study was limited to a single cement type and a single concrete class (35 MPa cube strength). To study the influence in the vicinity of a crack, a single crack width of 0.2mm was caused by deformation controlled pre-cracking. A single CFRP type was used. After removal of the pre-cracking load, the CFRP strip was applied to the concrete face and allowed to cure to the prescription of the supplier.

In addition to the physical tests, 2D plane stress finite element (FE) modelling was used to investigate the debonding behaviour of the CFRP strips from the concrete. Linear elasticity was modelled for the concrete, but the crack and epoxy bond was modelled with interface elements and a suitable non-linear material model to allow Coulomb-friction shear behaviour and direct tension debonding governed by adhesive shearing and tensile strengths and shearing and tensile fracture energies respectively. These model parameters were carefully calibrated to measured data from other characterising tests.

3 RESULTS

By comparison of the carefully calibrated FE model with experimental response to monotonic pull-off, as well as to cyclic loading at 65% and 85% of the static peak pull-off resistance, the FE model was accepted as representative for extrapolation to other load cases. Figure 1 shows the computed responses to the mentioned monotonic and cyclic load cases, as well as a schematic view of the inverted T-section specimen.

In Figure 2 the computed responses to cyclic loading at levels ranging from 45% to 85% of the peak static resistance are shown. Note that the inelastic shear-slip deformation in the interface representing the epoxy bond between the concrete and the CFRP is shown on the vertical axis. In particular, the shear-slip directly above the pre-crack is shown. It appears that a constant shear-slip deformation of about 65 μm is a threshold value for final pull-off.

A threshold number of load cycles appear to be required before initiation of debonding, or inelastic shear-slip in the bond in the vicinity of the concrete crack. This threshold increases with lower cyclic load level. However, for high cyclic loads, here 75% and above, debonding arises already in the first cycle.

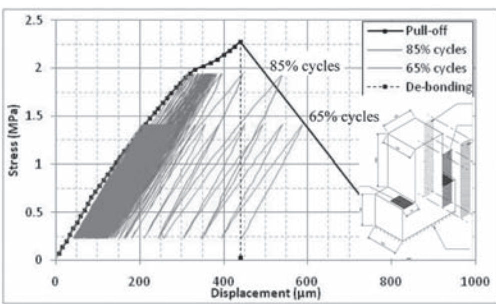

Figure 1. Computed cyclic and monotonic responses.

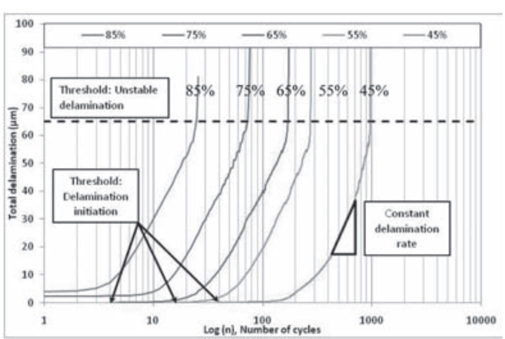

Figure 2. Total plastic relative displacement.

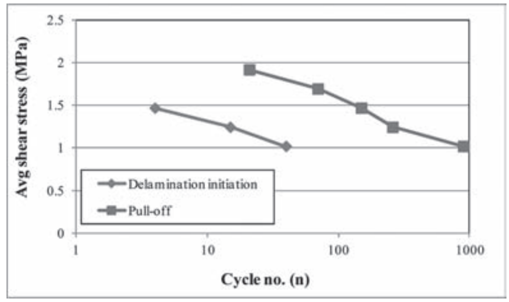

Figure 3. Computed number of cycles to shear-slip initiation and final pull-off.

After initiation, an increased debonding rate occurs until the final unstable debonding rate is reached, followed by abrupt pull-off. The computed numbers of load cycles to these two threshold levels of debonding are shown graphically in Figure 3.

4 CONCLUSIONS

The shear-slip debonding process in the epoxy bonded interface between reinforced concrete and CFRP reinforcing strip has been studied in a combined physical and computational experimental program. The link of this accelerated test remains to be developed clearly, to allow design of such CFRP strengthening for particular loading cycle scenarios based on accelerated test data.

The following conclusions can be drawn:

- Debonding initiation starts after a threshold number of loading cycles have occurred. This threshold appears to be dependent on the cyclic load level, with a higher threshold for lower load cycles.
- For high cyclic loads, here at 75% and beyond of the peak static pull-off resistance, debonding initiation starts already in the first cycle.
- In the accelerated test reported here, a cyclic load as low as 45% of the peak static resistance does lead to failure by CFRP pull-off. It remains to be established whether a lower threshold load level exists for which pull-off does not occur, irrespective of the number of loading cycles – a fatigue limit.
- It appears that a constant level of debonding in the vicinity of a concrete crack, in the case studied here at about 65 μm leads to pull-off. This is considered to be dependent on the particular materials, and likely to be governed by the elastic and fracture properties such as shear-slip fracture energy of the debonding process. In the case studied here, debonding occurred by shearing off the concrete surface.

Concrete Repair, Rehabilitation and Retrofitting III – Alexander et al. (eds)
 ISBN 978-0-415-89952-9

An improved damage model to predict the failure process in FRP/concrete assemblies

K. Benzarti & G. Ruocci
Université Paris-Est, IFSTTAR, MAT, Paris, France

P. Argoul
Université Paris-Est, Laboratoire Navier, Marne-la-Vallée, France

F. Freddi
Universita di Parma, Parma, Italy

ABSTRACT: An improved damage model is implemented for simulating the debonding behaviour of FRP/concrete assemblies and its evolution during hydrothermal ageing. This model has been developed within the framework of the principle of virtual powers and the bonded assembly is modelled as a "three-domain system" with concrete, glue and FRP laminate assumed as damageable materials, those domains being connected by two separate interfaces. An interaction between damage in the domains and damage along the interfaces is also introduced. This model was implemented in a Finite Element (FE) code, which made it possible to simulate the fracture behaviour of CFRP strengthened specimens tested in a single lap shear test configuration. Effects of hydrothermal ageing on the fracture behaviour were analysed by varying the properties of the adhesive layer in the modelling. Comparison between simulations and experimental tests showed the accuracy of the damage model prediction and its capability to distinguish between various failure mechanisms.

1 INTRODUCTION

The aim of this research is to investigate the failure mechanisms of FRP-strengthened concrete elements, through a damage modelling which considers both interfacial debonding and cohesive fracture. The proposed methodology relies on the model initially developed by Freddi & Frémond (2006) to predict the damage behaviour of bonded assemblies. It was recently adapted to the case of rate independent problems (quasi-static tests) by Benzarti et al. (2011a), with a reduced set of damage coefficients. This simplified formulation proved to satisfactorily describe the debonding process (2D fracture propagation) for a single-lap shear tests configuration.

In this study, different sets of mechanical and damage coefficients are considered to assess the variation in the debonding mechanism resulting from an alteration of the glue due to hydrothermal aging. Unlike in former studies, the actual thickness of the adhesive joint is taken into account in the model formulation, which makes it possible to distinguish between an adhesive interfacial failure and a cohesive fracture within the glue layer.

The first part of this paper presents the improved damage model and the main equations governing the progression of damage in the bonded assembly. Experimental and numerical examples of FRP-reinforced concrete specimens tested in a single shear configuration are then presented to investigate the effect of aging on the debonding process.

2 DESCRIPTION OF THE DAMAGE MODEL

A bonded assembly can be idealized by a system made of three domains Ω_i, with i = c, p, g, corresponding respectively to the concrete, FRP plate and glue layer. These domains are connected together by two interfaces noted Γ_{s1} and Γ_{s2}. Figure 1 presents a scheme of this representative three-domain pattern.

For each domain Ω_i, state quantities are the damage quantity β_i, $grad\beta_i$ and the deformation tensor ε_i, all depending on time t and position x. The damage quantity β_i can be interpreted as the volume fraction of undamaged material and its value varies between 0 and 1 (1 for the undamaged

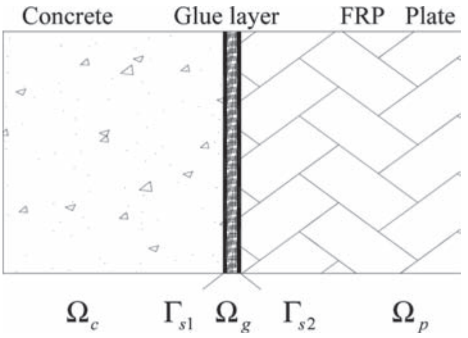

Figure 1. Geometry of the "three-domain model".

state, 0 for cracked zones). Similar state quantities can be defined for interfaces Γ_{s1} and Γ_{s2}, such as the surface damage quantities β_{s1} and β_{s2} and their gradients.

Combining the principle of virtual power with the constitutive laws leads to several sets of equations describing the damage evolution in the domains (1–2) and at interfaces Γ_{s1} (3) and Γ_{s2} (4):

$$div\,\sigma_i + \mathbf{f}_i = 0 \tag{1}$$

$$-k_i \Delta\beta_i = w_i - \frac{1}{2}\beta_i \varepsilon_i : \mathbf{C}_i : \varepsilon_i \tag{2}$$

$$-k_{s1}\Delta_s\beta_{s1} = w_{s1} - \frac{\hat{k}_{s1}}{2}\beta_{s1}\left(\mathbf{u}_g - \mathbf{u}_c\right)^2 - k_{s1,c}\left(\beta_{s1} - \beta_c\right) - k_{s1,g}\left(\beta_{s1} - \beta_g\right) \tag{3}$$

$$-k_{s2}\Delta_s\beta_{s2} = w_{s2} - \frac{\hat{k}_{s2}}{2}\beta_{s2}\left(\mathbf{u}_g - \mathbf{u}_p\right)^2 - k_{s2,g}\left(\beta_{s2} - \beta_g\right) - k_{s1,p}\left(\beta_{s2} - \beta_p\right) \tag{4}$$

With *div* the divergence operator, σ_i the stress tensor, $\mathbf{f}_i$ the volume exterior force, $\mathbf{C}_i$ the elasticity tensor and $\mathbf{u}_i$ the displacement field for each domain Ω_i. Δ and Δ_s are the Laplace operators. Key damage parameters considered in the model are:

- the damage extension parameter k_i for the domains. Similar parameters are defined on the two interfaces, and are noted k_{s1} and k_{s2},
- the initial damage threshold w_i. Its counterparts for the contact surfaces are w_{s1} and w_{s2}, which account for the cohesion of the two interfaces.
- surface rigidities of the interfaces, $\hat{k}_{s1}$ and $\hat{k}_{s2}$,
- surface-volume interaction parameters $k_{s1,c}$ and $k_{s1,g}$, that quantify respectively the influence of damage at interface Γ_{s1} on the damages in concrete and in the glue layer. Similarly, $k_{s2,g}$ and $k_{s2,p}$ accounts for the relationship between damage at the second interface Γ_{s1} and damages in the glue layer and in the FRP plate, respectively.

Equations (1) to (4) have to be coupled with adequate initial and boundary conditions; further details are available in (Ruocci et al., 2012).

3 EXPERIMENTS VERSUS FE SIMULATIONS

3.1 *Experimental campaign*

Numerous FRP reinforced concrete blocks were mechanically tested, before and after hydrothermal aging at 40°C and 95% R.H. Single lap shear tests were carried out using a 100 kN hydraulic jack, at a constant displacement rate of 6 *μm/s*, until complete debonding of the FRP plate. A full description of the tests campaign is given in (Benzarti et al., 2011b).

Shear tests revealed an evolution of the fracture mode, from a cohesive concrete failure for the initial specimens (Fig. 2a) to a cohesive failure in the glue layer for specimens aged over 3 months (Fig. 2b).

Complementary tensile tests showed that properties of the bulk epoxy adhesive are very affected by hydrothermal aging (~80% loss in strength and stiffness), which was ascribed to an extensive plasticization of the polymer network due to water sorption.

3.2 *FE simulations*

Numerical simulations of the shear tests were carried out by implementing the damage model in a FE code (Deal II software). Details regarding the FE mesh and the determination of damage parameters for initial/aged specimens are given in (Ruocci et al., 2012).

Figure 3 displays the volume damage patterns provided by the model for totally fractured specimens, both in the initial and aged states. Red zones

(a) 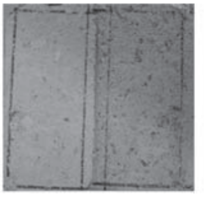 (b) 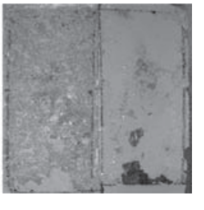

Figure 2. Fracture patterns of CFRP strengthened blocks, unaged (a) and aged for 12 months at 40°C – 95% R.H. (b).

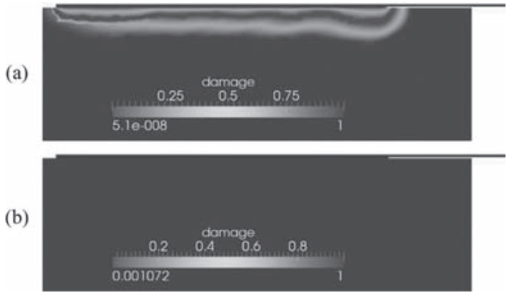

Figure 3. Simulated volume damage patterns for the fractured specimens, in the initial state (a) or after 8 months aging (b).

correspond to totally damaged regions ($\beta_i = 0$). The diagrams reveal a cohesive concrete failure at the initial state, which turns into a cohesive failure in the glue layer after hydrothermal aging. Such findings are in fair agreement with experimental evidences and demonstrate the accuracy of the model predictions.

REFERENCES

Benzarti, K., Freddi, F. & Frémond, M. 2011. A damage model to predict the durability of bonded assemblies—Part I: debonding behaviour of FRP strengthened concrete structures, *Construction and Building Materials* 25: 547–555.

Benzarti, K., Chataigner, S., Quiertant, M., Marty, C. & Aubagnac, C. 2011. Accelerated ageing behaviour of the adhesive bond between concrete specimens and FRP overlays, *Construction and Building Materials* 25: 523–538.

Freddi, F. & Frémond, M. 2006. Damage in domains and interfaces: a coupled predictive theory, *Journal of Mechanics of Materials and Structures* 1: 1205–1233.

Ruocci, G., Argoul, P., Benzarti, K. & Freddi, F. (in press 2012). An improved damage modelling to deal with the variability of debonding mechanisms in FRP reinforced concrete structures, *Int. J. of Adhesion and Adhesives*.

Concrete Repair, Rehabilitation and Retrofitting III – Alexander et al. (eds)

Mechanical fastening of multi-directional CFRP laminates in concrete

P. Desnerck & L. Vasseur
ECC Belgium NV, Wilrijk, Belgium

H. Van Hoecke
University College Ghent, Ghent, Belgium

ABSTRACT: Externally bonded CFRP (Carbon Fibre Reinforced Polymer) laminates are nowadays more frequently used in building industry for the strengthening, retrofitting or repair of existing structures. In most cases adhesive bonding is used for uni-directional laminates, but with the introduction of multi-directional laminates the possibilities of mechanical fastening, by means of bolts, are enhanced.

The use of additional mechanical anchoring has already been proven in previous research projects. This research project focussed on the mechanical anchoring of multidirectional CFRP composites. Besides the diameter and prestressing tension in the bolt, the dimensions of the spreader plate were varied. The results revealed a significant influence of the prestressing force in the bolt on the onset of failure, but a minor effect on the final failure load. In contrary, the bolt diameter had a minor influence on the onset of failure, but a more significant effect on the failure strength.

1 INTRODUCTION

During renovation or after accidental events, the engineer often faces problems with the available bearing capacity of existing elements. In such cases, a strengthening is needed to be able to carry the new loads. One of the frequently used methods for strengthening of existing concrete structures is externally bonded fiber reinforced polymers (FRP).

FRP materials are composed of non-metallic fibers embedded in a matrix. This matrix provides a force transfer between the concrete and the fibers on the one hand and between the individual fibers on the other hand. Frequently used fibers in civil construction applications are carbon fibers (CFRP).

Besides exceeding the bearing capacity and exceeding the criteria in the service limit state, the externally strengthened construction can fail in the anchorage zone. If premature failure can occur due to debonding, the external reinforcement is often extended to provide an adequate anchorage length. However, often the free length along which the CFRP can be applied is limited. In those cases, the only way to increase the anchorage capacity is by bolting the external reinforcement to the concrete.

This study discusses a research project into the possibilities of mechanical fastening of multi-directional CFRP laminates.

2 EXPERIMENTAL PROGRAM

To be able to quantify the influence of the dimensions of the spreader plate, the prestressing force in the bolt and the bolt diameter, an experimental program was developed. More than 110 different specimens were tested.

In the experiments a multi-directional CFRP laminate was used, produced by ECC NV.

Different types of spreader plates and washer have been used throughout the project. The following types of spreader plates have been selected ($b_v \times b_v \times t_v$): 50 × 50 × 5.1 mm; 30 × 30 × 5.1 mm; 50 × 50 × 10.2 mm and 50 × 50 × 3 mm.

Alternatively, washers can be used to distribute the forces. The following types have been used in the experimental program ($\phi_{inner} \times \phi_{outer} \times t_v$): $\phi 8 \times \phi 16 \times 1.4$ mm; $\phi 8 \times \phi 30 \times 5.6$ mm; $\phi 8 \times \phi 24 \times 1.9$ mm; $\phi 8 \times \phi 24 \times 1.9$ mm × 2 and $\phi 8 \times \phi 24 \times 1.9$ mm × 3.

As means for the mechanical fastening the possibility of using bolts or screw-threat is analyzed.

To be able to fully test the performance of the bold connection, the laminates were mechanically fastened to steel plates rather than a concrete surface. The final geometry consisted of a steel plate with a yield stress of 235 MPa and a thickness of 12 mm. Two of these plates were applied (one at each side of the specimen). At the passive side the laminate was not bolted to the steel plate but clamped in the claws of the tensile machine. At the active side the different bolt type/prestressing/spreader plate configurations were applied (Figure 1).

The specimens are tested in a servo-hydraulic testing machine with a maximum capacity of 250 kN. Both sides of the specimen (being the steel plates) are clamped in the machine before testing.

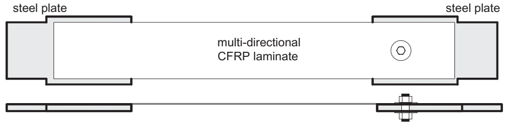

Figure 1. Specimen geometry.

3 RESULTS AND DISCUSSION

In the analysis two forces are of interest. The force $F_{l,rup}$ is defined as the force for which the laminate starts to rupture around the bolt. The force $F_{l,ult}$ is defined as the ultimate force the connection could bear before failure.

3.1 *Influence of the spreader plate and washer*

In a first phase, the thickness of the washer has been analyzed. A washer with an inner diameter of 8 mm and an outer diameter of 24 mm has been applied in 3 thicknesses. The influence of the washer thickness turned out to be not significant. However for small thicknesses, the washer was deformed after the experiment.

The influence of the surface of the washer or spreader plate is analyzed for bolt diameter 8 mm. Regardless of the type, the applied torque has been kept constant. This means that the contact pressure between the plate or the washer is varying according to the applied dimensions.

For the systems with washers, the rupture forces were comparable with the 50 × 50 mm spreader plate. The ultimate forces $F_{l,ult}$ were comparable for all configurations.

3.2 *Influence of prestressing force*

The influence of the prestressing force has been investigated on specimens with screw-threat of diameter 12 mm and steel quality 8.8. Spreader steel plates of 50 × 50 mm have been used and so only the torque has been varied within this set of experiments. The results are given in Figure 2.

As can be seen the prestressing force shows a linear relationship with the rupture force of the laminates. The ultimate failure load shows a less constant increase with the applied prestressing force.

3.3 *Influence of bolt diameter*

In the experiments the prestressing force has been kept constant regardless of the bolt diameter.

It can be concluded that the bolt diameter has little to no effect on the rupture force $F_{l,rup}$.

In Figure 3 the rupture force $F_{l,rup}$ is given as a function of bolt diameter and prestressing force F_m. It is seen that the bolt diameter is indeed of no influence on the obtained results.

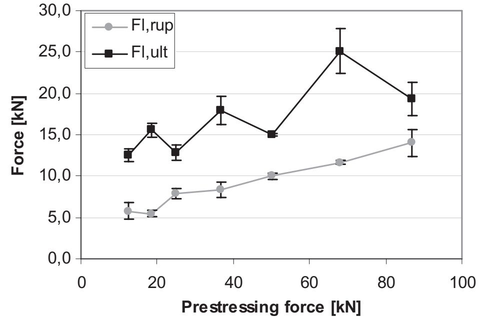

Figure 2. Influence of prestressing force on $F_{l,rup}$ and $F_{l,ult}$ for diameter 12 mm bolts.

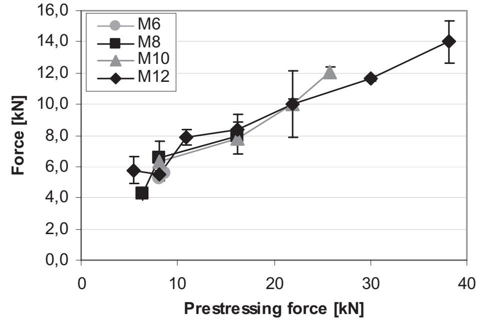

Figure 3. Influence of bolt diameter and F_m on $F_{l,rup.}$

4 DESIGN PRINCIPLES

Based on the obtained test results, design principles are derived for mechanical fastening of multi-directional FRP laminates. Two models have been developed: one taking into account the bolt characteristics and one neglecting these characteristics.

5 CONCLUSSIONS

Based on the obtained experimental results, the following conclusions can be stated:

– The influence of the fastener type, being bolts or screw threat, is small.
– The influence of the thickness of the spreader plate is negligible.
– The bolt diameter has little to no effect on the rupture force. The force $F_{l,rup}$ is only determined by the prestressing force of the bolt or screw-threat.
– The ultimate failure load is increasing for increasing bolt diameter.

Appropriate design models can be derived for the determination of the rupture forces corresponding to certain prestressing forces. These models are in good agreement with the experimental results.

Concrete Repair, Rehabilitation and Retrofitting III – Alexander et al. (eds)
© 2012 Taylor & Francis Group, London, ISBN 978-0-415-89952-9

TRM and UHPFRC: Retrofitting solutions for structural elements

A. Magri, M. Colombo & M. di Prisco
Department of Structural Engineering, Politecnico di Milano, Italy

ABSTRACT: Strengthening of existing concrete structures is becoming one of the most important issue for structural engineering. This requirement comes from that old buildings often were not designed for earthquake loads. Traditional methods of seismic retrofitting follow two main principles: the request for an increase of strength and stiffness and/or the attempt of mass reduction. A good combination of high compressive and tensile strength can be obtain by using Textile Reinforced Mortar (TRM) and Ultra High Performance Fiber Reinforced Concrete (UHFRC). For studying the contribution in the post crack behavior due to the retrofitting material, a new technique, Double Edge Wedge Splitting (DEWS), was adopted. The idea is to investigate the stress distribution on a repaired section of a notched original specimen loaded in pure tension. The uncoupling of tension and compression stress flows, that is the major advantage over bending and Brazilian tests of DEWS tests, is guaranteed by double notch of the specimen.

The experimental program included DEWS test on traditional concrete slab (30 cm × 30 cm × 10 cm) strengthened with two possible retrofitting solutions: TRM reinforced with Alkali Resistant glass fabric and Ultra High Performance concrete reinforced with steel fibers. Before casting the repairing layers, the traditional concrete was pre-cracked reproducing a crack opening corresponding to uncracked, and a SLS and ULS crack opening.

1 INTRODUCTION

The seismic retrofitting of reinforced concrete buildings not designed to withstand seismic actions is a current problem of social relevance. Conventional retrofitting methods provide the addition of new structural elements enlarging the existing members. Surface treatment includes different techniques like reinforced concrete jacketing, externally glued steel plates, shotcrete, ferrocement. Current research on advanced materials is mainly concentrated on fibre reinforced plastic (FRP), high performance fibre reinforced concrete (HPFRC), and textile reinforced concrete (TRC). FRP composites are considered to be the most favourable material in many strengthening applications, because they are light-weight and easy to install on site. The material costs of FRP composites are several times more than that of conventional materials (e.g. steel and concrete). Instead of FRP two possible solutions are Textile Reinforced with Alkali Resistant fabrics and Ultra high performance reinforced with steel fibres. The main advantages are the thickness that can vary from 6 mm for TRC to 20 mm for UHPFRC and the cost.

2 ADVANCED CEMENTITIOUS COMPOSITES FOR RETROFITTING

TRM was made by one Alkali Resistant (AR) glass fabric and fine grained concrete. The fabric is placed aligning the warp and weft wires to the principal stress directions of the element maximizing the performance of the composite. The reinforcement ratio is 3.45%. A tensile strength close to 25 MPa and an ultimate deformation of more than 2% characterize the uniaxial tension response. In the mix design of UHPFRC, 100 kg/m^3 of steel fibres, 13 mm long and 0.16 mm diameter, were introduced. The flexural tensile strength was about 26 MPa and the compressive strength was close to 126 MPa.

3 DEWS TESTS

A new technique has been developed to estimate the tensile strength and to analyze the post crack behaviour. As the well known indirect tensile tests such as Brazilian and Wedge Splitting test (WS), this technique called Double Edge Wedge Splitting test (DEWS) could carry out tensile tests by applying a compressive load, thus avoiding the typical problem of direct tensile test such as gluing plates to distribute the load at the ends of the specimen or other load-transferring devices. Furthermore, this technique allows to induce a tensile stress distribution on a specific section without any crosswise compressive stresses. The compressive load was applied through two steel cylinders acting on 45° shaped notches generating in the middle of the sample a tensile state of stress; two compressive

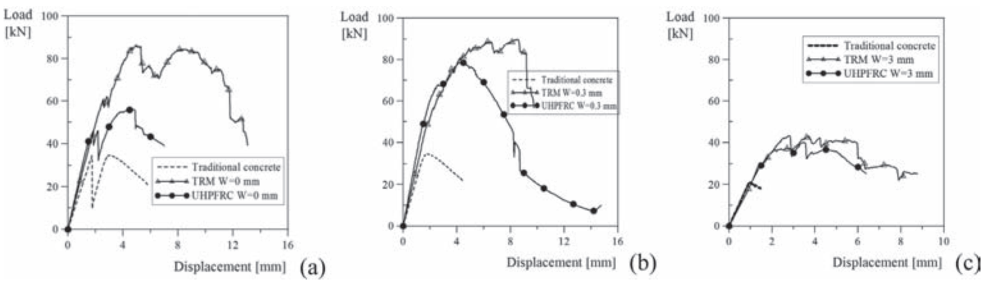

Figure 1. Comparison TRM and UHPFRC solutions at (a) w = 0 mm (b) w = 0.3 mm (c) w = 3 mm.

arches equilibrate the loading imposed on the punches. In the V notches two thin steel plates were placed to uniformly distribute the load. The friction between the steel plates and cylindrical tip of the load knife could reduce the efficiency of the loading device by introducing a tangential component. For this reason a graphite lubricant was applied.

DEWS technique was used to analyze the tensile strengthening resistance offered by the retrofitting layers. Traditional concrete plates (30 × 30 × 10 cm) were cast and pre-cracked after natural curing of more than 28 days imposing three different crack opening values (0 mm, 0.3 mm and 3 mm) and they were repaired by applying to both sides 6 mm of TRM or 2 cm of UHPFRC. The square specimens were made by 10 cm of concrete with a compressive strength of 34 MPa and they were reinforced with a steel welded mesh 6/150/150 mm. Before casting the retrofitting layer, to improve the bond, the concrete surfaces were treated by a sandblasting to make rough the interface. Two different casting procedures were adopted according to the repair technique. The matrix of TRM was cast in a horizontal plane after having placed the AR glass fabric and a roller was adopted to compact the mortar. UHPFRC was cast in vertical direction from one side to allow a alignment of the fibres in the tensile direction (Ferrara et al., 2010).

DEWS tests were carried out by using an electromechanical press DMG with a maximum load capacity of 100 kN. The tests were displacement-controlled by imposing a constant stroke rate (0.1 mm/min). Three displacement transducers (LVDT), at the tip of the upper and lower notch and in the middle of the plates were located at each side of the specimens (Front and Rear) and two LVDTs were positioned in the perpendicularly to the surface to measure the sliding of retrofitting layer with respect to concrete support and detect a possible delamination of the retrofitting layer.

The load versus vertical displacement curves are presented in Figure 1. Both retrofitting materials guarantee a load increase in the range of 40–60 kN.

Textile solutions reach higher peak loads than UHPFRC solutions. This result is due to the different failure mechanisms: textile layers multi-cracked in the middle of the plate and some parts of matrix, that covered the fabric, were played off. The detachment of the matrix could be explained by a compression stress field due to the eccentricity of the tangential stresses activated at the interfaces.

UHPFRC layers showed a failure caused by delamination in the case in which pre-cracks were equal to 0 mm and 3 mm. In the case of serviceability crack opening (w = 0.3 mm) localized cracks in the centre of the reinforcement occurred at both sides.

4 CONCLUSIONS

The Double Edge Wedge Splitting test is able to identify the tensile global performance by applying a compressive load and to detect the strengthening due to retrofitting materials. Both solutions, TRM and UHPFRC, enhance peak load and ductility with reduced thickness always smaller than 20 mm. TRM seems the best solution, because it is cheaper, the layer is thinner and the casting procedure is faster, because no formwork are needed. Furthermore, no fibre segregation can occur for casting large areas in vertical direction. Further analysis carried out looking to the best data showed to study the bond in the interface layer and the best treatment of original surfaces. Although the expected strengthening should be comparable and in the order of 75–90 kN, the results highlighted a contribution in the order of 15–40 kN due to partial delamination.

Concrete Repair, Rehabilitation and Retrofitting III – Alexander et al. (eds)
ISBN 978-0-415-89952-9

Analytical study on behavior of External shear wall and Internal shear wall as lateral load resisting systems for retrofitting a ten storey building frame

S.V. Venkatesh
Faculty of Civil Engineering, PES Institute of Technology, Bangalore, Karnataka, India

H. Sharada Bai & S.P. Divya
Faculty of Engineering—Civil, Bangalore University, Bangalore, Karnataka, India

ABSTRACT: Earthquakes are natural phenomena under which disasters are mainly caused by damage to or collapse of buildings and other man-made structures. Many existing buildings lack the seismic strength and detailing requirements as per standard codes of practice. An existing structure may need upgrading or retrofitting if the structure was initially not designed and constructed to resist an earthquake i.e. designed only for gravity loads. The present study consists of a comprehensive three-dimensional elastic analysis using Response Spectrum Method (RSM) of a ten storied building structure wherein External shear walls and Internal shear walls are considered as Lateral Load Resisting Systems (LLRS) as possible measures of retrofitting of structures. The behavior of the building in which LLRS are employed is compared with moment resisting Bare frame (without any LLRS). The building located in zone V (Most severe) of seismic zones of India, is subjected to seismic loads, non-seismic loads and their combinations to arrive at the critical deformations and forces in the structure. The following 3D frame models are considered for analysis.

Bare Frame without any special feature of LLRS

- Basic 3D moment resisting bare Frame 1 × 3 bays (7.5 × 3 m)—ten storey (BF) [Fig 1].

Frames with special feature of LLRS

- Basic 3D Frame 1 × 3 bays—ten storey, with External Shear wall of length equal to ¼ of span along X axis and ½ of span along Z axis at the corner of building (ESX4Z2) [Fig 2].
- Basic 3D Frame 1 × 3 bays—ten storey, with Internal Shear wall of lengths same as that of External shear walls (i.e. ¼ of span along X axis and ½ of span along Z axis) at the corner of building (ISX4Z2) [Fig 3].

Column & Beam cross-sections

- Column Size: 636 mm × 636 mm
- Beam Size:
  Along X axis: 300 mm × 750 mm
  Along Z axis: 300 mm × 375 mm
- Plinth Beam Size:
  Along X axis: 300 mm × 450 mm
  Along Z axis: 300 mm × 300 mm

The shear wall thickness considered is 200 mm.

The primary loads (dead and live load) on the frame have been calculated based on IS: 875 (Part I): 1987. The dead load consists of self weight of structural elements and wall load. The live load considered is as adopted for medium office, hospital or hostel building i.e., 4 kN/m^2. The Response Spectrum Method is adopted for the calculation of the lateral load at each floor level as per IS: 1893 (Part I): 2002.

Method of analysis

The structure is modeled as a three-dimensional space frame and analysis is carried out using FEM software package STAAD Pro. Beams and columns are modeled as 3D line elements, Slab and Shear walls are modeled as 2D plate element.

Figure 1

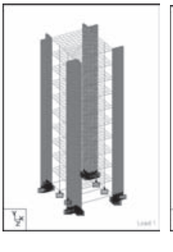

Figure 2

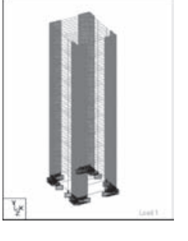

Figure 3

RESULTS

Out of 17 possible loads and load combinations the maximum Joint displacements, support reactions, and forces (except forces in global Y direction) are generally found to occur for the load combination, 10 or 11 i.e. 1.5 (DL + ELx), or 12 or 13 i.e. 1.5 (DL + ELz), showing that the critical load combination occurs when seismic loads are considered. Hence, it is important and necessary to consider seismic loads in analysis of structural systems.

It is found that non-seismic load combination 5 i.e., 1.5 (DL + LL) results in maximum forces in global Y direction for ESX4Z2. Whereas in all the other parameters considered maximum values occur due to seismic load combination and are very much higher than Non-seismic load combination. This highlights the importance of considering all load combinations in analysis of any structure.

In comparison to bare frame, the maximum displacement along X & Z directions reduce by 28% & 60% in ESX4Z2 & ISX4Z2 respectively showing that provision of LLRS in bare frame results in substantial increase in the lateral stiffness of the structural system.

It can be observed that there is considerable reduction in maximum support reaction Fx & Fz by 44% & 29% in ESX4Z2 and by 16% & 6% in ISX4Z2 when compared with bare frame. The maximum support bending moments, Mx & Mz also reduce by 52% & 66% by addition of shear walls externally & internally, which indicate shear walls are effective in resisting earthquake loads.

The value of maximum column axial force, Fx reduces by 8% & 22% in case of ESX4Z2 & ISX4Z2 in comparison to bare frame. Whereas the maximum column moments My & Mz reduce by 55% & 42% in both ESX4Z2 & ISX4Z2.

In comparison to bare frame, values of maximum torsion & bending moment in beams in ESX4Z2 & ISX4Z2 reduce by 26% & 42% respectively.

It is seen that the maximum column shear force Fy value in ESX4Z2 increases by 21% & beam axial force Fx value in ESX4Z2 and ISX4Z2 increase by 57% & 25% respectively, which needs design consideration.

The Principal stresses developed in shear walls are within the permissible stresses of reinforced concrete as applicable.

Internal shear walls show better performance in resisting lateral forces than External shear walls.

The fundamental period as obtained by software for the models considered do not match with the values obtained from the formula given in IS code 1893 (part I) 2002. This needs to be considered and revised as the fundamental period does not depend only on the height, but also depends on the structural configuration.

The multiplication factor Vb/VB are different along X and Z directions. It can be observed that in case of all the models considered the value of Vb/VB is greater than 1 which indicates that the values of Equivalent Static Force Method (ESLM) are greater than Response Spectrum Method (RSM).

CONCLUSION

Earthquake load and load combinations have to be considered for analysis as most of the maximum design forces occur due to earthquake loads.

The maximum storey sway reduces considerably because of the presence of LLRS.

Most of the maximum values of the parameters reduce substantially when compared to bare frame in frames with LLRS considered, so provision of these LLRS can be considered as a possible method for retrofitting.

The fundamental period as obtained by software do not match with the values obtained from the IS code formula and hence the IS code formula for fundamental period requires to be revised to include the effects of structural characteristics.

LIMITATIONS

The present study does not consider the effect of infill action of wall with the bounding frame.

The findings are applicable to single bay structure only.

ACKNOWLEDGEMENTS

The authors wish to thank the authorities of PESIT and Bangalore University for their support.

REFERENCES

Ashaf, M., Siddiqi, Z.A. & Javed M.A. 2008. Configuration of a multistorey building subjected to lateral forces, *Asian Journal of Civil Engineering (Building and Housing)* 9,(5): 527–537.

Indian Standard Code of Practice for Design Loads (other than Earthquake) for Buildings and structures, IS 875–1987, Part 1: Dead Loads, Part 2: Imposed Loads, Part 5: Special Loads and Load Combinations.

Concrete Repair, Rehabilitation and Retrofitting III – Alexander et al. (eds)
© 2012 Taylor & Francis Group, London, ISBN 978-0-415-89952-9

Retrofit of a reinforced concrete building with lead rubber bearing in Iran

M. Jamali Golzar
Sama Technical and Vocational Training College, Islamic Azad University, Sahand Branch, Tabriz, Iran

Y. Yasrebi Nia
Shabestar Branch, Islamic Azad University, Shabestar, Iran

M.A. Jamali Golzar
Ministry of Energy, East Azarbaijan Regional Watercorp, Tabriz, Iran

ABSTRACT: Waste of valuable natural resources and high death toll in recent strong earthquakes has led to revise seismic codes in the earthquake prone countries. The same is true for Iran as one of the most seismically active countries in the world that three revisions have been applied to its seismic code so far. Since Bam earthquake, the seismic assessment for the existing buildings has become a major issue for the construction engineering. In this regard a research has been carried out to assess seismic performance of a nine story reinforced concrete building. Nonlinear static analysis was conducted using procedures recommended in the rehabilitation provisions and results indicated that a large number of frames in both directions exceed life safety performance levels. Base isolation by lead rubber bearing adopted as alternative to retrofit entire building and it caused isolated structure support target displacement without failure on desired safety level.

1 INTRODUCTION

In this paper a reinforced concrete building that has been designed before the publication of third revision of code 2800 is selected as a case study. Since base isolation is one of the most widely accepted techniques to protect structures and to mitigate the risk of life and property from strong earthquakes, this building will be retrofit by utilizing lead rubber isolator. The building in this study is located in Tabriz, the fourth mega city in Iran and one of historically-rich cities of Iran as well as the capital city of Eastern Azarbaijan province. This city needs more attention to retrofit its old buildings and fortunately there is a high demand for such measures and studies. The reason why the building in this study is selected from among residential buildings is the proof of such a big demand.

2 CASE STUDY

Typical plan of the case study is shown in Figure 1. This building was constructed of reinforced concrete structure and the seismic force resisting system in both perpendicular directions is moment frame. The plan layout is 22.5 × 14 meter and its total height is 32 meter that consists of a story with height of 4.2 meter as parking in ground floor and 8 stories with height of 3.2 meter in upper floors. Entire structure were modeled and analyzed using the finite element program ETABS.

3 NONLINEAR STATIC PROCEDURE

Although entire structure meets some limitations to perform linear analysis, nonlinear static procedure can be adapted to assess its seismic performance. A three dimensional static pushover analysis is performed by utilizing displacement coefficient method.

In this paper two different patterns were used proportional to the product of mass and the first mode shape of structure. Also separate pushover analysis in positive and negative longitudinal direction was used as well. Thus for each directions of plan four lateral pushover cases was defined. The pushover curve is given for DYP nonlinear case in Figure 2. It is seen that structure cannot meets target displacement and it need to retrofit by a proper method. Figure 3 shows plastic hinges formation of frame 5 at performance point of structure on DXP case.

In Figure 4 the percentage of plastic hinges formation in structural elements for different pushover cases is presented.

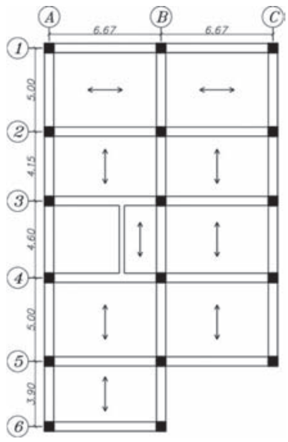

Figure 1. Typical floor plan of existing structure.

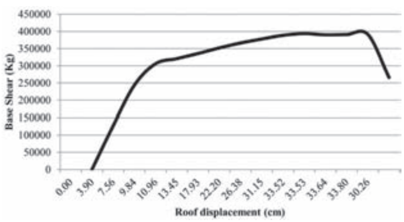

Figure 2. Pushover curve of structure in DYP case.

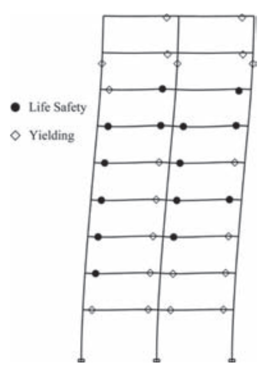

Figure 3. Plastic hinges formation of frame 5 in DXP case.

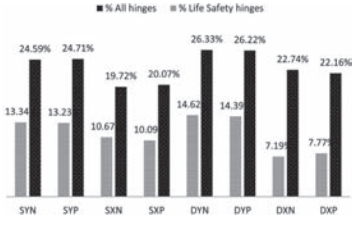

Figure 4. Percentage of plastic hinges formation of the structure.

Table 1. Properties of isolators for outer and inner columns.

Property	Outer LRB	Inner LRB
Effective stiffness (kg/m)	105000	143000
Initial stiffness (kg/m)	89000	120000
Yield strength (kg)	4400	6000
Effective damping	15%	15%

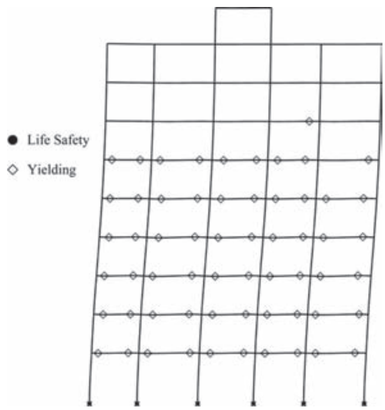

Figure 5. Plastic hinges formation of frame B in base isolated structure in DYP case.

4 RETROFIT OF STRUCTURE BY LRB

The analysis is performed for nonlinear static procedure by utilizing isolators with properties which is shown in Table 1. As it is seen in Figure 5 the LRB isolators restrict the spreading of plastic hinges and change the sequence of plastic hinges formation in the structure.

5 CONCLUSION

In this case, the target displacement estimated by the displacement coefficient method was greater than maximum displacement calculated by pushover analysis. Moreover, about 11% of plastic hinges formation occurred beyond the life safety level.

Based on the results of the analysis, the base isolation technique was selected as best method for achieving to retrofit objectives and providing the most favorable performance as for the reasonable cost. Then, nonlinear static procedure was performed again and it was concluded that:

All beams and columns satisfy life safety requirements at the design hazard level. Besides not only there is not any life safety hinges, but also there is about 13% reduction in overall hinge formation in the isolated structure.

This page intentionally left blank

Theme 4: Developments in materials technology, assessment and processing

This page intentionally left blank

Concrete Repair, Rehabilitation and Retrofitting III – Alexander et al. (eds)
 ISBN 978-0-415-89952-9

Influence of intensive vacuum mixing on the compressive strength of cementitious materials

J. Dils & G. De Schutter
Magnel Laboratory for Concrete Research, Ghent University, Belgium

V. Boel
Departement of Construction, Faculty of Applied Engineering Sciences, University College Ghent, Belgium

EXTENDED ABSTRACT: In the last decades the quality of cementitious materials increased enormously. New high performance construction materials such as Self-Compacting Concrete (SCC) and Ultra High Performance Concrete (UHPC) made it possible to build faster, higher and more elegant. Structural engineers are using the properties of these new materials up to the maximum performance possible. This means that a small variation in mechanical, rheological or durability properties can have a big influence on the final construction. For this reason the concrete industry shows a great interest in technology that can lower this undesirable fluctuations. One aspect is the uncontrollable air inlet during the mixing of the concrete. For this a lowered pressure in the mixing pan can be of great use. A vacuum mixer can control the air inlet during mixing and even lower the air content of the final product. This could have a positive effect on the mechanical properties such as the compressive and tensile strength and Young's modulus. This paper will try to verify whether this new type of mixing can have a positive effect on the compressive strength of cementitious materials.

1 INFLUENCE OF VACUUM MIXING ON THE COMPRESSIVE STRENGTH OF PASTE

In order to investigate the possible effect, compressive tests were performed on paste at an age of 28 days. The results for vibrated paste (VC) and SCC, given in Figure 1 are an average of 6 tests. Because UHPC is a concrete type of which little data is found in literature, the compressive strength (f_c) of the paste was determined as the average of 12 compressive pressure tests.

From Figure 1 can be seen that a lowered air pressure in the mixing pan has the greatest influence on a ultra-high performance paste followed by a vibrated paste. The lowest impact can be seen on a self-compacting paste.

It is reasonable to believe that the increase in strength comes from a lowered air content. Namely, less air bubbles implies more material that can help to withstand the increasing force during a compressive pressure test. This is verified by the measurements of the fresh air content given in Figure 02.

Figure 2 shows the greatest decrease in air content for UHPC which explains partially the strength increase. To know more in detail the effect of a lowered air pressure the hardened air content

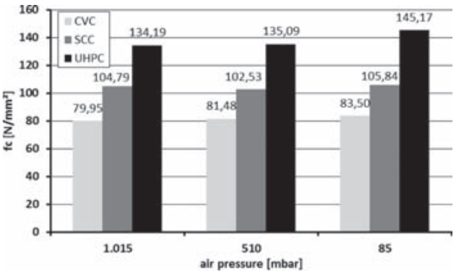

Figure 1. Compressive strength paste (f_c), determined on prisms 40 × 40 × 160 mm at 28 d, in function of the applied pressure in the mixing pan.

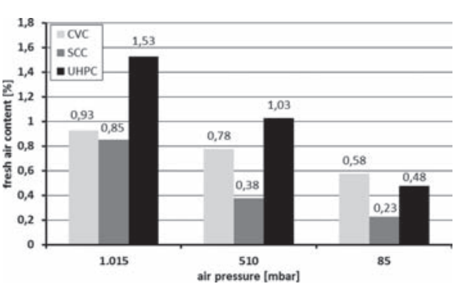

Figure 2. Air content of the fresh paste in function of the applied pressure in the mixing pan.

is determined by the use of air void analyses. The results give an influence on all air bubble sizes of VC and UHPC. Although all size fractions are reduced, the biggest reduction is found for the larger air bubbles.

2 INFLUENCE OF VACUUM MIXING ON THE COMPRESSIVE STRENGTH OF MORTAR

The same test samples as for paste were made for self-compacting mortar and vibrated mortar. The compressive strength (f_c) in Figure 3 is the average of 18 cubes in the case of SCC and 10 cubes in the case of VC. Because of the low d_{50} of the quartz sand, used in UHPC, this concrete can also be used in the comparison between mortar types. The test samples were cubes with size 100 mm and the results in Figure 3 are the average of three compressive pressure tests. The cubes were subjected to a steam treatment of 48 h. After demolding the cubes were placed in a container were a water bath of 90°C produced the necessary steam.

From Figure 3 can be derived, that similar as for paste, the greatest influence of a lowered air pressure in the mixing pan, is seen for UHPC, followed by VC. The smallest effect of the vacuum technique is again obtained for SCC. Furthermore the strength increase of the mortar samples are of the same magnitude as the paste samples. This indicates that the vacuum technique has the same effectiveness for mortar as for paste.

For each mixture the fresh air content was determined. Figure 4 summarizes the effect of the vacuum technique on the air content of mortar. Similar as for paste, the highest reduction is seen for UHPC. This explains partially the increase in compressive strength between atmospheric mixing conditions and almost vacuum mixing conditions.

As for the paste level, air void analyses were performed on mortar specimens. It can be concluded that a lowered air pressure in the mixing pan has an effect on all air bubble sizes. Although the effect is overall visible, the highest influence is again seen for the larger air bubbles. The effect on this air bubbles is even more pronounced for mortar than for paste.

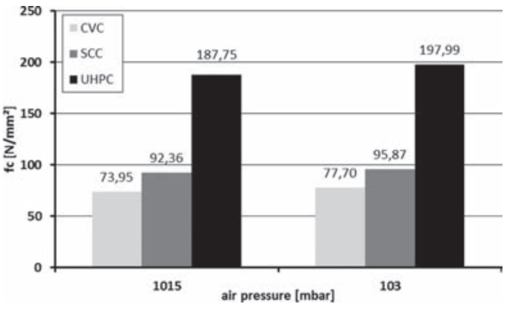

Figure 3. Compressive mortar strength (f_c), determined on prisms 40 × 40 × 160 mm (SCC & VC) and cubes 100 mm (UHPC) at 28 d, in function of the applied pressure in the mixing pan.

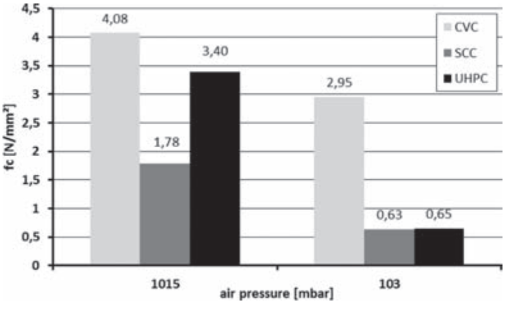

Figure 4. Air content of the fresh mortar in function of the applied pressure in the mixing pan.

ACKNOWLEDGEMENT

The financial support of the Hercules Foundation and of the Fund for Scientific Research Flanders is greatly acknowledged.

Concrete Repair, Rehabilitation and Retrofitting III – Alexander et al. (eds)
© 2012 Taylor & Francis Group, London, ISBN 978-0-415-89952-9

Underwater concreting by using two-stage concrete (Laboratory study)

H.S. Abdelgader & A.S. El-Baden
Department of Civil Engineering, Tripoli University, Tripoli, Libya

ABSTRACT: Placement of concrete underwater is necessary in the implementation of most in-shore, and off-shore structures. The pouring of underwater concrete is considered as a challenge for engineers, even during the design stage or during implementation and supervision. This is due to the fact that many precautions must be taken for the success of casting process. The most important precaution is to protect the fresh concrete during the casting process from the water to avoid the risk of washout of cement paste and segregation of aggregates. Concrete can be placed underwater successfully through good design of concrete mix, and through choosing the most suitable method for placing. There are new techniques for underwater concreting such as grouted aggregate which is known as Two-Stage Concrete (TSC) method. The main objective of the paper is to present the possibility of pouring the concrete underwater by using (TSC) method. A laboratory model was prepared and visually investigated and tested by extracting core samples, performing compressive tests, tensile tests and ultrasonic pulse velocity tests. From the obtained results it has been observed that, it is possible to pour concrete underwater by using two stage concrete in successful way, and it is recommended to develop this research by using different water cement ratios and cement sand ratios to get the optimum mix design and also, different types of aggregates which are available in local quarries.

1 INTRODUCTION

Two-stage concrete (TSC) is defined as concrete produced by placing the coarse aggregate in the place of destination then grouting the cavities (voids) of the coarse aggregate with a special mixture (grout) under pumping tubes extended to the bottom of the form, to fill the voids between aggregate particles, Figure 1. The aggregate that is used in (TSC) should be washed, free of surface dust and fines, the void content of the aggregate should be as optimum as possible. The grout that is used in (TSC) normally consists of ordinary Portland cement and well graded sand, the flow of the grout around the aggregate is essential (Abdelgader 1999). The cost of two stage concrete is less than the cost of normal concrete by nearly 40%. This is related to the reduction of cement content by 30% for the same compressive strength. The main material difference when compared also to normal concrete is that the aggregates are gap-graded with only fine sand commonly less than 2 mm and coarse aggregate usually greater than 20 mm used, thus cutting out the need to use expensive gravels. In addition, there is no need for compaction or vibrating of concrete (Abdelgader 1995). The drying shrinkage of two stage concrete is lower than that of ordinary concrete, due to the contact points between the large aggregate particles.

2 METHOD OF PLACEMENT

The placement of the concrete underwater was experimentally modeled as shown in Figure 2. The steel mold—diameter 600 mm and 600 mm height—was totally filled with water, and made sure there was no leakage or buckling that may occur. 700 mm height and 20 mm diameter two injecting PVC pipes were vertically soaked inside the water; the distance between the two pipes was 300 mm. The soaked height was 600 mm, the same height of the mold, and 100 mm was left above the

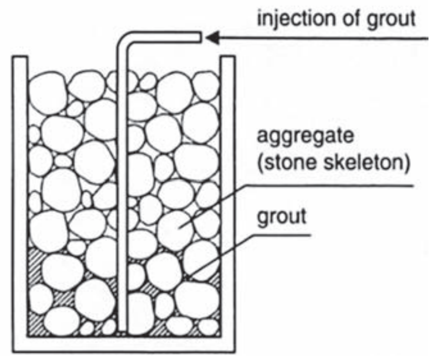

Figure 1. Two stage concrete.

Figure 2. Method of placement.

water level. The aggregate was casted gradually and slowly and distributed as uniformly as possible inside the mold. The aggregate was filled into the total size of the mold and then the grout mix was prepared for as previously described. The grout was pumped directly through the injecting tubes, and the water started to flood out of the mold.

3 CONCLUSIONS

- It is possible to use the local materials to produce underwater concrete by using two—stage concrete.
- Using two-stage concrete for underwater concreting has many advantages such as:
  - No segregation of the aggregate is expected because coarse aggregate is preplaced before adding other concrete mix components.
  - Reducing the amount of washout. This is mainly related to the fact that the amount of the water in the form was mostly replaced by the aggregate and the grout penetrated between the aggregate particles without wash-out.
  - The drying shrinkage of two-stage concrete is expected to be lower than that of normal concrete, due to the direct contact between the coarse aggregate particles. In fact, for the time being, the time dependent deformation properties of two-stage concrete still not clarified and it needs more researches.
- Based on the visual inspection of the extracted cores, the cement mortar totally filled the voids between coarse aggregate particles in addition that the aggregate particles had point-to-point contact.
- The obtained compressive and tensile strength from the extracted cores were considered as acceptable and better results could be obtained, if lower w/c ratio and admixtures were used.
- It is observed from the results of UPV in this research, that the values of pulse velocity measured are high, and that could be related in two stage concrete to the presence of direct contact between the coarse aggregate particles and large quantities of coarse aggregate used. More researches are needed to clarify the suitability of UPV for two stage concrete.
- Since the results obtained in this research is limited to only samples of 600 mm depth, which can not be compared to the field applications of underwater concreting, so more laboratory and field researches using samples of comparable size to the field applications are needed.

REFRENCES

Abdelgader, H.S. 1999. How to design concrete produced by a two-stage concreting method. *J.Cement and Concrete Research*, 29(3): 331–337.

Abdelgader, H.S. 1995. Experimental-mathematical procedure of designing the two-stage concrete. *Ph.D. Dissertation,* Technical University of Gdańsk, Gdańsk, Poland.

American Concrete Institute. 2005. Guide for measuring, mixing, transporting, and placing.

Concrete Society 2008. Underwater concreting. *Technical Report* No. 35. USA.

Warner J. 2005. Preplaced — aggregate concrete. J. *Concrete International*, 27(9): 34–38.

Concrete Repair, Rehabilitation and Retrofitting III – Alexander et al. (eds)
© 2012 Taylor & Francis Group, London, ISBN 978-0-415-89952-9

Robustness improvement of fresh concrete and mortar performance for challenging casting environments with focus on sub-Saharan Africa

W. Schmidt, N.S. Msinjili & H.-C. Kühne
BAM Federal Institute for Materials Research and Testing, Berlin, Germany

M.V.A. Florea
Eindhoven University of Technology, Eindhoven, The Netherlands

G. Senthil Kumaran
Kigali Institute of Science and Technology, Kigali, Rwanda

Paul Nibasumba
Université de Burundi, Bujumbura, Burundi

ABSTRACT: For various concrete applications, the early properties are a major specification, determining the functioning, the mechanical properties, and the durability of structures. The rheological properties of cementitious systems are depending on the water-cement interaction as well as on interactions of chemical admixtures with the cement hydration. The cement hydration, however, is strongly affected by the environmental boundary conditions, such as the climate or the available equipment for the proportioning and dispersion of concrete. This paper presents strategies for the robustness improvement of fresh properties of cementitious systems for challenging and particularly warm climate conditions. After explaining the basic mechanisms affecting the workability, practical conclusions are drawn with special attention on the circumstances of sub-Saharan Africa, where the climatic conditions are difficult and the casting technology is often limited. Solutions are suggested, how despite the disadvantageous circumstances, highly elaborate engineered concrete and mortar can be applied safely and with consistent quality.

1 ROBUSTNESS IMPROVEMENT FOR VERY HIGH TEMPERATURES IN SUB-SAHARAN AFRICANTRODUCTION

This paper focuses on the boundary conditions of sub-Saharan Africa. Here, in most countries and regions the environmental temperatures can be significantly high. Incomplete compaction of concrete due to poor workability at high temperatures can cause a critical reduction of the mechanical properties. It is therefore unavoidable to utilise superplasticizers to achieve steady quality and fully compacted concrete, since they prolong the workability period and make the flow properties independent of the water content.

Due to the fact that high charge density polymers can be consumed too quickly at elevated ambient temperatures, causing rapid loss of flowability, it is beneficial to compose concrete mixtures with superplasticizers that provide a low charge density.

A low charge polymer should also be used to reduce early shrinkage cracks. Low charge polymers are required in higher amounts than high charge polymers. The time of the final set is strongly depending on the amount of polymers, the early deformations caused by settlement, chemical and autogenous shrinkage, however, are less dependent on this. During the first 24 hours large deformations can be observed. Since accordingly mixes with low charge polymers set significantly later than mixes with high charge polymers, a prominent part of the large early deformations can be shifted towards a still plastic state, thus reducing the cracking risk.

For high temperatures it has furthermore been shown that despite the positive effect of dense particle packing on the mechanical properties, mixtures with rather high water to powder ratio should be preferred, since even at rapid crystal growth these leave sufficient clearance for particles to move between each other.

2 CONCRETE IN SUB-SAHARAN AFRICA

2.1 *Concrete technological needs in sub-Saharan Africa and solutions to overcome limitations*

Sub-Saharan Africa demands for special considerations regarding concrete technology. One of the major deficits that can be observed on the whole continent is a low number of cement plants, which is one of the reasons why cement in Africa has to be largely imported and is mostly extremely expensive.

In countries of the Northern hemisphere, concrete has been established for approximately 150 years. The established standards, which are often based on outdated data and can often not keep up with the escalating development during the last two decades, do not always allow engineers to act according to the best available practice. In Africa, concrete technology is rather new, which offers a unique opportunity for an African concrete technology that is based on the highest level of knowledge. In this context, the high cement prices should not be an obstacle for construction with concrete but they should foster concrete technology that does not require high amounts of cement:

– Optimised particle size distributions can reduce the concretes' dependency on the cement content and shift it towards the aggregates.
– Performance based cement blends can significantly reduce the required amount of Portland cement clinker.
– Fillers can be used instead of cement to complement the fines content.
– Superplasticizers typically increase the final strength since the better dispersion of particles causes a more homogenous hydration.

Such a concrete can be described as a sophisticated, engineered mixture composition. Considerations about optimised and robust mixtures, however, are significantly more important for sub-Saharan African countries than they are, for other countries, due to the climatic boundary conditions and the limited technological means. Typically, the words "sophisticated" and "engineered" are closely associated with high costs and a highly developed technology. Hence, in terms of economic and technical capacity, the question has to be discussed, whether good concrete technology is affordable in sub-Saharan Africa and whether it can be brought into practice.

2.2 *African solution for affordable good concrete mixtures*

Many African economies cannot afford expensive construction materials on a broad basis. However, high-level concrete technology does not inevitably have to be expensive. Furthermore, a specific African concrete technology should always take into account locally available raw materials. The main challenges of Africa are housing and infrastructure, which scarcely demand for high performance in terms of mechanical properties. For these applications, high w/cm values should not be considered as a taboo. Stability can be generated, e.g. by using starch-based viscosity modifying agents, which can be derived from Cassava—a widely available crop plant all over Africa. In summary, high performing concrete is rather a question of the awareness of options than a question of money.

2.3 *How to bring good concrete to practice, considering the African boundary conditions*

Another aspect to be discussed is how a good concrete can be brought to practice in sub-Saharan countries, where the boundary conditions for the application differ strongly from Europe, Japan and North America. Sub-Saharan Africa provides virtually no ready-mix industry. Concrete is typically mixed on the construction site, while cement is delivered and stored in 50 kg bags. In most countries of the sub-Saharan Africa, the dosage of constituents and mixing is often conducted manually, without recipe or adequate equipment.

A reasonable solution to bring elaborated concrete technology directly to the construction site can be found from the field of repair mortars and grouts, where pre-fabricated compounds are state of technology. The delivery of pre-fabricated concrete in bags, already including cements, fillers, admixtures, and sand and aggregates can be a reasonable solution for the sub-Saharan African construction site conditions. The compounds, containing engineered mixture compositions, only need to be amended by water. Pre-fabricated full concrete mixes have proven to work properly, even in case of self-compacting concrete under very challenging casting conditions. This practice would reduce the failure sources to a minimum and the pre-fabrication process would ensure a steady, reliable and robust quality throughout a large range of environmental boundary conditions.

3 CONCLUSIONS

Sub-Saharan Africa features many specific boundary conditions that need to be considered if state-of-the-art concrete technology shall be applied. Solutions were developed, how reasonable concrete mixture compositions should be composed to cope with the African environmental boundary conditions.

In order to master the challenging climate, concrete compositions need to be flowable or self-consolidating. A thorough mixture composition is thus of high importance.

Mixture components should be available locally. Bagasse and rice husk ashes can be a good solution to optimise and economise concrete technology. Both materials have not been well investigated world-wide yet. Furthermore, the Great Rift Valley areas have plenty of natural pozzolans available. These need to be taken into account in cement as well as concrete technology.

Without question, cement and concrete technology will play a major role in this context. Europe and North America had more than a century to develop good concrete practice. Sub-Saharan Africa does not have another century to develop good concrete practice. The need to solve infrastructure and housing problems is too urgent. A good way to bring modern concrete technology quickly to the construction site despite the disadvantageous infrastructure for concrete is the establishment of pre-fabricated full concrete compounds with specified performances.

Concrete Repair, Rehabilitation and Retrofitting III – Alexander et al. (eds)
© 2012 Taylor & Francis Group, London, ISBN 978-0-415-89952-9

Technical-economical consequences of the use of controlled permeable formwork

R. Torrent
Materials Advanced Services Ltd., Buenos Aires, Argentina

A. Griesser & F. Moro
Holcim Group Support Ltd., Holderbank, Switzerland

F. Jacobs
TFB (Technische Forschung und Beratung für Zement und Beton), Wildegg, Switzerland

ABSTRACT: A series of tests, applied on a 16-year old panel with one face de-watered by the use of "Zemdrain" CPF ("Z" face"), showed an improvement in hardness and a reduction in the "penetrability" of the treated surface, compared to that in direct contact with the formwork ("F" face). The series included NDT (Rebound and Air-Permeability) and tests on drilled cores: Chloride Migration, Water sorptivity and microscopy observation (both last conducted at different depths). The application of the CPF resulted in an improvement of all the properties tested and can be associated to a w/c reduction from 0.55 to about 0.40. The tests conducted at different depths showed that the CPF's effect of reducing the w/c ratio extends to a depth of 10–30 mm. The cost-efficiency of the use of CPF depends on the local conditions and the surface/volume ratio of the element; for Switzerland, the treatment may become convenient only for relatively thick walls. However, the spread of the use of CPF goes hand-in-hand with the adoption of performance-based specifications, particularly those specifying and controlling the "penetrability" of the concrete on site (end product).

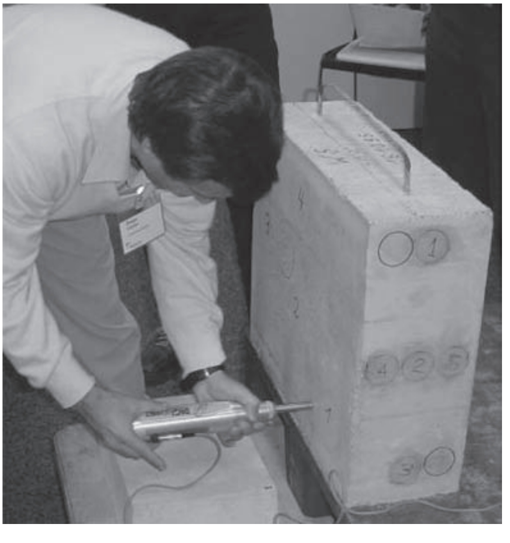

Figure 1. Application of Rebound Hammer on "Z" surface of the panel.

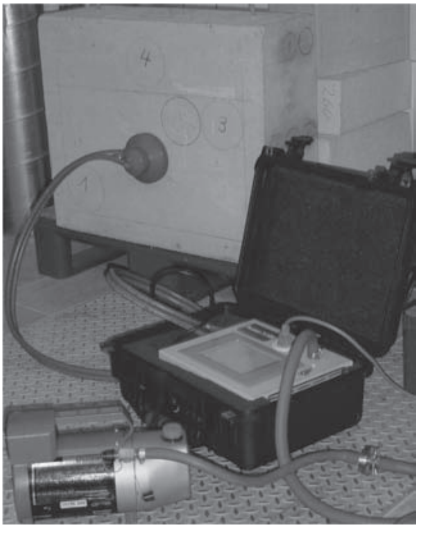

Figure 2. Application of site Air-permeability test on "F" surface of the panel.

1 TEST RESULTS

1.1 *ND tests*

The results of the ND tests conducted on both faces of the panel are summarized in Table 1.

Table 1. Results of ND Measurements on Test Panel.

Test	Rebound [-]		kT (10^{-16} m^2)	
Face	**Median**	**StDev.**	**GeoMean**	**sLOG**
Formwork face	46	4.8	6.6	0.16
Zemdrain face	54	2.1	0.79	0.14

1.2 *Carbonation test*

Table 2. Results of Carbonation test on cored samples.

Test	Carbonation Depth (mm)	
Face	**Mean**	**Maximum**
Formwork face	23	27
Zemdrain face	15	18

1.3 *Chloride Migration test*

Table 3 summarizes the results of Chloride Migration tests conducted on Ø50 mm × 50 mm specimens. The reported values are the Coefficient of Chloride Migration D_{Cl} and the penetration depth of the chlorides X_d

Table 3. Results of Chloride Migration test on cored samples.

	D_{Cl} (10^{-12} m^2/s)		X_d (mm)	
Face	**Mean**	**StDev.**	**Mean**	**StDev.**
Formwork face	29	3.3	43	4.4
Zemdrain face	18	1.5	26	2.2

1.4 *Water Sorptivity tests*

Table 4. Results of Water Sorptivity @ 24 h on cored samples.

	Water uptake (kg/m²) at depth from "Z" face:				
	0–50	**25–75**	**55–105**	**125–175**	**200–150**
Mean	**2.97**	**3.38**	**4.24**	**3.83**	**4.19**

2 COST-EFFECTIVENESS OF CPF

The cost-effectiveness of the CPF liner solution will depend on a number of factors, especially on its capability to reduce w/c ratio, specified strength, cost of installed CPF, price of concrete as function of w/c ratio and surface/volume ratio of the structure.

3 CONCLUSIONS

The results obtained in this investigation yield the following conclusions:

- As expected, the beneficial effects of the use of CPF seem to be permanent as they result from a change of structure of the pore system of the concrete rather than from a temporary sealing of pores.
- Significant improvement in the following properties were measured on the "Z" face of the 16-year panel, compared to the "F" face:
  - A ten-fold reduction in the coefficient of Air-permeability kT.
  - A 20% increase in surface hardness R.
  - A 33–45% reduction in Carbonation depth.
  - A 40% reduction in the coefficient of Chloride Migration D_{Cl}.
  - A 30% reduction in water sorptivity.
- That improvement allows the design of concretes, treated with CPF, of moderate strength (higher w/c ratio) and still of good durability in terms of low "penetrability" of the cover.
- The use of such leaner mix leads to a more sustainable solution and, particularly for rather massive elements, to reduced cracking susceptibility.
- The cost-efficiency of applying a CPF liner (to achieve the specified w/c ratio or durability performance) depends on local conditions and on the surface/volume ratio of the element. For Swiss conditions, a wall at least 1 m thick with one face exposed to an aggressive environment may benefit from the use of CPF (Fig. 3).
- The water sorptivity tests conducted at different depths and the microscopy observation of the microstructure indicate that the effect of CPF in reducing w/c ratio extends 10 to 30 mm from the treated surface.

Despite the advantages of using CPF to enhance the durability of concrete structures, its use is hindered by the strict application of prescriptive specifications (maximum w/c, minimum cement content) and/or specifications based on separately cast control specimens. The application of performance specifications, such as those proposed by the Swiss Federal Highway Administration, based on measuring the coefficient of Air-permeability on site, will certainly facilitate the diffusion of this technology.

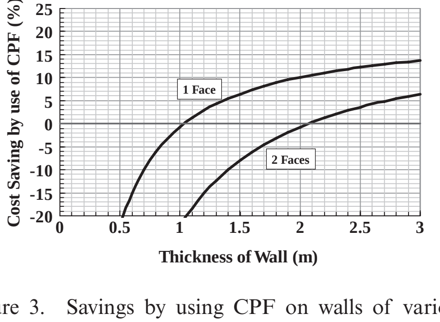

Figure 3. Savings by using CPF on walls of various thickness.

Concrete Repair, Rehabilitation and Retrofitting III – Alexander et al. (eds)
 ISBN 978-0-415-89952-9

An investigation on effect of aggregate grading on fresh properties of Self-Consolidating Mortar

N.A. Libre, A. Pourzarabi, A.M. Etemadrezaei & M. Shekarchi
Construction Material Institute (CMI), School of Civil Engineering, University of Tehran, Tehran, Iran

ABSTRACT: Self-Consolidating Mortar (SCM) due to its high fluidity is an appropriate material for repairing congested reinforced sections. As providing high fluidity may decrease stability, it's worthwhile to study the major factors affecting its fresh properties. Aggregates occupying a considerable volume of SCM have magnificent effect on its fresh properties. The study done in this paper is concerned with the effect of aggregate grading along with Maximum-Size Aggregate (MSA) on fresh properties of SCM. To this end, two series of aggregate grading has been selected, differing in MSA. Each series comprises a concave and an S-curved grading curve. Mortar mixes with each grading type are made in two fluidity levels of 26 ± 0.5 cm and 31 ± 0.5 cm. Fresh SCM experiments of mini slump flow, mini column segregation; bleeding and segregation probe tests are done with the purpose of comparison between mixes. Obtained results show that the S-curved grading mixes lead to enhanced fresh properties. On the other hand, the greater the MSA, the more probable is the risk of instability in fresh SCM.

Keywords: Self-Consolidating Mortar, Aggregate Grading, Maximum Aggregate Size, Fluidity, Stability

1 INTRODUCTION

Self-Consolidating Mortar (SCM) has been used as an efficient repair material. The self-compactibility of repair mortars may bring considerable advantages in narrow molds [2].

A highly workable SCM is being characterized by high fluidity and stability. On the other hand, providing higher fluidity may compromise stability which therefore requires countermeasures to be taken to ensure the good quality of the hardened concrete. Segregation and bleeding may be overcome by increasing the fine aggregate content, by limiting the Maximum Size-Aggregate (MSA); by increasing the powder content or by utilizing viscosity modifying admixtures [3]. Aggregates occupying a considerable volume of concrete, are the key ingredients when adjusting a SCC mix design; therefore it is of high importance to study how aggregates characteristic affect the fluidity and stability of a SCC mix design.

2 EXPERIMENTAL PROGRAM

In this paper the effect of aggregate grading along with MSA on the fresh properties of Self Consolidating Mortar is investigated. To this end, two series of aggregate distributions, as shown in Figure 1, has been selected, differing in MSA. Each series comprises a concave and an S-curved grading. Mortar mixes with each grading type are made in two fluidity levels of 26 ± 0.5 and 31 ± 0.5 cm. Fresh SCM experiments of mini slump, mini V-funnel, mini column segregation, bleeding and segregation probe tests are done with the purpose of comparison between mixes.

The fluidity and side bleeding of the mixtures was evaluated using the mini-slump flow test in conformity with EFNARC [6]. The static segregation resistance of fresh mortars was determined using segregation probe test and mini-column segregation test. The segregation probe test evaluates the vertical segregation in static state and the concrete was stable if the depth is less than 7 mm [8, 9].

The mini-column segregation apparatus was similar to the one described in ASTM C1610 [6]

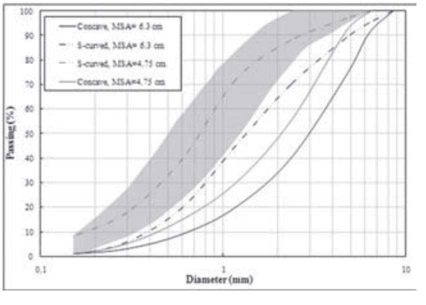

Figure 1. Aggregate size distribution.

but in a smaller size. Based on the previous experiments, the acceptable Static Segregation Index (SSI) for mortar mixtures is SSI ≤30% [4]. The amount of bleeding on top of the column segregation test was also collect as surface bleeding.

3 RESULT AND DISCUSSION

3.1 *Bleeding*

The relationship between MSA and bleeding of SCM for both S-curved grading and concave grading are given in Fig. 2a & b. As is shown, the greater the MSA, the more the bleeding for both types of aggregate grading is. This is due to the reason that the higher the MSA, the less would be the specific surface area of the aggregates and therefore less amount of water is required to surround the solid particles. As is seen, in a constant MSA, changing the grading type form concave to S-curved grading, leads to a decrease in bleeding in both fluidity levels.

3.2 *Segregation*

The results of mini column segregation test are shown in Figure 3. The results indicate that increasing the MSA tends to decrease the static segregation resistance of all mixes; leading to deterioration of workability.

It's worthwhile to note that modifying the aggregate grading curve from concave to S-curved grading, resulted in reducing the SSI for both MSAs. Such a decrease may be due to the fact that the finer the aggregates and the lesser the portion of the coarse aggregates to total aggregates, the higher would be the bond between the solid phase and the paste. As a consequent, the ability of cement paste to hold the aggregates increases and so does the resistance of concrete to segregate.

According to Figure 4, in which the results of probe segregation test are given, the more the MSA, the more the penetration depth of the probe is. This is as a result of the fact that coarse aggregates by their gravity force tend to deposit which leads to formation of a layer with high water content; and hence, very low yield stress, which accounts for the higher depth of penetration. Besides, comparing the results of the column segregation and probe segregation tests shows a good correlation as expected.

Overall, it seems that, in cases where the accessible materials and mechanical requirements impose the coarser aggregate size, more effort should be applied in modifying the aggregate grading by providing enough fine materials to control bleeding and segregation. To this end, one possible way is to modify the aggregate distribution (in this case the S-curved grading).

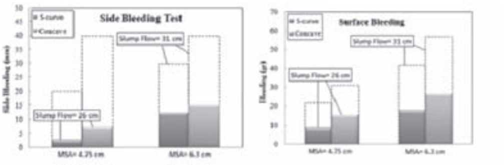

a) Surface bleeding test results b) side bleeding

Figure 2. The relationship between maximum sizes of aggregate and bleeding of mixtures.

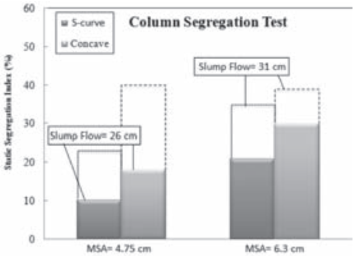

Figure 3. The results of the Column Segregation Test.

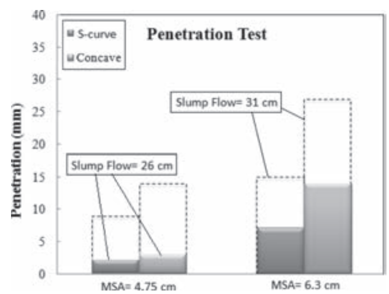

Figure 4. The results of the probe segregation test.

4 CONCLUSION

Based on the results of the investigation, the following conclusions can be drawn:

1. Increasing the MSA leads to an increase in the amount of bleeding for both side bleeding and the surface bleeding test. On the other hand, modifying the aggregate curvature from concave to S-curved grading decreases the bleeding; results in more stable mixtures.
2. Increasing the MSA causes lower resistance to segregation. As for the bleeding test, modifying the aggregate grading leads to a higher resistance of the mixtures to segregation.
3. The higher the fluidity level, the more prone mixtures are to bleeding and segregation.

Concrete Repair, Rehabilitation and Retrofitting III – Alexander et al. (eds)
 ISBN 978-0-415-89952-9

Strength of recycled aggregate concrete for structural uses

S.C. Paul
Civil Engineering Department, Stellenbosch University, South Africa

G.P.A.G. van Zijl
Civil Engineering Department, Stellenbosch University, South Africa

ABSTRACT: The suitability of using Recycled Concrete Aggregate (RCA) in structural concrete based on a better understanding of its strength and stiffness is reported here. Concrete containing RCA at replacement percentages of 0%, 30% and 100% was investigated experimentally for compressive strength classes in the range 30–40 MPa, using three sources of RCA. It was found that RCA replacement by 30% of Normal Aggregate (NA) does not show any significant difference in strength and stiffness compared to concrete containing 100% NA in concrete. Even though RCA100% replacement does show reduced strength and stiffness, this is not significant and can be compensated in standard ways. Concrete produced with the RCA from the three sources showed that better quality RCA in terms of lower absorption and higher strength produces better concrete, although the strength and stiffness improvement was not significant in this low-moderate strength class of 30–40 MPa. Based on the results, recommendations are made on limits for RCA absorption, flakiness index, density and 10% FACT values for this class of concrete made with RCA 30%.

1 INTRODUCTION

Approximately 16 billion tons of concrete was produced world-wide in 2010. This implies a significant environmental impact, amongst others due to aggregate collected from nature. It is important to find alternative sources of aggregate to meet our present and future demands and to reduce the environmental impact. Construction and demolition waste (C&DW), estimated to be 2–3 billion tons annually, place landfill sites in many countries under pressure. Recycling of suitable C&DW provides a solution to both the above impacts. Recycled concrete aggregate (RCA) has been used in several projects world-wide, dominantly in road construction, but also in structural concrete. Compared internationally, the use of RCA in the Republic of South Africa (RSA) is limited and little information is available on its application and performance, although significant quantities of C&DW (5–8 million tons in 2004) are produced in the RSA.

The percentage of replacement of NA with RCA in concrete varies internationally from 10% to 30% and up to 45% for specific applications. Internationally it has been found that RCA30% can be used for structural concrete without significant difference in workability, strength and stiffness compared with NA. Some researchers reported that concrete containing RCA is prone to higher shrinkage, creep and reduced durability even at 30% replacement of NA, but these results vary from country to country and also from different sources of RCA. Therefore there remains a need for more research in this regard.

This paper reports the results of a recent study at Stellenbosch University on the feasibility of RCA replacement of NA. Aggregate physical properties, and fresh and hardened properties of RCA concrete were studied and compared with the associated properties of Natural Aggregate Concrete (NAC).

2 EXPERIMENTAL PROGRAM

Four types of coarse aggregates were used in this work namely three RCAs and one NA. A natural fine aggregate was used. Four stages of experiments used RCA from three different sources, using RCA-1 and RCA-2 in stages 1 and 2 respectively, and RCA-3 in stages 3 and 4. Aggregate physical properties are given in Table 1. Reference mixes (see Table 2) containing 100% natural (Greywacke) aggregate (NA100%) were prepared and tested in stages 1, 2 and 4. Mixes were prepared in accordance with the physical properties for 0%, 30% and 100% replacement of NA with RCA. All aggregates (except RCA-1) were saturated surface dry (SSD) before mixing of the concrete. Tests conducted on these concretes included the slump test and the air content of fresh concrete—see Table 3. For the hardened concrete, the 7, 14, 28 and 56-days cylinder compressive strength and 28 day E-modulus (5 × 150 mm diameter × 250 mm high cylinders per test) and 28-days splitting tensile strength

Table 1. Physical properties of NA and RCA's.

	NA	RCA-1	RCA-2	RCA-3
Used in stage	1–4	1	2	3–4
Size (mm)	9.5–19	9.5–19	9.5–19	9.5–19
Relative density	2.74	2.48	2.52	2.54
Absorption (%)	0.65	5.24	4.40	3.49
10% Fact value (kN)	370	88	125	135
Flakiness index	25	18	19	21

NA - Natural aggregate (Greywacke)
RCA-1 - RCA from the Stellenbosch landfill
RCA-2 - RCA from the Portland quarry, Durbanville
RCA-3 - RCA from the Athlone cooling tower, Cape Town.

Table 2. Concrete mix proportions in kg/m^3.

		NA mixes		RCA mixes	
Materials	Used in stage	70%	100%	30%	100%
CEM II 32.5	1	333		333	
CEM I 42.5	2–3	350		350	
	4	175		175	
GGCS slagment	4	175		175	
Water	1	183		183	
	2–4	175		175	
Malmesbury	1	575	821	246	821
sand FM = 2.46	2–4	469	670	201	640
19 mm stone	1	753.5	1076	322.5	968.5
	2–4	868	1240	372	1185

Table 3. Slump value and % Air of concrete.

	NAC100%		RAC30%		RAC100%	
Stage	Slump (mm)	% Air	Slump (mm)	% Air	Slump (mm)	% Air
1	80	–	55	–	30	–
2	65	2.2	65	2.2	70	2.2
3	65	2.2	50	2.4	30	2
4	40	1.8	50	1.4	30	1.2

(5 × 150 mm cubes per test) and flexural strength (3 × 150 mm square × 450 mm spanning beams per test), were determined experimentally.

3 EXPERIMENTAL RESULTS

Characteristic (5 percentile) cylinder compressive strengths and E-moduli are summarized in Table 4. The compressive strength reduces slightly upon replacement of NA with RCA. The E-modulus appears to be virtually unaffected at a replacement level of 30%, but a consistently lower E-modulus is found for RCA100%.

Table 4. Characteristic (5 percentile) compressive cylinder strengths and E-moduli.

Stage 1			Stage 2		
Case No	$f_{k,cy}$(MPa)	E_k(GPa)	Case No	$f_{k,cy}$(MPa)	E_k(GPa)
NCA100	27.18	35.03	NCA100	30.24	31.67
RCA30	26.4	34.01	RCA30	27.33	32.22
RCA100	26.74	29.91	RCA100	26.45	23.42
Stage 3			**Stage 4**		
Case No	$f_{k,cy}$(MPa)	E_k(GPa)	Case No	$f_{k,cy}$(MPa)	E_k(GPa)
NCA100	30.24	31.67	NCA100	34.09	28.56
RCA30	28.23	34.55	RCA30	33.9	32.02
RCA100	28.29	28.11	RCA100	32.41	25.76

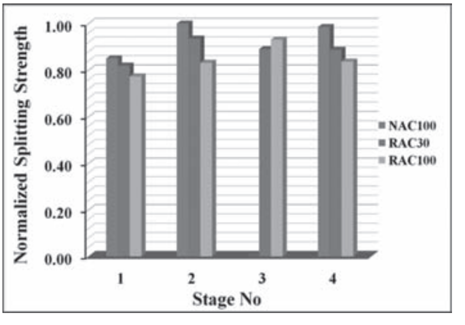

Figure1. Average splitting strength of concrete of different stages.

Both flexural and splitting strengths (see Figure 1) are slightly reduced upon NA replacement with RCA.

4 CONCLUSIONS

Higher quality RCA is represented by a higher density and 10% Fact value, and lower absorption. There are no clear indications that higher **quality RCA** produces higher strength concrete, for the concrete strength class considered here. However, the RCA quality had no significant influence on E-modulus, or on flexural and splitting strengths.

The **amount of RCA** does influence concrete stiffness and indirect tensile strength. At 30% replacement of NA the E-modulus is virtually unaffected or even slight increased, but at 100% replacement it is consistently reduced.

A 30% replacement level of NA with RCA of reasonable quality is recommended in this concrete strength class, based on strength and stiffness considerations. It may be possible to use 100% replacement, but this must be confirmed by experimental data on dimensional stability and durability, as well as a larger statistical base of stiffness and strength data.

Concrete Repair, Rehabilitation and Retrofitting III – Alexander et al. (eds)
© 2012 Taylor & Francis Group, London, ISBN 978-0-415-89952-9

Concrete containing steel slag aggregate: Performance after high temperature exposure

I. Netinger
Faculty of Civil Engineering, Josip Juraj Strossmayer University of Osijek, Osijek, Croatia

M. Jelčić Rukavina & D. Bjegović
University of Zagreb, Zagreb, Croatia

A. Mladenovič
Slovenian National Building and Civil Engineering Institute, Ljubljana, Slovenia

ABSTRACT: Due to the fact that steel slags are made at the temperatures up to 1600°C, utilisation in concretes with improved properties after the exposure to high temperatures is considered in this paper. An experimental program was designed and carried out to study properties of four steel slag based concrete mixtures with different types of cement pastes and conventionally used dolomite concrete prior and after heating up to 800°C. The results obtained have shown that residual mechanical properties of concrete made with steel slag aggregate are comparable to the reference dolomite concrete up to the temperature of ca. 550°C, while at higher temperatures, steel slag exhibits mineral transformation which reflected negatively on the residual properties of slag based concrete mixtures. This expansion become stable if the slag was previously heated up to 1000°C.

1 INTRODUCTION

Theure primary aim of this study, as a part of E! 4166 EUREKABUILD FIRECON project was to ascertain the properties of concrete prepared with steel slag aggregate after the exposure to high temperatures. Four concrete mixtures, made from steel slag aggregate from a Croatian steel plant landfill were studied with respect to different types of cement pastes including portland cement, fly ash as 20% replacement of portland cement and polypropylene fibres in the amount of 1% by volume respectively. The fire performance of the steel slag aggregate concretes obtaining compressive strength, modulus of elasticity, weight loss, ultrasonic pulse velocity, SEM and dilometrical analysis before and after heating was compared with the dolomite aggregate concrete.

2 EXPERIMENTAL STUDY

2.1 *Concrete mixture details*

The mix proportions of studied concretes are listed in Table 1. The reference mixture (M1) was completely prepared with dolomite aggregate, while the other four mixtures, M2 to M5, were prepared from the slag from Sisak steel plant as a coarse aggregate (4–8 mm and 8–16 mm) and dolomite fines (0–4 mm).

3 RESULTS AND DISCUSSION

3.1 *Residual compressive strength*

Figure 1 presents the variation of the residual relative compressive strength (in percent of the initial value) versus the temperature.

It is worth pointing out that at temperature range between 600°–800° a sharp drop of around 35% for all steel slag based mixtures occurred. It is obvious that type of the used aggregate has predominant influence on the residual compressive strength of slag based mixtures.

3.2 *Residual modulus of elasticity*

Figure 2 presents the variation of the modulus of elasticity (in percent of the initial value) versus the temperature. As per compressive strength, after heating to temperature of 800°C residual modulus of elasticity of dolomite based mixture is higher (19%) than in the case of all slag based mixtures (0–8.5%).

3.3 *Microstructural investigation*

Figure 3 a,b show SEM images of concrete mixtures after exposure to temperature of 800°C.

The grain of dolomite suffered more microcracks (Figure 3a) than grain of slag which remained almost intact (Figure 3b). Wider microcracks occured at the interface of slag grain and cement matrix (Figure 3b) for slag based mixture.

Table 1. Concrete mixtures details.

Constituent/Mixtures	M1 (D-pc)	Mixtures with steel slag aggregate M2 (SL-pc)	M3 (SL-pc-ppf)	M4 (SL-pc-fa)	M5 (SL-pc-fa-ppf)
Cement (kg/m^3)	400	400	400	320	320
Fly ash (kg/m^3)	–	–	–	80	80
Water/binder	0.43	0.43	0.43	0.43	0.43
Superplasticizer (l/m^3)	3.20	3.20	3.20	3.00	3.00
Dolomite, 0–4 (kg/m^3)	807	864	864	864	864
Dolomite, 4–16 (kg/m^3)	1028	–	–	–	–
Slag, 4–8 (kg/m^3)	–	422	422	422	422
Slag, 8–16 (kg/m^3)	–	723	723	723	723
Polypropylene fibres (% by vol)	–	–	1	–	1

Upper case letters denote type of used coarse aggregate (D—dolomite, S-slag), while lower case letters denote constituents of cement pastes (pc—portland cement, ppf—polypropylene fibres, fa—fly ash).

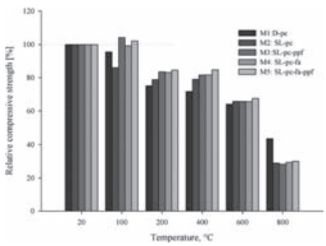

Figure 1. Relative compressive strengths of studied types of concrete vs. temperature.

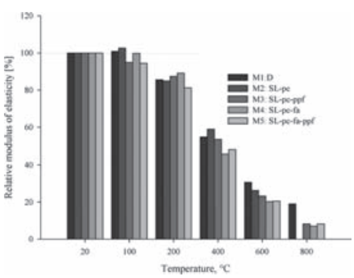

Figure 2. Relative modulus of elasticity of studied types of concrete vs. temperature.

3.4 *Dilatrometrical investigation of aggregate*

The linear thermal expansion of the dolomite and slag grains during exposure to temperature of 1000°C is presented in Figure 4 (full lines).

It seems that observed phase transformation (which is proved by literature review) of steel slag aggregate at temperature between 550°–800°C could be connected to pronounced microcracks occurrence at the interface of slag and cement matrix. Dotted curve at Figure 4 presents the stable expansion of slag heated before utilization in concrete to temperature of 1000°C with heating rate of 5°C/min.

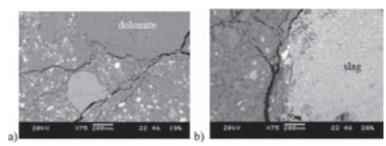

Figure 3. SEM analysis of a) Dolomite based concrete and b) Slag based concrete after heating to 800°C.

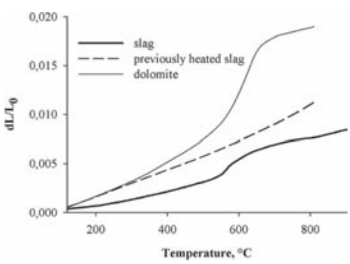

Figure 4. Results of the dilatometrical analysis.

4 CONCLUSIONS

Residual mechanical properties of steel based mixtures are comparable with dolomite based mixture up to the temperature of 550°C.

Mineralogical and dilatometrical analysis show that steel slag aggregate at temperature higher than 550°C experience the unstable expansive mineralogical transformation, find in available literature as transformation from wüstite into magnetite which results in pronounced microcracking at the interface aggregate—cement matrix. These microcracks, in turn, affect negatively the mechanical performance of slags based concretes. Literature review shows that this transformation is irreversible and if heated to temperature of 1000°C prior to use in concrete, slag become stable which is proved in this study. Further research will be based on testing of the concrete made with previously heated slag.

Concrete Repair, Rehabilitation and Retrofitting III – Alexander et al. (eds)
© 2012 Taylor & Francis Group, London, ISBN 978-0-415-89952-9

Completely Recyclable Concrete: How does the cement paste behave during reclinkering?

M. De Schepper, R. Snellings & N. De Belie
Magnel Laboratory for Concrete Research, Department of Structural Engineering, Ghent University, Ghent, Belgium

K. De Buysser & I. Van Driessche
SCRIPTS, Department of Inorganic and Physical Chemistry, Ghent University, Ghent, Belgium

ABSTRACT: It is known that the concrete industry has a big impact on the environment: large amounts of natural resources are used for aggregate and cement production, the cement manufacturing process is energy intensive and is responsible for 5–8% of the global anthropogenic carbon dioxide emissions. Last but not least, the construction sector is an important producer of waste. For this reason the concept of Completely Recyclable Concrete (CRC) has been developed. After the demolition of a CRC construction, the material cycle is closed as the concrete rubble is given a second life as raw material for cement production, without need for ingredient adjustments. Therefore, the concrete mixture is designed to be chemically equivalent to the raw material for cement production. Of course, cement is an important ingredient within CRC and in this study, it is investigated how the hydrated cement paste behaves during reclinkering. Therefore, the reactions occurring during heating and reclinkering of a hydrated cement paste and of a CRC sample were investigated and compared.

A hydrated cement paste and a hydrated CRC sample were ground in a planetary ball mill. Samples were fired at predefined temperatures up to 1450°C and quenched in order to study the clinker or pre-clinker phase assemblage. A series of X-ray Diffraction (XRD) analyses were then performed on the obtained clinkers. Microscopic analyses were used to visualize the different clinker minerals with a water and nital etch.

1 INTRODUCTION

Concrete production has a big impact on the environment. The manufacturing of cement, an important concrete ingredient, is energy intensive and responsible for 5–8% of the global anthropogenic carbon dioxide emissions [ISO (2005); Damtoft et al. (2008)]. The concrete industry is also known as a big waste producer and last but not least, the concrete production process uses large amounts of natural resources for aggregate and cement production.

Nevertheless, the concrete industry is fully aware of these problems and takes efforts to repair, rehabilitate and retrofit today's concrete constructions, which is one of the roads towards a more sustainable construction industry. However, the life of a concrete construction will eventually end and at that moment the problem of waste treatment occurs, and recycling seems the best option. Regarding concrete it is easily seen that cement and concrete production share some common base materials. From this, the idea came up to connect both life cycles and to design a Completely Recyclable Concrete (CRC) that will become a technical resource for cement production after demolition. In order to make CRC a suitable cement raw material, without the need for ingredient adjustments, the concrete mixture should be chemically equivalent to a traditional cement raw meal. Obviously, a CRC also contains cement and in this study it was investigated how the hydrated cement paste behaves during reclinkering, the main intermediary product within cement production.

2 MATERIALS & METHODS

For this study a CRC and a hydrated cement paste (CEM I 52.5 N, W/C 0.4, 28 days old) were used as raw materials for clinker production. These raw materials were ground in a planetary ball mill and pelletized. The pellets were then heated in an electric furnace up to 1050, 1150, 1250, 1350 and 1450°C. The clinker was immediately cooled in air.

A series of X-ray diffraction (XRD) analyses were then performed on the obtained clinkers. Microscopic analyses were used to visualize the different clinker minerals with a water and nital etch.

3 RESULTS & DISCUSSION

3.1 *X-ray diffraction analysis: The clinkering reactions from 1050 up to 1450°C*

At 1050°C the main phases are free lime and belite, besides ferrite (C_4AF) and early intermediate phases such as mayenite ($C_{12}A_7$) and ye'elimite (C_4A_3S) for both clinkers and gehlenite (C_2AS) for CRC clinker. The latter also contains already some aluminate (C_3A).

Free lime and most of the belite phase will be consumed for the formation of alite (C_3S) at higher temperatures. For the CRC clinker, the lime/belite to alite transformation takes place from 1150 up to 1350°C. In case of the cement paste, the main conversion happens between 1150 and 1250°C. For both clinkers the intermediate phases such as mayenite and ye'elimite transform into aluminate and gehlenite changes to alite between 1150 and 1250°C. Ferrite is present at all temperatures for both clinkers, but the amounts can vary little.

At a final temperature of 1450°C, the major clinker phases are present in both clinkers. The alite to belite ratio of the CRC clinker is higher, which is favourable as alite is the most reactive. The CRC clinker contains mostly aluminate and some ferrite, while the opposite is true for the cement paste clinker.

3.2 *Light microscopy: The spatial distribution of the clinker phases*

The porosity in both clinkers decreases with increasing temperature. Comparing both clinkers with each other, the clinker obtained from CRC seems more porous than the one originating from a hydrated cement paste.

At a temperature of 1050°C, melt phases are already formed for both clinkers, which contain some well-formed belite crystals in case of clinker obtained from the cement paste. Increasing the burning temperature stimulates the melt formation in both clinkers, although more melt is formed in case of the cement paste clinker. Besides this, the cement paste clinker is also characterized by an earlier formation of well-formed belite and alite crystals, at a temperature of 1050 and 1150°C, respectively. In the CRC clinker, such alite and belite crystals are observed from 1350°C onwards, although the distribution of these minerals will never be as nice as in the cement paste clinker, in which the alite and belite phases are nicely surrounded by a melt.

3.3 *The effect of sulphates on the clinkering process*

By microscopic investigation it is shown that the burnability of the cement paste clinker is better. This effect is probably caused by the higher SO_3 content of the cement paste, which is known to lower the temperature of the melt formation and to reduce the melt viscosity [Taylor (1997)]. However, SO_3 is also known to stabilize belite at the expense of alite.

This effect is seen for the cement paste clinker when the potential mineralogical composition is calculated using the traditional formulas of Bogue [Taylor (1997)]. According to these calculations, the cement paste should have a higher alite and lower belite content compared with the CRC clinker. However, XRD and microscopic analysis of clinker burned at 1450°C showed that the opposite is true. The cause of error in the Bogue calculations is found in the composition of the major phases which contain significant proportions of substituent ions, and phases thus do not have the assumed compositions.

In order to optimize the Bogue calculation, it is best to use the best available estimates of the composition of the four major phases, which can be found in literature. In this paper the modified Bogue calculations described in Taylor (1997) are used. It is shown that the XRD and microscopic results indeed have a better agreement with the modified Bogue calculations.

4 CONCLUSION

This paper proves that the sulphate present in a cement paste has important consequences for the alite to belite ratio of the clinker sintered from this material. However, regarding the regeneration of cement from CRC, this effect is diluted due to the rather low cement content of a CRC.

ACKNOWLEDGEMENTS

Financial support for this study from the Institute for the Promotion of Innovation through Science and Technology in Flanders (IWT-Vlaanderen) and the Research Foundation—Flanders (FWO) is gratefully acknowledged.

REFERENCES

Damtoft, J.S., Lukasik, J., Herfort, D., Sorrentino, D. & Gartner, E.M. 2008. Sustainable development and climate change initiatives. *Cement and Concrete Research* 38(2): 115–127.

ISO 2005 Business Plan. ISO/TC 71 Concrete, Reinforced Concrete and Prestressed Concrete.

Taylor, H.F.W. 1997. Cement Chemistry. London, Thomas Telford Publishing.

Concrete Repair, Rehabilitation and Retrofitting III – Alexander et al. (eds)
© 2012 Taylor & Francis Group, London, ISBN 978-0-415-89952-9

Influence of particle packing on the strength of ecological concrete

S.A.A.M. Fennis, J.C. Walraven & J.A. den Uijl
Delft University of Technology, Delft, The Netherlands

ABSTRACT: Energy consumption and CO_2-emission of concrete can be reduced when cement is replaced by secondary materials such as residual products from other industries. However, for the application of such environmentally friendly concretes, predicting their performance is very important. In this article the relation between packing density and strength of mortar mixtures is presented. 50 mortar mixtures were tested on flow value and cube compressive strength at 7 and 28 days. The packing densities were calculated with the Compaction-Interaction Packing Model, using the experimentally determined packing densities of the cement, sand and quartz powder. The increased packing density in mixtures with fine quartz powder M600 resulted in a 14% strength increase compared to the reference mixture. The presented relationship between the cement spacing factor and strength can be used to design ecological concrete mixtures and predict their strength based on their packing density.

1 INTRODUCTION (SUMMARY)

In a concrete mixture the cement is responsible for more than 50% of the CO_2-emission. Energy consumption and CO_2-emission of concrete can be reduced when cement is replaced by secondary materials such as residual products from other industries.

Water/binder ratio and types of binders and fillers are the main factors influencing the hydration process and the resulting internal microstructure of concrete, and thus also the material properties such as strength. Therefore, it is very important to select the right type of fillers and control the water demand, especially in defined-performance concrete with high amounts of fillers, such as ecological concrete or high strength concrete. For this reason a new particle packing model was developed to optimize the particle packing in concrete.

In this article it is shown in which way particle packing influences the particle structure of concrete and thus the water demand and strength.

2 RESULTS

Replacing part of the cement by the coarse fillers M6 and M300 decreases the packing density, while replacing cement by the fine filler M600 shows an improvement of the packing density. With increasing amount of filler the strength decreases, which was expected based on the water/cement ratio. However, compared to the use of M6 and M300, replacing cement by M600 leads to higher strengths at each replacement level, Figure 1.

The flow value measurements of the mortar mixtures show that replacing cement by quartz powders M6 and M300 has less influence on the workability of the mixtures than replacing cement by M600. Increasing the amount of M600 in a mixture increases the workability. This is contrary to the idea that increasing the specific surface area of the powders will reduce the workability. The results can be explained by the higher packing density of the mixtures containing an increasing amount of M600 (up to 40%). When the packing density increases, such as in mixtures E10–E13 the voids content ε decreases and more water becomes available to make the mixtures flow.

The increased packing density and increased flowability that are the result of replacing cement with M600, can be used to optimize mixtures. This was done for mixtures E14 and E15 which were designed to have the same flowability as the reference mixture E1. Because of the increased packing density, these mixtures require less water to fill the

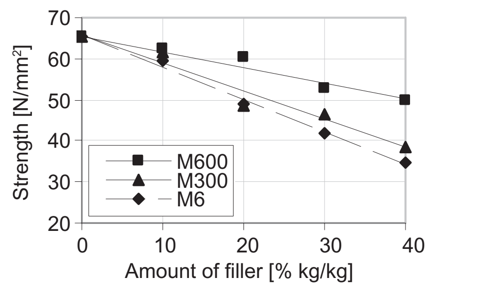

Figure 1. 28-day cube compressive strength of mortar beams series E.

voids. Therefore, the required amount of water at this consistency level could be reduced by more than 20%. In this way it is possible to use the increased packing density to reduce the cement content as well as the water demand. Mixture E15 with 20% [kg/kg] M600 shows a 14% strength increase compared to the reference mixture. The water/cement ratio was constant, so this strength increase might be explained by the improved packing density combined with possible pozzolanic activity and increased nucleation area (Kronlöf 1997, Poppe & Schutter 2005). The mixtures show clearly the suitability of filler M600 and the advantage of the increased particle packing density to replace cement while retaining a constant water/cement ratio.

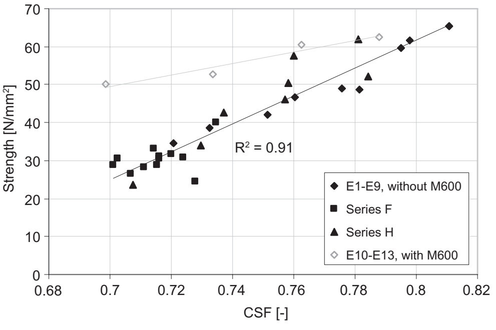

Figure 2. The cube compressive strength in relation to the cement spacing factor CSF for mixtures of series E, F and H ($K_t = 9$).

3 PACKING DENSITY AND STRENGTH (SUMMARY)

The strength measurements on the mortar mixtures of series E, F and H did not show a direct relation between packing density and strength, due to varying amounts of water present in the mixtures. The different water/cement ratios in the mixtures should be taken into account when evaluating the influence of packing density on strength. For that reason, a new factor is introduced: Cement spacing factor (CSF).

Hypothetically, the spacing between the cement particles should be related to the strength of the concrete or mortar mixture. With a higher amount of water and higher water/cement ratio, the cement particles are further apart. In that case, during the hydration process, the hydration products of the cement particles need to bridge a larger distance, eventually leading to a lower strength. With a high packing density in the mixture, cement particles and other particles are close to each other, making the space that needs to be filled by hydration products smaller.

For the total cement spacing this leads eventually to Eq.1.

$$CSF = \frac{\varphi_{cem}}{\varphi_{cem}^{*}\frac{\alpha_t}{\varphi_{mix}}} = \frac{\varphi_{cem}}{\varphi_{cem}^{*}}\frac{\varphi_{mix}}{\alpha_t} \qquad (1)$$

Fifty mortar mixtures were analyzed on the CSF compared to the experimentally determined 28-day cube compressive strength, Figure 2.

4 CONCLUSIONS AND RECOMMENDATIONS

The packing density of a powder or mixture in itself is a powerful parameter in the design of concrete mixtures. It helps to determine the suitability of fillers as cement replacing material and is related to the flowability and strength of mixtures. Very fine fillers, with high surface area can increase packing density to such an extent that the water/cement ratio can be decreased when cement is replaced by them. This shows water demand is not just surface area related as often stated in water layer theories.

The maximum packing density of the tested mixtures was not directly related to the flow value or compressive strength. However, in each mixture part of the added amount of water is used to fill voids, while the rest (the excess water) is used to lubricate particles and provide flowability. The relative amount of excess water pushes the cement particles further away from each other, thus increasing the volumetric distance between the cement particles. In that case, higher water/cement ratios and lower packing densities lead to a larger spacing between the cement particles and thus eventually to a lower strength due to the fact that the hydration products of the cement particles need to bridge larger spacings. The spacing between the cement particles is expressed as the cement spacing factor, which depends on the maximum packing density, the amount of water and the volume fraction of the cement particles. Mortar tests show a good relation between the cement spacing factor and the compressive strength of a mixture.

These results were used to design ecological concrete mixtures and predict their strength based on their packing density in the Ecological Concrete project at Delft University of Technology. The project showed that by selecting the right types of fillers as cement replacing materials, concrete could be designed with reduced cement contents, while at the same time the concrete mixtures still satisfied the demands for appropriate use.

Concrete Repair, Rehabilitation and Retrofitting III – Alexander et al. (eds)
 ISBN 978-0-415-89952-9

Development of geo-polymer based Ductile Fibre Reinforced Cementitious Composites (DFRCC)

S.F.U. Ahmed, M. Hossain & Y.Y. Lu
Department of Civil Engineering, Curtin University, Perth, Australia

ABSTRACT: This paper presents the development of geopolymer based Ductile Fibre Reinforced Cementitious Composites (DFRCC) containing steel and two types of Polyvinyl Alcohol (PVA) fibres. The fibres are used in mono form in the development of both cement based and geo-polymer based DFRCCs. The effects of two different sand sizes (1.18 mm, and 0.6 mm) and sand/binder ratios (0.5 and 0.75) on the deflection hardening and multiple cracking behaviour of both types of DFRCC are also evaluated. Results revel that the deflection hardening and multiple cracking behaviour can be achieved in geo-polymer based DFRCC similar to that observed in cement based system. For a given fibre type, sand size and sand content, comparable Modulus of Rupture (MOR) and the deflection at peak load are observed in both cement and geo-polymer based composites. The newly developed geo-polymer based DFRCC exhibit a significant benefit over cement based system as the former one is *green* in terms of *no cement use*.

1 INTRODUCTION

High performance fibre reinforced cementitious composites (HPFRCC) have been steadily developed in the last two decades. One of the salient features of HPFRCC is its strain hardening and multiple cracking behaviours in both tension and bending (Naaman & Reinhardt, 2006). It is a short fibre (metallic and/or non-metallic) reinforced cement based composites where fibre content between 2% and 3% by volume appears to be the most attractive due to ease of processing. Great interest in this area is observed through the development of engineered cementitious composites (ECC) (Li & Wu, 1992) and ductile fibre reinforced cementitious composites (DFRCC) (JCI, 2003). Ductile fibre reinforced cementitious composites (DFRCC) is cement based composite reinforced with short random fibres which exhibits deflection-hardening and multiple-cracking behaviours in bending. It is a special class of HPFRCC that has higher deflection capacity than that of regular fibre reinforced concrete (FRC) and exhibit deflection hardening and multiple cracking behaviours. However, current version of DFRCC is limited to cement rich matrix, although the replacement of cement with fly ash is reported in few studies (Ahmed, et al., 2007).

The need for environmentally friendly construction materials for sustainable development is an important issue in the present time. The concrete industry is said to be one of the significant contributors to global warming. This fact is due to the use of Portland cement as the main component in making concrete and cement based composites. The cement industry is responsible for about 6% of the CO_2 emission, which is the main cause of the global warming. However, the use of concrete and cement based composites as the most widely used construction materials are still unavoidable in the foreseeable future. In this respect, the efforts of using supplementary cementitious materials or finding alternatives to Portland cement are necessary. The introduction of "geo-polymers" as a novel binder promises to be a good prospect for introduction into the concrete industry as an alternative to Portland cement. Geo-polymer concrete is a 'new' material that does not use Portland cement as a binder. Instead, a source of material such as fly ash, that is rich in Silicon (Si) and Aluminium (Al), is reacted by alkaline liquids to produce the binder (Hardjito & Rangan, 2005). Considerable research have been conducted on geopolymer concrete (Rangan, 2007). However, very little is reported on the fiber reinforced geopolymeric composites (Yunsheng et al., 2009; Dias & Thaumaturgo, 2005; Li & Xu, 2009; Bernal, et al., 2006). However, none of the above studies reported deflection hardening or strain hardening behaviour in bending or tension.

This paper reports the preliminary results on the development of geo-polymer based DFRCC where the cement binder in DFRCC is replaced by fly ash based geo-polymer binder. The fly ash is activated by alkaline liquids (sodium hydroxide and sodium silicate). The newly developed geo-polymer based

DFRCC is the first of its kind in the field of HPFRCC where Portland cement is completely replaced by class F fly ash.

2 RESULTS

2.1 *Deflection hardening behaviour of geopolymer based DFRCC*

Generally, the composite containing 2% steel fibre exhibited much higher modulus of rupture (MOR) that those containing PVA-1 and PVA-2 fibres of the same volume fraction irrespective of matrix system, sand contents and sand sizes. But its deflection capacity (deflection at peak load) is much lower than that containing PVA-2 fibre. However, its deflection capacity is comparable to that containing PVA-1 fibre. The higher MOR and smaller deflection capacity of steel fibre reinforced DFRCC compared to its counter parts PVA fibres system is due to the high modulus of steel fibres. The lower MOR with considerable higher deflection capacity of PVA fibre reinforced composites are due to low modulus of PVA fibres. Other researchers also observed similar behaviour in both steel and PVA fibre reinforced cement based composites (Ahmed, et al., 2007). The geopolymer based DFRCC exhibits comparable deflection hardening and multiple cracking behaviour to cement based system with only exception with the composite containing PVA-2 fibre, where no deflection hardening behaviour is noticed. It could be attributed to the high fibre/matrix bond and the low strength of PVA-2 fibre. Previous research suggests that, in addition to friction bond, chemical bond also develops between PVA fibre and cement matrix (Kanda & Li, 1999). In the case of geopolymer matrix, the chemical bond might be even higher than that of cement based matrix, which might adversely, affected the deflection hardening behaviour of the composite containing PVA-2 fibre. But it is not in the case of geopolymer based DFRCC containing PVA-1 fibre, whose deflection capacity is higher than that of cement based system, which is still not clear and need to be thoroughly investigated through measuring the frictional bond of PVA fibers in geopolymeric matrix.

2.2 *Effects of sand/binder and sand sizes on the deflection hardening behaviour*

By lowering the sand content, the improvement in the deflection hardening behaviour in cement based DFRCC containing PVA fibre is observed. However, the same composite containing steel fibre does not exhibit such improvement. Improvement in deflection hardening behaviour of geopolymer based DFRCC is also observed similar to that observed in cement based system except the composite containing PVA-2 fibre. In case of cement based system, the deflection hardening behaviour is affected by increasing the sand size, especially in the case of steel and PVA-1 system. Interestingly, no such adverse effect is noticed in PVA-2 fibre reinforced composite. In the case of geopolymer based system, a different scenario is observed, where better deflection hardening behaviour is observed by increasing the sand size in the case of PVA-1 fibre system. No such improvement is observed in steel fibre reinforced composite similar to that observed in cement based system. No deflection hardening behaviour is also observed in geopolymer based DFRCC containing PVA-2 fibre.

3 CONCLUSIONS

Within the limited fibre types, sand contents and sand sizes used in this study, the following conclusions are made:

- Deflection hardening behaviour is achieved in the geopolymer based DFRCC containing 2% steel fibre by volume.
- Deflection hardening behaviour is also achieved in the geopolymer based DFRCC containing 2% PVA-1 fibre by volume.
- No deflection hardening behaviour is noticed in the geopolymer based DFRCC containing PVA-2 fibre by volume. This could be due to high bond of fibre/matrix interface and the low strength of PVA-2 fibre.
- The increase in sand content and sand size adversely affected the deflection hardening behaviour of cement based DFRCC.
- An opposite trend is observed in case of geopolymer based DFRCC system where deflection hardening behaviour is improved by increasing the sand size and sand content.

Concrete Repair, Rehabilitation and Retrofitting III – Alexander et al. (eds)
© 2012 Taylor & Francis Group, London, ISBN 978-0-415-89952-9

Load-deformation behavior of hybrid elements of PCC and CC under flexural stress

A. Flohr & A. Dimmig-Osburg
Bauhaus-Universität Weimar, F.A. Finger-Institute of Building Material Science, Professorship Polymer Materials, Weimar, Germany

ABSTRACT: Alongside many advantages, PCC (Polymer-modified Cement Concrete) also has some drawbacks. Compared to CC (Cement Concrete) the advantages of PCC are the improvement of workability, adhesive bonding and elasticity, as well as the increasing of flexural and tensile strength, ductility and not least of durability. Drawbacks are the increased viscous and plastic deformation under loading, the decrease of degree of hydration and the lower compressive strength. One solution to be able to use the advantages of PCCs to their full capacity and to compensate for the drawbacks is the use of hybrid elements of PCC and CC. Initial tests were performed on statically loaded samples to determine the deformation behavior of PCC and of CC. Then load tests were performed on hybrid beam elements, which consisted of a 70 mm layer of CC cast wet-in-wet on a 30 mm layer of reinforced PCC. It was found that the load-deformation behavior of the hybrid elements differs significantly from that of the reference samples made solely of CC, and can be regarded as favorable. An increase of flexural strength as well as an increase of the initial crack load could be observed on the hybrid elements. The crack distribution was similar on both samples, with reduced crack widths on the hybrid element beams. By applying PCC to the tensile zone of flexural loaded concrete beams, the deflection is increased.

1 INTRODUCTION

In recent years, the polymer-modified concretes have developed rapidly, but the assessment of the structural properties of the PCC is still difficult. The ongoing development of the polymers in which even small changes can have large effects on the properties of the concrete is one of the reasons for this. Of particular importance is the time-dependent load resistance of the PCC. Crucial here is not only the characteristic value of compressive strength, but the material behavior during continuous load in the limit range. Mostly unobserved in the studies of structural properties of the PCC was the load-deformation behavior of hybrid elements of PCC and CC under flexural stress. The here presented study shows how PCC in the tension zone of flexural stressed concrete members influences the load deformation and fracture behavior of these hybrid elements.

2 MATERIALS

The concretes were produced with a CEM I 32,5 R. Three different polymers were used, a re-dispersible powder (polymer 1) and a dispersion (polymer 2) on the basis of styrene/acrylate as well as a dispersion (polymer 3) on the basis of styrene/butadiene. The polymer-cement-ratio was 0.10. The consistency of the concretes was set at a uniform flow-table test of 480 mm by varying the water-cement-ratio.

3 METHODS AND RESULTS

3.1 *Characterization of the base concretes*

Generally a liquefaction of the concrete by the polymer modification was observed. The liquefying effect of the polymers was compensated by a reduction of the water-cement-ratio. All fresh concretes were set on the class of consistency F 3.

The hardened concrete properties show that the reduction of the water-cement-ratio can compensate the reduction of compressive strength. The tensile and flexural strength are increased. The Young´s modulus and the tensile modulus are decreased.

3.2 *Properties of the hybrid elements*

In order to investigate whether there is a relation between the characteristic values of the base concretes and the hybrid elements of PCC and CC, beams were produced for testing flexural strength and the load deformation relationship. The hybrid beam elements consisted of a 70 mm layer of

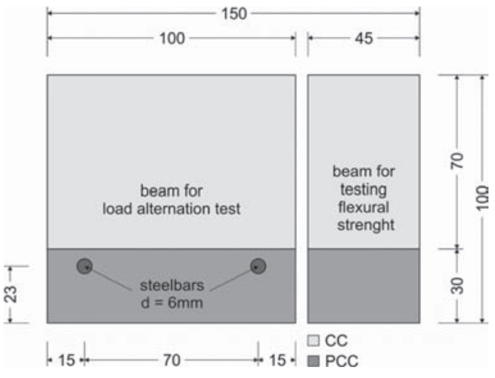

Figure 1. Cross-section of the beams.

CC cast on a 30 mm layer of reinforced PCC. Fig. 1 shows the entire cross-section of the beams.

3.2.1 *Testing flexural strength*

The flexural strength was determined in the 4-point bending test. The distance of the bearings was 600 mm. It can be stated, that it is possible to increase the flexural strength of concrete members due to the application of PCC in the tensile zone. This effect is attributed to the higher tensile strength of PCC.

3.2.2 *Load alternation tests on reinforced hybrid elements*

The experimental setup of the load alternation tests was equivalent to the experimental setup of the flexural test. For reasons of comparability the tests were made with the same load regime (Fig. 2) for all samples. As load steps 2, 4, 6, 8 and 10 N/mm² were chosen each with three load cycles. The retaining time between the load steps and the load cycles was 3 minutes.

The results of the load alternation tests show the influence of the layer of PCC in the tensile zone on the load-deformation behavior of flexural loaded hybrid elements. The individual states of the crack formation are visible in the load-deflection curves. For a clear representation of the loading-deflection curves the loading and unloading part of the curves of the load cycles were removed (Fig.3). The deflections of the uncracked samples are very small and of similar values. During crack formation the deflections are very different. The load to produce cracks is higher in the hybrid elements. When the crack formation is completed the cracks just wide on and the curves run almost parallel. The hybrid elements show larger deflection as the reference sample, but that has no negative influence on the average crack width, because the deformability of the PCC is generally higher in comparison to the CC.

The crack pattern was similar for all samples. Small differences are visible in the number of cracks, in the crack spacing and crack width. The

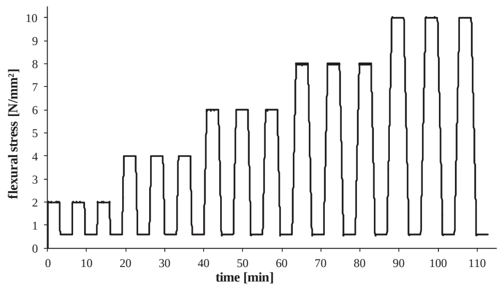

Figure 2. Load regime.

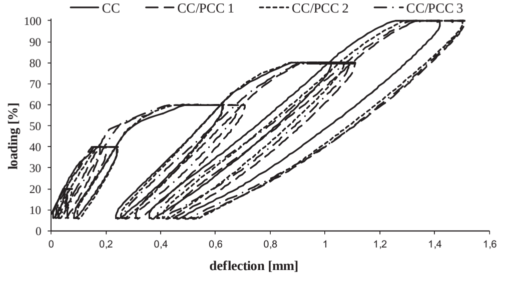

Figure 3. Loading-deflection relationship during the load alternation tests.

crack widths of the hybrid elements are generally smaller as these of the reference sample. The smaller crack widths can be advantageous for the durability of concrete constructions.

3.2.3 *Testing tensile bond strength*

The tensile bond strength between PCC and CC was determined after the load alternation tests. No delaminations or failures of bond could be detected. The tensile bond strength of PCC and CC showed no significant differences.

4 CONCLUSIONS

Coherences between the tensile strength PCC and the statical behavior of hybrid elements of PCC and CC were found. The flexural strength of the hybrid elements was generally higher in comparison to the reference samples. The load alternation tests show the positive effects by applying PCC in the tensile zone of concrete members. Cracks occur at a higher load than in the reference sample. This is due to the increased tensile strength of the PCC in comparison to normal concrete. The crack formation was independent of the polymer modification and similar at all samples. The higher deflections are possibly problematic in terms of serviceability of the concrete member and must be compensated by appropriate design measures.

Concrete Repair, Rehabilitation and Retrofitting III – Alexander et al. (eds)
© 2012 Taylor & Francis Group, London, ISBN 978-0-415-89952-9

Fatigue behaviour of self-compacting concrete

S. Korte, V. Boel & W. De Corte
Department of Civil Engineering, Faculty of Applied Engineering Sciences, University College Ghent, Belgium
Magnel Laboratory for Concrete Research, Department of Structural Engineering, Faculty of Engineering and Architecture, Ghent University, Ghent, Belgium

G. De Schutter
Magnel Laboratory for Concrete Research, Department of Structural Engineering, Faculty of Engineering and Architecture, Ghent University, Ghent, Belgium

ABSTRACT: It is well known that many civil engineering constructions may experience fatigue loading which can cause failure at a stress level much lower than in case of a single static load. Continuous degradation of the concrete during the loading process, due to propagation of microscopic cracks in the cement matrix and consequent strength decrease, may lead to extreme deformation and excessive crack widths, followed by structural collapse. This phenomenon is extensively documented in literature for normal, Vibrated Concrete (VC), whereas this is not so for Self-Compacting Concrete (SCC). Since both concrete types have a substantially different composition, it is unsure whether their mechanical properties regarding fracture behaviour and fatigue resistance are similar or not. In this paper the results of static and dynamic four point bending loading tests (with stress levels from $0.10f_{cc}$ to $0.80f_{cc}$) on reinforced concrete beams (made from VC and SCC) are reported. During the static and fatigue tests, deflection, strain, crack width evolution, and failure mechanism are observed. Subsequently, further analysis is carried out and both types of concrete are compared.

1 INTRODUCTION

Although a substantial amount of research has been carried out on the fresh, mechanical and transport properties and on the durability of SCC (De Schutter & Audenaert 2007, De Schutter & Boel 2007, De Schutter et al. 2008), there is still a lack of knowledge regarding its fatigue resistance. Therefore, in this experiment, the deflection, strain, and crack width evolution of reinforced concrete beams during static and dynamic loading tests are examined. Comparing VC to SCC, clearly indicates that there are differences regarding deformation and crack pattern.

2 EXPERIMENTAL PROGRAM

2.1 *Specimens*

Five VC beams (of the same batch) and five SCC specimens (of the same batch) with identical geometry, are tested up to failure. To achieve concrete crushing at ultimate load, while the steel rebar deformation remains fully elastic, the upper part of the geometrical beam section is narrowed (Figs. 1–2) in order to generate larger concrete bending stresses. In addition, the shear reinforcement (vertical stirrups) is overdimensioned, hence providing abundant resistance against shear collapse.

2.2 *Test procedure*

The four point bending tests are carried out with a load controlled hydraulic actuator. During the static and dynamic tests, the vertical displacement

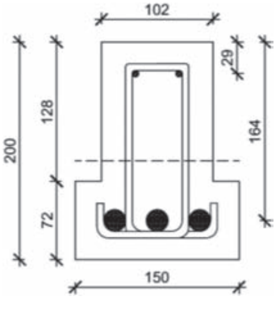

Figure 1. Beam cross section.

Figure 2. Beam geometry.

is measured by using deflection gauges with an accuracy of 10 µm, while five strain gauges automatically and continuously record the structural behaviour of the specimen. Furthermore, crack width evolution is measured using a crack width microscope with an accuracy of 20 µm.

The static destructive tests are performed on two reference beams (VC-0 and SCC-0) in order to determine the ultimate load value (P_{ult}), which is used to determine the lower and upper limit (0.10 P_{ult} and 0.80 P_{ult}, respectively) of the sinusoidal loading function for the dynamic tests. These cyclic tests, with a load frequency of 1 Hz, are executed on the eight remaining VC—and SCC specimens.

3 MAIN RESULTS OF THE STATIC TESTS

3.1 *Deflection*

A comparison of the theoretically determined deflection, according to EC2 (CEN 2004), with the experimental results indicates that EC2 underestimates the actual vertical deformation for both VC and SCC. In addition, it is observed that SCC deflects slightly more, compared to VC, considering an equal load.

3.2 *Strain*

The deformation diagrams, obtained by the strain recordings, are linear along the cross section of the specimens. Moreover, the concrete strain at the top surface of the beam, (practically) attains the failure limit of 3.5‰, for both concrete types, which confirms the concrete crushing failure mode. Furthermore, at a certain load, the deformation of SCC is again larger than that of VC.

3.3 *Crack pattern and crack width evolution*

Regarding the number of cracks and the crack pattern over the beam span, it can be concluded that the SCC specimen shows slightly more cracks, compared to the VC beam. These findings are in agreement with the results of De Corte & Boel (2011).

The experimental crack width evolution of the cracks in the constant moment region (between the point loads) of SCC-0 shows a good correspondence with the calculated average crack widths, based on EC2 (CEN 2004). However, the characteristic values exceed the measured ones with 21%. Related experiments (De Corte & Boel 2001) found similar results and concluded that SCC generates on average smaller crack widths, compared to VC, which indicates that the formulas, proposed by EC2, are better applicable to VC.

4 MAIN RESULTS OF THE DYNAMIC TESTS

4.1 *Number of cycles to failure*

Regarding the total number of cycles to failure large scatter is observed, for both VC and SCC. A conclusive explanation cannot be found.

4.2 *Deflection*

For all the specimens, both VC and SCC, a logarithmic S-shaped evolution of the vertical deformation is present. In the first short period of this evolution deformation is important. Subsequently a longer period of slightly increasing deformation is observed and finally there is a rapid growth until fatigue failure occurs. A similar trend was found in the deflection data of previous research (De Corte & Boel 2001). However, a comparison of the two concrete types does not reveal any difference in deflection.

4.3 *Strain*

In agreement with the findings of De Corte & Boel (2011) and Zanuy et al. (2007), again an S-shaped curve appears in the concrete strain evolution, which reflects the macroscopic result of well known internal material changes (bond deterioration, micro-cracking, macro-cracking, and fatigue failure).

Considering the magnitude of the concrete strain, again, no clear difference between VC and SCC is present. Furthermore, for both concrete types, the rebar strain does not reach the yield strength, which demonstrates that no plastic deformation occurs.

4.4 *Crack pattern and crack width evolution*

The observed cracks (in the constant moment region) widen during the entire loading process. However, neither VC, nor SCC shows a clear trend and consequently, no mutual differences appear.

Regarding the number of cracks, the SCC beams generate slightly more cracks than the VC specimens, as was also the case in the static tests.

5 CONCLUSION

All the tested beams collapse due to direct compressive fatigue failure, as was aimed for. Furthermore, the static tests point out that SCC deforms more than VC at a certain load. However, the dynamic tests yield conflicting results. For that reason, more extensive research is required concerning deformation and crack widths, as well as regarding the number of cycles to failure, since large scatter occurs.

REFERENCES

CEN Eurocode EN 1992-1-1: 2004. Design of concrete structures: General Rules and Rules for Buildings.

De Corte, W. & Boel, V. 2011. Fatigue Resistance of Dynamically Loaded Self-Compacting Concrete, *Magazine of Concrete Research* (approved to be published).

De Schutter, G. & Audenaert, K. 2007. *Durability of Self-Compacting Concrete.* State-of-the-art report of RILEM Technical Committee 205-DSC. RILEM Report 38.

De Schutter, G. & Boel, V. 2007. *Self-Compacting Concrete SCC2007*, RILEM Publications S.A.R.L., Proceedings PRO 54.

De Schutter, G., Bartos, P., Domone, P. & Gibbs, J. 2008. *Self-Compacting Concrete*. Caithness: Whittles Publishing.

Zanuy, C., de la Fuente, P., Albajar, L. 2007. Effect of Fatigue Degradation of the Compression Zone of Concrete in Reinforced Concrete Sections, *Engineering Structures* 29: 2908–2920.

Concrete Repair, Rehabilitation and Retrofitting III – Alexander et al. (eds)
© 2012 Taylor & Francis Group, London, ISBN 978-0-415-89952-9

Velocity profile of self compacting concrete and traditional concrete flowing in a half open pipe

H.D. Le & G. De Schutter
Magnel Laboratory for Concrete Research, Ghent University, Ghent, Belgium
Laboratoire de Mécanique et Matériaux du Génie Civil (L2MGC), Université de Cergy-Pontoise, Cergy-Pontoise, France

E.H. Kadri & S. Aggoun
Laboratoire de Mécanique et Matériaux du Génie Civil (L2MGC), Université de Cergy-Pontoise, Cergy-Pontoise, France

J. Vierendeels & P. Troch
Hydraulics laboratory, Ghent University, Belgium

ABSTRACT: The behavior of concrete flowing in a pipe is a key factor for mastering the concrete pumping technique. Due to the non-homogeneity of concrete, the concentration of particles (aggregate, sand, cement…) is not the same everywhere in the pipe. Particularly in the highly sheared zone near the wall, the concentration of coarse particles is much lower than that in the bulk. As a result, the rheological properties across the cross section vary with the distance from the wall. This phenomenon affects directly the velocity profile across the section. However, the velocity profile of concrete flowing in a pipe has never been quantitatively measured. This paper shows an experimental method to accurately measure the velocity profile. On the other hand, the influence of the variation of the rheological properties on the velocity profile across the pipe is also studied. Finally, a comparison between experimental analyses and numerical simulations shows reasonable correlation. This paper concentrates on the difference between the flow of a self-compacting concrete and that of a traditional concrete based on their different rheological properties.

1 INTRODUCTION

In a first part, the rheology of fresh concrete followed by the pumping of concrete will be briefly introduced. In a second part, this paper shows the results from a series of test: rheology of concrete, rheology of mortar and velocity profile measurement. In the last part, a numerical simulation of the velocity measurement test will complete the paper.

2 RHEOLOGY OF FRESH CONCRETE

2.1 *Rheometry*

For this project, the Tattersall MK-II rheometer is employed to measure the rheological properties of both concrete and mortar. This device is based on the principle of the coaxial cylinders, but the inner cylinder has been provided with a helical screw in order to prevent or at least slow down segregation.

Rheological properties have been determined by adapting the rotation to a pre-shear period until time independent toque id reached following by decreasing the rotational speed in 10 steps, from 75 rpm to 10 rpm (Feys D., 2009).

2.2 *Time independent rheological behavior*

In general, fresh concrete behaves like a Bingham fluid showing a yield tress and a plastic viscosity. Depending on the concrete composition, some SCC can behave like a Herschel-Bulkley fluid (Feys D. et al, 2008) but in this paper this type of concrete is not studied. The Bingham model is show in the equation 1.

$$\tau = \tau_0 + \mu\dot{\gamma} \tag{1}$$

Where τ = shear stress (Pa); τ_0 = yield stress (Pa); μ = viscosity plastic (Pas); $\dot{\gamma}$ = shear rate (1/s).

3 EXPERIMENTATION

3.1 *Experimental principle*

The optical method called PIV (Particle Image Velocimetry) has been used to study the flow in the free surface of concrete flowing in a half-open pipe.

3.2 *Test configuration*

The principal equipment of the test is a half open inclined pipe. A pump is used to collect the concrete at the outlet of the pipe and pump it up to the inlet of the pipe. In consequence, a fully automatic close pumping circuit in which there is a permanent flow created. A camera is situated above the free surface and located at the distance of 5 meters from the inlet. At this distance, the perturbation and the entrance effect from the inlet has no longer an influence and a permanent regime is also established.

3.3 *Measuring technique*

By using the PIV (Particle Image Velocimetry) technique, the velocity profile on the free surface is accurately determined.

3.4 *Testing procedure*

In order to maintain a permanent flow in the circuit, the pump must always be filled. Then, the camera starts to record the images. In parallel to the flow test, 15 liters of concrete is extracted from the mixer for the rheological test in the Tattersall Mk-II rheometer. The rheological test of mortar is performed later with the mortar produced by the Concrete-Equivalent Mortar method (Schwartzentruber A. et al, 2000). A

3.5 *Concrete mixes*

1 SCC and 1 TC were studied.

3.6 *Results and discussions*

3.6.1 *Rheological tests*

The test results show a linear relationship between torque and rotational speed. As a result, the Bingham behavior for both 2 concretes and 2 mortars is determined..

3.6.2 *Velocity measurement*

The images issued from each test have been analyzed with PIVlab program

During the experimentation, a layer of maximum 4 millimeters in thickness is observed situated next to the pipe wall. It can be assumed that the value of the slip velocity the maximum value of the local velocities in the slip layer.

4 NUMERICAL SIMULATION

4.1 *Hypothesis*

The rheological properties of the mortar in the concrete are smaller than these of concrete. Hence, it can be assumed that there exists a mortar layer of $D_{max}/2$ in thickness that plays the role of lubrication layer and contributes a slip velocity to the total velocity

4.2 *Geometry and initial conditions*

In order to validate the hypothesis, the flow of concrete in the half open channel is simulated by decomposing the fluid volume into 2 sub fluid volumes. The

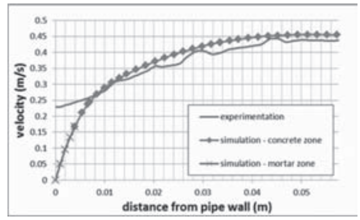

Figure 1. Velocity profile (V_x) across the pipe on the free surface of the flow for SCC.

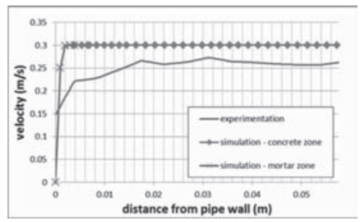

Figure 2. Velocity profile (V_x) across the pipe on the free surface of the flow for TC.

first fluid volume covers all cells situated at a distance smaller than or equal to $D_{max}/2$ from the pipe wall. This volume is assigned the rheological properties of the fluid in this zone are those from the experimental values of mortar. The second fluid volume covers the rest of the fluid volume and is assigned the rheological properties of concrete. One volume of air of 10 mm in height is situated above the free-surface of the fluid volume. The Volume Of Fluid (VOF) method has been used for the simulation.

4.3 *Results and discussions*

The velocity profile on the free surface shown below has been taken at the level of z = -5 mm, under the real free surface level (z = 0) to be sure that it is located in the fluid volume. The numerical results comparing to the experimental results is shown in the figure 1 and 2.

5 CONCLUSION

The objective of this work is to study the influence of the rheological properties on the flow profile of concrete and to confirm the existence of the slip layer. According to the literature (Wallevik O. H. et al, 2009), this study shows that the slip layer has lower rheological properties than the concrete on the plug flow. It contributes a slip velocity to the total velocity. The proportion contributed while pumping a self-compacting concrete is lower than in the traditional concrete. As a result, the movement of traditional concrete in a pipe is governed by the slip layer.

Concrete Repair, Rehabilitation and Retrofitting III – Alexander et al. (eds)
 ISBN 978-0-415-89952-9

Deformation of concrete subject to freeze-thaw cycles combined with chloride salt solution

Zhendi Wang, Yan Yao, Ling Wang & Yin Cao
States Key Laboratory of Green Building Materials, China Building Materials Academy, Beijing, China

ABSTRACT: To investigate the deformation of concrete under the combination action of freeze-thaw cycles and chloride salt solution, strain of the concrete matrix and temperature in specimen center were determined using the dual-purpose strain gauge. Saturation and weight loss of the specimen were also measured by means of weighing method. The results show that strain of the matrix increased cycle by cycle with the increase of exposure time. Further, the strain decreased on thawing stage and increased on freezing stage in the temperature range of –20°C ~ –5°C. Gradual rise in weight loss and slight increase of saturation with the augment of strain were found in this study. The relationship between strain of concrete matrix and saturation, weight loss were also analyzed. The result of the present work implied that phase transition affects the deformation of concrete matrix seriously and the strain of concrete matrix can be split into two parts, namely, plastic deformation and the propagation of cracks.

1 INTRODUCTION

This study is an attempt to study the deformation of concrete matrix subject to freeze-thaw cycles and chloride attack.Single effect of chloride on concrete was not considered.

2 EXPERIMENTAL MATERIALS AND TEST PROCEDURE

Portland cement (P.I 42.5) with the specific surface area of 343 m^2/kg and river sand with the fineness modulus of 2.6 was used. The water/cement ratio of 0.65 was used to highlight the freeze/thaw attack to maximize the deformation that the sensor can monitor. No water reducer and air en-training was used. Prismatic concrete specimens with the dimension of 100 mm × 100 mm × 400 mm were prepared. Strain variation at the center of the specimens was measured by the strain gauge, and recorded by the computer.

3 RESULTS AND DISCUSSION

3.1 *Evolution of concrete deformation*

Figure 1 shows the incremental of specimen's strain during the experimental period. The strain decreased upon thawing and increased upon freezing in every cycle during the steady system state. Similarly, the amplitude of strain increase with increasing of the time was also found from the comparison of anterior cycle to the posterior cycle. There are a number of factors that can be extracted to account for this behavior. Firstly, once the temperature goes down below freezing point, high expansion pressure might be act on the pore walls due to the volume increase from water to ice. The expansion pressure is more likely to accumulate in the porous matrix to cause plastic deformation. Next, when the expansion pressure is higher than the cracking strength of the pore walls, the pore wall is ruptured and cracks initiated. The formation and propagation of cracks in concrete matrix will also cause the incremental strain in concrete matrix.

3.2 *Relationship between deformation and temperature*

Plot of the deformation versus the temperature is shown in Figure 2. It can be seen from the figure

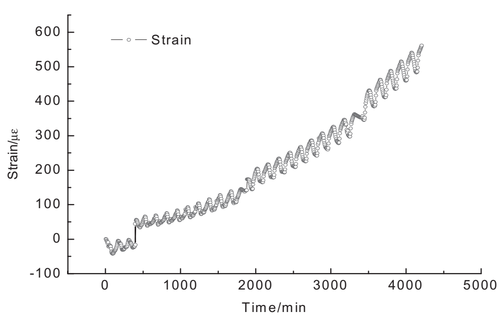

Figure 1. Deformation of specimens subject to freeze-thaw cycles and 3.5 wt.% chloride salts.

that concrete matrix continually contracts with the decreasing of temperature during the freezing process in the first cycle. Actually, The internal temperature is higher than that of surface in the beginning of freezing stage. Consequently, concrete surface expansions while the internal matrix contracts with the decrease of temperature. In addition to the above two factors, dimension and thermal conductivity may also influence the contraction behavior.

Next, concrete matrix begins expanding due to the chloride sodium solution starting freezing around −5°C in the following freezing process On the whole, temperature plays a significant role in the process of concrete matrix deformations during the whole period. Furthermore, strain in the last cycle is 11 times as large as strain in the fourth cycle. This clearly shows that severe damage has been produced in the concrete matrix by the action of freezing and thawing. The damage amount is equal to the residual strain in quantity.

3.3 *Relationship between deformation and weight loss, saturation*

Figure 3 shows the relationship between the expanding deformation of concrete matrix and weight loss, saturation.

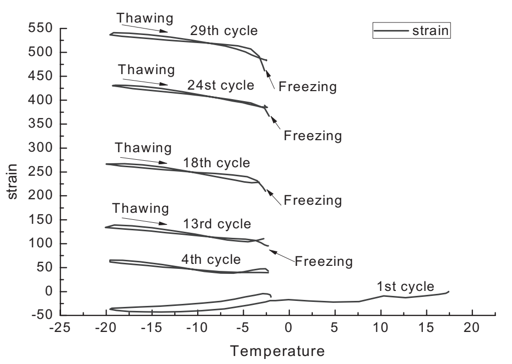

Figure 2. The relationship between deformation and temperature in specimen's center.

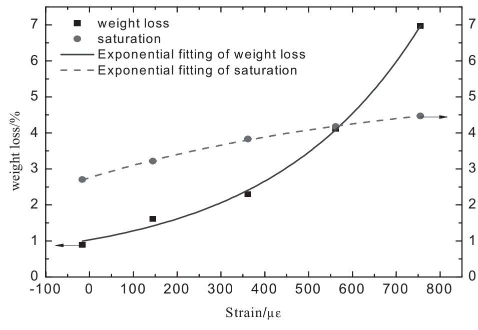

Figure 3. the relationship between deformation and weight loss, saturation.

The two curves cross each other when the strain is to reach 600 με. It is meaningful that weight loss of the concrete matrix retains a rapid increase after the strain beyond 600 με while increase of the saturation slows down. Since the degree of saturation and surface scaling are closely related to the internal cracks, the propagation of internal crack or the increase of concrete matrix deformation may bring about the rising of strain. At the same time, the relationship can be fitted as exponential function.

4 CONCLUSIONS

1. Deformation of concrete matrix increase with the time rolling. Plastic deformation and the propagation of cracks are responsible for the increasing of strain in concrete matrix.
2. Temperature plays a significant role in the process of concrete matrix deformations during the whole period. High residual strain has been found in concrete matrix. The damage may come from the crack initial and propagation.
3. The relationship between strain and weight loss, saturation can be described by exponential function. Weight loss and saturation can be obtained by measured strain.

Concrete Repair, Rehabilitation and Retrofitting III – Alexander et al. (eds)
© 2012 Taylor & Francis Group, London, ISBN 978-0-415-89952-9

Thermal expansion of high-performance cement paste and mortar at early age

M. Wyrzykowski
Empa, Swiss Federal Laboratories for Materials Science and Technology, Switzerland
Technical University of Lodz, Department of Building Physics and Building Materials, Poland

P. Lura
Empa, Swiss Federal Laboratories for Materials Science and Technology, Switzerland
ETH Zurich, Institute for Building Materials (IfB), Switzerland

ABSTRACT: Self-desiccation in high performance concrete may lead not only to autogenous shrinkage, but at the same time may also increase the risk of thermal cracking of the material. It is well known that the thermal expansion coefficient, which describes the deformation of the material due to a unit temperature change, increases considerably with a drop of water saturation in the pores. Hence it is expected that an increase will also accompany the self-desiccation process. In this work, an experimental investigation regarding the evolution of the thermal expansion coefficient in cement paste and mortar is presented. Results of the volumetric method for determining the coefficient of thermal dilation are verified with measurements of relative humidity evolution in cement pastes exposed to changing temperature. The observed change of RH due to temperature change is substantially higher than reported in the literature; however it can be directly correlated with the measured thermal expansion coefficient.

1 INTRODUCTION

Thermal stresses and the risk of cracking of concrete will depend on the characteristics of the structure (size, degree of restraint) and properties of the material, among which the tendency of the material to deform due to the temperature change will play an important role. The latter property can be quantified with the coefficient of thermal expansion (CTE), e.g. Sellevold & Bjøntegaard (2006). It has long been observed that the CTE increases during maturing of the material and after further drying to the environment. Sellevold & Bjøntegaard (2006) suggested that the total thermal expansion in partially saturated concrete origins from the following mechanisms: pure thermal dilation of constituents, thermal shrinkage (manifested in delayed contraction as temperature is increased, which is due to the redistribution of water from gel to capillary pores) and RH changes due to temperature changes. This work deals in particular with the latter mechanism. The first observation is that in capillary porous media as concrete the internal RH change due to the unit change of temperature, expressed with a coefficient $\Delta RH/\Delta T$, takes positive values, i.e. the increase of temperature leads to an increase of RH, and in consequence the resulting deformation occurs in the same direction as the immediate part of the pure thermal dilation. This effect of changing RH becomes more apparent as RH and saturation in pores decrease (Radjy et al. 2003). Since, the $\Delta RH/\Delta T$ mechanism governing the CTE increase is of paramount importance in HPC undergoing self-desiccation, the motivation of this work was to investigate the evolution of $\Delta RH/\Delta T$ and in parallel of the CTE in cement pastes and mortars of water-to-cement ratio (w/c) 0.3 maturing in autogenous conditions. Next, it was possible to relate the evolution of the measured $\Delta RH/\Delta T$ in time with the evolution of the CTE, using a model proposed by Bentz et al. (1998) for drying shrinkage. In this work, the emphasis is on continuous observation of the evolution of the mentioned quantities in sealed conditions in low w/c materials at early ages, which has not been performed before. In this way it was possible to verify against each other the experimentally observed $\Delta RH/\Delta T$ and CTE values.

2 EXPERIMENTAL INVESTIGATION

The investigation was performed on cement pastes of w/c 0.3 and corresponding mortars with 40% aggregate volume fraction.

The internal RH in the cement paste exposed to temperature cycles of 17–23°C was measured using water activity sensors. As a result, the continuous evolution of the coefficient $\Delta RH/\Delta T$ in the material undergoing self-desiccation was obtained (Fig. 1). As can be seen, the drop of internal RH due to

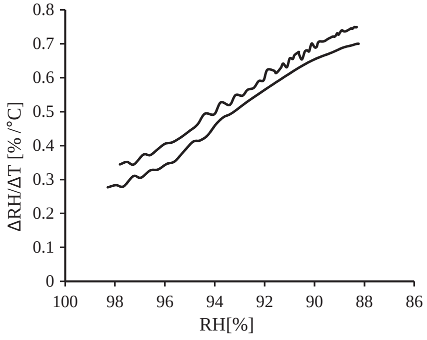

Figure 1. Evolution of *ΔRH/ΔT* as a function of RH in w/c 0.3 cement paste shown for duplicate specimens.

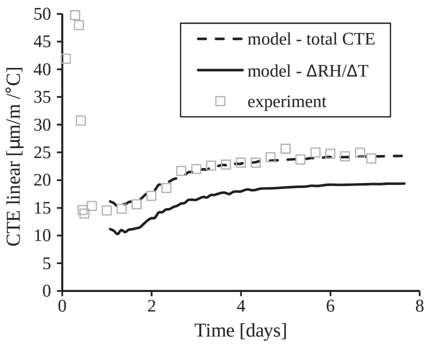

Figure 2. Measured and modeled evolution of CTE in w/c 0.3 cement paste. The continuous line was obtained based only on the RH related part of the CTE. The dashed line as shifted due to the pure thermal dilation assumed as 5 μm/m/°C.

the self-desiccation process is accompanied by the increase of *ΔRH/ΔT*. The values of the *ΔRH/ΔT* coefficient presented in Figure 1 (more than 0.70%RH/°C at 7 days) are considerably higher than those reported by e.g. Selevold & Bjøntegaard (2006) which did not exceed 0.15%RH/°C at 90% RH. As shown in the following section, the high values can be validated with the CTE tests.

The CTE of cement pastes and mortars was measured using the volumetric method as described in detail by Loser et al. (2010) (Fig. 2). It can be observed that the CTE of the cement paste increases by about 70% between 1 day and 7 days. For the mortar, the CTE increases by about 60% from 1 day to 7 days (not presented here).

3 MODELING

The mechanism investigated can be schematically described as follows: the CTE evolution in time is due to CTE dependence on RH which in turn is due to the *ΔRH/ΔT* dependence on RH. Since an increase of temperature leads to an increase of RH in the cement paste, the corresponding deformation resulting exclusively from the RH increase can be calculated using e.g. the capillary stress theory for partially saturated media as proposed by Bentz et al. (1998) for describing drying shrinkage. In order to account for the pure thermal dilation, the lines in Figure 2 were simply shifted up in order to agree with experimental data at the initial point of calculations, i.e. approximately 1 day.

It can be seen that the development of the CTE after setting can be described exclusively with the *ΔRH/ΔT* mechanism with a very good agreement. This confirms the observations by Sellevold & Bjøntegaard (2006) who stated that the moisture dependence of the CTE can be attributed mainly to the *ΔRH/ΔT* mechanism. Also, such a good agreement of the RH-related modeled development of the CTE and the measured development of the CTE supports the observed high values of the *ΔRH/ΔT* coefficient.

4 CONCLUSIONS

The measured CTE increased up to the age of 7 days by about 70% and 60% respect to the values at 1 day for the cement paste and mortar, respectively. High values of the *ΔRH/ΔT* coefficient were found for the cement paste, starting from about 0.3%RH/°C at 1 day to more than 0.7%RH/°C at 7 days. Modeling of the CTE based on the measured high values of the *ΔRH/ΔT* coefficient allowed obtaining an excellent agreement with the measured CTE evolution, which supports the *ΔRH/ΔT* data observed. It also confirms the statement that moisture dependence of the CTE can be attributed mainly to the temperature-induced RH changes.

REFERENCES

Bentz, D., Garboczi, E.J. & Quenard D.A. 1998. Modelling drying shrinkage in reconstructed porous materials: Application to porous Vycor glass. *Model. Simul. Mater. Sci. Eng.* 6: 211–236.

Loser, R., Münch, B. & Lura, P. 2010. A volumetric technique for measuring the coefficient of thermal expansion of hardening cement paste and mortar. *Cem. Concr. Res.* 40(7): 1138–1147.

Radjy, F., Sellevold, E.J. & Hansen, K.K. 2003. Isosteric vapor pressure—temperature data for water sorption in hardened cement paste: Enthalpy, entropy and sorption isotherms at different temperatures. Report BYG-DTU R-057, Techn. Univ. of Denmark, Lyngby, 2003.

Sellevold, E.J. & Bjøntegaard, Ø. 2006. Coefficient of thermal expansion of cement paste and concrete: Mechanisms of moisture interaction. *Mater. Struct.* 39(9): 809–815.

Concrete Repair, Rehabilitation and Retrofitting III – Alexander et al. (eds)
© 2012 Taylor & Francis Group, London, ISBN 978-0-415-89952-9

Development of new lime binder for building bio-aggregate materials

T.M. Dinh
Truong Dai hoc Thuy loi, 175 Tay Son—Dong Da—Hanoi, Vietnam
Université de Toulouse; INSA, UPS; LMDC (Laboratoire Matériaux et Durabilité des Constructions); Toulouse Cedex 04, France

C. Magniont, M. Coutand & G. Escadeillas
Université de Toulouse; INSA, UPS; LMDC (Laboratoire Matériaux et Durabilité des Constructions); Toulouse Cedex 04, France

ABSTRACT: The purpose of the present study is to investigate the new lime binders from two types of limes (Natural Hydraulic Lime—NHL3.5 and Slaked Lime—SL) and Metakaolin (MK). Several mixtures composed of MK, lime and admixtures were made to explore their mechanical properties, hardening and shrinkage. The incorporation of glycerol carbonate and potassium sulfate into alternative binders resulted in a greater improvement of compressive strength and limitation of shrinkage.

1 INTRODUCTION

Binder always plays a very important role in composite building materials. From the standpoint of sustainable development in the area of construction, it not only improves the mechanical properties but also limits the impact on the environment. In the special case of biocomposites including plant aggregates, its mechanical properties, its shrinkage and its compatibility with plant aggregates determine the performance of the composite.

Previous results have shown the potential of an eco-friendly innovative binder based on a mix of hydraulic lime and MK (Magniont et al 2010).

However, the initial mechanical performance with this type of binder is still too low. In order to enhance this property, mineral (potassium sulfate—PS) and organic (glycerol carbonate—GC) admixtures have been tested.

Finally, dimensional variations have to be controlled in order to avoid early-age cracking. Previous work has shown the shrinkage reducing effect of glycerol carbonate (Magniont et al, 2010) but it is necessary to assess its influence on the different compositions of binder tested in this study and to evaluate its interaction with potassium sulfate.

2 MATERIALS AND METHODS

2.1 *Materials*

The materials used in this investigation were metakaolin (MK), natural hydraulic lime (NHL3.5) and slaked lime (SL). The chemical composition data are presented in Table 1.

The main mineralogical phases of NHL3.5 were the C_2S, $CaCO_3$ and $Ca(OH)_2$ (Table 2).

SL is a commercial product from Calcinor. The major mineralogical ingredient is $Ca(OH)_2$.

X-ray diffraction analyses were realized to confirm the mineralogical components of the raw materials by.

Table 1. Chemical composition of materials.

	Content (% by weight)		
Oxides	MK	NHL3.5	SL
SiO_2	67.10	18.20	0.61
Al_2O_3	26.80	3.68	0.46
Fe_2O_3	2.56	1.36	0.17
CaO	1.12	56.68	70.20
MgO	0.11	2.10	0.40
K_2O	0.12	0.85	–
SO_3	< LD	1.22	–
TiO_2	1.30	0.18	–
Na_2O	0.01	0.04	–
Loss on ignition	0.84	15.04	26.67

Table 2. Mineralogical composition of NHL3.5 from Socli.

	$Ca(OH)_2$	$CaCO_3$	C_2S	C_3A	$CaSO_4$	Qz	Geh
NHL3.5	31.90	16.92	35.67	6.18	1.63	4.35	3.31

Qz: Quartz; Geh: Gehlenite.

In addition, superplasticizer (Sika Viscocrete 20 HEVP) was also used to reduce the water content.

2.2 *Methods*

The binders were made from MK and limes according to a MK to NHL3.5 ratio of 1 and a MK to SL ratio of 7:3. Admixtures were introduced in different proportions. The ingredients of the binders are presented in table 3 and table 4.

GC and superplasticizer were dissolved in water before mixing, PS was added to the binders at the time of dry mixing.

Specimens were cast in 40 × 40 × 160 mm molds and kept in a room at 20°C and 100% relative humidity (RH) for 2 days. The samples were demolded and continuously cured in the same conditions until day 7, then at 65% RH, 20°C until the mechanical properties were tested.

3 RESULTS

3.1 *Compressive strength*

The results show that the compressive strength of the MK-SL binders is generally higher than that of the MK-NHL3.5 binders, except MS binder at 2 and 7 days of age and S binder at 2 days of age.

Table 3. Components of binders from MK and NHL3.5.

	Content (% by weight)				
Components of binder	MH	H	HC	HP	HCP
Metakaolin	50	50	50	50	50
NHL3.5	50	50	50	50	50
Viscocrete 20 HEVP		0.8	0.8	0.8	0.8
Glycerol carbonate			0.5		0.5
Potassium sulfate				3	3
Water/binder	0.5	0.4	0.4	0.4	0.4

MH: control binder

Table 4. Components of binders from MK and slaked lime.

	Content (% by weight)				
Components of binder	MS	S	SC	SP	SCP
Metakaolin	70	70	70	70	70
Slaked lime	30	30	30	30	30
Viscocrete 20 HEVP		1.6	1.6	1.6	1.6
Glycerol carbonate			0.5		0.5
Potassium sulfate				3	3
Water/binder	0.6	0.4	0.4	0.4	0.4

MS: control binder

The influence of superplasticizer on the evolution of binder strengths because of porosity reduction was easily confirmed at both early age and in the long term.

The addition of GC did not have a positive effect on the mechanical performances of the binders except for SC binder at 2 days. In contrast, PS increased the strength of binders significantly at the age of 2 days.

The results also show that incorporating both GC and PS gave the best compressive strength (HCP and SCP binder).

3.2 *X-ray diffraction analyses*

The XRD analyses show the appearance of ettringite (Et) in the binders containing PS, which explains the influence of PS on the strength increase of binders at early age.

The differences of hydrates between MK-NHL3.5 binders and MK-SL binders can explain the difference of compressive strength. For the control binder, because hydraulic components are ingredients of NHL3.5, early age compressive strength of MK-NHL3.5 binder (MH) is much higher than that of MK-SL binder (MS).

Incorporation of PS and higher pH leads to the rapid formation of Et and thus the strength of MK-SL binder (SP) is higher than that of MK-NHL3.5 binder (HP), especially at early age.

Magniont indicated a slight increase of pH in MK-NHL5 binder with GC admixture after five hours (Magniont et al, 2010). This explained the good effect of a combination of GC and PS in strength development of binders (HCP and SCP). It can be seen that the compressive strengths of HCP and SCP are slightly higher than those of HP and SP respectively.

3.3 *Shrinkage*

The considerable shrinkage-reducing effect of GC is confirmed for both types of MK-lime binders.

The measurements of shrinkage also illustrate the best shrinkage-reducing effect of PS incorporated into PS binders (HP and SP binder). The combination of both GC and SP in binder also reduced shrinkage significantly. The shrinkage reducing effect of this association was almost the same as that of PS binders in endogenous shrinkage and was only a little lower than that of PS binders in total shrinkage.

4 CONCLUSION

This study shows the potential of lime binders for building bio-aggregate materials, which are formed from metakaolin, lime (natural hydraulic lime NHL3.5 or slaked lime) and glycerol carbonate or potassium sulfate admixtures.

It appears that, with metakaolin, slaked lime is more interesting than hydraulic lime (better strength with less lime).

Moreover, the incorporation of potassium sulfate brings about rapid formation of ettringite and consequently increases compressive strength considerably, especially at early age. On the other hand, it leads to the best shrinkage reduction with potassium sulfate and glycerol carbonate.

This study also shows the effect of a combination of glycerol carbonate and potassium sulphate in binders. The results indicate that this combination not only improves the mechanical properties, especially at early age, but also significantly reduces shrinkage.

These new binders appear highly suitable for making prefabricated blocks based on plant aggregate.

Concrete Repair, Rehabilitation and Retrofitting III – Alexander et al. (eds)
© 2012 Taylor & Francis Group, London, ISBN 978-0-415-89952-9

'Buffer' effects of natural zeolites in blended cements

R. Snellings
Magnel Laboratory for Concrete Research, University of Ghent, Belgium

ABSTRACT: One of the primary sources of natural supplementary cementitious materials are natural zeolite deposits. Natural zeolites present interesting potential both in terms of pozzolan reactivity and availability. Additionally to being consumed in the pozzolanic reaction, the unreacted zeolite fraction interacts with the cement pore solution and the internal cement environment as a water regulator and cation exchanger.

Zeolites can reversibly adsorb and release large amounts of water up to 20% of their weight or more. The uptake of water depends on the availability of water in the surrounding environment. The initial expansion of the zeolite lattice parameters as observed by in situ XRD measurements during the hydration of blended cements show that zeolites respond to the introduction of liquid water by adsorbing water into the zeolite microporous framework. In this manner, the effective water/cement ratio and the macroporosity of the system are reduced. Subsequently, the water contained in the zeolites will be released when the latter are consumed in the pozzolanic reaction or when the availability of water in the binder starts to drop. In this respect, zeolites can be considered as water carriers that gradually liberate their water over the hydration period to promote the completion of the hydration reactions.

Natural zeolites also thoroughly affect the pore solution chemistry of blended cements. Chemical analysis (AAS and ICP-OES) of the pore solutions in a range of zeolite blended cements show that the addition of zeolites generally increases alkali, Si and Al levels and decreases Ca concentrations in the pore solution. It was observed that the evolution of the pore solution is considerably affected by the zeolite type. The alkali concentration in the contact fluid is affected by the extra-framework cation content and the cation exchange characteristics of the zeolite. Most common natural zeolites (i.e. heulandite-clinoptilolite, mordenite, phillipsite, chabazite) selectively take up K and release Na and Ca to the pore solution.

1 NATURAL ZEOLITES AS INTERNAL WATER REGULATOR

Natural zeolites are well-known to adapt their water content to ambient humidity conditions. Their excellent water adsorption capacity has found direct application in their utilisation as desiccants. Adsorption of H_2O in the zeolite framework is generally accompanied by a slight expansion of the unit cell volume. The extent of expansion depends on the zeolite structure type, the framework charge deficiency (Si/Al ratio) and the nature of cations occupying the extra-framework sites. The smaller the ionic radius or the higher the charge of the extra framework cations, the larger the number of H_2O molecules that can enter the zeolite cages. The observed expansion of clinoptilolite and chabazite unit cells upon wetting of zeolite-portlandite and zeolite-cement mixes are to be interpreted along similar lines. Depending on the exchangeable cation content the expansion varies. Ca-clinoptilolite noted a 0.83 vol.% increase, Na- and K-clinoptilolite a 0.65 and 0.40 vol.% increase, respectively, when liquid water was mixed into the zeolite-lime mixes (Snellings et al., 2009). The adsorption of free water by the zeolite thus slightly lowers the water available for the pozzolanic and hydration reactions. In addition, the macroporosity of the pastes is lowered by both the expansion of the solid zeolite phase and the adsorption of water.

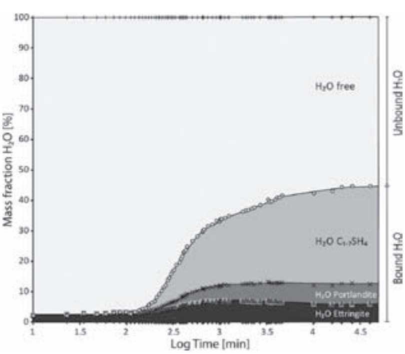

Figure 1. Evolution of bound water in a CEMI 52.5R Portland cement at w:b of 0.6 calculated by mass balance equations departing from the amounts of clinker phases reacted over time.

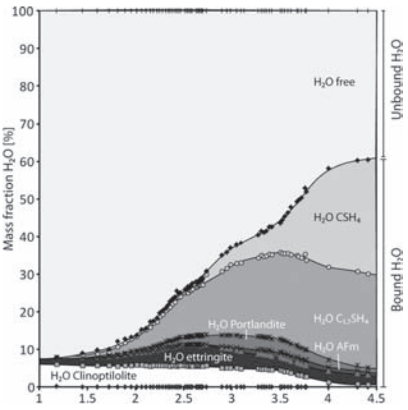

Figure 2. Distribution of water during hydration of a zeolite (Cli2) blended cement. A distinction is made between CSH derived from the hydration of clinker phases and CSH formed in the pozzolanic reaction. The former was assumed to have a C/S molar ratio of 1.7, the latter a C/S of 1.

Mass balance calculations based on in situ synchrotron hydration experiments show that a large amount of water is bound when an essentially anhydrous (gypsum excepted) ordinary Portland cement is hydrated (Fig. 1). The main phases containing water are C-S-H, portlandite, ettringite and small amounts of AFm. Ettringite is formed upon wetting by reaction of C_3A and Ca-sulphates (Snellings et al., 2010).

Figure 2 shows that in a zeolite (clinoptilolite type) blended cement H_2O is initially mainly present in the liquid and in the clinoptilolite. First, clinker phase hydration results in the formation of ettringite, C-S-H of high C/S and portlandite. Subsequently, the pozzolanic reaction starts consuming the formed portlandite and the clinoptilolite pozzolan. C-S-H of low C/S is assumed to be the main reaction product.

When comparing the levels of bound water in the ordinary cement paste and the zeolite blended cement, it can be observed that the amount of water bonded in pore space filling hydrates is estimated to be almost 20% higher in the blended cement. This also means that in order to reach the complete hydrate formation potential substantially more water is needed for the blended cement. In this respect zeolites may prove to be beneficial in both lowering initial macroporosity by water adsorption and in releasing substantial amounts of zeolite water at later stages of hydration. The added zeolite can thus be considered as a water buffer or carrier that partially removes water when it is initially abundant and that delivers water when it is needed in the hydration reactions.

2 NATURAL ZEOLITES AS CATION EXCHANGERS

Natural zeolites containing or exchanged to alkali cations increase the alkalinity of the cement pore fluid by releasing alkali into solution (Fig. 3). The higher solution alkalinity gives rise to higher Si and Al concentrations and lowered Ca concentrations. At early ages all tested natural zeolites except analcime selectively exchanged Na for K. An increased solution alkalinity at early ages is beneficial for the pozzolanic reaction rate as aluminosilicate dissolution rates and solubility increase exponentially with pH.

REFERENCES

Snellings, R., Mertens, G., Hertsens, S. & Elsen, J. 2009. The zeolite-lime pozzolanic: Reaction kinetics and products by in situ synchrotron X-ray powder diffraction. *Microporous Mesoporous Mater.* 126: 40–49.

Snellings, R., Mertens, G., Cizer, Ö. & Elsen, J. 2010. Early age hydration and pozzolanic reaction in natural zeolite blended cements: Reaction kinetics and products by in situ synchrotron X-ray powder diffraction. *Cement Concrete Res.* 40: 1704–1713.

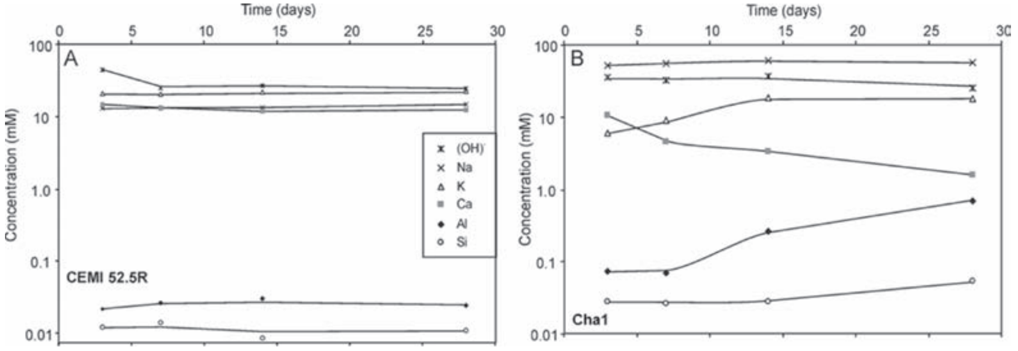

Figure 3. Pore solution composition during hydration of a CEMI 52.5R (A) and a chabazite tuff (Cha1) blended cement (B).

Concrete Repair, Rehabilitation and Retrofitting III – Alexander et al. (eds)
© 2012 Taylor & Francis Group, London, ISBN 978-0-415-89952-9

Evaluation of steel fiber distribution in a concrete matrix

S.A. Yehia
American University of Sharjah, Sharjah, United Arab Emirates

ABSTRACT: Steel fiber concrete is being used to improve plastic cracking characteristics, tensile and flexural strength, impact strength, and post cracking behaviour. Many guidelines by ACI 544 committee and steel fiber producers are available to provide directions for proportioning and mixing of steel fiber in concrete. In addition, recommendations and other mixing suggestions are given to avoid balling during mixing to ensure uniform distribution of the steel fiber in the mix. However, many concerns have been raised about the fiber distribution especially when a higher ratio of the steel fiber is used.

This paper will discuss an approach, which was followed during the evaluation of a steel fiber concrete mixture to ensure homogeneous distribution of the fiber within the mixture.

1 INTRODUCTION

Fiber-reinforced concrete has been used for roadway pavements in the United States since 1971. The benefits from adding steel fibers to concrete mix are not limited to increasing the ultimate flexural strength, shear and torsional strength, fatigue strength and impact resistance. Other benefits include increasing the ductile behavior, energy absorption capacity, ultimate strain capacity and post-crack load carrying capacity. The steel fiber content used in different concrete overlays has ranged from 36 to 157 kg/m^3 (60 to 265 lb/yd^3), with aspect ratios ranging from 40 to 200. Steel fibers have varied in length from 13 to 64 mm (0.5 to 2.5 in.). Using 2 percent of steel fibers by volume is considered an upper limit beyond which poor surface finishability will result.

However, to achieve the discussed benefits uniform distribution of the fiber in the concrete matrix should be achieved. Therefore, this paper focuses on the efforts by many committees, organizations, steel fiber producers, and researchers to ensure uniform distribution of the steel fiber in the matrix. In addition, results from a current evaluation will be presented and discussed.

2 FACTORS AFFECTING FIBER DISTRIBUTION

Several factors affect fiber distribution, which include steel fiber geometry (shape, aspect ratio), concrete mix design, batching and mixing process.

3 EVALUATION OF STEEL FIBER DISTRIBUTION IN THE MIX

Efforts before and during mixing are directed towards achieving uniform distribution of the steel fiber in the mix; however, long transportation time, long mixing and speed of mixing in transit truck, and workability of the mix might alter the SF distribution. This might lead to uneven fiber percentage within the same truckload. Therefore, evaluation of the fiber distribution in the mix needs to be conducted for every truckload.

3.1 *Fresh stage evaluation: Collecting the SF from known volume*

This process is usually conducted during mockup mixes to apply any adjustment to the mixing procedure. Samples with known volume (cube or cylinder) are collected from the beginning and the end of each truckload, and then the SF is collected after washing the concrete sample. Volume of the SF with respect to the known volume is calculated and compared with the target SF percentage.

3.2 *Hardened stage evaluation: Electrical resistivity of SFRC sample*

3.2.1 *Electrical resistivity test*

Electrical resistivity of SFRC samples are evaluated utilizing AC and DC current to ensure uniform distribution of the SF within the sample. Heat generated during resistivity testing could be used as an indication if there was fiber balling or increased fiber concentration in certain areas of the sample if an even heat distribution on the sample surface occurred.

3.2.2 *Cross section evaluation*

Horizontal and vertical cross sections from samples are prepared for inspection. This will provide addition information about the fiber distribution within the sample.

3.2.3 *SEM scan*

Scanning electron microscope (SEM) is a technique used to produce very high-resolution images of a sample surface; in addition, it can provide information about the distribution of different elements in the sample. Magnification capabilities in SEM scans can help examining fiber distribution in a sample.

3.2.4 *Computed tomography (CT)*

CT is another non-destructive technique, which could be used to check fiber distribution in a hardened concrete sample. This technique can produce 2-D and 3-D cross sectional images from flat X-ray images.

3.2.5 *Inductive scanning (IC)*

Inductive scanning technique can provide images for fiber distribution in a sample due to the interaction between metal targets with AC magnetic fields. Conductivity, permeability, and material size cause resistance and inductance of the current path, which determine the current value and phase.

4 RESULTS FROM CURRENT EVALUATION

Results from ongoing research at the American University of Sharjah (Yehia et al. 2011) to develop a steel fiber self consolidated high strength lightweight concrete mixes while maintaining the unit weight, workability, and strength requirements is briefly discussed in the following section.

4.1 *Collecting SF from cube samples*

Samples were collected from five batches with different steel fiber percentages (0.25, 0.5, 0.75, 1.0, and 1.25%) at the beginning and at the end of each batch. Then, washed and SF was collected. Batches with low SF dosage (0.25 and 0.5%) showed good distribution of the fiber; however, high SF dosage (0.75 to 1.25) showed variation in the results, which reflects the sensitivity of the self consolidated mixes. In addition, the lightweight aggregate was lighter than the steel fiber added.

4.2 *Cross section evaluation*

Horizontal and vertical cross sections from 150 mm × 150 mm × 150 mm (6 in × 6 in × 6 in) cube were prepared and evaluated. The visual inspection of both cross sections showed that random distribution of the fiber was achieved; however, some areas with high fiber concentration were detected. This will require re-evaluation of the mixing process to ensure uniform distribution of the fiber within all samples.

5 CONCLUSIONS

Technical notes from organizations, researchers, and steel fiber producers are available to provide directions for proportioning and mixing of steel fiber in concrete. Achieving uniform distribution of the steel fiber in the mix could be achieved if careful selection and preparation of the mix proportions. In addition, availability of the right batching equipment at the ready mix producer plant or at the job site will help achieve this goal. Fiber collection from samples at fresh stage, evaluation of electrical resistivity, and cross section inspection at hardened stage provide additional techniques to evaluate steel fiber distribution in concrete mixes.

Concrete Repair, Rehabilitation and Retrofitting III – Alexander et al. (eds)
© 2012 Taylor & Francis Group, London, ISBN 978-0-415-89952-9

Contribution to study of the self-healing effect activated by crystalline catalysts in concrete structures when subjected to continuous exposure to water

E.M. Takagi & M.G. Lima
Department of Aeronautical Infrastructure Engineering, Instituto Tecnológico de Aeronáutica, São José dos Campos, Brazil

P.R.L. Helene
Department of Civil Engineering, Escola Politécnica, University of São Paulo, São Paulo, Brazil

ABSTRACT: This paper aims to contribute to the study of the self-healing effects on high performance concretes activated by crystalline catalysts when subjected to continuous water exposure, as part of a post-graduate research program developed at the Instituto Tecnológico de Aeronáutica (ITA) in Brazil. For this purpose, a specific crystalline catalyst was selected to investigate the potential to act as a self-healing agent in concrete. Specimens of high performance concrete were prepared having a constant water/cement ratio of 0.50, with and without addition of these crystalline catalysts. A uniaxial compression load was applied to generate microcracks in cylindrical concrete specimens pre-loaded up to 90% of the ultimate compressive load determined at 28 days for 2 minutes. Later, the extent of damage was determined as a percentage of loss in mechanical properties by determining compressive strength recovery and percentage of increase in permeation properties and water absorption rate by monitoring for 28 and 56 days after preloading, during a period necessary for self-healing of these microcracks. The results of the recovery of strength and permeability will be attributed to the self-healing of these pre-existing microcracks, due to hydration of anhydrous particles of cement and especially by the activating effect of the crystalline catalyst, on the surfaces of these microcracks. This is determined as a percentage of gain of mechanical properties and the percentage of decrease in the permeability properties. The knowledge developed in this study makes it possible for the self-healing technology to be specified in the high performance concretes mix design in various applications in air transportation and airport infrastructure buildings, especially in hydraulic structures and underground constructions.

The term self-healing phenomenon has puzzled researchers for over a hundred years. In most studies the apparent decrease in permeability is incorrectly ascribed to a self-healing phenomenon. This mistake is especially common in investigations where only the inflow is recorded and through flow remains unknown. The latter is of primary importance, as the self-healing phenomenon is not a product of a particular testing procedure, but results from the interaction between the microstructure and permeating fluid.

Therefore, the aim of this study is to develop self-healing concrete technology for practical application in the near future, but it is also significant to know about the actual individual healing mechanism and its conditions. It is well-known that as concrete hydrates its permeability decreases. Continued hydration, however, is not the only mechanism which causes such reduction. Autogenous healing refers to carbonation of dissolved $Ca(OH)_2$ from concrete, with narrower cracks sealing faster than wider ones; and the self-healing mechanism, which is largely attributed to the dissolution and redeposition of hydrates, which can also significantly reduce the flow. In order to provide a systematic design of robust healing abilities to even aged high performance concrete, optimization methods can be applied, such as, use of mineral geo-materials and carbonate-based chemical agents, acting as a crystalline catalyst to supply the effect of cementitious recrystallization in voids of cracked concrete, in order to improve chemical stability and self-healing time.

The experimental program was performed with a standard mix design of a high performance concrete was prepared having a constant water/cement ratio of 0.50 and using two types of blended cement: a Type IS (MS) blast-furnace slag cement (slag content <70%) and a Type I (SM) slag-modified Portland cement (slag content <25%) according to ASTM C595, with and

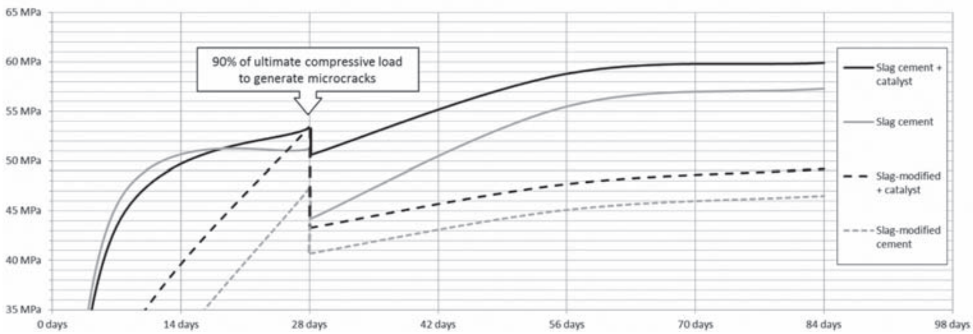

Figure 1. Loss of compressive strength and recovery due to self-healing of microcracks.

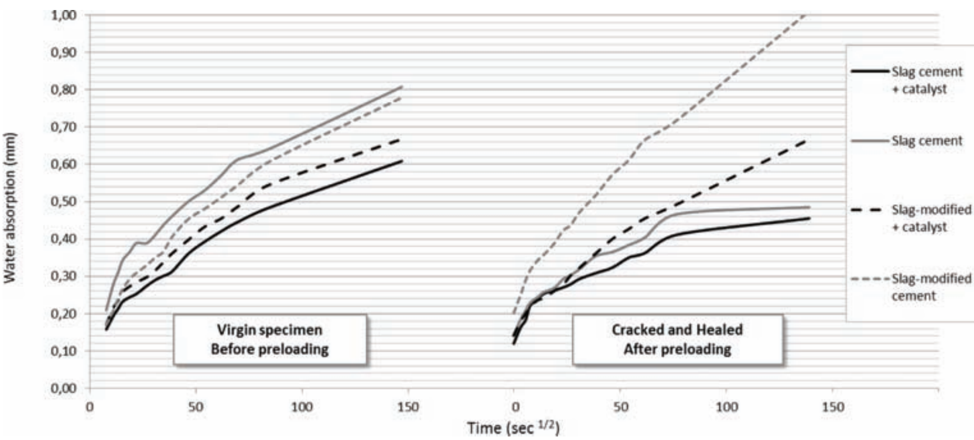

Figure 2. Comparison of water absorption rate of virgin specimen and cracked/healed concrete specimen.

without addition of crystalline catalysts at the rate of 2.5% by weight of cement content. Altogether, four different mixtures of HPC with addition of AR glass fibers were produced for the test program.

After a 28 days curing, a uniaxial compression load up to 90% of the ultimate compressive strength, determined at 28 days, was applied to generate microcracks in cylindrical concrete specimens for 2 minutes. Immediately after the release of pre-loading, the samples were tested to determine the loss in mechanical properties by determining compressive strength. The results of the recovery of compressive strength can be attributed to the self-healing of these pre-existing microcracks, due to hydration of anhydrous particles of cement and especially by the activating effect of the crystalline catalyst, on the surfaces of these microcracks, this is determined as a percentage of gain of mechanical properties. Based on ASTM C1585, the registered increase in mass of cracked and healed concrete specimens at given intervals of time, when permitted to absorb water by capillary suction.

From this experimental research, it was clear that the crystalline catalyst was effective in improving the durability of the high performance concrete stressed by continuous and repeated mechanical loading. It was confirmed that C-S-H cement crystals are increased in the cracks of the concrete and hence an improved compressive strength and waterproofing which also contributed to understanding the self-healing phenomenon study. In order to systematically design a robust self-healing technology for concrete structures subjected to continuous exposure to water, the use of a Type IS (MS) blast-furnace slag blended cement (25% < slag content <70%) with addition of crystalline catalyst and ductile-type fibers is highly recommended.

ACKNOWLEDGEMENTS

This postgraduate research developed at Instituto Tecnológico de Aeronáutica is supported by MC-Bauchemie Brasil, is gratefully acknowledged, and we would like to thank Dr. Pat McGrath of Xypex Chemical Corporation for the advices provided.

Concrete Repair, Rehabilitation and Retrofitting III – Alexander et al. (eds)
 ISBN 978-0-415-89952-9

Strength behaviour of clay-cement concrete and quality implications for low-cost construction materials

F. Solomon & S. Ekolu

School of Civil and Environmental Engineering, University of the Witwatersrand, Johannesburg, Republic of South Africa

ABSTRACT: Incorporation of clay soil into concrete mixtures is one means of designing low-cost, low strength construction materials. However the influence of clay on material properties should be understood as it affects engineering performance. This paper argues that the use of concrete for low-cost cementitious building materials has special requirements. A significant demand exists for physical infrastructure in developing countries. Usually, concrete or mortar blocks of sufficient integrity for low-cost housing, are made from cement with clay-contaminated sand by artisanal builders.

The work presented is based on experimental results of a laboratory study done for clay-cement concrete material. The clay-cement concrete studied was designed to be a low-strength material and its properties fall between those of soil and concrete. Four control concrete mixtures of 350 kg/m^3 CC (cementitious content) and w/cc (water to cementitious ratio) = 0.70, 0.75; 280 kg/m^3 CC and w/cc = 0.80, 0.85 were prepared. Further mixtures were made by substituting the OPC (Ordinary Portland Cement) in control mixes with 10, 20, 30, 40, and 60% local raw clay. Compressive strengths were measured at ages of 7, 28, 56, 270, and 365 days for all the mixtures. The laboratory test results show that clay-cement concrete mixtures with a maximum of w/cc = 0.80 and 20 to 30% clay replacement can be suited to fulfill the requirement of strength and workability for low–cost, low strength applications such as including housing, roads and dams. Interestingly, clay-cement concretes gave higher strength performance factors at later ages than the corresponding plain cement concretes, suggesting a possible pozzolanic behaviour, however minimal. Further investigations are being undertaken to determine the behavior of the clay-cement mixtures through study of drying shrinkage, creep, abrasion resistance, and fluid permeability.

1 INTRODUCTION

Building materials are often the largest component of costs for housing construction in developing countries, accounting for up to 70% of standard low-cost housing unit (Erguden 2001).

2 BACKGROUND

Strength is one of the main properties of hardened concrete. Concrete without adequate strength is of no use. With clay in the mix, the amount of water required for good workability can be considerably higher than that needed for hydration. Therefore, once the clay-concrete is cured and a portion of the water is chemically bound by hydration, a greater remainder of it evaporates, leaving an increased content of voids leading to lower strength (Neville 1987).

3 EXPERMENTAL

3.1 *Clays*

The research started by collecting undisturbed raw soil samples in Gauteng province guided by maps in the areas of Springs (RD) and Soweto (S2). The soil samples were tested to determine their engineering properties such as Atterberg limits, ASTM soil group classification, Casagrande`s soil classification systems and particle specific gravities.

3.2 *Mixtures*

Four control concrete mixtures having CC of 350 Kg/m^3 and w/cc = 0.70, 0.75; CC of 280 Kg/m^3 and w/cc = 0.80, 0.85 were made. Further concrete mixtures were prepared by substituting ordinary Portland cement with 10, 20, 30, 40 and 60% raw clay in all control mixtures. The workability of fresh concrete was measured for each mix and compressive strengths of the hardened concretes were determined at ages of 7, 28, 56, 270 and 365 days.

4 RESULTS

4.1 *Soil types*

The soils obtained from Springs/Brakpan and from Soweto were tested and their properties in terms of Atterberg limits, particle size distribution and soil classification.

According to the international society of soil science (Jumikis 1967, Lambe and Whiteman 1969), the soils can be classified as:

- Soil-I (RD)—Reddish sandy silty clay.
- Soil-II (S2)—Deep red sandy silty clay.

5 DISCUSSIONS

The results (figures 1&2) show the trends to be expected from the interaction of various parameters and, where applicable, the form of possible empirical equations describing this interaction. The analysis presented has also shown the relative performance of the different local raw clay-cement concretes tested. The results of Figure 1 on workability trends, shows that increasing the w/cc ratio has different effects on workability of the clay-concrete mixes. The RD clay showed increasing workability and S2 clay gave decreasing global workability, while the control exhibited a relatively constant workability with increase in w/cc ratio.

In Figure 2 is shown the global strength relationship for both clay-concretes, basing on the data generated from this investigation. The expressions generally obey the second order polynomial function.

6 CONCLUSIONS

The presence of clay in the aggregate has a significant effect on the workability of concrete, depending on the clay type. It was found that RD clay decreases workability while S2 clay increases workability of the mixtures.

Global analysis of the strength effects of the clay contents appears to suggest that clay-concrete mixes may in fact give higher strength performance factors compared to plain cement concrete. This effect of clays is more pronounced at the later ages of curing.

The results may also suggest a possible pozzolanic effect of the clays and further investigation is needed on this aspect.

Structural concrete made with clay materials would need to be investigated with regard to durability, particularly the dimensional stability. Further research is being conducting on durability of clay concretes and will be reported in future.

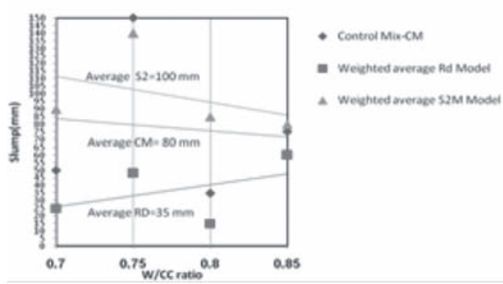

Figure 1. Workabiliy effect of the control and clay-concrete mixes of various w/cc ratios.

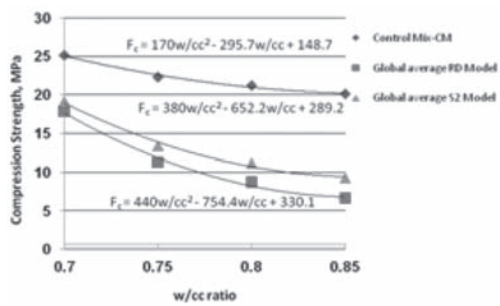

Figure 2. Strength effect of the control and clay-concrete mixes of various w/cc ratios.

Concrete Repair, Rehabilitation and Retrofitting III – Alexander et al. (eds)
© 2012 Taylor & Francis Group, London, ISBN 978-0-415-89952-9

Characterisation and description of the structure of metakaolin by total scattering, density functional theory, and X-ray spectroscopy

C.E. White
Department of Chemical & Biomolecular Engineering, University of Melbourne, Victoria, Australia
Lujan Neutron Scattering Center, Physics and Chemistry of Materials and Center for Non Linear Studies, Los Alamos National Laboratory, Los Alamos NM, USA

J.L. Provis
Department of Chemical & Biomolecular Engineering, University of Melbourne, Victoria, Australia

D.P. Riley
Department of Mechanical Engineering, University of Melbourne, Victoria, Australia

Th. Proffen
Powder Diffraction Group, Oak Ridge National Laboratory, Oak Ridge TN, USA

L.M. Perander
Department of Chemistry, University of Auckland, Auckland, New Zealand

J.S.J. van Deventer
Department of Chemical & Biomolecular Engineering, University of Melbourne, Victoria, Australia
Zeobond Pty Ltd, Somerton, Victoria, Australia

ABSTRACT: The structure of metakaolin (calcined kaolinite clay; a common SCM used as a blending agent in many concretes as well as in geopolymer synthesis) has been a source of controversy for more than 50 years, with its disordered ("X-ray amorphous") layered structure resisting traditional crystallographic analysis. Total scattering analysis using both high-energy synchrotron X-rays and neutrons from a spallation source, in combination with density functional theory, has finally given insight into the details of this complex layered structure. An iterative methodology involving both neutron total scattering data and Density Functional Theory (DFT) computations has shown the ability to generate a metakaolin structural model which is both experimentally and thermodynamically plausible. Furthermore, the process of kaolinite dehydroxylation has been simulated directly using density functional modelling, which provides insight into the mechanism of this transformation from crystalline to disordered, and the means by which the strained, reactive alumina sites in metakaolin are formed. These sites are seen to be predominantly 4-coordinated, with some sites that are strained 5-coordinated and a small number of 3-coordinated alumina sites; these identifications are supported by X-ray Absorption Near Edge Spectroscopy (XANES), although the results conflict with the current understanding of the system according to Nuclear Magnetic Resonance (NMR) spectroscopy. We will provide discussion of the factors—experimental and sample-related—which may contribute to this apparent discrepancy.

1 INTRODUCTION

With the increasing utilisation of supplementary cementitious materials (SCMs) to enhance both the environmental and performance credentials of concretes, and in the development and commercialisation of concretes based on alkali-activated binders, it is becoming very important to develop a detailed understanding of the chemical structures and reactivities of these materials. However, there has until recently been very little reliable data available in the literature regarding the atomic structure of metakaolin, which is one of the key SCMs utilised worldwide. This paper summarises some recent work aimed at remedying this uncertainty, by the application of advanced experimental and computational techniques, resulting in a plausible structural model for this complex disordered material.

2 PAIR DISTRIBUTION FUNCTION ANALYSIS

This paper presents two different approaches to the determination of the structure of metakaolin, one of which approaches the structure by iterative refinement between experimental neutron pair distribution function (PDF) data and density functional theory (DFT) calculations (White et al. 2010a), and the other based on direct DFT simulation of the dehydroxylation of metakaolin (White et al. 2010b). These two very different approaches are both able to provide structures which are thermodynamically plausible and in good agreement with the experimental PDF data, and which show structural environments and atomic coordinations consistent with the data obtained through XANES analysis (White et al. 2011).

Figure 1 displays the metakaolin structure which was obtained through the iterative DFT-PDF procedure, and a comparison between the PDF of this structure and the experimental PDF of kaolinite calcined at 750°C. The agreement between the experimental and simulated PDFs is very good. The original layers of the kaolinite structure are intact, but buckled, which is consistent with previous reports of a modulated but crystallographically disordered structure in metakaolin. The main changes from kaolinite to metakaolin are observed in the Al layer of the structure, which changes from 6-coordinated in kaolinite to predominantly 4-coordinated (with some 5-coordinated and a few 3-coordinated sited) in metakaolin.

Figure 2. shows an example of the procedure used in direct computational simulation of kaolinite dehydroxylation, where hydroxyl groups are sequentially selected for removal from the kaolinite structure, and the unit cell subjected to geometry optimisation after each step (White et al. 2010b).

The final computed metakaolin structure can then be compared with the experimental PDF data (Fig. 3). Figure 3 also shows a very good fit to the experimental PDF.

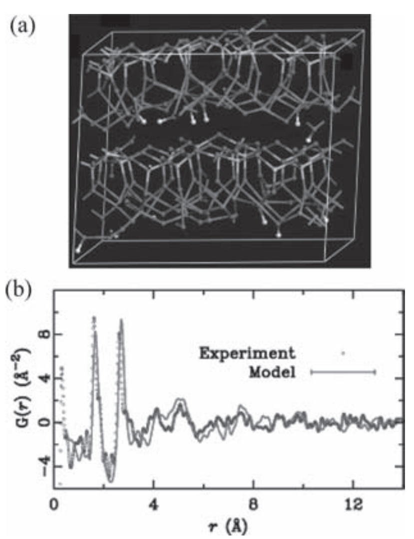

Figure 1. (a) The structural model for metakaolin obtained by the iterative PDF-DFT methodology of White et al. (2010a), and (b) a comparison between the experimental and model PDFs. Adapted from (White et al. 2010a).

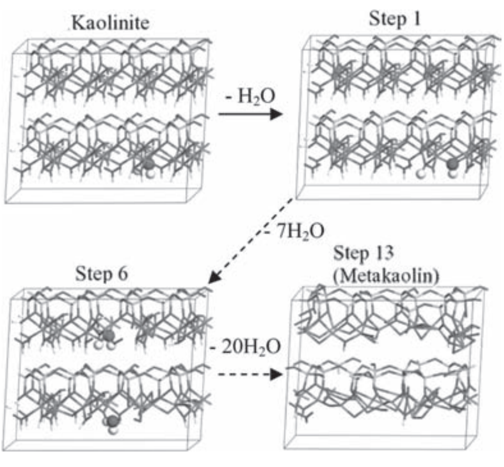

Figure 2. Schematic of the removal of water from the kaolinite structure to form metakaolin by DFT simulation of dehydroxylation. Dashed arrows represent multiple computational steps. Adapted from (White et al. 2010b).

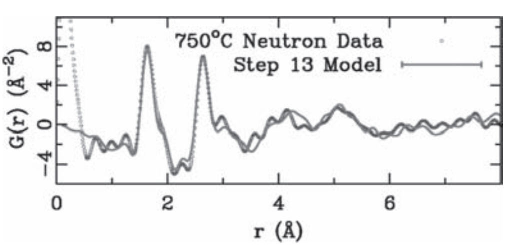

Figure 3. Comparison of the calculated neutron PDF of the final simulated metakaolin structure with the experimental neutron PDF of kaolinite calcined at 750°C. Adapted from (White et al. 2010b).

3 CONCLUSIONS

The analysis of metakaolin by several advanced experimental and computational techniques has led for the first time to the development of realistic structural models for this material. Metakaolin retains a characteristic layered structure, but lacks long-range order following the removal of the hydroxyl groups from the parent kaolinite, which leads to buckling of the layers in the structure. The structural representations developed here are in good agreement with experiment, and show a predominance of 4-coordinated Al environments. Some 3-coordinated Al is also observed, which is consistent with XANES data. The disagreement between the data presented here and the 'standard' structural understanding of metakaolin derived from NMR spectroscopy, which predicts higher Al coordinations (i.e., up to 6-coordinated Al sites) remains to be resolved.

REFERENCES

White, C.E., Perander, L.M., Provis, J.L. & van Deventer, J.S.J. 2011. The use of XANES to clarify issues related to bonding environments in metakaolin: a discussion of the paper S. Sperinck et al., "Dehydroxylation of kaolinite to metakaolin-a molecular dynamics study," J. Mater. Chem., 2011, 21, 2118–2125. *Journal of Materials Chemistry* 21(19): 7007–7010.

White, C.E., Provis, J.L., Proffen, T., Riley, D.P. & van Deventer, J.S.J. 2010a. Combining density functional theory (DFT) and pair distribution function (PDF) analysis to solve the structure of metastable materials: the case of metakaolin. *Physical Chemistry Chemical Physics* 12(13): 3239–3245.

White, C.E., Provis, J.L., Proffen, T., Riley, D.P. & van Deventer, J.S.J. 2010b. Density functional modeling of the local structure of kaolinite subjected to thermal dehydroxylation. *Journal of Physical Chemistry A* 114(14): 4988–4996.

Concrete Repair, Rehabilitation and Retrofitting III – Alexander et al. (eds)
© 2012 Taylor & Francis Group, London, ISBN 978-0-415-89952-9

The comparison between the cracking behaviour of bending and tension for Strain Hardening Cement-based Composites (SHCC)

P.D. Nieuwoudt & W.P. Boshoff
Department of Civil Engineering, Stellenbosch University, South Africa

ABSTRACT: Strain Hardening Cement Based Composite (SHCC) is a type of High Performance Fibre Reinforced Cement-based Composite (HPFRCC). SHCC contains randomly distributed short Polyvinyl Alcohol (PVA) fibres and exhibits a pseudo strain hardening or deflection hardening effect when subjected to uni-axial tensile loading or flexural loading respectively. Recent studies have been done to quantify the cracking behaviour of SHCC subjected to uni-axial tensile loading, but little work has been done to quantify the cracking behaviour subjected to flexural loading. This paper presents a comparison between the cracking behaviour of SHCC subjected to both uni-axial tensile loading and flexural loading to determine whether the cracking behaviour obtained in direct tension can be used to quantify the cracking behaviour of the tensile region of bending.

1 OBJECTIVES/DESCRIPTION

Strain Hardening Cement Based Composites (SHCC) is part of the High Performance Fibre Reinforced Cement-based Composite (HPFRCC) family and was designed to overcome the weaknesses of conventional concrete. SHCC contains randomly distributed short fibres which improve the ductility of the material and can resist the full tensile load for strains up to 5%. When SHCC is subjected to tensile loading or flexural loading, fine multiple cracking occurs that portrays a pseudo strain hardening effect as a result. It is this multiple cracking that sets SHCC aside from conventional Reinforced Concrete (RC) as conventional RC forms one large crack resulting in durability problems.

Concrete structural elements are mainly subjected to bending and not to direct tension, therefore the quantification of the cracking behaviour under flexural loading needs to be investigated. In this paper the cracking behaviour of bending and tension is compared to see whether the cracking behaviour in direct tension can be used to quantify the cracking behaviour of the tensile region of bending.

2 EXPERIMENTAL TEST PROGRAM/ RELEVANT RESULTS

2.1 *Crack width observation*

The surface deformations were measured using the ARAMIS system which is a non-contact digital image correlation system that can be used as a 2D or 3D measuring system.

2.2 *Experimental test program*

Fourteen dogbone shaped specimens were used during the quasi-static tensile tests. The specimens were tested at a crosshead displacement rate of 0.02 mm/s in a Zwick Z250 Universal Materials Testing Machine.

A total of four, four point bending tests were performed. The same SHCC mix as for the tensile tests was used for the bending specimens. A crosshead displacement rate of 0.02 mm/s was used and the tests were also done in a Zwick Z250 Universal Materials Testing Machine.

2.3 *Results*

In Figure 1 it is evident that the average number of cracks per metre for bending is lower than compared to tension for strains up to 1.5%, whereas for strains higher than 1.5% the average number of cracks per metre is approximately the same for both bending and tension.

In Figure 2 it is observed that the average of the average crack width in bending is lower than that found for tension for strains up to 1.5%, whereas the average of the average crack width at strains higher than 1.5% is about the same for both bending and tension.

In Figure 3 it is observed that the average standard deviation of the crack widths for bending is lower than in tension for strains up to 1.5%, however at strains higher than 1.5% it is about the

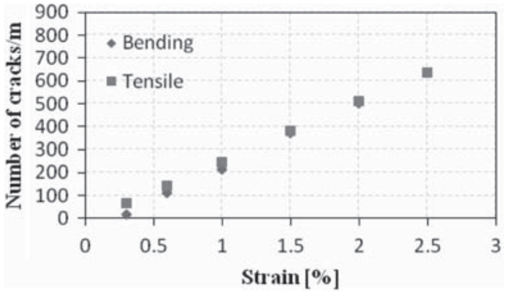

Figure 1. The comparison of the average number of cracks of cracks per metre between bending and tension.

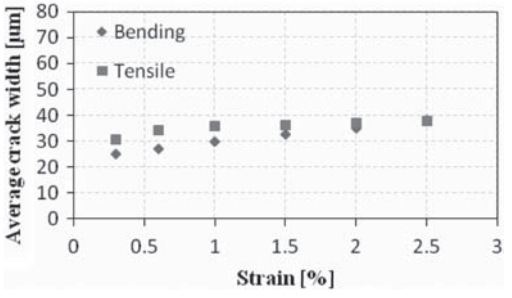

Figure 2. The comparison of the average of the average crack width of bending and tension.

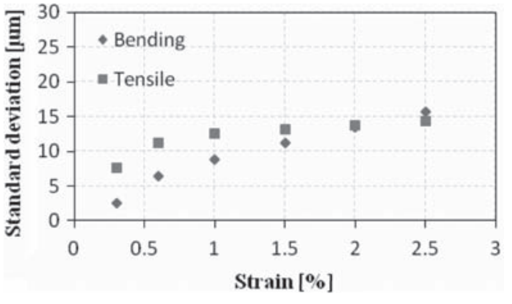

Figure 3. The comparison of the average standard deviation of the crack widths of bending and tension.

same for bending and tension. This indicates that in bending the distribution of the crack widths is less compared to those found in tension up to a strain level of 1.5%.

In Figure 4 it is observed that the average skewness of the crack widths is lower in bending than in tension, for strains up to 2.5%. This means that the maximum crack width is typically larger in tension compared to bending.

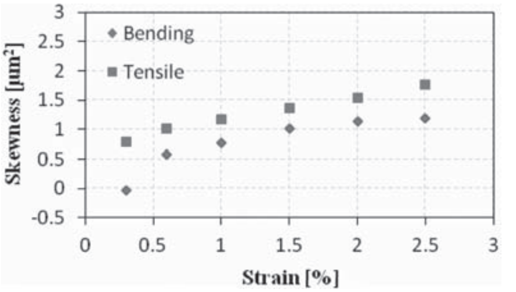

Figure 4. The comparison of the average skewness of the crack widths of bending and tension.

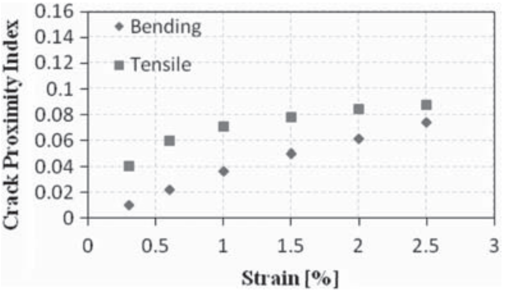

Figure 5. The comparison of the average CPI between bending and tension.

A model is proposed to quantify the crack pattern of SHCC, namely the Crack Proximity Index (CPI). The model describes the spacing of the cracks relative to each other. In Figure 5 it is observed that the CPI is lower for bending than for tension, which indicates that the cracks are more evenly spaced in bending.

3 CONCLUSIONS

A study was conducted to compare the cracking behaviour of bending and tension to see whether the cracking behaviour in direct tension can be used to quantify the cracking behaviour of the tensile region of a beam in flexure.

It was concluded that the cracking behaviour in direct tension cannot be used to quantify the cracking behaviour of the tensile region of bending up to a strain level of 1.5%. Further investigation is required to explain the mechanisms behind the different crack patterns in tension and flexure.

Concrete Repair, Rehabilitation and Retrofitting III – Alexander et al. (eds)
© 2012 Taylor & Francis Group, London, ISBN 978-0-415-89952-9

Influence of temperature on the hydration of blended cements

B. Lothenbach & G. Le Saout
Laboratory for Concrete & Construction Chemistry, Empa, Duebendorf, Switzerland

ABSTRACT: Blending of Portland cement with silica-rich materials leads to changes in composition of the hydrated cement and of its pore solution. In blends rich in SiO_2 all the portlandite formed by the Portland cement reaction is consumed within a few weeks and the formation of more C-S-H with a lower Ca/Si ratio is observed. This leads to an increased binding of alkalis and lower hydroxide concentrations. With time as more SiO_2 reacts monocarbonate and monosulfate are destabilised and in the very long term also ettringite. Higher temperatures increase the reactivity of both, the Portland cement and of the silica fume. Thus, at 50°C AFm phases and ettringite are destabilised within a few weeks, while gypsum is formed due to the low hydroxide concentrations in the pore solutions. This destabilisation of ettringite and AFm phases is in contrast to unblended Portland cements, where monosulfate and either ettringite or monocarbonate are stable at 50°C.

1 INTRODUCTION

The use of supplementary cementitious materials (SCMs) such as blast furnace slag or fly ash represents a viable alternative to Portland cements and utilizes by-products of industrial manufacturing processes. An industrial application of SCMs, however, is often hindered by the different and varying chemistry and that other hydrates are formed during hydration than in Portland cements. In Si-rich systems, portlandite can be absent and a calcium silicate hydrate phase (C-S-H) with a low Ca/Si ratio develops. A lower Ca/Si ratio leads also to an increase in alkali uptake by C-S-H and to a reduction of pH values in the pore solution. Most of the available studies on the properties of blended systems focus on mechanical or on durability aspects of a specific silica fume, fly ash or slag, while little is known about the fundamental connection between the composition and hydrates formed and its impact on the long-term development of such systems. In this paper, the hydration of a 50 wt% of a Portland cement and 50 wt% of silica fume (SF) was investigated at 7, 20 and 50°C experimentally. Thermodynamic modelling was used to predict the changes during hydration and the changes associated with the presence of different amounts of SiO_2.

2 HYDRATION

The temperature has a significant influence on the reaction of the silica fume as shown in Fig. 1. The reaction was considerably slower at 7°C than at 20 or 50°C. After 1 year, however, a similar degree of reaction of approximately 70 to 80 wt% was reached, such that from the 50 wt-% silica fume originally present, 10–15 wt-% silica fume had not yet reacted (Fig. 1).

During the first day, the hydration of the blended cement at 20°C proceeded similarly to OPC hydration. Ettringite formed during the first minutes; its quantity increased during the first day. The presence of portlandite was observed between 1–7 days and the presence of hemi- and/or monocarbonate up to 28 days. The relatively low amount of portlandite formed and its consumption with time is related to the reaction of the silica fume. During the first days, the reaction of the Portland cement is faster than the reaction of the silica fume. However, the silica fume continues to react during the first month (Fig. 1) and consumes

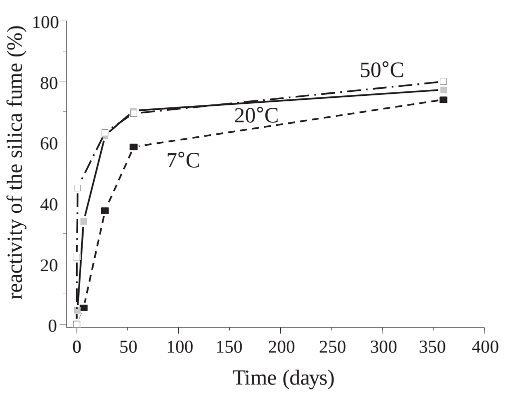

Figure 1. Reaction of silica fume.

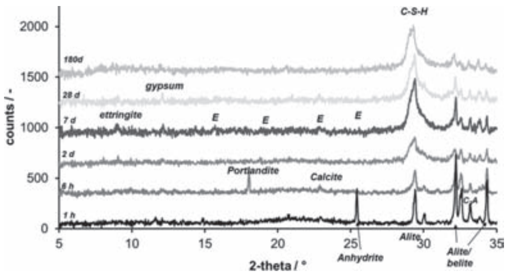

Figure 2. XRD of the hydration of 50% PC-50% silica fume at 50°C. E: ettringite.

the portlandite by the pozzolanic reaction. After 6 months, the main hydration products that could be identified by XRD and TGA were ettringite and tobermorite-like C-S-H.

At 7°C, the reaction of the silica fume was much slower (Fig. 1), thus the presence of portlandite was observed up to 28 days. The main hydrates formed at 7° were identical to those at 20°C.

At 50°C, the reaction of both the cement clinkers and of the silica fume occurred much faster. Portlandite formation was observed after 6 hours only and the portlandite was consumed after 1 day already due to the faster reaction of the silica fume (Fig. 2). During the first days, some ettringite had formed, which was destabilised at later reaction times again and the formation of poorly crystalline gypsum was observed. The destabilisation of ettringite and the formation of gypsum would be consistent with the higher reaction of the silica fume already at early age at 50°C than at 20 or 7°C (Fig. 1).

In contrast to the Portland-silica fume cements studied, monosulfate and either ettringite or monocarbonate have been observed to be persistent at 50°C in unblended Portland cements. The strong decrease of the hydroxide concentration due to the uptake of the alkalis by the low C/S C-S-H led in the experiments presented here to a destabilisation of monosulfate and ettringite.

The temporary occurrence of portlandite, ettringite and/or monocarbonate during the first few days emphasizes that not only the composition of solids but also their reactivity determines the composition of the phase assemblage.

The temperature had also a significant influence on the composition of the pore solution. The fast reaction of the silica fume at 50°C is mirrored by the fast decrease of K concentrations. The sulphate concentrations increased by a factor of 2 between 7 and 20°C and factor of 5 between 20 and 50°C, as the solubility of ettringite increases with increasing temperature. The strong decrease of the alkali concentration with time was also mirrored in the decreasing hydroxide concentrations. The hydroxide concentrations at 7 and 20°C decreased parallel to the decrease of the K and the increase of sulphate concentrations.

3 CONCLUSIONS

The composition of the solid phases and the pore solutions of a 50:50 Portland cement:silica fume blend was clearly affected by the temperature between 7 and 50°C. The changes were comparable to the changes observed in Portland cements within the same temperature range, with some important exceptions. In the blended cements studied, the reaction of the silica fume

- lowered the alkali and the hydroxide concentrations strongly,
- resulted in the consumption of portlandite and the formation of low Ca/Si C-S-H and
- destabilised hemicarbonate, monocarbonate and monosulfate with time.

At 50°C, ettringite was unstable and gypsum formed instead due to the strong decrease of the hydroxide concentrations.

Thermodynamic modelling indicated that the replacement of PC by SiO_2 leads to significant changes in the composition of the hydrate assemblage. Not only portlandite was depleted to form more C-S-H but also the amount and kind of AFm and AFt phases were affected. Monocarbonate and monosulfate were calculated to be unstable with regard to strätlingite and calcite as more and more SiO_2 becomes available. If even higher quantities of SiO_2 are available, eventually also ettringite is calculated to be unstable as the pH decreases.

Concrete Repair, Rehabilitation and Retrofitting III – Alexander et al. (eds)
 ISBN 978-0-415-89952-9

Thermodynamic modeling of sulfate interaction

B. Lothenbach & W. Kunther
Laboratory for Concrete & Construction Chemistry, Empa, Duebendorf, Switzerland

A.E. Idiart
Amphos 21 Consulting S.L., Barcelona, Spain

ABSTRACT: The expansion of mortars caused by external sulfate attack is significantly reduced by the presence of bicarbonate in the interacting solution. $CaCO_3$ is formed near the surface. Thermodynamic modeling confirms that $CaCO_3$ binds most of the available CaO and thus reduces the formation of ettringite. Thermodynamic modeling is a versatile tool to predict the changes in the phase assemblage associated with cement-sulfate interaction. Direct linking of the amount of ettringite and/or other solids formed with the macroscopically observed expansion, however, is not possible. Although sulfate attack generally leads to macroscopic expansion, the amount of newly formed solid is typically too small to fill all the available pores. Previous modeling efforts following crystallization pressure theory indicated that the consideration of an oversaturated solution and the subsequent development of crystallization pressure in small pores is not sufficient to adequately model the experimentally observed expansions. An improved understanding of the microstructural features responsible for expansion is thus needed.

1 INTRODUCTION

Chemical degradation of cementitious materials is a serious threat to the durability and performance of concrete structures. Recent advances in modeling have enabled adequate description of the changes associated with sulfate ingress either using simple "0-dimensional" models or 1-dimensional reactive transport models, which gave comparable results and were able to reproduce the changes observed in experiments.

In this work "0-dimensional" thermodynamic modeling is compared to experimental results and used to illustrate how adequate modeling can help to understand and illustrate the experimental observations. The limitations of such an approach are also discussed.

One of the major ions present in many ground waters is bicarbonate, HCO_3^-. Mortar prisms were exposed to solutions containing 50 g/L Na_2SO_4 or 50 g/L Na_2SO_4 + 30 g/L $NaHCO_3$ at 20°C. Control samples were exposed to limewater.

2 THERMODYNAMIC MODELING

The changes in the phase assemblage caused by the interaction with the sulfate solutions was calculated as a function of the ratio of Na_2SO_4 (or Na_2SO_4 + $NaHCO_3$) solution to the amount of cement as shown in Fig. 1. Thermodynamic modeling predicted in the hydrated core of the mortar sample the presence of C-S-H, portlandite, monosulfate, and smaller quantities of hydrotalcite and hemicarbonate (Fig. 1), which agrees with the experimental observations. Upon ingress of Na_2SO_4 solution, the AFm phases and portlandite were calculated to convert to ettringite until all aluminium available was present as ettringite (Fig. 1). The remaining portlandite reacted with the sulfate to form gypsum. Closer to the sample surface, the gypsum and the C-S-H were leached. The porosity was never totally filled as shown by the line indicating the initial volume in Fig. 1A.

The sample immersed in Na_2SO_4 + $NaHCO_3$ was predicted to show a similar sequence (Fig. 1B), destabilisation of AFm phases and portlandite while ettringite formed. However, nearer to the exposed surface, ettringite was destabilised and no gypsum was calculated while considerable quantities of calcite precipitated (Fig. 1B). The interaction of $NaHCO_3$ with ettringite led to its destabilisation as $CaCO_3$ is thermodynamically more stable under these conditions.

3 EXPERIMENTAL OBSERVATIONS

The mortar samples exposed to Na_2SO_4 solution showed much more expansion than the samples exposed to Na_2SO_4 + $NaHCO_3$ solutions. The samples showed after the interaction with

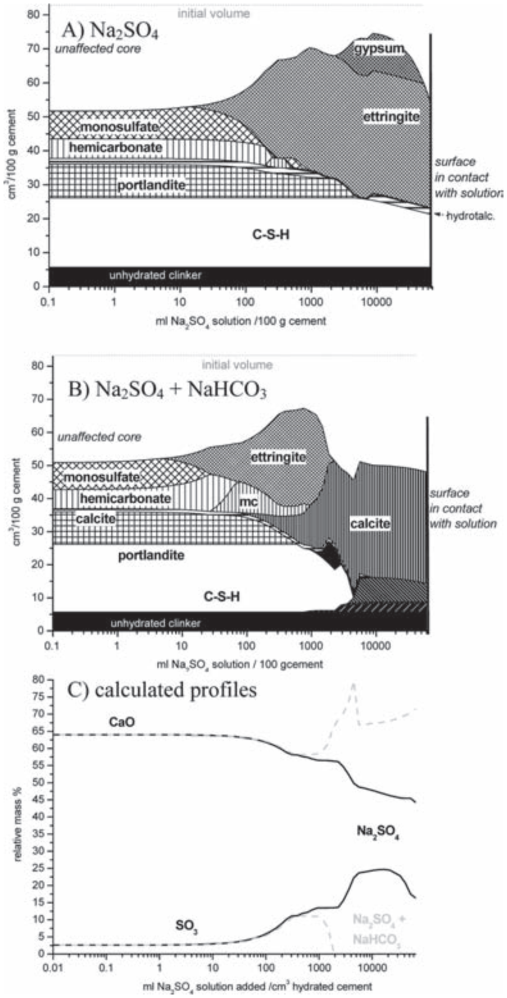

Figure 1. Calculated phase assemblage of the mortar immersed in A) Na_2SO_4 and B) Na_2SO_4 + $NaHCO_3$. C) calculated measured CaO and SO_3 profiles.

Na_2SO_4 solutions the formation of gypsum and more ettringite, while in the samples exposed to Na_2SO_4 + $NaHCO_3$ mainly calcite was observed, in agreement with the modelling results.

A clear decrease of CaO near the surface was observed for Na_2SO_4 exposed mortar. In contrast, the mortar exposed to $Na_2SO_4 + NaHCO_3$ exhibited no such decrease as the CaO was bound as calcite.

4 CURRENT LIMITATIONS OF MODELING SULFATE ATTACK

Thermodynamic modeling is a versatile tool to predict the changes associated with sulfate interaction. Direct linking of the amount of ettringite and/or other solids formed with the macroscopically observed expansion, however, is not possible. This is mainly due to the fact that it is the microstructural processes within the cement paste which dictate to a large extent the macroscopic behaviour. On the other hand, thermodynamic modeling as presented in this work is limited to the continuum scale. With this model, the amount of ettringite predicted is too small to fill the total available porosity although expansion has been observed. The consideration of oversaturated solution and thus the development of crystallization pressure in small pores has been found to be insufficient to adequately model the experimentally observed expansions at least in the present state.

More research is needed to consider other possibilities like introducing explicitly the effect of pore size distribution on the generation of oversaturation or exploring pore-scale reactive transport modeling.

It may be concluded that the mechanism by which ettringite formation leads to expansions is still not well understood and needs to be elucidated. Even though sulfate attack is very well characterized from a macroscopic perspective, some key aspects related to the hydrated cement microstructure are still largely unknown. One of the main concerns is how to realistically upscale the crystallization pressure calculated at the micro- or nano-scale to the macroscopic level. Another unresolved issue is how to deal with downscaling of solution concentrations from the continuum scale (the scale of thermodynamic modeling predictions as presented in this work) to the micro- or nano-scale (or vice versa). A further central issue regarding the role of ettringite is the determination of the precipitation sites within the microstructure of cement paste (which in turn depends on the initial distribution of AFm and AFt phases within the hardened cement paste): ettringite is typically found intimately mixed with the C-S-H phase, and also within large pores, voids and cracks. It is thought that only ettringite that is intimately mixed with C-S-H is the main responsible behind expansions.

Concrete Repair, Rehabilitation and Retrofitting III – Alexander et al. (eds)

An ongoing investigation on modeling the strength properties of water-entrained cement-based materials

Luís Pedro Esteves
Porto Engineering Institute/Technical University of Denmark, Copenhagen, Denmark

ABSTRACT: Water-entrained cement based materials by superabsorbent polymers is a concept that was introduced in the research agenda about a decade ago. However, a recent application in the production of high performance concrete revealed potential weaknesses when the proportioning of this intelligent material is not well performed, raising doubts among both academic and industrial society about the usability of superabsorbent polymers in cement-based materials. This work constitutes the baseline tentatively to be used on modeling the compressive strength of SF-modified water-entrained cement-based materials. Beyond the discussion of whether or not the introduction of superabsorbent polymers leads to a strength reduction, this paper uses both experimental and theoretical background to separate the effect of SAP in both pore structure and internal relative humidity and the effect from the active restrained desiccation on strength of the composite material.

1 INTRODUCTION

The prediction of compressive strength in cement-based materials is a topic with more than a century of research. The present work emerges from the actual necessity of adapting or creating a model that is able to predict the compressive strength of cement-based materials with the inclusion of superabsorbent polymers. It is shown that the existing models are not appropriate for the prediction of strength properties of low water and low porosity systems subjected to change in relative humidity, porosity and where restrained desiccation is active.

2 THE DIMENSIONS OF COMPRESSIVE STRENGTH IN LOW WATER AND LOW POROSITY SYSTEMS: A REVIEW

The paper identifies the relevant dimensions affecting strength of water-entrained cement-based materials. A review is given with focus on three different dimensions: the effect of porosity, the effect of relative humidity and the effect of microcracking (due to restraint of the free deformation of the paste). Experimental data is given to define the characteristics of water-entrained cement systems, whereas discussion is made about the role of the SAP pores, and the impact of internal curing on the RH-profile of the cementitious system. The role of aggregate in low porosity and low water systems is also addressed.

It is concluded that the modeling of the strength properties of cement-based systems entails the knowledge of different physical properties, which is beyond a simple mechanical characterization. A framework is established to to pursue the study of each individual parameter.

3 PART I: THE EFFECT OF POROSITY

The porosity in concrete is a crucial parameter. Not only the total porosity influences the strength of the material, but also the shape and distribution the pores affects differently the mechanical properties of cement-based materials. This is particularly important in the case of cement systems with superabsorbent polymers. The structural response of a material is the inverse of the force field that is applied to the solid surface. In the case of a porous surface, the non-solid regions are not able to transfer any load. The effective area being compressed in a water-entrained cement system should be reduced of the SAP porosity, so that the section that is effectively transferring load can be analysed. Such a concept, similar to that proposed by Hasselman (1963) for polycrystalline materials subjected to uniaxial tensile stress, could be described by the system of equations (1) and (2), where SAP_{pores} is given in vol.-%.

$$\alpha_y = \frac{F}{A_{ef.}} \tag{1}$$

$$A_{ef} = A \cdot \left(1 - SAP_{pores}\right) \tag{2}$$

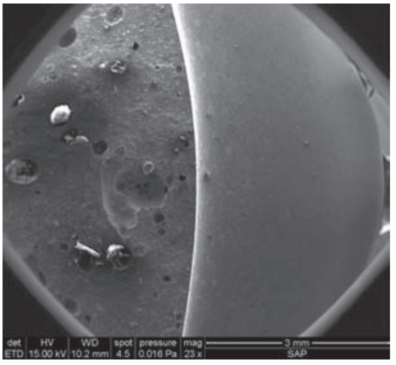

Figure 1. SEM-image taken from a water-entrained cement-based system by superabsorbent polymers. Both internal and external surface of the specimen is shown.

Substituting, equation (1) will assume the form of equation (3). Let k be a factor of strength conversation according to (4). Then (3) will reduce to (5).

$$\alpha_y = \frac{F}{A \cdot \left(1 - SAP_{pores}\right)} \tag{3}$$

$$k = \frac{1}{\left(1 - SAP_{pores}\right)} \tag{4}$$

$$\alpha_y = \frac{F}{A} \cdot k \tag{5}$$

The size distribution of the expanded SAP particles will determine the SAP porosity, assumed to match the size of the inclusions. This approach relates the physical properties of the system with the mixture proportioning. Also, desorption process will be initiated when the system has developed its final geometry, making the absorption capacity of superabsorbent polymers the sole variable affecting the SAP porosity (Fig. 2).

The SAP porosity is calculated with an absorption coefficient of 12.5 ml/g of dry SAP, a value that has achieved reproducibility (Jensen 2002, Esteves 2011). In any case, the prediction of porosity may be promptly modeled for other types of superbasorbent polymers through the proposed methodology. Fig. 3 and Fig. 4 were developed considering the model assumptions made about the effect of porosity as describe in the theoretical approach. It is seen that the values of theoretical strength approximate to the experimental values of strength, in particular for the matured cement pastes, and exceeds such values when coupled effects of aggregate addition, viz. microcracking, and internal curing are active.

A second part of this framework, on the effect of relative humidity on the strength is expected in autumn 2012.

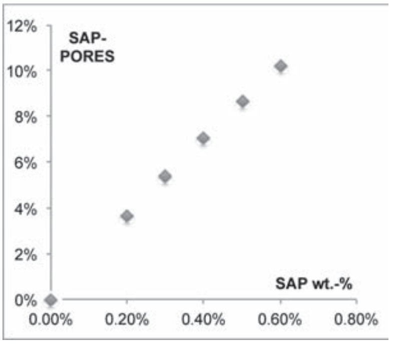

Figure 2. Relation between the mixture proportioning and the SAP porosity. SAP is calculated as wt.-% of cement. Absorption coefficient was 12.5 ml/g.

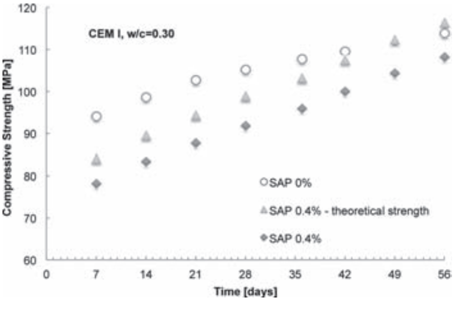

Figure 3. Theoretical strength of cement systems with superabsorbent polymers. The experimental values were taken from Lura et al. (2006).

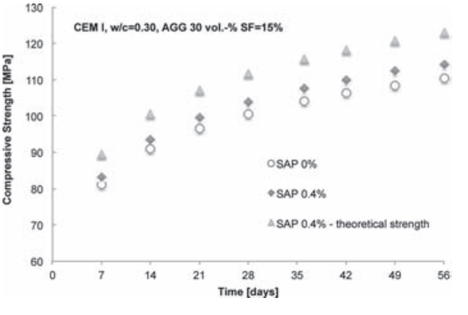

Figure 4. Theoretical strength of cement systems with superabsorbent polymers. The experimental values were taken from Esteves (2009).

ACKNOWLEDGEMENTS

A relevant part of this work was done at Technical University of Denmark. The opportunity to do so in conjunction with many other experiments, and also the thorough discussions with Ole Mejlhede Jensen are greatly acknowledged.

Theme 5: Concrete technology and structural design

This page intentionally left blank

Concrete Repair, Rehabilitation and Retrofitting III – Alexander et al. (eds)

Concrete knowledge improvement in sub-Saharan Africa

N.S. Msinjili, W. Schmidt & G.J.G. Gluth
BAM Federal Institute for Materials Research and Testing, Berlin, Germany

M.V.A. Florea
Eindhoven University of Technology, Eindhoven, The Netherlands

G. Senthil Kumaran
Kigali Institute of Science and Technology, Kigali, Rwanda

A.A. Akindahunsi & H.C. Uzoegbo
University of the Witwatersrand, Johannesburg, South Africa

I. Stipanović Oslaković
University of Twente, The Netherlands

ABSTRACT: The building situation in Africa is overwhelmed with high-priced materials and lack of adequate concrete technology, which provides a challenge in the concrete industry. Worldwide, cement and concrete experts are at the cutting-edge to sustainable, green and healthy but nonetheless high-performance concrete, which is more sustainable and safer than traditional methods of construction with clay and wood. Since concrete in Africa is rather a new construction material, this sustainability experience can offer the continent a unique opportunity to begin a constantly growing building sector with the newest state-of-the-art technology. This can be achieved without subordinating to existing standards by establishing a sustainable "African concrete technology". The major challenge for most sub-Saharan countries is the deficiency of experts, which would be required to establish such state-of-the-art technology. Based on the examples of two African-European scientific networks—SPIN and LightSHIP—this paper presents possible solution strategies for the establishment of a scientific cooperation between Europe and Africa, with links to policy making bodies that can help accelerate the progress of cement and concrete industries in Africa.

1 INTRODUCTION

Cement and concrete can be produced and applied nearly everywhere in the world with local materials. Concrete is very versatile and can be designed to withstand any natural threat. Furthermore it is sustainable and more durable than most other construction materials, particularly at high temperature and in humid climate conditions. This situation indicates that, cement and concrete technology will play a major role in the future construction technology of sub-Saharan Africa, where the steady growing population urgently demands for housing and infrastructure.

In comparison to Europe or North America, which have both approximately 150 years of experience, cement is a relatively new material for sub-Saharan Africa. However, the need for construction and the growing populations cannot afford another 150 years of slow learning process. Sub-Saharan Africa needs state-of-the-art technology, which however, has to be modified according to the specific African boundary conditions.

1.1 *Infrastructure for cement and concrete*

The whole infrastructure of Africa, with long distances between urban structures, cannot compare with Europe and thus offers different challenges, which have to be identified and taken into account to sustainably build with concrete.

1.2 *Cement types*

Most African countries do not have a significant steel production. Hence, slag blended cements are not an option. However, natural pozzolans and mineral wastes can be used as innovative materials to develop specific African novel binder types.

1.3 *Prices for construction materials*

All standards and established practices from countries of the northern hemisphere are based on high cement consumption with minimum manpower with the aim to lower the price of the construction process. Due to the scarcity of cement all over Africa, prices are extremely high. On the other hand labour power is extremely cheap in Africa. For Africa, it would thus be a fatal mistake to blindfold copy these practices. Africa has to develop novel and innovative approaches towards concrete technology, which do not require excessive volumes of cement.

1.4 *Construction technology and quality*

Construction sites in sub-Saharan Africa are typically not well equipped for high quality and high performance materials. Proportioning is made by rule of thumb and mixing of constituents is often conducted manually, with shovels. Fresh concrete quality control is often not well established.

1.5 *Environmental boundary conditions*

Sub-Saharan Africa is exposed to various climatic conditions. Numerous countries have long coastal lines. Many sub-Saharan countries suffer from natural hazards like earthquakes and floods. Heat is particularly a problem during the casting and the early hydration, often yielding uncompacted zones and cracks in a construction. Finally, heat in combination with humidity is fostering transport of aggressive media and thus accelerating the damage processes.

1.6 *Availability of raw materials*

Africa provides a large number of prospective materials that can be used in concrete technology, such as bagasse ash, rice husk ash, natural pozzolans, pumice aggregates, organic fibres, or even cassava starch as rheology modifier. Africa thus provides a high potential for new ways in concrete technology, but the key to the effective use is education and research.

1.7 *Standards*

The low level of standards in many African countries to date can be considered as a unique opportunity to filter existing standards with care and establish regulations that refer to what is really the best available practice. Developing novel technologies without reinventing the wheel requires a high level of expert knowledge, so again the importance of research and education needs to be emphasised. In this context, it is most important to have a reasonably high number of local experts available, which have the capacity to filter out the appropriate technology to be adopted, and the technology that needs to be redeveloped specifically for African boundary conditions. These experts are scarce all over the region, and the deficient number of educated people who stay in Africa is a serious threat to the progress of the construction industry.

2 HIGH LEVEL EDUCATION AS VEHICLE FOR A SPECIFIC AFRICAN CONCRETE TECHNOLOGY

As concrete technology has different histories on different continents, and technology varies all over the world, surely sub-Saharan Africa needs to develop an individual technology, based on the local traditions and boundary conditions. Unmindful use of standards that were developed for different geographical and economical areas does not yield the optimum technology.

The key to develop such technology is education throughout all levels of the educational system. A major drawback to be observed all over sub-Saharan Africa is the lack of researchers that remain on the ground, and those researchers that exist suffer from administrative obstacles and lack of funds. Multi-national cooperation networks with significant impact hardly exists in the field of cement and concrete technology. Therefore Africa needs to concentrate resources on joint and international research activities and networks. The major objective of sub-Saharan African countries should be high level scientific capacity that remains on site. It should be considered that high level technology fosters economic growth probably in a more sustainable way than any other measure. In Africa today, most universities are rather educational units than research centres. In order to achieve excellence, research activities should take place at minimum on PhD or post-doc level. Research centres of excellence with facilities of international standard could be a sustainable solution that can be implemented with shared economic responsibility as regional centres with funds from several surrounding countries.

3 CONCLUSIONS AND OUTLOOK

A more sustainable development in Africa is viewed to be challenging, taking into consideration the necessary requirements to have an initial investment, which can support the development and production of appropriate technologies and suitable building materials. This will involve the sharing of responsibilities between industries, research institutions, the local government and other public sectors. International cooperation projects between African and European countries like SPIN and LightSHIP give examples of initiatives that support scientific capacity in concrete and materials research. These initiatives, however, can only be a start-up to bring state of the art technology to a broader user group. For the sustainable development of a technology that is best for a specific region, this technology has to be founded on the knowledge of local experts. External experts can only support processes. Therefore, Africa needs to foster research excellence and needs to make it attractive also for international top level researchers to conduct activities in Africa. This might only be possible on a reasonably short term by pooling resources in order to implement few but excellent multi-national research facilities.

ACKNOWLEDGEMENTS

The SPIN and LightSHIP consortia would like to acknowledge the European Commission, ACP-ST programme (by the ACP Group of States), the Federal Ministry of Education and Research (BMBF), and the Federal Ministry of Economics and Technology (BMWi) for their continued support and cooperation throughout the run-time of the projects.

Concrete Repair, Rehabilitation and Retrofitting III – Alexander et al. (eds)
© 2012 Taylor & Francis Group, London, ISBN 978-0-415-89952-9

Evaluation of concrete quality in Libya

Mohamed S. Alazhari & Milad M. Al Shebani
Department of Civil Engineering, Tripoli University, Tripoli, Libya

ABSTRACT: The quality of concrete used in current and past 20 construction projects were evaluated based mainly on the concrete compressive strength achieved. The projects are different in nature and are at various levels of completeness. In Libya, concrete compressive strength was usually obtained from test results of a 150 mm standard cube mold. Data collected from all 20 projects showed that the 28-day concrete compressive strength follow in general Normal Distribution pattern. The study dealt with concrete quality aspects such as: quality control, strength range, data standard deviation, data scatter, and ratio of minimum strength to design strength. Site quality control for these projects ranged from very good to poor according to ACI214 criteria. The ranges (Rg) of the strength (max. strength–min. strength) divided by average strength are from 34% to 160%. Data scatter is measured as the range (Rg) divided by standard deviation (σ) and is found to be (1.82 to 11.04), indicating that the range is $\pm 3\sigma$. In lieu of national unified procedure, international construction companies working in Libya are free to use the assessment criteria for concrete compressive strength that suit them. Therefore, the study reveals that concrete quality assessments conducted by these construction companies usually meet their adopted (internal) standards, but sometimes fail to meet internationally known standard requirements. The assessment of concrete presented in this paper is based on ACI, British standards and proposed Libyan concrete strength assessment criteria.

1 INTRODUCTION

In Libya, concrete is probably the only materials used for building constructions. In lien of national unified concrete quality acceptance criteria, concrete batching plants and contractors use a variety of concrete quality assurance standards. Such a practice resulted in confusions some times, as to what constitutes an acceptable level of the quality of concrete.

2 ACCEPTANCE CRITERIA

Two widely used concrete quality's acceptance criteria:-

For ACI-code, the acceptance criteria lead to

$$\rho.A(\rho) \le 2\% \tag{1}$$

For BS-code, the general acceptance criterion is written as

$$\rho.A(\rho) \le 5\% \tag{2}$$

Where, ρ is % (portion) of strength values below the average design strength, fd, and $A(\rho)$ is the acceptance probability.

3 EVALUATION OF FIELD DATA

Four different methods of evaluation are used in this study:

3.1 *Method one*

The standard deviations and coefficient of variation were used to evaluate the level of control of conventional strength concrete mixtures. These two types of classifications showed an agreement in 9 out of 20 projects.

3.2 *Method two*

The relation between ρ and $A(\rho)$ is used to determine the quality control acceptance and non acceptance range as shown in Fig (1), for ACI, BS and a proposal Libyan criteria (PLC). Each criteria has a specified parameter "$\boldsymbol{\lambda}$" such that:

$$\rho \times \rho(A) \le \lambda\% \tag{3}$$

Overall, the evaluation by this method gives about 44% of the projects are being accepted.

3.3 *Method three*

In this method the whole data for all projects considered as one project. Then both the standard

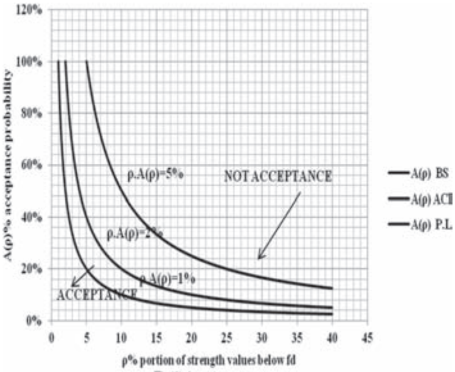

Fig (1) Acceptance curve

deviation, coefficient of variation and the range R are determined. In this method, concrete acceptance criteria is based on the following inequality:-

$$fcr \geq fd + \rho\sigma \tag{4}$$

$$\rho = (fcr - fd)/\sigma \tag{5}$$

Where fcr is the required strength. It is found that the changes of falling below lower limit is about 30%

3.4 *Method four*

This method addresses both conformity and strength safety. The evaluation of concrete quality was done based on ACI-Code, BS-Code and a proposed Libyan criteria(PLC). The system of evaluation is based on the relation of average required strength, average design strength and strength's standard deviation. The ACI and BS criterion gave a close evaluation level. The proposed Libyan criteria (PLC), however, is more conservative than the other two criteria.

4 CONCLUSIONS

The quality of concrete of twenty construction projects in Libya was assessed by using both ACI & BS quality control criteria. The assessment of site concrete quality of these projects revealed that the quality ranged from very good to poor according to ACI214 criteria. Statistical analysis of data considered in this study show a normal distribution pattern of the actual field data with a bias factor for concrete compressive strength ranging from 0.693 to 2.078 with a COV ranging from 5.58 to 25.19%. The proposed Libyan criteria of accepting concrete compressive strength gave an upper limit for both ACI & BS codes. This proposed criterion can be used to overcome the deficiency in concrete produced locally, as well as the lack of accuracy in testing method.

Concrete Repair, Rehabilitation and Retrofitting III – Alexander et al. (eds)
© 2012 Taylor & Francis Group, London, ISBN 978-0-415-89952-9

Who will be making high performance concrete?

Michael Khrapko
CBE Consultancy Ltd, New Zealand

ABSTRACT: There is an increasing demand for high performance concrete all around the world. Self-compacting concrete is growing in popularity, especially in precast factories; ultra high strength concrete attracts the interest of architects and designers, other high performance cement-based materials such as strain hardening composites, textile reinforced concrete and others are gaining their acceptance in the structural repairs and new product development sectors. Production and supply of high performance concrete is very technologically specific as it is highly sensitive to external influences, such as quality and uniformity of raw materials, batching (weighing) accuracy, mixing, personnel qualifications and capabilities, formwork quality, and many others.

The main medium for production and delivery of concrete in mass volumes these days is readymix (or pre-mixed) concrete, which originated in the 1920–30s. Concrete mixing technological advances enable to manufacture concrete even quicker and of better quality and uniformity, but the main objective of any readymix (RMC) organization—the fast production of a large volume of concrete—hasn't changed. RMC plants achieve this goal through the production of plain concrete.

Self-Compacting Concrete (SCC) is one of the most used types of high-performance concretes. Despite the intensive effort of commercializing Self-Compacting Concrete (SCC) in concrete construction industry in the last 15 years, globally SCC makes up approximately only 7% of total concrete produced (this excludes precast concrete). One the main reasons for this is that RMC industry, by the nature of the business organization, does not have enough incentive to be attracted to supply High Performance Concrete, as requirements for HPC production go beyond the routine daily operation. This paper discusses the problem in more detail and looks at whether the RMC industry can become the prime vehicle for the manufacture and delivery of high performance concrete.

The purpose of this paper is to simply bring up an awareness of the potential issues and in no way to criticize ready mix concrete and concrete construction industries.

High performance concrete (HPC) is concrete that possesses high workability, high strength and high durability. It has also been defined as concrete in which certain characteristics are developed for a specific application and environment, concrete that is designed to exceed the performance of ordinary concrete.

It has become evident that the quantitative precision and consistency in properties of HPC mix design is much higher than it would be for conventional vibrated concrete (CVC).

Self-Compacting Concrete (SCC) is the most well-known, used and researched type of High Performance Concrete.

SCC is a prime example of the current challenge the concrete industry is facing: neither RMC nor the concrete construction industry in their current organisational state are quite prepared to take up challenges presented by new technological advancements.

Globalization, advances in technology, environmental factors and changes in the structure of the economy are presenting new and serious challenges to the construction industry. To capture new opportunities, the industry must respond positively. New challenges require new approaches. Construction industry worldwide is largely made up of small firms, and is fragmented, with low profit margins, low-bid tendering, inequitable risk sharing, and poor investment in technology.

Production of conventional vibrated concrete (CVC) is a worldwide-established practice. Concrete is premixed at a specialized concrete batching plant, batched using reasonably accurate weighing equipment and mixed either in stationary or transit mixers. An average batching plant has limited storage capacity Thus, there would be a restricted number of aggregates and powder materials available for special concrete.

With the basic quality control and quality assurance in place, the required quality of CVC is achieved. Serving solely the construction industry, RMC suffers the same problems: in order to be profitable it has to survive in a highly competitive market, the products have to have low margins, and the operation must be low cost.

At the current point of development, demand on HPC, including SCC, is small, and, when it occurs, RMC delivers good quality products. But it comes at cost, as every HPC (SCC) supply project requires special management and high concentration of resources from RMC. The question is that if RMC will be able to supply consistent quality HPC when demand is high, whenever it is going to happen.

Two quite distinct approaches to future HPC manufacture and supply are envisaged: (a) upgraded RMC batch plant, and (b) a mobile unit solely specialized on production of HPC (this can be either part of RMC set up, or construction company). The former will only work efficiently when two problems are resolved:

Problem 1: Reasonable demand on HPC is necessary to justify investment into RMC upgrade (machinery, knowledge, training, etc.), and;

Problem 2: On site responsibility transfer from concrete supplier to concrete user.

It seems that the first problem will be sorted out naturally when the second problem is resolved. However, in order to resolve the second problem, some serious organizational changes are necessary.

The main attraction to the specialized HPC production units is that such units can be fully integrated into the construction process and the whole high performance concrete construction process would be similar to a concrete precast factory where concrete production and concrete placement are under one management roof. However, if such specialized unit is part or extension of RMC operation, the responsibility transfer issue can still be presented.

Quality and serviceability of structures made of HPC is entirely determined by the quality of fresh HPC. Approaches to the manufacturing processes of CVC and HPC are distinctly different in the sense that manufacturing of quality HPC is by far more complex. Therefore, there is a concern that at its current state RMC industry would not be able to adequately supply high volumes quality HPC of different kind when demand grows.

Concrete Repair, Rehabilitation and Retrofitting III – Alexander et al. (eds)
© 2012 Taylor & Francis Group, London, ISBN 978-0-415-89952-9

The role of the structural engineer in the design of low embodied energy concrete-frame buildings

R. Muigai, M.G. Alexander & P. Moyo
Concrete Materials & Structural Integrity Research Unit, Department of Civil Engineering, University of Cape Town, South Africa

ABSTRACT: Concrete is a widely utilized construction material in both residential and commercial buildings, which in turn makes it have a large influence on the environment. This paper reviews past studies on the Life-Cycle Assessment (LCA) of concrete-framed buildings with the objective of investigating the influence of the structural frame and materials on the environmental performance of concrete buildings. The study found that the structural frame has a dominant impact on the embodied energy compared to other building assemblies (finishes, roof, window and non-structural frame). Within the structural frame, the slab system has the highest contribution to the overall embodied energy of a building, representing 27% to 77% of the initial embodied energy. Thus the structural engineer can contribute to reducing embodied energy of RC frames by selecting suitable structural assemblies and construction technologies that can help reduce the embodied energy of concrete-frame buildings.

1 INTRODUCTION

Building construction has a large influence on the environment through consumption of massive amounts of resources and generation of wastes. Since 1990, life-cycle assessment (LCA) has proved useful for decision making as it establishes the impacts of a building over its life-cycle, and with this information the designer is able to make decisions that improve the environmental efficiency of buildings. A LCA tracks the inputs and outputs (for example, energy and materials, wastes and emissions) generated throughout the building's life (cradle-to-grave) and the potential impacts (ISO 14040:2006; ISO 14044:2006).

A number of researchers have reviewed past LCA studies for different reasons. Ramesh et al. (2010) reviewed life-cycle energy of 73 buildings located in 13 countries. They showed that operation and embodied energy formed the significant contributors of a building's life-cycle energy demand. Ortiz, et al. (2009) compiled 25 case studies on LCA in buildings. The studies reviewed were for the period 2000–2007. Sartori and Hestnes (2007) reviewed energy use in the life-cycle of conventional and low-energy buildings, for 60 buildings located in 9 countries. All these reviews compare the results of different types of buildings constructed using different materials: wood, steel or concrete. Hence the LCA studies presented in the aforementioned reviews are not fully comparable. At present there is no comprehensive review of past LCA studies focusing on concrete framed structures. Such a review is important as it would determine the specific impacts of concrete framed buildings hence allowing designers to focus their efforts on those areas with major impacts and in turn select structural systems that will reduce the overall negative impacts of the building.

In this paper, eighteen journal articles describing forty LCA studies on various concrete residential and commercial buildings are reviewed with the objective of investigating the influence of the structural system on the life-cycle energy use of a building. The term 'structural system' as used in this study refers to the materials and structural elements required to withstand and support all anticipated loads on a building.

2 EMBODIED ENERGY OF MATERIALS AND BUILDING COMPONENTS

2.1 *Contribution of materials to embodied energy*

In general, studies on the embodied energy of construction materials in buildings show that although concrete has smaller amounts of embodied energy (0.78 MJ/kg) (Hammond and Jones, 2008) compared to other materials such as aluminium (155 MJ/kg) (Hammond and Jones, 2008) and steel (57 MJ/kg) (Hammond and Jones, 2008), its application in massive quantities results in concrete having the largest share of the total embodied energy in buildings.

2.2 *Contribution of parts of a building to its embodied energy*

The structural frame of buildings forms a dominant proportion of the total embodied energy of a building, representing 27%–62% of the total initial embodied energy of the building. Hence, the structural system can be used as a target to reduce the embodied energy impact of a building.

All the LCA studies reviewed assumed that the building structure would last the full life of the building and hence replacement and repair activities of the structural frame were not considered in these studies. However, in reality this is not the case due to durability issues and further studies should be carried out to investigate the energy consumed in repair of structural systems.

2.3 *Contribution of structural elements to the embodied energy*

Within the structural frame, the floor slab system contributes the highest value to the embodied energy, representing 27% to 77% of the initial embodied energy. Thus, the designer has to select a suitable floor assembly (e.g. waffle slab or flat slab) that will result in minimal embodied energy.

2.4 *Influence of choice of construction technology on the embodied energy*

The construction phase has been found to represent 11–25% of the total initial embodied energy of buildings (Cole, 1999). This amount can be reduced by careful choice of the construction technology.

3 ROLE OF THE STRUCTURAL ENGINEER

Currently, the structural designer bases decisions on the choice of materials for the structural frame mainly on cost. However, decisions based on the construction costs for different alternatives will not necessarily have a positive influence on the environment. There are functional and material properties that influence the environmental performance of a concrete structure and which need to be considered as a priority in design. From a review of literature, it is apparent that with the construction of low-energy buildings, the embodied energy will form a dominant part of a LCA (Blengini, 2009; Thormark, 2006). This means that the structural designer will need to adopt a life-cycle approach in order to specify construction materials and building technologies that have a minimal life-cycle energy impact.

In addition, this review found the structural frame, to have a dominant impact on the embodied energy compared to other building assemblies (finishes, roof, window and non-structural frame). Within the structural frame, the slab system contributed highest to the overall embodied energy of the building, representing 27% to 77% of the initial embodied energy. To reduce these impacts, the structural engineer should aim at: (i) selecting appropriate construction technologies (e.g. precast as opposed to in-situ), (ii) selecting appropriate structural assemblies (e.g. waffle slab as opposed to solid slab for the floor system) and, (iii) reducing the concrete volume needed for building construction by optimizing the size of the structural elements particularly the slab thickness.

In order to incorporate these factors in design, further work is needed on the review of the current structural design practice and to show how these factors can be integrated into the design and optimized.

4 CONCLUSION

The paper gave a review of life-cycle assessment studies on concrete buildings, with the intention of identifying various aspects of a building which the structural designer can influence in order to reduce the overall life-cycle impacts of buildings. From the review it was noted that the structural engineer is faced with a major role in selecting materials which not only moderate building indoor performance (for human comfort and energy impacts) but in addition have minimal initial and recurring embodied energy. In addition, selection of: suitable structural assemblies, construction technologies and optimum sizing of structural components can help reduce the embodied energy of concrete buildings.

Concrete Repair, Rehabilitation and Retrofitting III – Alexander et al. (eds)
© 2012 Taylor & Francis Group, London, ISBN 978-0-415-89952-9

Synthetic climate modeling for estimating the impact of global warming on construction materials

D. Breysse, M. Chaplain & A. Marache
University of Bordeaux, I2M, UMR 5295, Talence, France
CNRS, I2M, UMR 5295, Talence, France
Arts et Metiers ParisTech, I2M, Talence, France

1 INTRODUCTION

The climatic variability at various space- and time-scales is an issue of interest for many reasons in civil engineering and building. Air temperature and humidity variations have a main influence on the ageing processes of building materials, either because they directly influence material properties or because they govern heat and mass transfer RC corrosion, timber durability…). Synthetic weather generators can be used as input data for material modeling. They are not affected by the scarcity of data and they enable to simulate and compare various scenarios. They can also be used so as to anticipate in a realistic way the possible consequences of global warming.

One can distinguish four types of weather modmodels: those based on extrapolation of data-series, on typical-years, on stochastic models and global models. The main difference is the quality of the physical modeling and the choice of mechanisms/variables which are directly accounted for, as shown on Figure 1.

Very few studies have, up to now, considered the influence of temporal fluctuations on building materials ageing. However, since their response can be driven by local events like crack propagation, or water movements inside a crack, which is itself very sensitive to local fluctuations, it seems useful to consider stochastic models, whose random nature (including frequency and magnitude of extreme events) can have a significant influence. In this paper, we will develop a stochastic model of local weather, considering temperature and humidity variations, but which will also (implicitly) account for solar radiations and evapo-transpiration mechanisms.

2 FIELD DATA AND MODELING METHODOLOGY

Input data are weather records from 1997 to 2009 on four French sites covering a variety of national climates: Brittany and Bordeaux (Oceanic), Corsica (Mediterranean) and Clermont-Ferrand (Continental). They amount to about 800 000 measurements, with temperatures at +/−0.1°C and relative humidity HR (in%). The first step was to analyze data in order to identify statistical patterns which will have to be reproduced by synthetic signals.

Temperature time variations write T(t):

$$T(t) = T_{D1}(t) + T_{D2}(t) + T_A(t)$$

where $T_{D1}(t)$ and $T_{D2}(t)$ are two deterministic components linked with seasonal and daily natural variations (driven by astronomic constraints) and where $T_A(t)$ is a stochastic signal, whose characteristic have to be identified. This part will explain the statistical variability between consecutive days, but also between years at a given date. The magnitude and the time correlation of this stochastic signal have both to be identified.

The seasonal component $T_{D1}(t)$ is modelled with a sine function:

$$T_{D1}(t) = T_{ref} + M_T.\sin [\, 2\pi(t - t_o)/8760]$$

The daily variation $T_{D2}(t)$ is identified by studying the deterministic part of the residual $T_{res1}(t) = T_m(t) - T_{D1}(t)$. It is a zero-mean signal which is governed by the solar radiations intensity and by the air cooling during the night. This variation is modeled considering that there is a linear decrease of the temperature between sunset (t_{ss}) and next sunrise (t_{sr}) and that a [linear + half-sine] function describes the temperature variation during the day time.

The stochastic component is:

$$T_A(t) = T(t) - T_{D1}(t) - T_{D2}(t)$$

It is characterized by using variographical analysis, which comes to compute the experimental semi-variogram function for each year:

$$\gamma(h) = (\, \Sigma\, [T_A(t+h) - T_A(t)]^2\,)/(2\, N(h))$$

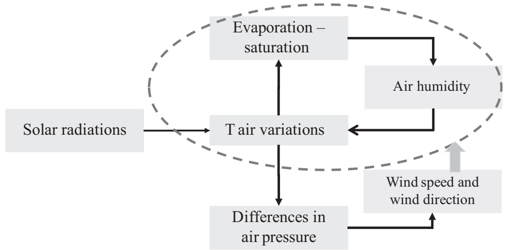

Figure 1. Relations between weather variables and mechanisms (after Guan, 2009).

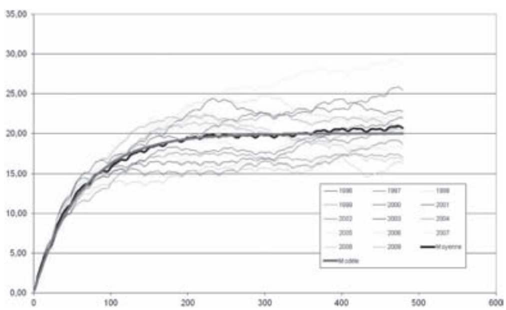

Figure 2. Experimental variograms and model variogram (Clermont-Ferrand case).

where h is the delay between two measurements (or lag-) and N(h) the number of pairs of data for a given h value. The average yearly variances of these stochastic signals amounts respectively 17.2, 10.2, 7.1 and 20.5°C² for Bordeaux, Brittany, Corsica and Clermont-Ferrand. Figure 2 plots the semi-variograms identified for 14 years of record in Clermont-Ferrand, the average variogram and the model varigram. In this case, the model is exponential.

About half of the correlation is lost after 24 hours and 90% of the correlation is lost after about 5 to 6 days. The correlation time is of prime importance for the temperature variability. It represents the « memory » of the stochastic fluctuations, very probably due to the atmospheric phenomena at a regional scale, which have not been explicitly modeled (cf fig. 1).

3 MODELING OF HUMIDITY SIGNALS

The time variations of absolute humidity are governed by two physical processes: the condensation process, and the movement of air masses because of the wind. The choice was done to consider humidity as a secondary parameter, governed by temperature variations. Its temporal variation and statistical distribution (which depends on the temperature value) have been analyzed and reproduced.

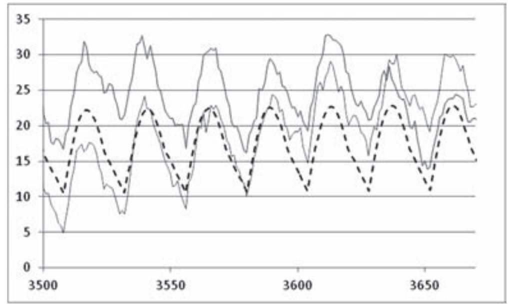

Figure 3. Two simulations of the temperature signal and deterministic part (dotted curve) in Bordeaux.

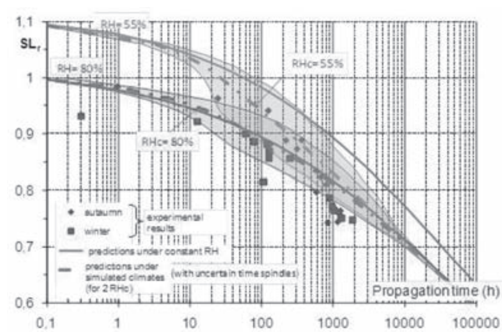

Figure 4. Experimental propagation times and average predictions under 10 000 RH simulations, as a function of stress level SL (i.e. normalized magnitude of loading).

4 SIMULATING SYNTHETIC SIGNALS AND APPLICATIONS

The comparison between synthetic signals and real ones with real signals is fully satisfactory, as well regarding statistical distributions as regarding time correlations.

Figure 3 shows the result of two simulations for the T signal in Bordeaux during a week at the end of May. The dotted curve is the deterministic component, at which the simulations add (here) two different statistical components. The daily variations as well as the time correlation can clearly be seen.

The synthetic models have been used in Monte Carlo simulations. order to simulate the time to failure of notched timber beams subjected to varying climatic conditions.. The relative contributions of the average component and of temporal variability have been analyzed and confronted with experimental results. Figure 4 shows what are the respective influences of the magnitude of mechanical loading, of the average humidity RHc, and of its stochastic variations on the service life of timber beams.

A second application was the use of the synthetic generator to simulate the RC corrosion activity by using an empirical model predicting the current of corrosion.

5 CONCLUSIONS

Combined models for temperature and humidity fluctuations have been built after an in-depth analysis of real data sets for four French climates. The models are able to reproduce: the seasonal variations for both variables, the day/night fluctuations, with cycles in the T-HR diagram, reproducing the humid air physics, and the time correlation of signals. A time scale of 5–7 days has been identified.

Two applications to timber service life and corrosion of reinforces concrete have been illustrated. It is expected that these studies will provide a basis for a better evaluation of structural reliability and monitoring of service life. Another perspective is the study of the consequences of climate change (global warming), since it is very easy to compare scenarios, like an increase of average annual temperature, an increased magnitude of random fluctuations, or more abrupt changes with a higher probability of extreme events.

Concrete Repair, Rehabilitation and Retrofitting III – Alexander et al. (eds)
© 2012 Taylor & Francis Group, London, ISBN 978-0-415-89952-9

Resistance factors for shear capacity of ordinary and lightweight R/C beams

A.S. Nowak & A.M. Rakoczy
University of Nebraska-Lincoln, USA

ABSTRACT: The objective of this study is to develop reliability model for shear strength of reinforced concrete beams, and compare the differences between ordinary concrete and lightweight concrete. The analysis is based on recent material and component test data. The research is focused on the development of statistical parameters of the shear capacity for reinforced concrete beams. Resistance is considered as a product of three random variables representing the uncertainty in material properties, dimensions and geometry (fabrication factor) and analytical model (professional factor). Material test data is presented in form of the Cumulative Distribution Functions (CDF) plotted on the normal probability paper for an easier interpretation of the results. The most important parameters are the mean value, bias factor and the coefficient of variation. It was observed that the quality of material and workmanship has been improved over the last 30 years and this is reflected in reduced coefficients of variation. However, the lab tests of the beams show that current shear design procedure is less conservative for lightweight concrete compared to normal weight concrete. It means that the resistance factor for lightweight concrete has to be revised according to statistical model of resistance.

1 INTRODUCTION

The new Load and resistance are treated as random variables. They are represented by statistical parameters, i.e. bias factor and coefficient of variation. Bias factor is the ratio of mean value and nominal (design) value. The load is considered as a combination of dead load, D, and live load, L. The statistical parameters are assumed based on the available literature. The statistical parameters of materials were determined from the test data provided by industry, including compressive strength of concrete cylinders for normal weight concrete (NWC) and light-weight concrete (LWC), and yield strength of reinforcing bars.

The statistical parameters were obtained directly from the CDF's and bias factors are shown in Fig. 1 and coefficients of variation in Fig. 2. Values of λ and V recommended for the reliability analysis are also given. The industry provided test data of yield strength for the reinforcing steel bars with the nominal yield strength of 420 MPa, and for sizes from #3 to #14 (diameters from 9.5 mm through 44 mm). It is observed that bias factors and coefficient of variation are practically the same for all rebar sizes, with $\lambda = 1.13$ and $V = 0.03$. The parameters of resistance, R, were calculated using Monte Carlo simulations.

2 RELIABILITY ANALYSIS

The reliability indices were calculated for a full range of dead load and live load ratios. For each considered design case, the results are presented for three values of ϕ for light-weight concrete, $\phi = 0.70$, 0.75 and 0.80. For comparison, the calculations

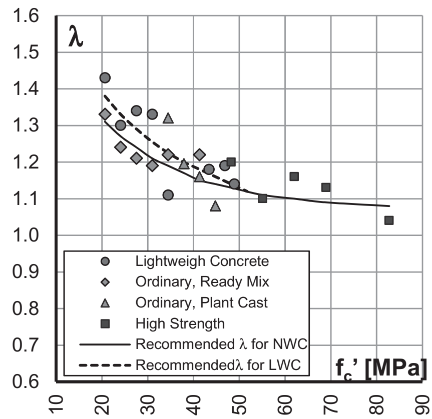

Figure 1. Bias Factors of Compressive Strength of Concrete.

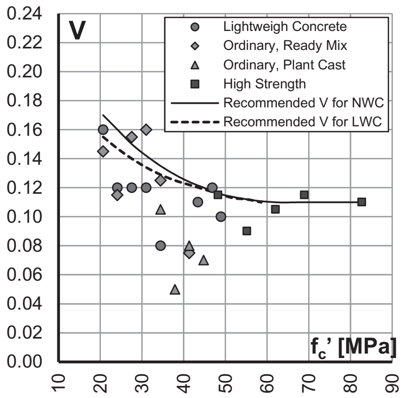

Figure 2. Coefficient of Variation of Compressive Strength of Concrete.

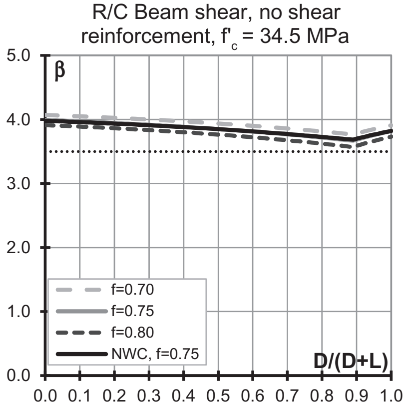

Figure 3. Reliability Index vs. Load Ratio for No Shear Reinforcement.

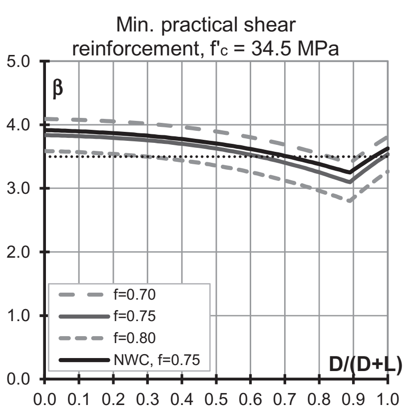

Figure 4. Reliability Index vs. Load Ratio for Minimum Practical Shear Reinforcement.

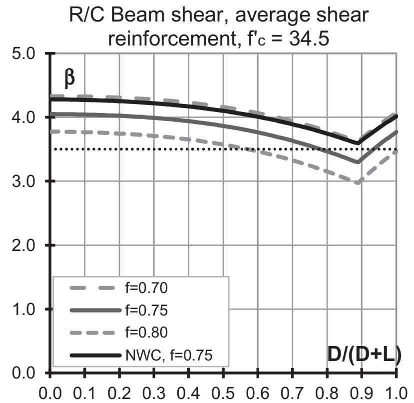

Figure 5. Reliability Index vs. Load Ratio for Average Shear Reinforcement.

were also performed for normal weight concrete and $\phi = 0.75$. The results are shown in Fig. 3 for the case of no shear reinforcement, Fig. 4 for the minimum practical shear reinforcement, and Fig. 5 for the average shear reinforcement. For lightweight concrete, the resulting reliability indices are practically between 3.5 and 4.0 for $\phi = 0.75$.

3 CONCLUSIONS

The statistical parameters of shear capacity depend on the shear reinforcement ratio and strength of concrete. The bias factor and coefficient of variation decreases with concrete strength. For larger reinforcement ratio, the resistance parameters are affected more by rebar properties rather than concrete.

It was observed that the bias factor for compressive strength of lightweight concrete is slightly higher than that for the ordinary concrete and high strength concrete. This is an indication of a more conservative approach to the application of a relatively new material. However, additional properties of lightweight concrete also influence the member capacity in shear resulting in a lower value of professional factor. It was found that the resistance factor for shear strength of lightweight reinforced concrete beams should be 0.70.

Concrete Repair, Rehabilitation and Retrofitting III – Alexander et al. (eds)
 ISBN 978-0-415-89952-9

Global safety factor for slender reinforced concrete structures

D.L. Allaix, V.I. Carbone & G. Mancini
Politecnico di Torino, Torino, Italy

ABSTRACT: The use of a non-linear analysis in the safety verification of reinforced concrete columns is the topic of the paper. A safety format based on the mean values of the material properties and a global resistance factor is presented. The global resistance factor is derived from the distribution of the failure load, using a probabilistic approach. The effect of the slenderness on the global resistance factor is investigated by a parametric analysis.

1 INTRODUCTION

The present paper concerns the use of the non-linear analysis for the safety verification of slender reinforced concrete columns at the semi-probabilistic level. A safety format based on the non-linear structural analysis should specify the following issues.

The first one is related to the representative values of the material properties. It is generally agreed that the design values may lead to an erroneous assessment of the load bearing capacity. For example, unrealistic redistribution of internal actions may occur in case of beams. Even a worse effect is observed in the case of slender columns. In fact, the design values of material properties lead to an overestimation of the deformability of the structure. Consequently, the load bearing capacity is strongly penalized. Following this reasoning, the mean values of the material properties have been suggested [CEB 1995]. By this choice, the most probable values of internal actions are obtained from the non-linear analysis.

The second issue is the choice of the domain where the safety verification is performed. In the recent Model Code 2010 [fib 2010], the domain of the actions is suggested. However, the domain of the internal actions is more appropriate, as considered in the EN1992-2 [CEN 2005]. Indeed, the structural design using the semi-probabilistic approach is based on the comparison of internal actions and corresponding resistances. In addition, only in the internal action domain it is possible to distinguish between linear, under- and over-proportional behaviour.

2 SAFETY FORMAT BASED ON THE MEAN MATERIAL RESISTANCES

The framework of the safety format of the EN1992-2 is maintained. The two modifications concern the material resistance and the global safety factor.

In accordance to the suggestions of the CEB [CEB 1995], the mean values of the resistances of steel and concrete are used in the non-linear analysis.

The safety verification is performed in the region of the structure whose failure determines the attainment of the ultimate load. In the case of a column, the safety verification is written as follows:

$$M_{Ed} \le M_R\left(\frac{q_u}{\gamma_R}\right)$$
$$N_{Ed} \le N_R\left(\frac{q_u}{\gamma_R}\right) \tag{1}$$

Where M_{Ed} and N_{Ed} are the internal actions due to the design actions, M_R and N_R are the corresponding resistances, q_u is the collapse load and γ_R is the global resistance factor.

The global resistance factor is estimated using a probabilistic approach, on the basis of the distribution of the failure load. Therefore, the randomness of the material properties and its effect on the failure load are directly taken into account.

3 PROBABILISTIC DERIVATION OF GLOBAL RESISTANCE FACTORS

In general terms, the global resistance factor is defined as the ratio between the mean and the design value of the resistance [Allaix et al. 2007, Allaix & Mancini 2007, Cervenka 2007, fib 2010]:

$$\gamma_R = \frac{R_m}{R_d} \tag{2}$$

Assuming a lognormal distribution with coefficient of variation V_R less than 0.25, the global resistance factor can be expressed as:

$$\gamma_R = \frac{R_m}{R_d} = \frac{R_m}{R_m \exp(-\alpha_R \beta V_R)} \tag{3}$$

where α_R and β are, respectively, the sensitivity factor and the reliability index. Considering the ULS, the values $\alpha_R = 0.8$ and $\beta = 3.8$ are suggested by the EN1990 [CEN 2002].

Hence, the global resistance factor γ_R is simply related to the coefficient of variation V_R:

$$\gamma_R = \exp(3.04 V_R) \tag{4}$$

The Monte Carlo method is used to estimate the coefficient of variation V_R. During each simulation, the relevant properties of the structure are generated randomly. A non-linear analysis, considering both material and geometrical non-linearities, is performed. The outcome of each simulation is the failure load level. A statistical analysis of its distribution enables an estimation of the coefficient of variation.

4 APPLICATION EXAMPLE

A pier of a slab bridge is analyzed in the present paper. A rectangular cross section with base *b* and height *h* of 4 m and 1 m is assumed. The characteristic values of the actions applied on the top are:

$F_{gk} = 10000$ kN;
$F_{qk} = 2500$ kN;
$H_{qk} = 4000$ kN.

The steel S500 and the concrete grade C35/45 are considered.

A parametric analysis with respect to the slenderness λ has been conducted. The objective is to analyse the variation of the global resistance factor γ_R when the second order effects become more important. The values λ = 40, 60, 80, 100, 120 and 140 are considered. The probabilistic model used in the Monte Carlo simulations concerns the compressive strength of concrete f_c, the yielding stress f_y and tensile strength of steel f_t, the out of plumbness ϕ and the resisting model uncertainties ϑ_R [JCSS 2006].

The global resistance factor γ_R is plotted in Figure 1. The global resistance factor decreases as the slenderness of the column becomes more important. The coefficient of variation V_R is between 0.08 and 0.14.

In the cases $\lambda = 40$ and $\lambda = 60$, the failure is characterized by the reinforcement steel in tension in the elastic range. For higher values of slenderness, the reinforcement steel is yielded at failure.

The decrement of the global resistance factor can be related to the ultimate strain configuration at the base of the column. The variation of the global resistance factor based on the failure load can be explained by the variability of the resisting bending moment at the cross-sectional level.

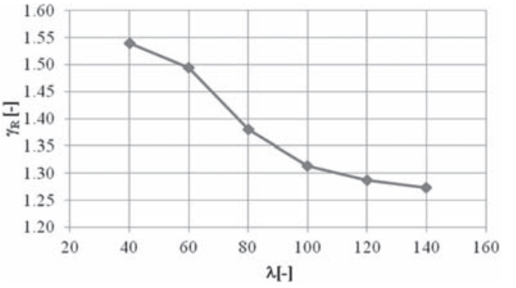

Figure 1. Global resistance factor vs. slenderness.

5 CONCLUSIONS

In the present paper a safety format for non-linear analysis based on the mean values of the material resistances is presented. The safety verification is performed in the domain of the internal actions. A global resistance factor obtained from the distribution of the failure load is applied on the resisting side.

REFERENCES

Allaix, D.L. et al. 2007. Global resistance factor for reinforced concrete beams. *Proc. 5th International Probabilistic Workshop, Ghent 28–29 November 2007.* Ghent: Acco.

Allaix, D.L. & Mancini, G. 2007. Assessment of a global resistance factor reinforced concrete columns by parametric approach. *Proc. International Symposium on Innovation & Sustainability of Structures in Civil Engineering, Ghent 28–30 November 2007.* Shanghai: Southeast University Press.

CEB 1995. New developments in non-linear analysis methods. Bulletin d'Information N°229.

CEN 2002. EN1990: Eurocode – Basis of structural design.

CEN 2004. EN1992-1-1: Eurocode 2—Design of concrete structures—Part 1-1: general rules and rules for buildings.

CEN 2005. EN1992-2: Eurocode 2 - Design of concrete structures—Part 2: concrete bridges—Design and detailing rules.

Cervenka, V. 2007. Global safety format for nonlinear calculation of reinforced concrete. *Proc. 5th International Probabilistic Workshop, Ghent 28–29 November 2007.* Ghent: Acco.

fib 2010. Model Code 2010.

Holicky, M. 2007. Probabilistic approach to the global resistance factor for reinforced concrete members. *Proc. 5th International Probabilistic Workshop, Ghent 28–29 November 2007.* Ghent: Acco.

JCSS 2006. Probabilistic Model Code.

Concrete Repair, Rehabilitation and Retrofitting III – Alexander et al. (eds)
© 2012 Taylor & Francis Group, London, ISBN 978-0-415-89952-9

Time-dependent analysis of segmentally constructed cantilever bridge comparing two different creep models

G.F. Giaccu
Dipartimento di Ingegneria Strutturale, Università di Cagliari, Italy

D. Solinas
Freelancer in Cagliari, Italy

G.P. Gamberini
Dipartimento di Ingegneria Strutturale, Università di Cagliari, Italy

ABSTRACT: Segmentally constructed balanced cantilever bridges are often subjected to larger deflections then those predicted calculations, which could be a problem for the vehicular traffic especially in the case the deflections increase during the lifetime of the bridge. It is the case of the "Navile" and "Sa Pruna" bridge, two similar viaducts located in Sardinia (Italy), both subjected to the same problems with large deformations involving considerable problems for vehicular traffic. In the present work a time analysis, related to "Navile" bridge, was performed as to compare the results obtained by two different creep-models the CEB-FIP Model Code 1990, the most common model and the B3 Model, which leads to different results from those obtained by the previous model. For the purposes of a comparison both two models have been introduced in the computation. The two different models lead to different results especially in the case of long time deformations, particularly the results obtained through the B3 model, are more in agreement with the real data.

1 INTRODUCTION

The Prestressed concrete segmental bridges are often subjected to considerable stress during the launch. These conditions, can lead to substantial displacements on the structure. Usually these effects are appropriately evaluated during the launch in order to reach a final straight configuration of the bridge. Under certain conditions, due to creep, shrinkage and relaxations effects, the displacements may increase during the entire life of the structure, leading to significant inconvenience to traffic and to the structure. For both of bridges have occurred, already a short time after the entry into service, large deformations at the ends of the cantilevers in correspondence of both shoulders and although to a lesser extent, in the middle point, where the joint is located. The restoration work carried out was mainly to level the road surface paved with asphalt injection, which, over the years have worsened the situation by increasing the displacements. It was found that after 16 years, the vertical displacements have a significant tendency to increase over time.

1.1 *Description of the "Navile"end "Sa Pruna" bridges*

Navile e Sa Pruna bridges are two structures built in Sardinia between 1990 and 1994. The two bridges are very similar to one another and differ only in number of spans. The "Navile" bridge consists of 8 spans with a total length of 560 m whereas "Sa Pruna" bridge consists of 10 spans with a total length of 700 m.

The static scheme adopted is the same for both bridges and consists of a continuous beam interrupted by a joint in the middle point and connected to the shoulders by a floating slab for the union between the shoulder and deck (figure 1).

The structures are a prestressed continuous hollow box-girder bridges launched by precast segmental construction technique (over head method).

For the sake of simplicity only the case of "Navile" bridge has been studied in this paper.

2 RESULTS

The results obtained are explained in the following points by evaluating the comparisons between the two rheological models used respectively for: bending moments, shear forces and vertical displacements.

2.1 *Bending moments*

The diagram of bending moments shows the differences between the model- (CEB MC 90) and the model (RILEM B3), differences between the results

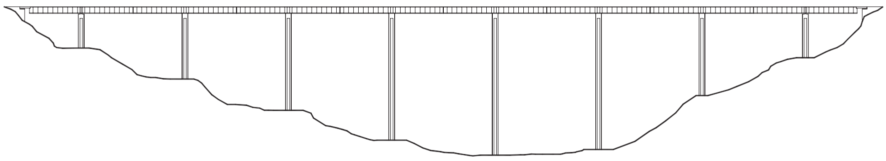

Figure 1. Elevation of the “Navile” bridge.

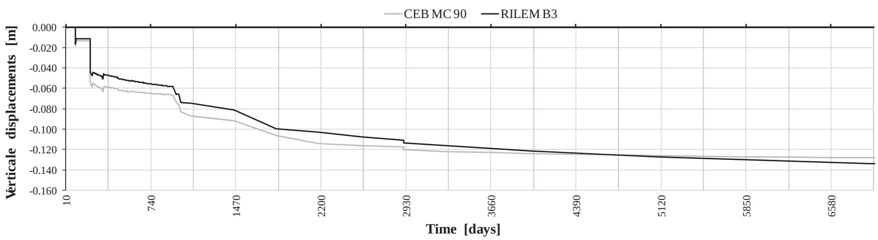

Figure 2. Comparison between the vertical displacements of the bridge in correspondence of the south shoulder.

obtained are limited to those parts of the deck in the middle of the span. The diagram emphasizes the presence of peaks of bending moments near to the lateral spans and in correspondence of the expansion central joint, where the structural continuity is lost because of the presence of joints. The prestressing tendons are not sufficient to balance the negative bending moments.

2.2 *Shear*

The shear diagrams do not show particular differences between the two rheological models, whose plots are almost overlapped. In this case the presence of the prestressing tendons is sufficient to ensure that the shear actions are distributed almost uniformly over the whole deck.

2.3 *Vertical displacements*

The vertical displacements are those values that represent the fundamental differences between the two rheological models utilized.

The displacements given by CEB MODEL occur almost immediately, but then tend to stabilize over time, while those obtained through the RILEM MODEL continue to evolve over time (figure 2).

Both models have shown the problems that arise in the process of launching; in fact the vertical displacements are not compatible with the serviceability limit state.

3 CONCLUSIONS

This paper shows the results obtained beam finite element model of the “Navile” bridge, where are taken into account all of the time dependent effects and all phases of the structure since its launch.

The results obtained by the use of the RILEM model qualitatively confirm those measured in situ, the displacements of the structure do not stabilize and tend indeed to evolve over time. The CEB models instead lead to results, which tend to stabilize in time.

The beam element model used in the present paper tends to underestimate the long term displacements, due to other tridimensional effects, but highlights the conceptual difference between the two modeling of creep used and confirms the fact that the RILEM model is, in this case, more appropriate. Future work will aim to draw up, for long term Displacements, a more complex modeling that takes into account all those tridimensional effects, which cannot be evaluated using the classical theory of bending.

REFERENCES

Bažant, Z.P. & Baweja S. 2000. Creep and Shrinkage Prediction Model for Analysis and Design of Concrete Structures: Model B3, ACI SP–194, Adam Neville Symposium: Creep and Shrinkage—Structural Design Effects, Am. Concrete Institute, 1–83, Farmington Hills, Michigan.

Bažant, Z.P., Li, G.-H., Yu, Q., Klein, G. & Křístek, V. 2009. Explanation of excessive long-time deflections of collapsed record-span box girder bridge in Palau, Structural Engineering Report No. 08–09/A222e, McCormick School of Engineering and Applied Science, Northwestern University, Evanston, Illinois.

Comitè Euro-International Du Beton. 1993. CEB-FIP Model Code 1990, Thomas Telford Services Ltd., London.

Malm, R. & Sundquist, H. 2010. Time-dependent analyses of segmentally constructed balanced cantilever bridges, Engineering Structures 32, Elsevier, 1038-1045, Amsterdam.

The Third International Conference on Concrete Repair, Rehabilitation and Retrofitting (ICCRRR 2012) was held in Cape Town, South Africa, from 3 to 5 September 2012. The conference was the latest in a sequence of ICCRRR international conferences, the two previous ones having also been held in Cape Town in 2005 and 2008. It was again a collaborative venture of the Universities of Cape Town and The Witwatersrand, and the Construction Materials Sections at Leipzig University and MFPA Leipzig in Germany.

The conference was also an occasion to honour the considerable achievements of Professor Joost Walraven of TU Delft who has made, as a researcher and as an engineer, outstanding and international contributions to the development and application of new construction materials, new structures, and structural models.

This 3rd ICCRRR was held in conjunction with the Annual RILEM Week – marking the first time that RILEM had held its annual event in sub-Saharan Africa. The African continent is on the move, and the next decades will provide great opportunities for expansion on this continent of science and technology, industry and culture. For this reason, it was timely that the RILEM Week was held in Cape Town.

Considerable progress has been made in recent years in understanding deterioration mechanisms for concrete, and in repair and rehabilitation technologies. Nevertheless, a vast stock of concrete infrastructure worldwide remains in a serious state of disrepair, and substantial work is needed to maintain and possibly restore it to acceptable levels of service, cost-effectively. Confidence in concrete as a viable construction material must be retained and sustained, particularly considering the environmental challenges that the industry and society now face.

The conference proceedings contain papers presented at the conference, classified into a total of 12 sub-themes which can be grouped under the five main themes of (i) Concrete durability aspects, (ii) Condition assessment of concrete structures, (iii) Concrete repair, rehabilitation and retrofitting, (iv) Developments in materials technology, assessment and processing, and (v) Concrete technology and structural design. In terms of submissions, major foci of interest are the fields of innovative materials for durable concrete construction, integrated service life modelling of reinforced concrete structures, NDE/NDT and measurement techniques, repair methods and materials, and structural strengthening and retrofitting techniques. The large number of high-quality papers presented and the wide range of relevant topics covered confirm that these proceedings will be a valued reference for many working in the important fields of concrete durability and repair, and that they will form a suitable basis for discussion and provide suggestions for future development and research.

CRC Press
Taylor & Francis Group
an informa business
www.crcpress.com

6000 Broken Sound Parkway, NW
Suite 300, Boca Raton, FL 33487
Schipholweg 107C
2316 XC Leiden, NL
2 Park Square, Milton Park
Abingdon, Oxon OX14 4RN, UK

ISBN 978-0-415-89952-9
9 780415 899529
an informa business